Elsevier
30 Corporate Drive, Suite 400, Burlington, MA 01803, USA
Radarweg 29, PO Box 211, 1000 AE Amsterdam, The Netherlands
Linacre House, Jordan Hill, Oxford OX28DP, UK



**British Library Cataloguing-in-Publication Data**
A catalogue record for this book is available from the British Library

**Library of Congress Cataloging-in-Publication Data**
A catalog record for this book is available from the Library of Congress

ISBN: 978-0-444-53757-7
ISSN: 1571-9197



Printed and bound in Great Britain
11 12 10 9 8 7 6 5 4 3 2 1

# Dedication

This book is dedicated to Dr. Chrysostomos L. Nikias, the eleventh President of the University of Southern California, Los Angeles, California, for his outstanding contributions to the education of University students.

# Foreword

Science progresses by continuous testing of theories. Today, the Earth sciences are intertwined with both economic and social policies in a complex world, more so than most of us could ever have imagined. Challenging the first principles of science and developing alternative explanations for observations are inherent in geological science, but seem to have been ignored when addressing concepts that have social and financial repercussions, such as climate change, environmental degradation, and catastrophic Earth events. Floods, volcanic eruptions, earthquakes, and landslides—all are demanding political and policy attention. Sorohktin, Chilingar, and Sorohktin are meeting that challenge with a book that documents the basis of the Earth sciences and prepares the reader to make better informed decisions about Earth-process-related problems.

Before delving into the book's contents, some historical and personal background might be useful to the reader.

Geology is the youngest of the physical sciences. Its organized beginnings were defined by the development of a theory of Earth's origin in 1787 (Werner, 1787) by Abraham Gottlieb Werner. He formulated the first encompassing theory of the Earth, Geognosy, or "Earth Knowledge" based on his own explorations around the Bergakademie in Freiberg, Saxony, and foundations laid by previous scientists. His theory was predicated on "exhalations and vapors" with unknown driving forces making fluids repeatedly spill onto the surface of the Earth, deposit rocks, and then return to the abyss, only to come forth again, a total of four times. On the other hand, Werner did recognize one of the fundamental aspects of the Earth. He noted the underlying basement of crystalline rocks (his "Primary"), later covered by layered rocks (his "Secondary"), then volcanics, and lastly, unconsolidated sands and gravels. In the immediate region around Freiberg, where he worked, this was a plausible sequence. The major stimulus for study of the Earth at the time was diagnosing mineral occurrences and their exploitation, a focus on economic implications of scientific study that persists today. It was a start, but lacked a real-world mechanism to drive the history he created.

At nearly the same time, James Hutton articulated his Theory of the Earth, based on comparison of present-day processes compared to those interpreted to have occurred in rocks. Uniformitarianism, as it is called today, is encapsulated in the simple statement, "The Present is the Key to the Past." It was likely presented in public in 1788 (Hutton, 1788), although officially published in two volumes in 1795 (Hutton, 1795). The beginning of modern geological science really dates from that publication. Hutton simply agreed that the mechanisms that drive the present were also the ones that drove the past, without speculating unduly on those mechanisms.

Before belittling either of these theories, it is important to place their evolution in the technology and travel opportunities of the times. Werner, for instance, never traveled

beyond Saxony, whereas Hutton traveled extensively, but only in the British Isles and Europe.

For nearly 200 years, we geologists could not understand how mountains were built or how rocks became to be deformed as Hutton (and now we) observed them. We developed many theories, several of which were diametric opposites. Some believed that the Earth was expanding, others argued forcefully that the Earth was shrinking. All kinds of simple dynamic models were proposed, from shriveled apples with wrinkled skins that mimicked folded mountain ranges (shrinking Earth) to glass Christmas tree balls filled with water and then frozen, to prove that the Earth was expanding through the pattern of cracks in the glass, so reminiscent of the rift valleys of Africa.

My early academic career was complicated by these conflicting theories. Kay's (1971) geosynclines dominated discussions during the late 1950s, and much class time was wasted on classifying all the tectonic features of the Earth into one or more geosyncline types, until it seemed that every feature was its own unique type. When I asked professors what forces caused the depressions and consequent mountain-building, I got blank stares in return or words that meant nothing to me, words related to either Earth contraction or expansion, polar wandering, or self-perpetuating gravity-driven dynamics. In short, after 200 years of study, we had not developed a unified field theory of the evolution of the dynamic Earth. It was as if we were blind men and women, each feeling some different part of an elephant.

For me, everything changed in 1963. Lurking in the background of the roiling tectonic debates was a theory called "continental drift." Maligned by nearly every geologist and geophysicist in the northern hemisphere, but kept alive by scientists in Africa and Australia, this theory argued that now separate continents had been joined in the past. This theory had been ridiculed and lambasted by many, but kept returning because of the coincidence of opposite shorelines, matching tectonic trends, and mammal distribution. One of the main arguments opposing this theory was that there was no known mechanical force that could drive such a dynamic phenomena.

In 1963, I attended a lecture series by the famed Carl Dunbar, newly retired from his professorship at Yale University. Among other stratigraphic lectures, he presented evidence that demanded the presence of a landmass to the east of the present Catskill Mountains of New York in Paleozoic time. When I protested that there was no data suggesting such a land mass existed out on the continental shelf, the famous professor, in his grandfatherly way, just showed me the stratigraphic data requiring the presence of an eastern source for the sedimentary wedges at issue.

I immersed myself in tectonic readings, including du Toit (1937) and evidence in the southern hemisphere for continental drift, Runcorn's paleomagnetism (Runcorn, 1963), and Clemen's mammalian evolution and distribution patterns (Clemens, 1963). Finally, during my oral doctoral examination, I was asked to explain the mechanisms for mammalian distribution. My mind knew exactly how to respond to this question, but my words darkened the faculty's faces and stunned my major professor: "Continental drift."

Fortunately for me, I knew the literature better than the faculty, and they passed me on that basis of that knowledge.

This is our modern dilemma about climate change. We have observations and data that do not fit current theory, but many

scientists deride the observations in order to defend their pet theory, while ignoring alternative theories that do explain all the data and observations, explaining them as being "not possible."

Just 2 years later, J. Tuzo Wilson (1965) gave his famous transform fault paper at the Geological Society of America Annual Meeting, followed shortly by papers discussing the seafloor spreading and, thus, geosynclinal theory went into full retreat and the "New Global Tectonics" was born.

For the first time in our science history, we had a unified field theory of the dynamic Earth. It explains all of the observational data, even though we do not fully understand the mechanisms that drive the system.

The foregoing story illustrates the difficulty in gaining acceptance of new ideas and the reticence of many scientists to rigorously test hypotheses against data, if the hypothesis is popular. In all the cited cases, discarded theories failed the test of explaining *all* of the data, rather than just part of the data. This is the issue that the proponents of anthropogenic climate change face today.

For the tectonic theory, it took nearly 50 years for observational data to override the contrary hypotheses. The scientific method makes science progress by developing new hypotheses, testing them against data and observations, and then modifying the concepts if the data do not support the hypotheses. This method is simple and straightforward. Frequently, this scientific method is ignored by highly schooled and largely uneducated people who *believe*, rather than *know.* This setting is not so far removed from Wernarian geognosy (Werner, 1787), an attitude that set back progress in geological science for 50 years.

Today, another 40 years later, we face the same reticence to test currently popular hypotheses on a variety of issues, including the causes of climate change. It has been more than 20 years since the quasi-religious anthropogenic climate-warming hypothesis first gained popular momentum. This hypothesis of human-caused global warming has been scientifically falsified by data demonstrating that the peaks of temperature historically precede peaks of carbon dioxide contents in atmosphere, that carbon dioxide is already at near saturation for absorbing heat, that there is no correlation between temperature change and concentration of carbon dioxide, and by demonstration that current rates and absolute values of temperature change are well within historical norms. In addition, the authors of this book have established that increasing the carbon dioxide content in the atmosphere will cool the atmosphere, rather than warm it. Yet, popular public figures and media call for persecution of those who have the temerity to argue that natural forces control temperature change, calling to mind the theocratic inquisitions of Galileo (Hansen, 2008).

"Evolution of Earth and its Climate: The Birth, Life, and Death of Earth" challenges the reader to critically analyze both theory and data. What a refreshing approach!

The authors of this new study of Earth history did not constrain themselves with currently popular concepts. Instead, they have developed a unified exposition of the Earth, including not only its history but also, based on that history, a projection of its future. The authors are internationally recognized scientists, representing a broad spectrum of knowledge and experience. For many, this volume contains new theories and concepts, in part presented first in the Russian language literature that is not widely read in the western world. The authors expect the reader to at least be better able to argue effectively from data and

observations for any other alternate theory, whether or not they agree with the writers' arguments. They fully understand that debate over unsettled theory is always useful and, frequently, crucial to resolution of knowledge.

Part 1, Chapter 1, is a discussion of how theory is developed and how the tectonic understanding of Earth's dynamic systems was constructed. Coupled with Chapter 2, it outlines how information about the Earth has been gathered and interpreted, and describes the various units of Earth's construction. Along with physical descriptions of hard materials of Earth's core, mantle, and crust, they also describe the origin and evolution of the atmosphere and hydrosphere. The viscosity, strength, and temperature of the inner Earth are described next.

Once the reader has grasp of the theory logic and the physical characteristics of the Earth, the authors use Chapter 3 to integrate the preceding into the interpretation of Earth origin, origin of Moon, and the placement of the Earth in the Universe. The early evolution of this green and blue planet is discussed as a consequence of early Earth dynamics. The culmination of these interpretations resides in a forecast for the probable "death" of the planet in the future.

Chapters 4–6 develop and expand upon the dynamics of the mechanical Earth systems, starting with differentiation of the core and mantle. Also included are discussions on the Earth's energy sources and heat and energy balance, with comments on the development of the magnetic field.

Part 2 (four chapters) is a full discussion of the evolution of the Earth's crust, combining the chemical evolution with tectonics and development of lithospheric plates. The relative movement of continents during the Precambrian and Phanerozoic is outlined. This is followed by an extensive treatment of the origin of mineral and energy deposits, relating emplacement processes to the dynamics of the Earth. Part 2 is devoted to the study and analysis of the solid Earth.

Part 3 (five chapters) addresses the "Evolution of the Oceans, Atmosphere, and Life on Earth." For those readers who have interest in the current debate over a possible human role in our constantly changing climate, Part 3 is a "back to first principles" study of the origin, evolution, and dynamics of the atmosphere. Before making statements about current climate change, the atmospheric dynamic system must be analyzed from its origin through its evolution to modern-day composition. Placed in a chemical and historical context, the changing composition of the atmosphere through time is examined. Alternative theories of how these changes will affect global temperature are also presented.

In the latter section, the authors express an opinion in their review of the Kyoto Protocol. However, it is only a minor portion of the discussion of atmospheric evolution and does not detract from the overall scientific authenticity. Considering the volume of background information they have presented, it is more surprising that they have restrained themselves from further comment. Readers should take extra care to fully understand the background, derivation, and significance of their empirically tested adiabatic theory of the greenhouse effect.

Sorokhtin, Chilingar, and Sorokhtin conclude this volume with a discussion of the biosphere, its origin, its impact, and its future. These Earth scientists do not hold a religious reverence for the biosphere. Rather they regard the biosphere as a part of the natural evolution of a solar system body, dependent upon its geological foundation, dynamic and chemical processes, and the laws of physics. Their forecast of its future

is dominated by their clinical analysis of relevant data.

This book is a compendium of our knowledge of the origin of Earth, tempered by advanced theories, and international concepts, some of which are unfamiliar to many readers. It lays the groundwork for additional research in many geological arenas owing to stimulative ideas.

For understanding modern climate change, the major step forward will be development and general acceptance of a set of metrics that define historical trends and permit the identification of changes that could have a human cause. The slope (rate) of natural temperature changes can be developed from the historical record. The limits of natural temperature variability can also be derived from the geological record. Testing current or future decadal or multidecadal trends against these norms can provide an absolute definition of "unprecedented" change.

Every century, humankind seems to be afflicted by a rebirth of catastrophism. For instance, in the 18th Century Werner (1787) prevailed, in the 19th Century, Cuvier (Wendt, 1956), and in the 20th Century, Hansen and Gore and the IPCC (Intergovernmental Panel on Climate Change of the United Nations). Earth scientists discount these episodes of catastrophism as fantasy, but they persist in political and social agendas. The Earth's dynamic systems change in character over time, but they change gradually. Claims to the contrary have always been proved false.

In closing, it may be worthwhile to consider a different view of geologic theory. Hutton's uniformitarianism has been simply stated as "the present is the key to the past." But with today's available technology and data sets, we can also confidently state, "the past is the key to the future." We should study the past carefully and project the lessons learned wisely.

DR. LEE C. GERHARD
Director (ret.) Kansas Geological Survey
Senior Scientist Emeritus
University of Kansas

# Introduction

*Science is built of facts as a house is built of bricks but a simple collection of facts is no more science than a heap of bricks, a house.*

*From Henri Poincare*

A theory is a system of guiding ideas and concepts. Its role in any science of natural history is, first of all, in facilitating the right understanding of observed natural phenomena, answering the "whys," and therefore allowing us to identify the causal relationships controlling the evolution of these phenomena and the processes they represent. This is not all, however. Besides a simple explanation of the already known domain of phenomena, a modern theory must enable a quantitative estimation of their major parameters and must possess a prognostic force: to forecast the existence of the phenomena unknown prior to the appearance of the theory, and gauge the course of such processes in the future. Of course, the adequate and most complete scientific theories must consider and include all facts and phenomena within the given scientific domain, without any exceptions.

There are several criteria to check on the correctness of a theory under consideration.

First of all, such theory must be internally consistent and firmly based on modern physics, and not contradict its laws and fundamental principles.

Second, the theory which is an objective reflection of reality must be self-congruent and, in principle, must be able to explain, from a unique position and quantitatively, all phenomena and processes under the auspices of the given natural–scientific discipline, and within the tolerances inherent in the subject theory. Well-known examples of theories describing natural phenomena with different degrees of approximation are the Newtonian, relativity and quantum mechanics in physics, the evolutionary and molecular genetics in biology, etc.

And lastly, any scientific theory must have a prognostication capacity and allow for the quantitative check by way of direct or indirect experiments for testing its forecasts.

A correct scientific theory is highly important in the solution of practical problems as it allows for the correct calculation and sometimes control of practically useful natural processes. On the other hand, practice and experiment are the main criteria of the verity of cognition which usually materializes in the form of the creation of scientific theories.

In this book, the authors aim to describe the most general physical theory of the Earth's evolution. The theory reflects as fully as possible the geologic record and the aforementioned requirements. They demonstrate that an adequate description of the Earth's geologic evolution may be performed using a relatively simple physical model of global processes. The theory is based on just two basic assumptions and one physical concept.

According to the most substantiated hypotheses of the origin of the planets in our Solar system, it is believed that the Earth formed about 4.6 billion (BY) years ago as a result of homogenous accretion of a gas–dust protoplanet cloud (Schmidt,

1948; Safronov, 1969). From here follows the first assumption: the young Earth has a uniform composition; it did not have either a dense core or a light crust. One may recall that the oldest Earth crust rocks are about 600–800 million years (MMY) younger than the likely age of the Earth. This is singular evidence of the fact that the primordial Earth was a cold cosmic body. Contrary to that, the oldest igneous rocks of a thick lunar crust (anorthosites) are 4.6–4.4 BY old, which is a convincing indication of the originally hot, melted, and differentiated state of the Moon. This conclusion is supported by the lead isotope ratios in Earth's and lunar rocks (see Chapter 3 for a more detailed discussion).

It is worthwhile mentioning here that new data appeared lately describing the find of embryonic type detrital zircons with the age of 4.2 to 4.4 BY. Some scientists are treating this fact as a proof of existence of not only magmatic rocks but even the crust-forming processes in Katarchaean (Hadean). We will detail this issue in Chapters 3 and 4 but we can state here that in our belief this phenomenon is associated with the planetary accretion processes and melting the planetesimal mutual impact surfaces. The released impact energy on the one hand, and high heat release rate on the other hand unavoidably resulted in the formation of a contact magmatic foci on the surfaces, and these magmatic phenomena had been very short-living.

As the chemical composition of the primordial Earth predetermined the entire endogenous energy of the planet, it was necessary to assign the composition of the Earth's crust, mantle, and core. The composition of the first two geospheres is known from empirical data, whereas the core composition is and will always be just a hypothesis. From this follows a second assumption: we suggested and tried to substantiate that the composition of the Earth's core external shell corresponds to the eutectic alloy of iron and iron oxide, which is the oxide of the univalent phase of iron, whereas the internal core is composed of an iron–nickel alloy (Sorokhtin, 1971). If this is correct, then the primordial Earth matter contained approximately 13% of free (metallic) iron and 22–24% of its bivalent oxide.

Thus, the proposed theory is based on two main assumptions: (1) the young Earth was a compositionally uniform and relatively cold planet with no melted foci under the surface and (2) the Earth's crust formed later and consisted of the oxide of the univalent iron phase and iron proper within the Earth's center. Under the first law of thermodynamics, Earth's evolution is based on a physical concept that the largest contribution to the planet's evolution was from energy processes that lowered to its minimum the potential (internal) energy of the Earth proper and of the Earth–Moon system. Heat released in these processes was eventually lost to outer space. Thus, the evolution of the Earth and of the Earth–Moon system was irreversible.

Data on the structure and composition of the present-day Earth as well as its historic geologic record serve as the boundary conditions of the evolutionary theory. Besides, a condition of the kinetic momentum conservation in the Earth–Moon system, and a remarkable coincidence of this momentum with its value at which the Moon gets beyond the Roche limit and both planets have synchronous angular velocities of *eigenrotation* (with a period of about 6 h), should be taken into account. This fact indicates a close tidal interference between the Earth and the Moon at the early stages of the planetary system's evolution. Considering a strong interaction between the young Earth and the Moon, it is also important to note the following: The Moon's basalt magmatism coincided with the occurrence about 4.0–3.8 BY ago of the

Earth crust's oldest igneous rocks that manifest at the beginning of the Earth's tectonic activity. It is also important that at the Archaean–Proterozoic boundary, about 2.6 BY ago, the most grandiose event in the Earth's history occurred: the Kenoran orogeny and the most radical change in the Earth crust formation processes. It is enticing to associate these events with a catastrophic formation of a dense core in the Earth's center, the core which was the "embryo" of the present-day iron-oxide core.

Under the most general geologic theory described, the main planetary process controlling the Earth''s evolution was the chemico-density differentiation of the Earth's matter. This process resulted in the separation in the Earth's center and growth of a dense iron-oxide core, and in the emergence of the chemico-density convection in its silicate shell (mantle) (Sorokhtin, 1974).

This process currently releases about 90% of the endogenous energy. In the second place in terms of its capacity is radioactive decay (less than 10%). The tidal deformations in the Earth's body release additional 1% of the endogenous energy.

The quantitative relationships between these energies changed with time. During the Earth's origin, the planet's accretion gravity energy almost totally dominated. The young Earth was dominated by the tidal energy release. Beginning in Archaean, that is, at the time when the Earth's endogenous tectonic energy first appeared, and through the present, the Earth's matter gravity differentiation energy releases dominated. The radioactive energy release in the Earth's bowels never played a leading role.

Forced by the mantle convection, the upper rigid Earth's shell, the lithosphere, broke into a number of plates moving on the surface of hot plastic mantle. Wherever the plates diverge, a new lithosphere forms with the oceanic crust on the surface and the mid-oceanic ridges with the rift zones at their crests occur. Wherever the plates converge, one plate is subsided into the mantle, and at the edge of the other plate appear the conjugated structures of deep-water troughs with island arcs or Andean-type active continental margins. Continental crust forms within these plate subduction zones as a result of remelting of the subducted oceanic crust and of the sediments.

The present-day mantle, similar to the primordial matter of the young Earth, has on average a uniform composition with a very low content of most ore and rare elements. This is the reason why the formation of endogenous economic minerals under our theory is a result of the interaction between the hydrosphere and the oceanic crust, with numerous recycling of the continental crust matter and the sedimentary matter within the lithospheric plate subduction zones. The formation of exogenous economic minerals was always controlled by the continental drift and the Earth's climatic zones.

Based on the unified position of the proposed general theory, the book reviews various aspects of the Earth's evolution. They include its tectonic activity, structure, geochemistry of its shells, lithospheric plate tectonics, the formation of the Earth's crust and its associated economic minerals, the origins of oceans, the atmosphere, and other evolutionary issues. A continuous check of the theory's conclusions for their match with the geologic data gives the authors hope that the theory provides a more or less adequate description of the Earth's evolution. Nevertheless, the authors are far from believing that the theory is complete. They believe, on the contrary, that it will further deepen, improve, and develop.

Any theory is tested by a comparison with actual facts and events. The more matches, the more correct is the theory. The proposed general theory of the Earth's

evolution explains most of the known geologic events and processes in the Earth's history. Besides, it is in complete agreement with the current geologic theory, tectonics of lithospheric plates. As of today, the theory provides a natural explanation, from unified positions, of most seemingly diverse global events and processes cited in the conclusions to the book.

A physical approach to the Earth's evolution problems involves some calculations. They are not possible without the use of mathematical physics equations. This, naturally, can make it a somewhat difficult reading for the reader who is not thoroughly versed in mathematics. The authors took this into account and tried to avoid complex mathematical computations, and always attempted to provide a simple explanation of the computational results. This makes the book readable by the mathematically uninitiated reader.

All the diagrams in the book were constructed using the program Grapher-2 based on quantitative calculations of the processes and phenomena described by equations of mathematical physics which were solved using the program Mathcad-2001.

Our computations of physical phenomena and processes are conducted using the absolute physical system of units (CGS) where the basic units are centimeter, gram, and second. The CGS to CI (base units: meter, kilogram, second) conversion may be performed through the following relations:

| | |
|---|---|
| Length | $1\ \text{cm} = 10^{-2}\ \text{m}$ |
| Mass | $1\ \text{g} = 10^{-3}\ \text{kg}$ |
| Area | $1\ \text{cm}^2 = 10^{-4}\ \text{m}^2$ |
| Volume | $1\ \text{cm}^3 = 10^{-6}\ \text{m}^3$ |
| Force | $1\ \text{dyne} = 10^{-5}\ \text{N}$ |
| Density | $1\ \text{g/cm}^3 = 10^3\ \text{kg/m}^3$ |
| Work and energy | $1\ \text{erg} = 10^{-7}\ \text{J}$ |
| Capacity | $1\ \text{erg/s} = 10^{-7}\ \text{w}$ |
| Pressure, Young's modulus | $1\ \text{dyne/cm}^2 = 10^{-1}\ \text{N/m}^2 = 10^{-1}\ \text{Pa}$ |
| Dynamic viscosity | $1\ \text{poise} = 10^{-1}\ \text{N s/m}^2 = 10^{-1}\ \text{Pa s}$ |
| Acceleration of gravity | $981\ \text{cm/s}^2 = 9.81\ \text{m/s}^2$ |

Besides, the authors use some convenient extrasystemic units:

**Pressure**

$\text{bar} = 10^6\ \text{dyne/cm}^2 = 10^5\ \text{N/m}^2 = 10^5\ \text{Pa} = 10^2\ \text{kPa}$
$\text{kbar} = 10^3\ \text{bar} = 10^8\ \text{Pa} = 10^2\ \text{MPa}$
$\text{Mbar} = 10^6\ \text{bar} = 10^{11}\ \text{Pa} = 10^2\ \text{GPa}$

**Heat energy**

$\text{cal} = 4.1868 \times 10^7\ \text{erg} = 4.1868\ \text{J}$
(thermochemical calorie:
$1\ \text{cal}_{\text{tch}} = 4.1840 \times 10^7\ \text{erg} = 4.1840\ \text{J}$)

**Acceleration of gravity**

$1\ \text{gal} = 1\ \text{cm/s}^2 = 10^{-2}\ \text{m/s}^2$

Finally, the expressions with parameters derivatives with time are common in the text. To abbreviate the writing, the authors use the parameter notation "with a point", such as $\frac{dx}{dt} = \dot{x}$
or

$$\frac{dE}{dt} = \dot{E}.$$

Other derivatives are represented in the conventional format.

CHAPTER

# 1

# Major Stages and Methodology in the Evolution of Geological Concepts

## 1.1 EARLIER SCIENTIFIC HYPOTHESES OF EARTH'S EVOLUTION

The appearance of a new scientific idea is usually preceded by protracted periods when new data are accumulated, most of which do not fit into the old concepts of certain phenomena and processes (Kuhn, 1977). The process of acceptance and especially incorporation of new scientific theories into practice is frequently very prolonged. The reason is that revolutionary ideas in science usually impinge on long settled perceptions that became too habitual. Even after the new theories are mostly developed, they do not immediately enjoy recognition in the scientific world. The new theory needs to be proved. It takes time for conducting control experiments and comprehensive testing against practical results. Plenty of time as well is spent to retrain and persuade the majority of the scientific community. All these create long delays in the recognition of new ideas and theories.

In geology, new ideas are very difficult to consolidate. Most general geological hypotheses of Earth's evolution played a very important role in forming the natural-scientific *weltanschauung* of the geologists. We will not dwell here on the prehistory of developing the scientific concepts of Earth's origin and geological evolution as the issue was diligently studied and publicized. We will just note that the first strictly physical theory of the formation of the Solar System was published by a genial mathematician, P. S. Laplace in early nineteenth century. He suggested that the stars, including Sun, formed as a result of gravity concentration and compression of the cosmic gas whose existence was already known to astronomers. Gas compression is accompanied by its heating. That is why, Laplace believed, all stars are hot and are radiating heat and light (at those times, the existence of radioactive processes was not even suspected). As the cosmic gas is in permanent motion, it not only heats up when compressed but also spins up. As a result, beside the central star a gas disk occurs around it, which concentrates into hot planets.

It is interesting that when Laplace presented Napoleon Bonaparte his book with a description of the cosmogonic picture that he had developed, the Emperor asked Laplace:

*Developments in Earth and Environmental Sciences*, Volume 10
DOI: 10.1016/S1571-9197(11)10001-4

"And where is God in your constructions?" the scientist replied that his theory does not need a hypothesis of the Creator.

A first scientifically grounded, rather progressive and most general geological hypothesis of Earth's evolution was put forward by Jean-Baptiste Élie de Beaumont in 1830. The hypothesis was clearly conceptual and allowed the search for causal association in geological phenomena. This hypothesis, named "the contraction hypothesis," was based on Laplace's idea of the "hot" origin of Earth which ostensibly formed of a compressing clot of a heated gaseous matter. It was, therefore, concluded that as Earth cooled down, its size substantially declined. Correspondingly, its external shell—the Earth's crust—shrank in the area and compressed. As a consequence, mountain ranges and folded belts of sedimentary rocks occurred.

The theory was physical in appearance for the nineteenth century but was not able to stand quantitative checks for the correspondence with the laws of physics, was unable to explain major patterns in Earth's geological evolution and did not in any way fit the present-day concept of a "cold" origin of the Solar System planets due to accretion of the protoplanetary dust cloud. Nevertheless, this apparent physicality and internal beauty of the contraction hypothesis literally fascinated geologists, and reigned in geology for almost a century, through the 1930s.

In 1940s, after the fundamental works by Schmidt (1946, 1948) have been published, the geological science acquired a reliable base for its development. Schmidt considered it essential that Earth and the planets of the Earth's group formed not out of a hot cosmic gas but out of a cold intergalactic dust. The reason for that was that after "kindling" of nuclear reactions in the Sun's bowels, even prior to the Sun going through the stellar evolution stage of the τ-Taurus type stars, all the cosmic gas and mobile elements were "swept out" off the near-Sun space by the solar wind (the flow of the protons and atom nuclei) into the Solar System's periphery where the giant planets formed. Thus, the primordial Earth turned out to be not a hot, gaseous planet but a cold, solid planetary body, which moreover was devoid of a gas atmosphere and impoverished in many volatile elements and compounds.

As for longevity of the contraction hypothesis, it finds its explanation in certain conservatism of the geologists. Not unlike the Ptolemeian system of macrocosm, the contraction hypothesis was fed by "obviousness" of our trivial ideas about the evolution of natural processes. In particular, geologists believed that rocks are so firm, and the continental masses are so great that there were no forces, except for compression, capable of moving the continents and changing their mutual positions on the surface of Earth. Based on these ideas, as if by itself, like the "obvious" one, the fixist concept emerged in theoretical geology. Under this concept, all geological structures (the continents included), mountains, oceans, the ocean floor, and islands were always positioned on Earth's surface in rigidly fixed positions. Even the folded mountains, under this concept, arose due to vertical motions only, without any noticeable horizontal displacements. Any significant horizontal motions of geological structures were totally banned within the constraints of such a fixist concept.

The fixist barrier of "obviousness" was first stepped over at the end of nineteenth century by an English pastor and talented physicist, Osmond Fischer. He published his idea in an undeservedly forgotten book under a rather present-day title of "Physics of the Earth's Crust" (Fischer, 1889). It is noteworthy that, based on the idea of isostatic equilibrium of the continents and way before geophysical study methods were developed, Fischer

was first to correctly determine the average thickness of the continental Earth's crust at 20–25 geographic miles, that is, 37–46 km (40 km on the average).

Contrary to the then prevailing ideas of the domination of compression stresses, Fischer proceeded from the fact of the coexistence on Earth of structures both extension and compression. He included among the former structures rift zones running through Island, Mid-Atlantic plateau (as the Mid-Atlantic ridge was called at those times), East Africa, and other similar structures. Among the latter structures were listed the Pacific mobile belt with its andesite magmatism and highly elevated seismicity. Fischer assumed the motion patterns of lava crusts forming at cooling down in the Kilauea volcano (Hawaii) Lava Lake as the base of Earth's core evolution model. These crusts always moved from the open fractures that were filling with the molten lava (which formed the crust when cooling down) to the places of their pipe-up and sinking into the depth of the Lava Lake's molten lava. Fischer extrapolated his observations onto the Earth's crust and concluded that the oceanic crust also forms as a result of basalt effusion from fractures in its extension zones such as Iceland, the axial Atlantic ridge, and other similar structures. And, the consumption of the oceanic crust occurs along the Pacific periphery in the compression zones where the ocean floor sinks under the island arcs and continental margins. This very oceanic crust dive under the continental crust caused earthquakes underneath the Pacific mobile belt. A moving mechanism shifting the crust's blocks, Fischer believed, was the convection flows of the undercrust substrate.

It is simply astounding that 70–80 years before the publication of foundational works in modern geological theory (tectonics of lithospheric plates), a model of the evolution of geological processes on Earth that is very close to this theory was drawn. Fischer's ideas were so much ahead of his time that they were not duly appreciated by his contemporaries. Moreover, geologists then knew very little about the ocean floor structure. Also, factual data supporting Fischer's hypothesis about the very important role the oceanic crust played in Earth's tectonics were not yet available. We can only guess now how much sooner modern geology would have developed if Fischer's ideas were perceived by his contemporaries. But that did not happen.

Fischer recognized the existence of large-scale horizontal motions of the continents and individual crust blocks. Thus, as opposed to the previous concepts of fixed position of the geological structures under the contraction hypothesis, his theory was the first scientifically substantiated mobilist concept.

The next step in the development of the mobilist ideas was made by an outstanding German geophysicist, Alfred Wegener, who in 1912 published his renowned hypothesis of continental drift (Wegener, 1912). Not only did he suggest a possibility of large-scale continental motions but also proposed an entire system of substantiated proof in favor of this phenomenon. As the major evidence of the reality of continental drift and breakage of the previously unique supercontinent Pangaea, Wegener mentioned the following: the extraordinary similarity of the western and eastern Atlantic shorelines; the same type of geology in the adjacent continents surrounding Atlantic Ocean; the commonality of the Paleozoic and Mesozoic flora and fauna in the presently divided continents; and the traces of almost simultaneous (Late-Paleozoic) blanket glaciation in South America, South Africa, India, and Australia, that is, on the continents which are presently located at distances of 10,000–15,000 km (Wegener, 1912–1922). Wegener tragically died in 1930 in Greenland

where he went to look for additional evidence in support of his ideas. After his death, his valiant hypothesis was all but forgotten.

Why, again, were the progressive ideas not accepted by geologists? We already mentioned conservatism of the scientific community. Such conservatism is sometimes well justified as it protects science against the acceptance of shallow hypotheses. But there was something else: the main reason was that Wegener's explanation for the continental drift mechanism was wrong. Wegener's background was in meteorology. He knew well about the great influence of Earth's rotation and the tidal interaction of atmosphere and hydrosphere with the Moon on the mechanism of air mass motion and on oceanic currents. Thus, he assumed that the continental motions also occurred under the influence of Earth's rotation and tidal interaction between the Earth and the Moon, that is, as a result of purely external forces. Simple calculations showed that rotation and tidal forces are weaker by many orders of magnitude than those that could really move the continents. The paradox was that, together with the erroneous mechanism, the scientists "threw the baby out with the bath water," that is, Wegener's correct argumentation in favor of the reality of continental drift: the point is that not a single of his geological arguments was ever refuted.

Even the publication by a known geologist, Arthur Holmes (1928), of his support for the existence in the subsurface of, as it was then called, convection flows of the subcrustal substrate did not help salvage the mobilist ideas. Holmes believed that the energy for these motions came from radioactive decay.

Should Wegener have used Fischer's or Holmes's convection mechanism to explain the continental drift, the mobilist ideas might not have been assigned to oblivion, and a state-of-the-art geological theory might have been created 30–40 years earlier. A long time elapsed before the new facts which did not fit the Procrustean bed of the fixist concept were gathered, helping to relaunch the progressive idea and not only to support continental drift but also to discover a new phenomenon, ocean floor spreading.

## 1.2 DEVELOPMENT OF THE MODERN THEORY OF EARTH'S LITHOSPHERIC SHELL FORMATION

Paleomagnetic studies on continents played a large role in the rebirth of the mobilist ideas and in the creation on that basis of the modern geological theory. Studies of rocks' magnetic properties showed that the rocks containing magnetic minerals are capable of "remembering" the ancient magnetic field of Earth. Determining the magnetic field parameters in rock samples from different continents enabled known physicists such as Blackett (1961), Runcorn (1962), and others to come in the early 1960s to a very interesting and important conclusion. Its substance was that the positions of all continents on Earth's surface substantially changed with time. If, however, the continents were placed such that their Late-Paleozoic and Early-Mesozoic paleomagnetic poles coincided with the present-day geographic poles, then all of a sudden a reconstruction occurred of the ancient supercontinent Pangaea (whose model was first constructed by Wegener 25 years prior to the appearance of paleomagnetic data).

The major impact on the theory, however, occurred only in the 1950–1960s after wide-ranging international studies of the ocean floor geology and the associated magnetic

anomalies. At that time, especially during the studies under the International Geophysical Year (1957), banded magnetic anomalies of the ocean floor and the major underwater ranges, running along the axial zones of young oceans and girding the entire Earth as a continuous chain over 60,000 km long, were discovered. It turned out that along the crestal zones of these ranges were deep tension fractures. These are the rift zones from which fresh young basalts were always extracted. It gave birth to the idea that the rejuvenation of the ocean floor was occurring simultaneously with the continental motions. Some oceans could open up, whereas the other ones could shrink in their area. And, the ocean floor age, based on the results of bottom deposits dredging, is always, without exception, relatively young, no older than 140–150 MMY. At the same time, the average age of the continents is usually older than 2.5 BY.

After these studies, the old hypothesis of the continental drift began to resurge rapidly but this time on a higher scientific level. Thanks to the efforts of geophysicists and geologists from different countries, and first of all Hess (1962), Dietz (1961), Wilson (1965), Morgan (1968), Le Pichon (1968), Dewey and Bird (1970a,b), and others, this hypothesis grew by the end of 1960s into a modern and orderly scientific concept called the theory of lithospheric plate tectonics.

Especially, great contribution into its creation came from geophysicists and geologists who studied structure and evolution of the ocean floor. Thus, in 1961 and 1962, American scientists (a geologist, Hoess and a geophysicist, Ditz) repeatedly formulated Fischer's basic ideas about the origins of the oceanic crust in the mid-ocean ridges, about the ocean floor young age and spreading, and also about sinking of the ocean crust into Earth's mantle in the area of conjugated structures of the island arcs and Andean-type active continental margins with deep troughs.

In 1963, British geophysicists Vine and Matthews (1963) came up with a bold suggestion: that banded magnetic anomalies of the ocean floor represent a record of Earth's magnetic field inversions in basalts of the spreading ocean floor, which plays the role of a natural magnetic tape in a giant "tape recorder" Earth. Based on this concept, American and French geophysicists (Heirtzler et al., 1968) theoretically calculated the age of the ocean floor. It turned out that the ocean floor in practically all regions of the World ocean formed relatively recently (during Cenozoic and Late Mesozoic), and that its age regularly increases with distance from the crests of mid-ocean ridges.

In 1965, a Canadian geologist, Wilson (1965), was first to note that the rigid Earth's shell (the lithosphere) was broken into a number of plates bounded by three types of borders: rift zones, plate subduction zones, and transform (often strike-slip) faults.

At the same time, a well-known British geophysicist Bullard and colleagues (Bullard et al., 1965) used Euler's theorem, describing the motions of rigid shell fragments on the surface of a sphere, and computer technology to generate quantitative reconstructions of drifting continental positions in the past geological epochs.

In 1968, an American geophysicist Morgan (1968) and a French geophysicist Le Pichon (1968) identified the largest lithospheric plates and computed parameters of their motion on the surface of the globe. At the same time, American seismologists B. Isaks, J. Oliver, and L. Syks (Isaks et al., 1968) showed that Earth's seismicity concentrates mostly along the lithospheric plate boundaries and is completely determined by their mutual motions on the Earth's surface.

In 1970, American geologists Dewey and Bird (1970a,b) reviewed from the positions of the new theory: the evolution of the geosynclinal process, origins of the rock folding, and emergence of Earth's mountain belts. A Japanese geologist, Miyashiro (1976), studied the formation and manifestation forms of regional metamorphism of the rocks and sediments within the plate subduction zones. Another Japanese scientist, the geophysicist Ueda (1978), studied in detail the mechanism of the lithospheric plate sinking into the mantle in the subduction zones. An American geologist, Sillitoe (1972a,b), studied ample data on the distribution of commercial ore deposits and came to the conclusion that many of them form only above the plate subduction zones. He also discovered a clear zoning in ore element distribution depending on their mobility: more mobile ore elements usually concentrate closer to the deep-water troughs, that is, they are carried to the surface in the beginning of the plate subduction process, whereas less mobile and more refractory elements and compounds accumulate at larger distances from the ocean shores, that is, they are brought in from greater depths in the plate subduction zones.

At the base of the new concept lay the new ideas of the Earth origins not from a hot gas but from a cold cosmic dust.

In the mid-1970s through late 1980s, the chemico-density mechanism of Earth matter differentiation in the gravity field was proposed (Sorokhtin, 1974; Ushakov, 1974; Monin, 1977, 1988; Monin and Sorokhtin, 1981, 1982a,b,c, 1984). It was shown that this process results in the separation in Earth's central portion of a dense core, most likely of an iron-oxide composition (Sorokhtin, 1972), and in the emergence in the mantle of nonstationary chemico-density gravitational convection (Sorokhtin, 1972) which is the direct cause of the continental drift. These discoveries enabled the determination of the core's age, its growth rate, speed of convectional mass-exchange in the mantle and of Earth's crust formation, of Earth's degassing, and so on (Sorokhtin and Ushakov, 1989a,b, 1991, 1993, 2002; Sorokhtin, 2007). The application of these concepts allowed to reconstruct the history of the continents, formation of the oceans and to construct a model of Moon formation and its tidal interaction with Earth (Sorokhtin, 1988; Sorokhtin and Ushakov, 1989a,b, 1991, 1993).

## 1.3 METHODOLOGY OF CONSTRUCTING A GENERAL THEORY OF EARTH'S GLOBAL EVOLUTION

Looking back on the history of geology evolution we can maintain that prior to the emergence of the lithospheric plate tectonic theory, this science did not possess a general and strictly scientific theory satisfying all high-bar requirements imposed onto a modern scientific theory. Up until the end of 1960s, geology was in fact just a descriptive science.

It does not mean, however, that geology then did not have its partial theories. There were numerous such theories, for instance, seismic wave in laminated media propagation theory, sedimentary-migration oil–gas generation theory, lithogenesis theory, thermodynamic theory of magmatic differentiation, and so on. These narrowly directed theories described individual geological processes torn out of the general geological environment, and did not create a unique *Weltanschauung* approach in the studies of Earth. And, some attempts to create a general geological theory either did not stand quantitative check (like the

contraction theory) or simply did not meet elementary requirements of modern scientific theories (like hypotheses of oceanization of the Earth's crust, expanding, pulsating or hydride Earth, etc.) Using Kuhn's (1977) terminology, geology up until the end of the 1960s was still at the pre-paradigmatic level of scientific evolution.

Many geologists belonging to the "classical" school of thought believed at that time that there were too little data collected about the crust structure in various areas of the continents for the creation of a genuine and all-encompassing geological theory. There was a paradoxical side of the "classical" approach. The more additional data on the detailed structure of individual continental areas were collected, the more confusing and contradictory was the general concept of Earth's evolution. As a known nineteenth century physicist O. Fresnel once mentioned, nature was sneering at our analytical difficulties: it used only simple means whose combinations gave birth to an almost unsolvable mess.

Additional geological information indeed was necessary to untangle this mess. However, it should not have been ever more detailed information on the continental structure but radically new information about the structure and evolution of the ocean floor. Also, needed were new and constructive ideas enabling a new approach to all earlier accumulated geological data and knowledge. In order to see the forest one would need to leave it and to look at it from aside.

Such radically new data that forced the scientists to throw out the old concepts of Earth's crust origins and of the nature of geodynamic processes in Earth's lithospheric shell were obtained only recently, over the last 55–60 years. It was a result of broad integrated studies of the geological structure, composition, and dynamics of the World ocean floor. These data provided an opportunity to put forward new ideas about the nature of global processes defining the evolution of Earth's crust and Earth as a whole.

A new geological theory, the tectonics of the lithospheric plates, was created based on these new ideas and resulted in a deep transfiguration of the classical geological concepts and an actual revolution in Earth sciences. The new theory did not contradict at all the positive geological knowledge collected during the time of the existence of geology as a science. On the contrary, it organically soaked them into itself and gave them a new meaning. Without any exaggeration, the value of this new theory for geology may be only compared with the value of the Newtonian or quantum mechanics for physics, of molecular biology for biology, and of cybernetics for technology.

We understand now why geology, one of the oldest sciences, did not have its own general theory through the mid-twentieth century. The reason was that the key to cognition of processes of Earth evolution lay on the ocean floor and could have been obtained only by setting up broad-range oceanological studies in all areas of the World Ocean. Such studies did begin in the late 1950s under the program of the II International geophysical year and other international projects.

The situation in geology drastically changed with the emergence of the theory of the lithospheric plate tectonics. We can responsibly state today that there is now in geology its own strict theory that is in complete harmony with the high requirements imposed on modern scientific theories. It is also important that this theory merged in itself three major branches of the Earth sciences: geology proper, geochemistry, and geophysics.

Certainly, there are limitations to lithospheric plate tectonics: it describes processes occurring only within the upper rigid Earth's shell, its lithosphere (including the Earth's Crust).

To create a more general theory of planetary evolution for Earth as a whole (which would naturally encompass also the lithospheric plate tectonics), a unique and consistently physical approach to the entire issue is required. For this purpose, the following basic items must be taken into consideration:

**(1)** Earth is a physical body and evolves under the strict laws of physics. It follows that Earth's evolution, under the first law of thermodynamics, must occur along the processes to the maximum extent decreasing its potential (internal) energy that is eventually converted to heat. The heat generated by endogenous processes is radiated by Earth to outer space, that is, irretrievably lost. Therefore, Earth evolution is irreversible.

**(2)** Earth revolution about the Sun, the Solar System's center of mass, the Galactic center of mass, and in the Universe is occurring on the equipotential surfaces of the gravitational field. Such a motion does not require any expense of energy *per se*. The energy transfer from the external gravitational field to the body of Earth may occur only if this field is variable, that is, if tidal forces are generated. In Earth, such forces emerge during its revolution about its own axis within the Lunar and Solar gradient gravitational fields. However, the present-day fraction of the tidal energy dissipated inside Earth does not exceed 1% of the total heat loss of Earth. An important inference is that the main sources of Earth's endogenous evolution must be searched for, first of all, within Earth itself, whereas the evolution of its exosphere (including the planetary climates, rock weathering processes, and depositional events) is to a greater extent ruled by the solar energy.

**(3)** As for any physical theory, the global evolution of Earth must be described by the equations of mathematical physics, and their solution may be searched only by assigning the problem's initial and boundary conditions. The formation time, structure, and composition of primordial Earth must be assumed as the initial conditions, the structure and layer-by-layer composition of the present-day Earth and its entire geological record must be assigned as the boundary (or edge) conditions.

**(4)** Earth with all its geospheres (the core, mantle, crust, hydrosphere, atmosphere, and biosphere) should be viewed as a unified and physically interacting dynamic system joined by internal connections. Apparently, mechanical displacements within the Earth cannot be detached from physicochemical processes evolving in it, resulting in changes in the composition, density, and volume of its matter. It also needs to be taken into account that the mechanical deformations *per se* result in matter's heating and even melting. All these require joint consideration of the evolution in all geological processes including Earth's tectonic activity in space and time.

**(5)** The speed of most endogenous processes on Earth is slowed down by a high-diffusion viscosity of Earth's matter. For this reason, many such processes are very slow and evolve during many millions and even billions of years. This calls for the consideration of all interacting geological processes, including Earth's tectonic activity, in space and time.

It is important that such an energy-oriented approach to studies of Earth's global evolution, tied up with the specific geological record (i.e., with the boundary conditions for the planet),

provides an opportunity to identify and rank the main planetary processes controlling such evolution (in terms of their capacity).

After studying each of such processes, it is possible to determine their combined effect on the tectonic activity of Earth and on individual manifestations of this activity. In its turn, this comprehensive approach to the studies of individual geological events and processes as to the particular manifestations of the global evolution of Earth as a whole provides a way to explain the origin and evolution of the oceans and atmosphere, to identify the main patterns in the continental growth, to find out the causes of a unique Proterozoic metallogenic epoch and even of the Earth climates.

The origin of the Precambrian iron ore formations is especially illustrative in this respect. To solve it, it is necessary to review most fundamental and diverse problems of Earth's formation and global evolution. These problems encompass the chemical differentiation of the matter in the protoplanet gas–dust cloud from which Earth formed, composition of the Earth's crust and the nature of its separation from the mantle, the evolution of the mantle's chemical composition and its convection mass-exchange, Earth degassing and the conditions of formation of oceans and atmosphere, of Earth's climates evolution (including the glaciations), the origins and evolution of life on Earth, biosphere productivity during Precambrian and of the following epochs, and so on.

A solution of this complicated problem became possible based on the most general geological theory of Earth's global evolution.

As mentioned, this theory arose from the organic merging and subsequent combined development of several disciplines. They include tectonics of the lithospheric plates, modern cosmogonic concept of Earth origins, Earth's matter differentiation processes, and hydrodynamic theory which describes the mantle's convective mass-exchange and its degassing that gave birth to the hydrosphere and atmosphere, the natural environment of life on Earth.

This book is a description of this general geological theory.

CHAPTER

# 2

# Structure and Composition of Modern Earth

## 2.1 GENERAL INFORMATION ABOUT EARTH

The structure of our planet is well known today based on seismic data and oscillations of the Earth. The composition of the external shells (Earth's crust, hydrosphere, and atmosphere) is supported by the geological data and direct measurements. Our knowledge of the composition of Earth's mantle is not as definitive. Still, from a consolidated mass of geological and geophysical data, we can have a reasonably certain knowledge about the structure and composition of this shell. As for the composition of Earth's core, here for understandable reasons we can only come up with more or less substantiated hypotheses. Numerous books and papers were published regarding study methodology of Earth's structure and composition (Bullen, 1956, 1963, 1973, 1975; Magnitsky, 1965; Sorokhtin, 1972; Botte, 1974; Verhoogen et al., 1970; Monin and Sorokhtin, 1981, 1982a,b,c; Zharkov, 1983; Bolt, 1984; Anderson, 1989 and numerous other publications). We will not be dwelling on it and will just provide the results.

Earth is the third planet from the Sun in the Solar System. It revolves around the Sun in an orbit that is close to circular (the orbit eccentricity $\varepsilon = 0.0167$) at the average distance of 149.6 million km. Looking from the side of the celestial sphere's North Pole, Earth and the other planets revolve around the Sun counterclockwise. The average velocity of Earth's motion on its orbit is 29.765 km/s, the revolution period (duration of a year) is 365.24 solar days or $3.147 \times 10^7$ s. Earth has its own direct (i.e., also counterclockwise looking from the side of the north pole) axial revolution whose period is 24 h 56 min 4.1 s, or $8.616 \times 10^4$ s.

Earth's mass is $M_g = 5.977 \times 10^{27}$ g, average radius $R_g = 6371$ km, the surface area is $5.1 \times 10^{18}$ cm$^2$ (510.08 million km$^2$), average density $\rho = 5.52$ g/cm$^3$, average gravity acceleration at the surface reaches $g = 981$ gal. Earth's shape is described as a geoid which represents equipotential gravity surface (Fig. 2.1). Outside of the continents, the geoid coincides with the undisturbed water surface of the World Ocean. On the continents, the surface is calculated from gravity data or satellite observations. The best approximation of the geoid is ellipsoid of


DOI: 10.1016/S1571-9197(11)10002-6

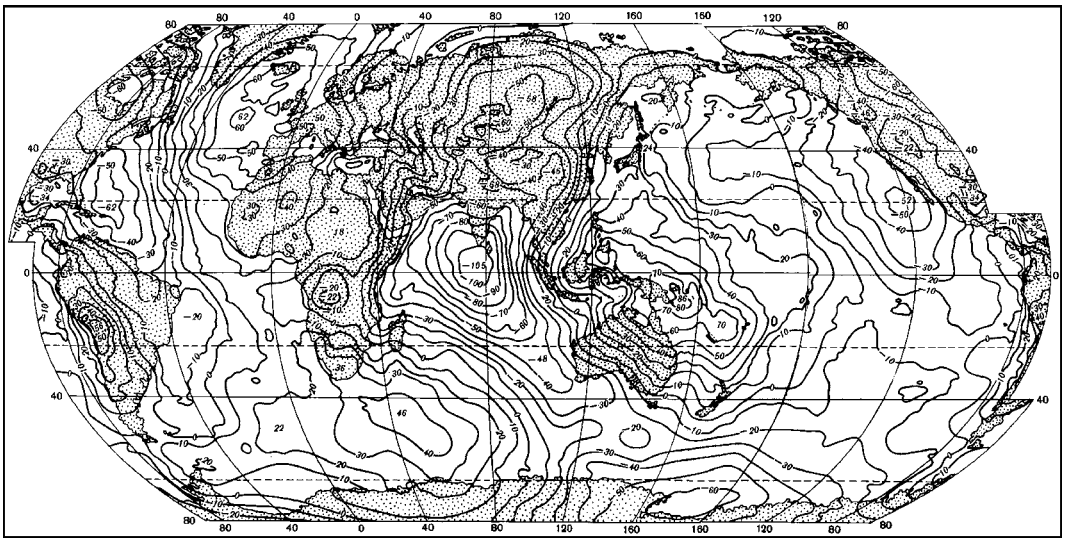

**FIGURE 2.1** Geoid's elevation map, in meters, relative to an equilibrium ellipsoid of liquid body revolution (Vincent and Marsh, 1975).

revolution (the equilibrium shape of a revolving uniform liquid). The geoid deviations from such an ellipsoid are between $+86$ and $-105$ m. They are caused both by a nonuniform mass distribution within Earth and by dynamic processes developing in the mantle and Earth's lithospheric shell. Geoid's (elipsoids of revolution) flattening depends on the Earth's revolution velocity around its polar axis. The polar radius of the present-day Earth $R_p = 6356.78$ km, the equatorial radius $R_e = 6378.16$ km. Thus, its flattening equals $e = (R_e - R_p)/R_e = 1/298.3$. The centrifugal gravity acceleration at the equator is $g_{cf} = -3.392$ gal.

The quoted data about the geoid's shape show that Earth's figure corresponds well (at 1% accuracy) with the equilibrium form of revolving liquid. A plausible conclusion from that is that Earth's matter in its depths is also effectively in a liquid state although viscosity of such a "liquid" may be very high (a superficial analogy of Earth's matter with the hard black pitch).

Earth's moment of inertia relative to the spinning axis $I = 8.04 \times 10^{44}$ g cm$^2$, whereas its dimensionless average moment of inertia equals $J = I/MR^2 = 0.33076$. It testifies to a significant increase in Earth's matter density toward the planet's center (for a sphere of uniform density medium $J = 0.4$).

The precession angle of Earth's own revolution currently is $\psi = 23.44^\circ$. It can change with time depending on lunar–solar tides and the continental drift (a reminder: the precession angle is the deflection of a planet's revolution axis from the perpendicular to the ecliptics, i.e., planetary revolution plane around Sun) or, which is the same, the angle between the Earth's equator plane and the plane of the ecliptic.

Earth has its own magnetic field. Its maximum intensity of about 0.6–0.7 Oe (oersted) is observed near the magnetic poles. It decreases to 0.25–0.42 Oe at the equator. The magnetic field's main component is the magnetic dipole field, or that of a uniformly magnetized sphere. The magnetic dipole axis is presently inclined toward the Earth's revolution axis

at 10.5°. However, its average position over the time periods on the order of a few tens of thousands of years nicely fits Earth's geographic axis.

Earth constantly loses part of its internal heat through its surface. The present-day total heat flow crossing Earth's surface is approximately $(4.2/4.4) \times 10^{20}$ erg/s (Sorokhtin, 1974; Sclater et al., 1981) and may be assumed to be equal to $4.3 \times 10^{20}$ erg/s. The average heat flow through the continents is approximately $1.43 \times 10^{-6}$ cal/cm$^2$ s, and through the ocean floor $2.37 \times 10^{-6}$ cal/cm$^2$ s. In total, about $1.2 \times 10^{20}$ erg/s is lost through the continents and approximately 2.5 times this amount ($3.1 \times 10^{20}$ erg/s) through the ocean floor.

## 2.2 EARTH'S ATMOSPHERE AND HYDROSPHERE

High-density gas and gas–liquid shells may exist only around relatively massive planets whose gravitational fields are capable of retaining gas molecules of a medium molecular weight, and whose surface temperature is above the ice's melting point but below the water's boiling point. Of all Solar System planets, these conditions exist only on Earth. Mercury, for instance, due to its small mass (0.06% of Earth's mass) and closeness to the Sun, lost almost all its atmosphere (atmospheric pressure on Mercury is $< 2 \times 10^{-14}$ atm.). Venus has a high-density atmosphere (surface atmospheric pressure there is about 90 atm.). However, due to a strong greenhouse effect, its surface temperature ($\sim$470 °C) is way above the critical water-to-gas (fluidal) state conversion temperature (374 °C). Mars has the mass which is 0.11% of Earth's mass. It preserves only a very rare atmosphere (close to $6 \times 10^{-3}$ atm.). The hydrosphere on this cold planet is currently completely frozen. The external planets (Jupiter, Saturn, Uranus, and Neptune) have very high-density atmospheres but miss liquid hydrospheres. All their satellites, as on Mars, have surface water only in a frozen state.

### 2.2.1 Earth's Atmosphere

The mass of Earth's atmosphere is approximately $5.15 \times 10^{21}$ g. Average air pressure at the sea level is $p_0 = 1.0132$ bar $= 1013.2$ mbar (760 mm Hg). Its density is $\rho_0 \approx 1.27 \times 10^{-3}$ g/cm$^3$. With the elevation, the air pressure and density rapidly decrease under the exponential law

$$p = p_0 \exp\left\{-\frac{g\mu}{RT} z\right\}, \tag{2.1}$$

where $g$ is gravity acceleration, $\mu$ is average molecular weight of the atmospheric gases (at $p = p_0$; $\mu = 28.97$ g), $R = 8.314 \times 10^7$ erg/deg mol is gas constant, $T$ is absolute temperature in degrees Kelvin, and $z$ is elevation above the sea level, in centimeter. Correspondingly, air density also decreases with elevation.

The nitrogen–oxygen composition of Earth's atmosphere is a unique feature of the Solar System planets. The dry air contains 75.51% (mass) of nitrogen, 23.15% of oxygen, 1.28% of argon, 0.046% of carbon dioxide, 0.00125% of neon, and close to 0.0007% of other gases (Reference Book, 1990). Water vapor (and the water in cloud drops) is an important active component of the atmosphere. The water vapor and water content in the atmosphere reach $(0.12–0.13) \times 10^{20}$ g, which is equivalent to a 2.5-cm (25 mm) water layer over the entire

Earth (or 2.5 g/cm). Taking into account the annual average evaporation and precipitation (~780 mm of water column), it is easy to calculate that the water vapor in the atmosphere changes approximately 30 times a year or once every 12 days. In the upper atmosphere, the oxygen molecules absorb the energy of this radiation and dissociate. This process is saving life on the Earth's surface from the deadly ultraviolet (UV) rays. The by-product of this process (not its cause!) is the emergence of the so-called ozone layer of the stratosphere composed of triatomic oxygen molecules (see Section 12.7 for details).

The classic version of the atmospheric and Earth's surface regime is determined by the Stephan–Boltzmann equation

$$T_e^4 = \frac{(1-A)}{4\sigma} S = (1-A) T_{bb}^4, \tag{2.2}$$

where $T_e = 255$ K is effective temperature (deg Kelvin) at which Earth is seen from the outer space with the precession angle of zero, $T_{bb} = 278.8$ K is temperature of absolutely black body at the average Earth's distance from the Sun (deg Kelvin) also with the precession angle of zero, $A \approx 0.3$ is the total spherical albedo (reflectivity) of the atmosphere and Earth's surface; $S = 1.367 \times 10^6$ erg/cm$^2$ s is average value of the solar constant that determines the per-unit area flow of the Sun energy impacting Earth directly under the Sun; $\sigma = 5.67 \times 10^{-5}$ erg/cm$^2$ s deg$^4$ is the Stephan–Boltzmann constant. Classic equations determining Earth effective temperature and absolutely black body temperature at the Sun–Earth distance divide the Solar constant $S$ by 4 as it is assumed that the illuminated Earth's disk is exactly four times smaller than the Earth areal extent. However, it is valid only if the precession angle $\psi$ is equal to zero or when the precession angle lies in the plane perpendicular to the direction to the Sun. In all other cases, when calculating $T_e$ and $T_{bb}$, one needs to account for the precession angle (see Chapter 13 for the details).

As Eq. (2.2) shows, 30% of the solar radiation is reflected by the atmosphere and Earth's surface back into the outer space, and the rest of the energy (70%) is dispersed in the atmosphere and absorbed by Earth's surface. The main Sun energy absorbers in the atmosphere are water vapor, carbon dioxide, and the oxygen dissociation process in the stratosphere. The cloud cover creates a strong negative feedback between the effective temperature and atmospheric albedo. It is known that any such feedback in a system results in the system's stabilization and linearization of the reaction at the system's output relative to its action at the input. As a result, the average near-surface temperature $T_s$ becomes a linear function of the temperature, the function describing the Sun radiation, that is, of the black body temperature at the distance of the planet from the Sun

$$T_s \sim T_{bb}. \tag{2.3}$$

The heating of the lowermost and densest atmospheric layer (the troposphere) results in the emergence of convective mixing of the air in this layer. As is known (Landau and Lifshits, 1976), for adiabatic processes

$$T = C^{\alpha} p^{\alpha}, \tag{2.4}$$

where $p$ is pressure, $\alpha = (\gamma - 1)/\gamma$; $\gamma = c_p/c_v$, $c_p$ and $c_v$ are heat capacities of the gas, respectively, at the constant pressure and constant volume. For all triatomic gases ($CO_2$ and $H_2O$), $\gamma \approx 1.3$, $\alpha = 0.2308$, and for biatomic gases ($N_2$ and $O_2$), $\gamma \approx 1.3$ and $\alpha = 0.2857$. At the water vapor condensation in a humid troposphere, heat is released, and the air

temperature rises. A result is the lowering of the adiabatic exponent $\alpha$. As an example, average value of this parameter for Earth's humid troposphere is $\alpha = 0.1905$ (Sorokhtin, 2001a,b).

The two quoted conditions are sufficient for a unique determination of the average temperature distribution in the troposphere and of the greenhouse effect $\Delta T$ of the atmosphere

$$T = T_s - T_e. \tag{2.5}$$

See details in Chapter 13.

The troposphere concentrates about 80% of the atmospheric air. Its thickness ranges between 8–10 km in near polar areas and 17–18 km near the equator (average is 10–12 km). The average value of the temperature adiabatic gradient for a humid troposphere is about 6.5 K/km (for the dry air, 9.8 K/km). As opposed to the convective heat release from the troposphere, the major heat-transfer mechanism in the upper atmosphere (the stratosphere, mesosphere, and thermosphere) is radiation. For this reason, temperature distribution in the upper atmosphere becomes more complex. In particular, the absorption of the Sun's UV radiation occurs within the stratosphere and mesosphere due to oxygen molecule dissociation into the atoms

$$O_2 + h\nu \rightarrow 2O, \tag{2.6}$$

where $h\nu$ is the energy of the Sun's UV radiation, $h = 6.626 \times 10^{-27}$ erg s is the Planck's constant, $\nu$ is the frequency of the absorbed UV electromagnetic fluctuations. For reaction (2.6), $h\nu = 5.12$ ev; $\nu \geq 1.24 \times 10^{15}$ Hz at the wave length $\lambda \leq 2420$ Å. The reverse reaction of oxygen atoms joining into a molecule occurs with the heat release

$$O + O \rightarrow O_2 + 118 \text{ kcal/mol} \tag{2.7}$$

expended for heating of the stratosphere and mesosphere (see Section 12.7).

As a result of the atmospheric radiation–convection balance, average temperature at the surface of Earth is positive $+15\,^{\circ}C$ although its fluctuations in different climatic zones may reach 150 °C.

Absorption of the Sun's UV radiation in the tenuous air of the troposphere and mesosphere is caused mostly by the photochemical dissociation of oxygen and water molecules which is accompanied by the absorption of the Sun's hard radiation

$$O_2 + h\nu \rightarrow 2O,$$
$$H_2O + h\nu \rightarrow OH + O.$$

The ozone formation, on the other hand, occurs with heat release, whereas the ozone dissociation, again, is caused by the absorption of the Sun's UV radiation

$$O_2 + O \rightarrow O_3 + 31.7\,\text{kcal/mol},$$
$$O_3 + h\nu \rightarrow O_2 + O.$$

Heat release in the ozone molecule formation results in the heating of the tenuous air mass in the stratosphere and mesosphere which is clearly seen on a temperature profile of these atmospheric layers (see Fig. 2.2).

There are transitional layers between the troposphere and stratosphere, mesosphere, and thermosphere. They are, respectively, the tropopause (temperature, 190–220 K) and mesopause (temperature close to 180–190 K).

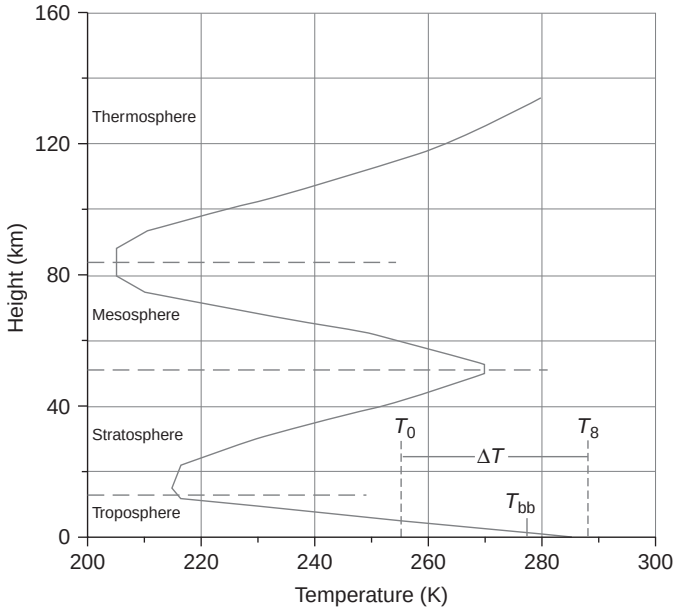


**FIGURE 2.2** Temperature distribution in the standard model of Earth's atmosphere.

Over the mesosphere is the thermosphere where the ionized gas temperature rises with height to 1000 K and greater. At the elevations above 1000 km, the thermosphere gradually turns into the exosphere, and higher up into the outer space.

## 2.2.2 Earth's Hydrosphere

Earth is the only planet in the Solar System on whose surface water may be present in the liquid state. The water mass in the present-day hydrosphere reaches $14.6 \times 10^{23}$ g. Most of it is concentrated in the World Ocean, and $1.42 \times 10^{24}$ g, in the continental glaciers. The fresh water on the dryland is responsible for only $0.023 \times 10^{24}$ g. Average salinity of the ocean water is 35‰, therefore, about $5 \times 10^{22}$ g of the salt is dissolved in the ocean water.

Part of the water is bonded in the Earth crust hydrosilicates. We estimate that about $0.422 \times 10^{24}$ g of water is bonded in the continental crust, and $0.358 \times 10^{24}$ g, in the oceanic crust. The total water content in the upper Earth's shells (Earth's crust and hydrosphere; we disregard the atmospheric humidity) is approximately $2.224 \times 10^{24}$ g.

Seas and oceans cover nearly two-thirds of the entire Earth's surface. The total water-covered area is 361.46 million km$^2$. The average depth of the World Ocean (accounting for the depths of the epicontinental seas) is close to 3.8 km.

The ocean water includes practically all elements of the periodic table. However, the main components (in ‰) are: $Na^+ = 10.764$; $Mg^{2+} = 1.297$; $Ca^{2+} = 0.408$; and $K^+ = 0.388$, and cations $Cl^- = 19.353$; $(SO_4)^{2-} = 0.701$; $(HCO_3)^- = 0.143$; $(CO_3)^{2-} = 0.070$; $Br^- = 0.066$; $F^- = 0.0013$; $(H_3BO_3)^- = 0.0265$‰. Some gases are also dissolved in the ocean water. Each liter from the upper layers of the ocean water contains about 50 ml of carbon dioxide, 13 ml of nitrogen, 2–8 ml of oxygen, 0.32 ml of argon, and minuscule amounts of the other

noble gases. Gas solubility in water increases with growing temperature. For this reason, cold oceanic waters at high latitudes are saturated with the dissolved gases noticeably greater than warm waters in tropical areas. The total amount of $CO_2$ dissolved in the ocean is around $2.19 \times 10^{20}$ g ($HCO_3$ plus $CO_3^{-2}$), that is, almost 90 times the amount in the atmosphere ($2.4 \times 10^{18}$ g). The amount of oxygen in the ocean water is nearly $8 \times 10^{18}$ g or about 150 times less than in the atmosphere ($1.19 \times 10^{21}$ g). With temperature increase in the oceanic water the gas solubility declines. This is one of the reasons of a correlation between the paleotemperatures and carbon dioxide concentrations as determined from oxygen isotopes in the ice samples and from air composition analyses in air bubbles from the Greenland and Antarctic firn. For this reason, natural (not manmade) changes in $CO_2$ concentration in the atmosphere were always a consequence of changes in the average water temperature of the ocean, and not the other way around how it is still sometimes interpreted.

The ocean water has a slightly alkaline reaction with $pH \approx 7.5$–8.5. This alkalinity level is maintained due to the equilibrium between the calcium carbonate of the sediments and water-solved calcium bicarbonate $Ca(HCO_3)_2$: in the environment of excessive $CO_2$, the carbonate dissolves and converts to the bicarbonate and vice versa. Under the $CO_2$ shortage, the bicarbonate converts to the carbonate and precipitates as a sediment. In the cold depth water of the present-day ocean, the carbonates begin to dissolve at a depth of about 4.5 km. Because of that, carbonate sediments currently are not deposited on the ocean floor.

Rivers annually bring into the oceans around $2.53 \times 10^{16}$ g of clastic material from the dryland. Of this amount, approximately $(2.21–2.26) \times 10^{16}$ g is in the form of suspension, and the rest is dissolved and organic matter.

## 2.3 EARTH'S CRUST

Earth's crust is the upper layer of Earth's rigid shell (its lithosphere). It is different from the subcrustal lithosphere in its structure and chemical composition. Earth's crust is separated from its underlying lithospheric mantle by the Mohorovicic discontinuity at which the seismic wave propagation velocity increases in a jump-like way to 8.0–8.2 km/s.

The Earth's crust surface is formed by three differently directed actions. These are: tectonic movements which create topographic features; denudation of this topography by way of destroying and weathering-out of its component rocks; and depositional processes. As a result, the constantly forming and simultaneously denuding Earth crust surface turns out to be rather complex. The maximum topographic contrast is observed only in the locations of maximum current tectonic activity. An example is the South America's active continental margin where the difference in topographic elevations between the Peru–Chili deepwater trough and the Andean summits reaches 16–17 km. A significant elevation contrast (up to 7–8 km) and great topographic roughness are typical of the present-day continent collision zones, such as Alpine-Himalayan fold belt. In both cases, maximum differences in the topographic elevations are determined not only by the intensity of Earth's crust tectonic movements and speed of its denudation but also by rheologic properties of the crust rocks which, affected by the surplus and noncompensated stress, convert into the plastic state. That is why large topographic differences in Earth's gravitational field lead

to the appearance of excessive stress exceeding rocks' plastic limit, and to the plastic flow of excessively large topographic features.

Older mountain ranges, for instance, Hercynian, such as the Urals and Appalachians, are already denuded to such an extent that the elevation differences there do not exceed 1–2 km. The Caledonian and especially Proterozoic folded zones are denuded even stronger. Quite often they have no topographic expression at all. Along with it, sedimentary sequences are being constantly accumulated in the accumulative depressions and basins and bury underneath them ancient topographic features of Earth's crust bedrock.

A generalized description of Earth's crust topography is represented by the hypsometric curve (Fig. 2.3). Vertical elevations of the firm land are placed along the vertical axis, and the total areas of the territories below a given elevation, along the horizontal axis. A very demonstrative differential format of the hypsometric curve was proposed by Wegener (1922). It shows the fraction of the Earth's surface positioned at a given elevation (Fig. 2.4). Having interpreted this curve, Wegener came in 1915 to the right conclusion that a bimodal nature of the curve indicates the existence of two types of crust, a denser basalt crust underneath the oceans and the granite crust underneath the continents.

## 2.3.1 The Oceanic Crust

The oceanic crust is primitive in its composition. In effect, it is the upper differentiated layer of the mantle overlain by a thin layer of the pelagic deposits.

Usually, three layers are identified within the oceanic crust. The first (upper) one is the sedimentary layer.

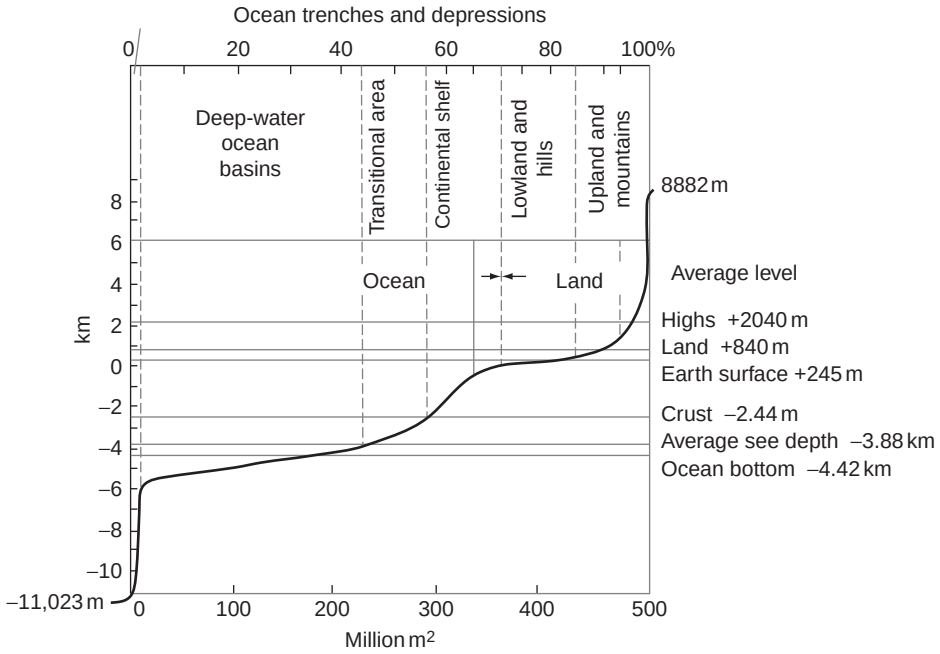


**FIGURE 2.3** Hypsometric curve of Earth's crust surface.

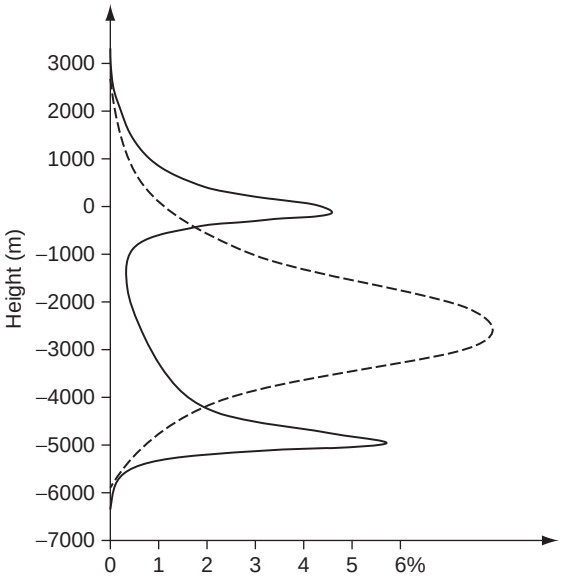


**FIGURE 2.4** Differential format of the Earth's crust surface hypsometric curve (after A. Wegener). Dashed line is normal distribution.

At the base of the sedimentary layer are often found thin and discontinuous metal-bearing sediments dominated by ferric oxides. The lower portion of the sedimentary layer is usually composed of carbonate sediments deposited at depths less than 4–4.5 km. As a rule, carbonate sediments do not deposit at greater depths as their component microscopic shells of single-cell organisms (foraminifers and coccolithophores) easily dissolve in the marine water under pressure of over 400–450 atm. Due to that, in the oceanic depressions, deeper than 4–4.5 km, the upper part of the sedimentary layer is composed mostly of noncarbonate deposits (red deepwater clays and siliceous silts). Near the island arcs and volcanic islands the sediment sequence often contains volcanic lenses and interbeds, and near large river deltas, clastic sediments. In open ocean, the sedimentary layer thickness increases from the crests of oceanic ridges (where the sediments are almost absent) to their periphery. Average sedimentary thickness is not great and is close to 0.5 km (Lisitsin, 1974a, 1978). Near the Atlantic type continental margins and in the areas of large river deltas it may reach 10–12 km. The reason is that almost the entire clastic material brought in from the dryland is deposited in the near-shore oceanic areas and on the continental slopes.

The second or basalt layer of the oceanic crust is composed in its upper portion of tholeiitic basalt lavas (Fig. 2.5). Erupting under water, these lavas acquire weird shapes of corrugated tubes and pillows so they are called pillow lavas (layer 2-a). Positioned lower are dolerite dykes of the same tholeite composition. They are the former feeding channels through which basalt lava in the rift zones erupted onto the ocean floor (layer 2-b).

The oceanic crust basalt layer is exposed in numerous locations on the ocean floor adjacent to the crests of mid-oceanic ridges and to the transform faults feathering them. This

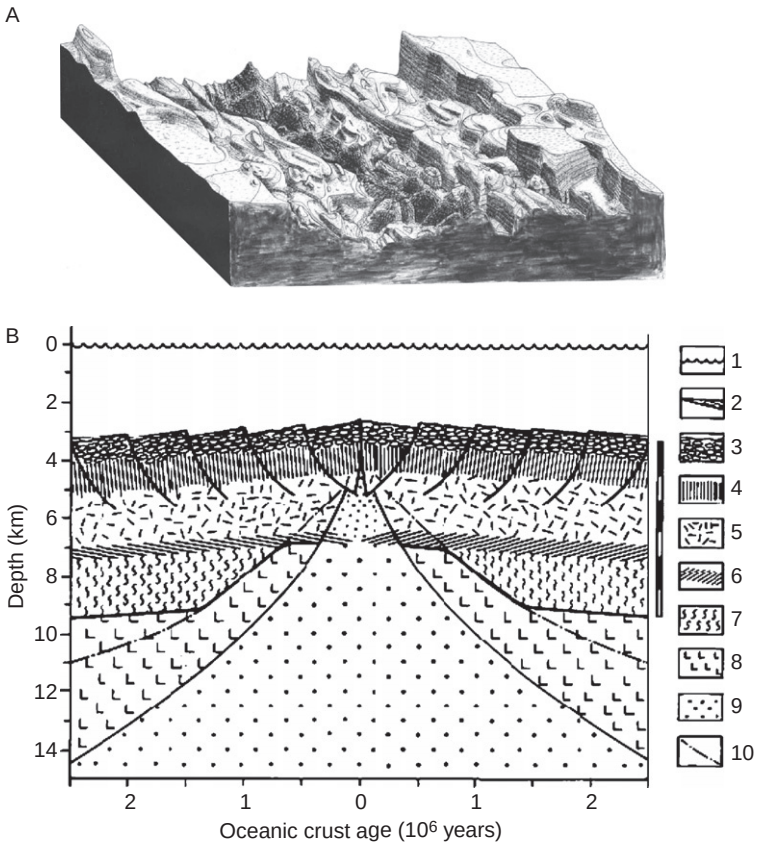


**FIGURE 2.5** Red Sea rift zone topography (A) and the structure of the mid-oceanic ridge oceanic crust (B): 1, ocean level; 2, deposits; 3, basalt pillow lavas; 4, dyke complex (dolerites); 5, gabbro; 6, laminated complex; 7, serpentinites; 8, lithospheric plate lherzolites; 9, astenosphere; and 10, 500 °C isotherm (start of serpentinization).

layer was studied in detail by traditional study techniques of the ocean floor (dredging, tube samplers, and photography) as well as by manned underwater vehicles. Those enabled the geologists observe geology of selected targets and collect samples purposefully. Besides, over the recent 25 years the surface of the basalt layer and its upper portion were drilled so that some wells penetrated the pillow lava layer and entered the dolerites of the dyke complex (layer 2-b). The total thickness of the basalt or second layer of the oceanic crust based on seismic is up to 1.5, sometimes 2 km.

Frequent finds in large transform faults of tholeitic gabbro inclusions indicate that these high-density and coarse-crystalline rocks are also part of the oceanic crust composition. Ophiolite nappes in the folded regions are fragments of the ancient oceanic crust thrown within these folded belts over the former continental margins (Peyve, 1969). Taking their structure into account, it is possible to conclude that the dyke complex in the present-day oceanic crust is also (like in the ophiolite nappes) is indeed a system of the conducting channels for the layer 2-a. This complex is underlain by the gabbro layer which comprises the upper portion of the oceanic crust's third layer (layer 3-a).

Based on seismic data, the lower portion of this Earth crust layer is also identified at some distance from the crests of mid-ocean ridges. Numerous encounters of serpentinites corresponding in their composition to hydrated peridotites and similarly structured serpentinites of the ophiolite complexes are known in the large transform faults. It shows that the lower portion of the oceanic crust may also be composed of serpentinites.

Seismic data indicate that the thickness of the gabbro–serpentinite (third) layer of the oceanic crust reaches 4.5–5 km. The oceanic crust under the crests of the mid-oceanic ridges is usually thinner, 3–4 and even 2–2.5 km immediately underneath the rift valleys.

Thus, the total thickness of the oceanic crust, without the sedimentary layer, reaches 6.5–7 km. The oceanic crust is underlain by crystalline rocks of the upper mantle that compose subcrustal areas of the lithospheric plates. Underneath, the crests of mid-oceanic ridges the oceanic crust is positioned directly over the foci of basalt melts released from the hot mantle's matter (i.e., from the astenosphere).

The area occupied by the oceanic crust is approximately $3.06 \times 10^{18}$ cm$^2$ (306 million km$^2$), its average density (without deposits) is close to 2.9 g/cm$^3$. Therefore, the mass of the consolidated oceanic crust may be about $(5.8–6.2) \times 10^{24}$ g. The volume and mass of sediments in the World Ocean's deepwater troughs is 133,000,000 km$^3$ and about $0.1 \times 10^{24}$ g (Lisitsin, 1980). The sediment volume concentrated on the shelves and continental slopes is somewhat larger, about 190,000,000 km$^3$ which translates (accounting for the deposits compaction) into approximately $(0.4–0.45) \times 10^{24}$ g.

The ocean floor (which is the surface of the oceanic crust) has a characteristic topography. Its depth in abyssal depressions is 6–6.5 km, whereas on the oceanic ridge crests (sometimes cut with deep precipices— the rift valleys) it decreases to 2–2.5 km. In some places, the ocean floor is exposed on the surface (e.g., in Iceland and in the Afar Province, Northern Ethiopia). In front of the island arcs surrounding the western periphery of the Pacific Ocean, northeast of the Indian Ocean, in front of the Small Antilles and South Sandwich Islands in the Atlantic Ocean, and in front of the active continental margin of the Central and South America the ocean floor sags, and its surface subsides to 9–10 km forming narrow and long deepwater troughs. Seismic data indicate that the oceanic crust, together with the sedimentary layer, is carried farther and dives underneath island arcs and active continental margins.

The oceanic crust is formed within the rift zones of the mid-oceanic ridges as a result of basalt melts separating from the hot mantle underneath these ridges from Earth's astenosphere and erupting on the ocean floor (Fig. 2.5). Annually, at least 12 km$^3$ of basalt melts rises from the astenosphere, erupts on the ocean floor, and crystallizes and forms the entire second and part of the third layer of the oceanic crust. These grandiose tectonomagmatic processes constantly occurring under the mid-oceanic ridge crests have no comparison on continents and are accompanied by elevated seismicity (Fig. 2.6).

In the rift zones over the mid-oceanic ridge crests, the ocean floor expands and spreads. That is why such zones have frequent but shallow earthquakes dominated by the expansion offsets. Contrary to that, the earthquakes underneath island arcs and active continental margins (i.e., in the plate subduction zones, see Fig. 2.7) are usually strong and dominated by the compression and shear deformations. According to seismic data, the dive of the oceanic crust and lithosphere is carried within the upper mantle and mesosphere to depths

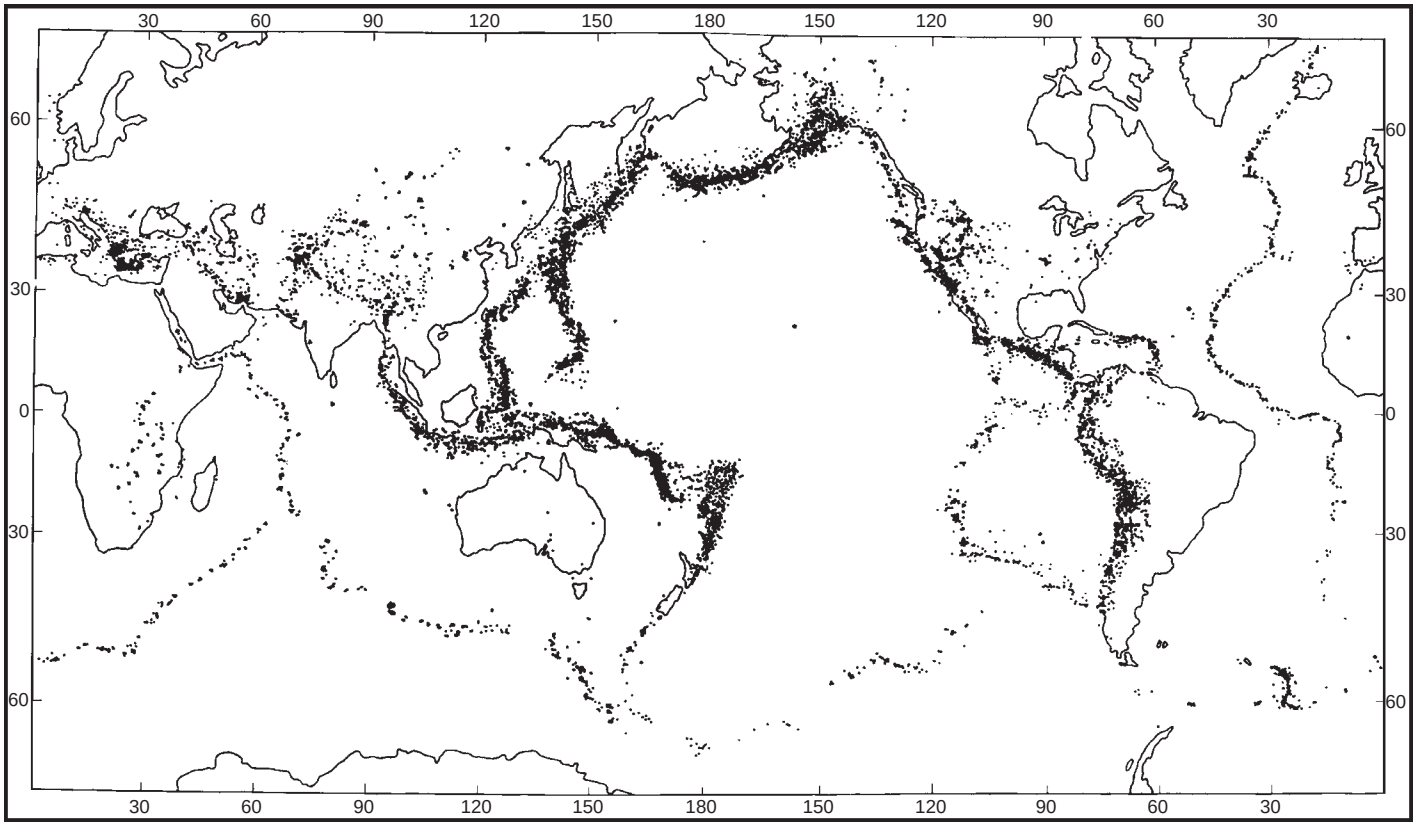


**FIGURE 2.6** Earth's seismicity: earthquake locations (Barazangi and Dorman, 1968).

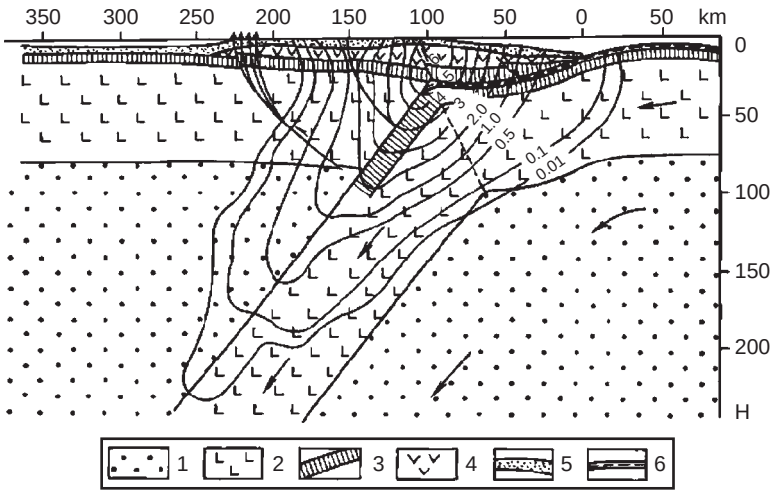


**FIGURE 2.7** Structure of the Kuril Islands subduction zone: 1, astenosphere; 2, lithosphere; 3, oceanic crust; 4–5, sedimentary-volcanic sequence; 6, oceanic deposits (the contours show seismic activity in $A_{10}$ units (Fedotov et al., 1969); $\beta$ is the Wadati–Benioff zone dip angle; $\alpha$ is plastic deformation zone dip angle.[2]

of 600–700 km. And tomography carries the oceanic lithospheric plates to 1400–1500 km (Jordan, 1975), and possibly even deeper, down to the surface of the Earth's core.

However, the strongest earthquakes with significant Earth's crust deformations occur when the continents collide. These deformations create the largest mountain ranges (Fig. 8.23). Many such mountain belts existed on Earth as each formation of a new supercontinent created its own system of large mountain buildups accompanied by strong earthquakes. Presently, most of such belts, especially ancient, are eroded and long gone. Their previous grandeur is indicated not by the topographic forms but only by the size, structure, and metamorphism of their roots.

The most spectacular modern collision mountain range is the Alpine-Himalaya fold belt. It formed due to the closing of the Tethys Paleo-Ocean and collision between the continents of Gondwana and Eurasia. This very belt also generates intraplate seismicity of the present-day Earth. This seismicity increases in terms of its repetitiveness and magnitude from the Alps through the Carpathians, Caucasus, Kopet-Dag, and Pamir to the Himalayas. Without delving into details, following are the causes of earthquakes in belt's characteristic points.

The northward drift of the Arabian Peninsula at a speed of about 5 cm/year imposes strong pressure onto the Caucasus Minor region which is an area of elevated seismicity (the testimonies to it are the Spitak earthquake of 1988, and the earlier earthquakes in Armenia). The Caucasus Minor, in turn, pushes the Caucasus Major which causes seismicity of Dagestan, Chechnya, and other piedmont areas. The Arabian drift resulted in earthquakes in Turkey and Iran (such as in 2006) as well as the devastating Askhabat quake of 1948. The strongest troublemaker, however, is the Indian subcontinent which is also rapidly drifting north-northeasterly at a speed of over 5 cm/year. Among the most seismic areas

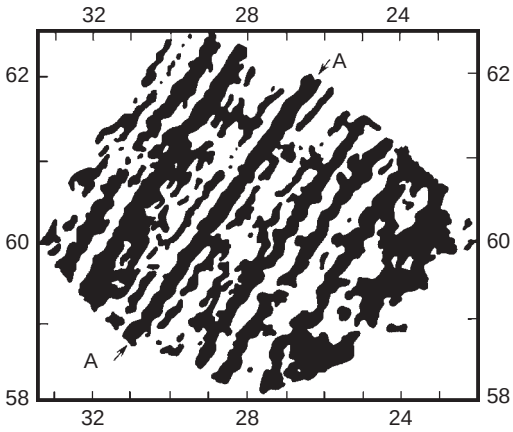


**FIGURE 2.8** Magnetic anomalies near the underwater Reykjanes Ridge in the north Atlantic Ocean (Heirtzler et al., 1966). The positive anomalies are shown in black. AA is the zero anomaly of the rift zone.

are the Hindu Kush in Pakistan and Afghanistan, and also Pamir, Karakorum, and Tibet. An event to remember is a devastating Pamir earthquake of 1911.

Under pressure from Indostan, the Himalayas and Tibet are continuing their growth accompanied by frequent and strong earthquakes up to the Bangladesh border.

A May, 2008 Sichuan quake on the Chinese Platform (magnitude 7.9) was also associated with pressure from the Indostan Plate on Tibet, and from Tibet on the Chinese Platform. And from the other side, the Chinese Plate was pushed by the Pacific Plate which was the causative factor of this earthquake that destroyed the city of Chengdu and killed over 20,000 people.

The effect of India's northeasterly drift expands over many thousands of kilometers. Modern scientific data indicate that Lake Baikal emerged in association with it. Lake Baikal is continuing to expand which is supported by a strong earthquake of 2008 in the southern part of the lake. The seismic belt extends farther east along the Baikal-Amur railway. The entire area from Pamir and Tyan-Shan to Baikal, 2500-km long, is a seismic area. The belt housed a strong Altay quake of February, 2003.

In the past epochs, such earthquakes, although much stronger, shook Earth many times, especially during the formation of supercontinents. Their consequences may only be seen now through the deformations in the ancient mountain belts, and in their numerous olistostromes.

The ocean floor displays very characteristic and rather contrasting banded magnetic anomalies. They are usually parallel to the crests of mid-oceanic ridges (Fig. 2.8). The origin of these anomalies is associated with the ocean floor basalts' property to magnetize while cooling thereby remembering the field direction at the moment of their eruption on the ocean floor. Taking into account the phenomenon of the magnetic field numerously changing its polarity in time, Vine and Matthews (1963) dated individual anomalies and showed that these anomalies are more or less parallel to the crests on the opposite flanks of the mid-oceanic ridges. What they did they showed that the ocean floor is relatively young. They identified major patterns in plate motions over the individual areas of the oceanic crust of the mid-Atlantic and showed that the ocean floor is spreading more or less symmetrically away from the mid-oceanic ridge crests at a speed of about a few centimeters per year.

Similar studies were later conducted all over the World Ocean and everywhere supported this pattern. Moreover, a detailed comparison of the ocean floor anomalies with

magnetic polarity reversal geochronology of the continental rocks (whose age was established independently) enabled the extension of the anomaly dating to the entire Cenozoic, and later to Late Mesozoic (Heirtzler et al., 1968). Thus, a new reliable technique of the ocean floor age determination was discovered.

The technique was used to support an earlier idea of a relative youth of the ocean floor: its paleomagnetic age, without exception, turned out to be only Cenozoic and Late Mesozoic. This conclusion was later totally supported by deep-sea drilling in many locations of the World Ocean. And it so happened that the age of the young oceans (the Atlantic, Indian, and Arctic oceans) is the same as the age of their floor, whereas the age of the ancient Pacific is much older than the age of its floor.

Indeed, the Pacific Ocean depression exists at least from Late Proterozoic (maybe even earlier), and the age of its floor's oldest areas is no older than 160 MMY, whereas its major portion formed in Cenozoic, that is, it is younger than 65.5 MMY.

The ocean floor renewed itself as a conveyor belt. The older areas of the oceanic crust with the deposits accumulated on them were constantly diving into the mantle under the island arcs. This was the reason why the oceanic depressions did not have time over the life of Earth to accumulate sediments.

Indeed, at the current rate of the oceanic depressions' fill-up with terrestrial clastic deposits ($2.2 \times 10^{16}$ g/year), the entire volume of the depressions (close to $1.37 \times 10^{24}$ cm$^3$) would be filled in about 1.2 BY. We may state with reasonable certainty that the continents and oceanic depressions exist together nearly 3.8–4.0 BY. No substantial fill-up of the depressions occurred over that log time.

Moreover, based on drilling results in all oceans we now know with reasonable certainty that there are no ocean floor deposits older than 160–190 MMY. This may have happened only if an efficient deposit removal mechanism existed. As it is presently known, this mechanism is sucking-in the deposits under the island arcs and active continental margins in the subduction zones (Sorokhtin and Lobkovsky, 1976). There, these deposits are remelted and merge again with the continental crust, which is forming in these zones, in form of granitoid intrusions (Sorokhtin et al., 1971). This process is called the deposit recycling.

### 2.3.2 Continental Crust

The continental crust is very different from the oceanic crust in its composition and structure. Its thickness ranges between 20–25 km under island arcs and the areas with a transitional type crust, and 80 km under young fold belts, such as Andes or Alpine-Himalayan belt. Average thickness of the continental crust underneath ancient platforms is about 40 km, and its mass, including the subcontinental crust, reaches $2.25 \times 10^{25}$ g (Ronov and Yaroshevsky, 1978). The continental crust topography is quite rugged. However, it includes wide plains filled up with sediments (they are usually positioned under the ancient Proterozoic platforms), highs of the oldest (Archaean) shields, and younger mountain systems. The continental crust topography displays the largest elevation gradients (reaching 16–17 km) between the feet of the continental slope in deepwater trenches and highest mountain peaks.

As opposed to the oceanic crust, most of the continental crust is very old. Based on the age of the oldest rocks on Earth (3.9–3.8 BY), the continental crust began forming in the

earliest Archaean. By the beginning of Proterozoic 2.6 BY ago, that is, during the initial 1.4 BY of Earth's tectonic activity, about 70% of the present-day crust was formed (Taylor and McLennan, 1985). The remaining 30% of the crust formed during the last 2.6 BY.

The continental crust is highly nonuniform. However, similar to the oceanic crust it may be sometimes subdivided, especially in the ancient platforms, into three layers. The upper one is sedimentary and the lower two are composed of crystalline rocks. The structure of the crust is more complex underneath the young mobile belts, although in general it is similar to the dual-layer structure (Broun and Mussett, 1981).

The sedimentary layer on the continents is reasonably well studied by geophysical methods and drilling. The structure of the consolidated crust surface wherever it is exposed on the ancient shields was studied by direct geological techniques and geophysical methods. On continental platforms covered by the sediments, the techniques were mostly geophysical and drilling. It was established that the seismic wave velocities within the crust layers increase down the section from 2–3 to 4.5–5.5 km/s in the lower sediment sequence, to 6–6.5 km/s in the upper layer of crystalline rocks, and to 6.6–7.0 km/s in the lower layer of the crust. The continental crust, likewise the oceanic one, is underlain almost everywhere by high-velocity rocks of the Mohorovicic discontinuity with seismic wave velocities of 8.0–8.2 km/s, but these are the properties of the subcrustal lithosphere composed of the mantle rocks.

The thickness of the upper, sedimentary layer of the continental crust widely ranges between 0 on the ancient shields and 10–12 km and even 15 km over the passive continental margins and within the platform foredeeps. Average sediment thickness over the stable Proterozoic platforms is usually close to 2–3 km. The sediments on such platforms are dominated by sandy–clayey deposits and carbonates of the shallow-water marine basins. The sedimentary rocks on the Atlantic type passive continental margins usually begin with coarse clastic facies replaced up the section by sandy–clayey deposits and carbonates of the near-shore marine facies.

Chemical deposits are sometimes developed at the base and in the upper section of the sedimentary sequences in the foredeeps. They are evaporites manifesting depositional environments of narrow semiclosed marine basins with arid climate. Such basins usually arise on the initial or final stages of marine basins and oceans (provided these basins and oceans at the time of their emergence or closing were located in the arid climate belts).

Among the examples of such formations associated with the early evolutionary stages of the ocean, basins are evaporites at the base of the sedimentary sections over the African Atlantic shelves and salt-bearing Red Sea deposits. Examples of salt-bearing formations within the closing basins include evaporites of the Reno-Hercynian zone in Germany and the Permian salt- and gypsum-bearing sections in the Urals Foredeep of the eastern Russian Platform.

The upper section of the consolidated continental crust is usually composed of old, mostly Precambrian granite–gneiss composition rocks or of alternating granitoids and greenstone belt rocks of base composition. This portion of the rigid crust is sometimes called "the granite layer" which underlines the prevalence of granitoid rocks and a secondary role of basaltoids. The "granite" layer rocks are usually altered by the processes of regional metamorphism up to the amphibolite facies.

The upper portion of this layer is always a denudation surface on which tectonic structures and magmatic formations of the old folded (mountainous) belts were eroded long

time ago. For this reason, the sediments covering the continental crust bedrock always overlie it with a structural unconformity and with a large age hiatus.

A dispersed and discontinuous boundary is quite common in deeper portions of the crust (at about 15–20 km). The compression wave velocities along this boundary increase by approximately 0.5 km/c. This is so-called "Conrad discontinuity" separating the lower layer of the continental crust tentatively called "the basalt layer" although there are very little definitive data about its composition. Most likely, the lower continental crust comprises rocks of medium to base composition metamorphosed to the amphibolite or even granulite facies (Broun and Mussett, 1981; Taylor and McLennan, 1985). It is possible that fragments of the old oceanic crust with not only base but even serpentinized ultramafic rocks may be located at the base of the continental crust blocks formed long ago in the collisions of island arcs.

The continental crust heterogeneity is quite clear at just looking on a geological map of the continents. Usually separate and closely interlocked, compositionally nonuniform crustal blocks represent vari-aged geological structures, remnants of ancient fold belts sequentially accreted to one another as the continental massifs grew. Sometimes, however, such structures are testimonies of past splits in the ancient continents (e.g., aulacogens). Such blocks contact with each other on the suture zones often called (and it is not a very good name) deep-seated faults.

Studies of the crust's deep structure conducted over the recent decades using signal stacking method of reflection seismic (Consortium for Continental Reflection Profiling project) indicated that the suture zones separating vari-aged fold belts are as rule giant overthrusts. These overthrusts are steep in the upper portions of the crust and rapidly flatten out with depth. In the map view, such overthrust structures are tens, sometimes hundreds of kilometers long. In depth, they sometimes approach the very base of the continental crust thereby marking ancient and now dead lithospheric plate subduction zones or secondary overthrusts conjugated with them.

The present-day earthquakes usually also occur along such younger zones. The strongest quakes with significant crust deformations happen when the continents collide. The resulting deformations usually form major mountain ranges (Fig. 8.23). There were plenty of such mountain belts on Earth as each process of the supercontinent formation created its own system of major mountain buildups accompanied by very strong earthquakes. Today, most of these mountain belts, especially the ancient ones, are eroded. Their past majesty may only be judged not from the topographic forms but from the size, structure, and metamorphism of their root portions.

The most majestic present-day collision mountain belt is the Alpine-Himalayan fold belt which arose due to the closing of the Tethys Paleo-ocean and collision between the Gondwanan continents with Eurasia. The main intraplate seismicity of the present-day Earth is also associated with this belt. This seismicity regularly increases in its repetitiveness and magnitude from west to east, from the French Alps, Carpathians, Caucasus, Kopet-Dag, and Pamir to Himalayans in the east of India. Not going into a detailed description of the belt's seismicity, we will just mention the earthquake caused at its characteristic points.

The Arabian Peninsula northward drift at a rate of about 5 cm/year exerts a strong pressure on the Caucasus Minor region. The region displays elevated seismicity as demonstrated by the 1988 Spitak quake and earlier quakes in Armenia. In turn, the Caucasus Minor pushes the Caucasus Major causing seismicity in Dagestan, Chechen Republic, and other piedmont regions. The drift of Arabia caused earthquakes in Turkey and Iran (e.g.,

in 2006) as well the Askhabat quake of 1948. However, the strongest "troublemaker" in the Alpine-Himalayan belt is the Indian Subcontinent which is also drifting north-northeastward at a rate of over 5 cm/year. One of the most seismic areas is Hindu Kush with Pakistan and Afghanistan, and also Pamir, Karakorum, and Tibet. The 10-ball Pamir quake of 1911 is especially memorable.

Pushed by Hindustan, Himalayans, and Tibet continue to grow accompanied by frequent and rather strong earthquakes up to the Bangladesh latitude. One such event was the Sichuan (Chinese Platform) quake of 2008 with the magnitude of up to 7.9. Its origin is associated with the pressure from the Hindustan Plate on Tibet, and from Tibet on the Chinese Plate. And from the other side, the Chinese Plate was pushed by the Pacific Plate. The result was a very strong earthquake which almost totally destroyed the city of Chengdu and killed over 20,000 people.

The effect from the northeasterly India drift extends over thousands of kilometers. The current data indicate that this drift caused the emergence of the Lake Baikal. The lake is continuing to expand which is supported by a strong earthquake of 2008 in the southern portion of the lake. The seismic belt extends farther east along the Baikal-Amur railroad. The entire area between Pamir–Tyan-Shan and Baikal, 2500 km in length, is a high seismicity area as testified by a strong Altay earthquake of February, 2003.

In the past geological epochs such quakes, only much stronger, numerously shook Earth, especially at the time of the supercontinent formation. Their results may only be judged from the residual deformations in the ancient mountain belts and their numerous olistostromes.

## 2.4 THE EARTH'S MANTLE

The mantle is a silicate shell positioned between the base of the Earth's crust and the surface of the Earth's core at a depth of around 2900 km. The mantle conventionally is subdivided based on seismic data into the upper mantle (layer B) to a depth of 400 km, the Golitsin transitional layer (layer C) in the 400–1000 km depth interval, and the lower mantle (layer D) at a depth of 2900 km. Usually, two more layers are identified at the base of the lower mantle. In the layer D″ (about 200-km thick), the velocity increase gradient decreases with depth. In the boundary Berzon layer, around 20-km thick, the shear wave velocity declines almost to zero. An additional layer (the Gutenberg crustal waveguide) is separated underneath the oceans. It is a layer of lowered seismic wave velocities usually identified with Earth's astenosphere where the mantle matter is partially melted. This layer is either not present or weakly expressed under the continents.

Under-crustal portions of the lithospheric plates where the mantle matter is cooled-down and totally crystallized are usually included into the upper mantle. The lithospheric thickness underneath the oceans changes from 0 under the rift zones to 60–70 km under the oceanic abyssal depressions. The lithosphere thickness under the continents may reach 250 km.

Our knowledge of the mantle and core structure and of the state of the matter in these geospheres is mostly based on seismologic observations. The seismic wave time-depth curves were interpreted using hydrostatic equations which associate the compression and shear wave propagation velocity values and the density gradients. The technique was introduced by an Australian geophysicist, K. Bullen, in the mid-1940s and later significantly

improved (Bullen, 1958, 1966, 1978; Zharkov, 1983). Figure 2.9 demonstrates density distributions in the mantle for some popular Earth models as constructed using these techniques, in comparison with the shock compression data for mantle silicates or the oceanic lherzolite composition silicates (modelHC-1).

As the figure shows, the upper mantle density (layer B) increases with depth from 3.3–3.32 to approximately 3.63–3.70 g/cm$^3$ at about 400 km. Deeper in the Golitsin transitional layer (layer C) the density gradient drastically increases, and density grows to 4.55–4.65 g/cm$^3$ at 1000 km. Average mantle density is approximately 4.54 g/cm$^3$.

The mantle density increases with depth due to the compaction of its matter under the ever increasing pressure of the overlying mantle layers reaching 1.35–1.40 Mbar at the mantle base. The upper mantle matter compaction with depth goes through several consecutive jumps, at the first kind phase transition boundaries, to denser mineral associations. Especially, strong compaction of the mantle matter silicates occurs in the 420–1000 km depth interval. According to Ringwood (1981), these are the depths where many minerals experience polymorphic transformations.

In particular, the most common mantle mineral olivine first acquires the spinel crystalline structure (at a depth of about 420 km), and then falls apart into enstatite and magnesiowustite. Pyroxenes first change to the ilmenite structure, and then to the most dense perovskite structure (at about 670 km).

At the same depths, most silicates (probably except enstatite which changes to the perovskite structure) decompose into simple oxides with the densest atom packing in their corresponding crystallites.

Motions of the lithospheric plates and the continental drift are convincing testimonies to the existence in the mantle of the intense convective flows which stirred the entire matter within this geospheres many times during Earth's life time. A conclusion from this is that

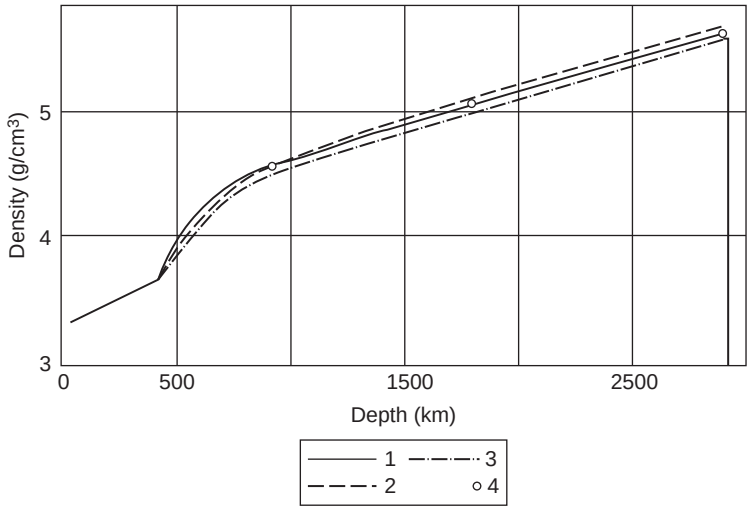


**FIGURE 2.9** Density distribution in the mantle under different models: 1, Naimark–Sorokhtin model (1977a); 2, Bullen model A1 (1966); 3, Zharkov's "Earth-2" model (Zharkov et al., 1971); and 4, Pankov and Kalinin data (1975) recalculated for the lherzolite composition under adiabatic temperature distribution.

the composition in the upper and lower mantle is, on the average, similar. The upper mantle composition is reliably determined from the finds of ultrabasic rocks in the oceanic crust and from the composition of ophiolite complexes.

Ringwood (1962a,b) proposed, based on his study of the ophiolites from fold belts and basalts of the oceanic islands, a hypothetical composition of the upper mantle. He called it "pyrolite." It resulted from mixing three parts of the alpine-type peridotite—hapsburgite with one part of the Hawaiian basalt. The Ringwood's pyrolite is close in its composition to the oceanic lherzolites studied in detail by Dmitriyev (Dmitriyev, 1969, 1973; Dmitriyev et al., 1969).

Contrary to the pyrolite, the oceanic lherzolite is not a hypothetical mixture but a real mantle rock raised from the mantle in the rift zones and exposed in the transform faults near these zones. Besides, Dmitriyev demonstrated complementarity of the oceanic basalts and restite harzburgites (residual after basalt's melt-out) with the oceanic lherzolites. Therefore, he proved the priority of lherzolites from which the tholeite basalts are melt-out, and the residue is the restite harzburgites. So, the oceanic lherzolite described by Dmitriyev (see Table 2.1) is closest in its composition to the upper mantle, hence, to the entire mantle.

Geochemistry of the basalt magmatism on the ocean floor significantly depends on the basalt melt-out depth and temperature (Green and Ringwood (1967a, 1977b)). Therefore, it is determined mostly by the thickness of the oceanic lithosphere. Permanency in the composition of the oceanic toleites (Lisitsin, 1974a,b; Ringwood, 1981, 1982), which melted-out along the entire rift zone system at the crests of the mid-oceanic ridges (i.e., under approximately similar conditions), is a convincing evidence in favor of the high uniformity of the upper mantle under the oceans (Ringwood, 1982). Taking into account the continental drift, continuous changes in the ocean and the continents positions on Earth's surface, and the mantle convection, this conclusion may be extended to the entire sub-lithospheric and upper and lower mantle (Sorokhtin and Ushakov, 1991, 1993).

Besides, the recognition of convective flows in the mantle enables the determination of its temperature regime. Indeed, the mantle temperature distribution under convection must be close to the adiabatic (see Section 2.8). As a reminder, the adiabatic process is such where there is no heat-exchange between the adjacent areas of the matter. All mantle heat loss occurs through its upper boundary layer, that is, through Earth's lithosphere. For the same reason, temperature distribution in the lithosphere is very different from the adiabatic.

The conclusion about a similar average chemical composition of the upper and lower mantle may be theoretically persuasive but still requires an experimental check. Ringwood (1981, 1982) experimentally studied the restructuring of the silicate crystalline structure under high pressure and found the following. All changes in the upper and lower mantle matter density (including in the Golitsin layer) are easy to explain by pyrolite compaction with no change in its chemical composition. Besides, to check the hypothesis about the similar composition of the upper and lower mantle, density of the oceanic lherzolite from a transform fault of the Karlsberg ridge in the Indian Ocean was estimated through the calculations of the silicate shock compression at the pressure of about 1.5 Mbar.

There is no need for a real compression in such experiment. It is sufficient to know the chemical composition and the results of previous experiments with the shock compression of individual rock-forming oxides. The results of a calculation performed for the adiabatic temperature distribution in the mantle (Naimark and Sorokhtin, 1977a,b) were compared with the known distributions derived from seismologic data (Fig. 2.9).

**TABLE 2.1** Composition of Present-Day Earth and of Primordial Earth Matter

| Oxides | Composition of continental crust[a] | Model composition of Earth mantle[b] | Model composition of Earth core | Composition of Earth's primordial matter (calculated) | Average composition of chondrites[c] | Average composition of coaly chondrites[d] |
|---|---|---|---|---|---|---|
| $SiO_2$ | 59.3 | 45.4 | – | 30.71 | 38.04 | 33.0 |
| $TiO_2$ | 0.7 | 0.6 | – | 0.41 | 0.11 | 0.11 |
| $Al_2O_3$ | 15.0 | 3.7 | – | 2.54 | 2.50 | 2.53 |
| $Fe_2O_3$ | 2.4 | 4.15 | – | – | – | – |
| FeO | 5.6 | 4.37 | 49.34 | 22.24 | 12.45 | 22.0 |
| MnO | 0.1 | 0.13 | – | 0.09 | 0.25 | 0.24 |
| MgO | 4.9 | 38.4 | – | 25.81 | 23.84 | 23.0 |
| CaO | 7.2 | 2.3 | – | 1.57 | 1.95 | 2.32 |
| $Na_2O$ | 2.5 | 0.43 | – | 0.3 | 0.95 | 0.72 |
| $K_2O$ | 2.1 | 0.012 | – | 0.016 | 0.17 | – |
| $Cr_2O_3$ | – | 0.41 | – | 0.28 | 0.36 | 0.49 |
| $P_2O_5$ | 0.2 | – | – | – | – | 0.38 |
| NiO | – | 0.1 | – | 0.07 | – | – |
| FeS | – | – | 6.69 | 2.17 | 5.76 | 13.6 |
| Fe | – | – | 43.41 | 13.62 | 11.76 | – |
| Ni | – | – | 0.56 | 0.18 | 1.34 | – |
| Total | 100.0 | 100.0 | 100.0 | 100.0 | 99.48 | 98.39 |

[a] *Ronov and Yaroshevsky (1978).*
[b] *Our model using the data from Dmitriyev (1973) and Ringwood (1966).*
[c] *Urey and Craig (1953).*
[d] *"Outlines of comparative planetology." Nauka (1981), 184–185.*

The comparison shows that the oceanic lherzolite density distribution at high pressure and adiabatic temperature is a good approximation of the independently derived real density distribution in the mantle. That definitely testifies in favor of validity of the suggestions about the lherzolite composition of the entire (upper and lower) mantle and the adiabatic temperature distribution in those geospheres.

Knowing the matter density distribution in the mantle, we can calculate its mass. Together with the oceanic crust, it turns out to be $4.035 \times 10^{27}$ g, i.e., 67.5% of the total Earth's mass.

Another layer is identified at the base of the mantle. This is layer D″. It is about 200-km thick. Seismic wave propagation velocity gradient decreases within this layer and the shear wave decay increases. Moreover, analyzing dynamic signature of the waves reflected by the

core surface Berzon and her colleagues (1968, 1972) identified a thin (20 km) boundary layer between the mantle and the core which we call "the Berzon layer." The shear wave velocity within this layer, in its lower portion, declines from 7.3 km/s to almost zero. The shear wave velocity can be only a result of a decrease in the rigidity modulus, therefore, a decrease in the matter's effective viscosity in this layer.

Still, the very mantle-to-core transition boundary remains quite distinct. Based on the intensity and spectrum of the seismic waves reflected by the core, the thickness of such boundary layer may be 1 km or even less.

## 2.5 EARTH CORE

The Earth core is clearly identified by seismic data. The indications are a clear shadow on the depth–time curves of seismic waves refracted within the mantle, compression and shear waves reflected from core's surface, and a total decay of the shear waves within it. At that, the compression wave velocity significantly declines (by about the factor of 1.7; see Fig. 2.11).

An important conclusion from this is that the matter in the external shell of the Earth's core (the external core or layer E) is in the liquid state. On the other hand, the existence of converted waves transformed from the compression waves to the shear waves and back again discovered by Lehmann (1934, 1936) in the central areas of Earth indicates the presence in Earth of the internal, effectively rigid core (Bullen, 1978).

Radius of the rigid internal core (layer G) is approximately 1200–1250 km, the thickness of the transitional layer between the external and internal core (layer F) is about 300–400 km, and the liquid layer E has the radius of 3450–3500 km (and the respective depths of 2870–2920 km). The core matter density within the external core changes monotonously from 9.5–10.1 on its surface to 11.4–12.3 $g/cm^3$ at the base (see Fig. 2.12). Density within the internal core increases by about 8–10% and reaches 13–14 $g/cm^3$ in the Earth center. The core mass is in various models on the order of $(1.85-1.91)\times10^{27}$ g. Our estimate is $M_c \approx 1.94\times10^{27}$ g, which is 32.5% of the Earth's mass.

An interpretation of the core's seismic tomography (Morelli and Dziewonski, 1987) showed that the core surface is uneven, with noticeable deviations by up to $\pm$(6–10) km from the equilibrium shape of an ellipsoid of the revolution (see Fig. 2.10). This core surface topography, most likely, is a reflection of the roots of ascending and descending convection flows in the lower mantle. We predicted this phenomenon (Sorokhtin, 1974) long before the discovery of this topography. Indeed, mantle lows (the roots of the descending flows indented into the core) must form underneath the descending convective flows (i.e., under heavier portions of the mantle), whereas the surface highs must be observed under the ascending flows.

The upper limit of viscosity value for the external (liquid) core layer may be estimated from the degree of absorption in this geosphere of compression seismic waves. It was determined that average matter viscosity in the liquid core portion is much lower than $\eta_c = 10^9$ poise (P) and probably does not exceed $10^3$ P (Zharkov, 1983). Studying variable components of the Earth magnetic field and energy balance of the geomagnetic dynamo, Loper (1975) concluded that core's kinetic viscosity is close to that of the water and most likely is $\nu_c \approx 4\times10^{-2}$ $cm^2/s$. Then, the core matter dynamic viscosity is $\eta_c \approx 0.4$ P. It is worth noticing here that the external core viscosity that low indicates its clear overheating or, which is

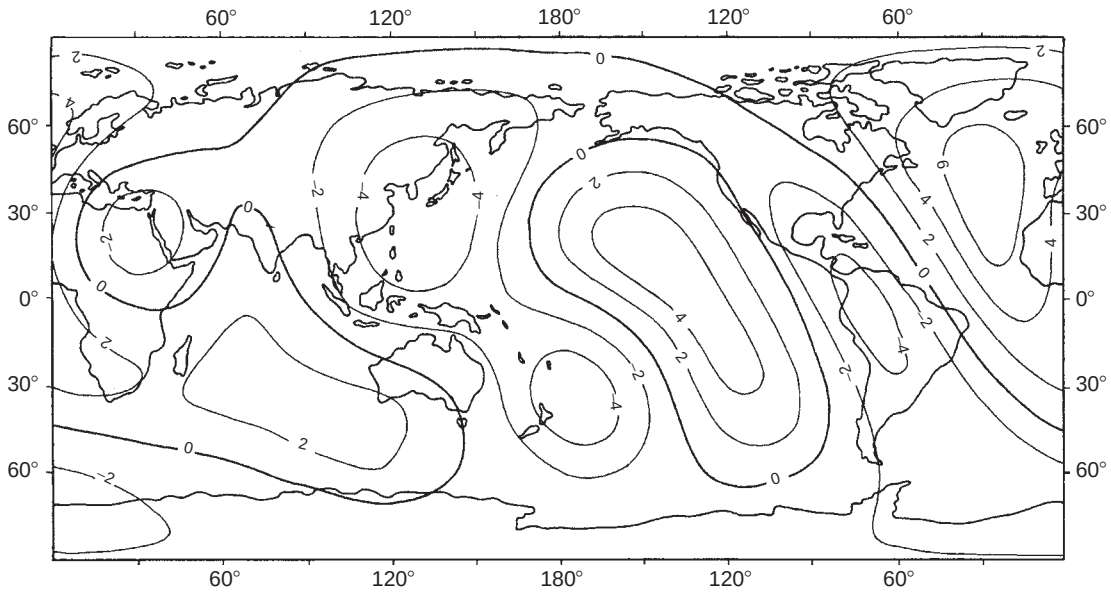


**FIGURE 2.10** Earth's core topography based on seismic tomography (contours are drawn every 2 km) (Morelli and Dziewonski, 1987).

the same, its low-melting temperature, and is a necessary condition for the generation of a geomagnetic field.

As already mentioned, the internal core with its mass of $1.1 \times 10^{26}$ g (or about 1.8% of Earth mass) is solid and, most likely, is different in its composition from the external core.

The fact that the oldest igneous rocks appeared only 600–800 MMY after Earth formation is a convincing testimony toward the "cold" origin. On the other hand, the Earth core formation at early stages of Earth evolution requires its hot and even melted state. It follows from this that the young Earth indeed did not have a high-density core. It is also supported by the lead isotope ratio in Earth rocks (see a detailed discussion in Section 5.2).

It is ever clearer now that many important processes were initiated and controlled by the planetary process of Earth core separation. These processes included tectonic activity, Earth crust formation with its economic mineral deposits, geochemical evolution of the mantle, its degassing and genetically related processes of the ocean and atmosphere formation as well as the emergence of life on Earth. This planetary process is continuing for about 4 BY now but is still not completed although most of the core matter has already sunk into Earth crust. The development of the main planetary process of Earth global evolution is completely defined by the composition of the Earth matter and Earth core. As this is an exceptionally important issue, we will dwell in some detail on the determination of the chemical composition of the core matter.

## 2.6 EARTH CORE COMPOSITION

Obviously, there are no direct data about the Earth core composition. Nevertheless, modern experiments with static and shock compression of metals and the data about the distribution of chemical elements in the Solar System and on Earth enable very reliable inferences on the matter. It is believed that the core contains about 90% iron (Birch, 1958; Altshuler et al., 1968; Altshuler and Sharipdzhanov, 1971a,b).

However, the external core cannot be composed of pure iron and even more so of its alloy with nickel. The reason is that the iron and nickel–iron densities in meteorites, under pressures dominant within the Earth core, are 10–15% higher than that of the external core matter. That is why a purely iron core could in no way be melted within Earth although the liquid state of the matter within the external core is doubtless.

The data quoted earlier force a conclusion that the core matter must include lighter additives beside iron. These additives decrease somewhat the matter density and significantly, its melting temperature. Among such additives different writers considered silicone, sulfur, and oxygen. For thermodynamic reasons, silica is the least likely component of the core matter. Indeed, based on the least differentiated meteorites (the coaly chondrites, type 1), the cold matter of the protoplanetary gas–dust cloud contained up to 25% of an iron oxide, FeO. The iron silicides $FeSi_2$ and FeSi are unstable in its presence and disintegrate forming $SiO_2$ and the metallic iron. The reaction is highly exothermic, therefore irreversible:

$$2FeO + FeSi \Rightarrow SiO_2 + 3Fe + 68 \text{ kcal/mol}. \tag{2.8}$$

Besides, the iron silicides were never found in the meteorite matter, be it primitive undifferentiated coaly chondrites or highly differentiated iron–nickel meteorites.

In selecting a most likely light additive to the core matter between sulfur and oxygen, the thermodynamic conditions of the planet formation and the core separation conditions at the planetary stage must be taken into account.

Without delving into much detail of the Solar System planet formation, we will mention here only solidly established and most general patterns in the planetary matter distribution with the increasing distance from the Sun.

Drastic differences in the planets' density within the Earth planetary group clearly indicate that the intense segregation in chemical composition of the primordial protoplanetary cloud predated (or accompanied) their accretion. It is now established that the total content of the iron–nickel phase in Earth group planets decreases with their distance from the Sun. The only exception is the Moon which "dropped" its iron core on Earth as its mother-planet proto-Moon was being destroyed on the Earth's Roche limit (see Chapter 3 for more detail).

Based on the planet density (accounting for their compression), Mercury contains about 65% of the iron–nickel phase; Venus, 28.8%; Earth (together with the "dropped" proto-Moon iron), 32.5%, and Mars, 20%. On the other hand, huge amounts of volatile components ($H_2$, He, $CO_2$, $CH_4$, $H_2O$, $NH_3$, $N_2$, etc.) are concentrated in the atmospheres of the internal planets. These amounts, in terms of their mass, sometimes exceed the silicate cores of the planets by one or two orders of the magnitude. To compare, the total mass of Earth atmosphere and hydrosphere is just 0.024% of the solid Earth, and for Venus it is even smaller, 0.0085%.

A similar segregation (maybe to a slightly lesser extent) must have occurred also with easily mobile elements, including sulfur. We know now that the surface of a Jupiter's

satellite Io is totally covered with the "ocean" of sulfur. We believe that it is a convincing testimony to the sulfur removal to the periphery of the Solar System as early as in the time of the protoplanetary cloud differentiation. Thus, it may be expected that the Earth group planetary matter was substantially impoverished in sulfur even prior to their accretion (at least in comparison with average composition of the protoplanetary cloud).

Ringwood (1982) noted that a hypothesis of sulfur in the core meets with great difficulties for a reason of significant impoverishment of the Earth core in a number of elements less volatile than sulfur (Cr, Mn, Na, K, F, Cs, Zn, and Cl). The impoverishment factors for these elements, compared to their primary occurrences in the first type coaly chondrites and in the Sun, are in the range of 0.3–0.03. A similar situation is typical for many meteorites. For instance, regular chondrites formed out of the primordial matter impoverished in sulfur by 80%, whereas Na, K, Rb, Mn, and Cr in them are almost completely preserved. Moreover, there is a contradiction. If the parent bodies of the meteorites contained average solar concentration of sulfur (5–6%), most of it must have concentrated in the metallic phase as the iron sulfide. In such a case, sulfur concentration in iron meteorites must have been substantially higher than 6%. But in fact sulfur content in the iron meteorites is close to 1%.

Taking into account what we just mentioned, and also the quoted facts and estimates, we may assume that the Earth matter as a whole is impoverished in sulfur by about the factor of 10 compared with the Sun matter.

At the same time, like the matter of coaly chondrites, the Earth matter is sufficiently oxidized and there is no oxygen deficiency on Earth. At least, the Earth mantle matter is reasonably completely oxidized albeit not to the limit as the ratio $FeO/Fe_2O_3 > 1$ there.

Thus, based on the comparative planetology data, Earth, compared with average composition of the planets and meteorites, is slightly enriched in iron (by the factor of 1.3–1.4), significantly impoverished in sulfur and other mobile elements (approximately by the factor of 10) and very significantly impoverished in all volatile compounds (by the factor of $10^5$–$10^7$).

But let us assume that there was no sulfur loss from the protoplanetary cloud in the Earth formation area, and that it has average sulfur content (around 5–6%). Even in this case the available amount of sulfur would not be sufficient for the Earth's core formation because a core of a FeS composition must contain about 11% of sulfur relative to the Earth mass. And as the Earth matter was substantially impoverished in sulfur, its remaining amount would be even more insufficient for the formation of a sulfide–iron core. At the same time, a reasonably complete oxidation of the Earth mantle matter suggests the existence of iron oxides also within the Earth core.

Let us now review the purely geophysical and geological information related to the composition of a possible light additive to iron in the Earth core matter.

We conducted a detailed analysis of the planet's energy balance (see Chapter 5). It indicates that the main source of the endogenous energy in the present-day Earth is the mantle gravity differentiation. It resulted in the separation of a high-density core and in existing of convective motions in the residual silicate mantle.

Due to this process, nearly $3 \times 10^{20}$ erg/s of gravity energy is presently generated in the mantle. The fraction of the radioactive decay is close to $0.35 \times 10^{20}$ erg/s of the heat energy (the remaining larger part of the radiogenic energy, approximately $0.9 \times 10^{20}$ erg/s, is released in the continental crust and does not take part in Earth's tectonic activity). Calculations show that in such a case about 150 billion tons per year of the core matter is currently

being transferred from the mantle to the core. The only components in the present-day mantle suitable for such function are iron oxides FeO and $Fe_2O_3$. Their total content in the mantle matter is currently close to 8%. At the same time, the iron sulfide concentration in the present-day juvenile mantle does not exceed 0.1%. Therefore, from this viewpoint as well, it is most likely that the light additive to iron in the Earth core is oxygen.

It follows from the theory of homogenous planetary accretion that the young Earth immediately upon its origin was a planet, most likely, uniform in its composition and devoid of high-density core. Studies of Earth stratification process and lead isotope ratios in Earth's rocks showed that the core was separated gradually. One conclusion from it is that the entire core matter was in the beginning of the geological history uniformly dispersed in the primordial mantle. We know that the origin of the oldest crustal rocks one way or the other resulted from their separation from the mantle. If so, these rocks must include plentiful components that descended into the core. Indeed, the Archaean ultramafic and base rocks usually contain elevated amounts of FeO, and ancient basalts from the Disko Island in Greenland were found to contain metallic iron (Levinson-Lessing, 1940). At the same time, there are no noticeable sulfur anomalies in Archaean rocks. And a fraction of the sulfide metallogeny at that time is disappearingly small compared with the total iron oxide amount in the rocks. Thus, geological data also testify in favor of the iron oxide and not sulfide composition of the Earth core.

Based on the above data and considerations, we proposed and substantiated a hypothesis of the iron–oxide composition of the external liquid Earth's core (Sorokhtin, 1972). The internal solid core was traditionally considered to be comprised of a meteorite-composition iron–nickel alloy $Fe_{0.9}{\cdot}Ni_{0.1}$.

To determine stoichiometry of an iron–oxygen compound at high pressure, one needs to remember that iron belongs to the transitional group of elements. Its external electron shell $4s^2$ is totally occupied, and its internal $3d^6$ shell is partially vacant. Just a reminder: electrons in atoms may have only certain energy levels, and the group in electron shells indicated s, p, d, f, and so on, and the shell number is denoted by a number. Each shell of a neutral atom may contain no more than certain number of electrons: s shell, no more that 6 electrons, shell d, 10 electrons, shell f, 14 electrons, and so on.

The number of electrons in a given shell is usually denoted by a superscript to the shell name. For instance, the iron's atomic number is 26; therefore, each neutral iron atom has 26 electrons grouped in seven electron shells as follows: $1s^2 2s^2 2p^6 3s^2 3p^6 3d^6 4s^2$.

Chemical bonds of an element may occur only with the electrons in the external and incompletely occupied shells. For this reason, the internal, totally full shells are usually not marked when describing the chemical properties of specific elements. In this case, the electron configuration of iron is: $3d^6 4s^2$.

The external shell 4s of iron atoms is completely occupied by the electrons. Thus, under normal pressure chemical properties of this element are determined only by the vacant electron levels of the 3d shell.

As is known, under high pressure electron-phase restructuring occurs in atoms of the transitional metals. As a result, external electrons transfer to the internal orbits, but after that chemical properties of the element change. In iron, a first electron-phase transfer is observed at pressure $p > 130$ kbar (Altshuler and Bokanova, 1968). After that one of the external s-electrons transfers to d-orbits changing the electron configuration: $3d^6 4s^2 \rightarrow 3d^7 4s^1$. As a result of such transfer, a single unpaired electron remains in the iron's external s shell. This electron may now append one of the electrons from the other atom, for

instance, oxygen forming with it a strong sσ univalent covalent bond (Sorokhtin, 1972). S-bonds are always stronger than d-bonds. Therefore, under high pressure iron should acquire properties of the univalent metal, and the chemical composition of the external core iron must correspond to an iron oxide with an unusual stechiometry $Fe_2O$.

At high pressure $p > 130$ kbar there is a possibility for $Fe_2O$ of a stable molecular structure where valence (s–p)σ bonds between iron and oxygen atoms operate only within the molecules proper. Intermolecular connections are working only through much weaker (d–d)π bonds between iron atoms and dipole (Vanderbilt) interactions between the $Fe_2O$ molecules (Sorokhtin, 1972). These properties of iron chemical bonds under high pressure suggest a relatively low-melting temperature of $Fe_2O$. That is very important for the explanation of a liquid state of the core matter within the external core and for a physical substantiation of the liquid core separation mechanism without melting of the lower mantle silicates.

At even greater pressure $p \approx 3$ Mbar a second electron-phase transition occurs in iron: $3d^7 4s^1 \rightarrow 3d^8$. After that, iron becomes a chemical analog of nickel ($3d^8 4s^2$), in which chemical properties are also completely defined by the analogous electron configuration ($d^8$) in the three-dimensional shell of its atoms.

Nickel can also experience the electron-phase restructuring and change its chemical properties but it occurs at even higher pressure. That is why the second electron-phase transition in iron, probably, explains the formation of a Fe·Ni alloy within the Earth's internal core and its greater density than of iron at the same pressure (Sorokhtin, 1972).

When high pressure is relieved iron returns to its usual state $3d^6 4s^2$. Under this state, the total identity of iron and nickel chemical properties is disrupted. As a result, the crystals of Fe·Ni composition which formed under higher pressures must disintegrate. That is exactly what is observed in iron–nickel meteorites: so-called Widmanstatten structures that appear in the iron–nickel meteorites after etching their polished surfaces with strong acids. Such meteorites have probably formed in the destruction of a relatively large planet within which pressure exceeded 3 Mbar. It could have been the hypothetical Phaeton destroyed by the Jupiter's powerful gravity field and having given birth to the asteroid belt between Mars and Jupiter.

In mid-1970s, we tested a hypothesis of iron oxide ($Fe_2O$) composition of the external core and the iron–nickel ($Fe_{0.9}{\cdot}Ni_{0.1}$) composition of the internal core by calculations based on experimental data from shock compression of metals and their oxides (Naimark and Sorokhtin, 1977a). The results showed a complete compatibility of the accepted hypothesis and the density distribution within Earth derived from the independent seismologic data (see Fig. 2.12).

At about the same time the iron oxide composition hypothesis of the core's external shell was supported by an Australian seismologist Bullen (1973, 1978) and a petrologist Ringwood (1982, 1977). Later experimental studies (Ohtani and Ringwood, 1984; Ohtani et al., 1984; Ringwood and Hibberson, 1990) demonstrated that under high pressure ($p > 200$ kbar) the iron oxide almost completely dissolves in the metallic iron melt with the formation of a Fe·FeO alloy stechiometrically similar to the $Fe_2O$ composition.

It turned out that the melting temperature of eutectic alloy Fe·FO was noticeably lower than that of the source components and also noticeably lower than adiabatic temperature distribution in the mantle (Fig. 2.17). Moreover, the experiments discovered the theoretically predicted volume decrease in the Fe·FeO alloy by about 3.8 $cm^3$/mol compared with

the combined molar volume of the source components (at normal pressure, $\sim$19.1 $cm^3$/mol). A compaction of the Fe·FeO alloy so substantial (by more than 20%), probably, may be explained only by electron-phase transitions in iron atoms and by the emergence in the melt at high pressure of strong covalent chemical s-bonds in the $Fe_2O$ molecules as was proposed by the source hypothesis. Computations by Ringwood and his colleagues also confirmed that under pressures common in the external core the density of a eutectic alloy Fe·FeO matches well with the core matter densities derived from seismology data.

The origins of Earth magnetic field and its nonstationary (variable) nature are usually associated with convective flows in the Earth core liquid matter. To excite Earth's magnetic field, however, the core matter must have high electric conductivity. Although so far there were no direct measurements of electric conductivity in the $Fe_2O$ or Fe·FeO alloy under high pressure and temperature, it follows from general physical and quantum-mechanics considerations that a compound of such composition must have metallic electric conductivity under the core conditions.

We now summarize the aforementioned theoretical considerations about the nature of Earth's core matter and experimental data about the melting temperature and density of iron eutectic alloys with its oxide under high pressure. It may be maintained with high probability that the external (liquid) portion of the core is composed of a melt of the univalent iron oxide $Fe_2O$ stable only under high pressure. The internal core is most likely comprised of an iron–nickel alloy $Fe_{0.9}{\cdot}Ni_{0.1}$. It is natural in this case to consider the composition of the transition layer F between the external and internal core as being a sulfide, FeS.

## 2.7 THE DENSITY OF THE DEEP EARTH

Despite the inaccessibility of the deep Earth to direct observations, it was possible to determine quite reliably the matter's density distribution in the mantle and Earth core from the earthquake waves propagation data in these geospheres.

The technique was first developed by Bullen (1958, 1966) and subsequently significantly improved on by him and by the other scientists through the use of additional information about Earth's moment of inertia and free oscillations (Haddon and Bullen, 1969; Zharkov and Trubitsin, 1980; Zharkov, 1983), which substantially raised the reliability of such determinations.

The technique of determining the density distribution within Earth is based on hydrostatic and thermodynamic equations connecting the radial density gradients within Earth with the medium's seismic parameters $\varphi(r)$:

$$\begin{aligned} \frac{dp}{dr} &= -\gamma m(r)\frac{\rho(r)}{r^2}\varphi(r), \\ \frac{dm}{dr} &= 4\pi r^2\rho(r), \\ \varphi(r) &= \frac{dp(r)}{d\rho(r)} = v_p^2 - \frac{4v_s^2}{3}, \end{aligned} \tag{2.9}$$

where $r$ is the current radius with its origin at the center of Earth, $\rho(r)$ is the matter density at the level $r$, $p(r)$ is pressure at the level $r$, $\gamma$ is gravitational constant, $m(r)$ is the mass

enclosed in a sphere of the radius $r$, and $v_p$ and $v_s$ are, respectively, compression ($P$) and shear ($S$) wave velocity. At that,

$$v_p = \sqrt{\frac{\lambda + 2\mu}{\rho}} \text{ and } v_s = \sqrt{\frac{\mu}{\rho}}, \tag{2.9'}$$

where $\lambda$ is compression modulus and $\mu$ is shear modulus.

As seismic velocities usually increase with depth, the interpretation of time–depth curves in order to determine velocity versus depth correlations is done by the Herglotz-Wichert technique (Jeffreys, 1959; Bullen, 1966) specially developed for the studies of gradient media. The compression and shear wave distributions within Earth so determined are shown in Fig. 2.11. The most striking feature of this distribution is a drastic and significant decrease of the compression wave velocities within the Earth's core. The reason for it is that the compression wave velocity is a function not only of the compression modulus but also of the shear modulus. The latter turns to zero within the external liquid core. Therefore, shear waves cannot propagate in a liquid matter of the external core.

Equations (2.9) may be used only for the layers of the constant composition and unchanging phase state of the matter. As we showed above, the constant composition condition is acceptable. However, polymorphous crystalline restructuring occurred in the mantle, and that led to the formation of denser mineral associations. That is a substantial complication.

However, the main phase transitions occur at depths between 400 and 800–900 km, that is, within the Golitsin transitional ("C" layer). In view of this, it may be accepted that the condition of the permanent composition is approximately met in the upper and lower mantle, and in the Golitsin transitional layer the mantle matter equation of state was approximated by a simple (for instance, quadratic) equation:

$$\rho(r) = ar^2 + br + c, \tag{2.10}$$

where $a$, $b$, and $c$ are the constants selected so that $\rho(r)$ is a continuous function at both the boundaries of the "C" layer, and the $d\rho/dr$ gradient is continuous at the base of the layer.

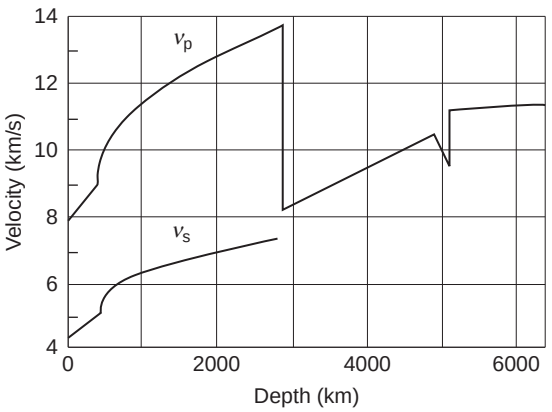


**FIGURE 2.11** Compression $v_p$ and shear $v_s$ seismic wave propagation velocities within Earth.

Equations (2.9) allow for the determination of only density gradients so, to generate a correlation for $\rho(r)$ it is necessary to assign boundary values of the density at the surface of Earth or in its center. The solutions derived for the individual geospheres (the core, lower mantle, transitional Golitsin layer, and the upper mantle) are stitched under the condition of pressure continuity at the boundaries of these geospheres. The density value in Earth center and parable (2.8) parameters are found from the equality of the calculated Earth mass $M$, average moment of inertia $I$, and density $\rho$ at the mantle's surface with the measured values of these parameters $M = 5.977 \times 10^{27}$ g; $I = 0.80187 \times 10^{45}$ g/cm$^2$ (moment of inertia relative to the Earth revolution axis $C = 0.8036 \times 10^{45}$ g/cm$^2$); $\bar{\rho}_0 = 2.9$ g/cm$^3$. These parameters are calculated from the following equations:

$$M = \int_0^R 4\pi r^2 \rho(r) \mathrm{d}r, \tag{2.11}$$

$$I = \int_0^R \frac{8}{3} \pi r^4 \rho(r) \mathrm{d}r, \tag{2.11'}$$

$$\rho_0 = \rho(R),$$

where $R = 6371$ km is average radius of Earth.

Additional fine-tuning of the density distribution in depth (especially in Golitsin's transitional layer) enables the introduction of the spectrum data for the frequency of Earth own oscillations caused by strong earthquakes (Haddon and Bullen, 1969; Zharkov and Trubitsin, 1980; Zharkov, 1983). Using the described technique, Bullen (1966, 1969), Zharkov et al. (1971), and Dzivonsky et al. (1975) generated a number of well-known models of the density distribution within Earth (see Fig. 2.12). For comparison, the same figure displays the frequency distributions we constructed based on the shock compression data for the Earth's model with a lherzolite mantle, iron oxide external and iron–nickel internal core, at the adiabatic temperature distribution in Earth depth, as well as the density distribution within the primordial, undifferentiated Earth (Naimark and Sorokhtin, 1977a,b, modified). Figure 2.13 and Table 2.1 also show the density distribution generated from our model.

Figure 2.13 shows that the density of the upper convecting (hot) mantle is 3.28 g/cm$^3$ on the surface and gradually increases with depth due to compression. Starting at the depth of 400 km, it increases faster and in a stepwise way. At about 900 km, the density gradient declines. After that the density increases monotonously to 5.6 g/cm$^3$ at the mantle base. As mentioned earlier, a drastic increase in the density gradient within the mantle transitional layer (layer C) is due to polymorphic transitions at those depths of the mantle matter into denser phases: the olivine, into the spinel phase; the pyroxene, into the ilmenite phase and further down, into the perovskite phase, and so on (Ringwood, 1981).

As opposed to this, there are no significant changes of the crystalline structure in the lower mantle as all oxides within that geosphere already have their atoms maximally densely packed, and the mantle matter compresses only due to the compression of the atoms proper.

At a depth of about 2900 km the Earth density jumps up almost by the factor of two, from 5.6 g/cm$^3$ at the mantle base to 9.9–10 g/cm$^3$ at the core surface. That is an indication of a drastic change in the Earth's matter chemical composition.

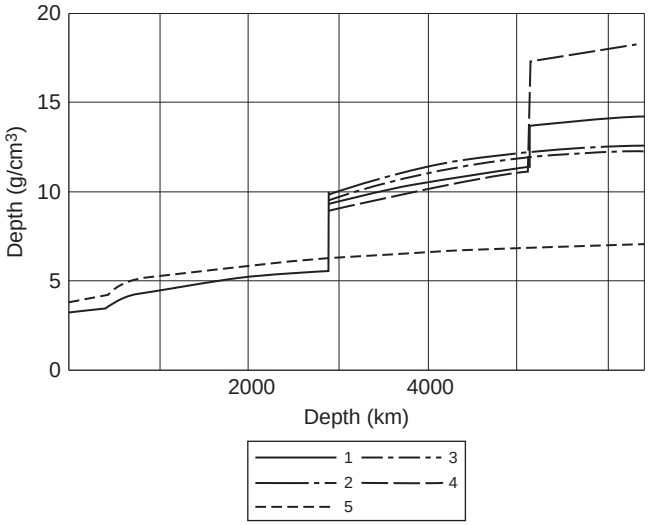


**FIGURE 2.12** Density distribution under various Earth models: 1, Neimark–Sorokhtin model (1977a); 2, Zharkov model "Earth-2" (Zharkov et al., 1971); 3, Bullen A1 model (1966); 4, Bullen A2 model (1966); and 5, Neimark–Sorokhtin primordial Earth model (1977a).

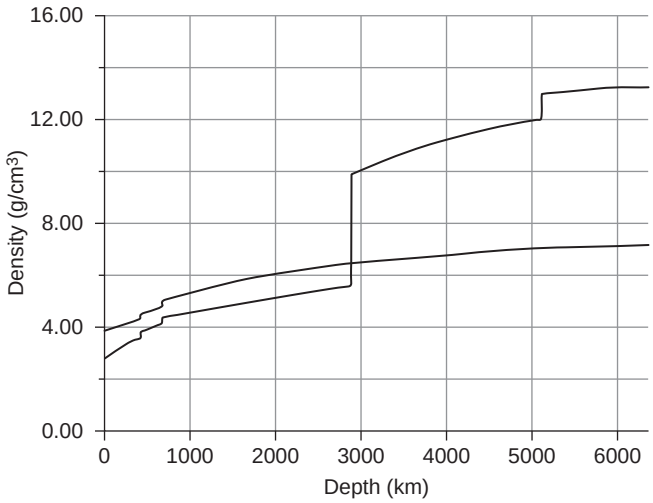


**FIGURE 2.13** Accepted density distribution within present-day and primordial Earth.

Within the core, the matter density again monotonously increases. Some models assume that another, although less-significant, density jump occurs in the layer F between the external and internal core. This jump also testifies to a change at that depth in the chemical composition of the core matter or its phase state.

And the last noticeable density jump must occur at a depth of about 5150 km. This jump manifests the transition from the external liquid shell of the core to its internal solid part.

Our estimate is that the core matter density on that boundary jumps from 11.92 to 13.7 g/cm$^3$ (i.e., by 15%) and reaches 14.19 g/cm$^3$ in Earth's center.

As already mentioned, knowing the assumed Earth's matter composition, it is possible to construct a density distribution model within Earth. Experimental data on the shock compression of major rock-forming oxides and metals may be used for that purpose. This technique allows for an independent evaluation of the matter density within Earth, and on the other hand, for a validity check of the assumptions made about the planet's chemical composition.

Besides, by selecting the composition of the present-day Earth according to seismic data and assigning the major patterns for its differentiation, this technique produces the density distribution within Earth at any stage of its evolution.

In particular, Fig. 2.13 shows the density distributions in the present-day and primordial (nondifferentiated) Earth for the lherzolite mantle composition and iron oxide composition of the core. Currently, the silicate, oxide, and metal density determination methodology at high pressures and temperatures based on shock compression of the matter is well developed and well published (Altshuler, 1965; Zharkov and Kalinin, 1968). The accuracy of density versus pressure and temperature function determination in the equation of state $\rho(p,T)$ based on shock compression is usually within 2–3%, which is quite acceptable for most geophysical problems.

There are many estimations of the mantle and core density for hypothetical mixes of various compositions (Altshuler and Sharipdzhanov, 1971a,b; Pankov and Kalinin, 1975; Kalinin and Sergeyeva, 1977). All these works, however, used a static (nonconvecting) mantle and temperature distribution model similar to the one by Reynolds and Summers (1969) artificially fit to the hypothesis of the external core iron composition. All such models assumed the temperature distribution at base of the mantle such as to provide for melting of the metallic iron within the entire volume of Earth's external core (close to 4000 K). As we saw, however, the external core is most likely composed of iron oxides with a much lower melting temperature. Besides, temperature of the convecting mantle should have a much lower adiabatic distribution (see Section 2.8). As a result of the artificial overestimation of the lower mantle temperature, the apparent density of this geospheres in such models was always undervalued. To compensate the mass deficiency, the authors of these models had to accept higher iron concentrations in the lower mantle, that is, just at the levels where the difference between the assumed and adiabatic temperatures reached its maximum value (about 1200 K).

The publication by Naimark and Sorokhtin (1977a) accounts for these pitfalls. The temperature distribution within the "sub-lithospheric" Earth was assumed strictly adiabatic because the drift of continents and oceanic plates undoubtedly indicates the existence of an intense and large-scale convection.

The value of the mantle temperature normalized for the surface was determined from maximum temperatures of basalt lavas and was assumed equal to 1280 °C ≈ 1550 K. The mantle composition was considered the same all over its thickness and was determined from the composition of the lherzolites in the oceanic rift zones (Table 3.1). For the external core, it was assumed $Fe_2O$, and for the internal, $Fe_{0.9}{\cdot}Ni_{0.1}$. In this book, it is additionally considered that phase transitions of the mantle matter into denser mineralogical associations occur at depths about 400 and 670 km. In calculating density distribution in Earth, it was assumed that its mass is $5.977 \times 10^{27}$ g, and its moment of inertia $I = 8.038 \times 10^{44}$ g·cm$^2$ The calculation results are included in Table 2.2 and shown in Figs. 2.9, 2.12, and 2.13.

**TABLE 2.2** Present-Day Earth: Density, Temperature, Pressure, and Gravity Acceleration Distribution[a]

| Depth (km) | Density ($g/cm^3$) | Temperature (K) | Pressure (kbar) | Gravity acceleration ($cm/s^2$) | Depth (km) | Density ($g/cm^3$) | Temperature (K) | Pressure (kbar) | Gravity acceleration ($cm/s^2$) |
|---|---|---|---|---|---|---|---|---|---|
| 0 | 2.85 | 288 | 0 | 981 | 2886 | 5.60 | 3130 | 1384 | 1067 |
| 200 | 3.30 | 1770 | 65.5 | 990 | 2886 | 9.92 | 3130 | 1384 | 1067 |
| 430 | 3.60 | 1940 | 138 | 997 | 3000 | 10.06 | 3310 | 1503 | 1041 |
| 430 | 3.82 | 2010 | 138 | 138 | 3400 | 10.60 | 3880 | 1909 | 945 |
| 600 | 4.09 | 2130 | 218.6 | 1000 | 3800 | 11.06 | 4400 | 2287 | 841 |
| 670 | 4.16 | 2170 | 247.2 | 1001 | 4200 | 11.43 | 4870 | 2628 | 732 |
| 670 | 4.37 | 2110 | 247.2 | 1001 | 4600 | 11.72 | 5280 | 2926 | 622 |
| 800 | 4.49 | 2170 | 305.7 | 1000 | 5000 | 11.97 | 5620 | 3175 | 517 |
| 1000 | 4.61 | 2260 | 397.7 | 996 | 5120 | 12.04 | 5710 | 3242 | 490 |
| 1200 | 4.72 | 2360 | 491.7 | 994 | 5120 | 13.00 | 5710 | 3242 | 490 |
| 1400 | 4.83 | 2450 | 587.8 | 993 | 5400 | 13.10 | 5890 | 3382 | 386 |
| 1600 | 4.94 | 2540 | 686 | 993 | 5800 | 13.23 | 6060 | 3518 | 227 |
| 1800 | 5.04 | 2640 | 786.3 | 995 | 6000 | 13.27 | 6110 | 3559 | 155 |
| 2200 | 5.25 | 2820 | 994.9 | 1006 | 6200 | 13.29 | 6140 | 3580 | 68 |
| 2600 | 5.45 | 3010 | 1216.2 | 1033 | 6371 | 13.29 | 6140 | 3583 | 0 |

[a] *The following major parameters were used in the calculations: Earth mass* $M = 5.9771 \times 10^{27}$ *g, dimensionless moment of inertia of a spherical Earth* $J = 0.33053$.

We compared a calculation of the lherzolite mantle density (Fig. 2.9), the iron oxide external and iron–nickel internal core (Fig. 2.12) with most common density distributions within Earth based on seismic data. It shows that a model of Earth chemical composition we accepted matches well with the commonly accepted density models of Earth structure. Thus, it may be concluded that our Earth composition model also well reflects the real situation within Earth.

There is one interesting result of the calculations: density of the oceanic lherzolites (exposed on the surface in transform faults of the oceanic rift zones) under high pressure and adiabatic temperature coincides to a high accuracy with the lower mantle matter density determined independently from seismic data. This coincidence occurs without any assumptions of the changes in lherzolite chemical composition with depth. This result is very important. It indicates the general similarity in the chemical composition of the mantle as a whole (both the upper and the lower).

This calculation result can only be explained by the existence of convective flows in Earth's mantle. These flows actively stir the entire mantle matter. Despite this, undoubtedly there are in the mantle local density nonuniformities of no more than $0.1-0.15\ \mathrm{g/cm^3}$. Moreover, these nonuniformities are the very reason for the convective flows in the mantle developed. These nonuniformities are constantly generated by the process of the mantle matter differentiation at the core surface and by the descent in the subduction zones of cold lithospheric plates into the depths of the hot mantle.

Another important consequence of the reviewed Earth's density model built from the given composition of its shells is that the Earth's external core may consist of the univalent iron-oxide $Fe_2O$ (or alloy Fe·FeO), and the internal core, of iron–nickel alloy $Fe_{0.9}{\cdot}Ni_{0.1}$. The core under this model has the following parameters: the mass $M_c = (1.94 \pm 0.01) \times 10^{27}$ g; the volume $V_c = 0.180 \times 10^{27}\ \mathrm{cm^3}$; pressure at the core's surface $p_c = 1.384$ Mbar; pressure in Earth's center $p_0 = 3.614$ Mbar; average core density $\rho_c = 10.6\ \mathrm{g/cm^3}$. Pressure and gravity acceleration distribution within Earth are displayed in Fig. 2.14.

## 2.8 TEMPERATURE DISTRIBUTION WITHIN EARTH

Earth's temperature regime is dependent on the Earth's matter composition and geodynamic processes deep within Earth. For instance, if mantle's viscosity is exceptionally high, and there are no convection movements in it, then the temperature distribution within this geospheres may be superadiabatic. If, however, the mantle is engulfed in convective movements, then average temperature distribution within it must be close to the adiabatic law. As the external Earth core is effectively liquid, temperature distribution within it cannot be but adiabatic or, if the core is noticeably heated at the mantle base (i.e., from above), it will be below adiabatic.

The continental drift and continuous renewal of the ocean floor are doubtless an indication of the convection flows in the mantle matter. Numerous studies were devoted to this issue. For instance, density calculations of the upper and lower mantle based on shock compression of silicates show that at certain pressure and at the adiabatic temperature within these geospheres, the density distribution as calculated from seismic data are well approximated by the density of oceanic lherzolites (Naimark and Sorokhtin, 1977a).

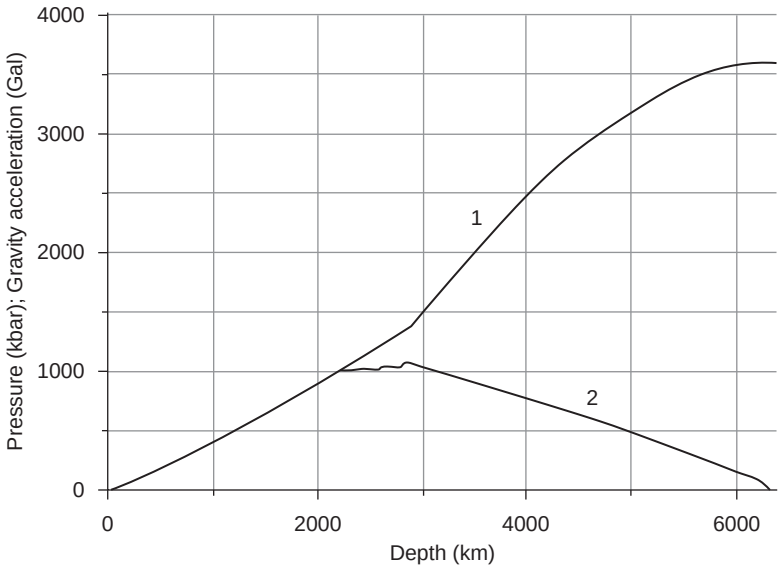


**FIGURE 2.14** Pressure (1) and gravity acceleration (2) distribution within Earth.

This result indicates approximate uniformity in the chemical composition of the entire mantle. It provides an indirect evidence of a large-scale convection within the mantle which continuously agitates its matter. It is also a testimony to adiabatic temperature distribution in the mantle.

Another clear evidence of a single system of convection flows in the mantle, the system encompassing both the upper and lower mantle, is topographic features on the core surface identified with the help of seismic tomography (Morelli and Dziewonski, 1987). As it turned out, there is good correlation between these topographic features and the spreading and subduction zones on Earth's surface. For instance, there are depressions on the core surface under the subduction zones in South and Central America and along the entire western "subductional" framework of the Pacific Ocean, that is, under clearly descending flows in the mantle.

On the contrary, underneath the Northern and Central Atlantic Ocean, in the central parts of the Indian and Pacific oceans (i.e., under the main spreading zones manifesting the ascending mantle matter) there are uplifts of the core surface.

Mathematical modeling of the mantle convection (Monin et al., 1987a,b; Trubitsin et al., 1994; Trubitsin and Rykov, 2000) also testifies to the existence in the Earth's shell of the large-scale convection encompassing both the upper and lower mantle. Lobkovsky et al. conducted recently a study taking into consideration the existence of phase transitions in the mantle which obstruct the development of a "smooth" convection. The study showed that the general mantle convection is maintained but becomes pulsating (Lobkovsky and Kotelkin, 2000, Lobkovsky et al., 2004). Therefore, in this case as well, adiabatic temperature distribution in the mantle is preserved.

The quoted publications prohibit us from accepting a mantle model with approximately uniform chemical composition corresponding to the mid-oceanic ridge lherzolites (Dmitriyev, 1973) or Ringwood's (1981) pyrolite, and the temperature distribution close to adiabatic.

Adiabatic temperature distribution is described by a relatively simple equation

$$\frac{dT}{dr} = -g\alpha\frac{T}{c_p} \tag{2.12}$$

where $g$ is gravity acceleration, $\alpha$ is matter's volume expansion factor, $c_p$ is per-unit mass heat capacity at constant pressure, and $r$ is the current value of the polar distance.

A fact of liquid state of the external Earth's core suggests that rather intense convective flows may be taking place there. And usually, the origin of Earth's magnetic field is associated with this phenomenon. It is obvious that temperatures within the external core must be above the melting temperature of its anticipated composition and close to the adiabatic distribution. However, the geomagnetic field in the Earth core may also be generated by surficial flows of a disintegrated mantle matter which close the convective flows in the mantle (Sorokhtin and Ushakov, 1993). In this case, it may be that the core is heated up from its surface, and the temperature distribution within it may be below the adiabatic one. Nevertheless, we will assume for our model adiabatic temperature distribution in the Earth's core. As mentioned in Section 2.6, the most probable hypothesis is that of the external core composed of $Fe_2O$ or its equivalent eutectic alloy $Fe_{0.44}{\cdot}FeO_{0.56}$. The external/internal core transition zone (layer F) comprises FeS and the central core is composed of the $Fe_{0.9}{\cdot}Ni_{0.1}$ alloy.

Studies of silicate, iron, and Fe–FeO–FeS melting regimes at high pressure (Boehler, 1993, 1996; Zerr and Boehler, 1993), in static experiments, in diamond cells, and with the samples heated by laser reached the enstatite melting temperature of about 5000 ± 200 K at pressure of close to 625 kbar. Enstatite is the major mineral in the external mantle in the perovskite structure. The enstatite–perovskite melting temperature at the core boundary is estimated by various researchers to be between 7000 and 8500 K. Boehler suggested that the mantle matter melting temperature must be within a similar range.

Boehler's results for phase transitions in iron at high pressures of up to 2 Mbar (Boehler, 1993) are shown in the states of iron diagram (Fig. 2.15). Extrapolation of the experimental data to high pressures was performed under Clausius–Clapeyron law. The law parameters were selected by the criterion of the theoretical curve best fit with the experimental data for ε-Fe melting:

$$\frac{dT_л}{dp} = \frac{TV}{q_л} \tag{2.13}$$

or

$$T_л = T_0 \exp\left\{\frac{pV}{q_л}\right\}, \tag{2.13′}$$

where $T_{melt}$ is ε-Fe melting temperature at pressure $p$; $T_0$ is melting temperature of this iron normalized to the value of $p=0$; $\Delta V$ is change in the specific volume at melting of iron; $q_{пл}$ is heat of melting. The best fit between the theoretical curve and the experimental data on ε-Fe melting was obtained at $T_0 = 2080$ K and $\Delta V/q_{melt} \approx 0.31$ Mbar$^{-1}$.

Melting temperature of the eutectic alloy $Fe_x{\cdot}FeO_{1-x}$ at low and moderate pressure of 300 and 600 kbar was assumed from Ohtani et al. (1984) and Ringwood and Hibberson (1990), at pressure of up to 1.4 Mbar, from Boehler, and at higher pressure, from Clausius–Clapeyron equation coordinated with Boehler's experiments (Fig. 2.15). The experimental data confirm that at low and moderate pressure (approximately up to 600 kbar) the eutectic

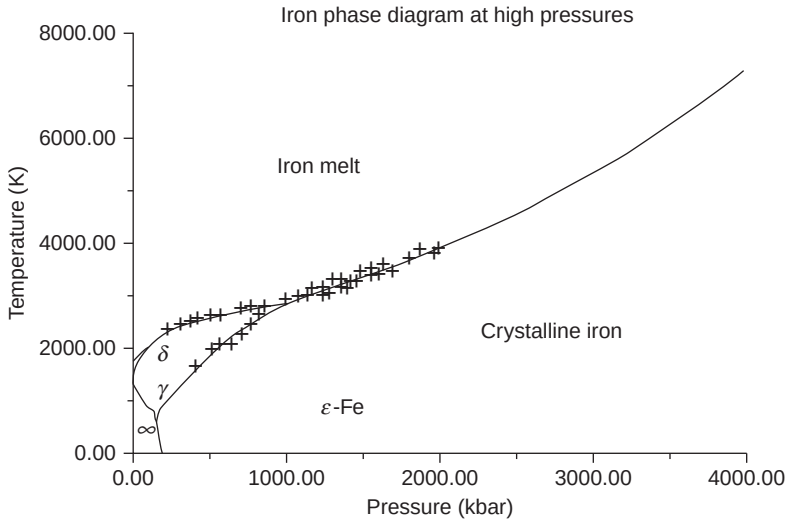


**FIGURE 2.15** States-of-iron phase diagram at high pressure. Crosses indicate experimental data (Boehler, 1993), curve extrapolation to higher pressure is done under the Clausius–Clapeyron law. Note that at pressures $p > 1$ Mbar the ε-iron melting curve gradient significantly increases.

temperature depression of $Fe_x{\cdot}FeO_{1-x}$ alloys melting is quite noticeable, in excess of 100–200 °C. At greater pressure, however, as Boehler showed, this depression declines to the experiment's accuracy limits. That is why it is accepted that eutectic depression of $Fe_x{\cdot}FeO_{1-x}$ system melting at very high pressure plays only insignificant role in Earth's core thermodynamics.

Adiabatic temperature distribution within the mantle and core is usually calculated from the classical equation (2.11) or from temperature versus pressure correlation

$$\left(\frac{\partial T}{\partial p}\right)_S = \frac{\alpha}{c_p} \cdot \frac{T}{\rho}, \tag{2.14}$$

where $S$ is the constant entropy, $\alpha$ is temperature volume expansion factor, $c_p$ is heat capacity of the matter at constant pressure, and $\rho$ is matter density. Then, the adiabatic temperature distribution is found from a relatively simple equation

$$T_S = T_0 + \sum_i T_i + \int_0^p \frac{\alpha}{c_p} \cdot \frac{T}{\rho} \cdot \mathrm{d}p, \tag{2.15}$$

where $T_0$ is mantle temperature normalized for the surface (as determined from maximum temperature of basalt magmas erupted on Earth's surface), $\Delta T_i$ is temperature difference in the convecting mantle on the phase transition boundaries between the mantle matter mineral associations (occurring, e.g., at depths about 100, 420, and 670 km) (Fig. 2.16).

Obviously, temperature jumps at the first kind phase transition boundaries occur in the mantle only when its matter, in the convection mass exchange process, crosses such boundary (in a static mantle any temperature jumps would be rapidly smoothed out due to the conventional heat conductivity). The temperature jumps in a matter of mass $m$ crossing

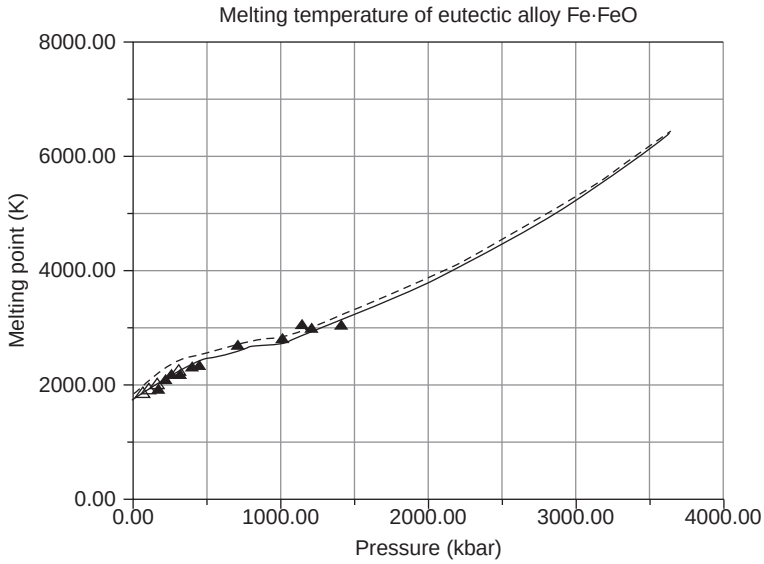


**FIGURE 2.16** Melting temperature of eutectic alloy $Fe_x{\cdot}FeO_{1-x}$ versus pressure. Hollow triangles are data by Ohtani, Ringwood, Hibberson (1984), filled-up triangles: to 500 kbar, data by Ringwood and Hibberson (1990); 700–1400 kbar, data by Boehler (1993), farter up, extrapolation from the Clausius–Clapeyron law; dashed line is the iron melting temperature from Fig. 2.15.

the phase boundary arises due to the release or absorption at such boundaries of the phase transition heat $q_{\text{phase tran}}$. The phase transition heat may be written up as $q_{\text{phase tran}} = \Delta T m c_{\text{p}}$, where $\Delta T$ is the temperature change caused by a phase transition (e.g., the transition olivine–spinel phase at a depth of about 400 km or by a transition of enstatite into a perovskite phase and by disintegration of other silicates into simple oxides at about 670 km. If the phase transition pressure does not change with temperature, and $\mathrm{d}p/\mathrm{d}T \neq 0$, then, from a generalized Clausuis–Clapeyron law,

$$T = \frac{VT}{mc_{\text{p}}}\frac{\mathrm{d}p}{\mathrm{d}T}. \tag{2.16}$$

Depending on the value of the difference $\Delta V$ and on the sign of the $\mathrm{d}p/\mathrm{d}T$ derivative, the temperature difference $\Delta T$ may be either positive or negative. Any transition in the mantle from the state 1 with lower pressure to the state 2 with higher pressure is always accompanied by the matter density increase so for the mantle usually $\Delta V = V_1 - V_2 > 0$. If the transition is exothermal (i.e., associated with a release of the internal energy), the derivative $\mathrm{d}p/\mathrm{d}T > 0$. Conversely, if the transition is endothermal and is accompanied by absorption of the energy, $\mathrm{d}p/\mathrm{d}T < 0$.

Experiments by Ito and Takahashi (1989), Kuskov and Fabrichnaya (1990), Kuskov and Panferov (1991a,b) indicated that the olivine transition to the spinel modification at 420 km is an exothermal transition for which $\mathrm{d}p/\mathrm{d}T > 0$. This is a single boundary as observed on seismic but it actually consists of two closely positioned phase boundaries with different mineral associations. As opposed to this, the silicate disintegration into simple oxides at about 670 km is endothermal, with $\mathrm{d}p/\mathrm{d}T < 0$.

Change in the volume and mass of the mantle matter crossing a phase transition boundary may be expressed through density. In this case, the total temperature change at the *i*th transition will be

$$T_i = \frac{T_1}{c_p}\left(\frac{1}{\rho_1} - \frac{1}{\rho_2}\right)\frac{dp}{dT} \tag{2.17}$$

From Kuskov and Panferov (1991b), for pyrolites at high temperature and at a depth of 400 km, $\rho_1 = 3.5\ g/cm^3$ and $\rho_2 = 3.64\ g/cm^3$, at a depth of 470 km, $\rho_1 = 3.7\ g/cm^3$ and $\rho_2 = 3.85\ g/cm^3$ at the average temperature $T_{430} = 1970$ K (this publication). From Kuskov and Panferov (1991a), at 670 km $\rho_1 = 4.01\ g/cm^3$ and $\rho_2 = 4.32\ g/cm^3$ at $T_1 = 2140$ K (this publication).

At the same depths (400 and 470 km), the pressure and temperature derivatives are, respectively: $dp/dT = 1.9$ MPa/K $= 1.9 \times 10^7$ dine/cm$^2$ K, $dp/dT = 1.3$ MPa/K $= 1.3 \times 10^7$ dine/cm$^2$ K, and at 670 km $dp/dT = -1.7$ MPa/K $= -1.7 \times 10^7$ dine/cm$^2$ K.

Inserting these data and the average mantle heat capacity value of $1.3 \times 10^7$ erg/g K into Eq. (2.17), we come up with: $\Delta T_{400} \approx 31\ ^\circ$C; $\Delta T_{470} \approx 20\ ^\circ$C, or in total $\Delta T_{430} \approx 51\ ^\circ$C, and $\Delta T_{670} \approx -50\ ^\circ$C. Ito and Takahashi (1989) found that $(dp/dT)_{420} \approx +2.08 \cdot 10^7$ and $(dp/dT)_{670} \approx -2.78 \times 10^7$ dine/cm$^2$ K, then $\Delta T_{420} \approx 80\ ^\circ$C and $\Delta T_{670} \approx -81\ ^\circ$C.

We assumed the intermediate option ($\Delta T_{430} \approx +70\ ^\circ$C; $\Delta T_{670} \approx -60\ ^\circ$C) although there is no major temperature distribution difference between these two source options (because in both cases $(dp/dT)_{420} + (dp/dT)_{670} \approx 0$). Besides, a small temperature jump, $\Delta T_{100} \approx 10\ ^\circ$C, as we calculated, must also occur at the transition boundary pyroxene lherzolite–garnet lherzolite at depths about 100 km.

Based on recent studies of possible compositions in mantle's mineralogical associations, some other phase transitions must exist deep in this geospheres (Pushcharovsky and Pushcharovsky, 1999). Seismic indicates, however, that these transitions are substantially less drastic than those at 420 and 670 km. Besides, we do not know yet how the physical properties of the mantle matter change at such transition boundaries. For this reason, as a first approximation, we consider that the mantle properties between major boundaries at 100, 420, and 670 km change gradually.

An important issue for the temperature distribution within Earth is the correct determination of the mantle temperature $T_0$ normalized for the surface. This parameter in Eq. (2.15) is determined taking into account the maximum temperatures of basaltic magmas erupting on the ocean islands and in the rift zones. Direct pyrometer measurement of liquid lava temperature at the Kilauea volcano (Hawaii) is within the range of 1100–1200 °C (Macdonald et al., 1990).

In the shield volcanoes, however, some cooling-down and differentiation of the primary magma occurs in the intermediate foci. However, the lava temperature at fissure eruptions occurring directly on the oceanic floor is a more realistic representation of the astenospheric matter melting temperature. It was concluded from the Fe/Mg ratios in the lavas at the base of an underwater Loihi volcano (south of the Hawaii Island) that the primary melt temperature at the magma origination depth (around 60−80 km) could reach 1456−1517 °C, which is higher by 250−300 °C than the lava temperature in Hawaiian volcano craters (Matveyenkov and Sorokhtin, 1998). Accounting for the adiabatic correction for the basalt melting-out and

limited accuracy of petrologic temperature determinations, we assumed that the basalt eruption temperature is approximately 1330 °C, in which case $T_0 \approx 1330$ K.

It was usually assumed from the traditional temperature distribution in Earth that the temperature at the mantle boundary with the core was 2600–2800 K. To reconcile these distributions with of iron and iron compounds melting results, Boehler (1993) had to assume the existence in the transitional layer at the core surface of a temperature jump on the order of 1300 K. Such an assumption, however, is not substantiated and contradictory with the basics of hydrodynamics: over billions of years of Earth's existence and presence of intense convection flows in the mantle, all excessive heat would have long ago been brought out, and the very external core would have crystallized. Besides, models of Earth evolution based on a gradual growth of the core due to the differentiation of the mantle matter (Monin and Sorokhtin, 1982b; Sorokhtin and Ushakov, 1991), heating of the core must precede beginning from its surface. For this reason, the core temperature distribution should not exceed the adiabatic one, and of course there cannot be any temperature jumps within it. It is quite likely that for the same reasons there may not be convection flows within the external, liquid core, and Earth's magnetic field is generated by surface flows only, as already mentioned above. And the suggestion that large sources of the radiogenic heat exist within the core is in complete contradiction with the geochemical data: all most common radioactive elements ($^{40}$K, U, and Th) are typically lithophilic and concentrate mostly in the Earth's crust (Gast, 1972). The same is supported by chemical analyses of meteorites: iron meteorites are practically sterile of these elements (Dodd, 1986).

Density $\rho$ in Eq. (2.14) is determined rather reliably in one of the seismic data-based Earth's density model such as Bullen (1978), Zharkov (1983), Zharkov and Trubitsin (1980) or is calculated using the conventional technique. Most uncertain terms in Eq. (2.14) are heat expansion factor $\alpha$ and Earth matter heat capacity $c_p$. All existing determinations of these parameters and their ratios for deep Earth are either hypothetical or extrapolated from the moderate pressure areas into the high pressure. For instance, heat expansion or heat capacity factors for iron determined for the α- or γ-iron are mechanically transferred onto the $P$–$T$ conditions of the Earth core. However, iron is a transitional metal with completely filled external electron 4s shells and a partially filled internal 3d shell. Under the core conditions, affected by high pressures one of the external s-electrons of iron switches onto the internal d-shells. The result is an electron-phase transition $3d^6 4s^2 \rightarrow 3d^7 4s^1$ (Sorokhtin, 1972). Thus, it is reasonable to expect that the phase of ε-iron existing at $p > 1$ Mbar has a different configuration of the external electron shells: for the α, β, δ, and γ-Fe it is $3d^6 4s^2$, whereas for the ε-Fe it is $3d^7 4s^1$. Therefore, the ε-Fe should have different, compared to the other forms of iron, physical parameters. Similarly, the decay of most chemical compounds into simple oxides occurs in the lower mantle (Pushcharovsky and Pushcharovsky, 1999) which may cause significant alterations in thermophysical properties of the matter, in particular, the $\alpha$ and $c_p$ parameters.

As the $\alpha/c_p$ ratios are uncertain, we relied in our constructions on the accepted values of this ratio only to a depth of 670 km (after Zharkov and Trubitsin, 1980). For great depths, the $\alpha/c_p$ values were selected so that the theoretical temperature distribution in the lower mantle and the core constructed from Eq. (2.15) would match the best way possible experimental data on the melting of iron and eutectic alloys $Fe_x{\cdot}FeO_{1-x}$.

We assumed as a second condition the requirement of the temperature distribution continuity at the mantle/core boundary. The results are displayed in Table 2.3 and Fig. 2.17.

**TABLE 2.3** Temperature Distribution in Deep Earth

| Depth (km) | Earth's density ($g/cm^3$) | Earth temperature (K) | Fe melting temperature (K) | Fe·FeO melting temperature (K) | Depth (km) | Earth temperature (K) | Fe melting temperature (K) | Fe·FeO melting temperature (K) | Earth temperature (K) |
|---|---|---|---|---|---|---|---|---|---|
| 0 | 2.85 | 288 | 1840 | 1750 | 2886 | 5.60 | 3130 | 3200 | 3100 |
| 200 | 3.30 | 1770 | 2000 | 1860 | 2886 | 9.92 | 3130 | 3200 | 3100 |
| 430 | 3.60 | 1940 | 2170 | 1960 | 3000 | 10.06 | 3310 | 3320 | 3220 |
| 430 | 3.82 | 2010 | 2170 | 1960 | 3400 | 10.60 | 3880 | 3760 | 3670 |
| 600 | 4.09 | 2130 | 2320 | 2110 | 3800 | 11.06 | 4400 | 4230 | 4140 |
| 670 | 4.16 | 2170 | 2350 | 2140 | 4200 | 11.43 | 4870 | 4710 | 4620 |
| 670 | 4.37 | 2110 | 2350 | 2140 | 4600 | 11.72 | 5280 | 5160 | 5090 |
| 800 | 4.49 | 2170 | 2420 | 2240 | 5000 | 11.97 | 5620 | 5590 | 5520 |
| 1000 | 4.61 | 2260 | 2510 | 2350 | 5120 | 12.04 | 5710 | 5710 | 5650 |
| 1200 | 4.72 | 2360 | 2590 | 2430 | 5120 | 13.00 | 5710 | 5710 | 5650 |
| 1400 | 4.83 | 2450 | 2660 | 2530 | 5400 | 13.10 | 5890 | 6000 | 5940 |
| 1600 | 4.94 | 2540 | 2710 | 2580 | 5800 | 13.23 | 6060 | 6280 | 6230 |
| 1800 | 5.04 | 2640 | 2770 | 2650 | 6000 | 13.27 | 6110 | 6370 | 6320 |
| 2200 | 5.25 | 2820 | 2840 | 2750 | 6200 | 13.29 | 6140 | 6410 | 6360 |
| 2600 | 5.45 | 3010 | 3040 | 2940 | 6371 | 13.29 | 6140 | 6410 | 6360 |

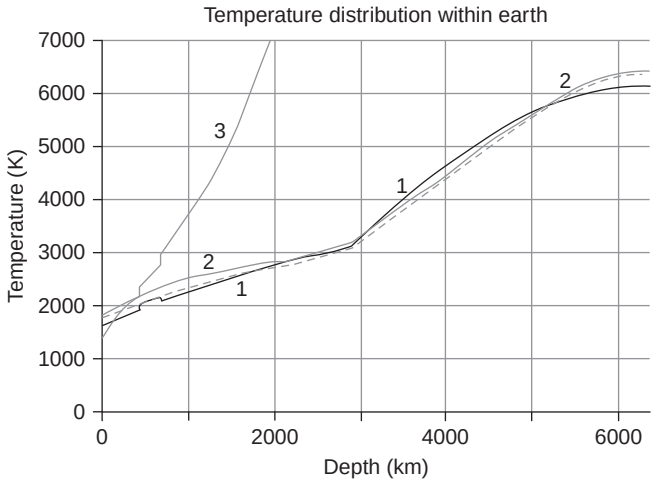


**FIGURE 2.17** Temperature distribution within the present-day Earth: 1, Earth's adiabatic geotherm coordinated with iron and Fe–O–S system melting experiments; 2, iron melting temperature (below 2 Mbar, static experiments by Boehler, 1993, farther up, extrapolation of this temperature under the Clausius–Clapeyron law); dashed curve is melting temperature of the eutectic alloy Fe·FeO (below 300 kbar, experimental data by Ohtani and Ringwood, 1984, below 1400 kbar, after Boehler, 1993; farther up, extrapolation under the Clausius–Clapeyron law accounting for a diminished eutectic depression Fe–FeO in the high pressure domain); 3, silicate melting temperature (at $p \geq 240$ kbar, the enstatite (Mg,Fe)$SiO_3$ melting temperature: below 625 kbar, from experiments by Zerr and Boehler (1993), farther up, extrapolation under the Clausius–Clapeyron law.

It so happened that in our model the $\alpha/c_p$ ratio for the lower mantle changes from $2.2 \times 10^{-12}$ g/erg at a depth of 670 km to $1.33 \times 10^{-12}$ g/erg at its base. These differences for the core are about twice that: the $\alpha/c_p$ ratios range between $4.7 \times 10^{-12}$ and $2.6 \times 10^{-12}$ g/erg rather than $2.3 \times 10^{-12}$ and $1.2 \times 10^{-12}$ g/erg after the standard models (Zharkov and Trubitsin, 1980). The explanation is in that the ε-Fe structure we assumed (which is characteristic of the core) significantly differs from the usual iron's electron configuration at lower pressure (which we already mentioned above).

As Fig. 2.17 shows, it is possible to directly reconcile the model of adiabatic temperature distribution in Earth with the current data about iron melting in the system Fe–FeO–FeS. The derived distribution is only slightly more high temperature than is usually accepted and closely corresponds with Zharkov's (1983) estimates. For instance, in accordance with the new determinations temperature at the mantle/core boundary reaches 3130 K rather than conventional determinations of about 2800 K.

And as was expected, there is no disruption in the temperature curve at this depth. Nevertheless, adiabatic temperature through the entire depth of the external core is above the melting temperature of the Fe–FeO–FeS system, which is in a total concert with the liquid state of the external core. The calculated temperature on the surface of the internal core is equal to the iron solidus temperature and reaches nearly 5710 K. This is close with the determinations of this temperature from iron shock compression (Broun and McQueen, 1986) and Zharkov's (1983) estimates. And temperature of the internal (solid) core, as it should be, is everywhere below the iron melting temperature.

The temperature estimate in the Earth center is 6140 K, whereas the iron melting temperature at the same pressure is approximately 6400 K. It is possible, however, that at pressure of about 3.3 Mbar, that is, near the external/internal core boundary, iron has a second electron-phase transition $3d^7 4s^1 \rightarrow 3d^8 4s^0$ after which its chemical properties change again

and become similar to the properties of nickel allowing for a complete miscibility with it (Sorokhtin, 1972).

Adiabatic temperature distribution generated in consideration of experimental data explains well the liquid state of the external core and solid state of the internal core. The geotherm in the mantle is positioned above expected at this level melting temperature of the core matter. Therefore, the proposed temperature model of Earth is also in good concert with the functioning conditions of the suggested barodiffusion mechanism of the mantle matter differentiation (due to this mechanism, the release of the gravity energy and growth of the core may currently occur without melting the silicates; Monin and Sorokhtin, 1981).

The quoted temperature calculations are appropriate only for a convecting mantle. Earth surface is covered by a cold lithospheric shell which actually represents a heat boundary layer whose temperature distribution drastically differs from the adiabatic law. The temperature distribution in Earth lithospheric shell is determined from the heat-transfer equation. In a single-dimension approximation, for a model of the horizontally laminated medium it is:

$$\rho c_p \frac{\partial T}{\partial t} = \frac{\partial}{\partial z}\left(\lambda \frac{\partial T}{\partial z}\right) + \Theta, \tag{2.18}$$

where $T(z,t)$ is medium temperature, $\rho$ is medium density, $c_p$ is matter heat capacity under the constant volume, $\lambda$ is heat conductivity, $\Theta$ is bulk density of the radiogenic heat sources within the medium, $t$ is time, and $z$ is vertical coordinate directed from Earth surface down.

The mantle matter melting temperature is found experimentally by way of melting the lherzolites (peridotites) under elevated pressure (Green and Ringwood, 1967a,b; Ringwood, 1975; Takahashi, 1986; Litvin, 1991). Thus, the mantle matter melting start (solidus) curve, at least to pressures of 70–80 kbar or depths of 200–250 km, may be plotted with a reasonable certainty.

Figure 2.18 displays Eq. (2.18) solutions for different ages of lithospheric plates, and a geotherm of an old (Archaean) continental plate in comparison with the generalized curve of the mantle matter solidus temperature generated with the data from Takahasi, Ringwood, and Litwin. Temperature distribution in the hot mantle was determined from Eqs. (2.13) and (2.14) on condition that the surface-normalized mantle temperature is 1330 °C.

As the graphs show, adiabatic temperature of the present-day mantle intersects with the mantle matter solidus temperature at depths about 85–100 km. In particular, a very important geological conclusion follows from that: nowhere deeper than 85–100 km, that is, deeper than the eclogite transformation, can melt-out and exist the mantle (basalt) melts in the juvenile mantle (in Fig. 2.18 the mantle melt existence area is shown in dotted shading).

For this reason, only the oceanic lithosphere can be represented as a relatively simple physical model of a rigid fully crystalline plate overlying a partially melted mantle matter. Such model is in many respects analogous with the ice floating in a frosty day on the surface of a freezing lake. The difference is that the ice is always lighter than the water, whereas cold lithospheric plates can be heavier than hot and partially melted mantle matter. This, in particular, explains why the oceanic plates live for a relatively short time compared with the “longevity” of lighter continental plates whose average density is much lower than the density of the convecting mantle.

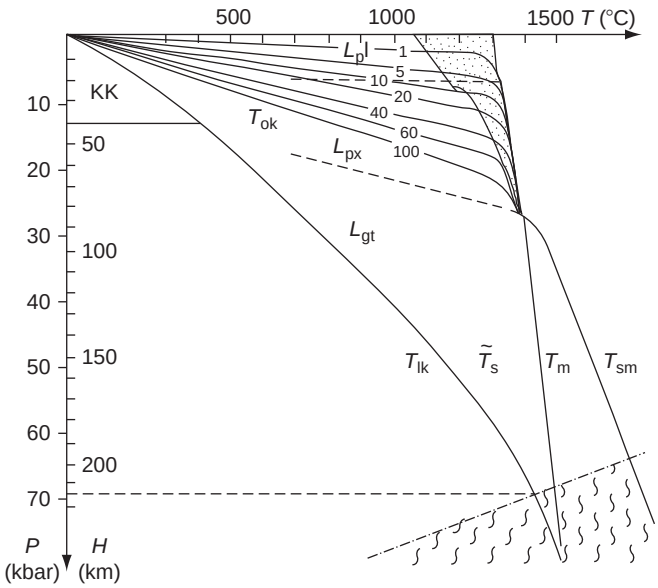


**FIGURE 2.18** Temperature distribution in the upper mantle and position of lithospheric plate geotherms versus their age (numbers in geotherms are the lithospheric plate age, MMY). KK is the continental crust, $T_m$ is the upper mantle adiabatic temperature, $T_{sm}$ is the temperature of mantle matter solidus, $T_{lk}$ is the geotherm ao ancient (Archaean) continental lithospheric plates. Zones of stable lherzolites: $L_{pl}$, plagioclase lherzolites; $L_{px}$, pyroxene; and $L_{gt}$, garnet. The dotted shading is the existence area in the mantle of basalt composition juvenile melts, the wavy shading is the area of a possible existence of elastic deformations, and dot–dash line is the mantle matter phase transition boundary from the rigid to the elastic state.

It is much more difficult to demonstrably determine the transition nature of the continental lithosphere into the underlying convecting mantle. The reason is that the continental geotherm asymptotically approaches the mantle temperature in that mantle area where any partial melting of the mantle matter is totally excluded (because at these depths the mantle temperature is below the mantle matter melting temperature by 200–300 °C).

Therefore, the position of the lithosphere's base underneath the thick (up to 250 km) continental plates is determined not by the geotherm of the start of mantle matter melting but by pressure and temperature of its transition from effectively rigid to effectively liquid (plastic) state. The physical nature of such transition can probably be associated with disintegration of the mantle matter. In this process, for instance, within the polycrystalline mantle matter intercrystalline connections are disrupted under high pressure and temperature with the preservation of the crystalline structure of mineral grains proper. As a result of such disintegration the rigid and firm mantle matter as if falls apart into small grains and becomes a "friable body" which behaves like a high-viscosity plastic body. As mentioned earlier, the temperature gradient at the transition boundary in the mantle matter from the rigid to the plastic state is negative, same as it is at a depth of 670 km.

## 2.9 VISCOSITY OF EARTH'S MANTLE MATTER

In order to understand correctly the processes occurring within the mantle, it is insufficient to know its composition and density. Also, important are its rheologic (viscoplastic) properties. The fact that the shape of Earth (the geoid) with a good approximation corresponds to an equilibrium revolution ellipsoid of a liquid body is an unquestionable indication on the effectively liquid state of the mantle.

Indeed, the difference between the geoid and the revolution ellipsoid is no greater than $\pm 100$ m (Fig. 2.1), whereas the ellipsoid's equatorial bump reaches 21.38 km. On the other hand, seismic S-waves with periods of a few minutes run through the mantle. That is an indication of its effective rigidity with respect to short-time mechanical actions.

These data may be conjugated only on condition that the mantle matter behaves similar to a hard bitumen, that is, very high-viscosity liquid. Under a short-term stress, such liquids have the properties pertaining to elastic and even brittle bodies. But under a long action, they behave like a highly viscous liquid.

As is known, some areas were recently (about 12,000 years ago) relieved of the glacier load. These areas include, for instance, the Baltic and Canadian shields. These areas were in a state of upheaval the speed of which enables an estimate of a rather high viscosity of the mantle matter under the continents. It is $\eta_m > 10^{21}$ poise, and most likely is within the $3 \times 10^{21}$–$2 \times 10^{22}$ poise range (Heiskanen and Vening Meinesz, 1958; McConnel, 1965; Ushakov, 1968; Ushakov and Krass, 1972).

Theoretical determinations of the lower mantle viscosity based on the velocity of the apparent pole drift produce values on the order of $6 \times 10^{23}$–$5 \times 10^{24}$ poise (Goldreich and Toomre, 1969; Sorokhtin, 1979). In the astenosphere underneath the oceanic lithospheric plates, the mantle matter viscosity probably declines to $10^{19}$–$10^{20}$ poise.

The quoted deflection value of the geoid form from the equilibrium shape of a liquid body revolution ellipsoid is approximately $\pm 100$ m the characteristic thickness of the mantle is approximately 3000 km and the likely average velocity of the convection flows in the mantle is approximately 10 cm/year. Based on these data, it is possible to estimate average viscosity of the mantle proper. It turns out to be approximately $\bar{\eta} \approx 3 \times 10^{22}$ poise. Ranelli and Fischer (1984) who assumed the adiabatic temperature distribution in the mantle estimated the viscosity of this geospheres in the range of $10^{20}$–$5 \times 10^{20}$ poise in the astenosphere, and up to $6 \times 10^{23}$ poise in the lower mantle at a depth of about 2700 km. (To compare: the water viscosity at room temperature is $10^{-2}$ poise; glycerin, 7 poise; basalt melt viscosity, depending on the temperature, $10^2$–$10^4$ poise; asphalt, $10^{10}$–$10^{12}$ poise; glass at the annealing temperature, $\sim 10^{13}$ poise; copper at 200 °C, $\sim 10^{18}$ poise; steel at 450 °C, about $10^{18} - 10^{20}$ poise).

The type of change in the mantle rheological properties is demonstrably seen in the behavior of the so-called quality factor $Q_\mu$, which defines the seismic wave and Earth's own oscillations decay at different depths in the mantle. This factor is in the inverse proportion to the dissipative function and is determined from the following equation:

$$Q_\mu^{-1} = \frac{E_\omega}{2\pi E_\omega}, \tag{2.19}$$

where $E_\omega$ is the elastic deformation energy of the oscillating process with the frequency $\omega$, $\Delta E_\omega$ is the energy of deformations dissipated within the medium over a single oscillation cycle. For this reason, the mechanical quality factor describes a degree of the real matter approach to the ideally elastic body. The higher the $Q_\mu$, the closer is the matter in its properties to the ideally elastic body. And conversely, the lower the $Q_\mu$ factor, the closer it is in its properties to the effectively liquid bodies. At that, the decline in the quality factor corresponds to the decrease in the effective viscosity of such matter.

For mechanical actions, whose duration is much longer than the characteristic heat oscillation periods of the atoms in a crystalline grid of the matter, the dissipative function $Q_\mu^{-1}$ is practically independent of the frequency. For this reason, seismic wave decay data and Earth's own oscillations (such as from strong earthquakes) as well as Earth's tidal deformations may be used for the $Q_\mu$ determination.

Based on all these experimental data about the decay of elastic oscillations within Earth, it was possible to construct a number of the factor's distribution models in the mantle. Two of such models are displayed in Fig. 2.19.

As the graphs show, the maximum values of the mantle quality factor $Q_\mu \approx 500$ is observed at depths about 1800–2500 km. In the astenosphere and at the base of the lower mantle, the quality factor declines to the values of about 100 (Zharkov et al., 1974). An expectation is that in the direct vicinity of the core surface the mantle matter mechanical quality declines even greater.

It is important that not only the quality factor $Q_\mu$ but also propagation velocity gradients of P-waves and especially S-waves decline in the lower mantle's lower layer (usually indicated as D″) (Bullen, 1978). Moreover, analyzing dynamic features of the seismic waves reflected by the Earth's core surface it was possible to identify a thin transitional layer, about 20-km thick, between the mantle and the core. We called it the Berzon layer. Within the lower portion of this layer, the S-wave velocity declines with depth from 7.3 km/s practically to 0 (Berzon et al., 1968; Berzon and Pasechnik, 1972). This is a very important result. It shows that rigidity modulus rapidly declines with depth within a thin transitional layer at the base of the lower mantle.

Viscosity distribution in the mantle should have similar nature of change. The partially melted mantle matter viscosity in the upper mantle astenosphere under the lithospheric plates, at a depth of 85–100 km, should not exceed $10^{19}$–$10^{20}$ poise. At depths of 250–300 km, under the continental plates the mantle viscosity increases to the values on the order of $10^{21}$–$10^{22}$ poise. In the lower mantle, viscosity everywhere increases with depth reaching $10^{24}$–$10^{25}$ poise at a depth of about 2000 km. Deeper yet in the lower mantle the matter viscosity declines again, probably to the values of $10^{19}$–$10^{20}$ poise within the transitional layer D″. And at last, at the base of the lower mantle within the Berzon layer (where the mantle matter disintegrates) viscosity rapidly drops by many orders of magnitude and approaches in the boundary layer at the core's surface to the core matter viscosity. The most likely viscosity distribution within the mantle is shown in Fig. 2.20.

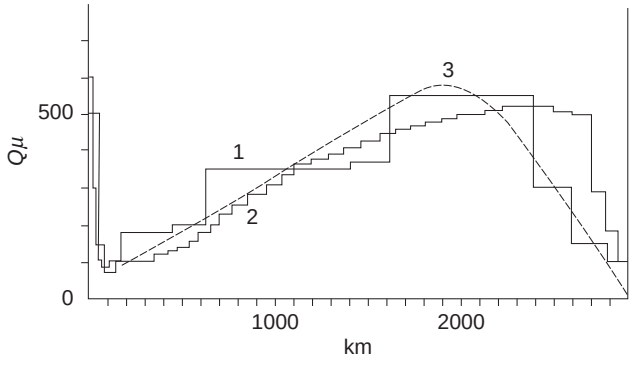


**FIGURE 2.19** Shear quality factor $Q_\mu$ distribution in Earth's mantle: 1, Dorofeyev–Zharkov model (1978); 2, Anderson-Hobart model (1976) (curves 1 and 2 are borrowed from the monograph by Zharkov (1983); and 3, assumed model.

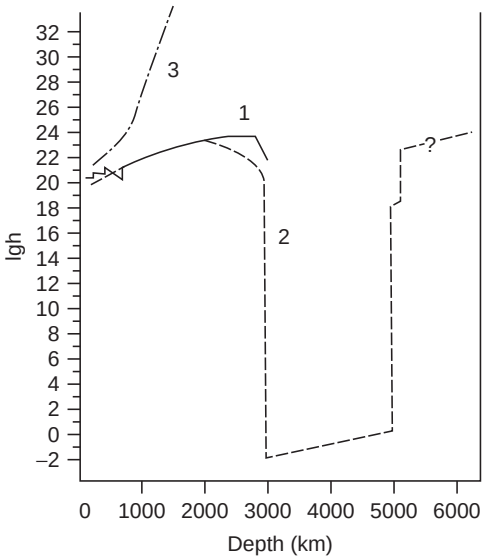


**FIGURE 2.20** Viscosity distribution within Earth: 1, Under Ranalli–Fischer model at adiabatic temperature distribution in the mantle (Ranelli and Fischer, 1984); 2, accepted viscosity distribution within Earth; and 3, viscosity distribution within the young Earth (before the beginning of differentiation).

The mantle viscosity substantially depends on its temperature. Under the Arrhenius' law, dynamic viscosity is determined as follows:

$$\eta = \eta_0 \exp\left\{\frac{W}{RT}\right\}, \tag{2.20}$$

where $\eta_0 \approx 10^{-5}$ Poise is the "limit" viscosity of the melted matter at "infinitely" high temperature $T$, $R = 1.987$ cal/deg mol is the gas constant, and $W$ is the viscous flow activation energy which depends on pressure (for the mantle viscosity values referred to above $W \approx 200$–$330$ kcal/mol).

The upper limit of the core matter viscosity within the external core may be estimated from decay in it of seismic P-waves. It was calculated that $\eta_c \ll 10^9$ poise. On the other hand, for generating within the core a dipole magnetic field with the axis closely coinciding with Earth's revolution axis it is necessary for the core matter flow velocity to be high enough, so that noticeable Coriolis inertial accelerations could start in it. These accelerations would be capable of "cork-screwing" such flows into structures with substantial latitudinal components.

For that to happen, the core matter flow velocity should be centimeters per second or even decimeters per second. Flows at such velocities may only occur on the core surface if the core matter viscosity is low enough for the appearance of rapid flows. It was determined from the geomagnetic field variable components and from energy balance of its generation that kinematic viscosity of the liquid matter within the Earth's core is about or below $\nu_c \approx 10^2$ cm$^2$/s (Loper, 1975). From that, dynamic viscosity is found: $\eta_c \leq 0.4$ poise.

Taking this into account, and also remembering that the core temperature is approximately 150–200 °C above the core matter melting point (i.e., it is overheated), we accept as a first approximation its viscosity at around $\eta_c \approx 10^{-1}$–$10^{-2}$ poise.

We do not know anything about viscosity of the internal core except that it must be higher by many orders of the magnitude than viscosity within the external core. A possible viscosity distribution within the deep Earth can be seen in Fig. 2.20.

As opposed to the modern Earth, the young Earth matter temperature was much lower (see Section 3.10). Thus, its viscosity was very high and in the central areas may have been substantially higher than $10^{30}$ poise. That made it practically impossible for any possibility of the Earth's matter convection in Katarchaean. Therefore, after the Earth's emergence about 4.6 BY ago there was absolutely no possibility for any differentiation processes in her depths; hence, there could not have been a high-density core and the crust. These geospheres formed much later, after a preliminary heating of the young Earth's matter due to her tidal interactions with Moon and the radioactive decay (see Chapter 4).

CHAPTER

# 3

# Origin of Earth, its Past and Future

## 3.1 ORIGIN OF THE SOLAR SYSTEM

To approach the issue of the origins of stars and their surrounding planetary systems, it is necessary to identify the source of the matter from which these systems formed. This very interesting and highly complex problem was studied in detail and profusely published (Tayler, 1975; Zeldovich and Novikov, 1971, 1975; Shklovsky, 1975, 1976; Aller, 1971; Alven and Arrhenius, 1976; Kaufman, 1979). We here remind the reader about the major concepts at the base of the origins of the Sun and its planets.

The present-day cosmogonic concept is that the initial gas–dust Proto-Sun-protoplanetary cloud formed from interstellar gas and dust accumulations typical of our and other galaxies. The origin of the matter in these accumulations goes back to explosions of large stars (several times more massive than the Sun) which completed their evolution. Usually, the final blowups of such large stars are called supernovas: for a brief time their luminosity increases by a factor of billions, they become the brightest objects in their galaxies and are perceived as flare-ups of new stars against the habitual background of the "old" skies.

As is now believed, at the moment our Universe formed (in a "big bang" about $13.73 \pm 0.12$ BY ago), the space was being filled up only by radiation and violently expanding matter (protons, electrons, helium nuclei—up to 25%—neutrinos and some other elementary particles). Heavier elements did not have time to form at those distant times, they just did not exist.

First, protogalaxies occurred from the matter fluctuation coagula. Those protogalaxies were composed of massive and primitive hydrogen–helium protostars. Gradually, ever heavier elements, up to iron, began forming in their bowels on the account of nuclear synthesis reactions (nuclear "burning").

Theory (Zeldovich and Novikov, 1971) indicates that this type of large stars (several times heavier than the Sun) are unstable, their evolution ends up in giant explosions. The heavier the initial star, the faster this fatal evolution occurs. The "supernova" explosions proper occur only when the light elements in their bowels are completely exhausted, and the core of iron and nickel forms (iron and nickel are the elements with the lowest internal energy of proton and neutron bonding in atom nuclei). As the reader may recall, the

*Developments in Earth and Environmental Sciences*, Volume 10
DOI: 10.1016/S1571-9197(11)10003-8

potential energy of the particle bonding in atomic nuclei is negative, so the elements with the lowest internal energy are most stable.

As a result, all nuclear reactions stop in the cores of these massive stars that ended up their evolution. The heat energy is no longer generated. There is nothing to prevent them from compressing. They collapse under no longer restrained gravity. Affected by the immense pressure in the stellar cores during their collapse, the electrons are squeezed-in into iron nuclei turning protons into neutrons, and the very stellar core, into a clot of neutrons, or even into a "black hole."

Gravity collapse of the stellar nucleus causes no less violent collapse of the star's gas shell.

A result is a catastrophic, temperature and pressure increase within the shell. It produces shock waves which throw the stellar shell away into the outer space. As opposed to the iron core of a collapsing star, its shell is still holding plenty of hydrogen, helium and other light elements (C, O, Mg, Si, etc.). These light elements are capable of participation in nuclear synthesis reactions. Besides, the stellar shell matter at that time is intensely irradiated by neutron flows released by the star's collapsing nucleus. For this reason, a drastic increase in temperature, pressure, and neutron flows in such star's shell causes no less violent avalanche of all synthetic nuclear reactions with huge energy release over a short period of time.

As a result, an amount of energy is released in the collapsing star's shell within minutes or even seconds which would otherwise be released during many millions of years of its evolutionary development. It causes the accelerated occurrence of various nuclear reactions synthesizing stable and radioactive elements and the whole gamut of their isotopes including those heavier than iron. The release of colossal energy from the lower portion of the stellar shell results in throwing out of the shell into the interstellar space. The transformed shell matter violently flows in all directions, and in place of the former normal star remains a small but very dense ($\rho \approx 10^{14}$ g/cm$^3$) neutron star (pulsar) or even a "black hole."

The dispersed matter from many exploded stars gradually forms in the galaxies interstellar gas–dust clouds. When the mass of such cloud (in its clots) reaches some critical value, the cloud self-gravity process begins. It becomes denser, heats up, and condenses into a new star. Several generations of the stars which dispersed their matter all over the interstellar space, changed one after another over the life of the Universe. And the matter thrown out by the previous generation of supernovas served as the source material for each new stellar generation.

Our Solar System is relatively young (4.7 BY) compared to the age of the Universe ($\sim$13.7 BY). For this reason, the summary composition of the matter that served as a basis for our Solar System must bear the footprints of the Universe's long history. However, the decay traces of some short-lived elements (such as $^{244}$Pu, $^{129}$I, and $^{26}$Al) found in meteorites indicate that at least two supernovas blew up shortly before the formation of the Solar system. And the latest one, which enriched the protoplanetary matter with $^{26}$Al and $^{129}$I isotopes, most likely, was a direct push toward the beginning of the formation from the interstellar cloud of our Sun and its planetary system.

The origin of the Solar system's planet is well elucidated in numerous publications (Schmidt, 1946; Safronov, 1969; Cameron, 1972, 1973; Ruskol, 1975; Alven and Arrhenius, 1976; Voytkevich, 1979; Fisher, 1987; Vityazev et al., 1990; Kaufman, 1982). So, we provide

here a most general description of the process. We, however, review the emergence and evolution of the Earth–Moon system in more detail and based on a totally new approach.

According to the modern cosmogonic concepts, the Earth group's planets, including Earth and the Moon, formed due to accretion of solid particles in the gas–dust protoplanetary cloud. Usually, the initial density of the interstellar clouds is not high enough for gravity compression and development of the independent star- and planet-forming processes. Supernova explosions, however, are accompanied by shock waves in the interstellar medium. If such waves hit a gas–dust cloud, pressure and matter density drastically increase on the wave-front. A result may be clots capable of the subsequent compression, now due to the self-gravity. That is why supernova explosions not only deliver the new matter into the cosmic space but also serve as the mechanism which eventually leads to the formation of new generations of stars and their surrounding planetary systems.

Apparently, such a situation arose about 4.56 BY ago in the vicinity of the protosolar gas–dust cloud. After having received an impulse of the initial compression and evolution and having been added a new matter, the cloud subsequently began to compress irreversibly, now affected by its own gravity field. With the compression, pressure and temperature in the cloud's center rapidly increased. Gradually, a giant gas clot, the Proto-Sun, formed in that zone. However, prior to "kindling" of the nuclear reactions and the Proto-Sun entering the main sequence of the stellar evolution, its temperature was relatively low, not above 1000–1500 °C, and the radiation was mostly in the IR and red spectral bands.

Simultaneously with the compression, the peripheral portions of the protosolar cloud, affected by the centrifugal and gravity forces, gradually shrank toward the equatorial revolution plane converting into a lentil-like disk—the protoplanetary cloud. The matter density in the protoplanetary cloud also rapidly increased, especially near the equatorial revolution plane. Particle trajectories under the influence of ever more frequent collisions and turbulent slowdown gradually approached the circular Kepler orbits.

Interstellar clouds usually are composed of the mixture of gas and micron-size dust particles. The gases are substantially dominated by hydrogen and helium. Volatile compounds like $H_2O$, CO, $CO_2$, $CH_4$, $NH_3$, $N_2$, and some others also play a significant role. Most likely, the dust particle composition corresponds to a mixture of relatively refractory metal oxides and silicates with the metals proper, their sulfides and, to a smaller extent, hydrosilicates, and carbonates. In the cosmic space, such dust particles may grow only by way of sorption from the gas phase of metallic atoms and their oxide or sulfide molecules on the surface of the particles. Due to a highly tenuous interstellar matter, this process was developing very slowly.

A different situation occurred in the protoplanetary cloud that began to contract. With the increasing density of the matter, the probability of particle collision and agglomeration drastically increased. As a result, first lumps of the matter appeared although very loose and small (on the order of centimeters, and later meters) and probably remindful of a dirty snow. A further compaction of swarms of this primordial matter facilitated their accelerated growth and gradual conversion into larger bodies—fetuses of the future planets: planetesimals. Their size may have reached many kilometers. The largest planetesimals, hundreds of kilometers in size, already had their own gravity fields. That ever more increased their effective capture cross-section of smaller bodies. The smaller bodies precipitated onto the larger ones increasing their size. As a result, large planetesimals grew faster than the

smaller ones. One of such largest planetesimal bodies positioned in the internal belt of the protoplanetary cloud eventually converted into the Earth's fetus.

The formation of the Sun as a normal yellow star, not very big, out of the compacting primordial gas and dust clot was going on much faster than the formation of planets. It took just a few millions of years. At the very beginning of the "kindling" in the Sun's bowels of helium-synthesizing nuclear reactions but prior to the entry under the regime of the main sequence of the stellar evolution, our Sun must have gone through a brief stage of τ-Taurus. Typical of this regime is rapid revolution, strong magnetic field and a very high intensity of the "stellar wind" radiation.

These particulars in the evolution of a young Sun must have affected the matter accretion conditions in its surrounding protoplanetary cloud disk. First of all, a very strong "solar wind" (a flow of high-energy charged particles) typical of the stars at the τ-Taurus stage, all gas and volatile components of the source protoplanetary cloud must have been swept out from the near-solar space to the distant periphery of the Solar system.

The reason for that was that the ionizing effect of the flow of high-energy charged atomic particles onto the surrounding protoplanetary disk matter resulted in a strong interaction between the disk and Sun's magnetic field. Apparently, as a result of such effective "adhesion" of the rapidly revolving young Sun with its surrounding matter, kinetic momentum was redistributed from the central celestial body to the periphery of the protoplanetary disk. After that Sun's axial revolution slowed down, whereas the orbital revolution velocity around the Sun of the protoplanetary disk matter increased. The same mechanism, probably, resulted in a noticeable matter separation in the protoplanetary cloud as all easily ionized elements were swept under the effect of the pressure from magnetic field lines of force out of the near-Sun space to the periphery of the protoplanetary disk.

Besides, chemical differentiation of the matter in the protoplanetary cloud must have been under a substantial influence of a greater heating by the Sun of the disk's central areas even at the stage of its compression and especially after "kindling" of nuclear reactions in the Sun. For that reason, many volatile elements and compounds (such as sulfur and its volatile compounds, water, carbon dioxide, etc.) converted to the gaseous state, after which they were removed by the Sun radiation pressure from these areas into the remote periphery of the Solar system.

As a result of these mechanisms, refractory elements and compounds with high-ionizing potential (refractory metals including Fe and Ni, and oxides $Al_2O_3$, CaO, MgO, $Ti_2O_3$, $SiO_2$, $Cr_2O_3$, FeO, etc.) predominantly concentrated in the central areas of the protoplanetary disk. At the same time, the average concentrations of easily fusible and easily ionizing elements (Li, Na, K, Rb, Cs, In, Ba, rare earth elements, Hg, Pb, etc.) in this part of the protoplanetary cloud were very low. To a somewhat smaller extent the Earth group planetary matter turned out to be impoverished in sulfur, zinc, tin and some other elements. The gas components ($H_2$, He, and other rare gases, $H_2O$, CO, $CO_2$, $CH_4$, $NH_3$, $H_2S$, $SO_2$ and $SO_3$, HCl, HF) were swept out of the internal area of the protoplanetary cloud and concentrated on its periphery where the giant planets with massive, high-density gas atmospheres later formed. Apparently, the internal areas of the protoplanetary cloud were also impoverished in hydrosilicates and carbonates which dissociated under the Sun radiation with the subsequent loss of volatile components.

A result was that even prior to the beginning of planetary formation, the source protoplanetary gas–dust cloud was substantially differentiated. This is a possible explanation of the clear correlation between planetary density and the planets' distance from the Sun (Mercury, 5.54 g/cm$^3$; Venus, 5.24 g/cm$^3$; Earth together with the Moon, 5.49 g/cm$^3$; Mars, 3.94 g/cm$^3$; Jupiter, 1.33 g/cm$^3$; Saturn, 0.67 g/cm$^3$; Uranus, 1.3 g/cm$^3$; Neptune, 1.67 g/cm$^3$). The same explains the fact that only the external planets have massive gas atmospheres, and their satellites are covered with thick armor of water ice, sulfur, and other solidified or liquefied gases ($CO_2$, $CH_4$, $NH_3$, etc.)

The Earth's atmosphere has a relatively small mass not exceeding $2.4 \times 10^{-4}$ of the planet's mass. Based on this and on the composition of the atmosphere, Earth, as the other planets of the Earth group, was formed out of the matter almost completely devoid of all gas components. Indeed, the Earth's atmosphere has practically no heavy primary noble gases, and the Earth's matter is drastically impoverished in hydrosilicates, carbonates, sulfur, and its compounds, and is noticeably poor in alkali and other easily fusible metals.

Most likely, the described differentiation of the primary matter in the protoplanetary cloud occurred rather rapidly, just over several millions or tens of millions of years. It must have happened during compression of the protoplanetary gas–dust cloud and during the young Sun passing through the τ-Taurus evolution stage. The planets formation, on the other hand, began after the disk's planetesimals had already acquired circular orbits, and continued for a relatively long time, on the order of 108 years (Safronov, 1969). An important inference from this is that the planetary accretion in their feeding ring zones (which, at that, had definite widths) was mostly homogenous (uniform). What it means is that the average chemical composition of the growing planets (with the differentiation processes in them absent) was more or less constant all along the radiuses of such planets.

Safronov (1969), who was one of the creators of the modern planet-formation theory, calculated that the Earth's growth continued for about 100 MMY. In the beginning, it was occurring under the ever accelerating accretion regime. Later, due to the exhaustion of solid matter in the near-Earth swarm of the protoplanetary cloud planetesimals, it slowed down again. The total amount of the gravitational energy released during Earth's accretion was enormous, about $23.3 \times 10^{38}$ erg. This energy was more than sufficient not only for melting the entire Earth's matter but also for its complete evaporation at the temperature above 30,000 °C. However, most of this energy was released in the most near-surface portions of the growing Proto-Earth and was lost with its heat radiation. And the slower Earth grew, the greater was the heat loss.

This is an important result. It shows that as Earth grew, not only did it heat up from the impacts of the planetesimals falling onto its surface but it also had time to cool down releasing into the outer space a larger part of the accretion heat energy.

As a consequence, the temperature inside Earth over the period of its growth (about $10^8$ MMY) was apparently everywhere below the melting temperature of Earth's primordial matter. Therefore, Earth was at that time a relatively cold, undifferentiated planet without a core and Earth's crust.

This is supported by direct geological data.

First, it is a complete absence on Earth of igneous rocks in the age interval of 4.6–4.0 BY. It tells of its initial cold state (first magmatic rocks in the Earth's crust showed up only 700–800 MMY after Earth formation).

Second, most exceptional and practically irrefutable proof of it is lead isotope ratios on the Moon and Earth. The lunar rocks clearly emerged after a complete melting and differentiation of the planet. The ratios of radiogenic lead isotopes with atomic weights of 206, 207, and 208 (formed due to the decay of Uranium 238 and 235, and also Thorium 232) to the stable (primordial) isotope 204 are extremely high. In lunar rocks, these ratios are as high as 207, 100, 226, and higher. For Earth rocks averaged in the oceanic reservoir of pelagic deposits the same ratios are 19.04, 15.68, and 39.07.

And for the primordial lead (composition data from iron meteorite "Diablo Canyon," Arizona, USA), these ratios are even lower, only 9.50, 10.36, and 29.45 (Voytkevich et al. (1990)).

The quoted lead isotope ratios *practically uniformly* indicate the fact of a total melt and differentiation of the lunar matter, and *no less convincingly prove* that Earth never totally melted and as not subjected to such a radical differentiation.

## 3.2 FORMATION OF A DUAL PLANET EARTH–MOON

Earth and the Moon actually form a dual planetary system. Their mutual influence is not great now but quite noticeable. However, at the early evolution stages of this system, it was exceptionally strong. It led to catastrophic consequences and radical changes in the evolution process of both planets.

That is why we reviewing the origins of Earth and the Moon together. It needs to be stated here in order to justify the heightened attention to the Moon in this monograph devoted to Earth evolution and its geodynamics that the Moon, as a satellite of our planet, served as the trigger mechanism which started and substantially activated Earth's tectonic evolution in Archaean. Besides, the Moon spun our planet. As is known, the origin of the magnetic field is associated with the rotation. On top of it, the lunar capture orbit defined the initial inclination of Earth's revolution axis, and that was the cause of all its initial climatic zoning. Moreover, it may now be stated with certainty that the Moon, by accelerating Earth's evolution, predetermined the emergence on its surface of highly organized life.

These are, of course, purely earthly problems which are impossible to disentangle without developing an adequate evolution theory of the Earth–Moon dual planet and of the Moon proper.

As opposed to the previous section, we describing here not the conventional concepts of the Earth–Moon system formation but a new model developed by the authors (Sorokhtin, 1988) of the origin due to tidal destruction at the Roche limit of a more massive planet, Proto-Luna. The model was described in publications with Ushakov (Sorokhtin and Ushakov, 1989a,b, 2002).

It appears to be explaining better than other models the entire aggregate of the modern knowledge about the composition, structure, and geological evolution of both Earth and our satellite. It also explains the origin of Earth axial revolution and the existing distribution of the kinetic momentums between Earth and the Moon.

In our belief, a major difficulty for the construction of an adequate theory of the Moon origin is its drastic impoverishment in iron, siderophilic, and chalcophylic elements. Judging by the average Moon density ($\rho_L = 3.34\ g/cm^3$), it contains no greater than 5% of the iron–nickel phase (Ringwood 1975a,b, 1979), or taking into consideration average FeO concentration in the lunar mantle, just 13–14% of the heavy fraction. This is much lower than average iron compounds content in the non-differentiated matter of carbonaceous chondrites (22%) and especially in Earth's matter (nearly 37%).

Taking these differences into account, hypotheses were proposed of Moon origin in other areas of the Solar System impoverished in iron compounds with subsequent capture by the Earth's gravity field (Alfven, 1954, 1963; Urey, 1972).

Hypotheses in this group have two drawbacks.

First, the probability of gravity capture from a distant orbit of a large cosmic body like the Moon is disappearingly small (practically zero). Second, it is impossible to come up with an explanation as to why the lunar matter is so deficient in iron when its content in the most primitive carbonaceous chondrites is about twice as large. Besides, the carbonaceous chondrites are rich in volatile and very mobile elements, whereas the Moon is drastically impoverished in them.

A difficulty explaining the capture by Earth of a large satellite from a distant area of the Solar System resulted in the formation of another group of hypotheses. Now, the Moon emerged in the Earth's formation area and made together with it a dual planet system.

Most developed of such hypotheses is the one by Ruskol (1960–1975). A similar hypothesis was suggested by Harris and Kaula (1975). It proposes the joint accretion of the Earth and Moon which began at the time when Earth had only 0.1 of its present-day mass. According to these hypotheses, the Moon was forming during a large part of its growth at a distance of about 10 Earth radiuses.

These hypotheses postulate the emergence of our planets from a single reservoir of the protoplanetary matter. But they were also incapable of explaining the deficiency on the Moon of iron and siderophilic elements as well as a high degree of the lunar matter differentiation and "tornadic" values of ratios of the radiogenic lead to the primary $^{204}Pb$. Besides, these models were based on the assumption that Earth's axial revolution existed from its very inception and acted in the same direction as the satellite revolution but at the angular velocity of own revolution exceeding the satellite's orbital revolution axial velocity.

Of interest is Gerstenkorn's (1967) hypothesis of the Moon capture and subsequent tidal evolution of its orbit. During this evolution, the Moon approached the Roche limit, that is, the closest distance from the satellite to the central plant (at a closer distance a massive satellite would be destroyed by the planet's gravity field). Under this concept as well, the Moon remained unchanged from its birth to our days, so there was no explanation to the origin of the existing iron deficiency in the lunar matter. Besides, Gerstenkorn's calculations have some errors. The Hannes and Alvén's hypothesis (1963) describes the Moon as a satellite captured by Earth onto the orbit close to the Roche limit. The present-day orbit formed through the tidal interactions with Earth.

As mentioned, the Moon is anomalous in terms of its iron content. At the same time, its basalts are wonderfully close in their composition to the primitive basalts of the Earth's mid-oceanic ridges. Oxygen isotope data also support "consanguineous" origins of the

Moon and Earth and a different origin of the carbonaceous and regular chondrite meteorites. Based on that, Ringwood (1975a,b, 1979) was able to show convincingly the geochemical affinity of the lunar matter with Earth's mantle matter. However, Ringwood made a rather exotic inference from this fact: soon after its formation and separation of the dense core, Earth rapidly spun up and, due to so formed rotational instability, a large lump was torn off its mantle, and later became the Moon.

This is an old idea which was put forward about a hundred years back by Darwin (1865), a talented geophysicist and son of Charles Darwin. Unfortunately, this hypothesis as well was mechanically wrong.

When dealing with the Moon's origin, one needs to take into account the extreme degree of its differentiation that led to iron separation from silicates and their substantial impoverishment in siderophilic elements. Such total differentiation of the matter may have occurred only within the body of a rather large and melted planet.

This is an important point which cannot be discarded. That the Moon was formed from the originally melted planet is supported, in particular, by the composition of its thick (up to 80 km) anorthosite crust composed mostly of a calcium feldspar anorthite. Such thick crust could only have separated from the totally melted matter of a large cosmic body, three to four times greater than the present-day Moon. As was found from the lunar anorthosite age determination (Tera and Wasserburg, 1974), this process was taking place about 4.6–4.4 BY ago, that is, during the period close in terms of timing to the formation of the very Earth–Moon system. Therefore, it is plausible to expect that the parent Moon body underwent the fool planetary melting and differentiation prior to the formation of the Moon proper.

One needs to take into consideration a second and quite remarkable fact important for the Moon's origin hypothesis. The total Earth–Moon system revolution kinetic momentum with accuracy to the third decimal point fits a situation when the satellite and the central planet were positioned at Roche limit distance from one another and had a synchronous axial revolution velocity. That cannot be just a coincidence. On the contrary, it is a convincing evidence of the situation where the Moon during its origin was indeed at the Roche limit and could have been destroyed.

It appears quite plausible based on the provided data and considerations that the Moon is a remnant of some larger planet, the Proto-Moon, which was captured by the growing Earth from an adjacent (closest) orbit and destroyed by Earth's gravity field at the Roche limit. Similar considerations, in a qualitative form, were published earlier by Wood and Mitler (1974) and Opik (1961). Analogous to these ideas, we have earlier proposed (Sorokhtin, 1988) a hypothesis under which the Moon formed as only a remnant, the tidal hump of a melted and totally differentiated Proto-Moon preserved from destruction in the Roche "bubble."

## 3.3 TIDAL INTERACTION OF THE PLANETS

Before turning to the Moon formation process, we briefly review the very nature of the tidal interaction. This phenomenon was studied by numerous scientists. Among the first was Newton who understood that the ocean tides are caused by the Moon's and Sun's

gravity pull of the water shell. The problem was considered by D. Bernoulli and L. Euler but the largest contribution in the studies of the nature of Earth's tidal interaction with the Moon and Sun was made by a mathematician, Pierre-Simon Laplace (1749–1827), who formulated the tidal problem in a modern format, and G. Darwin who proposed in 1898[1] some practical ways to solve this problem. In our days, the evolution of the tidal interaction in the Earth–Moon system was studied by MacDonald (1964a,b), Goldreich (1966a,b), and Ruskol (1975). Subtle effects of the planets' tidal interactions were studied by Avsyuk (1996).

The tidal interaction between Earth and the Moon, due to their closeness, is stronger than between Earth and the Sun. Currently, the effect of a static solar tide is about 20% of the lunar one MacDonald (1964b). In the past geological epochs, a relative effect of the lunar tides was even stronger. To make the problem simpler, we will review the influence on Earth of the Moon alone.

We also use Laplace's approximation for interacting planets' Keplerian orbits. We disregard the correction terms accounting for the tidal disturbances on this orbits (as described by Avsyuk, 1996 with the correcting terms accounting for the planets' rotation around their common center of mass and the tidal effect on their orbits). As a first approximation, we will regard the lunar orbit circular and positioned in Earth's equator plane. The latter condition is currently invalid as the plane of Earth's equator is inclined at the precession angle of 23.5° to the ecliptic (the plane of Earth's revolution about the Sun), and the lunar orbit plane is inclined at nearly 5° to the ecliptic. Earth's precession angle, however, changes with time being affected by the continental drift, emergence of ice sheets and gravity interaction between Earth's equatorial hump with the Sun and Moon (see details in Chapter 14 and the publication by Sorokhtin, 2006a,b).

As a result of planets' gravity pull, tidal deformations (swellings and humps) occur in their bodies. Each planet forms two humps, one facing the disturbing "neighbor" and the other, on the opposite side (Fig. 3.1). These disturbances are not limited to the oceanic waters (on the account of their overflow to the sublunar areas) but also affect the solid land.

Earth's axial angular velocity (one revolution every 24 h) is substantially higher than Moon's orbital revolution angular velocity (one revolution every 27.32 days = 655.7 h). As a result, the tidal humps are as if "running" on the surface of Earth following the Moon's apparent motion in the sky. As we have already mentioned, Earth's matter is not ideally elastic and has properties of a viscous liquid. In consequence, deformations in the lunar humps do not have time to dissipate after they have run through the culmination points with the Moon, and are carried by Earth's revolution running significantly ahead (approximately by 2.16°) of the Moon's motion. To an Earth observer, however, it appears that the maximum tides on Earth are always late and occur on its surface somewhat later than the Moon culmination (Fig. 3.1).

Additional pull from the excessive mass of the tidal humps affects the motion of the planets proper. The pull from both tidal humps on Earth generates a pair of forces acting on both the Earth and the Moon. However, the influence of the closer hump facing the Moon is slightly stronger than that of the farther one. Absolute values of the tidal attraction forces between the Moon and Earth are presently small. But their accumulation over time resulted in a noticeable breakage of Earth revolution and in the acceleration of Moon's orbital revolution and its distancing from Earth.

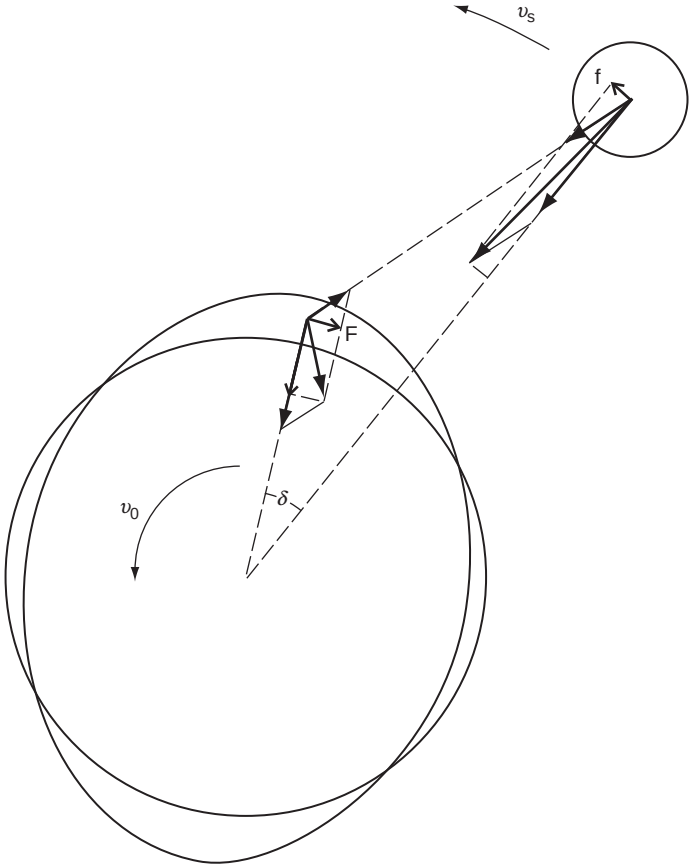


**FIGURE 3.1** Schematic presentation of Earth–Moon tidal interaction: $F$ is the tidal force, braking Earth revolution; $f$ is the tidal force speeding-up orbital revolution of the Moon; and $\delta$ is the tide delay angle.

In order to determine how the mutual positions of the Moon and Earth evolved, it is necessary to utilize the laws of the celestial mechanics (third law of Kepler) and the law of kinetic momentum (impulse) conservation in the system as well as to take into account the tidal deformation energy which is dissipated in the planets. The tidal interactions redistribute the kinetic momentums between the planets but the total kinetic momentum of the system always remains constant

$$I_e\Omega + \frac{Mm}{M+m}L^2\omega = K \equiv \text{const}, \tag{3.1}$$

where $I_e = 8.0363 \times 10^{44}$ g cm$^2$ is moment of inertia of the present-day Earth relative its revolution axis, $\Omega$ is angular velocity of Earth revolution about its axis (the present-day value is $\Omega = 7.292 \times 10^{-5}$ rad/s), $\omega$ is angular velocity of Moon's orbital motion around Earth (the present-day value is $\omega = 2.672 \times 10^{-6}$ rad/s), $M = 5.977 \times 10^{27}$ g is the Earth's mass; $m = 7.35 \times 10^{25}$ g is the Moon's mass ($m \ll M$), $L$ is the distance between the centers of Earth and the Moon (the present-day value is $L = 3.844 \times 10^{10}$ cm), and $K = 3.4458 \times 10^{41}$ g cm$^2$/s. Moon's revolution about Earth is ruled by the third law of Kepler

$$\omega^2 L^3 = \gamma(M+m) = \mu \equiv \text{const}, \tag{3.2}$$

where $\gamma = 6.67 \times 10^{-8}$ cm$^2$/g s$^2$ is the gravitational constant and $\mu = 4.03575 \times 10^{20}$ cm$^3$/s$^2$.

The energy of Earth's own revolution $E_\Omega$ and the full orbital energy of the Moon may be found from the following simple equations:

$$E_\Omega = I\frac{\Omega^2}{2}, \tag{3.3}$$

$$E_\omega = -\gamma\frac{mM}{2L}. \tag{3.4}$$

The present-day values of Earth rotation energy and of Moon's revolution are, respectively, $E_\Omega = 2.13 \times 10^{36}$ erg and $E_\omega = -0.38 \times 10^{36}$ erg (the Moon's orbital revolution energy is in essence the potential energy, so $E_\omega < 0$).

The tidal interaction results in the energy "pumping over" from one planet to the other. However, as opposed to kinetic momentum, the revolution energy in the system is not maintained constant and, due to tidal deformations, gradually converts to heat and dissipates in the outer space. Presently, Earth's revolution energy is being transferred to the Moon. As a consequence, the axial revolution of our planets gradually slows down, and simultaneously the Moon retracts from the Earth.

These patterns have an important consequence. If during its origin or capture a satellite had its own revolution at an angular velocity not equal to its revolution velocity around the massive central planet, then a tidal force pair must have arisen and acted on such satellite slowing down its motion. As for the satellites usually $m_s \ll M_0$ and $I_s \ll I_0$ (for the Earth–Moon system, $m_s/M_0 = 0.0123$ and $I_s/I_0 = 1.08 \times 10^{-3}$), the own revolution energy of such satellite $(E_\Omega)_s = I_s(\Omega_s - \omega)^2/2$ is small and is quickly dissipated converting to heat.

Therefore, suc satellite relatively rapidly turns to the synchronous revolution, its axial angular velocity becomes equal to its orbital revolution velocity ($\omega = \Omega_s$), and it stays turned by the same side to the central planet, which is observed currently in the Moon.

## 3.4 HYPOTHETICAL PLANET: PROTO-MOON

We now review the earliest history of the Earth–Moon system at the stage when the planets were better called Proto-Earth and Proto-Moon. The suggested events were coincidental with the epoch when the Solar System's planets were completing their formation due to the accretion of planetesimals. It happened nearly 4.6 BY ago.

The events may have evolved along several different scenarios.

The Proto-Earth and Proto-Moon may have originated under the "classical" mechanism of dual planet formation. First, Earth formed and then, from the remaining material of the Proto-Earth planetesimal swarm, formed the Proto-Moon (Ruskol, 1975). This does not explain, however, how such a Moon could have become overheated due to the tidal deformations, got melted and undergone the complete differentiation. For this to have happened, the eccentricity of its initial orbit must have been very large, close to 1 but due to the

averaging in the planetesimal motions in the near-Earth swarm, the orbit of a satellite that would have formed out of them must have been about circular. Besides, a suggestion of the Proto-Earth planetesimal swarm in itself assumes early capture of the celestial bodies (such as planetesimals) by the planet's gravity field.

Most common present-day Moon origin models assume its formation as a result of a tremendous tangential mega-impact on the Proto-Earth from some Martian size planet (Hartmann and Davis, 1975; Cameron and Ward, 1976). Later studies suggested that a single mega-impact or numerous smaller macro-impacts formed a Proto-Earth disk of fragments, and the Moon was a result of further accretion of such a disk (Cameron and Benz, 1990; Cameron, 1997; Ida et al., 1997).

Modeling of gravity interactions between numerous bodies within a nonuniform protoplanetary disk (Ohtsuki and Ida, 1998) showed the following. Gravity captures of celestial bodies always occur in the straight direction and ends up in their transfer to the near planetary orbits with the subsequent tangential planetesimal drop-off on the planet's surface. This indicates that the satellite capture from the orbits closest to the planet is quite possible. And such captures are the main cause of the planet spin. Unfortunately, the quoted numerical experiment did not include a modeling of massive captured bodies' destruction on the Roche limit. For this reason, the modeling scientists traditionally associated Moon's origin either with a sliding impact of a larger protoplanetary body or with the accretion of the Proto-Earth fragment disk.

We believe that the gravitational capture of the relatively large Proto-Moon by the growing Earth from the adjacent (closest) orbit is a more likely scenario. Contrary to a satellite capture from a distant orbit (the event of a very low probability), the probability of a satellite transfer from the nearest heliocentric orbit onto an orbit around the growing planet (i.e., the planet of an increasing mass) may be quite finite. That was assumed, for instance, by Singer (1972) and Alven and Arrhenius (1976).

In view of Kaula and Harris (1973), collisions of a passing-by satellite with planetesimal swarm bodies still revolving about the growing planet would be a much more efficient capture mechanism. Such collisions would substantially slow down the cruising speed of the satellite. As a result, its trajectory could have changed from a hyperbolic (relative to the central planet) to elliptical, and then to circular.

We need to mention here again that in the absence of a finite probability of the gravitational capture by massive bodies of other celestial bodies it would be impossible to explain the origin of the near-planet satellite swarms, from which, under the classical scenario, the planets' satellites then formed.

This concept is supported by the existence around all external planets of the satellite systems with multiple satellites usually revolving in the equatorial planes of their planets (one of the planets, Neptune, is revolving as if on its side). Besides, it would not be possible otherwise to explain the reverse revolution of Phoebe's satellite (the Saturn' system) and the Triton around the Neptune. Moreover, we witnessed in 1994 a demonstrative natural experiment, the capture by the Jupiter's gravity field of a comet (the Shoemaker-Levy-9), its destruction on the Roche limit and the drop-off of the fragments onto the central planet.

We consider this phenomenon to be the best testimony in favor of the reviewed model of the Proto-Moon capture and its subsequent destruction on the Earth's Roche limit.

One way of the other, the Proto-Moon turned out to occupy a near-Earth orbit. Let us now assume, contrary to the classical Moon formation hypotheses, that the Proto-Moon mass was originally much larger than the present-day lunar mass (may it be by the factor of 4) but still significantly smaller than the Proto-Earth mass.

In such a case, the Proto-Moon mass would be approximately $m_{\rm pl} \approx 2.94 \times 10^{26}$ g, and its average radius $r_{\rm pl} \approx 2.56 \times 10^{8}$ cm (the present-day Moon radius is $1.738 \times 10^{8}$ cm, and its mass is $7.35 \times 10^{25}$ g). Remember that the Proto-Earth own revolution (acquired exclusively due to the drop-off onto its surface of planetesimals from the adjacent—internal and external—belts of the protoplanetary cloud) could not be rapid. The explanation is in the statistical compensation of the protoplanetary bodies' impacts (these bodies impacted the growing planet from all directions on the Earth's orbit). On top of that, the planetesimals from the cloud's internal belt had a slight excess in their angular revolution velocities. For this reason, the initial Proto-Earth revolution could have been not only slow but also reverse (as in the satellite-free Venus). This condition, however, is not critical.

It so happened therefore that the original angular velocity of the Proto-Moon orbital revolution (regardless of its formation mechanism) was significantly higher than the angular velocity of the Earth's own axial revolution. To be definite, let us assume that the Proto-Moon was captured to the orbit with the average radius of about six Earth's radiuses ($L \approx 6R_g \approx 38{,}200$ km; again, this is not a critical condition) and revolved about Earth with a period of about 20 h. Let us also assume that the Proto-Moon revolution velocity was substantially higher than Earth's own revolution velocity.

As we agreed, the angular velocity of the satellite's orbital motion exceeded the angular velocity of the central planet ($\omega > \Omega$). Based on this and on the law of system's kinetic momentum conservation (3.1), it unavoidably follows that in the process of the planetary tidal interaction, the Proto-Moon orbital momentum gradually transferred to Earth. It accelerated its own revolution in the direction of the satellite's motion. The Proto-Moon, losing its kinetic momentum, must have equally unavoidably and irresistibly approached Earth. Otherwise, at $\omega < \Omega$, the satellite captured in the Earth's gravity field must have retreated from the Earth.

At the time of the Proto-Moon capture on the near-Earth orbit, its initial eccentricity must have been very big, approaching a one. This enables us to estimate the average value of the tidal energy released in the satellite after its transfer to an almost circular orbit.

$$\Delta E_{\rm pl} \approx \gamma \frac{M_{\rm pg} m_{\rm pl}}{2\bar{L}}, \tag{3.5}$$

where $\bar{L}$ is the average radius of the Proto-Moon's quasi-circular orbit after it absorbed the eccentricity of the initial capture orbit. The release in the satellite of the tidal energy must have rapidly transferred it to the stationary revolution regime $\omega = \omega_{\rm s}$ when the satellite was always facing the central planed by the same side.

The estimates show that after the capture of the Proto-Moon about $1.5 \times 10^{37}$ erg (or $1.5 \times 10^{30}$ J) of heat energy must have been released in its body only on the account of radial tidal deformations. That is equivalent to the release of 1200 cal of heat per gram of the Proto-Moon. The melting heat of most magmatic rocks is close to 100 cal/g, and their heat

capacity is ≈0.3 cal/g deg. Taking these into account, it is easy to determine that the heat so released would be sufficient for a complete melting of the Proto-Moon and its temperature rises to almost 3700 °C. Added to this, heat must be additional energy of the Proto-Moon gravity differentiation which must have unavoidably occurred after its melting. That would have added another $10^{36}$ erg in heat energy and the additional heating by 250 °C.

As a result, the Proto-Moon should have not only melted but also substantially overheated. That, in turn, would have resulted in a complete density differentiation of its matter and loss of volatile elements and compounds. As the Proto-Moon mass was small, and as it was later destroyed, these volatiles could not have been preserved in the satellite's atmosphere.

The system's evolution period from the moment of the Proto-Moon capture to its transition to the circular orbit was very brief (close to 10,000 years). So, despite intense surface cool-down, it must have for a long time remained a totally melted and strongly overheated celestial body.

Naturally, the tidal energy dissipation occurred on Earth as well. The heat energy of tidal interaction with the satellite released in the central planet was supplied by the energy of the satellite orbital revolution. Part of this energy was spent for "spinning" Proto-Earth (Earth's equatorial plane must have at the time coincided with the Proto-Moon's revolution plane around Earth), and part of it, for heating-up the planet. It was calculated that from the moment of the capture of the massive satellite to its transition on the Roche limit about $1.25 \times 10^{37}$ erg of the heat energy must have been released in Earth's body on the account of the tidal interaction between the Proto-Moon and Earth. This heat was sufficient to raise the Proto-Earth temperature by approximately 180 °C but far from sufficient to begin its melting. This is supported by the earlier mentioned geological data about the appearance of the most ancient magmatic rocks on Earth only after 600–800 MMY after its formation.

## 3.5 PROTO-MOON CATASTROPHE AND THE BIRTH OF THE MOON

As the massive satellite approached to the central planet, its body was ever more strongly deformed by tidal forces and extended along the lengthwise axis connecting the satellite's and planet's centers of mass. Starting at a certain distance between the central planet and satellite's orbit (known as the Roche limit) the tidal force acting upon the satellite becomes greater than its self-gravity. For the satellite destruction the difference between these forces must exceed the satellite rocks' rupture strength. Only under such conditions the satellite loses its stability and begins to fall apart. Therefore, for a solid satellite to be destroyed, it must as if sink into the Roche "bubble" to a depth at which the pull from the central planet exceeds the satellite's own gravity by the amount equal to the strength of its rocks. Contrary to that, the destruction of a melted (liquid) satellite begins as soon as it transfers to the orbit equal to the Roche limit.

The Roche limit depends on average values of the planet $\bar{\rho}_0$, satellite $\bar{\rho}_s$, and planet's radius $R_0$. It usually is computed from the approximate Alvin and Arrhenius (1979) equation

$$L_R \approx 2.44 \left( \frac{\bar{\rho}_0}{\bar{\rho}_s} \right)^{1/3} R_0. \tag{3.6}$$

As the satellite approaches the Roche limit, its body is experiencing ever greater deformations. At the Roche limit, the shape of a massive satellite may be determined from the equation of its equipotential surface

$$V = V_{\mathrm{g}} + V_{\mathrm{t}} + \delta V_{\mathrm{t}} + V_i \tag{3.7}$$

where $V$ is the resulting potential at the satellite's surface, $V_{\mathrm{g}}$ is the potential of the satellite not distorted by the tides, $V_{\mathrm{t}}$ is the tide-forming potential, $\delta V_{\mathrm{t}}$ is additional tidal potential caused by the satellite's deformations, and $V_{\mathrm{i}}$ is the potential of centrifugal forces expanding the satellite. These potentials are determined from the following equations (at $m \ll M$)

$$\begin{gathered} V = -\gamma\frac{m}{r}, V_g = -\gamma\frac{m}{r_0}, V_i = \gamma\frac{Mr^2}{L^3}, \\ V_{\mathrm{t}} = \gamma\frac{Mr^2}{L^3}\left[P_2(\theta) + \frac{r}{L}P_3(\theta) + \cdots\right], \\ \delta V_{\mathrm{t}} = \gamma\frac{Mr^2}{L^3}\left[k_2P_2(\theta) + k_3\frac{r}{L}P_3(\theta) + \cdots\right], \end{gathered} \tag{3.8}$$

where $r$ is the radius-vector of the satellite surface, $r_{\mathrm{o}}$ is the radius of the satellite not distorted by tides, $M$ is the central planet's mass, $m$ is the satellite mass; $P_2(\theta) = 0.5(3\cos^2\theta - 1)$ and $P_3(\theta) = 0.5(5\cos^3\theta - 3\cos\theta)$ are Legendre polynomials of the second and third power, $\theta$ is angle between the line connecting the planet's and satellite's centers of gravity and radius-vector $r$, and $k_2$ and $k_3$ are Love's tidal numbers dependent on the elastic modulus and mass distribution within the satellite. The number $k_2$ is equal to the ratio of the additional potential arising due to the planet's tidal deformation and tide-forming potential on its surface. The number $k_3$ is the ratio of the tide's height and the height of the equipotential surface rise of the rigid planet from the tide-forming potential (Zharkov, 1983). At $\theta = 0$, $P_2(\theta) = P_3(\theta) = 1$. Then, in the $r \ll L$ approximation, it is possible to determine the ratio of the long half-axis of the satellite deformed by the tide to its undeformed radius

$$\frac{r}{r_0} = 1 + \frac{Mr^3}{mL^3}(2 + k_2). \tag{3.9}$$

The equation of forces acting on the point at the satellite's surface with radius-vector $r$ may be found by the differentiation of Eq. (3.7) over the parameter $r$. In the accepted approximation, $r \ll L$ and $\theta = 0$; the equation of the forces, acting on the satellite's surface point facing the central planet, at the Roche limit is

$$\gamma\frac{m}{r^2} = \gamma\frac{M}{L_{\mathrm{R}}^3}2r + \gamma k_2\frac{M}{L_{\mathrm{R}}^3}2r + \gamma\frac{M}{L_{\mathrm{R}}^3}2r. \tag{3.10}$$

And from this, the very equation for the Roche limit is

$$L_{\mathrm{R}} \approx (4 + 2k_2)^{1/3}\left(\frac{M}{m}\right)^{1/3} r. \tag{3.11}$$

Inserting (3.11) into (3.9) we find that on the Roche limit the long half-axis of the tidally deformed liquid satellite is half again the length of its undistorted radius, that is,

$$r = 1.5r_o. \tag{3.12}$$

Therefore, the melted (liquid) satellite on the Roche limit acquires the shape of a revolution ellipsoid with the long axis directed toward the central planet and exceeding by the factor of 1.84 its equatorial radius (and looking like a huge baseball).

Unfortunately, we do not know the value of the Love's number $k_2$ for the melted Moon on the Roche limit. So, it is necessary to calculate the numerical value of this limit $L_R$ from a condition that on the lunar surface facing Earth, on this limit, the resulting gravity acceleration, taking the inertia term into account, is equal to zero. Then we can write

$$\gamma\frac{m}{(1.5r_0)^2} - \gamma\frac{M}{(L_R - 1.5r_0)^2} + (L_0 - 1.5r_0)\ \Omega_0{}^2 = 0. \tag{3.13}$$

We know that during the Moon emergence after the Proto-Moon destruction on the Roche limit, at some point in time the equality $\Omega_0 = \omega_0$ must be true. Therefore, we may insert (3.2) into Eq. (3.13):

$$\gamma\frac{m}{(1.5r_0)^2} - \gamma\frac{M}{(L_R - 1.5r_0)^2} + \gamma(M+m)\frac{(L_R - 1.5r_0)}{L_R^3} = 0. \tag{3.13'}$$

We find from this that the Roche limit for the Earth–Moon system $L_R = 17{,}151$ km. Judging from Eqs. (3.1) and (3.2), Earth's equatorial moment of inertia is

$$I_{e0} = \frac{K - Mm/M + m\ \sqrt{\mu L_R}}{\sqrt{\mu/L_R^3}} = 1.0047 \times 10^{45}\text{g cm}^2. \tag{3.14}$$

Currently, this momentum is equal $I_e = 8.0363 \times 10^{44}$ g cm$^2$.

Now, we can easily find from the same Eqs. (3.1) and (3.2) the Earth's axial revolution angular velocity and the lunar orbital revolution velocity on the Roche limit:

$$\begin{aligned}\Omega_0 &= \frac{K - Mm/M + m\ \sqrt{\mu L_0}}{I_{e0}} = 2.828 \times 10^{-4}\text{s}^{-1}\\ \omega_0 &= \sqrt{\frac{\mu}{L_0^3}} = 2.828 \times 10^{-4}\text{s}^{-1}.\end{aligned} \tag{3.15}$$

As we see, the condition $\Omega_0 = \omega_0$ for the Earth–Moon system on the Roche limit is complied with quite accurately.

The Earth's equatorial radius, when the planet was spun by tidal interactions with the Proto-Moon to the maximum satellite revolution velocity on the Roche limit with the period of 6.17 h, was about $R_{e0} \approx 6716$ km. It is easy to calculate that at the time the Moon was on the Roche limit orbit it was hanging over the Earth surface at a height of just 7828 km.

The destruction of a liquid and stratified (differentiated) Proto-Moon while in transfer onto the orbit of the cosmic limit with the subsequent gradual sinking into the Roche sphere must have occurred on the account of the melted matter from the internal (facing

the central planet) tidal swell flowing in the Proto-Earth direction. Silicate matter torn off the Protolunar surface formed small solidified sprays. They should have rushed, on a broad spiral, to the central planet and formed around the Proto-Earth (in its equatorial plane) rather dense rings of a fractured meteorite matter (similar to the present-day Saturn rings). The radius of such swarm-ring may be determined by the joint solution of Eqs. (3.1) and (3.2)

$$L_r = \frac{(L_R - r_R)^4}{L_R^3}, \tag{3.16}$$

where $r_R$ is the large half-axis of the Earth satellite figure on the Roche limit. If $L_r < R_{e0}$, then the fragments torn off the satellite surface unavoidably fall-off on the central planet surface and transfer to it their kinetic moment. On the Roche limit $r_R = 1.5r_0$. In our example, the Proto-Moon radius is $r_0 = r_{pl} \approx 2.56 \times 10^8$ cm, so $L_r \approx 6.1 \times 10^8$ cm but $R_{e0} \approx 6.72 \times 10^8$ cm, so the condition $L_r < R_{e0}$ was met. Therefore, at least in the first stages on the Proto-Moon destruction the fragments of its internal tidal hump must have been dropping off onto the Proto-Earth surface as shown in Fig. 3.2.

As the Proto-Moon was being destroyed, its size was gradually getting smaller. So, at the second stage of this process the rings of revolving small meteorite bodies similar to the Saturn rings must have formed around the young Earth. Under the Proto-Moon gravity and mutual impacts of the meteorite bodies, the ring matter must have gradually dropped off on the Earth surface. As a result, the Earth axial revolution velocity $\Omega$ increased, and the speed of the Proto-Moon remains sinking into the Roche sphere decreased.

Many features in the development of the Proto-Moon catastrophe were determined by the speed of its sinking into the Roche sphere. To determine this speed $\dot{L} = dL/dt$, it is necessary to find from Eqs. (3.1) and (3.2) the connection between the parameters $\Omega$ and $L$

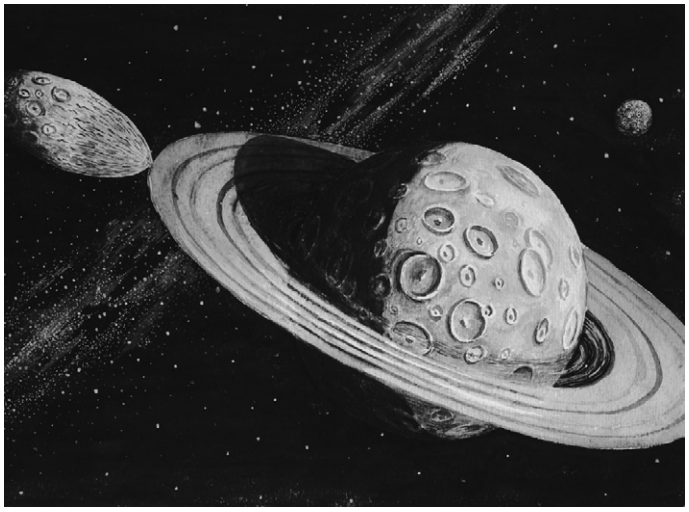

**FIGURE 3.2** Destruction of the Proto-Moon on the Proto-Earth Roche limit.

$$\Omega = \frac{K}{I_e} - \frac{\gamma^{1/2} Mm}{I_e (M+m)^{1/2}} L^{1/2}, \tag{3.17}$$

then

$$\dot{\Omega} = -\frac{1}{2} \frac{\gamma^{1/2} Mm}{I_e (M+m)^{1/2}} L^{-1/2} \dot{L}. \tag{3.18}$$

The derivative $\dot{\Omega}$ is determined from the Pariysky (1960) equation:

$$\dot{\Omega} = -\frac{3}{2} \frac{k_2 \gamma m^2 R_0^5}{I_e L^6} \sin 2\delta, \tag{3.18'}$$

where $k_2$ is the Love's number (it is determined from the ratio of the potential arising from the planet's tidal deformations to the tide-forming potential at the planet's surface), $\delta$ is the delay angle between the Moon culmination and the time of the tidal wave coming (for the case $\omega > \Omega$, the sign in Eq. (3.18′) should be changed to the opposite). It is known from the tide theory (MacDonald 1964b; Goldreich and Soter 1966) that

$$tg 2\delta = Q_\mu^{-1}, \tag{3.19}$$

where $Q_\mu{}^{-1}$ is, as earlier, the dissipative function determined from (2.18).

Comparing now Eqs. (3.18) and (3.18′), taking into account a small size of $\delta$ angles, with (3.19), we get eventually

$$\dot{L} = -3\gamma^{1/2} k_2 \frac{m(M+m)^{1/2}}{M Q_\mu L^{5.5}} R_0^5. \tag{3.20}$$

For a young and still relatively cold Earth, we may assume $k_2 \approx 0.3$ and $Q_\mu \approx 5000 \div 1500$. Then, it turns out that the speed of the satellite and the planet approach at that distant time was quite large. During one revolution the Proto-Moon, with its orbital revolution period of about 6 h, sunk into the Roche sphere by approximately 35 m, which was 50 km/.

As may be seen from the above estimates, the approach between the Proto-Moon and Earth was very rapid. At this speed of the Proto-Moon sinking into the Roche sphere, even the melted but still viscous Protolunar silicate matter from the satellite's internal tidal swell just did not have enough time to flow from its surface towards Earth. As a result, at that "tragic" time it could sink into the Roche sphere much deeper than theoretically acceptable without consideration of the satellite's final viscosity in the process of destruction.

The overflow from the Proto-Moon onto Earth of the gas components, degassed fractions of its primary atmosphere and hydrosphere must have been even more active. As the Proto-Moon was a substantially overheated planetary body which underwent a practically total differentiation, its early degassing at the time was practically complete. An important conclusion, therefore, is that Moon should have no traces of the primary atmosphere and hydrosphere. Thus, there cannot be on its surface any accumulation of free water, even frozen, as some experts expect to find there. All Moon's water is in its exceedingly dry rocks and only bonded, at a concentration below 0.05% (Mason and Melson, 1973).

The destruction problem of a layered satellite with low-viscosity (on the order of a few poise) but high-density (about 7–8 g/cm$^3$) core and more viscous (about $10^{10}$ poise) but light (about 3.3 g/cm$^3$) shell during a rapid sinking into the Roche sphere does not as yet have a strict solution. Perhaps, the situation must have rapidly changed as soon as the tidal acceleration from Earth exceeded the gravity acceleration at the Proto-Moon core surface. After that moment, at a reasonably rapid satellite sinking into the Roche sphere, significant expanding stresses emerged in most of its core. Under such conditions, after most of the Protolunar internal tidal hump was destroyed, most likely, a rapid outflow of low-viscosity melted iron from its core onto the Earth surface must have occurred. From Eq. (3.20), it appears that the entire Proto-Moon destruction took no longer than 100 years.

As all Proto-Moon matter fell on Earth, its mass increased to the present-day Earth mass, and its axial angular velocity increased due to the tidal interaction with the Proto-Moon. It reached the value of the satellite's orbital revolution axial velocity on the Roche limit $\Omega = \omega_R \approx 2.83 \times 10^{-4}\ s^{-1}$ (one revolution in 6.17 h). However, this status ($\Omega = \omega_R$) is unstable (metastable) because even a slight deviation from this equation toward a decrease in the satellite revolution axial velocity should have led to the sign change of the tidal interaction and to the sign change in Eq. (3.20). After that the satellite approach to the central planet should have changed to their repulsion from one another. The cause of such change in $\omega$ could have been the tidal interaction between the Sun and the young Moon: at $L_R > R_0$, Sun's tidal effect on Moon's revolution angular velocity must have been greater than on the angular velocity of Earth's own revolution.

Due to the law of the kinetic momentum conservation in the (3.1) system, a decreased angular velocity of Moon's revolution around Earth should have unavoidably resulted in an increase of Earth's revolution angular velocity, that is, $\Omega > \omega_R$ inequality would have occurred. But as soon as Earth's own revolution angular velocity exceeded the velocity of Moon's orbital revolution $\Omega > \omega$, the tidal interaction between the planet and the satellite would have changed their sign for the opposite. After that, Earth would have slowed down, and the Moon would have pulled off from Earth, and that must have saved it from the ultimate destruction.

That was a moment when the real Moon formed on the near-Earth orbit. The event took place approximately 4.6 BY ago at the price of the destruction of a larger mother-planet, the Proto-Moon.

## 3.6 NATURE OF THE PLANETS' AXIAL REVOLUTION AND THE ORIGIN OF METEORITES

Let us now review how unique is the destiny of the Earth–Moon system compared to the other planets. Can it be that the emergence mechanism of this planetary couple is more universal, especially for the planets revolving in the forward direction and possessing their own satellite systems? This is a legitimate question as in the planet formation only due to the direct fall-out of planetesimals (moving along the Kepler's circular heliocentric orbits) only the backward planets' revolution $\Omega < 0$ may occur (Giuli, 1968a,b), that is, the revolution in the same direction as Venus. Just a reminder: if we look at the ecliptic from the Polar Star side, all planets except Venus are revolving counterclockwise. The revolution is called

"forward" if the planets as if are rolling along their orbits around the Sun, that is, if their axial revolution is also occurring counterclockwise. The gravity capture of satellites from the adjacent closely positioned circular orbits usually occurs only in the forward direction (Alven and Arrhenius, 1976). Therefore, their tidal interaction with the central planet must spin it also only in the forward direction as in such a case initially the inequality $\omega > \Omega$ always holds. This inference, as mentioned earlier, was recently confirmed in mathematical modeling of the planetary accretion within a nonuniform protoplanetary cloud (Ohtsuki and Ida, 1998).

Recently, a hypothesis of the so-called mega-impacts became fashionable. Under this hypothesis, the planets acquire axial revolution due to tangential impacts of smaller mass planets with them. The central planet begins to spin and the "projectile" planet either completely merges with it or what remains of the "projectile" converts into a satellite. It is completely unclear why most of the Solar System's planet acquired the forward revolution. The point is that under this mechanism the impacts from either side are equiprobable. Besides, this hypothesis is incapable of explaining why practically all tidally "uninhibited" planets have their axial revolution angular velocities closely coincident with the axial revolution angular velocities of the satellites on their Roche limits (see Fig. 3.3). Indeed, under the mega-impact mechanism of the planetary spinning the velocities of their angular revolution should have been statistically distributed, that is, together with the forward and rapidly revolving planets, backward spinning and slowly revolving planets would exist. And in any case, their axial velocities would not have coincided so in concert with the satellite revolution velocities on the Roche limits (the only exceptions from this rule are Mercury and Venus as their axial revolution is strongly slowed down by the Sun-caused tides).

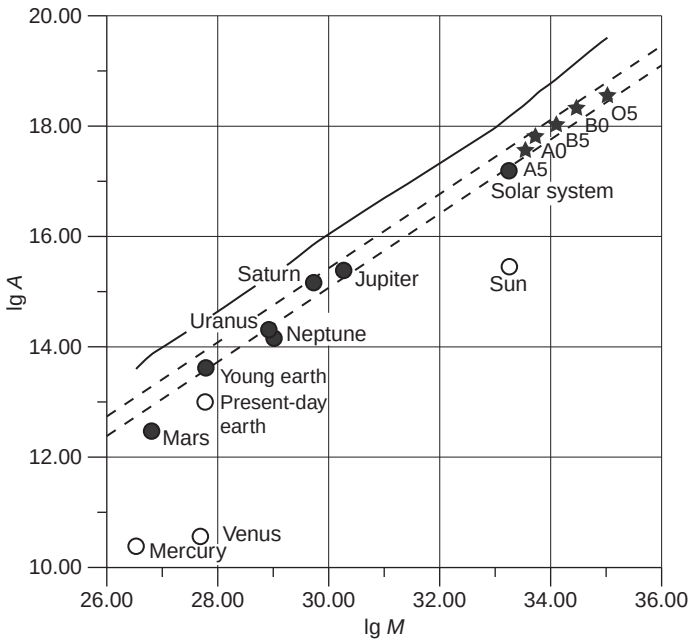


**FIGURE 3.3** Revolution of Solar System planets and some fast-revolving stars versus their mass plotted using Eq. (3.24) (Sorokhtin, 1999; Sorokhtin, 2001a,b): Solid dots are undamped objects; hollow dots are damped objects; and asterisks are stars. The dashed lines are specific momentum $A$ at planets and stars spinning up to the angular velocity of the satellites revolution on the Roche limit versus dimensionless revolution momentum of inertia of the planet (star), its density and the density of satellites destroyed on the Roche limit. The solid line is the maximum value of the momentum $A$ for a case of revolutionary instability of the same planets and stars. The data for the calculation are from the Reference book (Physics of the Cosmos, 1986).

In consideration of the aforementioned, and taking into account the obvious failure of the mega-impact hypothesis, let us see how universal may be the model of planet spinning by their satellites captured by them from the nearby orbits. In such a case, at the capture of a satellite, its orbital revolution angular velocity in the forward direction always turns out greater than the initial axial revolution angular velocity of the planet acquired by it earlier, in the process of its formation as a result of planetesimal fall-out. As a result, under the condition $\omega > \Omega$ and due to the tidal interactions, such satellites must have been gradually approaching their central planets.

When small planetesimals were captured and then fell on the planet's surface their total orbital kinetic momentums were transferred to the central planets. These processes were capable of significantly spinning the central planet. But this could only have continued until the central planet angular revolution velocity reached a maximum velocity determined by the satellite revolution velocity on the Roche limit (as all other satellites with $\omega < \Omega$ would now be repelled from the central planet).

Let us look now into which conditions satisfy the Solar System planets' rotational momentums. Did they correspond to the satellites' revolution velocities on the Roche limits or noticeably exceed them as it was during the planets' spinning to the velocity of their rotational instability?

Empiric data indicate that the specific revolutional momentum $A$ for most of the Solar System's planets is a function of their mass $M$ (Fish, 1967; Hartman and Larson, 1967)

$$A = 1.6 \times 10^{-5}\ M^{2/3} \tag{3.21}$$

$$A = JR_e^2\Omega, \tag{3.21'}$$

where $J$ is the dimensionless moment of inertia of a planet, $R_e$ is its equatorial radius, and $\Omega$ is the angular velocity of planet's own axial revolution. Equation (3.21) was derived by way of averaging the distribution of the real $A$ and $M$ parameters for rapidly revolving Solar System planets (Jupiter, Saturn, Uranus, and Neptune), and also for the summary revolutional kinetic momentum of the Earth–Moon system.

The angular velocity of a planet spun by the dropping fragments of satellites from the Roche limit may be found from Eqs. (3.2) and (3.6)

$$\Omega_R = \omega_R \approx \left[\frac{\gamma(M+m)}{K^3R_0^3}\right]^{1/2}, \tag{3.22}$$

where $K \approx 2.44(\bar{\rho}_0/\bar{\rho}_s)^{1/3}$ is the coefficient in (3.6) determining a relative size of the Roche limit for the given planet and $\gamma = 6.67 \times 10^{-8}$ cm$^3$/g s$^2$ is the gravitational constant. As $m \ll M$ and $\bar{\rho}_0 = 3M/4\pi R_0^3$, Eq. (3.22), taking (3.6) into account, may be rewritten as

$$\omega_R \approx \left[\frac{\gamma 4\pi}{3(2.44)^3}\right]^{1/2} \rho_s^{1/2} = 1.39 \times 10^{-4}\rho_s^{1/2} \tag{3.23}$$

and

$$A = J\left[\frac{\gamma}{K^3(4\pi\bar{\rho}_0/3)^{1/3}}\right]^{1/2} M^{2/3}. \tag{3.24}$$

Equation (3.24) says, in particular, the following. In the absence of the tidal spinning of the planet, of the satellites dropping on the planet, of their fragments and of the matter from the protoplanetary swarm (which is equivalent to the condition $\rho_s = 0$), no regular direct axial revolution $A = 0$ of the planet arises. This is logical: averaging the action of planetesimals dropping onto the planet from the near-Sun swarm (due to the intersection of their orbits with that of the planet, and without their preliminary capture by the planet's gravity field) results in a very slight (close to zero) and reverse own revolution (Giuli, 1968a,b), as in Venus.

Equation (3.23) leads to an interesting pattern. It turns out that the satellite revolution angular velocity at the Roche limit does not depend on either mass or size of the planet but only on the density of the satellites being destroyed. Therefore, both large and small celestial bodies (stars or planets) having been spun to the maximum velocities by the tidal interactions with their satellites of equal density would always have equal angular velocities.

The revolving planet's equatorial radius is found as

$$R_e \approx R_0\left(1 + J\frac{\Omega^2 R_0^3}{\gamma M}\right), \tag{3.25}$$

where the first term in parentheses is an approximate ratio of centrifugal acceleration to average gravity acceleration on the planet's equator. At rotational instability this ratio becomes larger than a one. Therefore, the condition of the planet's stable revolution is as follows:

$$\Omega < \sqrt{\frac{\gamma M}{J R_e^3}} = \sqrt{\gamma \frac{4\pi\bar{\rho}_0}{3(1+J)^3}} \tag{3.26}$$

As we can see from Eq. (3.26), the maximum angular velocity of a stable planet revolution depends on the dimensionless moment of inertia $J$ and average planet's density. The momentum may range between 0.4 and 0.2 ($0.4 > J > 0.2$) depending on the extent of planet's differentiation. The planet's revolutional instability may occur at:

$$\Omega_r > 5 \times 10^{-4}\rho^{1/2} \text{ and } \Omega_r > 9 \times 10^{-4}\rho^{1/2}. \tag{3.26'}$$

Under real conditions, $\rho_0$ and $\rho_s$ are usually commensurate with one another. So, comparing Eqs. (3.22) and (3.26′), we find that the planet's revolution velocity on the Roche limit is lower than its revolution velocity at the rotational instability $\omega_R = \Omega_R < \Omega_r$. Therefore, the destruction of the satellites on the Roche limit cannot cause planet's rotational instability.

Moreover, if even the planet had already been spun to the Roche angular velocity, its differentiation resulting in a noticeable decline of the dimensionless moment of inertia $J$ could have not resulted in the rotational instability. For this reason, all hypotheses of the Moon pullout from Earth ostensibly due to its rotational instability (Darwin, 1965; Ringwood, 1982), are totally inacceptable.

Equation (3.24) was derived on the assumption that the planets spun due to the tidal interaction with their satellites which then are destroyed on the Roche limit. This equation shows that the empiric correlation $A \sim M^{2/3}$ is also confirmed theoretically.

Let us now review this correlation quantitatively.

Most uncertain in Eq. (3.24) is $K$ coefficient which depends on the average density $\rho_s$ of the dropping fragments of the destroyed satellites. When analytically calculating the specific revolutional momentum $A$ versus mass $M$ for the young Earth, one has to keep in mind that under the accepted model a matter dropped off onto its surface which was significantly enriched in iron (compared with the average Proto-Moon composition). One also needs to remember that the young Earth had not yet been differentiated into the mantle and core.

So, we should assume for Earth $J \approx 0.373$; $\rho_0 = 5.52$ g/cm$^3$ and $\rho_s = 4.5$ g/cm$^3$. From these, we find $A_{\text{theor}} = 1.34 \times 10^{-5} M^{2/3}$.

Let us assume for Jupiter the density of the matter dropping from the Roche limit equal to the average density of its present-day large satellites. In this case, $\rho_s \approx 2.12$ g/cm$^3$, besides, $J = 0.262$; $\rho_0 = 1.33$ g/cm$^3$, therefore, for that planet $A_{\text{theor}} = 1.68 \times 10^{-5} M^{2/3}$ (and from empiric data, $A_{\text{emp}} = 1.54 \times 10^{-5} M^{2/3}$).

Similarly, for Saturn $\rho_s \approx 1.27$ g/cm$^3$; $\rho_0 = 0.69$ g/cm$^3$; $J = 0.227$, then $A_{\text{theor}} = 1.75 \times 10^{-5} M^{2/3}$ (and from empiric data $A_{\text{emp}} = 2.05 \times 10^{-5} M^{2/3}$).

On the average, for the young Earth, Jupiter and Saturn $\bar{A}_{\text{theor}} = 1.59 \times 10^{-5} M^{2/3}$. That is very close to the empiric equation (3.21). Such a comparison of $A_{\text{theor}}$ with (3.21) for Uranus and Neptune is not so gratifying due to the uncertainty of major parameters in Eq. (3.24).

Our calculations of $A_{\text{theor}}$ for the young Earth from Eq. (3.24) and the empiric data for the other planets are included in Fig. 3.3. Also, plotted on the graph are the positions of the Solar System's specific revolutional momentum values (actually, of the young Sun prior to its slowing down due to electromagnetic interaction with the primordial protoplanetary cloud). Also, plotted are the values for some young, massive and rapidly revolving stars which we calculated based on the data from the Reference book (Physics of the Cosmos, 1986, p. 20, 51, and 181).

The reviewed celestial bodies differ in their mass by seven orders of the magnitude. But when we compare the data, we see that the theoretical analytical correlation (3.24) we derived based on our hypothesis fairly approximates the earlier found empirical equation (3.21).

This coincidence cannot be accidental. Most likely, it is an indication of a commonality of gravity capture by the planets of their satellites and spinning the planets (and stars) due to the tidal destruction of the satellites at least on the planetary systems formation stage.

Apparently, this is not a universal mechanism as there are planets clearly deviating from this pattern. For instance, Venus revolves slowly and in the opposite direction. Possibly, this was associated with Venus' formation process only on the account of accretion and direct dropout of planetesimals without a gravity capture of the satellites onto its near-planetary orbits. Besides, the Venus revolution currently is clearly slowed down by the Sun tides, and it turned out to be captured even by the tidal interactions with Earth into the resonance state of the second kind.

It is not possible to tell anything definite about the former Mercury's revolution. It is now totally slowed down by the Sun tides and its orbital revolution is strictly resonance: it always faces the Sun with the same side (probably from the very moment of its formation).

The Mars situation is not totally clear at this time. Most likely, because of its small mass only very few large satellites were captured onto its near-planetary orbits in those far-away times. For this reason, it did not have time during its life to spin up to the maximum Roche

velocity. This is supported, in particular, by the position of its satellite Phobos on the Roche limit. The satellite's fate is sealed: it will unavoidably be destroyed or will drop on Mars intact thereby slightly accelerating its axial revolution. It appears that the destruction is already in progress. The indications are groves on Phobos' surface reminiscent of snow avalanche descendance: the upper layers are individual cliffs being torn away, whereas Neptune, most likely, was slowed down by the reverse revolution of its Moon-size satellite Triton.

Two important conclusions follow from the comparison of theoretical calculations with the empiric data. This comparison (see Fig. 3.3) shows their fair match, so:

First, this non-accidental coincidence indirectly confirms a suggestion by Alven and Arrhenius (1976) that the probability of a gravity capture by the growing planets of their satellites from the closest heliocentric orbits is finite. It is impossible to expect that the law shown in Fig. 3.3 would be fulfilled when large planets were spun by oblique planetesimalian impacts ("mega-impacts") without their first having been captured by the gravity field of the central planet because the impacts were randomly distributed on the target surface.

Numerous geochemical evidences (will be mentioned later) are also in contradiction with the "mega-impact" hypothesis. Besides, as mentioned earlier, such mega-impacts without a preliminary gravity capture would most likely result in the inverse rather than direct planet revolution. Moreover, without the concept of the planetesimals and satellites gravity capture by the growing planets (i.e., the planets with increasing mass), it is impossible to explain the emergence of the very same near-planetary swarms of primordial bodies and planetesimals from which the tradition attempts to "create" planetary satellites.

Ohtsuki and Ida (1998) conducted modeling of gravity interactions between multiple bodies within a nonuniform protoplanetary disk around the growing planet. The exercise showed that the gravitational capture at the planet's growth stage may be quite realistic. It usually happens in one (straight) direction and is a major cause of the planet spin.

Second, a conclusion may be made that most meteorites and asteroids, most likely, are small fragments of satellites or even planets that have already undergone differentiation and then been destroyed by the tidal forces after having entered the Roche sphere of more massive planets. This is especially true for differentiated meteorites, such as iron–nickel meteorites. Their matter had undergone deep and complete separation of the elements by their siderophilic properties so it is quite reasonable to invoke a hypothesis of the destruction of a large stratified planet with a metallic core. Such planet may be alike the hypothetical Phaeton (the assumed planet whose destruction gave birth to the asteroid belt between Mars and Jupiter).

Beside iron–nickel meteorites, such "Phaeton" fragments may also include mesosiderites (iron-stony meteorites), usual chondrites of the "mantle" composition and basaltic achondrites. Many such meteorites display the traces of intense plastic deformations and rapid cooling of a hot matter (such was probably the origin of enigmatic spherical granules or chondres). If it was really so then it turns out that most stony meteorites carry in themselves characteristic indications of a catastrophic destruction of planetary size *differentiated* bodies.

The mechanism for throwing out the fragments of such bodies outside of the gravity field of the planet that destroyed them may be the inertia slingshot effect. It occurs when a celestial body of the lunar size runs through the Roche sphere of a much larger planet at a speed close

to parabolic. As Wood (1980) showed, some of the formed fragments assume elliptical orbits around the central planet, and some others are accelerated to the hyperbolic velocity and forever leave its vicinity becoming the eternal wanderers of the Solar system. A similar event was recently observed when the Shoemaker-Levy-9 comet hit Jupiter.

In the period when planets formed around 4.6 BY ago, similar events may have been common. That is exactly why the primary ages of overwhelming number of all meteorites have this age.

So, it is quite possible that the remains of primordial planetesimals that formed the Solar System planets (or rather its external members) are comets. Even the coaly chondrites, as the other meteorites, are probably not the remains of the source (primordial) protoplanetary matter but rather originated on the Solar system's periphery due to the tidal destruction of the external and weakly differentiated planets rich in mobile and volatile elements.

It follows from this, in particular, that it is incorrect to determine the composition of Earth and other Earth group planets directly from the composition of the known meteorites. One has to always remember that the meteorites are not the remnants of primordial protoplanetary matter but are fragments of planets or planet-like bodies which sometimes undergone a deep differentiation.

Later, when determining average composition of the source Earth matter, we will again dwell on this issue.

## 3.7 EVOLUTION OF THE EARTH–MOON SYSTEM

The satellite–planet tidal interaction energy is strongly dependent on the distance between their centers of gravity $L$ and increases in direct proportion with the sixth power of such distance. Thus, any rapprochement between the planets results not only in strengthening of the tides but also in a violent intensification of all tide-associated processes. That is why it is important to determine the major evolutionary patterns of the Earth–Moon system versus time $t$ and the $L(t)$ function.

In general, the sought-for equation for $L(t)$ may be found by integrating (3.20) within the time interval from $t_1$ to $t_2$:

$$L_{t_2}^{6.5} - L_{t_1}^{6.5} = 19.5 \frac{\gamma^{1/2} k_2 m (M+m)^{1/2}}{M Q_\mu} R_0^5 (t_2 - t_1). \tag{3.27}$$

Judging from this equation, the Earth–Proto-Moon rapprochement and the Proto-Moon destruction on the Roche limit were very rapid. Thus, during the Proto-Moon capture on a close near-Earth orbit (let us say, $L \approx 6R_g \approx 38 \times 10^8$ cm), the entire satellite rapprochement process with the Proto-Earth (the quality factor may be assumed analogous to the factor of the present-day cold Moon equal $Q_\mu \approx 5000$) took only 190 MY. The very Proto-Moon destruction on the Roche limit ($L_R \approx 2.7R_g \approx 1.7 \times 10^9$ cm) took no longer than 400–500 years.

The spinning of Earth was also short. Within about 500 years its own revolution velocity increased by more than the factor of 2, from one revolution in 14.5 h ($\Omega_1 \approx 1.2 \times 10^{-4}\ \mathrm{s}^{-1}$) to one revolution in 6 h 10 min ($\Omega_2 \approx 2.828 \times 10^{-4}\ \mathrm{s}^{-1}$). These were just seconds in terms of geological time.

Taking into account the kinetic energy of falling Proto-Moon fragments, the rotational kinetic momentum accrued by Earth was equivalent to a huge energy of $3.8 \times 10^{37}$ erg. Under (3.3)–(3.5), part of this energy $\Delta E_t$, about $1.1 \times 10^{37}$ erg, converted to heat. If uniformly distributed in the entire Earth's volume, it would be sufficient to raise temperature by approximately 160 °C.

The actual heating was less than that, however, as the major effect from the falling Proto-Moon fragments was in the equatorial zone. On impact, heat explosions occurred and even some melting of Earth's surface layers. However, they cooled down rapidly releasing almost all their heat into the outer space in the form of radiation. So, the Proto-Moon catastrophe spun Earth up and somewhat heated it due to the tidal deformations but did not radically affect its external heat balance. It appears that the contribution from the destroyed Proto-Moon and from the dropped-off fragments to the Earth energetics should be attributed to the energy effects of our planet's accretion. These effects are in a general form accounted for in the modern planet-formation theory (see, for instance, Safronov, 1969; Alven and Arrhenius, 1976).

### 3.7.1 Earth's Tidal Quality

We need to calculate the further evolution of the Earth–Moon system and to determine the correlation between the distance $L$ and time $t$ from Eq. (3.27). To perform that, we need first to find out the origin of changes in the tidal (mechanical) Earth quality $Q_\mu$ over the entire evolution of out planet (see Section 2.9 for the definition of the quality factor).

This is a complex problem. But it may be solved at least as a first approximation.

As we showed, the young Earth after its formation was a cold celestial body. Nowhere in its depth had temperature exceeded the melting point of its matter. There were no seas or oceans on its surface at that time. If there was some atmosphere, it was composed almost entirely of nitrogen and very tenuous, with the pressure of about $10^{-3}$ atm. For that reason, Earth's effective mechanical quality factor $Q_\mu$ during that early period (we call it Katarchaean) was relatively high. Remember, seismic data indicate that the rigid oceanic lithosphere has the quality factor $Q_\mu \approx 1000$, the lunar cold upper mantle, $Q_\mu \approx 5000$, and its more heated middle mantle, $Q_\mu \approx 1500$ (Zharkov, 1983). By analogy with the quality factor of cold matter of the lunar upper mantle, we assumed the tidal quality factor of the young Earth at $Q_\mu \approx 5000$. In Katarchaean (4.6–4.0 BY), due to a release of the tidal energy and radioactive decay, Earth matter was being gradually heated up, so the tidal quality factor must have been gradually decreasing, say, from $Q_\mu \approx 5000$ to 1500.

The provided estimate of the Earth quality factor in Katarchaean enables us to determine from Eq. (3.27) that the Moon over that period, due to the tidal interactions with-Earth, was thrown out from the Roche limit (17,150 km) to a distance of up to $L_{4.0} \approx 1.52 \times 10^{10}$ cm = 152,000 km (the subscripts are Earth ages in billion years). The Moon pullout from Earth was nonuniform: first, very rapid, and later, more slow (see Fig. 3.4).

After tectonic activities began on Earth in Archaean, first, the melts in the mantle, then shallow-water seas and later ocean emerged. All these must have resulted in a substantial lowering of Earth tidal quality. The total Earth's quality factor $Q_g$ in Archaean and post-Archaean times may be found as:

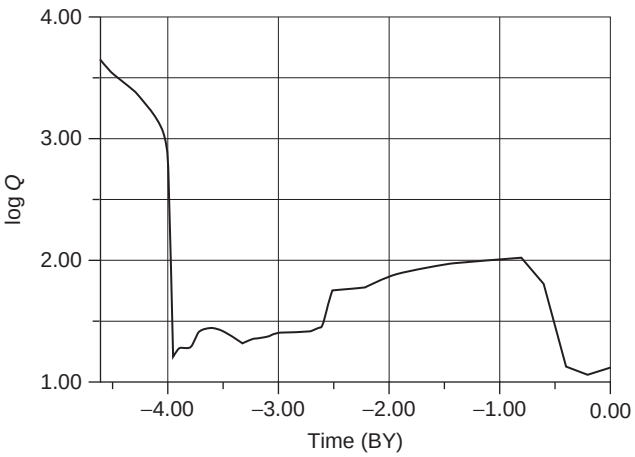


**FIGURE 3.4** Evolution of Earth's tidal quality factor (the factor is reduced to the log-scale).

$$\frac{\sum S_i}{Q_g} = \sum \frac{S_i}{Q_1}, \tag{3.28}$$

where $S_i$ and $Q_i$ are the area and the quality factor of an external geosphere (such as the World Ocean, shallow-water epicontinental and shelf seas, and the convecting mantle underneath the oceans and continents).

During Archaean, the area of the convecting mantle $S_m$ that gradually widened from lower to higher latitudes was, obviously, in proportion with the heat component of the energy $EmT$ released in the mantle. In this case, the area of the tectonically active mantle is determined from:

$$S_m \approx S_g \frac{EmT_{4-t}}{EmT_{2.6}}, \tag{3.29}$$

where $S_g$ is the area of Earth, $EmT_{4-t}$ is the heat energy released in Archaean, $EmT_{2.6}$ is the heat energy released in the mantle by the end Archaean. The area of seas and oceans in Archaean may be presented as a difference $S_{oc} = S_m - S_{cont}$, where $S_{cont}$ is the area of the continental crust. The growth in the continental crust mass and area was determined earlier (Sorokhtin and Ushakov, 1991) and will be described in Chapter 7 (see Fig. 7.4).

After Archaean, the area of deep oceans is determined as a difference $S_{oc} = S_g - S_{cont}$. In Vendian and Phanerozoic, first large marine transgressions occurred. Therefore, the area of shallow-water epicontinental and shelf seas must be taken into account for that time. We estimate from the present-day and paleogeologic data that currently the shallow seas account for 11% of Earth's area, 100–200 MMY ago it was up to 20%, during Paleozoic, 8%, and in Vendian (about 600 MMY ago), no greater than 1%. In Proterozoic, there were practically no epicontinental seas.

The present-day quality factor of the upper mantle under the ocean is close to 150 (Zharkov, 1983), and under the continents, to 500. Considering the overheating of the convecting mantle in Archaean, we assumed its quality factor at 60. Outside the convecting mantle belt, the Earth's quality factor was 1000 as at the end of Archaean. We believe that the oceans' $Q_{oc}$

and seas' $Q_s$ quality factors were in proportion to the water mass concentrated in these reservoirs. Then it turns out that the shallower the marine or oceanic basin, the lower its tidal quality factor. The proportionality factor between the water mass in the ocean or sea, and their quality factor may be determined from Eq. (3.28). At that, we need to take into account that the present-day Earth's tidal quality (determined by MacDonald (1964b), based on the Moon from Earth pullout speed, at $Q_{g0} \approx 13$. In this case, $Q_{oc} \approx 3.66 \times 10^{-21}\, m_{oc}$ and $Q_s \approx 3.66 \times 10^{-21}\, m_s$, where $m_{oc}$ and $m_s$ are, respectively, water masses in the oceans and shallow seas expressed in grams (the water accumulation in the World Ocean is reviewed in Chapter 11 and is shown in Fig. 11.4).

So, derived model of Earth tidal quality factor evolution is shown in Fig. 3.4. As we may see, immediately after the tectonic activity began about 4.0 BY ago and after the appearance of first shallow-water marine basins in Early Archaean, the Earth tidal quality factor drastically declined (by about the factor of 60). Subsequently, the hydrosphere played a major role in dissipating Earth's tidal energy.

As the water mass in the oceans grew, the tidal quality factor increased. The reason was that less tidal energy was dissipated in the deep ocean that it was in the shallow seas. In Archaean and Proterozoic, the continents stood high enough over the ocean surface (Sorokhtin and Sorokhtin, 1997). Shallow-water continental seas did not exist.

However, as the water gradually accumulated in the World Ocean and the continental elevations decreased, by the end Proterozoic (about 600 MMY ago) the ocean surface rose to the average level of the continent stand. After that, marine transgression began and first epicontinental seas emerged.

The tidal energy dissipation in the Earth hydrosphere immediately increased and, as the figure shows, Earth tidal quality factor drastically declined again (by about the factor of 9). The actual quality factor distribution may have been changing in time under a more complex law but its major features, as we believe, are determined correctly.

### 3.7.2 Moon from Earth Removal Speed

Figure 3.5 displays the correlation between Earth and Moon centers of gravity versus-time. It was calculated from Eq. (3.27) and aforementioned model of Earth tidal quality factor. Figure 3.6 illustrates the Moon from Earth removal evolution calculated from Eq. (3.20).

A very important feature of the model is the coincidence of the lunar orbit evolution time with the age of the planets proper. Today, this conclusion is quite natural. Do not forget, however, that the classical models of the Earth–Moon tidal interaction usually resulted in their normal evolution having been too short (about 1.8 BY). The reason for it was that in these models the current low value of the quality factor was extended to the entire Earth evolution.

To get out of this clear contradiction with the age of our planetary system the authors of such hypotheses (first of all, a German geophysicist, Gerstenkorn, 1967) invented very exotic concepts. In particular, Gerstenkorn suggested that originally the Moon revolved in the opposite direction and about 1.8 BY ago approached Earth almost to a distance of the Roche limit but then, after having gone through the polar orbit, its revolutions became straight. After that, it began its pullout off Earth.

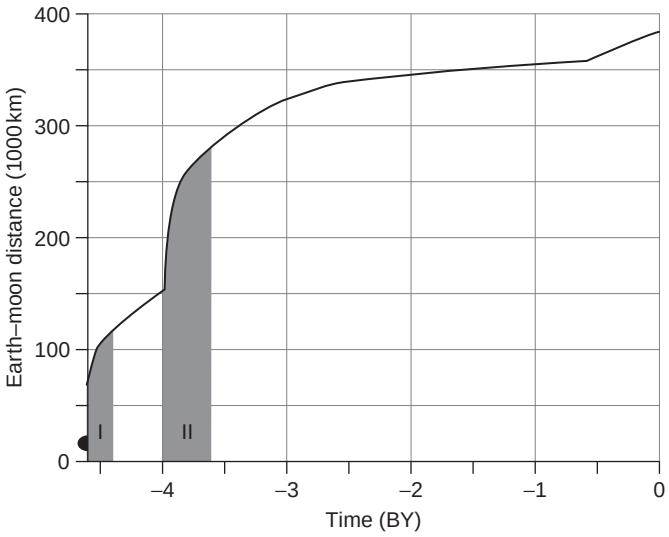


**FIGURE 3.5** Earth–Moon distance evolution. Interval I is duration of the anorthosite magmatism development on the Moon; interval II is duration of the basalt magmatism development on the Moon (see details in the text).

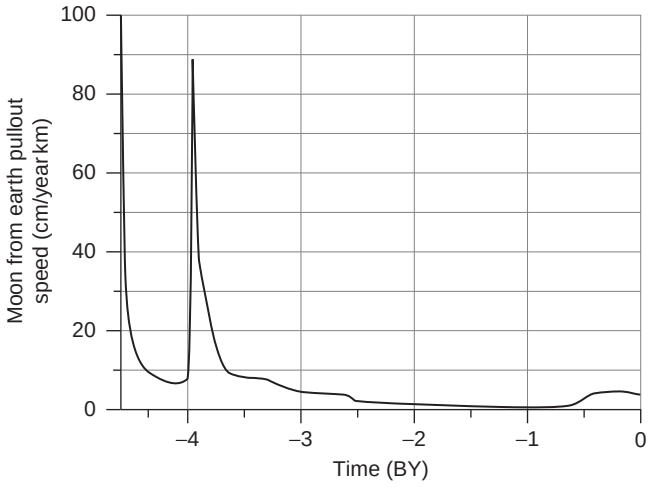


**FIGURE 3.6** Moon from Earth pull-off speed calculated from Eq. (3.20), centimeter per year. Maximum value of 240,300 cm/year (or 2.403 km/year) was reached about 4.6 BY ago; in 1 MMY it decreased to 7.54 m/year, in 10 MMY, to 1.09 m/year.

A well-known American geophysicist, Munk (1968) provided a vivid description of the hypothetical "Hernstenkorn event." In his estimate, during the short period of the closest Earth–Moon approach the oceanic tides must have reached the height of 1 km, and every 2.5 h they would attack the continents denuding them. The energy of lunar tides dissipation at that period would be so high that all Earth oceans would have boiled out and formed a thick water vapor atmosphere around Earth. In view of the greenhouse effect, the near-surface temperature would have risen to 500 °C, and all indications of life would have been eradicated. We may add to this terrifying picture that under temperatures so high carbonates (limestones and dolomites) would have almost totally dissociated releasing enormous

amounts of carbon dioxide into the atmosphere. It would have led to the emergence of a Venus-like *irreversible* greenhouse effect with the near-surface temperature on the order of 500–600 °C.

Undoubtedly, such a catastrophe could not but have left the indelible footprint in the geological record. But no such traces were discovered. And we are now living under comfortable climatic conditions rather than in a "steam boiler." This is a convincing evidence in favor of the fact that the "Gernstenkorn event" have never happened, and a beginning of the Earth–Moon system's normal evolution coincided with the timing of its formation as of a dual planet system 4.6 BY ago when there were no oceans on Earth.

Another thing worth mentioning is nonuniformity of the Moon pullout from Earth (see Figs. 3.5 and 3.6). The Moon was pulling away from Earth at its fastest in the very beginning of its evolution (immediately after the destruction of its mother-planet Proto-Moon) about 4.6–4.4 BY ago. A second substantial impulse to a drastic pullout speed increase occurred at the boundary of Katarchaean approximately 4.0 BY ago. And at last, a third, although a much slower one happened in Phanerozoic. Only the first impulse is connected with a small initial distance of their formation (remember that the Moon from Earth pullout speed, under (3.20), is in the inverse proportion of the distance to a power of 5.5). The origin of the second impulse was associated with the emergence in the deep Earth of the first rock melts (asthenosphere) and, as a result, with the mantle degassing and the formation on the Earth surface about 4.0 BY of the first shallow-water seas. The third impulse was also caused by purely earthly reasons. It was the raise of the growing ocean surface and of the flooding nearly 0.6 BY ago of the average level of the continental shelves. That resulted in the formation during Phanerozoic of large and also shallow-water epicontinental seas which lowered the Earth's effective quality to 13 (Macdonald, 1975). That time, however, the Earth–Moon distance was quite great so the pullout speed was relatively slow, about 2.5–3.4 cm/year.

It is interesting that the tidal interactions between Earth and Sun (where Earth plays a role of the satellite) lead to similar results. For instance, let us in Eq. (3.20) the Sun's mass $M_s = 1.99 \times 10^{33}$ g instead of the Earth's one, and the Earth's mass $m_g = 5977 \times 10^{27}$ instead of the lunar mass, the Sun–Earth distance $L_{sg} = 150 \times 10^6$ km $= 1.5 \times 10^{13}$ cm, the Sun's radius $R_s = 6.06 \times 10^{10}$ cm and the lowermost quality factor of the Sun's ionized gas shell $Q_s \approx 1.3 \times 10^{-4}$ we find that $\dot{L} \approx 4.81 \times 10^{-7}$ cm/s $\approx 15$ cm/year. That is exactly the value of the experimentally determined (2004) Earth from Sun distancing. We took into account the Earth distancing from Sun due to the Sun's radiation mass loss but this effect is much smaller than that of the tidal interactions.

The provided description of the Earth–Moon system evolution is based on the problem's solution under the Kepler approximation. It does not take into account the role played by the system's orbits disturbances caused by the Sun. Recently, such a consideration was given by Avsyuk (1996) who showed that due to the position difference in the center of gravity of the Earth–Moon system and Earth's center of gravity, the system is as if being rocked by the solar pull. As a result, the lunar orbit expands and contracts with a period of about 200 MMY and amplitude of a few Earth's radiuses. So, a monotonous Moon from Earth pullout curve (Fig. 3.5) should be modified in the second approximation by this rocking process.

Let us now check the obtained results against the empirical data. We use data from paleontology. Wells (1963) showed based on the daily micro-lamination of the Devonian corals that a Devonian year had on the average 400 days, and the day duration was no more than 22 h. The current geochronology scale gives the age of 380 MMY to Middle Devonian. Panella (1972) studied the micro-lamination in the Proterozoic stromatolites from the Gunflint Fm. in Canada and found that 2.2 BY ago the year had about 445 days.

The number of days in a year may be determined from Earth revolution angular velocity $\Omega$, for instance, from Eqs. (3.1) and (3.2). In Eq. (3.1), however, the angular velocity participates as a product with the Earth moment of inertia. But the moment of inertia relative to the revolution axis is itself a function of the planet's equatorial radius $I_e = JMRe^2$, and therefore depends on the angular velocity of its revolution ($J$ here is the dimensionless moment of inertia of the planet which describes the degree of its differentiation). So, we have to use an independent way of determining the function $R_e(\Omega)$.

To do this we may use the solution of the Clerot's equation determining the equilibrium shape of revolving liquid (see, for instance, the publication by W. Kaula (1971). We are using here an approximate form of this solution:

$$\frac{5}{2}\frac{\Omega^2 R_e^3}{\gamma M} + \frac{R_0^3}{R_e^3} - 1 = 0. \tag{3.30}$$

And from this we find the sought-for solution:

$$R_e \approx \sqrt[3]{\frac{\gamma M}{5\Omega^2} - \sqrt{\left(\frac{\gamma M}{5\Omega^2}\right)^2 - \frac{2\gamma M}{5\Omega^2}R_0^3}}. \tag{3.31}$$

In this case we can write Eq. (3.1) of the kinetic momentum conservation in the Earth–Moon system, taking into account the Kepler's law (3.2) and the definition of Earth moment of inertia

$$I_e = JMR_e^2,$$

as:

$$JM\Omega\left[\frac{\gamma M}{5\Omega^2} - \sqrt{\left(\frac{\gamma M}{5\Omega^2}\right)^2 - \frac{2\gamma M}{5\Omega^2}R_0^3}\right]^{2/3} + \frac{Mm}{M+m}\sqrt{\mu L} = K. \tag{3.32}$$

The main parameters in this equation were determined earlier and the dimensionless Earth's moment of inertia is found through the evolutionary parameter $x$ introduced by Monin. The evolutionary parameter determines the degree of the planet's differentiation (4.23):

$$x = \frac{M_c}{MC_0}, \tag{3.33}$$

where $M_c$ is the mass of the core and $C_0$ is the total iron and iron oxide ("the core" matter) concentration in Earth. Equations determining the function $x(t)$ are included in Section 5.4, and the diagram $x(t)$ is displayed in Fig. 4.11. The current value of the parameter $x_0 = 0.863$.

As a first approximation for the young Earth we can assume $J \approx 0.37$, and for the present $J \approx 0.33$. Then for all intermediate cases

$$J \approx 0.33 + \frac{0.37 - 0.33}{0.863}(0.863 - x). \tag{3.34}$$

Now we can use Eqs. (3.30) and (3.32) to construct the function $\Omega(t)$, in which the association with time is given through the functions $L(t)$ and $x(t)$ from Eqs. (3.27) and (4.22) to (4.24). Now the number of days in a year is found from:

$$N = \frac{3.1471 \times 10^7}{2\pi}\Omega, \tag{3.35}$$

where the parameter $3.1471 \times 10^7$ is the number of seconds in a year.

Number of days in a year is shown in Fig. 3.7. All empirical data for the determination of the number of days in a year from coral and stromatolite micro-lamination (after Schopf, 1982) are also plotted. They clearly fit the curve. It supports the validity of our results.

### 3.7.3 Evolution of the Lunar Orbit's Position

The reviewed mechanism of the Moon formation indicates that in the beginning its orbital plane must have been positioned strictly in Earth's equatorial plane. At a small distance between the planets, such situation was efficiently maintained stable by the lunar gravity to the Earth's centrifugal equatorial swelling. In this case, if the Moon strayed from Earth's equatorial plane, a pair of the attraction forces would have emerged which would tend to return the Moon back into the same plane. Nevertheless, the lunar orbit is currently inclined at 5° to the ecliptic, and the Earth equatorial plane, at 23.44°.

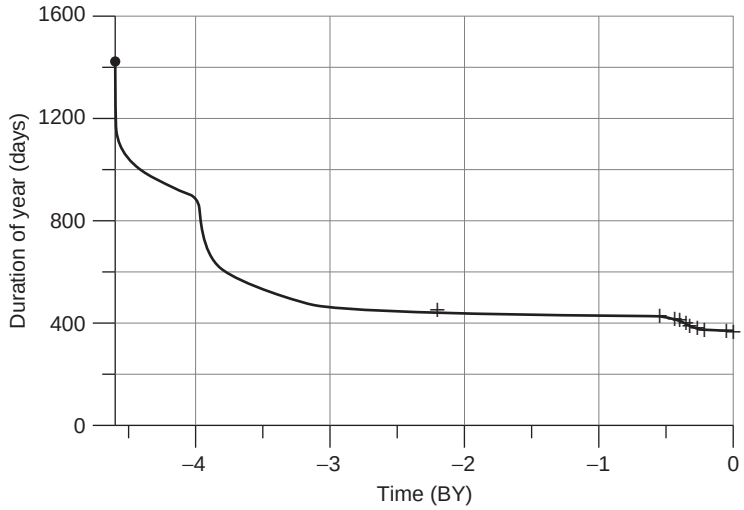


**FIGURE 3.7** Change in year length (days) with the Earth–Moon distance change. The crosses are empiric determination of the year length (in days) from the micro-lamination of Phanerozoic corals and stromatolites of the Gunflint Fm. (2.2 BY ago). After Panelli (1972).

There are two reasons for that:

First, as the Moon was pulling out from Earth, the effect of the Earth's equatorial swelling onto the lunar orbit progressively declined (in the inverse proportion with the sixth power of the distance between them). Therefore, the tidal interaction between the Moon and Sun became relatively stronger. The momentum of the forces acting from the Sun on the lunar orbit and trying to return it to the ecliptic plane increased at that in a direct proportion with the fifth power of the lunar orbit's radius. So, starting at some critical radius of the lunar orbit, the force momentum acting on the orbit from the Sun exceeded the force momentum generated by Earth equatorial swell.

Second, Earth precession angle did not remain constant. It changed due to the continental drift, the supercontinent formation, the emergence of thick ice covers and the action of the lunar–solar attraction on Earth equatorial hump (Sorokhtin, 2006). The total changes in the precession angle could have reached 30°, and the minimum changes, about 5° (see Chapter 14 for more detail).

From this viewpoint, the current 5° deviation of the lunar orbit from the plane of the ecliptic is just a "remembrance" of a distant past when the Moon could have revolved about Earth, possibly, at a higher angle toward the ecliptic but strictly within the Earth's equatorial plane, although it lasted only during the first 100 MMY of Moon's existence.

### 3.7.4 Lunar Geochemistry

The reviewed Moon formation model explains the main geochemical feature of our satellite, namely, a drastic impoverishment of its matter in iron. After the complete melting, differentiation and destruction of the Proto-Moon at the Roche limit most iron were lost due to the fall onto Earth of the Protolunar iron core which immediately followed the destruction of its internal tidal hump. Because of that, the Moon lost most of siderophilic (Ni, Cu, and especially Au, Ce, As, Sb), and chalcophylic (Ag, Cd, Tl, Pb, Zn) elements which transferred to the Protolunar core earlier, at the stage of the planet's melting and differentiation (prior to its destruction).

Lead is very demonstrative in this respect. The astronauts and unmanned cosmic apparatuses brought enough information from the Moon so we now have rather satisfactory data about the lunar rocks composition and geochemistry. According to Mason and Melson (1973), lead in the lunar rocks is mostly radiogenic. This is an indication of the fact that almost all primary lead was lost (due to the evaporation at high temperature) before the Moon formed as a celestial body. The lead currently in the rocks was almost completely generated in the radioactive decay of uranium and thorium.

The quoted authors believe, however, that the loss of the primary lead occurred on the preplanetary stage of the system evolution and was associated with the lead evaporation at high temperatures which, in their view, reigned within the protoplanetary cloud even prior to the planets formation. That would be strange because Earth, formed under the similar conditions, did not lose the primary lead.

Indeed, in the lunar basalts the ratios of the radiogenic lead 206, 207, and 208 formed due to radioactive decay of uranium 238, 235, and thorium 232, to non-radiogenic (primary) lead 204 are extremely high: $^{206}Pb/^{204}Pb \approx 207$; $^{207}Pb/^{204}Pb \approx 100$; $^{208}Pb/^{204}Pb \approx 226$ (Voytkevich et al. (1990)). For the primary lead from iron meteorites these isotope ratios are, respectively, 9.5,

10.4, and 29.5. Average ratios of the same isotopes in Earth rocks (averaged in the oceanic pelagic deposits) are 19, 15.7, and 39.1.

The quoted ratios show that practically the entire lead in lunar rocks is radiogenic. The primary lead was removed prior to the time when the Moon emerged as the satellite of Earth. At the same time, the primary lead in Earth rocks was preserved in great amounts. For this reason, the aforementioned Mason and Melson hypothesis cannot be accepted.

It follows from the review of the lead isotope ratios that during the Proto-Moon melting the lunar matter indeed lost (to the Protolunar core) 96–98% of the primary (non-radiogenic) lead, and almost only the radiogenic lead accumulated in the lunar core and basalts. There is no other way but the total melting of the Protolunar matter, liquefaction of the melts, and transfer of the lead sulfides into the planet core to explain the loss of the primary lead by the lunar matter. The "Diablo Canyon" iron meteorite where the lead isotopes indeed closely correspond to their primary ratios should be viewed as a core fragment of a satellite that, similar to the Moon, underwent the tidal melt, differentiation, and destruction at the formation stage of the Solar System planets.

Therefore, two things follow from the analysis of the quoted lead isotope ratios. First, the ratios practically singularly establish the total melting and differentiation of the lunar matter. Second, they show no less convincingly that Earth had never totally melted and had never been subjected to the equally radical differentiation. Earth core formed gradually, beginning 4 BY ago and henceforth during the entire geological evolution under the barodiffusion mechanism without the melt of silicates and sulfides. On the other hand, lead is a dispersed element. It does not form an independent phase in the mantle matter and usually is a component in the crystalline grids of sulfides and silicates. Besides, both primordial lead and its radiogenic isotopes (those that have time to accumulate by the time of the Earth matter differentiation) were in equal measure transported into the Earth core composition. That is why we observe in Earth rocks intermediate and close to initial (primordial) lead isotope ratios (compared to the similar ratios in the lunar matter).

We emphasize again that from the described view on the Moon origin mechanism, the identified anomalies in the distribution of siderophilic and chalcophylic elements (including lead) are completely understandable. Indeed, the Protolunar core formed only after the complete melt of the entire Protolunar matter. As a result, both liquid iron in an alloy with siderophilic elements and heavy sulfide melts of chalcophylic elements (including PbS), in the course of the density differentiation of melted and overheated Protolunar matter, were flowing under the force of gravity to the planet's center where they formed a heavy Protolunar core.

After the tidal destruction of the Proto-Moon and falling of its almost entire core onto Earth, the remaining lunar matter from the external tidal hump (mostly of a silicate composition) was significantly impoverished in all reviewed elements, including primordial lead (and its $^{204}$Pb isotope). All lithophilic (i.e., gravitating to aluminosilicates) elements transferred into the remaining silicate lunar matter. These elements included uranium and thorium whose decay resulted in the accumulation in lunar rocks of radiogenic lead isotopes $^{206}$Pb, $^{207}$Pb, and $^{208}$Pb.

Earth never melted. Its high-density core began to form gradually, long after the origin of Earth. And not only primordial but also radiogenic lead transferred into the Earth core so moderate lead isotope ratios (close to the primordial ones) were maintained in the Earth rocks.

The planetary melt of the Proto-Moon was accompanied by a substantial overheating of its matter and emergence of intense convective flows in the mantle. That could have resulted in an increased degassing of the Protolunar (lunar) insides and, as a consequence of this process, in the loss by the lunar matter of volatile elements and compounds.

Ringwood (1975a,b, 1979), Mason and Melson (1973), Taylor (1973), and many other experts who studied lunar rocks believe that such Moon impoverishment in volatile elements is a second and very distinctive feature of the lunar rocks. The lunar rocks are exceptionally dry, with the water content of 0.015–0.046%; carbon content in basalts is 0.006–0.007%; nitrogen 0.003%; fluorine 0.015%; chlorine 0.0014%; and so on.

Thus, one of the most indicative features of the lunar matter was the anomalous content of iron, siderophilic, chalcophylic elements, and the loss of volatiles. The other one was its high content of titanium, 4.3–7.4%, which is about one order of the magnitude above its concentration in the oceanic basalts. Beside Ti, lunar rocks display high contents of Cr, Zr, and Y, that is, typically lithophilic elements (Mason and Melson, 1973).

Apparently, this phenomenon may have only one explanation. The Proto-Moon, where magmatic differentiation of the primordial matter was going on, significantly exceeded the Moon in terms of its mass. The Moon proper was formed only from the external tidal hump of the Proto-Moon, that is, from its external portion enriched in lithophilic elements. Ringwood (1975a,b, 1979) and some other scientists studied earlier the occurrence of lithophilic and chalcophylic elements (as well as phosphorus and tungsten) in the lunar rocks and found that the lunar matter differentiation was proceeding within a different and much more massive body. They believed that a large iron core may have been formed in this planetary body. This core should have accounted for at least 26% of the planetary mass and consumed all these elements. Only Ringwood assumed that Earth itself was this celestial body (he, however, suggested totally unrealistic mechanisms of Moon's separation from Earth). In the model we are discussing it was the Proto-Moon.

Both Earth and the Moon originated on the closely positioned initial orbits as a dual planet. Their source was the ring dust cloud of the Solar System. They got their matter from a single source of the compositionally uniform protoplanetary matter. That is exactly why there is close genetic correlation in main petrogenic elements between the earthly and lunar matter (except for titanium which was discussed previously).

It is especially clear on comparison of the lunar basalts from which all excessive ilmenite was subtracted, with the tholeitic basalts of Earth's mid-oceanic ridges. We explain their close genetic affinity in the main rock-forming oxides by the fact that both emerged due to the similar chemico-density differentiation processes in the planet masses of a similar initial composition. The difference was that the differentiation in the Moon was in the environment of a total melt and very rapid (it took just a few thousand years), whereas in Earth the process was evolving without the mantle matter melt (or a partial melt in the upper mantle) and stretched for 4 BY.

Nevertheless, a drastic difference in the differentiation rate of the planetary insides was clearly reflected in the particulars of the potassium/uranium and potassium/thorium ratios in the lunar and earthly basalts. Lunar basalt analyses from the Sea of Tranquility indicate the noticeably low potassium/uranium ratios $K/U \approx 2.3 \times 10^3$ and potassium/thorium ratios $K/Th \approx 0.72 \times 10^3$ compared with the present-day earthly analogs, respectively $(8.3 \div 16.6) \times 10^3$ and $(2.1 \div 2.8) \times 10^3$.

The reason for this is as follows. Thorium and uranium are more mobile elements. In the course of a long differentiation of the Earth matter, which was occurring simultaneously with the formation of the continental Earth crust, they to a greater extent moved from the mantle to the crust. At the same time, the lunar basalts inherited the initial K/U and K/Th ratios. In this form, they were preserved even in Katarchaean after the lunar crust solidified, and subsequently was changing with time only depending on the different decay rate of U and Th.

We may notice here in-passing that, based on the lunar rock geochemistry and in particular lead isotope ratios, we cannot accept the so-called "mega-impact" or "macro-impact" origin of the Moon from fragments of the Earth mantle thrown out into the near-Earth outer space by tangential impacts of planetary bodies in the process of Earth formation. Indeed, in such a case the lead isotope ratios in the lunar and earthly rocks would be the same.

### 3.7.5 Evolution of Lunar Magnetism

Simultaneously with the Proto-Moon formation or capture, a number of smaller satellites or micro-moons could have emerged, also revolving around Earth. All those satellites and micro-moons surrounding Earth, like the Moon itself, experienced the effect of Earth tides. After the destruction of the Proto-Moon and emergence of the Moon, Earth had the maximum angular revolution velocity in the entire geocentric planetary–satellite system. Therefore, beginning at that time all satellites in the system, large as well as small, became repelled by the tidal interactions away from the central planet. As Eq. (3.20) shows, the speed of a satellite pullout from Earth was in proportion with its mass. So, massive satellites, and first of all, the Moon were pulling out faster than the smaller ones.

This resulted in the "sweep-out" of the smaller celestial bodies by the large satellites from the near-Earth outer space. The smaller bodies could not but fall onto the surface of their more massive neighbors when their orbits closely approached or intersected.

It is only natural that the Moon, being the most massive satellite–planet, "swept out" the entire content of the near-Earth satellite swarm more efficiently that the other bodies. That was especially so in the periods of its most rapid pullout from Earth at the dawn of the system evolution in Katarchaean and Early Archaean. Therefore, the most frequent collisions between the Moon and the swarm bodies must have occurred within the two relatively brief time intervals between of 4.6–4.4 and 4.0–3.6 BY ago (Fig. 3.5).

Simultaneously with the Moon, the orbits of all other swarm bodies expanded at the rates in proportion with their mass. Thus, by the time of the collisions with the Moon more massive satellites pulled out from Earth farther than the smaller ones. So, in Katarchaean the Moon must have collided with bodies of a small or medium mass, whereas on the second pullout stage (in Early Archaean) the collisions must have been with the largest and most massive of the remaining satellites which by that time also grew by the absorption of smaller bodies from the satellite swarm.

We now review the consequences for the Moon from such bombarding of its surface.

So, under our hypothesis the Moon was formed out of the melted and strongly overheated matter from the external tidal hump of the originally larger planet. This planet, the Proto-Moon, was destroyed on the Earth's Roche limit. Because of that, the Moon's insides remained overheated and melted for a long time. The primordial melts may still

remain in its central part. Moon's total melt led to the efficient gravity differentiation of the lunar matter. As a result, the upper layer, about 80-km thick, turned out to be composed of lighter rocks—anorthosites (density $\rho \approx 2.7\ \mathrm{g/cm^3}$). Deeper down must have been melted basalt layers ($\rho \approx 2.9\ \mathrm{g/cm^3}$) underlain by the ultrabasic (komatiite) composition melts, and with a remainder of the iron–nickel core in the center. It follows that the young Moon had a relatively thin lithosphere which increased in thickness, due to its cool-down, under the known law (Sorokhtin, 1973a,b):

$$H_l = k\sqrt{t}. \tag{3.36}$$

If the lithosphere thickness $H_l$ in this equation is in kilometers and its age $t$ in millions of years, then $k \approx 6$.

From Eq. (3.27), only during the first million years of its existence the Moon pulled away off Earth from a distance of about 17,000 to 60,000 km, that is, by 43,000 km. The lunar lithosphere at the time was no thicker than 6 km. So, all falling meteorite bodies of about 1 km in size easily cracked the primordial lunar crust and punched it through thereby opening the way for its sub-lithospheric melts to the surface. As we have already mentioned, the uppermost layer of the melts was at that time composed of the lightest derivatives of the primordial matter, that is, anorthosite magmas. And these magmas erupted then on the lunar surface.

The further Moon pullout from Earth was also accompanied by the simultaneous and gradual increase in the thickness of the lunar lithosphere. As a result, ever larger celestial bodies were able to crack it and punch through it. Their size must have been on the order of tens of kilometers. Most of the smaller bodies from the near-Earth satellite swarm left on its surface only traces of their falls, the impact craters of various sizes.

High intensity of anorthosite magmatism at the first stages of the Moon existence was promoted by a rapid change in its surface. Thus, near the Roche limit the shape of the Moon was a stretched ellipsoid with the long axis (directed toward Earth) almost twice the satellite width. Therefore, the lunar tidal humps at that time reached incredible 1300 km. As the Moon pulled out from Earth, its shape rapidly approached a spheroid. In about 200 MMY the tidal humps declined in size to 0.5 km.

This strong change in the lunar surface curvature over a relatively short time must have unavoidably resulted in the intense splitting and breaking of its young lithosphere. Lighter sub-lithospheric melts, that is, the same anorthosite magmas, were profusely fed through the splits and fractures to the lunar surface. That is why, as Ringwood (1975a,b, 1979) graphically noted, the anorthosite magmatism literally raged at the very earliest stages of the lunar evolution. The isotope age determination of lunar crust rocks (Tera and Wasserburg, 1974, 1975; Tera et al., 1974) indicates that it happened about 4.6–4.4 BY ago (see Fig. 3.5).

In about 200 MMY after its formation the Moon pulled out from Earth to a distance of close to 118,000 km. By that time, the thickness of its lithosphere increased to 70–80 km. Practically the entire upper layer of the anorthosite melts cooled down and completely crystallized turning into a solid anorthosite (so-called "continental") lunar crust. Just at that time, 4.4 BY ago, the lunar anorthosite magmatism almost completely stopped although the lunar crust continued to be underlain by the "magmatic ocean," although now it had only basalt composition.

A second impulse of the lunar magmatism 4.0–3.6 BY ago coincided with the second accelerated period of the Moon from Earth pullout. That time, as we have already mentioned, the increased tidal interaction between the planets was caused by purely earthly events. These events were the beginning of Earth tectonic activity and the emergence on its surface of shallow seas and ocean basins. However, the chemistry of the lunar magmatism was now totally different.

The event occurred 600 MMY after the Moon formation, at the Katarchaean/Archaean boundary. As during the first period, the Moon, due to its large mass, must have been, under Eq. (3.20), pulling at a great speed from Earth and sweeping out of the near-Earth outer space all other remaining satellites of a smaller mass. Some of such satellites might have however been preserved at that time on the external near-Earth orbits (at distances of 150,000–300,000 km). As was mentioned, during the time since the Moon emergence all largest bodies from the near-Earth satellite swarm, due to the tidal interaction with Earth, must have moved to the periphery of the system. If so, the most massive satellites and micro-moons of the near-Earth satellite swarm must have concentrated within the noted distance interval.

The time period between the origin of the Moon and the beginning of Archaean was about 600 MMY. During that period the lunar atmosphere increased in thickness to approximately 120–140 km. Only large celestial bodies, at least 100 km in size and with the mass of $10^{20}$–$10^{21}$ g could punch through this lithosphere. We believe that in the beginning of Archaean up to 10 or 12 such satellites beside the Moon were revolving about Earth on the external geocentric orbits.

As the Moon swept out these more massive satellites some of them fell on the lunar surface. They punched not only through the anorthosite crust but through the underlying gabbro layer. That opened a way to the surface for the sub-lithospheric basalt magmas. Basalt eruptions from the so formed impact craters and their feathering faults created the well-known pattern of the basalt covers in the lunar "seas." The so-called lunar mascons (abnormally heavy masses underneath the craters of the lunar "mares") may be associated with the invasion of the basalt masses into the satellite-punched holes in the anorthosite crust. These anomalies are generated by the excess density of basalts ($\rho \approx 2.95$) compared to lighter anorthosites of the lunar crust ($\rho \approx 2.7$–$2.75$). The absolute geochronology of lunar samples (Jessberger et al., 1974; Tera and Wasserburg, 1974, 1975; Tera et al., 1974) indicates that the impact crater formation and their fill-up with basalts occurred during the period of 4.0–3.6 BY ago which was totally coincident with the beginning of tectonic activity on Earth (see Fig. 3.5). And that is exactly what follows from the discussed origination and evolution of the Earth–Moon system.

It is noteworthy that the dropout of large satellite bodies on the lunar surface could have occurred only from one frontal side of Moon (in the direction of its revolution around Earth). For this reason, the basalt eruptions with their underlying mascons must have occurred only in one lunar hemisphere. The effect of the Earth's gravity on the shift of the satellite's center of gravity relative to its geometric center resulted in a gradual rotation of the Moon's body so that all basalt eruptions and mascons eventually turned out to be concentrated on one side facing Earth. At the same time, no basalt eruptions ("lunar mares") must have been on the opposite side. It appears that this coincidence was first noticed by Khain (1977).

It is important that the differentiation of the lunar matter which gave birth to the Early Archaean basalt eruptions occurred not at the time of the eruptions but much earlier, about 4.6 BY ago, that is, at the time of the Moon formation (Ringwood (1975a,b, 1979)). This conclusion is based on isotope composition of lead and on rubidium/strontium ratios. The conclusion is that the basalts of the lunar mares indeed were erupted on the lunar surface due to the integrity disruption of its lithospheric shell and opening of the "magmatic windows" that existed from the moment of the Moon formation, as it follows from our hypothesis of its formation.

After a second accelerated Moon pullout from Earth its motion became more quiescent (see Fig. 3.5). By about that time (3.2 BY ago) the "micro-moons" totally disappeared from the near-Earth satellite swarm. As a consequence, the bombardment of the lunar surface by the former Earth satellites stopped. Since then only the meteorite bodies whose orbits by accident intersected with our two planets fell on the Moon and Earth. So, the lunar magmatism stopped about 3.5–3.2 BY ago, and the Moon became a tectonically dead planet.

In conclusion of this section, we would like to draw the reader's attention to the two important circumstances related to Earth tectonic evolution in Katarchaean and Archaean.

First, the fact that meteorite bodies and even medium size satellites profusely fell on the Moon's surface does not mean that Earth was also subjected to such bombardment in Katarchaean and Archaean. The opposite is true. Only those celestial bodies from the near-Earth satellite swarm fell on the Moon which, due to their tidal interaction with Earth, must have moved out of it but not have fallen on the lunar surface.

Second, after a long hiatus of about 600 MMY the lunar surface was bombarded again, this time by large celestial bodies. It caused a flare-up of the basalt magmatism on the Moon. This flare-up clearly marked Earth transition from a tectonically passive state in Katarchaean to its active tectonic evolution in Archaean. In fact, the basalt magmatism on the Moon is clearly marking a beginning of the tectonic activity on Earth.

## 3.8 PRIMORDIAL EARTH COMPOSITION AND STRUCTURE

As mentioned in Section 3.1, Earth was formed due to a homogenous accretion of a cold protoplanetary dust cloud. At the pre-accretional stage, that cloud underwent a very strong differentiation affected by the solar wind, light pressure, short-lived temperature rise, and magnetic separation. As a result of such differentiation of the protoplanetary matter, all gas components of the source matter were removed from the primordial cloud in the Earth and Moon formation zone. The source matter was drastically impoverished in hydrosilicates, carbonates, and sulfur as well as bases and some other easily fusible elements.

A hypothesis of Earth and other Solar System planets origin was first proposed by Schmidt (1946) and developed in detail by Safronov (1969). It was very fruitful in explaining the planet-formation mechanism and in studying Earth evolution on its planetary stage. These publications were stage-setting and exceptionally important as they defined the initial conditions for the existence of our planet.

In particular, two conclusions of the planet-formation theory are critical for understanding the future Earth evolution.

First, immediately upon its origin the young Earth was a relatively cold celestial body. Nowhere within it had temperature exceeded the melting point of the Earth matter.

Second, the primordial Earth had a relatively uniform composition. Therefore, there was no Earth core at that time, and there was no chemical stratification into the mantle and crust.

As we show later, the young Earth was also devoid of a hydrosphere and had just a moderately dense (about 1 atm.) atmosphere composed then mostly of nitrogen with some admixture of noble gases (see details in Chapter 13).

If we accept these as initial conditions, then all further Earth evolution (of its core, mantle, crust, hydrosphere, and atmosphere) must have been totally defined by the initial composition of the Earth matter, by the planet's initial stored heat, and as we have already seen earlier, by the history of its interaction with the Moon. It is assumed here that the endogenous energy sources in fact controlling the entire global evolution of Earth (gravity differentiation of the Earth matter and energy of radioactive decay) eventually were also defined by Earth initial composition.

So, we shall start indeed with the composition of the primordial Earth matter.

### 3.8.1 Composition of Primordial Earth

Average composition of the Earth matter from major petrogenic oxides and elements may be determined by conceptually mixing the matter of the major geospheres, that is, the mantle, crust, and core (the core composition was detailed in Section 2.6). See the results of such calculation in Table 3.1 in comparison with the compositions of the modern crust, mantle, core, and stony meteorites.

As Table 3.1 shows, the primordial Earth matter was a clearly expressed ultramafic rock with a low silica saturation factor (similar to that of olivine) and high relative dual valence iron content. Therefore, the primordial Earth matter had a clear ortho-silicate composition and comprised 75% of olivine $(Mg_{0.62}Fe_{0.38})_2SiO_4$, 11% of other silicates, and 13.6% of kamacite $Fe_{0.9}{\cdot}Ni_{0.1}$.

These calculations indicate that relative to the average Sun matter composition (therefore, average composition of the Solar System's meteorites and planets) Earth is somewhat enriched in iron and its oxides (by about 50–60%), substantially (by the factor of 10) impoverished in sulfur, by the factor of 4–5 impoverished in potassium and other mobile elements but has oxygen content (relative to silicon) almost equal to average for the Solar System.

It is a much more difficult problem to estimate the contents in the primordial Earth matter of volatile, mobile, and rare (dispersed) elements. Unfortunately, this may be done only using indirect techniques. And the samples of deep rocks collected from the surface are significantly contaminated, still in the process of intrusion or subsequent effects, by the water and dispersed elements getting into them from the external geospheres (hydrosphere or Earth crust).

As an example, deep rocks like kimberlite and lamproites are totally unfit for the determination of the mantle or mantle-contained water composition. The reason is that they and related rocks were generated by sucking-in oceanic deposits of Early Proterozoic oceans to great depths. In effect, these rocks are oceanic deposits remelted and highly metamorphosed

**TABLE 3.1** Composition of the Present-Day Earth and of Primordial Earth Matter

| Oxides | Composition of continental crust[a] | Model composition of Earth mantle[b] | Model composition of Earth core | Composition of Earth primordial matter (calculated) | Average composition of chondrites[c] | Average composition of coaly chondrites[d] |
|---|---|---|---|---|---|---|
| $SiO_2$ | 59.3 | 45.4 | – | 30.71 | 38.04 | 33.0 |
| $TiO_2$ | 0.7 | 0.6 | – | 0.41 | 0.11 | 0.11 |
| $Al_2O_3$ | 15.0 | 3.7 | – | 2.54 | 2.50 | 2.53 |
| $Fe_2O_3$ | 2.4 | 1.97 | – | – | – | – |
| FeO | 5.6 | 6.55 | 49.34 | 22.76 | 12.45 | 22.0 |
| MnO | 0.1 | 0.13 | – | 0.09 | 0.25 | 0.24 |
| MgO | 4.9 | 38.4 | – | 25.81 | 23.84 | 23.0 |
| CaO | 7.2 | 2.3 | – | 1.57 | 1.95 | 2.32 |
| $Na_2O$ | 2.5 | 0.43 | – | 0.3 | 0.95 | 0.72 |
| $K_2O$ | 2.1 | 0.012 | – | 0.016 | 0.17 | – |
| $Cr_2O_3$ | – | 0.41 | – | 0.28 | 0.36 | 0.49 |
| $P_2O_5$ | 0.2 | – | – | – | – | 0.38 |
| NiO | – | 0.1 | – | 0.07 | – | – |
| FeS | – | – | 6.69 | 2.17 | 5.76 | 13.6 |
| Fe | – | – | 43.41 | 13.1 | 11.76 | – |
| Ni | – | – | 0.56 | 0.18 | 1.34 | – |
| Total | 100.0 | 100.0 | 100.0 | 100.0 | 99.48 | 98.39 |

Mass of Earth: $M = 5.9772 \times 10^{27}$ g; mass of core: $M_{core} = 1.9404 \times 10^{27}$ g; mass of internal core: $M_{core1} = 0.1083 \times 10^{27}$ g; mass of transition zone: $M_{core2} = 0.1299 \times 10^{27}$ g; mass of external core $M_{core3} = 1.8321 \times 10^{27}$ g; mass of mantle: $M_m = 4.0143 \times 10^{27}$ g; mass of continental crust: $M_{cc} = 2.25 \times 10^{25} = 0.0225 \times 10^{27}$ g.

[a] *Ronov and Yaroshevsky (1978).*

[b] *Our model using the data from Dmitriyev (1973) and Ringwood (1966).*

[c] *Urey and Craig (1953).*

[d] *"Outlines of comparative planetology." Nauka (1981), pp. 184–185.*

under high pressure. Ultramafic and eclogite xenoliths within them, at close study, turn out to be the fragments of the ancient oceanic crust (eclogites, of the basalt layer, and ultramafics, of the serpentinite layer; see Chapter 10).

All deep rock xenoliths in volcanic lavas must be completely screened off because of uncertainty of their formation history. Probably, only contents analyses of sought-for components in quenching glasses of fresh basalts from rift zones of mid-oceanic ridges (after thermal treatment for the removal of sorbed $H_2O$ and $CO_2$) may be used for these purposes. The contents of radiogenic argon in the atmosphere have to be used to estimate the potassium concentration in Earth.

This analysis is discussed in detail in Section 4.2. Here, we provide just its conclusions.

Compared with the coaly chondrites which are close in composition to the source protoplanetary matter, the Earth matter is impoverished in water by the factor 200–250, in potassium, by the factor of 5–7, carbon, by the factor 1000, and so on. The compounds like methane and ammonia have apparently been completely swept out of the Earth group planetary formation area and therefore have not reached Earth at all. The deficiency in noble gases (except for the radiogenic argon) reaches $10^{-6}$–$10^{-14}$ (Mason, 1966). All these elements and compounds may have reached Earth in small amounts in a bonded state (the water, with hydrosilicates; carbon dioxide, in carbonates, nitrogen, in nitrides and nitrates; etc.). Only minuscule amounts of primordial gases, including the noble gases, may have reached Earth adsorbed on the surface of loose or porous particles of the source protoplanetary matter.

### 3.8.2 Structure of the Primordial Earth

We know the composition of the original Earth matter. We reasonably assume that the young Earth was chemically uniform. So, we can calculate the density distribution in Earth, for instance, from the shock compression data of silicates and iron.

We conducted this calculation for the most likely temperature distribution within the just-formed Earth. See the results of the density distribution estimate, as well as temperature, gravity acceleration, and pressure in Tables 3.2 and 2.13. As seen, there were no separation boundaries except the phase transition zones at depths of 400–700 km. Neither the Earth crust nor mantle and especially core existed on Earth at those distant times. All these geospheres separated much later, in Archaean. Earlier (in Katarchaean) there was just a compositionally uniform Earth subdivided into zones only by polymorphic mineral associations depending on the pressure at a given depth. Earth matter surface density was 3.9–4.0 increasing to 7.2 g/cm$^3$ at the center.

Apparently, the young Earth radius did not significantly differ from its modern value. The reason is that two oppositely directed factors simultaneously affected Earth's size in the process of its evolution.

On the one hand, it was the Earth matter differentiation. It was accompanied by the separation of a high-density core, by pressure increase in Earth's central portion and by the gravity acceleration redistribution in its insides. These factors tended to a decrease in Earth volume, and its radius by 150–200 km.

On the other hand, the density of Earth's upper layers must have noticeably decreased after the differentiation (from 3.9–4 to 3.3 g/cm$^3$). This would have decreased pressure in the upper mantle and increased the depth to major phase transition boundaries in the underlying Golitsin layer. That must have resulted in Earth expansion (Table 3.2 does not include the shift in phase transition boundaries). A similar effect occurred due to additional heating of Earth's insides by about 1000 °C. A composite expansion from these two actions was also approximately 150–200 km.

We estimated the primordial Earth's radius at 6370 km.

An important factor is that not only the temperature inside Earth rose during its global evolution (see Fig. 4.2) but so did the pressure (see Fig. 3.8). The latter was undoubtedly associated with the core separation. See Fig. 2.13 for density distribution within the young and present-day Earth.

**TABLE 3.2** Density, Temperature, Pressure, and Gravity Acceleration Distribution in the Young Earth[a]

| Depth (km) | Density ($g/cm^3$) | Temperature (K) | Pressure (kbar) | Gravity acceleration ($cm/s^2$) | Depth (km) | Density ($g/cm^3$) | Temperature (K) | Pressure (kbar) | Gravity acceleration ($cm/s^2$) |
|---|---|---|---|---|---|---|---|---|---|
| 0 | 3.92 | 260 | 0 | 985 | 2200 | 6.15 | 1379 | 1042 | 764 |
| 200 | 4.15 | 1147 | 82 | 980 | 2400 | 6.25 | 1378 | 1133 | 734 |
| 400 | 4.38 | 1385 | 168 | 973 | 2600 | 6.35 | 1377 | 1223 | 703 |
| 400 | 4.50 | 1385 | 168 | 973 | 2800 | 6.44 | 1376 | 1309 | 670 |
| 600 | 4.76 | 1457 | 261 | 986 | 3000 | 6.52 | 1375 | 1393 | 638 |
| 670 | 4.85 | 1294 | 285 | 955 | 3400 | 6.66 | 1373 | 1548 | 569 |
| 670 | 5.02 | 1294 | 285 | 955 | 3800 | 6.78 | 1371 | 1688 | 498 |
| 800 | 5.16 | 1433 | 358 | 941 | 4200 | 6.90 | 1369 | 1810 | 425 |
| 1000 | 5.36 | 1411 | 456 | 921 | 4600 | 6.99 | 1367 | 1912 | 350 |
| 1200 | 5.53 | 1400 | 556 | 898 | 5000 | 7.07 | 1365 | 1995 | 273 |
| 1400 | 5.68 | 1393 | 656 | 874 | 5400 | 7.11 | 1363 | 2057 | 196 |
| 1600 | 5.81 | 1387 | 754 | 848 | 5800 | 7.15 | 1361 | 2097 | 119 |
| 1800 | 5.93 | 1384 | 852 | 821 | 6200 | 7.18 | 1359 | 2116 | 52 |
| 2000 | 6.,04 | 1381 | 948 | 793 | 6360 | 7.18 | 1358 | 2116 | 0 |

[a] *Calculating density, gravity acceleration, and pressure, Earth mass used was* $M = 5.977 \times 10^{27}$ *g, and dimensionless momentum of inertia for a spherical Earth turned out to be 0.374.*

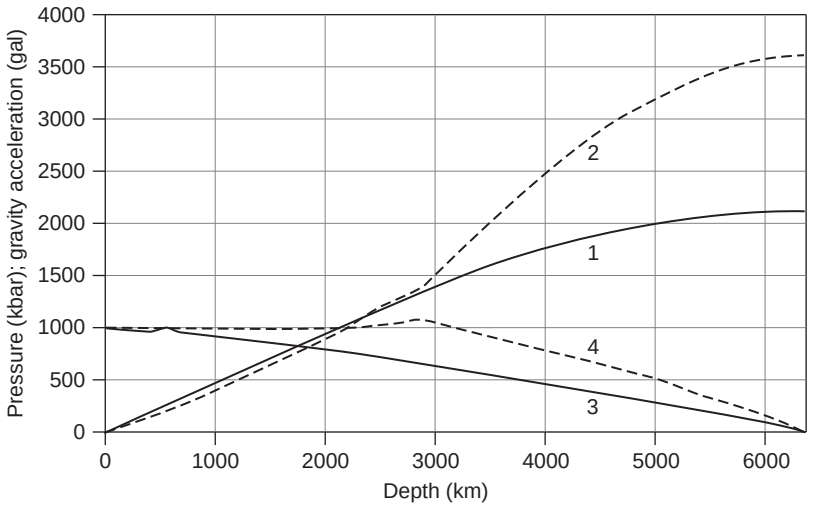


**FIGURE 3.8** Pressure distribution in: 1, young Earth; 2, present-day Earth; 3, gravity acceleration on young Earth; and 4, same, present-day Earth.

Beside the density distribution within the young and present-day Earth, it is useful to know also the heat capacity distribution within the same geospheres (as this parameter is used to calculate the planet's heat content). Estimates of these distributions in the young Earth are shown in Fig. 3.9. For the intermediate Earth evolution stages, we calculated the approximate values of its average heat capacity as follows:

$$\bar{c}_{\mathrm{p}} \approx \frac{M_{\mathrm{G}}}{m_{\mathrm{c}}/\bar{c}_{\mathrm{pc}} + m_{\mathrm{m}}/\bar{c}_{\mathrm{pm}}}, \tag{3.37}$$

where $M_{\mathrm{G}} = 5.977 \times 10^{37}$ g is Earth's mass, $m_{\mathrm{c}}$ is the current value of Earth's core mass, $m_{\mathrm{m}}$ is the current value of the mantle's mass, $\bar{c}_{\mathrm{pc}} \approx 0.622 \times 10^{7}$ erg/g deg is average heat capacity of the core's matter, $\bar{c}_{\mathrm{pm}} \approx 1.12 \times 10^{7}$ erg/g deg is average heat capacity of the mantle, and then $\bar{c}_{\mathrm{p}} \approx 0.889 \times 10^{7}$ erg/g deg.

Earth's surficial layers during almost the entire time of its formation were composed of thinly porous regolite. It was constantly generated from the precipitation of thin dust and condensation of the impact-evaporated planetesimals. The sorption capacity of such ground was extremely high. It actively absorbed that all remnants of the volatiles released in heat explosions of the planetesimals or were captured by the growing Earth from the protoplanetary space, which was almost completely devoid of all its volatiles by the time of Earth origin.

The same goes with currently so common volatiles such as the water or carbon dioxide. The water and carbon dioxide, part of them released when the falling planetesimals evaporated, immediately and actively bonded with the compositionally ultrabasic regolite, for instance, due to serpentinization:

$$4Mg_2SiO_4 + 4H_2O + 2CO_2 \rightarrow Mg_6(Si_4O_{10})(OH)_8 + 2MgCO_3. \tag{3.38}$$

As indicated earlier, the protoplanetary matter in the Earth formation zone was already impoverished in $H_2O$ and $CO_2$. Thus, serpentinization and other similar regolite hydration reactions almost entirely absorbed and buried under new layers of Earth matter almost all water and carbon dioxide arriving on Earth. Only heavy noble gases (Ne, Ar, Kr, and Xe)

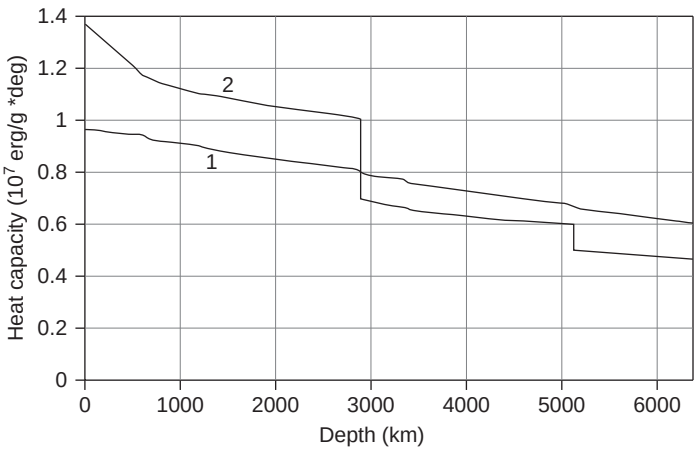


**FIGURE 3.9** Accepted heat capacity distribution within Earth: 1, Young Earth and 2, Present-day Earth.

arriving in very small amounts (possibly with the solar wind) and some amount of the inert nitrogen may have been preserved as gases in the Proto-atmosphere of the young planet.

Sometimes, noble gas isotope ratios are used for a proof of catastrophic events that ostensibly happened with the young Earth and led to its early heating and differentiation. Excessive amounts of radiogenic xenon $^{129}Xe$ in the atmosphere are especially demonstrative in this respect. However, as we will show in the next Chapter, this fact is no indication of the early catastrophic differentiation but is just a degassing result of the planetesimals dropping on Earth.

The above theoretical discussion and calculations lead to an important geological conclusion. The primordial Earth did not have hydrosphere, and its atmosphere could not have been high density and was comprised, most likely, of nitrogen with a small admixture of noble gases. The hydrosphere and high-density atmosphere appeared later, about 600 MMY after the formation of Earth.

## 3.9 YOUNG EARTH: ENERGETICS AND HEAT REGIME

Temperature distribution within the primordial Earth may be estimated only theoretically, based on the ideas about the Solar System planets formation. Such estimate for the reviewed Earth formation model due to accretion of a cold protoplanetary dust cloud was performed by Safronov (1969).

Under this model, most of the growing Earth heat energy was generated in its depths through transfer to heat of kinetic energy of falling planetesimals. Another substantial energy source was Earth tidal interaction with the Proto-Moon and Moon.

Total energy of Earth accretion is huge (see Section 5.1). It would be sufficient to totally evaporate Earth matter and heat the formed plasma to 30,000 °C. However, the accretion energy was released within the near-surface portions of the growing planet, and the generated heat was easily lost with the heat radiation into the outer space. The fraction of the lost heat was substantially dependent on the planet accretion rate and sizes of falling planetesimals.

Theory shows that simultaneously with the growth of the Proto-Earth the size of the planetesimals and energy of their fall on Earth surface also increased. By force of this pattern, temperature within the young Earth grew from the center out but near the surface it declined due to a faster cool-down of its near-surface parts. In such a situation total heat reserves of the young Earth and, hence, temperature distribution in its depths were completely determined by the planet's growth rate.

All hypotheses assuming a short planet accretion (on the order of ten or several tens of millions of years) and overestimated depth of Earth matter stirring on impact from planetesimals required melting of Earth in the process of its formation. For this to happen it was necessary to assume that Earth overheating at that time reached several thousand degree Kelvin (Earth matter melting temperature rapidly increases with depth and at the core depth significantly exceeds 6000–7000 K). However, if it had so happened then a rapid matter differentiation would have occurred (as in the Proto-Moon) and added substantial energy to Earth melting. As a result, in the very beginning of Earth evolution (about 4.6 BY ago) a high-density iron core would have separated, a thick melted layer of

anorthosite crust would have formed, and the early Earth matter degassing would have happened with the formation of a fluidal water–carbon dioxide atmosphere.

If a thick (up to 80 km) and relatively light (2.7 g/cm$^3$) anorthosite crust had indeed separated 4.6 BY ago, it should have been preserved on Earth forever (it is required by the Archimedes law). No indications of such crust or other traces of an early planetary catastrophe were found on Earth despite numerous attempts by geologists. As mentioned earlier, geological data testify to a gradual Earth crust formation, and it began approximately 3.9–3.8 BY ago. Moreover, if indeed a metallic core had separated, and a thick anorthosite crust had formed 4.6 BY ago then, as on the Moon, most radioactive elements would have transferred to this crust. After that Earth, deprived of all energy sources, would have turned into a tectonically dead planet like the Moon.

The planetary formation hypothesis reviewed here was developed by Safronov (1969) based on Schmidt (1948) also leads to the conclusion of a relatively "cold" Earth origin. Safronov estimated that the Earth's formation time took at least 100 MMY so that its insides always remained below the melting temperature of the Earth matter. And the temperature distribution within the young Earth significantly depended on the mass of planetesimals that formed the planet in the accretion process.

Based on that, Safronov provides two extreme cases of the temperature distribution within the young Earth (Fig. 3.10).

One of them assumes the planet growth due to accretion of small bodies and particles. Temperature gradually increases from 300 K near the surface to 800 K in the center of Earth. Another one assumes that the size of planetesimals falling onto the growing Earth gradually increased, and the young Earth temperature increases with depth then declines again toward the center. Under this case, the young Earth temperature reached its maximum of 1600 K at a depth of around 800 km and declined again to about 800 K in the center (Fig. 3.10). Under the second distribution, the temperature rapidly increases from 300 to 1400 K at a depth of about 800 km then smoothly increases to 1500 K in the Earth's center (Vityazev et al., 1990). Now we find out (see Section 3.2) that additional $1.25 \times 10^{37}$ erg of the tidal energy was released during the gravity capture of the Proto-Moon, and this energy

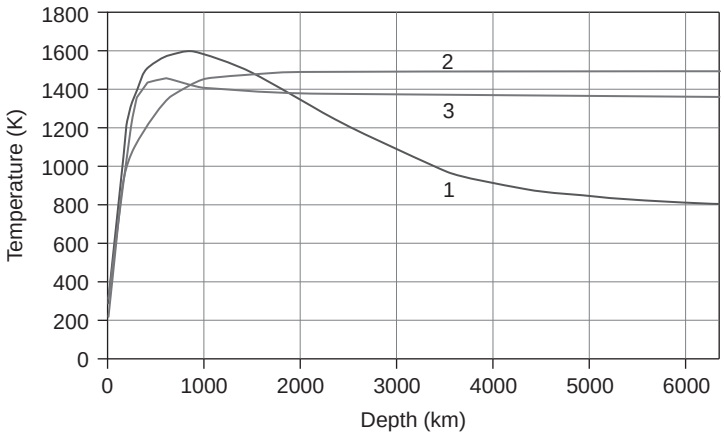


**FIGURE 3.10** Temperature of young Earth: 1 and 2, Max distributions of Earth's initial temperature: 1, after Safronov (1969) accounting for the body impacts (first, small, and later—larger); 2, after Vityazev et al. (1990) accounting for the large body impacts at the start of Earth's accretion; 3, accepted initial temperature distribution in young Earth constructed in consideration of its energy balance.

was mostly released in the near-surface portions of the young planet having raised their temperature by 500–600 °C.

Safronov in his calculations did not take into account the energy of the Proto-Moon–Proto-Earth tidal interaction. Besides, he significantly overestimated Earth heating due to radioactive decay. For these reasons this writers had to introduce some corrections into his distributions.

We assumed that the tidal deformations are in proportion with the tide-forming potential, which in turn is proportionate to the squared radius of the sphere being deformed. We estimated that the total radiogenic heating of the young Earth over the time of its formation, based on our estimates of the Earth matter radioactivity (Section 5.2), did not exceed 30–50 °C.

The resulting initial temperature distribution in the young Earth is somewhat below Safronov's distributions but its shape is intermediate between the two extreme distributions.

A test of the derived temperature distribution may be performed based on Earth energy balance by way of calculating the upper mantle temperature during Archaean and comparing it with the experimental komatiite lava melting temperatures.

Such a calculation (see Section 4.3, Fig. 4.4) showed a fair match of the theoretical temperatures with the experimental data. That indicates that the derived initial distribution of the young Earth temperature is fairly reflecting real life.

## 3.10 PRE-GEOLOGICAL EARTH EVOLUTION IN KATARCHAEAN

The structure, composition, heat status, and the "tidal tectonics" were drastically different from all subsequent stages of Earth's geological evolution. For this reason, that unique epoch, about 600 MMY in duration, from the moment of the planet's birth approximately 4.6 BY ago through the beginning of Early Archaean, should be identified as an independent chapter in Earth's evolution.

So far, there is no commonly accepted term for this period in the geological nomenclature. Sometimes, the epoch from Earth origin through Archaean is called "lunar." As we, however, tried to show, such term is totally unacceptable for Earth. In substance, this epoch may be called pre-Archaean. However, long time ago, in 1893, a Swedish geologist Sederholm introduced the term "Katarchaean" with about the same meaning—below the Archaean, that is, prior to Archaean. At that time, the concept of Archaean was not well established and understood as the age of the oldest granite–gneiss complexes of Scandinavia.

It was found later that Archaean should be extended to at least the ages of 3.8 BY (including, for instance, the Isua Iron Formation in the Western Greenland). After that the term "Katarchaean" was used as the synonym of Early (the Lower) Archaean, which is semantically wrong.

For this reason, we believe it is legitimate to move the notion "Katarchaean" in Earth's history time scale onto the epoch from its inception 4.6 BY ago to the beginning of Archaean 4.0 BY ago.

We later show that after the Archaean episode of the upper mantle melting in the Earth's equatorial belt, and of the "magmatic ocean" emergence in this geosphere, all primordial Earth surface, together with its primary, relatively dense (around 3.9–4.0 $g/cm^3$) lithosphere, literally sank in the upper mantle melts, that is, subsided into the mantle.

Thus, a translation of the Greek prefix κατα—down—may apparently be understood as a reminder that all geological objects of the pre-Archaean (i.e., Katarchaean) age subsided into Earth's melted upper mantle and thereby totally disappeared from its geological record.

We now review the external conditions on the surface of the young Earth and the particulars of the tidal tectonics in Katarchaean. This is a useful exercise as there are plentiful arbitrary and speculative ideas of the initial conditions on Earth. Some believe that violent volcanic and hydrothermal activities were going on under the cover of a dense atmosphere. These ideas came mostly out of popular science literature from the epoch when the contraction hypothesis ruled. And it is known that this hypothesis was based on the "hot" origin of Earth.

The conditions on the surface of the young Earth were unusual but in the directly opposite sense. At those distant times, only cold, inhospitable, severe desert landscapes existed on the planet, with cloudless skies (as the atmosphere was tenuous and devoid of humidity), a yellow and barely warming Sun (its luminosity was 25–30% lower than the present-day one) and a huge lunar disk without the habitual lunar "seas." Earth topography at that time reminded the crater-pitted lunar surface. Due to strong and practically continuous tidal earthquakes, the topography was substantially smoothed and composed of monotonously dark-gray primary matter overlain by no less dark and relatively thick regolite layer. No other, more differentiated rocks like basalts, peridotites, and especially granites were in existence on Earth.

From time to time, the desert landscape of the primordial Earth was disturbed by shakes and explosions of the falling residual planetesimals. But the frequency of the falls was becoming lower with time. Only within the equatorial zone of the young Earth at that time profuse, literally torrential flows of small rock and iron fragments continued to fall out of the satellite swarms of the recently destroyed Proto-Moon. Because of that, Earth surface in the equatorial zone for some time after the Moon formation (for a few hundred or even thousand years) remained hot.

However, no volcanoes erupting lava flows, gas or steam jets on the young Earth surface were existing as there were no hydrosphere or dense atmosphere. And the small amounts of gas and water vapor released at heat explosions of planetesimals and Proto-Moon fragments falling on the Earth surface were actively and rapidly gathered by the ultrabasic porous regolite that covered the entire young Earth surface in a thick layer.

The Sun movement at that time was very fast. It took just 3 h to cross the skies, and in 3 h was a new sunrise in the east over a lifeless horizon of the primordial Earth. The year duration was about the same as it is now but the year consisted of 1500 days! Moon's motions were noticeably slower as it revolved about Earth in the same direction. But the lunar phases changed very rapidly going through all stages in 6–8 h. In the very beginning of the Earth–Moon system evolution, the month was also about equal to the satellite revolution period at the Roche limit, that is, approximately 6 h. With time, this period rapidly lengthened. The apparent size of the moon was huge, 300–350 times the apparent area of the present-day lunar disk.

At the very beginning of its existence, the Moon was a substantially hot planet and radiated energy in the red portion of the spectrum. So, day and night it not only reflected the Sun light but also had its own dark-red luminosity and, due to its huge apparent size, noticeably heated Earth surface. Nonetheless, Earth surface was dominated by below-freezing temperatures.

From time to time, especially on the eastern side of the lunar disk, bright orange flares were visible. Those were spots of overheated magma erupted on the lunar surface impacted by meteorite bodies swept out by the Moon from the near-Earth satellite swarm. Besides, the entire huge lunar disk once in a while was covered with zigzag-shaped bright fractures that formed in a thin crust of the lunar rocks at rapid curvature changes of the tidal swells in the Moon which rapidly distanced itself from Earth.

Earth was also accompanied by a disk of small particles revolving about it on close orbits in the equatorial plane. The trajectories of individual particles merged together and created an illusion of continuous semitransparent rings resembling the Saturn's disks. At certain angle, the disks reflected the Sun light. Then they appeared to be solid but in effect they as always remained ephemeral, and all their matter soon fell on Earth (Fig. 3.2).

Earth also had several smaller than the Moon satellites ("micro-Moons"). They were much more remote than the "main Moon" but also visible well in the reflected Sun light as small disks or just bright starlets. Probably, there were at least 10 or 12 such satellites. Later, they fell on the Moon having given rise to large basalt-filled craters called now "the lunar mares."

The most impressive were probably the swarms of destructive earthquakes continuously following one after the other, which were caused by intense tidal deformations of Earth. Following the Moon, and together with the tidal humps these quakes literally shuddered the primordial face of Earth. The tidal quake periodicity depended on the difference between the period of Earth's axial revolution and Moon's orbital revolution, so it was constantly changing.

In the beginning, the Moon was still at the Roche limit, and angular velocities of Earth and Moon revolution were the same (a case of the stationary but metastable revolution of the planets). At that time, tidal swells were practically not moving on Earth's surface, so the quakes of this kind must have been temporarily absent. But as soon as the Moon left the Roche limit and began moving off Earth, intense tidal earthquakes immediately returned and shook Earth surface twice every time the Moon made the apparent revolution around Earth.

Height of the tides may be found from the equation of Earth's equipotential surface

$$V = V_g + V_t + \delta V_t, \tag{3.39}$$

where $V = -\gamma M/R$ is the total gravity potential of Earth; $V_g = -\gamma M/R_0$ is the gravity potential of the equilibrium rotating Earth not disturbed by the tides; $V_t \approx \gamma m R^2 P_2(\phi)/L^3$ is the tidal potential of the Moon acting on Earth surface; $\delta V_t \approx k_2 \cdot V_t$ is an additional tidal potential arising due to tidal mass redistribution in Earth; $P_2(\phi) = 0.5(3\cos^2\phi - 1)$ is the first even term of the Legendre polynomial; $\phi$ the is polar angle of the radius-vector for a given point on Earth surface counted from the direction connecting the centers of the interacting planets; $k_2$ is, as earlier, the second (tidal) Love's number; $\gamma$, $m$, $M$, and $R$ are, respectively, gravitational constant, Moon's mass, Earth's radius, and mass.

Considering that the height of Earth's tides was always much smaller than Earth's radius ($\Delta R \ll R \approx R_0$), we find from Eq. (3.39)

$$\Delta R \approx (1 - k_2)\frac{mR_0^4}{ML^3}P_2(\phi). \tag{3.40}$$

It shows that the tidal height on Earth is in the reverse proportion with the cubed distance between the planets' centers of gravity. At the Roche limit, the lunar center of gravity was 17,200 km from Earth's center (the Moon's center hung over Earth's surface at a distance of just 8200 km). So, the height of the lunar tides on Earth was at that time very large, about 1.5 km. Such tides, moving on Earth surface, caused swarms of numerous and strong earthquakes that continuously shook the surface of the young Earth.

Due to a rapid tidal Moon repulsion from Earth (in the inverse proportion to the distance between them to a power of 5.5), a million years from the planets formation the lunar tides on Earth declined to 130 m. After another 10 MY their amplitude decreased to 45 m, and in 100 MY, to 15 m. By the end of Katarchaean 4.0 BY ago, the tidal height was 7 m. The current Earth–Moon distance is 384,400 km, and the solid Earth tides near the sublunar point reach about 46 cm.

Rapid Moon pullout off Earth in Early Katarchaean and, as a result, a drastic decrease in the tidal energy dissipated within the young Earth saved it from overheating but quickly lowered the level of tidal seismicity in our planet. Let us assume that only 1/1000th of the tidal energy was spent on exciting earthquakes. Let us take the total energy of the present-time earthquakes at $10^{25}$ erg/year. It then turns out that the tidal earthquake energy in the very early Katarchaean (about 4.6 BY ago) exceeded by the factor of approximately 17,000 the modern level of Earth seismicity. However, in about just 100 MMY total intensity of the tidal earthquakes dropped to a level only about 2.2 times the current seismicity. By the end of Katarchaean (4 BY ago) it declined again, by the factor of 6.

Talking about the young Earth seismicity in Katarchaean, it is important that its nature and manifestation was totally different from the present-day earthquakes.

First, the Katarchaean tidal quakes were purely exogenic and not associated with any fixed tectonic zones (such zones did not exist on Earth). And second, these quakes, together with the running tidal wave, regularly moved in the body and on the surface of Earth at a speed determined by the apparent Moon revolution around Earth. As with conventional tides, quake culminations occurred twice every Earth revolution relative to the Moon. Third, the quakes reached their greatest intensity in the equatorial/tropical belt, and they were at their minimum in the polar areas.

## 3.11 CATASTROPHE OF EARTH IN THE DISTANT FUTURE

As Earth evolution and the Solar System evolution bear menacing changes and indications of catastrophic events, the comfortable conditions on Earth cannot continue ad infinitum. We will show in the next Chapter that the Earth core separation results in the emergence within the mantle of an oxidizing environment. When all iron in the mantle is oxidized to the magnetite stechiometry, further growth of the core will be accompanied

by a profuse release of the abiogenic oxygen. In the absence of oxidizable elements, this oxygen will eventually be entering the atmosphere.

A result will be a tremendous increase in the atmospheric pressure and the emergence of a very strong greenhouse effect. After the oceans boil, temperature on Earth will exceed 550 °C. Under such an environment, no life, even the most primitive, is possible. We are lucky in that these events will occur not too soon, in about 500–600 MMY.

After the initiation of nuclear reactions in the stars and their entering the main sequence of the star evolution (the Hertzsprung–Russell sequence), stars' luminosity and their size increase under an accelerated regime (Aller, 1976). The example for the Sun is shown in Fig. 3.11.

After the star transferred to the red giant class and reached the instability, it begins to collapse with a rapid formation of very dense and small objects. Depending on the mass of a source star, a "black hole" may emerge (if the star's mass exceeds 8–10 Sun masses; $M_{\text{star}} > (8\text{–}10)M_{\odot}$), a neutron star (at $M_{\text{star}} > (2\text{–}4)M_{\odot}$) or a white dwarf (at $M_{\text{star}} \approx M_{\odot}$).

That is how a known astrophysicist Aller (1976) is describing the upcoming Solar System evolution during the next 5 BY: over that period both Sun's radius and luminosity will be increasing. But the temperature increase in the Sun's surface will be going on slower than the changes in the Sun radius and luminosity. A result, in Aller's lively description, is that "...the Sun will gradually become brighter, and correspondingly the temperature on Earth will be increasing until, at last, the oceans boil out, and Earth converts to an incandescent slug... The Sun will continue to increase until, at last, it reaches a size of the Mercury's orbit, and the planet will be destroyed... For a relatively short period the Sun will turn into a giant, but its external shell will soon evaporate into the outer space, and its core will shrink into a white dwarf with the density of one hundred thousand to a million times that of the water..."

If the mass of the evaporated Sun shell is significant, the "slingshot effect" may happen, in which case the Solar System planets, Earth included, will leave it forever and turn into the eternal wanderers of the cold Universe. As the publication Physics of the Cosmos states, the planets' "take-off" off the Solar System may happen if the mass of the released shell is greater than half of the former Sun mass: $\Delta M_{\odot} > 0.5M_{\odot}$. This is not an unrealistic possibility but all these catastrophic events will happen in a very distant future, possibly, 5–5.5 BY from now.

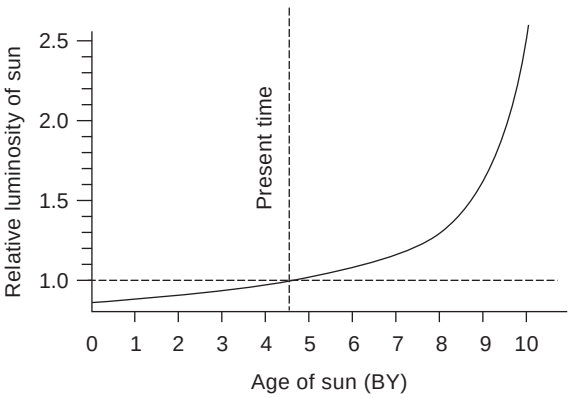


**FIGURE 3.11** Sun luminosity versus time (Aller, 1976).

CHAPTER

# 4

# Process of Earth's Core Separation

After the issue of Earth's origin, the timing and regime of Earth's core separation occupy a highly important place in planetary geophysics. In studying mechanisms and ways of Earth's planetary evolution, energy sources of its tectonic activity or major patterns of its geological evolution, the issue of timing and, most importantly, the regimes of the core separation becomes central. That is natural as the core currently concentrates nearly two thirds of Earth's mass, the process of radical differentiation of its matter could not but have left indelible traces in the geological record.

## 4.1 LATE BEGINNING OF EARTH'S CORE SEPARATION

An important conclusion from the theory of Earth's origin developed in Chapter 3 is that the young Earth did not have a high-density core. It does exist now, and a huge energy release, close to $17 \times 10^{37}$ erg, was associated with its formation. It is very important to find out exactly when this core appeared and how it was formed, at once or gradually.

This issue is closely connected with the heat regime of Earth's formation. Many quite serious studies merely postulate the early Earth heating accompanied by the core separation. Sometimes it is substantiated by way of solving, not always correctly, problems of heating the growing Earth by falling planetesimals of different sizes (Tozer, 1965; Oversby and Ringwood, 1971; Jacobs, 1975; Vityazev et al., 1990).

On the other hand, Schmidt (1946) proposed a hypothesis of a "cold" Earth origin. Runcorn (1962, 1965) suggested that the Earth's core began growing much later than Earth's time of formation and is continuing to grow even now. The hypothesis of the "cold" Earth origin and late core separation was supported by Elsasser (1963). The most detailed and substantiated concept of a "cold" Earth origin, therefore, of a late core separation, was proposed by Safronov (1969). It is an important issue so we review it in some detail.

Some hypotheses were based on a brief planetary accretion (on the order of ten of a few tens of millions of years) and overestimated Earth's matter stirring depth on impact from planetesimals. The result of these assumptions was that Earth had to melt in the process of its formation. Should that have happened this way, Earth, like the Proto-Moon, would

*Developments in Earth and Environmental Sciences*, Volume 10
DOI: 10.1016/S1571-9197(11)10004-X

have undergone a rapid and complete differentiation which would have added its significant fraction of energy into Earth melting. It would have resulted very early in Earth evolution (about 4.6 BY ago) in the separation of a high-density iron core, in the formation of a thick melted anorthosite crust layer and in the early degassing of Earth's matter, and the formation of a very thick fluidal water–carbon dioxide atmosphere.

Should it have so happened that indeed about 4.6 BY ago the metallic core separated and a thick anorthosite crust formed, then, as on the Moon, most of the radioactive elements would have transferred into the crust, and Earth, devoid of all endogenous energy sources, would have, like the Moon, converted into a tectonically dead planet.

It should be mentioned, however, that recent publications by Australian geologists informed of the clastic zircon finds with the age of 4.2–4.3 and even almost 4.4 BY. They were discovered in Archaean sandstones and conglomerates apparently aged approximately 3.5 BY (Wilde et al., 2001).

It does not mean, however, that the continental crust began to form in those remote times as some geologists believe. Indeed, as we show later, during almost entire Archaean the primordial Earth's matter was exposed on Earth surface. It was covered by a layer of the Moon-type thinly porous regolite formed during the planet formation and first 600 MMY of its life (Fig. 6.15). This matter must have contained zircons of the oldest ages ($t > 4$ BBY). They were generated in a local melting of the near-surface layers of young Earth as a result of planetesimal drops. Subsequently, after the emergence in Archaean of a dense atmosphere and hydrosphere, these zircons might have been washed out of the primordial rocks and deposited in Archaean sedimentary rocks reminding us that Earth is much older than its crust.

Sometimes, data on the noble gas isotope distribution in the atmosphere and mantle are used to prove early heating and differentiation of Earth. Especially, demonstrative in this respect is the excess content in the atmosphere of the radiogenic $^{129}$Xe. Its atmospheric concentration is about 7% above that assumed for the primordial xenon. The $^{129}$Xe isotope forms in the decay of short-lived radioactive iodine isotope $^{129}$I with the decay constant $\lambda_{129} = 4.41 \times 10^{-8}\,\text{years}^{-1}$. A conclusion is made from this that the excess $^{129}$Xe in Earth atmosphere is a testimony to early differentiation and degassing of Earth which occurred prior to $^{129}$I isotope disappearance from the Earth's matter (Oshima and Podosek, 1983; Tolstikhin, 1986; Azbel and Tolstikhin, 1988). However, excessive $^{129}$Xe is also found in Earth rock samples. The concentrations may be even higher than in the atmosphere which rather indicates a late degassing.

Oshima and Podosek who are unquestioning authorities in the noble gas geochemistry noted that the increase in the radiogenic xenon isotope concentration in the atmosphere and the excessive $^{129}$Xe require a very rapid degassing. This not only contradicts the models for argon and helium but is also internally contradictory. On the other hand, the isotope composition of most of the mantle xenon is similar to the atmospheric one, and there is no substantial excess of $^{136}$Xe associated with $^{129}$Xe. That indicates a slow degassing (Oshima and Podosek, 1983, p. 310).

To solve this conundrum, Oshima and Podosek proposed a two-step model. First, at a very early stage of Earth evolution, its rapid and tempestuous degassing occurred. In this process, most of the noble gases were lost to the atmosphere. After that, during the entire consequent evolution, a gradual degassing proceeded.

The Oshima–Podosek model is very attractive except for a "small" detail. The early degassing happened not to Earth but the dropping planetesimals. Of course, the process was violent as on impact with Earth surface and in heat explosions planetesimals could have even evaporated. All chemically active gases ($CO_2$, $H_2O$, and other volatiles) reacted with the ultramafic regolite that covered the growing Earth and were rapidly removed from the primordial atmosphere (Sorokhtin and Ushakov, 1989a,b, 1991; Sorokhtin, 2007). Only the noble gases and nitrogen were preserved and accumulated in the atmosphere. It is obvious that in no way such violent degassing of the planetesimals could describe the heat regime of Earth proper and even less so could be an indication of its early differentiation.

The early melting of Earth and the core separation would have been accompanied by a complete degassing of the entire planet. About $5 \times 10^{23}$ g of $CO_2$ currently bonded in carbonates, and more than $2.5 \times 10^{24}$ g of water would have over a relatively short time been released to the atmosphere. A rapid formation of a dense carbon dioxide atmosphere with pressure of close to 100 atm would have resulted in the emergence of a very strong greenhouse effect and the temperature raise above the critical temperature for water (+374 °C). After that the oceans would have boiled out, and the atmospheric pressure would have risen by about 500 atm more. An irreversible greenhouse effect would have emerged on Earth with average temperatures over 550–600 °C. Earth would not have liquid water and any traces of even the most primitive life.

We are lucky that it had not happened.

There are, however, direct evidences indicating that the young Earth never melted and did not have a high-density metallic core. For instance, many differences in the lunar rock geochemistry may only be understood if the parent body of the Moon (i.e., the Proto-Moon), contrary to Earth, was totally melted soon after its formation. At that, the Proto-Moon would have undergone a complete differentiation with the separation of the metallic core and anorthosite crust. This is supported by a thick anorthosite crust on the Moon and a drastic impoverishment of the lunar rocks (compared with Earth's) with all siderophilic and chalcophilic elements (Ringwood, 1982).

The strongest and practically irrefutable proof, however, is in the lead isotope ratios on the Moon and Earth (which was already mentioned in Section 3.7). For the same reason it is impossible to accept numerous hypotheses of the Moon formation as a result of the so-called "mega-impacts" or "macro-impacts." Let us assume that the Moon was indeed formed from the fragments of the Earth's mantle catapulted into the near-Earth outer space by a tangential shock or shocks. In this case even now, the lead isotope ratios on the Moon would be the same as in Earth's mantle rocks: $^{206}Pb/^{204}Pb \approx 18/19$; $^{207}Pb/^{204}Pb \approx 15/16$, and $^{208}Pb/^{204}Pb \approx 37/38$, and not the avalanche values of 100–220 quoted in Section 3.7 (Voytkevich et al. (1990)).

As opposed to the Moon's matter, the Earth's matter had been never subjected to a rapid and radical differentiation. The reason was that the Earth's core was being formed gradually, without silicate melting. The process was due to, initially, the zonal differentiation mechanism, with the iron melts separating from silicates. Then barodiffusion mechanism of the matter differentiation took charge. The rate of both mechanisms was constrained be very low heat conductivity and diffusion in the mantle silicates. Besides, both primordial lead and its radiogenic isotopes were in the core. They accumulated by the time of the differentiation process of Earth's matter. That is why the lead isotope ratios in Earth rocks are intermediate and relatively close to the primordial (compared to the same ratios in the lunar matter).

Based on the above data and considerations, it was proposed that the core separation process began 800–600 MMY after the Earth origin, that is, 4.0–3.8 BY ago (Monin and Sorokhtin, 1982a,b,c).

## 4.2 A SCENARIO OF THE CORE SEPARATION PROCESS

According to the most probable Earth origin model under the Schmidt (1948) hypothesis (later detailed by Safronov, 1969), Earth and other Solar System planets formed due to accretion of cold, homogeneous matter from the protoplanetary cloud (see Chapter 3). Two general scenarios of a high-density core separation within Earth may be suggested: (1) the core formed simultaneously with the planet growth or immediately upon its formation and (2) the high-density core separation began much later, after Earth heated up, and the differentiation process of Earth's matter expanded over billions of years and is even continuing today.

The first scenario is the least probable. It could have occurred only under the "hot" origin of Earth and a brief accretion period on the order of 10 MMY. For a rapid planet differentiation with the separation of a high-density core within it, the planetary matter should undergo a practically global melting, as happened with the Moon. For Earth such a suggestion is in direct contradiction with the available geological and geochemical data (see Sections 3.5, 3.6, 4.1 and also Sorokhtin, 1999). Repeating again, under this scenario the Earth's crust should have been forming simultaneously with the core separation. Nowhere on Earth was such most ancient (Katarchaean) crust discovered. Besides, lead isotope ratios in Earth rocks practically singularly indicate that Earth was never completely melted. Therefore, the differentiation of its matter, hence, the formation of the core was gradual and extended over time from about 4 BY ago. Analysis of Earth's energy balance shows that the process is continuing. The absence of an old, 4.5–4.0 BY, and thick Moon-type anorthosite crust which is a product of the early planet melting also suggests that the young Earth did not go through global differentiation immediately upon its formation. Moreover, Earth's crust does not include at all the rocks which are older than 3.8–3.85 BY. This is a convincing indication of Earth's tectonic passivity at that time.

The second scenario appears to be much more likely, and maybe the only one possible. Indeed, the modern theory of the planetary origin briefly described in Chapter 3 is based on a homogeneous and relatively long (on the order of 100 MMY) accretion under which the Earth depths remained relatively cold, with the temperature not to exceed 800–1500 K (Safronov, 1969; Ringwood, 1982; Safronov and Vityazev, 1983). Initial stages of the Earth differentiation process were determined by its initial heat-store estimated in Section 5.5. With the insufficient heat-store of the young Earth the core separation, as mentioned, could have begun only much later, after a preliminary heat-up of the insides of the Earth by the released radiogenic and tidal energy. And that is what actually happened as the age of the oldest crust rocks turned out to be 700–750 MMY younger than the age of Earth herself.

As we can see, temperature distribution within the young Earth turns out to be by hundreds or even thousands of degrees below the anticipated melting temperature of the Earth's matter at great depths. For any practical purpose this totally eliminates the possibility of the planet's global melting. We show again in Section 4.7 that the radiogenic-to-primordial lead ratios in Earth rocks singularly testify in favor of Earth, as opposed to the Moon, having never been completely melted.

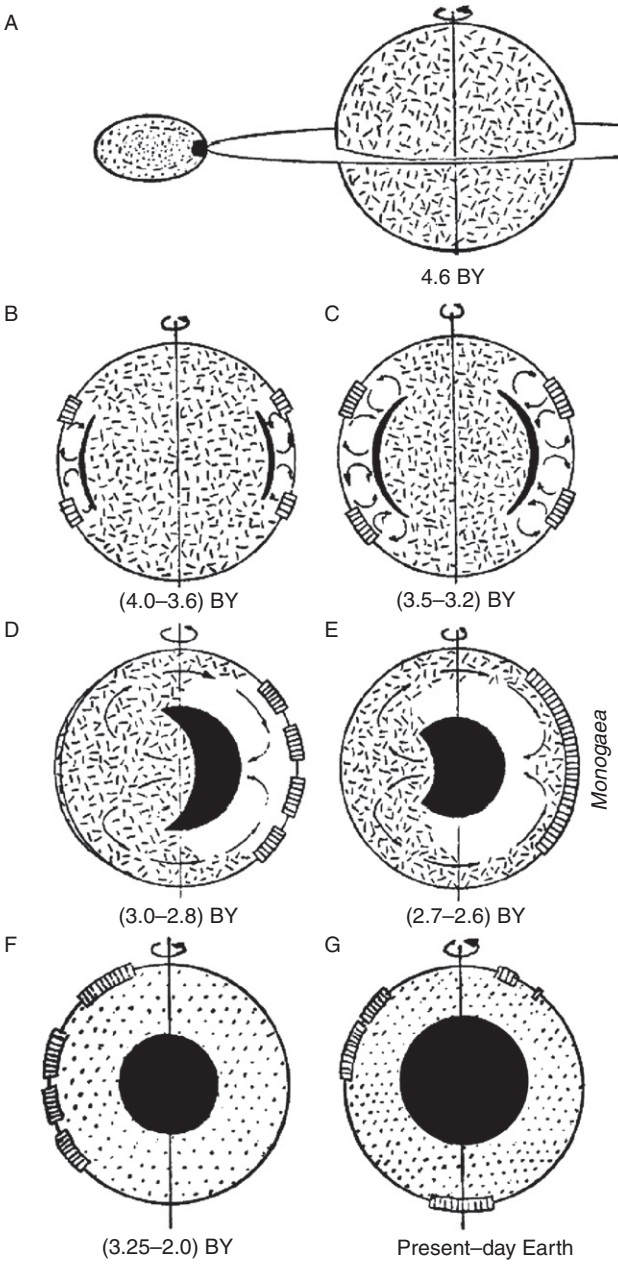


**FIGURE 4.1** Earth structure evolution: (A) the young Earth and Moon formation; (B–F) consecutive stages of the Earth's core separation and formation; (G) present-day Earth. The dashes represent the primordial matter; solid black is iron and its oxides melts; white is the Archaean depleted mantle impoverished in iron, its oxides, and siderophilic elements; the dots are the current-type mantle; and the boxes are continental massifs.

However, in order to explain a mechanism of the Earth's core separation there is no need in melting of the entire Earth matter. In Archaean, Earth differentiation proceeded only under the mechanism of Earth's matter zonal melting. Afterward, the mechanism changed to that of the barodiffusion differentiation (Sorokhtin and Sorokhtin, 2005). It is illustrated in Fig. 4.1.

Both mechanisms accept the process evolution in Earth depths at temperatures way below those of the silicate melting. However, both mechanisms are slow acting. For instance, the evolution of the zonal differentiation was limited by a low rate of heating of the Earth layers directly underlying the differentiation fronts (i.e., by low heat-conductivity factors of Earth matter, on the order of $10^{-7}$ erg/cm s deg). And the evolution of the baro-diffusion differentiation was limited by exceptionally low values of the diffusion factors in silicates, approximately $10^{-20}$–$10^{-22}$ $cm^2/s$. These specifics of the most probable Earth's matter differentiation mechanisms totally eliminate any possibility of a rapid separation of the present-day core. That is why the process of the high-density core formation expanded over billions of years and is still going on.

It is important that the differentiation of Earth's matter could only begin on the equator as that was the area where the maximum release of the Moon–Earth tidal interaction energy occurred (see Chapter 5). That was also the reason why the initial tectonomagmatic activity of Earth occurred only within the narrow low-latitude belt (Sorokhtin, 1988). Later, a similar idea of the continental crust formation in Early Archaean within a "hot equatorial belt of Early Earth" was forwarded by Glukhovsky et al. (1994).

The zonal differentiation process subsequently expanded into high latitudes. The evolution of this process in Archaean resulted in the planet's strong gravitational instability: a high-density (heavy) ring of the melted iron and of its oxide formed through the zonal melting was positioned over lighter matter of the primordial Earth's "kernel" (see Fig. 4.1B and C).

How could this situation of instability be resolved? There was only one way, floating-up of the rigid Earth "kernel" in the equatorial belt of one of the hemispheres and sinking of heavy melts to Earth center from the side of the opposite hemisphere (see Fig. 4.1D and E). Such event undoubtedly created strong asymmetry in the Late Archaean planet which resulted in a drastic increase of the precession angle (Fig. 14.16). Simultaneously, it provided for a stable orientation of the main Earth's axis of inertia, hence, for the stable revolution of the planet.

The process had to evolve under the surging-up avalanche scenario with the formation in the end of a high-density core. The explanation is in a substantial nonuniformity of heating in the young Earth. Indeed, after Earth captured the Proto-Moon, after the Moon formation and further evolution of its orbit, a major fraction of the tidal energy (and it was huge, about 4 or $5 \times 10^{37}$ erg) was being released mostly in Earth upper layers and within its equatorial ring belt. As a result, Earth turned out to be much more heated in the lower latitudes than in the polar areas. So, the first astenosphere and the associated iron separation zone had to arise within the upper mantle right beneath the equatorial belt. In Middle Archaean, the differentiation zone broadened to the moderate latitudes and engulfed the middle mantle. Late in Archaean it covered most of Earth area, and by the end of Archaean it encompassed Earth in its entirety (Figs. 4.1E and 4.3). Within the Early Archaean equatorial belt arose all the oldest Archaean continental shields and platforms.

Simultaneously with these processes, temperature of the upper and middle mantle underneath the both Earth poles remained relatively low. Because of that, the astenosphere layer had a much longer time to form there. Thus, the ring-like layer of high-density core matter melts could have existed in Early and Middle Archaean, could have expanded, and surrounded the cold and rigid ($\eta > 10^{30}$ P) kernel of the young Earth only from the side of its low-latitude belt. At the same time, through the high-latitude and polar areas the kernel was still rigidly connected with the middle and upper mantle, so it preserved its stable position.

Gradually, the high-latitude areas were heated up at the expense of the then proceeding gravity differentiation of the Earth's matter in the adjacent areas, by the radioactive decay and tidal disruptions. Their viscosity gradually declined to $10^{24}$–$10^{23}$ P, and the rigid connection between the cold kernel and the mantle was destroyed. Beginning at that time, the earlier generated gravity instability of Earth could have been resolved by way of heavy core matter melts sinking toward the planet's center and the compensatory squeezing-out of its rigid but lighter kernel toward the surface (Fig. 4.1D).

A large amount of the core matter accumulated by the middle of Late Archaean in the ring zones of differentiation (up to 12–13% of Earth mass). This matter had high density compared with the primordial Earth's matter ($\Delta\rho \approx 4$ g/cm$^3$). Because of these, pushing out the young Earth kernel from its central areas must have been proceeding in an accelerated way and been catastrophic. The speed of Earth's core separation was restrained by high viscosity of the cold primordial matter in the former Earth kernel. That kernel was at that time spreading along the active belt of the mantle under the influence of a huge excess pressure from the forming Earth's core and from a large uncompensated high on Earth surface over the area of the deep matter ascent (Fig. 4.1D).

Earth's core formation was accompanied by the release of a huge amount of energy, on the order of $5 \times 10^{37}$ erg. It was mostly spent on the additional heating of the mantle and of the matter from the former Earth kernel. These, in turn, accelerated the core separation process. The entire core formation process apparently lasted about 200 MMY. It was evolving in an accelerated way and was completed by the very end of Archaean (2.6 BY ago) with a catastrophic event of a high-density core formation in Earth center.

The core separation was accompanied by the emergence of exceptionally intense convection flows in Earth mantle. These flows completely transfigured the entire preexisting tectonic plan of the lithospheric shell. The presented scenario includes the emergence at the very end of Archaean of a single-cell convection structure with one ascending flow over the emersion spot of the former Earth kernel and one descending flow over the core matter drain area. This is the reason to suggest that a first supercontinent in Earth evolution which we called Monogaea (Sorokhtin and Ushakov, 1989a, 1990a, 1991, 1993) formed over this descending mantle flow at the Archaean/Proterozoic time boundary 2.6 BY ago. Independently and based on geological data, Khain and Bozhko (1988) proposed an Early Proterozoic continent they called "Pangaea 0."

Taking the above into consideration, it is enticing to associate the described geodynamic catastrophe with the most outstanding epoch of the Kenoran tectonomagmatic diastrophism. This event closed Archaean stage of Earth evolution. The result of this stage was the emergence of the Monogaea supercontinent.

The first and most turbulent stage of Earth's core separation was completed with the fill-up of Earth's central areas with the core matter and with the movement of the primordial Earth kernel to Earth periphery. At the same time, the first stage of Earth differentiation under the mechanism of iron and its oxides zonal separation from Earth matter ended. The further core matter separation and core growth occurred under the barodiffusion mechanism described in Section 4.4.

A drastic asymmetry in the distribution of Earth masses occurred in the process of the core separation. As a result, Earth precession angle might have significantly increased, maybe to 40° (Fig. 14.16). In the process, the disturbing masses of the descending and

ascending mantle flows should have been positioned in Earth equatorial plane which was at the time significantly tilted compared the ecliptic plane. The conclusion is that the first supercontinent in Earth history, the Monogaea, was also located on the equator.

## 4.3 MECHANISM OF EARTH'S MATTER ZONAL DIFFERENTIATION

Temperature within the young Earth was low (see Figs. 3.10 and 4.2), so the barodiffusion mechanism could not work at that distant time. That is why the separation of a high-density core matter (Fe and Fe·FeO) from the silicate matrix could start only after Earth temperature has risen, due to the radioactive decay and the tidal interaction with the Moon, to a level of the iron and iron oxides melt in the area of the local maximum of the young Earth geotherm in the upper mantle.

Most likely, the separation process of iron from the Earth's matter silicates began at depths of 200–400 km under pressure of 80–170 kbar. These conditions are commensurate with the pressure on the order of 130 kbar of the first electron-phase transition in iron between α-Fe and ε-Fe (Fig. 2.15), that is, in the area of the stable existence of the $Fe_2O$ oxide. However, based on the concentration $C^*$ of the silicates maximum saturation by the FeO solution (Fig. 4.8), at these depths $C^* > 50$ %, whereas the iron oxide concentration in the primordial matter was about two times lower: $C(FeO)_0 \approx 24\%$.

Therefore, the separation of easily fusible core matter component from the mantle silicates could not occur at depths of around 400 km within the young Earth. The reason was that at those times the critical depth for triggering the barodiffusion separation mechanism of $Fe_2O$ from the silicates was approximately 1200–1400 km (presently it is

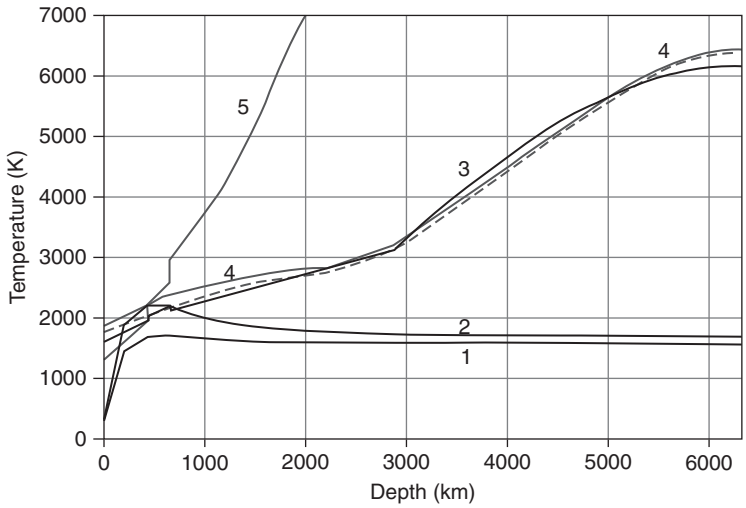


**FIGURE 4.2** Temperature distribution in the young and present-day Earth: 1, during Earth formation about 4.6 BY ago; 2, in the beginning of Archaean, about 4.0 BY ago; 3, temperature distribution in the present-day Earth; 4, iron melting temperature; 5, silicate melting temperature; and the dashed line is melting temperature of the eutectic melt Fe·FeO.

1900–2000 km). That is why the first astenosphere on Earth could emerge in the lower parts of the upper mantle only due to a partial silicate melt. But the then existing intense tidal disturbances from the closely positioned Moon (see Section 5.3) must have mostly concentrated within the upper mantle layers in the equatorial belt. This resulted in additional temperature raise in that layer up to the free iron melting point (Fig. 4.2). That initiated in the primordial astenosphere the density differentiation process of Earth matter.

As we remember, the initial free iron concentration in the primordial Earth's matter reached 13–4% (see Table 3.1). As soon as the free iron contained in the young Earth's matter began to melt, the further Earth's matter differentiation could expand up and down Earth independently, just due to the release of the gravitational energy.

This process was stable and self-sustaining. The silicate melting temperature in the upper mantle is always below the iron and iron oxide melting temperature, and the easily fusible oxide $Fe_2O$ does not emerge under the pressure prevalent within that geosphere. So, the initial Earth's matter differentiation on these levels could have proceeded only under the zonal melting mechanism (see Vinogradov and Yaroshevsky, 1965, 1967).

There are no in the present-day Earth energy sources capable of supporting the zonal melting process under continuous regime (Magnitsky, 1965). There are too little radioactive elements in the mantle (see Section 5.2) to support such process and the gravitational liquation or flotation energy of only silicate composition mantle melts. It also concerns the energy of the present-day lunar tides. As for the young Earth, such energy sources capable of supporting the process of the upper mantle matter zonal melting process under the continuous regime definitely existed within it.

First, it was the lunar tidal energy: the Moon during Early Archaean was positioned much closer to Earth, and its tidal effect on the heating of the astenospheric layers was exceptionally strong.

Second, after melting of some areas of the upper mantle, such energy was generated by the very process of the Earth's matter gravity differentiation at the expense of separating the metallic iron and its oxides (not bonded in the silicate phase) from lighter silicates.

A thermodynamic calculation of the upper mantle matter zonal melting process in the young Earth was performed. It showed that significant amounts of the gravitational energy are released in the process (Naimark, 1984a,b). The so released gravitational energy totally supported the self-sustenance and development of the process within the entire upper and middle mantle. The tidal energy dissipated then in the matter melt zones accelerated and strengthened the zonal melting process. For this reason, in Archaean the zonal melting process of the upper mantle in the Earth equatorial belt was developing rather violently and resulted in melting-out of most ancient continental crust areas of anorthosite and basalt composition. Simultaneously, already in the first half of Early Archaean occurs significant overheating of the upper mantle.

The Earth's matter differentiation in the deeper mantle (where the silicate melting temperature was substantially over the iron melting temperature) could occur only due to a simple separation of the melted iron from solid, unmelted silicates. That was helped by the property of the metallic iron, when in concentration close to 13%, to remain as a separate phase and be contained within intergranular spaces of the silicate crystals (similar to what is observed in meso-siderite meteorites).

The mantle differentiation front downward advance was evolving due to the emersion (flotation) of lighter silicate crystals from the base of the melted iron astenospheric layers toward their top.

In such a situation the heavy melt, in its descent, should have gradually increased in mass and thickness due to the addition of new portions of the iron melt from the underlying primordial Earth matter. It follows from the very nature of the reviewed process of Earth's matter zonal differentiation that the temperature at the base of the descending melted iron layer was always equal to the iron melting temperature at a given depth. Because of the iron-from-silicates separation and silicates flotation (emersion) through the layer of the liquid iron, this layer should have been significantly heated in the direction from down up. As a result, the temperature distribution in such melted iron layer may have been substantially under the adiabatic one and might have even become negative (i.e., rising up). That led to two important consequences. First, the overlying mantle should have experienced significant overheating. The reason would be that in the differentiation process the "current" mantle temperature was set by the top of the overheated zonal differentiation layer (melted iron). Second, the Earth's matter zonal differentiation process must have been accompanied by the emergence in the overlying portion of the mantle (which have already experienced primary differentiation) of intense heat convection.

Despite a substantial energy release, the zonal separation of the melted iron from the silicate matrix could not spread deeper than a certain maximum level. The reason was that the matter temperature in the young Earth declined with depth, and the iron melting temperature increased. Therefore, their difference substantially increased in the same direction (Fig. 4.4). Therefore, the fraction of energy expended for a preliminary heating of the Earth's matter must have been significantly increasing with depth. That is exactly why, beginning at some level, the released gravity energy might have been insufficient to maintain the continuous regime of the process. Obviously, for the process to continue it was necessary for the energy released in the differentiation to be sufficient for heating the underlying medium to the level where iron contained in it would melt.

The amount of energy released in the emersion of a unit volume ΔV of the differentiated silicate matter through an $h$-thick layer of melted iron is:

$$\Delta E = [1 - C(\mathrm{Fe})]\Delta\rho h g \Delta V, \tag{4.1}$$

where $C(\mathrm{Fe}) = 0.131$ is the metallic iron and its oxides concentration within the free phase of Earth's primordial matter; $\Delta\rho = \rho_{\mathrm{Fe}} - \rho_{\mathrm{Si}}$; $\rho_{\mathrm{Fe}}$ is density of the melted iron and its compounds; $\rho_{\mathrm{Si}}$ is the silicate fraction density; and $g$ is the gravity acceleration. This energy is expended for heating of a relatively cold primordial matter $\rho_0 c_p \Delta T \Delta V$, for melting and overheating of new portions of iron and its compounds.

In this case, the energy balance of the differentiation process may be described as follows:

$$[1 - C(\mathrm{Fe})]\Delta\rho h g \approx \rho_0 c_{\mathrm{p}} \Delta T + C(\mathrm{Fe})\rho_{\mathrm{Fe}} q + \delta T_H \rho_{\mathrm{Fe}} c_p(\mathrm{Fe}), \tag{4.2}$$

where $\rho_0$ is density of the primordial Earth's matter; $c_p \approx 10^7$ erg/g deg is its heat capacity; $\Delta T = T(\mathrm{Fe})_{\mathrm{m}} - T_0$; $T(\mathrm{Fe})_{\mathrm{m}}$ is iron melting temperature at depth $H$; $T_0$ is initial temperature at the same depth (see Fig. 4.2); $q \approx 2.77 \times 10^9$ erg/g is iron fusion heat; $\delta T_H$ is the amount iron

and iron oxide melts overheating compared with their fusion temperature at depth $H$; and $c_p(\mathrm{Fe}) \approx 0.5 \times 10^7$ erg/g deg is heat capacity of the melted iron.

The overheating amount $\delta T_H$ of the melt emerging at Earth's matter differentiation at a given level $H$ may be found from (4.2) as follows:

$$\delta T_H \approx \frac{[1 - C(\mathrm{Fe})]\Delta\rho h g - \Delta T \rho_0 c_p - C(\mathrm{Fe})\rho_{\mathrm{Fe}} q}{\rho_{\mathrm{Fe}} c_p(\mathrm{Fe})} \tag{4.3}$$

As usual,

$$\frac{1}{\rho_0} = \frac{C(\mathrm{Fe})}{\rho_{\mathrm{Fe}}} + \frac{1 - C(\mathrm{Fe})}{\rho_{\mathrm{Si}}} \quad \text{and} \quad g = \gamma \frac{m(r)}{r^2}, \tag{4.4}$$

where $\gamma = 6.67 \times 10^{-8}\ \mathrm{cm^3/g\ s^2}$ is the gravitational constant; $m(r)$ is the mass of Earth's insides within a sphere of radius $r$.

Normalization of $\delta T_H$ values for the surface conditions in Archaean is made using the following equation:

$$\delta T_0 = \delta T_H \frac{T(\mathrm{Fe})_0}{T(\mathrm{Fe})_H}, \tag{4.5}$$

where $T(\mathrm{Fe})_H$ is iron melting temperature at depth $H$ (found experimentally, see Fig. 2.15); $T(\mathrm{Fe})_0 \approx 1803$ K $= 1530$ °C is iron melting temperature on Earth's surface in degrees Kelvin and Celsius. Mantle temperature $T_{\mathrm{m}0}$ normalized for the surface (in °C) is found as:

$$T_{m0} = 1530\ ^\circ C + \delta T_0, \tag{4.5'}$$

where 1530 °C is iron melting temperature at normal pressure $p \approx 1$ atm.

The thickness $h$ of melted iron at depth $H$ may be found from the mass balance of the already differentiated Earth matter:

$$h = \frac{H + \left[\left[R^3 - (R-H)^3\right]\frac{\rho}{\rho_{\mathrm{Fe}}} C(\mathrm{Fe}) + (R-H)^3\right]^{1/3} - R}{S_{\mathrm{AR}}}, \tag{4.6}$$

where $H$ is the depth of the zonal differentiation front; $R = 6370$ km is Earth radius; it is assumed that the width of the ring separation zone between iron melts and mantle silicates is proportionate with the mantle heat energy, so the factor

$$S_{\mathrm{AR}} = \frac{E_{\mathrm{m}} T}{E_{\mathrm{m}} T_{2.6}} \tag{4.7}$$

takes into account gradual widening of the equatorial differentiation zone in Archaean (after the start of Earth's matter partial meltdown about 4 BY ago at depths of 200–400 km and through the time when it covered the entire Earth area at the end Archaean); here, $E_{\mathrm{m}}T$ is the current value of the mantle's endogenous heat energy, and $E_{\mathrm{m}}T_{2.6}$ is the mantle's endogenous energy at the end Archaean nearly 2.6 BBY ago (see Fig. 5.13, curve 3). And the width of a tectonomagmatic zone on Earth surface is (see Fig. 4.3)

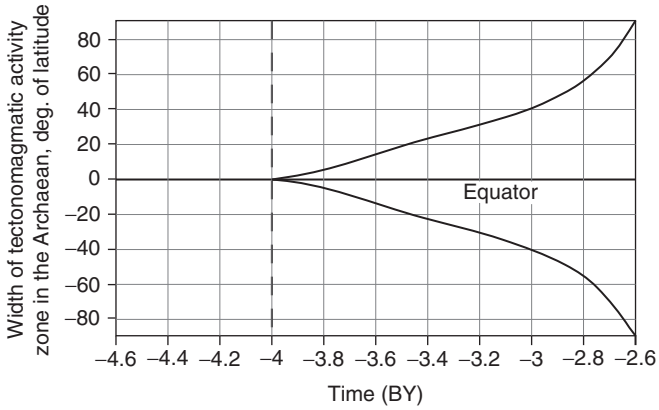


**FIGURE 4.3** Width of the tectonomagmatic activity ring-zone on Earth surface in Archaean, in degrees of latitude (the dashed line indicate the beginning of the core separation). The area outside of the ring-zone was represented in Katarchaean and Archaean by the primordial Earth's matter overlain by the ultramafic regolite.

$$S_{\mathrm{Tm}} = \frac{E_{\mathrm{m}}T - T_{\mathrm{m}}T_{4.0}}{E_{\mathrm{m}}T_{2.6} - E_{\mathrm{m}}T_{4.0}}. \tag{4.7'}$$

For a qualitative estimate of the process parameters we may assume, as a first approximation, that the compressibilities of Earth's matter, silicates, and iron are about equal. As $\rho_0 \approx 3.98$, $\rho_{\mathrm{Fe}} \approx 7.8$, and $\rho_{\mathrm{Si}} \approx 3.71$ g/cm$^3$, in this case we may assume $\Delta\rho/\rho_0 \approx 1.043$, $\rho_{\mathrm{Fe}}/\rho_0 \approx 1.96$, and $\rho_{\mathrm{Fe}}/\rho_{\mathrm{Si}} \approx 2.1$, where $\Delta\rho = \rho_{\mathrm{Fe}} - \rho_{\mathrm{Si}}$. Then from Eq. (4.6) we find that, for instance, at the depth of 200 km the melted iron layer was about 212-km thick. Similarly, as the differentiation front crossed the depth of 1000 km, the melt layer increased to 305 km, and crossed the depth of 1600 and 3200 km, the thickness of such melted iron and iron oxide layers increased, respectively, to 337 and 400 km (see Fig. 4.6). For the sake of a comparison, the young Earth's core formed at the very end of Archaean was 3010 km, and the core radius today is 3485 km.

The mantle heat-up in Archaean $\delta T$ substantially depended on the initial temperature distribution within the young Earth (Fig. 3.10). When selecting the initial temperature distribution, we used, as mentioned in Section 3.9, calculations by Safronov and Vityazev (1983). They estimated temperature values within the primordial Earth base on the "cold" model of the planet accretion. Their calculations, however, did not take into account either the energy of the Earth–Moon tidal interaction or the young Earth energy balance. We introduced certain corrections in their distributions as shown in Fig. 3.10.

Additional heating of the convecting Earth mantle in Archaean at the expense of radioactive decay, tidal interaction with the Moon, matter differentiation and the core separation is equal to $\Delta T_W$.

$$\Delta T_W = \frac{\Delta E_{R+T}}{M_{\mathrm{m}} c_p}, \tag{4.8}$$

where $\Delta E_{R+T}$ is the sum of the radiogenic and tidal energy released in Archaean within the convecting mantle and $M_{\mathrm{m}}$ is mass of the convecting mantle:

$$M_{\mathrm{m}} = \frac{4\pi}{3}\left[R^3 - (R-H)^3\right]\bar{\rho} S_{\mathrm{AR}}, \tag{4.9}$$

where $S_{\mathrm{AR}}$ is the width of the Earth's matter differentiation equatorial zone (see Fig. 4.3).

Temperature distribution in Earth depths at the Katarchaean/Archaean time boundary and the iron melting temperature at high pressure (Fig. 4.2), the difference $\Delta T$ rapidly increases with depth. Estimations based on Eq. (4.2) indicate that the metallic iron zonal differentiation in the pure form could have occurred within the young Earth only to a depth of about 2400 km. In this case, at the average rate 0.2–0.15 cm/g of the process development, Earth gravity differentiation must have stopped sometime in Middle Archaean. However, solid silicate solutions decomposed under high pressures (see Section 4.4). So, at depths of around 1400–1600 km iron oxides began segregating as a free phase forming Fe·FeO eutectic melts of the $Fe_2O$ core matter. From that moment on, that is, approximately since 3.2 BY ago, total concentration of such melts rapidly increased. This significantly accelerated the advance of the Earth's matter zonal differentiation (up to 0.4 cm/year) as well as energy efficiency of the differentiation process. As a result, temperature distributions within the Archaean mantle substantially changed with time as shown in Fig. 4.4.

Calculations indicate that the upper mantle overheating occurred rather drastically in about 200 MMY after the process of Earth's matter zonal differentiation became operational. In the beginning, the overheating rapidly increased but later slowed down gradually.

A decline in the mantle temperature over the first overheating maximum is associated with a gradual increase with depth in the iron melting temperature difference and the temperature within Earth depths against the background of the zonal differentiation. And the second maximum in the mantle overheating was above all connected with the iron oxide introduction into the core matter melting process and with the core separation process that began by the end of Archaean (see Fig. 4.1D and E). Our estimates are that at that time nearly $4.2 \times 10^{37}$ erg of heat energy must have been released within Earth over 200 MMY (see Section 5.5). Over the same time interval, Earth lost about $1.8 \times 10^{37}$ erg with the heat radiation. Therefore, approximately $2.4 \times 10^{37}$ more erg of gravitational energy was spent in Late Archaean for Earth heating. That resulted in its additional heating by about 330 °C. Besides, close to $1.35 \times 10^{37}$ erg of the radiogenic energy was released in Archaean, which added 190 °C.

As a result, despite an increase in the temperature difference $\Delta T$, we estimate the surface-normalized mantle temperature at the end of Archaean (about 2.7–2.6 BY ago) at higher

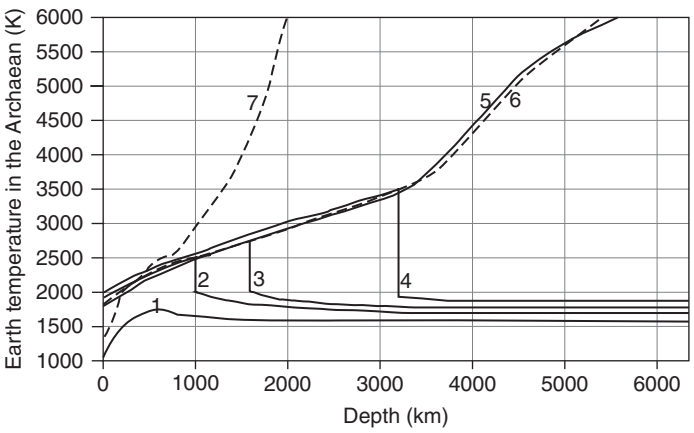


**FIGURE 4.4** The young Earth temperature in Archaean: 1, temperature distribution within Earth after its origin about 4.6 BBY ago; 2, Earth temperature in Archaean about 3.6 BBY ago; 3, sbout 3.2 BBY ago; 4, about 2.8 BBY ago; 5, Earth temperature after the crust separation about 2.6 BBY ago; 6, iron melting temperature; and 7, silicate melting temperature.

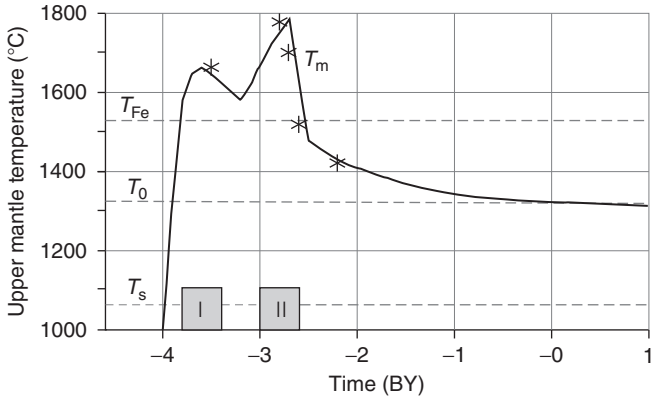


**FIGURE 4.5** Upper mantle temperature in Archaean normalized to the surface (°C): $T_s = 1060$ is the mantle matter solidus temperature; $T_0 = 1320$ is the present-day mantle temperature normalized to the surface; $T_{Fe} = 1530$ is iron melting temperature under standard conditions; the stars are basalt and komatiite temperatures after petrologic data (determined by the authors with the Perchuk program); and I and II are overheated komatiite lava eruption epochs (after Kovalenko et al., 1987).

than 1700 °C, and its overheating compared with the current temperature (≈1320–1330 °C) was at that time 460 °C (see Fig. 4.5).

The reviewed Earth zonal differentiation mechanism explains well the overheating of the Archaean mantle and the presence in time of two temperature maximums.

The first one appeared in Early Archaean about 3.8–3.2 BY ago. The second overheating impulse occurred in Late Archaean, during a period of 3.2–2.6 BY ago. At about 3.2 BY ago, there was a temperature minimum. This process reliably explains an important peculiarity in the development of the Archaean mantle magmatism, which is the existence of two impulses when overheated high-temperature komatiite lavas were melted out from the mantle. This event exactly coincides in time (Kovalenko et al., 1987) with the mantle temperature maximums determined earlier.

Iron and its oxides were released in Archaean in relatively narrow differentiation layers. Because of this, the density distributions in Earth at that time were highly contrasting (Fig. 4.6). The main distinction between the Archaean Earth and the modern earth, however, was the absence of the core through the end Archaean. The estimates show that by the time 2.8 BBY ago, close to $1.01 \times 10^{27}$ g of the core matter was separated which is 52.8% of the current core mass of $1.942 \times 10^{27}$ g.

In 200 MMY (i.e., by the end Archaean), $2 \times 10^{26}$ g more of the core matter (or 10.7% more) was released. As a result, the mass of the core formed by the end Archaean reached $1.21 \times 10^{27}$ g, which is around 62.3% of the present-day core.

Therefore, 62.3% of the core matter was released during 1.4 BBY of Archaean. And during Proterozoic and Phanerozoic (total duration, 2.6 BBY), only 37.7% of the core matter was released. Thus, the differentiation process of Earth's matter proceeded in Archaean at least 3 times more intensely than during the subsequent epochs.

Let us now review the young Earth's matter viscosity using a well-known correlation between viscosity and temperature:

$$\eta = \eta_0 \exp\left\{\frac{W}{RT}\right\}, \tag{4.10}$$

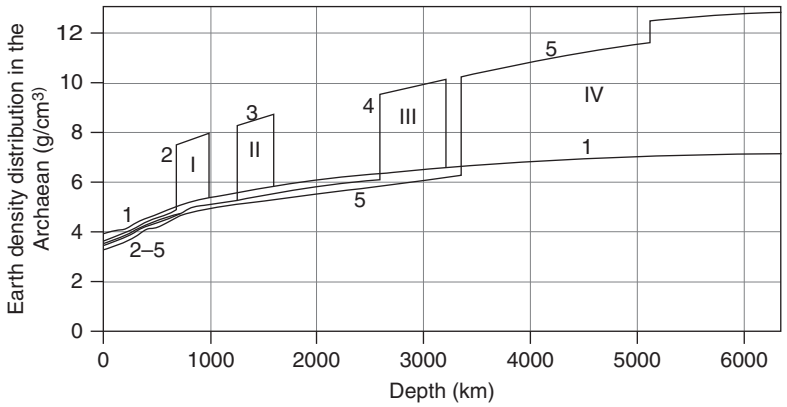


**FIGURE 4.6** Earth density distribution in Archaean: 1, primordial Earth's matter density prior to differentiation; 2–5, densities of differentiated mantle matter: I and II, density of ironish melts separated in the zonal differentiation of the Earth's matter about 3.6 and 3.2 BBY ago; III, iron oxide melt density about 2.8 BBY ago; IV, density of the core separated at the end of Archaean.

where $\eta_0 \approx 10^{-5}$ P is maximum viscosity of the melted matter at infinitely high temperature $T$ and $W$ is the viscous flow activation energy; $R = 1.987$ cal/mol deg is the gas constant. The activation energy is strongly dependent on pressure $p$ (Zharkov, 1983)

$$W = W_0 + Vp\,, \tag{4.11}$$

where $W_0$ is the activation energy at $p = 0$, $V$ is the factor accounting for the value of the activation volume $\Delta V$. Let us assign the most probable temperature and viscosity distributions (for instance, those shown in Figs. 2.17 and 2.20). Now we can determine probable $W(p)$ values within the present-day Earth. For the depth interval 200–2000 km (i.e., to the depth where the separation of the univalent iron melt into intergranular spaces begins) the coincidence with the viscosity distribution as shown in Fig. 2.20 occurs under the following values of Eq. (4.11) parameters: $W_0 = 210$ kcal/mol and activation volume $\Delta V = 6.91$ cm$^3$/mol. One calorie is equal to $4.187 \times 10^7$ erg/s, and $p$ is measured in kilobars, we find $V = 6.91 \times 10^6 / 4.187 \times 10^7 = 0.165$.

Equation (4.11) is very approximate but still may be utilized at pressure $p \ll K$, where $K$ is rock isothermal compression modulus (Zharkov, 1983). For the mantle rocks, $K \approx (1.5 \div 2)$ Mbar. Because of this, Eq. (4.11) may be used for a description of the convecting mantle in the young Earth upper section. It is even more justified as in Archaean practically all metallic irons were removed from the convecting mantle, and its composition, except for the iron oxide concentrations, was close to the composition of the present-day mantle with the already determined parameters of Eq. (4.11).

About 22–23% of the iron oxides were contained in the young Earth's matter (and in the Archaean convecting mantle). Elevated FeO content in silicates lowers their melting temperature. It is, therefore, reasonable to expect that activation energy of the convecting mantle matter in Archaean was much lower than its just determined value for the present-day mantle. We assumed in Eq. (4.11) half activation energy $W_0$ value. Then we find for the convecting mantle in Archaean:

$$W \approx 100 + 0.165p. \tag{4.11'}$$

To describe the iron melt viscosity within the Earth's matter differentiation zones, we assumed even smaller $W_0$ value:

$$W = 45{\cdot}10^5 + 0.165{\cdot}p. \tag{4.11''}$$

Under elevated pressures approaching in their value to compression modulus $K$ it is better to use a different equation (Zharkov, 1983):

$$W = W_0\left(\frac{\rho}{\rho_0}\right)^L, \tag{4.12}$$

where $\rho$ is the matter density at pressures $p \gg 0$, $\rho_0$ is the matter density at $p = 0$, and parameter $L$ is determined as:

$$L = \frac{V}{W_0}K \tag{4.12'}$$

(usually $L \approx 2$). To determine viscosity within Earth's primordial matter (accounting for high concentration in it of the metallic iron) we assumed for our calculations $W_0$ value approximately 2.5 times smaller than in the present-day mantle ($W_0 = 84$ kcal/mol) and $L = 2$.

The young Earth was cold so its insides had very high viscosity reaching the values on the order of $10^{30}$ P in the planet's center. That eliminated any possibility of convection. The reason is that the convection rate is always inversely proportional to the matter viscosity, therefore, disappearing small. That is why a rapid formation of the core was impossible at the early stages of Earth evolution. That included also a mechanism proposed by Elsasser (1963) of high-density iron melt flows through such medium. Subsequently, the process of zonal differentiation of the matter emerged in near-surface layers of Earth (200–400 km deep and with viscosity on the order of $10^{16}$ P). The process was evolving and its front was gradually moving down into the depths. The heating of the relatively cold young Earth's matter was slow in its advance, about 0.2–0.15 cm/year in Early and Middle Archaean and closer to 0.4 cm/year in Late Archaean (after Fe·FeO eutectic melt began to melt out). That is why we estimate the duration of the Earth's core separation process at about 1.4 BY (from 4 to 2.6 BY ago; Fig. 4.7).

Again, due to an exceptionally high viscosity of the primordial matter in Earth's center, the only mechanism of the core formation could be squeezing to the surface of the primordial matter of the Earth kernel by much heavier iron and iron oxides melts as it is shown in Fig. 4.1. After the core formed at the Archaean/Proterozoic time boundary and after the onset of a more quiescent barodiffusion mechanism of the mantle matter, the mantle temperature began gradually coming down. In calculating the mantle cool-down rate, we assumed that the current mantle temperature normalized for the surface is close to 1330–1320 °C.

As a result of such change in the differentiation mechanism from the zonal separation of the metallic iron and its oxides to the barodiffusion mechanism of the eutectic Fe·FeO melts release, the chemical density convection must have emerged in the entire mantle. In the

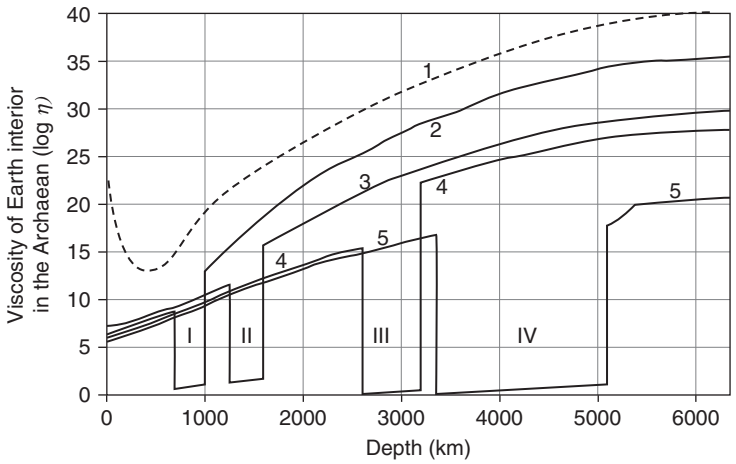


**FIGURE 4.7** Viscosity logarithm of the young Earth: 1, Earth viscosity after its formation about 4.6 BBY ago; 2–5, Earth viscosity in Archaean (respectively, about 3.7, 3.2, 2.9, and 2.8 BBY ago); I and II, iron melt viscosities in Earth's matter differentiation zones; and III and IV, core matter viscosity (univalent iron in $Fe_2O$) in Earth's matter differentiation zone about 2.9 and 2.8 BBY ago.

process, the mantle temperature evened out under the adiabatic law (2.11) according to the $Fe_2O$ core matter melting temperature at the core surface.

This theoretical conclusion matches well with the empirical data of a rapid disappearance of high-temperature komatiites at the Archaean/Proterozoic time boundary (Kovalenko et al., 1987).

## 4.4 BARODIFFUSION MECHANISM OF EARTH'S MATTER DIFFERENTIATION

Thus, the differentiation process of Earth's matter is currently operating. It resulted in the separation within the Earth's center of a high-density core. The development of a theoretical model for such a process is exceptionally difficult. Indeed, the process *per se* is unobservable. We can make a judgment from its indirect manifestations on the surface and using the data of experimental and theoretical physics.

One of the difficulties in studying the process is associated with a significant excess of the silicate melting temperature at great depths over the adiabatic temperature of the mantle. The most likely estimates of the mantle silicate melting temperature under high pressures at the mantle's base are greater than 8000 K. At the same time, the mantle temperature at such depth is close to adiabatic temperature of around 3200 K (see Section 2.8 and Fig. 2.17). It is obvious that such a grandiose temperature barrier of over 5000 °C completely eliminates any possibility of the core separation by way of its melt-out from the mantle.

This difficulty forced us to come up with a different mechanism. We assume that currently the iron oxide separation from mantle silicates occurs due to the decomposition of solid solutions affected by high pressure and iron oxide diffusion from silicate crystals

and from oxide crystallites into the intergranular space of the mantle matter (Monin and Sorokhtin, 1981).

This assumption is based on the Le Chatelier's principle and on the experimentally established phenomenon of solid solution disintegration under high pressures in cases when the molar volume of these solutions $V_s$ exceeds the total of the molar volumes $V_i$ of their components

$$V_s > \sum_i^n V_i. \tag{4.13}$$

Such solutions disintegrate due to a decrease in the maximum concentration $C_i^*$ of the solution components under pressure $p$:

$$\left(\frac{\partial \ln C_i^*}{\partial p}\right)_T = \frac{\Delta V_i}{RT}, \tag{4.14}$$

where $\Delta V_i$ is the change in the total volume at dissolving 1 mol of the component $i$ in the saturated solution, $R$ is gas constant, and $T$ is absolute temperature.

Experiments (Kirkinsky, 1975) showed that the disintegration of real solid solutions is adequately described by Eq. (4.14). This enables us to utilize it for the description of the iron oxide separation process from the mantle silicates. Unfortunately, we do not know from the experiment the value of the volume effect from mixing iron oxides with silicates at superhigh pressure. It may be expected, however, that after the first electron-phase transition in iron, the stereometry of its $Fe_2O$ oxide will be drastically different from the other silicate-forming oxides. Experimental data indicate that the miscibility of components with different crystalline structure drastically declines under elevated pressure. An assumption follows that solid silicate solutions containing the iron oxide under pressures above the level of the first electron-phase transition in iron ($p \approx 130$ kbar) may disintegrate.

The very process of the silicate disintegration, however, is insufficient for the iron oxide separation from the mantle matter because these iron oxides must be released out of the silicate crystalline grid into the intergranular space. The mechanism of such release may obviously be associated only with diffusion. Thermal diffusion usually results in homogenizing the matter, whereas in our case we must have the opposite phenomenon of iron oxide concentration in the intergranular space and films. Such a situation may occur only if there are energy barriers in the way of the diffusing atoms. These barriers must be such as to allow the movement in one direction and to obstruct any reverse movement.

If the condition (4.13) is accomplished, such natural energy barriers arise on the facets of crystals and individual grains. Indeed, at the diffusion from a crystal of some volume $V$ of iron oxides, the energy $\delta E$ is released proportionate to the decrease in total volume of the matter $\delta V$ and pressure $p$:

$$\delta E = p\,\delta V. \tag{4.15}$$

It is obvious that the reverse diffusion for the iron oxides into the crystal would require additional work $A$ for overcoming the pressure and the volume of the matter by the same $\delta V$ value so that:

$$\delta A = \delta E. \tag{4.15'}$$

This phenomenon prevents the iron oxides diffused from silicate crystals and grains from returning back under high pressures and temperatures in the lower mantle. They must, therefore, gradually accumulate in the intergranular spaces and films.

When dealing with the diffusion processes, one has to keep in mind that in actuality only atoms, not their compounds move through the vacancies and imperfections of the crystalline grid. That is why it would be more correct to refer to the iron and oxygen diffusion with their partial diffusion factors $D$(Fe) and $D$(O). These factors differ in value so the atoms move at different rates, and a result is the distortion in stoichiometric compositions of equilibrium compounds of the diffusing elements. In turn, the distortion in stoichiometric ratios causes the emergence and growth of chemical potentials in the boundary layers separating the atoms that went apart. The result of the newly added energy is that the iron and oxygen diffusion rates must equalize according to the composition of the compound or eutectic melt stable under these $P$–$T$ conditions.

Thus, here and thereafter we will be mentioning the oxide diffusion in a tentative way, for the simplicity. What we will actually have in mind will be their effective diffusion as only the atoms can diffuse in solid media.

High pressure exceeding the pressure of the first electron-phase transition drastically affects the physical and chemical properties of iron. Indeed, after such transition the atoms of iron as well as of copper have only one electron remaining on the external s-shell. But there are no endogenous copper silicates, so it is expected that within the lower mantle iron silicates as well become unstable and must disintegrate. As mentioned in Section 2.6, under such conditions the eutectic melt Fe·FeO (equivalent to the univalent iron oxide $Fe_2O$) is a stable iron compound (Sorokhtin, 1972).

It may also be suggested that the bivalent iron oxide decomposition reaction $2FeO \rightarrow Fe_2O + O$ will be taking place on the crystalline facets due to the diffusion of iron and oxygen atoms from iron silicates. On the other hand, the same reaction will be controlling the values of the diffusion factors $D$(Fe) and $D$(O) such that within the crystalline space behind the crystalline facets a stable compound $Fe_2O$ would form.

Physically, this may be explained so: average diffusion rates of iron atoms under high pressure out from the crystals $u_-$ and in the opposite direction, $u_+$ to a greater extent change for iron because after the electron-phase transition this metal drastically changes its physical and chemical properties. If in the process the diffusion of iron indeed is accompanied by the energy release (4.15), then $u(\mathrm{Fe})_- > u(\mathrm{Fe})_+$. At the same time, the oxygen atoms diffusion rate from the crystals $u(\mathrm{O})_-$ and back $u(\mathrm{O})_+$ in themselves, without accounting for the chemical interactions with iron, most likely remain at equilibrium, that is, $u(\mathrm{O})_- \approx u(\mathrm{O})_+$. But part of the oxygen atoms which diffused from the crystals now enters chemical reaction with iron and form a new stable compound $Fe_2O$ outside of the crystals. As a result, the equilibrium diffusion is distorted as now $u(\mathrm{O})_- > u(\mathrm{O})_+$, and therefore, the effective value of the oxygen diffusion factor $D$(O) changes.

It may be expected due to this reaction mechanism that a eutectic melt Fe·FeO (or iron protoxide $Fe_2O$) will form and accumulate only within the intergranular space outside the silicate crystalline grids. At the same time, iron oxide FeO and oxygen released in the reaction will be preserved within the crystal imperfections and with the excess of oxygen will form magnetite molecules:

$$3FeO + O \rightarrow Fe_3O_4. \tag{4.16}$$

Magnetite has the spinel crystalline grid with the most dense atom packing, and for this reason magnetite is very stable mineral under high pressure. It is quite possible that often observed magnetite impregnations—fringes of the mantle-originated olivine (fyalite) are consequences of the reaction (4.16).

Equation (4.14) indicates that with the positive volume effect of dissolution $\Delta V > 0$, that is, if the condition (4.13) is accomplished, maximum concentration $C_i^*$ of the component in the solution will decrease with the increase in pressure:

$$C_i^* = C_{0i}^* \exp\left\{-\frac{\Delta V(p_H - p_0)}{RT}\right\}, \tag{4.17}$$

where $C_{0i}^*$ is the concentration of the component $i$ in saturated solution at $p = p_0$ and $p_0 \approx 130$ kbar $= 0.13 \times 10^{12}$ dyne/cm$^2$ is the pressure of the first electron-phase transition in iron within the mantle at about 400 km depth (pressure at which iron oxides begin to decompose). It follows from Eq. (4.14) that the fraction separation process can develop only if the initial concentration of the component $C_i$ exceeds the maximum concentration $C_i^*$ for given pressure and temperature values (Fig. 4.8):

$$C_i > C_i^*. \tag{4.17'}$$

A total miscibility of iron oxide (e.g., in olivine) with the silica is observed to pressure $p \leq 130$ kbar in the presence of MgO, up to the stoichiometric ratio in fayalite ($Fe_2SiO_4$). That is why it is possible to accept for olivine $C_0^*(FeO) = 0.706$, or normalizing for the core matter, $C_0^*(Fe_2O) \approx 0.628$. The current average iron oxide concentration in the mantle (normalized for FeO) is $\bar{C}(FeO) = 0.083$ (see Table 2.1), and normalized for $Fe_2O$: $\bar{C}(Fe_2O) = 0.074$. So, no iron oxide differentiation can occur under low pressure.

We know that maximum concentration of the silicate saturation with iron oxides $C^*(FeO)$ rapidly declines with pressure as indicated by Eq. (4.14). So it is reasonable to expect that there is a depth in the mantle below which the condition $\bar{C}(Fe_2O) > C_0^*(Fe_2O)$ of solid solution decomposition is accomplished. We assumed that this depth coincides with the maximum at 2000 km on the mantle mechanical quality $Q_\mu$ curve of Fig. 2.19. This maximum corresponds with pressure $p = 0.89 \times 10^{12}$ dyne/cm$^2$ and temperature close to 2730 K.

We now assume that the molar volume ratio $\Delta V/V$ in the lower mantle is relatively unchanged with pressure. Then the volume effect $\Delta V_j$ at any $j$th level (depth) in the mantle

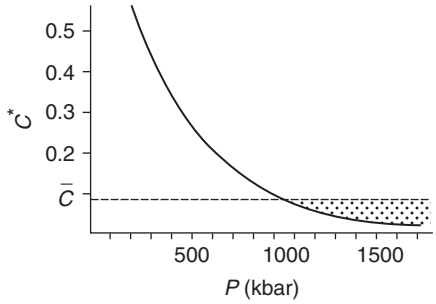


**FIGURE 4.8** Maximum concentration of iron oxide solid solutions in the mantle silicates versus pressure. The dotted area is zone of iron oxide barodiffusion from mantle silicates.

may be expressed through the change of the molar volume $\Delta V$ and density $\rho$ at the critical level (depth) of 2000 km: $\Delta V_j = \Delta V \rho / \rho_j$ (see $\rho$ and $\rho_j$ values in Table 3.2).

Equation (4.14) was derived for the depth of the start of iron oxide decomposition at about 400 km ($p \approx 0.13 \times 10^{12}$ dyne/cm$^2$). It follows from this equation that $C_0^* = 0.628$. From the same equation derived for the critical depth of the separation start of iron oxide from silicates at about 2000 km, $\Delta V_{2000} \approx 0.655$ cm$^3$/mol; in this case at the base of the mantle $\Delta V_{mc} \approx 0.655 \times 5.16/5.6 \approx 0.604$ cm$^3$/mol. Pressure at the core surface is approximately $1.4 \times 10^{12}$ dyne/cm$^2$. Then from Eq. (4.14) we find the sought-for value of the maximum iron oxide saturation concentration of the mantle silicates at its base as $C^*_{mc} \approx 0.027$. The correlation curve (4.14) for the mantle conditions is displayed in Fig. 4.8.

Barodiffusion separation of the core matter from the silicates is accompanied by the release of noticeable energy. According to Eq. (4.15), at depth of 2000 km this energy is $5.5 \times 10^{11}$ erg/mol or 102 cal/g of the released oxide $Fe_2O$. At the base of the lower mantle it increases to $8.15 \times 10^{11}$ erg/mol or 151.6 cal/g. In total, over the life of Earth about $1.3 \times 10^{37}$ erg or almost 9% of the entire Earth gravity differentiation energy was released. Most of this energy was expended for elastic compression of the matter.

The quoted estimates of the medium compaction in barodiffusion differentiation of the mantle matter were published in 1981 (Monin and Sorokhtin, 1981). As mentioned in Section 2.6, somewhat later was published the experimental study by Ohtani et al. (1984). It showed that the formation of eutectic alloys $Fe_x \cdot FeO_{1-x}$ under high pressure is also accompanied by strong compaction. These results manifest that the formation of the core matter with large negative volume effects arising under high pressure must follow toward the formation of an eutectic alloy $Fe_x \cdot FeO_{1-x}$ with the smallest molar volume.

A suggestion that the mantle matter differentiation occurs only in the lower mantle is indirectly supported by some geophysical data. For instance, the seismic wave decay noticeably strengthens at depths between 1800–2000 and 2900 km, and the quality factor $Q_\mu$ for P-waves (see Fig. 2.19) declines in this interval approximately from 500 to 115 near the core surface (Teng, 1968).

The lower mantle layer D″ is also identified by the decay of Earth own oscillations and the quality factor within the layer drops almost by the factor of 10 (Zharkov et al., 1974). This anomaly is so clear that the authors of these publications even proposed to call the D″ layer "a second asthenosphere."

From the viewpoint of the described Earth's matter differentiation mechanism, such comparison is quite justified as it is natural to expect a drastic decrease in the matter viscosity within the release zone of the liquid $Fe_2O$ phase (or eutectic melt Fe·FeO). Moreover, a relatively thin boundary layer (only 20-km thick) was identified based on the dynamic signature of seismic waves reflected from the core surface (Berzon et al., 1968; Berzon and Pasechnik, 1972). We named it "the Berzon layer." Within it, the mechanical rigidity of the lower mantle matter monotonously declines with depth almost to zero.

This fact indicates that through the fill-up of intergranular space in the polycrystalline mantle matter by the $Fe_2O$ melt, this layer gradually acquires the properties of a low-viscosity liquid without any silicate melting.

We now review the changes with time occurring due to diffusion of the heavy fraction (iron oxides) concentration in silicate crystals. For this purpose, we track one of the silicate crystals falling within a descending convective flow from the upper mantle to the lower

one, toward the core surface. Let us assume that the mantle matter differentiation is evolving only within the lower mantle, that is, within the depth interval of 2000–2900 km. Let us further assume that the heavy fraction separation from the mantle matter and iron oxide migration into the core occurs only within a very thin layer at the mantle base. Let us also assume that before crossing the 2000 km level the heavy fraction was uniformly distributed in the crystal volume at the concentration $C_0 < C^*$. Until the crystal crosses the level of the critical pressure $0.89 \times 10^{12}$ dyne/cm$^2$, the diffusion of iron and oxygen atoms from the crystal will be prevented by chemical bonds of these elements with the silica.

After the critical level of $C_0 = C^*$ at about 2000 km is intersected, the $C_0 > C^*$ inequality becomes valid. The diffusion movement of iron and oxygen atoms through the silicate crystal facets is no longer equilibrated because diffusion of these atoms from the crystals is now proceeding with energy release (4.15). As a result, the iron oxide concentration $C$(FeO) on the internal side of the crystal facets will begin declining. At any given moment in time it will be determined, under Eq. (4.14), by the value $C^*$(FeO) of the maximum concentration of the saturated iron oxide solution in the silicates at the temperature and pressure within the lower mantle.

The concentration changes $C$(FeO) in the process of a crystal descent through the lower mantle (which takes the time on the order of $10^7$ years) can spread into the crystalline grid only over a very short distance. The reason for this is that the diffusion factors in silicates under the pressure over $10^{12}$ dyne/cm$^2$ and temperature much lower than the silicate melting point must be very small, something like $D \approx 10^{-21}$–$10^{-22}$ cm$^2$/s.

We need to find the major patterns of the fraction separation process. For this, we search for the solution of the diffusion equation under some simplifying assumptions. We assume, for instance, that the diffusion factor is isotropic and constant in its value all over the descent interval from 2000 to the core surface at 2900 km. In such a case, the problem boils down to the solution of a unidimensional diffusion equation

$$\frac{\partial C}{\partial t} = D \frac{\partial^2 C}{\partial \xi^2}. \tag{4.18}$$

Here, $\xi$ is a coordinate axis perpendicular to the crystal facet. The solution is provided in our earlier publications (Monin and Sorokhtin, 1981; Sorokhtin and Ushakov, 1991, 1993).

We assume that the FeO concentration change depth into the crystal over the mentioned time interval of approximately $10^7$ years is small compared to the crystal size. We put the time origin $t = 0$ at the moment when the crystal intersects the critical pressure level at a depth of 2000 km. The iron oxide concentration $C^*$(FeO) at the crystal facets is determined by Eq. (4.14). According to Table 3.2, pressure within the differentiation level changes insignificantly compared with its average value (0.891–1.384 Mbar). So, we use as a first approximation the linear term of the expansion of this function and assume $C^* = C_0 - ap$. Taking into account the linear pressure increase with depth at these levels and assuming a constant descent rate of the matter in the convection flow, the concentration changes at the crystal facets may be approximated by a liner time function

$$C* = C_0 - at. \tag{4.19}$$

The diffusion and heat-conductivity equation, as is known, are completely analogous. This enables us, under the accepted restrictions, to use a solution of the heat-conductivity equation for the linear flow in a semi-restricted solid published by Carslow and Eger (1964). In this solution, the solid at the initial time has zero temperature, with a source of heat with temperature linearly changing in time acting on it. Then, considering the equivalency of the heat-conductivity and diffusion equations, we receive:

$$C = C_0 - at\left\{\left(1+\frac{\xi^2}{2Dt}\right)\left[1-\Phi\left(\frac{\xi}{2\sqrt{Dt}}\right)\right]-\frac{\xi}{\sqrt{\pi Dt}}e^{\xi^2/4Dt}\right\}, \tag{4.20}$$

where $\Phi(z)=\frac{2}{\pi}\int_0^z e^{-\zeta^2}d\zeta$ and $C_0$ is the initial FeO concentration in the crystal at $t=0$ ($C_0=\text{const}$).

Equation (4.20) determines the iron oxide concentration only within the iron silicate crystals. Outside of these crystals, in the intergranular space, a pure iron protoxide $Fe_2O$ is accumulated so we can assume that between the silicate crystals $C(Fe_2O)=1$.

Figure 4.9 demonstrates the iron oxide concentration distribution in the silicate crystals derived from Eq. (4.20), and the core matter $Fe_2O$ concentration in the intergranular space. The assumption was made that these crystals descended to the core surface together with the convection flow over the period of $10^7$ years.

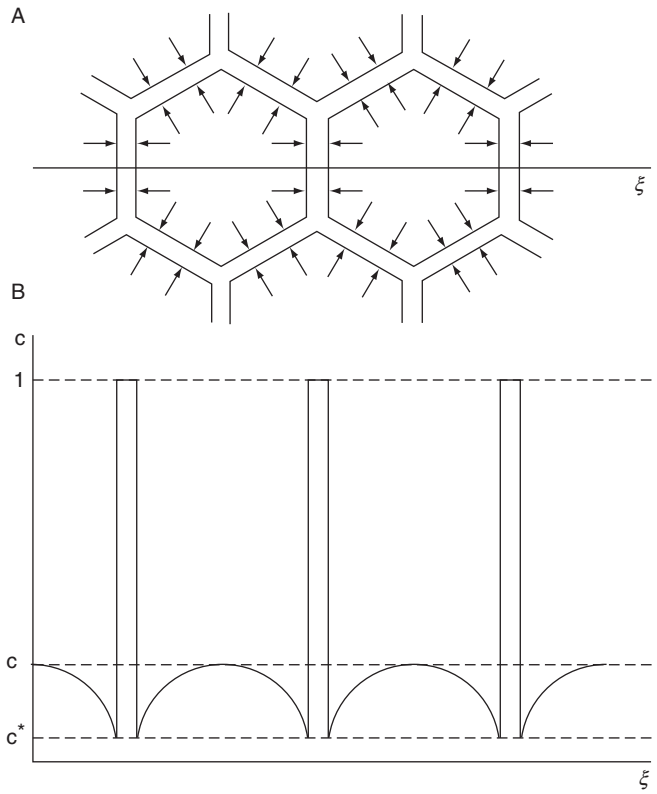


**FIGURE 4.9** Barodiffusion distribution of $Fe_2O$ concentration in silicate crystals within the lower mantle D″ layer: (A) directions of iron oxide diffusion in silicate crystals and (B) iron oxide concentration distribution in the same crystals intercrystalline space after diffusion.

As the mantle matter within the descending convection flow approaches the core surface, the fraction of iron oxides that diffused from the silicate crystals and grains into the intergranular space increases. The liquid status of the external core is an indication that the core matter (i.e., $F_2O$) in the granular space must also be melted. Therefore, the rigid bonds between the crystals in the lower mantle gradually weaken with the approach to the core. This is exactly the reason for a drastic decrease in mantle matter seismic quality within the D″ layer and especially the Berzon layer. As soon as individual inclusions of the melted iron oxide $Fe_2O$ merge near the Earth's core into a single system of the connected liquid films and discharges coating the crystals, grains or separate volumes of the mantle matter, it begins to disintegrate.

Obviously, the mantle depressions squeezed into the core surface must occur underneath the descending convective flows (i.e., underneath the heavier mantle volumes). The opposite must be true for the ascending flows as shown in Fig. 4.10 (Sorokhtin, 1974; Geodynamics, 1979).

The reality of this prediction was proven in mid-1980s (Morelli and Dziewonski, 1987) through the core's seismic tomography: the topography gradients on the core surface reached $\pm 6$ km (see Fig. 2.10).

Therefore, large imperfections exist at the base of the lower mantle and large density gradients between the core matter and the mantle matter ($\Delta\rho_{mc} \approx 4\ g/cm^3$). These, naturally, must cause the emergence of significant extension stresses at the roots of the descending mantle flows. We estimated these stresses at about 10 kbar (Sorokhtin, 1974). The final disintegration of the polycrystalline mantle matter into the individual crystals and granules suspended in the $Fe_2O$ melt occurs due to these stresses at the mantle base underneath the descending flows and results in the emergence of the aggregate state remindful of a "magmatic gruel." The oxide of the univalent iron (the core matter) released earlier from the mantle matter crystals migrates into the Earth's core providing for a gradual increase in its mass.

Apparently, this phenomenon is the cause of a gradual rigidity loss by the mantle matter with its transition to the effective liquid state at the core surface (Berzon et al., 1968; Berzon and Pasechnik, 1972). We emphasize again that the described processes of the core matter separation from the mantle evolve without any silicate melt.

Seemingly, the mantle matter spread from under the roots of the descending flows in the direction of the ascending flows should result in the leveling of the core surface topography. However, such topography leveling in the environment of the convecting mantle is constantly compensated by the descent to these levels of new portions of the fresh mantle matter and ascent

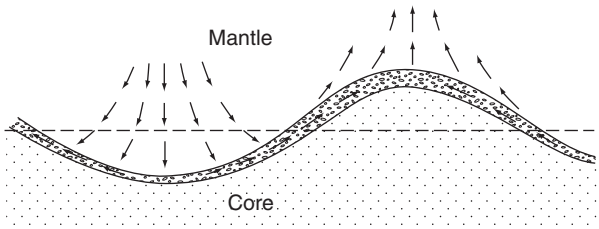


**FIGURE 4.10** Schematics of convective flows near the mantle–core boundary and the formation of ascending mantle flows.

of already differentiated matter in the areas of the ascending flows. As a result, some equilibrated movement is established of the disintegrated mantle matter at the boundary of the mantle and core. This movement connects the convective mantle flows into single closed cells.

The opposite processes develop within the mantle matter ascending flows. Affected by confined pressure, the major part of the melted iron oxide is gradually squeezed out of the emerging mass into the core. Due to the plastic deformations and the intergranular diffusion, the silicate crystals and grains are gradually soldered again into a "continuous" medium. But the differentiated silicates contain less iron oxide than the source mantle matter. For this reason, the mantle matter density in the ascending flows is always substantially lower than that in the descending ones. It causes the emergence of lift (the Archimedes force) in the Earth gravity field which eventually puts to action convective mass exchange in the mantle.

Iron oxide diffusion in the ascending flow matter will be evolving in the opposite direction from the intergranular space into the silicate crystals. Simultaneously, the $Fe_2O_3/FeO$ ratio will increase in the crystals. Magnetite $Fe_3O_4$ molecules will form as well as the iron oxide zonal distribution within the crystals.

The provided qualitative interpretation of undulations (wave-like irregularities) on the core surface gives us an opportunity to determine average density between the primordial and differentiated mantle matter within the descending and ascending flows. Indeed, the mantle pressure on the core surface underneath the ascending mantle flow is somewhat smaller that under the descending flow: $\Delta p = \Delta\rho\Delta h g$. Here, $\Delta p$ is the difference between average pressure and the core underneath the ascending and descending mantle flows, $\Delta\rho$ is the density difference between the mantle and core matter, $\Delta h$ is the amplitude of the core topography difference underneath the ascending and descending mantle flows, and $g$ is the gravity acceleration at the Earth core's surface.

From Table 2.2, we have $\Delta\rho = 9.92 - 5.6 = 4.32\ \mathrm{g/cm^3}$ and $g = 1067\ \mathrm{cm/s^2}$, and from Fig. 2.10 $\Delta h = 12$ km. In this case $\Delta p = -5.53 \times 10^9\ \mathrm{dyne/cm^2} = -5.53$ kbar. On the other hand, using the pressure difference between the ascending and descending flows it is possible to determine parameters of the flows proper: $\Delta p = \delta\rho H_\mathrm{m}\bar{g}_\mathrm{m}$, where $\delta\rho$ is the difference of average density values between the source matter in the descending mantle flow and the differentiated matter in the ascending flow, $H_\mathrm{m} = 2886$ km is average thickness of Earth's mantle, and $\bar{g} \approx 1000\ \mathrm{cm/s^2}$ is average gravity acceleration in the mantle. Then we find

$$\delta\rho = \frac{\Delta p}{H_\mathrm{m}\bar{g}_\mathrm{m}} = 0.019\ \ \mathrm{g/cm^3}. \tag{4.21}$$

As we see, the density difference is not great but over a long period of Earth's tectonic activity the mantle density had enough time to decline substantially. The calculations indicate that after the core formed at the very end Archaean and through present, the average mantle density decreased by about $0.38\ \mathrm{g/cm^3}$. It means that over the recent 2.6 BY each volume of the mantle matter went through the differentiation on the core surface close to 20 times. This helps to estimate average rate of the convective movements in the viscous matter of the lower and middle mantle. It turns out to be nearly 4.6 cm/year, which looks reasonable. To compare, based on the Pacific oceanic plate motion velocities, the mantle matter speed within a relatively thin and low-viscosity asthenosphere (where it can be much higher) reaches only a few tens of centimeters per year.

## 4.5 PROCESS OF EARTH'S CORE GROWTH

It is convenient to review the quantitative side of the Earth's core separation process (same as Earth differentiation process) beginning with the present-day situation where the core grows due to the action of barodiffusion Earth's matter differentiation mechanism. The process rate under the barodiffusion mechanism of the core matter ($Fe_2O$) separation from the mantle silicates is obviously proportionate to the difference between the iron oxide concentration in the mantle $C$ (normalized for $Fe_2O$) and the maximum saturation $C^*$ by these oxides of the solid silicate solutions at the mantle base $C-C^*$ (see Section 4.4).

On the other hand, the rate of iron oxide flow from the boundary layer at the base of the lower mantle (the Berzon layer) into the core, that is, the rate of the core matter separation from the mantle matter must be proportionate to gravity acceleration $g_c$ on the core surface, to the size of this surface and to some constant $K$, which depends on the rate of the barodiffusion. Therefore, the total core mass separation rate is:

$$\dot{M}_c = K(C - C*)4\pi r_c^2 g_c, \tag{4.22}$$

where $r_c$ is the radius of the growing Earth's core. Gravity acceleration on the core surface is:

$$g_c = \gamma \frac{M_c}{r_c^2}, \tag{4.22'}$$

where $\gamma = 6.67 \times 10^{-8}\ \mathrm{cm^3/g\ c^2}$ is the gravitational constant. At $M_c \approx 1.942 \times 10^{27}$ g and $r \approx 3.47 \times 10^8$ cm, the present-day value of $g_c \approx 1.075\ \mathrm{cm/s^2}$ ($K$ is the proportionality factor).

To determine the correlation between the core matter concentration in the mantle $C$ and the core mass $M_c$, we utilize a concept of the evolution parameter or relative core mass (introduced by Keondzhyan and Monin, 1975, 1976):

$$x = \frac{M_c}{C_0 M}, \tag{4.23}$$

where $M = 5.977 \times 10^{27}$ g in the Earth's mass and $C_0 = 0.376$ is the total concentration in Earth of the core matter (iron, iron oxides, and other heavy siderophilic elements migrating into the core).

The present-day value of the $x$ parameter may be determined from the chemical composition of the present-day Earth. Currently, the core matter amount within Earth's core is $1.942 \times 10^{27}$ g, and the modern mantle (whose mass is $4.012 \times 10^{27}$ g) still contains about 4.15% of $Fe_2O_3$ and 4.37% of FeO, which, normalized for the eutectic composition Fe·FeO, gives 7.646% or $2.249 \times 10^{27}$ g of the core matter. Total content of this matter in Earth, accounting for iron oxides within the continental crust, is $2.251 \times 10^{27}$ g.

Therefore, the total concentration of the potential core matter in Earth $C_0 = 0.376$, and the current value of the Earth evolution parameter (which actually determined the relative value of the dimensionless mass of Earth's core) is $x_0 = 0.864$.

The concentration in the mantle and continental crust of the remaining core matter (i.e., iron oxides normalized for $Fe_2O$) is determined from equation

$$C = C_0 \frac{1-x}{1-C_0 x}. \tag{4.24}$$

The calculation shows that the mantle and the crust still must contain about 7.57% of the potential core matter.

It appears that average Earth core density little changed with time as simultaneously with the core growth, pressure on its surface somewhat declined, and increased in its center. Our estimate shows that the initial core density was 10.7 g/cm$^3$, and the current value is 10.6 g/cm$^3$. Considering this, we get from Eq. (4.23):

$$\dot{M}_c = C_0 M \dot{x}. \tag{4.25}$$

Using now Eqs. (4.23)–(4.25), we find the correlation between the growth rate of the relative Earth's core mass and parameter $x$:

$$\dot{x} = \frac{1}{\tau}\left(C_0 \frac{1-x}{1-C_0 x} - C^*\right)x, \tag{4.26}$$

where $\tau = K_c/4\pi\gamma$ is a constant with the time denomination, $K_c$ is a factor describing the rate of the core matter migration from the mantle to the core under the barodiffusion mechanism of Earth's matter differentiation.

To determine the function $x(t)$ we integrate Eq. (4.26) over time and parameter $x$. The gravity acceleration in the Earth center is equal to zero. Thus, from (4.22), the barodiffusion differentiation process could not start in the Earth center but could only occur after the core "fetus" formed. We reviewed a possible scenario of such process in Section 4.1.

Geological data and the aforementioned theoretical constructions indicate that the "fetus" formation process, with a relative mass $x_e$, lasted almost 1.4 BY. But by the Archaean/Proterozoic time boundary about $t_e \approx 2.6$ BY ago such core fetus had already been formed (see Fig. 4.1). After that, the further core growth proceeded only due to the barodiffusion mechanism s described in Section 4.4.

This view is supported, in particular, by the drastic and radical change of Earth's core tectonic regimes. In Archaean, domal–fluidal structures of the granite–greenstone belts dominated but were replaced by geosynclinal and riftogenic lineaments in Proterozoic.

By integrating (4.26) from $t_e$ to $t$ and from $x_e$ to $x$ we obtain (Monin and Sorokhtin, 1982a):

$$t - t_e = \frac{\tau}{1-C^*}\left[\ln\frac{a-x}{a-x_e} - \frac{1}{aC_0}\ln\frac{x_e(a-x)}{x(a-x_e)}\right], \tag{4.27}$$

where $a = (C_0 - C^*)/C_0(1-C^*)$, $t_e$ is the time when the core fetus completely formed, and $x_e$ is the relative mass of fetus at the time $t_e$.

The value $C_0$ of the total core matter concentration in Earth may be determined from its current chemical composition. Presently, the core contains $1.94 \times 10^{27}$ g of the core matter, remaining in the mantle is close to 4.15% $Fe_2O_3$ and 4.37% FeO, which, if normalized for the Fe·FeO eutectic composition, gives 7.65% or $0.307 \times 10^{27}$ g of the core matter. Total content in Earth, accounting for iron oxides within the continental crust, is $2.25 \times 10^{27}$ g of this matter. Thus, total concentration of the core matter in Earth is $C_0 = 0.376$, and the present-day value of the evolution parameter, based on Eq. (4.23), is $x_0 = 0.864$.

The time constant $\tau$ in Eqs. (4.26) and (4.27) may be determined based on energy considerations. In Section 5.5, when analyzing Earth energy balance we show that presently nearly $3.07\times10^{20}$ erg/s or $9.67\times10^{27}$ erg/year of heat energy is generated in the Earth's matter gravity differentiation. Let us assume as a first approximation that the total energy of Earth gravity differentiation is more or less proportionate with the core mass (or core matter) released by this time, that is

$$E_g \approx E_\infty x \tag{4.28}$$

$$\dot{E}_g \approx E_\infty \dot{x}, \tag{4.28'}$$

where $E_\infty$ is the heat component of the total Earth gravity energy. Over the life of Earth, $E_g \approx 1.26\times10^{38}$ erg of the Earth's matter gravity differentiation associated heat energy was released in its depths. From this, $E_\infty \approx 1.458\times10^{38}$ erg. Knowing the present value of $\dot{E}_g \approx 3.065\times10^{20}$ erg/c, we determine from Eq. (4.28′) that $\dot{x}_0 \approx 0.664\times10^{-10}$ year$^{-1}$.

Knowing $C^* = 0.027$ (see Section 4.4) and the parameter values $x_0 = 0.864$ and $C_0 = 0.376$ determined above, we find that $a = 0.954$, and from Eq. (4.26) $\tau \approx 0.635\times10^9$ years. Inserting these parameters values into Eq. (4.27) and assuming $t_0 - t_e = 2.6\times10^9$ years, the relative mass of Earth core fetus at the time when it was completely formed at the Archaean/Proterozoic time boundary about 2.6 BY ago is $x_e = 0.543$.

Equations (4.26) and (4.27) define Earth's core growth only within the main sequence of the Earth group planet evolution under the barodiffusion mechanism of iron oxide separation from the mantle silicates at $t > t_e = -2.6\times10^9$ years. For the time interval of the core fetus formation ($-4\times10^9 < t < t_e = -2.6\times10^9$ years, i.e., in Archaean), the analytical function $x(t)$ may be determined from the mass of the convecting mantle (4.9), therefore, from the mass of the released core matter, and from Eq. (4.29):

$$x = \frac{4/3\left[(R-H+h)^3 - (R-H)^3\right]S_{AR}\rho_{Fe}}{MC_0}, \tag{4.29}$$

where $R$ is earth radius; $H$ is depth to the base of the Earthy matter zonal differentiation layer in Archaean; $h$ is the thickness of the iron melt layer as determined from Eq. (4.6); $\rho_{Fe}$ is iron melt density; $S_{AR}$ is, as before, the factor taking into account a gradual expansion of the equatorial zone of Earth tectonic activity in the Archaean mantle (4.7); $\Delta t$ is the running time from the beginning of Archaean (4 BY); and $1.4\times10^9$ years if the duration of Archaean.

The evolution parameter $x$ value in Eq. (4.29) depends on the concentration $C$(Fe) of the core matter coming into melt through the thickness $h$ of the iron melt layer, and the thickness is found from Eq. (4.6):

$$C(\mathrm{Fe}) = 0.136 + 0.239\left[1 - \exp\left\{\frac{-\Delta V(p-p_{cr})}{RT}\right\}\right], \tag{4.30}$$

where $\Delta V$ is the change in total volume of the saturated iron oxide solid solution in silicates at dissolving one mole of the iron oxide in this solid solution; $p$ is pressure at the depth $H$; $p_{cr}$ is pressure at the critical depth where iron oxides begin to separate (in our case $H_{cr} \approx 1400$ km, and $p_{cr} = 656$ kbar); $R$ is the gas constant; $T$ is Earth temperature at depth $H$.

We select the $\Delta V$ value so that parameters $x$ in Eqs. (4.27) and (4.29) for the Archaean/Proterozoic time boundary coincide with one another ($x_{2.6}=0.544$) and find $\Delta V \approx 0.026$ cm$^3$/mol.

The derived correlation between of the Earth evolution parameter versus time enables the determination of the Earth's core growth curve. The present-day core mass is $1.94\times10^{27}$ g, the present-day parameter $x=0.864$, thus, the curve values in Fig. 4.11 must be multiplied by $2.212\times10^{27}$ g. Then, using Eq. (4.26) we can determine the rate of change of the evolution parameter $\dot{x}(t)$ as shown in Fig. 4.12, as well as the rate of the core matter separation from the mantle (see Fig. 4.13). In a similar way, the Earth's core mass growth may be determined from the graph of the evolution parameter (Fig. 4.14).

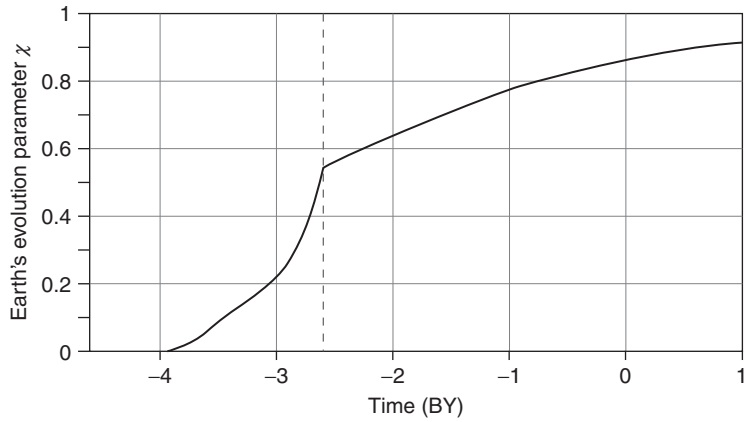


**FIGURE 4.11** Earth's evolution parameter describing the Earth's core relative growth (in Archaean, a relative mass of the separated core matter). The dashed line denotes the end of the core separation process.

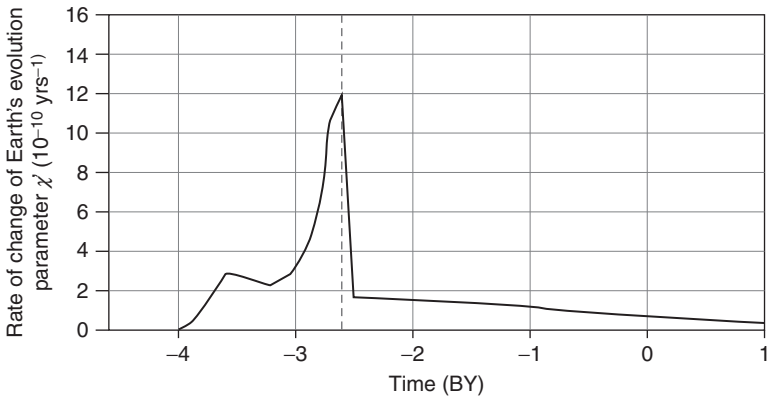


**FIGURE 4.12** Rate of change of Earth's evolution parameter describing relative speed of core matter separation and core growth.

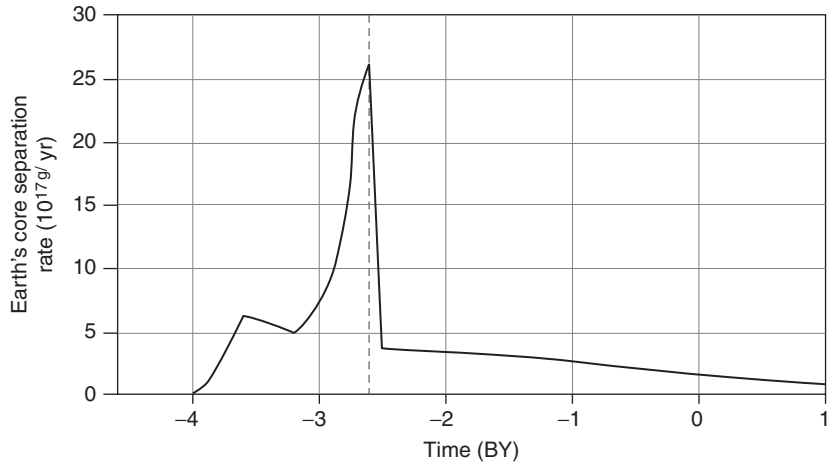


**FIGURE 4.13** Earth's core growth rate.

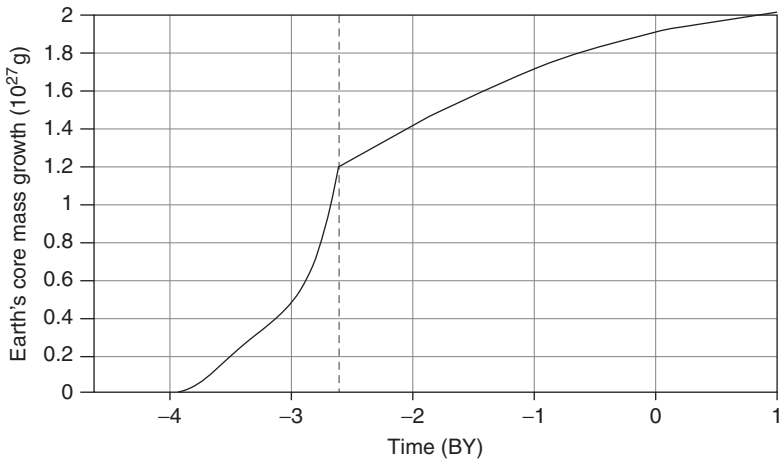


**FIGURE 4.14** Earth's core mass accumulation (core growth).

Earth's gravitational instability emerged in Archaean due to the functioning of the matter zonal differentiation mechanism. As mentioned in the previous section, it resulted, most likely, in the catastrophic events at the end Archaean of a rapid shifting of the previously separated core matter to the Earth center. For this reason, it is reasonable to believe that at the Archaean/Proterozoic time boundary 2.6 BY ago the young Earth's core completely formed, and the further differentiation of Earth's matter changed to a quieter mechanism of the barodiffusion separation of the univalent iron oxide $Fe_2O$. The moment when Earth transferred to a new evolution regime (which may be called the main sequence of the planet's evolution) is clearly seen in Fig. 4.13 at the time of about 2.6 BY ago. As Fig. 4.14 shows, approximately 63% of the current core mass had been formed during the first

1.4 BY of Earth's geological evolution. The remaining 37% separated in Proterozoic and Phanerozoic, over the time period of 2.6 BY.

Thus, under our Earth model evolution the core had not yet existed in Archaean. Instead, there have been a ring belt of heavy iron and its oxides melt of the eutectic composition. This liquid iron–iron oxide asthenosphere was slowly descending into Earth depths gradually broadening and increasing in thickness.

Accordingly, the geomagnetic field at the time must have been substantially different from the present-day one. The real Earth's core, although somewhat smaller in size and mass ($M_{2.6} \approx 1.22 \times 10^{27}$ g) then the present-day one ($M_{0.0} \approx 1.94 \times 10^{27}$ g), formed only by the Archaean/Proterozoic time boundary. So, we may take it that the Earth's matter was accumulating in the Archaean mantle, and beginning in Proterozoic, after its separation, the core proper was growing (see Fig. 4.14).

After the real iron oxide core formed, the present-day kind of a dipole magnetic field apparently emerged. Paleomagnetic data indicate (Hale, 1987) that this theoretical conclusion finds its experimental confirmation (Fig. 4.17).

We determine from Eqs. (4.25) and (4.26) and from the present-day value of the parameter $\dot{x} \approx 0.664 \times 10^{-10}$ year$^{-1}$ that currently nearly $1.45 \times 10^{17}$ g/year or 145 billion tons per year of the core matter ($Fe_2O$) or approximately 127 billion tons per year of the metallic iron migrate from the mantle to the core. During Late Archaean 2.8 BY ago, however, close to 1.9 trillion ($10^{12}$) tons per year of metallic iron was melted out.

## 4.6 EVOLUTION OF CHEMICAL COMPOSITION OF THE MANTLE

The provided description of the Earth's core separation process enables us to theoretically determine the evolution of the mantle's chemical composition.

First of all, we will be interested in the composition of the convecting mantle. In Proterozoic and Phanerozoic, after the young core formation process was completed, the notions of the convecting Earth mantle and just mantle were one and the same. It was different in Archaean. The convecting mantle at that time included only those areas of the Earth shell which underwent zonal differentiation of the Earth's matter and were involved in the convective flows.

The convecting mantle in Early Archaean was relatively thin and, most likely, existed as a ring geosphere underneath the Earth equatorial belt. Only by the very end Archaean did the convective mantle spread to cover almost the entire Earth (see Fig. 4.1). Besides, at the time of the core formation 2.6 BY ago there was an addition to the convecting mantle of the matter from the former Earth "kernel" with its primordial concentrations of iron, iron oxides (nearly 13% and 23%), siderophilic elements, sulfides of chalcophilic metals, and other ore elements, including platinoids.

This is directly supported by unique differentiated base and ultramafic Early Proterozoic rocks intruded in Early Proterozoic many old shields. The most typical classical complexes of this type are laminated intrusive Bushveld massif in South Africa, Great Dyke intrusion in Zimbabwe, Sudbury norites in Canada, gabbronorite complex Pechenga and Pan Intrusions on the Kola Peninsula in Russia, all rich in platinum, cobalt, nickel, copper, and other ore elements. What is important is that these type intrusive buildups with very high contents of ore elements never repeated, before or after.

Thus, iron, its compounds, and other siderophilic elements were moved from the primordial Earth's matter into the heavy fraction separation zones. They subsequently migrated to the emerged Earth's core, and the mobile and lithophilic elements migrated to the Earth's crust, hydrosphere, and atmosphere. All these events must have caused significant changes in chemical composition of the convecting mantle. The removal of the heavy fraction (the core matter) from the mantle matter must have unavoidably resulted in relative growth of the concentration for the remaining elements and compounds.

For instance, in Early Archaean, when the zonal differentiation began and the removal from the convecting mantle of the entire iron ($C_0(\mathrm{Fe}) = 0.131$) contained in the primordial Earth matter, the contents of other elements and compounds $C(i)$ in the residual mantle drastically increased by about 15% (Fig. 4.15) to the level determined by the following equation:

$$C(i) = \frac{C_0(i)}{1 - C_0(\mathrm{Fe})}, \tag{4.31}$$

where $C_0(i)$ is the initial concentration of a given element (compound) in Earth's primordial matter. During Proterozoic and Phanerozoic (i.e., after the barodiffusion differentiation of Earth's matter began functioning), the residual element and compound concentration in the mantle, as a result of iron and iron oxides migration into the core, started to increase under the following law:

$$C(i) = \frac{C(i)_0}{1 - C_0 x}, \tag{4.32}$$

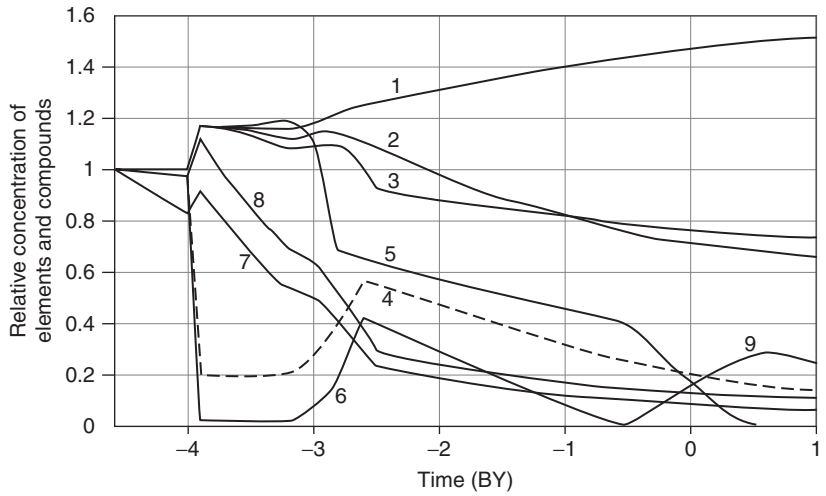


**FIGURE 4.15** Evolution of convecting mantle's chemical composition in relative concentrations (the concentration of a given compound in the primordial Earth's matter is taken for the one): 1, $SiO_2$, $TiO_2$, MgO, CaO, $Al_2O_3$; 2, $H_2O$; 3, $K_2O$; 4, Ni and other siderophilic and chalcophilic elements and compounds; 5, FeO; 6, Fe; 7, U; 8, Th; and 9, $Fe_3O_4$.

where $C_0 = 0.376$ is, as previously, the source core matter (Fe + FeO + FeS + Ni) concentration in Earth's matter normalized for $Fe_2O$. The total core matter concentration in the Proterozoic and Phanerozoic mantle (normalized for $Fe_2O$) declined with time as follows:

$$C = C_0 \frac{1 - x}{1 - C_0 x}. \tag{4.33}$$

The changes in the post-Archaean mantle in the content of the nickel, gold, platinoids, iron sulfides, lead, copper, and some other siderophilic elements which also gradually migrated into the core, followed a similar law:

$$C(i) = C(i)_0 \left[\frac{1 - \alpha x}{1 - C_0 x}\right], \tag{4.33'}$$

where $\alpha$ is the mobility factor of the element or compound, which defines its fraction migrating from the mantle to the core: at $\alpha = 0$ Eq. (4.33′) turns into Eq. (4.32), and at $\alpha = 1$, into Eq. (4.33). Figure 4.15 shows relative contents of the major petrogenic elements as derived from Eqs. (4.31) to (4.33′).

We may now determine the percentages of the elements and compounds (Fig. 4.16) by way of inserting the initial concentration values from Table 2.1 or from the publication by Sorokhtin (1974).

The zonal differentiation of Earth's matter began 4 BY ago. After that, the iron content in the convecting mantle must have declined to the equilibrium iron concentration of this metal in the upper mantle silicate melt over the iron separation zones. The miscibility of such melts was low and the density difference was great. Thus, it may be suggested that during most of the Archaean time the metallic iron content in the convecting mantle was close to zero: $C(\text{Fe}) \approx 0$. In Late Archaean about 2.8 BY, ago the metallic iron content in the convecting mantle began to grow and reached 5.5% by end Archaean. The reason was that in the end Archaean a great amount of the primordial Earth's matter with the initial concentration of iron of 13.1% entered in the convecting mantle (see Fig. 4.1).

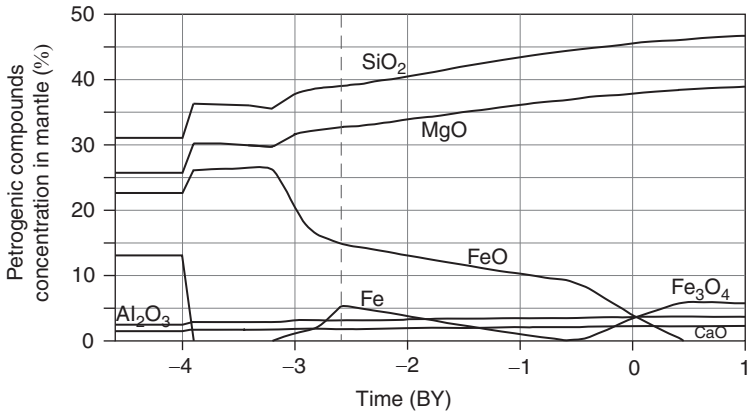


**FIGURE 4.16** Evolution of major petrogenic elements and compounds in the convecting mantle.

In Proterozoic, the metallic iron content in the mantle began declining again due to its migration into the emerged core (see Figs. 4.15 and 4.16). Changes of iron and iron oxide concentrations in mantle during the post-Archaean stages of Earth evolution may be determined from basic reactions of the core matter formation. For instance, in Proterozoic (as well as late in Archaean, between 2.8 and 2.6 BY ago) the formation of this substance followed this reaction:

$$\mathrm{FeO} + \mathrm{Fe} \rightarrow \mathrm{Fe_2O}. \tag{4.34}$$

For each 56 parts of the metallic iron and 72 parts of its bivalent oxide, 128 weight parts of the core matter formed

$$m(\mathrm{Fe}) = \frac{56}{128}\widetilde{C}_0 M x, \tag{4.35}$$

where $\widetilde{C}_0 = 0.363$ is the total content of Fe and FeO in Earth normalized for $Fe_2O$ (not accounting for other core matter heavy components such as FeS and Ni) and $M$ is Earth mass. Part of iron remained in the post-Archaean mantle:

$$C(\mathrm{Fe})M_\mathrm{m} = C(Fe)_0 M - \frac{56}{128}\widetilde{C}_0 x M. \tag{4.36}$$

As we know that the mantle mass $M_\mathrm{m}$ after Archaean decreased under the following law:

$$M_\mathrm{m} = M(1 - C_0 x) \tag{4.37}$$

we finally find:

$$C(\mathrm{Fe}) = \left[C(\mathrm{Fe})_0 - \frac{56}{128}\widetilde{C}_0 x\right]\frac{1}{1 - C_0 x}. \tag{4.38}$$

Similarly, we find that the content of the bivalent iron oxide in the post-Archaean mantle changed as follows:

$$C(\mathrm{FeO}) = \left[C(\mathrm{FeO})_0 - \frac{72}{128}\widetilde{C}_0 x\right]\frac{1}{1 - C_0 x}. \tag{4.39}$$

An important conclusion from Eq. (4.38) is that the free (metallic) iron could be preserved in the mantle only till a certain critical time $t_{cr1}$ when $C(\mathrm{Fe}) = 0$ and the critical evolution parameter value $x = x_{cr1}$. We know that $C(\mathrm{Fe})_0 = 0.131$, so we determine from (4.38) $x_{cr1} \approx 0.825$, and from (4.27) we find the time of the total metallic iron disappearance from the mantle: it turns out to be approximately 500 MMY ago.

Despite the approximate nature of the calculations, the determined time is surprisingly close to the timing of the major biologic boundary in the evolution of highly organized life on Earth (the Proterozoic/Phanerozoic boundary about 570 MMY ago).

This coincidence cannot be accidental. Indeed, the event of the metallic iron disappearance from the mantle and rift zones (where it previously was in contact with the oceanic water) predetermined a radical change in reduction potential of the external Earth shells. The reason was that free iron is the major chemical agent which actively absorbed oxygen from the hydrosphere (and atmosphere) during the entire Precambrian evolution.

Only after the metallic iron totally disappeared from the convecting mantle, oxygen generated by the plants and produced from the water vapor photodissociation could accumulate in the atmosphere in the amounts sufficient for the appearance and normal functioning of live forms on Earth surface (Sorokhtin, 1974) (see in more details in Chapters 12 and 15).

We discuss the iron transition mechanism from the mantle into the hydrosphere, with the subsequent oxygen absorption from the atmosphere, in Section 10.5.

Equations (4.38) and (4.39) may be used only within the evolution parameter range of $x_{2.6} \le x \le x_{0.5}$, that is, for Proterozoic when the core matter formed under reaction (4.34). For the time corresponding with $x \ge x_{cr1} = x_{0.5}$, it is necessary to remember that after the metallic matter disappeared from the mantle the core matter in the lower mantle formed differently:

$$2FeO \rightarrow Fe_2O + O. \tag{4.40}$$

And the oxygen released under this reaction above the stability level of iron oxides with silicates solutions (see Section 4.4) bonded again with iron oxides forming the magnetite component of the mantle:

$$3FeO + O \rightarrow Fe_3O_4. \tag{4.41}$$

For this reason, until the total oxidizing of the bivalent iron at $x = x_{cr2}$, the core matter formation occurs according to the following summary reaction:

$$5FeO \rightarrow Fe_2O + Fe_3O_4, \tag{4.41'}$$

Under which 128 weight parts of the core matter and 232 parts of magnetite forms for every 360 weight parts of the bivalent iron oxide.

Using reaction (4.41′), the total balance of masses participating in iron oxide differentiation is:

$$C(FeO)M_m = C(FeO)_1 M_{m1} - \widetilde{C}_0 M(x - x_{cr1}) - \frac{232}{128}\widetilde{C}_0 M(x - x_{cr1}), \tag{4.42}$$

where $C(FeO)_1$ and $M_{m1}$ are, respectively, FeO concentration and the mantle mass at $x = x_{cr1}$. From this, for the evolution parameter range $x_{cr1} \le x \le x_{cr2}$:

$$C(FeO) = C(FeO)_1 \frac{1 - C_0 x_{cr1}}{1 - C_0 x} - \frac{360}{128}\widetilde{C}_0 \frac{x - x_{cr1}}{1 - C_0 x} \tag{4.43}$$

and

$$C(Fe_3O_4) = \frac{232}{128}\widetilde{C}_0 \frac{x - x_{cr1}}{1 - C_0 x} \tag{4.44}$$

A second critical value of the parameter, $x_{cr2}$, is determined from condition $C(FeO) = 0$ at $x = x_{cr2}$ considering that at $x_{cr1} = 0.825$, $C(FeO) = 0.102$, then $x_{cr2} = 0.894$, and from Eq. (4.27) $t_{cr2} \approx +0.6 \times 10^9$ years. The trivalent iron oxide is unstable at high pressure and changes into the denser magnetite $3Fe_2O_3 \rightarrow 2Fe_3O_4 + O$. Thus, in the future (in about 600 MMY) all iron that still remains in the mantle will be oxidized into the stable under high pressure magnetite phase $Fe_3O_4$. So, at the stage three of the Earth's matter barodiffusion differentiation the core matter will be forming as follows:

$$2Fe_3O_4 \rightarrow 3Fe_2O + 5O \tag{4.45}$$

And the content of the magnetite component in the mantle will be determined as

$$C(Fe_3O_4) = \frac{464}{384}\tilde{C}_0\frac{1-x}{1-C_0x}. \tag{4.46}$$

Another conclusion is important for the understanding of how life on Earth will further evolve. After the total mantle iron is oxidized into the migmatite phase (in about 600 MMY), oxygen released at the core matter formation under reaction (4.45) will no longer be held in the convecting mantle and will be entering Earth atmosphere and hydrosphere. Since the time it happens the oxygen partial pressure will begin to grow significantly (Sorokhtin, 1974). That will kill all land life. The limited oxygen solubility in the water will delay the end of life in the world ocean. However, this will result in an increase of the atmospheric pressure which will lead to a drastic increase in the greenhouse effect and the emergence on Earth to the irreversible environment of a Venus-type hot climate (see Chapters 13–15).

Obviously, there will be no direct filtration of the volatile and mobile elements and compounds dispersed in the mantle. It will not happen because the mantle matter is dense and highly viscous ($\eta \approx 10^{20}$–$10^{23}$ P), so the diffusion factors in such matter are on the order of $D \approx 10^{-21}$–$10^{25}$ cm$^2$/s. Therefore, the migration of lithophilic and volatile components from the mantle to the external geospheres (the continental crust, hydrosphere, and atmosphere) may develop only through melting of the mantle matter. That, however, is only possible within the near-surface portions of the mantle (see Fig. 2.18), and not anywhere but only wherever Earth rigid shell (its lithosphere) is cut by deep-seated faults through which basalt magmas are erupting.

So, in order to estimate concentration changes of the volatile and mobile elements and compounds which migrate in the process of Earth evolution from the mantle into the crust, hydrosphere, and atmosphere, we need an additional parameter characterizing the mobility of the components under consideration.

The mobility of elements and compounds depends not only on their chemical properties but also on the degree and depth of melting of the mantle matter underneath Earth's rift zones which are the main channels feeding juvenile basalt magmas and its dissolved volatile and mobile elements to the surface.

If we take the mobile elements, which concentrate predominantly within the continental crust, their mobility parameters depend also on the reworking regimes of the oceanic crust and deposits in the subduction zones where the secondary mobilization of the mobile elements occurs and their migration from the oceanic crust into the continental happens. Besides, part of the elements and their compounds (such as $H_2O$, $CO_2$, $K_2O$, etc.), which earlier migrated into the external geospheres (the Earth crust, hydrosphere, and atmosphere), can again be sucked into the mantle through the subduction zones and get involved again in the matter recirculation. That is why only the effective values of such elements and compounds should be treated as their mobility.

It needs to be noted here that the very degassing processes of volatile compounds become possible only due to the existence of the convective mass exchange in the mantle. This exchange continuously delivers into the rift zones on Earth surface new amounts of the mantle matter capable of separation and release of the mobile elements. It follows from

this that the migration rate of mobile elements from the mantle to the external geospheres must be proportionate with the rate of the mantle convective mass exchange. In this case, the removal rate of such component from the mantle is:

$$\dot{m}_i = -(m_i)_{\mathrm{m}} \chi_i \dot{z}, \tag{4.47}$$

where $(m_i)_{\mathrm{m}}$ is the mass of $i$th component in the convecting mantle, $\chi_i$ is its mobility factor, and $\dot{z}$ is the parameters characterizing Earth tectonic activity (and convective mass exchange in the mantle). In general, Earth tectonic activity is proportionate with the depth heat-flow coming from the mantle $\dot{z} \propto \dot{Q}_{\mathrm{m}}$ (see Section 5.6)

$$z = (Q_{\mathrm{m}} - Q_{4.0})/(Q_{\mathrm{m}0} - Q_{4.0}), \tag{4.48}$$

where $Q_{4.0} \approx 1.6 \times 10^{37}$ erg is the Earth's heat loss by the beginniong of its tectonic activity about 4 BBY back; $Q_{\mathrm{m}0} \approx 10.77 \times 10^{37}$ erg is the total heat loss by the mantle by the present. In such a case, Earth tectonic activity is described by the time derivative of the parameter $z$:

$$\dot{z} = \dot{Q}_{\mathrm{m}} / \left|\dot{Q}_{\mathrm{m}0}\right|, \tag{4.48'}$$

where $\dot{Q}_{\mathrm{m}}$ is the current value of the depth heat-flow and $\left|\dot{Q}_{\mathrm{m}0}\right| = 3.39 \times 10^{20}$ erg/s is absolute value of the current heat Earth's heat loss.

Now, to the concentrations of elements and their compounds:

$$C(i) = \frac{(m_i)_{\mathrm{m}}}{M_{\mathrm{m}}}. \tag{4.49}$$

For Archaean:

$$C(i) = \frac{C(i)_0}{1 - C(\mathrm{Fe})_0} \mathrm{e}^{-\chi_i z}. \tag{4.50}$$

And similarly for Proterozoic and Phanerozoic:

$$C(i) = \frac{C(i)_0}{1 - C_0 x} \mathrm{e}^{-\chi_i z}. \tag{4.50'}$$

In general, the mobility factors $\chi_i$ could have differed in Archaean and during post-Archaean time due to different mantle matter differentiation mechanisms and different formation conditions of the continental crust, hydrosphere, and atmosphere in those epochs. This makes the solution of Eqs. (4.50) and (4.50′) more difficult and forces the involvement of additional data about the development of the components under consideration in Archaean and Proterozoic.

In some cases, it is possible to fulfill this condition. For instance, let us assume (after Taylor and McLennan, 1985) that up to 70% of the continental crust mass formed in Archaean (which is close to our theoretical calculations). Let us further assume that it contained approximately 1.8% of $K_2O$. Let us also assume that for the modern crust $C(K_2O) \approx 2.1\%$ (see Section 2.3). Then it turns out that the potassium mobility factor in Archaean was close to $\beta(K_2O)_{\mathrm{AR}} \approx 0.56$, and during the subsequent epochs it was $\approx 1.07$.

A similar estimate for the water performed under a technique described in Chapter 11 shows that in Archaean $\chi(H_2O)_{\mathrm{AR}} \approx 0.123$, and the post-Archaean $\chi(H_2O)_{\mathrm{PAR}} \approx 1.45$.

It means that the effective value of the water mobility factor after Archaean increased approximately by the factor of 12. Thus, there are significant differences in the effective values of the water mobility factors at its degassing from the mantle in Archaean and during the subsequent epochs. These differences are apparently associated with the fact that we took into account the water thermally dissociated within the layers of the melted metallic matter in the overheated Archaean mantle (see Fig. 4.1). Besides, the water dissociation after its degassing from the mantle could have also introduced its share. It could have been, for instance, due to the oxidation of the metallic iron in the Early Cambrian oceanic crust or due to the water vapor photodissociation by hard solar radiation in the Early Cambrian no-oxygen atmosphere.

Average values of the mobility factor for uranium ($^{238}U$) and thorium turn out much higher: $\chi(U) \approx 2.26$ and $\chi(Th) \approx 2.65$. That, as well as the uranium and thorium radioactive decay, was the reason why the concentration of these elements in the mantle declined very strongly.

The calculation results of the evolutionary changes in the convecting mantle chemical composition (not accounting for the mass of the water dissociated on the iron melts) are shown in Figs. 4.15 and 4.16 in absolute and relative concentrations.

As the diagrams show, after the zonal separation of the metallic iron began evolving within Earth at the Katarchaean/Archaean time boundary about 4 BY ago, the chemical composition of the convecting mantle drastically changed through the removal of approximately 13% of the metallic iron. Since then the mantle concentration of the most common and slow-moving oxides $SiO_2$, MgO, $Al_2O_3$, and CaO was regularly increasing. Their current contents in the mantle are about 1.4–1.5 times the primordial Earth's matter (see Table 2.1). The contents of such slow-moving components as $Na_2O$ also increased somewhat although substantially less than the previous group of compounds (increase in the $Na_2O$ content is not shown in Fig. 4.16).

The compounds $H_2O$, $K_2O$, and $Rb_2O$ were released from the mantle to a much greater extent, so their concentration decreased with time by the factor 1.4–1.3. The mantle content of the radioactive elements U and Th decreased even stronger by several times. As mentioned earlier, there were several reasons for it. First, it was the decay of these very elements, their great lithophility and the prevalent migration into the continental crust. Since mid-Archaean (about 3.0–2.9 BY ago) the Earth's matter zonal differentiation process switched to the release of eutectic melts Fe·FeO (see Section 4.3). After that, the oxide FeO content began declining with time. And total content of the core matter in the mantle was regularly declining since 4 BY ago to its current value of no greater than 7.5% (compare with the initial content of 37%).

The free (metallic) iron behavior in the convecting mantle was unusual. The upper mantle areas involved in convection melted in Early Archaean. These melts underwent the density differentiation. Immediately after that iron content in them drastically declined from 13% to almost a zero level of the metallic iron dissolved in silicate melts. By the end of the Archaean the primordial Earth's matter from the former "kernel" began entering the convecting mantle (see Fig. 4.1). It resulted again in the mantle iron concentration increase. Perhaps, this is an explanation of the native iron encountered in some Late Archaean and Early Proterozoic basalts (for instance, on the Disco Island in West Greenland, Levinson-Lessing, 1940).

By the time of the Earth's core separation about 2.6 BY ago average iron content in the mantle rose to 5.5%. Subsequently, however, iron content in the mantle began gradually declining again, and it totally disappeared from this geosphere, based on calculations, approximately 500 MMY ago. This date was determined by way of calculating the Earth differentiation rate at the given composition of its core (the external core composition is $Fe_2O$ and the internal core is comprised of the $Fe_{0.9}{\cdot}Ni_{0.1}$ alloy). And it closely corresponds with the most radical boundary in Earth evolution, that is, with the time boundary between Proterozoic and Phanerozoic (more details in Chapter 15).

After the metallic iron disappeared from the mantle, oxygen released in the core matter formation began to bond into the magnetite phase under reaction (4.41). Naturally, magnetite content in the mantle matter began climbing and reached its current value of 3.7%. Increase in $Fe_3O_4$ content in the mantle will be continuing for about 600 MMY in the future until the entire silicate (bivalent) iron disappears from this geosphere. Since that time all mantle iron will be represented by the magnetite phase. As a result, the endogenous oxygen released under reaction (4.45) will be able to reach Earth surface. Under the equilibrium mantle degassing, oxygen partial pressure will grow by about 1 bar every million years erasing in the process all life on Earth (see Chapters 14 and 15 for more detail).

## 4.7 EMPIRICAL EVIDENCE OF THE CORE SEPARATION TIMING

We reviewed the theory of Earth's core formation. Together with general concepts and data about Earth's evolution in the Early Precambrian, it shows that the core began emerging at the Katarchaean/Archaean time boundary about 4 BY ago and completely formed only by the end of Archaean nearly 2.6 BY ago. It is insufficient, however, to invoke only theory in the determination of the core separation start and the moment of its formation. It is necessary to utilize additional geological and geophysical data and direct determination of the age of the lunar and the oldest Earth rocks. Indeed, the formation of Earth crust rocks could begin only after powerful energy processes began developing within Earth, the processes that initiated tectonomagmatic activity of the planet.

We mentioned above the late separation of Earth's core, and also in Section 3.7 when referring to the crust formation start time and the ages of the oldest rocks which are about 3.8 BBY. Indeed, Earth crust could begin to separate only after the upper mantle melt. The beginning of Earth gravity differentiation (i.e., the core separation start) also must have corresponded with this event. For this reason, the start of Earth crust separation (marked by the age of the oldest rocks) is a convincing indicator of the core separation process start. Reliably determined ages of the oldest crust rocks are usually no older than 3.75–3.8 BY (Murbat, 1980; Taylor and McLennan, 1985).

As already mentioned, a significant effort and futile by the geologists all over the world to find rocks older than that. What happened with those older rocks? How would it be possible to explain such a total "memory lapse" in the geological record from the moment of Earth origin about 4.6 BY ago to the ages of around 3.8 BY ago? There is only one explanation: during approximately first 600–800 MMY of its life the young Earth was indeed a cold and tectonically inactive planet. That was the reason why the differentiation processes did

not develop then within its depths, and thus no light crust rocks (basalts, anorthosites, and plagiogranites) were melted out.

Analyzing the causes of Earth's first tectonomagmatic activation, Khain (1977) noted that an intense granitization about 4 BY ago was, most likely, stimulated by external causes with regard to Earth. It was because large tectonic events on a comparable scale happened at the same time on the Moon (discussed in detail in Section 3.7). The explanation is that it was then that Earth apparently first formed the astenosphere which accelerated the Moon distancing from Earth. As a result, the remaining large bodies of the near-Earth planetesimal swarm began falling down on the Moon. The astenosphere, as is well known, played in the future a very important role in the tectonic life of our planet. Khain associates the very emergence of the first granitization in Earth evolution with melting and differentiation of the primary basalt crust or with its metasomatic transformation in the differentiation of the juvenile mantle.

We show in Chapters 3 and 5 that such a decisive external action which could have excited Earth's tectonomagmatic activity might have been "pumping" of the tidal energy into Earth's astenosphere which emerged 4 BY ago. That is exactly why its formation and rapid expansion with the subsequent overheating of the astenospheric matter served as a real push to the beginning of the major energy process on Earth, the chemico-density differentiation of Earth's matter. The overheating of the emerged astenosphere must have been accompanied by the beginning of iron melts (i.e., the future core matter) separation. Besides, it must have been accompanied by the mantle degassing with the formation on Earth surface of the first shallow-water marine basins which dissipated most of the tidal energy.

For this reason, we may associate the beginning of the core separation process with the time of a drastic increase in the Earth–Moon tidal interaction and with the start of the second stage in the accelerated Moon-from-Earth pullout at the Katarchaean/Archaean time boundary (see Figs. 3.5 and 3.6).

As shown in Section 3.7, a second intense bombardment of the lunar surface with large celestial bodies corresponded with this stage. These celestial bodies were satellites and micro-Moons swept out at that time by the accelerated Moon-from-Earth pullout from the still preserved near-Earth satellite swarm. Based on the absolute age of the lunar basalts (Jessberger et al., 1974; Tera and Wasserburg, 1974, 1975; Tera et al., 1974), the beginning of those catastrophic phenomena on the Moon may be attributed to the time about 4 BY ago. That is why we are justified in our belief that the core separation process began around 4.0 BY ago.

After the beginning of the core separation (when Earth was heated to the extent of the appearance of the initial melts and the emerged convective flows broke the primordial lithospheric shell), the first igneous crustal rocks showed up on the Earth's surface. The entire primordial lithosphere, which was in essence an equivalent of the primitive but heavier oceanic plates, must have rapidly sunk into the mantle. Its traces were completely destroyed on the young Earth's surface. That was facilitated by the fact that the primordial lithosphere was comprised of iron-rich, therefore rather heavy (about 4 $g/cm^3$), primordial matter. At the same time, the density of the melted upper mantle after the beginning of the zonal differentiation began rapidly declining to 3.2–3.3 $g/cm^3$. The igneous rocks, which even at that time were extremely differentiated from the base composition of Earth's matter,

must have been much lighter, on the order of 2.9–3.0 g/cm$^3$. It is exactly because of this that they were preserved to our times and form the oldest crustal areas on the Earth's surface, about 3.8 BY old. After "pumping-in" the tidal energy into the Earth's equatorial belt, some time was required to separate the Earth's crust rocks. During that time melting and differentiation of Earth's matter occurred at the level of the upper mantle. Assuming that the zonal iron melt began in the upper mantle at depths of close to 400 km (see Fig. 4.1) and spread up at a rate of about 0.2 cm/year, in 200 MMY it would have reached the surface, thereby starting the melt-out of the oldest crustal rocks. Thus, the core separation began about 200 MMY earlier than the oldest continental crust rocks formed. This is a reason to assume that the core began separating nearly 4 BY ago, that is, exactly at the time when the first basaltic magmatism occurred on Moon, whereas the Earth's crust began to melt out about 200 MMY after that, that is, approximately 3.8 BY ago.

The combination of all arguments quoted here and in Chapters 3 and 5 enables us to assert that the Earth's core separation process indeed began 4 BY ago and that the Earth's tectonic activity noticeably manifested itself on the surface only 200 MMY since (i.e., about 3.9 BY ago). That was indeed the time when the oldest igneous rocks emerged, and the hydrosphere and high-density atmosphere started to form. It is most likely that the first and most primitive life forms appeared at that time, with only a slight delay.

Thus, there is an indirect connection between the timing of the start of the core separation and the time when the oldest continental crustal areas emerged. Beside this indirect connection, there is also a direct evidence of the late core separation derived from the paleomagnetic data. It is suggested that the revolving planets' (Earth included) magnetic fields are associated with the flows of the electro-conductive core matter within the core's liquid layers (see Section 4.5). If that is so, the Earth's magnetic field must have appeared only after the core separation process began, and the modern-type dipole field must have appeared only after the core separation happened. Paleomagnetic data (see Fig. 4.17) indicate that the core separation process began in Early Archaean about 4 BY ago and was completed by the end of Archaean, about 2.6 BY ago (Hale, 1987).

Beside the geomagnetic data, there are strong lead isotope evidences of the late core separation. For instance, the checks of the lead deposit age determinations using the standard lead isotope technique were conducted. The technique is based on the assumption of a single

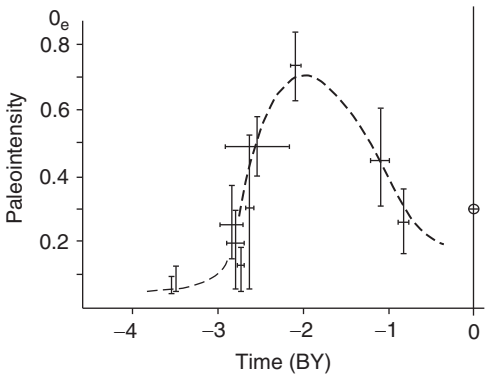


**FIGURE 4.17** Changes in Earth's magnetic field intensity based on paleomagnetic data (Hale, 1987). Horizontal and vertical bars are measurement confidence intervals; the crossed circle denotes intensity of the present-day magnetic field.

unchanging mantle–crust lead, uranium, and thorium reservoir under the Holmes–Houtermans (1946) model. It turned out that all such determinations underestimated the Earth's rock ages by about 400–500 MMY (Faure, 1977). The systemic discrepancies between single-stage Pb-dating with the ages of the same rocks determined from other isotope of geological data required improvements in the Earth's lead evolution model. Stacey and Kramers (1975) proposed a two-stage model of isotope ratio change in leads of different age. The model parameters were selected so that it best approximated empirical age data from most of the world lead deposits whose ages were reliably determined by other techniques. Such techniques included the rubidium/strontium, potassium/argon, and samarium/neodymium ratios as well as the geological data based on the uranium/lead ratios in zircons. Under the Stacey–Kramers model, the evolution of the lead isotope ratios began 4.57 BY ago in a closed reservoir but later, approximately 3.7 BY ago the U/Pb and Th/Pb isotope ratios drastically changed as a result of the Earth's matter chemical differentiation. It needs to be emphasized that the beginning of the accumulation of excess radiogenic lead under this model approximately coincides with the beginning of the crust formation (the chemical differentiation of Earth's matter), therefore with the beginning of the core separation process.

Under our model, the U/Pb and Th/Pb ratios in the 4.6–4.0 BBY interval, as in the Stacey–Kramers model, evolved within the young Earth's closed reservoir without any leak of lead. After the moment in time 4.0 BBY ago (3.7 BBY under the Stacey–Kramers model), the ratios of the radiogenic lead to the primary lead $^{204}$Pb in the mantle were affected by a gradual lead migration into the core matter. And the preferential migration of radioactive elements into the continental crust was occurring under the laws similar to those governed by equations of the mantle degassing (4.47) and (11.1). Under these equations, the migration rate $m_i$ of the mantle component $i$ into the crust is proportionate with the mantle contents of this component $(m_i)_{\mathrm{m}}$, its mobility factor $\chi_i$ and the rate $\dot{z}$ of the mantle mass exchange (4.47).

To simplify the format of the subsequent equations, we introduce the following designations:

$$\frac{^{206}\mathrm{Pb}}{^{204}\mathrm{Pb}} = a; \quad \frac{^{207}\mathrm{Pb}}{^{204}\mathrm{Pb}} = b; \quad \frac{^{208}\mathrm{Pb}}{^{204}\mathrm{Pb}} = c. \tag{4.51}$$

We add the subscripts denoting the age (in BY) of the moment where the corresponding parameter belongs. For the initial (Katarchaean) stage of the Earth evolution, we format the usual correlations of lead isotope ratios and the lead age under the one-stage Holmes–Houtermans model (Fore, 1989):

$$\begin{aligned} a_i &= a_{4.6} + \mu\left(\mathrm{e}^{\lambda_1 t_{4.6}} - \mathrm{e}^{\lambda_1 t_i}\right) \\ b_i &= b_{4.6} + \mu\frac{\left(\mathrm{e}^{\lambda_2 t_{4.6}} - \mathrm{e}^{\lambda_2 t_i}\right)}{137.88} \\ c_i &= c_{4.6} + \omega\left(\mathrm{e}^{\lambda_3 \cdot t_{4.6}} - \mathrm{e}^{\lambda_3 t_i}\right), \end{aligned} \tag{4.52}$$

where $\lambda_1 = 0.15513 \times 10^{-9}$, $\lambda_2 = 0.98485 \times 10^{-9}$, and $\lambda_3 = 0.49475 \times 10^{-9}$ years$^{-1}$ are the decay constants of $^{238}$U, $^{235}$U, and $^{232}$Th; $\mu = \frac{^{238}\mathrm{U}}{^{204}\mathrm{Pb}}$ and $\omega = \frac{^{232}\mathrm{Th}}{^{204}\mathrm{Pb}}$, the factor 137.88 determines the isotope $^{238}$U/$^{235}$U ratio in Earth matter.

Under the two-stage Stacey–Kramers model, at the initial stage, prior to the geochemical differentiation, $\mu_1 = 7.192$ and $\omega_1 = 32.208$. At the second stage, after the beginning of the differentiation of Earth's matter, $\mu_2 = 9.735$ and $\omega_2 = 36.837$.

In our model, the source values of the factors $\mu = 7.767$ and $\omega = 33.593$ were slightly changed but amended by the introduction of the corrections $X_i$ for the lead migration into the core. These corrections may be determined under a proposition that lead migration into the core was also defined by Eq. (4.51) although with a somewhat different mobility factor $q$. In this case, the remaining lead isotope concentrations in the mantle are determined as:

$$\begin{aligned} a_i &= a_{4.6} + \mu \frac{\left(e^{\lambda_1 t_{4,6}} - e^{\lambda_1 \cdot t_i}\right)}{X_i} \\ b_i &= b_{4.6} + \mu \cdot \frac{\left(e^{\lambda_2 t_{4,6}} - e^{\lambda_2 t_i}\right)}{137.88 \cdot X_i} \\ c_i &= c_{4.6} + \omega \frac{\left(e^{\lambda_3 t_{4,6}} - e^{\lambda_3 t_i}\right)}{X_i}, \end{aligned} \tag{4.53}$$

in which:

$$X_i = 1 - q\left[1 - \frac{(1 - x_i)}{1 - C_0 x_i}\right], \tag{4.54}$$

where $x$ is the relative mass of the Earth's core matter separated from the mantle, and in Proterozoic and Phanerozoic the mass of the core proper (see Eq. (4.23)).

We now assume for our model the same primordial and modern lead isotope ratios (i.e., the problem's edge conditions) as in the Stacey–Kramers model: $a_{4.6} = 9.307$; $b_{4.6} = 10.294$; $c_{4.6} = 29.476$; $a_{0.0} = 18.700$; $b_{0.0} = 15.628$; $c_{0.0} = 38.630$. In this case, Eqs. (4.53) determine for Archaean and subsequent epochs the lead isotope ratios in the mantle.

Remember that the mobility factor $q$ in Eq. (4.54) determines not the very migration of lead into the core but only associated changes in the isotope ratios formed over the core separation period (i.e., the recent 4 BY). The radiogenic lead isotope formation rate, however, is also different. For instance, over the geological interval (again, 4 BY) the $^{206}Pb/^{204}Pb$ isotope ratio increased by 42%, whereas the ratios $^{207}Pb/^{204}Pb$ and $^{208}Pb/^{204}Pb$ increased only by 19% and 21%.

Correspondingly, the effective mobility factors $q$ turn out to be different for different lead isotopes: 0.184 for the isotope $^{206}Pb$ to 0.074 and 0.087 for the isotopes $^{207}Pb$ and $^{208}Pb$.

It is now possible to determine correlation between $b_i$ factors and $a_i$; and between all parameters $a_i$, $b_i$, and $c_i$ at the time $t_i$. The results of such calculations in comparison with the Stacey–Kramers model are shown in Figs. 4.18 and 4.19. As can be seen, both two-stage models neatly match one another. The Stacey–Kramers model was coordinated with other independent age determinations of actual lead deposits, so our model we are presenting here must also match these empirical data.

Thus, we may maintain that the model of lead migration into Earth's core presented here indeed matches the available empirical data on isotopy of Earth's lead.

As lead gradually migrated into the growing Earth's core, the fraction of its radiogenic isotopes in the total mass of the mantle (and core) lead, naturally, must have gradually

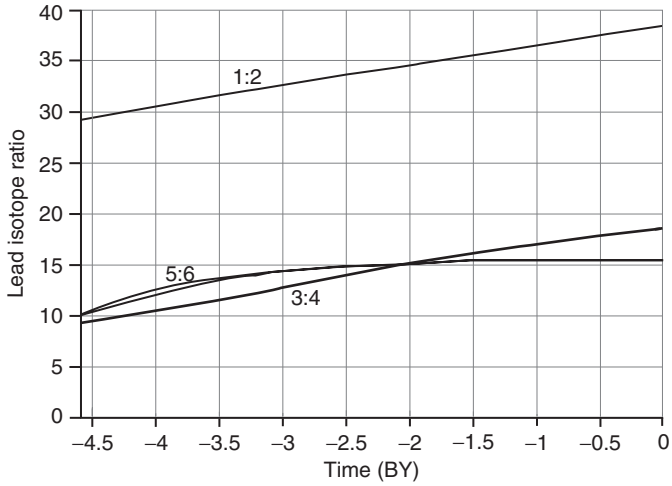


**FIGURE 4.18** Comparison of lead isotope ratios evolution under a two-stage model (Stacey–Kramers) coordinated with empirical data, and the theoretical model accounting for a partial lead transfer to the core: 1 and 2, ratios $^{208}Pb/^{204}Pb$; 3 and 4, ratios $^{206}Pb/^{204}Pb$; and 5 and 6, ratios $^{207}Pb/^{204}Pb$ under the reviewed models.

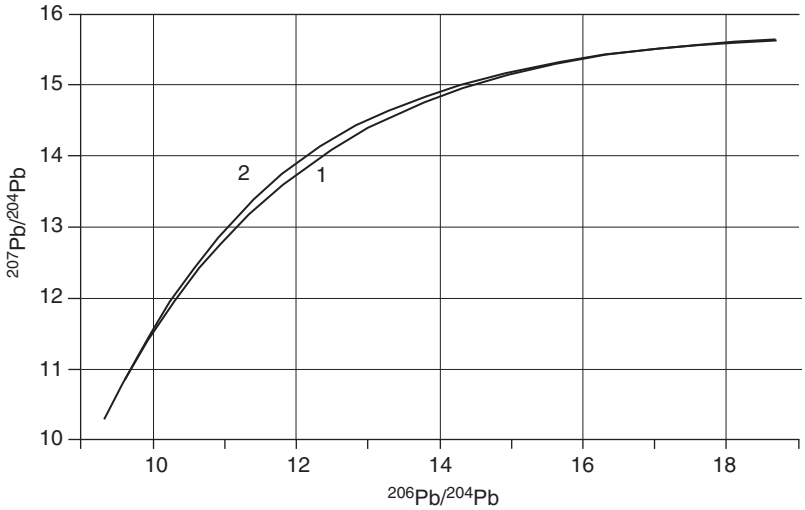


**FIGURE 4.19** Lead isotope evolution: 1, under a two-stage model (Stacey–Kramers); 2, under a two-stage model taking into account lead transfer to the core.

increased. If lead had not migrated into the core, then under the Stacey–Kramers model the current isotope ratios would have been $(a_0)' = 16.8$; $(b_0)' = 15.04$; and $(c_0)' = 37.71$, and under our model, respectively, 17.32; 15.3; and 38.0. That is instead of the conventional values for the present-day core isotope ratios: 18.7; 15.63, and 38.63.

Taking the quoted lead isotope values into account, the estimate is that close to 30% of this metal sank into the Earth's core. We amended these data by the determinations of the radioactive elements distribution within Earth from Table 5.1 (Sorokhtin and Ushakov, 1991). It enabled a determination of the lead amount that migrated over Earth's geological

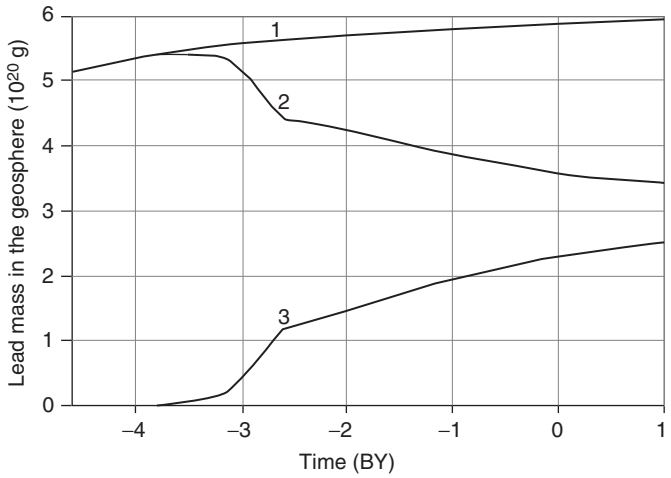


**FIGURE 4.20** Evolution of lead mass within Earth taking into account lead isotope formation in uranium and thorium radioactive decay: 1, total lead mass in Earth; 2, total lead mass in the mantle and continental crust; and 3, lead mass transferred to the core.

evolution interval into its core: $2.29 \times 10^{20}$ g (see Fig. 4.20). This example provides the expected evolution of the lead relative concentration in the convecting mantle as calculated from Eq. (4.33).

Coming back to the lead ratios in the lunar matter ($a_L \approx 200$; $b_L \approx 100$; and $c_L \approx 230$) we find that 96–97% of the primordial lead was removed from the lunar matter reservoir at the Proto-Moon melting and differentiation. A question then arises: why are the lead-to-planetary core transfer factors so drastically different in the differentiation of the planets with similar initial composition? The answer is quite simple: the Proto-Moon was overheated by the tidal deformations; it underwent a complete melting and no less complete differentiation by way of melt liquation. At the same time, Earth was never completely melted (only the upper mantle partially melted), and the core separation was gradual and without melting of silicates. On the other hand, lead is a dispersed element. It does not form a free phase in the mantle matter and enters the crystalline grids of silicates and sulfides. That is why the lead separation from the mantle matter and its migration to Earth's core, most likely proceeds under the same barodiffusion mechanism (although with different diffusion factors) under which the core-forming iron oxides are separated, that is, without melting of the mantle matter (Monin and Sorokhtin, 1981).

Thus, the evolution of the lead isotope ratios, like many other geological data, also supports our model of a late and gradual core separation. Stratification of an originally uniform and relatively cold earth into a high-density core and its silicate shell (the mantle) says that an effective mechanism of chemical-density differentiation of Earth's matter was operative at the planetary stage of Earth's evolution. A detailed study of Earth's energy balance leads to the conclusion that this process not only continues presently but is also the most powerful of all other endogenous energy processes. Due to this process, an intense convection arises and evolves within the mantle. It results in the stirring of its matter and lithospheric plate drift on Earth's surface.

CHAPTER

# 5

# Earth Energetics

One of the fundamental issues in planetary geophysics is the sources of energy determining the heat regime and supporting tectonic activity on Earth. It may be resolved only in a close association with the modern data about Earth's composition, structure, and evolution.

As mentioned in numerous publications (Sorokhtin, 1974, 2007; Sorokhtin and Ushakov, 2002), the major processes controlling tectonic activity on Earth may only be those deep-seated energy processes which lower to the highest extent the potential (internal) energy of our planet and of the Earth–Moon system. The lowering of potential energy occurs at the expense of its conversion into heat and kinetic energy of Earth mass movements (the convection, lithospheric plate motions, continental drift, mountain building, etc.).

In its turn, any displacements of landmasses are also accompanied by the dissipation of the kinetic energy and heat release. Those result in the partial melting of the upper mantle matter or the continental crust rocks thereby feeding Earth's magmatism with energy.

Eventually, this entire heat is gradually lost with Earth's heat radiation through the surface and is lost in outer space. Thus, an important theoretical conclusion: the heat coming from the Earth's depths and eventually radiated to outer space is the natural and quantitative measure of its tectonic activity.

Therefore, if, based on an analysis of Earth's energy balance, we can estimate its heat loss during the past geological epochs, we will thereby be able to define the evolution of the planet's tectonic activity.

Three global energy processes dominate inside Earth:

First, it is Earth's matter gravity differentiation by density. It results in Earth's stratification into the high-density iron-oxide core, the residual silicate mantle, the light aluminosilicate crust, and the hydrosphere with the atmosphere.

Second is the decay of radioactive elements causing the release of heat energy.

Third is the tidal interaction between Earth and the Moon.

All other endogenous energy sources are either immeasurably smaller than the three listed above or totally reversible due to the mass exchange of the mantle convection. For instance, the transition energy of mineral associations affected by the pressure in the

*Developments in Earth and Environmental Sciences*, Volume 10
DOI: 10.1016/S1571-9197(11)10005-1

ascending and descending convective flows has opposite signs. That is why any effect of such reactions onto the summary endogenous energy balance of Earth may be disregarded although they may affect the configuration of the mantle convective flows.

## 5.1 EARTH ACCRETION AND GRAVITY DIFFERENTIATION ENERGY

Among the major Earth's energy sources stored as early as during the planet's formation process is part of the Earth's matter gravity accretion energy and the Earth's insides compaction energy.

As mentioned earlier, the Earth's formation process at the expense of accretion of the protoplanetary gas–dust cloud took about 100 MMY and was completed about 4.6 BY ago in the emergence of a young and more or less compositionally uniform Earth.

At the geologicalal stage of our planet's evolution (beginning $\sim$4.6 BY ago), a different powerful gravitational energy release process began to develop. It was associated with density differentiation of Earth's depths. This process eventually resulted in the separation in Earth's center of a high-density iron-oxide core and in the emergence within the residual silicate shell (the mantle) of intense convective flows, which are the direct cause of the planet's tectonism.

The planet's accretion occurred through the transfer of a dispersed protoplanetary matter from remote orbits to the local space where it was condensed into a unique celestial body. So, for any planet including Earth, the accretion energy is equal to the work necessary to collect the dispersed protoplanetary matter from "infinity" and to concentrate it in the body of the planet; in other words, to totally destroy the planet and disperse the planetary matter to infinitely large distances.

Numerically, the planet accretion energy $E_a$ is equal to its potential (gravity) energy $U$ with the opposite sign (as potential energy is always negative by definition). Potential energy of any system depends on the system's configuration, in our case on the density distribution within the planet.

$$U = -4\pi\gamma \int_0^R rm(r)\rho(r)\,\mathrm{d}r, \tag{5.1}$$

where

$$m(r) = 4\pi \int_0^r \rho(r)r^2\,\mathrm{d}r. \tag{5.1'}$$

Here, $m(r)$ is the mass of Earth's insides within a sphere of radius $r$; $\rho(r)$ is the Earth matter density at radius $r$; $\gamma = 6.67 \times 10^{-8}$ cm$^3$/g s$^2$ is the gravitational constant; $R = 6.371 \times 10^8$ cm is Earth's average radius. The heat store (heat content) of Earth may be determined from the following equation:

$$W = 4\pi \int_0^R \rho(r)\,T(r)c_p(r)r^2\,\mathrm{d}r, \tag{5.2}$$

where the density distributions within the present-day and the young Earth are shown in Fig. 2.13, the temperature distribution within the present-day Earth, in Fig. 2.17, and that of the young Earth, in Fig. 3.10. The assumed heat absorptions of the present-day and the young Earth are shown in Fig. 3.9.

To determine the young Earth's accretion energy, the density distribution within it is necessary. As mentioned earlier, such a distribution for the young Earth was prepared based on the average composition of Earth's matter (see Table 2.1) and on the silicate and metal shock compression data (Naimark and Sorokhtin, 1977a,b). The current technique of rock-forming oxides (not the rocks proper) density determination at high pressure based on shock compression data has accuracy of 2–4%. The density distribution within the young Earth so determined is shown in Fig. 2.13.

We used Eqs. (5.1) and (5.1′) to calculate the accretion energy released in the process of Earth's formation about 4.6 BY ago. This energy, approximately equal to its original potential energy, was immense: $U_{(4.6)} \approx -23.255 \times 10^{38}$ erg. Part of this energy, around $E_{\mathrm{com}(4.6)} \approx 3.25 \times 10^{38}$ erg, was spent in the process of Earth's formation for the elastic compression and initial heating of Earth whose heat store turned out to be $W_{(4.6)} \approx 0.838 \times 10^{38}$ erg.

However, an overwhelmingly larger part of the accretion energy (nearly $E_{\mathrm{T}(4.6)} \approx 19.17 \times 10^{38}$ erg) was lost with the heat radiation. This amount of energy would be sufficient to raise the planet's average temperature to 30,000 °C, which would have resulted in the total evaporation of Earth's matter. It has not happened, however. The reason is the long period of the planet's formation, on the order of 100 MMY. And the planetesimal impact energy was released only within the near-surface layers of the growing planet and was rapidly lost with the planet's heat radiation. Besides, as mentioned earlier, geological data and the supporting calculations indicate that the initial heating of Earth was not substantial (Fig. 3.10).

The accretion energy was being released only while Earth grew. At the geological stage, however, the main source of endogenous energy was the gravity differentiation of Earth's matter into the high-density core and lighter silicate shell, that is, the mantle. Quantitatively, the gravity differentiation energy is equal to the difference between the potential energy of the uniform Earth immediately before the beginning of the differentiation process (i.e., about 4 BY ago), and the potential energy of the present-day stratified Earth:

$$E_{\mathrm{g}} = U_{4.0} - U_{0.0}. \tag{5.3}$$

The present-day Earth's potential energy is $-24.952 \times 10^{38}$ erg. Therefore, by definition the total energy of the gravity differentiation is $[-23.255 - (-24.952)] \times 10^{38}$ erg $= 1.698 \times 10^{38}$ erg. Part of this energy was spent on additional elastic compression of Earth ($0.4355 \times 10^{38}$ erg) but most of it ($1.2625 \times 10^{38}$ erg) converted first to the kinetic energy of the mantle matter convection flows, and then to heat. This is exactly a part of the total energy feeding Earth's tectonic activity.

The derived value of Earth's gravity differentiation energy is immense and substantially exceeds the total release in its depths of all other kinds of energy. Indeed, over the same time, that is, from Earth's origin to the present, close to $0.3106 \times 10^{38}$ erg of radiogenic and $0.2238 \times 10^{38}$ erg of tidal energy were released in the mantle. The total energy release

in the mantle was $(1.698+0.3106+0.2238-0.4355)\times10^{38}=1.7969\times10^{38}$ erg of heat energy. Together with about $0.1223\times10^{38}$ erg of radiation energy, the total amount of energy released within Earth was nearly $2.3547\times10^{38}$ erg.

The present-day Earth heat store is equal to $W_{(0)}\approx1.592\times10^{38}$ erg. Therefore, over the period of geological evolution Earth's heat energy increased by $\Delta W_{(0)}=W_{(0)}-W_{(4.6)}\approx 1.592\times10^{38}-0.838\times10^{38}=0.754\times10^{38}$ erg. Energy released in the mantle was spent for additional Earth heating $\Delta W_{(0)}\approx0.754\times10^{38}$, heat radiation $\Delta Q_{\mathrm{m}(0)}\approx1.077\times10^{38}$ erg and the additional Earth compression in its differentiation $\Delta E_{\mathrm{com}(0)}\approx0.436\times10^{38}$ erg, the total being: $E_{\mathrm{m}(0)}\approx0.754\times10^{38}+1.077\times10^{38}+0.436\times10^{38}=2.267\times10^{38}$ erg.

Certain issues are important for the determination of major patterns in the release of the energy of Earth's gravity differentiation. One of the most important issues is the determination of the planet's core formation timing. As mentioned in Chapter 4, many hypotheses of Earth's origin (e.g., Jacobs, 1975) postulate early core separation. We believe, however, that based on the geological and geochemical data we provided it may be stated with certainty that no such process occurred within Earth prior to 4.0 BY ago.

Moreover, in analyzing the joint evolution of the Earth–Moon system we attempted to show that the core separation process had just begun 4.0 BY ago. However, the convincing arguments in this issue are, as mentioned, paleomagnetic data (Fig. 4.17) and lead isotope ratios (see Section 4.7 and Figs. 4.18–4.20). In the preceding chapter, we used the lead ratios in lunar and earthly rocks to show that the Moon experienced the total melt and early differentiation, whereas Earth never melted and did not have any early differentiation. Thus, the evolution of the lead isotopic ratios and numerous other geological data also support the proposed model of a gradual Earth crust separation.

We also mentioned that no traces of magmatic rocks older than 3.8–4.0 BY have ever been found in the Earth crust despite active searches. If the hypothesis of early Earth's differentiation was true, such ancient light derivates of Earth's matter, similar to the rocks of the Moon's light anorthosite crust, would have not only been preserved but also been dominant in the Earth's core now, which is not true. The conclusion is that the process began without the total melting of Earth's matter about 600 MMY after the origin of Earth herself. This is also supported by paleomagnetic data (e.g., Fig. 4.17).

Only the heat portion of gravity differentiation energy had the definitive importance for Earth's tectonic activity. The energy spent for additional Earth compression does not count. The release of the heat energy fluctuated during geological evolution of Earth. As a first approximation, the generation rate of the gravity energy is proportionate to the separation speed from Earth's matter of the heavy fraction, that is, of the core matter which subsequently (about 2.6 BY ago) descended into the core.

To describe this process, we used the evolution parameter $x$ defined in Eq. (4.23) and quantitatively determined in Section 4.5. The present-day value of the parameter is $x=0.864$. In this case, the heat portion of Earth's gravity differentiation energy is equal to

$$E_{\mathrm{gT}}\approx1.458\times10^{38}\ \ x\,\mathrm{erg} \tag{5.4}$$

and the release rate of this energy is

$$\dot{E}_{\mathrm{gT}}\approx1.468\times10^{38}\ \ \dot{x}\,\mathrm{erg/year} \tag{5.4'}$$

(for Early Archaean, the factor in front of $x$ and $\dot{x}$ is equal to $1.25\times10^{38}$ erg).

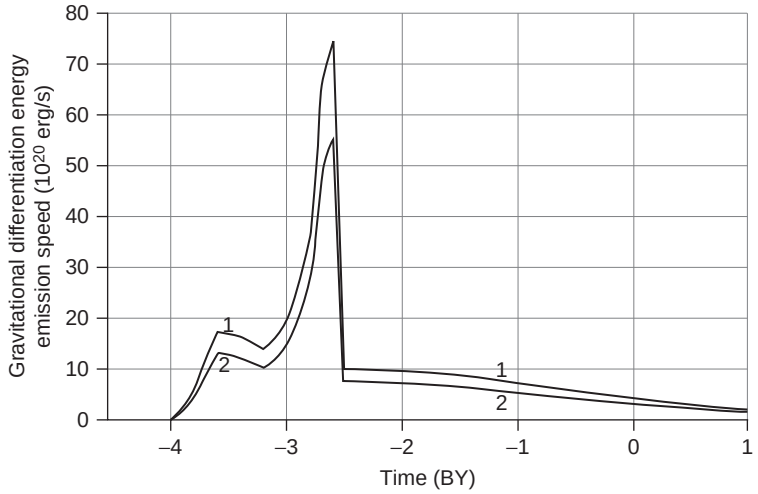


**FIGURE 5.1** Earth's gravity differentiation energy release rate: 1, total gravity energy (including the energy of additional Earth's elastic compression on the account of core separation) and 2, heat component of the gravity energy. A burst in the energy release rate at about 2.6 BY ago was associated with the core formation at that time.

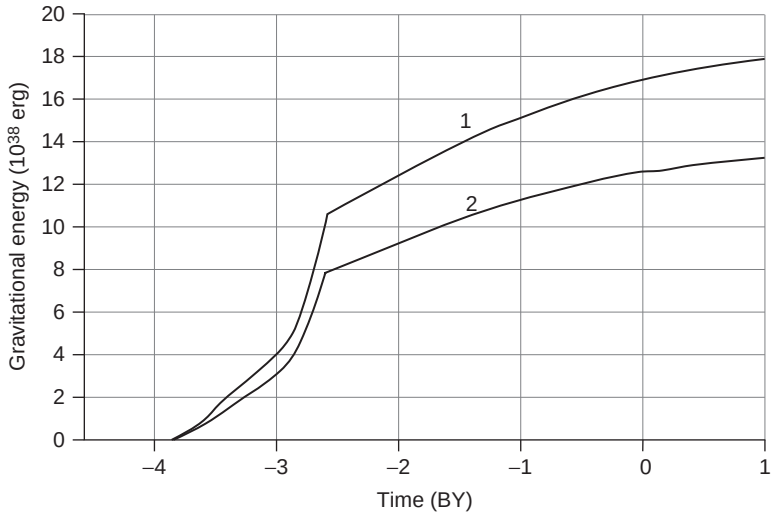


**FIGURE 5.2** Earth's gravity differentiation energy release versus time: 1, total energy (including additional heat release at adiabatic Earth and 2, kinetic (heat) energy of Earth's differentiation.

We review the major patterns of Earth's tectonic activity in the next chapter. Here, using these patterns, we only include diagrams of the generation rate of the gravity differentiation energy (see Fig. 5.1) and a graph of gravity energy versus time (see Fig. 5.2).

Earth's gravity differentiation energy release began rather abruptly approximately 4.0 BY ago. By about 3.8 BY ago almost three times more energy was being released as heat than

it is presently (the present amount is close to $3 \times 10^{20}$ erg/s). In Early Archaean, this energy was being released only within a relatively narrow equatorial belt (Fig. 4.3) where the tectonic activity of Earth began. Thus, per-unit-area heat flows at the time were much higher than now. A significant increase in the gravity energy release occurred in Late Archaean. The reason was a change in the Earth's matter differentiation process from metallic iron separation to the release of Fe·FeO eutectic melts. In that process about 2.8 BY ago, gravity energy release rate exceeded its present-day level by about the factor of 14 and reached $43 \times 10^{20}$ erg/s.

The gravity energy release rate reached its maximum only at the very end of Archaean, approximately 2.6 BY ago, at the time of a catastrophic event—the high-density core separation (see Section 4.2). Gravity energy release rate at that time reached $70 \times 10^{20}$ erg/s. The amplitude of its heat component was almost $53 \times 10^{20}$ erg/s, that is, 18 times its current release rate.

It is noteworthy that the maximum of the Earth's matter gravity distribution energy rate falls onto a unique epoch of the Late Archaean Kenoran diastrophism, that is, a period when geological data indicate the maximum tectonic activity. Obviously, the gravity distribution energy could be released only after the upper mantle matter began melting. As already noted, this event happened, most likely, approximately 4.0 BY ago. Then, affected by the tidal interaction with the Moon, a melted layer of the Earth's matter (the asthenosphere) was formed in the equatorial zone of the upper mantle at a depth 200–400 km.

That moment in Earth's evolution, as we could see, was clearly marked by the beginning of the basalt magmatism on the Moon and, with some lag time, by melting-out of the oldest Earth's crust rocks. That is why the proposed model of Earth's evolution assumes that the release of gravity differentiation energy within Earth began about 600 MMY after its origin (i.e., at the time of the asthenosphere emergence in the upper mantle) and was initially associated with the separation of metallic iron melt from Earth's matter silicates.

After the core separation in the end Archaean, the rate of heat component in the gravity energy significantly declined in Early Proterozoic to $7 \times 10^{20}$ erg/s. The subsequent gravity differentiation occurred quiescently. It gradually declined to its current heat energy release level of about $3 \times 10^{20}$ erg/s. The decline will continue in the future.

The accumulation of the gravity energy was going on much more quietly. As Fig. 5.2 shows, the total gravity energy released through the present is $16.85 \times 10^{37}$ erg. Out of these, $4.36 \times 10^{37}$ erg was spent on additional compression of Earth. The heat component of the gravity differentiation energy (converted to the convective flow energy) is approximately $12.63 \times 10^{37}$ erg.

The graphs of Figs. 5.1 and 5.2 are just average heat release parameters. In real life, the gravity convection in the mantle is nonstationary, hence, so are the gravity differentiation processes. Thus, the energy release rate is described by a more complex curve than shown in Fig. 5.1, as if superimposed by the fluctuating process of cyclical restructuring corresponding to the tectonic cycles (see Fig. 6.8). However, it is suggested that the amplitude of such deflections is small compared with the average background.

## 5.2 CONTENTS OF RADIOACTIVE ELEMENTS IN EARTH AND THEIR DECAY ENERGY

The establishment history of the concept of radiogenic Earth heat sources is very demonstrative and didactic.

It played a significant role in the criticism of and rejection by the geologists of the formerly very popular contraction hypothesis of Eli de Beaumont which dominated earth sciences for almost an entire century and even survived through the 1930s.

As a reminder, under this hypothesis based on the Laplace's ideas of "hot" origins of the Solar System planets, our Earth formed from the primordial gas cloud, and after it compacted and became denser, from the overheated fiery-liquid magma. As Earth cooled down, covered herself ever thicker crust and compacted, its size decreased (i.e., it underwent contraction). As the proponents of this hypothesis believed, such contraction (as of a drying-off apple) resulted in wrinkles on the surface of Earth's crust. That was the explanation of folded (mountain) belts on Earth and the earthquakes. Breakthroughs of the subcrustal magma created volcanoes, and its intrusions into the Earth crust resulted in granite plutons.

Anry Bekerel discovered in 1996 the phenomenon of radioactivity. It was found later that Earth crust contained massive reserves of radioactive elements ostensibly sufficient to melt the entire Earth without the involvement of Laplace's hypothesis about the hot origin of the planets. This discovery and its application to Earth which apparently was suggested by Raley in 1906 radically disrupted the old concepts of Earth's origin and the nature of its geological processes. Somewhat later, radioisotope techniques of rock age determination overturned old ideas of a relatively young age of Earth. It became obvious that the planet lasted not millions of years as was thought at the turn of the XXth century but billions of years.

That was the death nail for Laplace's cosmogonic hypothesis as it estimated the age of Earth, based on its concepts and earlier determined heat flows through the Earth's surface, at no longer than 100 MMY.

All these stimulated the development of new ideas in planetology, geophysics, geology, tectonics, and other allied Earth science disciplines. Among them was, for instance, a modern hypothesis by Schmidt of a "cold" origin of Earth and other Solar System planets. We mentioned this hypothesis in Chapter 3. One of the reasons of its appearance was undoubtedly the discovery of a new powerful source of the radiogenic energy capable of providing all energy necessary for Earth's tectonic activity.

All these positive moments of the radiogenic hypothesis undoubtedly played an important role in the progress of modern geology. However, it also had its problems, some of them serious. In particular, when estimating the capacity of the radiogenic energy source within Earth, the radioactive element concentration in the mantle was always a great unknown. And the problem was being solved as the scientists' weltanschauung dictated.

Majority of geologists and geophysicists were total adepts to the radiogenic hypothesis of Earth's depths heating. For this reason, the radioactive element concentration in the mantle was usually determined from the condition of the equality between heat they generated and the heat flow through the Earth's surface.

This approach by default completely eliminated from consideration all other possible sources of endogenous energy. And those eliminated sources might have been tremendous and, combined, could have significantly exceeded the actual contribution to the planet's heat balance from the radiogenic sources.

That is exactly what happened. Detailed estimates discovered that over the life of Earth the other energy sources released within Earth the amount of heat about 4–4.5 times the radiogenic heat. Such neglect toward the other and much more powerful endogenous energy sources could not but play a negative role. It delayed the development of a state-of-the-art

geological theory by many years. That was the major drawback of the overblown infatuation with the "obvious" radiogenic hypothesis.

Thus, the weakest place of the radiogenic hypothesis and at the same time the most methodologically difficult issue were the radioactive element contents within the depths of the mantle inaccessible to a direct experiment. The major attention was devoted only to most energy-capacious and long-living isotopes with the half-life periods commensurate with the age of Earth itself. Such isotopes are uranium 235 and 238, thorium 232, and potassium 40 ($^{235}U$, $^{238}U$, $^{232}Th$, and $^{40}K$).

What is usually taken into account when estimating the radioactive element contents within Earth is that these isotopes are lithophilic chemical elements concentrated mostly in light aluminosilicates. This property determines the direction of their migration during the differentiation to the places of the greatest concentrations of aluminosilicates with elevated contents of the silica ($SiO_2$), alumina ($Al_2O_3$), and bases (Li, Na, K, R, etc.), that is, to the continental crust. These elements are much rarer in aluminum-impoverished and enriched in magnesium high-density ultramafic rocks of the mantle. They must be practically absent from the core (which is supported by the composition of iron meteorites and their sulfide phase, troilite).

The radioactive element concentration in the crust is usually estimated from their content in the most common crustal rocks, and in the mantle, by analogy with their concentration in chondrite meteorites (Birch, 1958; MacDonald, 1964a,b) or in the ultramafic rocks (Tilton and Read, 1963; Lyubimova, 1968a,b).

This approach, however, renders uncertain solutions. The reason is that the meteorites taken as samples might have originated in other than Earth parts of the Solar System with totally different properties of the protoplanetary matter differentiation. This was empirically shown by Gast (1972).

Another way, determination of the mantle radioactivity by directly measuring the radioactive element content in Earth's ultramafic rocks, is also dubious due to a large scatter of the experimental data, especially as related to uranium and thorium.

There is a simple explanation to the instability of radioactive element content values determined in the mantle rocks reaching Earth's surface. These rocks almost always undergo the strongest influence from the metamorphogenic factors which substantially distort the original composition of rare and dispersed elements. Usually, the ultramafic rocks are contaminated by bases simultaneously with their hydration. It is especially so for such dispersed elements as uranium and thorium.

As was shown by Peyve (1969), Peyve et al. (1971), Coleman (1971a,b), Dewey and Bird (1970a,b), and some others, all ophiolite nappes which contain the mentioned mantle-associated ultramafic rocks are in actuality the fragments of an old oceanic crust thrown over the continental margins. The oceanic crust usually forms under a thick layer of the oceanic water saturated with bases and other dissolved elements including potassium, uranium and thorium.

For similar reasons, the composition of mantle rock xenoliths from kimberlite tubes or from volcanic eruptions in the island arcs cannot be used for the determination of radioactive element contents in the mantle. The connection here is that the ultramafic and eclogite xenoliths from the kimberlite tubes are actually the fragments of the Early Proterozoic oceanic crust sucked in through the Svekofenian subduction zones deep underneath

lithospheric plates of the Archaean continents (Sorokhtin et al., 1996, 2001). And the island arc and active continental margin volcanoes function only at the expense of remelting and deep reworking of the oceanic crust thrust under them. One needs to be very careful when selecting and analyzing ultramafic xenoliths from the Hawaiian type ocean volcanoes. Many such samples are of cumulative origin and emerge at the level of intermediate magmatic foci. Besides, magmatic melts in such volcanoes are contaminated by the sea water penetrating into the hot zone through the laminated lava sheets of stratovolcanos.

Thus, it appears to be impossible to determine "most probable" radioactive element concentrations in Earth based on empirical data only, and we have to use indirect techniques. For instance, we could begin with the determination of the concentration in Earth of most common radioactive element potassium. Then, using K/U and K/Th ratios, we could determine the concentrations of uranium and thorium. This way, however, is somewhat unreliable as the determined concentration values of these ratios in the mantle rocks have a wide scatter.

There is a way to lower uncertainty of the calculations in determining the contents of radioactive elements in the continental crust. We may utilize a restriction imposed on the possible contents of these elements in the crust by the value of average heat flow through the continents $q_{cr} \approx 1.41 \times 10^{-6}$ cal/cm$^2$ s (Sclater et al., 1980). The total heat flow through the continents is composed of two parts: the radioactive and the mantle (depth) heat flows. The mantle flow on the Precambrian platforms aged $t > 1.8$ BY (accountable for about 75% of all continental area) is currently stationary and may be found as:

$$\bar{q}_m \approx \lambda_l \frac{\Delta T}{\Delta H_l}, \tag{5.5}$$

where $\lambda_l \approx 6.21 \times 10^{-3}$ cal/cm s deg (2.6 w/m K at 1300 K (Reference book "Physical properties. . .", 1976) is the heat conductivity of the subcrustal lithosphere; $\Delta T \approx 1100$ °C is the temperature gradient within the subcrustal lithosphere; $\Delta H \approx 250 - 40 = 210$ km is the subcrustal lithosphere thickness on the old platforms. In this case, average heat flow through old platforms is equal to $\bar{q}_m \approx 0.33 \times 10^{-6}$ cal/cm$^2$ s. For the young platforms ($t < 1.8$ BY), the mantle heat flow must depend on their age

$$\bar{q}_m \approx 2\lambda_l \frac{\Delta T}{\sqrt{\pi a \tau}}, \tag{5.6}$$

where $\tau = 1.8$ BY is the maximum age of the platform with still not settled heat regime; $a = 5.7 \times 10^{-3}$ cm$^2$/s is lithosphere thermometric conductivity factor. From (5.6) we find that average depth heat flow through the platform younger than 1.8 BY is approximately $0.43 \times 10^{-6}$ cal/cm$^2$ s, and average depth heat flow for all continents is equal to $0.35 \times 10^{-6}$ cal/cm$^2$ s. In such a case, the remaining fraction of the average radiogenic heat flow is $(q_R)_{cc} \approx 1.41 \times 10^{-6} - 0.35 \times 10^{-6} = 1.06 \times 10^{-6}$ cal/cm$^2$ s, and total radiogenic heat flow through the entire continental crust (areal extent, $2.04 \times 10^{18}$ cm$^2$) is equal to $\left(\dot{Q}_R\right)_{cc} \approx 0.9 \times 10^{20}$ erg/s. This is 21% of total Earth heat loss of $\dot{Q} \approx 4.3 \times 10^{20}$ erg/s. A similar estimate by Sclater et al. (1981) gives a somewhat smaller share of the radioactive energy of $0.71 \times 10^{20}$ erg/s (or ~17% of total Earth radiation ($\dot{Q} \approx 4.2 \times 10^{20}$ erg/s as determined by Sclater et al. (1981)).

Based on publications by Taylor (1964), Gast (1975), and Ronov and Yaroshevsky (1978), average concentration of potassium in the continental crust is reasonable to accept at 2%. Let us also

accept that $^{40}K/(^{39}K + ^{41}K) = 1.167 \times 10^{-4}$ (Faure, 1989). Total mass of the crust is $2.25 \times 10^{25}$ g, so it contains $4.5 \times 10^{23}$ g of potassium and $5.24 \times 10^{19}$ g of radioactive potassium isotope $^{40}K$.

Let us assume for our energy calculation specific energy releases by radioactive isotopes (Turcotte and Schubert, 1985) are: $^{40}K = 0.279$; $^{238}U = 0.937$; $^{235}U = 5.69$; and $^{232}Th = 0.269$ erg/g s. From these, the fraction of the radiogenic heat flow associated with the potassium radioactive isotope decay is $0.146 \times 10^{20}$ erg/s. Let us accept average Th/U ratio in the crust at $Th/U \approx 4$. In such a case, from the summary rate of radiogenic energy generation in the crust ($0.91 \times 10^{20}$ erg/s) the uranium $U = 0.367 \times 10^{20}$ g and thorium $Th = 1.52 \times 10^{20}$ g contents may be determined. In this case, the ratio $K/U \approx 1.2 \times 10^4$ and $K/Th \approx 3.0 \times 10^3$.

The determination of radioactive elements content in the mantle is a much more daunting problem. It may be accomplished only using indirect techniques. One such technique was proposed independently by Gast (1975, 1968) and Hurley (1968). Their idea was finding the content in Earth of the radioactive isotope $^{40}K$ (hence, the entire potassium) was using the atmospheric concentration of the radiogenic argon isotope argon $^{40}Ar$ which entered this geosphere at potassium transition from the mantle to the crust. Gast believed that the potassium mobility is the same as of rubidium, and that one may be determined from the strontium ratios $^{87}Sr/^{86}Sr$ in the crust and mantle rocks.

Utilizing this technique Gast concluded that the potassium concentration in the mantle is exceptionally low, about $6.5 \times 10^{-5}$. In our studies, we somewhat perfected this technique (Sorokhtin, 1977; Sorokhtin and Ushakov, 1991, 2002) by the application of Earth's evolutionary model and comparing the isotope ratios of radiogenic elements in Earth and lunar basalts. We determined that the most likely potassium concentration in the mantle is approximately two times of that determined by Gast, and reaches 0.012%. Therefore, the present-day mantle contains $4.81 \times 10^{23}$ g of potassium and $5.62 \times 10^{19}$ g of the radiogenic isotope $^{40}K$, and the total contents within Earth are $9.31 \times 10^{23}$ g of potassium and $1.086 \times 10^{20}$ g of $^{40}K$.

The other determination of potassium content in the mantle rocks were: by Vinogradov (1962), close to 0.03%; by Tilton and Read (1963), 0.01%; by Ringwood (1981, 1982), 0.03%; by Taylor (1973), 0.015%; and by Gast (1975), $<0.01\%$. As can be seen, our value is close to the average of these values.

Estimates of uranium and thorium content in the mantle may only be made indirectly, for instance, based on the potassium–uranium and potassium–thorium ratios. As a rule, relatively refractory elements (uranium and thorium) are concentrated in the continental crust to a noticeably greater extent than the alkali metals (Gast, 1975). For this reason, it is anticipated that the potassium–uranium and potassium–thorium ratios in the present-day mantle will be higher than in the crust. On the other hand, the total contents of uranium and thorium in Earth may exceed their mass in the continental crust. This enables the finding of the ranges for these elements in Earth:

$$\begin{aligned} 3.76 \times 10^{19} < U_g < 7.76 \times 10^{19} g, \\ 1.51 \times 10^{20} < Th_g < 3.10 \times 10^{20} g. \end{aligned} \tag{5.7}$$

These ranges are not that wide in themselves but in real life they must be even narrower. Indeed, the left parts of the inequality (5.7) are outright unrealistic as that would indicate total absence of U and Th in the mantle, which is improbable. The right parts are also not

very probable: due to high mobility of Th and U (compared to K), the K/Th and K/U ratios must be much higher, and the Th/U ratio, lower in the mantle than in the crust.

But let us disregard, for the sake of the argument, this limitation and use the right limits in the (5.7) inequality for the determination of the radiogenic energy released within Earth. Even in this case total heat generation by these elements (together with $^{40}$K) is about $1.89 \times 10^{20}$ erg/s. That is much lower than total heat loss by Earth of $\dot{Q} \approx 4.3 \times 10^{20}$ erg/s.

An important conclusion is that there must be additional and quite powerful endogenous energy source within the planet: $\dot{E}_g > 2.41 \times 10^{20}$ erg/s. As we showed previously, only the currently functioning process of the gravitational (chemical density) differentiation may be such a source. This energy results in the high-density iron-oxide core separation in its central areas and in the generation of intense convective flows in the mantle.

In our calculations detailed in Sorokhtin and Ushakov (1991), we assumed for the mantle $K/U = 4.5 \times 10^4$ and $K/Th = 1.7 \times 10^4$. The uranium content in the mantle is $U_m = 1.05 \times 10^{19}$ g, and thorium, $Th_m = 2.89 \times 10^{19}$ g. Together with potassium, these elements generate nearly $0.34 \times 10^{20}$ erg/s of the heat energy in the mantle. The total radiogenic energy released currently by Earth is about $1.25 \times 10^{20}$ erg/s.

The quoted calculations, based on methodology independent of the hypothesis of exclusively radiogenic Earth heating, show that the contribution to Earth energetics from radioactive elements is much more modest than believed earlier (and sometimes even now). However, it is still noticeable (see Table 5.1).

As the above estimates show, the bulk of radioactive elements is currently concentrated in the continental crust. It was earlier clearly demonstrated by Gast (1975). One needs to

**TABLE 5.1** Radioactive Element Contents in Earth

| | **Continental crust, mass $2.25 \times 10^{25}$ g** | | **Mantle, mass $4.07 \times 10^{27}$ g** | | **Entire Earth, mass $5.98 \times 10^{27}$ g** | |
|---|---|---|---|---|---|---|
| | **Element contents** | **Released energy (erg/s)** | **Element contents** | **Released energy (erg/s)** | **Element contents** | **Released energy (erg/s)** |
| $^{238}$U | $3.64 \times 10^{19}$ r | $0.341 \times 10^{20}$ | $1.047 \times 10^{19}$ r | $0.098 \times 10^{20}$ | $4.69 \times 10^{19}$ r | $0.439 \times 10^{20}$ |
| $^{235}$U | $0.026 \times 10^{19}$ r | $0.015 \times 10^{20}$ | $0.008 \times 10^{19}$r | $0.004 \times 10^{20}$ | $0.034 \times 10^{19}$r | $0.02 \times 10^{20}$ |
| $^{232}$Th | $15.18 \times 10^{19}$ r | $0.408 \times 10^{20}$ | $2.89 \times 10^{19}$ r | $0.078 \times 10^{20}$ | $18.07 \times 10^{19}$ r | $0.486 \times 10^{20}$ |
| $^{40}$K | $5.24 \times 10^{19}$ r | $0.146 \times 10^{20}$ | $5.62 \times 10^{19}$ r | $0.157 \times 10^{20}$ | $10.86 \times 10^{19}$ r | $0.303 \times 10^{20}$ |
| K/U | $1.23 \times 10^4$ | – | $4.6 \times 10^4$ | – | $1.98 \times 10^4$ | – |
| K/Th | $3 \times 10^3$ | – | $1.67 \times 10^4$ | – | $5.16 \times 10^3$ | – |
| Th/U | 4 | – | 2.74 | – | 3.83 | – |
| $\dot{E}_{\Sigma}$ | – | $0{,}91 \times 10^{20}$ | – | $0.337 \times 10^{20}$ | – | $1.248 \times 10^{20}$ |

remember, however, that whereas it is possible to determine the radioactive element contents in the crust with some accuracy, estimates for the mantle are quite approximate. Still, the main conclusion that much less radiogenic heat is dissipated in the mantle than in the crust may be considered quite reliable.

Radioactive elements brought up from the mantle into the crust are mostly concentrated in its granite layer or the sedimentary shell. Their generated heat is relatively rapidly lost through Earth's surface and does not have any practical participation in heating of Earth's depths. Therefore, in identifying the endogenous energy sources feeding Earth's tectonic activity only that fraction of the radiogenic energy released in the mantle is of a special interest. The above calculation shows that currently this fraction of the radiogenic energy ($0.337 \times 10^{20}$ erg/s) is responsible for only 8% of the total Earth heat loss ($4.3 \times 10^{20}$ erg/s) or about 10% of the depth heat generated within the mantle ($3.39 \times 10^{20}$ erg/s). In the past geological epochs, however, the radiogenic energy release in the mantle might have been much higher.

To find this energy fraction it is necessary to take into consideration that the radioactive element concentration in the mantle declined with the passing of time not only due to the decay of these elements but also because of their predominant migration into the continental crust. That is why the mantle content $R_i$ of a radioactive element $i$ declined in time under a somewhat more complex resulting rule. We can assume as a first approximation that the radioactive element migration into the continental crust is proportionate with the rate of the mantle convective mass exchange. The latter, under (4.48), is described by the rate of heat energy release in the mantle.

We need to perform a quantitative estimation of the radioactive element migration process from the mantle to the continental crust. For this purpose it turned to be convenient to use, by analogy with Earth's evolution parameter $x$, also Earth's tectonic parameter $z$ (see Section 4.4) and Eqs. (4.48) and (4.48′). Here they are again:

$$z = (Q_{\mathrm{m}} - Q_{4.0})/(Q_{\mathrm{m}0} - Q_{4.0}), \tag{5.8}$$

where $Q_{4.0} \approx 1.6 \times 10^{37}$ erg is Earth's heat loss by the time its tectonic activity began about 4.0 BY ago and $Q_{\mathrm{m}0} \approx 10.77 \times 10^{37}$ erg is the total heat loss by the mantle by the present time. In this case, Earth's tectonic activity is characterized by the derivative over time of this parameter. This derivative, in normalized format, is

$$\dot{z}_{\mathrm{n}} = \dot{Q}_{\mathrm{m}}/|\dot{Q}_{\mathrm{m}0}|, \tag{5.8′}$$

where $\dot{Q}_{\mathrm{m}}$ is the current value of heat flow from the mantle and $|\dot{Q}_{\mathrm{m}0}| = 3.39 \times 10^{20}$ erg/s is the absolute value of the current heat loss by Earth. Then the present-day value of the parameter $z_{\mathrm{o}} = 1$ and the derivative $\dot{z}_0 = 1$ (for the comparison, $x_{\mathrm{o}} = 0.864$ and $\dot{x}_0 = 0.664 \times 10^{-10}$ years$^{-1}$).

In this case, the migration speed of the element $i$ from the mantle to the crust (hydrosphere or atmosphere) is

$$\dot{m}_i = -m_{0i}\chi_i\dot{z}. \tag{5.9}$$

And from this

$$m_i = m_{0i}(1 - e^{-\chi_i z}), \tag{5.9'}$$

where $m_i$ is mass of the element $i$ which migrated from the mantle into the other geosphere; $m_{0i}$ is the initial mass of this element in the mantle; $\chi_i$ is the element $i$ mobility parameter. As parameter $z$ is normed, the mobility parameters $\chi_i$ become dimensionless values and the derivative $\dot{z}$ acquires the dimension of 1/time.

In this case, the content $R_i$ of radioactive element $i$ in the mantle is

$$R_i = R_{0i}e^{-(\chi_i z + \lambda_i t)}, \tag{5.10}$$

where $\lambda_i$ the decay constant $R_i$ of the element; $t$ is time from the moment of Earth's formation; $i$ is the index of one of the four radioactive elements $^{238}$U, $^{235}$U, $^{232}$Th, or $^{40}$K. In this particular case, the radioactive energy release speed $\dot{E}(R)$ in Earth and the mantle is

$$\dot{E}(R_i)_g = \sum_{i=1}^{4} R_{0i}\dot{q}_i e^{-\lambda_i t} \tag{5.11}$$

$$\dot{E}(R_i)_m = \sum_{i=1}^{4} R_{0i}\dot{q}_i e^{-(\chi_i z + \lambda_i t)}, \tag{5.11'}$$

where $\dot{q}_i$ is the heat generation by a unit mass of the radioactive element $R_i$ per unit time ($^{238}$U = 0.937; $^{235}$U = 5.69; $^{232}$Th = 0.269; $^{40}$K = 0.279 erg/g s). Now, we can determine total radiogenic energy released in Earth and the mantle during time $t$ by integrating Eqs. (5.11) and (5.11′) over all radioactive elements

$$E(R_i)_g = \sum_{i=1}^{4} R_{0i}\frac{\dot{q}_i}{\lambda_i}\left(1 - e^{-\lambda_i t}\right) \tag{5.12}$$

$$E(R_i)_m = \sum_{i=1}^{4} R_{0i}\dot{q}_i \int_0^t e^{-(\chi_i z + \lambda_i t)} dt. \tag{5.12'}$$

The initial masses of radioactive element are found as

$$R_{0i} = R_i e^{\lambda_i t_g}, \tag{5.13}$$

where $R_i$ is the total mass of the element $i$ in the present-day Earth and $t_g = 4.6$ BY is Earth's age.

To calculate Eqs. (5.10)–(5.12), we need to first determine the value of the mobility parameters $\chi_\iota$ from Eq. (5.9′). The sought-for mobility parameters of these elements may then be determined from this expression and earlier determined radioactive element contents in the mantle and continental crust: $\chi_K \approx 0.79$; $\chi_U \approx 1.8$; and $\chi_{Th} \approx 2.2$. The values of function $z$ are given by (5.8) and were determined in (Sorokhtin and Ushakov, 2002).

From the data published by Faure (1977): $^{40}K/(^{39}K + ^{41}K) = 1.167 \times 10^{-4}$; $^{238}U/^{235}U = 137.88$; $\boldsymbol{\lambda}_{238} = 1.551 \times 10^{-10}$ years$^{-1}$; $\lambda_{235} = 9.849 \times 10^{-10}$ years$^{-1}$; $\lambda_{232} = 4.948 \times 10^{-11}$ years$^{-1}$; $\lambda_{40} = 5.543 \times 10^{-10}$ years$^{-1}$. Then $^{238}U_0 = 9.76 \times 10^{19}$ g, $^{235}U_0 = 3.22 \times 10^{19}$ g, $^{232}Th_0 = 2.22 \times 10^{20}$g, and $^{40}K_0 = 1.39 \times 10^{21}$ g.

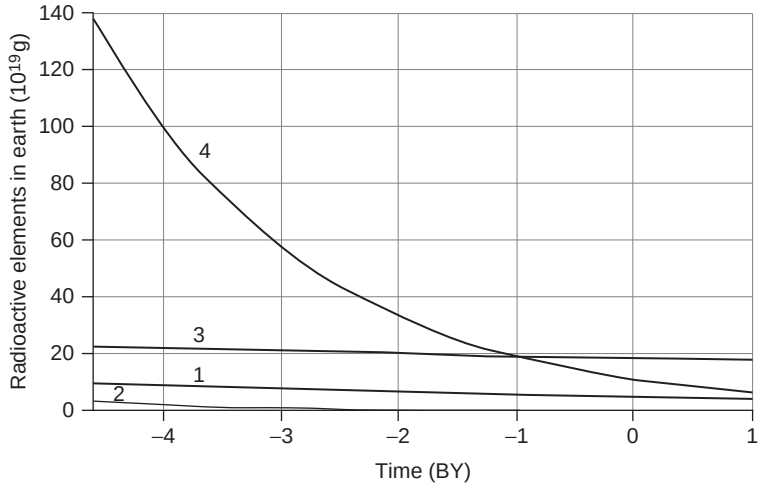


**FIGURE 5.3** Evolution of radioactive element contents in Earth (element mass in $10^{19}$ g): 1, $^{238}$U; 2, $^{235}$U; 3, $^{232}$Th; and 4, $^{40}$K.

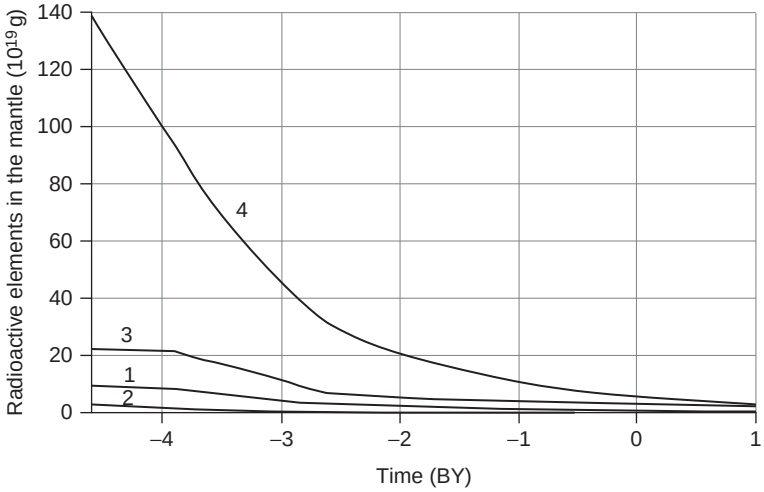


**FIGURE 5.4** Evolution of radioactive element contents in Earth's mantle (element mass in $10^{19}$ g): 1, $^{238}$U; 2, $^{235}$U; 3, $^{232}$Th; and 4, $^{40}$K.

Using these and aforementioned data on the radioactive element contents in the continental crust we can determine the evolution of these elements in Earth, the mantle and the continental crust (Figs. 5.3–5.5).

As the diagrams show, the radioactive element content in Earth gradually declined according to their decay constant $\lambda_i$. The decline rate for the same elements in the mantle turned out to be somewhat higher as a noticeable portion of them migrated to the continental crust. As for the continental crust, when it was forming at the greatest rate in Archaean,

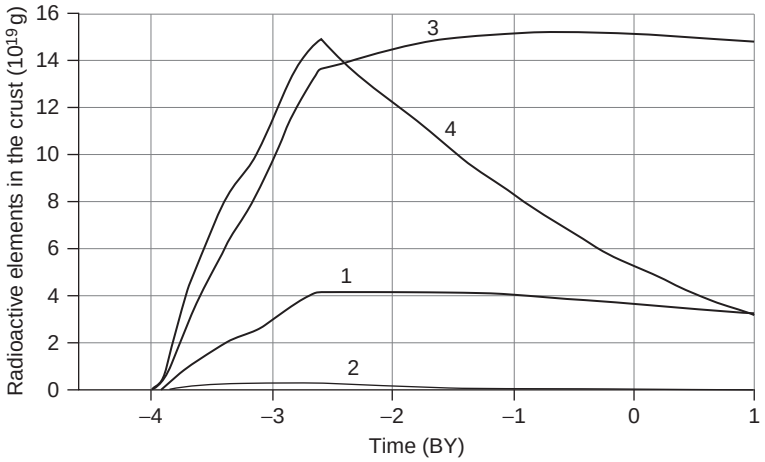


**FIGURE 5.5** Evolution of radioactive element contents in the continental crust (element mass in $10^{19}$ g): 1, $^{238}$U; 2, $^{235}$U; 3, $^{232}$Th; and 4, $^{40}$K.

and relatively high concentrations of the radioactive elements were still present in the mantle, their concentrations were also increasing most rapidly. Earth's tectonic activity and the continent formation rate drastically declined after the formation of the Earth's core 2.6 BY ago. After that, in Proterozoic and Phanerozoic the $^{238}$U and $^{232}$Th concentrations somewhat stabilized, whereas the $^{235}$U and $^{40}$K concentrations after Archaean continuously declined due to their higher decay constant values.

The diagrams in Fig. 5.6 demonstrate drastic differences in the relative concentrations of the reviewed elements in Earth associated with their migration into the continental crust. The concentration of these elements in the primordial Earth's matter is taken for a one.

We will now insert the aforementioned parameters of the reviewed radioactive elements and the value of their specific heat generation in Eqs. (5.11) and (5.11′). The result shows that $7.18 \times 10^{20}$ erg/s of radiogenic energy was being initially released within the young Earth. Figure 5.7 displays the radiogenic energy release rate diagrams within Earth, the mantle, and the continental crust.

As we see, the radiogenic energy release intensity in the mantle was noticeably declining, especially in Archaean, as it was the time of the fastest radioactive element migration into the continental crust. The current radiogenic energy release in the mantle does not exceed $0.337 \times 10^{20}$ erg/s. This is just 4.7% of the initial rate and 8% of the total heat loss by the present-day Earth.

The same is indicated also by a calculation of the total energy from Eqs. (5.12) and (5.12′). It so happened that over the life of Earth, $4.33 \times 10^{37}$ erg of the radiogenic energy was released within it. Out of that, approximately $1.16 \times 10^{37}$ erg was released during Katarchaean over the first 600 MMY, that is, prior to the beginning of any geological activity. During the entire Archaean (4.0–2.6 BY ago), about $1.67 \times 10^{37}$ erg of radiogenic energy was released within Earth ($1.35 \times 10^{37}$ erg in the mantle and $0.32 \times 10^{37}$ erg in the continental crust). Only $0.6 \times 10^{37}$ erg was released within the mantle over the remaining 2.6 BY of the geological evolution. This is about 14% of the radiogenic energy (Fig. 5.8). Total radiogenic energy release within the mantle was circum $3.11 \times 10^{37}$ erg and in the continental crust $1.22 \times 10^{37}$.

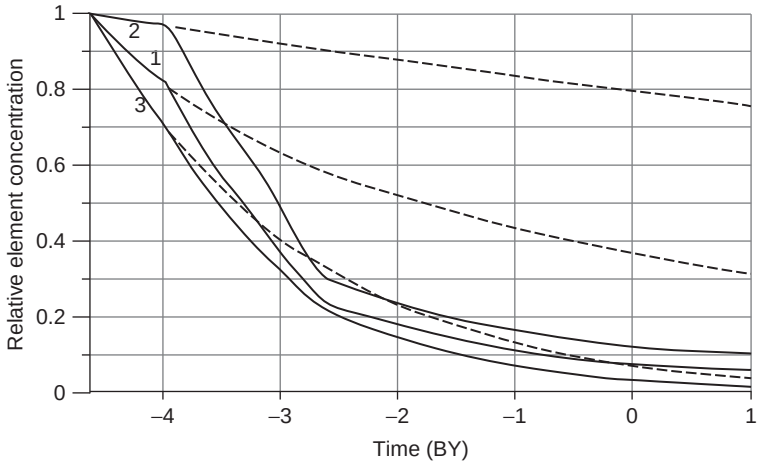


**FIGURE 5.6** Relative concentration of radioactive elements in the mantle (solid curves) and in Earth (dashed curves). The element concentration in Earth's primordial matter is taken as the unit: 1, total concentration of $^{238}U$ and $^{235}U$; 2, concentration of $^{232}Th$; and 3, concentration of $^{40}K$.

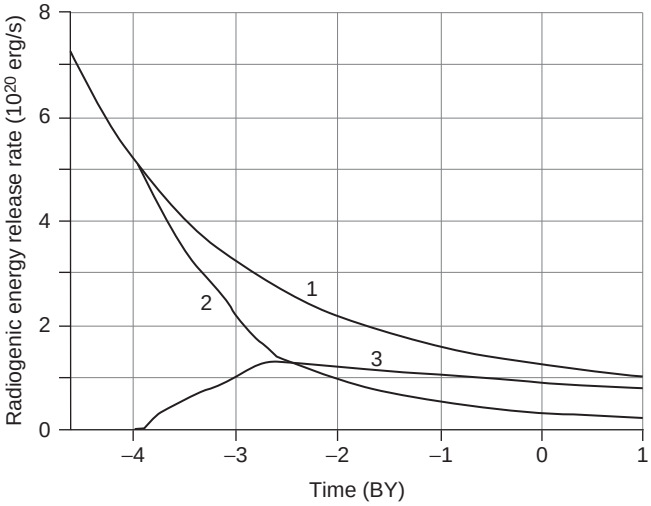


**FIGURE 5.7** Radiogenic energy release rate (in $10^{20}$ erg/s): 1, in Earth; 2, in mantle; and 3, in continental crust.

## 5.3 ENERGY OF EARTH'S TIDAL SLOW-DOWN

Total kinetic momentum (3.1) in the system of a planet with the satellite tied by the gravity-tidal connections remains unchanged although the momentums are redistributed between the planet and the satellite. Such changes occur only under the release

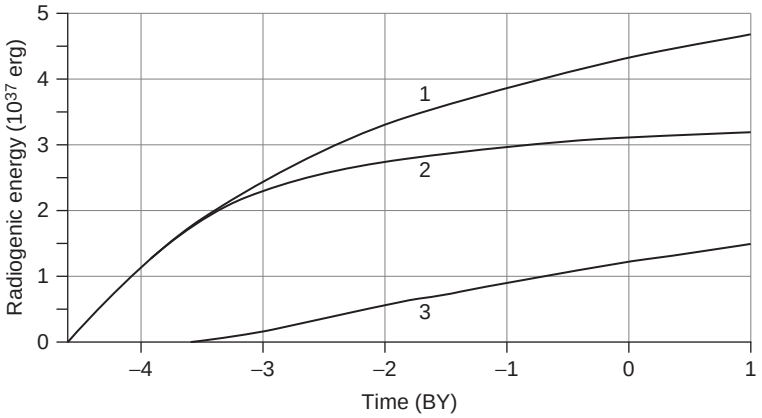


**FIGURE 5.8** Radiogenic energy release (in $10^{37}$ erg): 1, within Earth; 2, within mantle; and 3, within continental crust.

and dissipation of the kinetic energy initially stored within the system. This kinetic energy is defined by Eqs. (3.3) and (3.4).

After the formation of the Moon, the angular velocity of Earth's axial revolution was always higher than the angular velocity of the Moon's orbital revolution ($\Omega > \omega$). Thus, the tidal energy dissipation within the body of Earth resulted in a decline of both $\Omega$ and $\omega$. Therefore, under Kepler's third law (3.2), the distance $L$ between Earth and the Moon continuously increased (see Section 3.7). The changes in the mentioned system's parameters strongly depended on the dissipation rate of the tidal energy $\dot{E}_t$ within the body of Earth.

Presently, most of the tidal energy is being released in the shallow seas and a much smaller part, in deep oceans and in Earth's asthenosphere. MacDonald (1975) determined that the present-day rate of the tidal energy release is $\dot{E}_t \approx 0.25 \times 10^{20}$ erg/s. About two-thirds of it is dissipated within the shallow seas due to the friction of intense near-bottom marine currents about the sea-floor. Our estimate is $\dot{E}_t \approx 0.287 \times 10^{20}$ erg/s; 94% of the tidal energy is dissipated in the hydrosphere. The present-day heat flow through Earth's surface reaches approximately $4.3 \times 10^{20}$ erg/s (see Section 2.1). Therefore, the current tidal energy fraction dissipated within the "solid" Earth does not exceed 0.5–1% of the total energy generated in its depths.

It shows that the lunar tides now play a very modest role in feeding Earth's tectonic activity. At the same time, the tidal deformations of the lithospheric shell may reach a few tens of centimeters in amplitude and apparently may sometimes serve as the earthquake trigger mechanisms. The Solar tides are even less significant as their effect does not exceed 20% of the lunar tides.

Solar tide amplitude was always insignificant. The effect of the lunar tides during the past geological epochs was much stronger. The theory of the tides shows that the intensity of such action is in the inverse proportion with the distance between the planets to the power of six (Pariysky, 1960; MacDonald, 1975; Ruskol, 1975). A conclusion is that during distant geological periods when the Moon was much closer to Earth, its tidal action on our planet was much stronger. At the earliest stages of Earth's evolution the lunar tide amplitude according to (3.40) reached 1.5 km. Therefore, it may be expected that at that

time the tidal energy dominated all other sources of the endogenous energy and for that reason substantially determined Earth's tectonic evolution.

MacDonald (1975) and Ruskol (1975) found that the heat released due to the tidal deformations is extracted from the kinetic energy of Earth's axial revolution (3.3). Today this energy is relatively small, $(E_\Omega)_{0.0} = 0.214 \times 10^{37}$ erg. In the beginning of the Earth–Moon evolutionary path (about 4.6 BY ago) it was much greater, up to $(E_\Omega)_{4.6} \approx 4.019 \times 10^{37}$ erg.

Part of this energy released in the deceleration process of Earth's revolution was spent on the increase of the Moon orbital motion energy which is determined by Eq. (3.4). The rest of it dissipated within Earth. At the time of the Moon formation its distance from Earth was $L_{4.6} \approx 1{,}72 \times 10^9$ cm (see Section 3.7). Using (3.4) we find Moon's initial orbital motion energy $(E_\omega)_{4.6} = -8.54 \times 10^{36}$ erg (Moon's initial orbital motion energy is potential energy, so $E_\omega < 0$). Similarly, currently $L_{0.0} = 3.844 \times 10^{10}$ cm and $(E_\omega)_{0.0} = -0.38 \times 10^{36}$ erg.

Therefore, over the life of the Earth–Moon system, that is, over 4.6 BY, Earth's revolution kinetic energy declined by $\Delta E_\Omega = 3.81 \times 10^{37}$ erg, and Moon's orbital motion kinetic energy increased by $\Delta E_\omega \approx 0.81 \times 10^{37}$ erg. So, over the same period the energy dissipated in Earth and converted into heat was

$$E_t = \Delta E_\Omega - \Delta E_\omega, \tag{5.14}$$

which is about $3 \times 10^{37}$ erg of the tidal energy.

We can find major patterns of the tidal energy release in Earth through Eq. (3.27), which determines $L(t)$ correlation, and then use the basic planet motion Eqs. (3.1) and (3.2) enabling the determination of $\Omega$ versus $L(t)$ correlation.

In this case, the rate of the tidal energy release may be found from a differential Eq. (5.14) taking into account Eqs. (3.3) and (3.4)

$$\dot{E}_t = I\Omega\dot{\Omega} - \gamma\frac{Mm}{2L^2}\dot{L}, \tag{5.15}$$

where $I$ is Earth's momentum of inertia; $\Omega$ is angular velocity of its own revolution; $\gamma$ is the gravitational constant; $M$ and $m$ are, respectively, Earth and Moon masses; $L$ is the distance between Earth and Moon mass centers.

The evolution correlation between a derivative $\dot{\Omega}$ and the Earth–Moon system parameters may be determined from Pariysky equation (3.18′) by replacing the tide delay angle with the dissipative function $\sin 2\delta \approx tg2\delta = Q_\mu^{-1}$

$$\dot{\Omega} = -\frac{3}{2}\frac{k_2\gamma m^2 R^5}{IQ_\mu L^6}, \tag{5.16}$$

where $k_2$ is the second Love number; $R$ is Earth's radius; and $Q_\mu$ is Earth's mechanical quality factor (3.19).

Now, we can find the sought-for correlation between the tidal energy in Earth's release rate through Eqs. (3.1) and (3.2) (Sorokhtin and Ushakov, 1991):

$$\dot{E}_t = -\frac{3}{2}\frac{k_2\gamma m^2 R^5}{Q_\mu L^6}(\Omega - \omega). \tag{5.17}$$

Here, the correlation between $E_t$ and time $t$ is done through the parameter $L$ from Eq. (3.27), and the correlations $\Omega$ and $\omega$ versus distance $L$ are determined from Eqs. (3.1) and (3.2) in consideration of evolutionary changes in Earth's momentum of inertia $I$ described in Eqs. (5.15) and (5.16). The other parameters are either constant or assigned by the assumed Earth's evolution model.

We showed in Chapter 3 that Earth's tidal quality factor $Q_\mu$ substantially changed in time over the entire evolution of the planet. Based on geological data and a condition of the Earth and Moon age equality, we substantiated in Section 3.7 an approximate $Q_\mu$ change with time model (Fig. 3.4). Figure 5.9 shows the rate of the tidal energy release in time $\dot{E}_t(t)$ calculated from Eq. (5.17) using the aforementioned equation $Q_\mu(t)$. The values of this energy $E_t(t)$ derived from Eq. (5.14) are displayed in Fig. 5.10.

The tidal energy was released within Earth most intensely at the very beginning of its formation, prior to the Moon's origin. During those far away times, immediately upon the capture of the Proto-Moon 4.6 BY ago the rate of the tidal energy release reached a tremendous value of close to $5.2 \times 10^{24}$ erg/s. This is 13,000 times the rate of the current endogenous heat energy generation within Earth. Remember, the tide height in the "solid" Earth at that time was almost 1.5 km, and the seismic activity was likely higher than its present-day level by three orders of magnitude (see Section 3.9).

At the moment the Moon transferred to a stationary orbit of the Roche limit, the tidal energy release, under Eq. (5.17), dropped practically to zero as on such Roche limit orbit $\Omega = \omega$. In one million years, however, the tidal heat generation rose again to approximately $20 \times 10^{20}$ erg/s, and in 100 MMY since it declined again to $7 \times 10^{20}$ erg/s, which exceeds the current total heat generation within Earth only by the factor of 2.

Subsequently, the tidal energy dissipation continued its gradual decline to approximately $2.2 \times 10^{20}$ erg/s by the end of Katarchaean nearly 4 BY ago. As mentioned in the previous chapter, in Katarchaean the young Earth did not have asthenosphere or hydrosphere. For this reason, the tidal energy then was distributed in Earth's body more uniformly and in accordance with the tidal deformation amplitudes as determined by Eq. (3.40). It follows

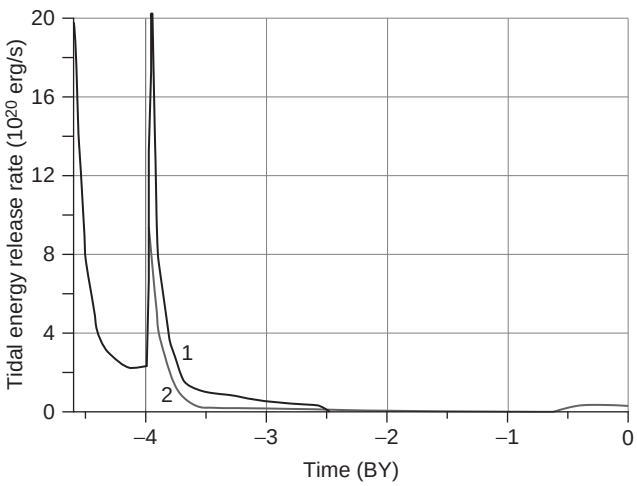


**FIGURE 5.9** Tidal energy release rate in Earth: 1, total energy release rate in mantle and hydrosphere and 2, energy release in mantle.

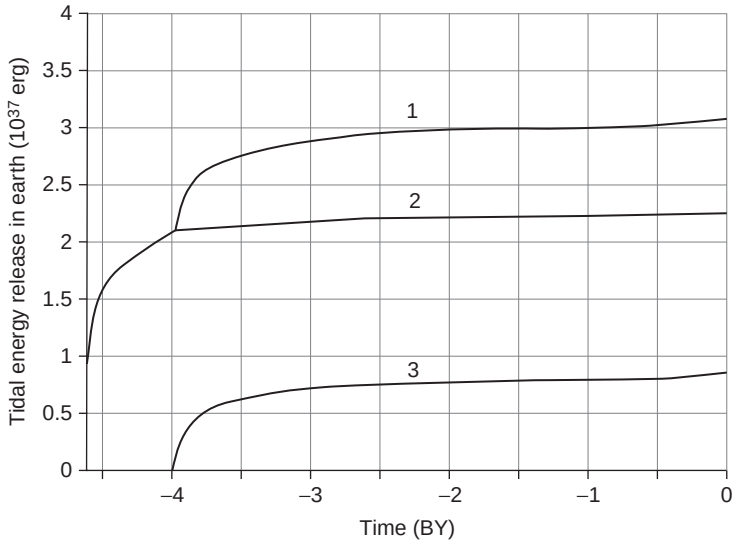


**FIGURE 5.10** Tidal energy release: 1, in Earth; 2, in mantle; and 3, in hydrosphere.

from this equation that the most intense Katarchaean tidal deformations were happening on the equator and in the low latitudes. At 55° of the latitude they turned into zero, and at higher latitudes the deformations changed their sign but became weaker. On the poles, their variable component again became equal to zero. That is why the bulk of the tidal energy in Katarchaean was released within the equatorial ring belt and in the low latitudes. As a result, Earth could have heated up within this belt by additional 600 °C, and on average within its entire mass, by 400 °C. This additional heat-up should, however, most likely be attributed to the primary Earth heat-up.

A second tide-associated "heat shock" occurred at the Katarchaean/Archaean boundary about 4 BY ago, immediately upon the asthenosphere emergence on the equator and appearance of the first shallow-water marine basins. The explanation is that the planet's tidal deformations mostly concentrate within the layers with the lowermost rigidity and viscosity moduli, that is, within the easiest deformable layers. After Earth heated-up in Katarchaean, and the mantle began degassing with the hydrosphere formation in Early Archaean, the tidal deformations tended to concentrate mostly in shallow-water seas of the low-latitude ring-like equatorial belt and in part within the mantle's upper asthenosphere underneath the same belt. The released tidal energy resulted in the additional overheating and melting of the mantle matter, and also to broadening of the asthenosphere layer. This, in turn, lowered Earth's tidal quality and, therefore, increased even more the rate of the tidal energy release.

The amplitude of this tidal energy peak in the very beginning of Archaean was much lower than the Katarchaean peak but still reached $1 \times 10^{22}$ erg/s, that is, it was 20 times higher than the current endogenous energy generation rate within Earth. This energy, however, was releasing not within the entire Earth mass but mostly in the seas and in the upper mantle asthenospheric layer (Fig. 4.1). As a result of such avalanche release of the tidal

energy, the upper mantle matter within the equatorial ring belt melted. A new and most powerful energy process of the Earth's matter gravity differentiation within this melted belt began.

The tidal energy release in Late Archaean and even more so in Proterozoic became more placid. By that time real oceans appeared on Earth so most of the tidal energy was being dissipated in the hydrosphere. The tidal energy release rate again increased somewhat only during Phanerozoic. This time, such activation of the tidal interaction with the Moon, was insignificant and associated only with the evolution of Earth's hydrosphere. This evolution was the development in that epoch of the first broad oceanic transgressions over the continents and the formation of shallow-water epicontinental seas where currently most of the tidal energy is spent.

The model of a change in time of Earth's effective quality reviewed in Section 3.4 enables approximate estimate of the energy fraction dissipated now within the shallow-water seas, oceans, and the mantle. The present-day Earth's tidal quality factor is equal about 13. So, it is possible to calculate that currently around $0.287 \times 10^{20}$ erg/s of the tidal energy is dissipated within Earth. The dissipative functions have a property of additivity. So, we find that $0.27 \times 10^{20}$ erg/s is dissipated in the hydrosphere, and only $0.018 \times 10^{20}$ erg/s, in the mantle, which are, respectively, 93% and 7%. Thus, the tidal energy fraction of Earth's endogenous energetics ($3.39 \times 10^{20}$ erg/s) is approximately 0.5%.

The total tidal heat energy release in Earth during Katarchaean (first 600 MMY of Earth's existence) was $2.1 \times 10^{37}$ erg (Fig. 5.10). In Archaean, Proterozoic, and Phanerozoic, about $1.2 \times 10^{37}$ erg of the tidal energy was released in Earth. Of this amount, nearly $0.96 \times 10^{37}$ erg was released in the hydrosphere and only $0.24 \times 10^{37}$ erg in the mantle. Altogether, from the moment of the Moon emergence on the near-Earth orbit 4.6 BY ago approximately $3.08 \times 10^{37}$ erg of the tidal energy was released within Earth including about $2.24 \times 10^{37}$ erg in the mantle (Fig. 5.10).

The above calculations show that the tidal energy dominated only Katarchaean and the very beginning of Archaean. The lunar tide contribution to the total Earth energetics in Late Archaean, Proterozoic, and Phanerozoic was very modest, never more than 1–2%.

## 5.4 HEAT LOSS BY EARTH

As was shown in the preceding sections, $E_{gT} \approx 16.95 \times 10^{37}$ erg of Earth's matter gravity differentiation energy, nearly $3.11 \times 10^{37}$ erg of the radiation energy and about $2.24 \times 10^{37}$ erg of the tidal energy were released from within Earth over its life. The total is $22.3 \times 10^{37}$ erg including $17.94 \times 10^{37}$ erg of the heat energy and $4.36 \times 10^{37}$ erg of the energy of additional Earth compression released in the core formation. This heat was quite sufficient to heat Earth and overheat it to 4000 °C. It did not happen, however. The conclusion is that part of this heat was lost by Earth with its heat radiation into the outer space. We will determine this fraction quantitatively in the next section. Here, we will review only the current heat loss of Earth.

There are now over 40,000 experimental measurements of the heat flow at different points of Earth's surface. It would be methodologically wrong, however, to average these heat loss values and determine from that the total Earth heat loss $\dot{Q}$.

The present-day Earth's heat loss may only be determined using a semiempirical–semitheoretical technique. The reason for this is that a significant fraction of the depth heat flow from the mantle is carried out with thermal waters. The hydrothermal heat release on the continents is relatively small. At the same time, the heat release with the oceanic waters circulating within the Earth's crust fractures in the oceanic rift zones and on the slopes of the mid-oceanic ridges is tremendous. Our estimates indicate that such heat release may be up to 24% of the total Earth's heat loss (Sorokhtin, 1974). Unfortunately, so far it was impossible to experimentally measure the total convective heat flow. That is why it is necessary, beside empirical data, to utilize theoretical estimates of the heat flow convective component for the determination of Earth's depth heat loss.

Oceanic lithospheric plates form due to the cooling and total crystallization of the partially melted upper mantle matter (Sorokhtin, 1973). A conveyor of the oceanic lithospheric plates is continuously moving from the rift zones over the crests of the mid-oceanic ranges where they emerge, to the plate subduction zones where they again submerge into the hot mantle. That is why the most of the planet's heat loss indeed occurs through the ocean floor (Ushakov and Fedynsky, 1973). The continents and continental plates play a modest and mostly passive role in regulating Earth's heat balance. The heat flow through the ocean floor is more than 2.5 times greater than the total heat flow of the continents. Most of the continental heat is generated by the decay of radioactive elements concentrated in the upper layers of the crust. This taken into account, more than 90% of the endogenous (mantle) heat of Earth is lost through the ocean floor (Sorokhtin and Ushakov, 1990, 1993).

It follows from the crystallization model of the oceanic plate origins that the heat flow through a plate is in the reverse proportion with square root of its age $t$:

$$q = \lambda_1 \frac{T_m}{\sqrt{\pi a (t_0 + t)}}, \tag{5.18}$$

where $t_0$ is the effective time of the oceanic crust formation in the rift zone of a mid-oceanic ridge (usually about 30,000–40,000 years); $\lambda_1$ is the heat conductivity of the lithosphere; $a$ is its thermometric conductivity; $T_m$ is the temperature of the upper mantle. The reference book (Physical properties... 1976) suggests for a lherzolite-composition lithosphere a value $\lambda_1 \approx 6.2 \times 10^{-3}$ cal/cm s deg and $a \approx 5.7 \times 10^{-3}$ cm$^2$/s. Average temperature of melted basalt foci underneath the rift zones may be assumed to be 1300–1400 °C (see Fig. 2.18). Let us now express the lithospheric plate age in millions of years (1 MY $\approx 3.156 \times 10^{13}$ s) and the heat flow in units of $10^{-6}$ cal/cm$^2$ s, then

$$q \approx \frac{12}{\sqrt{t_0 + t}}. \tag{5.19}$$

A comparison was made of the theoretical equation (5.19) with the experimental measurements of the heat flows through quiescent areas of the ocean floor off the transform faults and volcanic areas (see, e.g., Sorokhtin, 1974; Gorodnitsky and Sorokhtin, 1981; Anderson and Hobart, 1976). It showed that the theoretical curve averages only the maximum values of the measured heat flow (see Fig. 5.11). The reason is that the Earth's crust in the mid-oceanic ridges is cut by a dense network of fractures and faults arising during extension of the lithospheric plates in their spreading away from the rift zones. These fractures are draining the

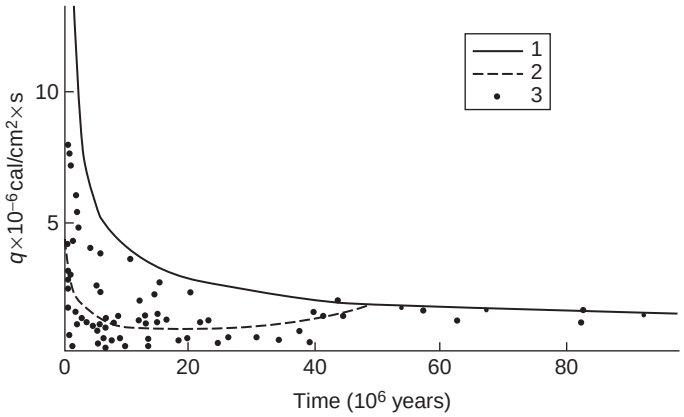


**FIGURE 5.11** Heat flow through the ocean floor versus lithospheric plate age (Sorokhtin, 1974): 1, theoretical curve of the total heat flow from Eq. (5.19); 2, conductive component of the heat flow (average value from experimental determinations); and 3, experimental heat flow measurements in the South Atlantic and Pacific Oceans.

oceanic crust. The oceanic water is freely circulating through them and carrying from the still warm lithospheric plates a substantial fraction of heat from the crust to the oceans.

As a result, the total heat flow through the ocean floor falls apart into two components, the conductive and the convective. The possibility of convective heat release from the mid-oceanic ridges and of the existence of hydrothermal springs was first predicted theoretically (Lister, 1972; Sorokhtin, 1973a,b, 1974), way ahead of the actual discovery of the springs on the ocean floor in 1977–1978 (Hekinian et al., 1978, 1983; Edmond et al., 1979; Francheteau et al., 1979). At that time an estimate of the hydrothermal heat release through the ocean floor was first given. It was approximately $2.4 \times 10^{12}$ cal/s$\approx 1 \times 10^{20}$ erg/s, which is about 23% of the total Earth's heat loss (Sorokhtin, 1974).

A similar correlation between the heat flow value and the ocean floor age was arrived at by Gorodnitsky and Sorokhtin (1981). This one, however, utilized a much broader set of actual data from the Pacific, Atlantic, and Indian oceans. The averaging is done according to Eq. (5.19) but with somewhat greater approximation factors: 13, 14, and 15 (see Fig. 5.12).

The appearance of the convective component results in an increase of the oceanic crust heat conductivity effective value $\lambda_{cr}$, therefore, in a decrease in it of the temperature gradient. The heat flow may be experimentally measured only on the sea-floor areas slightly covered with deposits. The heat flow is measured from the temperature gradient in the deposits and the heat conductivity of the deposits $\lambda_s$. In the presence of the convective heat release, we have always $\lambda_{cr} < \lambda_s$. Because of this, the heat flows measured in deposit-filled topographic pockets of the mid-oceanic ridges with thermal sondes using conventional techniques usually undervalue true (total) flows. Only in rare cases (under favorable conditions), in the ocean-floor areas with fractures completely filled-up with deposits, the measured convective components correspond with the total heat flow. For this reason, the theoretical heat flow curves through the ocean floor are always above the cloud of the experimental points. Actually, the total heat flow curve through the mid-oceanic ridges and the ocean floor should average maximum values of the flow measurements. With this and the data from Fig. 5.12 taken into account, we can now fine-tune Eq. (5.19) providing the correlation of the heat flow through the ocean floor versus its age:

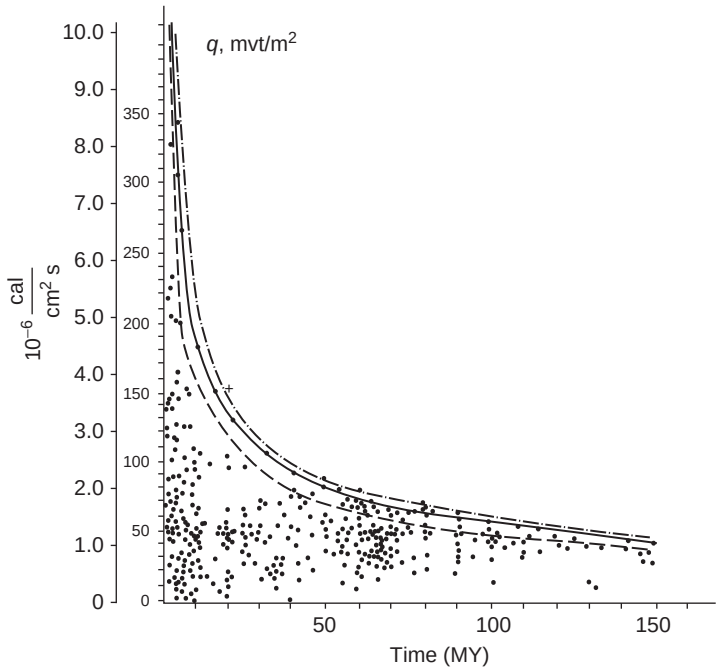


**FIGURE 5.12** Heat flow through the ocean floor versus ocean floor age. Experimental data in this diagram were collected from rift zones and quiescent areas of the ocean floor between the transform zones and away from young intraplate volcanic areas (Gorodnitsky and Sorokhtin, 1981).

$$q \approx \frac{13.2}{\sqrt{t_0 + t}}, \tag{5.19'}$$

where $q$ is in $10^{-6}$ cal s and $t$ is in millions of years. In this case, the average specific heat flow through the ocean floor is:

$$\bar{q} = \frac{26.4}{\sqrt{\tau}}, \tag{5.20}$$

where $\tau$ is average life time of the oceanic plates.

The average maximum age of the present-day oceanic lithospheric plates is probably close to $\tau \approx 120$ MMY. If so, the average specific heat flow through the ocean floor is approximately: $q_{oc} \approx 2.41 \times 10^{-6}$ cal/cm$^2$ s. Total area of the oceanic crust (without the shelf and marginal seas with the continental and transitional type crust) is $3.06 \times 10^{18}$ cm$^2$. Thus, the total heat flow through the oceanic crust is $\dot{Q}_{oc} \approx 7.37 \times 10^{12}$ cal/s $= 3.09 \times 10^{20}$ erg/s.

Based on empirical data, average specific heat flow through the continents equals approximately $1.42 \times 10^{-6}$ cal/cm$^2$ s (Sclater et al., 1981). Given the continental crust area of $2.04 \times 10^{18}$ cm$^2$ (accounting this time for the shelf and marginal seas areas with the continental type crust), total heat flow through the continental crust is $\dot{Q}_{cc} \approx 2.9 \times 10^{12}$ cal/s $= 1.21 \times 10^{20}$ erg/s. The radiogenic heat flow of the continents equals to $0.91 \times 10^{20}$ erg/s, then the depth heat flow through the continents is $1.21 \times 10^{20} - 0.91 \times 10^{20} = 0.3 \times 10^{20}$ erg/s runs through the continents. Then the depth heat flow coming from the mantle through the entire Earth is

$$\dot{Q}_m = 3.09 \times 10^{20} + 0.3 \times 10^{20} = 3.39 \times 10^{20} \text{erg/s}. \quad (5.21)$$

Therefore, the total heat loss by the present-day Earth reaches $\dot{Q}_G \approx 3.39 \times 10^{20} + 0.91 \times 10^{20}$ erg/s. For a comparison, the similar estimates of Earth's total heat loss previously made are: $4.2 \times 10^{20}$ erg/s (Sorokhtin, 1974; Sclater et al., 1981) and $4.3 \times 10^{20}$ erg/s (Gorodnitsky and Sorokhtin, 1981)

## 5.5 EARTH'S ENERGY BALANCE AND TECTONIC ACTIVITY

The integral format of Earth's energy balance is:

$$W_T = E_g + E_R + E_t - Q_G, \quad (5.22)$$

where $W_T$ is Earth's heat store; $E_g$is Earth's gravity differentiation energy; $E_R$ is radioactive element decay energy; $E_t$ is the tidal energy in solid Earth; $Q_G$ is total heat loss through Earth's surface. Main components of Eq. (5.22) have already been determined (see Figs. 5.2, 5.8, and 5.10). The primary and present-day Earth heat stores may be determined from Eq. (5.2) with heat capacities of the young and present-day Earth shown in Fig. 3.9. Density and temperature distributions shown in Figs. 2.13 and 2.17 are, respectively, $W_{4.6} = 8.38 \times 10^{37}$ and $W_{00} = 5.915 \times 10^{37}$ erg. We analyzed the temperature distribution at end Archaean taking into consideration the potential energy released in the core separation ($\Delta U_c = -8.08 \times 10^{37}$ erg) and the virial theorem stating that half of such energy (with the opposite sign) converts to heat. As a result we determined Earth's heat store value at the end of Archaean: $W_{2.6} = 14.69 \times 10^{37} + 4.04 \times 10^{37} = 18.73 \times 10^{37}$ erg. Thus, after the Archaean mantle overheating and the core separation, Earth began gradually cooling down. Its heat store declined over this time by $\Delta W_T = 2.81 \times 10^{37}$ erg (see Fig. 5.13, curve 3).

We determined individually and in total the value of main energy sources in Earth ($E_g + E_r + E_t$) and the nature of change of Earth's heat store $W_T$. Now it is simple to determine Earth's heat loss:

$$Q_G = E_g + E_R + E_t - W_T. \quad (5.22')$$

We can similarly determine total heat loss by the mantle $Q_m$. The difference will be equal to the continental crust heat loss $Q_{cr}$. It is associated with decay of the radioactive elements contained in it: $Q_G - Q_m = Q_{cr}$.

Thus, over the life of Earth the following amounts of energy were released: in the mantle, $16.95 \times 10^{37}$ erg of the Earth's matter gravity differentiation energy (together with the Earth's depths compression energy); about $3.11 \times 10^{37}$ erg of the radiogenic energy and approximately $2.24 \times 10^{37}$ erg of the tidal energy (not accounting for its dissipation in Earth's hydrosphere). The total is nearly $22.29 \times 10^{37}$ erg.

This heat would be sufficient for additional Earth overheating by almost 4400 °C. It did not happen, however, which means that most of the heat was lost by Earth with its heat radiation to outer space. The estimate, taking into account the total energy generation in the mantle and Earth's primary and current heat stores, determined that over Earth's life it lost about $10.77 \times 10^{37}$ erg of the depth (mantle) heat with its heat radiation. This very value describes the total energy of tectonomagmatic processes on Earth. To determine total Earth heat loss, the radiogenic energy released within the continental crust,

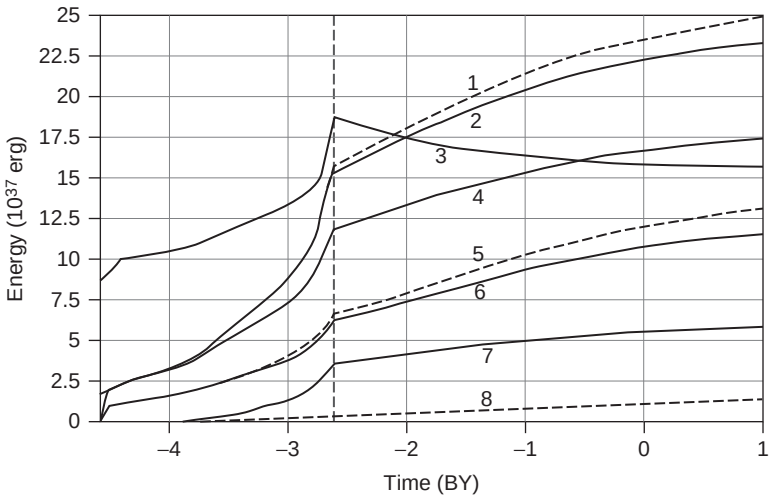


**FIGURE 5.13** Integral form of Earth's energy balance: 1, total energy $E_G$ released in Earth (not including the tidal energy dissipated in the seas and oceans); 2, energy $E_m$ released in Earth's mantle; 3, Earth's total heat store $W$; 4, heat component $E_mT$ of energy released in the mantle; 5, total Earth's heat loss $Q_G$; 6, heat loss of the mantle caused by the depth heat flow $Q_m$; 7, energy of Earth's additional compression $E_{com}$ due to the core separation; and 8, radiogenic energy $E_{rcr}$ dissipated in Earth's crust.

$E_{rcr} \approx 1.22 \times 10^{37}$ erg (curve 8 in Fig. 5.13) should be added to the mantle component. With this energy added, total Earth's heat loss by the present time reached approximately $10.77 \times 10^{37} + 1.22 \times 10^{37} = 11.99 \times 10^{37}$ erg.

By summing-up all data about the energy release rate as shown in Figs. 5.1, 5.7 and 5.9 we can find the total endogenous energy generation rate in Earth: curve 4 in Fig. 5.14.

Figure 5.14 shows that after the formation of the Earth–Moon system, energy within Earth was generated most rapidly only in Archaean and especially in Late Archaean. At that time, at the peak of the endogenous energy release its level was about 17 times the present-day level. Beginning in Proterozoic, the endogenous energy release rate was continuously declining. The decline will continue in the future until 1.5–2 BY from now and Earth will become a tectonically dead planet.

At the earliest stages of Earth's life (in Katarchaean), its energetics were clearly dominated by the tidal energy, and beginning in Archaean, only by the gravitational energy. The radiogenic energy, especially as it is dissipated within the mantle, contrary to common belief, had never defined Earth's energy regime. This is an important conclusion in theoretical geology and can no longer be disregarded.

Earth's heat balance in the differential format (which determines, e.g., the total rate of heat energy accumulation in the mantle)

$$\dot{E}_{mT} = \dot{E}_{gT} + \dot{E}_R + \dot{E}_t, \tag{5.23}$$

or the depth heat flow $\dot{Q}_G$ coming from the mantle

$$\dot{Q}_m = \dot{E}_{mT} - \dot{W}_T = \dot{E}_{mT} - \dot{W}_T, \tag{5.23'}$$

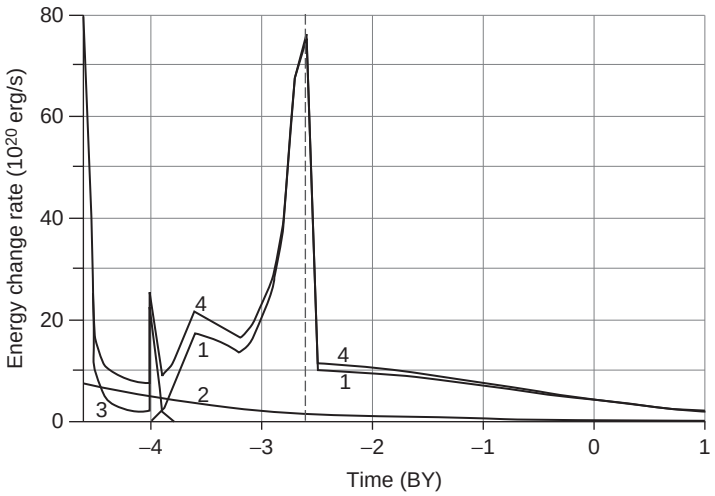


**FIGURE 5.14** Rate of endogenous energy release in the mantle: 1, Earth's gravity differentiation energy; 2, radiogenic energy; 3, lunar tide energy; 4, total energy. Vertical dashed line is the moment of the core formation.

where $\dot{E}_{mT}$, $\dot{E}_{gT}$, $\dot{E}_R$, and $\dot{E}_t$ are, respectively: the release rate of the total heat energy in the mantle, of the mantle gravity differentiation energy heat component, of the radiogenic, and tidal energy in the mantle; $\dot{Q}_m$ is depth heat flow coming from the mantle (see Fig. 5.15); $\dot{W}_m$ is the rate of change in heat content in the mantle (in its heat store).

The present-day depth heat flow is equal to the difference between the total Earth heat loss ($4.3 \times 10^{20}$ erg/s) and the rate of radiogenic energy generation in the continental crust ($0.91 \times 10^{20}$ erg/s), that is, $\dot{Q}_0 = 3.39 \times 10^{20}$ erg/s. The fraction of the change in Earth's heat store $\dot{W}_0$ is $\dot{W}_0 = -0.27 \times 10^{20}$ erg/s (i.e., $\dot{W}_0 < 0$). What it means is that after the Archaean upper mantle overheating (as mentioned above) Earth still continues its slow cool-down at a rate of close to 0.015 °C in a million years.

## 5.6 EARTH'S TECTONIC ACTIVITY

The above calculation under Eq. (5.23′) enables us to determine the tectonic activity of Earth expressed in units of the mantle heat flow $\dot{Q}_m$. Keep in mind that first, the area of the oceanic crust grew due to the expansion in Archaean of the Earth's matter differentiation belt from the low latitudes to the high ones, and then, during post-Archaean, it gradually shrank due to the growth in the continental area (see Fig. 7.4). Using this pattern, it is possible to estimate average specific heat flows piercing during the past geological epochs the oceanic crust ($\bar{q}_{occr}$) and the surface of ancient continents ($\bar{q}_{concr}$). The following diagram of Earth's tectonic activity (Fig. 5.16) was put together in view of such corrections.

As this figure shows, the general tectonic activity of Earth (curve 1) is a double-peaked curve with an overwhelming domination of the second activity hump. The Early Archaean maximum describes the zonal separation process of the metallic iron from the mantle's silicate matrix. A drastic activation during Late Archaean is caused by two reasons: (1) by

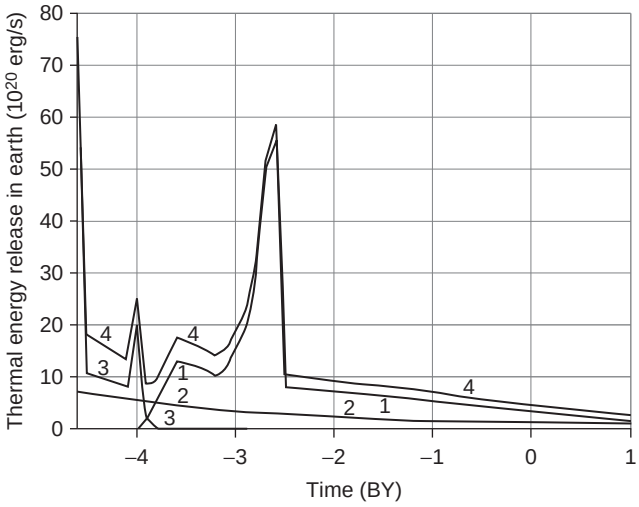


**FIGURE 5.15** Rate of heat energy release in the mantle: 1, heat component of Earth's gravity differentiation energy $\dot{E}_{gT}$; 2, radiogenic energy release $\dot{E}_R$; 3, tidal energy release $\dot{E}_t$; 4, total rate of the heat energy generation in Earth $\dot{Q}_G$.

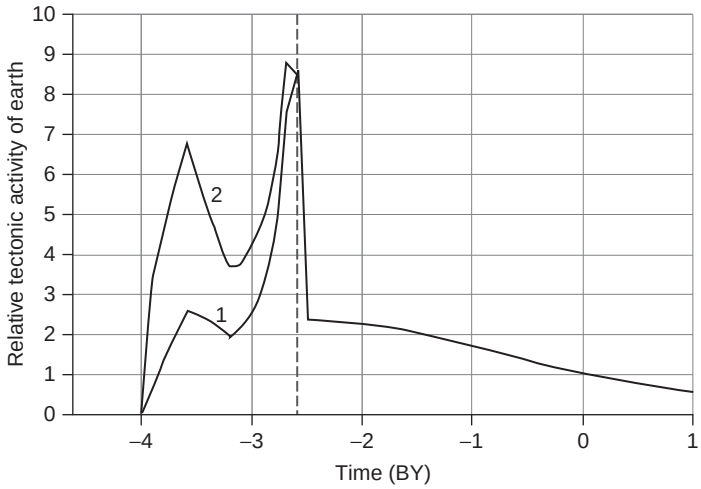


**FIGURE 5.16** Relative measure of Earth's tectonic activity or its normalized tectonic parameter (5.8): 1, Earth average and 2, Archaean (within a latitudinal ring over the Earth's matter differentiation zone).

switching on into the differentiation process (beside the metallic iron) of iron oxides and (2) by the beginning at the end Archaean of the core separation.

The tectonic activity on Earth's surface is described in this figure also by a double-humped curve (curve 2). But its parameters are different. The first maximum is much higher than the curve 1 maximum, whereas the second maximum is commensurate with the main maximum of the total Earth's tectonic activity. The explanation is not so much in the intensity of the

endogenous energy generation at the time as in a relatively small area of its exposure on the surface within the relatively narrow equatorial belt where this activity was manifested (see Fig. 4.3). Maximum intensity of the local tectonism in Early Archaean (about 3.6 BY ago) exceeded the current activity of our planet more than 6.5 times. And the average Earth activity at that time was just 2.5 times its current level. It was so because the area of the zonal differentiation ring belt of Earth's matter at that time was just 0.37% of Earth's surface at the level of the zonal differentiation front of Earth's matter. Because of that, Earth's local activity at that time was approximately $2.5/0.37 = 6.73$ times the current activity.

In Mid-Archaean, both the local and medium tectonic activities were significantly lowered over a slow-down in the differentiation rate of Earth's matter (as mentioned in Section 4.3). During Late Archaean, however, a new and most intense burst of tectonic activity occurred. Its amplitude was almost 8.5 times the present-day level (see Fig. 5.16). It was associated with the start of the core separation process 2.8 BY ago (see Fig. 4.1). Both bursts of Earth's tectonic activity in Archaean correlate well with changes in surface temperature of the upper mantle during episodes of its overheating in Archaean (see Fig. 4.5). It is convenient to quantitatively describe Earth's tectonic activity through the total rate of the endogenous energy generation in the mantle (see Fig. 5.17).

In Proterozoic and Phanerozoic, the gravity energy generation was occurring under a much more quiescent regime of barodiffusion differentiation of the mantle matter. For this reason, Earth's tectonic activity became more quiescent although it is necessary to remember that the Fig. 5.17 curve describes its averaged value, with the averaging scale on the duration order of the tectonic cycles (i.e., on the order of hundreds of millions of years). The real correlation of Earth's tectonic activity versus time is more complex although the amplitude of the tectonic cycles superimposed over the averaged curve is much lower than the main maximum at the time of about 2.6 BY ago (see Fig. 6.8). The store of the core matter in the mantle was being gradually exhausted so that the Proterozoic and Phanerozoic tectonic activities gradually declined. This trend will continue in the future.

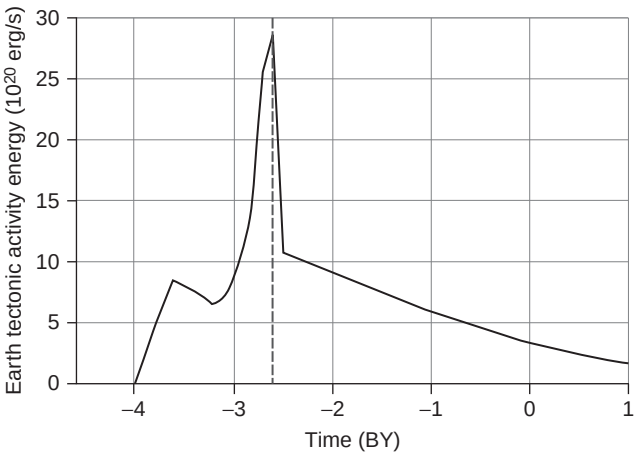


**FIGURE 5.17** Energy expression of Earth's tectonic activity (vertical dashed line denotes the core formation time).

Let us try to determine Earth's heat loss in Archaean, that is, before the tectonism began. Let us assume that during the completion period of Earth's formation process and profuse fallout of large planetesimals on its surface, any volume of Earth's near-surface layers underwent the melting stage (due to the planetesimal impacts). In this case:

$$\dot{Q} \approx \frac{\lambda T_m S_g}{\sqrt{\pi a (t + t_0)}}, \tag{5.24}$$

where $\lambda \approx 5 \times 10^{-3}$ cal/cm s deg is heat conductivity; $T_m \approx 1000$ °C is Earth's matter melting temperature at pressure $P = 0$; $S_g = 5.1 \times 10^{18}$ cm$^2$ is Earth's area; $a \approx 5 \times 10^{-3}$ cm$^2$/s thermometric conductivity factor; $t_0 \approx 10^7$ years $\approx 3.16 \times 10^{14}$ s is the time of Earth's formation closing stage during which its mass increased, for instance, from 97% to 100%.

Inserting these parameter values into Eq. (5.24) and remembering that 1 cal $\approx 4.19 \times 10^7$ erg, we come up with the heat flow in the beginning of Archaean of $\dot{Q}_{4.6} \approx 4.8 \times 10^{20}$ erg/s, whereas it declined to $0.6 \times 10^{20}$ erg/s by the end of that epoch.

Thus, average heat flows in Katarchaean were quite modest compared with the present-day one of $\dot{Q}_0 = 4.3 \times 10^{20}$ erg/s. By integrating Eq. (5.24), we determine that the total Earth heat loss in Archaean was exceptionally low and did not exceed $0.2 \times 10^{37}$ erg. Over the same time Earth's heat store increased from $8.38 \times 10^{37}$ to $9.98 \times 10^{37}$ erg, that is, by $1.6 \times 10^{37}$ erg.

Estimations of the energy release rate in Earth (see Fig. 5.14) and of total energy, accounting for changes in Earth's own heat store (Fig. 5.13), enable the evaluation of the past heat flows $\dot{Q}(t)$. As a first approximation, such flows turn out to have been in proportion with the intensity of the convective mass exchange. In general, the intensity of the convective mass exchange in the mantle (or, which is the same, Earth's tectonic activity) may be described by Eq. (5.23′).

It is known that the main portion of the total Earth heat loss was always happening through the oceanic crust (see Section 5.4). Over 4 BY, that is, during the time of Earth's geological evolution (minus heat loss in Katarchaean), approximately $10.77 \times 10^{37} - 1.6 \times 10^{37}$ erg $= 9.17 \times 10^{37}$ erg of the heat energy was lost through its surface. Of this, 90% was lost through the oceanic crust.

Taking into account the reviewed endogenous energy generation mechanisms and major heat loss by Earth, it is possible to determine the evolution of heat flows through the ocean floor. It turns out to be close to curve 2 in Fig. 5.16. A reminder: elevated heat flows through the ocean floor in Early Archaean were associated with a narrow equatorial belt where the young oceanic crust was then forming.

## 5.7 EVOLUTION OF AVERAGE TEMPERATURE IN THE CONVECTIVE MANTLE

As shown above, significant overheating of the upper convecting mantle existed in Archaean (Fig. 4.5). A reminder: the convecting mantle during Early and Middle Archaean encompassed only small part of Earth. Only by the end of Archaean, at the moment of the core origin, its mass significantly increased (Fig. 4.1). The calculations in Section 4.3 enable to determine the evolution of the convecting mantle average temperature in Archaean. The calculation results are shown in Fig. 5.18. As the aforementioned energy balance of our

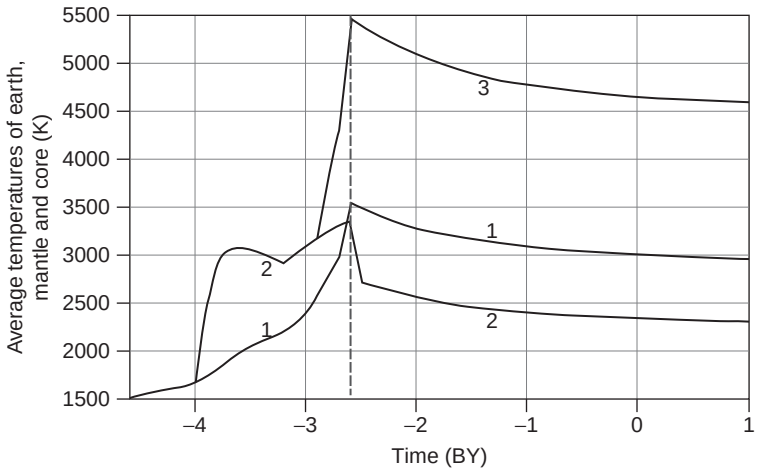


**FIGURE 5.18** Evolution of average Earth temperature (curve 1), mantle temperature (curve 2), and Earth core temperature (curve 3).

planet shows, in Proterozoic and Phanerozoic Earth gradually cooled down, and its energy store W declined (Fig. 5.13, curve 3). We can now determine based on Earth's heat store Earth's average temperature and that of the mantle. Earth's average temperature may be found from its mass $M_G$ and heat store $W_G$

$$T_G = \frac{W_G}{M_G c_{PG}}. \tag{5.25}$$

Here, Earth's heat store $W_G$ is given by curve 3 in Fig. 5.13, Earth's mass $M_G = 5.9772 \times 10^{27}$ g, its average heat capacity is assumed at $0.887 \times 10^7$ erg/g.

As a first approximation, the heat store of the mantle and core are:

$$W_m = W_G \frac{M_m}{M_G}, \tag{5.26}$$

$$W_C = W_G \frac{M_C}{M_G}, \tag{5.26'}$$

where $M_m$ and $M_C$ are, respectively, the mantle and core masses. Then average temperatures of these geospheres are:

$$T_m = \frac{W_G}{M_G c_{Pm}}, \tag{5.27}$$

$$T_C = \frac{W_G}{M_G c_{PC}}, \tag{5.27'}$$

where $W_G = 15.915 \times 10^{37}$ erg is the present-day Earth's heat store; $C_{PG} \approx 0.89 \times 10^7$; $C_{Pm} \approx 1.106 \times 10^7$; and $C_{PC} \approx 0.574 \times 10^7$ erg/g·deg are the assumed values of the average heat capacity for, respectively, the entire Earth, the mantle, and the core.

Utilizing Eqs. (5.25), (5.27), (5.27′) and the graph in Fig. 3.9, we may now approximately determine average temperatures of the present-day Earth (≈3000 K), of the mantle (≈2400 K), and the core (≈4600 K). The obtained estimates in comparison with the temperature distribution within the present-day Earth are included in Fig. 5.19. As it shows, the derived estimates of average temperatures match quite well the temperature distribution within the present-day Earth. What it means is that Earth's heat store values (curve 3 in Fig. 5.13) and the heat capacity of Earth's geospheres (Fig. 3.9) are both close to their actual values.

## 5.8 EMERGENCE OF EARTH'S MAGNETIC FIELD: POSSIBLE CAUSES

Endogenous energy sources also excite Earth's magnetic field. The capacity $\dot{E}_\mu$ of this field is relatively small. Different estimates range between $2\times10^{16}$ and $10^{19}$ erg/s (Parkinson, 1983). It is almost obvious today that the generation of the geomagnetic field is associated with convective processes going on within the liquid and electro-conductive matter of the external (liquid) Earth core. The main difficulty in developing a theory of the geomagnetic field is in that the Earth core is lacking in substantial energy sources capable of generating such a field. Indeed, neither the iron-oxide external nor the iron internal core should include radioactive elements as they are all lithophilic elements and migrate from the mantle only into the crust. It is supported by the geochemistry of iron–nickel meteorites which are, most likely, the fragments of lunar-size protoplanetary bodies destroyed sometime in the past. Such meteorites do not have even traces of radioactive elements but do include sometimes in noticeable concentrations the products of their decay (e.g., lead isotopes).

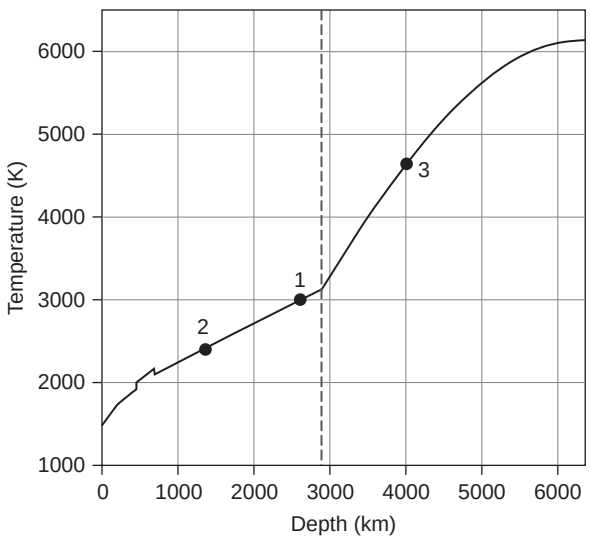


**FIGURE 5.19** Temperature distribution within Earth as compared with average temperatures in Earth's geospheres: dots 1, 2, and 3 are the average Earth, mantle, and core temperatures (the dots are the intersection points of the determined average temperatures with Earth's temperature distribution). The dashed line is the mantle/core boundary.

For this reason, the Earth core can now be heated only from its surface. Therefore, no convective flows may arise within it and the origin of the Earth's magnetic field is usually believed to be associated with such flows. From the viewpoint of the theory of Earth's global evolution we are proposing here, the possible cooling of the Earth core after its overheating at the Archaean–Proterozoic boundary could be a source of the geomagnetic field energy: about $1 \times 10^{37}$ erg of gravitational energy was then released over a short period deep within Earth. The rate of the heat energy release by the cooling-down core may be estimated from the following equation:

$$\dot{E}_c \approx \Delta\bar{T} \frac{M_c}{\Delta t} c_p e^{-\Delta t/\tau_c}, \tag{5.28}$$

where $\Delta\bar{T} \approx 400\ ^\circ\mathrm{C}$ is the difference between expected average temperatures of the young and present-day core (taking into account the adiabatic heating of the core matter due to its compression in Earth's central areas); $M_c \approx 1.5 \times 10^{27}$ g is average core mass over the time interval $\Delta t = 2.6$ BY; $c_p \approx 0.63 \times 10^7$ erg/g deg is average specific heat capacity of the core matter; $\tau_c \approx 8 \times 10^8$ years is average period of the convective megacycles (see Fig. 6.8). Inserting these parameter values into (5.28) we find that the heat energy release by the core due to its cooling may currently reach $1.8 \times 10^{18}$ erg/s. This is in sync with the aforementioned possible values of the geomagnetic field energy.

A second and more realistic mechanism of the geomagnetic field generation may be associated with the emergence on the core surface of stream flows of a mantle matter disintegrated into individual granules and crystals. These flows close by themselves the mantle convective flows thereby forming singular closed structures. They are always directed from the base of descending mantle flows to the centers of the ascending mantle flows (Fig. 4.10). The capacity of this process is determined by the topographic gradient of the lower mantle base (i.e., the top of the core) which reaches $\Delta h_c \approx 14$ km $= 1.4 \times 10^6$ cm (Fig. 2.10), by the decay rate of the mantle matter $\dot{m}_m \approx M_m/\tau_c \approx 1.6 \times 10^{11}$ g/s and by the gravity acceleration at the core surface $g_c \approx 10^3$ cm/s$^2$

$$\dot{E}_c \approx \frac{\Delta h_c g_c \dot{m}_m \Delta\rho_{cm}}{\rho_c}, \tag{5.29}$$

where $\Delta\rho_{cm} = \rho_c - \rho_m$; $\rho_c \approx 9.7$ g/cm$^3$ is the matter density at the surface of the external core; $\rho_m \approx 5.66$ g/cm$^3$ is the mantle matter density at the base of the lower mantle. Inserting these parameter values into (5.29) we come up with $\dot{E}_c \approx 9.3 \times 10^{19}$ erg/s.

The provided estimate shows that the gravity energy released on the surface of Earth core is about 50 times greater than possible energy of the core cool-down and much higher than the magnetic field energy $\dot{E}_c >> \dot{E}_\mu$. Therefore, the process of gravity differentiation of the Earth's matter, the most powerful source of endogenous energy on Earth, can at the same time feed Earth's magnetic field. This, in particular, can explain the changes in the magnetic field inversion frequency during the past geological epochs with varying tectonic activity.

As shown in Section 2.9, viscosity of the core matter is relatively low, $\eta \leq 0.4$ poise. Gans (1972) estimated that the upper core matter viscosity hardly exceeds $0.1 - 0.01$ poise. So, the viscosity is low, and the density gradient between the core matter and crystals and silicate grains suspended in it is great. Under this environment, the flows of the mantle matter that disintegrated into granules on the core surface may be very rapid and relatively narrow. As

topography of the core is very rugged, such flows must cause strong erosion of the mantle's lower surface (i.e., its base). As a result, the flows of the mixed disintegrated mantle and core matter on the core surface must fall apart into individual streams similar to the rivers flowing upside down, from the bottom up. If so, the velocity of such stream flows may reach meters per second.

At a speed so high, these stream flows would obviously be subjected to the Coriolis acceleration which would deflect them toward the equatorial plane. And the movement of the core matter captured by the streams would result in the emergence of powerful electric currents and magnetic fields.

It is quite possible that the geomagnetic field of our planet was generated by such stream flows on the surface of the core. The streams closed by themselves the convection mass exchange in the mantle. At least this connection between the geomagnetic field and the mantle convective flows can explain the identified correlation between the field remagnetizing frequency and Earth's evolution tectonic periods.

Indeed, the stream flows of electro-conductive core matter should flow away in different directions from the roots of descending mantle flows and should generate magnetic fields of varying polarity. Usually, however, there is no complete symmetry in such fields. For this reason, under the action of the Lorentz forces the field of one direction would always prevail over the field of a different direction, creating the corresponding magnetic field polarity on the Earth's surface.

The Coriolis accelerations emerging on the surface of the core would make the stream flows to meander. Closing of such meanders may result in the direction change of dominating flows, therefore in the geomagnetic field polarity change.

The provided schematic descriptions of the possible nature of Earth's magnetic field are, of course, very tentative. They require a more thorough work and quantitative solutions. Nevertheless, this mechanism enables the merging of the energy model of Earth's evolution with the very fact of geomagnetic field occurrence.

CHAPTER

# 6

# Earth's Tectonic Activity and its Nature

## 6.1 POSSIBLE CAUSES OF EARTH'S TECTONIC ACTIVITY

After the demise of the contraction concept of Earth's evolution (see Chapter 1), it was replaced by a number of purely conceptual tectonic hypotheses which only have historic value. Some of them, however, despite clear contradictions with geological data and the laws of physics, turned out to be surprisingly durable with some geologists and were even contraposed to the modern theory of lithospheric plate tectonics. It is especially true for the Earth's crust basification, expanding, pulsating, and hydride Earth hypotheses.

These hypotheses were criticized in many publications, including those of Sorokhtin (1985b) and Sorokhtin and Ushakov (1991). We will not dwell here on their analysis and will just note certain drawbacks and, sometimes, outright blunders of such hypotheses.

For instance, no versions of the expanding or "pulsating" Earth describe and even more so quantitatively estimate physically acceptable mechanisms capable of changing Earth volume to the assumed size. And most of the suggested mechanisms clearly contradict the laws of the modern physics or experimental data about the matter behavior under high pressure and temperature (such as the hypothesis of a hybrid Earth) and cannot for this reason be accepted as serious hypotheses. In particular, many versions of the hypothesis of expanding Earth use the assumption of changes in the gravity constant or self-growth in the mass of celestial bodies (due ostensibly to the generation of the mass from vacuum). They do not take into account, however, that the same factors must have been active not only in Earth but also in the Sun. But any noticeable changes in defining Sun parameters unavoidably would lead to catastrophic results for the Sun and Earth, up to the Sun exploding and formation in its place of a "white dwarf" or even a black hole.

Sometimes purely exogenous actions are used to explain Earth tectonics such as the Solar system's revolution about the galactic center of mass or nonuniformity of Earth's own revolution. Speaking about the first mechanism we must remember that Earth and likewise the other celestial bodies move in space only on the equipotential surfaces of the gravity

*Developments in Earth and Environmental Sciences*, Volume 10
DOI: 10.1016/S1571-9197(11)10006-3

field. Deformation forces from such fields on Earth may arise only if noticeable gradients of the exciting field exist, which generates tidal forces. The action of tidal forces on Earth was reviewed in Chapters 3 and 4. It was shown that currently their effect from the Moon's side is disappearingly small, not exceeding 1%. Nevertheless, the gravity acceleration gradient from the lunar tides ($1.7 \times 10^{-13}\,s^{-2}$) is much higher than the solar gradient of $7.87 \times 10^{-14}$ and greater by many orders of magnitude than the gradients generated by the galactic gravity field $1.5 \times 10^{-30}\,s^{-2}$. Thus, the gravity gradient of the lunar tides is greater than the gradient generated by the galactic gravity field by the factor of about $10^{17}$, so there may be no effect from the "galactic year" on Earth tectonics.

The same goes with the effect of a nonuniformity in Earth's own revolution on its tectonic activity. The total Earth revolution energy is currently nearly $2.1 \times 10^{36}$ erg. In the time of the Moon formation 4.6 BY ago, this energy reached $3.4 \times 10^{37}$ erg. It shows the following. During Earth life about $3.19 \times 10^{37}$ erg of its revolution energy could have been released this way. It includes $2.24 \times 10^{37}$ erg released in its depths. Over the time of geological evolution (i.e., after 4 BY ago) only $0.2 \times 10^{37}$ ergs were released (all this energy is taken into account in the aforementioned energy balance as the energy of Earth–Moon tidal interaction, see Chapter 5).

The other additional portion, $0.95 \times 10^{37}$ erg, must have been released in the hydrosphere. A reminder: over the same period of time approximately $23.5 \times 10^{37}$ erg of heat energy was released within Earth.

As for the nonuniformity of Earth revolution caused by the tectonic movements and by fluctuations of the Sun–Earth connections, the capacity of these energy actions does not exceed $1.6 \times 10^{17}$ erg/s. This is lower by 3.5 orders of magnitude than the total of all endogenous energy sources feeding Earth's tectonic activity.

We could similarly criticize some other conceptual hypotheses, such as the Earth's crust oceanization (basification) hypothesis which clearly breaks the Archimedes law. There probably is no need to do it now as over the recent years such hypotheses moved from the domain of science to a shelf of history.

Thus, all exogenous factors of Earth's tectonic activity but the lunar tides may be disregarded. The lunar tides, as shown in Chapter 3 (Sections 5.3 and 5.5) made noticeable contribution into the general Earth heating only in Katarchaean (i.e., at the pre-geological stage of the planet evolution) and Early Archaean. Thereby they served as a trigger mechanism which started Earth's tectonic evolution. During all other time the lunar tide contribution into Earth tectonics was modest. Therefore, beginning 3.8 BY ago Earth's tectonic activity was fed only by endogenous energy.

Stating a minor effect of the external factors on the planet's tectonic activity we should not forget a large, often definitive influence of the solar radiation, that is, as a purely exogenous factor, on the general geological development of Earth. This is natural as the total flow of the solar energy on the surface of Earth (close to $1.75 \times 10^{24}$ erg/s) is about 4000 times the capacity of the depth heat flow of Earth proper ($4.3 \times 10^{20}$ erg/s). The upper geospheres of Earth (the atmosphere, hydrosphere, Earth's crust, and even the lithosphere) are in a constant mass exchange with one another.

Although these external geospheres formed due to endogenous processes of degassing and differentiation of Earth's depths, the existence of liquid water, comfortable climatic conditions, highly organized life, rock weathering processes, sedimentogenesis, the

formation of evaporites, combustible, and other commercial deposits—all these are associated exclusively with the solar radiation.

The modern tectonic theory (tectonics of the lithospheric plates), substantiated scientifically and tied-in with practically all geological data, as mentioned in Chapter 1, was introduced only in the 1960s. The very nature of the global processes controlling Earth's tectonic activity became better known even later, in mid-1970s (Sorokhtin, 1974; Geodynamics, 1979). At present, these processes are theoretically studied although not always really in-depth. The theoretical conclusions well match geological data (see Conclusions), there are no blatant contradictions, and the theory is broadly checked for its compliance with the modern physics. All these say that a modern, strictly scientific physical theory of Earth's evolution was born in geology.

It was mentioned in the Introduction that Earth's evolution and its tectonic activities must be controlled by most powerful endogenous processes which lower to the maximum extent Earth's potential (internal) energy. Such processes can only include the chemico-density differentiation of Earth matter, decay of radioactive elements and the lunar tides. The contribution from the lunar tides was noticeable only at the very initial stages of Earth evolution. At the geological evolutionary stage, beginning approximately 4.0–3.8 BY ago, the chemico-density (gravity) differentiation of Earth's matter became the most important process which resulted in Earth stratification into a high-density iron-oxide core and the residual silicate mantle.

This process was accompanied by the emergence in the mantle of large-scale convective movements. They engulfed the entire mantle (both the lower and upper) and formed convection cells whose sizes were commensurate with the size of the mantle itself. This explains the very fact of the continental drift and the existence of large lithospheric plates whose size may often reach many thousands of kilometers.

The lithospheric plate motions cause a set of geological processes and phenomena which we usually associate the notion of Earth's tectonic activity (such as earthquakes, volcanism, mountain building, etc.). Average rate of lithospheric plates' relative movements may serve as a demonstrative measure of Earth's tectonic activity (currently it is close to 4.5–5 cm/year). However, as the energy of any dynamic (tectonic) processes in Earth's depths is eventually converted into heat, the most natural measure of Earth's tectonic activity is the depth heat flow coming from the mantle. Its total present-day value reaches $3.39 \times 10^{20}$ erg/s (see Fig. 5.17).

As shown in Chapter 5, the most powerful endogenous process controlling Earth's tectonic activity is the process of chemico-density differentiation. It results in the separation of the Earth core and generates convective motions in the mantle matter. It appears that the first scientist who understood the importance of the core separation in Earth's tectonic activity was Runcorn (1962, 1965). Later, the issue was studied by Artyushkov (1968, 1970), Sorokhtin (1972, 1974, 2007), Monin (1977, 1999), Monin and Sorokhtin (1981, 1982), Sorokhtin and Ushakov (1991, 1993, 2002), and so on.

Presently, there is numerous evidence that tectonic processes in Earth's lithospheric shell are directly associated with the matter convection in the mantle's depths. The main evidence is believed to be: continental drift; the young age of the ocean floor; a global system of the rift zones (where the mantle matter ascends to the surface and the young oceanic crust is forming); the presence of global compression belts underneath which the oceanic crust is sinking into the mantle. There are other facts supporting this conclusion. Some of them will be reviewed further in this book.

The chemico-density differentiation of Earth's matter plays a leading role in the nature of the emergence of the mantle convection. The heat component of the convection should also be remembered. Its contribution depends both on the matter heating due to the convection energy dissipation within the viscous mantle and on the additional heating of the mantle matter by radioactive decay and by the tidal disturbances.

Energy estimates in Chapter 5 indicate that the radiogenic heat contribution into the convective mass rotation of the mantle matter is presently no more that 10%, and the tidal deformations contribute less than 1%. The main portion of the endogenous energy feeding Earth's tectonic activity (almost 90%) is coming from the Earth's matter differentiation process.

Considering these estimates, the nature of tectonic (or, more accurately, tectonomagmatic) activity of Earth must be associated not with just gravity but with gravity-heat convection. Further down we will be using the term "chemico-density convection" in an understanding that density irregularities in the mantle occur not only due to the changes in chemical composition but also due to its temperature irregularities.

## 6.2 POSSIBLE MECHANISMS OF LITHOSPHERIC PLATE MOVEMENT

We now review the motivating forces arising within the lithospheric shell proper. Disregarding the side pressure from the adjacent lithospheric plates, two major factors are usually identified which are capable of causing the plate motions relative to one another and to the mantle.

A first one is sliding of the oceanic plates from the slopes of asthenospheric lenses positioned underneath the mid-oceanic ridges (Fig. 6.1). A second one is associated with sinking of the cold, therefore heavier oceanic plates into the hot mantle through the subduction zones. The lithospheric edge sinking into the mantle as if pulls behind it the major, "buoyant" portion of the plate still remaining on the Earth surface (see Fig. 6.3).

The lithospheric plate sliding down from the asthenospheric lens may abut the adjacent plate, push it and compress its peripheral areas. The compression $\Delta p$ generated by the oceanic plate at the expense of its sliding from the asthenospheric lens underneath the mid-oceanic ridge in the absence of friction at the plate's base may be estimated from the condition of hydrostatic equilibrium. In this case the compression acting on the plate's base, aged about 100 MMY, reaches approximately 800 kg/cm$^2$, that is, it approaches the limit of the long-term rock shear strength of about 1 ton/cm$^2$.

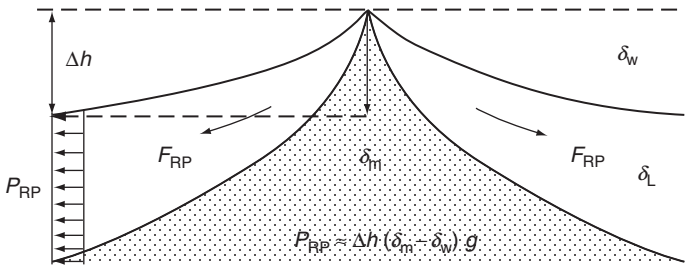


**FIGURE 6.1** Mechanism of oceanic lithospheric plate sliding from hot mantle uplift areas underneath the mid-oceanic ranges.

This excess pressure may be the reason for a somewhat elevated seismicity of the passive Atlantic oceanic and continental margins. Probably, this phenomenon manifests itself in particular in the Northern Atlantic. In that region, under the stress from the mantle flow underneath it, the oceanic plates are uplifted 2–2.5 km above their average elevation, and in the Iceland area the ocean floor rose even above the water surface. It creates the additional pressure of about 200–400 kg/cm$^2$. Thus, the composite pressure on the mid-oceanic ridge flanks in the Northern Atlantic may exceed the long-term strength of the lithospheric rocks. It appears that such was the nature of the known Lisbon quakes in 1531 and 1755 in Portugal and some quakes on the East Coast of the United States and on the western shores of Northern Europe.

The forces that suck-in lithospheric plates into the mantle may be substantially greater. To estimate them, it is necessary to take into account the existence in the mantle of phase transitions in the mineral associations of its matter (Fig. 6.2). The restructuring in such mantle associations occurs under influence from high pressure and temperature. It happens with the pressure increase due to the restructuring in the crystalline structure of the minerals into higher density modifications. Such restructuring in the crystalline structure of the

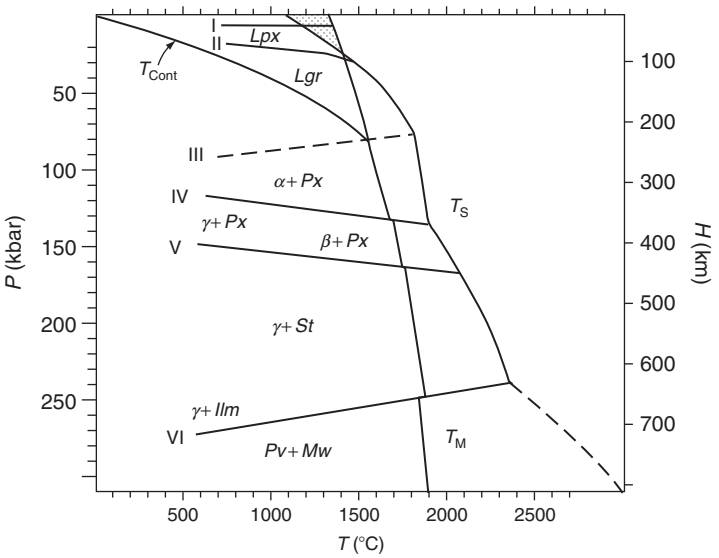


**FIGURE 6.2** Temperature distributions in the mantle and phase transitions in the mantle matter: $T_S$ is mantle matter solidus temperature (based in particular on the data by Green and Ringwood, 1967a,b and Takahashi, 1986); $T_M$ is adiabatic temperature of the convecting mantle (Sorokhtin, 2001); $T_{cont}$ is the continental geotherm under Archaean cratons (Sorokhtin and Ushakov, 1996); shaded is the area of existence of juvenile melts in the mantle. Exothermal phase transitions: I, transition from plagioclase lherzolites to pyroxene lherzolites (*Lpx*); II, transition from pyroxene lherzolites to garnet lherzolites (*Lgr*); IV, transition from olivines (α) to spinel structures (γ and β); V, transition from silica to the stishovite structure (*St*) and pyroxenes to the ilmenite structure (*Ilm*). Endothermic transitions: III, transition from the rigid polycrystalline matter to its plastic state proposed by us (see Section 2.8 and Fig. 2.18); VI, pyroxene transition to the perovskite (*Pv*) and magnesiowustite structure (*Mw*). Phase transitions I and II are based on the data by Green and Ringwood, 1967a,b, generalized transitions IV, V, and VI, based on the data by Kuskov and Fabrichnaya (1990).

mantle's mineral associations can occur with the heat release or consumption. In the former case, the transition is exothermal, the position of its boundary on the pressure/temperature plane has a positive gradient (phase transitions I, II, IV, and V in Fig. 6.2). In the latter case, the transition is endothermic, with a negative pressure gradient (phase transitions III and VI in the same figure).

Let us assume that the oceanic lithosphere sunk into the mantle through the subduction zone to some depth $h$ (Fig. 6.3). As a result, the negative Archimedes force will arise due to a higher density of its cold rocks compared to a hot mantle matter.

In the absence of the friction, this sucking-in force would create an extension stress in the near-surface lithospheric cross section. For instance, if the sinking plate descended to a depth of 400 km, the extension stress in the oceanic lithosphere in front of the deep trough, depending on the sinking angle, may reach 2–3 kbar. It needs to be taken into account that the descent of a cold oceanic lithosphere to the level of the exothermal phase transition in the hot mantle will result in an increase of its density, therefore, in strengthening of the plate sucking-in into the mantle. As an example, the IVth phase boundary at a depth of 400 km corresponds to the olivine transition under high pressure from the rhombic syngony (α-phase) to the spinel modification (β-phase), and is accompanied by the mineral density increase by approximately 8% (Ringwood, 1975a,b).

The sinking plate temperature at the depth of this phase transition (about 400 km) is about 500 °C lower than the surrounding hot mantle. Because of this, the discussed exothermal polymorph transition of its matter and a corresponding plate "weighing" will occur at a somewhat shallower depth of approximately 380 km (see Fig. 6.2). Therefore, additional pressure of about 0.2 kbar will arise at these depths and will strengthen the lithospheric plate sucking-in into the mantle. A similar process will be observed also at the intersection by the sinking plate of phase boundary V at a depth of close to 470 km, and pressure will again increase by the same amount.

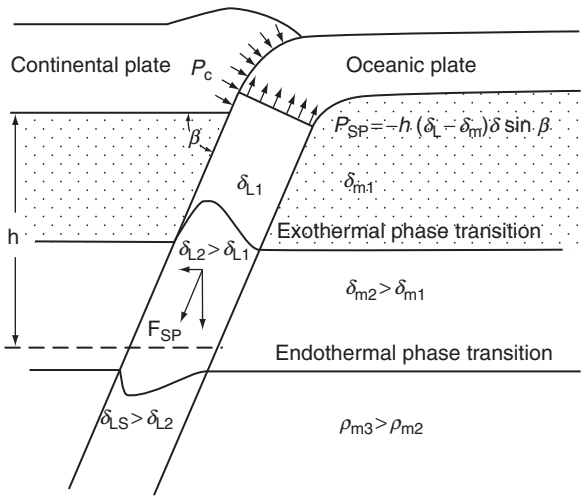


**FIGURE 6.3** Sucking-in of the oceanic lithosphere into the mantle through subduction zones.

Contrary to that, when the plate intersects an endothermic boundary at a depth of 670 km its pressure will decline by about 0.2 kbar. However, at this depth the total excess pressure of the sinking plate is equal to approximately 5–6 kbar. So, albeit the endothermic phase transition boundary at 670 km weakens the sucking-in gravity force of the oceanic lithospheric plate, it cannot prevent its subsidence into the lower mantle depths. Similarly, exothermal phase transitions in the mantle matter will facilitate the ascent of hotter mantle flows, and the endothermic ones, will somewhat slow down the ascent but not block it.

We now estimate the ascending convection flow heating compared with its descending branch. We assume that under the equilibrium conditions heat energy excess of the ascending flow is being almost entirely radiated by the oceanic plates during the time of their motion from rift zone to subduction zones, that is, during their average life time $\tau \approx 120$ MMY or $3.8 \times 10^{15}$ s. As determined in Chapter 5 (see Eq. 5.20), average present-day mantle depth heat flow through the ocean floor is equal to $\dot{Q}_m \approx 3.09 \times 10^{20}$ erg/s. Then average temperature gradient between the ascending convection flow and the surrounding matter will be approximately:

$$\Delta T \approx 2\frac{\dot{Q}_m \tau_m}{M_m (c_p)_m}, \tag{6.1}$$

where $M_m \approx 4 \times 10^{27}$ g is the mass of the present-day mantle, $(c_p)_m \approx 1.11 \times 10^7$ erg/g deg is average heat capacity of the convecting mantle. The result is $\Delta T \approx 52$ °C.

In this case, for instance, the transition boundary of the olivine α-phase to the β-phase (boundary IV in Fig. 6.2) descends within the ascending flow by about 2.5 km. Additional lift will emerge in the flow with excess pressure on the order of 0.07 kbar. Opposite to it, the endothermic phase transition boundary at 670 km (boundary VI in Fig. 6.2) will rise by about the same amount. That will result in a blocking pressure of about 0.1 kbar and some slowing-down of the ascending flow.

The difference in average mantle matter density before and after its differentiation on the core surface (i.e., within the descending and ascending flows) will be approximately 0.01–0.02 g/cm$^3$.The ascending mantle flows form on the core surface (at nearly 3000 km). Their lift is about 1.0–1.5 kbar and is much higher than the "blocking" action of the endothermic boundary at 670 km. For this reason, the global convection remains unified for the upper and lower mantle although the "blocking" action of such boundary may somewhat complicate the convection and result in its pulsating functioning.

Based on the quoted estimates of the forces sucking-in oceanic plates into the mantle Forsyth and Uyeda (1975) suggested that the observed rates of the lithospheric plate movements depend on the length of the encircling subduction zones. Indeed, the purely oceanic and relatively thin (60–80 km) plates with the relatively long subduction zones turned out to be "fast" plates. Under the same classification, almost all continental plates of a large thickness (up to 250 km) and their attached oceanic plates turn out to be "slow." It was also found that the larger the continental plate's area, the slower its drift rate. It may indicate that the thick continental plates, like grounded icebergs, dip their roots into the mantle's mesosphere, and the horizontal components of the mantle flows are small or are counterbalanced over a large area of the major continents.

In substance, it is still the same heat convection moved not by the cool matter heating from beneath but by the hot matter cooling from above. As we can see, the gravity instability of the oceanic lithospheric plates may initiate their movement and generate the mantle convection. An illustration may come from observations of cooled-down lava crust on the surface of the melted lava lake in the Kilauea volcano in Hawaii. They were conducted over a century ago by reverend Fisher (mentioned in Section 2.1). He observed those cooled-down and heavier crusts, like micro-lithospheric plates, slide down from the surface of the fiery melted lava and form structures similar to the mid-oceanic ridges on the one side and a semblance of the subduction zones on the other where the cooled-down crusts are sinking again into the incandescent lava and are completely melting in it. Based on his observations, Fisher (1889) came to a far-reaching conclusion about the nature of Earth's tectonic activity. These long-forgotten observations were repeated in about 80 years by Duffield (1972) who compared the lava crust motion with the then discovered movements of the lithospheric plates.

In actuality, however, both the oceanic lithosphere compression on contact with a passive continental margin and the lithosphere extension stress in front of a subduction zone may be very different from the simple estimates. The reason is the interaction between the moving plates with the other plates and with the mantle matter. As under this plate movement model, the plates are moving relative to the stable mantle, forces of viscous friction with the mantle matter must occur, and the opposing tangential braking stresses. Plate friction in the subduction zones and in the active portions of the transform faults is adding to this. As a result, the plate movement is substantially slowed down and the corresponding forces sucking-in the plates into the mantle are substantially weakened. The forces of viscous breaking increase with the increase in the plate movement rate. For this reason, the plates move at approximately constant rate of a few centimeters per year. Under a stationary scenario, the sum of the moving forces is totally counterbalanced by the sum of the breaking forces.

Let us now review the nature of the mantle convection in a broader sense and try to elucidate the issue of whether the described oceanic lithospheric plate "self-motion" mechanism is sufficient to initiate the convection. Keep in mind that this lithospheric plate motion mechanism could operate only beginning 2.6 BY ago. In Archaean, as it is now on Venus, subduction zones most likely did not exist. Their functions were performed by the basalt sheet pile-up zones over the continental shield edges (see Fig. 7.5).

For the described convection to exist long-term, as in any other case of the heat convection, the mantle matter must be supplied with the energy which is no less that the convection-associated heat loss. The intensity of the mantle convective mass exchange, and in our case the average velocities of the oceanic plate movements (i.e., average intensity of Earth's tectonic activity) will apparently be totally controlled by the rate of energy generation in the mantle. It is associated with a strong exponential correlation of the mantle matter viscosity with temperature, therefore with energy supply to this matter. If heat generation rate in the mantle declines, its viscosity will increase. Correspondingly, viscous friction forces will increase and slow down the plate movement under the described mechanism. Vice versa, if additional energy is supplied, the mantle viscosity and friction forces will decrease and the plate "self-motion" rate will increase.

This is the reason why Earth's tectonic activity within the framework of the proposed plate motion model is rigidly defined by the heat energy generation within the mantle, that

is, is actually defined by the heat flow through the ocean floor. As shown previously, the main contribution to the depth heat flow comes from the main energy process on Earth, the Earth's matter chemico-density differentiation into a high-density iron-oxide core and the residual silicate mantle. Therefore, the mantle heat convection must also be defined mostly by the same process of the core formation.

At present, approximately $7.6 \times 10^{17}$ g/year or nearly 230 $km^3$/year of cooled-down oceanic lithospheric plate rocks annually sink into the mantle through the subduction zones. We showed in Section 5.4 that the major endogenous heat loss occurs and always occurred through the oceanic crust in the process of oceanic plate formation. We also showed in Chapter 5 that Earth's tectonic evolution under the laws of the lithospheric plate tectonics began only in Early Proterozoic, after the Earth core separation 2.6 BY ago (as we indicated, in Archaean there could not have been the lithospheric "self-motion" mechanism). Total loss of heat energy through this mechanism over the last 2.6 BY was close to $4.5 \times 10^{37}$ erg (see Section 5.5). Presently, around $3.09 \times 10^{20}$ erg/s (see Section 5.4) or approximately $9.7 \times 10^{27}$ erg/year of the heat energy is lost through the ocean floor.

The oceanic lithospheric plates form due to crystallization and cooling-down of the mantle matter. Their average temperature changes little in the process. Thus, it may be accepted as a first approximation that the quoted heat loss is proportionate with the mass of the lithospheric plates that formed and sunk into the mantle. Average oceanic lithospheric plate density is about 3.3 $g/cm^3$. Thus, nearly $1.25 \times 10^{12}$ $km^3$ or $4.13 \times 10^{27}$ g of the lithospheric plates sunk into the mantle over the last 2.6 BY. The mass of the present-day convecting mantle without the continental crust is approximately $4 \times 10^{27}$ g. Therefore, over the period when the lithospheric plate tectonics mechanism was in operation (2.6 BY) the lithospheric plate mass sunk into the mantle was somewhat greater than the mass of the mantle itself. It shows that under the oceanic plate "self-motion" mechanism over the same time period the entire mantle matter must have at least once turned around in the convection cycle. It follows from this that the reviewed lithospheric plate "self-motion" mechanisms could have indeed generated a large-scale convection with a relatively minor mass exchange in the mantle.

Later we will show that about six convection cycles initiated by the chemico-density convection indeed existed after Archaean. Therefore, the Earth convection chemico-density differentiation mechanism is approximately six times greater in its intensity than the reviewed heat convection mechanism.

## 6.3 NATURE OF LARGE-SCALE MANTLE CONVECTION

We now review physical mechanisms capable of inciting convective motions of the mantle matter. Most geophysicists traditionally prefer only the classical format of the heat convection. It is believed that it is fed by the energy of radioactive decay or by gradual Earth cooling. Among the early publications on the subject are the already mentioned Fisher (1889) who believed that the subcrustal matter convection was caused by the general cooling of Earth, and a publication by Holmes (1928) who also believed that the heat convection causing the continental drift may be generated by radioactive element decay.

A strict solution of the velocity field for the convective movements in the mantle matter may be arrived to only by way of the joint solution of the Navier–Stokes equation for compressible liquids and the continuity equation. The boundary conditions must be the real mantle structure (in consideration of the phase transitions) and the mantle matter equations of state. It is quite difficult to meet all these conditions. Besides, from the start not all patterns in Earth structure and evolution were known with sufficient accuracy. That is why the earlier attempts in the heat convection studies (such as in a fundamental publication by Chandrasekhar (1961) and some others) usually found perhaps mathematically correct solutions but for very crude Earth models. Such models could be based on a constant viscosity or the viscosity as a monotonous function of the radius, or the models wherein the mantle was heated up by the core.

The results were cumbersome solutions only barely reflecting the nature of the real phenomena.

Heat convection as applied to the mechanism of the lithospheric plate tectonics was studied by Richter (1973), McKenzie and Richter (1976), Turcotte and Schubert (1985), Trubitsin and Rykov (2000), and Trubitsin et al. (1994).

Conditions for the emergence of heat convection in the mantle are conventionally determined using the Rayleigh criterion (Rayleigh number)

$$R_a = \frac{\rho H^3 \Delta T \alpha g}{a\eta} \tag{6.2}$$

where $\rho$ is mantle density; $H$ is the thickness of the mantle layer; $\Delta T$ is super-adiabatic temperature gradient in the layer; $\alpha$ is the volume expansion factor of the mantle matter; $g$ is gravity acceleration; $a$ is thermometric conductivity factor; and $\eta$ is the mantle matter dynamic viscosity. For a spherical layer, the critical Rayleigh criterion value at which heat convection can start is about 2000 (Zharkov and Trubitsin, 1980). The current belief is that the effective mantle viscosity is $10^{23}$–$10^{24}$ poise (Ranelli and Fischer, 1984), so the temperature gradient of 1–10 °C is sufficient to initiate through-going heat convection. With such gradient only an exceptionally sluggish convection would occur. However, actual values of the super-adiabatic temperature gradients may well reach a few tens of degrees.

It shows that heat convection in its classical meaning (i.e., due to the mantle matter heating from underneath of from within the mantle itself) may indeed arise in the mantle. The only problem is sufficient heat sources. The radiogenic elements are insufficient for the purpose. The only sufficient energy source is the chemico-density differentiation of the mantle matter. Besides, this process not only generates heat in the mantle but also creates variability in its body, and this variability substantially exceeds the effect of heat expansion of the matter. That is why, to model a more realistic environment, it is necessary to involve not just heat convection or purely chemico-density convection in the mantle but their combination in form of the chemico-heat density convection.

The chemico-density convection emergence condition may be derived analogous to the Rayleigh criterion for heat convection. The dimensionless Rayleigh number (6.2) is the ratio of two factors: of the lift arising at heat expansion of the matter and the factor resisting the convection and describing the dissipation rate of heat variabilities in the variable medium and its resistance to shear deformations. In view of this, we may replace the product $\Delta T \cdot \alpha$

in Eq. (6.2) by its equivalent ratio $\delta\rho/\rho$. Here, $\delta\rho$ is average density gradient emerging due to a change in the mantle matter chemical composition after its differentiation on the core surface (see Eq. (4.21)). We will extend the analogy between the diffusion equation (which determines the dissipation rate of the chemical composition variability) and the heat-conductivity equation (which determines the rate of temperature equalizing in the medium): we will replace the thermal conductivity factor $a$ in the denominator of Eq. (6.2) by the diffusion factor $D$. Then the modified Rayleigh criterion (which determines the development of chemico-density convection in the mantle; Sorokhtin, 1974) may be reformatted as follows:

$$R_g = \frac{\delta\rho H^3 g}{D\cdot\eta}. \tag{6.2'}$$

Most uncertain in Eq. (6.2) is the product $D\cdot\eta$. To estimate it, we will use the diffusion viscosity theory (Zharkov, 1983) under which the crystalline matter viscosity and the diffusion factor are related as follows:

$$\eta = A\frac{kT}{Dd}\left(\frac{l}{d}\right)^2 \tag{6.3}$$

where $A$ is a constant equal approximately 0.03; $k = 1.38\times10^{-16}$ erg/deg is the Boltzmann constant; $T \approx 2500$ K is average mantle temperature; $l \approx 0.1$ cm is the characteristic size of the mantle matter crystals; $d \approx 3\times10^{-8}$ cm is the characteristic parameter of the crystalline grid cell in the mantle matter. In this case $\eta\cdot D \approx 3.8\times10^6$ dyne.

By inserting the found $\eta\cdot D$ value into Eq. (6.2') and assuming, according to the (4.21) definition that $\delta\rho \approx 0.02$ g/cm$^3$, $g \approx 10^3$ cm/s$^2$, $H \approx 2.9\times10^8$ cm, we find that the modified Rayleigh number has values of about $1.3\times10^{20}$. That is many orders of magnitude above its critical value of $2\times10^3$ and may be considered infinite.

This large modified Rayleigh number does not mean at all a greater intensity of convection. It only shows that the intensity of chemico-density convection is totally defined by the medium viscosity $\eta$ and density gradients $\delta\rho$ of its chemical variations and is completely independent of the diffusion process of these density variabilities. Thus, at given $\eta$ and $\delta\rho$, chemico-density convection within the mantle will always be developing at a maximum possible rate. It may be very sluggish, however, if the mantle viscosity $\eta$ is high enough and the density gradients $\delta\rho$, generated on the core surface, are small. In the natural conditions, the rate of chemico-density convection must self-regulate so that the rate in lowering of Earth potential energy is at its maximum and the energy spent to overcome the viscous friction forces in the medium is at its minimum. And the convection structure organizes itself so that both these conditions are satisfied to a greatest extent.

If the matter reacts to slow deformations like a viscous liquid, an important conclusion follows from the above dissertations: almost any changes in the mantle matter chemical composition arising during its differentiation on the core's surface will unavoidably result in the emergence of convective movements in the mantle. It is true even when these differentiation-caused density fluctuations barely disturb gravitational stability of the mantle. The evolution rate of such process will be fully determined by the mantle matter density gradients and its viscosity.

The intensity of the mantle stirring changed in time approximately closely related to Earth tectonomagmatic activity (see Fig. 5.17). However, two periods of elevated convective and tectonomagmatic activity are identified on the Earth surface in Archaean (see Fig. 5.16, curve 2). A first one occurred in the beginning of Archaean and was associated with the zonal differentiation of the metallic iron. The convective mass exchange at that time was mostly heat-generated and included only the upper mantle and its transitional layer to a depth of 400–800 km within a narrow tropical belt.

The Early Archaean burst of convective (and tectonic) activity turned out to be relatively high not so much due to a high rate of the Earth's matter gravity differentiation release as because all this energy then was dissipated within small volumes of the convecting mantle underneath a narrow tropical belt. Because of that, the Early Archaean convective structures must have been small, a few hundreds to a little over a thousand kilometers in size. Therefore, at least 80 convective structures could have existed in Early Archaean. Remember, first embryos of the future continental shields formed over the descending flows of such structures. It means that $80/2=40$ such continental cores formed in Early Archaean (see Figs. 6.4 and 9.1). What is interesting is that about the same number (37) of the primary and most ancient continental crust nuclears composed of gray gneisses, trondhjemites, and tonalites, are identified based on geological data (Glukhovsky, 1990; Glukhovsky et al., 1994).

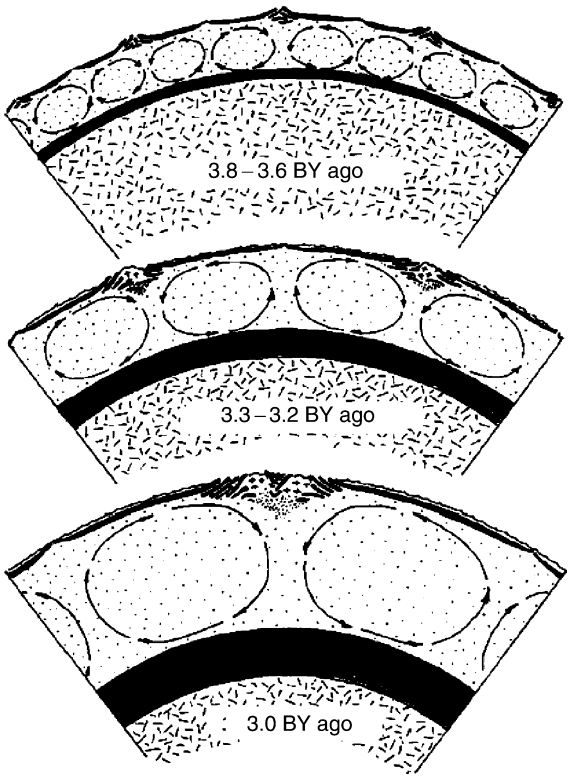


**FIGURE 6.4** Change of cell number in the Archaean convecting mantle and the formation of embryos (nuclears) of the Archaean continental shields (the cross sections are through the equatorial plane and to arbitrary scale).

As the differentiation front descended, the size of the convective cells must have increased, individual nuclears must have merged, and their number must have declined. So, by the end of Early Archaean the number of such continental embryos should not have exceeded 20 (Fig. 6.4).

A second period of drastically increased Earth convective and tectonomagmatic activity in Late Archaean, as previously mentioned, was associated with the start of Earth core separation and involvement in the zonal differentiation process, beside iron, also its oxide with the formation of eutectic melts Fe·FeO. The new burst of Earth's tectonomagmatic activity was now stimulated by a significant increase in the core matter separation rate and of the core proper formation (see Fig. 4.13). These processes induced a proportionate increase in the generation rate of the Earth's matter gravity differentiation energy (see Fig. 5.1).

By that time the differentiation belt substantially expanded, hence, the convecting mantle mass did as well. At the same time, the number of continental massifs (the future Archaean shields) possibly dropped to 12 or 14. After such transition the matter differentiation belt was substantially activated. It particularly strengthened after the Earth core formation process began in the second half of Late Archaean (about 2.8 BY ago). During the same period, the most significant transfiguration of the mantle convection flows happened: the most powerful single-cell convective structure began to form within the mantle which led in the end Archaean to the collision of all earlier emerged continental massifs into a single supercontinent which we called Monogaea (see Fig. 4.1). Under the mechanics law about a stable rotation of free bodies (see Section 4.2), the supercontinent formed over the center of the descending mantle flow must have been positioned on the equator. That, most likely, happened 2.6 BY ago and is marked in the geological record by a grandiose diastrophism of the Kenoran orogeny.

Despite the tentative nature of our estimates, the established general pattern in changes of the convection cell number during Archaean appears to reflect correctly the general evolution of the convection processes in that ancient eon. In particular, it follows from these estimates that only small convection cells with short-life span (tectonic cycles) could form in Early Archaean. As the Early Archaean convection was to a small scale (on the order of a few hundred kilometers), individual cycles overlapped in time. It created a continuous chain of pulsating but not globally correlated processes in separate cores of the growing continents. Correspondingly, numerous Early Archaean tectonic cycles in the most ancient cores of different continents made up a mosaic picture of individual and not synchronous bursts of tectonic activity.

First globally synchronous tectonic cycles could emerge only in Late Archaean. The zonal differentiation front of Earth's matter at that time significantly sunk into the mantle, causing the size of convective cells to grow substantially to a few thousand kilometers. Clearly, however, the synchronicity of tectonic processes must have shown up only by the very end Archaean, at the moment of the core separation.

According to the geological data analyzed by Condie (Fig. 6.5), a noticeable global correlation of the tectonic events in the Archaean granite–greenstone belts on various shields appeared only about 2.9 BY ago. However, its most clear manifestation was in the 2.7−2.6 BY interval. The last Archaean convective cycle coinciding in time with the core separation is at the same time the first and most grandiose global tectonomagmatic event in Earth evolution. It left its inexorable footprint during the Kenoran diastrophism.

After the matter gravity differentiation switched from the mechanism of the core matter zonal separation to a relatively slow barodiffusion mechanism, the mantle convection

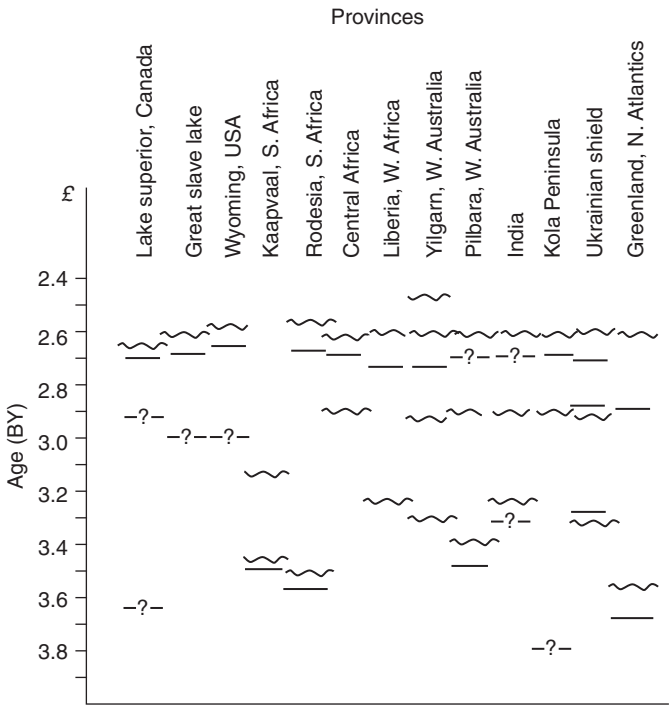


**FIGURE 6.5** Correlation of tectonic events at the formation of Archaean granite–greenstone belts (after Condie,1981, modified): straight segments are the periods of greenstone belt formation and wavy segments are periods of folding.

beginning in Early Proterozoic became much more quiescent. Because of that, a relatively quiet (after the stormy Archaean tectonic events) and the longest Earth's evolution stage, by analogy with the stellar terminology, may be named the main succession of the Earth group planetary evolution.

As the mantle matter differentiation barodiffusion mechanism was gradually extinguishing due to the depletion of the core matter reserves in the mantle, a gradual decline in the intensity of the endogenous energy release was occurring. Calculations indicate that the endogenous energy release after the gravity differentiation switched to the barodiffusion mechanism about 2.5 BY ago declined by the factor of 2.3. Now, compared to the Archaean peak, it declined by a factor of 7–8. The decline will continue in the future.

From the time when Earth core was formed about 2.6 BY ago, its mass was regularly increasing (see Section 4.5). And the mass of the mantle correspondingly decreased from $4.76 \times 10^{27}$ g at the Archaean/Proterozoic time boundary to $4.035 \times 10^{27}$ g at present time. Apparently, under the chemico-density convective mass exchange in the mantle the single-cell and dual-cell convective structures alternate (Sorokhtin, 1974; Monin et al., 1987a,b). At the emergence of single-cell convective structures single supercontinents should form; based on geological data, there were four such continents: Monogaea, Megagaea (by Hans Stille), Mesogaea (Rodinia), and Pangaea (by Wegener). Therefore, beginning 2.6 BY ago, during Proterozoic and Phanerozoic four complete single-cell convective structures existed. Between them, dual-cell convective structures evolved at which times the

supercontinents were destroyed and the separated continents drifted from one another moved by centrifugal forces (see Fig. 6.7).

The above estimate of the number of convective structures is certainly approximate. It may be fine-tuned, for instance, by using the synergistic approach to the issue and coordinating the calculation results with the field data. The convecting mantle is and open dissipative system engulfed in strong positive and negative feedback connections. It suggests the existence in the mantle of a self-organizing tendency with the emergence of intermediate quasistable states. These states are defined by the mantle's most general parameters, such as the mass, the core matter concentration, by the energy the mantle generates, and by the balance of the positive and negative feedback connections acting in the mantle.

We assume that the convective mass exchange in the mantle is controlled by the activity of the strong positive and negative feedback connections within the system. An example of the positive feedback is the correlation between the convection rate and the heat generation. As the mantle temperature increases its viscosity exponentially declines. Correspondingly, the iron-oxide diffusion rate from the silicate crystals to the intergranular space increases and, as a result, so does the rate of the core matter migration to the core (see Section 4.4). This, in turn, leads to increased density variability within the mantle and to a renewed activation of the mantle mass exchange.

A strong negative feedback emerges due to Earth heat loss. For instance, with the increase in the rate of convective mass exchange, the movement of the oceanic plates accelerates, heat flows through the ocean floor increase, and the total Earth heat loss increases. These decrease the mantle average temperature, increase its matter viscosity which, in turn, results in a decline of the mantle convective mass exchange. Another negative feedback mechanism is ingrained in the very mantle matter barodiffusion differentiation process.

Iron-oxide diffusion from the silicate crystals into the intergranular space occurs only in the lower mantle at a depth of over 2000 km (see Section 4.4). So, the higher the convection rate, the shorter time will the mantle matter spend in the lower mantle active layer, and the less core matter will diffuse from the silicate crystals and migrate into the core. And the slowdown of the differentiation process will unavoidably result in the convection rate declining.

Thus, Earth heat engine is an open nonlinear dissipative system with feedback that determines a possibility of the emergence in it of self-oscillatory processes and self-organizing of the geodynamic processes. It means that the chemico-density convection in the mantle is in its nature a nonstationary process. It is characterized by a variable distribution of the heavy fraction concentration in the mantle matter and the associated constantly changing structure of the convective cells. So, it is to be expected that self-organization of the mantle convective cells will be constantly disrupted by the instability of the process. Nevertheless, from time to time such self-organizing states (on average corresponding with minimum dissipation rates of endogenous energy) should arise.

It is shown in the publication by Sorokhtin and Ushakov (1993) that, at the permanent mass of the mantle and in the absence of its heating or cooling, average convective mass-exchange rate in this geosphere remains constant over long time intervals although it may vary significantly fluctuate due to the restructuring of the convective cells. If, nevertheless, the mantle on average cools down after the Archaean overheating, the convection rate will gradually decline. Therefore, the periods of the complete convective mass-exchange cycles in the mantle will be lengthening.

However, the mantle mass was decreasing with time due to the core separation. The result is speeding up of the convective mass exchange. This may cause the mantle convection processes to stabilize. This conclusion is apparently supported by the geological data. If it is so, then an important geodynamic law follows: Earth energy balance on average stabilizes the development of the mantle convection processes.

What was happening in actuality and which factor (mantle cool-down or a decrease in its mass) dominated may be determined from the geological record. For instance, the emergence of the supercontinents Monogaea, Megagaea, Mesogea, and Pangaea must be juxtaposed against the closing times of the Kenoranian, Svekofennian, Grenvillian, and Hercynian tectonic eras (orogenies) at, respectively, $2600 \pm 100$, $1800 \pm 100$, $1000 \pm 70$, and $230 \pm 10$ MMY ago.

If this is so then the supercontinent formation periodicity in Precambrian changed little between 800 and 780 MMY. Obviously, the megacycle periodicity in post-Archean, accurate to the orogenies age determination, remained approximately constant in Proterozoic. This indicates that simultaneously with the decrease in the mantle mass (see Fig. 6.6), which resulted in the convection speeding-up, its slight cool-down occurred (see Fig. 5.13, curve 3), which increased its viscosity, hence, slowed down the convection. Both oppositely acting factors stabilized the mantle convection and maintained approximately constant megacycle periods of the supercontinent formation.

Therefore, a decline in Earth's tectonic activity due to decreasing endogenous energy generation in the mantle (hence, the mantle temperature) was compensated in Proterozoic by a decrease in the mantle mass thereby stabilizing the periodicity of tectonic events on Earth. In the future, however, because of the depleting Earth's energy store and slowing-down of the mantle matter differentiation the mantle cool-down begins to play more

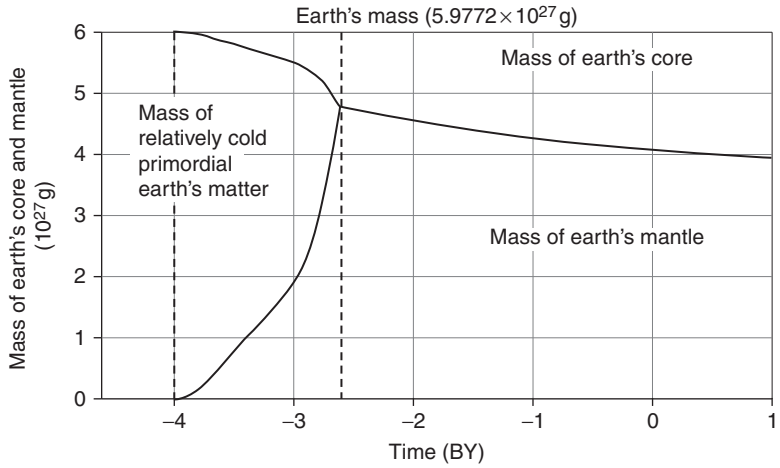


**FIGURE 6.6** Gradual increase of the mantle mass in Archaean due to the expansion of Earth's matter differentiation zone and in its mass in Proterozoic and Phanerozoic due to the core growth. Dashed lines are the times when the core matter separation began about 4 BY ago and when a high-density iron-oxide core separated in the center of Earth about 2.6 BY ago. Since the origin of Earth 4.6 BY ago and through the very end of Archaean the primordial Earth's matter saturated with ore elements was preserved within Earth.

important role. As a result, the mantle convective mass exchange will slow down and the tectonic megacycle length will noticeably increase.

As noted earlier, the Archaean evolution completed by the formation of a real high-density Earth core and the emergence of a powerful single-cell convective structure in the mantle. For this reason, it is convenient to accept this natural time boundary (the moment of the final heavy Earth core formation about 2.6 BY ago) for the beginning of the post-Archaean geological history corresponding to the main succession in Earth evolution. That is even more justified by the emergence at the end Archaean for the first in Earth's evolution supercontinent Monogaea. This boundary is most clear in the geological record as it was accompanied by the change in mechanisms and geochemistry in the continental crust formation and besides it was immediately preceded by a most powerful tectonism (Kenoranian orogeny) which formed the first supercontinent Monogaea.

In this case, accounting for the alternating single-cell and dual-cell mantle convective structures and the provided geological data on the supercontinent formation timing, it is possible to fine-tune the derived estimate of the convective cycle number in Proterozoic and Phanerozoic.

It turns out that till present time approximately 6.2 convection cycles, 380–420 MMY each, were completed. Kenoranian orogeny which completed the Archaean tectonic events may be taken for the origin of all subsequent tectonic cycles (both single- and dual-cell). Then it turns out that by present at $N_0 \approx 6.3$ the integer numbers $N_0 = 0$, 1, 2, 3, 4, 5, and 6 correspond in post-Archaean to the ages of 2.6, 2.22, 1.84, 1.45, 1.05, 0.65, and 0.23 BY ago. They are very close to the ages of the main tectonic events in Proterozoic and Phanerozoic (Fig. 6.7). As mentioned, in the future, due to depletion of Earth's energy store, a decrease in its tectonic activity will be playing ever more important role. Because of this, the mantle convective mass exchange will significantly slow down and, as a result, the time duration between tectonic megacycles will noticeably lengthen.

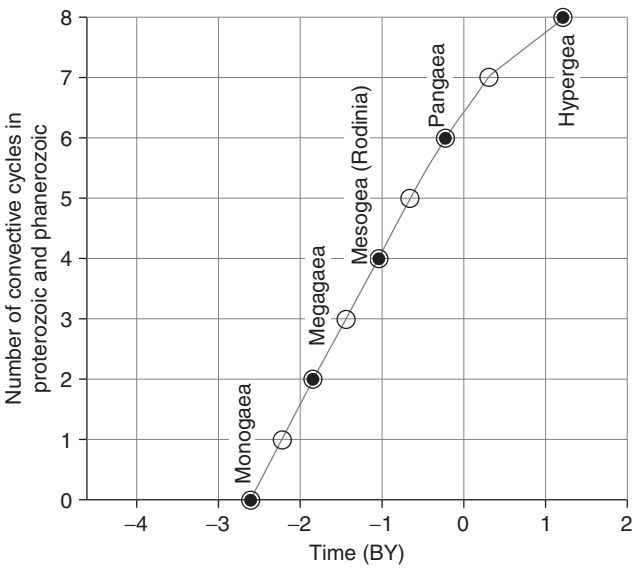


**FIGURE 6.7** The number of convecting (tectonic) megacycles in Proterozoic and Phanerozoic $N_C(t)$ versus time. Solid dots are single-cell convective structures and the supercontinent formation times; hollow dots are dual-cell convective structures and the times of maximum continent split.

Assuming that in the chemico-density convection one convection cycle corresponds to the complete turnaround of the mantle matter, 6.3 convective cycles existed in Proterozoic and Phanerozoic.

$N_C = 0$ corresponds to the emergence time of the first supercontinent in Earth history (see Fig. 9.2). By analogy with the unified continental massifs later emerged during the subsequent geological epochs, the Megagaea by Hans Stille and Pangaea by Alfred Wegener we called this first supercontinent the Monogaea.

The supercontinents are unstable. After they emerge, they rapidly fragment into individual parts (see Chapter 9 for possible reconstruction of the supercontinents and continents—remains after their fragmentation). The cause is changes in the mantle convection flow structure and the emergence of a new ascending mantle flow in place of the descending one underneath the former supercontinent. The ascending flow is a direct cause of the supercontinent's fragmentation (see Figs. 6.13 and 9.14). But each time a single-cell convective structure formed within the mantle, a new supercontinent emerged (Fig. 6.8).

Taking relatively brief supercontinent lifespan into account we suggest that at $N_C = 1$ by the moment in time 2.22 BY ago a more complex, possibly dual-cell convective structure was established in the mantle. For Earth stable revolution, the laws of mechanics require for its main axis of moment of inertia to coincide with its own revolution axis. Thus, Earth must have rotated so that the center of mass of most continents at that time (e.g., fragments of the Monogaea) was on the equator or in low latitudes.

The next supercontinent, the Megagaea by Stille (see Fig. 9.4) began to form about 2.0–1.9 BY ago, but finally emerged only 1.84 BY ago as a result of the global Svekofenian (Karelian) orogeny. Therefore, at the time to which parameter $N_C = 2$ may be attributed a single-cell convective structure must have functioned within the mantle. A conclusion was quoted in Section 4.2 that the orientation of Earth's momentum of inertia depends on the continental masses positions on the surface (Monin, 1988). Based on that, we suggest that a second supercontinent Megagaea formed on the low latitudes with the center of mass on the equator (see Section 9.4).

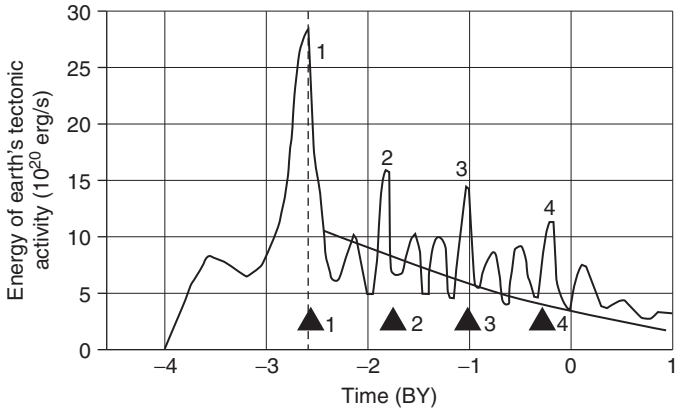


**FIGURE 6.8** Summary diagram of Earth's tectonic activity based on the analyzed model (see Fig. 5.17) but using the calculations by Keondzyan and Monin (1976) accounting for the cyclicity in the release of endogenous energy. Each significant maximum on the curve at the times 2.6; 1.8; 1.0 and 0.2 BY ago had the corresponding single-cell convective structure in the mantle and the formation of the supercontinents. The real time-positions of the supercontinents are marked by the triangles: 1. Monogaea; 2. Magagaea; 3. Mesogea (Rodinia); 4. Pangaea (we modified the amplitude of the 4th tectonic activity impulse). The dashed line denotes the time of Earth core separation.

Its lifespan was also brief: general crust fragmentation occurred in the beginning of Riphaean. The parameter value $N_C = 3$ corresponds in time (1.45 BY ago) to Early Riphaean. The Megagaea split began somewhat earlier, about 1.6 BY ago, and is closely coincident with the next outstanding epoch of a great renewal in Earth structural plan. Some use that time as the beginning of the Neogean epoch.

The parameter value $N_C = 4$ corresponds with time 1.05 BY ago. It is close to a no less radical Grenville epoch of tectonomagmatic activation. This activation began the formation from Megagaea fragments of a new, third supercontinent Mesogea (called sometimes Rodinia, see Fig. 9.6).

The new supercontinent, similar to the Megagaea, was positioned close to the equator and lived a relatively short life, 100−150 MMY. Soon thereafter the single-cell mantle convection was replaced by the dual-cell convective structure. It had two descending flows near Earth poles and a single ring-like ascending flow underneath its equatorial belt. This situation, with the parameter value $N_C = 5$ and time 800 MMY ago, corresponded with the Mesogea split into two large supercontinents, Laurasia and Gondwana (see Fig. 9.7).

But about 650 MMY ago, a secondary ascending mantle flow emerged underneath the northern fragment, the Laurasia. It literally tore the supercontinent into pieces with the formation of the Pro-Atlantic Ocean Japetus and the Paleo-Urals Ocean. The Gondwana experienced only partial destruction and was welded again into a supercontinent by the Katanga (Pan-African) orogeny (see Section 9.5).

A fourth single-cell convection structure emerged and a new supercontinent Pangaea (see Fig. 9.10) formed at the Paleozoic/Mesozoic time boundary about 230 MMY ago. Corresponding to this event were parameter $N_C = 6$, the calculated timing of 230 MMY, and the maximum tectonic activity during the Phanerozoic Hercynian orogeny. As all other supercontinents, Pangaea did not live long and already early in Mesozoic (about 200 MMY ago) experienced the first impulses of destruction. About 190 MMY ago first transcontinental faults split Pangaea and soon grew over into young oceans: the Atlantic, the Indian, and the Arctic.

These $N_C(t)$ estimates are of course approximate especially in view of substantially nonstationary nature of the mantle convection. Still, it appears that they correctly reflect the main feature of Earth's tectonic activity evolution, that is, its cyclicity. The provided estimates (see Fig. 6.7) suggest that in the post-Archaean geological history there were six alternations in the convective cycle structures between single-cell and dual-cell structures: 2.6–2.22–1.84–1.45–1.05–0.65–0.23 BY ago, with the duration of about $380-420 \pm 10$ MMY.

If we extend this pattern into the future, taking into consideration a progressive decay of Earth's convective activity, then the next full convective cycle will be completed about 300 MMY from now at $N_C = 7$. And the fourth, last megacycle with $N_C = 8$ may end about 1.2 BY from now in the future. As the Earth's matter barodiffusion differentiation process is gradually weakening, and so does the mantle convective activity, it is not clear whether the slackening mantle convection has enough capacity to form the last supercontinent, the hypothetical Hypergea.

The energy approach enables to estimate the total mass of the mantle matter that went through the differentiation and participated in the convection. It was determined above that the rate of the present-day convective mass exchange in the mantle is approximately $6 \times 10^{18}$ g/year or $1.9 \times 10^{11}$ g/s.

Over the entire Earth's tectonic period (beginning 4.0 BY ago and through present), its heat loss due to the convective heat transfer was about $10.773 \times 10^{37}$ erg (see Fig. 5.13). The corresponding depth heat flow, minus the effect of the post-Archaean Earth cooling, is $3.39 \times 10^{20} - 0.27 \times 10^{20} = 3.12 \times 10^{20}$ erg/s. This allows for the determination of the total mantle matter that participated in the convective mass exchange. It turns out to be $5.2 \times 10^{28}$ g. Earth and the present-day mantle masses are, respectively, $5.977 \times 10^{27}$ and $4.035 \times 10^{27}$ g. Thus, presently the total mass of the mantle matter that went through the convective mass exchange is almost 8.7 times the mass of Earth and 13 times the mass of the present-day mantle. This approximate estimate is very demonstrative and shows that the convective mass exchange is huge and cannot be disregarded.

Now we can estimate the overheating $\Delta T$ of the matter in the ascending mantle flows compared with average mantle temperatures. As the mantle convection is "heating up" Earth, including the core from its surface, we may write

$$\Delta T = \frac{\Delta E_{m_{2.6-0}}}{M_G 8.7 (c_p)_G}, \tag{6.4}$$

where $\Delta E_{m_{2.6-0}} = 4.576 \times 10^{37}$ erg is the heat component of the energy released within the mantle after Archaean; $M_G = 5.977 \times 10^{27}$ g is Earth mass; $(c_p)_G \approx 1 \times 10^7$ erg/g deg. We find $\Delta T \approx 88$ °C, which is somewhat higher than the previous estimate from Eq. (6.1) but still commensurate with it, therefore, temperature of the ascending mantle matter so far exceeds average mantle temperature by less than 100 °C.

The scale of the mantle matter differentiation may also be determined. Indeed, the rate of the gravity energy release is connected with the rate of the mantle matter differentiation on the Earth's core surface $\dot{M}_m$:

$$\dot{E}_g \approx \dot{M}_m \left[ \Delta \bar{h}_c \frac{\Delta \rho_{cm}}{\bar{\rho}_c} + H_m \frac{\Delta \rho_m}{\bar{\rho}_m} \right] g_c. \tag{6.5}$$

The current rate of the heat energy component of the Earth's differentiation gravity energy is $\dot{E}_g \approx 2.77 \times 10^{20}$ erg/s. The average core surface topographic gradient $\Delta h_c$ may be found from the map in Fig. 2.10. It is about 7 km. $\Delta \rho_{cm}$ is the matter density gradient at the mantle/core boundary according to Table 2.2: $\Delta \rho_{cm} = 9.92 - 5.6 = 4.32$ g/cm$^3$; $\bar{\rho}_c \approx 10.6$ g/cm$^3$ is the average core density; $H_m \approx 2875$ km is the average thickness of the mantle; $\bar{\rho}_m \approx 4.54$ g/cm$^3$ is the average mantle density; $g_c = 1067$ cm/s$^2$ is gravity acceleration on the core's surface (see Table 2.2). The descending and ascending flow matter density difference $\Delta \rho_m$ may be determined from the condition of their isostatic equilibrium (keeping in mind that $\Delta h_c \ll H_m$)

$$\Delta \rho_m \approx \Delta \bar{h}_c \frac{\rho_c - \bar{\rho}_m}{H_m}. \tag{6.6}$$

From this, $\Delta \rho_m \approx 0.0165$ g/cm$^3$. A somewhat different although close estimate, $\Delta \rho_m \approx 0.019$ g/cm$^3$, was derived in Section 4.4 (see Eq. 4.21). Inserting now all these values into (6.5), we obtain the migration rate of the Fe·FeO melt from the mantle to the core $\dot{M}_m \approx 2.8 \times 10^{11} \div 3.2 \times 10^{11}$ g/s or $8.8 \times 10^{18} \div 10.1 \times 10^{18}$ g/year. In terms of the metallic iron the numbers are, respectively, $7.7 \times 10^{18} \div 8.8 \times 10^{18}$ g/year or $7.7 \times 10^{12} \div 8.8 \times 10^{12}$ t/year.

## 6.4 CONVECTION IN EARTH MANTLE

There is undoubtedly intense and large-scale convection in the mantle. It is caused by endogenous energy processes. The most important such process is the mantle matter gravity differentiation energy with some contribution from the radiogenic heat and currently insignificant additions from the tidal energy. The boundary conditions on Earth surface are associated with the ancient and thick continental plates and with the emergence on the surface of the convecting mantle of cooled-down and mobile oceanic lithospheric plates. These boundary conditions impose a specific footprint on the mantle convection and often subrogate its structure to the lithospheric plate and subduction zone locations.

There are indirect indications of a large-scale convection simultaneously within the upper and lower mantle. These are the calculation data about the calculated lower mantle matter density based on the shock compression of silicates. The calculations showed that, under the corresponding pressure and adiabatic temperature, the density distribution in both upper and lower mantle is accurately approximated by the density of the oceanic lherzolites recovered from the ocean floor transform faults (see Fig. 2.9). This indication of a uniform mantle matter chemical composition is at the same time an indirect testimony of the existence of the large-scale convection in the mantle, the convection that is continuously stirring its matter.

And what about direct indications?

Seismic observations show that the tails of the oceanic plates sinking into the mantle are observed underneath the subduction zones much deeper than the maximum depth of earthquakes. These tails are observed to 800 km, maybe even to 1400 km, that is, already in the lower mantle. This is a direct testimony to the existence of a single mass-exchange structure penetrating the lower as well as the upper mantle.

There are convincing evidences of the depth mantle convection flows totally dissociated from the "self-motions" of the oceanic lithospheric pales in the subduction zones. Such evidences are apparently represented by the African continent split along the Red Sea–Bay of Aden–East-African rifts system; by the spreading of the Atlantic and in part Indian Oceans; by the oceanic floor rise above the water level in the Northern Atlantic (Iceland) and in the northeastern Ethiopia (the Afar Province), and so on. All these phenomena cannot be caused by sucking-in of heavy oceanic plates into the mantle. They require the involvement of the independent convection flows of the mantle matter acting from beneath on the base of the lithospheric plates.

The split of the Wegenerian Pangaea into separate parts—the present-day continents—is apparently the clearest proof. This event occurred in mid-Mesozoic but the continental drift (and the split of Africa) is still continuing. This phenomenon cannot be explained using gimmicks such as the "self-immersion" of heavy oceanic plates into the mantle.

Now, back to the aforementioned correlation between the lithospheric plate movement rate and the length of the surrounding subduction zones. It may be interpreted quite differently from the Forsyth and Uyeda (1975) interpretation. All "fast" plates are as if grouped within two adjoining regions. On the one hand, these are the Nazca, Cocos, Pacific, and Philippine Plates, and on the other, the Indian Plate. But assuming the powerful ascending mantle flows exist underneath the southeastern and eastern Pacific and underneath the central Indian Ocean, and between them, somewhere under New Zeeland, Indonesia, Eastern Asia, and South America are the descending flows, the same result happens due to a simple mantle matter spreading

underneath the mentioned plates (see Fig. 2.10). Lo and behold! There are indeed ascending and descending mantle convection flows underneath those areas. However, in such a case the viscous adhesion between the mantle matter and the lithospheric plate bases will no longer hamper the plate movement but quite to the contrary will facilitate it.

There is a rather large ascending convection flow underneath the North Atlantic. This is supported by several facts. First, it is spreading of the continents framing this part of the ocean. Then, it is the uplift of the ocean floor. It is also the Earth's core topographic map showing a noticeable high under the North Atlantic similar to such underneath the southeastern and eastern parts of the Pacific (see Fig. 2.10). The plates are moving at a very slow rate in the North Atlantic region, 2 cm/year. In the Pacific, however, the rate reaches 15–18 cm/year (see 8.6). Apparently, this difference in the plate movement rate over the ascending flows is due to the effect of the lithospheric shell *per se* on the formation of the horizontal branches of the mantle convection flows. For instance, the asthenosphere in the mantle underneath the Pacific is clearly expressed and the region's oceanic plates are surrounded from almost all sides by the subduction zones. And in the Northern Atlantic there are hydrodynamic barriers in the form of thick continental plates which hamper the asthenospheric flows spreading outside of the ocean boundaries. And the viscous matter convection flows are usually organized in such structures that at a given mass-exchange rate the viscous friction energy dissipation rate was minimal. The mass-exchange rate under the proposed model is determined by the mantle matter differentiation process on the core's surface.

This is a fundamental tenet. In particular, it follows from it that the convective flows in a viscous medium always tend to cover as much volume of space as possible, with the emergence of the broadest flows, and within relatively narrow asthenospheric layers, of the largest area. Given the medium with a variable thickness of the oceanic and continental lithospheric plates (as in Atlantic Ocean), the convective flows always concentrate within the least viscous layers (i.e., asthenosphere) and can spread only along the trend of the oceanic rift zones.

That is the reason why the convective flows in a stratified mantle with a clearly low-viscosity asthenosphere must draw together into this layer of the lowered viscosity. As a result, the lower mantle and the lower part of the upper mantle are dominated by the vertical matter flows, whereas mostly horizontal flows form in the asthenosphere. Therefore, most of the convective flow matter runs through the thin asthenospheric layer forming in it relatively rapid (up to several dozen centimeters per year) horizontal asthenospheric flows. These very flows pull with themselves the relatively thin (10–80 km) Pacific oceanic plates from the ascending convective flow underneath the East-Pacific uplift toward the descending mantle flows, that is, toward the subduction zones surrounding the ocean. These flows do not obstruct the plate motion if they are caused by the mechanism of sucking-in of a denser lithosphere into the mantle because in this case the plate movement directions toward the subduction zones indeed coincide with the anticipated direction of the asthenospheric flows under these plates.

A totally different development occurs underneath thick continental plates submerged into the mantle to a depth of up to 200–250 km. There, the asthenospheric layer is practically absent or substantially degenerated. For this reason, viscosity underneath the continental plates must be more uniformly distributed, and the horizontal components of the convective flows under them are formed within a much greater volume of the middle

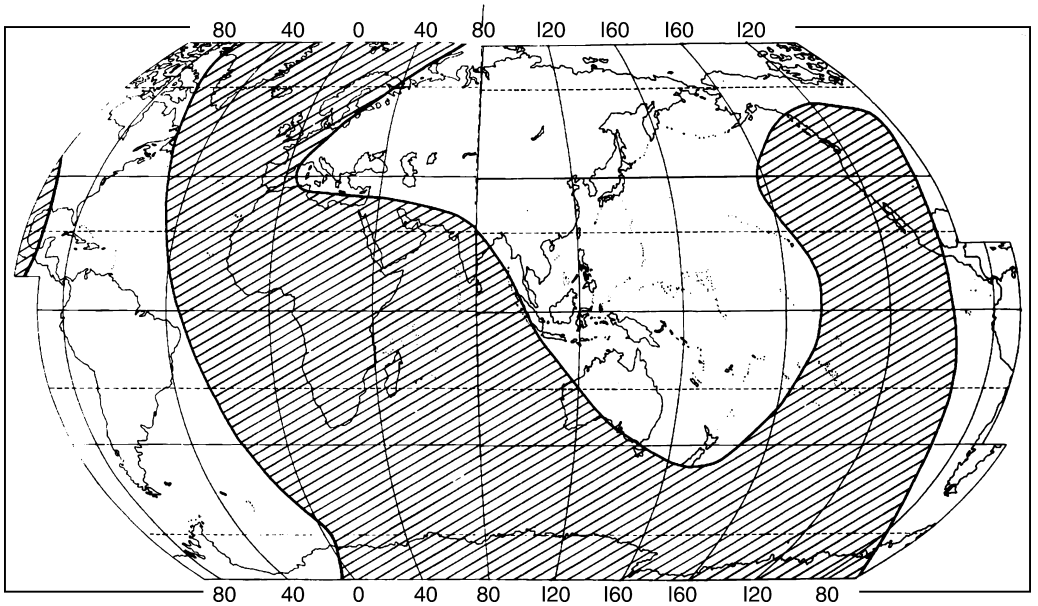


**FIGURE 6.9** Location map of probable ascending and descending convective flows in the present-day Earth mantle (Ascending flows are shaded (Sorokhtin, 1979)).

and lower mantle with the greatest viscosity. However, the cross-sectional area of these horizontal flows under the continental plates is much greater, so their velocities are correspondingly lower (a few centimeters per year). Most likely, that is why we observe much slower continental drift, especially for large continents firmly rooted in the Earth's mesosphere. The motion rate of the oceanic plates welded with them is also lower. This occurs, for instance, in the Atlantic.

The mentioned distinctions in geodynamic reaction from the oceanic and continental plates to the mantle convection flows are apparently well illustrated by the aforementioned Forsyth–Uyeda correlation. In actuality, this correlation defines a connection between the lithospheric plate motion rate and their structure, continent size and plate positions relative to the descending and ascending mantle flows. Our attempt on their reconstruction is shown in Fig. 6.9.

The Forsyth–Uyeda correlation clearly divided large lithospheric plates into two groups, the continental and purely oceanic plates of the Pacific region. The Indian Plate holds an intermediate position in this classification—perhaps because the continental massifs welded into it (India and Australia) are relatively small continents. Besides, the Indian Plate, similar to all Pacific plates, is favorably positioned between the ascending and descending mantle flows which in the final analysis caused a relatively high rate of its movement toward Indonesia.

The asthenosphere in the Northern Atlantic is developed only under the ocean floor. It is overlain from the east and west by thick continental plates. These plates play role of giant dams preventing spreading in these directions of the asthenospheric flows from the

ascending flows located there. That is why, as was previously mentioned, the asthenospheric flows in the region can spread only along the Mid-Atlantic Ridge.

This shrinkage in the effective cross section of the asthenosphere results in a substantial increase in its hydrodynamic resistance. It is known that there is a law in hydrodynamics similar to the Ohm's law in electric engineering. The electric resistivity analog in hydrodynamics is pressure which involves a viscous matter in the convective mass exchange. The flow of the matter in this mass exchange plays the role of the amperage. Thus, one finds hydrodynamic resistivity of the medium as the quotient from the division of the pressure by the matter flow. In our case, the matter flow is assigned by the mantle matter differentiation mechanism on the core surface. That is why increase in the asthenospheric hydrodynamic resistivity unavoidably leads to the corresponding increase in the excess pressure acting upon the matter within this layer.

The action of such excess pressure is very demonstrative in the North Atlantic. First of all, this phenomenon causes a significant general uplift of the ocean floor in the region. The amplitude of the hydrodynamic "swelling" is such that the Mid-Atlantic Ridge over the center of the ascending flow rises above the water surface and forms the island of Iceland. The average depth to the mid-oceanic ridge crests is usually 2.5–2.7 km below the sea level. Thus, one can estimate the excess pressure from the ascending convection flow which uplifted the North Atlantic sea-floor at 700−800 bar.

This excess pressure, together with the pressure from the oceanic lithospheric plates sliding off the asthenospheric lens underneath Atlantic Ocean (this pressure is also about 700–800 bar), is acting on the edge zones of the Europe, Greenland, and North America's continental plates and is creating here excess compression stresses on the order of up to 1−1.5 kbar. These stresses often result in the unpleasant consequences as shock bumps, rock bumps in mines, and even earthquakes in the near-shore continental areas around the North Atlantic (such as the Lisbon earthquakes of 1531 and 1755).

The raise of the ocean floor in the North Atlantic creates in that region a large positive gravitational anomaly. The dynamic nature of this regional anomaly is clearly manifested in the isostatic reduction, after the subtraction from it of a correction for the effect of "excessive" topography, that is, the difference between the real ocean floor topography in the region and average topography of the mid-oceanic ridges in "unaffected" regions. After such recalculation performed by Ushakov (Sorokhtin and Ushakov, 1991) for the "normal" topography, the North Atlantic residual gravity field becomes negative. Together with the data about the ascent in the region of the Earth core level (see Fig. 6.10) and the ocean floor spreading, this result of the regional gravity field analysis is serious evidence in favor of a powerful ascending convection flow existing there and piercing the entire mantle from the core surface to Earth surface.

It is worth mentioning that the gravity field of Earth and the geoid shape are not always sufficient for a judgment about the structure of the mantle convection flows. Indeed, there is a positive gravitational anomaly and the corresponding rise of the geoid level by 60 m over North America, despite the existing underneath it of a powerful ascending flow of a light mantle matter. On the other hand, there clearly is underneath the Western Pacific no less powerful descending convection mantle flow marked by a series of subduction zones. Still, its apparent manifestation in the Earth's gravity field is the same as in North America: a positive gravity anomaly and an 80-m geoid "swelling" (see Fig. 2.1). An explanation

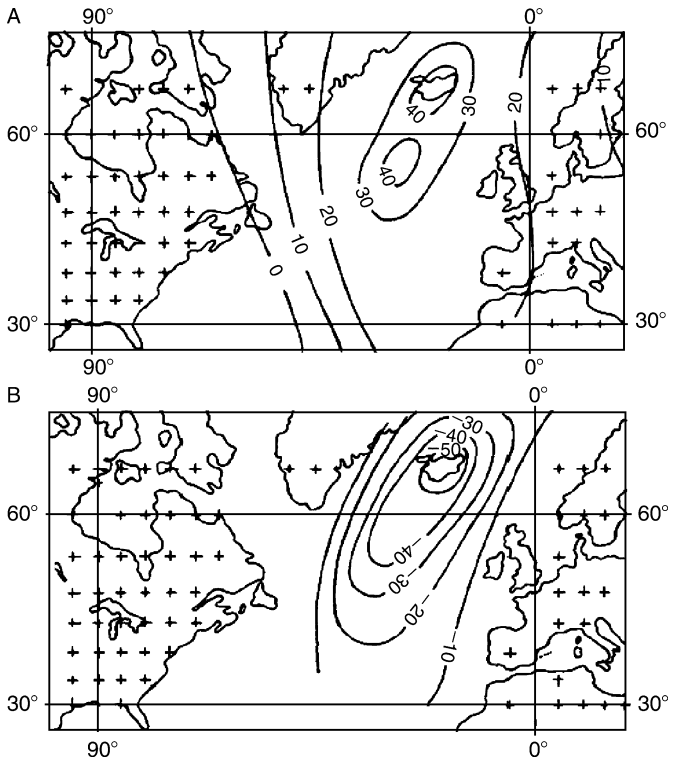


**FIGURE 6.10** (A) Averaged free air gravity anomaly (positive Faye anomaly) over the North Atlantic, mgal and (B) residual anomalous gravity field after the removal of the "excessive" effect of the Mid-Atlantic Ridge topography in the North Atlantic (negative isostatic anomaly, mgal; Sorokhtin, Ushakov, 1991).

may be as follows. In the first case, the gravity field "dynamic" component is dominant. It is caused by the rise of the ocean floor due to the excess pressure from the ascending flow. In the second case the dominant component is "static," associated with the excessive mass of the cold (hence, heavy) lithospheric plates sunk into the mantle (although here as well some dynamic component may be present).

Should the lithospheric shell have been uniform, unmoving, and had the same thickness everywhere then the large-scale undations (wave-formed surface bends) should have uniquely reflected the structure of the mantle convection flows. The actual situation is much more complicated as the asthenospheric hydrodynamic conditions underneath the oceans and the continents are significantly different. If, however, the space between the ascending and descending mantle flows is overlain only by the oceanic (or only by the continental) plates it may be expected that the large-scale gravity anomalies and undations in such regions of the geoid will remain the least distorted.

For instance, two positive geoid undations may be identified from the geoid topography in the Pacific Ocean and the adjoining regions (see Fig. 2.1). They are positioned in the west and east of the ocean and well coincide with the plate subduction zones there. Between these geoid "swellings" there is a broad band of the lowered and negative geoid elevations covering the entire southern and central parts of the ocean. Such kind of the geoid topography in the Pacific Ocean may be with certainty interpreted as an indication of the ascending

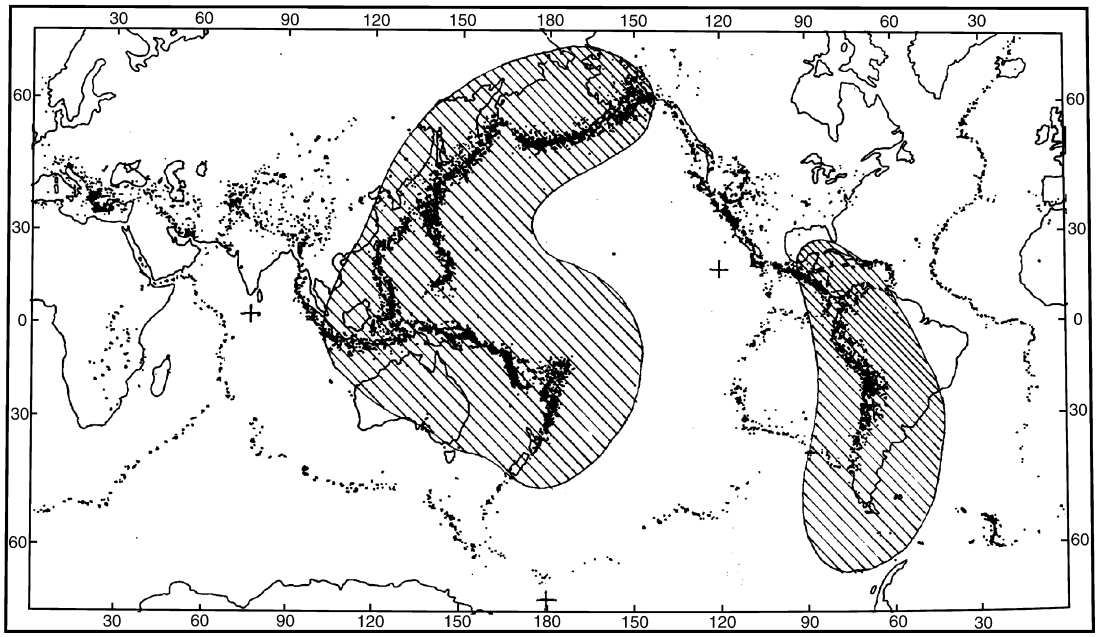


**FIGURE 6.11** Location map of the descending mantle convective flows in the Pacific Ocean and the adjacent areas against the background of Earth tectonic activity map (Barazangi and Dorman, 1968) shown in Fig. 2.6; crosses are centers of the negative geoid undulations in the Pacific, Southern and Indian Oceans (respectively, −52, −60, and −105 m).

mantle flows underneath the lowered elevations and of the descending flows, underneath the positive undations (Fig. 6.11).

A comparison of this interpretation with the Earth's core topographic map (see Fig. 2.10), albeit a very schematic and probably still not very accurate, confirms nevertheless such an interpretation. Indeed, negative topographic forms are observed on the core surface underneath the western portion of the ocean and underneath South America. They reliably mark the roots of the mantle descending flows. Under the central and southern Pacific, the core surface is uplifting which is no less reliable indication of the ascending flows there.

If the provided description of the geodynamic environments in the Pacific area is close to reality, it may be expected that the East Pacific and the southern branches of the convection flows farther join the powerful ascending flows underneath the Indian Ocean, Africa and North Atlantic (see Fig. 6.9). An impression is created that the interconnected chain of the ascending flows encompasses as a broad belt the descending flow center underneath the western Pacific, Indonesia, and North Australia.

It is also clear that there is a powerful ascending flow under North America (as already mentioned). But how is it connected with the just described convection flow system, through North America or Europe? It is not completely clear yet. Most likely, through North America because underneath Western Europe and Africa (and especially along the Mediterranean and Alpine-Himalayan mobile belts), there still are relics of sometime ago powerful descending convection flows which predetermined the closing of the Tethys Ocean.

The African situation remains unclear. On one hand, its relatively high stand above the ocean level and the geological data definitely indicate the split and continuing spreading of the East-African rift zone. These are easier to explain through the existence of the ascending flows underneath the continent. But on the other hand, the core topography does not show the roots of such flows. Thus, what remains is to assume that the larger (western) part of the African Plate as if is being torn away of the Somali block (probably along the weakened old sutures) and is drifting westward due to the action on its base of the horizontal mantle flows coming from the Indian Ocean ascending flow toward the descending flow underneath South America.

But this is just an assumption.

On the whole, the lithospheric plates tend to move under influence of the convection currents from the ascending flow areas to the mantle matter descending flow areas which usually coincide with the areas of the oceanic plate sinking into the mantle. Their displacements are often hampered by the plates' rigidity and their interactions with one another. It is anticipated nevertheless that this pattern is real.

The data about the plate drift directions and rates are important for the identification of a general structure of the mantle convection. One has to keep in mind that there is no absolute coordinate system for measuring plate motions. All determinations of their displacements are relative to the other plates. Perhaps, it would be better to do it relative to the least mobile continent, for instance Antarctic. It is located near the pole since Late Paleozoic and never left the pole in Cenozoic.

## 6.5 RESULTS OF MODELING THE MANTLE'S CHEMICO-DENSITY CONVECTION

The provided description of the mantle convection was qualitative. It would be desirable to test the conclusions and try to obtain new results by way of more rigid modeling and quantitative analysis of the major patterns of the process. Unfortunately, the correct description of a compressible liquid flow in the potential gravity field with the spherical Earth's mantle, with the variable liquid's viscosity depending on the temperature, and with a nonuniform and variable density is difficult as the describing equations are complex and cumbersome.

A complex chemico-density and heat convection is evolving in the Earth's mantle. Any viscous liquid convection in the gravity field may be only density convection regardless of the causes of the density variations. That is why in a broader sense, convection evolving in the mantle should be called the chemico-heat or concentration-heat convection. That would underline the issue that the mantle matter density variabilities $\delta\rho_m$ causing it emerge due to the changes in the chemical composition or concentration of the heavy fraction as well as due to effects of the matter's heat expansion (contraction):

$$\delta\rho_m = \bar{\rho}_m\left[\Delta C\cdot\frac{\bar{\rho}_m(\rho_C-\rho_{Si})}{\rho_C\rho_{Si}}-\alpha\Delta T\right], \tag{6.7}$$

where $\bar{\rho}_m$ is the average matter density at the given mantle's level; $\rho_C$ is the heavy fraction (Earth's core) density; $\rho_{Si}$ is the light fraction (the mantle matter's silicate fraction) density;

$\Delta C$ is the difference in concentration of the core matter in the mantle; $\alpha$ is the matter's volume expansion factor; and $\Delta T$ is super-adiabatic temperature gradients in the mantle matter.

In a general case, under Eq. (2.19), the mantle matter viscosity strongly depends (under the exponential law) on the temperature. So, this correlation needs to be taken into account in the modeling. In particular, if the matter's temperature within the lower mantle's ascending flow is greater by 100 °C than the surrounding medium's temperature, the matter's viscosity in this flow will be about 10 times lower than the viscosity in the descending flows. This is a substantial difference. It will significantly affect the structure of the mantle's convection flows. Nevertheless, most of the earlier publications on the convection did not account for the viscosity versus temperature correlation due to mathematical complexity in using it in the viscous liquid flow equations.

In the case of a purely heat convection, it is usually accepted that the chemical component concentration in the viscous liquid remains constant and all density changes are only due to the temperature changes. On the other hand, under a rigid approach there is no purely chemico-density convection in the nature. It always converts to the chemico-heat convection. Thus, it is obvious that the chemico-heat convection modeling is a more complex problem than the modeling of purely heat convection.

Although the chemico-density convection does evolve in the mantle, it was traditionally believed, beginning with Holmes (1928) that the Earth's tectonic activity is fed only by the energy of the radioactive decay and is caused by the heat convection. This viewpoint is still shared by many geologists and geophysicists. That is probably the explanation why most publications on the mantle convection are limited to the discussion of its heat form only.

Indeed, there is much in common between the heat convection and chemico-density convection. They are described by the similar equations, their external manifestations are also similar albeit in details, sometimes substantial, and their behavior differs. For instance, the heat and chemico-density flows react differently to the overlying continental plates, to the changes in the convection flow structure, to the intersection of phase transition boundaries, and so on.

The most thorough study of the heat convection as of today was conducted by Trubitsin and Rykov (2000). They performed three-dimensional modeling and took into account the effect of the "mantle heat-insulator" continents on the structure of the convection flows. It was found in the heat convection models that the mantle overheating can occur underneath large continental plates. It can cause the emergence in the mantle of new ascending flows destroying such plates. This is an explanation of instability and destruction of the supercontinents that existed in the past epochs. For this to happen powerful radiogenic energy sources should have existed which are practically not available as shown in Section 5.2 (the ascending flow emergence mechanism underneath the supercontinents under the chemico-density convection is illustrated in Fig. 9.14). Nevertheless, modeling of the mantle heat convection approximately but demonstrably shows the existing mantle matter mass exchange (Fig. 6.12).

In view of extreme difficulties in modeling the chemico-heat convection mass exchange in the mantle, initially the purely chemico-density convection was modeled disregarding its heat effects. A partial justification of such approach was that the purely heat convection was well studied experimentally and through mathematical modeling. The chemico-density convection in the mantle is in its nature an irreversible thermodynamic process. As the heavy fraction reserves are depleting it gradually declines and eventually must die out. That is why such convection is better studied using mathematical modeling techniques.

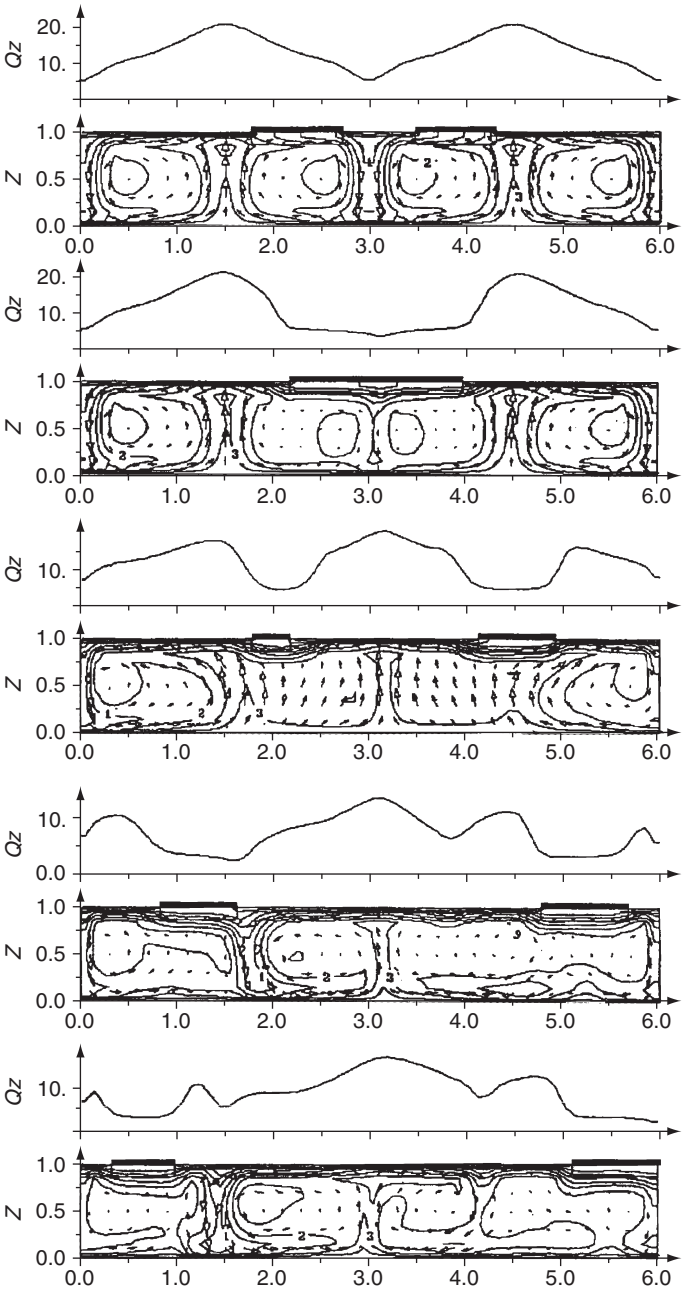


**FIGURE 6.12** 3D digital modeling of heat convection in Earth mantle (after Trubitsin and Rykov, 1995). The cross sections are for tentative times 0, 0.2, 0.5, 1.0, and 1.2 BY, drifting continents are shown at the top of the cross sections. Contours on the cross sections denote the excess temperature distribution (relative scale), the arrows are vectors of mantle flows. Curves over the cross sections are dimensionless heat flows (average and maximum heat flows for the oceans are, respectively, 75 and 120 mw/m$^2$).

The first studies of the subject were conducted as early as in 1970s. After the modern theory of the barodiffusion differentiation was developed (see Section 4.4), a possibility appeared to model the chemico-density convection based on more realistic concepts of the physical process of differentiation and using more sophisticated mathematical approaches.

The new technique (Monin et al., 1987a,b) utilized the spherical coordinates but, due to the computing power limitations at the time, was limited to axis-symmetrical options and actually studied only the two-dimensional convection.

Assigned in the models were the concentrations $C(r,\theta,t)$ of the core matter and $C_{Si}=1-C$ of the light silicate matter. Here, $r$ is the current radius-vector ($r_c \le r \le$); $r_c$ is the core radius; $R$ is the Earth's radius; $\theta$ is the polar angle or the addition to the latitude $0 \le \theta \le \pi$. The equation of state $\rho(p,T)$ for each component was calculated using the technique published in (Naimark and Sorokhtin, 1977a). The total density of the mantle matter was found as:

$$\rho = \left[\frac{C}{\rho_c} + \frac{1-C}{\rho_{Si}}\right]. \tag{6.8}$$

The mantle matter and its components were treated as uncompressible liquids as the compressibility was taken into account by the assignment of the equation of state $\rho(p,T)$. In this case

$$\text{div } \vec{u} = 0, \tag{6.9}$$

where $\vec{u} = \vec{u}\ (r,\theta,\lambda,t)$; $u_r$, $u_\theta$, $u_\lambda$ are the vector of velocity and its components; $\lambda$ is longitudinal angle; $t$ is time. The viscous liquid equation was assigned by the Navier–Stokes equation:

$$\rho \frac{d\vec{u}}{dt} = \rho\vec{g} - gradp + \eta\nabla^2\ \vec{u}\ , \tag{6.10}$$

where $\vec{g}$ is the vector of the force of gravity; $p$ is pressure; $\eta$ is dynamic viscosity of the medium; $\nabla^2$ is the Laplace operator in spherical coordinates; $\rho$ and $\eta$ are assigned by the matter equations of state $\rho=\rho(r,T)$ and $\eta=\eta(r,T)$ presented in Figs. 2.9 and 2.20. If $\varphi$ is the longitudinal angle then

$$r^2\nabla^2 u = \frac{\partial}{\partial r}\left(r^2\frac{\partial u}{\partial r}\right) + \frac{1}{\sin\theta}\frac{\partial}{\partial\theta}\left(\sin\theta\frac{\partial u}{\partial\theta}\right) + \frac{1}{\sin^2\theta}\frac{\partial^2 u}{\partial\phi^2} = 0. \tag{6.10'}$$

In order to close the system of equations defining the mantle convection it is necessary to add to the Eq. (6.10′) one more equation, the equation of the core matter balance in the mantle

$$\frac{\partial C}{\partial t} + u_r\frac{\partial C}{\partial r} + \frac{u_\theta}{r}\frac{\partial C}{\partial\theta} = \frac{1}{r^2}\frac{\partial}{\partial r}\left(r^2 D\frac{\partial C}{\partial r}\right) + \frac{1}{r^2\sin\theta}\frac{\partial}{\partial\theta}\left(D\sin\theta\frac{\partial C}{\partial\theta}\right), \tag{6.11}$$

where $D$ is the diffusion factor.

The chemico-density convection modeling technique was mostly developed by Monin, Seidov, and Sorokhtin (Monin et al., 1987a,b) who also conducted first experiments. The results follow.

Under the techniques, the high-density core matter concentration, major Earth's parameters, and spherical coordinates were assigned in the model. Besides, for each of the components were assigned the matter's equations of state defining the correlation of its density versus pressure and temperature. The mantle matter and its components were treated as uncompressible liquids (the matter compressibility was indirectly taken into account in its equations of state). The mantle viscosity was assigned from most likely distributions (see Section 2.9), the initial temperature distribution was assumed adiabatic. All mathematical details are published in (Monin et al., 1987a,b). In order to close the system of equations defining the mantle convection one more equation was added, the equation of the core matter balance in the mantle. The boundary condition was the condition of the convecting matter "sliding' without friction on the mantle base and its surface.

The composed equations were being solved over the uniform grid for the radius and polar angle: with the step for the radius of 175 km and for the angle of 3° (total of 1037 grid nodes). The step for the time was selected on condition of the iterations stability and, converted to the geological time, was 250,000 years. At the initial time, a uniform high-density fraction field was assigned with random fluctuations on the order of 0.001 (which corresponded with the density field disturbances about 0.003 $g/cm^3$).

Modeling of the chemico-density convection in spherical coordinates was complicated in regards the model symmetry with respect to the polar axes. Taking that into account, Sorokhtin modeled such convection in cylindrical coordinates but with a replacement of the cylindrical coordinates divergence parameter (inversely proportionate to the current radius) by the coordinates divergence parameter in spherical coordinates (inversely proportionate to the squared current radius). The resulting model is equivalent to the spherical model but describing the convection in the equatorial plane (Fig. 6.13).

The conducted experiment showed that the chemico-density convection is indeed unstationary and continuously changing its structure. The convective structure changes from the single-cell to the dual-cell (sometimes even more complex) and always returns to the single-cell structures. When rescaled to the Earth's timescale, the period of a complete convection

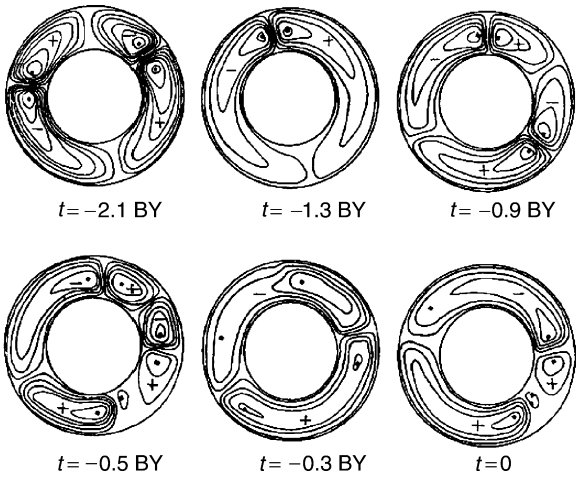


**FIGURE 6.13** Digital modeling of flow function fields for chemico-density convection in cylindrical coordinates but with the spherical divergence factor, analog of the equatorial cross section in spherical coordinates (after Yu. Sorokhtin).

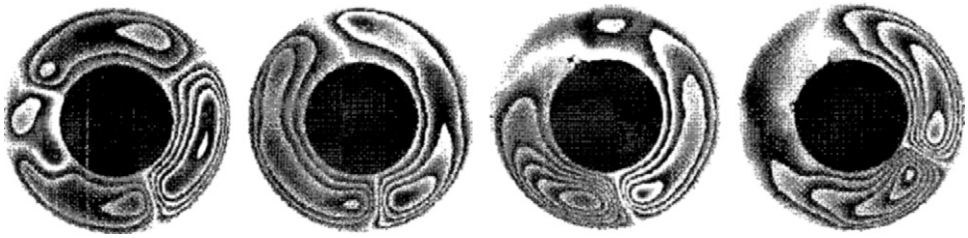

**FIGURE 6.14** Digital modeling of thermochemical convection in the mantle (Kotelkin and Lobkovsky): the high-density Earth core is in black, the mantle displays convective flows (half-tones are the flow intensity).

megacycle in the experiment was about 1 BY (it is close to 0.8 BY in actuality) and is clearly marked by the formation moments of the old supercontinents Monogaea, Megagaea, Mesogea, and Pangaea (see Figs. 9.2 and 9.10).

Recently, Lobkovsky and Kotelkin (2000) modeled the thermochemical convection in a round cross section. Despite that, their results for Proterozoic and Phanerozoic are also quite expressive (see Fig. 6.14).

There are in the mantle boundaries with the endothermic phase transitions. One such boundary at the depth of 670 km was mentioned in Section 6.2. They can complicate the convection structure but at the actual d$T$/d$p$ temperature gradients for such boundaries they do not result in the emergence of a stable "double-stage" convection. Thus, the common and now fashionable ideas about the double-stage convection functioning in the mantle are not supported by theoretical calculations and modeling. On the contrary, all such studies convincingly support a single convection for the lower and upper mantle, with a good stirring of the mantle matter.

Of course, the mantle convection experimentation is schematic. It would be unreasonable to expect from it the total match with the observed tectonic phenomena, even with the application of the scaling factors. One of the most important modeling results is a proof of the nonstationary nature of the chemico-density convection (which well explains the changes in the Earth's evolution tectonic regimes) and the cyclicity of this process. Demonstrative in this respect is the identified capacity of the chemico-density convection to create from time to time single-cell convective structures with their subsequent decomposition into more complex structures. This phenomenon is the reason for temporary aggregations in the Earth's evolution of previously separated continents (Monogaea, Megagaea, Mesogea, and Pangaea) into the unified supercontinents. It was also shown that not only the supercontinents formed at the periods when single-cell structures emerged in the mantle but also the tectonic activity bursts occurred (see Fig. 6.8). All these coincidences were obtained by inserting into the model either the totally independently derived parameters (such as the mantle viscosity and iron-oxide concentration in it) or earlier determined parameters based on the theory of the mantle matter barodiffusion differentiation. That is why these coincidences cannot be just accidental: they confirm once again that the mantle is indeed involved in unified chemico-density convection.

Especially, well studied based on paleomagnetic and geological data are the continent merging into the Wegenerian Pangaea and its subsequent split and the centrifugal

continental drift continuing till the present. These data are so convincing and well illustrated by numerous similar reconstructions that today there are no doubt about it.

The purely heat convection is controlled by heating the mantle matter from below (by the core heat) and by its cooling from the surface (by sinking the oceanic lithospheric plates into the mantle). Such convection should result in the emergence in the mantle of a Benard-type stationary convection with the unchanging positions within it of the ascending and descending flows. On a planet like this, the continent positions would be set and tied-in with the descending flows. On the periphery, they would be surrounded by subduction zones. Only the heat convection excited by the radioactive heating of the mantle matter itself (as assumed by Trubitsin and Rykov), similar to the chemico-density convection, is radically nonstationary. To initiate it at the observed intensity of the tectonic processes would require about 10 times the content of radioactive elements in the mantle compared to their most likely current concentration. As previously mentioned, the present-day contribution from the radiogenic energy into the Earth's endogenous energetics does not exceed 10% (see Sections 5.2 and 5.5). Besides, with the radiogenic mechanism controlling the tectonic activity the mantle overheating in Archaean and a drastic transition from the Archaean tectonics to tectonics of the lithospheric plates in Proterozoic and Phanerozoic would be impossible to explain because under the radiogenic mantle heating such transition must have been smooth.

Thus, digital modeling of the chemico-density mantle convection was another convincing evidence in the chain of proofs that the global evolution of Earth and its tectonic activity are mostly controlled by the major energy process of the Earth's matter chemico-density differentiation into a high-density iron-oxide core and the residual silicate mantle. This process is still ongoing.

## 6.6 EVOLUTION OF EARTH'S TECTONIC ACTIVITY

As mentioned earlier, the writers understand the Earth's tectonic activity as the intensity of the entire gamut of geological processes deforming its lithospheric shell (including the crust) and causing any forms of magmatism within this shell. When the lithospheric plate tectonics appeared, it became clear that some measure of the movement of the lithospheric plate ensemble may serve as a demonstrative estimate of the Earth's average tectonic activity. Such measure may be represented, for instance, by the rate of the plates' relative displacement. However, it appears that the most general, convenient, and physically justified estimate of the Earth's tectonic activity is its energy measure. This energy is eventually defined by the depth heat flow $\dot{Q}_m$ released from the mantle. Indeed, any motions of the matter and its magmatic transformations, which lead to the planet's tectonic activity, are eventually converted to the heat and are lost with the Earth's heat radiation. That is exactly why the depth heat flow $\dot{Q}_m$ may be a natural measure of the Earth's tectonic activity.

As mentioned previously, the Earth's tectonic activity within a broad Early Archaean ring belt was very intense and 3.7–3.5 BY ago substantially exceeded its current level. In the middle of Archaean (around 3.2 BY ago), the Earth's tectonic activity declined somewhat with the formation of more stable oceanic plates. The lithospheric plate movement rate at that time decreased to 20–25 cm/year. The slackened tectonic activity was due to the approach of the Earth's matter zonal differentiation front to a depth of 800–1000 km

where significantly increased the difference between the metallic iron melting temperature and the Earth's geotherm (see Fig. 4.4). As a result, beginning sometime about 3.4 BY ago a substantial portion of the gravity energy released in the separation of the iron melts from the silicates began to be expended not only for the excitement of the upper mantle convection (i.e., not only for the tectonic activity) but also for heating of the underlying and still relatively cold primordial kernel of the young Earth.

In Late Archaean, during the Earth's core emergence a new and most drastic burst of tectonic activity occurred. The plate movement rate at the time exceeded 350 cm/year and at the peak reached almost 400 cm/year, which is 70 times their present-day rate.

This burst was caused by two reasons.

The first was the transition in the Earth's matter differentiation process from the metallic iron separation (in Early Archaean) to the differentiation of more abundant eutectic alloys Fe·FeO.

The second was a catastrophic process of the Earth's core separation process 2.8–2.6 BY ago. It was going with the release of a large additional energy ($5 \times 10^{37}$ erg; see Chapter 5).

The combination of these processes caused a colossal burst in the tectonic activity which left an indelible trace in the geological record of a radical reworking of almost the entire continental crust formed by that time.

Beginning in Early Proterozoic, the average rate of the lithospheric plate motion was gradually declining from 50 cm/year to its current value of about 5 cm/year although it drastically increased at the time of the tectonic activity bursts (see Fig. 6.8). The decrease in the plate motion rate will continue in the future until such time when iron oxides will migrate to the core and their reserve in the mantle is depleted. It may take 1–1.5 BY.

A first and main conclusion from the provided theory of the Earth's global evolution is a clear division of the Earth's tectonic evolution into four major and radically different stages: (1) a passive Katarchaean (Hadean); (2) a very active Archaean; (3) a moderately active (quiescent) Proterozoic–Phanerozoic; and (4) the future Earth's tectonic death.

The oldest stage (pre-geological or Katarchaean) lasted about 600 MMY, that is, from the moment of the Earth's emergence 4.6 BY ago through the start of its tectonic activity 4.0 BY ago. The endogenous tectonomagmatic manifestations were completely absent as Earth was a relatively cold celestial body, and all the matter in its depths was under the temperatures way below the melting point.

Despite that, Earth in Katarchaean was not tectonically dead.

First, its depths were gradually heated by the radioactive decay energy and the tidal interaction with Moon. That served as a preparation for the transition to the tectonically active evolutionary stages.

Second, a significant role in Katarchaean (especially in Early Katarchaean) played the tidally induced exogenous tectonics which caused swarms of very strong earthquakes. This stage may be called a crypto-tectonic one.

First clear and intense endogenous tectonomagmatic events are reliably recorded only in the beginning of Archaean 3.8 BY ago (Murbat, 1980; Taylor and McLennan, 1985). The start of the Earth's tectonic activity was prepared by the radiogenic and tidal Earth's matter heating up to the appearance in the upper mantle of the primordial asthenosphere. It was followed by a drastic, maybe even "shock" activation of the tectonomagmatic activity. It occurred first, because of the "pumping" into the formed asthenosphere of the tidal energy

from the Moon–Earth interaction, and then, due to the release of the Earth's matter gravity differentiation energy (see Chapter 5 and Section 4.3).

The tidal energy "pumping" into the asthenosphere was going on mostly in the equatorial belt. For this reason, the first embryos of the continental massifs (about 40 in total) could emerge in the beginning of Early Archaean only within the near-equator areas (see Section 6.3 and Fig. 6.4). After a new and very powerful energy source (the gravity energy release under the Earth's matter zonal differentiation mechanism) began active, the tectonic activity belt was gradually broadened into higher latitudes. Conversely, the number of the continental massifs declined and simultaneously their mass was increasing.

By the end Archaean 2.6 BY ago, the tectonic movements engulfed the entire Earth and all continents merged into a supercontinent Monogaea.

During Archaean, the entire primordial matter-composed lithosphere within the expanding low-latitude belt of the hot upper mantle must have been assimilated into the mantle and completely remelted. That erased all direct traces of the Katarchaean evolution (see Figs. 4.1 and 6.15). Apparently, the only remelted and substantially changed remains of the Earth's primordial matter are the gray gneisses of the ancient Archaean complexes.

## 6.7 GENERAL PATTERNS IN EARTH'S TECTONIC EVOLUTION

As mentioned above, the most general, convenient, and physically justified estimation of the Earth's tectonic activity is apparently its energy measure. It is determined in the last analysis by the depth heat flow $\dot{Q}_m$ coming from the mantle. Indeed, any motion of the Earth's masses and magmatic transformations resulting in the tectonic activity eventually transform into the heat and are lost with the Earth's heat radiation. That is exactly why such depth heat flow $\dot{Q}_m$ may be a natural measure of the Earth's tectonic activity.

As we strived to show above, the tectonic activity in Archaean was most likely restricted to within a latitudinal Earth's belt whose size was gradually increasing with timer. Only by the end Archaean, at the time of the final core separation, the tectonic activity covered the entire planet (see Fig. 4.3). The so defined "local" tectonic activity in Archaean is represented by curve 2 in Fig. 5.16. As the diagram indicates, the Earth's tectonic activity within the Early Archaean latitudinal ring belt was quite intense. During the period 3.7–3.5 BY ago, it exceeded the modern level by the factor of 7 or 8.

In Mid-Archaean, such activity declined to approximately its present-day level. However, a new and most intense burst of the tectonic activity occurred in Late Achaean. It was about 17 times its present level. The explanation is that the Earth's matter zonal differentiation converted from the metallic iron separation to that of its oxide (see Section 4.3), and also the core separation process begun about 2.8 BY ago. Both tectonic bursts in Archaean correlate with the changes in the upper mantle surface temperature during the episodes of its Archaean overheating (see Fig. 4.5).

The provided scenario of the Earth's core separation (see Section 4.2 and Fig. 4.1) and the corresponding empirical data (see Sections 4.1 and 4.7) lead to an important conclusion already mentioned in Chapters 3 and 4. During the first 600 MMY of its existence, Earth was a relatively cold and tectonically passive planet. The tectonic activity began only after the core started to separate about 4 BY ago and only within a narrow equatorial belt. Therefore, in Katarchaean 4.6–4 BY ago the entire surface of Earth was composed of the

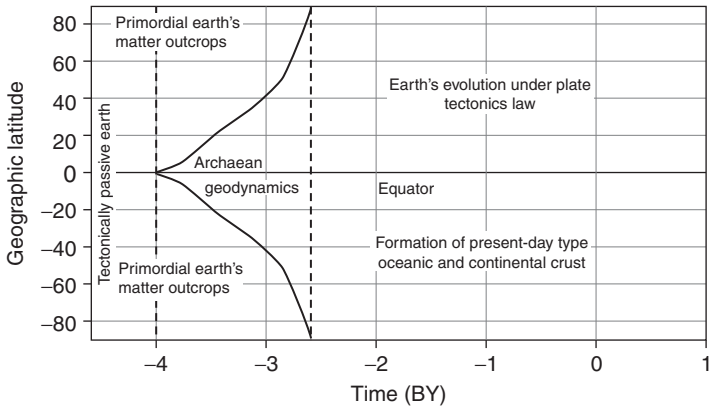


**FIGURE 6.15** Evolution of tectonic environments on Earth: in Katarchaean (4.6–4 BY ago) Earth was a tectonically passive planet. Tectonic activity began only in Archaean after the start of Earth core separation about 4 BY ago within a narrow equatorial belt. By end Archaean, about 2.6 BY ago, this belt expanded over the entire Earth. During entire Archaean a substantial part of the Earth surface was yet composed of the primordial Earth matter. Granite–greenstone belts are typical of Archaean geodynamics. After the separation of Earth core about 2.6 BY ago Earth evolved under the lithospheric plate tectonics laws with the formation of the modern-type oceanic and continental crust.

primordial undifferentiated Earth's matter overlain by a small-pore ultramafic regolite. The regolite was preserved from the times of the intense planet bombardment by the falling planetesimals (see Fig. 6.15). Beginning 4 BY ago, the tectonic zone gradually broadened. Still, during entire Archaean up to 2.6 BY ago a substantial portion of the Earth's surface was still composed of the primordial matter and of the overlying regolite.

The oceanic crust formation in Archaean occurred under the mechanisms not unlike the current ones except that the oceanic plate spreading (which in this case is better to call sheets) was much faster, many meters annually. The Archaean oceanic sheets remained thin and composed of only light derivatives of the Archaean mantle (the basalt and in part komatiite lavas). These were incapable of sinking into the denser mantle. That is why there was no subduction zones in Archaean, and the compensation of large areas of the forming oceanic sheets occurred in their pile-up zones above the descending mantle matter flows (see Fig. 7.5). Subsequently, due to the secondary remelting of the oceanic sheets, embryos of the Archaean continents began forming in the pile-up zones (see Fig. 6.4). A powerful single-cell convective structure emerged in the core separation at the very end Archaean. It gathered and welded together all Archaean continental crust blocks existing by that time into a single Archaean supercontinent (see Fig. 4.1E). That is the way the first supercontinent in the earth's evolution was formed. It was Monogaea (see Fig. 9.2). The Monogaea emergence 2.6 BY ago completed the Archaean era, the first stage of the Earth's geological evolution.

Earth core separation at the end Archaean caused a significant lowering in Earth's average tectonic activity (see Fig. 5.16). After that, the oceanic plate formation rate drastically declined, and the duration of their life and cool-down on Earth surface increased no less drastically (see Fig. 8.11). The cooled-down oceanic plates became denser than the mantle matter and could sink into the mantle's depths. The subduction zones emerged. After that, Earth's tectonic evolution followed the lithospheric plate tectonics laws. Still, during approximately 100–200 MMY (between 2.6 and 2.5–2.4 BY ago), the Archaean tectonics continued to have

some effect. Thus, this relatively brief period in Earth's evolution may be described as the transition from the Archaean geodynamics to the Phanerozoic lithospheric plate tectonics.

To repeat again, the core separation 2.6 BY ago predetermined the transition in Earth's tectonic evolution from the Archaean geodynamics to the post-Archaean tectonics of the lithospheric plates.

## 6.8 MEMBRANE TECTONICS (CRITIQUE OF "HOT SPOT" HYPOTHESIS IN THE MANTLE)

Discussing the issue of the mantle convective mass exchange it is impossible not to critique the notion of the so-called"hot spots." It was first proposed by Wilson (1963) that there are "hot spots" in the mantle above which Hawaiian-type volcanoes arise. Later, Morgan (1971, 1972) tried to provide a theoretical substantiation of the idea which unexpectedly became very popular among geologists. According to Morgan, there are hot streams—plumes—in the mantle. They rise from the lower mantle level to the base of the lithospheric plates and burn-through them. The result is the interplate volcanoes. Burke and Wilson (1976) counted 122 such hot spots on Earth. It was assumed that the "hot spot" positions were as if fixed relative to the lower mantle. Numerous publications attempted to determine the "absolute" lithospheric plate displacements based on the volcanic chains which ostensibly remained on the Earth's surface as the plate "burn-through" traces after their movements over such hot spots.

This concept has no more physical justification supported by the geological data than the "expanding Earth" idea.

First, the geological data.

Usually, the "hot spot" associated volcanoes erupt alkaline basalts. It is known (Green and Ringwood, 1967a,b) that such basalt melt-out in the existence domain of the spinel pyrolites (lherzolites) at a sub-solidus temperature. This means that the alkaline basalt magmas are not the hot but maximum-cooled melts. Such melts can exist only directly under the base of the lithosphere at a low degree of the mantle matter partial melting. The pykrite basalts or even the komatiites should have been melted out at high temperature, much higher than the mantle matter solidus, that is, at high degree of partial melting of the pyrolite. This is also supported by the basalt magmas fraction crystallization experiments. Indeed, the alkaline basalts form only as the residual liquid at the cooling and crystallization of the source olivine-basalt magmas under elevated pressure (Joder and Tilly, 1962) corresponding to the $P$–$T$ conditions directly underneath the mature oceanic plates with the age of 20–120 MMY and thickness of 40–80 km.

The alkaline lava temperature of the "hot spot" volcanic eruptions is usually 1100–1200 °C, whereas the mantle's adiabatic temperature normalized for the surface is 1320–1330 °C. Its intersection with the experimentally determined mantle matter melting temperature occurs at a depth of about 80 km (see Fig. 2.18). Therefore, the basalts may have been generated only within this depth limit.

Assuming the magmatic streams—plumes—were generated in the lower mantle as suggested by the proponents of the "hot spots" hypothesis (let us say 1000 km, and this is just the upper portion of the lower mantle), then that is the very depth where the source melt nodes would have emerged. The silicate melting temperature at these depths reaches

3500 °C. So, it is easy to determine that at the surface these melts would have the temperature of approximately 2100 °C, that is, the melts would be overheated by 800–1000 °C compared to the actual temperature of the basalt lavas. This did not happen even in Archaean when the mantle was overheated by 300–500 °C and generated profuse komatiite melts.

All attempts to seismically identify magmatic streams of overheated matter plumes in the deep mantle underneath the Hawaiian Islands were unsuccessful. No anomalies were discovered within the sublithospheric mantle. Broun and Mussett (1981) note that seismic studies did not confirm the existence of plumes in the mantle.

The "hot spot" hypothesis was developed as an explanation of the Hawaiian volcanism. And it contradicts the Hawaiian volcanic manifestations.

It was established based on geological data that the main volcanic phase that formed the island of Oahu ended about 3 MMY ago. Since then, the island was eroded, peneplanation planes and deep valleys were formed, and no volcanic activity occurred for more than 2 MMY. However, in Quaternary, a few hundred thousand years ago, the volcanic activity flared up again and ended only 30,000 years ago after having built fresh eruptions and volcanic buildups of the Honolulu series.

Over the 2 MMY-long interruption in the volcanism, the earlier existing magmatic channel must have been completely crystallized and plugged. Why then that new short-lived burst of volcanism on the Oahu Island? Maybe because of a new lithospheric "burn-through" above a new "hot spot"? The old one continued to "operate" at the same time on the southern island, Hawaii, whereas the island of Oahu moved over this interval of 2–3 MMY 200–300 km northwest of the location of active volcanism. We believe that such short impulse of the repeated volcanism of the Honolulu series (after a long interruption in the volcanic activity) may only be explained by the repeated formation of a fissure in the lithospheric plate under the island of Oahu.

We now briefly discuss the physical grounds of the "hot spots."

First, this concept is completely incompatible with the convecting mantle concept which is the basis of well-substantiated theory of the lithospheric plate tectonics. In the convecting mantle, whether it is the heat or even more so the chemico-density convection, the temperature distribution is always close to the adiabatic one with the normalized surface temperature about 1320–1330 °C. Thus, no juvenile melts can exist in such mantle deeper than 80 km (i.e., deeper than spinel lherzolite to garnet lherzolite transition boundary, see Fig. 2.18). This prohibition covers the lower mantle even more. Besides, the matter in the convecting mantle is continuously stirred. Any suggestion of the existence in its depths of some locally overheated areas (to 1000–2000 °C) is an impossibility. It would require natural radioactive generators with the avalanche concentrations of radioactive elements. These elements are scarce in the mantle and more or less uniformly distributed, and their contribution to the endogenous energy processes does not exceed 8–10% (see Section 5.2).

Some may object: what about the kimberlite, lamproite, carbonatite, and alkali-ultramafic magmas generated deeper than 80 km, up to 250 km? First, the temperature of such magmas does not exceed 1000–1100 °C. Then, the origin of this exotic melts may easily be explained by the remelting of the Precambrian water-saturated and iron oxide-rich carbonate–silicate oceanic deposits sucked-in to those depths underneath the Archaean continents through the ancient subduction zones (Sorokhtin et al., 1996, 2004). The possibility of sucking-in iron-rich (heavy) deposits to such depths was shown by Monin and Sorokhtin

(1986), and it is known that the water-saturated deposits melting temperature even at the pressure of 50–70 kbar does not exceed 600–900 °C (see Chapter 10 for more detailed discussion of the mechanism of the kimberlite and lamproite magma formation).

In order for the "cold" crystalline lithosphere to be melted-through, a sufficient heat must be supplied to its base. If the "burn-through" of a narrow magmatic channel is done by the same magma that is fed into the volcanic channel, then the initial temperature of such magma must exceed the asthenospheric temperature by the same 1000–1500 °C, which was shown above to be completely impossible. Hydrodynamically, narrow plumes cannot be generated by the convective mass exchange in the mantle. For this to happen, its matter should have been overheated by thousands of degrees, and instead of the alkaline lavas the volcanoes positioned over such "hot plumes" would erupt only the komatiites. In actuality, the excessive heating of the ascending mantle flows is no greater than 100 °C (see Eq. 6.4).

Sometimes the following is used as a proof of the "hot spots" and the introduction of matter to them from deeper, undepleted mantle reservoirs. The proof is strontium ratios $^{87}Sr/^{86}Sr = 0.7030–0.7036$, which are slightly but still noticeably above those for the tholeiites of the mid-oceanic ridges ($^{87}Sr/^{86}Sr = 0.7027$).

This difference in the isotope ratios, however, is easily explained without the involvement of such mechanisms as the "hot spot" plumes.

Indeed, the fraction melting of the mantle matter at depths of the sublithospheric mantle under moderate pressure (7–20 kbar) and near-solidus temperatures results first of all in the melting of alkaline clinopyroxenes containing also the radioactive rubidium $^{87}Rb$. The excessive radiogenic strontium $^{87}Sr$ is transferred to the melt and accumulates in the crystalline grid of such pyroxenes (at the expense of $^{87}Rb$ decay) before a given portion of the mantle matter gets to the asthenospheric level. At lower pressures and greater mantle matter partial melting underneath the mid-oceanic ridges the calcium pyroxenes (the main carriers of strontium) are transferred to the melt to a greater degree. They "remember" the $^{87}Sr/^{86}Sr$ ratios from the previous cycle of the mantle matter melting in the asthenosphere. It occurred during the preceding convection cycle with the lower value of such ratios.

Thus, magmatism of the so-called "hot spots" turns out to be very cold and in no way associated with the deep (lower) mantle. That is why all numerous attampts to determine from the "hot spots" the absolute displacements of the lithospherix plates are built on sand.

What then is the real nature of the intraplate magmatism? The answer today is certain and unique. The intraplate magmatism shows up only when there are through-going fractures in the lithospheric shell which drain the upper layers of the asthenosphere and are filled up with the melts coming from it. Under this mechanism, the intraplate magmatism geochemistry and thermodynamics are defined only by the pressure and temperature in the sublithospheric mantle as well as by the penetration depth of the draining fissures into it. This mechanism is fully supported by most geological data and experimantal results with the pyrolite (lherzolites) melting under various $P$–$T$ conditions. It does not require any additional hypotheses. The only remaining issue is the formation mechanism of the fissures and fractures in the lithospheric shell.

Naturally, such fissures can emerge from the mantle convection flows (an example is the East African rift system) and as a result of the plate collision and the pressure form the adjacent plates (as it happens in the East Asia and the Trans-Baikal region). Such splits, however, do not create an illusion of the resting magmatic centers like the Hawaiian

volcanoes. This may be explained through the Turcotte and Oxburg (1978) hypothesis. Under this hypothesis, the lithospheric plates, while moving on the hot mantle surface, must adjust to the variable curvature of the Earth's ellipsoid of revolution. Although the lithospheric plate curvature radiuses at that change little (just fractions on one percent), their defomation causes the generation within the bodies of large plates of excessive extension or shear stresses on the order of hundreds of bars. As the asthenosphere includes liquid melts capable of filling-in the forming micro-fractures and supporting the confined hydrostatic pressure from the overlying rocks, such stresses are sufficient to completely split the lithosphere from its base to the surface.

If now a large lithospheric plate, such as the Pacific Plate, is moving from lower to higher latitudes, extension stresses must be gradually increasing in its body (Fig. 6.17). Upon reaching the breaking point, the lithospheric shell overlying the asthenospheric layer soaked with liquid basalt will split and form the fissure which will be filled up with these basalts. As a result, the basalt magmas get access from under the base of the lithosphere to its surface. First, they form sheet eruptions and then, volcanic buildups. If this mechanism is working for an extended time in the critical latitudes of about 18–20° North, a "running" fracture will open, and basalt lava eruptions will be continuously happening at its extremity.

In 1990, one of these writers (O. Sorokhtin) descended in a manned submersible vehicle "Mir" onto the Pacific Ocean floor south of the active underwater volcano Laihi (south of the Island of Hawaii) near the start of newly forming lithospheric fissure. In the submersion location, completely fresh and not covered by deposits pillow basalt lavas, in form of a sheet, directly overlay the deposits. Open fractures (gjars) were clearly visible in the center of the sheet, about a meter in size, a clear indication of the rock extension stress. The lava thickness and lava-covered area increased northwesterly and gradually turned into the foot of the young underwater volcano Laihi. We believe that the observed basalt eruptions south of the Hawaiian Islands are a unique testimony to the functioning mechanism of the Pacific Plate rupture rather than its melting-through by the "hot spot" mantle matter.

We now discuss the quantitative side of the issue to what extent the membrane hypothesis matches the real occurrences of the Hawaiian-type intraplate volcanism on the Pacific Plate. The actual parameters of the Earth's ellipsoid of revolution are the equatorial radius $R_e = 6378.16$ km and the polar radius $R_p = 6356.78$ km. Thus, the ellipsoid eccentricity is very small, $e = 1/298.3$. This enables an approximate solution to the problem of the lithospheric plates moving on the Earth's surface using only simplified models.

Let us assume a large lithospheric plate, $L$ km-wide, is moving north from the equator. In such a case, the plate's displacement may be represented by the plate's rotation around the rotation poles positioned on the equator and distanced from the central meridian by $\pm 90°$. The ellipsoid's cross section through both rotation poles and a given point at the ellipsoid's surface at the latitude $\varphi$ and longitude $\theta = 0$ is an ellipse with the large half-axis $R_e$ and small half-axis $R_\varphi$ determined by the equation:

$$R_\phi = \sqrt{R_e^2 \cos^2\phi + R^2 \sin^2\theta}. \tag{6.12}$$

In this case, the radiuses of the selected ellipsoid cross section at the plate boundaries $\theta_i = \pm L/2R$ (see Fig. 6.16) are:

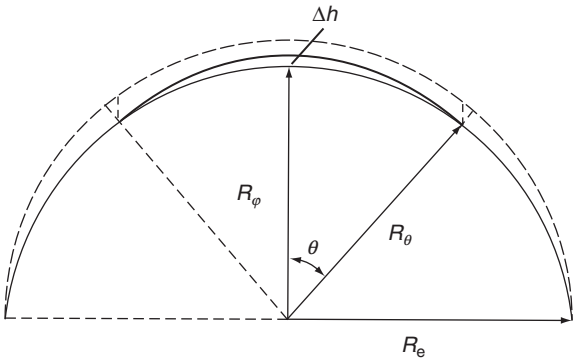


**FIGURE 6.16** Change in the lithospheric plate curvature while it moves from the equator into the high latitudes.

$$R_\theta = \sqrt{R_e^2 \sin^2\theta + R_\phi^2 \cos^2\theta}. \tag{6.13}$$

The difference between the radius "remembered" by the plate when at the equator and the radius of its cross section at the plate boundaries is $\Delta R_\theta = R_e - R_\theta$. Then the height of the arch formed by the plate in moving from the equator to the latitude $\varphi$ is

$$\Delta h = \Delta R_\phi - \frac{\Delta R_\theta}{\cos\theta}, \tag{6.14}$$

where $\Delta R_\varphi = R_e - R_\varphi$.

The oceanic lithospheric plate lies on the effectively liquid also very high-viscosity asthenosphere (i.e., Wincler's base). Thus, it is possible to estimate the extension stress in the arch's center at a hydrostatic approximation. Assuming that the plate can slip down from the asthenospheric bump formed underneath it and not balanced in the Earth's gravity field, the extension stress $\sigma$ applied to the plate is

$$\sigma \le \Delta h \Delta \rho g, \tag{6.15}$$

where $\Delta\rho = \rho_a - \rho_w$; $\rho_a \approx 3.2$ g/cm$^3$ is the density of the asthenosphere; $\rho_w = 1$ g/cm$^3$ is the oceanic water density; and $g = 980$ cm/s$^2$ is the gravity acceleration.

Calculations using Eqs. (6.14) and (6.15) show that at latitude 18° the height of the arch for the Pacific Plate absolute rigid model (not taking its elastic deformations into account) must reach $\Delta h \approx 800$ m and the extension stress $\sigma \approx -1.7 \times 10^8$ dyne/cm$^2$. These are commensurate with the long-term strength of lithospheric ultramafic rocks.

The estimate (6.15) is a maximum estimate. In the real elastic lithosphere the amplitude of the formed plate arch $\Delta h$ is much smaller than defined by (6.14). A decrease in the arch height occurs due to the plate's elastic deformations which arise under the excess weight of the uplifted rocks. Besides, it is limited by the maximum rock strength. Nevertheless, even in that case the extension stress is greater than the rock tensile strength. The point is that the lithosphere overlies the asthenosphere with its low-viscosity liquids—basalt melts capable of filling-in micro-fractures at the base of lithosphere thereby releasing the hydrostatic compression stress.

The arch under review does not have any support at the plate edges: in the west, it is diving into the mantle through the subduction zone and in the east it is just forming in the rift zones. That is why there is no the typically arch effect of compression in the Pacific Plate,

the compression which would be able to make the arch stronger. The opposite is actually observed: the plate is extending due to sliding from the asthenospheric protuberance under the arch. As soon as the extension stress exceeds the lithospheric rocks strength limit, a fracture occurs. As the plate moves into the higher latitudes, the fracture widens, and the basalt supply to the surface increases.

But the critical latitude of the fracture opening and its position in the center of the moving plate remain constant. This creates an illusion of an immovable "hot spot" and of the "fracture running from it" although in actuality it is just the permanency in the lithospheric plate destruction at critical latitudes as it is moving along Earth's ellipsoid of revolution (see Fig. 6.17).

After the split is fully developed, the lithosphere's curvature again adjusts itself to Earth's ellipsoid of revolution. Stress in the lithosphere relaxes. Basalt magmas which earlier intruded the emerged fractures completely cool down, crystallize, and solder the split plate into a monolith again. However, the extinct volcanoes remain on its surface and clearly mark the plate movement path over the critical latitude (but not longitude, and especially not over the "hot spot"!). Sometimes, the extension stresses continue to grow due to the continuing changes in the moving lithospheric plate curvature). In such a case, a new fissure can arise, and a repeated volcanism impulse can occur as it was observed in Holocene on the Oahu Island in Hawaii.

The described destruction of the Pacific oceanic plate is strongly supported by the gravity field. One particular testimony to it is a broad regional positive gravity anomaly of nearly $+10$ mgal extending northwest strictly in the central zone of the Pacific platform the equator through the Hawaiian Islands. From the west and east, the anomaly is bounded by broad gravity anomalies with amplitudes of $-5$ to $-20$ mgal (see Fig. 6.18).

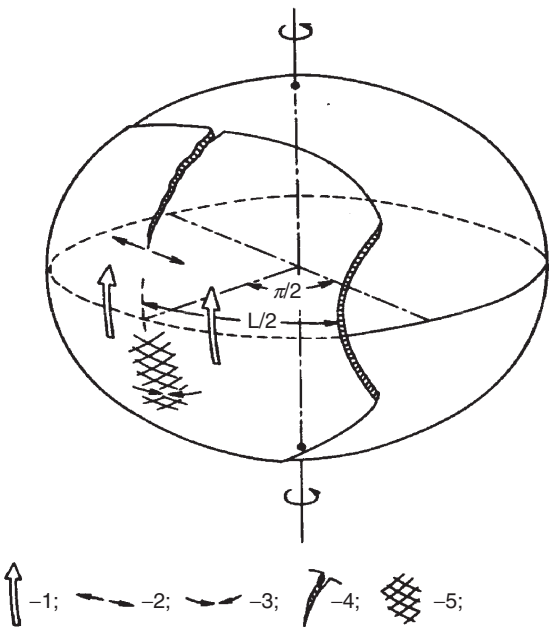


**FIGURE 6.17** Extension and split of a rigid lithospheric plate while it moves south to north on the surface of Earth ellipsoid of revolution: 1, direction of plate movement; 2, extension stresses; 3, compression stresses; 4, "Running" extension fracture; and 5, shear deformation zone in the plate compression area.

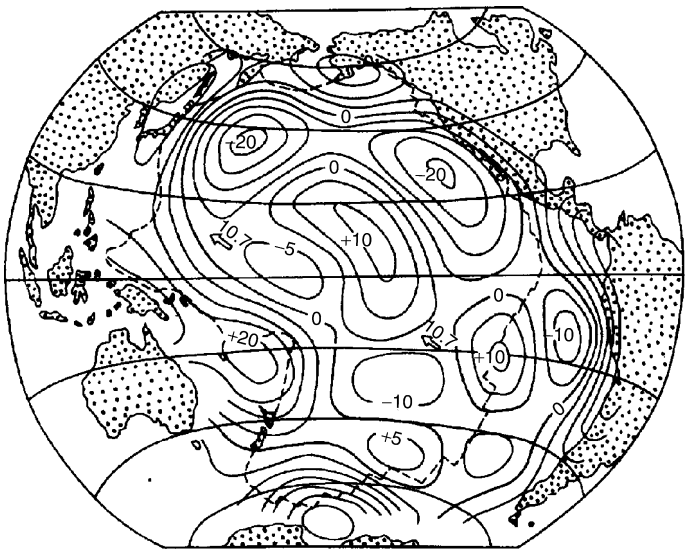


**FIGURE 6.18** Free-air gravity anomalies for the Pacific ocean averaged on the 10° grid (Geodynamic Map, 1985).

The map shows that the central Pacific Ocean gravity field completely fits the presented process of the Pacific Plate deformation. The total height of the Pacific Plate arch in the Hawaiian area, based on the gravimetric data, is

$$\Delta h = \frac{\Delta g}{2\pi\gamma\Delta\rho}, \tag{6.16}$$

where $\gamma = 6.67 \times 10^{-8}$ cm$^3$/g s$^2$ is the gravimetric constant. In the latitudes of interest (about 20°N), $\Delta g \approx 15$–30 mgal, hence, $\Delta h \approx 400$–500 m. The excessive high of this magnitude not compensated in Earth gravity field stress must arise in the body of the lithospheric plate on the order of $-1 \times 10^8$ dyne/cm$^2$ (from Eq. 6.15). Just a reminder: based on the intensity of most earthquakes and the sizes of their focal zones, ruptures in rocks occur at the excessive stress of a few units per $10^7$ dyne/cm$^2$ (Magnitsky, 1965).

Therefore, the stresses generated due to the membrane effect were quite sufficient for the breakup of an oceanic plate and the emergence in it of large fissures—magma feeding channels. The width of such fissure may be determined from a relative elastic deformation of the plate. Indeed, even before the rupture of the lithospheric shell, elastic extension deformations are generated within it: $\varepsilon = \Delta L/L$. They are defined by Hooke's law $\sigma \, E\varepsilon$, where $E$ is Young's modulus. Based on the seismic P-wave velocities $v_P \approx 8.1$ km/s and S-wave velocities $v_s \approx 4.2$ km/s, Young's modulus in the lithosphere is approximately $E \approx 1.8 \times 10^{12}$ dyne/cm$^2$. After the split formed and far from its vortex the fissure width will be

$$DL \approx L\sigma/E. \tag{6.17}$$

It follows from Eq. (6.17) that if the fracture formation in the Pacific Plate indeed begins somewhere around 18°N (near the location where the first indication of the fracture formation was observed), its width at the latitude of the Hawaii Island (20°N) may reach 1.3 km.

This is quite sufficient for extended feeding of the major volcanoes such as Kilauea and Mauna Loo on the Hawaii Island. South of the Hawaii Island is another young underwater active volcano Loihi. When observed in 1990 it was not active but all lava flows were fresh, and intense hydrothermal activity was going on (Sorokhtin and Sagalevich, 1994). We believe that as the Pacific Plate is moving north, in about 1–2 MY a new volcanic Island Loihi with active volcanoes will emerge south of Hawaii Island.

As follows from the membrane tectonics hypothesis, in the southern Pacific depression where the lithospheric plate is moving from the high southern latitudes to the low latitudes, a flat negative free air gravity anomaly is located over the center of the plate surrounded on the periphery by positive anomalies. The total anomaly amplitude is approximately 30 mgal. Therefore, the relative amplitude of the plate depression there also reaches 330 m, and the compression (and shear) stresses reach $+70$ bar.

In the southern hemisphere, when the plates are moving from the high to low latitudes, latitudinally directed compression stresses emerge in them. As a consequence, the orthogonal system of shear deformations is generated, oriented at 45° to the direction of the main compression stresses. Usually, isolated channels appear in the nodes of the shear deformation grid (at the intersection of strike-slip faults). Volcanic eruptions occur through these channels and create groups of volcanic islands. As in the previous case, these islands form mostly on the critical latitudes (not the longitudes!). On the Pacific Plate, for instance, archipelagos of such islands emerge at approximately 25–30°S, and always gravitate to the weak zones of transform faults. At the same latitudes, numerous volcanic islands emerged in the middle of Cretaceous. In Late Cretaceous, they turned into the flat-crested volcanic mountains—guyots (Bogdanov et al., 1990). By now, all these guyots moved to the northern hemisphere.

The quoted calculation examples show that the stresses emerging in the Pacific Plate due to the membrane effect are sufficient to cleave the plate and to enable the emergence in it of large fissures—feeding magma channels. Naturally, such wide fissures are excellent feeding channels for the basalt magma ascending from underneath the split lithosphere onto its surface. This is an explanation of the Hawaiian-type intraplate volcanism.

With time, the basalt magma filling-in the fissure must cool down and crystallize as gabbro. It may happen that upon total crystallization of the basalt melts within the feeding channel the lithospheric plate will again be soldered at some latitude $\varphi$ into a single-elastic shell. This time, it will acquire the curvature of Earth ellipsoid of revolution at the same latitude $\varphi$. Therefore, in calculating new stresses arising within the moving plate at higher latitudes it is necessary to rely on the parameters of the cross section through latitude $\varphi$ and both poles of the plate rotation rather than of the equatorial cross section.

Based on the map of gravity anomalies displayed in averaged format in Fig. 6.18, a complete restoration of the pacific plate integrity occurs only on latitudes near $\varphi \approx 25$–30°N. In this case, by the time the plate moved to a latitude of about 40°N the stresses close to the lithosphere strength (about to 47 bar based on gravity data) again accrue in its body. As we know, the Pacific plate did not split the second time, probably because of a rapid stress release due to decreased plate's linear dimensions in the northern Pacific. It cannot be excluded nevertheless that a relatively young Emperor's Trough structure on the ocean floor formed just due to the development of the initial stages of plate extension which did not reach its total rupture.

Thus, the quoted estimates show that, despite the smallness in the eccentricity of the Earth revolution ellipsoid, the membrane effect associated with deformations of the lithospheric plates moving on its surface is quite noticeable geologically and may cause ruptures in the large plates. Subsequently, the plates restore their integrity through the cooling and crystallization of magmas filling the faults. However, the scars remain as the chains of extinct volcanoes. They were active long time ago at the 18–20° latitudes and now clearly mark the traces of "running" cracks in the moving plates.

In the same way, a "running" fracture in the body of the Pacific Plate left an indelible trace in the form of Hawaiian Archipelago and underwater buildups of the Hawaiian and Emperor Ridges. These ridges and islands, however, have no traces of the so-called "hot spots."

Perhaps, another example of the membrane tectonics is the Whale Ridge in the South Atlantic.

CHAPTER

# 7

# Evolution of the Crust-Formation Processes in Earth's History

## 7.1 GENERAL PATTERNS OF OCEANIC PLATE FORMATION

The oldest stage of Earth's formation (the pre-geological or Katarchaean stage) lasted approximately 600 MMY from the moment of Earth's emergence 4.6 BY ago through the beginning of its tectonic activity in Early Archaean, about 4.0 BY ago. Earth at that time was a relatively cold celestial body. All matter within it was at temperatures way below its melting temperature. There was no tectonomagmatic activity.

Nevertheless, Earth during Katarchaean was not a tectonically dead planet.

First, its insides at that time were gradually warmed up by the radioactive element decay energy and by the energy of tidal interaction with the Moon. These events were preparing the conditions for Earth transitioning to tectonically active evolution. Second, the exogenous tectonics of the tidal origin played a significant role in Katarchaean (especially in Early Katarchaean). This evolutionary stage may be called the crypto-tectonic stage.

First clear and intense manifestations of the endogenous tectonomagnetic activity on Earth are reliably identified in the beginning of Archaean close to 3.8 BY ago (Murbat, 1980; Taylor and McLennan, 1985). The beginning of Earth's tectonomagmatic activity was prepared by the radiogenic and tidal heating of the primordial Earth's matter to the temperature when the primary melts appeared within the upper mantle. That was followed by a drastic and maybe even "shock" activation of the tectonomagnetic activity. First, it happened due to "pumping" into the then formed asthenosphere of the tidal energy from the Moon–Earth interaction. Later, it proceeded due to the energy release from gravity differentiation of Earth matter (see Section 4.3 and Chapter 5).

Rapid overheating of the asthenosphere with almost complete melting of its matter resulted at the Katarchaean/Archaean time boundary in a no less drastic thinning of the overlying lithosphere. The primary lithosphere at that time was rich in iron and its oxides (Fe≈13% and FeO≈24%). Thus, its density was quite high ($\rho_o \approx 3.9$ g/cm$^3$), much higher than the density of already differentiated young asthenosphere ($\rho_a \approx 3.3$–$3.4$ g/cm$^3$).

*Developments in Earth and Environmental Sciences*, Volume 10
DOI: 10.1016/S1571-9197(11)10007-5

Because of this, the primary lithosphere above the Earth's matter differentiation zone must have been sinking into the melted upper mantle and been completely remelted there.

The differentiation zone, however, expanded only gradually and covered the entire Earth only by end Archaean (see Figs. 6.15 and 7.4). Therefore, during entire Archaean the primordial Earth's matter was present on the surface and was overlain by a moonlike porous ground (regolite). As the zone of tectonomagmatic activity expanded, all this primordial matter was totally destroyed and did not get into the geological record.

Specifics of tectonic processes in Archaean were formed by "pumping" of the tidal energy into the asthenosphere mostly within the Earth's equatorial belt. That is why first marine basins and embryos of the continental massifs (in total, about 40) could emerge in the beginning of Early Archaean only in the equatorial areas (see Figs. 4.3 and 6.4).

Later, a new powerful process began, that is, the gravity energy release under Earth's matter zonal differentiation mechanism. After that the Earth's tectonic activity belt began to broaden engulfing ever higher latitudes. On the contrary, the number of the emerged continental shields was declining and the shields increased in their mass. By end Archaean 2.6 BY ago, the entire Earth was involved in tectonic movements. All emerged continents merged into a single supercontinent Monogaea.

For this reason during almost entire Archaean, in addition to the emergence of new oceanic crust areas and embryos of the future continents, areas of Earth's primordial surface were preserved. They were covered by a thick regolite layer whose composition was that of primordial Earth's matter.

With this in view, and considering that nearly 70% of the continental crust formed in Archaean, and only 30% during the subsequent epochs (Taylor and McLennan, 1985), it was possible to estimate the oceanic crust area increase in Archaean and its further evolution in Proterozoic and Phanerozoic (see Fig. 7.4).

As a first approximation, average volume of the basalt eruptions on the ocean floor is proportionate to the heat flow through it. The conclusion is that the basalt eruption thickness in Archaean $H_b \sim \dot{Q}_m$ could have reached significant values. We assume that the basalt layer thickness in the present-day oceanic crust is approximately 2 km. Then we find that in Early Archaean it could have reached 9 km and in Late Archaean, greater than 32 km.

The mass of the erupting basalts at that time was restricted by the depth at which the mantle matter began melting (Fig. 7.1), and the thickness of the consolidated layers (analogs) of the oceanic crust, by the surface cooling, and by the oceanic water penetration depth into the basalts. Our estimate is that in Archaean their thickness was nearly 4 km.

In mid-Archaean about 3.2 BY ago, the thickness of the consolidated sheets exceeded the basalt layer thickness and reached 11 km. In Late Archaean, it declined to 8 km and declined even further in Proterozoic when the oceanic crust (together with the gabbro layer) gradually got from 6 to 4 km (Fig. 7.1).

The quoted considerations lead to important geological conclusions.

First, there could not be any subduction zones in Archaean. The oceanic plate compression was compensated by their piling-up and obduction over the continental plate margins (see Fig. 7.5).

Second, plate subduction zones could appear only in Proterozoic about 2.5 BY ago. Therefore, Archaean tectonic evolution was going under the mechanism of thin lithospheric sheets deformation. The lithospheric plate tectonics on Earth began operating only in Early Proterozoic (starting $\sim$2.5 BY ago).

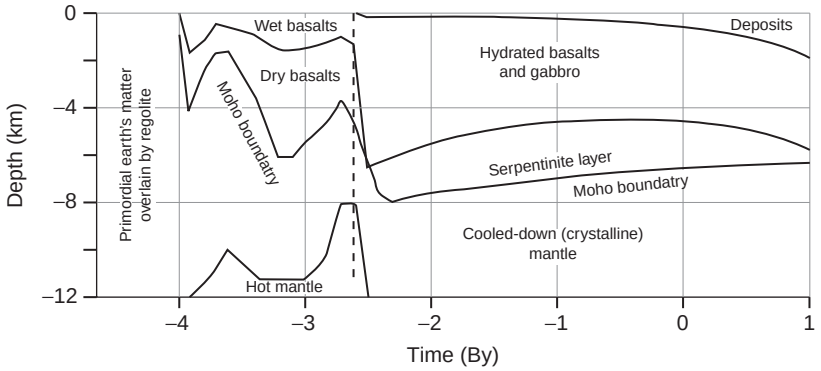


**FIGURE 7.1** Generalized model of the oceanic crust evolution.

Figure 7.1 displays an evolutionary model of the oceanic crust structure. As we see, the oceanic crust was substantially basaltic in Archaean, with only a thin layer of overlying sediments. At the times of the maximum upper mantle overheating (see Fig. 4.5), the crust bedrock composition became basalt–komatiite. Contrary to this, in Proterozoic and Phanerozoic the consolidated oceanic crust acquired the modern three-layer features: the upper basalt layer, the gabbro layer, and at the base of the oceanic crust, the serpentinite layer.

As we showed above (Section 5.4), most of the depth heat (Fig. 5.15) is lost through the oceanic plates. Presently, this fraction is 92%, and in the past geological epochs it was even greater. So, it may be assumed that after the Earth's endogenous tectonic activity arose, the parameter $\dot{Q}_m$ described, first, foremost and always, the oceanic lithospheric plate formation and destruction regimes.

Average heat flow through the ocean floor is approximately equal to the $\bar{q} = \dot{Q}_m/S_{oc}$ ratio and in the inverse proportion with square root of average life of the oceanic plates $\bar{q} \propto 1/\tau = \sqrt{u/S_{oc}}$. Here, $u$ is average rate of the oceanic plate formation (km$^2$/year) and $S_{oc}$ is total area of the oceanic plates (km$^2$). It follows from this that the average rate of the oceanic plate formation is in direct proportion with $u_1 \sim \dot{Q}_m^2/S_{oc}$ ratio (Sorokhtin and Ushakov, 1993). The heat flow through the oceanic crust was estimated in Section 5.5 by Eq. (5.23′), and also is shown in Fig. 5.15, curve 1 in Archaean and curve 4, thereafter.

We assume that the average rate of the oceanic plate formation is approximately 3 km$^2$/year (or about 5 cm/year: the length of all oceanic rift zones is 60,000 km). We also assume that the oceanic plate area in Archaean was gradually increasing together with broadening of the low-latitude tectonically active belt. Based on these, it is possible to estimate average rate of the plate formation during the past geological epochs (see Fig. 7.2).

The diagram shows that the first substantial burst in Earth's tectonic activity occurred in Early Archaean when the iron zone differentiation mechanism became operational.

At that time, the oceanic plate formation rate reached 40–50 km$^2$/year, that is, it was 16–20 times higher than the current rate. The plate formation rates were so high in substantial part due to the fact that their areal extent in Early Archaean was small, so the heat flow density through them was quite significant.

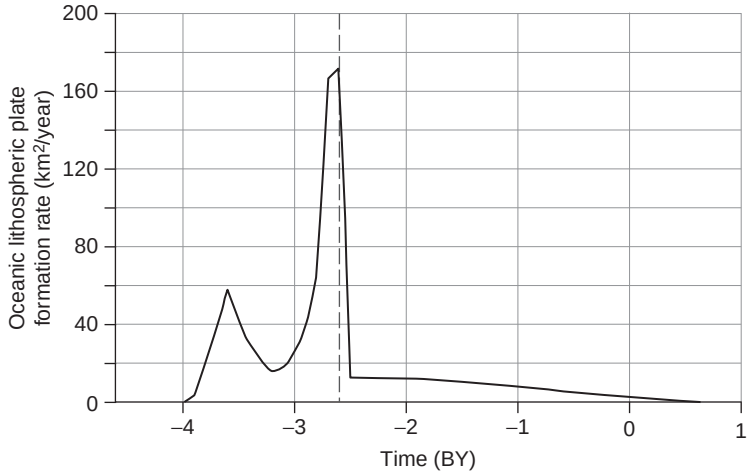


**FIGURE 7.2** Average rate of the oceanic lithospheric plate formation (present-day rate is approximately 2.6 $km^2$/year).

In mid-Archaean 3.2 BY ago, a significant weakening in Earth's tectonic activity occurred with the formation of more stable oceanic plates. Then, the lithospheric plate motion velocity declined to 20–15 cm/year. The explanation of this slackening was that the Earth's matter zonal differentiation front approached at that time the depths of approximately 800–1000 km where the difference between the metallic iron melting temperature and Earth's geotherm significantly increased (see Fig. 4.4). A result was that starting at that time (3.2 BY ago) substantial part of the gravity energy released in the iron melt separation from the silicates started to be expended not only for exciting of the convective movements in the upper mantle (i.e., Earth's tectonic activity) but also for heating of the underlying and yet relatively cold primordial kernel of the young Earth.

In Late Archaean, during the Earth core separation, new and most drastic burst of Earth's tectonic activity happened. The oceanic plate motion rate at the time reached 170 $km^2$/year, which is more than 50 times greater than currently.

There were two reasons for this drastic burst:

First was the transition in the Earth's matter differentiation from the metallic iron separation (in Early Archaean) to the differentiation of more prolific eutectic melts Fe·FeO. Second was a catastrophic process of the Earth core separation about 2.7–2.6 BY ago. This process was accompanied by the release of a huge additional amount of energy of nearly $5 \times 10^{37}$ erg (see Chapter 5).

The combined result of these two processes was a colossal burst in Earth's tectonic activity. It left in the geological record an indelible trace of the radical reworking of the entire continental Earth crust formed by that time.

Beginning in Early Proterozoic, the lithospheric plate advance rate was gradually declining from 13 to its present-day level of about 3 $km^2$/year ($\sim$5 cm/year). This decline will be continuing until such time when, due to the oceanic plate thickness increase and their friction one about the other, the movement completely stops. Our belief is that this will have happened about 1–1.5 BY from now.

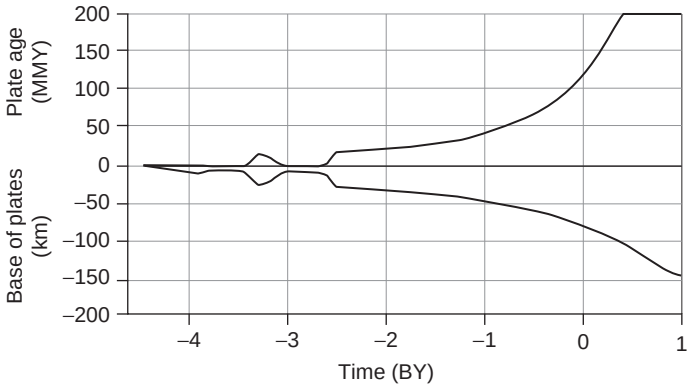


**FIGURE 7.3** Evolution of oceanic lithospheric plate life duration and average thickness.

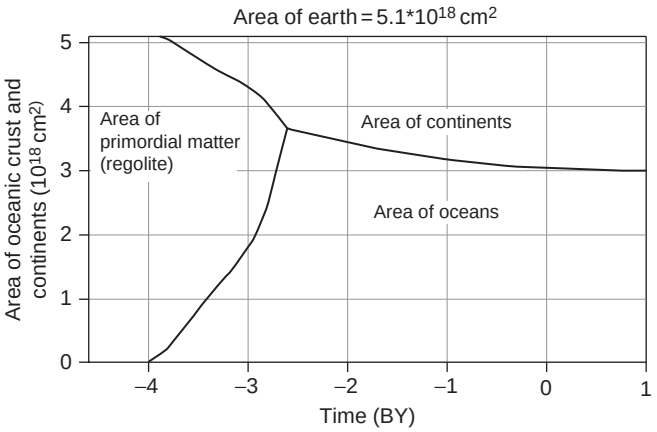


**FIGURE 7.4** Areas of the oceanic and continental crust versus time.

Figure 7.3 illustrates the evolution of average life span of the oceanic plates $\tau$ and the corresponding average thickness of the same plates.

When determining the oceanic crust (oceans) areal extent, the following needs to be taken into account. First, it is a substantial oceanic crust growth in Archaean due to the expansion of the tectonic belt from the equatorial zone in the beginning of Archaean to practically entire Earth (together with the continental crust blocks). And second, the corresponding growth in the area of the continents (see Fig. 7.4).

One of the main conclusions of the proposed theory of Earth's global evolution is a clear subdivision of Earth's tectonic evolution into four major and radically different stages: (1) a passive Katarchaen stage; (2) a very active Archaean stage; (3) a moderately active (quiescent) Proterozoic–Phanerozoic; and (4) a future stage of Earth's tectonic death.

## 7.2 CONTINENTAL CRUST FORMATION MECHANISMS IN ARCHAEAN

We now make a brief review of the tectonomagmatic processes of the continental crust formation in Archaean.

It follows from the lithospheric plate tectonics that presently the continental crust is forming only over the lithospheric plate subduction zones. It happens due to dehydration and partial remelting of the oceanic crust and its overlying deposits in the subduction zones.

However, only those plates can sink into the mantle through the subduction zones whose average density, accounting for a lower crust density of 2.9 $g/cm^3$ compared to the lithosphere (3.3 $g/cm^3$), is higher than that of a hot mantle (3.2 $g/cm^3$). Currently, these conditions are satisfied for the plates whose thickness (together with the oceanic crust $H_{oc} \approx 6.5$ km) exceeds approximately 26 km. In the past geological epochs, this critical thickness could have been different (see Fig. 8.11, curve 3). Remember, the continental plates, despite their great thickness of 200–250 km, never sink into the mantle. The reason is that they, due to their low density, always have the positive buoyancy reaching 0.02–0.03 $g/cm^3$.

In Section 8.2, we will describe in detail the correlation between the oceanic plate thickness and their age: $H_l \approx k\sqrt{t}$ (where $H_l$ is in kilometers, $t$ is in millions of years, and $k \approx 6.5$–7.5). Utilizing this correlation, we determine that the plate thickness in excess of 26–30 km corresponds to the ages of 16–21 MMY. Based on the paleomagnetic geochronology data, average life of the present-day oceanic plates is approximately 120 MMY. For this reason under the current conditions such plates, older than 16–20 MMY, not only can but indeed do sink into the mantle through the subduction zones. As the estimation of the ocean plate thickness evolution (see Fig. 8.11) shows, the condition for their sinking into the mantle was fulfilled only during the entire Proterozoic and Phanerozoic. That was because the thickness of the lithosphere (curve 4) at that time significantly exceeded the critical thickness of the plates (curve 3) after which the cooled-down oceanic plates became heavier than the hot mantle and began sinking into it through the subduction zones. This makes us to propose with certainty that beginning in Early Proterozoic (2.5 BY ago) all oceanic lithospheric plates formed in the mid-oceanic ridge rift zones after time interval exceeding 16 MMY must have sunk into the mantle through the then existing plate subduction zones.

Therefore, Earth's tectonic evolution during almost entire Proterozoic and Phanerozoic was developing under the lithospheric plate tectonics laws and in principle was no different that the modern tectonic regime.

Contrary to that, during most of Archaean average life of the lithospheric plates was much shorter than 16 MMY and a possible plate critical thickness significantly exceeded their actual thickness. Because of that, the thin Archaean plates (which are better called lithospheric basalt sheets) during Early and Late Archaean had lower density than the mantle. Therefore, such plates could not at that time sink into the mantle. An important tectonic conclusion from this is that there were no conventional subduction zones over most of Archaean. Instead, pile-up zones of thin oceanic lithospheric plates emerged in the compression areas of the lithospheric shell (i.e., over the descending convection flows of the mantle matter).

Affected by the compression forces caused by the convection flows of the mantle matter, the total thickness of the piled-up lithospheric plates, naturally, increased. Due to that, the

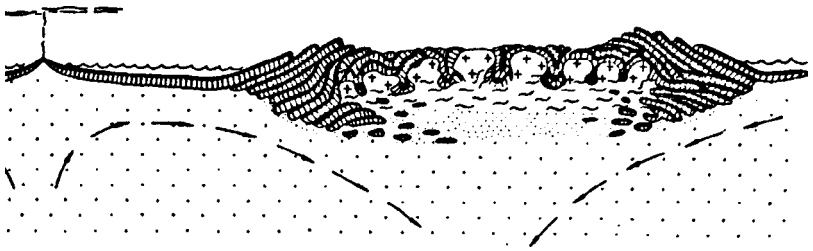

**FIGURE 7.5** Image of the continental crust formation in Archaean.

roots of such pile-up structures descended into the hot mantle to a depth of 50–80 km. In Archaean, the upper mantle was significantly overheated, its temperature then was 400–500 °C higher than currently (see Fig. 4.5).

As a result, the roots of the piled-up thin oceanic sheets immersed into the overheated mantle must have remelted. Melting of the water-containing basalts of the former oceanic crust and the subsequent melt differentiation led to the formation of lighter tonalite, trondjemites, and plagio-granite melts. These relatively light melts, naturally, must have floated and ascend in form of diapires and domes. They pierced from beneath the entire thickness of the piled-up oceanic sheets thereby forming the renowned Archaean granite–greenstone belts, the oldest areas of the continental crust (Fig. 7.5).

The theoretical grounds for the formation of Archaean continents through piling-up and partial melting of a relatively thin (just a few kilometers thick) oceanic lithosphere was published earlier (Sorokhtin and Ushakov, 1991). In 1998, this model of the continental shield formation got a factual support by the field studies in the South African Kaapvaal Archaean craton (Wit et al., 1992; Wit, 1998). These authors also believed that the Archaean oceanic crust could not be subducted due to its high buoyancy.

There is another noteworthy feature in the formation of the Archaean continental massifs. The heat flows in Archaean were intense, and a high-density thick ultramafic lithosphere could not form under continental crust of this massifs. So, a relatively light continental crust as if "floated" directly on the hot mantle. That was a reason why the continent stand during the entire Archaean and the beginning of Early Proterozoic was exceptionally high. Their surface at that time loomed 4–6 km over the ocean surface (Sorokhtin and Sorokhtin, 1997). This, in particular, is why all Archaean shields without exception are highly eroded.

Thus, the Archaean continental crust formed through the action of two major tectonic processes. At the first stage, thin basalt sheets of the oceanic crust formed. At the second stage these sheets were piled up and subjected to the secondary melt.

Two different petrogenetic processes identified by Moralev and Glukhovsky (1985) from empirical data in their studies of composition and structure of the Aldan Shield rocks correspond to these tectonic stages. The first stage was the formation of a basite crust at the expense of partial melt and differentiation of the mantle matter. The second one was a partial (15–20%) melting of the material in the lower part of the basite crust at 7–8 kbar, that is, at a depth of 25–30 km, with the release of silica and alkali in the amounts sufficient to form first high-temperature and low on potassium enderbites, first in Earth's history. The enderbites are rocks in the tonalite–trondhjemite series.

Some types of ancient anorthosites formed at the third stage due to the differentiation of the secondary melts apparently have similar petrogenesis.

In view of the aforementioned, we will define the Archaean tectonics as the thin basalt sheet tectonics. It emphasizes its radical difference with the conventional present-day Earth evolution tectonic regimes. Only in mid-Archaean, during the time of a drastic decline in Earth's tectonic activity 3.2 BY ago, the conditions may have emerged for the initiation of the plate subduction zone type. It is not clear at this time whether they were implemented.

Thus, as opposed to the processes of lithospheric plate tectonics which reign supreme on Earth since Early Proterozoic, the Archaean tectonomagmatic processes were evolving under different mechanisms which might have been similar to those occurring now on Venus. Radar images of the Venusian surface show clear indications of the rift zones and the likeness of mid-oceanic ridges but not the structures of the plate subduction zone type. Instead, there are compression or pile-up zones of the core material with typical small structures of small scales (tesserae) or long ridges as if flowing by the large hilly plateaus (analogs of the Archaean continental massifs and shields).

One characteristic feature on the Venusian surface is a merger zone of the plateau Lakshmi and Maxwell Mountains (see Fig. 7.6). The boundary between these different structures is indicated by a drastic transition from the plateau's plane (with the elevation of 4–5 km over the average planet level) to the steep slope of the Maxwell's Mountains (10–11 km high) which fringe the plateau from the east and northeast. Within the Maxwell Mountains, the ridges' slopes facing massif Lakshmi are often steeper than the opposite slopes (same as shown in Fig. 7.5).

A brief scenario of the Archaean crust formation is nothing new. Similar models were described in numerous publications (Glickson, 1976; Condie, 1981; Taylor and McLennan, 1985). What is important to us is that the proposed Earth's tectonic evolution model in Archaean well matches many known patterns in Earth crust formation at that distant time. In particular, the model apparently provides a correct explanation of the bimodal nature of Archaean crust magmatic rocks dominated by alkali (tholeite basalts) and acidic (tonalite composition granitoids) rocks with only subordinated amount of the medium vulcanites (andesites).

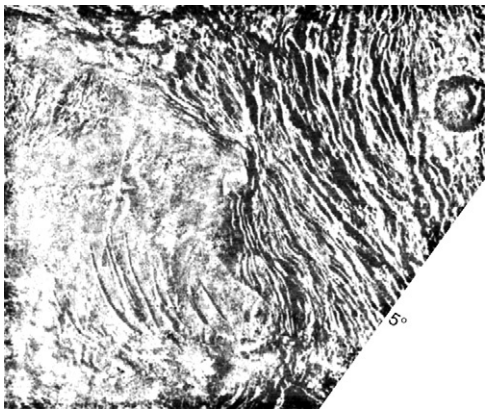

**FIGURE 7.6** Radar image of a Venus surface area (500 × 550 km) in the merger location of the Maxwell Mountains (analog of thin basalt plate pile-up) with the Lakshmi Plateau (analog of a continental massif). A large impact crater Cleopatra is seen in the upper right-hand portion.

The other features the model explains are the origin of the most ancient Archaean migmatites (gray gneisses), the mechanism of the continental crust buildup from beneath by the granitoid material, a noticeable age difference between the basaltoids, and relatively younger granitoids in the Archaean granite–greenstone belts. The model also explains the origin of the granulite massifs formed at depths of about 30 km but then floated to the surface as giant domes, or of lower crustal stages overthrusting along deep-seated faults on the Earth's surface, or a wide development of migmatites in Archaean, and many other patterns in the Archaean crust evolution.

## 7.3 EVOLUTION OF THE CONTINENTAL CRUST

At the end Archaean, the turbulent process of iron-oxide core separation within Earth was complete. It concentrated 63% of the present-day core mass. After that, the planet's tectonic evolution became much more quiescent. A drastic decrease in Earth's tectonic activity during Proterozoic resulted in a no less drastic increase in the longevity and thickness of the lithospheric oceanic plates (see Fig. 7.2). As a result, the plate density exceeded that of the mantle. So, normal subduction zones of the modern type replaced the pile-up zones of thin basalt sheets so typical of Archaean. Besides, the composition and structure of the oceanic crust substantially changed about 2.5 BY ago. In place of a purely basalt Archaean oceanic crust a third, serpentine layer formed in the beginning of Proterozoic. This layer was a main reservoir of the bound water in the oceanic crust.

All these changes led to the firm establishment on Earth at the beginning of Proterozoic of a tectonic regime described by the theory of lithospheric plate tectonics.

A theory of Earth's global evolution we are developing here enables us to identify the major patterns of the continental crust growth as well. We assumed that the growth of the continental crust mass was proportionate with the mantle-generated heat component of the total energy (it began 4 BY ago and did not include the energy of the additional Earth compression, as shown in Fig. 5.13)

$$m_{\mathrm{Ccr}} \sim E_{\mathrm{m}} T - 3.2 \times 10^{37} \mathrm{erg}. \tag{7.1}$$

We accepted the mass of the present-day continental crust, after Ronov and Yaroshevsky (1978): $m_0 \approx 2.25 \times 10^{25}$ g.

Utilizing this function, we plotted the theoretical curve of the continental crust growth (Fig. 7.7) in comparison with the most common model proposed by Taylor and McLennan, 1985. Our model accounts for the geochemical data, estimates of the oceanic deposition rates, and the consumption rates of the same deposits by the subduction zones.

As Fig. 7.7 shows the theoretical continental crust growth curve generated from our geodynamic model (curve 1) fits well with the empirical model by Taylor and McLennan (curve 2).

These models used the same mass value of the present-day continental crust. They, however, were generated based on different approaches and used independent suppositions and data. Nevertheless, their outcomes are similar. This may be interpreted as an indication of the veracity of the both models.

This is important because a theory of the tectonic activity being submitted in this publication will require more checks and proofs, and the curve comparison in Fig. 7.7 is one such proof.

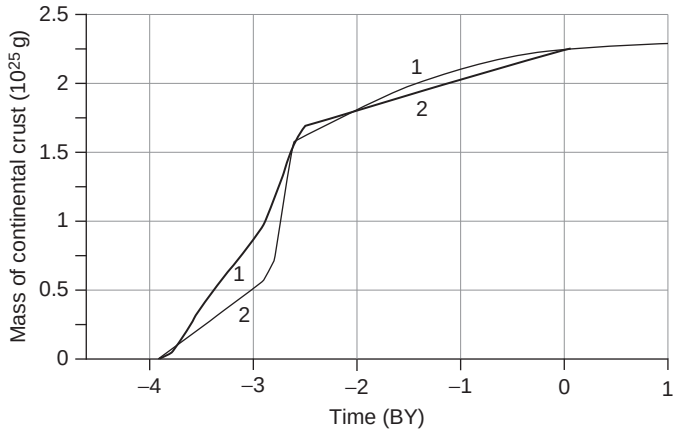


**FIGURE 7.7** Continental crust mass growth: (1) authors' version and (2) Taylor and McLennan (1985) curve.

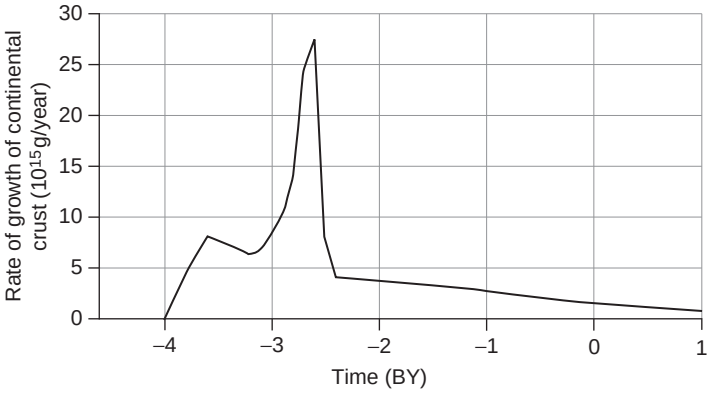


**FIGURE 7.8** Evolution of the continental crust growth rate.

The continental crust formation rate may be found by differentiating the function (7.1). The results are shown in Fig. 7.8.

As this diagram shows, the crust growth rate in Early Archaean was relatively high, almost up to $8 \times 10^{15}$ g/year or about 3 $km^3$/year. With time, it gradually declined due to the Earth's matter zonal differentiation front descent into the mantle. Mid-Archaean (3.3–3.2 BY ago) was a period of generally decreased Earth's tectonic activity (see Fig. 5.17). The crust formation rate declined as well. This period could be called an Archaean "lithoplate" period. It is possible that during these brief interval geodynamic environments typical of the lithospheric plate tectonics might have arisen someplace. These environments would have normal plate subduction zones and island-arc calcareous-alkali magmatism similar to the modern analogs. By the same token, the formation of Archaean greenstone belts must have stopped in the lithoplate period and had been replaced even by some ophiolite sheets usual in Phanerozoic.

The continental crust formation rate drastically increased in Late Archaean. The reason was a transition in the metallic iron differentiation process to the separation of the Fe·FeO eutectic melt, and most of all the process of the Earth's core separation begun in the end of

Late Archaean (see Fig. 4.1). Estimates indicate that at the peak of the Late Archaean tectonic activity burst the continental crust formation rate reached $27 \times 10^{15}$ g/year or 10 km$^3$/year.

In Late Archaean, the greenstone belt formation rate and the formation rate of the associated granitoid intrusions (mostly with elevated potassium content) must have significantly increased. At the same time, the heat flows through the oceanic sheets should have increased substantially. As a result, the amount of the komatiite lavas melt-out should have increased with the simultaneous growth in their basicity. Also raised at that time was the intensity of tectonic deformations. That is clearly identified in the structure of many greenstone belts on ancient shields of practically all continents. Apparently, for the first time in the Earth's evolution on most ancient shields might be observed approximately synchronous (3.2–2.9 BY) correlation between the tectonic deformations and magmatic events (see Fig. 6.5).

The continental crust formation regime must have reached its maximum brunt only by the end Archaean, at the time of the catastrophic process of the Earth's core separation. The geological timing of this event (see Fig. 6.5) is between 2.7 and 2.6 BY ago. It was accompanied on all continents by the practically simultaneous and very intense activation of all tectonomagmatic processes. They included really huge greenstone belts, the melt-out in tremendous amounts of granitoids (with a significant participation of potassium granites), the formation of high-stress folded deformations, and so on (Condie, 1981; Taylor and McLennan, 1985).

The major tectonic result of the core separation process must have been the formation 2.6 BY ago of the first supercontinent in Earth's history: the Monogaea.

Combined, tectonomagmatic formations of that age manifest the oldest and most intense Kenoran (or Belomor) global diastrophism epoch.

As the process of the young Earth core separation was complete approximately 2.5 BY ago, Earth's tectonic activity declined in Early Proterozoic. Together with it, the rate of the continental crust formation rate dwindled to $6 \times 10^{15}$ g/year or nearly 2 km$^3$/year. The continental crust mass accrual rate continued to go down, to $4.2 \times 10^{15}$ g/year 2.4 BY ago in Proterozoic, $1.4 \times 10^{15}$ g/year (0.5 km$^3$/year) in mid-Phanerozoic. We estimate the current rate at no greater than $0.8 \times 10^{15}$ g/year (0.28 km$^3$/year).

So far we estimated Earth's tectonic activity as defined by the mantle heat flow. Now, we can estimate average thickness of the lithospheric plates beneath the ancient continents.

It follows from a solution of the heat-conductivity equation that the cooled-down portion of the half-space penetrated by heat flow $q$ (in our case, the lithospheric plate thickness underneath the continents) is in inverse proportion with this mantle heat flow penetrating such continents. We assume that average thickness of the Archaean continental crust was at least as that of present-day Archaean shields (40 km).

On the other hand, theoretical estimates accounting for the upper mantle overheating in Archaean and possible heat flows through the continental crust indicate that the subcrustal lithosphere in Archaean was 15–23 km. In mid-Archaean, when Earth's tectonic activity declined, this thickness grew to 40 km but in Late Archaean it decreased again to 5–8 km (Fig. 7.9). That is why the continental shield stand over the ocean level during almost entire-Archaean was exceptionally high, 6.5 km on the average. That also defined a high erosion base of almost all Archaean shields.

In Proterozoic, continental lithospheric plate thickness reached the depth of the endothermal transition boundary from a solid matter of the subcrustal lithosphere to the plastic state (see boundary III in Fig. 6.2). After that time (about 2 BY ago), the thickness of the Precambrian

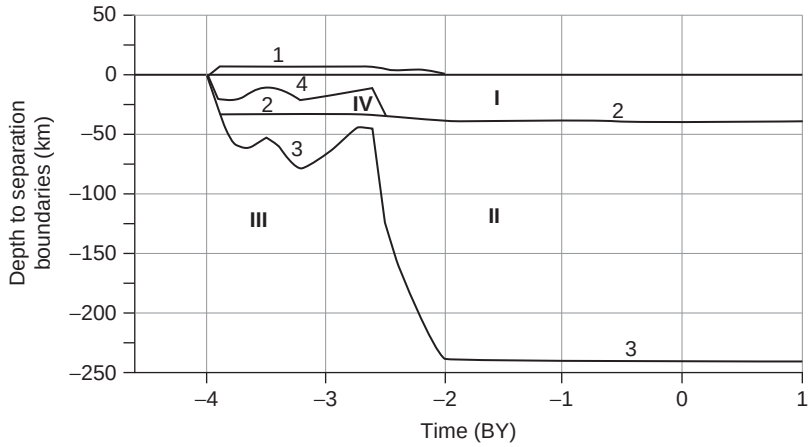


**FIGURE 7.9** Evolution of the continental plate structure: I, continental crust; II, continental lithosphere; III, sub-lithospheric (hot) mantle; 1, surface of the continents; 2, continental crust base (Mohorovicic boundary); and 3, base of the continental lithosphere.

continental lithospheric plates (together with the average thickness of the continental crust of ~40 km) was not changing and remained at a depth of about 240–250 km (see Fig. 7.9).

The continental crust melt-out regimes changed in Proterozoic. The upper mantle cooled down after its overheating in Archaean. All these changed the continent stand level. Remember, in Archaean thick and high-density ultramafic lithospheric plates could not form due to high heat flows under the continental crust. As a result, the lighter Archaean continental massifs raised high over the average stand level of the mid-oceanic ridges and ocean surface.

Contrary to Archaean, the upper mantle noticeably cooled down in Proterozoic and Phanerozoic, and thick high-density lithospheric plates formed, "soldered" under the continental crust (see Fig. 7.9) which substantially "sunk" the continental blocks. The ocean level rose (see Fig. 11.6), and under the Archimedes law, increased the lift force acting on the plates. These opposite forces made the balance fluctuate so that the average continent stand over the ocean level changed as shown in Fig. 7.10.

Presently, much of the Archaean crust is denuded, and its older and deeper portions, often metamorphosed to the amphibolite and granulite facies, are exposed on the surface of cratons.

## 7.4 MAJOR FEATURES OF THE CONTINENTAL CRUST COMPOSITION IN ARCHAEAN

The young primitive continental crust could form only from remelting of water-saturated basalts, that is, to be composed of tonalites and trondhjemites. There could not have been other crust components as the young Earth has not undergone the differentiation yet and was comprised of the primordial ultramafic planetary matter from which only basalts could melt out without a radical differentiation. For higher differentiated rocks to form, a deeper differentiation of Earth's rocks or addition to them of a new material with other geochemical parameters would be necessary. For instance, addition of the sedimentary material

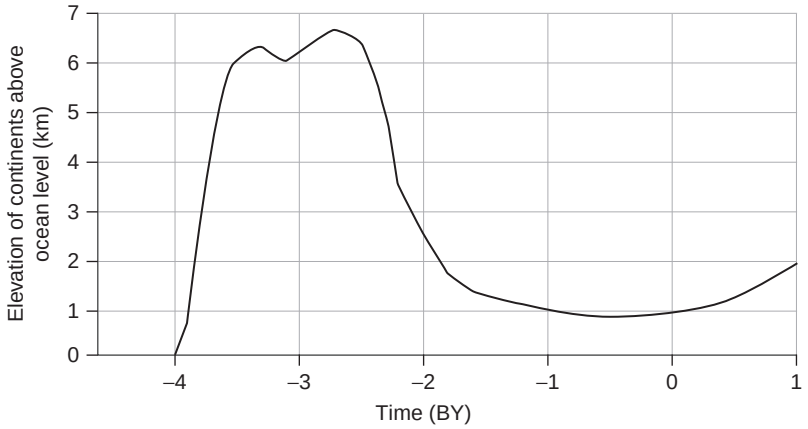


**FIGURE 7.10** Average continental massifs stand height over rift zones in Archaean and over the ocean surface in Proterozoic and Mesozoic.

which underwent preliminary weathering stage under various geodynamic conditions would be needed for the melt-out of the granitoids so common in Archaean.

The quoted calculations indicate that, due to a high stand of the continents and accelerated erosion of their crust in Archaean, large sedimentary masses must have accumulated. At the same time, very little sediments are preserved in the Archaean sections. Where did they go? Obviously, the bulk of the deposits must have been accumulated on the oceanic plates (sheets) at the foot of the continental massifs (see Fig. 7.5). In Archaean, however, the oceanic plate motion rate was very high, sometimes up to a few hundred meters per year. And their lifetime declined to a few million years or even few hundreds of thousands of years (see Fig. 7.2). Because of that, clastic deposits did not have time to accumulate in large masses at the foot of the continental massifs and, together with the oceanic sheets, rapidly got into their overthrust or pile-up zones (Fig. 7.5). Subsequently, under the burden of newly overthrusted oceanic crust fragments, the entire package of the previously piled-up sheets with their overlying sediments again sank into the hot mantle. In the process, the sedimentary rocks were also melted generating granitoid magmas. Those magmas formed granite diapires and huge crustal intrusions which intruded the continental massifs (see Fig. 7.5). Therefore, due to the recycling processes most of the Archaean sediments were converted into the granitoids of the granite–greenstone belts whose mass is indeed tremendous.

The aforementioned examples show that the Archaean to Proterozoic transition must be clearly marked by geochemical indicators. Taking into account the tectonic factors and the quoted theoretical constructions, it is possible now to maintain with great certainty that the nature of a major Archaean–Proterozoic geological time boundary is connected with the completion of a high-density core formation in the center of Earth. The core at that time contained about 63% of its present-day mass. What also happened after the young core separation was a transition in the endogenous Earth's matter differentiation regime from the zonal separation of iron and its oxides to a quieter barodiffusion differentiation mechanism.

The immediate cause of drastic changes in the geochemical and tectonic conditions of the Earth core formation that occurred between Archaean and Proterozoic was the transition from the thin basalt sheet tectonics in Archaean, with typical zones of Earth core pile-ups, to tectonics of the lithospheric plates with the subduction zones in Proterozoic and Phanerozoic.

The serpentinite layer of the oceanic crust, the major carrier of the bonded water on Earth, was formed in Early Proterozoic. That substantially changed the water regime of the continental crust melt-out. After Archaean, the crust formed in the environment of excessive overheated fluids coming from the subduction zones. Such fluids are aggressive mineralizers enriched in silica and alkali. A greater role belonged now to the continental slope deposits over the plate subduction zones. They numerously remelted in them forming crustal magmas, especially of the granitoid and alkali composition.

A special case is the origin of the Late Archaean potassium granitoids which challenged the sodium granitoids and tonalite–trondhjemite granitoids typical of the entire Archaean. The origin of these granitoids was studied in detail by Taylor and McLennan, 1985. We accept many conclusions of these writers and will now review the issue from the position of our model of the Early Precambrian geodynamics.

The mantle origin of most of these granitoids is supported by low primary strontium ratios $^{87}Sr/^{86}Sr \approx 0.702–0.703$. They are only slightly above the mantle readings for that period of 0.701–0.7015. This excess can probably be explained by partial involvement in their melt-out process of older crust rocks (including Early Archaean sodium granitoids) with some addition of the sedimentary material (Taylor and McLennan, 1985).

The Late Archaean Canadian granitoids also have the mantle origin which is supported by the analyses results of their Sm/Nd ratios. A substantial enrichment of the Late Archaean granitoids in potassium may be explained in such situation not only by the contamination with a crust material but also by the melt-out of the corresponding sial magmas from water-saturated basalts at great depths, which possibly exceeded the basalt-to-eclogite conversion depth or high depths of the granulite facies. Of course, for these magmatic processes to develop, the specific tectonic conditions were needed.

In Late Archaean, in connection with the change in Earth's matter differentiation regime, a strong burst of convective, therefore, tectonic Earth's activity occurred (see Fig. 5.16). Simultaneously, about 2.7–2.8 BY ago the maximum overheating of the upper mantle happened, temperature rose to 1800–1850 °C (see Fig. 4.5). Besides, due to a gradual water accumulation in the hydrosphere, the ocean surface during almost entire Late Archaean was over the crests of mid-ocean ridges and rift zones located within them. That naturally resulted in a substantial increase in water-saturation of Late Archaean oceanic crust basalts. Actually, at that time hydration of the oceanic basalt reached its maximum.

All these could not but affect the composition and growth rate of the continental crust being formed in Late Archaean. In particular, the lithospheric sheet pile-up processes must have drastically increased at that time. For this reason, the roots of the pile-up structures at that time might have deeply sunk into the hot mantle and remelted there. Currently, the maximum depth of the melt existence within the juvenile mantle does not exceed 80–100 km. In Late Archaean, the mantle overheating reached 400–500 °C and partial mantle matter melt spread to a depth of 350–400 km.

Because of that, if the piled-up oceanic sheet roots, together with the oceanic crust water-saturated basalts, sunk at that active time to depths exceeding 80–100 km, the sial magma

melt-out could have occurred at pressures over the basalt-to-garnet eclogite conversion pressure. The eclogites, being a heavy fraction, must have descended into the mantle depths carrying with them most of MgO, FeO, CaO, $TiO_2$, and excess of $Al_2O_3$, thereby enriching the residual melts with silica and alkali (Green and Ringwood, 1967b).

It is also not out of the question that the silicate magmas which generated potassium granitoids underwent additional fraction differentiation with the deposition at intermediate depths of the lower crust of sodium-containing pyroxenes and amphiboles (such as omphacite, zhadeite, and egirine). As a result, a light residual melt would definitely be enriched in $K_2O$. Besides, maximum hydration of the oceanic crust basalts led to another phenomenon. The sial magma melt-out in the lithospheric pile-up zones of that time was occurring in the presence of water. The water is a very strong mineralizer. It actively brings into solution all lithophilic (hydrophilic) elements, and first of all potassium, rubidium, uranium, and thorium.

Part of the crust material, including deposits, could have, in the environment of drastically increased heat flows and high-tension tectonic motions of the already formed oceanic crust, got into the lithospheric sheet pile-up zones and could have remelted there. That would mean additional differentiation and enrichment in lithophilic elements.

Altogether, these phenomena apparently resulted in the formation during late Archaean of first continuous series of potassium granitoids, from granodiorites, monzonites to adamellites and real potassium granites.

Great melt-out depth of the bulk of the Late Archaean potassium granitoids is supported by their rare-earth element distribution spectra (Fig. 7.11). Let us accept, for instance, that the granitoids indeed were melted out at the existence level of the garnet lherzolites. It is known that the garnets are the major depositories of heavy elements in this group. Then,

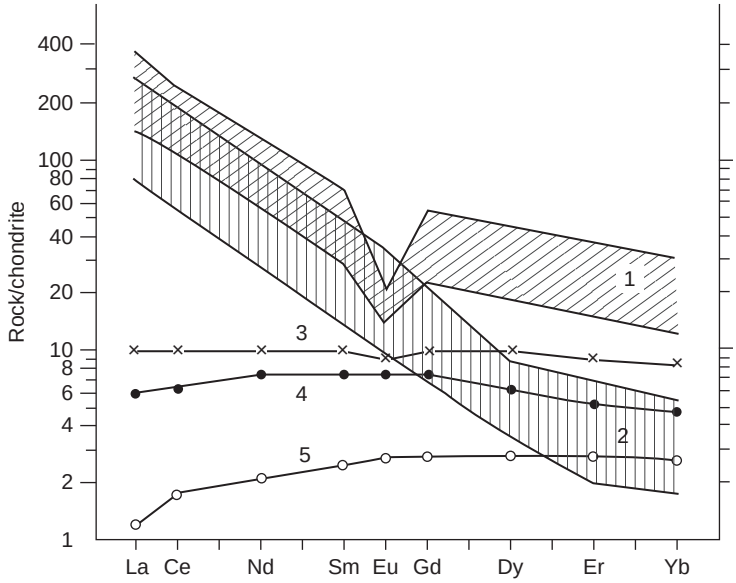


**FIGURE 7.11** Distribution of rare-earth elements in Archaean rocks: 1, the field of the Early Archaean Na–granitoids; 2, the field of the late Archaean K–granitoids; 3, Minnesota tholeite basalts; 4 Onverwacht komatiites; and 5, peridotite komatiites after Taylor and McLennan, 1985.

after the melt separation the rare-earth element spectrum in the granitoids must be substantially impoverished in heavy rare-earth elements. And that is exactly what is observed in actuality. All Late Archaean granites have relatively high ratios of La/Yb ≈ 20–30, whereas shallower Early Archaean and Proterozoic granitoids display lower ratios of La/Yb ≈ 5–10.

Despite the transition in Earth's tectonic evolution after Archaean to the tectonics of lithospheric plates, the calcareous-alkaline (andesite) magmatism was strongly suppressed or even totally disappeared in Early Proterozoic (Borukayev, 1985; Frolova and Burikova, 1992). The most likely association was the specificity of Early Proterozoic oceanic deposits because that was when the mass deposition of the iron ore formations occurred. Getting into the plate subduction zones heavy iron deposits could no longer be squeezed out of the slot between the plates and served there as a lubricant thereby preventing the heating and remelting of bedrocks in the subducted oceanic crust due to its dry friction with the obducted plate. That is exactly why the calcareous-alkaline magmatism of the subduction zones in its modern form showed up only in middle Proterozoic after the iron ore formations were deposited.

Another distinctive feature in the formation of the continental crust composition during the post-Archaean time was melting out of crust magmas and occurrence of regional metamorphism in the environment of the excessive water coming out of the plate subduction zones from dehydration there of the oceanic crust serpentinites.

It was estimated that during the entire Proterozoic and Phanerozoic almost $2.3 \times 10^{25}$ g of water filtered through the subduction zones. This is 16 times the amount of water in the world ocean! That is an important fact as the water is a strong chemical reagent and mineralizer which is actively transporting all lithophilic and hydrophilic elements into the continental crust.

Changed conditions of continental crust formation in the post-Archaean time are clearly manifested by geochemical relationships between the same-type rocks of different ages. Weizer (1980) studied variations of $K_2O/Na_2O$ ratios in crustal magmatic rocks of different ages (Fig. 7.12). All Early Archaean igneous rocks indeed have typically basalt ratios of $K_2O/Na_2O \approx 0.5$. In Late Archaean, these ratios gradually increase due to the start of potassium granitoid melt-out. Especially, rapid potassium accumulation in the crustal rocks happened in Early Proterozoic when the newly formed serpentinite layer of the oceanic crust began sucking-in the water. By the end of Early Proterozoic, however, because of the oceanic crust maximum saturation with the oceanic water $K_2O/Na_2O$ ratios reached the equilibrium value of 1.2–1.5. A local ratio minimum in Mesozoic is most likely associated with the global

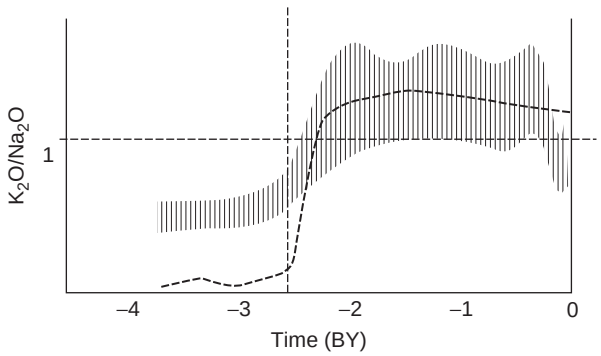


**FIGURE 7.12** Evolution of $K_2O/Na_2O$ ratio in continental crust rocks (after Ya. Weizer, 1980) in comparison with the bound water concentration in the oceanic crust (dashed line).

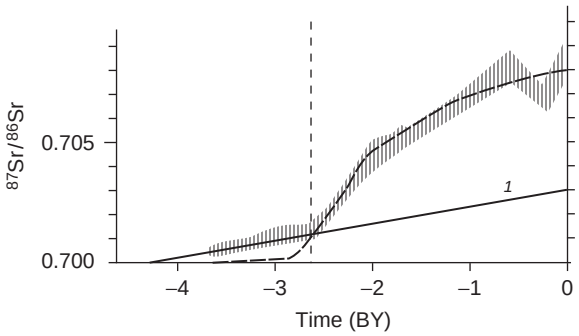


**FIGURE 7.13** Evolution of $^{87}Sr/^{86}Sr$ ratio in oceanic deposits (after Ya. Weizer, 1980) in comparison with the age trend of this ratio in the mantle rocks (*1*) and with the bound water content in the continental crust (dashed line).

transgression on the continents and, as a consequence, with the decrease in the core material supply into the ocean and farther, together with deposits, into the subduction zones.

No less demonstrative are the strontium isotope ratios $^{87}Sr/^{86}Sr$ in the oceanic origin limestones (Fig. 7.13). The reason is that effective averaging occurs in the oceanic water of isotope markers in the continental rocks which are being currently weathered and transported by rivers into the ocean. That is why the isotope composition of such sediments that are deposited in the equilibrium environment with the water must reflect the composition of the provenance areas. In this case, it is average composition of the continental crust and oceanic basalts erupting through the rift zones of mid-oceanic ridges.

As in the previous case, the $^{87}Sr/^{86}Sr$ diagram in Fig. 7.13 demonstrably shows that in Early Archaean the primary ratios $^{87}Sr/^{86}Sr$ in the crustal rocks completely coincided with the mantle source. In Late Archaean, the potassium granitoid melt-out and the beginning of the core material recycling (which led to predominant accumulation of potassium and rubidium in the crust) resulted in some increase of $^{87}Sr/^{86}Sr$ ratios in the crustal rocks.

The contribution from this process to the general composition of the Late Archaean crust was still insignificant, and on the whole it has about the mantle values of the primary $^{87}Sr/^{86}Sr$ ratio. Only beginning in Early Proterozoic, that is, after the first restructuring of Earth's tectonic regime, emergence of the serpentinite layer of the oceanic crust and mainly after the appearance of subduction zones which began sucking-in the deposits washed-out off the continents, the ratios $^{87}Sr/^{86}Sr$ drastically increased thereby marking the accelerated accumulation in the crust of rubidium, and therefore potassium.

As in the case of $K_2O/Na_2O$ ratios, the Mesozoic minimum on the $^{87}Sr/^{86}Sr$ curve for the marine limestones was caused by a decline in the carbonate material transport from the continents to the oceans and by "pumping out" of carbonates during the Late Cretaceous marine transgression from the oceans into Cretaceous epicontinental seas (see Fig. 10.32).

The Archaean–Proterozoic time boundary is marked by drastic changes in the concentration of the dispersed elements (Taylor and McLennan, 1985). For instance, the ratio of the light rare-earth elements to their heavy part in fine-grained sediments at this boundary drastically increased approximately from 6 to 11, the ratio Th/Sc increased from 0.4 to 1.1, La/Sc from 1 to almost 3, and the thorium concentration rose from $1.5 \times 10^{-6}$ to $3.5 \times 10^{-6}$.

Thus, geochemical parameters clearly indicate the transition from Archaean to Proterozoic. Based on tectonic factors and the quoted theoretical considerations, it is fair to maintain that

the nature of a major geological boundary between Archaean and Proterozoic is associated with the completion of the Earth core separation. The core at that time contained about 63% of its present-day mass. What also happened after the young core separation was a transition in the endogenous Earth's matter differentiation regime from the zonal separation of iron and its oxides to a quieter barodiffusion differentiation mechanism. The immediate cause of drastic changes in the geochemical and tectonic conditions of the Earth core formation that occurred between Archaean and Proterozoic was the transition from the thin basalt sheet tectonics in Archaean, with typical zones of Earth core pile-ups, to the tectonics of the lithospheric plates with the subduction zones in Proterozoic and Phanerozoic.

The serpentinite layer of the oceanic crust, the major carrier of the bonded water on Earth, was formed in Early Proterozoic. That substantially changed the water regime of the continental crust melt-out. After Archaean, the crust formed in the environment of excessive overheated fluids coming from the subduction zones. A greater role in the crustal magma melt-out (especially the granitoid and alkali ones) belonged now to the continental slope deposits pulled into the plate subduction zones.

## 7.5 CONTINENTAL LITHOSPHERE FORMATION TECTONIC REGIMES IN EARLY PRECAMBRIAN

Let us now review the particular tectonic regimes which formed the continental crust in Archaean. First tectonic activity of Earth must have showed up in the equatorial zone. Therefore, the first volume of the continental crust (the oldest embryos of the future continents) could form only in the low latitudes. In early times during Archaean, the Earth's matter zonal differentiation front was relatively shallow, 400- to 800-km deep. Only small convective structures (a few hundred, maximum a 1000 km in horizontal size) could have emerged in the overlying mantle. It means that several oldest continental crust embryos (similar in type to the Isua Formation in West Greenland) could exist and evolve simultaneously, and each of them had to be located over the center of a descending convection flow in the mantle (see Fig. 6.4).

As the differentiation front deepened, the size of the mantle convection cells must have increased and the belt of Earth's tectonic activity must have widened into the higher latitudes. As a result, the emerged kernels of the future continental shields increased in their mass and spread apart from one another. Our model indicates (Fig. 5.16) that in the middle of Archaean (about 3.2 BY ago) Earth's tectonic activity must have quieted somewhat. As mentioned earlier, it is possible that then for a short period the subduction zones formed instead of the thin basalt sheet pile-up zones. If so, then the continental crust in mid-Archaean could have been for some time increasing due to the island-arc (andesite) magmatism. However, in the beginning of Late Archaean (about 3 BY ago) a new and very strong activation of all tectonic processes occurred.

Beginning at that time, all processes of the continental crust formation drastically activated. Especially, significant changes in tectonic regimes of the Archaean crust formation happened by the end of Late Archaean, 2.8–2.6 BY ago. At that time, a catastrophic process of the core separation began developing in the Earth's center (see Section 4.1). That led to the establishment within the mantle of a single-cell convective structure with exceptionally strong mantle

flows directed from the equatorial zone of one hemisphere to the other hemisphere. As a result, at the end of Late Archaean all previously separate continental massifs began to rapidly move toward the center of the descending flow on the equator, collide with each other, significantly deform and join into a single continental massif. It appears that was the way how the first supercontinent in Earth's evolution, Monogaea, formed (see Fig. 4.1D).

If it really were so, then at the end of Late Archaean about 2.6 BY ago a practically simultaneous deformation of almost all basalt sheet pile-up zones surrounding the continental massifs should have happened. These zones were the future greenstone belts of Late Archaean. At about the same time with just a small lag, a powerful granitization impulse must have occurred and be accompanied by "squeezing-out" of huge amounts of the granite melts from under the basalt sheet pile-up zones into the upper layers of the newly forming continental crust. The squeeze was due to the intense compression of the continental margins. Condie's data (1981) indicate that it really happened. Figure 6.5 borrowed from his publication shows that the first clear correlation of the reviewed tectonic events occurred simultaneously on almost all Archaean continental shields only in the end Archaean about 2.7–2.6 BY ago.

The tectonomagmatic events in Middle Archaean are much weaker correlated: tectonic events of that period showed up on different continents far from simultaneously. In Early Archaean, it is difficult to identify tectonic events synchronous on all continents: Early Archaean continental embryos were evolving quite independently from each other, each of them was located within an individual descending flow area of the upper mantle multi-cell convection structure. In view of the latitudinal interdependence of convection intensity in the Archaean mantle, the observed time distinctions in the tectonic events on different continents during Early Archaean and first half of Late Archaean may be associated with the different latitudinal positions of the then already existing continental massifs.

It was shown (Monin, 1977, 1999) that under the laws of mechanics the planet's revolution becomes stable only if the supercontinent's center of gravity is located on the equator. Let us assume that such supercontinent formed in a different place, for instance at high latitudes. In this case, the planet's body affected by the forces of inertia will rotate relative to the planet's revolution axis so that the "center of gravity" of this continent got to the equator.

That means that Monogaea must have also been positioned on the equator. Despite that, in Early Proterozoic (2.4–2.5 BY ago) it was affected by a first glaciation in Earth's history (the Guron glaciation). It showed up simultaneously on several shields—in Canada, South Africa, India, Western Australia and on the Baltic Shield (Chumakov, 1978). The explanation is that in Early Proterozoic, after the ultramafic rocks began to be hydrated and the serpentinite layer of the oceanic crust was formed, the high-density Archaean carbon dioxide atmosphere was bonded in carbonates, the greenhouse effect disappeared, and Earth's climate drastically cooled down, with the average planet's temperatures of $+20\,^{\circ}C$ (instead of $+60$ to $+70$ in Archaean, Fig. 14.17).

At the same time, the continental stand over the sea level after Archaean (during a first half of Early Proterozoic) remained relatively high, close to 2.5–2 km (see Figs. 7.10 and 11.6).

So, the Huron equatorial glaciation was in fact a high-mountain glaciation of moderate climate (Sorokhtin and Sorokhtin, 1997) although the near-shore glaciers in middle latitudes may have slid to the sea level.

Crustal rocks are being melted out in the plate subduction zones and thereby help to grow the continental crust. The opposite processes of denudation are at work at the same time. They destroy the crust and transport the clastic material into the oceans. The oceans go through a complete evolution cycle from the opening to the eventual closing. After the cycle is completed, the entire amount of deposits in the oceanic basin eventually is reworked within the subduction zones or crushed into folds, is upthrown over the continental margins, and again merges with the continental crust.

This process is nonuniform. The continent denudation rate over the most of the cycle is substantially greater than the amount of the crust merged in the subduction zones. Garrels and Mackenzie (1971) found that the total amount of material transported into the oceans is currently around $25 \times 10^{15}$ g/year (close to 10 km$^3$/year). At the same time, the present-day crust accrual rate in the plate subduction zones is only 0.5–1.1 km$^3$/year (Taylor and McLennan, 1985). The material brought in from the continents is mostly deposited in the area of the continental slopes and on the shelves (Lisitsin, 1984). Therefore, it maintains the connection with the continental crust and technically may be considered its part, whereas the pelagic deposits totally torn apart from the continental crust accrue only by $3 \times 10^{15}$ g/year or 1.1 km$^3$/year in the equivalent crustal rocks.

That is the reason why the mass of the present-day continental crust currently decreases rather than increases.

By the end of tectonic cycles during the closing of the Atlantic-type oceans, all previously deposited oceanic sediments are involved in the process of the crust formation, crushing, granitization, metamorphism, and consolidation. The crust formation rate and its accrual drastically increase during such orogenic phases, and the crust growth becomes dominant.

In Phanerozoic, such phenomena occurred, for instance, in the closing of the Paleo-Atlantic Ocean (Yapetus) during the Caledonian phase, of the Paleo-Urals Ocean during the Itscynian epoch or of the Tethys Ocean in Cenozoic during the Alpine-Himalayan orogeny. According to our theoretical estimates, the continental crust mass accrual averaged over a period of about 1 BBY is currently positive and approximates $0.65 \times 10^{15}$ g/year (0.26 kn$^3$/year).

Based on averaging of the continental crust formation effects over various phases of this process and assuming the complete recycling of the sedimentary material to the crust within approximately 800 MMY, it is reasonable to believe that until now the balance of the continental crust growth was positive. Moreover, through mid-Phanerozoic this condition appears to have been fulfilled in-full. In the future, Earth's tectonic activity will slow down, and the balance of the oceanic sedimentation and the recycling of the sediments in the crust-formation processes will have to be ever more disrupted. It will be facilitated by the increase in the land basis level of erosion because the average ocean stand level in the future will be progressively declining (see Fig. 11.6). So, in the future, and especially after the almost total extinction of Earth's tectonic activity, the continental crust mass can only decrease.

Thus, as Fig. 7.8 shows, under our model of Earth's tectonic activity the continental crust formation was at its fastest in Late Archaean. Most of the present-day crust (nearly 70%) has already been formed by the end of Archaean 2.6 BY ago. Only 15% of the crust was formed in Early Archaean (4.0–3.8 to 3.2 BY ago), and in Late Archaean, over approximately the same time interval (3.2–2.6 BY ago) about 50% of the crust formed. Only 30% was generated during the remaining and longest Earth evolution (2.6 BY), and just a little over 3% (taking

the recycling into account) formed in Phanerozoic (close to 600 MMY). In the distant future, the continental crust growth will stop and the phase of irreversible destruction will onset.

The last, concluding stage in Earth's evolution will be associated with its upcoming tectonic death in about 1.6 BY after almost total exhaustion of its energy sources. Before that, however, in about 600 MMY, a very strong greenhouse effect will emerge on Earth due to the depth (abiogenic) oxygen supply released from the mantle in the core matter formation (see Section 12.7). With the cessation of tectonic activity and the emergence of a strong greenhouse effect, Earth's endogenous heat loss will unavoidably decline as after these events they will be occurring only due to the conductive component of the heat flow.

This may even result in a slight overheating of Earth's depths. That, however, will not save Earth from cooling and will just delay somewhat the process of its decay. Although the mutual lithospheric plate motions will have stopped, the residual tectonic movement will last on Earth for quite a long time. No magmatic phenomena will be observed after Earth's decay. And the exogenous effect on the surface will result in stronger rock weathering.

Due to a changed continental crust melt-out regime in Proterozoic and cooling down of the upper mantle after its overheating in Archaean, the continent stand level changed significantly (Fig. 7.10).

As the tectonic regime of the oceanic crust converting to the continental one changed, the very process of the continental crust formation in post-Archaean time transformed. The areal crustal magmatism, mostly tonalite–trondhjemite in composition, which emerged in the pile-up zones of the oceanic crust, was replaced by calcareous-alkaline magmatism of the plate linear subduction zones. The processes of granitoid formation also changed. In post-Archaean, they usually formed out of the crustal matter sources and mostly due to remelting of the terrigenous sandy–clayey sediments sucked-in into the subduction zones or due to metamorphic reworking of the sedimentary sequences by the overheated fluids (see Fig. 8.22).

## 7.6 CONTINENTAL LITHOSPHERE FORMATION PROCESS IN EARLY PRECAMBRIAN

As shown earlier, the high heat flow in Archaean resulted in mostly heat convection in the mantle. This convection, due to a small thickness at that time of the mantle lenses, was a small-cell convection and was organized as Bénard cells (see Fig. 6.4). Thin basite plates over the descending convection flows piled up and sagged into the hot mantle. There, they were remelted and gave birth to the granitoids—embryos of the future continents (see Fig. 7.5). Most favorable areas for that were apparently the conjugation areas of the Archaean mantle convective cells. That predetermined their isometric form, which sometimes close to polygonal (Figs. 7.14 and 7.15).

The obvious similarity in the configuration of individual crustal domains with the Bénard cells is most likely a result of their origin: the domains indeed emerged over the Bénard type descending convection cells (Figs. 6.4 and 7.16). It is important that this similarity is typical not only of the large crustal segments but also of their component domains. This is observed within the Russian Plate (Fig. 7.15) and within the Karelian greenstone area

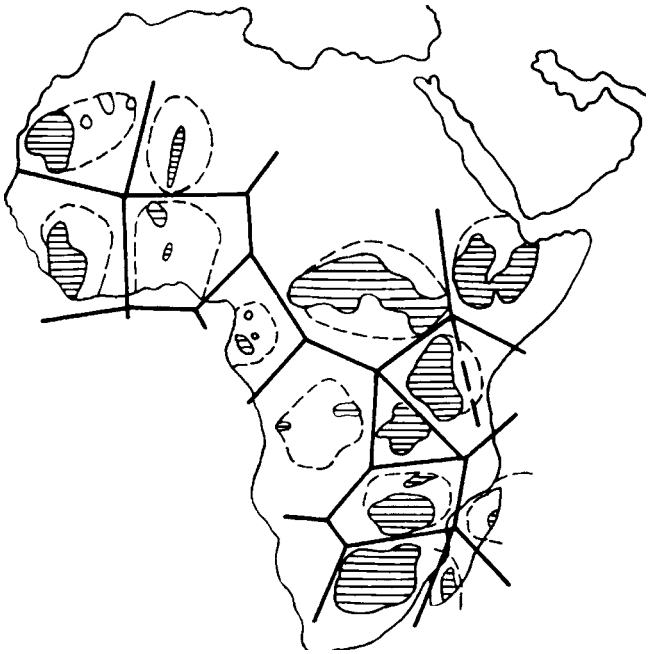

**FIGURE 7.14** Location of Archaean continental microplates in Africa (shaded) (Kushev, 1992). Solid lines indicate general trends of Archaean and Early Proterozoic mobile belts.

(Fig. 7.17), which is one of its components. There, the greenstone structure axes form two crustal segments clearly separated in space and different from one another age-wise; they both have polygonal shape.

The continental crust formation over the descending convective mantle flows resulted in the formation of small continental plates which up to Late Archaean evolved relatively separately from one another (Ringwood, 1981; Taylor and McLennan, 1985; Sorokhtin and Ushakov, 1991).

The following fact is demonstrative. The continental formations aged 3.8–3.2 BY do not bear any noticeable traces of collision interaction. There are just a few cases of the intense collisions aged about 3.5 BY (Condie, 1981).

This phenomenon is easy to explain taking into account that the intense heat convection materializes in the form of the Bénard cells which are stable enough in space and time. Then the emerging continental crust embryos must be separated and their lateral drift on the surface of Earth is practically impossible. The facts of lateral motions about 3.5 BY ago and in other epochs, as shown earlier, may indicate a jump-like enlargement of the Archaean mantle cellular structure as a result of its spatial excrescence (see Fig. 6.4).

Modeling of the Early Precambrian continental crust formation showed the nonuniform structure of the Archaean continental lithosphere (Sorokhtin, 1994, 2001a,b). As we show, a powerful heat flow through the continental crust must have resulted in the emergence and long-time durability within the lower crust layers of large zones of a partial substrate melting. The thickness of such zone might have reached 20–30 km at the total crust thickness close to the present-day one (close to 40–45 km). Thus, the Archaean continental lithosphere was a macro-layered system of physicochemically diverse media orderly positioned in space.


**FIGURE 7.15** Schematic positions of Archaean continental plates within the Russian plate (Kushev, 1992). Double and single lines are generalized Archaean and Early Proterozoic mobile belt trends.

The rigid crystalline crustal layer was at the top, lower followed a highly plastic layer of the lower crust. Lower yet was the layer of relatively rigid and totally crystallized subcrustal lithosphere overlying the partially melted substrate of the mantle asthenosphere (Sorokhtin, 1997). This continental lithospheric plate structure was only typical of Archaean and does have nothing to do with the present-day situation.

Taking all the aforementioned into consideration, we now review the effect of Earth's tectonic activity and of the depth heat flow on the structural evolution of the continental lithospheric plates and on the specifics of their Early Precambrian formation.

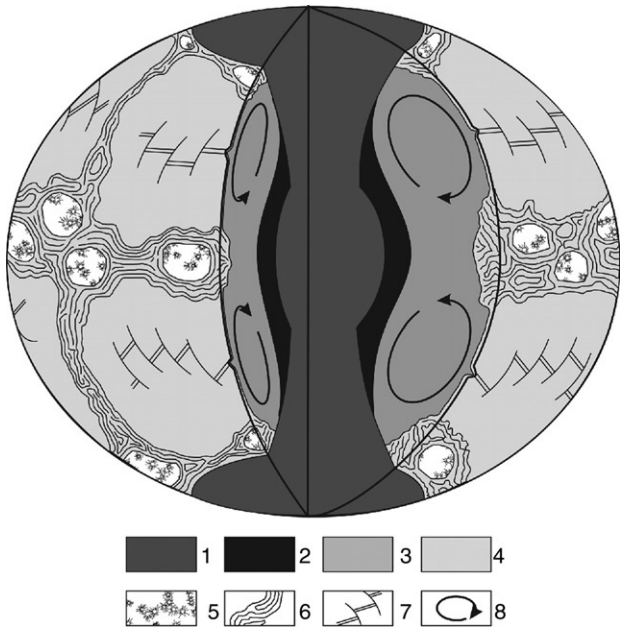


**FIGURE 7.16** Volume model of Earth's structure in Meso-Archaean. 1, primordial Earth's matter; 2, iron and iron-oxides melts (core matter); 3, depleted mantle impoverished in iron, its oxides and siderophilic elements; 4, proto-oceanic type crust; 5, continental crust; 6, proto-oceanic crust pile-up areas; 7, mid-oceanic ridges; and 8, directions of convective flows in the mantle (the scale is distorted).

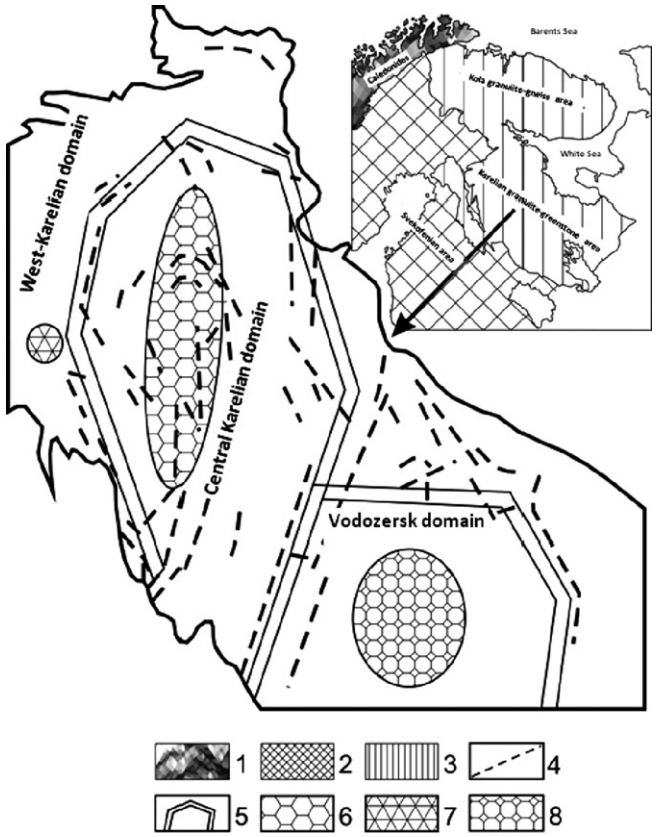


**FIGURE 7.17** Schematic map of Archaean greenstone structures within the Karelian granite–greenstone area and Vodlozer domain. The inset shows the location of different age continental crust areas within the Central and Eastern Baltic Shield: 1, Paleozoic; 2, Early Proterozoic; 3. Archaean; 4, Greenstone belt axes; 5, boundaries of identified polygonal structures; 6–8, continental crust cores of different ages (Early Precambrian..., 2005); 6, Continental crust area 3.0–2.9 BY old; 7, continental crust area $>3.1$ BY old; 8, continental crust area $\approx 3.1$–3.5 BY old.

To simplify the model, we may disregard the duration of a continental crust area formation and consider its heat history only beginning at the time $t_0$ marking the end of the core matter separation process. We assume that the continental crust thickness changed little since its formation and remained close to $H_{cc} \approx 40$ km (Taylor and McLennan, 1985). We also assume that beginning at time $t > t_0$ a rigid subcrustal lithosphere began forming under the newly emerged embryo of the continental crust. The lithosphere separated the crust from the direct contact with the hot mantle. The lithosphere formed due to cooling and total crystallization of the partially melted mantle matter. In this case, the lithosphere thickness $H_l$ and the position of its base were controlled by the crystallization (solidus) geotherm $T_s$ of the mantle matter.

To determine heat regimes of the Earth's crust existence and of the lithospheric plate formation, we need to solve the heat-conductivity equation; edge conditions corresponding with geodynamic environments of the past epochs should be inserted into the general solution. For our accepted simplified plate model, we use the single-dimensional approximation for the horizontally laminated medium, in which case the heat-conductivity equation has the simplest format:

$$\rho c_p \frac{\partial T}{\partial t} = \frac{\partial}{\partial Z}\left[\lambda \frac{\partial T}{\partial Z}\right] + \Theta, \tag{7.2}$$

where $T(z,t)$ is the medium temperature; $\rho$ is the medium density; $c_p$ is the matter heat capacity at constant pressure; $\lambda$ is heat conductivity; $\Theta$ is the bulk density of the radiogenic heat sources in the medium; $t$ is time; and $Z$ is the vertical coordinate directed down from Earth's surface.

As we assumed a horizontally laminated representation of the medium, we search for a solution of Eq. (7.2) for each of the identified lamina/layer. The defining parameters $\rho$, $c_p$, $\lambda$, and $\Theta$ may be considered constant within the layers. If we now disregard the temperature jumps at the phase transition boundaries within the convecting medium (at low convection rates), we may stitch individual partial solutions into one general solution. We also assume that within a layer containing radioactive elements

$$\Theta = q_R/h_R, \tag{7.3}$$

where $q_R$ is heat flow generated at the top of a layer by the radioactive decay and $h_R$ is thickness of this layer.

The temperature $T(z)$ correlation versus depth in Eq. (7.2) may be determined from its stationary solution $\partial T/\partial t = 0$ taking into account that the layered medium is penetrated, besides the radiogenic heat flow, also by the depth (undercrustal) heat flow $q_m$. The total heat flow on the surface, at $Z = 0$, is:

$$q_0 = q_m + q_R. \tag{7.4}$$

Then temperature at the depth $Z$ ($Z \le h_R$) will be:

$$T = T_0 + \frac{q_m}{\lambda} Z + \frac{q_R}{\lambda}\left[Z - \frac{Z^2}{2h_R}\right], \tag{7.5}$$

where $T_0$ is the Earth's surface temperature. The crustal stationary temperature at $Z \ge h_R$ is:

$$T = T_0 + \frac{q_R}{\lambda}\frac{h_R}{2} + \frac{q_m}{\lambda}Z. \tag{7.5'}$$

And temperature at the base of the crust (or at the top of the lithosphere) will be:

$$T_0^{KK} = T_0^l = T_0 + \frac{q_R h_R}{2\lambda} + \frac{q_m}{\lambda}H_{KK}, \tag{7.5''}$$

where $H_{cc}$ is the crust thickness.

The radiogenic elements are distributed within Earth very nonuniformly (see Chapter 5). The present-day mantle contains so little of these elements that their energy contribution to the heat flow does not exceed 10% (Sorokhtin and Ushakov, 1991). For this reason, in the solution of Eq. (7.2) for the medium's subcrustal layers (the subcrustal lithosphere and the convecting mantle) we may assume $q_R \approx 0$ (the mantle radiogenic heat contribution will be indirectly accounted for in the flow $\widetilde{q}_m$). The radioactive element distribution in the continental crust is also very nonuniform, most of them apparently are concentrated within the upper crustal layer (Lyubimova, 1968a,b; Taylor and McLennan, 1985). Should the radioactive element concentration in the continental crust be uniform and same as in the near-surface conditions, the hear flow on the surface of old continents would be at least twice their observed value.

Based on all the aforementioned we will assume that the meaningful radioactivity is concentrated only within the $h_R$-thick upper layer of the continental crust. For the other layer we will assume $q_R \approx 0$ at $q_m \neq 0$. Then the general solution of Eq. (7.2) may be expressed in a classical format as provided, for instance, in Tikhonov and Samarinsky (1966). In this case for the depth interval $H_{cc} \leq Z \leq H_{cc} + H_l$, where $H_l$ is thickness of the subcrustal lithosphere:

$$\left[T - T_0^l - \frac{\widetilde{q}_m}{\lambda}[Z - H_{cc}]\right] = \left[T_m - T_0^l - \frac{\widetilde{q}_m}{\lambda}[Z - H_{cc}]\right] erf\frac{[Z - H_{cc}]}{2\sqrt{at}}, \tag{7.6}$$

where $erfx = 2/\sqrt{\pi}\int_0^x e^{-\xi^2}d\xi$ is error integral; $\widetilde{q}_m$ is heat flow from the convecting mantle depth; $a$ is thermometric conductivity; $T_m$ is temperature at depth $Z$. And the stationary solution of the heat-conductivity equation (7.2) is:

$$T - T_0^l = \frac{\widetilde{q}_m}{\lambda}[Z - H_{cc}]. \tag{7.7}$$

It is impossible to determine temperature distribution in the sublithosphere mantle using a simple solution of Eq. (7.2) because it depends on the structure of the mantle's convection flows and especially on the parameters of boundary layers emerging under the lithosphere. That is where heat flows $\widetilde{q}_m$ are generated (due to energy dissipation from viscous friction within the deformed mantle matter).

If nowhere within the lower crust temperature exceeds its rock melting (solidus) temperature, that is, $T_0^l < T_s^{cc}$, and the matter within that layer maintains its effectively rigid state, then temperature at the crust base (at the top of the subcrustal lithosphere) is determined from Eq. (7.5''). But if $T_0^l \geq T_s^{cc}$, then within the partially melted (migmatized) lower crust rocks, $H_2^{cc}$-thick, convective flows with the temperature distribution close to adiabatic must unavoidably emerge:

$$\frac{dT}{dZ} = \frac{\alpha g}{C_p} T, \tag{7.8}$$

where $g$ is the gravity acceleration; $\alpha$ is the volume expansion factor; $C_p$ is crustal rock heat capacity. In this case:

$$\ln \frac{T_0^l}{T_S^{KK}} = \frac{\alpha g}{C_p} H_2^{cc}, \tag{7.8'}$$

where $T_s^{cc}$ is the crustal rock solidus temperature at the upper/lower crust boundary (at $H_1^{cc}$ the depth).

Using the actual parameter values in Eq. (7.8′) $g = 981\ \mathrm{cm/s^2}$; $\alpha \approx 3 \times 10^{-5}\ \mathrm{deg^{-1}}$; $c_p \approx 1.2 \times 10^7$ erg/g deg and $H_2^{cc} \approx 25$ km, we can see that the adiabatic distribution temperature changes little within the lower crust depth interval, that is, $T_0^l \approx T_s^{cc}$. However, the real temperature $T$ deviation from its adiabatic distribution (7.8) within the convecting layer of the lower crust may be estimated from the Rayleigh criterion

$$R_a = \frac{\alpha \rho g \Delta T \left(H_2^{cc}\right)^3}{a\eta}, \tag{7.9}$$

where $\eta$ is the crustal rock viscosity after their melting. For a noticeable convection to emerge, it is necessary for the Rayleigh number to be $R_a \geq 1500/2000$. So, in order for the stable heat convection within the lower portion of the Archaean crust the following condition must be met:

$$\Delta T \geq 2 \times 10^3 \frac{a\eta}{\rho g \alpha \left(H_2^{cc}\right)^3}. \tag{7.9'}$$

We assume that the ideal viscosity of partially melted (migmatized) lower crust rocks is $\eta \approx 10^{18}$ P. Then we can see that for the heat convection to emerge within this layer, the superadiabatic temperature gradient on its surfaces was just over 9 °C. At a lower viscosity, these gradients are even smaller, and temperature distribution approaches the pattern (7.7), that is, become practically isometric at the $T \approx T_s^{cc}$ level.

The above discussion is valid on condition of instantaneous temperature leveling within the crust if it rises or lower in the heat-generation area (i.e., the mantle). If medium's temperature drastically increased for some reason then the stationary temperature distribution within the crustal asthenospheric lens may become impossible. The heat removal through the external crustal shell is proportionate with some average temperature difference $T - T_0$ of the crustal asthenospheric lens and the external medium, depending on the nature of heat release within the lens. So, if the medium's temperature rapidly increased within the Archaean crust, the operating type of heat removal (such as convection) could have been insufficient to reach the system's equilibrium. In such a case, a heat "explosion" may have occurred in the individual crustal block expressed as a breakup of the upper rigid crustal crystalline layer and instantaneous heat release form the heat-generation area (the upper mantle) to the atmosphere. Naturally, the Late Archaean mantle temperature rise could not cause an instantaneous heat regime change in the entire lower crust layer and must have been somewhat delayed. A qualitative estimate of the temperature leveling time

may be made using a dimensional function proposed by Zharikov (1976): $\Delta t \sim (\Delta L)^2 / a$, where $\Delta L$ is the distance from the heat source to the observation point and $a$ is the thermometric conductivity factor ($5 \times 10^{-3}$ cm$^2$/s). Assuming the crustal asthenosphere convecting layer is 20- to 30-km thick, we find $\Delta t \sim 25 \times 10^6 - 50 \times 10^6$ years.

Such kind of processes may have occurred only next to the ascending convection flow within the crust and would result in the overheating of its lower layer. On the whole, due to the convective stirring, average temperature at the continental crust base might have been around 600 °C. It does not mean that large areas of a stronger heated matter could not have resided in the lower crust.

Granitoid series aluminosilicates with low water content begin to melt under high pressure $p > 2$–3 kbar at about 600–650 °C (Zharkov, 1976). Under the Arrhenius's law, the matter viscosity drastically declines. We assume that at 400 °C the continental crust rocks maintain their rigidity (effective viscosity on the order of $10^{23}$–$10^{24}$ P). At $T \approx 600$ °C, their viscosity drastically drops to about $10^{16}$–$10^{17}$ P. Under such environment, convective flows must unavoidably arise within the lower crust and remove the heat excess from the lower crust base to the base of the upper crustal layer. Indeed, under Rayleigh criterion (7.9) convection occurs even at small superadiabatic temperature gradients $\Delta T \approx 10$ °C and within relatively thin layers of approximately 10 km, not even speaking about the entire lower crust with the thickness of up to $H_2^{cc} \approx 25$–30 km.

The thickness of the underlying Archaean subcrustal lithosphere may be determined utilizing the condition $Z - H_{KK} = H_l$ at $T = T_s^l$, where $H_l$ is the thickness of the lithosphere; $T_s^l$ is the solidus temperature of the mantle lithospheric matter. Then:

$$\left[T_s^l - T_0^l - \frac{\widetilde{q}_m}{\lambda} H_l\right] = \left[T_m - T_0^l - \frac{\widetilde{q}_m}{\lambda} H_l\right] erf \frac{H_l}{2\sqrt{at}}, \tag{7.10}$$

where $\widetilde{q}_m$ is the depth heat flow arriving to the lithosphere base from the sublithospheric convecting mantle. A stationary solution of Eq. (7.10) determines the maximum thickness of the subcrustal lithosphere and is found as:

$$T_s^l - T_0^l - \frac{\widetilde{q}_m}{\lambda} H_l = 0. \tag{7.10'}$$

The heat flow generated by the cooling lithosphere is determined by the derivative over $Z$ of the function $T(z,t)$ found from Eq. (5) at $Z - H_{KK} = 0$:

$$q_m = q_l + \widetilde{q}_m = \lambda \frac{[T_m - T_0^l]}{\sqrt{\pi a t}} + \widetilde{q}_m. \tag{7.11}$$

The solution (7.11) of Eq. (7.10) is derived on the assumption of constant heat flow $\widetilde{q}_m$. In actuality, however, this heat flow substantially fluctuates. These fluctuations are slow compared with the changes in the vertical temperature gradient. So, this solution may be used but only as an approximation. Due to slow changes in $\widetilde{q}_m$, the stationary lithospheric regime (7.10′) may establish itself within a finite time. If it so happens that $T_s^l - T_0^l - \widetilde{q}_m H_l / \lambda < 0$, then the subcrustal lithosphere begins to gradually melt and get thinner until equilibrium onsets again at highest heat flow $\widetilde{q}_m$ value and a thinner $H_l$ of the lithosphere. The approximate heat flow value still maintains the format of Eq. (7.11).

Besides the heat flow associated with the lithosphere cool-down, its formation is also accompanied by the release of latent heat of the lithospheric matter crystallization:

$$q_s = \mu\vartheta\rho_l \frac{dH_l}{dt}, \tag{7.12}$$

where $\mu$ is partial melting of the sublithospheric hot mantle; $\vartheta$ is latent heat of the lithospheric (mantle) matter crystallization; $\rho_l$ is lithosphere density; $dH_l/dt$ is the crystallization front advance rate at the base of the lithosphere. The heat flow from the release of latent mantle matter crystallization heat is relatively low. Its change in time is the same as the changes in the heat flow $q_l$ as determined from Eq. (7.11).

As it is so and the major thermophysical process parameters ($\lambda$, a, $\mu$, and $\rho$) are known only approximately, we may as a first approximation disregard the effect of the $q_s$ component (indirectly, it is accounted for in the flow $q_l$ associated with the cool-down of the lithosphere).

The solutions (7.6) and (7.10) are still valid when $T_m(z)$ and $T_s^l(z)$ are linear functions of depth. This enables taking into account, as a first approximation, actual correlations between the boundary temperatures and depth. The present-day total thickness of the lithospheric plates (the crust plus the subcrustal lithosphere) on the ancient continental platforms is apparently close to 220 km and is probably marked by a seismic Lehmann boundary (Sorokhtin and Ushakov, 1991). If heat effects of polymorphic phase transitions in the mantle matter are disregarded, the temperature distribution within the convecting mantle must be governed by the adiabatic equation (7.8). In which case:

$$T_m = T_m^0 \exp\{g\alpha Z/c_p\}, \tag{7.13}$$

where $T_m{}^0$ is the mantle temperature normalized to the surface. At $T_m{}^0 \approx 1300\,^\circ$C, $g = 981$ cm/s$^2$, and ratio $\alpha/c_p \approx (5.16\text{–}4.77)\times 10^{-12}$ g/erg (Zharkov and Trubitsin, 1980), we may find that at depth 200 km ($2\times 10^7$ cm) temperature must reach $T_m = 1461\,^\circ$C, and at 220 km $T_m = 1477\,^\circ$C.

From the surface to a depth of 220 km, the mantle matter undergoes at least two polymorphic transitions: from plagioclase lherzolites to the pyroxene ones and to garnet lherzolites. At each such transition, a positive temperature jump must occur in the convecting mantle:

$$\Delta T = W/c_p, \tag{7.14}$$

where $W$ is specific heat of the exothermal phase transition. Ringwood (1981) found that densities of the plagioclase, pyroxene, and garnet pyrolite (compositionally close to lherzolite) at normal pressure and temperature are, respectively, $\rho_1 = 3.26$, $\rho_2 = 3.33$, and $\rho_3 = 3.38$ g/cm$^3$. At the same time, under the sub-solidus temperature the phase transitions occur at pressures $P$ close to 7.5 and 25 kbar. As $W = \Delta V \cdot P$ (where $\Delta V$ is volume effect of the phase transition), we determine that the temperature jumps at those levels are, respectively, 4 and 9 °C.

Thus, taking the phase transition heat effects into account, the mantle temperature at 220 km may reach 1500 °C, and that is what was assumed for the calculations. Then the sought-for correlation $T_m(z)$ may be presented as:

$$T_m = T_m^0\left[1 + 7\times 10^{-9} Z\right]. \tag{7.15}$$

Unfortunately, presently there are no reliable direct determinations of the lithospheric plate current thickness underneath the old continents. It may be because the transition boundary from the rigid lithosphere under the continents to the underlying viscous convecting mantle is transparent for the seismic waves and other geophysical fields. The oceanic lithosphere model is simple. It is represented as a rigid fully crystallized plate lying over a partially melted plastic mantle layer. The nature of the continental lithosphere transition to the underlying mantle is more difficult to model.

The reason is that the continental geotherm (without accounting for convection flows in the mantle) must asymptotically approach the adiabatic mantle temperature in the mantle area where partial melting of its matter is completely out of the question. Indeed, experimental data (Takahashi, 1986) indicate that at 220 km the mantle matter melts at about 1790 °C, which is 290 °C over the mantle temperature. In this case, Eq. (7.10) determining the thickness of lithospheric plates has no solution and makes no sense.

It was experimentally established that even at temperature much lower than the solidus temperature the silicates acquire plastic properties and they behave as very high viscosity but still effective liquid media (Botte, 1974). This phenomenon can explain the postglacial rise of the Fennoscandia and Canadian Shield. They clearly indicate effectively liquid state of the mantle matter underneath the continental lithosphere although mantle temperature at these levels is 200–300 °C below the expected matter melting temperature. Studies of this phenomenon (Haskell, 1935; Takeuchi, 1963; McConnell, 1965; Artyushkov, 1968; Ushakov and Krass, 1972) showed that the mantle viscosity underneath the old shields is $1\times10^{20}$–$3\times10^{21}$ P and on average may be $1\times10^{21}$ P. If so, then the mantle matter viscosity at 220 km and at sub-solidus temperature of about 1800 °C under the Arrhenius' law would be $2\times10^{17}$ P. It is by almost four orders of magnitude below the experimental value.

This parameter discrepancy shows that the position of lithosphere base underneath the thick continental plates is defined not by the geotherm of the mantle matter initial melting but by transition temperature of the mantle substrate from fully crystalline and affectively rigid state to effectively amorphous state of overcooled liquid. Similar conditions of the mantle matter existence at high pressure are well described by a model of the Newtonian viscous liquid (Magnitsky, 1965; Kaula, 1968). And the physical nature of a matter transition to the effectively plastic state at high pressure may be explained, for instance, by the development of shear dislocations on the intergranular boundaries without disrupting the structure of the crystalline grain comprising the mantle rocks. What it means is that the long-term strength of the matter is substantially lower than its "instantaneous" rigidity determined by the modulus of elasticity (see Section 6.2 and Fig. 6.2).

If so, it is reasonable to assume that, at given temperature, polycrystalline silicates acquire properties of effectively viscous liquids only if the external pressure exceeds the long-term strength of the matter's intercrystalline bonds. Usually, the long-term strength of polycrystalline materials is about one order of magnitude lower than their instantaneous rigidity modulus (Zharkov, 1976). Then, we can determine from the S-wave propagation velocity in the upper mantle at a depth of 220 km ($U_s = \sqrt{\mu/\rho} \approx 4.6$ km/s) that the critical value of approximately 70 kbar is currently reached at depths of 200–220 km.

Maximum thickness of the continental lithospheric plates of 200–250 km is also supported by petrological determinations of the maximum formation depth of mineral associations in depth xenolites from Kimberlites. Based on petrologic determinations (Kaminsky,

1984), the formation depth of diamond-bearing rocks and xenoliths usually does not exceed 220–250 km (70–80 kbar at $T \approx 1120$–$1290\ ^\circ$C). Maximum age of the diamonds determined from the inclusions isotopy (see below) indicates that at those depths the continental lithosphere preserved its rigidity for at least 2 BY. Otherwise, both the diamonds and xenogenic material would have been numerously assimilated in the mantle over such a long period from the time of their formation.

Thus, the above considerations and data provide certainty that the lithospheric plate thickness under the old continents is within a range of 200–250 km and on average may be assumed to be 220 km.

It also follows from the provided considerations that within the existence range of the mantle melts (at depths up to 100 km) it is possible to use the classical determination of the lithosphere and to take it that its base position is determined by the mantle matter solidus temperature $T_s^1$. Deeper, only a notion of the effective thickness may be used, assuming that the lithosphere base depth is determined by the temperature of the mantle matter transition from the rigid to the plastic, very high viscosity but still effectively liquid state. At the lithospheric base, such transition must occur at somewhat lower temperature but still close to the convecting mantle temperature. For a depth of 220 km, effective value of this temperature may be assumed equal: $\widetilde{T}_s^1 \approx 1450$–$1460\ ^\circ$C at $T_m \approx 1500\ ^\circ$C. In this case, the averaged correlation $\widetilde{T}_s^1(z)$ may be written, as a first approximation by a linear function, as:

$$\widetilde{T}_s^l = T_s^0\left[1 + 1.7 \times 10^{-8} Z\right] \tag{7.16}$$

where $T_s^0 \approx 1060\ ^\circ$C is the mantle matter solidus temperature on Earth's surface.

We now discuss the evolution of the depth and radiogenic heat flows running through the continental lithospheric plates. $\widetilde{q}_m$ is proportionate with the mantle heating, that is, the temperature difference $T_m^0 - T_s^0$. We assume that $T_s^0$ at low pressure changed little with time and remained on average 1060 °C. But mantle temperature $T_m^0$ normalized for the surface changed significantly in the course of Earth's evolution (see Fig. 4.5). These changes were most likely caused by the zonal differentiation of metallic iron whose content in the primordial Earth's matter reached 13%. It was evolving in Early and Middle Archaean (Sorokhtin and Ushakov, 1991). As Fig. 4.5 shows, the upper mantle surface temperature in Early Archaean exceeded 1500 °C, rose to 1700 °C by the middle of Late Archaean, rapidly declined to 1400 °C by the Archaean–Proterozoic time boundary, and to 1300 °C today. The Archaean overheating, in particular, was a reason for the komatiite lavas abundance in the Late Archaean greenstone belts.

We can determine the proportionality factor in the function $\widetilde{q}_m \sim \left[T_m^0 - T_s^0\right]$ by assigning the present-day value of the deep heat flow $\widetilde{q}_m$. For this, however, we have to first assign temperature at the top of the subcrustal lithosphere $T_0^1$ (or, which is the same, temperature at the base of Earth's crust $T_0^{KK}$). Smirnov (1980) indicates that underneath the Archaean platforms and shields $H_{cc} \approx 40$ km, and temperature at the Moho boundary is close to $T_0^1 \approx 400\ ^\circ$C. Remembering that the heat flows underneath the old shields are about stationary we determine from (7.16) that at depth $(H_{KK} + H_l) \approx 220$ km $\widetilde{T}_s^1 \approx 1456\ ^\circ$C. Then from Eq. (7.10′), at $2 \approx 5 \times 10^{-3}$ cal/cm s deg and $H_l \approx 180$ km, $\widetilde{q}_m = 0.29 \times 10^{-6} \approx 0.3 \times 10^{-6}$ cal/cm$^2$ s.

Another independent estimate gives for the total radiogenic release in the continental crust of about $0.91\,10^{20}$ erg/s (Sorokhtin and Ushakov, 1991). The total area of the continental crust is close to $2.04 \times 10^{18}$ cm$^2$, wherefrom average radiogenic heat flow is $\bar{q}_R \approx 1.06 \times 10^{-6}$ cal/cm$^2$ s.

At average heat flow through the continents of $\bar{q}_{KK} \approx 1.4 \times 10^{-6}$ cal/cm$^2$ s (Sclater et al., 1980), average depth heat flow is $q_m \approx 0.34 \times 10^{-6}$ cal/cm$^2$ s.

It is obvious that for the old shields the flow $q_m$ should be somewhat lower that the derived average value for the entire continental crust. Because of that, we assumed for the subsequent calculations that average value of the present-day depth heat flow through Precambrian areas of the continental crust is equal to $\tilde{q}_m \approx 0.3 \times 10^{-6}$ cal/cm$^2$ c. Then the sought-for correlation is

$$\tilde{q}_m \approx 1.25 \times 10^{-9}\left[T_m^0 - T_s^0\right]. \tag{7.17}$$

This equation shows that during the Archaean epoch of the upper mantle overheating to ${T_m}^0 \approx 1600$–$1700\,^\circ$C the stationary depth heat flows were approximately 2–2.5 times stronger than their current values.

After we determined the present-day parameters of the depth heat flow through the continental crust we can use Eq. (7.4) for the estimation of the average radiogenic component value on the old shields and platforms. For most of the Archaean shields $q_0 \approx (0.8\text{–}0.9) \times 10^{-6}$ cal/cm$^2$ s, thus $q_R \approx (0.5\text{–}0.6) \times 10^{-6}$ cal/cm$^2$ s. The provided examples show, in particular, that the Archaean shields rock radioactivity is much lower than is typical of average heat flow values within the continental crust ($\bar{q}_R \approx 1.06 \times 10^{-6}$ cal/cm$^2$ s).

To be able to calculate heat flows of the radiogenic origin, we need to know the rate of radioactive elements accumulation in the continental crust. We assume that this rate was approximately proportionate with the mass of these elements in the convecting mantle and with the rate of the continental crust formation. In Archaean, the mantle mass $M_m$ continuously increased on the account of gradual heating of Earth's primordial matter (which was at that time still available at great depths) and its involvement in the convective mass exchange. And the continental crust-formation rate $M^{cc}$ was fully determined by Earth's tectonic activity (Sorokhtin et al., 1996). Taking that into consideration,

$$\sum \dot{m}_R^i = -\sum (m_R^i)_0 e^{-\lambda i t} \frac{M_m}{M_g} \chi_i \dot{M}_N^{cc}, \tag{7.18}$$

where ${m_R}^i$ is the mass of the $i$th radioactive element ($^{238}$U, $^{235}$U, $^{232}$Th, and $^{40}$K); $({m_R}^i)_0$ are the initial contents in Earth of these elements; $\lambda$ and $\chi_i$ are, respectively, half-lives and mobility factors of the radioactive elements; $M_m$ is the mass of the convecting mantle; $M_g$ is the Earth's mass; $\dot{M}_N^{cc} = \dot{M}^{cc}/M_0^{cc}$ is the relative rate of the continental crust formation normalized to the current crust mass ${M_0}^{cc}$; a dot over the parameter denotation, as usually, indicated the derivative of this parameter over time.

Now, as the radioactive energy generation rate is always proportionate with the radioactive elements mass $\dot{\xi}_R \sim m_R^i$, the solution of Eq. (18) for Archaean may be formatted as follows:

$$\dot{E}_R^{cc} = \sum (\dot{E}_R^i)_0 e^{-\lambda_i t}[1 - e^{-\chi_i \mu}], \tag{7.19}$$

where $\mu = \int_0^{M^{cc}} M_m / M_g \, dM^{cc} / {M_0}^{cc}$; ${\dot{E}_R}^{cc}$ is the radiogenic energy dissipated in Earth's crust; $({\dot{E}_R}^i)_0$ is the initial radiogenic energy radiation level by an $i$th radioactive element at the moment of Earth's emergence.

After Archaean, all radioactive elements concentrated in the mantle or crust. Thus, the solution of Eq. (7.18) should be formatted somewhat differently:

$$\dot{E}_{\mathrm{R}}^{\mathrm{cc}} = \sum (\dot{E}_{\mathrm{R}}^{i})_{\mathrm{AR}} \mathrm{e}^{-\lambda_i \Delta t} + \sum (\dot{E}_{\mathrm{R}}^{i})_0 \mathrm{e}^{-\lambda_i \cdot t} \left[1 - \mathrm{e}^{-\chi_i \Delta M_N^{\mathrm{cc}}}\right], \tag{7.19'}$$

where $(\dot{E}_{\mathrm{R}}{}^{i})_{\mathrm{AR}}$ is the radiogenic energy generation by end Archaean; $\Delta t$ is the time counted from end Archaean; $\Delta M_N{}^{\mathrm{cc}} = M_N{}^{\mathrm{cc}} - (M_N{}^{\mathrm{cc}})_{\mathrm{AR}}$ is a relative change of dimensionless (normalized) continental crust mass after Archaean.

Sorokhtin and Ushakov (1991) determined the radioactive element masses within Earth $(m_{\mathrm{R}}{}^{i})_0$; $^{238}\mathrm{U}_0 = 9.62 \times 10^{19}$ g; $^{235}\mathrm{U}_0 = 3.04 \times 10^{19}$ g; $^{232}\mathrm{Th} = 2.22 \times 10^{20}$ g; $^{40}\mathrm{K}_0 = 1.29 \times 10^{21}$ g.

And their content in the present-day continental crust: $\mathrm{U} = 3.71 \times 10^{19}$ g; $\mathrm{Th} = 1.48 \times 10^{20}$ g; and $^{40}\mathrm{K} = 5.49 \times 10^{19}$ g.

These data enabled an estimate of the radiogenic energy generation within the continental crust during all its existence. The differential radiogenic heat flow

$$q_{\mathrm{R}}^{t} = \left(\mathrm{d}\dot{\xi}_{\mathrm{R}}^{i} / \mathrm{d}S^{\mathrm{cc}}\right)_t \tag{7.20}$$

is the rate of radiogenic energy dissipation in the core areas of given age $t$, and average flow

$$\bar{q}_{\mathrm{R}} = \dot{\xi}_{\mathrm{R}}^{\mathrm{cc}} / S^{\mathrm{cc}} \tag{7.21}$$

describes average value of the radiogenic flow on the whole over the entire area $S^{\mathrm{cc}}$ of the continental crust whose individual parts formed at different times.

We now review in more detail the continental crust heat regime evolution. The thickness of the upper rigid crust $H_1{}^{\mathrm{cc}}$ is determined by the position of the geotherm of the continental crust water-containing rock melting start which we tentatively assumed to be $T_{\mathrm{s}}{}^{\mathrm{cc}} \approx 600$ °C. The depth of this geotherm is determined from Eq. (7.5') by the insertion of $T = T_{\mathrm{s}}{}^{\mathrm{cc}} \approx 600$ °C and $Z = H_1{}^{\mathrm{cc}}$, provided temperature at the crust base $T_0{}^{\mathrm{cc}} = T_0{}^{1} > T_{\mathrm{s}}{}^{\mathrm{cc}} \approx 600$ °C. In such a case, the lower crust matter is partially melted (migmatized) and is intensely stirred by the heat convection. And the higher the depth heat flow $q_{\mathrm{m}}$, the more intense the convection and mass exchange in the lower crust $H_2{}^{\mathrm{cc}} = H_{\mathrm{cc}} - H_1{}^{\mathrm{cc}}$.

The determined boundaries positions of phase transition from the rigid upper crust to a partially melted lower crust are shown in Fig. 7.9. The diagram indicates that in Archaean the continental crust was very thin everywhere (its subcrustal portion did not exceed 40 km), and at the time of the maximum mantle overheating about 2.8 BY ago it dropped to 20–25 km.

Convection within the lower crust transported the differentiated light sialic material into the upper crust. However, as already mentioned, high efficiency of the convective heat release maintained in the lower crust the sub-solidus temperatures, at which only eutectic melts could be produced.

Thin Archaean plates certainly could not have the same strength as the present-day ones that reach 180–200 km in their subcrustal portion. That is why it is expected that the continental plates in Archaean were sufficiently plastic and could have been subjected to very significant deformations both in the oceanic basalt plate pile-up zones and at collisions of individual continental massifs. That was manifested with particular strength in the epoch

of maximum mantle heating and formation of a first supercontinent, Monogaea about 2.7–2.6 BY ago (Sorokhtin and Ushakov, 1991).

In the entire range of aluminosilicate crustal rocks, only granitoids have eutectic properties. This can explain very common development of granitoids and genuine granites intruded in Archaean from the lower into the upper crust. With granitoids, many lithophilic components including alkali, rare earths, and radioactive elements migrated into the upper crust. The lower crust matter, naturally, was losing all these elements, silicon and was enriching in calcium and magnesium oxides. As a result, after the emergence of the primary tonalite–trondhjemite continental crust this process led yet in Archaean to gradual separation of this crust into two layers. The upper one was enriched in lithophilic elements, mostly granitic, and the lower one, the enderbite–charnokite–diorite Archaean granulite layer impoverished in lithophilics. Calculations indicate that the lower crust anatectic layer (the continental crustal asthenosphere) existed underneath all without exception old shields during entire Archaean (see Figs. 7.5 and 7.9).

The continental crust formation in Proterozoic and Phanerozoic occurred under the lithospheric plate tectonics mechanism. The crust emerged over the plate subduction zones on the earlier formed lithosphere. Depth heat flow on such plates is usually low, $q_m < (1–0.5) \times 10^{-6}$ cal/cm$^2$ s. At the same time, although the heat flow radiogenic component reached $q_R \approx (2–3) \times 10^{-6}$ cal/cm$^2$ s, they were generated within the uppermost thin layers of the continental crust. That is why they could not make a substantial contribution to the heat regime of the entire crust. And that is exactly why underneath the Proterozoic and Phanerozoic age crust, contrary to the Archaean one, continuous and stable crustal asthenospheric layers usually did not emerge (see Fig. 7.9). Commonality and longevity of such partially melted layers within the crust are typical of Archaean only. This is a major and important distinction between the Archaean crust and the younger continental crust areas.

No less radical was the effect of specific Archaean conditions on the lithospheric plate structure. As follows from the (7.10) solution, the subcrustal lithosphere formation was definitively affected by the mantle temperature conditions $T_m$ and the conditions at the lithosphere base $T_s^l$ and top $T_0^l$ as well as by the depth heat flow $\widetilde{q}_m$. The $T_m$ and $\widetilde{T}_s^l$ parameters are temperature as a function of depth. They are calculated from Eqs. (7.15) and (7.16), the lithosphere surface temperature $T_0^l$ is found from (7.5″) and (7.7) at $T_s^{cc} \approx 600$ °C, the depth heat flow $\widetilde{q}_m$ is found from (7.17), and the radiogenic component $q_R$, from Eqs. (7.19), (7.19′), and (7.20).

The continental crust thickness began rapidly increasing in the end Archaean and in Proterozoic. Correspondingly, its strength increased as well, the tectonic evolution of the continents changed from the thin and mobile (plastic) plate geodynamics to the tectonics of lithospheric plates. At the same time, the present-day type of the subduction zones emerged. As depth heat flow declined, the young lithospheric plate thickness increase rate increased noticeably. By the end of Early Proterozoic (about 1.8 BY ago), the continental lithospheric plate thickness underneath the Archaean crust blocks had already increased to 180–200 km. These estimates are approximate so it is possible that their total thickness may have reached 220 km. Subsequently, the old plate thickness remained about constant.

Currently, only relatively young Phanerozoic continental plates remain relatively thin. That is exactly why the young areas of Earth's crust (such as the West Siberian epi-Paleozoic or the Sea of Okhotsk epi-Mesozoic platforms) are currently experiencing a stable subsiding trend.

Strength of a fully crystalline matter is determined by its elastic modulus of rigidity $\mu$. The same modulus controls S-wave propagation velocity in such matter:

$$v_s = \sqrt{\mu/\rho}. \tag{7.22}$$

If external pressure exceeds the modulus of elasticity of a crystalline matter, such matter must turn to the amorphous state of an overcooled liquid although the viscosity of such liquid may be very high. For the crystalline silicates such transition to amorphous state may occur only under pressures in excess of 2–3 Mbar, that is, way outside of the mantle pressure range.

For a polycrystalline matter, however, effectively amorphous state may only emerge after the external pressure exceeds the intergranular bond strength which is determined by the value of the long-term strength $\widetilde{\mu}$ of such matter. If such is a case, the matter at $P > \widetilde{\mu}$ remains polycrystalline but its component crystals acquire the capacity for reciprocal displacements even under small shear stresses

$$\tau \approx \eta \dot{\varepsilon}, \tag{7.23}$$

where $\eta$ is matter viscosity and $\varepsilon\cdot$ is the propagation rate of the emerging plastic deformations. For this reason, such a plastic state of the stressed polycrystalline matter may be treated as effectively a liquid state despite its temperature remaining way below the melting temperature. At that, under the Arrhenius law, temperature still remains the main controlling factor of the matter viscosity.

Usually, the long-term strength $\widetilde{\mu}$ of polycrystalline compounds is one order of magnitude lower that the "instantaneous" (elastic) strength $\mu$ (Zharkov, 1976). It may be concluded from the S-wave propagation velocity in the upper mantle underneath the continents ($\vartheta_s \approx 4.6$ km/s) that the "instantaneous" value of the elastic modulus of rigidity is $\mu \approx 7 \times 10^{11}$ dyne/cm$^2$. Based on this we assume that $\widetilde{\mu} \approx 7 \times 10^{10}$ dyne/cm$^2$ and from this we determine that the critical pressure $\widetilde{P} = \widetilde{\mu} \approx 7 \times 10^{10}$ dyne/cm$^2$ is reached at depths of about $\widetilde{H} \approx 216$ km which closely relates to the depth of the base of the continental lithosphere. As these estimates are approximate, we may assume that the critical pressure in the mantle is reached at the level of the Lehmann (1959) boundary, that is, at a depth close to 220–250 km (see Fig. 6.2, boundary VI).

The continental crust is drastically heterogeneous in its structure and composition. The reason is diverse environments in the lithosphere underneath the continents in post-Archaean. The crust was numerously fragmented, assembled again, reworked and formed anew together with the continental crust near the subduction zones where to the oceanic plates were sucked-in together with the oceanic crust and its overlying deposits. Within these zones, the oceanic crust rocks were dehydrated and remelted. Complex metamorphic and metasomatic processes were evolving there, transforming the lithospheric matter within the former plate subduction zones and forming the composition of the continental crust above them. After numerous overprinting and superposition of these processes, a complex mosaic of blocks welded along the deep suture zones must have emerged. Most of these sutures are former subduction zones.

At the same time, all these suture zones are the zones of weakness. Thus, with any changes in the lithospheric state of stress (such as caused by the restructuring of the mantle convection flow system, etc.) any intraplate motions occurred first of all along these zones

of weakness or the already existing faults. The consequence was the inherited nature of tectonic movements along the old faults and suture zones.

## 7.7 EARLY PRECAMBRIAN GEODYNAMIC REGIMES, THEIR EVOLUTION, AND LOCATION

Presently, Earth's upper shells include a thick rigid lithosphere (reaching ~200 km underneath the continents) and the underlying plastic mantle. Geodynamic processes in the mantle affect the lithosphere. As already mentioned, the Archaean continental crust was a dual layer formation. The upper layer (10–12 km, sometimes less) was rigid, and the lower was represented by a partially melted highly plastic layer (~28–30 km and thicker). It was in turn underlain by the crystalline layer of the subcrustal lithosphere overlying the mantle's asthenosphere. Based on this, it is possible to assume for Early Precambrian vertical alternation on the tectonic and geodynamic processes manifestation areas.

The attempts to reflect the Early Precambrian geodynamic processes on the specialized maps often are made difficult due to the lack of knowledge about their manifestation patterns in time and space. Until recently, it was practically impossible to generate a complete shield or continental area geodynamic map which would allow one to clearly discern all evolutionary patterns of either inter-domain or intra-domain structures from the moment of nascence to the present-day slice. Most of the available Early Precambrian geodynamic maps usually reflect Early Proterozoic, sometimes Late Archaean, events, whereas only very little attention is devoted to the earlier crust-forming processes (Minz, 1992; Sinitsin, 1992).

The major tenet in the generation of such a map should be to present the structural–material markers of geodynamic regimes which reflect a continuous chain of the crust-forming and crust-modifying processes within the subject region. As mentioned, we understand the geodynamic regime as a combination of characteristic indications allowing for the reconstruction of the depth forces and processes, identification of their interaction mechanisms and determination of their effect on the surface tectonic processes.

In deeply eroded continental areas where structural associations of the former crustal-asthenospheric layer are exposed, structural–material complexes may be classified by their attribution to a certain geodynamic regime whose markers they represent. We may assume that the picture we are observing is the reflection of events that occurred at that time at a certain depth, and the nature of these events was preserved as a result of the superimposed processes or other factors. That is why, before starting the identification of dynamic regimes' consolidated indicators, it was necessary to create a schematic map of the regimes positions in space and time, identify mechanisms of their interaction and hierarchy of their manifestation.

The processes and phenomena spatial inter-subordination enable the identification of cause-and-effect connections between the geodynamic regimes. The regimes may be subdivided into the planetary in scope, regional, and local. Assuming that the global convective stirring of the mantle matter existed in some form during the entire Earth's geological history, it is natural that it was the most efficient mechanism generating regimes of the regional and local rank.

The regimes may be identified at the Earth's crust compression due to which the continental-type crust was formed, as well as the aggradation and transfiguration of the continental lithospheric plates along the periphery. As mentioned earlier, during Precambrian

and especially Archaean, prerequisites were created within the surface geospheres for the emergence of large volumes of matter which caused the formation of the future continents. Thus, three independent geodynamic regime groups may be identified. Two of them reflect the compression or relative quiescence environments, and the third one, the extension environment over the ascending branch of the mantle cell.

The emergence of continental-type crustal nodules also enables the identification of the regimes reflecting their birth, differences in the evolution paths and regular deaths of the active endogenous processes. Although the present-day status of the continental kernels usually corresponds with the conditions of the end of tectonic evolution, we will make an attempt to recreate their evolutionary path from the moment of birth.

Glukhovsky (1990) and Moralev (1986) identify in the basement of ancient platforms large isometric structures which are nuclears (sialic cores) separated by mostly by simatic internuclear areas which have a thinner consolidated crust and lithosphere compared with the sial. The nuclears are focal geodynamic systems that emerged within the mantle in the environment of a high heat flow (Pospelov,1971). Their lateral and vertical growth defines the stage-by-stage irreversible processes of the primary basite crust transfiguration into the continental crust.

The earliest stage of the continental-type crust formation is defined by the sialic kernels emergence regime. This regime must have reflected the entire specifics of their formation time and rapid growth. If the system existed in a relatively uniform stress field (a geostationary conditions), the formation of large of domal (diapiric) structure fields was possible as a result of the density inversion and buoying of the granitoid material. Under the dominance of tangential (horizontal) compression, a combination of buoying and lateral compression may be observed, up to the formation of syn-tectonic flattened bodies of the squeezed granitoid matter (Polyansky, 1987).

The "domal swarms" or pile-up areas formation processes are always accompanied by the injection into the crust of a relatively lower density granitoid matter heated to almost sub-solidus temperature. The interdomal areas filled up with a colder and often more compositionally basic, therefore denser matter subsided. A pattern in the implementation of this process is nothing but nonstationary convective stirring of the crustal matter with the addition of a newly formed material.

Thus, the described events were followed not only by deoxidizing of the upper crustal layers but also by their compaction. These processes could not but show up within the near-surface levels of the Archaean crust and, most likely, formed the ascendant structures (i.e., the domal structures).

These typical tectonic formations are well known, studied in the Phanerozoic complexes, and do not require any detailed consideration. The long-term interactions between the described events as well as the high continental stand in Archaean facilitated the intense destruction of the surface and exposure of the depth levels. That may explain a paradox of the Archaean conglomerate pebbles composition discrepancy with the surrounding tonalite–trondhjemite formations of the Early Archaean continental crust. As a rule, the pebbles are composed of more acidic material that the framework granitoids. The reason was, most likely, that the rocks eroded on the surface are supplied to the continent foot and then, at the collision with the other similar formation, they turn out to be associated with the depth-derived more compositionally base tonalite–trondhjemites.

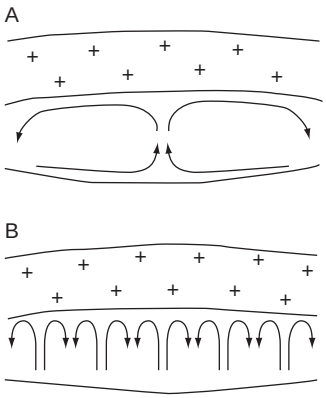


**FIGURE 7.18** Suggested convection types within the crustal asthenosphere. (A) Stationary and (B) nonstationary.

The next regime in its manifestation timing and also reflecting the evolution of the forming continent system is the crustal asthenosphere regime. As was shown above its typical feature was the lower continental crust layer capable of viscous or plastic flow whose state was that of unstable temperature equilibrium. The necessary condition for a normal evolution of such system is it relative closeness. It enabled the lower crustal layer to evolve as the volume of intense endogenous processes affecting the rigid surface layer.

The condition of unstable temperature equilibrium by definition assumes the presence of certain temperature leveling mechanism at the base and top of the layer, the mechanism depending first of all on the intensity of the heat-generating source. The two most common heat transfer types are the conductive and convective. Where the lower crustal layer was partially melted, the contribution from the conductive heat transfer must have been relatively small. Heat transfer was conducted mostly due to convection which occurred together with the mass transfer.

On the whole, the heat-mass-transfer within the lower crustal layer could have been orderly (stationary) or disorderly (nonstationary) convection (Fig. 7.18). Stationary convection reflected the maximum process manifestation and caused the presence of one or several cells within the entire volume of the convecting layer (the critical parameters determining the existence of such a cell are, for instance, the diameter of 100 km and the layer thickness of 30 km). Disorderly convection has several cells continuously changing their positions and may be compared with the conditions of pseudochaotic flotation for the granite diapires. So, if stationary convection occurred within the crustal asthenosphere, this could result in the emergence of a typical structure–material paragenesis reflecting this regime. For instance, an accumulation of domal structures may be observed in the central portion of the domain, and metamorphic parageneses can reflect a deeper level of metamorphism thereby indicating the conditions of the subvertical matter ascent. Over the domain, periphery may be observed the transfer of the metamorphic zoning vertical branch to a horizontal branch and the structures can reorient into the matter plastic flow zones in a subhorizontal plane.

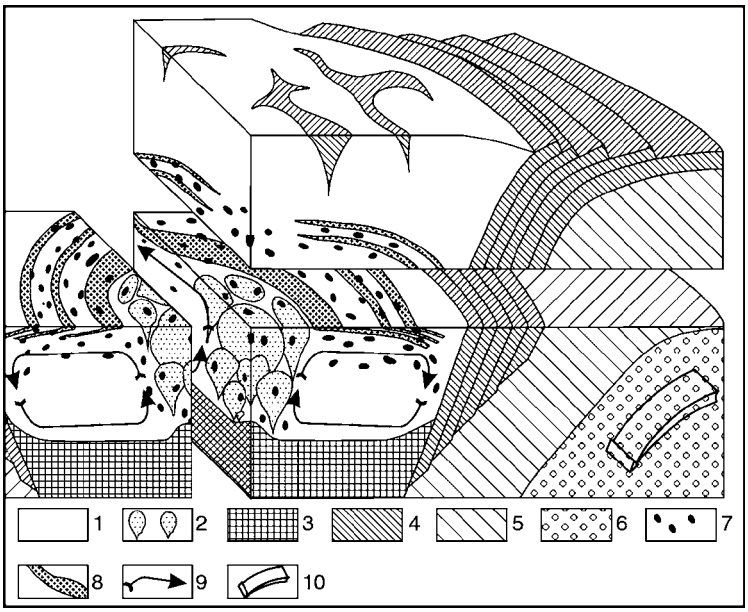


**FIGURE 7.19** Typical features in the evolution of the Kovdozer domain crust asthenosphere (White Sea mobile belt): 1, continental crust; 2, granite–gneiss domes; 3, subcrustal area of the continental lithosphere; 4–5, oceanic type lithosphere; 6, mantle's asthenosphere; 7, protolith xenoliths and restites in the crust asthenosphere; 8, transition area from the crust asthenosphere to the crystalline crust; 9, matter flow directions of the crust asthenosphere; and 10, flow directions of the upper mantle matter.

One example of the orderly convection in the lower Archaean crust is the pre-collision structural–material complexes in the Belomor mobile belt (Kozlov et al., 2006) (Fig. 7.19).

As shown above, temperature equalization within the lower crustal layer almost always had to lag when parameters of the heat-generating source in the subcrustal volume changed. If the heat inflow from underneath increased significantly and rapidly, then a local accumulation of the excess heat could form in the equalization area. If the convection was stationary, the appearance of such a node in the heated matter upfloating area could facilitate piercing of the rigid upper crustal layer and heat transfer directly from the heat-generation volume to the atmosphere. That would create the conditions for a rapid system cooling and draining of the matter from the subcrustal zone through fissures. On the whole, this phenomenon tended to stabilize the entire system and therefore resonates in substance with the processes occurring under the cratonization regime of the materially similar magmatic complexes (see below).

Rapid destruction areas of the continental crust upper portion facilitated the exposure for different levels of crustal–asthenospheric layer. That is why it is possible to encounter in a region with several generationally different crustal domains differences in the combinations of the marker rock associations, individual trends in metamorphism and structural forms.

There are certain features in the nature of the lithostatic pressure associated metamorphism, in its classic format, that are supposed to be found below the crustal–asthenospheric layer. These are: the granulite facies; slowed-down anatexis process of enderbite-charnokite

matrix; the presence of abundant mafite and ultramafite xenoliths; and restites as well as structures typical of subhorizontal viscous flow. The asthenospheric level of the Archaean continental crust must be easily diagnosable by the presence of polymigmatite associations (indicating the intensity of substrate anatexis), of metamorphism's amphibolite facies conditions and of the viscous flow structures. Zones of a wide manifestation of the depth metasomatosis processes may also be present in the same area. These processes are caused by high fluid-saturation of the granitoid matter.

The matter stirring in the crustal–asthenospheric layer provides an opportunity to identify the connection between the lower and upper levels based on the relics in the upper portion reflecting the matter state within the lower level. Thus, in the ascent areas of the crustal asthenosphere, the relic metamorphism of granulite facies may be observed in the ascended matter which underwent diaphtoresis (retrograde metamorphism) and serves the fragmentary carrier of memories of depth events. Such buttes may be found in central areas of the domal structures.

When studying the sequence of geodynamic regimes in a specific region, discrepancies may sometimes be encountered in the evolutionary processes within individual crustal domains and their separating structures. Such mosaicity of the regional structure may be caused not only by the genetic differences in the component structures but also by erosion depth of the continental crust. For instance, the surface of the crustal–asthenospheric may be represented by its upper, middle, or lower portions. Each of these levels must be different in the extent of metamorphic and metasomatic processes, in the nature of structure formation, granite generation conditions, and so on.

The uncertainty in diagnosing a geodynamic regime may arise when the erosion exposes transition zones from the crystalline (brittle) crustal layer to the crustal asthenospheric layer or from the crustal asthenospheric layer to the subcrustal lithosphere. These exposed transitional zones often cannot indicate the nature of the processes in the layers between which they were born. Some secondary issues may also cause difficulties in the identification of geodynamic regimes. Such secondary issues may be scarce previous studies, the lack of natural exposures, and so on.

Natural processes of the Archaean crust formation usually resulted in the emergence of a volcanosedimentary complex which was the protoplatform continental cover in Early Precambrian (Moralev, 1986; Khain and Bozhko, 1988). Some areas were subsequently subjected to the intense erosion which exposed depth crustal levels. In such areas, the stabilization processes may be identified from the characteristic intrusive magmatism. Most common of these magmatisms are the intrusions of alkaline and subalkaline granites and anorthosite–granite complexes.

We merged all the aforementioned processes of the continental crust ancient kernel formation into a single temporal chain. The result is the succession of the regimes manifestation: the sialic kernels emergence regime $\Rightarrow$ the crustal–asthenospheric regime $\Rightarrow$ the cratonization regime. This succession of the events often resulted in the deep portions of the crust being exposed by the time of cratonization in the micro-continent center.

In certain cases, however, well-preserved surface or near-surface formations are observed in the kernels of the ancient continents. Such are, for instance, the Isua Fm. in Greenland and the Pilbara craton in Australia. They indicate the absence of the destruction for the upper crust in those areas.

An explanation may be found using the described crust-formation process. This needs to be done in consideration of the fact that if metamorphism, partial melting, and differentiation of the basite matter over large areas (larger that the critical sizes of the continental crust developing kernels) occurred simultaneously, the focus of the continental mass melt-out underneath of the forming continent kernel may have been depleted. As a result, it rapidly cooled down, increased in density, and therefore sagged. Such events must have substantially slowed down the denudation of the micro-continent central areas relative to its periphery.

The manifestation specifics of these processes could result in the changed nature of the system evolution. The system might have jumped after its birth immediately into the cratonization regime and, hence, not have experienced lengthy upheaval leading to the intense surface erosion. In the described case, the domain evolution scheme would look like following: nascence of the sialic kernels ⇒ cratonization.

Apparently, just because of this phenomenon it was possible to identify sufficiently old rock ages in the tonalite–gneiss and amphibolite complexes (Isua Province, Western Greenland), in Southern Africa, in the Prince Charles Province in Antarctic, and in the Pilbara Block of Australia. When the system was undergoing normal evolution, the isotopic parameters of the continental crust complexes could have been rejuvenated due to a long-term evolution of the crustal–asthenospheric layer within the domain. It is possible that the Kola granulite–gneiss area and a number of other areas belong to this kind of the continental massifs.

It is possible to identify within each geostructural element of the crust (domains, microplates) in Early Precambrian sections the individual zones of the crust-forming geodynamic regimes. Various combinations of the regimes may be identified only in cases where there is some mechanism of a very rapid consolidation of the processes that are occurring within them.

On the other hand, we know that the Archaean–Proterozoic time boundary is marked on many continents by the event reflecting collision processes. This is certainly associated with the formation of the oldest supercontinent named Monogaea. One way or the other, the collision interactions facilitated rapid die-out of the processes which, under the described conditions, sequentially replaced one another within the crustal domains. That is why it is possible to observe in the specific regions the evolution of those pre-collision processes which occurred there prior to the time in Late Archaean when they were set by the superimposed processes.

The collision regime not only causes the buildup of new crustal volumes but also to a significant extent the transformation of those already formed. In detailed regional studies, it is sometimes possible to identify the differences in the collision regime manifestations within the Early Archaean crustal blocks, in their suture and internal zones. In general, however, this geodynamic environment should display the allochthonous position of the material complexes, a commonality of overthrusts and plastic flow zones, high pressure metamorphism, and strong manifestations of the granite formation and rock migmatization (Fig. 7.20).

Extended study was conducted by one of the authors (N. Sorokhtin) in the structure–material complexes of the Baltic Shield Belomor mobile belt and its surroundings. It was found that the Belomiride suture zone *per se* and the suture zone of the Kola granulite–gneiss area are covered by a greenstone-type supra-crustal allochthone and the protrusions

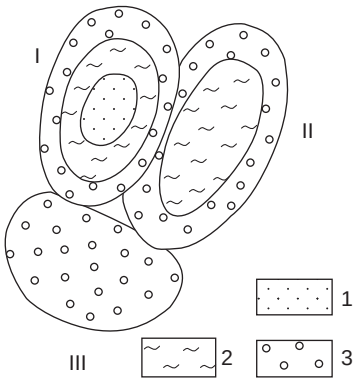


**FIGURE 7.20** Lateral zoning in derivatives of different geodynamic regimes within different crust domains (schematic presentation) (I–III). Regimes: 1, cratonization; 2, crustal–asthenospheric; and 3, birth of sial cores (crust-forming diapirism of the peripheral zones).

of the deep crust (the Lapland-Kolva granulite belt; Bogdanov et al., 1992). Thus, we have closely positioned material complexes different in their genesis and formation depth. Some of them are brought up from the crust/subcrustal lithosphere boundary, and some of them are subsided surface or near-surface formations. Such a situation is typical of the Archaean continental collision formations which may, in the current geodynamic environments, correspond with the development areas of the paired metamorphic belts (Miyashiro, 1976).

This issue, however, is not well understood and requires additional studies.

Based on the type of the process manifestation, the suture zone, foreland structure on the foot wall, and the back zone on the hanging wall may be identified in the collision zones. The deformation nature of the upthrowing plate edge suggests the formation of stress discharge zones under the general dominance of the compression environment. The matter from the acidic, medium, and base magma generation areas could have been released through these zones. Due to high core matter plasticity in Archaean, the lower crust matter may have been intensely squeezed out through these zones. The squeezed-out matter would have formed flattened domes or thin syn-tectonic bodies marking the strike-slip offsets. The situation in the underthrown plate (the foreland structure) would most likely differ mostly in the compression environment. The lower crust plastic matter may also have been squeezed out due to additional heating from the system deformation by the overlying allochthone.

No less important for the identification of the region's geodynamic regime are structural–lithologic complexes reflecting the conditions of Earth's crust expansion. Most Early Precambrian greenstone belts belong with them. Most of them reflect the formation conditions of the oceanic type crust within ancient oceans like Pantalassa. Some of them, however, are results of the riftogenesis process in the continental crust.

It is noteworthy that the intra-crust rift zones are readily recognizable approximately after the Archaean\Proterozoic time boundary (~2.6 BY) and are marked by associations of the alkaline and bimodal volcanic series, alkaline, alkaline–ultramafic rocks, and the sediments of graben facies (Minz, 1992).

Glickson (1976) studied the genetic nature of greenstone belts. He proposed to subdivide the Early Precambrian greenstone belts into the primary and secondary ones. He proposed

to include among the primary belts the base and ultramafic intrusive and eruptive formations as well as the associated clastogenic sediments. This type of greenstone belts is in his view a butte of the previously existed proto-oceanic type crust whose reworking resulted in the formation of the earliest continental shell.

If we accept that the continental crust is a derivative in the metamorphism, partial melting, and differentiation of the basite substrate, it becomes understandable why buttes of the oceanic proper type basalt crust (the proto-oceanic or oceanic proper regime) may be encountered within the sialic continental masses.

Condie (1981) analyzed the data about the Archaean greenstone belts based on their stratigraphy. He came to a conclusion that the primary greenstone belts formed during entire Archaean, whereas the secondary, that is riftogenic over the continental crust, only formed at the time boundary 2.6–2.7 BY ago. This is a very interesting conclusion indicating global changes in the nature of geodynamic processes by the end Archaean—beginning of Proterozoic. Crust domains identified within the study region often include xenoliths of older basite composition formations (greenstone associations). At the same time, these associations may be encountered within the inter-domain (inter-craton) space marking their merger zones.

This spatial position of the primary greenstone belts (Fig. 7.21) is very much understandable if it is accepted that a small-cell heat convection of the mantle substrate was possible in Archaean.

This, in turn, suggests the emergence and evolution of individual continental masses which did not experience any significant lateral movements up to the Late Archaean time boundary and were evolving independently (see Figs. 7.5 and 7.22). At the end Archaean they stuck together, resulting in the closure of their separating channels and in the emergence of ensimatic craton belts of a greenstone-type.

It may be concluded in general that the continental crust initiation and evolution processes in Early Precambrian were quite typical for all regions of the world. These issues were studied in minute detail over the eastern Baltic Shield (Kozlov et al., 2006). The geodynamic style of its development indicates a two-stage set-in of the continental lithosphere in

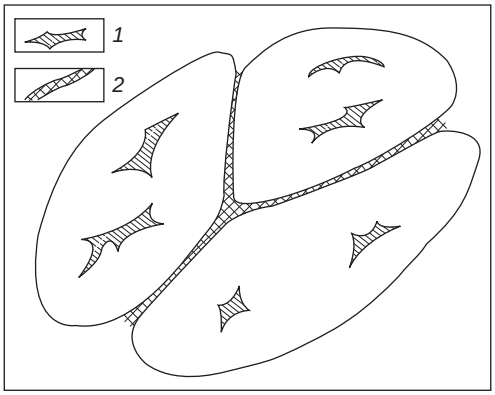


**FIGURE 7.21** Spatial distribution of the "primary" (after Glickson, 1976) greenstone belts: intra-block (1) and inter-block (2).

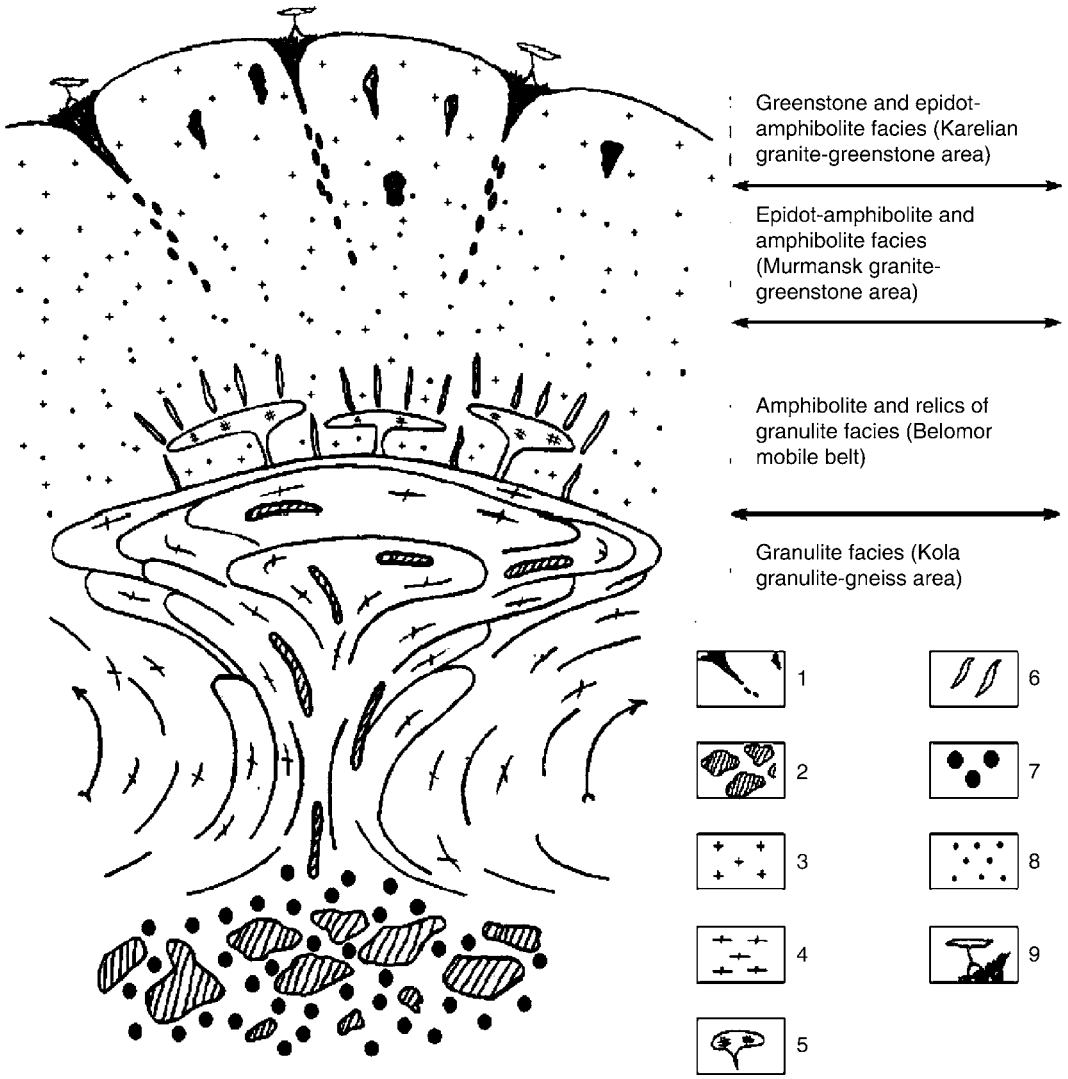


**FIGURE 7.22** Idealized schematics of the mature continental crust in Archaean. Legend: 1, greenstone belts and their fragments; 2, restites and fragments of the greenstone belts. Pyroxenites, olivinites, olivine gabbro; 3, tonalites, trondjemites, granodiorites, amphibolites; 4, enderbites, charnokites, base granulites; 5, microcline granites; 6, plagio-microcline pegmatoid vein granites; 7, area of partial melt and differentiation of proto-oceanic type crust; 8, processes of substrate microclinization; 9, volcanic buildups. ГЗО is granite–greenstone area, ПП is mobile belt, ГГО is granulite–gneiss area.

Archaean. Stage 1 was the emergence and initial development of individual spatially separated segments of the continental lithosphere (domains, terranes or nuclears, and microplates). It is restricted within the time window of 3.6–2.85 BY. Stage 2 (2.8–2.6 BY) is characterized by a massive collision of previously separated continental blocks into a single supercontinent Monogaea.

CHAPTER

# 8

# Lithospheric Plate Tectonics in Early Proterozoic and Phanerozoic

As a result of massive international geological and geophysical studies conducted in the 1950s and 1960s, a new geological theory was formed. It was called "Tectonics of lithospheric plates." It is vastly covered in publications (Le Pichone et al., 1973; New Global Tectonics, 1974; Unksov, 1981; Sorokhtin, 1984; Khain and Lomidze, 1995; Teslenko and Sagautdinova, 2006, and many others). We here briefly review it and show that it is the organic component of our wider and more general theory of Earth's evolution.

## 8.1 FUNDAMENTALS OF THE THEORY

The word "tectonics" means construction arts, the construction in ancient Greek. In earth sciences, it signifies geological structure and evolution patterns of the Earth's crust, and the lithosphere means the rock (i.e., rigid and firm) Earth's shell. As currently understood, the "lithosphere" includes the Earth's crust and part of the upper mantle where the mantle matter is so cooled down that it is totally crystallized and turned into rock. The word "plates" in the name of the new theory shows that Earth's lithospheric shell is broken into individual blocks whose vertical size is much smaller than the horizontal one.

Thus, we treat lithospheric plate tectonics as a geological theory dealing with the structure, emergence, and mutual displacements of the lithospheric plates accompanied by their deformations, magmatic manifestations, and other processes resulting in the formation of Earth's crust and the associated economic deposits. This definition does not discuss the causes of plates' displacements. It is the task of a closely related discipline, geodynamics, which was discussed in the previous chapters (see Chapter 6).

A typical feature of the lithospheric plates is their long-term rigidity and capacity to maintain unchanged shape and structure in the absence of external actions. In order to destroy or deform a lithospheric plate, additional mechanical stresses exceeding the strength of its rocks must be applied (the rock strength is about 1 $t/cm^2$).

*Developments in Earth and Environmental Sciences*, Volume 10
DOI: 10.1016/S1571-9197(11)10008-7

It was found that the upper, rigid Earth shell, the lithosphere, consists of Earth's crust and the underlying subcrustal lithosphere. As mentioned in Section 2.3, the continental crust is mostly composed of granitoids and rocks of medium composition usually overlain by sediments. The total thickness of the crust is 30–80 km (about 40 km on average). The consolidated oceanic crust is thinner, 6.5–7 km, and comprises, down the section, basalts, gabbro, and serpentinites. The sediment thickness over the oceanic crust is greater in the coastal zones and pinches out to zero over the crests of mid-oceanic ridges. On average, it is close to 500 m (Lisitsin, 1978). The oceanic crust is underlain by massive ultramafic rocks (peridotites and lherzolites). The total thickness of oceanic lithospheric plates ranges between 2–3 km in the oceanic rift zone areas and 80–90 km near the ocean shores. The thickness of ancient continental plates reaches 200–220 km.

Earth's temperature gradually increases with depth. Underneath the oceanic plates, the mantle temperature reaches partial melting of the mantle rocks (see Fig. 2.18). For this reason, the base of the lithosphere underneath the oceans is assumed to be the surface of the mantle rocks melting with its solidus temperature. Below the oceanic lithosphere the mantle matter is partially melted and plastic, with lowered viscosity. The plastic mantle layer is usually identified as an individual shell, the asthenosphere. The asthenosphere is clearly identified only under the oceanic plates where it was first discovered as a layer forming a seismic wave conductor. Under the thick continental plates, the asthenosphere is practically absent although they are also underlined by the upper mantle plastic matter (see Fig. 2.18).

The asthenosphere plays certain role in the formation of oceanic plate basalt magmatism and in the interaction between the mantle convective mass exchange with the lithospheric shell. The basalt magmatism can only show up if a hot mantle matter through a split in the plate rises to the melting level of this matter (at a depth of about 80–100 km).

As opposed to the lithosphere, the astenosphere does not have the strength limit. Its matter can deform (flow) under even a very low excess pressure. Because of the asthenospheric matter high viscosity (in the order of $10^{18}$–$10^{20}$ P), this process is very slow (to compare, the water viscosity is $10^{-2}$ P, that of a liquid basalt lava, $10^{4}$–$10^{6}$ P, of the ice, $10^{13}$ P and of rock salt, about $10^{18}$ P). Under high hydrostatic pressure within Earth, the silicate melting temperature increases with depth faster than the mantle temperature. Therefore, there should be no partial melting of the mantle matter below asthenosphere although it may become plastic and similar to a super-viscous liquid with viscosity of about $10^{22}$–$10^{23}$ P (see Fig. 2.20).

Seven large plates are identified on Earth, the Pacific, Eurasian, Indo-Australian, Antarctic, African, North-American, and South-American. There are also seven medium-size plates, the Nazca and Cocos in the Eastern Pacific, Philippine, Arabian, Somali, Caribbean and Scotia positioned between the South America and Antarctica. Sometimes medium-size plates are identified as independent units within the large continental plates. Such are the Amur, South China, Indonesian, and many more smaller plates: the Panonian, Anatolian, Tarim, and so on (see Fig. 8.6). All plates move relative to one another, so their boundaries are usually zones of elevated seismicity (see Fig. 2.6).

The lithospheric plate movements on the surface of the asthenosphere occur due to the mantle flows. Individual lithospheric plates can move apart, approach or slide relative to one another. In the former case, extension zones with rift boundaries along the plate boundaries occur between the plates. In the middle case, the compression zones

arise accompanied by thrusting one plate over the other. And in the latter case the strike-slip zones (transform faults) emerge along which the adjacent plates are offsetting.

The plate motion kinematics is governed by the Euler's law formulated late in XVIII$^{th}$ century. Under this law, any displacement of a rigid body on a sphere is equivalent to its own rotation around the axis running through Earth's center and an immobile point at Earth's surface. This point is usually called the body revolution pole. That is why any rigid plate displacements on the surface of a sphere are in effect just plate rotations about their revolution poles. An example is given by the Southern Atlantic Ocean formation at the Gondwana split in Mesozoic (Le Pichon et al., 1973; Fig. 8.1).

New oceanic crust emerges between the moving apart plates. The crust increment rate is measured from magnetic anomalies on the sea floor (Vine and Matthews, 1963). It was found that all rift faults are always directed toward the corresponding plate expanding poles, and the conjugated transform faults are always perpendicular to these directions. Therefore, the rift and transform fault grid arising between two sliding apart plates is always oriented with the longitudinal and latitudinal circles drawn from the pole of mutual rotation of the plates.

Euler's theory says that the rate of the mutual offset between two lithospheric plates changes with the distance from the rotation pole under the law of the polar angle sine of a given point taken from the plate rotation pole. Euler's theorem enabled the use of paleomagnetic anomalies on the ocean floor to quantitatively estimate the motion of all lithospheric plate ensembles and to reconstruct the paleogeodynamic positions of the ancient oceans and continents.

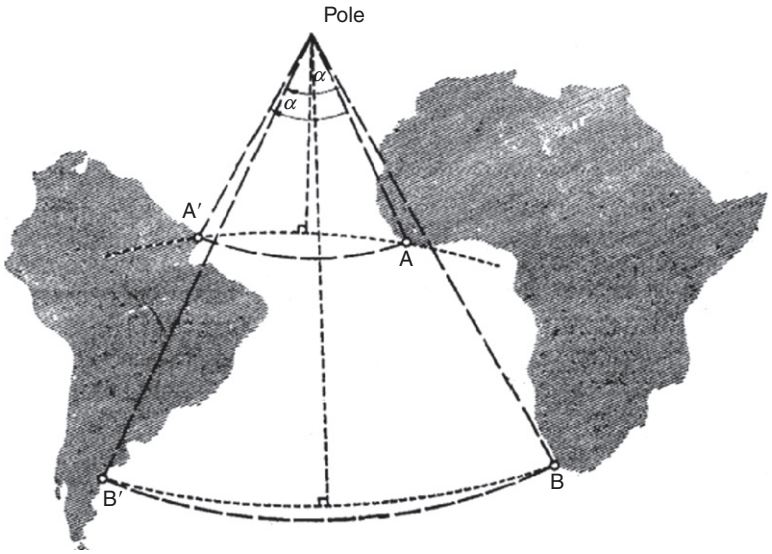


**FIGURE 8.1** Example of the South Atlantic formation as a result of the South America moving away from Africa rotating by the angle α around the plate revolution axis. The pole is at the intersection of the perpendiculars drawn through middle arches of the large circle AA′ and BB′ (dotted lines). The true plate rotation trajectory is shown by the concentric dashed lines (Le Pichon et al., 1973).

These estimates are important as they allow for a quantitative estimate of the present-day tectonic activity and the amount of magmatic eruptions from the present-day rift zones. The same technique provides the opportunity, by sequential superposing same-age magnetic anomalies, to reconstruct the precise ocean and continent positions in the past geological epochs (with the mid-oceanic ridges) and to determine the rate of spreading or subduction of the ocean floor under the island arcs. In 1970s, Zonenshein et al. (1976) and Zonenshein and Gorodnitsky (1977) performed a great number of such paleogeodynamic reconstructions for the entire time interval covered by the magnetic anomalies of the modern ocean floor (from Middle Mesozoic to the present).

The lithospheric plate motion rates are usually determined from the striped magnetic anomaly positions on the ocean floor (see Figs. 2.8 and 8.2). As noted, these anomalies appear in the oceanic rift zones due to magnetizing of basalts erupted from those zones by Earth's magnetic field at the time of eruption. It is established that the magnetic field from time to time reversed its direction to the opposite. Thus, basalts erupted during different inversion periods turned out to be oppositely magnetized. As the ocean floor spreads apart in the rift zones of the mid-oceanic ridges, the older basalts are always farther from these zones. Magnetic anomalies attached to the basalts spread apart together with the ocean floor.

The ocean crust spreading together with the magnetized basalts usually evolves symmetrically on both side of the rift. So are the magnetic anomalies symmetric on both sides of the mid-oceanic ridges and their surrounding abyssal depressions. These anomalies may now

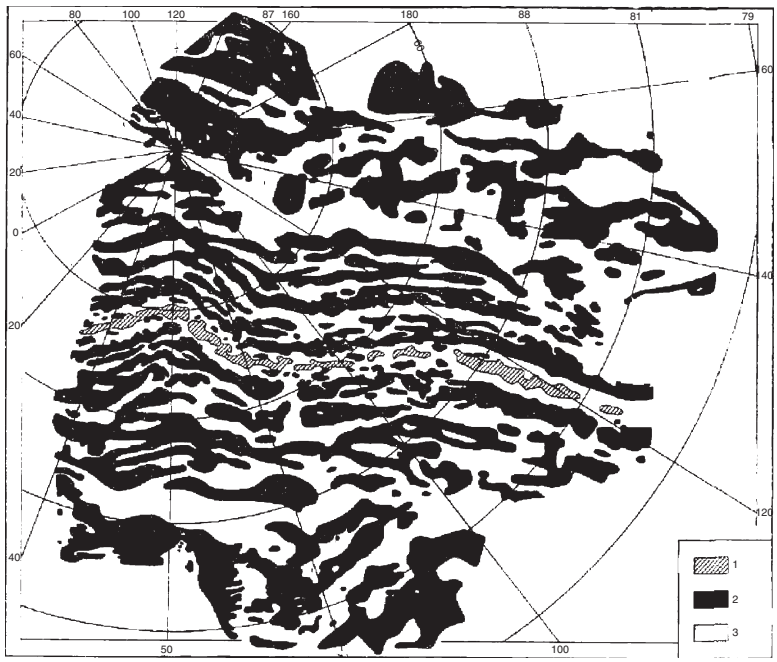


**FIGURE 8.2** Schematic map of magnetic anomalies. Eurasian basin of the Arctic Ocean (Demenitskaya and Karasik, 1971): 1, rift anomaly along the center of the Gakkel Ridge; 2, positive anomalies; and 3, negative anomalies.

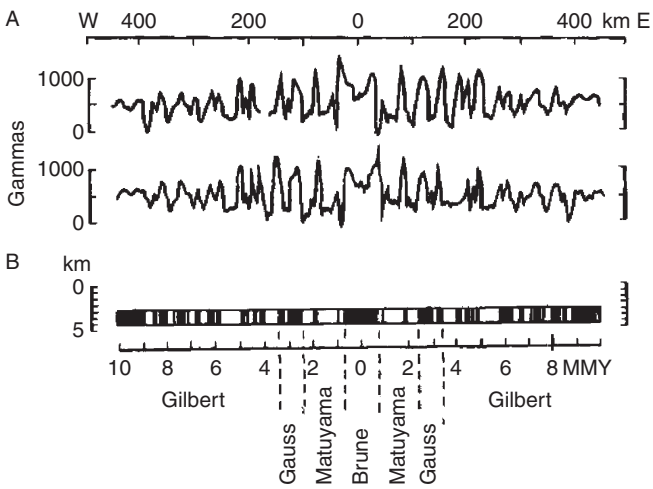


**FIGURE 8.3** Symmetry of magnetic anomalies relative to the axes of mid-oceanic ridges: (a) lower curve, magnetic cross section through the Pacific-Antarctic ridge (near 50°S and 120°W), upper curve is mirror reflection of the lower curve relative to the ridge axis and (B) duration of epochs of opposite geomagnetic field polarity (Geodynamics by Sorokhtin, 1979).

be used to determine the ocean floor age and its spreading rate in the rift zones. For this, however, it is necessary to know the age of individual magnetic field inversions and to compare these inversions with the observed ocean floor magnetic anomalies.

As Fig. 8.2 indicates, the magnetic anomalies are not continuous bands but rather chain of spots. It does not prevent the magnetic field symmetry relative to the mid-oceanic ridge axes to show up clearly (see an example in Fig. 8.3).

The age of the magnetic inversions was determined from well-dated basalt sheets and sedimentary rocks on continents and the ocean floor basalts (Fig. 8.4).

The provided theoretical conclusions enable quantitative estimates of the movement parameters for the adjacent plates, and then for a third plate as a pair with one of the two. This way it was possible to calculate the motions for the main identified plates and determine plates' mutual displacement on Earth's surface. This technique of comparing the derived geomagnetic timescale with the ocean floor magnetic anomalies enabled the determination of the ocean crust ages over the most of World Ocean (Minster et al., 1974; Larson et al., 1985; Fig. 8.5).

Based on the ocean floor ages, it was possible to estimate relative displacement speed of the lithospheric plates (Galushkin and Ushakov, 1978; Fig. 8.6). The maximum spreading rate was found in the southeastern Pacific, near the Easter Island. There, the annual increment of the oceanic crust is 18 cm. This is a large amount as a band of a young ocean floor 180 km wide forms over 1 MMY, about 360 $km^3$ of basalt lavas is erupted during the same period of time over each kilometer of the rift zone.

It was estimated that Australia moves from Antarctica by about 7 cm/year, the Southern America moves from Africa by about 4 cm/year, and the North America from Europe, by 2–2.3 cm/year. The Red Sea is spreading even at a smaller rate of 1.5 cm/year (correspondingly the amount of erupted basalts there is just 30 $km^3$ over 1 MMY for each kilometer of the Red Sea rift).

At the same time, the rate of India–Asia collision reaches 5 cm/year. This explains the intense current neotectonic deformations and the growth of Hindu Kush, Pamir, and

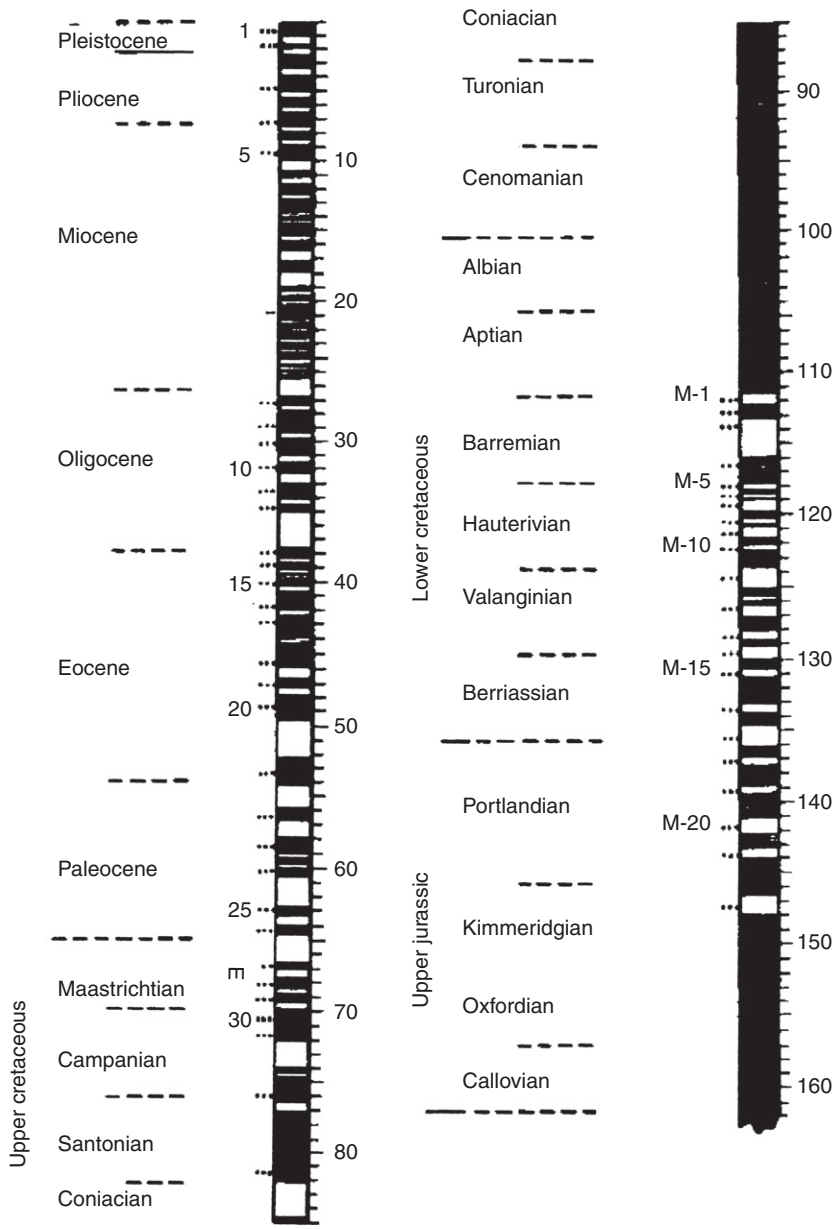


**FIGURE 8.4** Lamont paleomagnetic scale (time is in MMY).

Himalaya mountain systems. These deformations generate high level of seismic activity in the entire region. The effect of the India–Asia collision is felt way outside the immediate plate collision zone extending to Lake Baikal and to the Baikal-Amur railroad. The deformations of Caucasus Major and Caucasus Minor are caused by the pressure from the Arabian

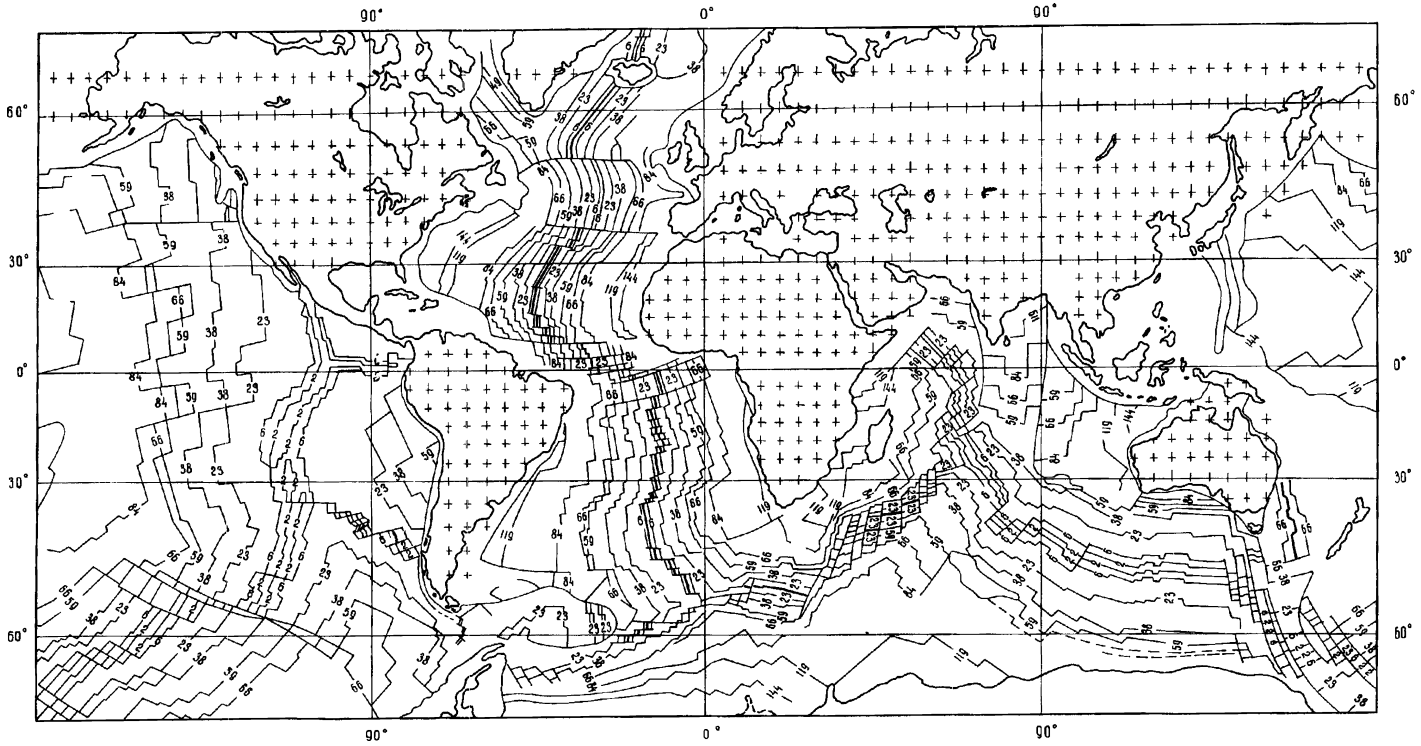


**FIGURE 8.5** Map of the ocean floor age, MMY (Larson et al., 1985).

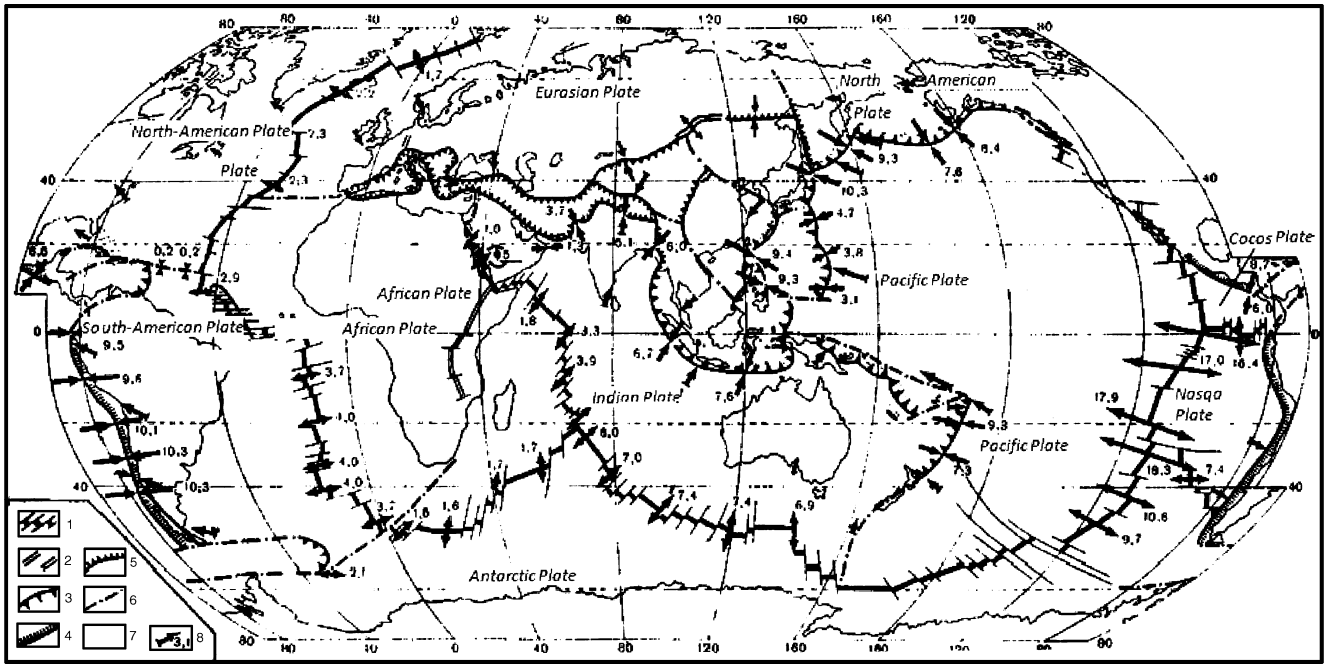


**FIGURE 8.6** Lithospheric plate velocity map (Galushkin and Ushakov, 1978): 1, oceanic rift zones and transform faults; 2, continental rift zones; 3, zone of oceanic lithospheric plate subduction underneath island arcs; 4, same, underneath Andean-type active continental margins; 5, continental plate collision zones; 6, transform (strike-slip) plate boundaries; 7, lithospheric plates; and 8, stresses and rates (cm/year) of relative plate movement.

Plate onto this Eurasian area. There, however, the rate is lower, just 1.5–2 cm/year. For this reason, the region's seismic activity is lower.

Many plates include both continental massifs and "welded" area of the oceanic lithosphere. Thus, the African Plate includes the African continent proper as well as adjacent eastern halves of the Central and Southern Atlantics, western portions of the Indian Ocean floor and the adjacent areas of the Mediterranean and Red Sea. These are the plates of a mixed continental-oceanic origin. Besides, there are plates composed exclusively of the oceanic lithosphere with the oceanic crust on the surface. These are the Pacific Plate, Nazca, Cocos, and Philippines plates.

All oceanic plates formed before Late Jurassic have already sunk into the mantle through the present-day or old subduction zones. Thus, the ocean floor does not include magnetic anomalies 160–190 MMY. That is why only approximate paleogeographic reconstructions may be performed for older geological epochs using paleomagnetic data from the continents. These reconstructions by Smith and Briden (1977) cover the time interval through Early Triassic (220 MMY). Similar reconstructions were conducted by Gorodnitsky, Zonenshein, and Mirlin for the entire Phanerozoic (1978).

Different types of deformations arising on a plate's periphery create three types of boundaries. Type one (divergent boundaries) includes the plate boundaries along which the lithospheric plates spread with the rift zone formation (see Fig. 2.5). Such are the mid-oceanic ridge crests: the Gakkel, Knipovich, Mona, and Kolbeinsey in the Arctic Ocean, Reykjanes, North Atlantic, South Atlantic, and African-Antarctic in the Atlantic Ocean, Arabian-Indian, West Indian, Central Indian ridges, and Australo-Antarctic uplift in the Indian Ocean, and South Pacific and East Pacific uplifts in the Pacific Ocean. On continents, such boundaries include the East-African rift zone and the Baikal rift in Asia. The Red Sea rift and Bay of Aden rift are examples of the rift zones recently converted from the continental to the oceanic.

A powerful basalt volcanism forming the oceanic crust in the mid-oceanic ridge rift zones as well as shallow-focus seismicity corresponds with the divergent plate boundaries. On the continents, the divergent plate boundaries are marked by trap basalt effusions and by contrasting bimodal basalt-sialic and alkaline magmatism, and somewhat deeper-foci earthquakes (up to 200 km).

The second, convergent type is formed by the plate subduction zones where the oceanic lithospheric plates subduct under the island arcs or under the Andean-type continental margins. These boundaries are usually marked by characteristic topographic forms. They include the conjugated deepwater trough structures (sometimes deeper than 10 km) with the chains of volcanic island arcs or very high mountain buildups (up to 7–8 km high) if the subduction occurs under the continent.

The examples are deepwater troughs in front of the Aleutian, Kuril-Kamchatka, Japanese, Marianas, Philippines island arcs, and deepwater troughs at the foot of New Britain, Solomon Islands, New Hebrides Islands, Tonga-Kermadek, and at the foot of Central and Southern Africa western shores in the Pacific.

In the Indian Ocean, these are the deepwater troughs of the Andaman, Small, and Great Sunda Isles. In the Atlantic, these are the Cayman and Puerto Rico troughs in front of the Large and Small Antilles in the Caribbean and Sandwich Trough in front of the Sandwich Islands in the Southern Atlantic.

The subduction zones are always inclined toward (under) the island arcs or continental margins and are usually easily identified by the chains of earthquake foci. As seismic wave decay in the sinking cold lithospheric plate is lower than in the surrounding hot and partially melted mantle, the sinking plates also have elevated seismic quality factor $Q$. The plate subduction zones are characterized by the calcareous-alkaline andesitic magmatism. Andesite volcanoes are usually positioned in the back portions of the island arc structures (see Fig. 2.7).

Unless the oceanic plate subduction compensated by the spreading in the mid-oceanic ridges, it results in gradual closing of the ocean, collision of the framing continents, and the emergence along the subduction zone of a collision folded belt. That is how the Alpine-Himalayan fold-belt formed in place of the ancient Tethys Ocean. The plate subduction is still continuing there which is supported by the elevated seismicity in the region, so the Alpine-Himalayan belt may also be treated as a convergent or collision boundary.

## 8.2 FORMATION OF THE LITHOSPHERIC PLATES AND ORIGIN OF MID-OCEANIC RIDGES

Earth's lithospheric shell is a cooled-down and totally crystallized part of the upper mantle. It is underlain by a hot, underneath the ocean partially melted asthenospheric matter. It is reasonable to assume that the oceanic lithospheric plates formed as a result of cooling down and total crystallization of the partially melted asthenospheric matter, the same way as it occurs in the river when the water freezes and ice forms.

Asthenospheric crystalline rocks are in essence the same as a "silicate ice" for the partially melted silicate asthenospheric matter. The difference is that the usual ice is always lighter than the water and the crystalline silicates are always heavier than their melt. If the assumption is true, the oceanic plate formation is not difficult to disentangle as the water crystallization is well studied.

This analogy is less valid for the continental lithosphere: although it is underlain by a hot mantle but with the temperature lower than the temperature when the mantle matter begins melting (see Fig. 6.2). This, in particular, explains the fact of the continental lithospheric plate solid state to a depth of about 250 km, with the plastic mantle lying deeper. As mentioned in Chapter 6, the physical nature of this transition from the rigid to the plastic state of the upper mantle under the continents may be associated with the disintegration of the mantle matter, for instance, at high pressure. Indeed, the following may be expected. Pressure increases to a level at which the energy of the mantle matter additional activation $\Delta W = p\,\Delta V$ caused by increase in pressure $p$ and compression $\Delta V$ exceeds the bonding energy between crystals in the polycrystalline matter. At that point, the intercrystalline bonds will be disrupted with the preservation of crystalline structures in the mineral grains proper.

Such disintegration occurs with the energy $\Delta W$ absorption. As a result, the rigid and strong mantle matter as if falls apart into individual small grains and turns into a granular material which behaves similar to a high-viscosity plastic matter. In such a case, the phase transition at the continental plate bases must have the properties of endothermic boundary (see Fig. 6.2).

The oceanic lithospheric plate formation under the crystallization mechanism model may be presented as follows. Basalts released from the partially melted asthenospheric matter rise into a gap between the spreading plates. On the ocean floor they cool down, harden,

and crystallize turning into the lithospheric rocks. As the plates spread, the earlier formed lithospheric areas "freeze" ever deeper. Now the asthenospheric mantle matter is crystallizing under the basalt composition rocks. They are replaced through new rift fissures by new portions of the basalts and asthenospheric matter, and the process repeats itself.

The lithospheric plate formation begun in the rift zones continues under the slopes of the mid-oceanic ridges and abyssal depressions. It happens due to a gradual cool-down and complete crystallization of the source hot mantle matter which "freezes" to the base of the lithosphere. It is obvious that the longer the mantle matter raised to the surface cools down, the greater the depth of its "freezing" and crystallization. Therefore, underneath the older areas of the ocean floor (which are farther from the rift zones) the lithosphere thickness (i.e., the cooled-down and crystallized mantle layer) will be greater.

It appears that a first suggestion as to the thickness of the oceanic lithosphere was by Dewey and Bird (1970a). They made a connection between the ocean depth increase with the distance from mid-oceanic ridges and increases in the thickness of the lithosphere. These authors, however, did not dwell on physical reasons for such deepening of the ocean floor. Later it was found that the melt "freeze-through" depth, whether it was the water, basalt magma, or partially melted asthenospheric matter, is determined by the heat-conductivity equation (Sorokhtin, 1973a,b).

The lithospheric plate formation and geodynamics substantially depend on the thermodynamic parameters of the upper mantle and on its cool-down regime. For this reason, temperature distribution within the upper mantle and the lithospheric plates must be studied especially carefully. Earth's mantle is involved in an intense convective mass exchange. It is supported, for instance, by the displacements of the lithospheric plates in the oceans and by the continental drift. Because of this, temperature within the hot convecting mantle must be close to the adiabatic distribution determined by the following equation:

$$\frac{dT}{dr} = -\frac{g\alpha T}{c_p}, \tag{8.1}$$

where $g$ is the gravity acceleration; $\alpha$ is the volume expansion factor; $c_p$ is heat capacity at constant pressure; and $r$ is the current Earth's radius. The lithosphere thickness may be determined from the Kelvin's solution of the heat-conductivity equation:

$$T_s = T_l \operatorname{erf}\frac{H_L}{2\sqrt{at}}, \tag{8.2}$$

where $T_s = 1060\ ^\circ\mathrm{C}$ is the temperature of the basalt solidus; $T_l = 1320\ ^\circ\mathrm{C}$ is the temperature of the asthenosphere (basalt liquidus); $H_L$ is the thickness of the lithosphere; a is thermometric conductivity factor; $t$ is time since the asthenospheric matter raise to the surface. Then from Eq. (8.2)

$$\operatorname{erf}\frac{H_L}{2\sqrt{at}} = \frac{T_s}{T_l} = 0.803. \tag{8.3}$$

From the special function reference book (Yanke et al., 1968) we find

$$\frac{H_L}{2\sqrt{at}} = 0.915 \quad \text{or} \quad H_L = 1.83\sqrt{at} \tag{8.3'}$$

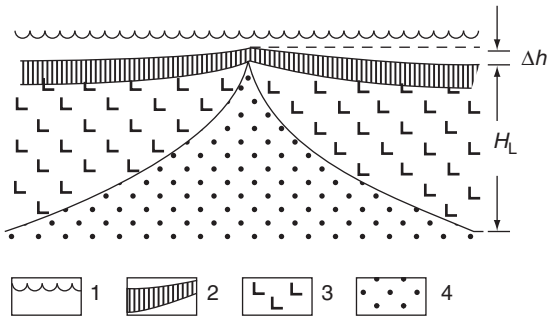


**FIGURE 8.7** Generalized structure of oceanic lithosphere: 1, ocean surface; 2, oceanic crust; 3, oceanic lithosphere; and 4, asthenosphere.

Equation (8.3′) provides the correlation between the oceanic lithosphere thickness $H_l$ and its age $t$ (Sorokhtin, 1973a,b; Parker and Oldenburg, 1973)

$$H_l = k\sqrt{t} \tag{8.4}$$

which gives us a generalized model of the oceanic lithospheric plates (Fig. 8.7).

Thermometric conductivity is determined from the equation $a = \lambda/(c_p\rho_L)$, where $\lambda$ is heat conductivity; $c_p$ is per-unit heat capacity, $\rho_L$ is the lithosphere density. The lithospheric heat capacity for the assumed lherzolite composition at average lithosphere temperature $T_L = 730\ ^\circ C$ as calculated from the Reference Book (1971) is $\bar{c}_p = 0.28$ cal/g deg. Extrapolating the heat conductivity factors for gabbro and dunite to average lithospheric temperature we find $\bar{\lambda}_L = 5.0 \times 10^{-3}$ cal/cm s deg. The lithosphere density may be assumed $\rho_L = 3.3$ g/cm$^3$, therefore, average thermometric conductivity of the lithosphere is $a_L = 5.41 \times 10^{-3}$ cm$^2$/s. Factor $a_L$ is defined in the CGS system but it is much more convenient to determine the time $t$ in millions of years and the lithosphere thickness $H_L$ in kilometers. For this case we have:

$$H_L = 7.56\sqrt{t}, \tag{8.5}$$

where $H_L$ is in kilometers and $t$ in MMY.

When basalt (diabase) crystallizes its density increases by approximately 8.6% (Reference Book, 1969). Taking into account this, and also the lithospheric average temperature, and assuming the rock volume expansion factor $a = 3.0 \times 10^{-5}$ deg$^{-1}$, we find $\rho_L = 3.3$ g/cm$^3$, $\rho_a = 3.21$ g/cm$^3$, and $\Delta\rho = 0.09$ g/cm$^3$.

Other scientists came up with different but close results (Fig. 8.8).

Using the most likely values of these parameters, it may be concluded that the real lithospheric plate thickness versus their age is within the range (see Fig. 8.9)

$$6.5\sqrt{t} \le H_l \ge 8.6\sqrt{t}. \tag{8.6}$$

The factor $k$ in Eq. (8.4) may also be determined from empirical data. For instance, the lithosphere thickness under the island of Hawaii, based on the seiamological data, is approximately $h \approx 60$ km (from the ocean-floor), and the crust age is 85–90 MMY. Then $h \approx 6.3\sqrt{t}$ (see Fig. 8.8).

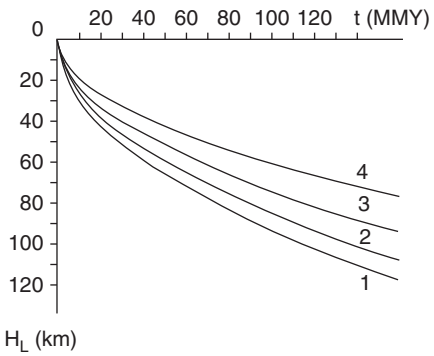


**FIGURE 8.8** Oceanic lithosphere thickness versus age: 1, Parker–Oldenburg model (1973) $k \approx 9.4$; 2. Model (Sorokhtin, 1973a,b) $k \approx 8.6$; 3, Yoshii model (1975) $k \approx 7.5$ and current Sorokhtin model $k \approx 7.56$; 4, curve based on seismic data of lithosphere thickness underneath Hawaii Island (60 km): $k \approx 6.3$.

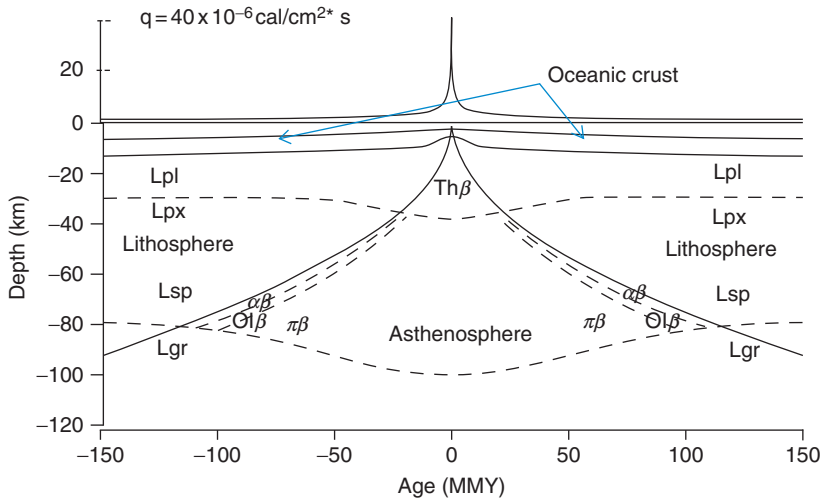


**FIGURE 8.9** Cross section through an oceanic lithospheric plate (at the top are heat flows $q$ penetrating these plates). Areas of existence: Lpl, plagioclase lhertzolites; Lpx, pyroxene lherzolites; Lsp, spinel lherzolites; Lgr, garnet lherzolites. Melt-out areas: Thβ, tholeitic basalts; αβ, alkaline basalts; Olβ, olivine basalts; πβ, pykrite basalts.

Nevertheless, we accepted the correlation as defined by Eq. (8.5). Figure 8.9 displays a typical cross section of the oceanic lithospheric plates taking into account their composition and heat flow that penetrates them. The heat flow value (in $10^{-6}$ cal/cm$^2$ s) was determined from the following equation (Gorodnitsky and Sorokhtin, 1981)

$$q = \frac{13.2}{\sqrt{t + t_0}}, \tag{8.7}$$

where $t_0 \approx 100{,}000$ years is the consolidation time of the rift zone.

Thus, the crystallization model fits well the real mechanism of the oceanic lithospheric plate formation. In this model, the thickness of the lithosphere is determined by the mantle

matter cool-down and crystallization depth; therefore, it depends on the mantle matter exposure time on Earth's surface. That is why the lithosphere thickness underneath mid-oceanic ridges is variable and regularly increases with the distance from the rift zones. The lithospheric thickness in the rift valley centers is at its minimum and the asthenosphere is almost exposed on Earth's surface. Contrary to the oceanic plates, the ancient continental lithospheric plates had enough time during their existence ($t > 1$ BY) to cool down to the level where stationary heat flows were established in them. For this reason, their thickness practically did not change with time and remained equal to about 200–250 km.

The lithospheric rocks are heavier than their overlying hot asthenospheric matter by about 0.1 g/cm$^3$. Therefore, the thicker the oceanic lithosphere, the deeper it is subsided into the mantle and the lower its surface is. Because of this, the ocean floor subsidence is determined by the same correlation (with the radical) versus the lithosphere age, that is, the ocean floor age. Based on this correlation, the highest ocean floor stand level must be wherever the lithosphere is at its thinnest, that is, in the oceanic rift zones located over the crests of the mid-oceanic ridges. With the distance from these ridges, the ocean depth must increase in proportion with the lithospheric thickness increase, that is, as follows:

$$\Delta h = \frac{\rho_L - \rho_a}{\rho_a - \rho_w} H_l, \tag{8.8}$$

where $\Delta h$ is average topographic gradient between the crest and any point on the slope of the mid-oceanic ridge; $\rho_L$, $\rho_a$, and $\rho_w$ are the densities, respectively, of the lithosphere, asthenosphere, and ocean water. Taking heat flows (8.7) in consideration we will accept, according to Eq. (8.5), $H_L = 7.56\sqrt{t}$, and assume most likely average densities of the lithosphere and asthenosphere equal to $\rho_L = 3.3$; $\rho_a = 3.2$ g/cm$^3$. Average oceanic water density is equal to its mass $M_{oc}$ divided by its total volume $V_{oc}$. According to the Reference Book (1990), $M_{oc} = 1.420 \times 10^{15}$ t and $V_{oc} = 1.370 \times 10^6$ km$^3$, then $\rho_w = 1.036$ g/cm$^3$, wherefrom

$$\Delta h \approx 0.35\sqrt{t}. \tag{8.9}$$

If the described oceanic lithospheric plate model is valid, then the theoretical pattern based on this model should correctly average the real ocean floor topography. This is easy to verify (see the results in Fig. 8.10A and B). As these and many other examples show, the averaged profiles of all mid-oceanic ridges are closely approximated by the same function $\Delta h \approx 0.35\sqrt{t}$. At that, the derived value of the proportionality factor in the equation matches well with its averaged empirical value. The ocean depth may be found from a no more complicated equation

$$h_{oc} \approx h_0 + 0.35\sqrt{t}, \tag{8.9'}$$

where $h_0$ is the depth of the oceanic rift zone location. On average, $2.5 > h_0 > 2$ km. Sometimes, however, $h_0 \approx 0$ or even somewhat above the ocean surface (as in Iceland or in the Afar province in northern Ethiopia).

It is obvious that at a uniform rate of the ocean floor spreading the distance $x$ from the mid-oceanic ridge crests will be proportionate with the ocean floor age. In this case (Sorokhtin, 1973a)

$$\Delta h \approx 0.11\sqrt{\frac{x}{u}}, \tag{8.9''}$$

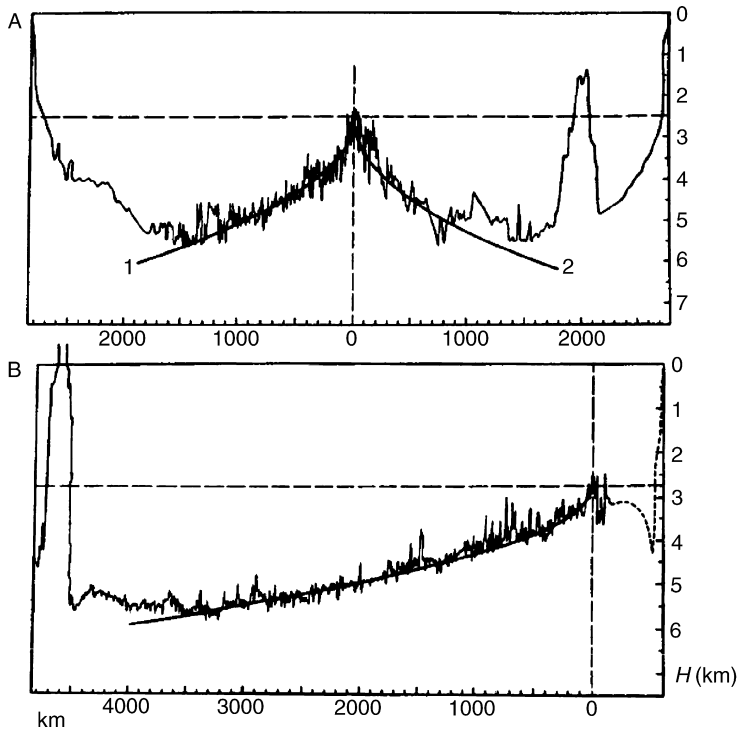


**FIGURE 8.10** Approximation of oceanic depth on the slopes of mid-oceanic ridges by the function $\Delta h \approx 0.35\sqrt{t}$ (Sorokhtin, 1973a,b): (A) Mid-Atlantic Ridge in Southern Atlantic Ocean (plate spreading rate $2 \times 1.8$ cm/year) and (B) Eastern Pacific uplift, latitudinal cross section through Hawaiian Islands (plate spreading rate about $2 \times 5$ cm/year).

where the distance $x$ and the depths difference $\Delta h$ are in kilometers and the spreading rate $u$ is in cm/year. In these coordinates, the calculation results are represented in Fig. 8.10.

As the ocean floor volcanoes are fed by basalt magmas directly underlying the oceanic lithospheric plates, it is natural that the underwater volcano and oceanic island height must be controlled by the plate thickness. It was noticed by Vogt (1974) and Gorodnitsky (1977). In particular, Gorodnitsky derived a simple equation for the height $H_m$ determination of both underwater volcanoes and Hawaiian-type oceanic islands:

$$H_m = H_L \frac{\rho_a - \rho_b}{\rho_b - \rho_w}. \tag{8.10}$$

Here, $H_L = 7.56\sqrt{t}$ is the lithospheric plate thickness (see Eq. 8.5); $\rho_a = 3.21$; $\rho_b = 2.9$; and $\rho_w = 1.03$ g/cm$^3$ are, respectively, the densities of the lithosphere, basalts, and seawater.

Estimation based on Eq. (8.10) corresponds well with the observations. Thus, for Hawaii $t \approx 85$ MMY, $h_w \approx 5$ km, and $\rho_w = 1.03$ g/cm$^3$, and the resulting height of the island over the ocean is 10 km (actually $H_m = 9.7$ km). The same equation supports the pattern (Gorodnitsky, 1977): the closer the volcano to the rift zone, the lower this volcano is.

Using Eqs. (8.1)–(8.5) together with the Eq. (5.23′) for Earth's tectonic activity, it is possible to identify major patterns in the oceanic lithospheric plate development throughout the entire evolution of Earth (Fig. 7.3).

In the very beginning of Earth's tectonic activity about 3.8 BY ago, maximum lithospheric plate thickness over the Earth's matter differentiation zone was greater than 12 km. By the time 3.6 BY ago, the plate thickness declined to 10 km, and their life duration as of the oceanic plates did not exceed 1 MMY (as the ocean width was very narrow as shown in Fig. 4.3). In mid-Archaean (about 3.2 BY ago), the maximum oceanic plate thickness again increased to 27 km and their longevity increased to approximately 10 MMY. In Late Archaean, about 2.9 BY ago, the plate thickness again dropped to approximately 8 km, and their life span, due to their large movement rate, dropped again to a few million years (the ocean significantly broadened at that time).

Figure 8.11 shows, together with the evolution of oceanic plate thickness, also the critical thickness of the oceanic lithospheric plates calculated from their thickness. If a real oceanic plate is thicker, it becomes heavier than the underlying hot mantle and can sink into it, that is, to be subducted. If a lithospheric plate thickness is less than the critical value, the plate cannot be subducted into the mantle. In the compression environment, however, such plate may override the other plate or a continental margin (obduct it).

The depth heat flow $\dot{Q}_m$ (see Fig. 5.17) enables the determination of the other important parameters of Earth's tectonic activity. One such parameter is average longevity of oceanic plates $\tau_l$, which is proportionate with square root of the oceanic plate area to their penetrating heat flow $\tau_l \sim S_{oc}^2/\dot{Q}_m^2$ (see Figs. 7.3 and 8.11). Another parameter is average thickness $H_l$ of oceanic plates at their maximum age $\tau_l$, which is proportionate with the

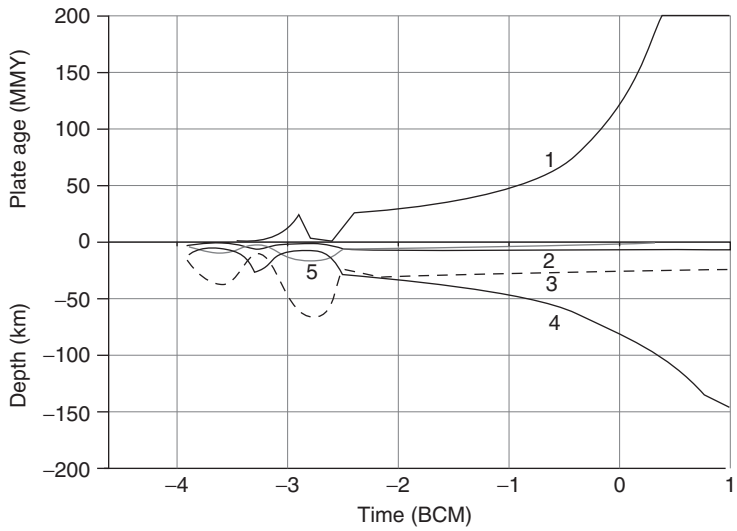


**FIGURE 8.11** Structural evolution of oceanic lithospheric plates and average duration of their life on Earth's surface: 1, average plate life; 2, oceanic crust thickness; 3, critical thickness of lithospheric plates determining the possibility of thicker plates sinking in the mantle; 4, oceanic plate thickness by the end of their average life duration; and 5, basalt layer thickness.

oceanic plate combined area to the same heat flow ratio $H_l \sim S_{oc}/\dot{Q}_m$ (curve 4 in Fig. 8.11). Assuming the present-day average oceanic plate longevity is approximately $\tau_l \approx 120$ MMY and $H_{ocl} \approx 7.56\sqrt{\tau_l} \approx 80$ km, it turns out that the plate thickness at the peak of the activity in Early Archaean (3.6 BY ago) was as low as 6.2 km, and their life was just 700 MY! In mid-Archaean (3.2 BY ago), the maximum oceanic plate thickness increased to 27 km and their longevity to almost 14 MMY. In Late Archaean (2.8 BY ago), $H_l$ dropped again to about 8 km and their longevity to 1.2 MMY.

As a first approximation, average volume of the ocean floor basalt eruptions is proportionate with its penetrating heat flow. So, using the same approach it is possible to determine the thickness of the oceanic crust basalt layer $H_b \sim \dot{Q}_m$ (see Fig. 7.1). In Archaean, however, the basalt layer thickness was limited not by the basalt eruption amounts but by the depth of the mantle matter melting, that is, by the lithospheric plate thicknesses. And those were approximately 6.2 and 8 km in Early and late Archaean. It is obvious from this that thin basalt plates with density 2.8–2.9 g/cm$^3$ directly overlay at that time the melted mantle with density of at least 3.3–3.2 g/cm$^3$. In the beginning of Archaean and in its middle 3.2 BY ago, the lithospheric plate thickness exceeded the basalt layer thickness. In Proterozoic, the oceanic crust basalt layer thickness (not accounting for the gabbro layer) gradually declined from 6.5 to 2 km (Fig. 8.11, curve 5).

If the oceanic lithospheric plates are indeed heavier than the asthenosphere matter then the question is why are not they sinking into the hot mantle?

This question would not be totally correct for the oceanic plates as sooner or later they sink into the mantle through the plate subduction zones. That is exactly why all modern day oceanic lithosphere is younger than 150 MMY as its older fragments long ago sank into the mantle. And within these 150 MMY the oceanic lithosphere is buoyant as metal ships floating on the surface of the water. Indeed, stable (not sinking in the mantle) oceanic plates are similar in their structure to giant saucers bounded on all sides by the raised flanks which are mid-oceanic ridges and continental margins (such as the lithosphere under the Atlantic Ocean).

This causes the emergence of neutral buoyancy in such plates as under the Archimedes law the density of the displaced asthenosphere is equal to the summary density of the plates proper and the water filling-up the lithospheric "saucers" (abyssal depressions). The faults emerging in such plates rapidly self-heal through crystallization of their penetrating basalt magmas.

When the lithospheric plates sink into the asthenosphere, their body experiences excessive stress. The deeper such plates sink into the mantle (i.e., the older the plates) the greater the stress. It is easy to estimate from the aforementioned correlation of the oceanic depth versus the age of its floor that the stresses must emerge in the lithospheric plates older than 150 MMY which exceed 1 t/cm$^2$, that is, breaking strength of the lithosphere. This is probably the reason why the maximum oceanic plate age is approximately 150 MMY.

The continental plates do not sink as the light continental crust with a reserve of positive buoyancy is "welded" to their heavy mantle portion, so average density of the continental plates is always lower than that of the hot mantle which they are immersed in.

It was established that the crests and rift valleys of mid-oceanic ridges are not continuous but as if torn apart into individual segments by transform faults along which the plates usually experience only strike-slip motions. These transform faults are a third type of the plate

boundaries. They are always perpendicular to the strike of rift fissures. The active parts of the faults are only those segments that connect two adjacent rift zones (i.e., transforming one of them into the other). Outside of these active areas there are no plate movements on the transform faults. The offsets in most cases are no greater than 10 km or a few dozen kilometers but sometimes they reach hundreds of kilometers.

Sometimes, the transform faults cross subduction zones or extend from them to the rift zones but most of them intersect only mid-oceanic ridges. The largest are Gibbs, Atlantis, Vima, and Romanche in the Atlantic, Owen and Amsterdam in the Indian Ocean, and Eltanin Challenger, and Udintsev in the Pacific. Besides, there are in the Northern Pacific traces of the now dead but sometime ago giant fault with offsets by many hundreds and even up to 1200 km. These are so-called great faults: the Mendocino, Pioneer, Murray, Molokai, Clarion, and Clipperton. An example of the third type boundary on continent is the San Andreas Fault in California.

The oceanic transform faults have a typical topography of conjugated parallel structures of narrow ridges and troughs with a steep common wall (Fig. 8.12). The lithospheric plates are "soldered" at passive flanks of the transform faults and the younger plates sink more rapidly. For these reasons, the transform faults are always framed by narrow ridges only from the side of the younger plates and have the troughs on the side of the older and slowly sinking plates. That is why the height difference between the ridges of the young plates and the troughs of the older plates as if memorize the different plate height at their contact ("soldering"), that is, on the flanks of the ridges displaced along the transform faults. As a rule, the transform faults are amagmatic although sometimes (when there is a move-out component in the plate movements) basalt volcanoes of alkali orientation may occur on their flanks.

Moving lithospheric plates rub against one another. That causes earthquakes on their edges (see Fig. 2.6). That is why the lithospheric plate boundaries are identified not only topographically but also by the elevated seismicity zones. Different plate boundaries

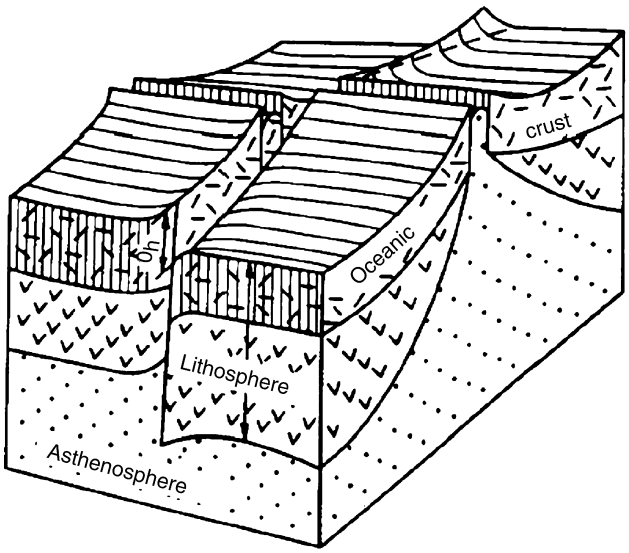


**FIGURE 8.12** Oceanic lithosphere transform fault block diagram.

correspond to different earthquake mechanisms. All earthquakes underneath the mid-oceanic ridge crests in the oceanic rift zones have the focus at a depth of 5–10 km and have extension mechanisms. The quake depths in the active segments of transform faults reach 30–40 km, and the mechanism is a pure shear.

Most seismically active are the plate subduction zones. Shallow earthquakes (the foci depths of up to 30 km), intermediate earthquakes (30 to 150–200 km), and deep-seated quakes (up to 600–700 km) are known there. The main seismofocal surface of the subduction zones usually dips at 30–50° from the deepwater trough axis under the island arc or the continental margin thereby bounding the body of a subducted oceanic plate. Different type earthquakes occur in the subduction zones. The shallow-foci quakes are dominated by the strike-slip or reverse fault strike-slip mechanisms, and medium and great depths are dominated by the strike-slip and compression mechanisms.

As a rule, the maximum depth of the deep-foci earthquakes corresponds with the endothermic phase boundary at a depth of about 670 km (see Fig. 6.2). Below this boundary crystalline bonds in the mantle matter are disrupted, apparently it acquires the properties of amorphous matter. Despite that, as seismic tomography indicates, the traces of the sinking oceanic plates are observed deeper within the lower mantle, down to the core. It may be observed in the core topography: underneath the subduction zones (for instance, those framing the Pacific and Indian Oceans) there are depressions up to 4 km deep on the core surface. Contrary to that, under the ascending flows in the center of these oceans and under the North Atlantic there are topographic uplifts with amplitude of up to 6 km (see Fig. 2.10).

Heat flow through the ocean floor may be found from the heat-conductivity equation. The flow is in the inverse proportion with the square root of the lithospheric plate ages. By comparing analytical calculations with the observed heat flows in the ocean floor areas where they are not distorted at $t > 50$ MMY (see Fig. 5.12), it was possible to determine empirical correlation of the specific heat flows $q$ (in heat flow units $10^{-6}$ cal/cm$^2$ s) with the ocean floor age $t$ (in MMY): $q \approx 13.2/\sqrt{t}$ (Gorodnitsky and Sorokhtin, 1981). Then average heat flow though the ocean floor of the age between 0 and $\tau$ is $\bar{q} \approx 26.4/\sqrt{\tau}$. Our estimate of average oceanic plate longevity is 120 MMY. In this case, average heat flow through the ocean floor is $\bar{q} \approx 2.41 \times 10^{-6}$ cal/cm$^2$ s. The areal extent of all oceans and marginal seas is approximately $3.06 \times 10^{18}$ cm$^2$ so the present-day heat loss through the ocean floor is about $7.375 \times 10^{12}$ cal/s or $3.09 \times 10^{20}$ erg/s. This is the depth heat flow through the oceanic crust only.

## 8.3 STRUCTURE AND FUNCTIONING OF THE LITHOSPHERIC PLATE SUBDUCTION ZONES

Fisher's idea of a possible oceanic floor subduction underneath the island arcs was confirmed 50 years thereafter, in the 1930s, by the gravity surveys over those structures and the adjacent deepwater troughs (Vening Meinesz, 1948, 1955). Negative gravity anomalies of up to 200 mgal were discovered over the island-side slopes of the troughs and over the troughs proper, whereas positive anomalies of up to 100–150 mgal were recorded over the island arcs. Vening Meinesz rightly attributed the origin of these conjugated gravity anomalies to a dynamic effect of the compression and subduction of the ocean floor under the island arcs.

The next step in the studies of active transition zones between the oceans and continents was made by a Japanese seismologist Wadati (1935) who established the presence of a depth seismofocal surface dipping from the ocean underneath the island arcs and by an American seismologist Benioff (1955a,b). Benioff studied these zones in more detail and showed that they are the surfaces on which the continental crust and upper mantle blocks were thrust over the oceanic crust.

Zavaritsky (1950) noted genetic relationships between the andesite volcanism and the Wadati's identified depth seismofocal zones. Thus, the continental crust formation process was united with tectonic movements.

The modern Kuril-type subduction zone model accounting for the elastoplastic properties of the lithosphere was developed in the Oceanology Institute of the USSR Academy of Sciences (Sorokhtin, 1974; Lobkovsky and Sorokhtin, 1976) and Moscow State University (Shemenda, 1983). Under this model, the subduction process reminds of the ice piling-up at compression. The subducted plate experiences strong pressure from the obducting plate. Affected by excess pressure from the horizontal compression stress and from the weight of the obducted plate, plastic deformations develop within the lower, subducted plate. It changes its direction and begins to steeply sink into the mantle. The major difference between the processes is in that the ice is lighter than the water, whereas the oceanic lithospheric plates are always somewhat heavier than the asthenospheric matter.

Lithospheric plate sliding on the inclined plane of the subduction zone disturbs the isostatic equilibrium and causes the emergence of positive and negative gravity anomalies over the island arcs (see Fig. 8.13). Under the condition of force equilibrium within the plate subduction zone, it is possible to derive the correlation between the amplitude of the

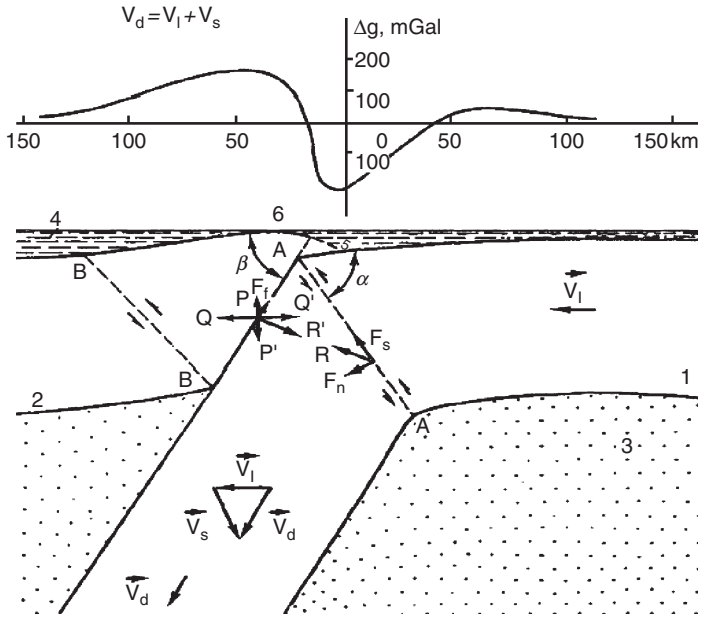


**FIGURE 8.13** Mechanical model of plate subduction zone (Lobkovsky and Sorokhtin, 1976): 1, subducted lithospheric plate; 2, obducted plate; 3, asthenosphere; 4, ocean and marginal basin; 5, deepwater trough; 6, island arc; $\beta$ is the Wadati–Benioff zone dip angle; $\alpha$ is plastic deformation zone dip angle; $\Delta g$ is free-air gravity anomaly.

emerging gravity anomalies and the lithosphere strength. Estimates are that this strength is close to 1 t/cm$^2$ which is coincident with empirical data about the shear strength of ultramafic rocks.

In Fig. 8.13, the plastic deformation area is marked by the AA line although it may be rather wide; angle $\beta$ is the plate subduction zone inclination; angle $\alpha$ is the inclination angle of the shear deformations surface; $V_l$ is the advance rate of the oceanic plate; $V_d$ is the advance rate of the descending plate branch; and $V_s$ is the shear rate of the layers offset in the plastic deformation zone. It may be formatted as:

$$V_d = V_l + V_s. \tag{8.11}$$

The deformation of the obducted lithospheric plate in the model develops along a scheme similar to metal cutting. The plate's frontal portion plays the role of a chisel and the descending branch of the subducted plate is as if shavings. If the oceanic plate thickness in front of the subduction zone is denoted $H_L$ and its thickness after the subduction zone is $H_d$ then

$$H_d = H_L \frac{\sin(\alpha + \beta)}{\sin\alpha}, \tag{8.12}$$

which shows that in general $H_d \neq H_L$.

From Eq. (8.11) we can find absolute values of the lithospheric plate shear velocity $u_s$ and descendance $u_d$ as the function of its subduction velocity $u_L$:

$$\begin{aligned} u_s &= u_L \frac{\sin\beta}{\sin(\alpha + \beta)}, \\ u_d &= u_L \frac{\sin\alpha}{\sin(\alpha + \beta)}. \end{aligned} \tag{8.13}$$

The described model (Lobkovsky and Sorokhtin, 1976) allows for the determination of gravity anomalies above the plate subduction zones. Indeed, the tangential stress $\tau_s$ may be expressed through the shear angle $\alpha$ and the internal friction angle $\varphi$, and also through the vertical force $P$ of excess pressure from the uplifted edge of the obducted plate:

$$\tau_s = \frac{P}{H_l} \frac{\sin\alpha \sin(\alpha + \varphi)}{|\cos(2\alpha + \varphi)|}. \tag{8.14}$$

The excess pressure is

$$p = \frac{P}{H_L \cot\beta}. \tag{8.15}$$

From this follows:

$$p = \tau_s \frac{|\cos(2\alpha + \varphi)| \tan\beta}{\sin\alpha \sin(\alpha + \varphi)}. \tag{8.16}$$

Excess pressure $p$ is connected with the gravity anomaly amplitude above the island arc as the free-air gravity anomaly $\Delta g$ above the layer with density $\rho$ and thickness $h$ is:

$$\Delta g = 2\pi\gamma\rho h, \tag{8.17}$$

where $\gamma = 6.67 \times 10^{-8}$ cm$^3$/g s$^2$ is the gravitational constant. Excess pressure generated by this layer is $p = \rho g h$, where $g$ is the gravity acceleration. Wherefrom

$$p = g\Delta g/2\pi\gamma. \tag{8.18}$$

It follows from Eqs. (8.16) to (8.18) that the free-air gravity anomaly over the island arc is

$$\Delta g = \frac{2\pi\gamma\tau_s}{g}\frac{|\cos(2\alpha+\varphi)|\tan\beta}{\sin\alpha\sin(\alpha+\varphi)} \tag{8.19}$$

To calculate $\Delta g$, we assume that average value of the maximum shear stress $\tau_s$ of the lithospheric material is approximately $\tau_s \approx 10^9$ dyne/cm$^2$ (1 t/cm$^2$). By inserting into Eq. (8.19) the values of the angles (such as $\alpha = \beta = 40°$, $\varphi = 30°$) we find $\Delta g \approx 200$ mgal. This is a good fit with average free-air $\Delta g$ anomaly value over the island arcs. The derived $\Delta g \approx 200$ mgal corresponds with the vertical offset of the obducted plate frontal edge on the order of $h \approx 2.8$ km (at the lithospheric bulge density $\rho_s \approx 2.7$ g/cm$^3$).

After having sunk into the plate subduction zone the oceanic crust is dehydrated, heated up, and partially remelted. The result is a decrease in the crust matter effective viscosity so that the crustal layer in the plate subduction zones may be treated as lubricant between the rigid surfaces rubbing against one another. (This process is reviewed in more detail in Section **8.4** using the deposit suck-in into the subduction zone as an example) In this case, the crustal matter experiences the shear deformations on the manner of the Cuetta flow (Schlichting, 1964), and

$$\eta_{cr} \approx \frac{\tau_c h_{cr}}{u_d}. \tag{8.20}$$

where $h_{cr}$ is the oceanic crust thickness within the subduction zone ($\sim 6.5 \times 10^5$ cm); $\tau_c$ is the tangential stress in the Cuetta flow; and $u_d$ is the lithospheric plate ascendance rate into the mantle (on the order of 5 cm/year $\approx 1.58 \times 10^{-7}$ cm/s).

Tangential stresses at deformations of the oceanic crust composed of basalt pillow lavas and serpentinite must be much smaller than in a massive material of the lithospheric plates (which we assumed to have been $10^9$ dyne/cm$^2$). Based on crustal earthquakes, tangential stresses causing these quakes reach $10^8$ dyne/cm$^2$. Then, the oceanic crust viscosity is approximately $4 \times 10^{20}$ P. Plate friction in the subduction zone results in a significant heat release which heats and remelts the nearby rocks. Heat release increases with depth so the lower and middle portions of the subducted plate are subjected to a stronger magmatic reworking and destruction than the upper one. Due to this, a relatively thin wedge-like lithospheric (crustal) protuberance is formed in front of the obducting plate. As a giant ledge it overlies the subducting plate in the area between the deepwater trough and the subduction zone (see Figs. 2.7and 8.15). Besides, due to constant erosion in the obducted plate frontal parts, this process under the Kuril-type island arcs results in the arc displacement toward the continent and in the gradual closing (at a rate of 0.3 cm/year) of the back-arc basins if they exist. Examples of such closing of back-arc basins are the South Okhotsk deepwater trough and the Sea of Japan.

Besides the Kuril- and Andean-type subduction zones with dominating horizontal compression stresses which "break" the subsiding plate, there are also plate subduction zones where the heavy oceanic lithosphere subsides into the mantle simply under the force of its gravity and under the pressure from the island arc. A typical example is the Marianas island arc in the Pacific. The plate which is subducting underneath it has age very close to the quoted maximum stability age of the oceanic plates, 150 MMY. The distinction of these island arcs from the previous type is in that there are no positive gravity anomalies under them or they are slight, whereas the negative anomalies above the deepwater troughs are pronounced. Besides, contrary to the Kuril-type zones, the Mariana-type back-arc basins are not closing but actively expanding with the formation within them of secondary rift zones.

When the lithospheric plates sink into the mantle under their own weight, extension stresses emerge in the back of the island arcs. Due to these stresses, the island arc body can move apart from the back portions of the island arc plate along the faults feathering the subduction zones (DG in Fig. 8.14(a)). As a result, at the back of such arc occurs a secondary rift zone, and spreading apart of the newly born plates and the island arc apart-movement in the direction of the subducted oceanic plate is compensated by way of young plate buildup (Fig. 8.14(b)). Excess pressure from the island arc on the subducted plate (at $h \geq 20$ km) exceeds the subsiding plate rock shear strength, deforms it, and gradually moves the subduction zone toward the ocean.

A distinction in the evolution dynamics of the Mauritanian and Kuril island arc types is mostly determined by the rate of the plate subduction. The Kuril-type arcs form at a great speed of the plate approach, and the Mauritanian type arcs, at a slow speed. The critical rate appears to be close to 5 cm/year. The Tonga-Kermadek island arc with the Lau back-arc spreading basin is the only exception as the Pacific Plate subduction rate underneath this arc exceeds 5 cm/year. It may be associated with the dynamic effect of the upper mantle matter squeezing out into the asthenosphere by the Australian continental plate moving northeastward or with the existence of a local ascending mantle flow underneath Fiji depression.

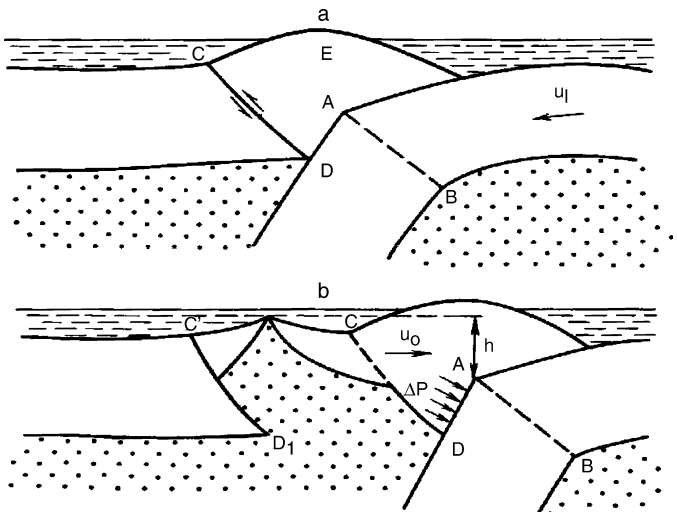


**FIGURE 8.14** Formation stages (a, b) of a second rift zone in the back of island arc and back-arc basin floor spreading.

## 8.4 GEODYNAMICS OF THE PLATE SUBDUCTION ZONES

Subducting plate friction about the base of the obducting plate lithospheric protuberance at the island arc or active continental margin frontal zone is naturally accompanied by earthquakes (see Fig. 2.7). The problem of earthquake frequency $\Delta t$ in the model of elasto-plastic medium is solved in (Magnitsky, 1965):

$$\Delta t \approx \frac{\sigma_s}{\mu \bar{\varepsilon}}, \tag{8.21}$$

where $\sigma_s$ is the material's tensile strength; $\mu$ is the modulus of elasticity (shear modulus) of the material; and $\bar{\varepsilon}$ is the material deformation rate. Using the publication by Sorokhtin (1974), we determine the rate of the deformation by the $u_L/L$ ratio, where $u_L$ is the rate of plate movement and $L$ is the width of the island arc's or active continental margin's crustal protuberance (frontal ledge). For a wide variety of materials and rocks, the ratio $\sigma_s/\mu$ is equal to approximately $10^{-4}$. We assume average plate subduction rate at 7 cm/year $\approx$ $2.22 \times 10^{-7}$ cm/s and the width of the crustal protuberance at 100 km (see Fig. 2.7). The resulting time interval between the earthquakes is then $\Delta t \approx 140$ years.

In 1988, Lobkovsky proposed more advanced model of the subducting plate frontal portions (Lobkovsky, 1988). He noticed that the lithospheric protuberance ledge on the side of the island arcs and active continental margins is cut not only with the lengthwise but also with crosswise fractures separated by distances of 100–200 km. As a result, the lithospheric protuberance ledges and the active continental margin ledges are split into individual "keys" pressed to one another but capable of independent movements (see Fig. 8.15).

It follows from the "keyboard" model that the crosswise faults affect only the crust and extend only to the top of the subducting plate. The interactions between the "keys" and between them and the subducting plate results in various seismic movements and the respective tsunami sources. It is important that the model explains observed patterns in the spatial and temporal distribution of the foci of the devastating earthquakes including those that produce tsunamis. In particular, the following conclusion may be made from the model. Assume that there were no earthquakes in some portion of the island arc or of the active continental margin for a long time. At the same time, in the adjacent areas

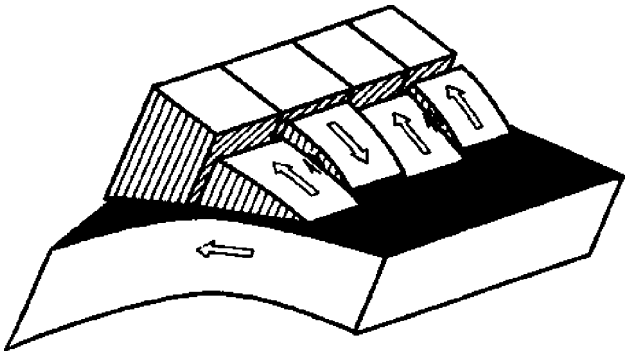

**FIGURE 8.15** "Keyboard" model of a crust high over the plate subduction zone, frontal part of the island arc (Lobkovsky, 1988).

of the active zone there earthquakes occurred constantly. Then one has to expect very strong earthquakes in the former areas (called seismic gaps).

This pattern was previously included into an empirical concept of the "seismic gaps" which is currently used as a basis for long-term prediction of devastating earthquakes and strong tsunamis in the island arcs and active continental margins. Now, however, there is the physical foundation of this concept and the pattern is no longer just empirical but physically understandable.

Modeling the displacements for the frontal portions of two adjacent key blocks and the expended energy is shown in Fig. 8.16. The modeling parameters were: block width, 200 km; critical energy of the faults $\approx 3 \times 10^{25}$ erg; thickness of the contact zone between the plates, 0.5 km; viscosity of this zone, about $10^{20}$ P; and width of the crosswise faults, 1 km. The subduction rate was assumed to be 6 cm/year.

Modeling showed that the interblock interactions were relatively weak and that the blocks moved by about 8 m and almost autonomously, at a period of close to 160 years (see Figs. 8.16 and 8.17).

As mentioned earlier, offsets of the "keyboard" blocks in the island arc frontal zone occur due to their friction with the subducted lithospheric plate. The "keyboard" blocks deformation results in the elastic energy accumulation within these blocks and in the emergence of shear stresses. As soon as these stresses exceed rock shear strength, the block's state of stress relaxes, the block "straightens up," and assumes the initial (unstressed) position; the frontal portion of the block protrudes drastically ahead displacing the contacting oceanic water toward the ocean.

That is the way strong tsunami-producing earthquakes are born (Lobkovsky and Sorokhtin, 1980). The examples are the Chilean earthquake of 1960 and the Indonesian earthquake of 2004 whose tsunami wrecked catastrophic consequences not only on the Island of Sumatra and the adjacent islands but also on almost the entire shores of the Indian Ocean. A distinctive feature of such tsunami is the strongest falling tide of the oceanic water over the epicenter of the source earthquake (see Fig. 8.18) followed in a while by a huge wave, sometimes in excess of 30–40 m.

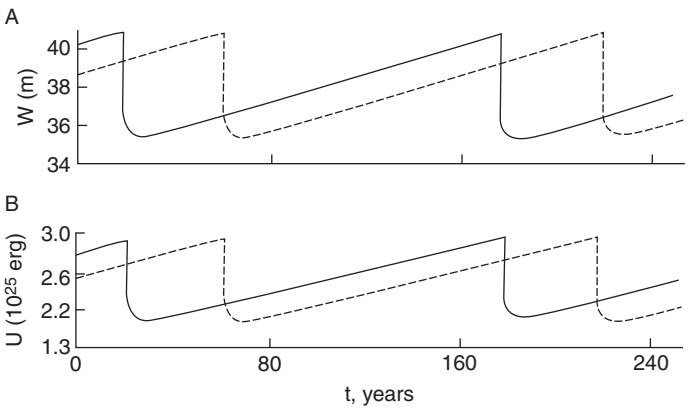


**FIGURE 8.16** Cyclic shifts of the external edge (A) and variations of the total elastic energy (B) for two adjacent blocks of the crust uplift in the island arc in the seismotectonic evolution of the arc's margin after Lobkovsky (1988).

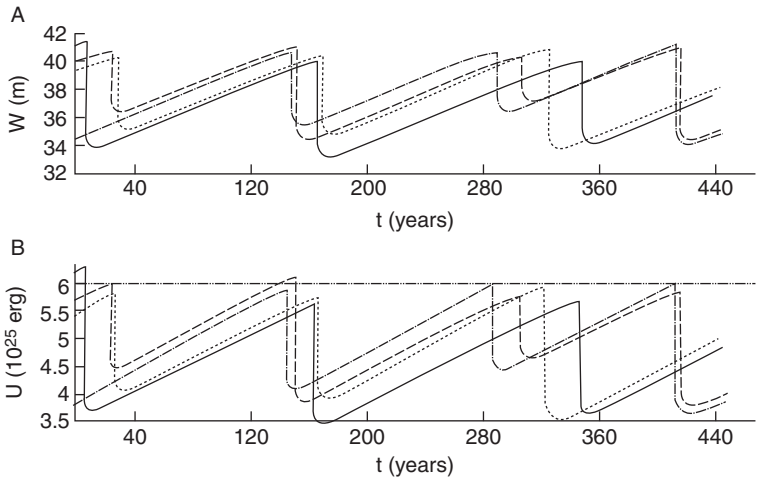


**FIGURE 8.17** Example of seismotectonic evolution in a group of central "keyboard" blocks—components of a system of 10 seismoactive blocks (Lobkovsky, 1988). See Fig. 8.17 for A, B.

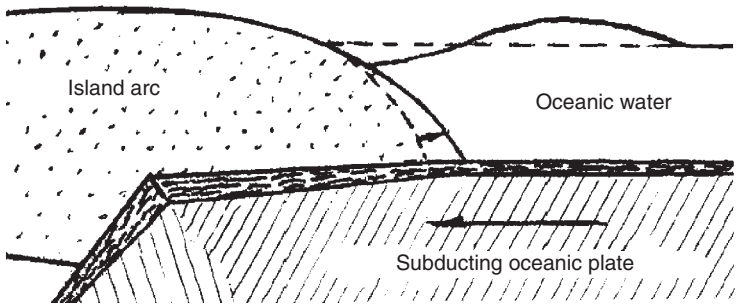


**FIGURE 8.18** Tsunami emergence due to elastic recoil of the island arc crustal edge compressed by subducted plate. Dashed lines mark compressed position of the island arc crustal edge and undisturbed ocean surface; solid lines, island arc position after the elastic recoil, and the resulting tsunami which then turns into a series of waves (scale distorted).

There is another tsunami-generating mechanism (although the tsunamis in this case are smaller). Such earthquakes occur when, under pressure from the subducting lithospheric plate, the frontal part of the island arc is moved over the edge of the arc itself (see Fig. 8.19). Under this mechanism, contrary to the previous case, the tsunami wave rolls on the island arc shore first and only then rolls back.

The Lobkovsky model shows that the greatest danger is associated with the seismic gaps, that is, the island arc and active continental margin areas where there were no earthquakes for a long time. Great danger is associated with the areas of oblique plate subduction as it was observed in the north of the Sunda island arc. Indeed, the initial push in the catastrophic earthquake of December 26, 2004 happened near the northern extremity of Sumatra Island. After that the "domino" principle acted. It activated the adjacent keyboard blocks

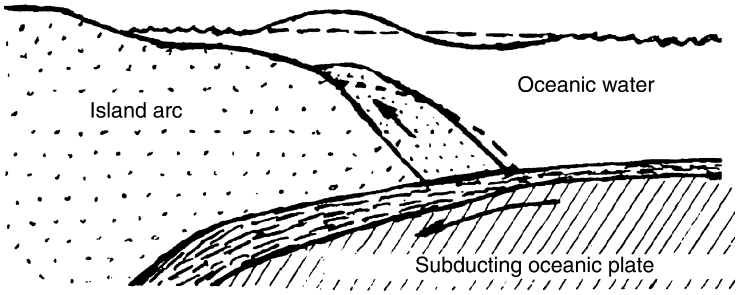


**FIGURE 8.19** Tsunami emergence from the overthrust of island arc frontal portion under pressure from the subducted plate on the arc's body.

thereby extending the tsunami-generating earthquake node by almost 1300 km (Lobkovsky, 2005). There is such a danger zone, a gap in about the middle of the Kuril-Kamchatka island arc. Although it is a place where the ortagonal subduction is occurring, still there were no large earthquakes there for at least 150 years. A strong tsunami-generating earthquake was predicted in this zone (Lobkovsky, 2005) and it indeed happened on November 25, 2006. So, this earthquake was predicted.

The tsunami wave propagation velocity in the open ocean is huge and may be determined from the following equation:

$$V_{\text{ts}} = \sqrt{gH_{\text{oc}}}. \tag{8.22}$$

Here, $V_{\text{ts}}$ is the tsunami wave propagation velocity in the ocean, $g$ is the gravity acceleration, and $H_{\text{oc}}$ is the depth of the open ocean. When $H_{\text{oc}} \approx 5000$ m, $V_{\text{ts}} \approx 211$ m/s $\approx 760$ km/hour. The height of the tsunami waves in the open ocean is small, close to 1 m, but their length is 500–1000 m. When such wave reach shallow water its velocity drastically decreases, and their height dramatically increases.

## 8.5 MECHANISM OF OCEANIC DEPOSIT SUCK-IN UNDER CONTINENTS

Together with the oceanic lithosphere, pelagic deposits are moved in the direction of the plate subduction zone. In most cases, however, there is no stripping-of and crushing of the deposits. There is usually no significant deposit accumulation in the deepwater trough although the sedimentation rate there reaches a few centimeters per thousand years. At this rate, most troughs should have been totally filled-in within a few tens of millions of years. In actuality, they remain "empty" although some of them are in existence and continue to evolve over hundreds of millions of years in a row (as, e.g., the Japanese ort Peruvian-Chilean troughs). It is a testimony of an effective deposit removal mechanism there. It was recently found out that such natural mechanism is deposit sucking-in into the subduction zones. The phenomenon is similar to the lubrication of moving mechanical parts by liquid oils when these oils get into the gaps between the rigid parts rubbing one about the other.

The very possibility of sucking-in the unconsolidated pelagic deposits into the gaps between the moving rigid plates was doubted by many geologists. This problem was solved theoretically (Sorokhtin and Lobkovsky, 1976), and later the sucking-in was confirmed by seismic studies (Garkalenko and Ushakov, 1978) and after that by drilling on the slopes of the Lesser Antilles (Biji-Duval et al., 1981). Somewhat later was found a theoretical solution for the problem of the pelagic deposits sucking-in to great depths under the continents (Monin and Sorokhtin, 1986).

The deposits in the gap between lithospheric plates are affected by the oppositely directed forces. One such force is the displacement of the subducted plate. The other one is the back-squeezing of the deposits from the zone by the excess weight of the obducted continental lithospheric block (Fig. 8.20).

The interaction of these oppositely directed forces controls the process evolution. If the sucking-in forces prevail, the deposits will be consumed within the plate subduction zone without the stripping effect. Oppositely, the excess deposit volume will be squeezed out of the zone, crushed in front of the obducting plate edge, and will form the folded structure of an accretion prism.

In order to determine the nature of viscoplastic flows within the deposit layer between the moving plates, we need to solve the Navier–Stokes equation for a given structure of the plate subduction zone. It is convenient to search the solution for the case of the viscous liquid stationary flow within a flat slit between two rigid surfaces moving relative to one another. In hydrodynamics, such flows are called the Cuetta flows (Schlichting, 1964).

Let as assume the subduction zone model as shown in Fig. 8.20. Let us direct $x$-axis along the subduction zone from its front into the zone's depth. Let us place $z$-axis perpendicularly to the subduction zone top and direct it downward. Let us select the origin next to the frontal edge of the obducting plate and assume that the subducting plate moves at a constant rate $u_0$. Then the Navier–Stokes equation is

$$\eta \frac{d^2u}{dz^2} = \frac{\partial P}{\partial x} - \rho_s g \sin\alpha, \tag{8.23}$$

where $u$ is the deposit flow rate in the gap between the plates; $\eta$ is the deposit viscosity; P is pressure; $\rho_s$ is the deposit density; $g$ is the gravity acceleration; and $\alpha$ is the subduction zone dip angle.

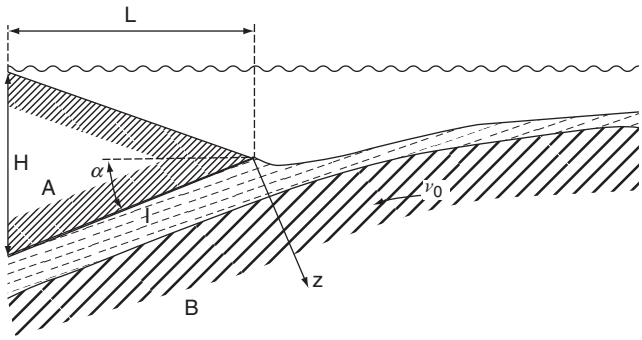


**FIGURE 8.20** Model of deposit sucking-in into subduction zone: (A) frontal edge of obducted plate; H and $L$, thickness and length of this edge; (B) subducted plate; $\alpha$, subduction zone incline.

The boundary conditions may be formatted as

$$\begin{aligned} u &= 0 \,\text{at}\, x = 0 \\ u &= u_0 \,\text{at}\, z = h, \end{aligned} \tag{8.24}$$

where $h$ is the gap thickness between the plates. In this case, the solution of Eq. (8.23) is

$$u = \frac{z}{h} u_0 - \frac{z}{h}\left(1 - \frac{z}{h}\right) \frac{h^2 \Delta\rho g}{2\eta} \sin\alpha, \tag{8.25}$$

where $\Delta\rho = \rho_l - \rho_s$; $\rho_l$ is the obducting lithospheric plate density; $\rho_s$ is deposit density. Then average rate of the sedimentary matter flow within the gap is

$$\bar{u} = \frac{u_0}{2} - \frac{h^2 \Delta\rho g}{12\eta} \sin\alpha. \tag{8.26}$$

Obviously, the deposit suck-in into the plate subduction zones may only occur if $\bar{u} > 0$. For usual pelagic deposits with density way below average density of the lithospheric plates $\rho_s < \rho_l$, this condition is satisfied only when

$$\frac{h^2 \Delta\rho g}{6\eta} \sin\alpha < u_0. \tag{8.27}$$

In the absence of the deposit stripping from the ocean floor and their crushing in front of the subduction zone, the deposit flows on the ocean floor and in the beginning of the subduction zone must be similar, that is, $h_0 u_0 = h\bar{u}$, where $h_0$ is the deposit thickness on the ocean floor. In such case,

$$h_0 u_0 = \frac{u_0}{2} h - \frac{h^2 \Delta\rho g}{12\eta} \sin\alpha. \tag{8.28}$$

On the other hand, the solution (8.25) indicates that the deposit back-flows may arise within the gap between the plates, the deposits being squeezed out under the weight of the obducting plate. Such flows may emerge at low and medium $z$ values. For them it may be that $u < 0$. The inequality $u \geq 0$ satisfied within the gap at all $z$ levels is the condition that such flows, therefore the deposit squeeze-out of the gap will not occur. Under this condition, at $\rho_l > \rho_s$ we find from Eq. (8.27):

$$0 < \frac{h^2 \Delta\rho g}{2\eta u_0} \sin\alpha \leq 1. \tag{8.29}$$

The same Eq. (8.29) may be formatted differently:

$$3\left(1 - \frac{2h_0}{h}\right) = \frac{h^2 \Delta\rho g}{2\eta u_0} \sin\alpha. \tag{8.30}$$

Comparing Eqs. (8.30) and (8.29), we find that at positive pressure gradient ($\rho_l > \rho_s$) and constant deposit viscosity $\eta$ their thickness $h$ in the gap is always

$$2h_0 < h \leq 3h_0. \tag{8.31}$$

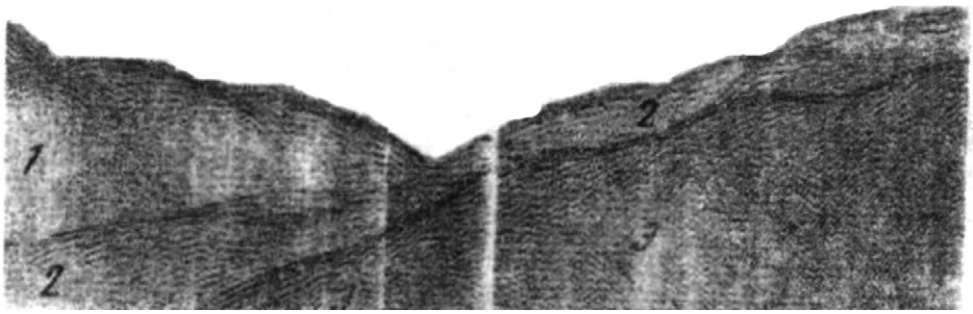


**FIGURE 8.21** Seismic cross section displaying sucking-in of oceanic deposits (2) together with oceanic plate (3) under Kuril island arc (1) (Bondarenko et al., 1977).

Practically, the condition (8.31) is almost always satisfied, especially at shallow depths (see Fig. 8.21). However, this inequality relates to the width only of the plate subduction zone frontal portion. In deeper portions, the gap width $h$ between the plates may significantly change depending on the deposit alterations and the respective viscosity changes, and also, at the deposit melting, on permeability for the melts of the plate area over the subduction zone.

Indeed, the deposit deformation accompanied by the viscous friction energy dissipation occurs in the deposit suck-in between the moving plates. As a result, deposit viscosity in the depths of the subduction zone rapidly declines under the Arrhenius law:

$$\eta = \eta_0 e^{w/RT}, \tag{8.32}$$

where $\eta_0 \approx 10^{-5}$ P is viscosity of strongly overheated silicate matter; $W$ is per-unit activation energy of viscous deformations; $R$ is the gas constant; T is temperature (Kelvin). In such an environment the inequality (8.31) is disrupted. Together with a decrease in viscosity of the deposit sucked into the plate subduction zone, the equilibrium gap width $h$ between the plates must significantly decrease. Practically, it means that the light deposit material $\rho_s$, as it heats up and loses viscosity, must be squeezed out of the subduction zone through the system of the associated faults which are usually abundant in the body of the island arc or the active continent margin. The estimate of heat generation by the deposits may be conducted using the dissipative function $q$ which determines the viscous friction energy release within the unit volume over the unit time (Eq. 8.33; Monin and Sorokhtin, 1986):

$$q \approx \frac{2\eta}{h}\int_0^h \left(\frac{du}{dz}\right)^2 dz = 2\eta\frac{u_0^2}{h^2} + \frac{(h\Delta\rho g \sin\beta)^2}{6\eta}. \tag{8.33}$$

It is also obvious that over the time while the deposits subside to the depth $H$ the following heat is released in each gram of their matter:

$$Q = q\frac{H}{\rho_s u_0 \sin\beta}. \tag{8.34}$$

The estimates using Eqs. (8.32)–(8.34) show that within a wide range of the deposit densities they will heat up the water-containing silicate melting point at depths of 20–30 km. Thus, the light deposits with density of about $\rho_s \approx 2 \div 2.5$ g/cm$^3$ do not get deeper than that, and are squeezed out from the subduction zone and intrude the back-zones of island arcs and active continent margins (see Fig. 8.22).

As in a case of lubrication, the deposit amount getting into the gap between the rubbing plates must depend on the plate movement rate and viscosity of the sucked-in deposits. Calculations based on the theory of mechanisms lubrication showed that the deposits may be sucked-in under the island arcs without stripping and crushing only if their thickness does not exceed some critical limit which depends on the plate subduction rate and deposit viscosity (Sorokhtin and Lobkovsky, 1976). At that, the thickness of the sucked-in deposits increases by two or three times, and the latter limit is a maximum and corresponds to stripping of the excess deposits and to the formation in front of the island arc of a sedimentary accretion prism. The critical thickness of the deposits $h_0$, depending on their viscosity $\eta_s$ and the plate subduction rate $u_0$, is found as:

$$h_0 \leq 5.5 \times 10^{-8} \sqrt{\eta_s u_0}. \tag{8.35}$$

Here, $h_0$ is in meters; $u_0$ is in cm/year; $\eta_s$ is in poise.

Up to 500–520 m of pelagic deposits may be sucked-in without stripping and crushing under such arcs as the Kuril, Japanese, and Tonga, and only 400–430 m, into the Peru-Chilean, Aleutian, and Java troughs. The deposit thickness near the Kuril, Japanese, and the central part of the Javanese deepwater troughs is no greater than 300–500 m, near the Tonga trough, 100–300 m and in front of the most of the Peru-Chilean trough, 100 m and less. So, the plate subduction under these structures is not accompanied by the deposit stripping

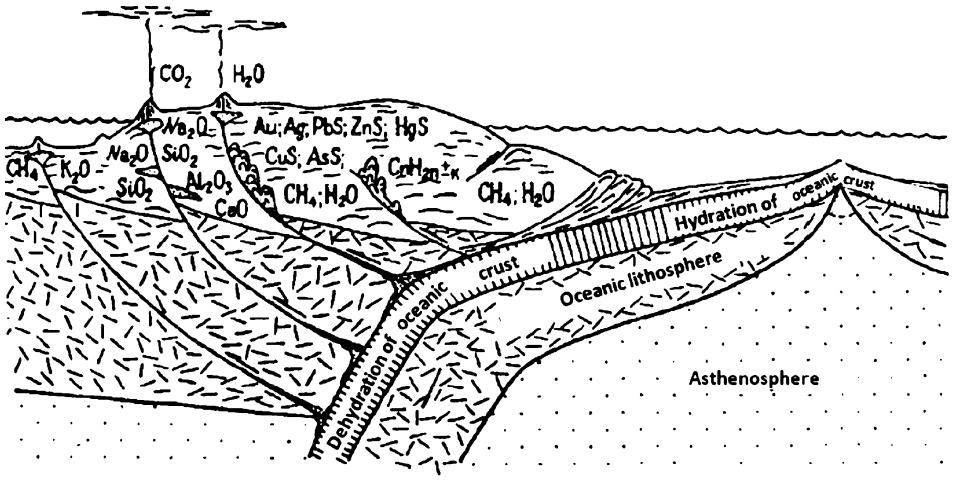


**FIGURE 8.22** Continental crust formation in Proterozoic and Phanerozoic due to partial remelting and dehydration of oceanic crust and overlying pelagic deposits within the oceanic plate subduction zones under island arcs.

and crushing in front of the obducting plate. Assuming that 500 m of deposits may be sucked into the aforementioned zones without stripping, the viscosity of the Pacific pelagic deposits is estimated at approximately $10^{19}$ P.

A totally different situation is encountered in the Alaska Bay (in the eastern part of the Aleutian arc) and in the north of the Javanese trough. The plate subduction rate in these areas is small (about 2–3 cm/year), the deposit thickness is over 500–700 m (sometimes 1000 m). Thus, everywhere it is over the critical value.

A similar situation occurs near the subduction zone of the Atlantic plate underneath the Lesser Antilles. The critical no-stripping, no-crushing deposit thickness for that zone is about 250 m, and the actual thickness is 500–1000 m. It means that the plate subduction there must go with the ocean floor deposits stripping and crushing in front of the island arc lithospheric protuberance, that is, with the formation of the accretion depositional prisms.

That may explain the emergence of nonvolcanic external ridges near these plate subduction zones (the Kodiak Island in the Aleutian arc, the Lesser Antilles in the Atlantic, and the Andaman Islands in the Indian Ocean).

As the viscous friction energy dissipates, the deposits in the slit between the rubbing plates are gradually heated up and even begin to melt. As a result, their viscosity within the subduction zones declines by many orders of the magnitude. The critical thickness of the deposits capable of being preserved within the zones at great depths also drastically decreases. For this reason regular deposits with density lower than that of the lithosphere cannot be sucked-in to the subduction zones to depths deeper than 20–30 km. As already mentioned, such deposits are usually squeezed up through feathering faults and intrude the body of the island arc structures or active continental margins over such subduction zones as migmatite granite–gneiss batholiths.

The deposits may be sucked-in to great depths and underneath the continental lithospheric plates only if their density is greater than that of the lithosphere. In such a case, the deposit suck-in rate into the subduction zones is always higher than the plate subduction rate. Therefore, the heavy deposits must "fall" into the subduction zones (Monin and Sorokhtin, 1986).

Any present-day deposits are lighter than the lithosphere whose density is $\rho_l \approx 3.3$ g/cm$^3$ so they cannot be sucked-in to great depths under the island arcs or active continental margins. It is known that there were epochs in the Precambrian history when abundant iron-ore formations (jaspelites) were deposited on the ocean floor and on the continental shelves. Their density reached 4–4.5 g/cm$^3$ and was much greater than that of the lithosphere. Such deposits could be without hindrance sucked-in (could "fall") to great depths under the continents.

These deposits were melted and differentiated with the formation of silicate–carbonate malts. Iron compounds were separated from them and went into the mantle. After that, nodes of the kimberlite, lamprophyre, carbonatite, and alkali-ultramafic rocks could form at the base of the continental lithosphere, at depths of 100 to 220–250 km. Subsequently, after liquation of the melts and iron separation these magmas became lighter. When the tectonic regime changed from compression to extension they could raise to the surface and intrude the continental crust (see Section 10.6).

## 8.6 MOUNTAIN AND MOUNTAIN BELT FORMATION

Mountain buildups and ranges usually form narrow linear or arcuate folded structures located as a rule along the periphery of stable continental platforms. The mountains are often comprised sedimentary sequences which are significantly metamorphosed, folded, and cut with faults (Fig. 8.23). Before the advent of the plate tectonics, formation mechanisms of the regional overthrusts and geosynclinal folding were actually unknown. There were many, often mutually exclusive hypotheses. Not a single one satisfied the aggregate of the geological knowledge about the structure of Earth's mountain belts. The new theory made it clear that all without exception folded mountain systems, often with regional overthrusts, emerge only in front of the plate subduction zones or in their immediate vicinity due to compression and deformation of thick sedimentary sequences which got into the zones, of the island arcs themselves or of the continental margins.

British geologists Dewey and Bird (1970a,b) identified major genetic types of the regional overthrusts and folded structures emerging in the deformation of island arcs and active continental margins (whenever the oceanic lithosphere is subducted underneath them and whenever the island arcs and Atlantic-type active continental margins are obducted) or when the continents collide (see Figs. 8.24 and 8.25).

The folding of sedimentary sequences, often with imbrication and nappes, arise only when these sequences are subducted underneath the frontal areas of island arcs and active continental margins, after the collision between island arcs or continents and in the back of these structures (see Figs. 8.25 and 8.26). The new theory not only allowed understanding the nature but also the quantitative estimates of the formation regimes of foredeeps where usually accumulate thick deposit sequences which are crushed into folds at the continental margins collision with island arcs.

Figure 8.27 shows, using the South-American Andes as the example, generalized deformation schematics of the active continental margins. As we see, these type mountain buildups (and most island arcs) are cut by two systems of strike-slip faults dipping toward one another. Main movements and deformations occur along these faults. Within the same faults happens the matter circulation in the active continental margins' and island arcs' bodies. The circulation occurs due to the friction and tectonic erosion at the base of the lithospheric (crustal) protuberance overlying the subducting oceanic plate.

As a result, the torn-apart matter of the obducting plate frontal areas, together with the worked-over matter of the subducting plate, gradually moves from the back to the frontal portions of the mountain buildup and gradually "rejuvenates" them. We estimated (Sorokhtin, 1979) that the tectonic erosion rate of the Kuril island arc reaches 0.3 cm/year. Therefore, the entire body of the arc, about 300 km wide, will be totally consumed in approximately 100 MMY. Apparently, there are no rocks older than Late Cretaceous on the Kuril Islands.

Still, all the diversities of the actual-folded structural forms in Earth's fold-belts are mostly controlled by complex combinations of the mentioned simpler deformations sometimes overrun later by additional tectonic processes of a different nature (such as rift-formation).

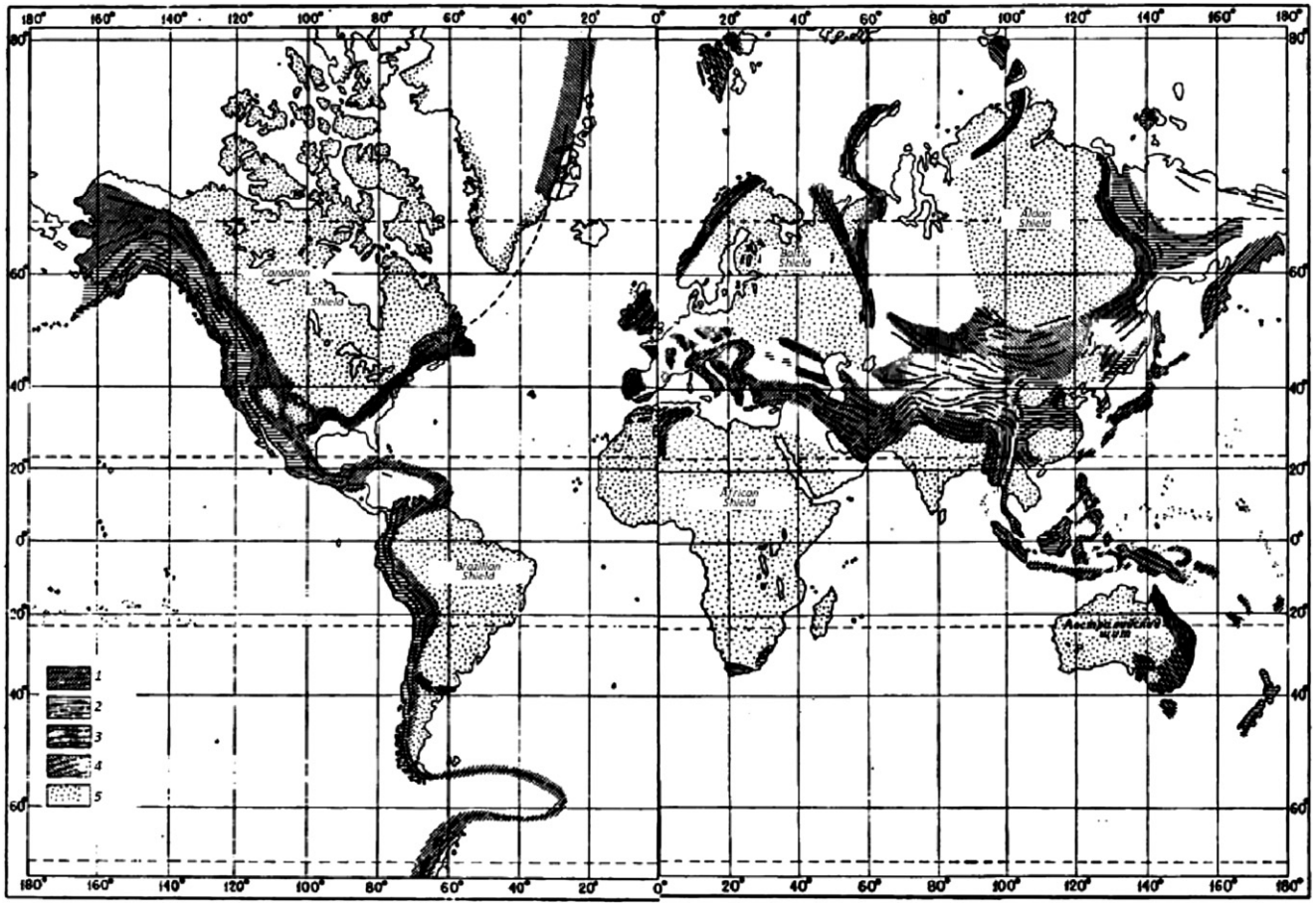


**FIGURE 8.23** Earth's mountain belts: 1, Cenozoic; 2, Mesozoic; 3, Hercynian; 4, Caledonian; and 5, Precambrian platforms (Umbgrove, 1947).

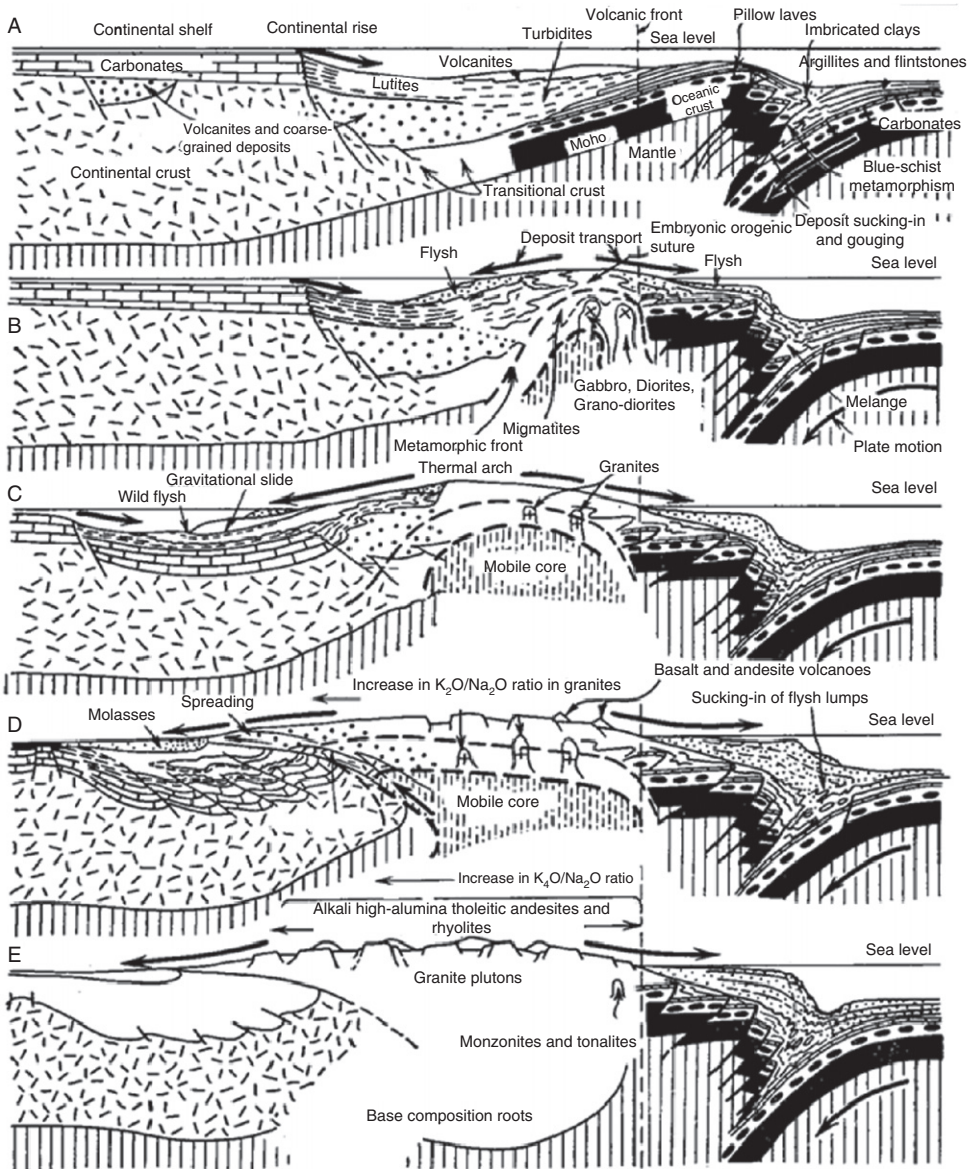


**FIGURE 8.24** Model of mountain belt formation (stages A through E) over the Cordillera-type active continental margin (Dewey and Bird, 1970a; it is assumed that the "mobile core" is represented by melts ascending from "hot" portion of plate subduction zone).

When Earth's tectonic activity increases, pressure from the subducting oceanic plates on the island arcs and back-arc spreading basins grows. As a result, the back-arc basins close up, and the island arc back portions or the adjacent continental margins are obducted by ophiolite nappes (the areas of the former oceanic crust of these basins). The ophiolite

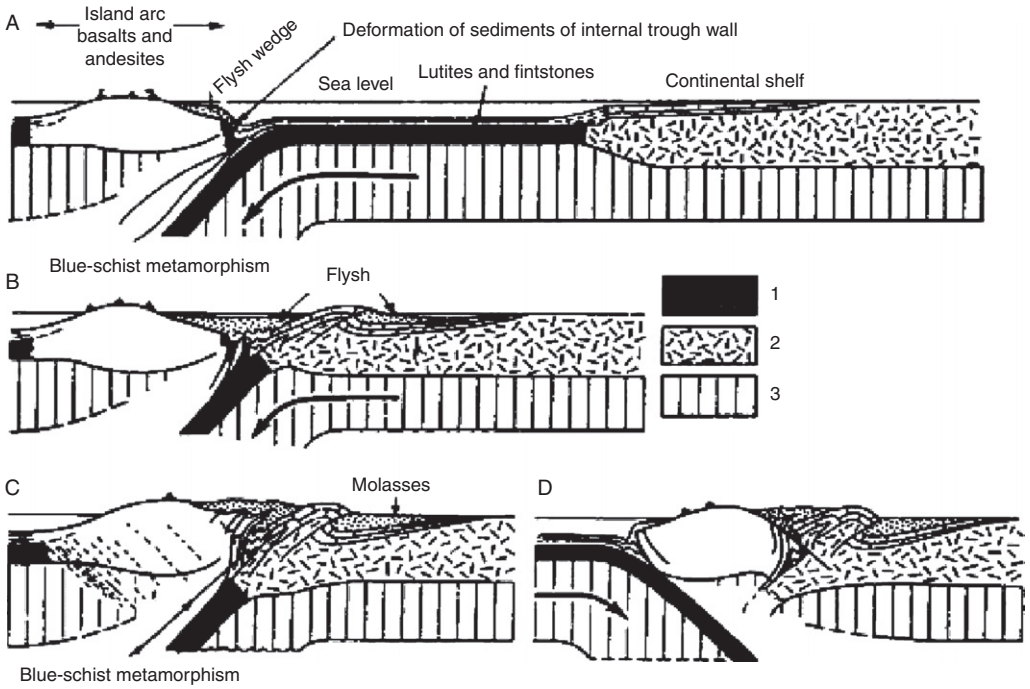


**FIGURE 8.25** Model of mountain belt formation (Stages A through D) in the collision zone of island arc and continent (Dewey and Bird, 1970b): 1, oceanic crust; 2, continental crust; and 3, lithosphere.

nappes may arise also during closing of the Red Sea-type narrow oceanic basins. This happens when the spreading regime in such basins converts to the compression.

The island arcs often start on the oceanic lithosphere so they frequently have former oceanic crust for a base. Subsequently, as deformations develop in the arc's body and as affected by the subducting plate, the island arc's base (i.e., the former oceanic crust now forming the ophiolite nappe) may be thrown over the arc (Fig. 8.28). The overthrusts (obduction) occur in such cases from the arc's frontal parts onto its back areas.

Often underneath the so formed ophiolite sheets are found glaucophane-schist rocks emerged under the island arc base and metamorphosed at relatively low temperature of 300–500 °C, but at high pressure of about 6–10 kbar corresponding to the depths of island arc base (25–40 km). Sometimes, these glaucophane-schist sheets are thrust over volcanic areas of the island arcs which have high-temperature metamorphism. In such cases the so-called paired metamorphism occurs.

The paired regional metamorphism belts with the opposite nature of pressure/temperature environment are quite common in many regions of the Pacific mobile ring. Usually, they are close of age and extend parallel to each other over great distances. One of such belts may be of a high pressure type, and another, of a low-pressure type although some segments of either may belong to a moderate pressure type.

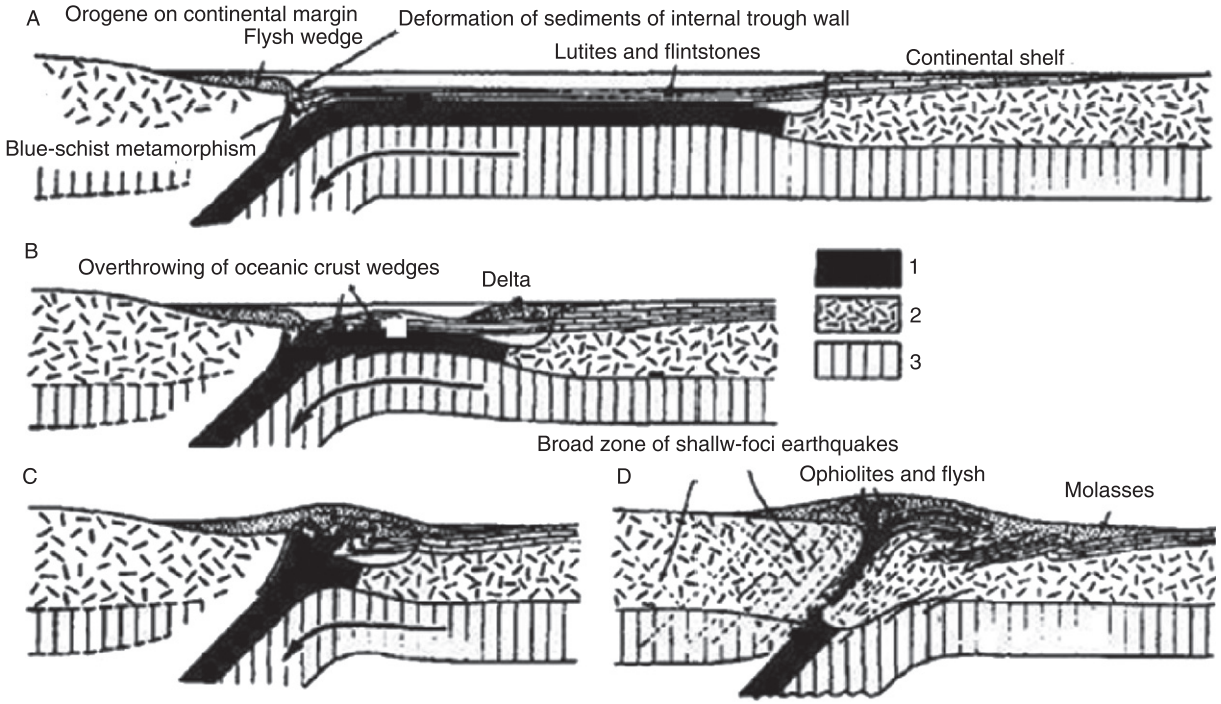


**FIGURE 8.26** Model of mountain belt formation (stages A through D) in the collision zone of two continents (Dewey and Bird, 1970b): 1, oceanic crust; 2, continental crust; and 3, lithosphere.

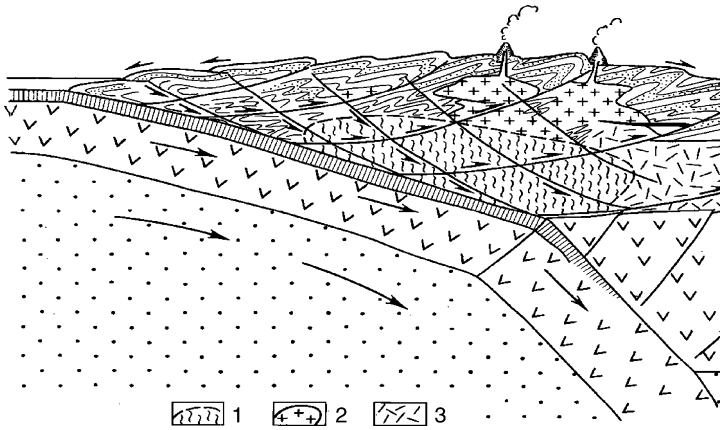


**FIGURE 8.27** Deformations of mountain buildups over Andean-type active continental margins: 1, melt and migmatite existence area; 2, granitoid intrusions; and 3, continental crust.

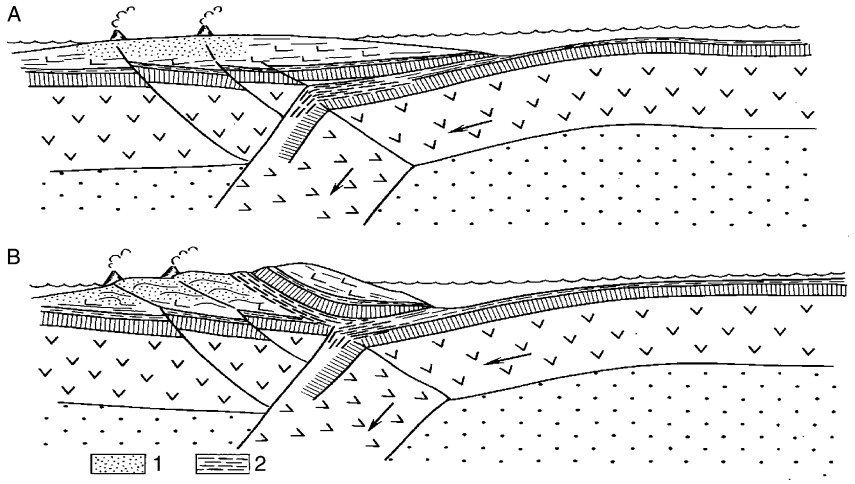


**FIGURE 8.28** Origins of ophiolite nappes and paired metamorphic belts in island arcs: 1, area of high-temperature low-pressure metamorphism and 2, glaucophane schists—products of low-pressure high-temperature metamorphism.

The paired metamorphism belts are well studied in Japan (Fig. 8.29), they are described in California, Chile, New Zeeland, in Scottish Caledonides (Miyashiro, 1976), and possibly in the Urals (Maksyutkov complex).

The high-temperature (600–700 °C and higher)–low-pressure (0.5–3 kbar) metamorphic belts are usually accompanied by numerous granite intrusions. The andesite volcanoes chains are surface indicators of the low-pressure metamorphic zones and the associated granite magmatism. Thus, a low-pressure metamorphic belt may be treated as the granite plutonism/andesite magmatism belt (Miyashiro, 1976).

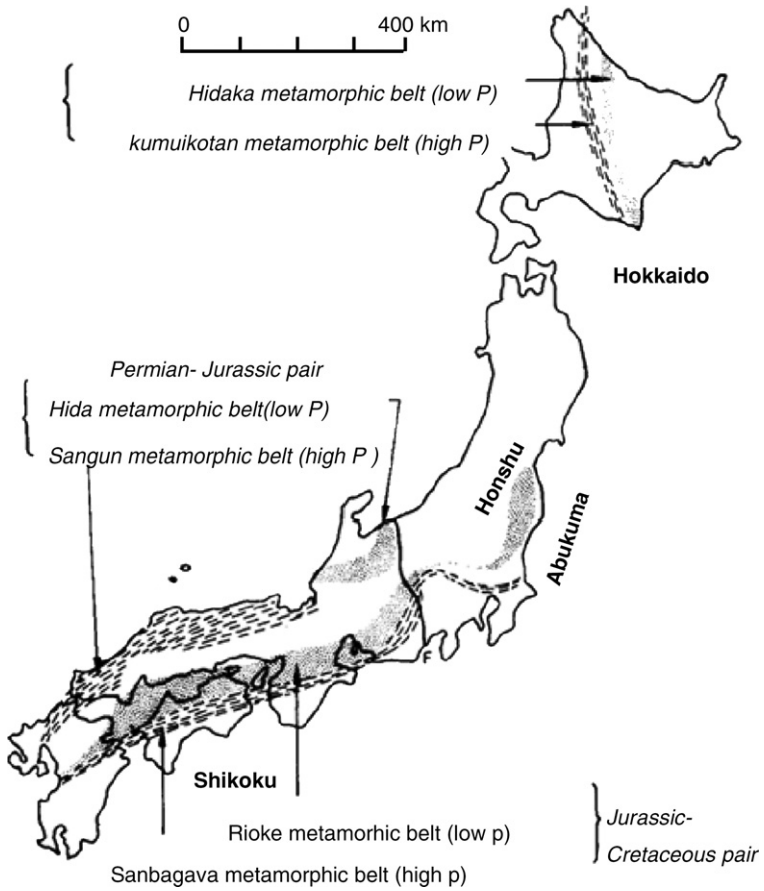


**FIGURE 8.29** Three paired regionally metamorphic belts of Japan (Miyashiro, 1976).

An important role in Earth's geology belongs to the intercontinental mountain ranges. They are in effect the sutures connecting the adjacent older continental platforms (see Fig. 8.26). Such ranges most of which are long eroded, compose most of the post-Archaean continental crust. An Early Paleozoic North-Atlantic belt which includes the Appalachian, Scottish, and Norwegian Caledonides formed in place of the Paleo-Atlantic Ocean Iapetus, and the Urals-Kazakhstan Hercynian fold-belt, both welding 230 MMY ago Gondwana and the northern continents into a supercontinent, Wegener's Pangaea, belong to the Phanerozoic mobile belts of this type.

Younger structures of this type include a Mesozoic Verkhoyansk-Kolyma fold-belt which emerged in place of the East-Siberian paleo-ocean and merged the Kolyma Massif and Chukotka to the Siberian Platform. And the youngest and most grandiose Alpine-Himalayan Cenozoic mountain belt formed at the closing of the Tethys paleo-ocean and joined Africa, Arabia, and India with Eurasia (see Fig. 8.23).

Worth mentioning out of the old intercontinental suture zones that merged the Precambrian platform and shield fragments are the Svekofenian fold-belts that soldered the fragments of the first supercontinent Monogaea which disintegrated in Proterozoic into a new supercontinent, Hans Stille's Megagaea. The next, third supercontinent Mesogea (Rodinia) was welded from fragments of the disintegrated Megagaea by the Grenvillian intercontinental mobile belts the same way as the Late-Riphaean and Phanerozoic belts joined the Mesogea fragments into the Wegener's Pangaea.

What are the common features in the evolution of all these intercontinental mountain belts?

The issue was first dealt with in the geosynclinal doctrine. However, it was always descriptive, the nature of Earth's crust formation process was not elaborated and the cause-and-effect relationships in this process were never disclosed. Besides, in recent decades the notion of Earth's crust geosynclinal evolution was vastly expanded. It now included diverse geological processes from the formation of ophiolite formation rocks to the emergence of fold-belts. The original term gradually lost its former information load and actually converted into a synonym of Earth's crust formation notion.

There are two options:

A first one is to restrict the notion of the geosynclinal process to Earth's crust formation above the plate subduction zones. The notion should not include the stage of ophiolite (i.e., the oceanic crust) complex formation.

A second and better one is to throw this term out as it no longer satisfies the requirements of the modern geological theory (as it was previously done in physics with phlogiston and ether).

It was found with the emergence of the lithospheric plate tectonics that it was more convenient and more accurate to describe the Earth's fold-belt and crust (both continental and oceanic) formation processes in terms of the new theory rather that of the geosynclinal doctrine.

From this viewpoint, we briefly review as an example the origin of the intercontinental mountain ranges of the previously mentioned types. Their common feature is a succession of events associated with the continental split, the formation and closing of the young Atlantic-type ocean basins, the deformation and magmatic reworking of the former continental margins, and the repeated mergers of the continental massifs into new continents.

A Canadian geologist Wilson (1968) was the first to describe this chain of events from the position of the lithospheric plate tectonics. Since then, the succession of the formation of intercontinental ocean basins and the mountain belts emerged in their place is called the "Wilson cycle" (Fig. 8.30).

Under his model (amended by the modern concepts of the supercontinent formation and destruction succession; see Chapter 9), the mobile belts of the type under review always emerge on the continental crust and have a long evolution on the order of 700–800 MMY. The formation of such a belt is usually started with the split impulse of the then existing supercontinent and the emergence under the crust extension environment of a continental rift system not unlike the East-African one, with the bimodal volcanism typical of such systems (Fig. 8.30, situation 1).

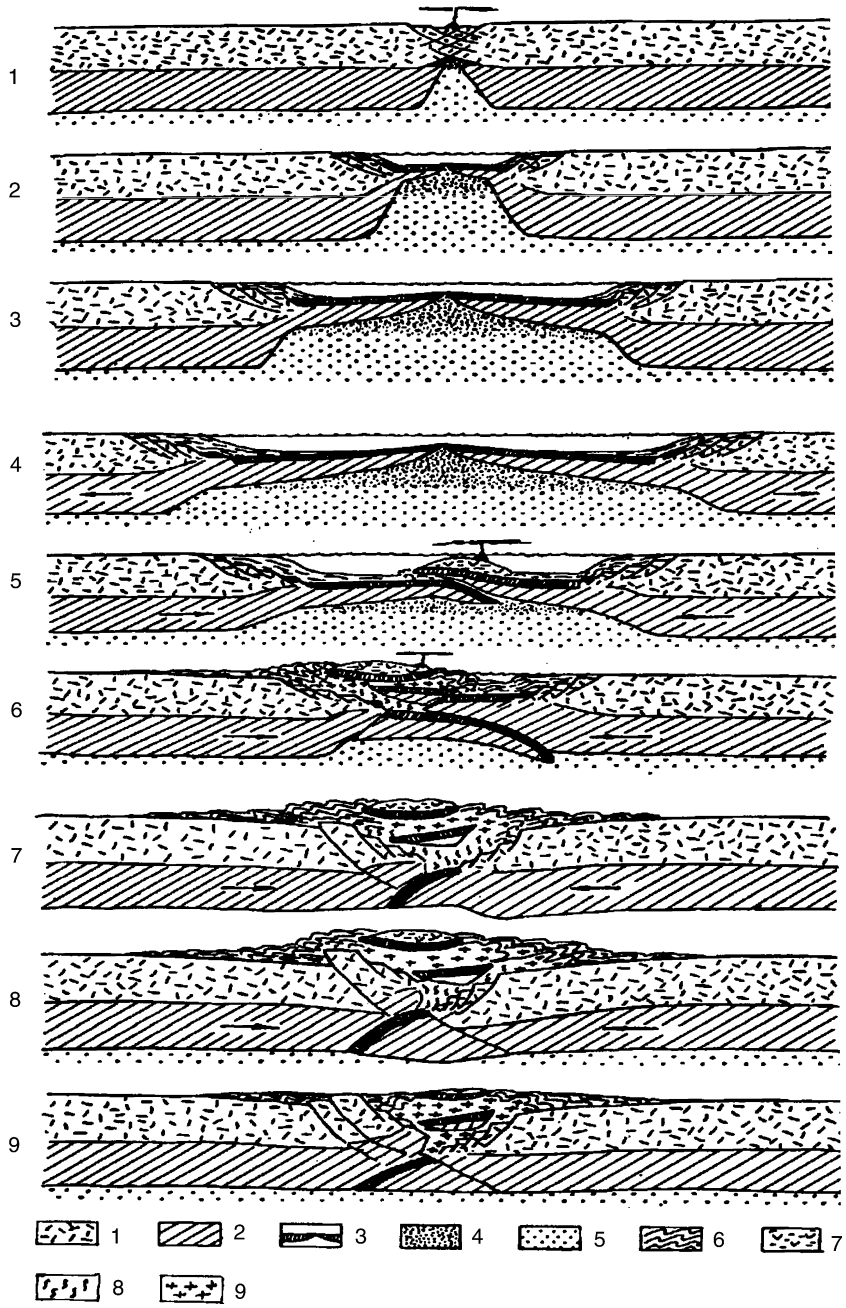


**FIGURE 8.30** Schematic formation of intercontinental mountain buildups under the Wilson cycle: 1, continental crust; 2, subcrustal lithosphere; 3, oceanic crust; 4, partially melted asthenospheric matter; 5, plastic mantle; 6, folded sedimentary sequences; 7, volcanosedimentary island arc formations; 8, granitoid composition melts and migmatites; and 9, granite intrusions.

As the separated continental massifs spread apart, first, a narrow Red Sea-type marine basin forms in place of the continental rift zone (the basin now has the oceanic crust and basalt magmatism, Fig. 8.30, situation 2), and then the real Atlantic-type ocean (Fig. 8.30, situations 3 and 4).

At his stage in the belt evolution, the continental margin (i.e., the future miogeosynclinal zone) experiences constant subsidence due to the sinking of the oceanic lithosphere "soldered" to such margin. Therefore, here as well the continent subsidence with time was determined as $\Delta h \sim \sqrt{t}$. The proportionality factor, however, is different as the continental lithosphere positive buoyance and elasticity resist such continental margin subsidence and, contrary to that, the deposition facilitates them. At this stage, corresponding to the initial subsidence phase of the classic geosynclinal scheme, thick continental sandy–clayey and marine carbonate sediments accumulate there. Over the time interval when such expanding ocean existed (about 200 MMY) thick (up to 15–18 km) clastic sequences accumulate on the continental margins.

Usually, the supercontinent disintegration process ends at this stage in the mobile belt evolution. Centrifugal spreading of the earlier separated continents is replaced by their centripetal approach. This stage is comparable with the mature stage in the geosyncline evolution. The extension environment is replaced by the compression one. The earlier formed ocean begins to close. A new island arc, the future eugeosynclinal zone with the characteristic andesite magmatism emerges in place of the former rift zone (i.e., where the lithospheric plate is the thinnest; Fig. 8.30, situation 5). At the ocean closing stage, the island arc calcareous-alkali volcanism mentioned earlier is very common.

In the further ocean closing, the continental margin also continues to subside, although now it is under pressure from the approaching island arc. This results in a drastic increase in its subsidence rate, especially in the latest stage when the island arc begins to obduct the continental margin. At the same time, the sediments deposited in front of the island arc over the entire oceanic period are crushed. The island arc obducts the passive margin of one of the continents and the ophiolite sheets form (Fig. 8.30, situation 6). After that, the still preserved former oceanic areas in the back of the island arc close. The entire ocean completely closes, sediments on both continental margins that earlier framed the former ocean are crushed (Fig. 8.30, situation 7).

Over a relatively short interval (a few million years) in the orogenic stage of belt's evolution, the sedimentary cover of the former continental margin (i.e., in the miogeosynclinal zone) was folded. In that time, often affected by ever increasing plate pressure, their subduction direction changed. As a result, vertical motions over the former continental margin may have changed its sign, then the emerged folded buildups began to rise. At the same time, the overthrust and faulted-folded deformations reached their maximum intensity within the body of a former island arc, that is, in the eugeosynclinal zone.

As a result of the remelting, the sedimentary sequences of the former continental margin within the subduction zone, the geosynclinal magmatism changed. The calcareous-alkaline typically island arc magmatism was replaced by an acidic magmatism with profuse granite intrusions and broad regional metamorphism (the nature of such magmatism and metamorphism was reviewed earlier).

The continued approach of the adjacent continents in the formation of a new supercontinent or of its fragments resulted in the compression of the mobile belt that emerged in place

of the former ocean. A consequence was mountain-building processes that raised the summits of such mountain belt to 7 or 8 km above the ocean level (as it is observed now in Hindu Kush, Pamir, and Himalayans (Fig. 8.30, situation 8).

Typical of this stage in the evolution of the intercontinental mountain ranges are intrusions of large granite batholiths and riolite magmatism. Upon the consolidation of so emerged mountain range, the stage of its denudation and erosion began which could last for hundreds of millions of years (Fig. 8.30, situation 9). After the almost complete mountain belt leveling, deeply metamorphosed rocks of its base were exposed and it turned into a portion of a regular continental platform.

This brief description of the emergence of a "typical" intercontinental fold-belt shows that the classic geosynclinal evolution scheme fits well with one possible version of the mobile belt development under the theory of the lithospheric plate tectonics. The new theory, however, gives a more accurate description of the process nature and goes further in reviewing the other ways in the mobile zones evolution (such as the Andean-type). What is especially important is that, as opposed to the geosynclinal doctrine, it helps uncover the cause-and-effect relationships in the formation of Earth's crust and individual mobile belts.

## 8.7 EARTH'S CRUST ORIGIN

As the lithospheric plates spread, open extension fissures form in the oceanic rift zones. Basalt melts rise from the asthenosphere through these fissures. These basalts erupt on the ocean floor surfaces pillow lavas and gradually form the upper portion of the second (basalt) layer of the oceanic crust (the first one is comprised by sediments).

Basalt composition is usually determined by the depth of their melt-out and differentiation. Underneath the rift zones, the basalt melt foci usually form at shallow depths of 10–15 to 2–3 km so the erupting basalts are of a toleitic composition. Under the pillow lavas is positioned the so-called dyke complex formed though filling-up of fissures occurring in rift zones with basalt magmas. This complex usually comprises dolerite dykes attached to one another ("dyke in dyke" type) and makes up the lower part of the basalt (second) oceanic crust layer.

Underlying the basalts is a third layer of the oceanic crust. Its upper portion is composed of gabbro (mostly also of a toleitic composition) and its lower part is serpentinites formed over hydrated ultramafic rocks (harzburgites and lherzolites). Gabbros are formed after a slow crystallization of basalt melts within the magmatic node which before that was feeding the rift zone basalt volcanism. Based on the nature of the ophiolite formations, the so-called laminated complex is usually observed in the gabbro portion of the oceanic crust third layer. This laminated complex comprises cumulates of denser minerals. Chromite deposits are often found within this complex. The third layer's serpentinite portion usually emerges at some distance from the rift zones due to the oceanic water penetration through fractures under the gabbro layer, that is, as a result of the lithospheric ultramafic rock hydration. Water penetration depth is limited by the lithostatic pressure of about 2.3 kbar. At a higher pressure, serpentinite becomes highly plastic, bloats, and closes up the fractures, hence, the water access to deeper horizons (see Fig. 2.5). Total thickness of the oceanic crust (seismic

data) is approximately 6.5–7 km, the deposit thickness is 0–1000 m (500 m on average), the basalt layer is 2– 2.5 km thick, and the gabbro–serpentinite layer, 4–4.5 km thick.

The rocks in all three oceanic crust layers (sedimentary, basalt, and gabbro–serpentinite) are substantially hydrated. The serpentinites alone include up to 10–11% of the irreducible water, and on the whole the crustal hydrosilicates bond at least 5% of water (by mass). The hydration process removes from the oceanic crust the silica, calcium, magnesium, iron sulfides, and other ore minerals which form ore deposits near the rift zones.

All hydration reactions of this type are exothermal, go with heat release, hence, are irreversible.

Following are the main such reactions:

$$\underset{\text{olivine}}{4Mg_2SiO_4} + 4H_2O + 2CO_2 \rightarrow \underset{\text{serpentine}}{Mg_6(Si_4O_{10})(OH)_8} + \underset{\text{magnesite}}{2MgCO_3} + 65.05 \text{ kcal/mol}; \quad (8.36)$$

$$\underset{\text{olivine}}{4Mg_2SiO_4} + 6H_2O \rightarrow \underset{\text{serpentine}}{Mg_6(Si_4O_{10})(OH)_8} + \underset{\text{brusite}}{2Mg(O)_2} + 33 \text{ kcal/mol}; \quad (8.37)$$

$$\underset{\text{enstatite}}{6MgSiO_3} + 4H_2O \rightarrow \underset{\text{serpentine}}{Mg_6(Si_4O_{10})(OH)_8} + \underset{\text{quartz}}{2SiO_2} + 26 \text{ kcal/mol}. \quad (8.38)$$

Hydration of basalts (wherein the main mineral is anorthite) proceeds under the following generalized reaction:

$$\underset{\text{anorthite}}{2CaAl_2Si_2O_8} + 4H_2O + 2CO_2 \rightarrow \underset{\text{kaolin}}{Al_4(Si_4O_{10})(OH)_8} + \underset{\text{calcite}}{2CaCO_3} + 110.54 \text{ kcal/mol}. \quad (8.39)$$

At the same time, the crust hydration results in its enrichment in potassium, sodium, and some other lithophilic minerals including uranium, all getting into the crust with the marine water.

As it is now known, the continental crust forms mostly in the lithospheric plate subduction zones as a result of the oceanic crust reworking and deposit suck-in (Sorokhtin et al., 1971). The subduction zone magmatism is drastically different from a relatively primitive ocean floor magmatism. In the subduction zone magmatism, base and more acidic rocks take the main part. These rocks are andesites, their intrusive equivalents diorites, granodiorites. When the island arcs obduct passive continental margins, the granite magmatism dominates. Andesites and especially granitoids radically differ from basalts in elevated contents of silica, alkalis (especially potassium), and other lithophilic elements and in low contents of magnesium, calcium, iron, and other transitional metals of the iron group. The andesites and granodiorites cannot be derived from differentiation of the mantle origins basalt magmas. They are specific crustal-continental rocks emerging as a result of complex reworking of the other rocks and deposits in the lowermost crustal levels or in the uppermost mantle levels.

The lithospheric plate friction within their subduction zones results in the release of massive amounts of heat, approximately 500–700 cal/g of the continental crust rocks. If heat were not carried out of the subduction zones it would have been sufficient to heating up of the crustal rocks to 1500–2400 °C. Water-saturated silicates begin to melt at much lower temperature of 700–800°C so the oceanic crust unavoidably must melt, and the surface

eruption of the formed magma and water fluids will lower temperature in the plate friction zone to about 1100–1200 °C.

The oceanic crust dehydration and anatexis within the plate subduction zones are complex and multi-step processes. A complete picture of the crust transfigurations is far from known but the general direction of the processes is clear.

First of all, the oceanic crust rocks that got into the plate subduction zones begin to actively dehydrate. First, they lose the pore water, the crystallization water. After that, a complex series of endothermal (i.e., with heat absorption) metamorphic transformations is developed in them, often with the release of water, silica, alkali (especially potassium), and lithophilic elements. As an example, deserpentinization goes along the following route:

$$\text{Serpentine} + Q \rightarrow \text{talcum} + \text{forsterite} + \text{water};$$
$$\text{Talcum} + Q \rightarrow \text{forsterite} + \text{silica} + \text{water},$$

where $Q$ is heat absorbed in the reaction.

The rocks of the greenstone metamorphic facies which are part of the oceanic crust, when heated within the plate friction zones, gradually dehydrate, lose part of their water, undergo the progressive amphibolite facies metamorphism and lose some silica. Getting into the amphibolite facies environment, such typical minerals of the greenschist metamorphic facies as pyrophyllite, chlorite, and chloritoid transform losing water and silica:

$$\text{pyrophyllite} + Q \rightarrow \text{andalusite} + \text{silica} + \text{water};$$
$$\text{chlorite} + \text{muscovite} + Q \rightarrow \text{staurolite} + \text{biotite} + \text{silica} + \text{water};$$
$$\text{chloritoid} + \text{andalusite} + Q \rightarrow \text{staurolite} + \text{silica} + \text{water}.$$

Other minerals from greenstone rocks can undergo similar transformations. At even higher temperature, amphiboles and micas begin to dehydrate and melt, and potassium and alkali are bonded in feldspars. Dehydration of clay minerals from the deposits undergoes similar reactions with the release of water and silica. For instance, the main clay mineral of the pelagic deposits montmorillonite is decomposed as follows:

$$\text{Montmorillonite} + Q \rightarrow \text{paragonite} + \text{albite} + \text{chlorite} + \text{silica} + \text{water}$$
$$\rightarrow \text{sillimanite} + \text{albite} + \text{cordierite} + \text{silica} + \text{water}.$$

In the course of oceanic crust rocks, metamorphic and subsequent transformations, olivine, enstatite, magnetite, and other refractory components forming at a depth of the eclogite transition are removed from the system together with the lithospheric plate sinking into the mantle. The water fluids, silica, and lithophilic compounds are assimilated by the silicate melts forming within the subduction zones. A result is their enrichment in silica and lithophilic compounds, and the melts acquire the properties of andesite rocks.

We now review under the new theory the origins of granites which is among the central problems in geology.

Currently, a view of anatectic and palingenetic (i.e., associated with rock melting and remelting) origin of most Phanerozoic granites dominates among the petrologists and geologists. It is recognized, however, that some granites may have formed due to a deep metamorphism of the sediments. The melting, remelting, and metamorphism mechanisms of the crustal rocks as well as the sources of energy, matter and fluids feeding these processes

remained unclear till recently. The situation changed with the emergence of the lithospheric plate tectonics. The new theory came up with a realistic mechanism showing how the oceanic crust matter saturated with the sedimentary material may be involved into the secondary reworking resulting in the granitoid formation.

Under the new theory, most magmatic granites (at least in post-Archaean) emerged from the remelting of the sedimentary sandy–clayey rocks. They were sucked into the plate subduction zones at obduction of the island arcs and active continental margins over passive margins of the adjacent continents with thick clastic sequences accumulated at their foot and over the continental slopes.

Such appears to be the nature of most granites in the Urals, Appalachians, Alps, and many other fold-belts that emerged on the periphery of the ancient platforms as a result of the obduction of island arc structures. Granitoid melts may also form as a result of the sialic matter secondary mobilization and remelting within the oceanic plate subduction zones underneath the Andean-type continental margins. That is the origin of the largest Andean granitoid intrusions in South America, of the Caledonian granites in the British Isles, Kazakhstan, South Siberia, Hercynian granites of the Eastern Australia South-East Asia, and some other world regions. When the Andean-type active margin is obducted over a passive continental margin, the melted-out granite mass may turn out to be especially large. Apparently, that is how giant Nevada granite batholiths in the western United States formed in the collision between the Rocky Mountains mobile belt and the North-American platform passive margin.

The new theory explains the origins of metamorphic granites, often with the preserved shadow structures (the footprints of sedimentary lamination). They emerged from metasomatic reworking of sedimentary–volcanic sequences by overheated saline waters ascending from the subduction zones at the back of the island arcs and Andean-type active continental margins. Composition similarity between the metasomatic and palingenetic granites is due to their eutectic composition which does not depend on the source melts differentiation paths.

The idea of granite origin due to metasomatic reworking of the surrounding rocks by hot solution flows and the associated melts is not a new one. However, only the new theory of tectonics of lithospheric plates provided a natural mechanism through which powerful flows of the overheated and highly saline solutions occur under Earth's geosynclinal zones (i.e., under the subduction zones). The mechanism is energized by the process of the oceanic water dehydration in the oceanic lithospheric plate subduction zones under the island arcs and Andean-type active continental margins.

It was estimated that presently up to 3 $km^3$/year of thermal waters is released underneath these structures, and it was even greater in the past geological epochs. In Early Proterozoic, up to 7 $km^3$ of overheated water fluid filtered annually through the plate subduction zones. Over the entire Evolution of Earth, nearly 16 billion $km^3$ of water (seven times the amount of water in the external Earth geospheres, that is, the oceans, the oceanic and continental crust together) filtered through the subduction zones.

Therefore, the entire hydrosphere water at least seven times filtered through the plate subduction zones over the duration of Earth's geological evolution. It was partially bonded in the continental crust (300 million $km^3$ of the irreducible water) but mostly it turned around and again entered the oceans and oceanic crust. Apparently, this amount of water

was more than sufficient for granitization of the entire continental crust as its volume (about 8 billion $km^3$) is approximately half of the water amount involved in the circulation.

Naturally, the composition of the magma forming in the course of rock melting substantially depends on the rock composition. When the carbonate rocks or evaporites are sucked into the subduction zones, the emerging melts must be enriched in alkali-earth or alkali elements. The carbonate assimilation leads to magma de-silicifying and to a relative increase in its alkali content.

The silicate magmas should also significantly change when evaporites get into the subduction zones. The reason is that after assimilating the salt-bearing sediments the originally acidic magmas are being saturated with alkali, chlorine, fluorine, and some other dispersed elements, and are losing calcium. As a result, the melt becomes a syenite one.

Similarly, when the phosphorus-rich sediments as phosphorites accumulated in the former near-shore upwelling areas on the shelf and slope of the old continental margins are sucked-in under the island arcs, the apatite-rich magmas may emerge.

And when the ore metal-bearing sediments get into the subduction zones, the magmas mat form that are enriched in ore minerals.

## 8.8 VERIFYING THE THEORY

Thus, over the short period of its life (since the late 1960s), the lithospheric plate tectonics was able to explain the nature of practically all major endogenous processes of the crust formation. They included the formation of the oceanic and continental crust, the nature of base and acidic magmatism, concentration mechanisms of ore and lithophilic elements in the continental crust, origins of the folding and of Earth's mountain belts, aulacogen and foredeep formation, and a number of other processes.

Today, the new geological theory underwent detailed experimental verification. Its major positions are supported by drilling, seismic, and magnetic observations. There are numerous examples of confirmed theoretical forecasts of previously unknown geological phenomena.

It followed from the theory that the ocean floor is relatively young, no older than 100–150 MMY and regularly ages with the distance from the crests of mid-oceanic ridges. In mid-1960s, this was a bold conclusion as the prevailing view was that the ocean floor was as old as the continents, that is, 2–3 BY. Drilling conducted for this purpose completely substantiated the theoretical forecast: wherever drilled (now there are more than 1000 points), the empirical ocean floor age determinations coincided with the theoretical predictions.

There are other examples of the theoretical forecasts substantiated by geological and geophysical studies. Observations of the rift zones in the mid-oceanic ridges by the French, American, and Soviet scientists from the manned submersible deepwater vehicles confirmed a theoretical conclusion about the ocean floor spreading in these zones, about the displacement direction of the transform faults and significant heat release from the oceanic rift zones.

As mentioned, it was theoretically predicted (Parker and Oldenburg, 1973; Sorokhtin, 1973a,b) that the lithospheric plate thickness increases with the distance from the rift zones as the square root of the ocean floor age, whereas previously it was believed that the oceanic plate thickness was constant. Experimental studies published in 1975 (Yoshii,

1975) totally confirmed this conclusion. At about the same time, the theory predicted the existence in oceanic rift zones of powerful hydrothermal systems (Lister, 1972; Sorokhtin, 1973a,b). Five to six years since such hot springs (black and white "smokers") have indeed been discovered in the rift zones of all oceans.

A view was common among the geologists in 1960s and early 1970s that the compacted old sediments play significant role in the basalt layer of the oceanic crust. Contrary to that, the lithospheric plate tectonics maintained that the role of sediments in that layer is disappearing small. This theoretical prediction was fully confirmed by drilling in mid-1970s, and all sediments overlying the basalts are young, no older than Middle Mesozoic.

Two more interrelated examples. As already mentioned, the new theory proposed that loose deposits together with their contained organic matter must be sucked-in under the island arcs and active continental margins (Sorokhtin and Lobkovsky, 1976). An important practical suggestion was that large hydrocarbon amounts must be generated in the subduction zones (Dickinson, 1974; Sorokhtin et al., 1974). Both sucking-in and the hydrocarbon generation within the subduction zones were theoretically substantiated in the early 1970s although at that time it was not supported by most geologists. In 1976, the deposit suck-in under Kuril island arc was confirmed by the deep seismic profiling (Garkalenko et al., 1978). And in 1981 the deposit suck-in under the Antilles arc was confirmed by drilling at the foot of the arc (Bijy-Duval et al., 1981).

In mid-1970s was checked and verified a second theoretical conclusion about hydrocarbon generation in the subduction zones. At the time, the Soviet and Cuban oilmen discovered commercial oil accumulations underneath the Cuban ophiolite sheet overlying the Cretaceous plate subduction zone. But the main confirmation of this important theoretical forecast came from drilling onto the subthrust zones of the Rocky Mountains and Appalachians conducted in the United States since 1975. These areas which were priorly believed to be lacking in potential turned out to be literally saturated with hydrocarbons, exactly as the theory forecast.

Lastly, the main theoretical conclusion, the continental drift was directly verified using the satellite triangulation (Smith et al., 1990). The measured displacement, both quantitatively and in terms of their directions, well matched the forecast value based on the paleomagnetic data.

Thus, even a brief review of the major positions, successes and results of experimental verification of the plate tectonics theoretical forecasts indicate that the concept is a stringently scientific and state-of-the-art geological theory. It is now well established, its main positions are well elaborated. It is now being detailed, fine-tuned and, which is practically important, used in exploration of commercial deposits (in particular, oil and gas).

CHAPTER

# 12

# Atmosphere: Origin and Physicochemical Aspects of Evolution

## 12.1 PRIMORDIAL ATMOSPHERE OF THE YOUNG EARTH

A specific feature in the origin and evolution of the Earth's atmosphere was a paucity of Earth's matter (compared with the Sun) in volatile and mobile elements and compounds. Had it been otherwise, the present-day atmosphere and hydrosphere would have been much thicker and denser. Maison (1971) estimated the relative hydrogen content on Earth (vs. silicon) is $10^{6.6}$ times lower than in outer space; nitrogen, $10^{5.9}$ times; carbon, $10^4$ times; noble gases, $10^6$–$10^{14}$ times. So despite the commonality in outer space of such volatile compounds as $H_2$, He, $N_2$, $H_2O$, $CO_2$, $CH_4$, $NH_3$, and so on, they turned out to be very scarce in Earth's matter. It is believed that such substantial differentiation in primordial Earth's matter occurred in the pre-planetary stage of the Solar system's evolution, when the Sun was at the τ-Taurus stage of stellar evolution. It may have happened due to the intense sweep of volatile and mobile components from the internal portions of the protoplanetary gas–dust cloud into its periphery, into the giant planet formation zone.

Those volatile compounds and elements found on Earth ($H_2O$, $CO_2$, $N_2$, HCl, HF, HI, etc.) could have gotten there only in a bonded state. The water must have been bonded with hydrosilicates; nitrogen, with nitrides and nitrates; carbon dioxide, with carbonates; halogens, with haloids, and so on. For this reason, as Earth grew, such components were buried into its depths. Some residual chemically active volatile compounds were released in the shock explosions of planetesimals hitting Earth. These residual volatiles must have been intensely sorbed by the ultramafic regolite on the surface of the growing planet and then buried under new layers of the precipitating meteoritic matter.

It may be assumed, therefore, that primordial Earth's atmosphere was composed only of inert and noble gases. For instance, due to a short helium "flight time" from the atmosphere (on the order of $10^6$ years) its partial pressure in the primordial atmosphere over the time of its formation (about $10^8$ years) had enough time to equilibrate, so it was no higher than the present one. The product of $^{40}K$ radioactive decay, $^{40}Ar$, also should not have been present in the

*Developments in Earth and Environmental Sciences*, Volume 10
DOI: 10.1016/S1571-9197(11)10012-9

atmosphere in noticeable amounts. Taking this into account it is reasonable to expect that the partial pressure of the noble gases in the primordial atmosphere did not exceed $2 \times 10^{-5}$ atm.

It is much more difficult to determine partial pressure of the other active components in the primordial atmosphere ($H_2O$, $N_2$ $CO_2$, and CO). To do this, it would be necessary to know the sorption and reactive capacity of the gases with the ultramafic regolite. And, besides, the regolite contained free metals (Fe, Ni, Pt, Co, C, etc.). It is anticipated, however, that their pressure did not exceed $10^{-4}$ atm.

## 12.2 DEGASSING OF CARBON DIOXIDE AND EVOLUTION OF ITS PARTIAL PRESSURE IN THE ARCHAEAN ATMOSPHERE

On the geological stage of the Earth's evolution, the only "purveyors" of carbon for the rocks could be carbon dioxide and the products of its reworking (carbonates, hydrocarbons, and organic matter). The primordial carbon could enter the crust, hydrosphere, and atmosphere only through the mantle degassing. There is a difference at the mantle degassing between the heat of formation of water and carbon dioxide. The carbon dioxide heat of formation is 94.05 kcal/mol which is much higher than 63.05 kcal/mol for iron oxide. For this reason, the carbon dioxide mobility factor $\chi(CO_2)$, as for nitrogen, should have not been dependent on the differentiation mechanisms of Earth's matter (iron zonal separation or barodiffusion mechanism of the core separation). This makes the determination of the pattern of $CO_2$ degassing from the mantle easier as it predetermines in advance the permanency of the carbon dioxide mobility factor and the proportionality of its degassing rate with the tectonic activity (see Fig. 5.17).

As one of the boundary conditions we assume (after Ronov and Yaroshevsky, 1978) that nearly $3.91 \times 10^{23}$ g of $CO_2$ is bonded in the crustal carbonates. Besides, the crust contains about $1.95 \times 10^{22}$ g of organic carbon ($C_{org}$). With this amount of $C_{org}$, prior to its reduction in the biologic processes, was bonded $5.2 \times 10^{22}$ g of oxygen. Therefore, the total $CO_2$ mass buried in the crust is $m(CO_2) \approx (3.91 + 0.72) \times 10^{23} = 4.63 \times 10^{23}$ g.

Carbon or $CO_2$ content determination in the mantle is much more complicated. Experimental data indicate that the high-temperature distillation fractions of volatile components in the oxygen atmosphere of the tempering glass from the tholeitic basalts in the oceanic rift zones contain 20–170 g/ton of the mantle-derived carbon with the isotopic shifts of about $-5$‰ (Watanabe et al., 1983; Sakai et al., 1984; Exley et al., 1986). The dispersed carbon is found in all igneous rocks in negligible concentrations of 10–100 g/ton with a substantial deficite of the heavy isotope $\delta^{13}C \approx -22$ to $-27$‰ (Galimov, 1988a). On the contrary, carbon in the crust is isotopically heavier, with $\delta^{13}C \approx -3$ to $-8$‰ (average value is $-5$‰). Part of the mantle carbon is dispersed among silicate crystalline grids in the atomic state (Watanabe et al., 1983) and, hence, is not a volatile component of the basalt melts. Therefore, carbon content in the $CO_2$ gas phase of basalt melt-outs may actually be noticeably smaller than the quoted total carbon concentrations.

For certainty, we assume the mobile carbon content in the mantle at about 30 g/ton, or 110 g/ton ($1.1 \times 10^{-4}$) normalized for carbon dioxide. In this case, the mantle carbon dioxide content is $m(CO_2) \approx 4.48 \times 10^{23}$ g of $CO_2$.

On this basis, the total $CO_2$ mass in Earth (with $C_{org}$ normalized for $CO_2$) is $m(CO_2) \approx 9.11 \times 10^{23}$ g. From Eq. (11.2), $\chi(CO_2) \approx 0.71$. Carbon dioxide from the mantle degassing rate

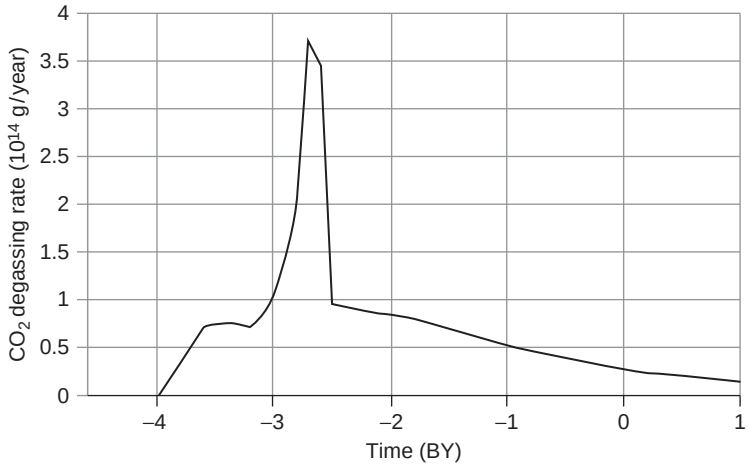


**FIGURE 12.1** Rate of carbon dioxide degassing from the mantle.

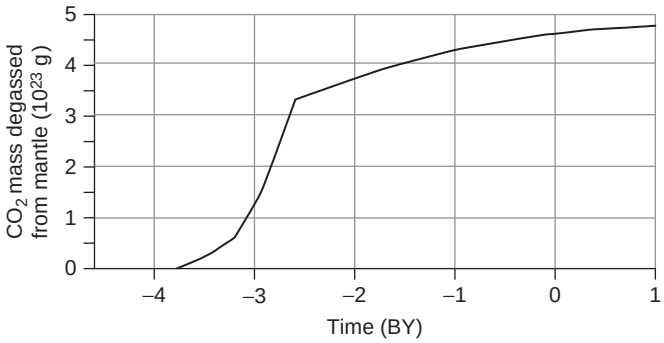


**FIGURE 12.2** Mass of carbon dioxide degassed from the mantle.

(Fig. 12.1) and $CO_2$ accumulation rate in the Earth's external geospheres (the atmosphere, hydrosphere, and the crust, see Fig. 12.1) are plotted based on Eqs. (11.1) and (11.2).

It is interesting how different the carbon dioxide degassing is from that of the water (compare Figs. 12.1 and 11.5). As mentioned above, the reason is the lower formation heat of water (for the molecular water $\Delta H_f^0 = 57.8$, for $CO_2$ $\Delta H_f^0 = 94.05$, and for FeO $\Delta H_f^0 = 63.6$ kcal/mol) and its dissociation on the metallic iron during the zonal differentiation of Earth's matter in Archaean. The $CO_2$ degassing rate peak coincided with the time of maximum tectonic activity, 2.6 BY ago. At the same time, the water degassing was at its maximum rate about 2.5 BY ago, that is, after the high-density Earth's core separation and after the switch in the differentiation of Earth's matter from the zonal melting mechanism to a more quiescent barodiffusion mechanism (Fig. 12.2).

Should the entire degassed carbon dioxide have been preserved in the atmosphere, its partial pressure today would have been approximately 91–100 atm, that is, about the same as it is on

Venus. Life on earth was lucky in that simultaneously with $CO_2$ entering the atmosphere it was being bonded in carbonates. For this reaction to occur, liquid water is needed. Only in such a case is the silicate hydration accompanied by $CO_2$ absorption with the emergence of carbonates under reactions similar to (11.7) and (11.7′). That is why the ocean evolution was so significant in the carbon dioxide partial pressure evolution in the atmosphere (Figs. 11.4 and 11.6).

Beside carbonates, the iron-containing ultramafic rock hydration in the oceanic crust is accompanied by the release of free hydrogen and by the generation of abiogenic methane (see Eqs. (11.8) and (11.9)).

As the type reactions (11.7) and (11.7′) show, for every two $CO_2$ molecules bonded in carbonates four water molecules are expended to hydrate the rock-forming minerals of the oceanic or continental crust. Therefore, under carbon dioxide excess in the atmosphere and hydrosphere practically all rock hydration reactions will be accompanied by bonding of $CO_2$ in the carbonates. And for every unit of the water mass bonded in the rocks there will be approximately 1.22 units of carbon dioxide mass. It there is a $CO_2$ shortage, the hydration of some part of the silicates will proceed without bonding carbon dioxide, for instance, under the brusite formation reactions (11.6).

The World Ocean covering the crests of the mid-oceanic ridges already existed in Late Archaean 2.8 BY ago (see Fig. 11.6). As a result, the hydration of the substantially basaltic oceanic crust noticeably strengthened and the $CO_2$ partial pressure growth rate in the Late Archaean atmosphere somewhat declined. The most drastic carbon dioxide pressure decline, however, occurred only at the Archaean/Proterozoic time boundary after the Earth's crust separation and the associated weakening in the tectonic activity (see Fig. 5.17). Because of that the oceanic basalt melt-out decreased no less drastically in Early Proterozoic. The oceanic crust basalt layer became noticeably thinner than it was in Archaean. Underneath it, the serpentinite layer was formed for the first time. And the serpentinite layer is the main and constantly renewable irreducible water reservoir on Earth (see Fig. 7.1). The serpentinites can contain up to 12% of the constitutional (i.e., bonded) water.

That was exactly the reason why by 2.4 BY ago (i.e., by the beginning of the Huron Orogeny; Chumakov, 1978) the carbon dioxide partial pressure in the Early Proterozoic atmosphere drastically declined (by about the factor 10,000) to the equilibrium level of about 1.0–1.5 mbar. Total atmospheric pressure decreased from 5–6 bar at the very end Archaean to 1.4 bar in Early Proterozoic (see Fig. 12.15). The entire $CO_2$ removal process from the atmosphere at the Archaean/Proterozoic time boundary likely did not last longer than 100–150 MMY. As a result, the composition of the Early Proterozoic atmosphere became mostly nitrogen (with a small addition of argon, about 9 mbar). A natural reaction to these events was significant climate cooling although the average continent stand level still remained rather high, 4 to 2–3 km. That was exactly the reason for the emergence of Huron Glaciation: the onset of cooling-down at a high-continent stand (Sorokhtin and Sorokhtin, 1997; Sorokhtin, 2002). As a result almost all continents (which at that time formed a unique supercontinent Monogaea, Fig. 9.2), despite their equatorial positions were above the snowline (see Fig. 14.20) and were shackled under a huge sheet glaciation.

Subsequently, carbon dioxide partial pressure in the atmosphere was controlled by the oceanic water average temperatures and by Henry's law. During ice periods it declined to 0.3 mbar (the current value is approximately 0.46 mbar), and in warm periods it increased to 0.7−1 mbar.

A little earlier we estimated the total amount of the water bonded within the rocks. It is a sum of the curves 3 and 4 in Fig. 11.4. As these figures show, the highest hydration rate of crustal rocks was indeed observed in Early Proterozoic. At the same time, the massive bonding of the atmospheric carbon dioxide in carbonates, especially dolomites, must have taken place. This gives a way to estimate carbon dioxide mass which could have been bonded in the carbonates. Life in the ocean is restricted by phosphorus content in the oceanic water. The phosphorus solubility is relatively low (Schopf, 1980). Thus, it may be assumed that the absolute organic matter mass in the ocean is proportionate with the oceanic water mass. Thus, the organic matter mass (normalized for $CO_2$) in Archaean and Proterozoic may be estimated assuming that it is, as a first approximation, proportionate with the water mass in the World Ocean (see Fig. 11.4, curve 2).

Figure 12.3 compares the mass of the mantle-degassed carbon dioxide (curve 1) with the $CO_2$ mass bonded in the carbonates (curve 2) and the mass of the organic carbon (normalized for $CO_2$ mass) in the biosphere (curve 3). A separate curve (curve 4) illustrates the evolution of the $CO_2$ mass in the atmosphere. As this figure shows, in Proterozoic and Phanerozoic almost the entire mantle-degassed carbon dioxide was bonded in the carbonate (as $C_{carb}$) or biogenic ($C_{org}$) reservoirs. At the same time, the $CO_2$ mass in the atmosphere and dissolved in the hydrosphere of these epochs (except for the far future) could not be shown at a scale of the provided diagrams.

The Archaean situation was different.

The water mass in the Archaean oceans was relatively small. Thus, the bonded $CO_2$ mass at the time was substantially lower than the mass of the mantle-degassed carbon dioxide. Therefore, a substantial part of carbon dioxide in Archaean must have been in the atmosphere (see Fig. 12.4) and dissolved in the oceanic waters.

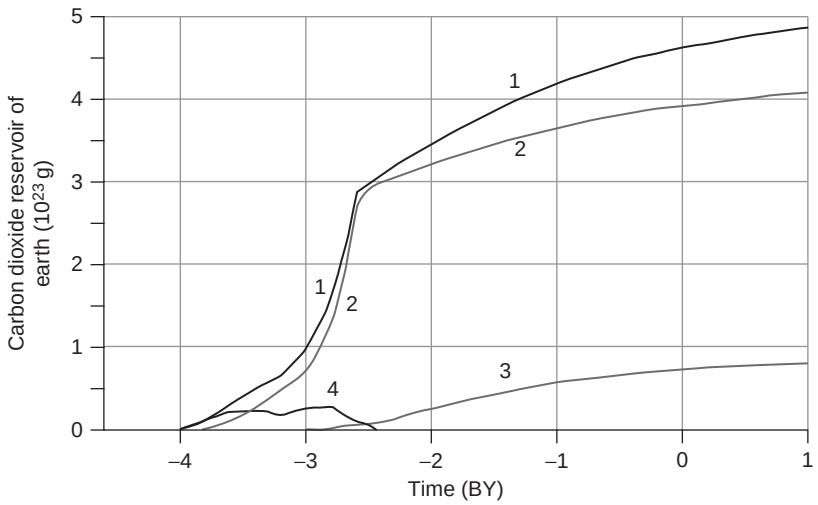


**FIGURE 12.3** Mass of carbon dioxide bonded in the Earth's crust and Archaean atmosphere: 1, mass of $CO_2$ degassed from the mantle; 2, mass of $CO_2$ in the Earth's crust carbonate reservoir; 3, organic carbon mass normalized for $CO_2$; and 4, $CO_2$ mass in the Archaean atmosphere.

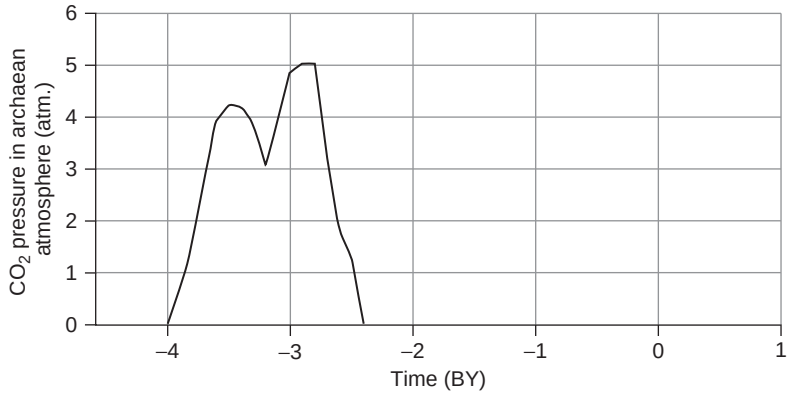


**FIGURE 12.4** Evolution of carbon dioxide partial pressure in the Archaean atmosphere.

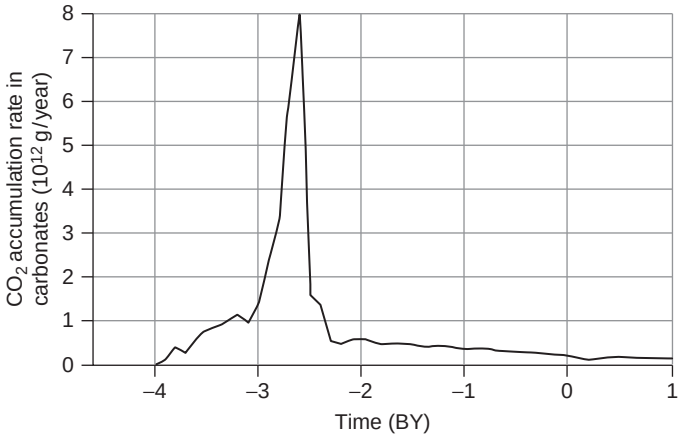


**FIGURE 12.5** Rate of carbon dioxide bonding (accumulation) in carbonates. In Early Precambrian those were mostly dolomites.

The serpentinite layer formed in the oceanic crust at the Archaean/Proterozoic time boundary (see Fig. 7.1). It resulted in a drastic increase of carbon dioxide bonding rate in carbonates under reactions (11.7) and (11.7′) and the carbonate sedimentation with the oceanic deposits. Thus, in Late Archaean already occurred a noticeable increase of the sedimentary carbonates (such as marbles and calciphyres of the Trans-Baikal Slyudyanka Series). In Early Proterozoic, huge masses of carbonates from the formerly carbon dioxide atmosphere and the ocean water-dissolved carbon dioxide were deposited. Of course, due to a poor carbonate rocks resistivity to weathering (Garrels and MacKenzie, 1974) most of them subsequently were redeposited in younger formations (Fig. 12.5).

Simultaneously with these events, carbon dioxide partial pressure drastically dropped and, together with it, total atmospheric pressure in Early Proterozoic. As a result, a hot Archaean climate gave way to a moderately warm Proterozoic epoch. The emergence of the Early Proterozoic Huron glaciation was due to a high-continent stand in Early Proterozoic (Sorokhtin and Sorokhtin, 1997; see more detail in Chapter 14).

Beside $CO_2$ bonded in rocks part of carbon dioxide (as anions $HCO_3^-$) was always dissolved in the oceanic water. Under the Henry's law, the carbon dioxide solubility in water is in direct proportion with its partial pressure in the atmosphere:

$$C(CO_2)_{ocean} = H(CO_2)p(CO_2), \tag{12.1}$$

where $C(CO_2)_{ocean}$ is the carbon dioxide concentration in the oceanic water, $H(CO_2)$ is Henry's constant, and $p(CO_2)$ is the carbon dioxide partial pressure in the atmosphere. The gas solubility in the water is an exponential function of its temperature $T$:

$$H(CO_2) = H_0 e^{\frac{-V(CO_2)p(CO_2)}{RT}}, \tag{12.2}$$

where $V(CO_2)$ is the partial molar volume of the water-dissolved $CO_2$ in an infinitely diluted solution, $R = 1.987$ cal/mol deg is the gas constant, and $H_0$ is the proportionality factor.

Approximately $1.4 \times 10^{20}$ g of $CO_2$ is dissolved in the modern oceans. Its partial pressure in the atmosphere is 0.46 mbar. Using Eq. (12.1), the estimate of the Henry's factor for the modern ocean is $H_{ocean} \approx 0.213$. The Earth's average surface temperature is currently 288 K ($\approx 15$ °C), and the proportionality factor in Eq. (12.2) $H_0 = 0.803$. The mass of the oceanic water-dissolved carbon dioxide may be found as:

$$\delta m(CO_2) = m(H_2O)_{ocean} H(CO_2)p(CO_2). \tag{12.3}$$

In Late Archaean, 2.7 BY ago, the calculated mass of ocean water-dissolved carbon dioxide reached $10^{23}$ g. It means that at the average temperature of the Archaean ocean of 55 °C (see below), the oceanic water in Late Archaean was hot and acidic, hence, an aggressive solvent of many substances (including ore elements). Again, only in Archaean did the conditions exist for emergence of a high-density carbon dioxide atmosphere. In Proterozoic, after the core separation and a drastic decrease in tectonic activity, the serpentinite layer formed in the oceanic crust (see Fig. 7.1) and strongly increased carbon dioxide bonding in carbonates under reactions similar to (11.7) and (11.7′). As a result, almost the entire carbon dioxide was rather rapidly (within 100–150 MMY) removed from the atmosphere in Early Proterozoic, and the Earth's atmosphere became nitrogenous with total atmospheric pressure of 1.4 atm. Whereas carbon dioxide of the Archaean atmosphere and hydrosphere almost in its entirety migrated to carbonates and, in part, to organic matter.

As Fig. 12.4 indicates, the carbon dioxide partial pressure in Archaean reached 4–5 atm. The explanation is the small amount of water in the Archaean oceans so the mass of bonded $CO_2$ at the time was substantially smaller than the mantle-degassed $CO_2$ (see Fig. 12.3). A conclusion is that in Archaean the bulk of the mantle-degassed carbon dioxide must have been in the atmosphere and dissolved in the oceanic waters.

Due to the elevated carbon dioxide pressure in the Archaean atmosphere, redox potential pH of the Archaean oceanic waters at the time declined to 6–5.5 (Makkaveyev and Sorokhtin, 2005). After Archaean and after a decrease in $CO_2$ partial pressure in the atmosphere it increased practically to its present-day level of about 8 (see Fig. 12.6).

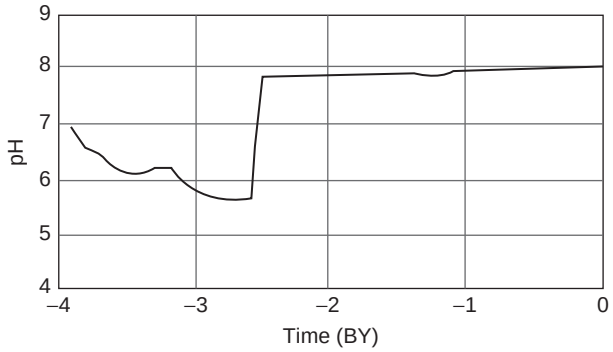


**FIGURE 12.6** Evolution of the World Ocean pH redox potential as defined by carbon dioxide partial pressure in the atmosphere (Makkaveyev and Sorokhtin, 2005).

## 12.3 NITROGEN-CONSUMING BACTERIA EFFECT ON THE NITROGEN'S PARTIAL PRESSURE

Nitrogen is a moderately active element weakly reacting with the natural organic compounds. There are, however, nitrogen-consuming bacteria removing this gas and bonding it in the organic matter. The first and most primitive bacteria (procaryotes and Archaeans) probably appeared soon after the emergence of life on Earth. It is possible that they included some nitrogen-consuming bacteria. Thus, nitrogen bonding in the organic matter and its burial in oceanic deposits (and after their exit onto the dry land, also in the continental deposits) may have already begun in Archaean. Besides, nitrogen may be bonded in nitrates and nitrites by thunderstorm activity. Thus, bacterial life activity and thunderstorms over a long geological evolution could have significantly lowered the partial pressure of nitrogen in the atmosphere, which would have changed Earth's climates.

The available estimates show that the nitrogen bonding by thunderstorms was substantially less than that by the biogenic effect. Besides, the thunderstorm-bonded nitrogen was in less stable nitrites and nitrates whose decomposition might have again released nitrogen into the atmosphere.

We assume, however, that nitrogen removal from the atmosphere was as well by bacteria as by the thunderstorm activity, and the effects are difficult to separate at this time. In calculating the nitrogen absorption effect, it needs to be taken into account that the organic nitrogen ($N_{org}$) accumulated in the oceanic deposits was continuously removed from the ocean waters, together with the deposits, through the oceanic crust pileup zones in Archaean and through the plate subduction zones in Proterozoic and Phanerozoic. After that nitrogen was partially included into the granite–metamorphic rocks of the continental crust or went into the mantle but was again partially degassed and released to the atmosphere.

One way to estimate the nitrogen amount buried with the oceanic deposits is from the mass of the buried organic carbon $C_{org}$. The only thing to do for this purpose is to determine the proportionality factor between $N_{org}$ and $C_{org}$. In the open ocean bottom deposits, the $C_{org}$:$N_{org}$ ratio is about 1:0.04 (Lisitsin and Vinogradov, 1982). Romankevich (1977, 1984) estimates this ratio in the deposits at 1:0.1 and Faure (1989) estimates at close to 1:0.05. We assumed for our calculations an intermediate value of $C_{org}$:$N_{org} \approx 1$:0.09.

The Ronov and Yaroshevsky (1978) and Ronov (1993) data show that currently $(2.7–2.86) \times 10^{21}$ g of $C_{org}$ is preserved in the oceanic deposits (pelagial plus shelves) and in the continental deposits, nearly $(9.2–8.09) \times 10^{21}$ g $C_{org}$. In view of the avalanche deposition of the solid clastic material in the oceanic near-shore areas and elevated organic carbon concentration in them (Lisitsin, 1984), we assumed for the calculations a somewhat greater amount of the present-day oceanic deposits, hence, of organic carbon: $C_{org} \approx 3.36 \times 10^{21}$ g in which case the present-day $N_{org}$ content in the ocean-floor deposits and shelves is approximately $2.35 \times 10^{20}$ g, and in the continental deposits, close to $5.0 \times 10^{20}$ g.

The quoted organic nitrogen amounts were deposited over the average existence time of the modern oceanic crust, that is, over the recent 120 MMY, and on the continents, approximately over 400 MMY. Now we determine $N_{org}$ accumulation rate during the past geological epochs. We take into account that the element controlling life evolution in the oceans is phosphorus whose solubility in the oceanic water is limited (Schopf, 1980). The ocean life evolves mostly within the photo-active water layer. Still, phosphorus-saturated depth water reaches this habitable layer through the upwelling zones. It follows from it that the oceanic biomass was always approximately proportionate with the mass of the ocean *per se* which is shown in Fig. 11.4, curve 2. With this taken into account it is possible to estimate the very biomass of the ocean (Fig. 12.7).

We assumed above that the oceanic biomass is proportionate with the mass of the oceanic water. Now we can approximately account also for the mass of the organic nitrogen $N_{org}$ bonded in the deposits and removed together with them during the Earth's geological history from the oceanic sedimento-sphere into the Earth's crust or mantle through the plate subduction zones:

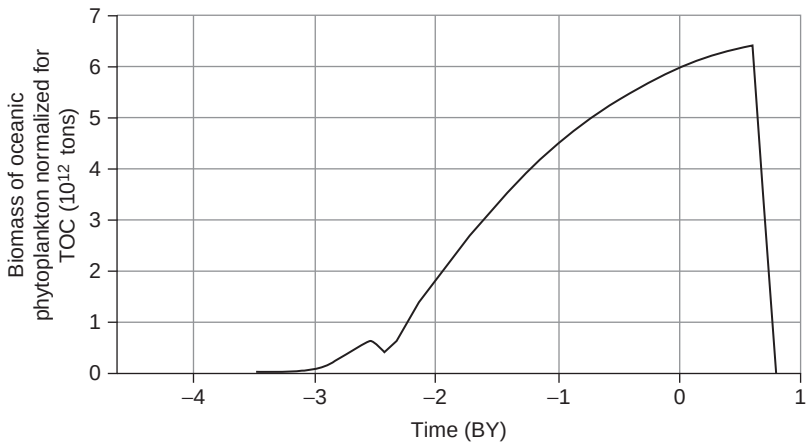


**FIGURE 12.7** Biomass evolution in the World Ocean. Biomass declines to 0–600 MMY in the future is due to the degassing from the mantle in large amounts of the abiogenic oxygen deadly for all living under reaction (4.45) and the associated significant greenhouse effect (Sorokhtin, 1974; Sorokhtin and Ushakov, 2002).

$$\left(N_{\text{org}}\right)_{oc}^{\Sigma} \approx \frac{\left(\dot{N}_{\text{org}}\right)_{oc}}{\left(m_{oc}^{\text{w}}\right)_0} \int_{t=-4\times10^9}^{t} m_{oc}^{\text{w}} \mathrm{d}t, \tag{12.4}$$

where $(N_{\text{org}})_{oc}^{\Sigma}$ is the total organic nitrogen mass removed from the oceanic reservoir over the time from $t=-4$ BY to the present $t=0$, $\left(\dot{N}_{\text{org}}\right)_{\text{oc}} = \left(N_{\text{org}}\right)_{\text{oc}}/\tau$ is the current $N_{\text{org}}$ burial rate in the oceanic deposits, $\tau \approx 120$ MMY is the average age of the present-day ocean floor, and $m_{\text{oc}}^{\text{w}}$ and $\left(m_{\text{oc}}^{\text{w}}\right)_0 = 1.42\times10^{24}$ g are the current value and current water mass in the World Ocean (see Fig. 11.4).

By the numerical integration of Eq. (12.4) over the accepted parameters, we determine that over the geological evolution time (i.e., recent 4 BY) about $4.3\times10^{21}$ g of nitrogen were removed from the atmosphere through the marine biota life activity. Added to this amount must be $N_{\text{org}} \approx 5.0\times10^{20}$ g of nitrogen preserved in the continental deposits over a period of close to 400 MMY. Thus, the total nitrogen removed from the atmosphere over the life activity on Earth is close to $4.82\times10^{21}$ g. That is equivalent to the atmospheric pressure decline by 945 mbar, which is slightly greater than the nitrogen partial pressure in the modern atmosphere (765 mbar).

One has to keep in mind that in Middle Proterozoic (2 to 0.8 BY ago) the atmosphere was almost pure nitrogen with some admixture of the radiogenic argon. It was much warmer than now, no ice sheets emerged anywhere on continents (Chumakov, 2004b). Therefore, at the average elevations of the continents at that time, nowhere did average annual temperature, even at the poles, drop below 0 °C. The adiabatic theory of the greenhouse effect says that for the positive temperatures to reign on the surface of the continents with the average elevations of 1–1.7 km which were found in Middle Proterozoic on the poles, the atmospheric pressure should have exceeded 1.2 atm.

How, then could we explain the nitrogen partial pressure changes from about 0 atm in Katarchaean to 1.4 atm in Proterozoic to 0.755 currently? Only by assuming that along with the mantle-degassed nitrogen there was an effective mechanism for its removal from the atmosphere (Sorokhtin, 2005a,b, 2008).

The best fit with these conditions is reached if we assume that the present-day atmosphere contains about 40% of the mantle-degassed nitrogen. The nitrogen partial pressure evolution in such a case is illustrated by curve 2 in Fig. 12.8.

The nitrogen removal rate from the atmosphere in itself is exceptionally low, presently just $7\times10^{-7}$ mbar/year. That is way below the accuracy of our observations although the total for Earth is $3.6\times10^{6}$ t/year. Keep in mind, however, that the nitrogen-consuming bacteria and thunderstorms operated almost during the entire geological evolution, that is, several billion years. The combined effect, therefore, becomes quite noticeable: by now, the nitrogen removed from the atmosphere corresponds to the pressure decline of 945 mbar, that is, almost the total physical atmosphere. We believe that the removal of such nitrogen amounts from the atmosphere and its migration to organic compounds in the Earth's sedimentary shell was impossible without the contribution from the nitrogen-consuming bacteria and thunderstorms. It is even more so that there are no natural chemical reactions bonding the inert nitrogen in the non-dissociating organic compounds. The thunderstorms indeed contribute to the nitrogen bonding but the products are mostly nitrates and nitrites, which are less stable and partially convert into the gas phase and back to the atmosphere. A similar effect on the Earth's climate could have been caused by a gradual distancing of

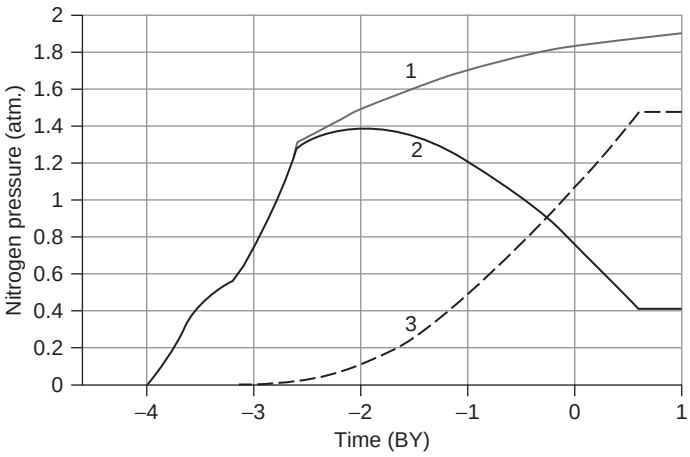


**FIGURE 12.8** Origin of the atmospheric nitrogen and its pressure evolution: 1, mantle-degassed nitrogen; 2, pressure of total atmospheric nitrogen; and 3, mass of nitrogen removed from the atmosphere normalized for pressure.

Earth from the Sun due to their tidal interactions (see Section 3.7) and the Sun's mass loss with radiation. The total cooling effect over 4 BY did not exceed 5.4 °C, whereas, according to the climatic paradox, the cooling over that period reached 70 °C (see Section 14.1).

We will show in Chapter 14 that due to the general decline of the atmospheric pressure in the future the climate severity will substantially increase. That may affect the general metabolism of the nitrogen-consuming bacteria. Thus, it may be expected that in the distant future will occur some slowdown in nitrogen removal from the atmosphere up to the establishment of a new equilibrium state of this process. However, this new activity level of the nitrogen-consuming bacteria will hardly be beneficial for the evolution of highly organized life.

## 12.4 EVOLUTION OF OXYGEN'S PARTIAL PRESSURE AND OXYGENIZING OF THE ATMOSPHERE

In calculating oxygen's partial pressure, we assume that oxygen was generated during Precambrian by micro-algae and some bacteria (such as cyanobacteria) which then populated the oceans and in Phanerozoic also by the dry land plants.

In the process of photosynthesis, oxygen is released through carbon dioxide dissociation under the following reaction:

$$CO_2 + H_2O \rightarrow CH_2O + O_2, \tag{12.5}$$

where $CH_2O$ is a generalized form of organic matter (Schopf, 1980).

Thus, the bulk of oxygen is biogenic. But it also may be released abiogenically in the water vapor and carbon dioxide dissociation by the hard Sun radiation:

$$H_2O + h\nu \rightarrow O + H_2, \tag{12.6}$$

$$CO_2 + (h\nu)_3 \rightarrow CO + O. \tag{12.6'}$$

This oxygen source, however, appears to be of low efficiency (Walker, 1977). Currently, only one one-millionth part of the atmospheric oxygen is so generated (Walker, 1974), although in Early Precambrian, in the practical absence of the ozone layer and low oxygen partial pressure, the fraction of the abiogenic photodissociation oxygen might have been somewhat higher.

After the oxygen-generating bacteria die out the inverse reaction usually occurs. The organic remains are being oxidized and oxygen being consumed with the formation of carbon dioxide (this time, of biogenic origin):

$$CH_2O + O_2 \rightarrow CO_2 + H_2O. \tag{12.7}$$

If, however, the organic remains get into a non-oxygen medium and are subsequently buried with the deposits, the organic matter decomposes without absorbing oxygen and with the release of the organic carbon $C_{org}$:

$$CH_2O \rightarrow C_{org} + H_2O, \tag{12.8}$$

or hydrocarbons:

$$2CH_2O \rightarrow C_{org}H_4 + CO_2. \tag{12.8'}$$

Comparing now the reactions (12.5) and (12.8) we see that every atom of the buried carbon corresponds to two atoms of the released biogenic carbon. That is why the burial of organic carbon also results in the accumulation of the biogenic oxygen in the atmosphere (Walker, 1977).

The atmospheric oxygen contributes to oxidizing the rocks in the weathering process or oxidizing water solutions of the ore elements. Thus, the biogenic oxygen accumulates in the deposits. Only the oxidized deposits and organic carbon buried on the continents and at the bottom of the present-day oceans are accessible to observations. Carbon and such oxides sunk into the mantle through the ancient subduction zones cannot be directly observed. There is a possibility of indirect estimates. They may be performed using, for instance, theoretical models of the ore formations accumulation as iron is the main and most active absorber of the atmospheric oxygen.

During Precambrian, oxygen was generated by marine organisms only in the ocean. The mass of oxygen released must have been proportionate with the oceanic biomass (see Fig. 12.7) or, which is the same, with the oceanic water mass (see Fig. 11.4, curve 2). In Phanerozoic about 400 MMY ago, the plants expanded onto the dry land, so the previous source was amended with oxygen generated by the land plants. Thus, in general the oxygen mass migrated from the ocean to the atmosphere must be directly proportionate with the oceanic water mass and inversely proportionate with iron ore formations mass on Earth. In Phanerozoic, the contribution from land plants must also be included:

$$p(O_2) = \frac{aM_{wo}}{b\dot{F}e + c} + p(O_2)_{cont}, \tag{12.9}$$

where $M_{wo}$ is the oceanic water mass (see Fig. 11.4); $\dot{F}e$ is the iron ore formations accumulation rate determined earlier (see Fig. 10.5); $p(O_2)_{cont}$ is the land plants contribution (beginning 400 MMY ago) into the total partial pressure of oxygen (we assumed $p(O_2)_{cont} \approx 0.1$ atm); the factors a, $b$, and c are selected so that the oxygen partial pressure

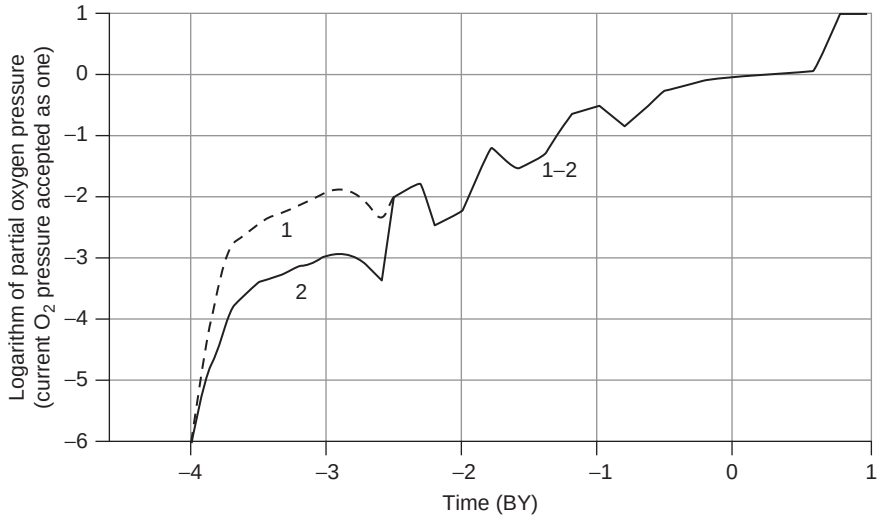


**FIGURE 12.9** Atmospheric oxygen partial pressure evolution (log–log diagram). In Precambrian, oxygen was generated only by the oceanic biota. In Phanerozoic, oxygen from the land plants was added. 1, iogenic oxygen pressure (assuming the intensity of its generation by the Archaean procariots was the same as by eucariote micro-algae and 2, same, assuming the intensity of its generation by the Archaean procariots was one order of magnitude lower than those by eucariote micro-algae after Archaean.

in the modern atmosphere were 0.231 atm, and in the atmosphere 600 MMY ago, lower by one order of the magnitude: ≈0.0231 atm. The calculation results from Eq. (12.9) (to a log scale) are shown in Fig. 12.9.

Comparing the results of oxygen partial pressure theoretical calculations with the geological data we have to recognize that the $O_2$ partial pressure in the Archaean and Early Proterozoic atmosphere was indeed very low. The $O_2$ partial pressure in Archaean could have been somewhat higher than in Early Proterozoic due to lower metallic iron content in the convecting mantle over the areas of the Earth's matter zonal differentiation (see Figs. 4.1B, C and 4.16). In Early Proterozoic, one may recall, massive iron ore formations were deposited. Besides, some contribution may have come in Early Precambrian from the oxygen abiogenic generation processes affected by the Sun's hard radiation under reaction (12.6). Our estimates indicate, however, that partial pressure of the photodissociation oxygen at that time did not exceed 0.1 mbar.

Usually, low oxygen partial pressure is substantiated by geochemical parameters of ancient sedimentary rocks. These parameters may be interpreted as indicators of a reducing environment and almost total absence of free oxygen in the atmosphere up through 2.0 BY ago. For instance, Late Archaean and Early Proterozoic Witwatersrand-type conglomerates are found in South Africa and Elliot Lake in Canada. Similar rocks are common on many ancient shields and formed between 3 and 2.1 BY ago. They include abundant clastic fragments of uraninite $UO_2$ and pyrite $FeS_2$. The formation of these minerals cannot be explained by the stagnation in the deep oceanic waters. Besides, during a massive Huron glaciation (2.4–2.2 BY ago) there were no conditions for the formation of stagnant water.

Therefore, at the time of their emergence uraninite and pyrite of the Early Proterozoic conglomerates were in geochemical equilibrium with the aerated oceanic water, that is, with the atmosphere.

The reducing environment in the ancient atmosphere is also supported by a high protoxidic to oxidic iron ratio in the Early Precambrian sediments and weathered crusts and massive deposition of chemical siderites.

A phenomenon of the simultaneous deposition at that time of the oxidic iron ore formations does not contradict at all the aforementioned conclusions of very low oxygen partial pressure in the atmosphere. Moreover, the very existence of the Precambrian sedimentary iron ore formations supports these conclusions. Indeed, under oxidizing atmospheric and oceanic environment the iron oxide solubility drastically declines. Thus, iron's migrating capacity must likewise decrease. In such a case the entire iron would oxidize to the insoluble trivalent state directly in the rift zones and would be there deposited forming the metal-bearing sediments of the ophiolite complexes. Under the proposed concept, the water-soluble iron bicarbonate emerged on contact between iron and the water in the presence of carbon dioxide under reaction (11.4). It was spread all over the ocean. In the shallow water, with the microorganisms participation, iron was oxidized under reaction (11.4′) to the insoluble trivalent iron oxide which formed the bulk of the iron ore deposits.

In particular, it follows from such iron-oxidizing mechanism that at the time of most intense iron ore accumulation the oxygen atmospheric partial pressure must have declined even lower as at those periods almost entire oxygen was consumed by the oxidizing iron. Conversely, during the period of slow iron ore accumulation the oxygen content in the Precambrian atmosphere might have increased somewhat. The scale of these partial pressure fluctuations is very difficult to determine but it is likely that they may have differed by the whole one order of the magnitude.

The oxygen partial pressure was slightly but continuously increasing during Middle and Late Precambrian. As a result, red-bed weathering crusts and red-bed continental clastic sediments appeared on the continents and continental margins 2 BY ago (Salop, 1973; Anatolyeva, 1978). Red-beds are indisputable testimonies of free oxygen in the atmosphere (and hydrosphere). The reason is that in the process the iron's migration capacity declines; and after it is oxidized to the trivalent state in the silicate or carbonate weathering it is preserved *in situ* in the rock destruction products coloring them in fulvous-reddish tinges. A demonstrative characteristic of the changed redox reactions in the ancient atmosphere is the europium conversion in the sediments from $Eu^{2+}$ to $Eu^{3+}$, which also occurred within the time interval 1.9–0.8 BY ago (Fryer, 1977).

Increase in oxygen partial pressure which began 2 BY ago was also marked in the Earth's biota. Just at that time tempestuous evolution of many single-cell bacteria and algae occurred. After the metallic iron totally disappeared from the atmosphere at the Proterozoic/Phanerozoic time boundary a renewed and most significant increase in the oxygen partial pressure began. A result was the most significant restructuring of the entire Earth's biots (see Chapter 15 for a more detailed discussion of the issue).

A third drastic Geologo-biologic boundary at the transition from Proterozoic to Phanerozoic not only indelibly reflected in the Earth biologic evolution but also radically changed the entire environment on its surface. The atmosphere turned from a neutral into an oxidizing one. Most efficient in this new situation turned out to be life forms whose metabolism

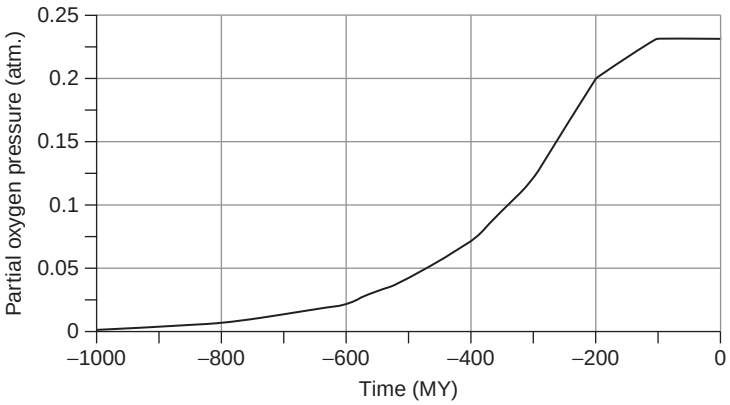


**FIGURE 12.10** Accepted oxygen partial pressure distribution over the last 1 BY (the present-day oxygen partial pressure is 0.2315 atm.).

was based on oxidizing reaction of organic compounds synthesized by the plants. In accordance with that, we assumed the oxygen generation in Vendian and Phanerozoic as shown in Fig. 12.10.

## 12.5 MAJOR PATTERNS IN GENERATION OF THE ABIOGENIC METHANE

Among the minor additions to the basic atmospheric composition is methane. At the early stages of the Earth's evolution it substantially affected the conditions of the life emergence on the planet. Besides, the abiogenic methane could serve as a nutrition base for the bacterial biota and probably played a noticeable role in the formation of gas-hydrate accumulations in the oceanic deposits.

The emergence of the Precambrian iron ore formations was based on iron-oxidizing processes by thermal dissociation of the $CO_2$-saturated oceanic waters and of hydration by the same waters of iron-containing oceanic crust rocks. In the process, methane was generated:

$$4Fe + 2H_2O + CO_2 \rightarrow 4FeO + CH_4 + \quad 41.8 \text{ kcal/mol.} \qquad (12.10)$$

Presently, the mantle does not contain free iron. The methane generation in the oceanic rift zones occurs only in the hydration of the oceanic crust rocks containing the bivalent iron, mostly under reactions like (10.4). Due to the isotope fractioning between carbon dioxide and methane, methane must have enriched in the light isotope $^{12}C$, whereas the heavy isotope $^{13}C$ mostly migrated to carbon dioxide. Such isotope shifts occur, for instance, in the hydrotherms of the "black smokers" which arise on serpentinites. Methane in such sources usually has $\delta^{13}C \approx -13$ to $-14‰$, whereas the oceanic water-dissolved $HCO_3^-$ and $CO_2$ have the shifts close to $\delta^{13}C = -5.5‰$ (Sorokhtin et al., 2001). It indicates that the isotopic exchange between carbon dioxide and methane, exactly as it follows from reaction (11.13), in the direction of lowering $\delta^{13}C$ in methane.

As the iron ore formations were highly developed in Precambrian, it is expected that iron release from the mantle to the hydrosphere as well as hydration of the iron silicates as

described by the reaction (11.9) was accompanied by the profuse abiogenic methane generation. We now compare the calculation results with the biological response to these iron accumulation events in Precambrian.

It is obvious that maximum iron transport to the ocean must have been accompanied by maximum methane generation rate. That, in turn, resulted in increasing mass of the methane-consuming bacteria. As follows from the reaction (11.3), fractioning of carbon isotopes always produces a lighter methane isotopic composition, hence, a lighter carbon composition in organic matter $C_{org}$ in the bacteria which consumed this methane. This is a likely explanation of usually extremely low shifts in $\delta^{13}C_{org}$ to $-50‰$ and even to $\delta^{13}C_{org} \approx -80‰$ in the methane-consuming bacteria. It may also explain local minima in $\delta^{13}C_{org}$ distribution right at the time when the largest iron ore formations masses were deposited in the end of Archaean and in Early Proterozoic.

We determined in Chapter 10 the iron ore formations accumulation rate in Precambrian. We will repeat the same diagram here (see Fig. 10.5) in comparison with the isotopic shift distribution curve in organic carbon borrowed from Schidlowski (1987) (see Fig. 12.11).

As the comparison shows, every epoch of a massive iron ore sedimentation on the ocean floor corresponds with a minimum in the organic carbon $\delta^{13}C_{org}$ shift. However, despite smaller intensity of the jaspelite formation rate in Late Archaean, the $\delta^{13}C_{org}$ isotopic

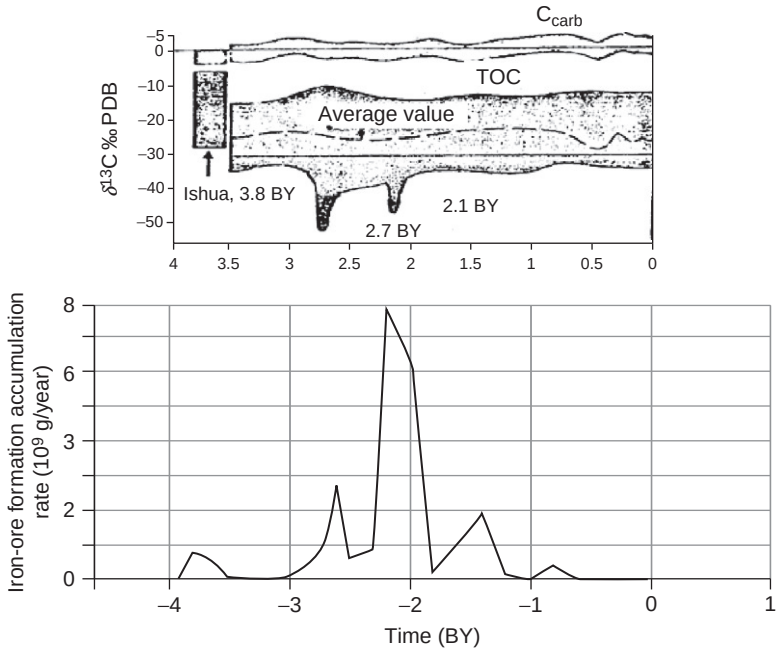


**FIGURE 12.11** Carbon isotopic shifts in organic matter versus epochs of the Precambrian iron ore formations accumulation. Upper diagram: $\delta^{13}C_{org}$ and $\delta^{13}C_{carb}$ distributions in Earth's evolution (Schidlowski, 1987). Lower diagram: Precambrian iron ore deposits formation rate in Precambrian as shown in Fig. 10.5. Two most outstanding Precambrian iron ore formation deposition epochs clearly correspond with the two local minima on the envelop of the minimum $\delta^{13}C_{org}$ values. Unfortunately, the upper diagram does not include their complementary positive $\delta^{13}C_{carb}$ anomalies which reached $+8$ to $+11‰$ PDB in Early Proterozoic (Semikhatov et al., 1999).

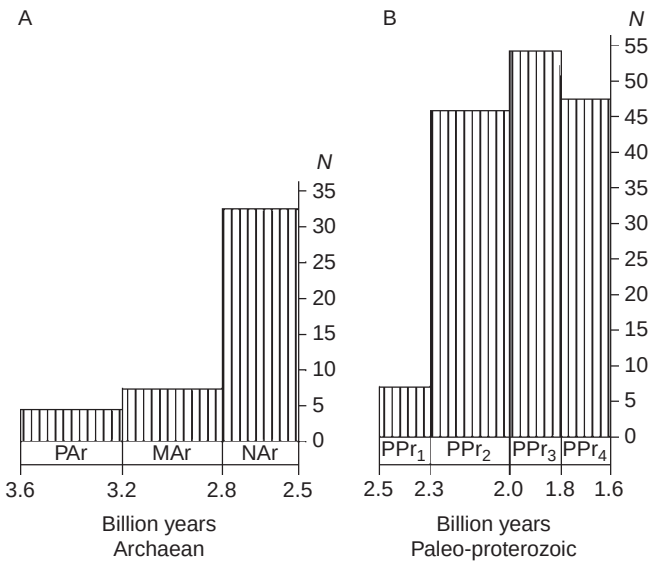


**FIGURE 12.12** Changing of the number of stromatolithic formations in Archaean (A) and Proterozoic (B) after Semikhatov et al. (1999): $N$ is the number of formations with stromatoliths. Comparing the histograms, remember that the Archaean stromatoliths are much smaller in mass that the Early Proterozoic ones ("Paleoproterozoic" by Semikhatov).

minimum amplitude at that time was the largest. The likely cause is the existence in Archaean of a high-density carbon dioxide atmosphere, whereas in Early Proterozoic the $CO_2$ partial pressure declined and the methane generation rate decreased as a consequence.

What is noteworthy is that the times of the iron ore accumulations in Late Archaean and Early Proterozoic also corresponded with the two periods of broad stromatolite development (Fig. 12.12). It is most likely that the nutrition base for the stromatolites was the same abiogenic methane generated in the metallic iron oxidation process under reaction (12.10) and hydration of the iron silicates under reactions similar to (11.9).

The abiogenic methane generation rate $\dot{m}(CH_4)$ is usually controlled by the oceanic crust formation rate (Dmitriyev et al., 2000; Sorokhtin et al., 2001) equal to $V(H_b + H_{sp})\rho$, where $V$ is the oceanic crust area increase rate in the rift zones (see Fig. 7.2); $H_b$ and $H_{sp}$ are, respectively, the oceanic crust's basalt-gabbroid and serpentinite layer thickness (see Fig. 7.1); $\rho \approx 2.9$ g/cm$^3$ is the oceanic crust average thickness. Besides, during the epochs of mass iron ore formations deposition additional methane release occurred at a rate proportionate to iron $\dot{F}e$ accumulation rate in such formations.

In Precambrian rift zones, the methane generation occurred due to the hydration of iron silicates under reactions similar to (11.9) as well as due to the participation of the free (metallic) iron under reaction (12.10). Both reactions proceeded within the oceanic crust at hydration of its rocks by the oceanic water. There is a possibility that the same reactions occurred in Archaean due to the saturation of the primordial regolite with rain water saturated with carbon dioxide as regolite at that time covered significant part of the Earth's surface (see Figs. 4.1B, C and 7.4).

In order to normalize the calculation results to a single scale it was necessary to normalize all methane generation reactions to its unit mass. For instance, under the iron-oxidizing reaction (12.10) one mole of methane (16 g) in the rift zones and primordial regolite forms due to the combination of 304 g of the source reagents. Thus, the scale factor for this reaction is: $k = 16/304 = 0.0526$. Similarly, the oceanic crust iron-containing rock and regolite hydration

under reaction (11.7) has the correction factor $n = 16/2876 = 0.00556$. Taking these into account, the abiogenic methane generation rate (with the excess of $CO_2$) may be presented so:

$$\frac{d(CH_4)}{dt} = U\rho n C_{FeO}\, 0.8\left(H_{sp} + 0.12H_b\right)\frac{S_O}{S_G} \times 10^{15} + k\frac{d(Fe)}{dt}0.1, \qquad (12.11)$$

where $S_O$ is the oceanic crust area (see Fig. 7.4); $S_G = 5.1 \times 10^{18}$ cm$^2$ is the Earth's surface area; $C_{FeO}$ is ion-oxide concentration in the mantle matter and the oceanic crust (see Fig. 4.16); factors 0.1 and 0.8 relate to the recovery extent of a given component (Fe·FeO from the oceanic crust layers). Under reaction (11.9), the methane generation in the present-day oceanic crust is $1.86 \times 10^{12}$ g/year. It is close to the determinations by Dmitriyev et al. (2000) of about $2 \times 10^6$ t/year (or $2 \times 10^{12}$ g/year). The calculation results are compared with organic carbon isotopic shifts in Fig. 12.13.

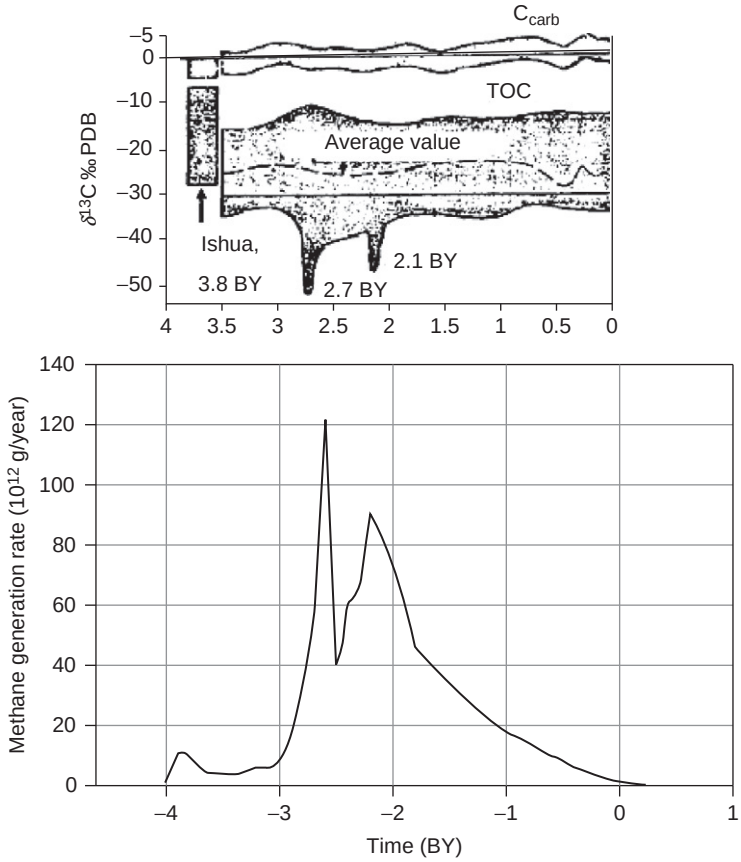


**FIGURE 12.13** Abiogenic methane generation in the oceanic crust plotted under Eq. (12.11) compared with the carbon isotopic shifts in organic matter. Upper diagram: $^{13}C_{org}$ and $\delta^{13}C_{carb}$ distributions versus time (Schidlowski, 1987); lower diagram: abiogenic methane generation rate. Two most outstanding Precambrian iron ore formation deposition and methane accumulation epochs clearly correspond with the two local minima on the envelop of the minimum $\delta^{13}C_{org}$ values.

As the diagram shows, the abiogenic methane generation in the oceanic crust began nearly 4 BY ago and reached 10 million t/year but rapidly declined to a few million tons per year in Mid-Archaean. Later, due to the beginning of the Earth's core separation (see Fig. 4.1D–E) and significant increase in tectonic activity (see Fig. 5.17), the methane generation drastically increased and reached by the end Archaean its absolute maximum of about 120 million t/year. At the Archaean/Proterozoic time boundary the tectonic activity diminished significantly, and so did the methane generation (to 40 million t/year). Massive deposition of iron ore formations began in Early Proterozoic about 2.2 BY ago (see Fig. 12.11). This resulted in renewed intensification of methane generation to approximately 90 million t/year. Subsequently, the abiogenic methane formation was gradually decreasing to only 1.8 million t/year presently. The process will stop in about 500 million years when, due to the Earth's core separation process, the mantle becomes totally devoid of bivalent iron (see Fig. 4.16).

It is noteworthy that there is strong correlation between the organic carbon isotopic shifts and methane generation rate, hence, the mass of the Early Precambrian iron ore formations. This is logical as iron oxidizing under reaction (12.10) and its further accumulation in iron ore formations is accompanied by generation of the abiogenic methane. Methane is the nutrition base for the cyanobacteria and methane-consuming bacteria, so that must have left noticeable traces in the geological record. Due to carbon isotope fractioning in the exchange reactions between carbon dioxide and methane under (11.13), methane always enriched in the light carbon isotope. Remaining carbon dioxide which later migrated to carbonates became isotopically heavier. Because of that, organic matter formed from the methane-consuming bacteria must always have lighter carbon isotope composition, sometimes as low as $\delta^{13}C_{org} \approx -50‰$ and lower.

This phenomenon may have been the cause of the local $\delta^{13}C_{org}$ distribution minima exactly at the times when the iron ore formations deposited at the end Archaean and Early Proterozoic at the greatest rate.

Accelerated methane generation during the massive iron ore formations deposition must have affected the evolution intensity of stromatolites which are remains of laminated bacterial mates (films). Assuming it is so, and a noticeable fraction of such films was indeed formed by the methane-consuming bacteria, the bloom of these life forms must have occurred during the massive deposition of the iron ore formations and profuse methane generation. That appears to be exactly what happened. Semikhatov et al. (1999) indicate that these time intervals are marked by the burst in the growth of stromatolite buildups (see Fig. 12.12).

Part of the abiogenic methane could have concentrated in gas-hydrate accumulations of the oceanic deposits. Massive shungite deposition occurred in Karelia during the Late Jatulian time (the second half of Early Proterozoic). The shungites are coaly matter, most likely, graphitized remains of the previous hydrocarbon accumulations.

Beside the methane generation in the oceanic rift zones, a nonrecurring abiogenic methane release into the atmosphere happened in the beginning of Archaean due to hydration of the ultramafic regolite still covering at that time most of the planet (see Figs. 4.1B, C and 7.4). The release intensity may be estimated by assuming that over the initial 100 MMY (4.0–3.9 BY ago) the entire primordial regolite layer was soaked with carbon dioxide rainwater. The initial iron concentration in the regolite is about 13%, and its oxides, about 23% (see Fig. 4.16). In this case, under the excess of $CO_2$, the original methane pressure may be determined as:

$$p(\mathrm{CH_4}) = \rho_r H_r (0.13k + 0.23n)\frac{S_r}{S_G \times 10^3} bar, \tag{12.12}$$

where $\rho_r \approx 2$ g/cm$^2$ is regolite density (by analogy with the lunar regolite); $H_r$ is unknown thickness of the rainwater-soaked regolite layer; $S_r$ is area covered by the regolite (see Fig. 7.4); $S_G = 5.1 \times 10^{18}$ cm$^2$ is the Earth's area. In the methane formation reactions (11.9) and (12.10), the limiting factor is the mass of the degassed carbon dioxide. Our estimate is that by the moment 3.9 BY ago about $m(\mathrm{CO_2}) = 6.4 \times 10^{20}$ g of carbon dioxide was degassed from the mantle. Assuming all this gas was spent for the methane generation, its mass would be $m(\mathrm{CH_4}) = m(\mathrm{CO_2}) \times 16/44 \approx 2.33 \times 10^{20}$ g, and its partial pressure would not exceed $p(\mathrm{CH_4}) \approx 46$ mbar. This methane pressure in Eq. (12.12) corresponds to a carbon dioxide rainwater-soaked regolite layer 37.5-m thick. The provided $p(\mathrm{CH_4})$ estimate appears to be maximal. The actual methane partial pressure in the beginning of Archaean was lower but most likely no lower than 20 mbar.

Methane could not accumulate in the sea basin water in the locations where it was generated (within the primordial regolite and outside the sediment sequences). Thus, it was released directly into the atmosphere making it very reducing. Therefore, the atmosphere in the beginning of Early Archaean was significantly reducing and carbon dioxide–nitrogen–methane in its composition. Subsequently, in about 100 MMY, after the total hydration of the primordial regolite the Archaean atmosphere's reducing potential must have declined due to methane photodissociation by the solar radiation and the formation of formaldehyde

$$\mathrm{CH_4} + \mathrm{CO_2} + h\nu \rightarrow 2\mathrm{HCOH}. \tag{12.13}$$

Besides, affected by the solar ultraviolet (UV) radiation, methane was oxidized in a humid and warm Early Archaean atmosphere under reaction: $\mathrm{CH_4} + \mathrm{H_2O} + h\nu \rightarrow \mathrm{CO} + 3\mathrm{H_2}$, with hydrogen evaporating. As a result, the Archaean atmosphere became the carbon dioxide–nitrogen one with minor methane content and at the equilibrium humidity content.

As was shown by Galimov (2001), in order for life to emerge abiogenically, some simple source organic compounds must have been accumulated first. One such compound may have been formaldehyde which, as methane, formed at iron oxidizing:

$$2\mathrm{Fe} + \mathrm{H_2O} + \mathrm{CO_2} \rightarrow 2\mathrm{FeO} + \mathrm{HCOH} + 3.05 \text{ kcal/mol}. \tag{12.14}$$

Beside formaldehyde, due to thunderstorm discharges in the Early Archaean reducing atmosphere with its nitrogen and methane, another "link" in the chain of the primary life, the hydrogen cyanide must have emerged:

$$\mathrm{N_2} + 2\mathrm{CH_4} + \mathrm{Q} \rightarrow 2\mathrm{HCN} + 3\mathrm{H_2}, \tag{12.15}$$

where $Q = 26.6$ kcal/mol is the part of the thunderstorm discharge energy absorbed by reaction (12.15). In the earliest Archaean, about 3.9 BY ago, bacteria probably have not emerged yet. If so, the isotopic shifts in organic matter at that time were determined only by the properties of the reactions like (11.9) and (12.10) with no addition of isotopic shifts due to the bacterial metabolism. Apparently, these oldest Earth's rocks were populated by bacteria only somewhat later and with no participation of the abiogenic methane. That may be one

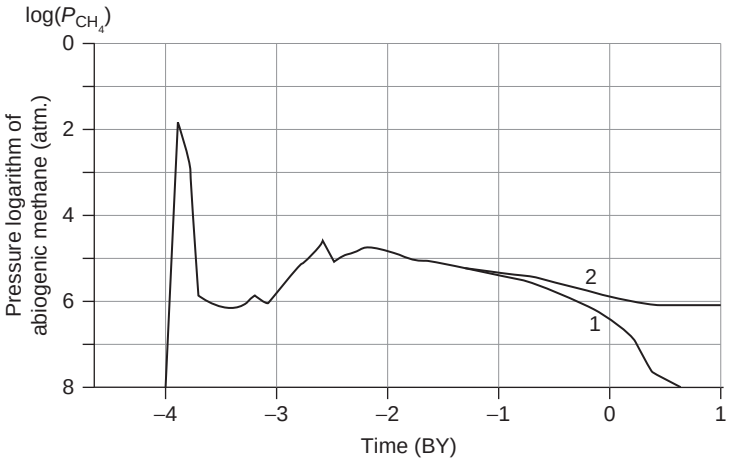


**FIGURE 12.14** Atmospheric methane partial pressure versus time: 1, methane generation in the oceanic crust and 2, total methane generation in the oceanic crust and on the continents

reason why the carbon isotopic ratios about 3.9–3.8 BY ago in the Shidlovsky diagram have slightly elevated $\delta^{13}C$ values compared to the subsequent epochs (see Figs. 12.11 and 12.13).

Using Eqs. (12.11) and (12.12) we came up with the evolution of the abiogenic methane partial pressure in the atmosphere shown in Fig. 12.14. To make the characterization of the methane generation on Earth more complete, Eq. (12.12) must be amended by the swamp methane in the northern Eurasia and Canada, by the soil-generated methane in the humid tropical areas and methane seeping up from the continental hydrocarbon accumulations.

We assume that the process began about 1.8 BY ago. The current methane partial pressure is approximately $p_0 = 1.216 \times 10^{-6}$ bar ($\log(p_0) = -5.92$). Thus, we may determine the total methane partial pressure in the atmosphere. Our estimates are that the present-day methane generation on continents is 3.3 times that generated by the oceanic crust rocks. As the methane partial pressure fluctuated in the Earth's evolution by at least four orders of the magnitude, we used logarithmic scale in Fig. 12.14.

Methane is rather unstable and under normal circumstances rapidly decomposes. For instance, it degasses from the oceanic water, gets into the stratosphere, and then rapidly decomposes under the hard solar radiation with carbon returning into the atmospheric carbon dioxide reservoir

$$CH_4 + 2H_2O + h\nu \rightarrow CO_2 + 4H_2, \tag{12.16}$$

$$CH_4 + 2OH + h\nu \rightarrow CO_2 + 3H_2. \tag{12.17}$$

In the oceanic water, methane is consumed by bacteria with the release of carbon dioxide (especially after the microorganisms die out)

$$CH_4 + \text{bacteria} \rightarrow CO_2 + (OB). \tag{12.18}$$

In the Early Precambrian active metamorphism zones the direct reduction of the methane carbon may have occurred with the formation of coaly matter (combustible shales,

shungites, and even graphite). And in Late Precambrian, especially in Phanerozoic, direct methane oxidizing began

$$CH_4 + 4O_2 \rightarrow 2H_2O + CO_2 + 131.2 \text{ kcal/mol}. \quad (12.19)$$

Despite all these losses, methane remaining in the sedimentary sequences, especially in the absence of oxygen, could form independent hydrocarbon accumulations, for instance, gas-hydrates. More complex hydrocarbons could also form from methane. Lein and colleagues (1998, 2000) believe that the "black smokers" sulfide ores are a unique target for studying organic matter genesis. The chemical peculiarity of hydrothermal systems which include dissolved $H_2$, $H_2S$, $CH_4$, $NH_4$, $Fe^{2+}$, $Mn^{2+}$, CO, $CO_2$ and NaCl (electrolyte), and sulfide minerals as a solid phase (electrode) gives rise to a possibility of organic compounds bacterial synthesis on the sulfide mineral matrix in this giant electrochemical cell. In particular, Lein et al. (1998) studied lipid fractions in the hydrothermal springs using single-dimensional and bidimensional chromatography and found that all similar samples included a broad range of neutral lipids and phospholipids, and in the water–methanol phase, proteins and DNAs.

Mass-spectrometric analysis of the lipid fraction from the organic matter in sulfide ores confirmed the presence of biogenic components including cellular material of microorganisms. Fatty acids from the present-day sulfide ores are compositionally close to lipids from the biomass of chemoautotroph bacteria in the hydrothermal community in the active fields of mid-ocean ridges (Lein et al., 1998; Lein and Sagalevich, 2000; Perisypkin et al., 1998).

## 12.6 EVOLUTION OF ATMOSPHERIC COMPOSITION AND PRESSURE

By putting together partial pressures of all major components of the atmosphere (carbon dioxide, nitrogen, in consideration of the additional generation of argon, oxygen, and water from the atmospheric humidity), it is possible to plot the summary picture of the atmospheric chemical composition from the entire Earth's evolution and even a forecast for the future (see Fig. 12.15).

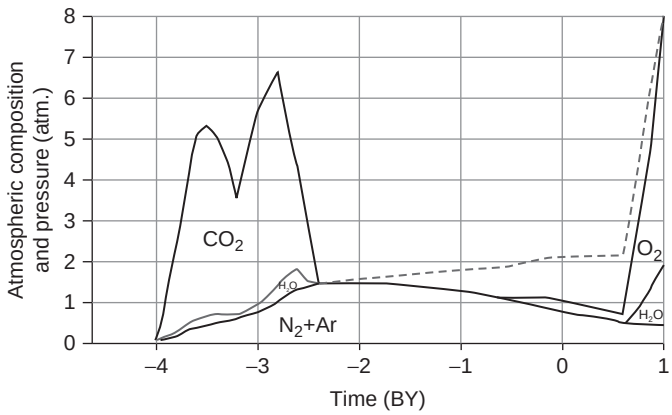


**FIGURE 12.15** Composition and pressure of the Earth's atmosphere versus time. The dashed line is based on an assumption that there is no bacterial nitrogen consumption.

When Earth emerged, its atmosphere contained insignificant amounts of inert nitrogen and just traces of noble gases. The atmospheric pressure did not exceed 1 mbar. There were no additions of chemically active gases (such as $CO_2$, CO, $O_2$, $H_2O$, or OH) in the Katarchaean primordial atmosphere as all such components were rapidly absorbed by the regolite of the still growing Earth.

The Earth's degassing began in Early Archaean. Partial pressure of carbon dioxide, nitrogen, and methane rapidly increased due to $CO_2$ reduction on iron. The atmosphere became carbon dioxide–nitrogen–methane and substantially reducing. Beginning at about 3.5 BY ago, after a significant rise in the atmosphere's average temperature (see Chapter 14), the carbon dioxide–nitrogen composition was amended by partial pressure of the water vapor. And after the methane dissociation approximately 3.8 BY ago the atmosphere became a neutral carbon dioxide–nitrogen gas-shell of Earth.

The nitrogen partial pressure noticeably increased in Late Archaean due to nitrogen degassing from the mantle. And the carbon dioxide pressure began declining at the end Archaean as the atmospheric carbon dioxide after that was being intensely bonded in carbonate deposits. And at last, after the core separation and the formation of the Earth crust's serpentine layer (see Fig. 7.1), which emerged as a result of drastic decline in the tectonic activity, almost entire atmospheric carbon dioxide was bonded in carbonate rocks. The Proterozoic atmosphere became almost purely nitrogen with minute admixture of argon and methane (see Fig. 12.15).

Nitrogen's partial pressure may have reached 1.4–1.5 atm in Early Proterozoic. Beginning in Middle Proterozoic it began noticeably to decline due to the life activity of the nitrogen-consuming bacteria. Simultaneously, in Late Riphean oxygen started to accumulate rapidly in the atmosphere, especially after a total disappearance of the metallic iron from the Precambrian mantle.

In Phanerozoic, nitrogen's partial pressure continued its decline although in Paleozoic and Mesozoic it was amply compensated by accelerated concentration of the biogenic oxygen. When the broad evolution of flowering plants, major oxygen generators, took place at the end Mesozoic, its partial pressure reached the stationary level of about 230 mbar, and together with nitrogen, about 1 atm. Later, in the Cenozoic, the atmospheric pressure began dropping again. The atmospheric pressure decline results in climate cooling. That may noticeably affect the life activity of the nitrogen-consuming bacteria. That, in turn, will have to result in a decreased nitrogen partial pressure decline rate in the future.

The nitrogen-consuming bacteria played positive role in the climate evolution and created favorable and comfortable conditions for the evolution of highly organized life on Earth. Without such bacteria the current atmospheric pressure would be approximately 2 atm, the average planet's temperature would be 54 and over 70 °C on the equator, which is above the coagulation temperature of some vitally important proteins. Favorable conditions for highly organized life may have been preserved only on the mountaintops at high latitudes. But vitally important oxygen could not have accumulated in sufficient amount under such extreme conditions. In fact, if not for the nitrogen removal from the atmosphere, Earth would be presently (as in Archaean) populated only by the thermophilic bacteria and maybe primitive multicellulars.

We mentioned above a drastic oxygen partial pressure increase in the distant future. It will be associated with the abiogenic oxygen degassing due to the core separation process after the complete oxidation of the mantle iron to the stoichiometry under reaction (4.45).

In the future, after 600 MMY the atmospheric pressure will rapidly rise and will significantly exceed 10 atm causing a strongest greenhouse effect on Earth.

Using the derived atmospheric composition and pressure, and the earlier proposed adiabatic theory of the greenhouse effect (Sorokhtin, 2001a,b), it is now possible to determine the temperature parameters of the former, present, and future Earth's climates. Before doing that, however, we must discuss the basics of the adiabatic theory of the greenhouse effect which will be done in the next chapter.

## 12.7 ABSORPTION OF THE SOLAR UV RADIATION BY THE EARTH'S ATMOSPHERE

It is traditionally assumed that the life-saving absorption of the UV portion of the solar radiation occurs in the stratosphere due the ozone (a triatomic oxygen) forming reaction and that the stratospheric ozone is exactly the medium that is absorbing the solar UV radiation. For instance, the textbook "Meteorology and climatology" (Khromov and Petrosyants, 2001) states that the ozone "absorbs the solar radiation with the wavelengths of 0.15–0.29 mkm," that is, exactly in the UV portion of the solar spectrum. How correct is this hypothesis? It needs to be verified.

A close review shows that the absorption of the solar UV rays within the tenuous stratospheric and mesospheric layers is associated mostly with the photochemical dissociation of the oxygen molecules accompanied by the absorption of the energy of hard solar radiation $E = hv$, where $h = 6.626 \times 10^{-27}$ erg s is the Planck's constant, $v$ is the electromagnetic frequency corresponding to this reaction

$$O_2 + hv \rightarrow 2O. \tag{12.20}$$

After the dissociation, the oxygen atoms merge into molecules again but now with heat $Q$ release:

$$O + O \rightarrow O_2 + Q. \tag{12.21}$$

Similar reactions occur with nitrogen:

$$N_2 + hv \rightarrow 2N \text{ and } N + N \rightarrow N_2 + Q. \tag{12.22}$$

The nitrogen effect may be disregarded as the solar hard radiation intensity at the frequency of the nitrogen molecules dissociation is about four orders of the magnitude lower than at the oxygen dissociation frequency (see Fig. 12.16).

The water vapor and carbon dioxide concentrations in the present-day stratosphere are too low to be taken into account. A different situation occurred in Archaean, under a dense carbon dioxide atmosphere whose pressure at that time reached 5 atm. Because of this, in Archaean the absorption of the solar UV radiation was at least as intense under reaction (12.23) of $CO_2$ dissociation and reaction (12.24) of water dissociation

$$CO_2 + hv \rightarrow CO + O \text{ and then } CO + O \rightarrow CO_2 + Q. \tag{12.23}$$

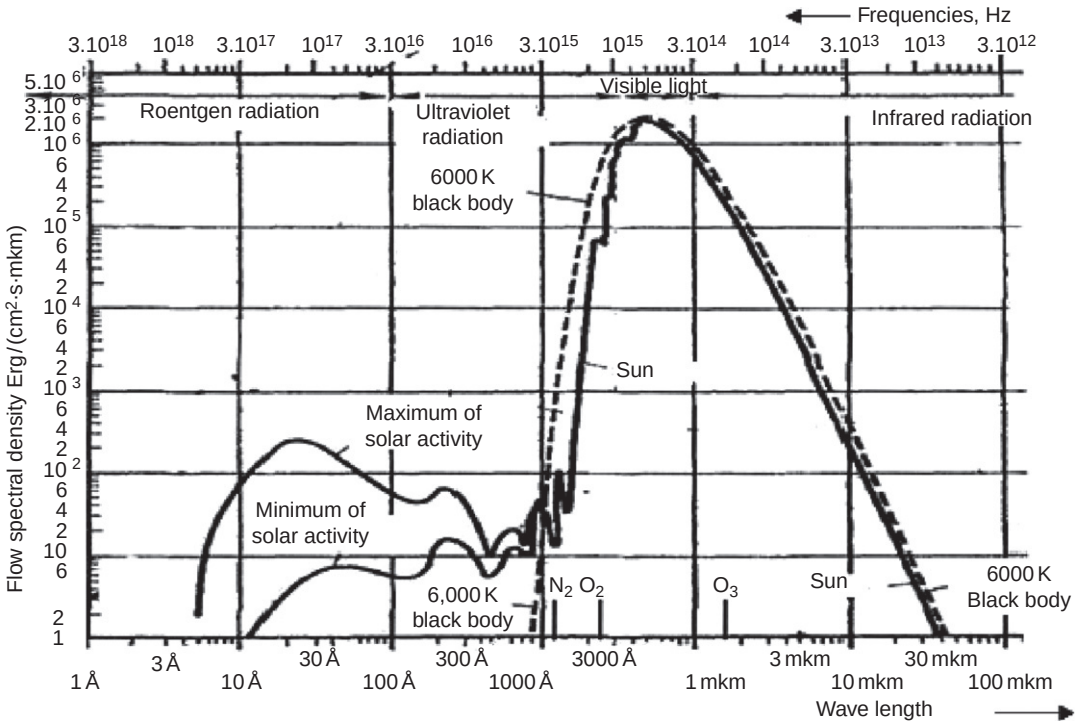


**FIGURE 12.16** Current solar radiation spectrum (solid line) compared to the spectrum of absolute black body at 6000 K (dashed line). Symbols $N_2$, $O_2$, and $O_3$ indicate the spectrum lines (Fraunhofer lines) of nitrogen, oxygen, and ozone molecules corresponding to the dissociation energy of these molecules.

Besides, in Archaean, like under the Proterozoic warm climate with its nitrogen oxygenless atmosphere the UV radiation was apparently also absorbed in the troposphere at the water (humidity) dissociation within the cloud cover under reaction (12.24):

$$OH + O \rightarrow H_2O + Q. \tag{12.24}$$

The solar energy absorption occurs only at the ozone dissociation. Under the energy conservation law, at the ozone dissociation into the source compounds the amount of the absorbed energy is exactly the same as in its formation, that is, $hv = 24$ kcal/mol:

$$O_3 + hv \rightarrow O_2 + O. \tag{12.24}$$

Ozone formation, on the other hand, always occurs with the heat release under an exothermal reaction and not with the absorption of the solar radiation energy as it is still sometimes believed:

$$O_2 + O \rightarrow O_3 + 24 \text{ kcal/mol}. \tag{12.25}$$

The absorption of the IR solar radiation occurs only at ozone dissociation. Under the energy conservation law, at ozone decomposition into the source components exactly the same energy amount is absorbed as at its formation, that is, $hv = 24$ kcal/mol:

$$O_3 + h\nu \rightarrow O_2 + O \tag{12.26}$$

The molecule dissociation energy is usually measured in electron-volts, $1\ \text{ev} = 1.602 \times 10^{-12}$ erg $= 23.045$ kcal/mol. The dissociation of one oxygen molecule is accompanied by the energy absorption E about $5.12\text{ev} = 8.203 \times 10^{-12}$ erg $\approx 118$ kcal/mol, and that of carbon dioxide, by the energy absorption $5.45\ \text{ev} = 8.731 \times 10^{-12}$ erg $\approx 125.6$ kcal/mol, at water dissociation, $5.11\ \text{ev} = 8.186 \times 10^{-12}$ erg $\approx 117.8$ kcal/mol is absorbed, and at ozone dissociation, about $1.04\ \text{ev} = 1.67 \times 10^{-12}$ erg $\approx 24$ kcal/mol more. Critical frequencies at absorption of the electromagnetic waves of these reactions are apparently $\nu = E/h$ (here, E is given in ergs), and the critical wave lengths $\lambda = c/\nu$ cm, where $c = 2.998 \times 10^{10}$ cm/s is the light velocity. We find from here that at the oxygen dissociation the absorbed frequencies are higher than $1.238 \times 10^{15}$ Hz, and the wave lengths are shorter than $2.422 \times 10^{-5}$ cm; at carbon dioxide dissociation, the frequencies higher than $1.318 \times 10^{15}$ Hz are absorbed, and the wave lengths shorter than $2.275 \times 10^{-5}$ cm; at the water molecule dissociation, the frequencies higher than $1.235 \times 10^{15}$ Hz are absorbed, and the wave lengths shorter than $2.427 \times 10^{-5}$ cm. Therefore, the dissociation of oxygen, carbon dioxide, and water molecules must result in the absorption of the solar UV radiation because all dissociation spectra of these molecules are within the UV portion of the spectrum. Indeed, the boundary of the visible and UV radiation in the solar spectrum is at about the frequency $\nu \approx 1 \times 10^{15}$ Hz ($\lambda \approx 3 \times 10^{-5}$ cm). The restoration of oxygen, carbon dioxide, and water molecules apparently results in the heat release $Q$ exactly equal to these molecules dissociation energy. For this reason, the described reactions actually convert the energy of the solar UV radiation into heat.

The frequency of the solar radiation absorption by ozone is $\nu \geq 0.252 \times 10^{15}$ Hz or $\lambda \leq 1.19 \times 10^{-4}$ cm. It is within the IR portion of the spectrum, so ozone can only absorb the short-wave portion of the heat waves and the adjacent low-frequency area of the visible solar radiation but not the UV (see Fig. 12.16).

The provided estimates and reasoning lead to a conclusion important for life on Earth: beginning in Archaean, that is, from the very moment of the appearance of life on Earth, the Earth's surface was never subjected to intense solar UV radiation which allowed for life to evolve directly on the Earth's surface. It is supported by the emergence in Early Proterozoic of the red-colored weathered crusts formed as a result of iron-oxidizing bacteria metabolism (Anatolyeva, 1978). The similar Archaean crusts apparently were not preserved due to an active erosion of Archaean continents.

Only the young Earth in Katarchaean (4.6–4 BY ago) was totally devoid of a hydrosphere and chemically active atmosphere so it was actively irradiated by the intense UV radiation which completely prohibited the emergence of life on Earth prior to Archaean.

Let us now go back to the present conditions and to the dissociation of only the atmospheric oxygen. If, after the oxygen molecules dissociation, all released oxygen atoms recombine, the released heat may be found as follows:

$$Q = \frac{h\nu N_A}{K_{td}} = \nu\left[\frac{hN_A}{K_{td}}\right] = \nu 9.531 \times 10^{-11}. \tag{12.27}$$

Here, $N_A = 6.023 \times 10^{23}$ is the Avogadro number and $K_{td} = 4.187 \times 10^7$ erg/cal is the thermodynamic conversion factor from ergs to calories. Then, for oxygen

$$1.24 \times 10^{15} \times 9.531 \times 10^{-11} = 118,184 \text{ cal/mol} \approx 118.2 \text{ kcal/mol}; \tag{12.28}$$

and for ozone:

$$0.252 \times 10^{15} \times 9.531 \times 10^{-11} = 24,018 \text{ cal/mol} \approx 24 \text{ kcal/mole}. \tag{12.28'}$$

Therefore, the inverse recombination reactions of the earlier dissociated oxygen molecules into the air molecules in actuality transform the energy of the solar UV radiation into the heat energy, and it is spent for the heating of a thin stratospheric and mesospheric air at a height of 15–80 km. This is clearly seen on the temperature profile of these atmospheric layers (see Fig. 13.2).

The confusion with the UV radiation absorption by ozone is likely associated with the assumptions in the calculations of the ozone molecules' complete dissociation into three oxygen atoms at once, with the absorption of $24.02 + 118.18 = 142.2$ kcal/mol. In actuality, the process is a two-step one. Initially, ozone easily releases only one atom (Nekrasov, 1973), with the absorption of 24.02 kcal/mol, and only then the remaining molecule mixes with the atmospheric oxygen and can dissociate with the absorption of 118.18 kcal/mol but only if affected by the other photons as is shown under reaction (12.20).

The atmospheric pressure at the elevation $h$ is approximately

$$P_h = P_0 \exp\left[\frac{g\mu}{RT}h\right], \tag{12.29}$$

where $P_0 = 1.013$ mbar is pressure at the Earth surface; $g = 981$ cm/s is the gravity acceleration; $\mu = 28.89$ is the air mixture molar weight; $R = 8.314 \times 10^7$ erg/mol deg is the gas constant; $T \approx 270$ K is the approximate temperature at the stratosphere/mesosphere boundary, that is, at the elevation of the maximum stratosphere heating of about 50 km (Fig. 13.2). Then pressure at that elevation is:

$$P_{50} \approx 1.013 \exp\left[-\frac{981 \times 28,89}{8.314 \times 10^7 \times 270} 5 \times 10^6\right] \approx 1.837 \text{ m bar}. \tag{12.30}$$

At the adiabatic air temperature distribution within the atmosphere its undisturbed value at the elevation $h$ (Sorokhtin, 2007) is:

$$T_h = 288\left[\frac{P_h}{P_0}\right]^{\alpha}, \tag{12.31}$$

where $\alpha = 0.1905$ is the atmospheric adiabatic exponent and 288 is the average Earth temperature at the sea level, degrees Kelvin. Then the adiabatic temperature at the elevation of about 50 km will be

$$T_{50} = 288\left[\frac{1.837}{1013}\right]^{0.1905} \approx 87 \text{ K}. \tag{12.32}$$

At a new recombination of the atomic oxygen into the molecules under reaction (12.21), additional stratosphere heating occurs. If, for instance, the fraction of the dissociated oxygen molecules was only 0.3% ($S = 0.003$), then such heating in the present-day atmosphere is

$$\Delta T = \frac{Q}{c_p} S = \frac{118,000}{1.962} 0.003 \approx 180 \text{ K}, \tag{12.33}$$

where $c_p \approx 1.962$ cal/mol deg is the air heat capacity at 87 K. And the resulting temperature at the 50 km elevation will be: $87 + 180 = 267 \approx 270$ K as shown in Fig. 13.2.

At the elevations below 50 km, the UV radiation intensity declines. Thus, the relative number of the molecule dissociation events significantly decreases, and so does the stratosphere heating. At the same time, at greater elevations the decrease in the number of the molecule dissociation events is in proportion with the exponential air pressure decline in the same direction.

The ozone's mass fraction in the atmosphere is about $3.6 \times 10^{-5}$%. Thus, even assuming that every single ozone atom takes part in the absorption of the solar IR radiation, a similar calculation of the stratosphere and mesosphere heating will be only 6.7 K. Therefore, the ozone formation may only result in a significantly smaller (by the factor of 30) atmosphere heating than the actually observed. This is an additional confirmation of the hypothesis according to which the responsibility for the absorption of the solar UV radiation lies not with ozone but with the oxygen molecules dissociation process into atoms.

The emergence of the atomic oxygen in the transition layer between the stratosphere and mesosphere results in the occurrence in that layer of the noticeable oxidizing environment which leads, for instance, to oxidizing of methane which happens to get there:

$$\underset{\text{Methane}}{CH_4} + O \rightarrow \underset{\text{formaldehyde}}{HCOH} + H_2 + 9.8 \text{ kcal/mol} \tag{12.34}$$

$$H_2 + O \rightarrow H_2O + 57.8 \text{ kcal/mol} \tag{12.34'}$$

$$HCOH + O \rightarrow CO_2 + H_2 + 66.4 \text{ kcal/mol} \tag{12.35}$$

$$H_2 + O \rightarrow H_2O + 57.8 \text{ kcal/mol}. \tag{12.35'}$$

These reactions decompose methane thus stabilizing its atmospheric concentration. They also contribute to the stratosphere and mesosphere heating which, however, is insignificant due to a low-atmospheric concentration of methane.

Therefore, ozone dissociation and even more so its formation cannot cause the absorption of the solar UV radiation as these reactions occur in the IR radiation domain. The solar UV radiation with the wavelength shorter than 0.24 mcm (2400 Å) is absorbed only by the oxygen dissociation process. Repeated recombination of the oxygen atoms into molecules results in the stratosphere and mesosphere heating to the observed temperatures. Thus, the ozone layer in the stratosphere is actually not a protective shield against the UV radiation that is deadly for all living things. The only real "shield" is oxygen. Still, ozone is generated due to merging of the atomic oxygen, released at the absorption of the UV radiation, with the oxygen molecules in the air. This is a reason why the ozone concentration in the stratosphere is a real indication but not the cause of the absorption of the solar UV radiation. This may justify a great deal of attention devoted to studies of the ozone layer and to the "ozone holes" problem although the ozone formation is just a consequence and not the cause of the absorption of the solar UV radiation.

In recent decades, there was much ado about the danger from the so-called "ozone holes" to all living things as these holes ostensibly open the way for the solar UV radiation to the Earth's surface. It is noteworthy that the "ozone holes" are usually understood as the stratospheric areas in the polar and moderate latitudes where the ozone concentration declined by about 20−30%. The holes usually emerge in winter and spring over stable anticyclones, for instance, in Antarctic or over Yakutia. The reason is that the solar insolation drastically decreases in winter and even totally disappears in the polar areas. On the other hand, the air masses rise over the anticyclonic areas and flow over into the stratosphere. As a result, the ozone layer over the anticyclones as if dispelled. In summer, however, the ozone "holes'" area drastically decreases or they completely disappear.

The "ozone hole" panic began only after the scientists learned how to measure the ozone concentration in the atmosphere in the 1950s. Before that everything was quiet, nobody worried. The ozone "hole" was first discovered in the Antarctic at the time when one of these writers participated in studies there. Soon after that, a plethora of assumptions of the anthropogenic effect emerged around the "hole" issue. The most fashionable was assault on the cooling industry which made household aerosol cans using easily liquefiable Freon gas. It was not explained why the deepest and widest ozone "holes" were observed in the Antarctic, that is, in the southern hemisphere, whereas maximum anthropogenic Freon releases occur in the Northern hemisphere (the real explanation was constant domination of the Antarctic by the largest anticyclone). It is also unclear why the industrial Freons are more dangerous than the similar but natural ones released in immeasurably greater amounts (many millions of tons annually) at volcanic eruptions over the subduction zones of oceanic plates underneath the island arcs and active continental margins.

A conclusion is that the role of the anthropogenic effect on the ozone layer in the stratosphere, where the ozone "holes" emerge, is negligible, three to four orders of the magnitude below the natural effect. That is why all fluctuations of the ozone concentration in the atmosphere are natural and in no way are associated with human activity. It was shown by Kapitsa and Gavrilov (1999) that the stratospheric ozone concentration fluctuates seasonally and bears no danger. There is no ozone "hole" problem, and still colossal amounts are expended to fight it. Some estimates indicate that just in order to comply with the Montreal protocol to the 1985 Vienna Convention on the ozone layer protection only in Russia $5 billion annually must be expended, and the single-time loss from the destruction and replacement of the Freon-using equipment is $10–15 billion. Certainly this money may be better used.

To summarize, the "war" against the anthropogenic Freon releases into the atmosphere had already cost many billions of dollars and is actually "tilting at windmills," so brilliantly described by Miguel de Cervantes in his immortal novel *The Ingenious Hidalgo Don Quixote of La Mancha*.

CHAPTER

# 9

# Continental Drift in Earth's Geological History

Earlier we showed, based on convincing geological data, that the continental crust formation began 4.0–3.8 BY ago. That was a delay of 600–800 MMY after Earth's origin. After the crust emerged, its mass continuously although nonuniformly grew to its current amount. The most intense crust formation happened in Late Archaean. During the entire Archaean, however, there were no large continents. Their embryos (nuclears and old shields) most likely evolved in isolation from one another (see Figs. 6.4 and 9.1). Probably, a first large supercontinent Monogaea formed at the Archaean–Proterozoic time boundary, about 2.6 BY ago, at the time of a dense iron-oxide Earth core separation. During the subsequent epochs, other supercontinents emerged time and again (see Fig. 6.7). They fragmented into individual continents which drifted away from one another and merged into new supercontinents like the Wegener's Late Paleozoic Pangaea.

A theoretical analysis and modeling of the mantle convection processes showed that the supercontinents could form at the interval of about 800 MMY, and only after Archaean. Only four such supercontinents could have formed over the entire post-Archaean time interval (see Section 6.7). In this chapter, we will reconstruct the spatial positions of these supercontinents and the continental (and ocean) drift in Earth's Precambrian evolution. We will review these reconstructions in their historical sequence, from the older to the younger, albeit the reconstructions were conducted the other way around.

## 9.1 CONTINENTAL SHIELD EVOLUTION IN ARCHAEAN

As mentioned earlier (see Section 7.2, Fig. 7.5), the continental crust in Archaean formed due to the secondary remelting of partially hydrated basalt sheets (oceanic crust), where they piled up over the descending convection mantle flows. The Early and Middle Archaean mantle convections were mostly heat-induced, with heating from below against the background of Earth's matter zonal differentiation. For this reason, it must have been organized into a system of stationary Bénard cells (see Section 6.3, Fig. 6.4). This way, the

*Developments in Earth and Environmental Sciences*, Volume 10
DOI: 10.1016/S1571-9197(11)10009-9

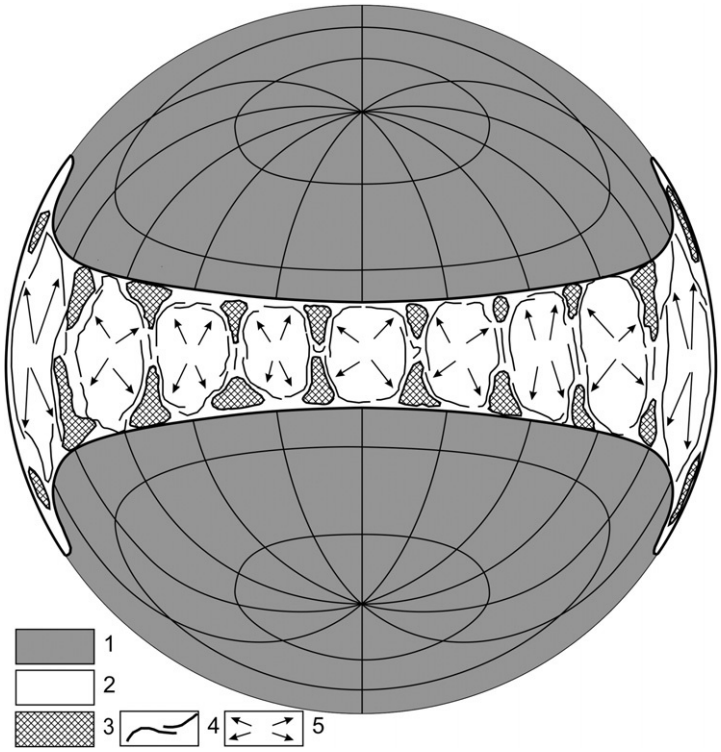


**FIGURE 9.1** Possible positions of the oldest (embryonic) continental crust blocks in Earth equatorial belt about 3.6 BY ago: 1, primordial Earth's ultramafic matter (overlain by small-pore regolite of the same composition); 2, basalt surface of the convection cells within latitudinal zone of Earth's tectonomagnetic activity; 3, continental crust embryos composed of greenstone rocks and sodium composition granitoids; 4, folding at the edges of convective cells; and 5, basalt plates movement directions.

number of the continental crust embryos in Early Archaean was most likely equal to the number of the then existing convection cells and could have reached 40 "nuclears" (using Glukhovsky, Moralev and Kuzmin, 1994 terminology).

The shields at that time formed in isolation from one another as if staying in place, without noticeable continental drift, and gradually acquiring the outlines of roundish structures. As the zonal differentiation front of Earth's matter descended and the differentiation zone expanded, the size of the stationary Bénard cells also increased. That must have resulted in the restructuring of convection and in the respective nuclears merging into larger shields. Nevertheless, at least 10–12 mutually unconnected centers of future continent formation (Archaean shields) must have been preserved by mid-Late Archaean.

It is not possible now to reconstruct the exact positions of old shields on Earth's surface in Archaean. It is possible, however, to sketch-in general patterns of the continental massifs distribution at that remote time.

It is most likely that first embryos of the future continental shields emerged about 3.8 BY ago in the equatorial zone of Earth's lithospheric shell over the oldest Earth's matter differentiation zone (see Fig. 4.1). Probably, many such embryos of the future continents did not survive to our days. Some of them, however, not only survived but also are now the stratotypic examples of the Earth's crust most ancient formations, such as the gray–gneiss complexes of West Greenland or the Yengr Series rocks on the Aldan shield.

Subsequently, during almost the entire Archaean the zonal differentiation of Earth's matter was fed mostly by gravitational energy but continued to evolve as if in an inherited way within the same expanding latitudinal Earth belt (see Chapter 7). Around 3.6 BY ago, the width of the tectonomagmatic activity belt exceeded 3000 km (see Fig. 9.1). The Archaean shield drift relative to one another still was insignificant as at that time the shields formed more or less independently in the environment of the Bénard-type stationary heat convection over the descending convection flows in the upper mantle, which were heated from beneath by the zonal differentiation process of Earth's matter (see Fig. 7.14).

As mentioned, a catastrophic event of the core separation at the end of Archaean must have been accompanied by the exciting of the exceptionally strong convection flows in the mantle belt over the differentiation zone of Earth's matter. These flows totally rebuilt the entire preexisting tectonic plan.

The geometry of the described events says that a single-cell convection structure must have formed at that time with a single ascending flow over the place where the former Earth kernel floated up, and a single descending flow over the area of the core matter "draining" toward the planet's center (see Fig. 4.1D and E). This is a reason to believe that at the Archaean–Proterozoic time boundary 2.6 BY ago, a first supercontinent in Earth's evolution was formed above this descending mantle flow from the previously separated continental shields. We named this supercontinent Monogaea (Sorokhtin and Ushakov, 1989a, 1990).

A possibility of a single supercontinent's existence at the Archaean–Proterozoic time boundary was previously suggested by Khain and Bozhko (1988) based on geological data. They called this hypothetical continent Pangaea 0.

Taking the aforementioned into account, it is enticing to tie in the described geodynamic catastrophe with the most outstanding Kenoranian planetary tectonomagnetic diastrophism which completed the Archaean stage of Earth's geological evolution. The prime cause of those radical geological events was a catastrophic process of Earth's core separation.

The primordial Earth kernel matter density at normal pressure (about 3.9–4.0 g/cm$^3$) was noticeably higher than the differentiated mantle matter (about 3.2–3.3 g/cm$^3$). For this reason, the core separation 2.7–2.6 BY ago could have occurred only under the influence of excessive pressure acting from the core under separation onto the former Earth kernel. Not only should the kernel have floated to Earth surface but it should also have raised high (several kilometers) over this plain surface (see Fig. 4.1-D). The floating-up of Earth's kernel in the environment of the revolving Earth should have occurred in Earth's equatorial plane. Thus, there are reasons to suggest that the then formed supercontinent Monogaea was also positioned over the equator and in the low latitudes.

## 9.2 SUPERCONTINENT MONOGAEA FORMATION IN THE END ARCHAEAN

Besides Monogaea formation specifics, as mentioned, the very positions of the continents on the surface of the revolving Earth substantially distorted the symmetry of its moment of inertia and forced Earth's body to rotate so that the center of gravity of the continents was on the equator (Monin, 1988, 1999). For the same reason, all subsequent supercontinents

must have been positioned only in the low latitudes with the geometric centers on the revolution equator. Apparently, that is exactly what happened. At least, no traces of ice sheet deposits were discovered on the subsequent supercontinents Megagaea, Mesogea, or Pangaea (Chumakov, 1978). However, the continent stand over the rift zones and oceans level in Archaean and Early Proterozoic was still very high (see Fig. 7.10). It was up to 6 km in Archaean and up to 4–3 km in Early Proterozoic. That is why, despite a hot Archaean climate and significantly cooled down but still warm Early Proterozoic climate, glaciations may have developed on the continents of the time. The evidence of this is numerous glacier tillites and tilloids of that time (Chumakov, 1978). An indirect support of this idea is provided by the conglomerate developments (like the Witwatersrand in the South Africa) in Early Proterozoic profusely deposited then on the margins of many other old cratons.

A first in Earth's history almost global Huronian glaciation covered most shields of the old continental platforms. Its timing was Early Proterozoic, about 2.5–2.2 BY ago. It might have been caused only by the almost complete bonding after Archaean of carbon dioxide from a dense atmosphere with pressure close to 6 atm by carbonates (see Chapter 12). The total pressure of an almost purely nitrogen atmosphere declined to 1.5 atm (see Fig. 12.15).

A reminder: this drastic decline in the atmospheric pressure occurred at a high average continent stand level of 5–3 km. That is why the atmospheric pressure decline at high continent stand level was the main cause of the broad-based high-elevation Early Proterozoic glaciation (Sorokhtin and Sorokhtin, 1997). Of course, the emergence of broadly developed glaciations in Early Proterozoic could also occur on the continents positioned in low latitudes.

Unfortunately, so far the Precambrian paleomagnetic (and in particular Early Proterozoic) data are not very reliable and their ties with stratigraphic horizons leave a lot to be desired. For this reason, we intentionally did not utilize the paleomagnetic data for the reconstruction of Precambrian supercontinents and individual continental massifs and continents within them as we believe that these data could distort such reconstructions beyond recognition. All our reconstructions are based on geological and paleoclimatic data. We aligned same-age or same-type structures, formations, and climatic provinces with one another. We used the geological data published in the special literature on the geology of Early Precambrian (Precambrian of the continents, 1976a,b, 1977; Kratz et al., 1981; Condie, 1983; Borukayev, 1985; Khain and Bozhko, 1988).

In particular, for the Monogaea reconstruction we used the data on tillite and tilloid distribution on the Early Proterozoic continents (Chumakov, 1978). We utilized the criterion of compact grouping of known Early Proterozoic tillite deposits in consideration of possible inherited continent locations on Earth's surface in the subsequent geological epochs.

Under such preconditions, the "center of gravity" for the geographic locations of the identified tillites and tilloids approximately defines the center of gravity for the supercontinent proper. We also took into account the distribution and trends of the Kenoranian and the equivalent orogenies ($\sim$2.6 BY ago). Besides, in Early Proterozoic eastern South America (the Brazilian craton) was still united with the Central and possibly South America but was separated from the southern part of the South-American (Amazonian) platform. Another restriction was that the West Africa, most likely, was still joined with the Guiana shield of South America. It appears that at the Archaean–Proterozoic time boundary the other

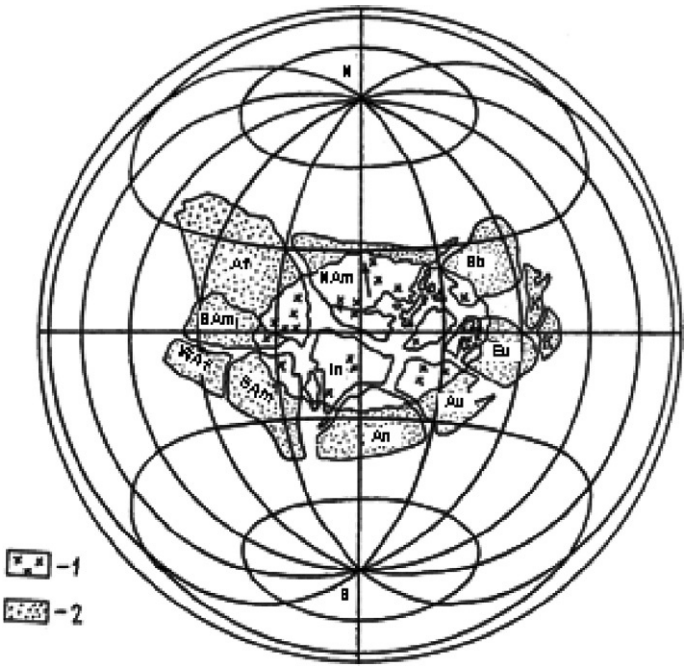


**FIGURE 9.2** Monogaea reconstruction for the period about 2.5–2.4 BY ago (Lambert projection): 1, tillites and tilloids; 2, consolidated continental crust devoid of tillites and tilloids; arrow on the Canadian Shield is the direction of glacial scour; unshaded areas within Monogaea are the sheet glaciation areas (actually may have been broader). Au, Australia; NAm and SAm, North and South America; AN, Antarctic; WAf and Af, West Africa and Africa; Eu, Europe; In, India; K, Kazakhstan; and Sb Siberia.

old platforms were fractured into parts and their fragments (Archaean shields) could occupy then different positions from what they are now. At this time, reliable geological data about possible displacements of the other shields at the end Archaean are missing. That is why our reconstruction of Monogaea (Fig. 9.2) tentatively shows the other platforms with their modern configurations with the current mutual positions of the component Archaean shields.

## 9.3 DISINTEGRATION OF MONOGAEA AND FORMATION OF MEGAGAEA SUPERCONTINENT IN EARLY PROTEROZOIC

Asymmetric mantle matter density distribution emerged at the Archaean–Proterozoic time boundary after the core separation (see Fig. 4.1D). It must have resulted in an equally strong asymmetry of the mantle matter barodiffusion differentiation process on the surface of the newly formed core. The primordial matter was rich in iron (nearly 13%) and its oxides (nearly 24%). Thus, most intense differentiation must have proceeded underneath the "dense" hemisphere with the formation there of powerful descending convection flows. Contrary to this, within the "light" hemisphere underneath Monogaea the equally powerful ascending convection flow must have emerged which eventually resulted in the supercontinent fragmentation (see Fig. 9.14).

First extension impulses may have showed up about 2.4 BY ago. This is supported by the age of the Great Dyke in Zimbabwe. The main phase of the supercontinent fragmentation, however, occurred somewhat later, about 2.3 BY ago. The continental lithospheric plates remained relatively thin (no greater than 100 or 150 km) after the Archaean mantle overheating. They were also weaker than the plates of the present-day continents whose thickness, together with the Earth crust underneath the Archaean shields, reaches 250 km. This gives us a reason to believe that, against the background of relatively active Early Proterozoic tectonic activity, Monogaea split in small blocks-cratons mostly along the old sutures which soldered Archaean shields during the Kenoranian diastrophism into a unified supercontinent.

As a result, many shields separated again in mid-Early Proterozoic and began a centrifugal drift away from the center of the former Monogaea (Fig. 9.3). In reconstructing Monogaea disintegration, we used a pattern described in (Sorokhtin et al., 2004) according to which the kimberlite diamond-bearing rocks formed due to sucking-in underneath the Archaean continents of carbonate pelagic deposits in tropical and low-latitude zones of the Early Proterozoic oceans. As opposed to the Kimberlites, the lamproites formed from the no-carbonate (mostly clayey) pelagic deposits of the Early Proterozoic high-latitude and near-polar zones.

The distribution of the Karelian (Svekofen) and equivalent orogenic belts which again soldered the cratons about 1.9–1.8 BY ago into a new supercontinent Megagaea helps restore the cratons separated in Early Proterozoic (fragments of the former Monogaea). To


**FIGURE 9.3** Monogaea disintegration about 2.2 BY ago. Archaean continental blocks and shields: 1, Australia; 2, Antarctic; 3, Africa; 4, Baltic shield; 5, East Siberia; 6, Greenland; 7, West Africa; 8, India; 9, Chinese shields; 10, Russian Platform; 11, North America; 12, Ukrainian shield; and 13, South America.

implement this pattern, we used a monograph by Khain and Bozhko (1988) on the Precambrian continental tectonics as well as additional criteria for diagnosing the edge zones of the Archaean shields and protoplatforms in Early Proterozoic. For instance, we took into account that the largest iron ore deposits of the same age were most likely formed on the passive margins of the continental blocks in the upwelling zones of that time.

Geological data (Khain and Bozhko, 1988) indicate that within the North-American Platform Archaean cratons Wyoming, Churchill, Kaminak and Slave from the one side, and cratons Superior, and North Atlantic from the second and third sides are separated by the Trans-Hudson and Labrador orogens with the folding age of 1.9–1.8 BY. With this in mind the North-American Platform of the Early Proterozoic reconstruction (see Fig. 9.3) is shown as broken into three portions: the eastern, western, and Greenland with the Baffin Land and Newfoundland Provinces.

Similarly, the European Platform is shown as broken into three cratons: the Kola-Karelian, Central Russian (including SW Fennoskandia, Voronezh Massif, Pri-Dnepr, and Pri-Azov blocks of the Ukrainian shield), and the third craton (Kirovograd and Belozer blocks of the Ukrainian shield—basements of Belorussia and of Baltic Republics).

The Siberian Platform is tentatively broken into four parts: the Anabar and Aldan shields with the adjoining areas although there may have been more such fragments in the Siberian platform.

Australia is split into three cratons: the Yilgarn and Pilbara blocks with the adjoining areas and a group of blocks in the north (Pain Creek, Kimberly, and some others).

Africa has four cratons: the Kalahari southern shield, the Congo protoplatform in the equatorial Africa, the Central African protoplatform (possibly merging several independent shields), and the West Africa protoplatform.

South America includes two protoplatforms: the Guiana shield with the Amazon craton and the East Brazilian craton which includes a number of smaller blocks with the Archaean crust for a basement. The East Brazilian craton is shown as still combined with the South African Congolese craton as the clear-cut separation of these blocks happened much later.

Thus, in mid-Early Proterozoic the Archaean continental crust was broken into numerous separate plates (see Fig. 9.3). Khain estimated the number of such plates at over 30 (we believe that there were 28 such plates) so he even proposed to identify Early Proterozoic as the epoch of small plates.

As mentioned, the Early Proterozoic mantle was very nonuniform in its composition. Thus, the descending flow of the next single-cell convection structure (formed 1.9 BY ago) must have been positioned as the antipode to the former supercontinent Monogaea. Accounting for that, a reconstruction of the second supercontinent Megagaea (proposed by Hans Stille in the 1940s) was generated by way of moving the Monogaea continental blocks to the opposite side of Earth plus the subsequent centripetal drift up to "gluing" them into a single continental massif. It so turned out that all the old continental massifs surrounded by the Karelian and age-equivalent foldings and by the Archaean crust activation and reworking areas of about 1.9–1.9 BY ago also merged together (Fig. 9.4).

Khain and Bozhko (1988) wrote: "By the time-boundary 1.7 BY practically all protogeosynclinal areas disappeared, all eocratons merged, and a single continental crust massif—

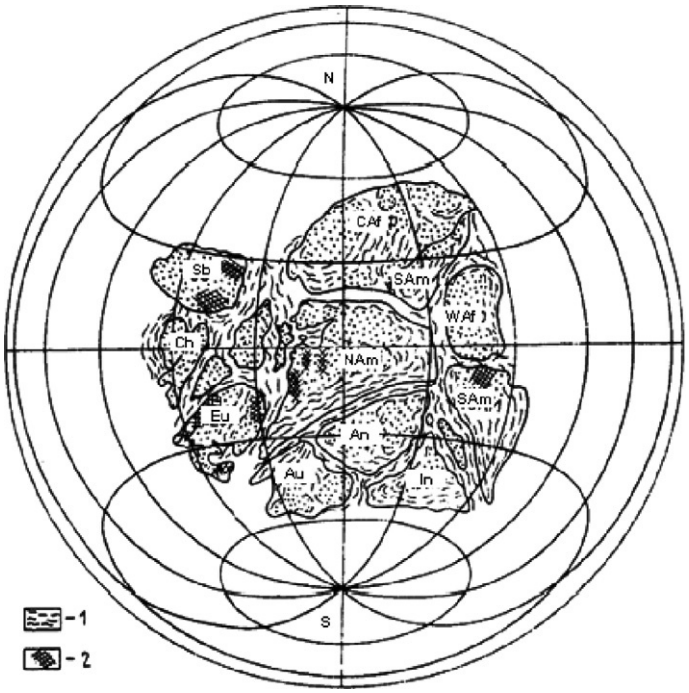


**FIGURE 9.4** Megagaea 1.8 BY ago: 1, folded belts and 2, red-beds (see Fig. 9.2 for the rest of the legend).

supercontinent must have emerged. It is logical to call it Pangaea I as opposed to the later, Wagnerian Pangaea II."

As mentioned earlier, Earth's moment of revolution's axes reoriented simultaneously with the continental drift. As a result, the newly formed supercontinent must have moved into the low latitudes again. Apparently that was exactly what happened as supported by the development of red weathered crusts (Anatolyeva, 1978; see Fig. 9.4).

Remember, Hans Stille was the first to suggest the existence of a hypothetical ancient supercontinent in 1944. He also proposed the name, Megagaea. His suggestion was based on his observation of a close similarity in geology of different ancient blocks often joined into a unit by the same-age folding at the time of the "Algonquian revolution" in the end of Early Proterozoic. A result was that Stille came to a right conclusion "of an unusually thick post-Algonquian continental massif Megagaea. It included the oldest continents from the subsequent Earth evolution. But it also included at least main portions of the later orthogeosynclinal regions which emerged as the oldest geosynclines within Megagaea after the global regeneration. At the same time, the oldest continents were preserved from this regeneration and may be considered as the residual humps of Megagaea" (Stille, 1964, p. 383).

Stille was no mobilist. He viewed the Megagaea origin from purely fixist positions and believed that the supercontinent was an ancient formation of Earth's crust, and the

separation of many modern continents as a result of the subsequent crust destruction and not of the continental drift.

A modern geological substantiation of Megagaea based on more accurate and massive absolute age determinations of geological events and on the mobilist approach to the issue was provided by Khain and Bozhko (1988). They called the supercontinent Pangaea I rather than Megagaea.

Although we used the same mobilist approach and the same geological data taken mostly from Khain and Bozhko's monograph, the Megagaea reconstruction provided here (see Fig. 9.4) is substantially distinct from the Khain and Bozhko reconstruction.

This may indicate that any continental reconstructions for the remote geological epochs are still far from unambiguity. As the Proterozoic rocks paleomagnetic data are unreliable, the paleomagnetic technique is so far impossible to apply for the reconstruction of the Precambrian history of the continental drift.

## 9.4 DISINTEGRATION OF MEGAGAEA AND MESOGEA (RODINIA) SUPERCONTINENT FORMATION IN MIDDLE RIPHEAN

As Monogaea, Megagaea was short-lived, just 100–150 MMY. Already 1.7 BY ago first indication of the supercontinent breakup appeared. For instance, first rift buildups and aulacogens were formed at that time in place of the future North-American Cordillera. The fault tectonics and the continental breakup were at their strongest about 1.5–1.4 BY ago. At that time, rift troughs and numerous aulacogens emerged on almost all platforms. About that age huge, sometimes unprecedented unorogenic volcanoplutonic belts formed over some rift structures as along the eastern framework of the North-American Platform or western edge of the Russian Platform. These broad, up to a few thousand kilometers-long, belts were intruded in Early Riphean by hundreds of large (up to 100 km in diameter) anorthosite, syenite, gabbro, granite–porphyre, and rapakivi granite plutons and by normal potassium granites.

This unique and never again repeated Early Riphaean phenomenon is still waiting for an explanation. It may be suggested that all these plutons were the result of secondary remelting of the sedimentary rocks accumulated over 200–300 MMY on the passive continental margins (fragments of Megagaea fragmented 1.7–1.6 BY ago). The end part of Early Proterozoic and the beginning of Early Riphaean were the epochs when massive iron ore formations accumulated on the continental shelves. So, it is possible that the remelting of huge shelf sequences (12–15 km thick) was facilitated by their high iron-oxide content. It is possible that the density of these sediments exceeded that of the mantle matter (the mantle matter density is about 3.3 $g/cm^3$ and the jaspelite density is over 4 $g/cm^3$). Because of that, during riftogenesis such sediments could have "fallen" into the hot mantle. After remelting of the sediments and liquation of the melts, the iron compounds sunk into the mantle, whereas the light silicate magmas floated up to the surface and crystallized there at shallow depths as granitoid or alkaline plutons (Sorokhtin and Ushakov, 2002; see Chapter 10).

This was even more likely because at that time the thickness of Middle Proterozoic oceanic plates did not exceed 40 km, that is, they were half of the present-day plates in thickness (see Fig. 7.3).

The originally depositional origin of anorthosite–rapakivi–granite magmas is supported by the strontium ratios in these rocks. The primary $^{87}Sr/^{86}Sr$ ratios for 15 anorthosite bodies in the North America and Norway are within the range of 0.703−0.706, the Vyborg rapakivi massif has 0.704. These are the ratios typical of the very end of Early Proterozoic and of Middle Proterozoic, whereas the mantle ratios for the same ages are in a narrow range between 0.7015−0.702 (see Fig. 7.13).

This was the reason why for the reconstructions we treated the anorogenic volcanoplutonic belts as the indicator complexes of passive continental margins. Besides, at the reconstruction of Megagaea disintegration its fragmentation into individual continents was done along the collision sutures of the Grenville orogeny (the orogeny occurred at the next consolidation stage of the third supercontinent, Mesogea = Rodinia). It was also assumed that the Megagaea fragments drifted centrifugally in various directions from the center of gravity of the former supercontinent. The so generated reconstruction of the continents—fragments of the disintegrated Megagaea at the time about 1.4 BY ago is shown in Fig. 9.5.

Our reconstruction of the next supercontinent, Mesogea was based on an assumption that the newly emerged descending flow of a single-cell convection structure, as in the case of Megagaea, occurred within the opposite Earth hemisphere. That theoretical assumption


**FIGURE 9.5** Megagaea disintegration about 1.4 BY ago (see Fig. 9.1 for the legend).

was relied on in combining the continents into a single structure of the new supercontinent. Also taken into account were inherited nature of the continent movements and the paleoclimatic data on the distribution of the red-bed weathered crusts in Middle Riphaean (Anatolyeva, 1978). Another issue taken into consideration was the event of the future glaciations, about 800 MMY ago, simultaneously in the South and North America, on the Brazilian craton and in the Eastern Australia. That was the reason why in our Mesogea reconstruction Australia is shown in a position of the approach with South Africa.

Paleomagnetic latitude determinations for Middle Riphaean are yet not very reliable so we did not use them the Mesogea reconstruction. At the same time, the paleomagnetic inclinations apparently may be used as secondary information. To do this, we took directions to the poles for each subcontinent for the time 1 BY ago from the reconstructions by Zonenshein et al. (Monin and Sorokhtin, 1986) and by Piper (1976). These directions are shown as arrows on our reconstruction (Fig. 9.6).

A distinctive Middle Riphean feature was a drastic weakening of riftogenesis so typical of the previous epoch and no less drastic increase in orogenies. Middle Riphaean Grenville diastrophism (about 1 BY ago) manifested itself on the periphery of almost all Early Proterozoic platforms.

Grenville folded belts were used as one of the major criteria in Mesogea reconstruction. We tried to superpose same-type Grenville mobile belts at the edges of the adjoining continents. For instance, in the eastern North America arose at that time the Grenville mobile belt which most likely was the collision zone with Northern Europe. Khain and Bozhko (1988) remarked

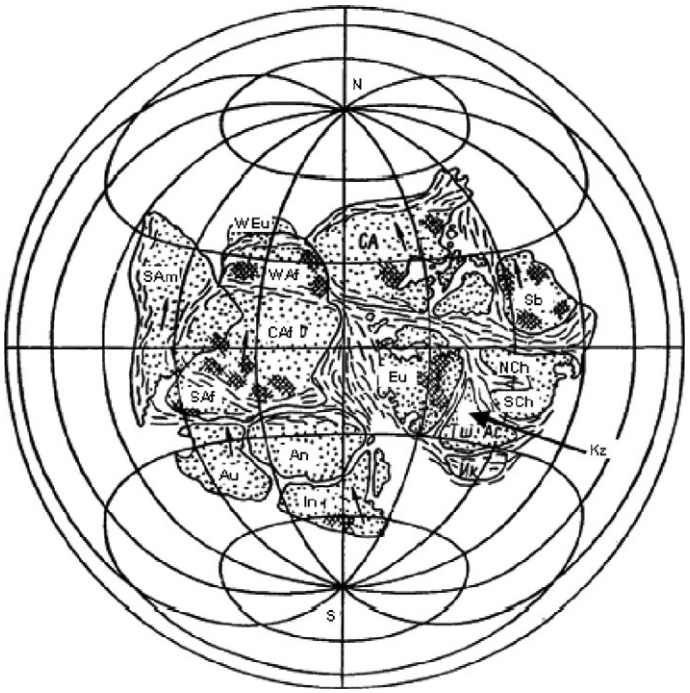


**FIGURE 9.6** Megagaea supercontinent reconstruction for the epoch about 1 BY ago. Arrows are paleomagnetic inclinations borrowed from Monin and Sorokhtin (1986) (see Figs. 8.2 and 8.4 for the legend).

in this respect that about 1 BY ago the Grenville mobile belt joined North America, Greenland, Ireland, North UK, Scandinavia, and North France into a single continental plate. We may add that merged with North America through these areas were also the Baltic Shield and the Russian Platform. However, the Northwestern Europe with the Armorican massif was still separated from the rest of Europe and most likely was adjacent to Africa.

The Timan structures and the subduction Masyutkov metamorphic complex of the Southern Urals were started in Middle Riphaean. The Grenville tectogenesis in Kazakhstan and in the basement of West Siberia actually united the Russian and Siberian platforms through the system of the Yenisey Range. Grenville age orogeny engulfed the Kazakhstan-Tyan-Shan, Altay-Sayan, and Baikal-Vitim folded regions as well as Northern Mongolia. By the end of Middle Riphaean, sedimentary sequences in the rift troughs and framework of the Chinese Platform were intensely folded; besides, the island-arc and marginal-sea environments existed in place of the South-China craton.

This brief list includes the geography of the collision fold-belts which soldered the adjoining platform. It shows that in Middle Riphean, about 1 BY ago, all northern continents merged into a single supercontinent, Laurasia, although its outlines were still different from the classical Wegener's Laurasia, which later was a component in Pangaea. The difference was associated with the probable position at the time of the Chinese Platform between the Siberian and Kazakhstan plates. This is supported in particular by age-equivalent glaciations in Europe, Kazakhstan, and the Chinese Platform dated about 650 MMY ago (Chumakov, 1978, 2006).

The southern continents about 1 BY ago were also joined into a second supercontinent, Gondwana. At that time, the Amazon Plate was joined along a sublongitudinal folded system Arasha-Estrondu with the Brazilian platform, and through it with the Central Africa. Simultaneously, the Southern Africa welded to the Central African Platform through the Cybaides folded buildup. It also merged through the longitudinal folded zone of Hoggar with West Africa. The eastern Gondwana including Australia, Antarctic, and India was merged with the eastern edge of the African mega-shield through the extension of the Kibar folding in the Mozambique mobile belt and the folded system of the Somali Horn and Arabian Peninsula. In the Antarctic, a tectonothermal basement reworking zone in the Trans-Antarctic Mountains (East Antarctica) corresponds with this belt.

Most likely, both Middle Riphean supercontinents were merged into a single large supercontinent Mesogea. This is supported by intense folding and magmatic activity in the Arabian-Nubian Gondwana area and in the folded belt of the Dalsland orogeny in the South-European framework of Laurasia. From the Europe's side, the basement of the Pannonian depression, the central portion of the Rodop Massif, and possibly of the Serbian–Macedonian Massif belong to the relics of this Grenville belt branch. The extension of the belt goes probably to the Crimea.

The reconstruction accounting for all the aforementioned criteria is shown in Fig. 9.7. It shows that the supercontinent Mesogea was a compact formation somewhat reminiscent in its outlines of the Paleozoic Pangaea (Fig. 9.11). Exceptions are the Eastern Gondwana turned at 90° to its position on the Wegener's Pangaea reconstruction and the Chinese Platform which is located on our reconstruction still between the Siberian and Kazakhstan plates.


**FIGURE 9.7** Mesogea disintegration into Laurasia and Gondwana about 800–750 MMY ago (triangles are tillite and tillitoid locations, after Chumakov, 1978).

## 9.5 DISINTEGRATION OF MESOGEA AND PANGAEA FORMATION AT THE END PALEOZOIC

Similar to the preceding supercontinents Mesogea existed over a relatively short period of time (no greater than 100–150 MMY) and some time around 900 MMY ago began to disintegrate into the northern part (Laurasia) and the southern part (Gondwana). Approximately 850 MMY ago, a wide oceanic basin of Proto-Tethys emerged between them. About 800–750 MMY ago, Laurasia moved into the northern near-polar area, and Gondwana, toward the South Pole. This is supported by numerous Late Riphaean tillite and tilloid finds on these two supercontinents (Chumakov, 1978).

At the end Proterozoic, the climate cooled down substantially. The snow lines went down—even below the continent stand level in the high latitudes. As a result, a new era of glaciation epochs engulfed Earth (see Fig. 14.20). Besides, due to convection the mantle by that time became rather uniform, without large lateral density variations. For this reason, only the continent and ocean positions on Earth surface determined now the orientation of the main axes of Earth momentum of inertia and the position of its body in relation to its revolution axis.

Thus, the positions of the continents and oceans in the near-polar areas helped establish cold climate in Laurasia and Gondwana by the end Riphean and in Vendian. But that was

not the only factor. At that time, a wide ring-like oceanic basin emerged in the low latitudes. That favored the birth of a single powerful equatorial passat current with weak anti-passat branch current in the modern latitudes. A result was that the "water-heating" system of Earth's continental portions was drastically weakened in the end Riphean. That facilitated the development in the second half of Late Riphean of the African-Australian glaciation in Gondwana and the Canadian glaciation in Laurasia as well as a broad Lapland glaciation in Europe, Kazakhstan, and China in the terminal Riphean or Vendian (Figs. 9.7 and 9.8).

In Late Riphaean and Vendian, as in Early Riphaean, most former Middle Riphaean Mesogean orogenic mobile belts died out. Riftogenic structures formed in their place. On the continental platforms emerged at that time a network of aulacogens which usually inherited the old sutures of Svekofenian (Karelian) age. New ocean basins were beginning to form along the younger sutures of Grenville folded belts. For instance, about 800 MMY ago a new Proto-Atlantic Ocean Japetus emerged in place of a Grenville mobile belt which welded in Middle Riphaean the east coast of North America and Greenland with the European platform.

At the same time, the West Gondwana was cut by Red Sea-type narrow oceanic troughs of the West African and Brazilian sub-oceans with the Katanga Bay. A rapidly expanding African-Australian oceanic basin emerged between the West and East Gondwana. This basin probably caused the transformation of the general Gondwanan structural plan (see Fig. 9.8).


**FIGURE 9.8** Laurasia and Gondwana disintegration about 650 MMY ago (see Fig. 9.1 for the legend).

Geology of the present-day eastern edges of Africa and Australia as well as the Trans-Antarctic Mountains does not contradict a hypothesis of a Late Riphaean oceanic basin between these continents. Indeed, the Mozambique belt in Africa, the Adelaide geosyncline in Australia, and the Trans-Antarctic Mountains were at that time passive continental margins.

It is important that the actual data about the ice sheet (tillites and tilloids) distribution on the southern continents in Late Precambrian are a very rigid requirement for Gondwana reconstructions in Late Riphaean and in earlier geological periods. These data (Chumakov, 1978) indicate that about 750 MMY ago glacial sheets simultaneously existed in the South and Central Africa, Australia, and Eastern South America. That forces us to build our reconstruction of the southern continents in Late Riphaean so that all glaciated continents were always located compactly around the southern geographic pole. The geological formations—glaciation indicators—are much more reliable than the Precambrian paleomagnetic data. For this reason, in our Middle and Late Riphean Gondwana reconstructions we show the juncture of the supercontinent's eastern and western fragments not in a conventional way but along the line of the Australian and Antarctic continents attachment to Africa (see Figs. 9.6 and 9.7).

The same goes with the locations of the northern continents in the Riphaean reconstruction of Laurasia. Our Late Precambrian reconstructions show the Chinese Platform not in the south Laurasia but in the territory adjacent to the Northern Europe (see Fig. 9.8).

In some cases, the paleoclimatic data help estimate also the width of the intercontinental oceanic basins. For instance, we estimate the width of the circum-equatorial Proto-Tethys in Late Riphaean at about 6000–10,000 km (see Fig. 9.7). Similarly, the width of the Japetus paleo-ocean in Vendian was at least 2000 km, whereas the Paleo-Urals Ocean was still narrow (see Fig. 9.8).

Folding in the second half of Riphaean occurred within the limited regions of both supercontinents. In Laurasia, orogenic activity was preserved only in the Indochina parts adjacent to the Chinese Platform and in the Yenisey Range. In Gondwana, mobile fold-belts continued to form only in the east of the Arabian craton and in the adjacent parts of the Antarctic Platform on the side of the modern Weddell Sea.

During Vendian, practically all Laurasian continents and cratons continued to be under the riftogenic structure formation environment, with the passive continental margin regime along their periphery. Only in the Timan-Pechora mobile belt folding and overthrusting developed at the end Vendian. In general, however, the Laurasian continental massifs in Vendian, like in Late Riphean, continued their centrifugal drift.

Contrary to that, in terminal Riphean (=Vendian) Gondwana moved into the area of a descending mantle convection flow. That predetermined a complete about face in the tectonic regime of this supercontinent. As a result, South America and Africa were involved in an intense compression with the closing of all preexisting narrow oceanic troughs in whose place inter-craton folded structured of the Pan-African orogeny now emerged. At the same time, the Eastern Gondwana again merges with the Western one along the Mozambique belt on the eastern edge of Africa. This is a partial explanation of the intense orogenic motions in the entire Mozambique belt by the end Vendian (~630–600 MMY ago). The final Gondwana consolidation, however, occurred somewhat later, in Cambrian and Ordovician, after the last activation phase of this belt about 550–450 MMY ago. This time,

the southern supercontinent outlines became the same as on the conventional reconstructions of the Wegener's Pangaea (see Figs. 9.9 and 9.10).

As we could see, the merged supercontinent position in the near-polar zone caused a strong instability in Earth's revolution. As a result, its body tended to rotate so that the center of gravity of such continental massif would eventually end up on the equator because it is the only situation where the main axis of the planet's moment of inertia maximum value coincides with its revolution axis. However, when two approximately equal supercontinents are positioned near the poles asymmetrically but within the same hemisphere, a quasi-stable situation may occur where the common center of mass of these continental massifs is within Earth's equatorial plane. Also, Earth's revolution may be stable when its revolution axis coincides with the third axis of the moment of inertia which is minimal for this axis. In such a case under the laws of mechanics Earth revolution is stable. This is the situation with modern-day Earth. The large axis of its main moment of inertia is somewhere in the Central Pacific South of the equator. The small axis is in the Northern polar basin near the geographic pole.

Figures 9.8 and 9.9 show the reconstruction options satisfying this condition.

The emergence in Late Riphaean (Vendian) of this quasi-stable situation can explain a relatively long (about 200 MMY) stay of significant continental masses in the Earth's near-polar areas without a noticeable rotation of its body into a position where both supercontinents (Gondwana and Laurasia) would turn out at the equator. If the supercontinents were positioned in these near-polar areas more symmetrically in relation to the geographical


**FIGURE 9.9** Mesogea disintegration at the time about 550 MMY ago (see Figs. 9.2, 9.4, and 9.7 for the legend),


**FIGURE 9.10** Wegener's Pangaea at about 200 MMY ago. After Smith and Brieden (1977).

poles such Earth's rotation and the movement of both supercontinents to the equator, at the average mantle viscosity $10^{23}$ P, would have occurred in less than 150 MMY.

Nevertheless, the continental drift in Late Riphaean and Vendian was continuously changing the orientation of Earth's moment of inertia's axes. As a result, the adequate rotations of its body relative the geographic poles must have been happening. During Late Riphaean and Vendian, frequent alternation of ice periods and warm periods occurred on the same continents (Chumakov, 2006). It is possible that the cause was just these Earth's rotations relative to its revolution axis in combination with the continental drift.

In particular, at the Vendian–Cambrian time boundary, during the final formation of the Paleozoic Gondwana about 550 MMY ago, due to the general Earth's rotation by 90°, West Africa turned out at the South Pole and North America, Europe, and Australia, at the equator (Fig. 9.9). By that time, the West Europe block probably separated from West Africa and began its drift to the European Platform with which it merged in Paleozoic along the Rhenohercynian suture. As a result, in Cambrian most continents were positioned at low latitudes and that predetermined the emergence of the warm climate so characteristic of this period. Sheet glaciers at that time were developed only within a limited area in West Africa. This may explain a rapid (at a rate of close to 5 cm/year) apparent pole movement on the continent of Gondwana from West Africa in Late Ordovician to Antarctica in Early Permian.

Paleomagnetic data become much more reliable for Phanerozoic, especially its second half. Thus, the outlines of the last supercontinent Pangaea (predicted by Wegener, 1922 as

early as in 1912) are usually determined from the paleogeomorphologic features in the near-shore areas of the adjoining continents and from paleomagnetic data. One of the best reconstructions (by Smith and Briden, 1977) is presented in Fig. 9.10.

As was the case with the previous supercontinents, the Pangaea's center of gravity was also located in the lower latitudes although by that time the continents increased and stretched in a broad band almost from one pole to the other. If we accept this reconstruction, it turns out that Pangaea (which emerged at the end Paleozoic) was in such a quasi-stable state relative to the Earth's revolution axis where the third, small axis of the planet's moment of inertia coincided with the revolution axis. With such configuration Pangaea could have preserved its orientation toward the Earth's revolution axis *ad infinitum* if not for its disintegration about 200 MMY ago and a new period of centrifugal continental drift.

The drift effects on Earth's position during Phanerozoic were discussed in detail in a publication by Monin and Keondzjan (Sorokhtin, 1979). A reminder: the small axis of the Earth's main moment of inertia currently coincides with the Earth's revolution axis. Despite this, the planet continues its stable revolution without any tendency for a significant apparent pole drift.

## 9.6 CONTINENTAL DRIFT EVOLUTION IN MESOZOIC AND CENOZOIC. FUTURE FORECAST

The history of Pangaea's split and subsequent centrifugal drift of the component continents in Mesozoic and Cenozoic up to their current positions is known in detail (Zonenshein et al., 1976; Zonenshein and Gorodnitsky, 1977; Smith and Briden, 1977). For this reason, we will only provide a single reconstruction for an intermediate epoch (around 60 MMY ago). It is presented in Fig. 9.11. For a comparison, the present-day continents' positions are provided in the Lambert projection in (Fig. 9.12).

Figures 9.10–9.12 show the gradual opening of the Atlantic Ocean and gradual closing of the Tethys Ocean in place of which a grandiose Alpine-Himalayan mountain belt arose at the end of Cenozoic. The figures show the Africa's and Arabia's northward drift that gradually closed the western part of Tethys. Only small relics of this old and large ocean presently remain as the Eastern Mediterranean, Black Sea, and the southern depression of the Caspian Sea. The emergence of the Alps and Caucasus was significantly related to the Afro-Arabian Plate collision with the island arcs that framed from the south the West European and Russian platforms.

Another and apparently most representative example of the formation of planet's highest mountain systems is given by the rush India drift from the southern into the northern hemisphere.

India separated from Antarctica about 100 MMY ago and collided 30 MMY ago with the southern edge of the Asian continent. Thus, over 70 MMY it rode 6600 km at a rate of over 9 cm/year. The collision of India with the Asian continent and its currently continuing northward movement resulted in the formation of the Hindu Kush, Pamir, and Himalayan mountain belts as well as the high-altitude Tibetan Plateau. Figure 9.10 shows an intermediate stage in the Indian Ocean formation with the Indian Subcontinent in the middle, with Madagascar already separated but Australia still connected to Antarctica (it separated somewhat later, about 50–40 MMY ago).

**FIGURE 9.11** Pangaea disintegration (about 60 MMY ago). After Smith and Brieden (1977).

Summarizing the supercontinent buildup and destruction, one can line them up by the time of their formation (see Fig. 9.13). A: Monogaea (2.5–2.3 BY ago); B: Stille's Megagaea (1.8–1.7 BY ago; C: Mesogea–Rodinia (1.0–0.9 BY ago); E: Wegener's Pangaea (230–100 MMY ago). The same figure shows the result of Mesogea split into two smaller supercontinents that played an important role during the last 900 MMY of the Earth's geological evolution, northern Laurasia, and southern Gondwana. For comparison, the present-day continental positions are shown. Still, only four first buildups, A, B, C, and D, were the genuine supercontinents.

When a single-cell convection structure emerges, all continental massifs drift toward the single descending flow and form above it a single supercontinent like Monogaea, Megagaea, or Pangaea. It was always accompanied by a burst in the Earth's tectonic activity at the time of supercontinents formation (see Fig. 6.8). After the formation of such a supercontinent, it naturally turns out to be as if surrounded from all sides by the subduction zones through which the oceanic plates of the surrounding single ocean, Pantalassa, sink into the mantle. At a regular subduction rate of about 5–10 cm/year, these plates in a few tens of millions of years will descend to the core level. There, they will be completely destroyed (disintegrated) due to the action of the iron-oxide differentiation barodiffusion mechanism (see Section 4.4).

The mantle matter barodiffusion differentiation effect depends on the time of its sojourn under a high pressure (over 0.9 Mbar). The descending matter itself is always somewhat colder, therefore denser than the surrounding mantle. For this reason, it is natural to expect

**FIGURE 9.12** Continental and ocean positions on present-day Earth; Lambert projection. After Smith and Brieden (1977).

that the mantle matter underneath the subduction zones will dent the core and form there the likeness of the descending flow roots (Fig. 9.14).

Therefore, after the differentiation the disintegrated mantle matter of these roots should, in the form of a liquid "magmatic gruel," flow off of them (i.e., rise) on both sides of the areas of the former lithospheric plates sinking into the core. Because of that, large masses of the differentiated, hence lighter, mantle matter begin accumulating under the center of the recently formed supercontinent. As a result, in the time on the order of a few tens of millions of years underneath the supercontinent a powerful ascending flow arises in place of the formed descending flow. This flow uplifts and breaks through the overlying lithospheric shell. The result is that the supercontinent splits and its fragments-continents centrifugally drift off its former center. That is probably why the supercontinents formed in the past geological epochs were unstable and existed only for short periods (no longer than 100 MMY) as unified continents. This pattern (actually, a law) may only be explained through the mechanism of a global chemico-density convection.

Reconstructions of the continent positions may be extrapolated into the future based on their present-day drift pattern. One such reconstruction advanced 50 MMY (Fig. 9.15) was performed in early 1970s by Dietz and Holden (1972). It shows that in 50 MMY both the Atlantic and Indian Oceans will be much wider. The Pacific Ocean will shrink correspondingly. North and South America will shift westward, Africa northeastward, Europe, Asia and India eastward, and Australia northward. They all will reach the equator. Antarctica will remain almost unchanged relative to the South Pole.

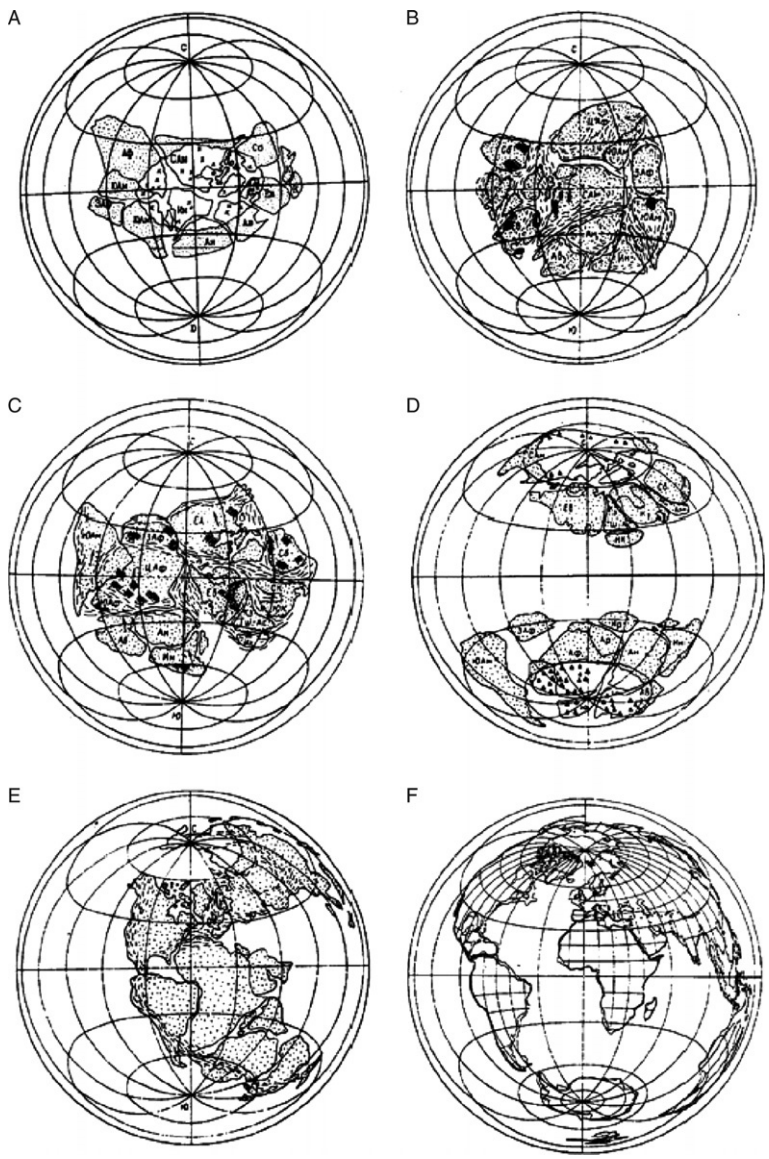


**FIGURE 9.13** Paleo-reconstruction of continent and ocean positions, Lambert projection: (A) Monogaea, 2.6 BY ago (unshaded areas of the continents are ice sheets; crosses are tillites and tilloids after Chumakov (1978); (B) Stille's Megagaea, 1.8 BY ago (wavy shading is folded belts; black spots are red-bed sequences after Anatolyeva (1978); (C) Mesogea, 1.0 BY ago; (D) Mesogea split into Laurasia and Gondwana, 750 MMY ago (unshaded areas of the continents are ice sheets; triangles are tillites and tilloids after Chumakov (1978); (E) Wegener's Pangaea, 200 MMY ago (reconstruction by Smith and Briden, 1977); (F) current continent and ocean positions.

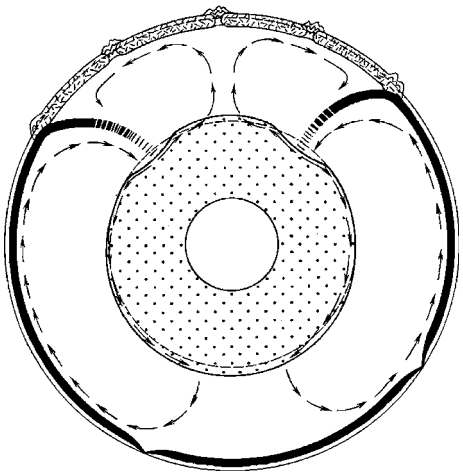

**FIGURE 9.14** Supercontinent destruction mechanism due to the emergence underneath it of a new ascending mantle flow instead of the previous descending flow.

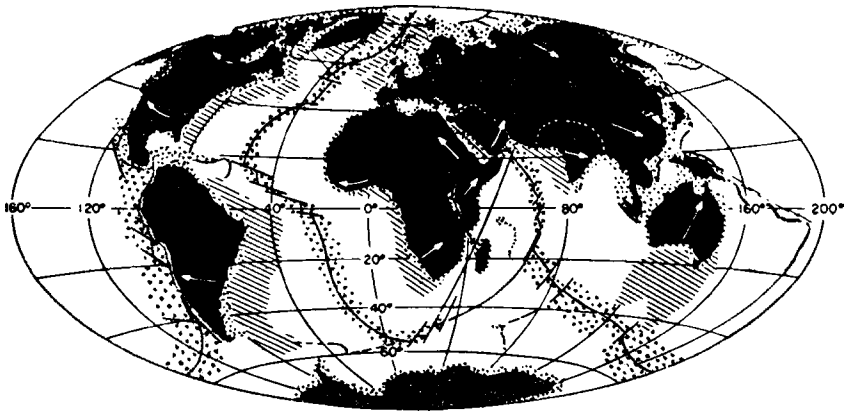


**FIGURE 9.15** Forecast of continent positions 50 MMY from now after Dietz and Holden (1972): oblique shading is the current continent positions, black shading is their positions 50 MMY from now; large dotted shading is build up of new oceanic crust; small dotted shading is shelves.

CHAPTER

# 10

# Major Patterns of Economic Deposit Concentration within Earth's Crust

Major patterns of ore matter concentration in the Earth's crust and the very origin of the economic deposits (especially endogenous deposits) are closely associated with the global evolution processes. On the other hand, the exogenically emerged commercial deposits are strongly related also with the evolution of the global climate. At the same time, the identified patterns in the spatial and temporal distribution of commercial deposits can often serve as reliable indicators of the very process of the Earth's evolution.

For this reason, numerous metallogenic concepts were mostly based on the once reigning theoretical ideas about the evolution of geotectonic and petrologo-geochemical processes. After the emergence of the global evolution theory based on plate tectonics, it became possible to discuss all these complex problems from a unified theoretical position.

In-depth analysis showed that metallogenic epochs are inimitable moments in the planet's evolution. This is understandable as, thermodynamically, Earth is an open dissipative system irreversibly losing its endogenous energy to outer space. Therefore, its evolution must be irreversible. Here, we discuss the issue of the origins of commercial deposits and the major patterns of their spatial and temporal distribution from the position of the most general physical theory of the Earth's global evolution.

## 10.1 EARTH'S CRUST ORE AND LITHOPHILIC ELEMENT CONCENTRATION MECHANISMS

There is a problem in explaining the formation of large local accumulations in the Earth's crust of ores and some other dispersed elements. Their concentration in the mantle is negligibly small but grows hundreds and thousands times in commercial deposits. The concentrations of uranium and gold in the present-day mantle do not exceed $2 \times 10^{-9}$, of mercury and thorium $8 \times 10^{-9}$, of lead $9 \times 10^{-8}$, of silver, tungsten, and platinum about $10^{-7}$, of lithium, niobium, molybdenum, and tin $10^{-6}$, etc. Besides, it follows from the modern

*Developments in Earth and Environmental Sciences*, Volume 10
DOI: 10.1016/S1571-9197(11)10010-5

views on the origin and evolution of Earth that over 4 BY of tectonic activity, the matter in both the upper and lower mantle was well stirred by the convection flows and is on the average uniform in its composition on different levels. Thus, the presence of local non-uniformities with elevated concentrations of ore elements should not be expected. Only the most common of the mantle ore elements (such as chromium) can form purely endogenous aggregations by way of a direct differentiation of the mantle melts. An example is given by the chromite commercial deposits in the Earth's ophiolite belts.

It is important that, based on the melt-out conditions of the oceanic basalts and their content of juvenile water, the mantle is practically dry; its water content does not exceed 0.05%. Thus, in the mantle, there cannot be any fluid flows capable of bringing ore elements into the crust.

With the emergence of a new geological theory—the tectonics of the lithospheric plates—new approaches opened to understanding the mechanisms through which the Earth's crust may be enriched in ore elements, carbonates, and silica rocks. In particular, it was found that the major mass of the endogenous commercial deposits within the continental crust may have formed only through a multi-step process of ore elements concentrating in the crust. And the first step in such concentration occurs in rift zones on the ocean floor.

It was found that very powerful hydrothermal systems are operating in the oceanic rift zones and on the slopes of the mid-oceanic ridges (Fig. 10.1). Through these systems, Earth loses more than 30% of its endogenous heat (Sorokhtin, 1974). Our estimates are that the average total water-exchange rate in all oceanic hydrothermal springs of the mid-oceanic ridges is approximately 2300 $km^3$/year. At such a rate, the entire oceanic water mass ($1.42 \times 10^{24}$ t) runs through the active hydrotherms and seepings of mid-oceanic ridges, with their wide and low-angle slopes, in about 0.6–1.0 MMY.

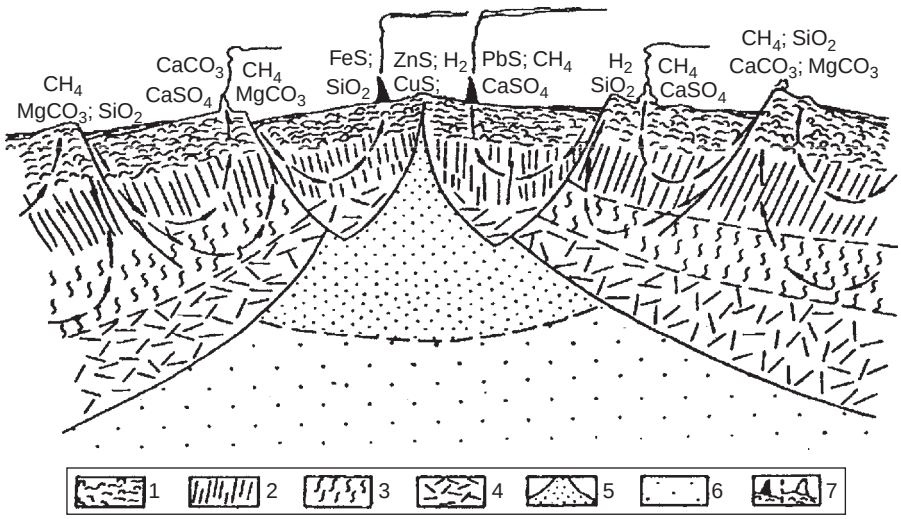


**FIGURE 10.1** Ocean crust formation and geochemistry of hydrothermal processes in mid-oceanic ridge rift zones: 1. Basalts (pillow lavas); 2. Dolerite dykes; 3. Serpentinite layer; 4. Subcrustal lithospheric layer; 5. Magmatic note underneath the crest of a mid-oceanic ridge; 6. Asthenosphere; 7. Black and white smoker buildups; the arrows show paths of the oceanic water within the oceanic crust.

Enormous amounts of endogenous matter (including chalcophilic ore elements and silica, zinc, copper, lead, and other metal sulfides; Lisitsin, 1978; Lisitsin et al., 1990) are brought into the oceanic crust and hydrosphere through the rift zone hydrothermal systems. In the Pacific alone, over the recent 150 MMY, about $(10–15) \times 10^{12}$ t of the polymetallic ore matter was supplied this way from the hydrothermal sources (Gurvich, 1998). In the rift zones, the hydration of the near-surface mantle layers occurs and the chemical reactions take place that are important for maintenance of the stable ecologic environment on Earth and for the formation of the carbonate and silicate facies. All reactions are exothermal so they are irreversible. The main reactions are those hydrating the oceanic crust. They bond carbon dioxide in carbonates, which later are consumed by living organisms and are buried in the oceanic deposits:

$$\underset{\text{olivine}}{4Mg_2SiO_4} + 4H_2O + 2CO_2 \rightarrow \underset{\text{serpentine}}{Mg_6(Si_4O_{10})(OH)_8} + \underset{\text{magnesite}}{2MgCO_3} + 72.34 \text{ kcal/mol}, \quad (10.1)$$

$$\underset{\text{anorthite}}{2CaAl_2Si_2O_8} + 4H_2O + 2CO_2 \rightarrow \underset{\text{kaoline}}{Al_4(Si_4O_{10})(OH)_8} + \underset{\text{calcite}}{2CaCO_3} + 110.54 \text{ kcal/mol}. \quad (10.2)$$

These reactions help maintain the equilibrium and relatively low partial pressure of carbon dioxide in the atmosphere and supply to the ocean the source material for the normal life activity of skeletal organisms (including corals, mollusks, foraminifers, and coccolithophorids) which eventually form carbonate rocks.

When the pyroxenes are hydrated, abundant amounts of silica are released from the rift zones:

$$\underset{\text{enstative}}{6MgSiO_3} + 4H_2O \rightarrow \underset{\text{serpentine}}{Mg_6(Si_4O_{10})(OH)_8} + \underset{\text{silica}}{2SiO_2} + 27.38 \text{ kcal/mol}, \quad (10.3)$$

It is the source of the material for the organisms with silica skeletons and for the deposition of siliceous sediments, for the formation of flints and jaspers. When the bivalent iron silicate is oxidized to the trivalent state, the abiogenic methane forms in the presence of carbon dioxide:

$$\begin{aligned} \underset{\text{fayalite}}{4Fe_2SiO_4} + \underset{\text{forsterite}}{12Mg_2SiO_4} + 18H_2O + CO_2 \rightarrow \underset{\text{serpentine}}{4Mg_6(Si_4O_{10})(OH)_8} \\ + \underset{\text{hematite}}{4Fe_2O_3} + \underset{\text{methane}}{CH_4} + 183.47 \text{ kcal/mol}, \end{aligned} \quad (10.4)$$

When iron is oxidized without $CO_2$, hydrogen emerges:

$$\underset{\text{fayalite}}{Fe_2SiO_4} + \underset{\text{forsterite}}{3Mg_2SiO_4} + 5H_2O \rightarrow \underset{\text{serpentine}}{Mg_6(Si_4O_{10})(OH)_8} + \underset{\text{hematite}}{Fe_2O_3} + H_2 + 30.72 \text{ kcal/mol}. \quad (10.5)$$

Calculations show that about 9 million tons/year of $CH_4$ and approximately the same amount of $H_2$ are generated in the oceanic crust rock hydration. At such a rate of methane generation, more hydrocarbons would emerge on Earth than there is now available. Therefore, most of this methane is oxidized by the methane-consuming bacteria or removed to the atmosphere together with hydrogen. However, a significant part of these volatile emanations may be preserved in the oceanic deposits and form in them hydrocarbon accumulations, for instance, in the form of gas-hydrates (Balanyuk and Dongaryan, 1994).

Many ore elements, including iron, zinc, lead, copper, manganese, and other dispersed elements, are carried out of the mantle in the oceanic rift zones. Sulfur is also carried out and forms sulfides of these ore elements, although a substantial portion of it enters the rift zone sulfides through the reduction of the sulfate sulfur from the oceanic water by methane and hydrogen from the same zones under the following reaction:

$$\underset{\text{magnesium sulfate}}{MgSO_4} + \underset{\text{methane}}{CH_4} \rightarrow \underset{\text{magnesite}}{MgCO_3} + \underset{\text{hydrogen sulfide}}{H_2S} + H_2O + 11.35 \text{ kcal/mol.} \quad (10.6)$$

The released hydrogen sulfide is a highly "aggressive" mineralizer (releases plenty of energy in reactions). It immediately reduces iron and other ore metals (copper, zinc, lead) to sulfides by literally "sucking them" out of basalts and oceanic crust ultramafic rocks, for instance, through the following reaction:

$$\underset{\text{fayalite}}{Fe_2SiO_4} + 2H_2S \rightarrow \underset{\text{pyrrotine}}{2FeS} + SiO_2 + 2H_2O + 56.68 \text{ kcal/mol.} \quad (10.7)$$

All these elements eventually transfer from the water into the deposit. They form ore element sulfide deposits around the rift zone hot springs ("black smokers"), and on the ocean crust, a layer of the metal-bearing deposits (Lisitsin et al., 1990; Bogdanov et al., 2006). The sulfide deposits are gradually oxidized and destroyed, and their ore matter migrates to the metal-bearing deposits.

Besides the hydrothermal concentration of ore elements in the oceanic crust, the magmatogenic-banded chromite ore deposits usually form in its lower part, at the gabbroids contact with dunites and peridotites. The ores' origin is due to the mantle matter's direct differentiation in the magmatic node underneath the rift zones. Actually, these ores are the residue of a dense phase of basalt melt accumulates descended to the bottom of the magmatic node underlain by restite mantle rocks. This determined the usual chromite ore position between the layers of gabbro and dunites in the ophiolite complexes. Examples of such cumulative deposits are the Kempirsay Paleozoic chromite deposit in the South Urals and Mesozoic chromite deposits of the Balkan Peninsula.

It follows from the lithospheric plate tectonics theory that the second step in the crust enrichment with both lithophilic and ore elements occurs within the plate subduction zones underneath the island arcs and active continental margins due to their release from the oceanic crust. The ore element mobilization and transfer into the continental crust occurs due to the dehydration and remelting processes within the subduction zones of the oceanic crust, and the pelagic and terrigenous deposits sucked-in into the same zone. In the process, the abundant water bonded in the silicates is released. Powerful, hot and mineralized flows emerge which transport plenty of previously dispersed elements into the continental crust.

The oceanic crust rock dehydration reactions in the lithospheric plate subduction zones usually follow in reverse compared with the rift zones. They consume the already released compounds (such as $SiO_2$ and $(Ca,Mg)CO_3$) and release new components. Contrary to the rift zones, the release occurs endothermally, that is, with the addition of energy which is generated there due to the heat release in friction of the subducting plate with the frontal portion of the obducted plate. The main water- and silica-releasing reaction occurs due to deserpentinization of the third (serpentinite) ocean crust layer:

$$\underset{\text{serpentine}}{Mg_6(Si_4O_{10})(OH)_8} + 38.12\ \text{kcal/mol} \rightarrow 3\underset{\text{forsterite}}{Mg_2SiO_4} + SiO_2 + 4H_2O. \tag{10.8}$$

The olivine (forsterite), being a refractory component, descends into the mantle and the silica solution in water, and alkaline and other lithophilic elements rise and enter the continental crust.

The oceanic deposits are usually also sucked-in into the subduction zones (Sorokhtin and Lobkovsky, 1976). These deposits are always saturated with salt water. When they get into hot areas of the subduction zone, alkaline aluminosilicates form. They are also carried out into the continental crust and enrich it in the alkaline and other lithophilic elements, for instance, under the albitization reaction:

$$\underset{\text{kaolin}}{Al_4(Si_4O_{10})(OH)_8} + NaCl + 26.98\ \text{cal/mol} \rightarrow \underset{\text{albite}}{Na(AlSi_3O_8)} + HCl + 2H_2O + \underset{\text{diaspor}}{SiO_2} + 3AlO(OH). \tag{10.9}$$

At great depths, the aluminosilicates are enriched in potassium:

$$\underset{\text{kaolin}}{Al_4(Si_4O_{10})(OH)_8} + KCl + 23.88\ \text{kcal/mol} \rightarrow \underset{\text{orthoclase}}{K(AlSi_3O_8)} + HCl + 2H_2O + SiO_2 + \underset{\text{diaspor}}{3AlO(OH)}. \tag{10.10}$$

Chlorine plays a significant role in hypergenetic processes. The proof is not only the formation of some chlorine-containing silicates (skapolites, sodalites) but also the release of enormous amounts of gaseous HCl in the active volcanism areas. For instance, in 1919, only in the Valley of Ten Thousand Smokes (New Zeeland), nearly 1.25 million tons of HCl and 0.2 million tons of HF were released with water vapors.

The carbonate dissociation also occurs within the plate subduction zones. The alkaline-earth elements enter into the silicate composition, and free carbon dioxide is released, for instance, as in the following:

$$\underset{\text{serpentine}}{Mg_6(Si_4O_{10})(OH)_8} + 4SiO_2 + \underset{\text{calcite}}{2CaCO_3} + 59.5\ \text{kcal/mol} \rightarrow 2CaMg(Si_2O_6) + \underset{\text{diopside}}{4MgSiO_3} + \underset{\text{enstatite}}{4H_2O} + 2CO_2. \tag{10.11}$$

Under this reaction, enstatite and diopside, as refractory minerals, are removed into the mantle, and water and carbon dioxide again enter the hydrosphere and atmosphere.

The mechanism of the oceanic-to-continental crust conversion is cumulative and powerful. Thus, only within the time interval of the lithospheric plate tectonics activity (which is about 2.6 BY), the total mass of the water-fluidal flows in the subduction zones was 8–10 times the mass of Earth's hydrosphere and 13–16 times that of the ocean and sea water mass. This is a very important theoretical conclusion showing that the actual fluidal-water flows in the subduction zones are millions of times more powerful than the juvenile flows.

Nevertheless, the continental crust enrichment in ore elements in the subduction zones results in more or less uniform increase of their content along the subduction zones.

However, commercial deposits of some minerals (such as the sulfide ores) can still form. This is especially typical of the long-functioning subduction zones. There, tectonic erosion occurs on the obducting plate's frontal part and the recycling of crustal rocks and the plate-overlying sediments happens. That was probably how the unique copper–molybdenum ores in the South American Andes formed. Based on paleo-geodynamic reconstructions, the Pacific and Pre-Pacific Ocean crust was subducted there almost continuously for 1.5 BY.

In addition to the theory of the lithospheric plate tectonics, there is a third mechanism controlling the ore element concentration in the endogenous economic deposits. The weathering and deposit accumulation exogenous processes often involve the participation of live organisms and plants and strongly affect the element redistribution within the crust. The sedimentogenesis is usually accompanied by intense differentiation of the matter. Good examples are phosphorite, carbonate, sandy–clayey, and other differentiated sedimentary sequences with a very characteristic and unique mineralization. For instance, the Russian Platform clayey sediments contain, on the average, 11 times the concentration of tin, 20 times lead, 200–250 times potassium, 500–700 times rubidium, 1500 times barium, 3000–3500 times uranium, and hundreds of times rare-earth elements compared to the mantle composition. If the sandy–clayey sediments were deposited in a stagnant environment (which was common in Precambrian), then iron sulfides, copper, zinc, lead and molybdenum sulfides, and sometimes uranium oxides, tungsten hydroxides, and gold could accumulate in the sedimentary sequences.

A similar situation occurs with other sediments. For instance, carbonates contain several times strontium concentrations compared to those in the mantle. The evaporites concentrate sodium, potassium, calcium, sulfur, chlorine, and fluorine.

Live organisms accumulate within themselves many of the dispersed elements, including uranium and rare-earths (lanthanum, cerium, neodymium, etc.). That is why the phosphorites always include their concentrations many times higher than those in the mantle (for uranium, 20,000–25,000 times, for the rare-earth elements, 500–1000 times).

The clastic sediments are usually brought by the rivers or temporary flows to the continental margins and are deposited there on the continental slopes through avalanche sedimentation (Lisitsin, 1984). At the base of such clastic sequences are often found the evaporites formed at the early stage of the parent supercontinent split (for instance, the evaporites are known on the Atlantic shores, in the Red Sea, in the Gulf of Mexico, etc.). When such sediments get into a subduction zone or a collision zone of two continents, the entire gamut of the crustal intrusive rocks can melt out of them, from granites to syenites and to alkali-ultramafic rocks with their appropriate mineralizations. This also explains the often observed motley spatial distribution of the commercial deposits.

A fourth step in the continental crust enrichment with ore elements happens sometimes through the new crustal rock destruction and the repeated sedimentogenesis. For this reason, the later ore deposits of this type may turn out to be richer as their ore mass goes through a greater number of the recycling episodes over the time of the Earth's geological evolution. An example is tin deposits. The tin concentration in younger aggregations is usually higher than in the old ones. Thus, the total tin content in the Mesozoic aggregations is at least two orders of magnitude higher than in the Archaean ore occurrences (Sobolev et al., 2000).

The same goes with molybdenum. Its concentration (as well as the tungsten's) was gradually increasing in the young sediments as a result of magmatic reworking of the sedimentary sequences (Sobolev et al., 2000).

It follows from this that seemingly clearly endogenous commercial deposits ran through recycling, that is, through the concentration due to the destruction of the crustal rocks and subsequent sedimentogenesis under clearly exogenous environments.

Another demonstrative example of the significant exogenous effect over the formation of commercial deposits is hydrothermal aggregations. The water content in the mantle is negligibly low. Thus, all hydrothermal deposits without exception, regardless of their type, form either through the mobilization of the surface or ground water flowing around the hot magmatic bodies or through the release by the cooling magma of its dissolved water. In the latter case, in the process of its formation, the water-saturated magma picked up water from the water-saturated deposits or from the hydrosphere.

Ore aggregations of most fumaroles or hot springs in volcanic areas may be attributed to the first type of hydrothermal deposits. The "black smokers" sulfide deposits in the rift zones of the mid-oceanic ridges belong to the same category. A second type of hydrothermal processes is often accompanied by the pegmatite mineralization which occurs, for instance, over granitoid massifs or due to the hot mineralized water rising from the plate subduction zones. The granite massifs in the Post-Archaean time usually emerged due to the remelting of the sandy–clayey sediments in the continent collision zones, and the water got into the plate subduction zones together with the oceanic crust rocks that it saturated, and with the pelagic deposits. Thus, the water in hydrothermal aggregations in all cases comes from the hydrosphere, that is, it is an exogenous reagent.

## 10.2 EARTH'S CORE SEPARATION AND THE EVOLUTION OF METALLOGENIC ENVIRONMENTS

The Earth's crust environments and formation conditions changed along with the geological evolution. So did the formation regimes of the crustal economic deposits. As previously mentioned, evolutionary processes on Earth are irreversible. Thus, a careful application of the principle of uniformitarianism (the present is a key to the past), with constant evolutionary corrections, may be utilized to find major evolutionary patterns in the emergence of the economic deposits. For instance, it was found that there were no subduction zones in Archaean (see Fig. 7.5). It means that the continental crust formation regimes, as well as those for most endogenous commercial deposits, were at that time totally different and quite unlike the present-day ones.

Keeping that in mind, we will now discuss the issue of commercial deposits evolution based on the most general theory of the Earth's global evolution. The theory is based on a concept of the Earth's core separation and growth being the main energy process controlling the Earth's evolution as a whole.

As discussed in Chapter 3, the current concept of the Earth's origin is its (and other Solar system's planets) emergence through the accretion of a "cold" gas–dust protoplanetary cloud. The concept is based in particular on the studies by Schmidt (1946, 1948) and Safronov (1969). For this reason, Earth, immediately upon its origin, was a "cold," tectonically passive and compositionally and structurally uniform planet. Therefore, all ore and other elements were more or less uniformly distributed in the just formed volume at their Clarke contents and did not form agglomerations which could be attributed to the commercial deposits.

Thus, there were no commercial deposits in the young Earth.

Three large eons can be identified in the Earth's history: Katarchaean (same as Hadean) (4.6 to 4.0–3.8 BY ago), Archaean (4.0–3.8 to 2.6 BY ago), and Proterozoic together with Phanerozoic (2.6–0.0 BY ago). All three eons are unique in themselves and closely associated with the three stages in the core separation process discussed in Chapter 4 (see Fig. 4.1).

Initially, Earth was heated only due to the release within it of the tidal and radiogenic energy. As estimated in Chapter 5, the total amounts of energy released within its depths in Katarchaean (i.e., during the first 600 MMY of the Earth's life) were $2.1 \times 10^{37}$ erg (tidal energy) and $1.1 \times 10^{37}$ erg (radiogenic energy). Due to this heating, the primordial Earth's heat reserves increased from $7.12 \times 10^{37}$ to $9.2 \times 10^{37}$ erg in the beginning of Archaean. As a result, about 4.0 BY ago at a depth of 200–400 km in the equatorial belt where the tidal deformations were at the strongest, the upper mantle matter began to melt. That triggered into action the most powerful source of endogenous energy, the Earth's matter chemico-density differentiation. It involved the separation of the iron and iron oxide melts from the mantle silicates. In Archaean, this process was evolving under the zonal differentiation mechanism which led by the end Archaean to a "catastrophic" event of the core separation (see Fig. 4.1D and E). In the subsequent epochs, the process was evolving a quieter mechanism of the barodiffusion differentiation. This process played (and is continuing to play) a major role in inducing a large-scale mantle convection which is the main factor in the Earth's tectonic activity.

## 10.3 ARCHAEAN METALLOGENY

Thus, during Early and Middle Archaean, most siderophilic and chalcophilic elements from the Earth's primordial matter migrated together with iron and its oxides into the melted ring belt. Because of that, in Early and partially Middle Archaean, the convecting mantle above the sinking ring layer of the zonal differentiation of Earth's matter was impoverished in iron and other siderophilic elements (see Figs. 4.15 and 4.16). That is exactly why the Early Archaean continental shields and the greenstone belts within them had a relatively low metallogenic potential (Smirnov, 1980; Khain, 2000) and relatively low metallogeny with reserves of iron and other commercial minerals.

The iron-oxide melt migration toward the Earth's center and squeezing the primordial kernel out of there (Fig. 4.1D and E) must have been accompanied by squeezing of ore element-rich primordial Earth's matter from its central areas (from the young Earth's kernel) into the upper mantle. As a result, the Late Archaean oceanic plates began forming at the expense of the mantle matter significantly enriched in ore elements. This explains why the end Mid-Archaean and especially Late Archaean greenstone belts are ore-bearing, saturated by numerous siderophilic and lithophilic elements including gold, copper, nickel, platinum, platinoids, and polymetals. When the greenstone rocks were remelted in the lower portions of the Archaean crust (see Fig. 7.5), the Late Archaean granitoids also became ore-bearing.

The Earth's core separation about 2.6 BY ago was accompanied by the release of enormous amount of energy, $5 \times 10^{37}$ erg. The result was the planet's overheating and the

melt-out of the komatiites. In the process, intense convective flows emerged in the mantle. They totally and radically rebuilt the entire preexisting tectonic regime and led to the formation of the first supercontinent, Monogaea, which most likely happened at the very end of Archaean. This scenario is supported, in particular, by the paleomagnetic data. They show that Earth acquired the modern-type dipole magnetic field only about 2.6 BY ago, that is, at the Archaean/Proterozoic time boundary (Hale, 1987; see Fig. 4.17). The analysis of the lead isotope ratios (see Figs. 4.18–4.20) also testifies unambiguously that the Earth's core separated without melting of the silicate matter. Moreover, the above scenario of the Earth's core separation is well described by a double-step lead isotope ratio change model. Under this model, the isotope ratio evolution before this process occurred in a closed reservoir, and after the process began, the evolution accounted for the migration of sole lead to the core. Presently, about 30% of the planet's lead (radiogenic and primary) migrated to the Earth's core (Sorokhtin, 1999).

The earth's core separation process reflected first of all on the planet's tectonic activity. As mentioned, during the entire Katarchaean (4.6–4.0 BY ago) the young Earth remained tectonically passive. After the Earth's matter zonal differentiation started (it was accompanied by the iron melts separation from the silicates, see Fig. 4.1B), a convecting mantle emerged in the Earth's equatorial belt for first time. The mantle temperature rapidly exceeded the melting temperature of iron. After that, the first mantle matter melts appeared at the upper mantle level, and the embryos of the oldest continents began forming.

As can be seen in Fig. 5.17, maximum tectonic activity occurred in late Archaean. The total heat flow at the time exceeded its present-day value approximately by a factor of 13. In Early Archaean, despite high local tectonomagmatic activity, no more than 15% of the continental crustal mass was formed (Taylor and Mac-Lennan, 1985). At the same time, in Late Archaean over a shorter time interval 55% of it was formed, that is, 3.7 times more. This is another indication that the tectonomagmatic activity in Early Archaean manifested itself only within a narrow portion of Earth, whereas most of the planer remained cold and tectonically passive.

The averaged Earth's tectonic activity versus time curve (Fig. 5.17) smoothes out the changes associated with the tectonic cycles. The real curve is different in the superposition of quasiperiodic fluctuations (see Fig. 6.8) pertaining to the tectonic cycles, especially at the times of the supercontinent emergence. Another example is Fig. 11.9 displaying the tectonic activity curve for Phanerozoic (at a significantly stretched horizontal scale). The curve is based on the marine transgression and regression data.

In the environment of a high tectonomagmatic activity in Archaean, the upper mantle overheated above the melted iron separation zones (see Fig. 4.5). Oceanic crust spreading rate in the Archaean rift zones was very high, up to 400 $km^2$/year (see Fig. 7.3). At the same time, the "independent life" of the oceanic crust formed in these zones was correspondingly short, no longer than 10–15 MMY (see Fig. 8.11, curve *1*). That is why there were no thick and high-density lithospheric plates in Archaean as their formation takes 50–150 MMY. Instead, basalt sheets, no thicker than 15–30 km, emerged.

For this reason, plate subduction zones could not exist in Archaean. The compensation of the ocean floor spreading occurred in their pileup zones where the basalt sheets obducted one another and the younger continental massifs which formed at the time over the descending flow of the convecting mantle. The secondary remelting of these water-saturated

basalt sheets and deposits occurred at the base of the oceanic sheet pileup zones. It led to the melt-out of huge amounts of lighter continental magmatic rocks, trondhjemites, tonalites, plagio-granites, and just granites. They rose into the upper layers of the growing continental crust as diapires and domes (see Fig. 7.5).

## 10.4 NATURE OF A UNIQUE EARLY PROTEROZOIC ORE-FORMATION EPOCH

The upper mantle enrichment in the primordial Earth's matter increased at the very end of Archaean and in Proterozoic. This resulted in the concentration of ore elements in the upper mantle of the time. During the core separation at the Archaean/Proterozoic time boundary, the upper mantle composition changed radically. As previously mentioned, the cause was the addition of the matter from the former kernel of the Earth (with the primordial iron content of about 13–14%, iron oxides of about 23–24%, and siderophilic elements, chalcophilic metal sulfides and other ore sulfides, including platinoids). Thus, at the end Archaean and especially in Early Proterozoic, most favorable conditions for the formation of unique endogenous ore commercial minerals arose, and the epoch became the most outstanding ore-formation period.

The unique differentiated base and ultramafic intrusions of Early Proterozoic (about 2.3 BY ago) are direct indications of this. They invaded many old shields in the first impulses of the extension and the split of the Archaean supercontinent Monogaea. The most typical and classical example of this type of formations is the Great Dyke intrusion in Zimbabwe. It is a laminated complex of the Early Proterozoic mantle matter invading the Earth's crust. The chromite deposits in the Great Dyke are developed on its lower levels and are associated with the dunites and harzburgites. Platinum (as sperrylite $PtAs_2$) and the platinoids are encountered within sulfide layers between the ultramafic rocks and gabbro-norites.

In the Early Proterozoic, ultramafic and gabbro-norite intrusives of the Bushveld laminated magmatic massif (South African Republic), iron, titanium, chromium, and tungsten reach high concentrations. The layer-like nickel sulfide deposits include platinoids in commercial concentrations. The Bushveld pluton invaded a thick Transvaal Early Proterozoic volcanosedimentary sequence. As a result, the upper (gabbro-norite) part of the mantle intrusion came into contact with the crustal granites formed in the remelting of volcanosedimentary rocks encompassing the pluton. Thus, the lithophilic (hydrothermal) tin and fluorite mineralization is also associated with the Bushveld granites.

The other examples of this type of mantle intrusions are: the Sudbury norites intruding the Canadian Early Proterozoic Huronian volcanosedimentary sequence (copper, nickel, cobalt sulfides, platinum); the Canadian Stillwater deposit (chromium, titanomagnetite, platinoids), the Kambalda deposit in Australia (nickel, copper, platinoids), the Burakovsky intrusive in the SE Baltic shield (Russia) (chromite, nickel, vanadium, platinum, and possibly gold metallogeny). Apparently, a closely related type includes gabbro-norite Pechenga and Monchegorsk gabbro-norite intrusives with the sulfide copper–nickel and cobalt mineralization, the Kola Peninsula Pan intrusive and the Olong Group magmatic formations (Karelia) with platinum mineralization.

It is important to emphasize that intrusive formation of this type, with high concentrations of ore elements, did not occur either before or after Early Proterozoic. This is a testimony in support of the proposed model of the convecting mantle enrichment on the Archaean/Proterozoic time boundary by the primordial matter which rose from the central areas of Earth in the process of the core separation at the end Archaean (Fig. 4.1E).

Besides intrusive ore-bearing rocks, Early Proterozoic had sedimentary ores. The classical examples are the sedimentary iron ore of jaspelite formations and ore-bearing of the Witwatersrand sedimentary sequence in South Africa (see below). Thus, Fig. 10.2 illustrates the gold reserves distribution in time for the entire geological history (Starostin and Sorokhtin, 2002). There was indeed a drastic burst of the deposited gold in Early Proterozoic, most of it in the Witwatersrand deposits.

In Phanerozoic, the chalcophilic element recycling (including the gold) was strongly activated. It was associated with a high mobility of the chalcophilic elements and their lower resistance to weathering processes. Because of these, the chalcophilic elements were gradually carried out of the old rocks and redeposited in younger sediments. If such sediments got into the plate subduction zones or were in contact with hot mantle melts, they remelted with the formation of new (young) magmatic deposits, but their ore matter was old. A good example is tin, rare-metal, and gold fields in the Verkhoyansk–Kolyma fold zone. They are found in the Mesozoic but are underlain by the Precambrian (we will discuss it in more detail in Section 10.7). Their ore matter, however, is old and is derived from Archaean and Early Proterozoic matter redeposited during Paleozoic and Early Mesozoic in the near-shore deposits of the East-Siberian paleo-ocean.

After the separation of the Earth's high-density iron-oxide core, its further growth proceeded under a quieter barodiffusion mechanism. The Earth's tectonic activity noticeably declined in Proterozoic, the chemico-density convection emerged, the ocean floor spreading rate declined, thicker and "heavier" lithospheric plates formed, plate subduction zones appeared, and the lithospheric plate tectonics mechanism began operating.

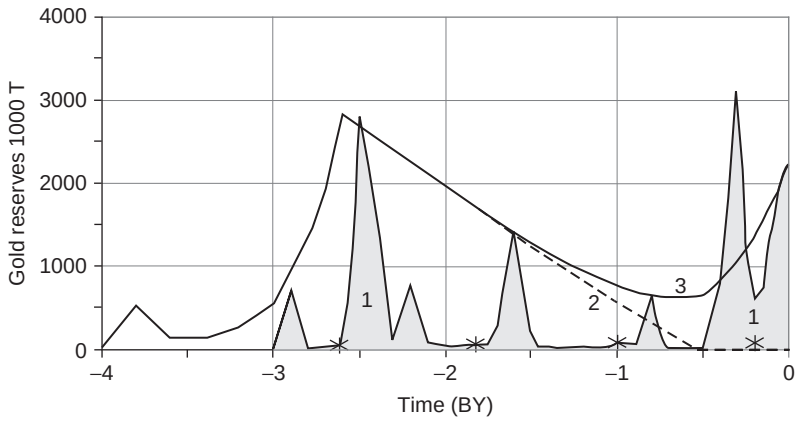


**FIGURE 10.2** Gold reserves distribution in Earth's geological history (after Starostin and Sorokhtin, 2002). 1. Golg reserves; 2. Relative concentration of metallic iron in the mantle shown in Fig. 4.15; 3. Curve accounting for the gold recycling in the young formations (asterisks are the supercontinent formation times).

The chemico-density convection is in its essence unstable and changes its structure. The result was that periodically, about once every 800 MMY single-cell mantle convective structures must have formed with one powerful ascending and one descending mantle flows (see Fig. 6.13). All then existing continents drifted to the center of such descending mantle flows and formed giant supercontinents on the like of the Wegenerian Pangaea. Four such supercontinents existed in the Earth's history (see Figs. 9.2, 9.4, 9.6, and 9.10): Monogaea (2.6 BY ago), Stille's Megagaea (1.8), Mesogea or Rodinia (1.0) which later (in 120–200 MMY) disintegrated into two large continents (Laurasia and Gondwana) and the Wegenerian Pangaea (about 220 MMY ago).

Sequential stages of the supercontinent emergence and destruction predetermined the manifestations of different metallogenic environments. Thus, at the time of the supercontinent formation the ophiolite sheets usually arose with characteristic chromite deposits like the Kempirsay massif in the South Urals, as well as the environments of the continent collisions with the melt-out of huge granite masses, the formation of abundant hydrothermal and pegmatite deposits and polymetallic and sulfide ore deposits.

The supercontinent longevity as unified continents usually did not exceed 100–120 MMY. The explanation is the particulars of the mantle chemico-density convection (see Fig. 9.14). Because of those, the supercontinent compression was rapidly replaced by the extension with the manifestations of younger than the supercontinent age alkali-ultramafic, syenite, carbonatite, and diamondiferous kimberlite magmatism. Most of the world's kimberlite blow-pipes are indeed associated with such periods of the initial supercontinent extension. The further supercontinent extension during their split led to massive intrusions of the continental crust by the trapp basalts and to the formation of the continental rifts with typical bimodal volcanism. Usually this process ended up in the supercontinent destruction into smaller centrifugally drifting continents with the formation between them of Atlantic type young oceans (see Figs. 9.3, 9.5, 9.7–9.9, 9.11 and 9.12)

It is important that the open fissures (the depth magma release channels) could sometimes appear at the supercontinent formation stage under the generally compressive environment of the continental lithosphere. It was especially typical if one of the colliding lithospheric plates had a wedge-like outline which happened at the Laurasia consolidation or in the closing of the North Paleo-Atlantic (Japetus Ocean) in Devonian (see Fig. 10.20). It is likely that such fissures were utilized in Devonian and Carboniferous by alkaline-ultramafic Kola Peninsula intrusions and diamondiferous kimberlite near Archangel in Russia.

## 10.5 EFFECT OF THE OCEAN AND OF EARTH'S CLIMATES ON THE FORMATION OF EARLY PROTEROZOIC SEDIMENTARY ECONOMIC DEPOSITS

It was known for a long time that the atmosphere and hydrosphere strongly affected the Earth's metallogenic environments, including in Early Precambrian (Voitkevich and Lebedko, 1975; Smirnov, 1982; Strakhov, 1963, 1976; Tugarinov and Voitkevich, 1970, etc.). However, only recently, after the lithospheric tectonics concept took hold and the fundamentals of the global evolution were developed, it became possible to evaluate a genuine scale of these processes and clarify the nature of their effect on the Earth's exogenous and endogenous metallogeny.

As will be shown in Chapter 12, in Archaean, the partial pressure of carbon dioxide reached 4–5 atm. (see Fig. 12.4). The cause was a small amount of the water in the Archaean oceans, so the mass of the dissolved $CO_2$ was significantly lower that the mass of $CO_2$ degassed from the mantle (see Fig. 12.3). Thus, the bulk of carbon dioxide degassed from the mantle in Archaean must have been in the atmosphere and dissolved in the oceanic water. The Archaean ocean was hot (see Fig. 14.19), and due to high $CO_2$ partial pressure in the Archaean atmosphere, up to 5 atm. (see Fig. 12.4), the oceanic water was saturated with the carbonic acid $H_2CO_3$ and had an acidic reaction (pH≈5–6). Hot and acidic water is an aggressive reagent and dissolves many ore elements and compounds. Therefore, it is to be expected that the water of the Archaean ocean was saturated with many ore elements including gold, uranium, iron, copper, lead, zinc sulfides, manganese oxides, bivalent iron oxides, etc. It is likely that all these compounds entered the hydrosphere at the oceanic crust basalt's hydration and interaction of hot and acidic rain waters with the rocks of the greenstone belts and granitoids of the continents.

The climate significantly cooled down in Early Proterozoic, and the atmospheric pressure declined (see Fig. 12.15). After that the oceanic water became neutral (pH≈7–8). That is how, in our view, at the very end of Archaean (about 2.7–2.6 BY ago) and in Early Proterozoic (about 2.5–2.3 BY ago) large stratimorphic deposits of gold, uranium, copper, polymetals, cobalt, sulfides, iron carbonates, manganese oxides and other commercial deposits were formed (see Fig. 10.3). An example of such fields is Witwatersrand deposits. Their ore bearing in the greenstone rocks was manifested about 3 BY ago, and the ore-bearing

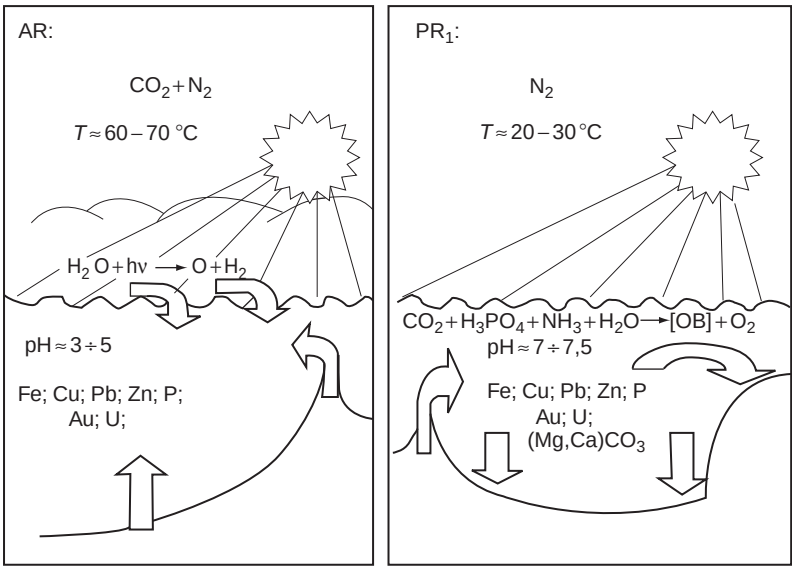


**FIGURE 10.3** Formation of unique Early Proterozoic stratiform ore deposits due to the ore element precipitation after bonding in carbonates of the Archaean atmosphere carbon dioxide and oceanic water cooling at the Archaean/Proterozoic time boundary (OM—organic matter). Arrows show the ore element supply paths to the oceans and their precipitation in Early Proterozoic (descending arrows in Archaean indicate washout from the continents).

conglomerates containing gold and uranium appeared only 2.5 BY ago. At the same time, Early Proterozoic gold-bearing conglomerates were deposited on the other old platforms as well as the Katanga–Rhodesia copper belt cupriferous sandstones in Africa, Udokan cupriferous sandstones in Siberia, etc.

Easily understood from the position of the proposed concept are the unique iron ore formations of the end Archaean–Early Proterozoic. Iron concentration within the convecting mantle over most of Archaean was relatively low (see Fig. 4.16) as iron at the time almost in its totality migrated into the underlying convecting mantle of the differentiation zone of Earth's matter (see Fig. 4.1). However, by the end Archaean, the primordial matter squeezed out of the central Earth's areas began transferring into the convecting mantle. This matter had high concentrations of iron and iron oxides (see Fig. 4.1D and E). Our estimate is that the average concentrations within the mantle at the end of Archaean and the beginning of Early Proterozoic were metallic iron, 5.5%, and bivalent iron, 15%. In the oceanic rift zones, the metallic iron rose to the Earth's surface and reacted there with the oceanic water. In the no-oxygen medium, the hot iron was oxidized at the expense of the water dissociation. Then, it reacted with carbon dioxide and formed the water-soluble iron bicarbonate:

$$4Fe + 2H_2O + CO_2 \rightarrow 4FeO + CH_4 + 41.8 \text{ kcal/mol}, \tag{10.12}$$

$$FeO + 2CO_2 + 2H_2O \rightarrow Fe(HCO_3)_2. \tag{10.12'}$$

In this form, iron was apparently spread around the entire ocean. Under the near-surface conditions, due to life activity of cyanobacteria and microalgae, the bivalent iron was oxidized to the trivalent state and precipitated:

$$2Fe(HCO_3)_2 + O \rightarrow Fe_2O_3 + 2H_2O + 4CO_2. \tag{10.13}$$

The trivalent iron could have been reduced again through the metabolism of iron-reducing bacteria, but this time only to the magnetite stoichiometry (Slobodkin et al., 1995). Simultaneously with iron, silica, released from pyroxene hydration (for instance, under reaction (10.3)), was also brought out of the rift zones. It explains the iron–silica paragenesis in jaspelites of the Precambrian iron ore formations (see Fig. 10.4).

Obviously, the mass release of iron and other metals from the mantle to the hydrosphere could occur only when the mantle matter contained noticeable amounts of these metals and when the ocean surface covered the average rift zone depths on the mid-oceanic ridge crests. It is important that only the combination of these two factors could provide for iron release from the mantle to the hydrosphere and subsequently in the Earth's sedimentary shell. The oceanic water composition was also significant. For instance, iron content in the Precambrian basalt crust was much lower (approximately 10 times lower) that in the serpentinites formed in hydration of the restite areas of the mantle matter.

After taking into account all these factors, it was possible to estimate the average accumulation rate of the Precambrian iron ore formations. The precondition was that these formations contain on the average about 50% of iron, and only 50% of iron is extracted from the oceanic crust rocks.

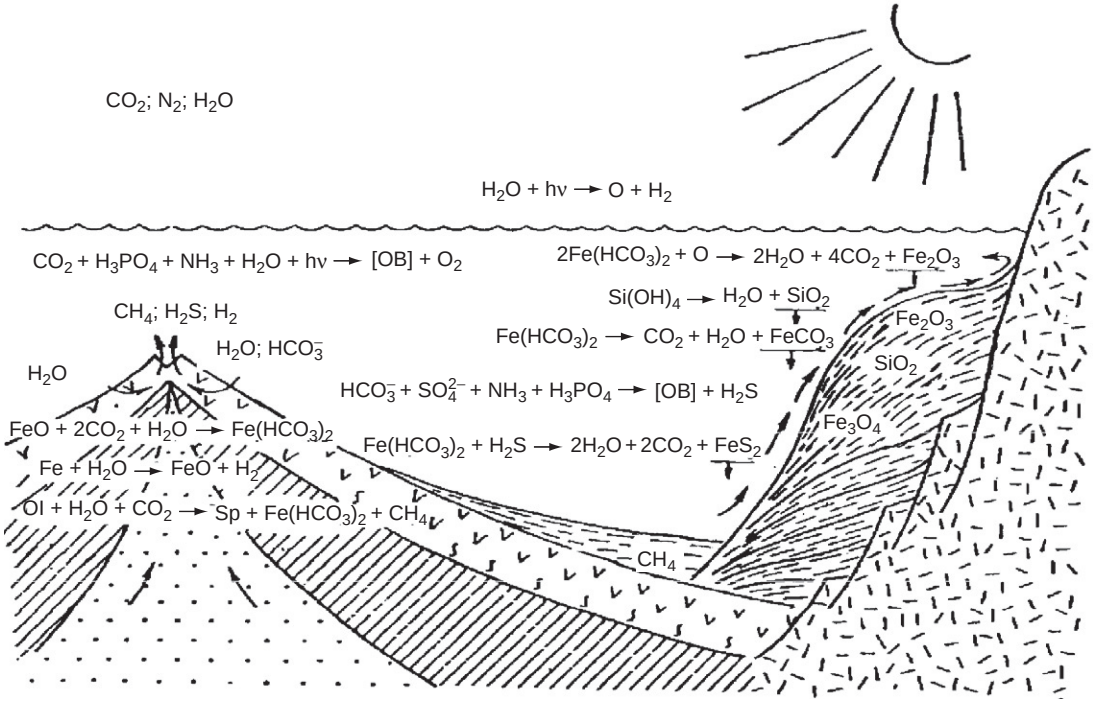


**FIGURE 10.4** Geochemistry of the iron transfer from the mantle to the rift zones and oceans in the formation conditions of iron-ore deposits on the continental margins in Early Proterozoic.

Besides the described mechanism whereby the Early Precambrian iron ore formations emerged due to iron release from the rift zones, the other mechanism may have existed in the beginning of Archaean.

As mentioned, formation of the Earth's crust in Early Archaean occurred only within the narrow equatorial ring belt. The remaining planetary surface was composed of the primordial Earth's matter (see Fig. 7.4) which contained approximately 13% of the metallic iron and 23% of its bivalent oxide (iron silicates). After the Earth's degassing began and the carbon dioxide atmosphere formed, iron from the surface layers of these primordial areas was carried out by the acidic rain water into the young marine basins where it was deposited and formed Early Archaean iron ore formations.

Galimov (1988a) associated the accumulation of iron ore formations with the biosphere evolution and generation of abiogenic naphtides, in particular methane. He also indicated that the Archaean oceanic water was substantially impoverished in $^{18}O$ compared to the modern ocean. Under the proposed concept, the $^{18}O$ isotope bonds with iron mostly within the mantle when water molecules go through the melted iron zones (see Fig. 4.1B and C) as follows:

$$Fe + H_2O \rightarrow FeO + H_2 \qquad (10.14)$$

The above calculations also assumed that iron release from the oceanic crust to the oceanic water was in proportion to the water content in serpentinites $m_{\mathrm{sp}}{}^{w}$ (nearly 11%) and basalts $m_{\mathrm{bs}}{}^{w}$ (about 2.5%) and to the average rate of the oceanic lithospheric plate area increase $u_{\mathrm{oc}} = k\dot{Q}_m^2/S_{\mathrm{okk}}$. Here, the heat flow $\dot{Q}_m$ determines the characteristics of the Earth's tectonic activity as shown in Fig. 5.17, and $S_{\mathrm{occ}}$ is the areal extent of the oceanic crust (Fig. 7.4)

In view of the aforementioned, a relative iron ore accumulation rate in Precambrian may be found as

$$\dot{m}(\mathrm{Fe})_{\mathrm{s}} \approx C(\mathrm{Fe})_m|\delta h|\left[m_{\mathrm{sp}}^{w} + m_{\mathrm{bs}}^{w}\right]u_{\mathrm{oc}} \tag{10.15}$$

Here, the delta-function $|\delta h| = 1$ at $\delta h_{\mathrm{oc}} > 0$ (i.e., when the ocean water covers the mid-oceanic ridge crests) and $|\delta h| = 0$ at $\delta h_{\mathrm{ок}} \le 0$ (i.e., when the ocean water is below the mid-oceanic ridge crests or exactly coincides with them). The iron release rate from the mantle into the sedimentary shell under Eq. (10.15) is displayed in Fig. 10.5 in $10^9$ ton/year.

As we see, four to five periods of a massive iron ore accumulation may have occurred in Precambrian. The earliest episode, 3.8 BY ago produced the Isua formation in west Greenland. The next iron ore accumulation epoch, the Late Archaean, brought in the accumulation of the Kivatin-type volcanosedimentary iron ore, and several locations in Russia (the Kostamuksha and other areas in Karelia and the Kola Peninsula, the Taratasha complex in the Urals and the Staro-Oskol series on the Voronezh crystalline massif).

However, the most outstanding iron ore accumulation period was the end Early Proterozoic epoch between 2.2 and 2.0–1.8 BY ago. Iron ore deposits of that epoch are known on practically every continent. Many of them were deposited simultaneously. These accumulations include unique Krivoy Rog jaspelite deposits in the Ukraine, the Kursk magnetic anomaly in Russia, Karsakpay in Kazakhstan, Hamersley in west Australia, deposits of the Lake Superior in the US and Canada, in Guyana (South America) and other regions. It is important that the silica-saturated iron sediments which later converted in the jaspelites could have been deposited only in the high-latitude boreal and near-pole zones. The reason was that in Early Proterozoic (as well as presently) only carbonate-rich sequences

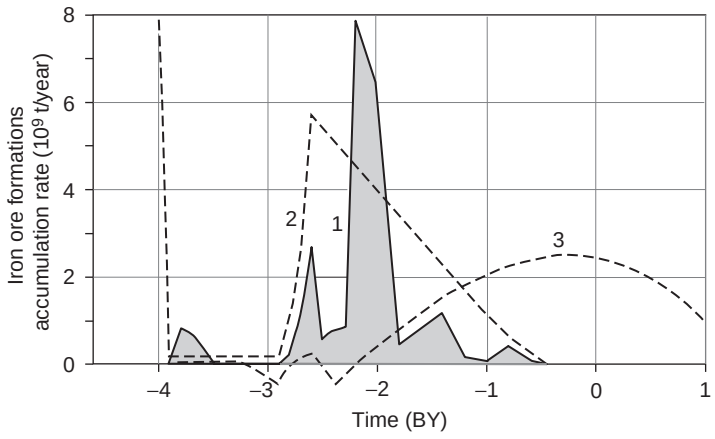


**FIGURE 10.5** Analytical calculation of the Precambrian iron ore formations accumulation rate: 1. Total iron ore sedimentation rate, $10^9$ ton/year: 2. Metallic iron concentration in the convecting mantle, % (see Fig. 4.16); 3. Ocean surface position relative to the average stand level of mid-oceanic ridge crests, km (see Fig. 11.6).

later converted into the siderite iron ores could have been deposited in the tropical belt. The siderites (as the other carbonates) are easier weathered and redeposited. That is probably why there are much fewer occurrences of the old siderite ores than the jaspelite ones.

In the second half of Early Proterozoic (which accounts for just 5–7% of the entire geological evolution), at least 70–75% of the world's iron ore reserves were formed. Our estimates are that at the time the iron accumulation rate reached 3.3 billion tons per year which is close to earlier estimates of $(1–3) \times 10^9$ ton/year (Hollend, 1989). The total Precambrian iron ore formations amount must have been around $3.3 \times 10^{18}$ tons. This is greater by many orders of the magnitude than the discovered resources of about $3 \times 10^{12}$ tons (Bykhover, 1984) and more than 30 times the iron oxide amount in the continental sedimentary rocks (close to $0.1 \times 10^{18}$ ton after Ronov and Yaroshevsky, 1978), although it is possible that somewhat greater iron amounts may be found in the metasedimentary rocks and the "granite" continental crust layer. It may indicate that most of the sedimentary iron sunk again in the mantle through the old subduction zones still in Precambrian.

A typical feature of this unique iron ore accumulation epoch was its practical simultaneity (about 2.2 BY ago) on all continents. It is understandable under the proposed model (general cause). Indeed, at that time, the oceanic crust was already totally saturated with water. After that, the ocean surface rose above the mid-oceanic ridge crests (curve *3* in Fig. 11.6) and the soluble iron hydroxides began to enter the ocean as shown in Fig. 10.4.

By the end of Early Proterozoic (about 1.8 BY ago), the massive accumulation of the sedimentary iron ore stopped almost as instantaneously as it started. A likely reason may have been that by that time the ocean surface rose approximately 400 m above the mid-oceanic ridge crests. That was the water layer thicker that the active oceanic layer. On the other hand, the Middle Proterozoic and Riphean Ocean most likely had a stable stratification with the stagnated deepest waters which is supported by the commonality of black shales at that time. Thus, since that time on, the hydroxides of bivalent iron from the rift zones entered only stagnant depth waters and could not be oxidized there to the insoluble state, and the iron ore formations of that time could only be deposited in the oceanic upwelling zones.

Nevertheless, as mentioned in Section 9, in Early Riphean (1.6–1.4 BY ago), the split of the Stille's supercontinent Megagaea occurred. At that time, during the split, one more small iron ore deposition burst could be observed. It was associated with the emergence on that former supercontinent of numerous rift structures which subsequently grew over into relatively shallow-water continental margins (Fig. 9.5). The shallow-water nature of the young oceans was because the Megagaea split was evolving above a powerful ascending mantle convection flow (see Fig. 9.14). It was similar to what is happening currently in the North Atlantic where the ocean-floor even reaches the daylight surface (Iceland).

By that time there was 2–2.5% of metallic iron in the mantle (see Fig. 4.16). Due to the shallow-water nature of the Riphean intercontinental oceans, the metallic iron that entered the oceanic rift zones got, after hydration, into the active layer and spread all over the ocean. After the oxidation in well aerated waters of the continental margins, iron precipitated on the sea-floor and gradually formed iron ore deposits there. This situation lasted for a relatively brief time between 1.6 and 1.4 BY ago. After that, a descending mantle flow reoccurred in the place of the split Megagaea's continents. This flow consequently formed about 1.0 BY ago a new supercontinent Mesogea.

Apparently, the stagnant world ocean water stratification lasted till a new glaciation impulse that engulfed in Late Riphean a number of the Laurasia and Gondwana continents (see Figs. 9.6 and 9.7). During glaciation periods, the oceanic water stirs and mixes, thus, iron oxides from the rift zones could at the end Riphean again reach the oceanic active layer. However, there was much less that 1% of metallic iron in the mantle as most of it had already migrated into the growing core. That is why the last Precambrian iron ore accumulation impulse was the weakest.

The basis of the Precambrian sedimentary iron ore formation is in the iron oxidizing through the thermal dissociation of the $CO_2$-saturated oceanic waters and hydration by these very waters of the iron-bearing oceanic crust rocks.

Simultaneously, abiogenic methane is generated under reaction (10.12). Obviously, the epochs when a maximum iron release into the ocean occurred must have been accompanied by the maximum methane generation rates. That, in turn, resulted in an increased mass of the methane-consuming bacteria. As the reaction (11.13) shows, the carbon isotope fractioning always results in lightening of the methane isotope composition, hence, in lightening of carbon $C_{org}$ in the bacteria which grew on this methane. This is probably why the organic matter of the methane-consuming bacteria is extremely low on the heavy carbon isotope $\delta^{13}C_{org}$ to $-50‰$. That may also be the reason for local $\delta^{13}C_{org}$ distribution minima in the sediments with the greatest iron ore accumulation rates at the end Archaean and in Early Proterozoic (see Fig. 12.11). However, despite the lower intensity of the jaspelite formation in Late Archaean, the $\delta^{13}C_{org}$ isotope minimum amplitude at the time was the largest. A probable cause was a high-density carbon dioxide atmosphere in Archaean whereas the $CO_2$ partial pressure declined, and the methane generation rate decreased as a result (Fig. 12.13).

The Early Archaean iron ore formation must have also been accompanied by the methane generation. But where methane was generated (outside the sedimentary sequences) it was unable to accumulate and directly entered the atmosphere. And in the warm and humid Early Archaean atmosphere methane, affected by the Sun UV radiation, was oxidized as follows: $CH_4 + H_2O + h\nu \rightarrow CO + 3H_2$, and hydrogen evaporated. Most likely, in Early Archaean, there was still no bacteria capable of consuming methane. Therefore, the isotopic shifts in the organic matter of the time were determined only by chemical reactions (possibly abiogenic) without any addition of methane's isotopic shifts (see Fig. 12.11).

## 10.6 SUBDUCTION PROCESSES AND THE FORMATION OF DIAMOND-BEARING AND AFFINED ROCKS

Besides the aforementioned unique endogenous (mantle-magmatic) and exogenous (primary-sedimentary) Proterozoic economic deposits, at the same time and for the first time, the lithospheric plate subduction zone was manifested. It was associated with the calcareous-alkaline or granitoid magmatism. For the first time appeared and widely spread paired metamorphic belts, pegmatite formations with muscovite-rare metal, lithium–beryllium, and phlogopite–apatite mineralization, and also crystal-bearing, gold–uranium, rare-earth, polymetallic and sulfide formations (Sokolov and Kratz, 1984).

The origin of this outstanding "geosynclinal" metallogenic impulse is clear from the position of the proposed concept. Indeed, in Early Proterozoic, the lithospheric plate tectonics began operating and first subduction zones appeared (in Archaean, only the basalt sheet pileup zones existed with the domination of the obduction not subduction, see Fig. 7.5). Also, in Early Proterozoic, as previously mentioned, drastically increase the oceanic crust hydration. Thus, the continental crust melt-out above the subduction zones was now occurring in the water-abundant environment as the water was released in these zones at the oceanic crust hydration. However, the mantle (see Fig. 4.16), hence, the oceanic crust in Early Proterozoic was still rich in the primordial Earth's matter which rose from the central areas of Earth at the core separation (see Fig. 4.1E). Most siderophilic elements in the subduction zones returned into the mantle and the lithophilic and partially chalcophilic elements and compounds, together with the released overheated water, rose up and become the components of the continental crust forming in it unique pegmatite and polymetallic deposits.

There was one more specific kind of depth formations closely associated with the subduction process of the Early Proterozoic oceanic deposits. It dealt with the origin of diamondiferous kimberlites, lamproites, carbonatites and the affined alkali-ultramafic rocks (such as the Khibin apatite-bearing nepheline syenites).

Most modern hypotheses derive the kimberlite and the affined magmas from the partial melt-out of the mantle matter enriched in volatile elements or from the emergence of the residual melts in the lengthy fractioning of the mantle matter. This approach is currently most commonly adhered to by many researchers of the diamondiferous rock and diamond origin. For instance, Orlov (1984) wrote that the diamond is a magmatic mineral that crystallizes at depth in an alkali-ultramafic magma which then forms the kimberlite rocks. The proponents of this view believe that the source of diamonds' carbon is the juvenile carbon of the magma, and that diamonds crystallize in this magma together with olivine, garnet, pyroxene, and other minerals which are found in diamonds as syngenetic inclusions.

Despite the mantle-magmatic hypotheses popularity, they have a number of major practically insurmountable drawbacks.

First, all modern petrologic determinations of the kimberlite magma formation environment indicate with certainty their low temperature (about 1000–1250 °C) at pressures of 45–65 kbar (Dowson, 1983; Kaminsky, 1984). That is at least 500 °C lower than the expected mantle matter melt-start temperature (the mantle matter begins to melt under the same pressure at 1570–1720 °C; Takahashi, 1986). An unavoidable conclusion is that the kimberlite and affined magmas simply could not emerge from melting (even a partial melting) of the mantle matter because the temperature barrier separating the existence areas of the kimberlite melts and mantle melts is too high.

Second, let us assume the kimberlite melts formed due to a partial melting of the lherzolite composition mantle matter. Even if it could happen it would result only in a moderate (in equilibrium with lherzolites) concentration in the emerging melt-outs of the lithophilic and volatile compounds. It, however, would happen without a drastic decrease in the silica concentration which is so typical of the kimberlites and especially carbonatites. Besides, such mechanism is unable to produce the "avalanche" increases in the contents of many rare-earth and dispersed elements (for instance, radioactive elements).

Third, an assumption could be made that the source material for the kimberlite melt-out was a garnet lherzolite which contains admixtures of phlogopite and carbonates so

common in the kimberlites and xenoliths. This assumption a priori relies on the existence in the juvenile mantle of significant variability in its chemical composition. We know now from the fact of the continuous lithospheric plate drift that the Earth's mantle is engulfed in an intense convection. Over the life of Earth, the mantle matter stirred and turned around many times and homogenized. This is supported, in particular, by the tholeite basalt melt-outs in the oceanic rift zones. Therefore, the current concept is that on the average the mantle is compositionally uniform (Ringwood, 1975b) with possible slight variations due to the continuing iron oxide migration from the mantle into the core (Sorokhtin and Ushakov, 1991, 2002). This makes it very difficult to accept all hypotheses deriving the kimberlites and the affined rocks from the melting of the juvenile mantle anomalies strongly enriched in the volatile compounds and lithophilic elements. There are simply no such anomalous areas in the mantle. Some narrow areas of local variability may form under the lithospheric plate subduction zones in connection with sucking-in of the oceanic crust and deposits. These, however, are not indigenous anomalies in the mantle composition but the exogenous variability introduced into the mantle together with the crustal matter and deposits. And this variability is again totally homogenized in the mantle matter differentiation and disintegration on the Earth's core surface. The contribution from such exogenous factors to the emergence of the diamondiferous and affine rocks is discussed in the other hypothesis. We will also review it later in the book.

A massive material on the isotopy of the discussed rock group and inclusions in the diamonds and on the carbon isotope shifts in the diamonds was accumulated over the recent years. It shed new light on the entire diamond and diamondiferous rocks formation problem. For instance, both Sobolev and Sobolev (1980) came to a conclusion that beside the juvenile (mantle) carbon, also the exogenous (from carbonates) carbon sucked-in together with the oceanic crust through the subduction zones to great depths underneath the continents, can contribute to the diamond origin. Automatically, the eclogite origin from the transformation of the former oceanic crust basalts got a natural explanation. Kuleshov (1986) concluded that the high-temperature carbonate genesis in kimberlites and carbonatites must be associated with the remobilization of the crustal matter and first of all the matter of the Earth's sedimentary shell (Fig. 10.6).

Indeed, the isotopic composition of the carbon in diamonds, enriched in light carbon isotopes, is impossible to explain without involving the core matter with its "light" organic carbon and low $\delta^{13}C$ values (Galimov, 1988a,b; see Fig. 10.7). Similar situation is observed in high-temperature depth rocks of the carbonatite and kimberlite association. Carbon isotope composition with significant negative $\delta^{13}C$ shifts and oxygen isotope composition with positive $\delta^{18}O$ values shows that in the formation of the carbonate matter in these rocks participates the crustal $CO_2$ of primary sedimentary origin (Kuleshov, 1986).

In the late 1970s, we studied the origin of the kimberlites and the affine rocks from the viewpoint of the lithospheric plate tectonics and came to a conclusion that the matter composing the kimberlite, carbonatite, and alkali-ultramafic magmas emerged due to the remelting of pelagic deposits sucked into the subduction zones to great depths under the continents (Sorokhtin, 1981a,b). Thus, we believe contrary to the common view that the diamondiferous kimberlites, lamproites, and carbonatites cannot be attributed to mantle rocks. This is rather a pseudo-mantle rock group.

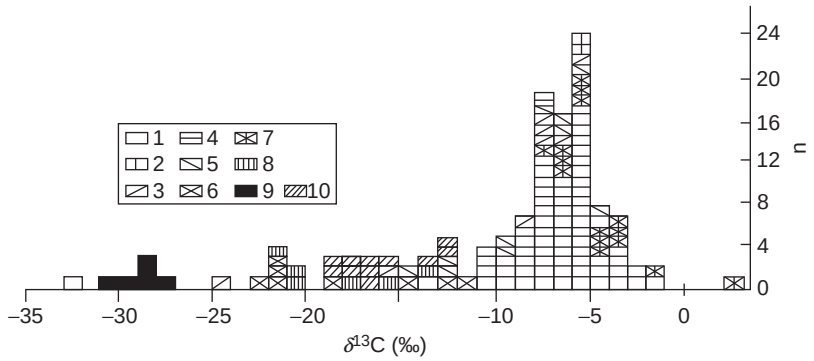


**FIGURE 10.6** $\delta^{13}C$ carbon isotope distribution histogram in diamonds and carbonado (Ilupin et al., 1990). Diamonds: 1. From Siberian, African, North American kimberlites; 2. From meteorites; 3–8. Placers (3. Urals, 4. Timan, 5. Sayan, 6. Ebelyakh, 7. Africa, America, Australia, 8. Ukraine); 9. Brazilian carbonados; 10. Diamonds from outer space; *n*. No of measurements.

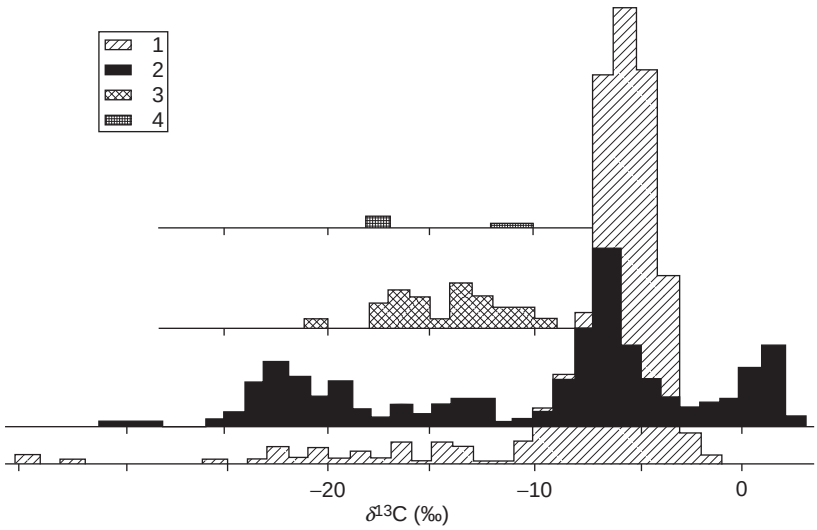


**FIGURE 10.7** Distribution of carbon isotope composition for different sources (Galimov, 1984): 1. Kimberlite pipes; 2. Placers; 3. Impact craters; 4. Metamorphic rocks.

Summarizing, we can state that the ocean deposits are a "cradle" of diamonds (Sorokhtin, 2006a). The issue of the deposits sucking into the plate subduction zones was resolved with the help from the theory of mechanical lubrication still in mid-1970s (Sorokhtin and Lobkovsky, 1976) (see Section 8.5). Somewhat later this solution was confirmed by seismic surveys in the Kuril Island Arc (Garkalenko and Ushakov, 1978) and even by drilling in the frontal portion of the lesser Antilles Arc (Bijy-Duval et al., 1981).

Regular modern deposits cannot be sucked-in to great depths due to their low density. For this to happen, the density of the deposits within the plate subduction zones must be

greater than the average density of the continental plates (Monin and Sorokhtin, 1986). Such iron-rich thus high-density (and heavy) pelagic sediments were only deposited in Early Precambrian. Only these deposits could be sucked-in (could "drop") through the old subduction zones to great depths underneath the Archaean continental shields. This mechanism could have been implemented only in Early Proterozoic, about 2.2–1.8 BY ago (Sorokhtin, 1981, 1985) when the heavy iron-rich sediments were deposited (see Fig. 10.5) and when the continental plate thickness increased to 200–250 km (see Fig. 7.9).

Similar conclusions were made by Eldridge et al. (1991) based on analysis of isotope shifts in sulfur and lead isotope ratios from sulfide inclusions in diamonds. They actually confirmed the old age of diamonds (about 2 BY) which we proposed earlier based on the lithospheric plate tectonics mechanism.

The origin of these exotic rocks was analyzed in detail in our publications (Sorokhtin et al., 1996, 2002; Sorokhtin and Sorokhtin. 2006). Under the developed model, the diamondiferous kimberlites and the affine rocks formed due to sucking-in the heavy (iron-rich) Early Proterozoic oceanic deposits through the old subduction zones into great depths (up to 200–250 km) underneath the Archaean shields. These sediments had to remelt at great depths and generate the kimberlite and lamproite magma nodes. If carbonate rich iron-rich deposits of the Earth's tropical areas were sucked-in into the plate subduction zones, the kimberlite and carbonatite melts formed. Where those were boreal and polar clayey deposits impoverished in carbonates but rich in silica, magnesium, and alkali, lamproite melts formed. This may be a partial reason why the jaspelite (silica–siliceous) iron ore of the Hamersley Province in western Australia is so common; it is the classical region of the lamproite diamondiferous magmatism. Besides, due to high density of the iron-rich deposits they had to "drop" into the plate subduction zones and serve there as a lubricant. That is probably why the plate subduction zones at the end Early Proterozoic (the time of the Svekofenian orogeny) and in Middle Proterozoic were mostly amagmatic. They did not have the calcareous-alkali volcanism typical of the island arcs and active continental margins which was early on indicated by Borukayev.

Remember, a condition for the heavy deposits "drop" in the space between the plates is an inequality where the average rate of the deposit flow within the slot between the plates is greater than the plate subduction rate: $\bar{u} > u_0$, at $\Delta\rho = (\rho_l - \rho_s) < 0$. This condition also gives rise to another inequality for the "dropping" deposits (Monin and Sorokhtin, 1986)

$$\frac{h^2(\rho_s - \rho_l)g}{2\eta u_0} \sin\beta > 1, \tag{10.16}$$

where $h$ is the thickness of the subducted deposits; $\rho_s$ the density of metalliferous deposits; $\rho_l$ lithosphere density; $g$ the gravity acceleration; $\beta$ the subduction zone angle; $\eta$ the deposit viscosity; and $u_0$ is the subduction rate.

$$\eta < \eta_{crit} = \frac{(\rho_s - \rho_l)gh^2}{2u_0} \sin\beta \tag{10.17}$$

For instance, with $h = 1$ km; $u_0 = 10$ cm/year; $\beta = 45°$ and $(\rho_s - \rho_l) = 0.5$ g/cm$^3$; critical viscosity of the deposits $\eta_{crit} \approx 5.5 \times 10^{18}$ poise. All heavy deposits with viscosity lower than $\eta_{crit}$ will "drop" into the plate subduction zones at a rate $\bar{u} > u_0$. If the deposit viscosity is

greater than $\eta_{crit}$, they will be sucked in at a rate $\bar{u} < u_0$ or maybe even will be squeezed out of the plate subduction zone.

Heat released in sinking of the heavy and light deposits decreases their viscosity. Contrary to the first option, however, the heavy deposits cannot be squeezed up out of the slot between the plates. Thus, the viscosity decrease will only result in an increased "drop" rate of the deposits into the subduction zone's depths and in a decrease of the heat-generation rate as defined by the dissipative function (Eq. (8.33)). For instance, if in the example above the heavy deposit viscosity declines due to the heating to $1 \times 10^{18}$ P (which is still very far from melting), then at their subsiding to a depth of 200 km they will release, under Eq. (8.34), only about 10 cal/g of heat, which corresponds to the temperature rise just by 30 °C.

Therefore, heavy iron ore deposits (such as belonging to Early Proterozoic) must have sunk into the subduction zones to a relatively great depth without melting. It follows from this that such subduction zones in themselves must have been "cold," amagmatic (with no noticeable manifestations of the calcareous-alkali magmatism).

At a depth about 150 km, the melting curve of the water-saturated deposits intersects the continental lithosphere's geotherm (see Fig. 10.11). Deeper than this, the deposits are additionally heated by the mantle's internal heat and begin to melt. The process is accompanied by the melts differentiation and liquation, melt's heavy fractions (sulfides and iron oxides) migrate downwards into the convecting mantle and are gradually assimilated by the mantle matter, and the light fractions (silicates, carbonates) remain within the lithosphere. As the subduction zones and the immediate surroundings are within the compression environment, the light silicate–carbonate melts usually are unable to rise to the surface from the depth of over 80–100 km because the lithostatic pressure at such depths is much higher than the rocks' plastic limit ($\tau_0 < 1$ ton/cm$^2$). This means that under the compression environment the emergence of magma-conducting channels (fractures) is practically impossible at those depths. Thus, the melts formed from the remelting of heavy deposits are preserved in the middle and lower portions of the continental lithospheric plates and gradually form there the nodes of the depth silicate–carbonate magmas (Fig. 10.8).

Under the proposed model, the formation time of depth melts is strictly limited to the second half of Early Proterozoic (2.2–1.8 BY ago) or, on rare occasions, to Middle Proterozoic. The reason is as follows. There were no conditions in Archaean for the generation of these magmas as the heat flows at the time did not allow the thickness of the continental lithospheric plates, together with the continental crust, to increase over 60–80 km. Subduction zones did not exist at that time. Instead, there were pileup zones of thin and mostly basaltic oceanic lithospheric sheets (see Fig. 7.5).

As mentioned, first subduction zones emerged only after the Earth's core separation in Early Proterozoic, and the Archaean continental plates began rapidly increasing in thickness. By the end of Early Proterozoic, the plate thickness reached maximum values of about 250 km. This created conditions for the formation of the depth (diamondiferous) melts. However, this opportunity was materialized only after heavy iron ore deposits of the jaspelite type began forming on the ocean floor 2.2 BY ago. This epoch of massive iron ore deposition lasted approximately to 1.8 BY ago. And during this period (2.0–1.8 BY), maximum number of the kimberlite and affine magmas was generated in the continental lithosphere depths.

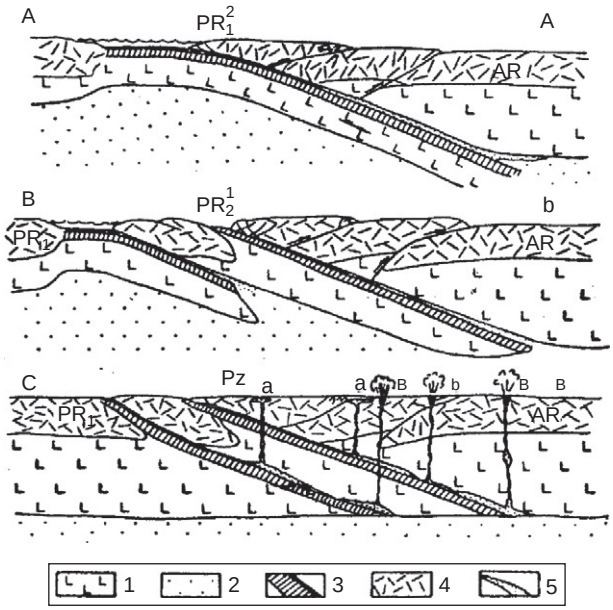


**FIGURE 10.8** Formation of alkali-ultramafic, lamproites and kimberlite composition depth melts (Sorokhtin et al., 1996): (A). Situation at the end of Early Proterozoic; (B). At the Early/Middle Proterozoic time boundary; (C). In Riphaean and Phanerozoic (shown is the breakthrough moment of depth magma to the surface and the formation of: a. Alkali-ultramafic intrusions; b. Melilite and carbonatite intrusions; c. Diamond-bearing lamproites and kimberlite sub-volcanic complexes). 1. Lithosphere; 2. Asthenosphere; 3. Early Proterozoic oceanic crust with the overlying heavy iron-rich deposits; 4. Continental crust (AR, Archaean; $PR_1$, Early Proterozoic), 5. Depth melts.

A second though less massive impulse of the depth melts generation could have happened during the destruction time of the second supercontinent, the Stille's Megagaea about 1.6–1.4 BY ago. Numerous relatively shallow-water intercontinental oceans emerged at that time. Iron was also released from their rift zones. If such deposits got to the plate subduction zones, they could have given birth to the depth pseudo-mantle alkali-ultramafic and even kimberlite melts.

Like the kimberlites, lamproites were also born in the lower portions of the continental lithosphere in the form of magnesium–potassium alkali silicate melts saturated with the silica and water. As previously mentioned, the kimberlites apparently formed out of carbonate-rich tropical zone deposits. Contrary to that, the lamproites originated from no-carbonate deposits such as iron–siliceous or iron–clayey sediments of the boreal or even polar climatic zones.

It is interesting in this connection that 2.2 BY ago in the classical diamondiferous lamproite region of the Western Australia the jaspelites and fluvioglacial deposits were very common as well (Chumakov, 1978). The lamproite magmas have a silicate composition so their viscosity must be noticeably higher that viscosity of the kimberlite silicate–carbonate melts. In particular, this is a reason for a more quiet rise regime of the lamproite melts. It is accompanied by only a slight turbulence incapable of bringing large depth xenoliths to the surface.

The proposed model enabled a description from the unified positions of the majority of specific features and sometimes even the fine details in the composition of the diamondiferous and affine rocks including the diamonds themselves and their mineral inclusions.

Thus, under the model, the kimberlites and lamproites are indeed depth rocks but they emerged from the pelagic deposits. This is supported by the coinciding rare-earth element

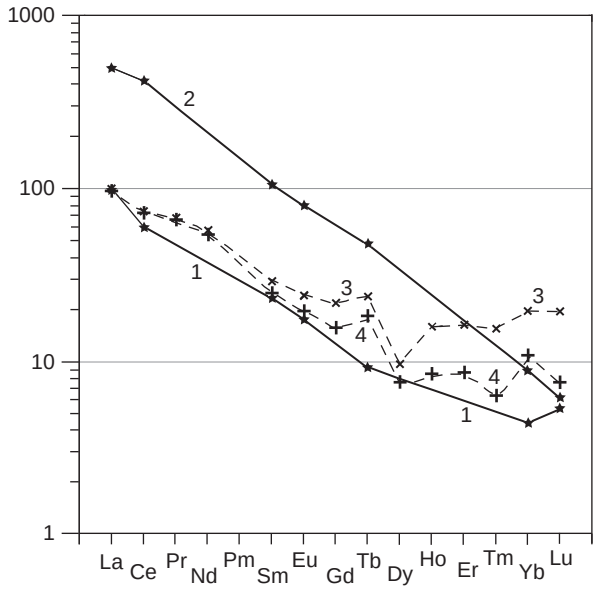


**FIGURE 10.9** Average rare-earth element distributions in kimberlites and deposits. The data are normalized over the average chondrite distribution (Kheskin et al., 1968): 1 and 2. Rare-earth element distributions in Premier and Wesselton kimberlite pipes, South Africa (Dowson, 1983); 3. Rare-earth element distributions in oceanic deposits calculated from the data by (Kheskin et al., 1968); 4. Corrected rare-earth element distribution in deposits taking into account that heavy rare-earth elements are mostly migrate to garnets.

distributions in the kimberlites and in the pelagic deposits (Fig. 10.9). Therefore, carbon, fluorine, most lithophilic elements (Li, B, F, Cl, K, Ti, Rb, Sr, Y, Zr, Nb, Cs, Ba, Ta, Pb, Th, U), carbonates, water, and other fluids in diamondiferous rocks have not the mantle but primary-sedimentary, that is, purely exogenous origin. The same conclusion is supported not only by high concentrations and spectrums of the rare-earth elements but also by the potassium/sodium, thorium/uranium ratios, by the hydrogen, oxygen, sulfur, and strontium isotopes in the kimberlites as well as gas–liquid inclusions ($H_2O$, $H_2$, $CH_4$, $CO_2$, CO, $N_2$, Ar, $C_2H_4$, and even the ethyl alcohol $C_2H_5OH$) in the diamonds (Melton and Giardini, 1974, 1975). Shifts in the carbon isotopic ratios of the diamond crystals with clearly biogenic markings are testimony to the same effect. Some other isotope data, such as neodymium/samarium, rubidium/strontium, strontium, uranium/lead, thorium/lead, and lead/lead ratios also smoothly enter the proposed model (Sorokhtin et al., 1996, 2002; Sorokhtin and Sorokhtin, 2006).

Eclogite xenoliths in the kimberlites also have indications of their near-surface origin. Despite the clearly depth-related mineral associations their bulk composition well corresponds with the oceanic tholeite basalts which are melted out only at shallow depths (up to 35 km) under the oceanic rift zones (Fig. 10.10). We believe that all these are convincing testimonies to a relatively near-surface formation level of the entire reviewed rock complex in Early Proterozoic.

Indeed, as is clear from the above example, practically all eclogite xenoliths are metamorphosed fragments of the basalt (tholeite) layer of the former oceanic crust. The example without any doubt indicates the oceanic crust sucking-in to great depths underneath the old continents. On the contrary, xenoliths in the garnet peridotites may have diverse nature. Most of them are the fragments of a third (serpentinite) layer of the former oceanic crust, and the rest of them may be the fragments of the subcrustal continental lithosphere torn away from the walls of the eruption channel. Correspondingly, the first type of these ultramafic xenoliths may be diamondiferous whereas the second one is always without the diamonds.

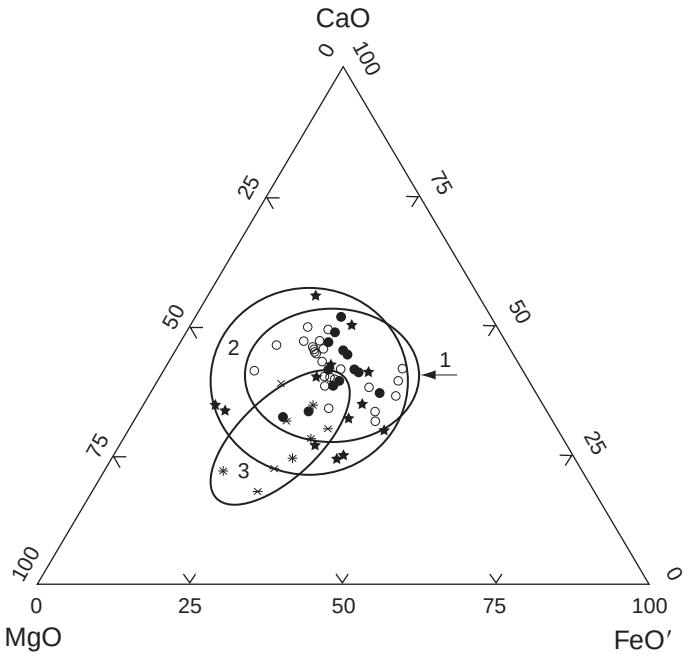


**FIGURE 10.10** CaO–MgO–$FeO_{tot}$ diagram: 1. Mid-oceanic ridge basalt field based on Frolov et al. (1979) and oceanic crust gabbro field (Kashintsev, 1991); 2. South Africa eclogite field (Dowson, 1983); 3. Yakutia eclogite field (Ilupin et al., 1990).

The deposits melt in the subduction zones due to dissipation of the deposit viscous friction energy and the lithospheric plate friction. However, when heavy deposits were sucked-in into Early Proterozoic plate subduction zones such heating was insignificant. At that time, the deposits were more heated by the depth heat flow penetrating the continental plates. Therefore, the temperature of the sediment flow in the slot between the plates corresponded with the continental plate geotherm. Because of that, the heavy deposits that got into the subduction zone began to melt only at depths where the continental plate geotherm intersected with the deposit melting temperature (see Fig. 10.11).

It is a well-known fact that the melting temperature of the most silicates in the presence of water declines to 600–700 °C when pressure rises to 5–10 kbar (Zharkov, 1976). Water-saturated carbonates and many other compounds behave similarly. However, when a system is saturated with a complex water–hydrocarbon fluid the rock melting temperature, first, declines with the pressure increase, but then gradually increases. The position of the temperature minimum depends on the $H_2O$ and $CO_2$ ratio in the fluid and is usually close to 5–10 kbar.

The lithospheric plate temperature at 200–250 km reaches 1400–1500 °C and is much higher than that of the water-saturated deposits. The mantle rock melting temperature at the same depth is close to 1800–1850 °C. For this reason, the deposits sucked-in to great depths into the subduction zones unavoidably melted and differentiated by the melt liquation. The heavy iron-rich fraction sank into the mantle, a lighter carbonate–silicate matrix was preserved in the lower lithosphere as nodes of the depths magmas. Thus, it is legitimate to say that "the oceanic deposits are a cradle of the diamonds" (Sorokhtin, 2006)

The density of most iron minerals in the Early Proterozoic deposits was very high. As an example, the goethite density is 4.0–4.4; hematite, 5.0–5.2; magnetite, 4.9–5.2; pyrrhotine, 4.6–4.7; pyrite,

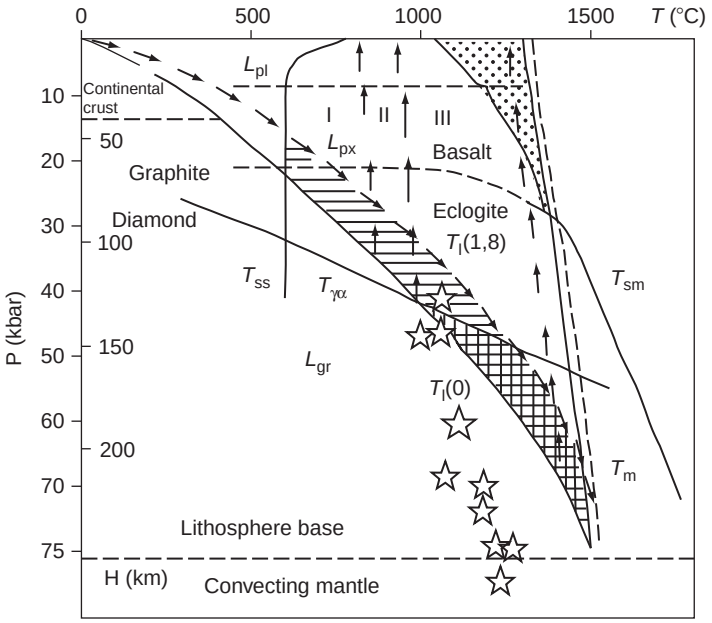


**FIGURE 10.11** Depth–temperature conditions for melt-out of alkali-ultramafic and kimberlite magmas: $T_m$, mantle temperature; $T_{sm}$, mantle matter solidus temperature; $T_{\gamma\alpha}$, graphite–diamond transition temperature; $T_{lk}$, present-day continental geotherm (the ancient geotherm is shown by descending arrows); $L_{pl}$, $L_{px}$, and $L_{gr}$, areas of stable coexistence of plagioclase, pyroxene, and garnet lherzolites; $T_{ss}$, water-saturated deposit melting temperature; horizontal shading is existence area of alkali-ultramafic, alkali-carbonatite, and calcium-carbonatite melts; cross-shading is existence area of diamond-bearing depth melts of kimberlites and lamproites under the reviewed mechanism; the stars indicate the positions of P–*T* conditions for the natural diamonds (Kaminsky, 1984); the arrows show P–*T* conditions for the movements of heavy iron-rich deposits about 2–1.8 BY ago and for the magma rise in Phanerozoic; I. Formation and rise to the surface area of alkali-ultramafic intrusions; II. Of carbonatites, melilites and no-diamond kimberlites; III. Of diamondiferous kimberlites and lamproites.

4.9–5.2 and siderite, 3.9–4.0 g/cm$^3$. After the deposit diagenesis and suck-in into the subduction zones where the pore and crystallization water was squeezed out of them, their density substantially increased. The estimates show that in the iron compound content in the Early Proterozoic pelagic deposits was over 40% (poor jaspelite ores with 28–30% iron), their density exceeds the average density of the continental lithospheric plates ($\rho_l \approx 3.2$ g/cm$^3$). Therefore, such deposits were easily sucked-in into the subduction zones to great depths, depending on their viscosity. If the viscosity was low they could just "drop" into the slot between the plates and sink to the base of the continental lithospheric plates at about 250 km (Fig. 10.12).

Knowing the mineralogical composition of the mentioned depth rocks and their melt-out temperature–depth conditions, it is possible to determine the formation areas of such rocks (Fig. 10.12). The field data supporting our diamondiferous rock formation model is discussed in much detail in our previous publications (Sorokhtin et al., 1996, 2002; Sorokhtin and Sorokhtin, 2006).

Significant role of iron in the composition of the source sedimentary matter sucked-in during Early Proterozoic underneath the Archaean crust is supported in particular by the

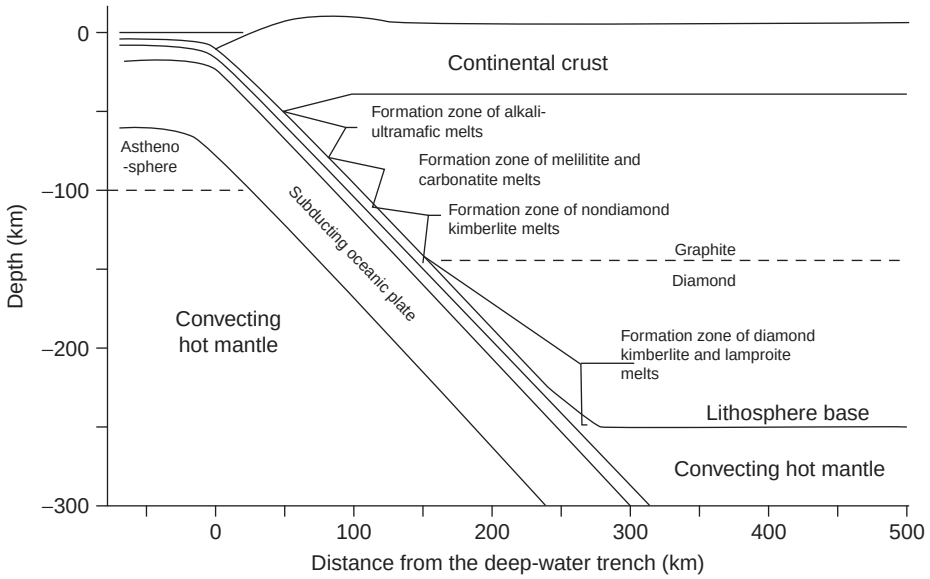


**FIGURE 10.12** Conditions of heavy (iron-rich) deposit suck-in to great depths (up to 250 km) with the oceanic plates into Early Proterozoic subduction zones under the Archaean continents and depth rocks formation areas.

carbonatite–magnetite and apatite–magnetite commercial deposits in the central type intrusions within the alkali-ultramafic provinces. Such are the magnetite deposits Kovdor and Afrikanda in the Kola Peninsula iron-rich intrusive complexes. Iron content there reaches 27%. Although the rock bulk composition (minus iron) is rather similar to the carbonate-clayey and phosphorus-rich deposits of the oceanic upwelling zones, they in no way correspond to the mantle rock composition.

Based on the strontium and lead-isotope ratios in the omphacites and diamond inclusions, the age of the kimberlites is also Early Precambrian and close to 2–2.5 BY (Dowson, 1983). This is exactly what follows from our formation model of these exotic rocks. Recently published information, based on the samarium/neodymium and rhenium/osmium ratios in the diamond inclusions, attribute older ages to the diamonds, up to 3–3.4 BY. The due diligence review of the age determination technique showed, however, that they used only the parameters of the uniform chondrite reservoir CHUR. It appears that such technique is not exactly appropriate for the mantle rocks and their derivatives. Traditionally, the diamonds are considered to be mantle formations. As we showed above, however, the diamonds formed from the matter of Early Proterozoic pelagic ocean deposits. Therefore, into geochrone equations should be substituted not the $(^{143}Nd/^{144}Nd)_{CHUR}$ values from the CHUR model but rather the values of these isotope ratios in the crustal rocks $(^{143}Nd/^{144}Nd)_{crust}$ or even better in the oceanic deposits

$$\left(\frac{^{143}Nd}{^{144}Nd}\right)_{diam} = \left(\frac{^{143}Nd}{^{144}Nd}\right)^{0}_{crust} - \left(\frac{^{147}Sm}{^{144}Nd}\right)^{0}_{crust} \left(e^{\lambda t} - 1\right), \qquad (10.18)$$

where $\lambda = 6.54 \times 10^{-12}$ years$^{-1}$ is the decay constant of samarium $^{147}$Sm; the superscript "0" means that the present-day values of the isotopic ratios are used. If we now insert into Eq. (10.18), for instance, the average crustal values of $(^{143}Nd/^{144}Nd)^0_{crust} \approx 0.5115$ (instead of 0.512638 from the CHUR model) and $(^{147}Sm/^{144}Nd)^0_{crust} \approx 0.2–0.22$ (instead of 0.1967 from the CHUR model), we will obtain the Early Proterozoic diamond ages of about 2 BY, exactly as it follows from the theory (rather than imprecise determinations of 3–3.4 BY). The same goes with all other determinations of the diamond age: when determining these ages, the old deposits' parameters should be included rather those of the rocks from the entire mantle (Sorokhtin, 2001).

The oxygen isotopic shifts and hydrogen/deuterium ratios in kimberlite hydrosilicates fit well the proposed model of the kimberlite formation. Moreover, Dowson (1983) indicates that the initial isotope ratios $^{87}Sr/^{86}Sr$ (in the kimberlite and affine rocks minerals with the minimum values of 0.703–0.705 for the no-phlogopite samples) are completely within the field of the same ratios in Early Proterozoic deposits (see Fig. 7.13). Maximum values are usually observed in phlogopite, that is, alkaline kimberlites with elevated rubidium content. For the eclogites, these ratios are within the 0.701–0.703 range, which for mantle rocks also corresponds to the Early Proterozoic age. The elevated $^{87}Sr/^{86}Sr$ ratio values in some eclogite samples may be due to the alkali contamination of basalts, probably at the hydration stage of the source oceanic crust by the chloride waters of the Early Proterozoic ocean.

Sorokhtin (2001) demonstrated that the proposed model of the kimberlite and carbonatite formation is in a complete accord with the neodymium isotopes distribution observed in these rocks. Indeed, as noted by Faure (1989), a partial mantle melting in the past gave birth to magmas with lower Sm/Nd ratios compared with the mantle matter. That is why the rocks formed from such magma (for instance, basalts and their transformation products—crustal rocks (granitoids and deposits)) currently have lower that mantle $^{143}Nd/^{144}Nd$ ratios. On the contrary, solid phases of the mantle matter (residue after the magma removal) have higher Sm/Nd ratios than in the mantle reservoir (Fig. 10.13). Faure emphasized that the rocks formed from such residual solid phases in the past geological epochs also will have higher $^{143}Nd/^{144}Nd$ ratios. Therefore, the carbonatites emerged in Early Proterozoic from such ultramafic restites by way of their serpentinization under reactions (10.1) and (10.2), also must have higher $^{143}Nd/^{144}Nd$ ration than the present-day mantle rocks.

The difference between the rocks due to their origin is demonstrably expressed by the $\varepsilon$Nd parameter as determined by the difference between the observed ratio $(^{143}Nd/^{144}Nd)_{rock}$ and its mantle value $(^{143}Nd/^{144}Nd)_m = 0.512638$

$$\varepsilon Nd = \left[ \frac{\left(^{143}Nd/^{144}Nd\right)_{rock} - \left(^{143}Nd/^{144}Nd\right)_m}{\left(^{143}Nd/^{144}Nd\right)_m} \right] \times 10^4 \qquad (10.19)$$

Eq. (10.19) shows that a negative $\varepsilon$Nd value corresponds to the rocks formed out of the mantle melt-outs through their reworking and the assimilation of the old crustal rocks. Positive $\varepsilon$Nd values indicate that the rocks formed from the restite solid phase of the mantle reservoir after the magma was removed from it at some earlier time (Fore, 1989). For instance, in the Archaean or Early Proterozoic sedimentary rocks formed from the mantle differentiates or their derivatives (basalts, tonalites, diorites or granitoids) the $\varepsilon$Nd parameter may be only negative. Conversely, carbonate deposits formed from the Early Proterozoic

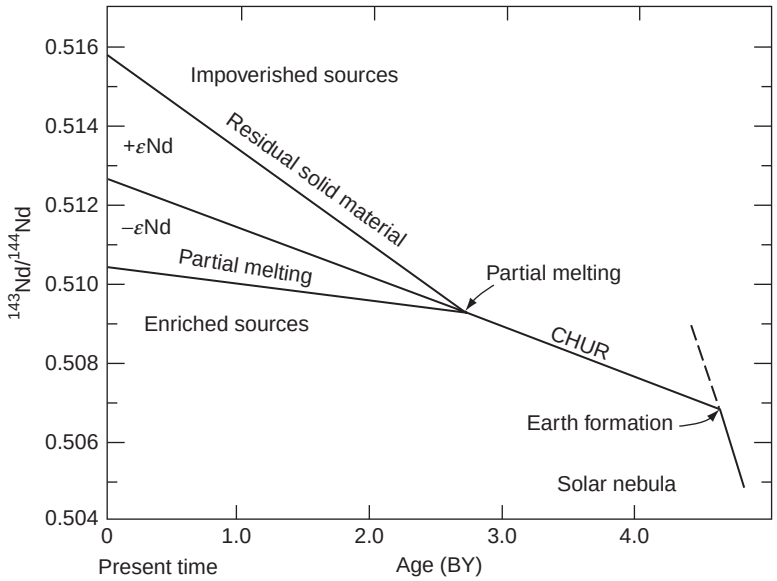


**FIGURE 10.13** Isotopic evolution of Nd in the mantle (within a CHUR chondrite reservoir) and in the melt-out from the mantle matter (Fore, 1989).

oceanic crust's ultramafic rocks after their serpentinization, judging from the reactions (10.1) and (10.2), must have positive εNd values (Fig. 10.13).

The deposits of different origin mix together. Depending on the mass ratio, the actual kimberlites and carbonatites can include the entire range of such values approximately between $-40$ and $+10$, including $\varepsilon Nd = 0$ as observed in the eruption products of some modern South African carbonatite volcanoes.

Under the proposed carbonatite and kimberlite origin model, these rocks should be dominated by the magnesium carbonates (magnesite and dolomite). In actuality, however, calcium carbonates prevail. The reason is the exchange reactions in the hot nodes of the kimberlite and carbonatite melts. Under these reactions, magnesium migrates to the silicates, and calcium, in carbonates, for instance, like follows:

$$\underset{\text{diopside}}{CaMg(Si_2O_6)} + \underset{\text{magnesite}}{MgCO_3} \rightarrow \underset{\text{enstatite}}{Mg_2(Si_2O_6)} + \underset{\text{calcite}}{CaCO_3} + 0.73\,\text{kcal/mol} \tag{10.20}$$

The proposed model forms diamonds by way of carbon reduction under a reaction between carbon dioxide or carbon monoxide with methane and other organic and abiogenic hydrocarbons sucked to great depths together with the deposits. In the subduction zones, carbon dioxide may be released through the thermal dissociation of carbonates:

$$\underset{\text{calcite}}{CaCO_3} + SiO_2 + 21.3\ \text{kcal/mol} \rightarrow \underset{\text{wollastonite}}{CaSiO_3} + CO_2 \tag{10.21}$$

$$\underset{\text{magnesite}}{MgCO_3} + SiO_2 + 15.3\ \text{kcal/mol} \rightarrow \underset{\text{enstatite}}{MgSiO_3} + CO_2 \tag{10.22}$$

$$\underset{\text{magnesite}}{2MgCO_3} + SiO_2 + 34.2\ \text{kcal/mol} \rightarrow \underset{\text{forsterite}}{Mg_2SiO_4} + 2CO_2 \tag{10.23}$$

$$\underset{\text{siderite}}{2FeCO_3} + SiO_2 + 35.8\ \text{kcal/mol} \rightarrow \underset{\text{fayalite}}{Fe_2SiO_4} + 2CO_2 \tag{10.24}$$

$$\underset{\text{calcite}}{CaCO_3} + \underset{\text{magnesite}}{MgCO_3} + 2SiO_2 + 31.4\ \text{kcal/mol} \rightarrow \underset{\text{diopside}}{CaMg(Si_2O_6)} + 2CO_2 \tag{10.25}$$

It is possible that at deeper levels where the deposit melting and melt liquation begin (i.e., in the area of emergence of the kimberlite magmas' silicate–carbonate fractions) phlogopite mega crystals form over the potassium feldspars:

$$\underset{\text{orthoclase}}{K(AlSi_3O_8)} + \underset{\text{magnesite}}{3MgCO_3} + H_2O \rightarrow \underset{\text{phlogopite}}{KMg_3(AlSi_3O_{10})(OH)_2} + 3CO_2, \tag{10.26}$$

olivines and pyrops over clay minerals and pyrophyllite

$$\underset{\text{magnesite}}{5MgCO_3} + \underset{\text{pyrophyllite}}{Al_2(Si_4O_{10})(OH)_2} \rightarrow \underset{\text{forsterite}}{Mg_2SiO_4} + \underset{\text{pyrop}}{Mg_3Al_2(SiO_4)_3} + 5CO_2 + H_2O \tag{10.27}$$

Carbon monoxide can form, for instance, in oxidizing of the bivalent iron hydroxide (amakinite) to trivalent hydroxide (goethite)

$$Fe(OH)_2 + CO_2 \rightarrow FeO(OH) + CO + H_2O + 3.4\ \text{kcal/mol}. \tag{10.28}$$

This kind of reaction is possible within the hot portion of the plate subduction zones. It is supported by the size of the olivine and garnet crystals sometimes exceeding 3–7 cm, and mostly the kimberlite inclusions in them (Dowson, 1983).

For carbon crystalline forms to emerge, it is necessary for it to be released through exothermal reactions (naturally, they release heat and lower the system's internal energy). These conditions are satisfied in the reactions between carbon compounds and carbon dioxide or carbon monoxide which proceed with the energy release, for instance:

$$CH_4 + CO_2 \rightarrow 2C + 2H_2O + 24.6\ \text{kcal/mol}, \tag{10.29}$$

$$CH_4 + 2CO \rightarrow 3C + 2H_2O + 65.9\ \text{kcal/mol}. \tag{10.30}$$

Besides hydrocarbons (often of organic origin), the abiogenic methane (forming in particular under reaction (10.4)) may participate in the diamond generation as well as hydrogen forming under reaction (10.5). In the latter case, the diamond generation reaction may be like follows:

$$2H_2 + CO_2 \rightarrow C + 2H_2O + 42.6\ \text{kcal/mol}. \tag{10.31}$$

Under moderate pressure, reactions (10.29)–(10.31) form graphite. Under high pressures, diamond crystallizes. All these reactions indicate that the diamond (and graphite) isotope composition must be substantially dependent on the composition of the reacting carbon compounds. For instance, in diamond formation under reactions (10.29) and (10.30) from the abiogenic or organic methane $C_{met}$ and carbonate carbon $C_{carb}$ (in the form of $CO_2$ or CO), the isotopic shifts in diamonds are determined as follows:

$$\delta^{13}C_{diam} = \frac{\delta^{13}C_{met} + \delta^{13}C_{carb}}{2} \tag{10.32}$$

$$\delta^{13}C_{diam} = \frac{\delta^{13}C_{met} + 2\delta^{13}C_{carb}}{3} \tag{10.33}$$

When diamonds form under reaction (10.31), obviously

$$\delta^{13}C_{diam} \approx \delta^{13}C_{carb} \tag{10.34}$$

Carbon isotopic shift in the abiogenic methane formed at the oceanic crust rock's hydration as measured in the hot springs of the mid-oceanic ridges (Sorokhtin et al., 2001) is about $-13\cdots-14‰$. The carbon isotope composition in organic matter ranges between $\delta^{13}C_{org} \approx -15$ and $-50‰$, and is on the average $-25‰$ (Hoefs, 1983). The carbonate carbon at the time of iron ore deposition nearly 2.3–2 BY ago had the positive isotope anomaly with the shift of up to $+13‰$ (Semikhatov et al., 1999). Thus, at the average value of $\delta^{13}C_{met} \approx -25‰$ we find from (10.32) $\delta^{13}C_{diam} \approx -6‰$. This is very close to the maximum in the histogram of $^{13}C$ isotope distribution in diamonds (see Fig. 10.7). If we assume the $\delta^{13}C$ isotope shift in the organic methane at approximately $-45‰$ (see Figs. 12.11 and 12.13), then $\delta^{13}C_{diam} \approx -16‰$. It is also within the limits of the isotope distribution in Figs. 10.6 and 10.7. Similar isotope shift distributions under Eq. (10.33) are within the $+0.3‰$ to $-6.3‰$ range.

The above estimates show that the diamonds mostly form from the mixture of the biogenic methane with abiogenic methane and carbonates.

The kimberlites are typical of drastically elevated ratio $MgO/CaO \geq 2$. It is even higher in the lamproites, up to 3–4. At the same time, in the affine alkali-ultramafic rocks this ratio is below 0.3–0.1, and in the carbonates it is 0.3–0.6. Its value in the modern oceanic deposits is only 0.05–0.12 (Chilingar, 1956; Lisitsin, 1978). A partial explanation of this discrepancy may be in that not limestones but dolomites most likely deposited in the Early Proterozoic oceans (Garrels and MacKenzie, 1974; Schopf, 1982; Ronov, 1993). In them, $MgO/CaO \approx 0.5–0.7$. Also, magnesite released under reaction (Eq. (10.1)) has $MgO \approx 46.7\%$.

Nevertheless, the carbonatites and kimberlite carbonates are usually dominated by $CaCO_3$. The reason is the exchange reactions of Eq. (10.20) in the kimberlite and carbonatite node melts. At even deeper elevations, garnet and corundum form with the release of calcite:

$$\underset{\text{anorthite}}{3Ca(Al_2Si_2O_8)} + \underset{\text{magnesite}}{6MgCO_3} \rightarrow \underset{\text{pyrop}}{2Mg_3Al_2(SiO_4)} + \underset{\text{calcite}}{3CaCO_3} + 3CO_2 + \underset{\text{corundum}}{Al_2O_3} \tag{10.35}$$

$$\underset{\text{anorthite}}{3Ca(Al_2Si_2O_8)} + \underset{\text{siderite}}{6FeCO_3} \rightarrow \underset{\text{almandine}}{2Fe_3Al_2(SiO_4)} + \underset{\text{calcite}}{3CaCO_3} + \underset{\text{corundum}}{3CO_2} + Al_2O_3 \tag{10.36}$$

Beside kimberlites, many shallower-originated but also clearly magmatic alkali-ultramafic rocks have similar geochemical features. Examples are the Kovdor and Africanda carbonatite intrusions as well as Khibin apatite–nepheline ore deposits on the Kola Peninsula. For instance, the Khibin syenites and apatites (nepheline, eudialyte, and feldspars) were found to contain hydrocarbon gases. Also encountered are high molecular weight (up to $C_{20}$) paraffin bitumoids, naphtene, and aromatic hydrocarbons, derivatives of compound

ethers, saturated steroids and carbon acids. Actually, all classes of compounds typical of sedimentary rock bitumoids were discovered among the bitumoids of these alkaline rocks (lubricants, benzene and alcohol–benzene resins, asphaltenes, etc.; Kostyleva-Lobuntsove et al., 1978).

The tectonic environment during subsequent geological epochs was periodically the one of the old shields' extension. The so emerged depth magmas together with the diamond crystals violently erupted onto the surface and formed there diamondiferous diatremes (see Fig. 10.14). Estimates of the kimberlite magma rise are up to 30–50 n/s (Sorokhtin et al., 2004).

We will now discuss the mechanism of the kimberlite magma rise to the surface. It is known that the chemico-density mantle convection is nonstationary and from time to time changes its configuration. That is why in place of the former descending convection flows in a while (usually, a few hundred million years) regularly emerge the inverse, ascending flows. The compression regime is being replaced by the extension regime. The latter emerges through extension forces acting on the base of the lithosphere from mantle flows diverging from the center of the ascending mantle flow, and due to the continental lithosphere "sliding" from the mantle uplift (swelling) which usually occurs over the center of an ascending mantle flow.

Open fractures cannot arise in the absence of liquid melts at great depths in the lithosphere. The reason is that the fracture walls will immediately "bloat" under the burden of overlying rocks (which is well above their strength) due to the plastic deformations in the surrounding lithosphere. If liquid fluids are present at the base of the lithosphere they assume the lithostatic pressure from the overlying rocks. After that, they are subjected to the extension stress only, and the fractures expand up at a rate of their fill-up with the fluid. Most publications about the mechanism of the kimberlite volcanism (Artyushkov, 1977; Anderson, 1979; Artyushkov and Sobolev, 1984; Sorokhtin et al., 1996, 2004) indicate that a rapid raise of the kimberlite magmas to the surface is facilitated by their low viscosity. The $CO_2$ release from magma as it is ascending the fracture must lower the melt viscosity

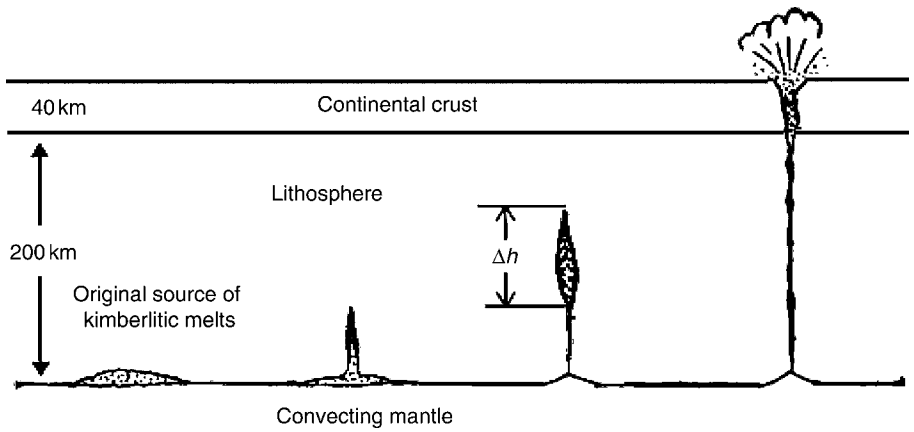


**FIGURE 10.14** Mechanism of magma-leading channels development at the kimberlite magmatism.

thereby drastically accelerating the fracture opening and the rate of its upward propagation (Anderson, 1979). The actual kimberlite ascension rates are so high that they easily carry with them even heavy eclogite and garnet peridotite xenoliths.

Therefore, due to the density gradient between the lithospheric rocks and kimberlite melts ($\Delta\rho \approx 0.5$ g/cm$^3$), the latter must be actively squeezed out of the lower part of the fracture and invade, after the fluid, the continental crust (Fig. 10.14) under high excess pressure

$$\Delta p \approx \Delta h \, \Delta p g, \tag{10.37}$$

where $\Delta h$ is depth interval in the lithospheric fracture filled up with the melts; $\Delta\rho$ is the density difference between the lithosphere and the kimberlite magma; $g \approx 10^3$ cm/s$^2$ is gravity acceleration. Obviously, this squeeze mechanism may work only if the excess pressure $\Delta p$ is greater than the rocks' tensile strength, that is, at $\Delta p > 10^8$ dyne/cm$^2$. For that, the inequality $\Delta h > 2$ km (see Fig. 10.14) must be satisfied, which appears to be realistic.

Thus, the opening of magma-conducting fractures under the effect of the lithosphere extension stresses, most likely, occurs only due to hydraulic fracturing of the overlying rocks by the excess pressure $\Delta p$ in the column of the rising magma (Fig. 10.14). Near the surface, the internal fluid pressure exceeds the lithostatic pressure. That usually results in a blow-up and the formation of diatremes. Such an explosion is accompanied by a drastic pressure drop and adiabatic decline in the magma temperature.

The kimberlite melts rise at a rate determined by the rate at which the opening fracture is being filled-up with fluids. Our estimate of kimberlite melt ascent rate (Sorokhtin et al., 2004) is within $4 < \bar{U} < 160$ m/s. Most likely, it is around $\bar{U} \approx 50$ m/s. At such a rate (nearly 180 km/hour), the kimberlite magma penetrates the entire lithosphere from the depths of 200–220 km within 1–1.5 h. The magma flow turbulence facilitating the capture of xenoliths begins under these conditions at a rate of $\bar{U}_{crit} > 4$ m/s. We would like to emphasize again that only due to high rate of the magma rise ($\bar{U} \geq 50$ m/s) high-density eclogite and lherzolite-garnet xenoliths may be carries up to the surface. High rate of the magma rise is apparently an explanation of the fact that diamonds, which are metastable at low pressure and high temperature, manage to rapidly "jump-through" a dangerous graphitization zone and be preserved within the fast-cooling kimberlite diatremes. Still, sometimes the blow-up tubes include diamonds in graphite "shirts."

### 10.6.1 Forecasting Criteria for the Location of the Bedrock Diamond Magmatism

Thus, under the proposed model:

1. Diamondiferous rocks (kimberlites, lamproites, and the affine rocks) mostly emerged underneath the Archaean continental crust. In some cases, they intruded the Proterozoic crust but should never be encountered on the young (Phanerozoic) platforms or even more so, on the ocean floor.
2. Diamondiferous kimberlite and lamproite blow-up pipes (diatremes) and the affine carbonatite and alkali-ultramafic intrusions are mostly positioned above the subduction zones of the Svekofenian (Karelian) plates. These zones functioned about 2.0–1.8 BY ago, although sometimes they could emerge over younger Grenville subduction zone.

3. According to the formation depth of a rock series in question and to the subduction zone dip angle, closest to the front of the former subduction zone (100 to 200–300 km from its front) are alkali-ultramafic intrusions and sodium carbonates. Farther away (200–400 km) is the calcite carbonatite and melilite, sometimes nondiamondiferous kimberlite zone. Diamondiferous kimberlite and lamproite diatremes are positioned farther than the other similar formations, at about 300 to 600–650 km from the Early Proterozoic subduction zone front.

Beside the already identified world diamond provinces no less prospective, based on the proposed depth melts emergence mechanism and the origins of the diamondiferous rocks, are the Baltic Shield, the Russian Platform with the Voronezh Shield and the Ukrainian Shield.

We will now discuss the extent to which the aforementioned search criteria of the bedrock diamondiferous rocks correspond with the identified kimberlite and lamproite blowpipes in the best known world diamond provinces.

*South Africa*. The kimberlites in the South African Republic (see Fig. 10.15) are developed within the huge Kaapvaal Archaean craton between the Early Proterozoic Limpopo foldbelt

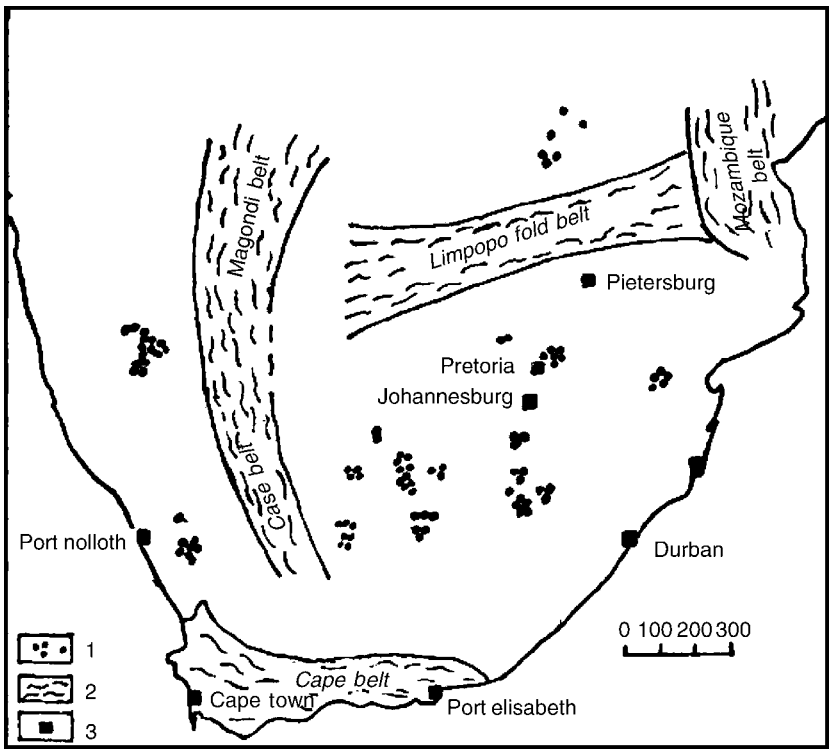


**FIGURE 10.15** Schematic South African kimberlite location map: 1. Kimberlite pipes (Trofimov, 1980); 2. Foldbelts: Limpopo, Case and Magondi formed about 2.0–1.8 BY ago, Mozambique belt (Lt. Paleozoic), Cape belt (Early Paleozoic) (Khain, 2001); 3. Cities. The kimberlite field south of Limpopo is located on the Archaean craton Kaapwal, and to the north of this belt on the Archaean craton Zimbabwe. The western kimberlite fields intrude through Proterozoic formations.

in the north and Early Paleozoic Cape mobile belt in the south. Zimbabwe craton adjacent to the Limpopo belt from the north is also diamondiferous. Both Archaean cratons were separated in Early Proterozoic and apparently were located within the equatorial belt far from each other. By the end Early Proterozoic (about 2.0 BY ago) they joined and formed the Limpopo foldbelt and a unique protoplatform Kalahari. The edge zones of the mobile belt were thrown over both cratons, Kaapvaal and Zimbabwe (Khain, 2001) which rises a suggestion that the oceanic plate subduction occurred simultaneously under both cratons, Kaapvaal (to a greater extent) and Zimbabwe. Besides, Archaean age of the Limpopo foldbelt central zone shows that in the collision of both cratons a small terrane of older crust was squeezed between them. After the Kalahari protoplatform emerged, the Magondi and Case mobile belts turned out attached to it from the west. Both belts, as the Limpopo belt, were evolving 2.0–1.7 BY ago (Khain, 2001). Similar situation is observed near the other African diamond provinces. They are everywhere are bounded by surrounded with Early Proterozoic foldbelts which were evolving in the formation of the supercontinent Megagaea about 2.0–1.8 BY ago.

Most North American diamondiferous kimberlites are associated with the cratons Slave and Superior. They are separated by a Svekofenian Trans-Hudson foldbelt which emerged 1.9–1.9 BY ago at Megagaea formation (Fig. 10.16). Besides kimberlites, the lamproite magmatism manifestations are known over the edges of the North American Platform (Bogatikov et al., 1991). Appraisal operations in 1990s showed that the craton Slave may become one of the best world diamond provinces (Kharkiv et al., 1998)

Most of the North American kimberlite bodies are located not on the Archaean but on the Proterozoic crust (Fig. 10.16). It may be that the origin of these kimberlites was either associated with Early Riphean iron ore accumulation impulses or with the fact that the North American Proterozoic formations were thrown over the Archaean crust.

A similar situation is observed in the Western Australia. A publication by Jaques et al. (1986) states that the major structural position of kimberlite and lamproite intrusions in the Western Australia is defined by their location within Early Proterozoic mobile zones. The zones are found on the boundaries of the Archaean cores, and some of these zones are covered by the Phanerozoic sediment cover (Fig. 10.17). It is worth mentioning that the Archaean block is suggested underneath a Riphean-filled Kimberley depression. The block is bounded from the south and east by Early Proterozoic folded systems, correspondingly King Leopold and Halls Creek. The final deformations (cratonization) age of this entire West Australian region is estimated at 1850–1890 MMY ago (Khain, 2001). A conclusion may be made that, as in North America, most of the kimberlite and lamproite intrusions in Western Australia emerged on the Archaean crust and the corresponding depth melts underneath it occurred during the Early Proterozoic plate subduction episode simultaneous with the Svekofenian orogeny on the Baltic Shield. As in North America, both kimberlites and lamproites are found in Australia. It may be an indication of both cratons sequentially drifting from the tropics to the boreal belt after Monogaea split, and then, during Megagaea formation, drifting back to the tropical belt.

One more classical example is the Yakut diamondiferous province on the eastern Siberian Platform. Tectonics of the Siberian Platform is sketched from Khain (2001). The basement is exposed on two large shields, the Anabar Shield in the north and the Aldan mega-block in the southeast. The Anabar mega-block and partially the Aldan mega-block

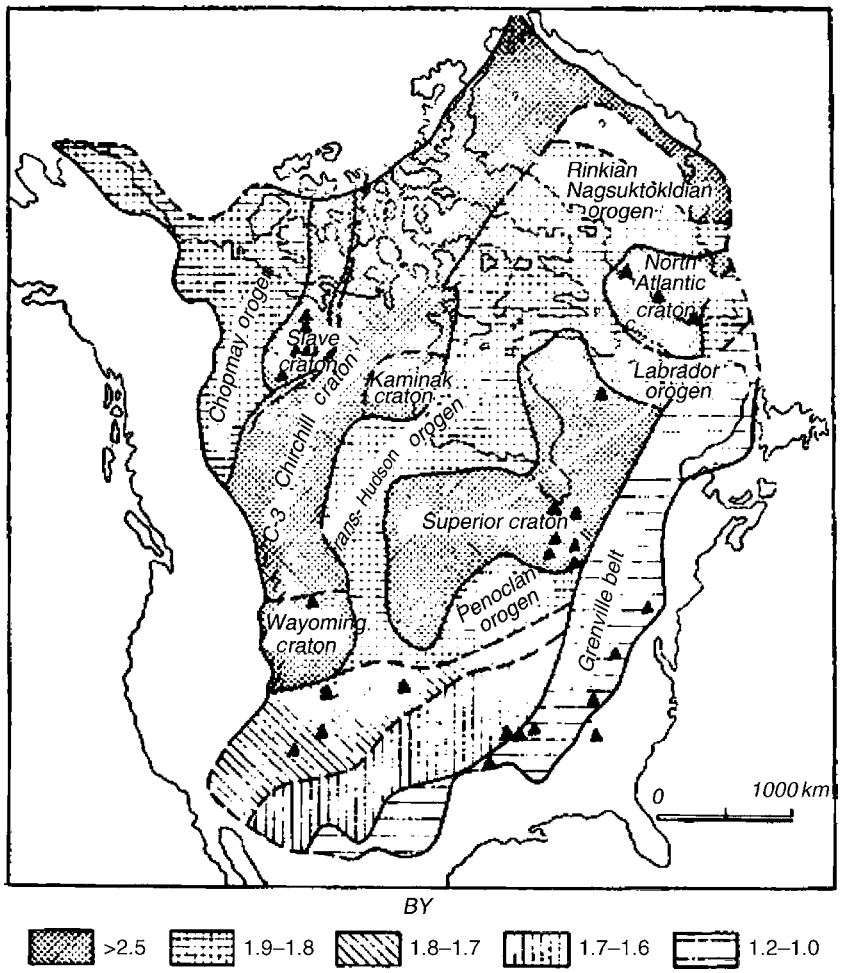


**FIGURE 10.16** Schematic geological map of the North American basement (after Hoffmann, borrowed from Khain and Bozhko, 1988). Trianfles are kimberlite bodies after Dowson (1983), and for the Slave craton, Kharkiv et al. (1998).

are diamondiferous (Fig. 10.18). The central part of the Aldan mega-block is composed of granite-greenstone rocks dominated by Late Archaean formations with the age of about 2.75 BY, although Middle Archaean ages are also encountered. The Anabar Massif includes three blocks separated by the foldbelts with the ages of 1.9–1.8 BY. Along those, the western blocks are underthrown under the eastern ones. The ages of the western (Magan) and the central (Daldyn or Central Anabar) blocks are 3.2 BY. The western (Tunguska) mega-block merged with the rest of the Siberian Platform probably in the second half of Proterozoic 1.9–1.8 BY ago. That was the time of the platform cratonization whereas in Early Riphean (i.e., during the supercontinent Megagaea destruction) the aulacogen stage began on the Siberian Platform.

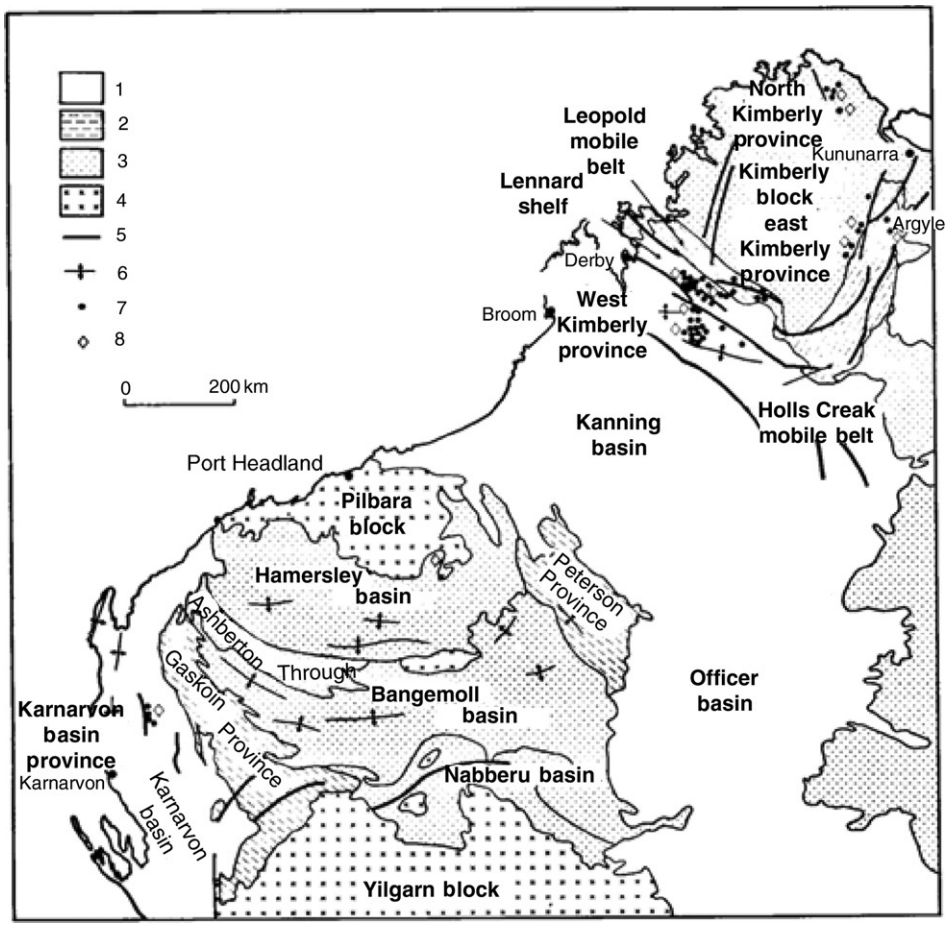


**FIGURE 10.17** Major tectonic structures in West Australia and locations of the kimberlite and lamproites provinces (Jakes et al., 1989): 1. Regions overlain by Phanerozoic sediments; 2. Proterozoic fold-belts; 3. Proterozoic basins; 4. Archaean cratons; 5. Faults; 6. Axes of anticlines; 7. Lamproite and kimberlite intrusions; 8. Diamondiferous deposits.

A judgment of the western (Tunguska) mega block is difficult as it is overlain by a thick platform cover. In our view, the fact that the Archaean rocks are exposed in the Yenisey Ridge and in the southwest of the mega block may indicate Archaean age of the mega block itself. Geophysical data show that the Baikal–Taymyr suture belt is a plate subduction zone along which the Tunguska mega block is subducted underneath the Anabar mega block. In this case, for instance, the origin of the kimberlite areas (from Mirny to Daldyn and Upper Mun) as well as the Mesozoic diatremes adjacent to the Anabar Shield (see Fig. 10.18) may be due to the Early Proterozoic iron-rich deposits of the Central Siberian paleo-ocean being sucked-in under the Magan and Anabar Archaean mega blocks. In all these cases, the distance between the front of the Baikal–Taymyr subduction zone and these kimberlite development areas is about 400–500 km. Still, the eastern kimberlite areas are apparently

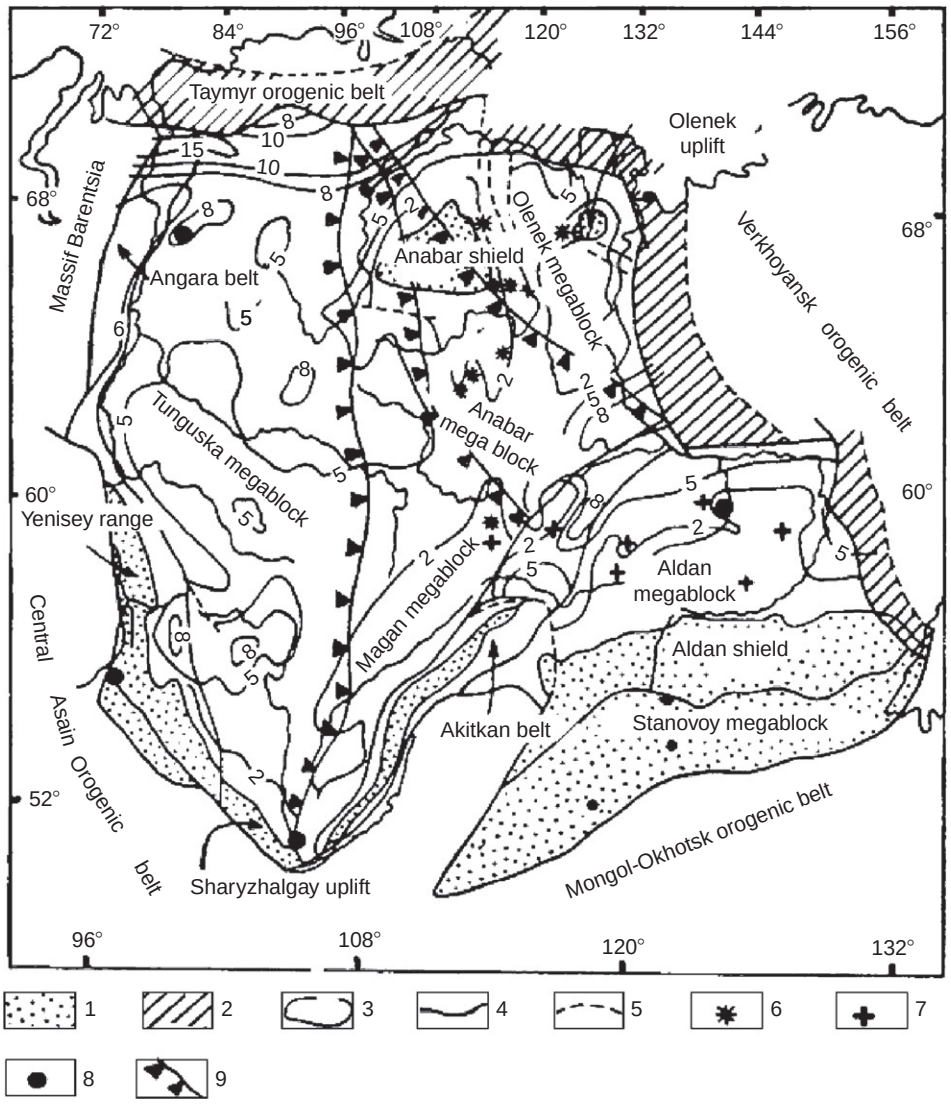


**FIGURE 10.18** Schematic tectonic map of the Siberian craton (Rosen et al., 1994; borrowed from Khaina (2001) with modifications): 1. Major basement outcrop areas; 2. Paleozoic and Mesozoic overthrust belts on the craton's periphery; 3. Platform cover thickness, km; 4. Main structures; 5. Faults in the platform cover; 6. Kimberlite belts; 7. Same, the crustal xenoliths; 8. Well penetrating the Precambrian basement; 9. Suggested plate subduction zones along the Baikal-Taymyr suture and eastern blocks of the Anabar massif (interpretation by these writers).

associated with the Magan block subduction zones underneath the Daldyn, and of the Daldyn block, underneath the East Khapchan block.

Thus, same as in South Africa on the Siberian Platform we are dealing with a classical example where the kimberlite rocks are formed due to sucking-in of the Early Proterozoic

pelagic (iron-rich) tropical deposits under the Archaean cratons. Contrary to that, the lamproite magmatism on the Aldan Shield indicates that the shield could have been for a while located in a boreal or even polar zone, and high-latitude deposits impoverished in carbonates but rich in silica, magnesium, and potassium were sucked-in under it.

We will now discuss possible formation conditions of the depth rocks in the north and northeast of the Russian Platform. Most important for the forecast of the position of alkali-ultramafic and diamondiferous magmatism is finding Svekofenian age Early Proterozoic sutures which are footprints of the former ocean crust plate subduction zones under the Archaean cratons and determining the direction of their dip.

The supercontinent Monogaea disintegrated 2.4–2.2 BY ago. The new supercontinent Megagaea formed during the period 2.1–1.8 BY ago. In the process, the Baltic Shield geodynamic environment changed to the overall compression regime. The closure of the Early Proterozoic oceanic basins 2.0–1.8 BY ago was accompanied by the oceanic crust consumption by subduction zones southwest of the Kola Archaean lithospheric plate. A result of the resulting collision of the previously separate microcontinents and terranes was the consolidation of the Karelian–Kola mega block and of the Svekofenian area with the formation of en echelon zones—footprints of the former plate subduction zones (Sorokhtin, 2001).

The spatial positions, internal structure, and the emergence age of the volcanosedimentary complexes suggest the presence in the Karelian–Kola mega block of at least four or five paleo-subduction zones dipping northeast (Fig. 10.19). Each of those may be accompanied by their own zone of kimberlite and alkali-ultramafic magmatism manifestations.

Previously, when describing the emergence mechanisms of the kimberlite and alkali-ultramafic magmas we emphasized a direct connection between the depths of their births and the distance to the front of the Early Proterozoic plate subduction zones (see Fig. 10.12). That is exactly the reason why the mutual positions of the Svekofenian subduction zones and the younger Caledonian and Hercynian rift faults are definitive in a forecast of the possible kimberlite magmatism areas.

The eventual Svekofenian oceans closing occurred 1.9–1.8 BY ago. Since then and through the present the Karelian–Kola mega block of the Archaean crust and the adjoining Early Proterozoic Svekofenian structures experienced only the platform regime of the continental crust evolution.

A new tectonic activation in the region occurred in Ordovician about 480–450 MMY ago at the closing of the Japetus Paleo-Atlantic Ocean (Sorokhtin et al., 2004). The Japetus closure may be restored from the present-day North Atlantic continental shelf outlines and from the striped magnetic anomalies. It may be also amended by the structure of the Caledonian allochthonous sheet in the northwestern Baltic Shield which marks the ancient merger zone. In the collision with the European Plate, the wedge-like shape of the East Greenland lithospheric plate must have resulted in extension stresses over the northern Baltic Shield along the line North Norway—Kola peninsula—the Archangel Province, that is, from northwest to southeast (Fig. 10.20).

Similarly, in closing of the Devonian Paleo-Urals Ocean and in the collision at the end Carboniferous between the West Siberian epi-Paleozoic platform and the Russian Platform an extension stress zone may have been initiated along the line Novaya Zemlya—Kolguyev Island—city of Kandalaksha—Bothnian Bay (Fig. 10.20). At that, the Karelian Plate protrusion

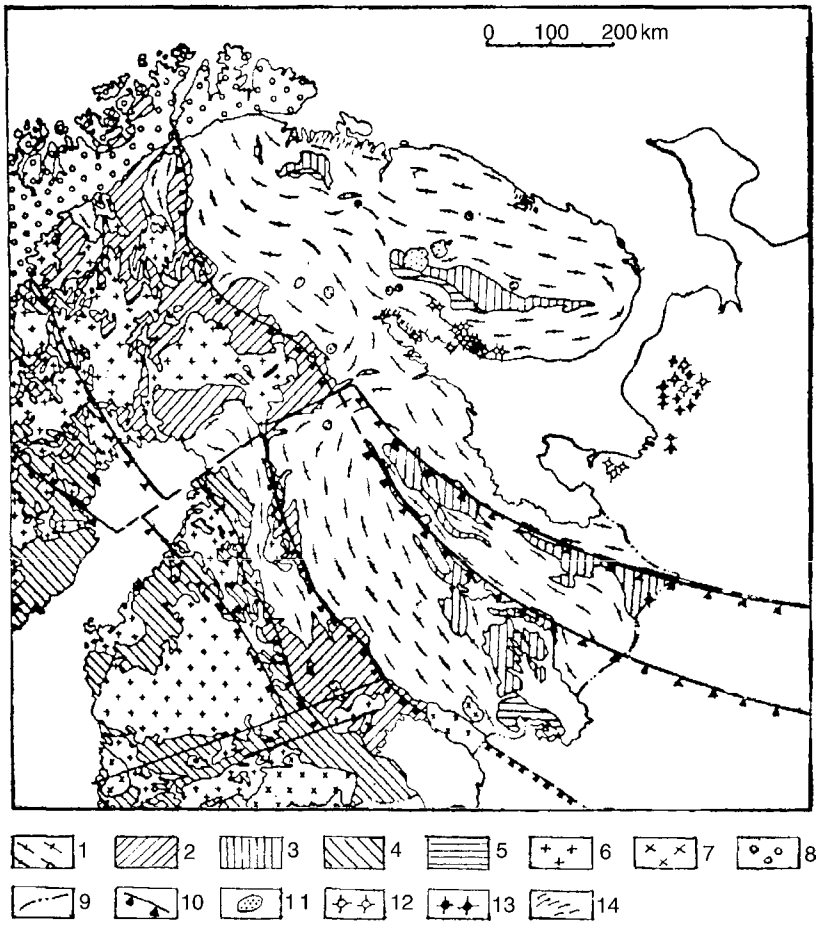


**FIGURE 10.19** Schematic geological map of the eastern Baltic Shield (Sorokhtin et al., 1996, 2004): 1. Continental-crustal Archaean associations; 2–3. Volcanosedimentary and intrusive complexes aged 2.5–2.2 BY: 2. Island arc and ophiolite; 3. Rift, island arc and ophiolite; 4–5. Volcanosedimentary and intrusive complexes aged 2.2–1.9 BY; 4. Island arc and ophiolite, 5. Rift, island arc and ophiolite; 6. Svekofenian (1.9 BY) granites and granitoids; 7. Rapakivi granites (1.4 BY); 8. Allochthonous Caledonian sheets; 9. Boundary of the Russian Platform Paleozoic sediment cover; 10. Early Proterozoic (1.9–1.8 BY) subduction zones and subduction directions; 11. Alkaline-ultramafic intrusions; 12. Pykrite and melilitite blow-pipes; 13. Kimberlites; 14. Alkali-ultramafic and base dykes.

(marked by a knee-shaped bend of the Novaya Zemlya folded structures) intruded as a wedge the Barentz Sea Platform.

The directions of the Baltic Shield compression 400 and 320 MMY ago were close to ortagonal. Thus, the compression and extension stresses formed at those times were also ortagonal to each other. Figure 10.20 illustrates the compression and extension axes in the northwestern Kola Peninsula. The compression and extension arose in the Japetus Paleo-Ocean closing 400 MMY ago. In the eastern Kola Peninsula and Archangel Province, these

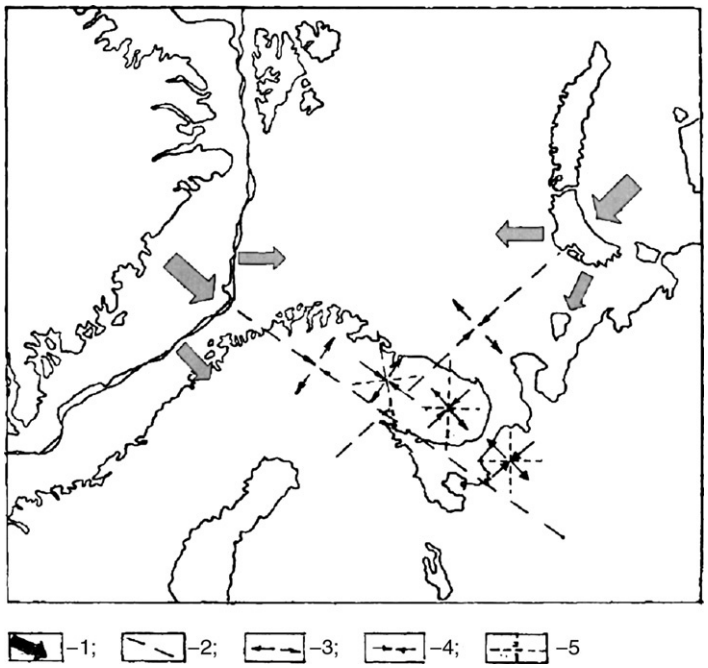


**FIGURE 10.20** Schematic map demonstrating the emergence of extension and compression environments at the collision of the America-Greenland and West-Siberia—Kara Sea plates with the Baltic-Barets Sea plate, respectively, about 400 and 320 MMY ago (Sorokhtin et al., 1996, 2004): 1. Plate pressure directions; 2. Basic trends of compression and extension zones; 3. Extension stresses; 4. Compression stresses; 5. Characteristic trends of sublatitudinal and sublongitudinal strike-slip faults feathering the main extension and compression zones at 45°.

stresses emerged at the closing of the Paleo-Urals Ocean about 320 MMY ago. In actuality, these both compression and extension systems may overlap.

As the result of these events systems of ortagonal strike-slip displacement occurred on the northeastern Baltic Shield. Their intersections formed extension faults which were natural channels for the release of the depth magmas on the surface. Apparently, the intense alkali-ultramafic and kimberlite magmatism on the Baltic Shield and the northern Russian Plate 450–320 MMY ago was associated with the birth and rejuvenation of these fault systems. The alkali-ultramafic intrusive massifs are found in the central Kola Peninsula (Fig. 10.19). The blow-pipe area is eastward from the alkali-ultramafic intrusives and occupies a compact location within the Yermakov graben. The blow-pipes in the Archangel Province were discovered in the early 1980s. They form the Zimne–Berezhnaya area of the kimberlite and melilite magmatism (Fig. 10.19). Individual diatremes were found in the area of Ivanov Bay on the Barentz Sea coast.

Most of the Kola Peninsula diatremes positioned on the Tersk shore of the Kandalaksha Bay are of a melilite composition whereas in the Archangel Province both melilite and deeper-rooted diamondiferous kimberlite magmatism took place. Beside intrusives and diatremes, the Kola Peninsula Caledonian and Hercynian magmatism was characterized by an abundant dyke complex forming two separate areas. One of them extends along the Murmansk shore from North Norway to the Ivanov bay in the east (Fig. 10.19). The dykes are mostly of the alkali-ultramafic composition. There are some dolerite dykes within the western area.

The plate subduction zones on the Karelian–Kola craton are positioned in an echelon pattern. Apparently, in such a situation there is a possibility of overlapping alkali-ultramafic, depth-transitional carbonatite, melilite and even kimberlite magmatism as shown in Fig. 10.8.

## 10.7 EFFECT OF ANCIENT ORE DEPOSITS REMOBILIZATION (RECYCLING)

Most ore manifestations, especially the Mesozoic ones, are a result of the remobilization and redeposition (recycling) of the Early Proterozoic ore deposits. Practically all Mesozoic gold, tin, rare metals and polymetals deposits belong to this secondary type. Some Phanerozoic iron deposits (such as contact-metasomatic titano-magnetites of the Magnitnaya Mountain in the Urals and some other world deposits) also belong to this group. Below, we will discuss two most demonstrative deposits of this type.

Rare metals and gold deposits of the Verkhoyansk–Kolyma folded zone. Tin, rare-metals, and gold deposits in the Verkhoyansk–Kolyma folded zone of Eastern Siberia are good examples showing the effect of the exogenous factors on the emergence of seemingly endogenous commercial deposits. In Early Paleozoic, the Kolyma Massif split from the East-Siberian Platform. The East-Siberian paleo-ocean arose between them (Fig. 10.21). Thick clastic sequences whose material was brought in by the paleo-rivers. They came from the Anabar Archaean Shield and from the Early Paleozoic sediment cover in the north, and from the Aldan Shield and the Vitim-Patoma Highlands in the south, and were deposited on the eastern passive margin of the Siberian Platform. Near-shore placers of heavy

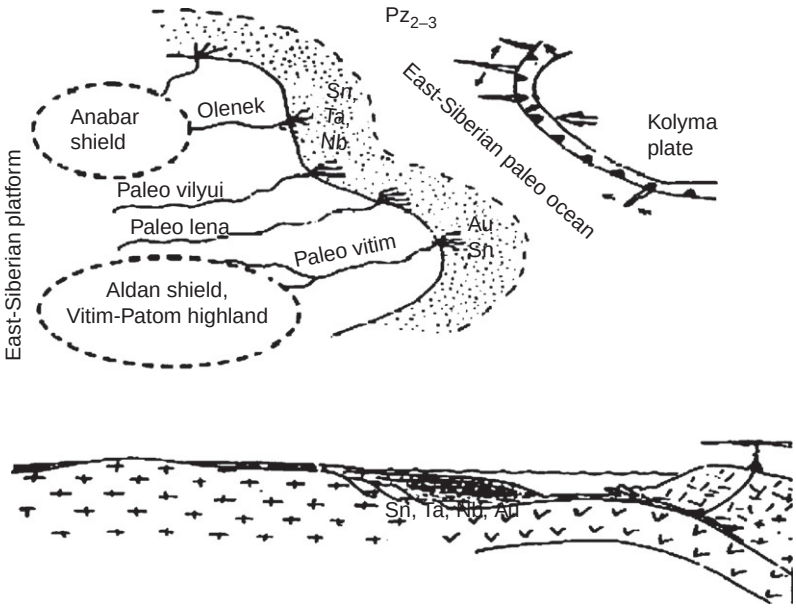


**FIGURE 10.21** East-Siberian ocean in Paleozoic and its geodynamic cross-section.

fractions carried in from the old shields were gradually accumulated in these deposits. They included cassiterite, gold, niobium, tantalum, and other rare metal minerals. This way, over the 250–300 MMY's existence of the East-Siberian Ocean at least 12–15 km of the clastic (including deltaic and channel) Devonian (although mostly Carboniferous through Jurassic) sediments accumulated on its western margin (i.e., in the eastern Siberian Platform).

In Mid-Mesozoic, a new convergence of the Kolyma Massif with the Siberian Platform began. As a result, the East-Siberian Ocean started to close. The paleo-ocean closure in Mid-Mesozoic was accompanied by the crushing of all continental-margin sedimentary sequence accumulated by that time on the oceanic crust, and its obduction of the Siberian Platform (Fig. 10.22). The Kolyma Massif, as an ice-breaker, crushed under itself the East-Siberian oceanic lithosphere. The crosswise extension fractures must have emerged in the oceanic lithosphere underlying the continental margin sedimentary sequence. These fractures were used by basalts melts that invaded the lower portion of the sedimentary sequence. The basalt melt density is about 2.8 $g/cm^3$ which is substantially higher that the average sedimentary density of 2.5–2.7 $g/cm^3$. For this reason, the basalts intruded only the lower part of the sequence. The basalt magma temperature at 12–15 km reaches 1350–1400 °C. The melting temperature of water-saturated deposits at the same depth is no higher than 700–750 °C. Therefore, on contact with the hot basalt magma the deposits must have melted, somewhat lowered their density due to the heating and then intrude

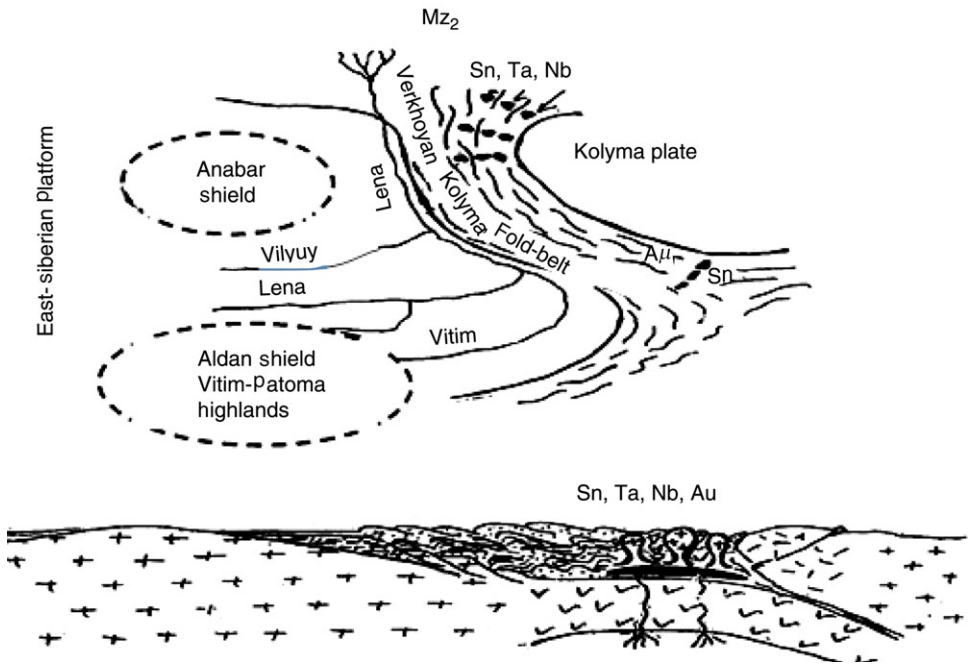


**FIGURE 10.22** Schematics of Mesozoic collision between the Kolyma Massif and the edge of the East-Siberian Platform and the geodynamic cross-section of the resulting Verkhoyan–Kolyma fold zone.

the upper horizons of the sedimentary sequence as granite intrusions—diapires. The average composition of these granitoids is from granite–porphyries to liparites. It corresponds with the average composition of the zone's sedimentary rocks.

Ore elements accumulated earlier in the deposits were subjected to the hydrothermal reworking. The result was a typical ore specialization of the granitoids and the corresponding hydrothermal manifestations in the northern Verkhoyansk–Kolyma zone where to the sediments from the Anabar Massif were mostly brought-in. This is the tin and tantalum–nyobium mineralization, and in the southeast of the zone (where to the sediments from the Aldan Massif and the Vitim-Patoma Highlands were brought in), mostly gold mineralization.

Another example of a similar recycling is Malaysian tin deposits.

The magmatic and metasomatic Urals titanomagnetite deposits of Kichkanar and iron ore deposits at Magnitnaya and Blagodat also belong to the recycling formations. In all those cases, the emergence of iron ore deposits was associated with the closing in Late Paleozoic of the Paleo-Urals Ocean and obduction over the eastern edge of the Russian Platform by the Urals island arc. Thick Riphean sedimentary sequences and older Taratash ore complex were sucked-in into the subduction zone. They were remelted and hydrothermally activated within this zone which caused the emergence of such ore deposits. It is important that, for instance, the Kachkanar ore bodies associated with the crust intrusion by large gabbroid massifs are lined up by pyroxenes. It means that, together with iron, the basalt melts carried silica out to the surface. And the iron–silica paragenesis is indeed observed at Taratash.

Tectonics of the lithospheric plates opened a new way to the discovery of the patterns in the distribution of economic deposits on the Earth's surface. For instance, it follows from the theory, and is supported by the empirical data, that most endogenous ore deposits form only over the edges of the lithospheric plates. Different types of plate boundaries contain different ore complexes differently positioned in relation to these boundaries. This enables the utilization of the geodynamic maps with the ancient plate boundaries marked for the forecast and search of the economic deposits.

Copper–nickel sulfide deposits (Norilsk type). Other examples of the mobilization of ancient ore formations are unique Norilsk and Talnak copper–nickel deposits. They are found in the Mesozoic trapps over the northwestern Siberian Platform (Starostin and Ignatov, 2004). Most of these trapps, however, extends far to the southeast from the Norilsk area and are almost totally empty of the ore. Besides, in Mesozoic, due to the repeated convection stirring of the mantle matter, its composition was reasonably uniform, without the volumes enriched in ore elements. This enables a suggestion that the Norilsk ores are genetically associated with basalts of the trapp formation. This is also supported by the basalt groups in other world regions, such as the Deccan trapps in India or Ethiopian trapps. They are similar in their composition with the Siberian trapps outside Norilsk and Talnak and do not include ores. A similar situation is identified with the mid-oceanic ridge basalts. The ridges expend 60,000 km on the ocean floor, the basalts were everywhere melted-out from the mantle, they are similar in their properties and all of them do not include ores. A conclusion from this is that the Norilsk and Talnak nickel ores got into the Siberian basalt trapps not from the mantle. This is also supported by the Earth's evolution theory. It says that after the core separation and the establishment of the geological evolution under the

laws of the lithospheric plate tectonics, the mantle convection over 2.5 BY well stirred its matter and made it uniform, without any substantial ore anomalies. Where did the platinum, nickel, copper, and iron sulfide ores come from?

The only possibility is for the Norilsk ore elements (maybe without most of iron) enter the basalts from the continental crust. To analyze this suggestion, it is necessary to determine a possible basement and the Early Proterozoic composition, the structure and the assumed composition of the Tunguska depression and the Talnak Trough. Khain (2001) stated that the basement of the Siberian Platform was composed of the Archaean blocks whose unification into a single platform and its consolidation apparently occurred in the end of Early Proterozoic. The Tunguska mega block is exposed in the extreme southwest. It is fringed in the west by the Yenisey mobile belt with exposures of the Early Precambrian. A distinct feature of this belt is thick lower Proterozoic sedimentary and magmatic rocks formed most likely in the active continental margins environment.

It may be expected therefore that the entire set of commercial deposits so typical of this unique metallogenic epoch (see Section 10.2) may be present in these thick Early Proterozoic magmatosedimentary sequences. If it is so, then that was exactly the remobilization of the ore elements from the Early Proterozoic deposits and rocks that served the source for the oreless basalt saturation with platinoids and sulfides of copper and nickel (and in part, iron). Iron could be supplied to the pyrrotins directly from the basalts.

The present-day (and the Mesozoic) mantle is and was practically sterile with regards to ore element aggregations. All such elements were uniformly distributed ("smeared-out") over the entire mantle mass and had relatively low concentrations. If so, the basalt melts which intruded Norilsk region could have been saturated with noticeable amount of ore elements only by breaking through the Early Proterozoic ore-bearing formations or the products of their subsequent reworking, such as Early Riphean weathered crusts. Apparently, an important role in the process was played by the ancient aulacogens intruded by the basalts. They were filled-in with sulfate (gypsiferous) deposits which contained substantial amounts of hydrocarbons. That opened the way to important endothermic reactions which released an active mineralizer, hydrogen sulfide $H_2S$, with the heat supplied by the hot basalts (for gypsum $Q \approx 34$ kcal/mol):

$$\underset{\text{gypsum}}{CaSO_4 \cdot 2H_2O} + \underset{\text{methane}}{CH_4} + 34\ \text{kcal/mol} \rightarrow \underset{\text{calcite}}{CaCO_3} + H_2S + 3H_2O \tag{10.38}$$

Anhydrite is reacting as follows:

$$\underset{\text{anhydrite}}{CaSO_4} + \underset{\text{methane}}{CH_4} + 9.5\ \text{kcal/mol} \rightarrow \underset{\text{calcite}}{CaCO_3} + H_2S + H_2O \tag{10.38'}$$

The iron sulfide formation over silicates is already happening under the exothermic reaction with the heat release and destruction of the source silicates:

$$\underset{\text{olivine}}{Fe_2SiO_4 + Mg_2SiO_4} + 2H_2S \rightarrow \underset{\text{pyrrotine}}{2FeS} + \underset{\text{enstatite}}{2MgSiO_3} + 2H_2O + 38.8\ \text{kcal/mol}, \tag{10.39}$$

Under these reactions, the water is released in the form of a vapor with $\Delta H_f^0 = 57.8$ kcal/mol and not the liquid water for which $\Delta H_f^0 = 68.3$ kcal/mol.

Basalt intrusions into gypsum-coaly sequences result in the formation of diopside under exothermic reaction

$$\underset{\text{olivine}}{Fe_2SiO_4 + Mg_2SiO_4} + 2CaSO_4 + 2C \rightarrow 2FeS + \underset{\text{Diopside}}{2CaMg(Si_2O_6)} + 2CO_2 + 210\ \text{kcal/mol}, \tag{10.40}$$

When the hot basalt intrudes hydrocarbon-saturated sediments, monticellite forms, this time under the endothermic reaction:

$$\underset{\text{olivine}}{Fe_2SiO_4 + Mg_2SiO_4} + 2CaSO_4 + 2CH_4 + 45.33\ \text{kcal/mol} \rightarrow 2FeS + \underset{\text{Monticellite}}{2CaMg(SiO_4)} + 2CO_2 + 4H_2O \tag{10.40'}$$

Copper could enter the melts directly from clastic sediments-filled Proterozoic and Riphean aulacogens very common on the Siberian Platform. Such sequences include red-bed weathered crusts, usually with copper sandstones and shales, mostly of a sulfide composition: chalcosine $Cu_2S$, bornite $Cu_5FeS_4$ and chalcopyrite $CuFeS_2$ (Lourie, 1988).

This is a solution of the copper and iron sulfide origins in the Norilsk ore belt within the constraints of our hypothesis of ore element recycling. It is a more complex problem to determine the origin of nickel sulfides. It is likely that most nickel sulfide is directly captured from the Precambrian sulfide ores, such as pentlandite very common in Early Proterozoic ore deposits. Part of nickel, however, could be supplied from the ultramafic rock weathered crusts, especially Precambrian, where nickel-containing analogs of the serpentinite, revdinskite, garnierite, and nepouite are often found. These rocks have been encountered in the South Urals, in the Maksyutov complex, Khalilov and Akkerman deposits, and also on the Island of New Caledonia. Pentlandite, revdinskite, and garnierite are important nickel ores (Betekhtin, 1950; Lazarenko, 1971). For the extreme nickel mineral revdinskite:

$$\underset{\text{Revdinskite}}{Ni_6(Si_4O_{10})\,(OH)_8} + 6H_2S \rightarrow 6NiS + 4SiO_2 + 10H_2O \tag{10.41}$$

Hot basalts rising from below assimilate all so formed metal sulfides and carry them into the upper levels of intrusions where the ore melts may be liquated, sometimes with the formation of massive ores.

The Norilsk and Talnak deposits sulfides were formed at the expense of hydrogen sulfide which emerged in the reduction of sulfate minerals. Thus, it is expected that the sulfur isotopic composition in the sulfides will be preserved from the sulfates. That is exactly what is observed. Based on the data published by Grinenko and Grinenko (1974), Almukhamedov and Medvedev (1982), the isotopic composition of the sulfides in the Norilsk copper–nickel deposit is clearly shifted in the direction of the sulfate sulfur: to $d^{34}S \approx +8$ and $+19‰$, at the mantle composition of around 0–2‰.

Thus, the isotopic composition of sulfur from the Norilsk sulfides also confirms that most of them were remobilized by the basalts from the Precambrian areas of the continental crust, that is, these sulfides are the result of recycling.

The provided discussion shows that the necessary condition for the emergence of the Norilsk type sulfide ores is the presence of a Proterozoic aulacogen filled up with clastic, gypsiferous, and coal-bearing deposits saturated with hydrocarbons. Basalts above such ore deposits usually have elevated magnesium content (see reaction (10.40)) and carbonate inclusions often represented by large Iceland spar crystals (see reactions (10.38) and (10.39)).

Therefore, as the discussed Norilsk-type sulfide deposits show, their external indication is the elevated basalt magnesium content and the presence of calcite often forming large Iceland spar crystals.

## 10.8 ORIGIN OF THE EXOGENOUS ECONOMIC DEPOSITS

The new theory opens additional opportunities in exploring for exogenous commercial deposits. They include bauxites, coal, salts (including potassium salts), gypsum, etc. These economic minerals are currently located in the different climatic belts but their formation could occur only under very specific and often very narrow climatic and tectonic environments. Lithospheric plate tectonics helps more accurately conduct the paleogeographic reconstructions of the past geological epochs and from them find areas with most favorable climatic conditions and tectonic regimes for the accumulation of various economic deposits. Thus, the search for evaporites (salt deposits) should be conducted only within the areas which, under the reconstructions, were positioned in the aridic (desert) climate where semi-closed marine basins could have emerged. Most favorable appear to have been young Red Sea-type oceanic depressions at the early development stages of the Atlantic Ocean type depressions. Such conditions may have, for instance, occurred at the very beginning of the disintegration of the last supercontinent Pangaea in Jurassic along the shores of the then nascent Atlantic Ocean (see Fig. 10.23) and in the Red Sea in Miocene.

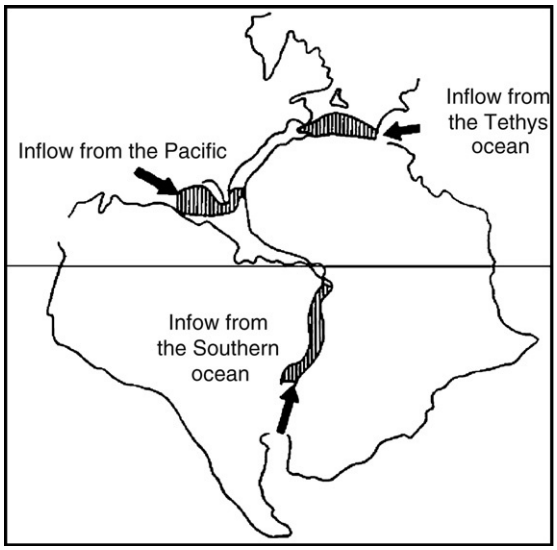


**FIGURE 10.23** Circum-Atlantic belt of salt deposits (shaded areas). After Burke (1975).

The salt deposition under arid environments might have occurred also in the residual basins emerging on the continental margins when they are obducted by the island arcs. This happened, for instance, during the Permian period in the east of the Russian Platform obducted by the Uralian island arc. Paleogeographic reconstructions indicate that the central and northern Urals foredeep was located at that time at approximately 25–30° N, that is, within the desert belt. This predetermined the deposition of thick salt sequences (including potassium salts) in a narrow semi-closed marine basin which existed then in front of the Urals. A similar situation existed at that time in the Central European Rhenohercynian tectonic zone which is also rich in the Permian salt deposits.

Contrary to the salts, coals form only in humid environments in the tropical or moderate climate at the continental margins continuous subsidence under the ocean level. Such conditions usually occur in gradually subsiding young continental rift zones which later convert to aulacogens, or on the passive continental margins at the early stages in the evolution of the Atlantic-type oceans. Besides, the conditions of rapidly subsiding continental margins occur under the weight of the obducting island arcs. These coal accumulation conditions existed, for instance, in Carboniferous within a broad band extending over almost the entire Eurasia from England and France through Middle Europe, southern Russian Platform into Kazakhstan and Southwestern Siberia. This entire area was then under a humid tropical climate and besides experienced intense subsidence due to the closing of the old Paleo-Tethys Ocean positioned to the south.

The following should be kept in mind when looking for phosphorite deposits. Especial attention must be paid to those surface areas which during the global transgressions (such as the Vendian, Ordovician–Devonian or Late Cretaceous) were located in the near-shore continental zones subjected to marine flooding in the tropical belt and in the upwelling zones (Figs. 10.24 and 10.25). Such zones were usually located on the eastern shores of the then contemporary oceans. Four major phosphorite accumulation epochs are identified. They are: (1) Early and Middle Cambrian (Karatau deposits); (2) Early and Middle Ordovician (Baltic state, Tennessee); (3) Early Permian (Rocky Mountains); (4) Late Permian–Cenozoic (the Volga and Morocco basins).

A similar potential in using the lithospheric plate tectonics approach is applicable in the bauxite exploration. These commercial deposits form only under a hot and humid climate in the equatorial belt due to the weathering of basaltic and clayey rocks. On the reconstruction, zones favorable for the bauxite formation are always positioned near the paleo-equator for a given epoch. Thus, the bauxites of the Tikhvin deposit, Urals, Kazakhstan, and South China (many of them are currently in relatively high latitudes of 50–60° N) formed in Early Carboniferous near the equator and only later, due to the continental drift, moved to higher latitudes.

We mentioned earlier (see Fig. 10.12) the Kola Peninsula nepheline–apatite deposits. It is important that the area was located during the deposition in Early Proterozoic of iron-rich sediments (from which later the Apatite alkali-ultramafic intrusions formed) on the southwest shore of the Baltic Shield in the tropical upwelling zone where phosphorites deposited. During the Svekofenian orogeny, this margin was subducted under the Kola craton which caused the emergence on it of the unique magmatic apatite deposits (see Fig. 9.3).

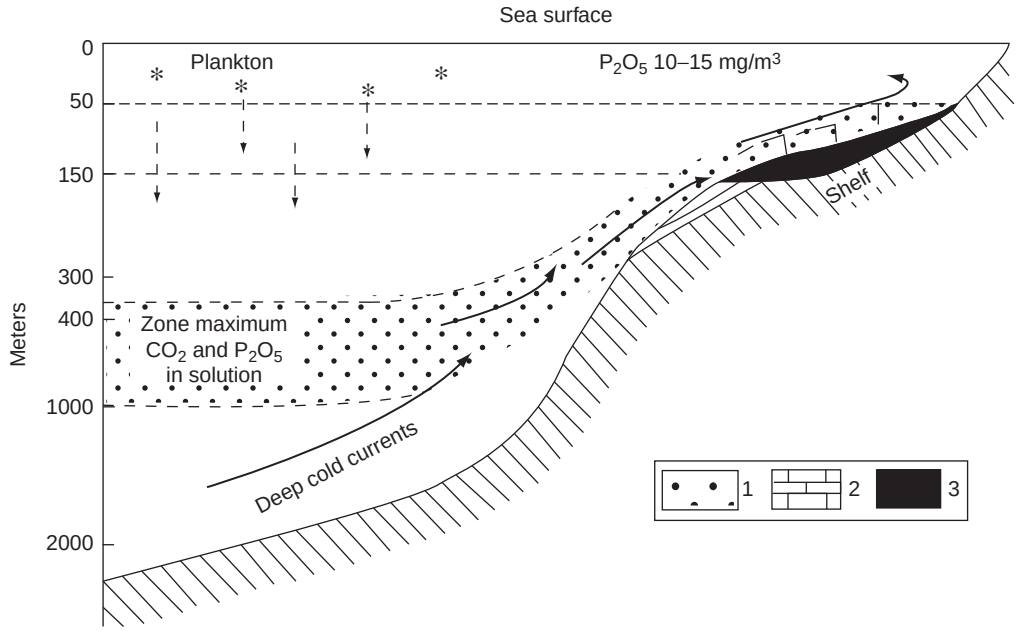


**FIGURE 10.24** Phosphate formation in the oceanic tropical upwelling zones on their eastern shores (after Kazakov, 1939): 1. Phosphorus—compound enriched oceanic waters; 2. Continental shelf carbonate deposits; 3. Phosphate deposits.

## 10.9 TECTONICS OF THE LITHOSPHERIC PLATES AND EARTH'S OIL AND GAS OCCURRENCES

Tectonics of the lithospheric plates introduced a very significant contribution to the petroleum geology. A first large-scale and successful application of the new theory into the practical combustible fuel exploration was performed in this important branch of the applied geology. This, however, happened only in the late 1970s. Before that, in early 1970s, in the US and Russia almost simultaneously appeared new ideas about the existence of a powerful hydrocarbon generation mechanism out of the organic matter sucked-in with the oceanic deposits into the plate subduction zones (Sorokhtin, 1974; Sorokhtin et al., 1974; Dickinson, 1974). Figure 10.26 illustrates the hydrocarbon accumulation mechanism in the body of island arcs and active continental margins when the oceanic plates and the overlying pelagic deposits are sucked-in into them.

The suggestion made in the early 1970s was a bold one but had to be verified. This proposed formation mechanism of oil and gas basins gravitating to the old and young plate subduction zones, and the hydrocarbon generation is illustrated by Fig. 10.26. What was needed was a proof that the oceanic deposits are indeed sucked-in into the plate subduction zones as in the early 1970s this suggestion was not obvious. Earlier we discussed this issue (see Section 8.5); we emphasized that the deposit sucking-in into the subduction zones phenomenon was initially just a hypothesis which later was substantiated by drilling. Besides,

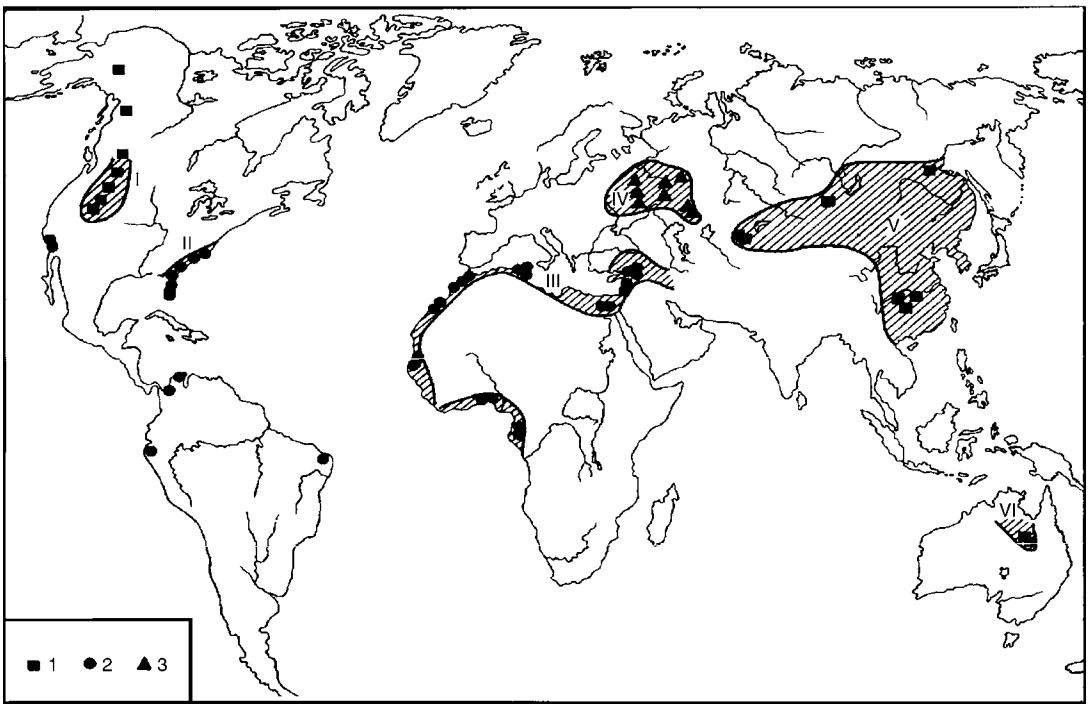


**FIGURE 10.25** World's phosphate provinces (after Sinyakov, 1987). Phosphate deposits: 1. Microgranular; 2. Granular; 3. Nodular phosphate provinces: I. Rocky Mountains; II. East-American coastal plain; III. Arabian–African; IV. Russian Platform; V. Asian; VI. Australian.

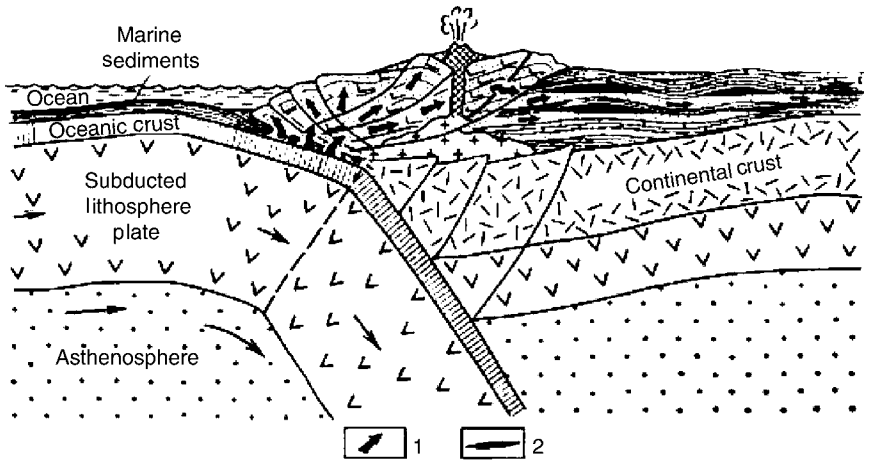


**FIGURE 10.26** Hydrocarbon generation in the oceanic plate subduction zones under island arcs and active continental margins: 1. Hydrocarbon migration paths from the subduction zone to the obducted plate structures; 2. Formed hydrocarbon accumulations.

it was necessary to identify the formation mechanisms and regimes of the foredeeps and submontane troughs where usually the bulk of hydrocarbons migrating from the adjacent plate subduction zones are concentrated.

It was illustrated by calculations (Sorokhtin et al., 1974). The combined length of the modern plate subduction zones reaches 40,000 km; the average oceanic deposit thickness is about 500 m and the average plate subduction rate is 7 cm/year. Thus, nearly 3 billion tons of the deposits annually are presently being sucked-in under all island arcs and active continental margins. The oceanic deposits usually contain approximately 0.5% of organic matter of which only 30% may be converted to hydrocarbons. Therefore, about 5 million tons of hydrocarbons may be generated annually in the plate subduction zones. The number does not appear to be impressive. But a highly organized life on Earth was evolving in Phanerozoic for 600–500 MMY. The total of $(2.5–3) \times 10^{15}$ ton of oil may have been generated this way which is 1000 times the reserves identified on Earth by the 1970s. The rate of oil and gas migration from the plate subduction zones into the foredeeps and submontane troughs, together with the abiogenic methane generation in the Earth's rift zones (see Section 12.6) are such that they may be able to compensate the world hydrocarbon production (Gavrilov, 2008).

Thus, the proposed mechanism turned out to be very powerful. Even if its efficiency rate were low it still would be adequate for the explanation of the origin of most world oil and gas provinces. We made a comparison of the world oil and gas basins distribution with the positions of both the modern and ancient plate subduction zones. It showed that at least 70–80% of world oil and gas reserves indeed gravitated toward the plate subduction zones of the past epochs (Sorokhtin and Balanyuk, 1982; Gavrilov, 1986). It includes the unique basins of the Persian Gulf, Venezuela, US Midwest, Canada, Alaska, Indonesia, and the classic fields in Appalachians, Urals Foredeep, Caucasus, Carpathians and many other world regions including the forecast provinces such as the eastern foredeep of the Siberian Platform and subthrust zones in the Verkhoyansk–Kolyma folded zone.

The largest oil and gas accumulations emerge in the foredeeps forming when the island arcs and Andean-type continental margins obduct the Atlantic-type passive continental margins with their thick sedimentary sequences accumulated on these margins over the life of the ocean (Fig. 10.27). Such events were frequent in the Earth's evolution. That was the way hydrocarbon accumulations formed in the Persian Gulf, in the piedmont of Appalachian, Urals, North American Cordilleras, in most of the Alpine–Himalayan mobile belt and in many other fore-mountain belts of the world. The island arc collision with the old continental margins in the Appalachians and in the Urals ended 350 and 250 MMY ago, in the Rocky Mountains such collision occurred 100 MMY ago, in the Persian Gulf, around 20 MMY ago although the northeastern flank of the Arabian Platform in still subducting under the Zagros arch (that is supported by numerous earthquakes in the region and the deformations of the youngest deposits). The initial stage of the Lesser Sunda Isles arc collision with the north margin of the Australian continent may be observed in the Timor Sea.

When the island arc or active continental margin obducts a passive continental margin it is sagging under the weight of the obducting structures, which causes the increase in the deposition rate. And when these structures collide, the subsidence and deposition rate rapidly increases under the weight of the obducting lithospheric plate as shown in Fig. 10.28. Possibly, the oil and gas-generation accelerates under the increased pressure.

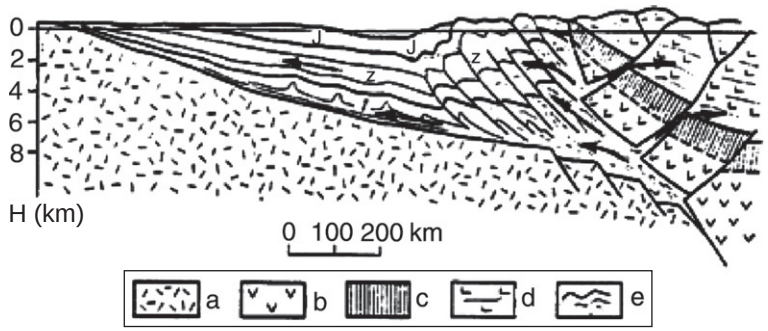


**FIGURE 10.27** Schematic cross-section through the overthrust zone of an island arc over the passive continental margin: a. Precambrian basement of the continental platform; b. Island arc basement; c. Oceanic crust rocks; d. Island arc volcanosedimentary sequence; e. Crushed foredeep sediments; 1–3. Sedimentary complexes. Arrows indicate hydrocarbon migration paths from the subduction zone.

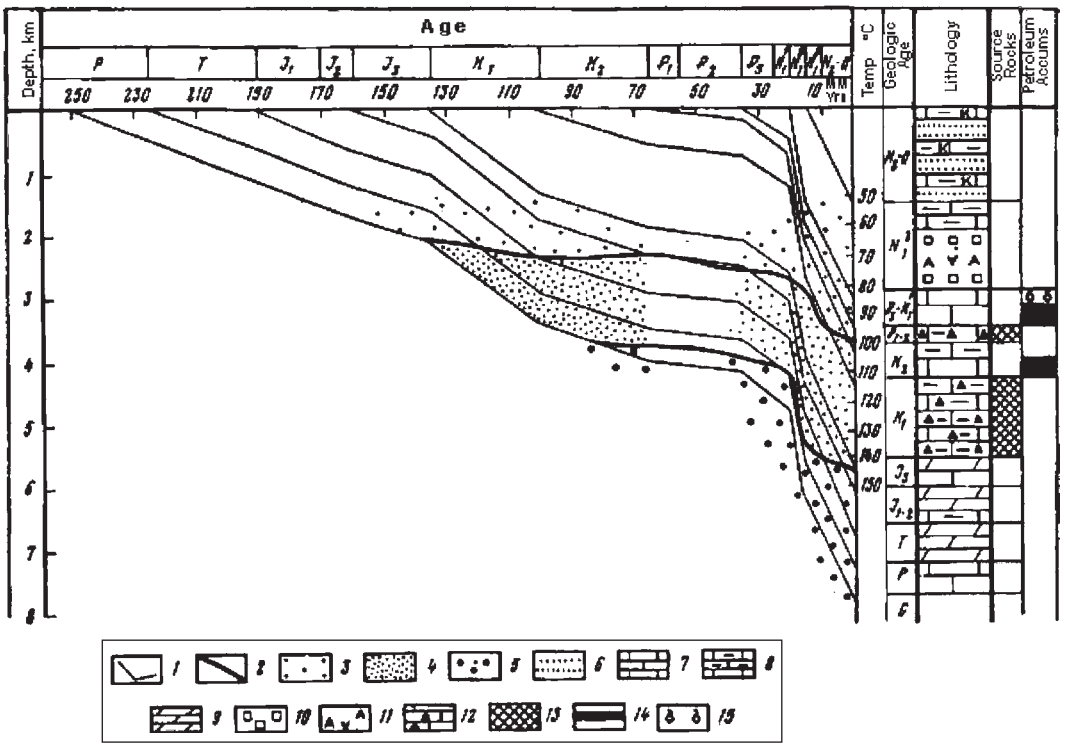


**FIGURE 10.28** Continental margin subsidence and sediment accumulation in the southern Mesopotamian trough (Agha-Djari Field area) after Vysotsky and Golenkova (1980): 1. Deposit paleodepth curve (from wells); 2. Oil window ranges; 3. Early katagenic gas generation and initial oil generation zone; 4.Oil window and medium-katagenic gas window; 5. Oil generation dwindling and continuing medium katagenic gas-generation zone; 6. Sands and sandstones; 7. Limestones; 8. Clayey limestones; 9. Dolomites; 10. Rock salt; 11. Gypsum and anhydrite; 12. Bituminous marls (deep-water facies); 13. Oil source-rocks; 14. Oil accumulations; 15. Gas accumulations.

The diagram also enables the determination of the interaction history between the adjoining plates. Indeed, the drastic bends in the deposition graphs clearly identify the critical moments in such plate interaction. Thus, the graph shows that the increase in the deposition rate in the Persian Gulf basin around 140 MMY ago was due to the Cretaceous sea transgression on the continents whereas the Zagros island arc collision with the Arabian Plate east edge happened much later, about 20 MMY ago (Fig. 10.29).

Oil and gas generation in such structures occurs not only due to mobilization of the oil and gas dispersed in the crushed sedimentary sequences of the former continental margin. It also happens due to the hydrocarbon supply from the plate subduction zones as stated above and shown in Fig. 10.27. Apparently, a combination of these two oil and gas concentration mechanisms in the foredeeps makes these structures into unique hydrocarbon accumulators. Good examples are the Persian Gulf basin and also the West Canadian, North Alaska, Venezuela and some other basins.

Giant bitumen and malt accumulations in the front portions of the West Canadian Cordillera overthrust structures over the Canadian Platform in the Athabasca area indicate large hydrocarbon flows from the subduction zones. If we converted these bitumens into the normal oil accumulations from which the bitumens formed, it would bring the West Canada oil accumulations on par with the Persian Gulf fields which are among the world largest (Fig. 10.30).

The same may apply to the bitumen deposits in the east of the Siberian Platform. They clearly indicate the existence thereof hydrocarbon flows running from under the Verkhoyansk–Kolyma folded zone along the strike of the sediments. Therefore, based on the proposed mechanism of the oil and gas basin formation within the continents' foredeeps the East Siberian region and the Verkhoyansk–Kolyma underthrust zones may have high hydrocarbon potential (Gavrilov, 1986).

Another potential oil and gas area is the western and southwestern Novaya Zemlya and Island of Vaygach shelves and the adjoining areas of the Barents Sea Baikalian-age platform. The evidence is in the rich gas-hydrate accumulations in the Shtokman Field on the

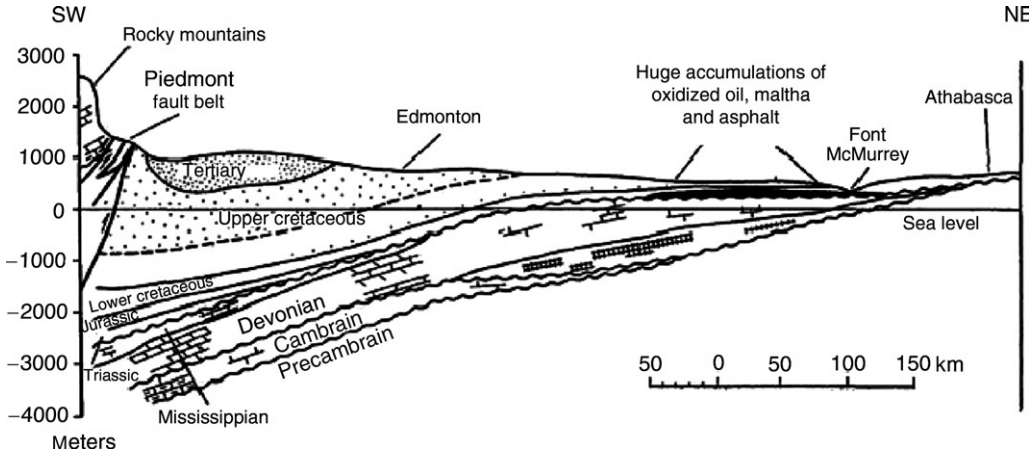


**FIGURE 10.29** Schematic cross-section through the West Canadian basin (Stewart, 1963).

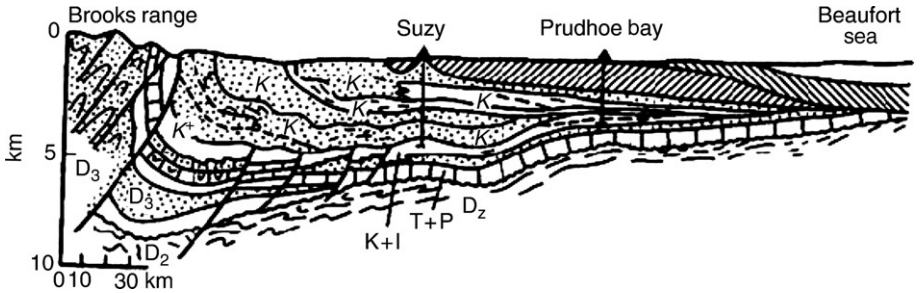


**FIGURE 10.30** Longitudinal cross-section through the North Alaska oil–gas basin (Brosge, Tailleur, 1971).

western shelf of Novaya Zemlya and the southeastern extension of this zone into the Timan–Pechora oil and gas basin. At the base of the Novaya Zemyla shelf must be Hercynian overthrust structures overlain by a thick Mesozoic and Cenozoic sequences.

Extremely important for the petroleum geology is the issue of marine transgressions as the richest world oil and gas provinces are associated with the transgressive periods. Examples are the Western Siberia, North Sea basins and the continental shelves. We will discuss the transgression origin and development and the eustatic world ocean level fluctuations in Section 11.4. Here we will just note that large marine transgressions on the continents usually occur at the disintegration of the supercontinents, and conversely, the large regressions are associated with the times of their formation. For instance, during the formation of a last supercontinent (the Wegenerian Pangaea) in Permian and Triassic a large regression of the oceanic water was indeed observed. Conversely, at the very beginning of the Pangaea destruction in Jurassic the last and largest marine transgression on the continents happened. It reached its maximum in Late Cretaceous when the oceanic water rose 400 m compared to its current level. Since then and till present, a general decline in the ocean water level is going on. It certainly is substantially modulated by both tectonic and glacioeustatic fluctuations reaching sometimes 100–120 m (see Fig. 11.8). Of course, the relatively short-lived sea level fluctuations play a very important role in the petroleum geology as they control the reservoir and seal rock alternation.

Figure 10.31 illustrates the positions of the Late-Cretaceous epicontinental seas. As we may see, at least one-third of the dry land was then flooded by the sea water, and most of the seas were located within the arid tropical or moderate climatic zones. As we will show in Section 14.3, each supercontinent epoch had its corresponding elevated near-surface temperatures. In particular, in Cretaceous (at the time of the Wegenerian Pangaea) the average Earth temperature at the sea level was $+22\,^{\circ}C$ (currently, $+15\,^{\circ}C$), and at the equator it reached $+32\,^{\circ}C$ (currently, $+20$ to $26\,^{\circ}C$). Even at the poles, the average temperature did not decline at the sea level below $+4$ to $+5\,^{\circ}C$ (currently, below $-10\,^{\circ}C$ (see-Fig. 14.21), and taking a high albedo of the snow cover in the Arctic Ocean it is even below $-20\,^{\circ}C$.

All these resulted in the intense water evaporation from the epicontinental seas which turned out to be in the arid or subtropical areas of the Earth's moderate climatic zones. Because of that, evaporation of the water fed into the epicontinental seas from the oceans resulted in a substantial elevation in salinity in these seas including the calcium carbonate

**FIGURE 10.31** Reconstruction of the Late-Cretaceous marine transgression about 80 MMY ago: the dry land is shaded, the epicontinental seas are blank within the continents. Positions of the continents and oceans are from the reconstruction by Smith, Briden (1977).

and, especially important, phosphorus. The epicontinental seas at the time were open seas so the salinity elevation was obviously small. However, a thorough heating-through and aeration of these shallow-water basins with the elevated concentrations of $CaCO_3$ and phosphorus compounds led to the development of life in such seas and to the intense deposition of limestones and phosphates (see Fig. 15.6), especially phytoplankton (Coccolithophoridae) and foraminifers composing thick chalk sequences. Simultaneously, corals and other skeletal animals emerged in the shallow water. They formed thick rudist-coral limestone sequences in the middle of Cretaceous.

Besides, the marginal seas are natural basins where the avalanche deposition develops and river load is discharged (Lisitsin, 1984). For this reason, the clastic and carbonate material brought in by rivers from the continents was mostly deposited in these seas and did not reach the open ocean. A result was that the World Ocean in Middle and Late Cretaceous was substantially impoverished in phosphorus compounds and in carbonates whereas the epicontinental seas were enriched in them. All these caused the accumulation in the Cretaceous epicontinental seas both deposits and organic matter that later served as sources for the formation of rich oil and gas fields.

A classic example of this type oil and gas basin is West Siberia which we will discuss here in more detail. The basin emerged in the place of the Early Paleozoic Paleo-Ural Ocean which in Khain's belief was a marginal sea of a larger Paleo-Asian Ocean. First island arcs formed beginning in the first half of Ordovician first volcanic island arcs formed in the Paleo-Ural Ocean. In Middle Devonian, the ocean began to close. By the end of Middle Jurassic (about 160 MMY ago), the entire region was engulfed by the Mesozoic marine transgression. In the very beginning of Cretaceous, high in organic matter content clayey Bazhenov deposits (a major source rock in the region) were accumulating. The

transgression peaked in Late Cretaceous. The regression began thereafter, and in Oligocene the sea finally left West Siberian basin which turned into a lacustrine-alluvial plane (Khain, 2001).

Basement of the West Siberian basin most likely formed in closing of the Paleo-Ural Ocean in Middle Devonian, nearly 380 MMY ago, after the collision of island arcs. Since then, the future basin's basement began subsiding due to the buildup underneath it of the subcrustal lithosphere. This subsidence, same as for the oceanic lithosphere, is described by Eq. (8.9) or (8.9′) with a different proportionality factor. In the earlier period, the basin was surrounded by the dry land from the west, east, and south. Thus, it may be assumed that after the marine transgression began 160 MMY ago the deposition in the basin was involved in the compensatory sedimentation. In such a case, our estimate of the proportionality factor in Eq. (8.9) is close to a one. If so, then about 3 km of sediments must have been deposited in the West Siberian basin during the time of the Cretaceous transgression (160–35.4 MMY ago). That is exactly what is actually observed (Fig. 10.32)

The other examples of such buildups are the North Sea and Gulf of Mexico basins (Fig. 10.33).

Sediments accumulating on the continental margins always contain organic matter. The usual content is no more than 1% although sometimes (like in the major river deltas) it may reach a few percent. As the continental margin subsides and the sediments are dumped on it, the lower sedimentary layers are compacted and heated by the upgoing heat flow. As a result, the sediments are lithified, and the organic matter is subjected to thermolysis and gradually turns into hydrocarbons.

This process is well studied and quantified. A number of geologists and geochemists developed these ideas and created a theory of oil and gas generation.

Using the theory and major positions of the lithospheric plate tectonics it was possible to calculate the oil- and gas-generation conditions within the sedimentary sequences on the passive continental margins and to show that the maturation within them of the organic matter to produce oil and gas occurs 20–30 MMY after the formation of the continental margin itself. Subsequently, the hydrocarbon generation area substantially expands.

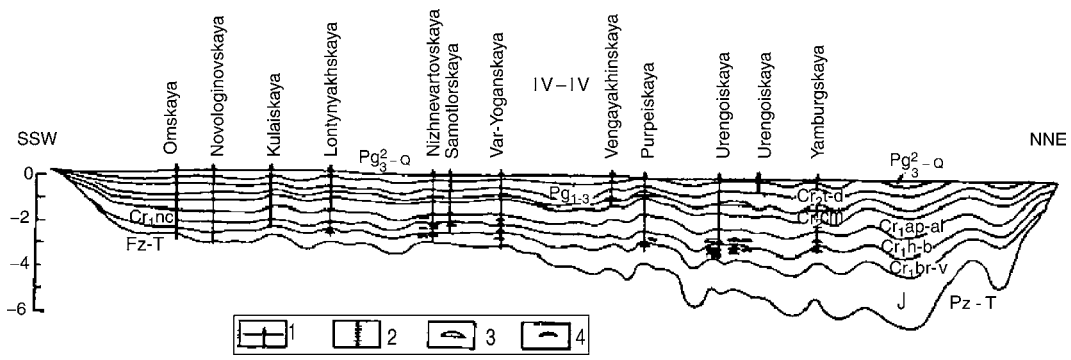


**FIGURE 10.32** Longitudinal cross-section through the West-Siberian Plate (after Rudkevich, 1974): 1. Wells; 2. Faults (absent in this cross-section); 3. Gas and gas-condensate accumulations; 4. Oil fields.

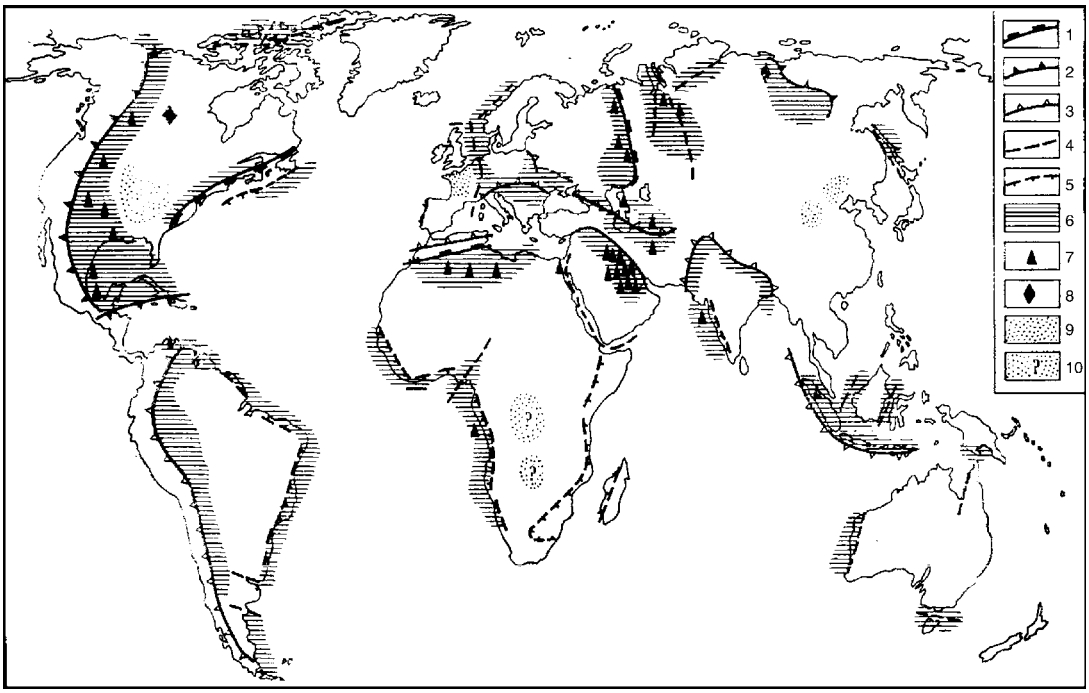


**FIGURE 10.33** Schematic map of major world oil and gas regions (after Gavrilov, 1986): 1, 2, 3. Paleozoic, Mesozoic, and Cenozoic subduction zones; 4. Some intracontinental rifts; 5. Marginal-continental rifts; 6. Oil and gas regions; 7. Large oil and gas fields; 8. Bitumen and heavy oil fields; 9. Inter-platform oil and gas depressions; 10. Same, suggested.

The oil migration within the sedimentary sequences on the passive continental margins occurs only as affected by compaction of the underlying sediments, their heating and dehydration, and is flabby. For this reason, the bulk of the hydrocarbons there are in a dispersed state, large oil and gas fields are rare (Zabanbark and Konyukhov, 2005). If the shelf deposits are associated with large river deltas which usually bring in large amount of deposits, very large oil and gas fields may form (Zabanbark, 2004, 2006). For a more complete mobilization of the dispersed oil and gas the deposits should be subjected to powerful tectonic motions capable of "squeezing" or "flushing" most hydrocarbons out of such them. Such motions usually occur at the second stage of the foredeep evolution when ancient oceans are closing and island arcs obduct the former continental margins. We have already discussed the nature of the ocean opening and closing (see Chapter 9). Here, we will only review those geological processes that result in the formation of oil and gas fields in the foredeeps.

As soon as the island arc closely approaches the continental slope, two events happen.

First, since this moment in time on the subsidence of the continental margin drastically accelerates under the weight of the obducting island arc. It is accompanied by an increase of the deposition rate within the forming foredeep (see Fig. 10.28).

Second, the pore water and migration-capable hydrocarbons in the deposits earlier positioned in the continental slope area and now underneath the island arc, begin to be squeezed out. The process is even more activated by thermal waters coming from deeper portions of the subduction zone. These waters are released in dehydration of the deposits and ocean crust rocks that got into the subduction zone. All these hot fluids are moving along the sedimentary lamination from under the island arc to the least pressure area, that is, to the continental platform. Simultaneously, the sediments located in front of the obducting arc are crushed into folds and form oil and gas traps which are gradually filling up with these hydrocarbons.

As soon as the young mountain belt arises, the foredeep formation is completed with the emergence of oil and gas basins in the foredeeps' sedimentary complex. The oil and gas accumulating in such foredeeps migrates there from two sources. First, the hydrocarbon accumulations concentrate due to the mobilization of the local micro-oil generated in the source rocks within the foredeeps. Second, they concentrate through the hydrocarbon migration from the part of the sedimentary rocks which by the time of the foredeep formation were sucked-in underneath the island arc obducting the continental margin.

The capacity of the latter hydrocarbon source is exceptionally high. Let us assume that along the 1000 km-long shoreline, the continental margin shelf with a sediment section of 15–17 km is obducted by the island arc's frontal overhang to a depth of 100–120 km. (That is what happened in the Persian Gulf when the Zagros island arc obducted the edge of the Arabian Platform). Several hundred billion tons of hydrocarbons could have migrated in this case toward the foredeep.

This was perhaps a reason why in many largest and unique world oil and gas basins (such as the Persian Gulf, Venezuela, Athabasca and others) the oil and gas reserves density is many times over the oil source potential of the sequences wherein the combustible deposits were generated. The actual hydrocarbon migration amounts turn out to be more modest that the calculations suggest. That happens because part of oil and gas remains in the underthrust zones and often forms large accumulations there. Among the examples are large oil and gas fields discovered in 1970s under the overthrusts in the Rockies and Appalachians, underneath the ophiolite sheet in Cuba, in the Swiss Alps, New Zeeland and some other areas of the world.

Very indicative in this respect the discovery of new oil and gas fields on Cuba and in the US.

The Cuban and Russian (Knipper) explorationists were familiar with the plate tectonics concept. In mid-1970s, they drilled the serpentinite ophiolite sheet and discovered underneath a large oil field formed in Cretaceous sediments of the Cuban underthrust zone.

Another successful application of the plate tectonics concept is the discovery and production of new oil and gas basins in the underthrust zones of the Rocky Mountains and Appalachians in the US. Prior to the 1970s these regions were traditionally regarded as low-potential and even no-potential areas. After the new concept got hold, the US geologists revisited their previous attitude to the underthrust zones at the front in the mountain belts marking the frontal parts of the former subduction zones. Exploration of the Cordillera, Wachita, and Appalachian subthrust belts.

This resulted in 1975 in the discovery in the Rockies of a first new type oil field, Pineview, with the recoverable reserves of 18.3 million tons. An estimate by American

geologists of the recoverable oil and gas reserves only in the Cordillera subthrust zone as of the beginning of 1981 was 2.1 billion tons of oil and 2.8 trillion cubic meters of gas which is about half of the current proved oil and gas reserves of the country. Recently, new oil and gas fields were discovered in the Wachita and Appalachian subthrust zones.

Another example of the application of the plate tectonics ideas in the petroleum geology is the discovery of a large oil field White Tiger in the granites of the Vietnam shelf crystalline basement. The field was formed over the Mesozoic plate subduction zone due to the fractured crystalline rocks saturation with hydrocarbons rising from the subduction zone (Areshev, 2003; Gavrilov et al., 1996).

No less prospective in Russia must be the East Siberian foredeep (along the middle and lower course of the Lena River) and the subthrust zones of the Verkhoyan–Kolyma foldbelt. Beginning in Devonian and through Jurassic, thick sedimentary sequences were accumulated within this continental margin area and on the passive margin of the Paleo-Siberian Ocean. By the end Mesozoic they got into the compression environment from the Kolyma Massif overriding the eastern edge of the East-Siberian Platform. Actually, the East-Siberian Province may have even greater hydrocarbon potential that the Urals Foredeep of the Russian Platform.

Thus, one environment favorable for the emergence of the largest oil and gas provinces in the world is old and young subduction zones. Beside that, significant concentrations of oil and gas arise within the continental rift and aulacogens buried underneath thick sedimentary sequences. In the bedrock topography (underneath the sediments), the rift structures are usually linear troughs extended over many hundreds of kilometers. These structures often have steep stepwise flanks formed by faults. Their width usually does not exceed a few dozen kilometers. Typical examples of the young rift troughs not yet filled with sediments are Lake Baikal in Siberia and the system of the East African rift faults. The sediment-filled rift zones (aulacogens) with abundant indications of oil and gas occurrences are, for instance, the North Sea grabens, Dnepr-Don trough, graben Benue in Africa and many other similar structures. The aulacogens form when the continents split but only if the continental block spread was relatively small and was not accompanied by the ocean formation. Such structures are as if the grooves and scars in the Earth's crust left after a failed attempt of the ocean formation.

The association between many oil and gas basins and the ancient rift structures and aulacogens occurred due to a relatively rapid subsidence of their central areas (rift valleys). Such subsidence usually involves the accumulation of thick continental or marine deposits. The nature of the continental rift zones subsidence is the same as for the sea floor subsidence. It occurs due to the emergence underneath the rift zones of fresh lithospheric areas. These areas appear as a result of cooling and the total crystallization of the hot mantle (asthenospheric) matter which prior to that rose within the space between the spread continental plates. As it is, the subsidence law remains the same: the rift depression depth increases with time in proportion with square root of its formation age.

The hydrocarbon generation occurs in the sedimentary sequences within the rift zones at the expense of thermolysis of their organic matter. The hydrocarbon migration in such structures, same as on the passive continental margins, occurs mostly due to squeezing-out of the pore and irreducible water in the process of the deposit compaction and heating in the central, deepest parts of aulacogens. The so released water migrates together with the hydrocarbons along the sedimentary lamination from the axes of the buried structures to

their flanks. This migration mechanism well explains frequent association of oil and gas fields with the flanks and peripheral areas of the ancient rift zones.

In some cases, the continental rift zone, after having been filled up with deposits, is compressed. In such a case, squeezing of the pore and irreducible water significantly strengthen. However, in these cases no unique basins (like the Persian Gulf, Venezuela, and Athabasca) emerge because all oil in the aulacogens is autochthonous, that is, it forms within the very sequence filling up the rift depression without any additional inflow from the side. Because of this, in all rift basins, as on the passive continental margins, the oil and gas reserves density is never higher (and in most cases much lower) than the oil source potential in the filling sediments.

The lithospheric plate tectonics also provided an opportunity to first predict (Sorokhtin and Ushakov, 1991; Dmitriyev et al., 2000; Sorokhtin et al., 2001; Sorokhtin, 2005) and then discover a new hydrocarbon source on Earth (Balanyuk and Dongaryan, 1996). Currently, the bulk of abiogenic methane forms in the serpentinization of iron-rich ultramafic rocks. It happens due to the bivalent iron oxidation into the trivalent state and carbon dioxide reduction to methane. Hydrogen is released through the marine water dissociation on the bivalent iron (see reaction 10.4). Such reactions are exothermal and at temperatures close to 400 °C occur with the substantial energy release (183.83 kcal/mol; Dmitriyev et al., 2000; Sorokhtin et al., 2001).

The methane formation rate in the oceanic crust reaches 2–9 million tons/year. Usually methane and hydrogen released in hydrotherms of the mid-oceanic ridge rift zones enter the oceanic water and disperse in it. In some cases, the spreading of the rift zones is slow; they turn out to be overlain by deposits. Some depositional basins on the oceanic periphery overlie the areas where the crust serpentinization is still proceeding. In these cases, the hydrocarbons can accumulate within the sedimentary sequence and form in them independent gas-hydrate deposits (Balanyuk and Dongaryan, 1994) or, with the bacterial participation, even oil and gas fields. At that, the bacteria serve as the main factor in the $CH_4$, $H_2$, and $H_2S$ transformation into more complex hydrocarbons. Such bacteria are consuming methane, hydrogen, and hydrogen sulfide as the abiogenic methane can serve as food for the bacteria which in their term generate organic matter later converted into the normal hydrocarbons (Lein and Sagalevich, 2000).

The classic examples of the hydrocarbon aggregation in the sedimentary sequences over the rift zones are the California Bay Basin and the Red Sea Basin. In the California bay, the rift zone is overlain by 400–500 m of the deposits. Due to the heat convection these deposits are actively flushed by the oceanic water and hot hydrotherms (Fig. 10.34). These sources feed the abundant bacterial flora within and on the surface of the sedimentary sequence. A testimony to this is the abundant bacterial mates and "oases" of the bottom fauna surrounding the hot and warm hydrothermal springs (Sorokhtin and Sagalevich, 1994). Besides, organic matter is also supplied into the basin from the California bay oceanic waters. A result is that the basin's sedimentary sequence near the hydrotherms' discharge is literally saturated by hydrocarbons which include up to 3–4% of liquid naphtoids. These naphtoids contain nearly 65% of aliphatic hydrocarbons, 15% of aromatic hydrocarbons and 20% asphaltenes (Lein et al., 1998).

The Red Sea basin is geodynamically similar. It is the youngest oceanic basin with the age of no more than 30 MMY. The near-shore and peripheral basin's areas are overlain by

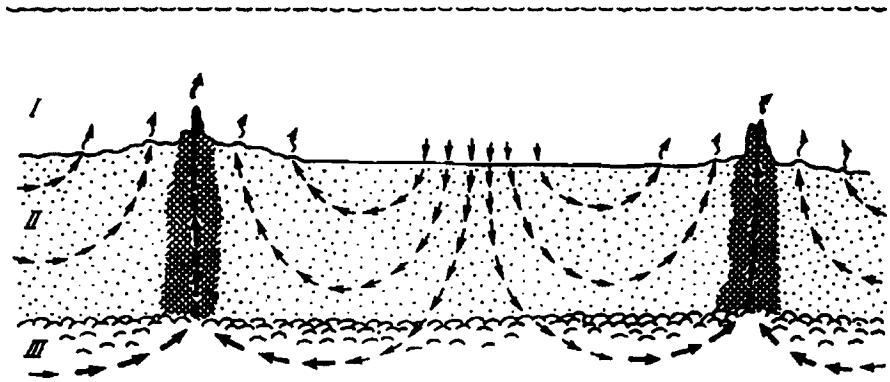


**FIGURE 10.34** Schematics of the marine water convective circulation within porous sediments and basalts of the California Bay rift zone (Sorokhtin and Sagalevich, 1994): I. Oceanic water; II. Ground water convection flows within the sedimentary sequence; III. Overheated water fluids flows within the oceanic crust's bedrock; cross-shading is hydrothermal sulfide deposits and buildups of "black smokers."

sediments with significant evaporite participation. Total thickness is up to 3 km. Wherever the rift zone is covered by the sediments, the entire abiogenic methane and organic matter, as in the California bay, are substantially converted into more complex hydrocarbons.

Very important for the formation of oil and gas fields were alternating marine transgressions and regressions. The latest Late Cretaceous transgression was especially important (see Fig. 10.31). At that time under a warm climate environment in the broad shallow-water seas that covered about 30% of the present-day dry land, the life bloomed. It was abundantly fed by organic substances coming directly from the open ocean. The remains of that life in the form of oil and gas are found in numerous Cretaceous sediments developed in the richest world oil and gas provinces. Large marine transgressions and regressions usually evolved very slowly, during about 100–200 MMY. Against this general trend, short-lived declines of the ocean level (with the duration of tens of thousands to a few millions of years) were observed. Their amplitude as a rule did not exceed 100 m (more often, 50–60 m). Their consequences for petroleum geology, however, are very important. It is important for the formation of oil and gas fields that the source rocks and seals in the sedimentary basin fill alternate with reservoirs and water-permeable layers (for instance, clayey and sandy sediments). Usually the clayey sediments are at the same time the source rocks, and the sandy layers form traps where oil and gas accumulate.

Such alternations of the depositional facies had numerous reasons. The most important were drastic changes of the erosion base level in the dry land surrounding the sedimentary basin and the intermittent communications between the ocean and the marine depressions where the sediments were accumulated. The erosion base level fluctuations in the mobile belts were caused by the superposition of tectonic motions and eustatic changes in the ocean level. On the platforms they were caused only by eustatic changes in the ocean level. But that were exactly the effects caused by the short-lived oceanic regressions. Their effect on the geological evolution of large regions may be illustrated by the following example.

Due to the development of an Antarctic glaciation at the end Miocene 5 MMY ago (Messinian time), the oceanic level significantly declined (by more than a 100 m). As a result, the

Mediterranean and the Red Sea were almost completely isolated from the ocean although the oceanic water continued to enter them through narrow straights of a river channel-type. Thus, these seas were gradually drying up with the accumulation of salt-bearing deposits on their bottoms (the salt thickness in the Red Sea reaches 3–4 km). Rivers emptying into the Mediterranean cut steep canyons, 1.5–2 km deep. The Black Sea was almost completely desalinated at that time. It turned into a giant fresh-water lake connected with the salt-bearing depression of the Mediterranean through a river flowing in deep canyons of Bosphorus and Dardanelles.

The shortest global marine regression with the amplitude 50–100 m and duration of a few thousand years may occur due to the emergence or increase in volume of the continental sheet glaciations. Lengthier regressions, one to a few million years, happen when the lithospheric plates "jam" and their movement slows down. Such events usually occur in the continent collisions or island arc collisions.

It is impossible to describe here all possible applications for the plate tectonics to the petroleum geology. The supplied examples should be sufficient to illustrate great potential in using this modern geological theory for the studies of the origin, structure, and evolution of the world's petroleum basins and for the forecasting the positions of the new oil and gas basins.

We will now briefly discuss the issue of the oil generation.

Despite lengthy and involved studies, the arguments between proponents of the organic and inorganic origin of petroleum do not subside although the voices of the opponents of the organic origin are not as loud. The main arguments of the organic proponents were purely geological data about the conditions of accumulation formation in sedimentary rocks, the optical activity of oils and mostly the petroleum geochemistry which found in the crudes biomarkers supporting its biogenic origin. The abiogenic proponents also relied on chemical reactions assuming that the Earth's mantle has plentiful carbon and water; oil and gas accumulations in the sedimentary shell were explained by the existence of deep fractures and fault zones in the crust. Sometimes they supported their arguments by the oil finds in definitely magmatic rocks of geosynclinal zones, for instance, in the Swedish and Norwegian fractured granites.

What does the modern theory of the Earth's evolution say about this issue?

First, there are no noticeable amounts of carbon or water in the mantle. Calculations in Sections 11.2 and 12.2 show that the water content in the mantle is no greater than 0.05–0.06%, and carbon content is even lower, no greater than 0.01%.

Second, and most important, no hydrocarbon could form and even be present in the mantle during Phanerozoic because of the oxidizing environment. This was associated with the Earth's core separation and growth which is still continuing. We discussed in Chapter 2 the core composition and showed that most of it is composed of the univalent iron oxide $Fe_2O$ (or eutectic alloy Fe·FO). This alloy is generated through partial reduction of the silicate iron bivalent oxide with the release of free oxygen:

$$2FeO \rightarrow Fe_2O + O. \tag{10.42}$$

This oxygen is generated at a huge rate of up to 20 billion tons per year. The Precambrian mantle contained some metallic iron which absorbed the released oxygen. At the Archaean/Proterozoic time boundary, about 600 MMY ago, the metallic iron completely

migrated into the core and disappeared from the mantle (see Fig. 4.16). After that, the environment drastically changed in the mantle and turned from a reducing to an oxidizing one. Oxygen released under reaction (10.42) is expended for oxidizing the bivalent iron to the magnetite stoichiometry:

$$3FeO + O \rightarrow Fe_3O_4 + 76.5 \text{ kcal/mol}. \tag{10.43}$$

If hydrocarbons were present in the mantle their oxidizing would have occurred with the release of a much greater energy, therefore, under a more preferred reaction:

$$CH_4 + 4O \rightarrow CO_2 + 2H_2O + 191.76 \text{ cal/mol} \tag{10.44}$$

Thus, 20 billion tons of oxygen is released annually by the mantle. Over $1.2 \times 10^{19}$ tons were released during the entire Phanerozoic. This is about a hundred million times the amount of all discovered oil and gas reserves together.

The conclusion is that no hydrocarbon could emerge in the mantle. Oil and gas formed only under xenogenic conditions, and the overwhelming majority of them, biogenically. A small part of methane could have formed abiogenically in the oceanic crust hydration under a reaction similar to (10.4). The abiogenic methane generation rate on the ocean floor is tremendous, 2–10 million tons per year. Most of this methane dissolves in the oceanic water and serves as food for the methane-consuming bacteria. They, in turn, may form organic matter, for instance, like follows:

$$CH_4 + \text{bacteria} \rightarrow CO_2 + (\text{organic matter}) \tag{10.45}$$

Part of the abiogenic methane, especially underneath the sediment cover overlying the oceanic crust bedrock, can form independent gas-hydrate accumulations. Thus, it is a possibility that part of the oceanic gas-hydrates could have formed this way (Balanyuk and Dongaryan, 1994; Balanyuk et al., 1995; Gavrilov, 2008). The rest of oil and gas fields are undoubtedly of the organic origin although part of their organics may have formed absorbing the abiogenic methane under reaction (10.45) (although in this case that part should be treated as organic).

Now, about oil and gas in fractured magmatic rocks of the geosynclinal zones. The so-called geosynclinal zones are in effect the plate subduction zones where hydrocarbons rising from deposits sucked-in between the plates penetrate all overlying rocks, including fractured granites and diorites, and saturate those with oil (see Fig. 10.27).

Yeremenko and Chilingar (1996) wrote that the available data "undoubtedly" support the organic origin of the known oil and gas accumulations. It is indicated by the oil composition (as well as that of coals, oil shales, bitumoids) containing chemofossils—biomarkers of organic compounds which preserved the structure of transitional bioorganic molecules. More than 300 such biomarkers are found in oils. Sometimes half of the oil is composed of such biomarkers. That means that they are not admixture but a constitutional component.

Summarizing the dispute, we strongly believe that the overwhelmingly large portion of the oil has organic origin whereas a substantial part of the ocean floor gas-hydrates could be abiogenic.

CHAPTER

# 13

# Adiabatic Theory of the Greenhouse Effect

## 13.1 INTRODUCTION

First and foremost, the Earth's climate is determined by the Sun's radiation intensity, the density of Earth's atmosphere and its capacity to absorb and retain this radiation. It is usually assumed that the heating of the atmosphere and Earth's surface is to a substantial extent due to the capacity of some gases (called the greenhouse gases) to absorb the IR (heat) radiation of Earth.

The idea of the Earth's atmosphere heating by the greenhouse gases was first stated by the well-known Swedish scientist Svante Arrhenius at the end of the nineteenth century. Since then it is postulated as obvious, accepted on faith, practically with no verification (Budyko, 1974, 2002; Greenhouse effect, 1989; Khromov, Petrosyants, 1994). This concept is now totally dominant in the conclusions of the Intergovernmental Panel on Climate Change (IPCC), Greenpeace, United Nations Environmental Program (UNEP), World Meteorological Organization (WMO) and the conclusions of the Russian ecological and scientific organizations. The same viewpoint was totally supported in the resolutions of the International ecological congresses in Rio de Janeiro, Brazil (1992) and Kyoto, Japan (1997). It is usually assumed that the main danger arises due to the industrial releases into the atmosphere of the greenhouse gases, especially carbon dioxide, which is the main product of burning hydrocarbons and coal (the fundamental energy sources of the modern economy). Under the forecasts of the proponents of the concept, the climate warming may reach 2.5–5 °C by the year 2100. The ocean level rise caused by this warming will reach 0.6–1.0 m. This may cause certain problems in the densely populated areas of the continental shores as well as for the oil and gas industry in the lowland areas. Other deadly consequences of the global warming are also forecast (the spread of deserts, permafrost melting, soil erosion, etc.).

Concerns about similar catastrophic situations and the pressure from environmental organizations, and sometimes just speculations on the subject, force many governments to

*Developments in Earth and Environmental Sciences*, Volume 10
DOI: 10.1016/S1571-9197(11)10013-0

allocate huge amounts of money to fight the consequences of the climate warming ostensibly caused by the human releases of the "greenhouse gases" into the atmosphere.

How justified are these expenses? Aren't we fighting windmills?

There are some seemingly "obvious" concepts accepted on faith as axioms without critical verification. Before Copernicus and for quite a long time thereafter it seemed obvious that the Sun revolves around an immobile Earth and not the other way around. Whoever doubted it could observe from a sunrise to a sundown the movement of the Sun in the sky from east to west around the "immobile" Earth. Was that not obvious? Certainly—but still impossible.

A similar pseudo-obviousness is happening currently with the concept of the greenhouse effect. We were inculcated from our school years with the idea that the greenhouse gases absorb the heat coming from the heated Earth's surface and heat the air above Earth. This is so indeed. But from this, an "obvious" conclusion is made that the more there are of such gases in the atmosphere (and especially carbon dioxide), the warmer the air above Earth and the warmer the Earth's surface. Obvious? Yes, but the likelihood of this needs to be verified.

A close review of the problem revealed that there was no theory of the greenhouse effect through the 1990s. All calculations on the effect on Earth's climate of the $CO_2$ and the other greenhouse gases concentration were conducted on the basis of various intuitive models with numerous and not always stable parameters (Greenhouse effect, 1989). The existing uncertainties in the estimates of many model parameters (there are at least 30 such parameters) make the solutions incorrect.

That was the reason we conducted the review of the nature of the greenhouse effect from the most general positions using the synergetic approach (Prigozhin and Stengers, 2003; Hacken, 1980, 1985).

The atmosphere is a clear example of the dissipative (energy dissipating) system described by nonlinear equations of mathematical physics. These two circumstances give us hope that there is a possibility in the Earth's atmosphere for self-organization of the physical fields and formation in it of the process parameters-defined stable thermodynamic structures in space and time. Such approach commands the use of only the most significant and reliably established parameters of the medium and definitive characteristics of the controlling process.

For instance, it is possible to take into account only such parameters as the mass of the atmosphere, its heat capacity, the average value of the solar radiation hitting Earth as well as a strong negative feedback between the planet's spherical albedo and its averaged near-surface temperature. With this set of parameters the local details in the greenhouse effect description as the first approximation model is single-dimension and averaged over entire Earth.

In certain cases, such an approach may have some advantages. It enables obtaining analytical and unique results in the solution of global problems as the influence of the atmosphere's composition on the total value of the greenhouse effect (for the entire Earth). Besides, it is possible to include in the single-dimension model additional and local parameters (the latitude of a locality, the Earth's revolution axis angle with the ecliptics, its precession, inflow of additional heat by the air flows (cyclones), the snow-cover

albedo, etc.). This way it is possible to build 3D and even 4D (with the time as the fourth dimension) greenhouse effect models.

Out of all our solar system's planets only Earth has a unique atmosphere and hydrosphere favorable for the development on its surface of higher life forms. This happened due to a confluence of many lucky circumstances: the Sun is a "quiet" star; Earth is positioned at the optimal distance; Earth has a massive satellite (Moon); the primordial chemical composition of Earth discussed in detail in our earlier publication (Sorokhtin, 2007).

We will make an attempt to demonstrate that the main factors responsible for the emergence on Earth of comfortable climatic conditions are the amount of solar radiation, the atmospheric pressure, the heat capacity, and Earth's precession angle (Sorokhtin, 1990, 2001, 2006; Khilyuk and Chilingar, 2003, 2004; Sorokhtin, Chilingar et al., 2007a,b).

## 13.2 MAJOR FEATURES OF THE PRESENT-DAY EARTH'S ATMOSPHERE

We will first review the major parameters of Earth's atmosphere. Its mass is approximately $5.15 \times 10^{21}$ g, the average atmospheric pressure at sea level $p_0$ is equal to one physical atmosphere or 1.0132 bar = 1013.2 mbar (760 mm mercury), its density $\rho_0 \approx 1.27 \times 10^{-3}$ g/cm$^3$. The air pressure and density rapidly decline with height under the exponential rule (Fig. 13.1):

$$p = p_0 \exp\left\{-\frac{g\mu}{RT}h\right\}, \tag{13.1}$$

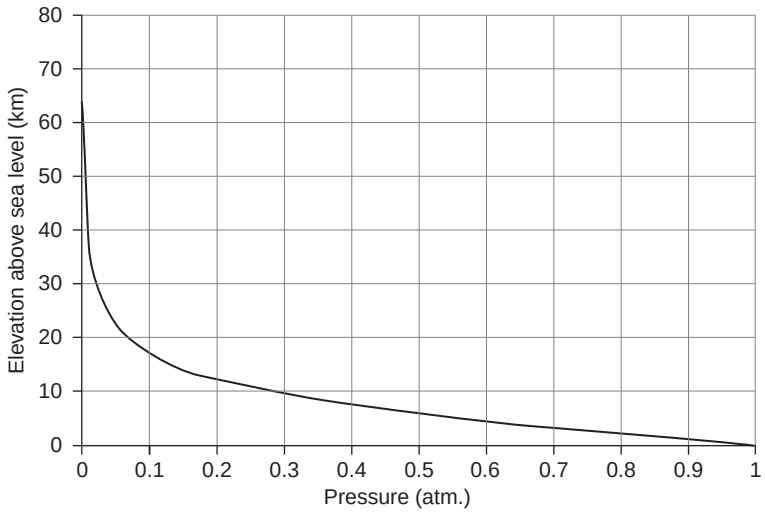


**FIGURE 13.1** Atmospheric pressure versus elevation (calculated from Eq. (13.1) and from the temperature versus elevation in Fig. 13.2).

where $g = 981$ cm/s$^2$ is the gravity acceleration; $\mu$ is the average molecular weight of the atmospheric gases (for Earth at $p = p_0$, $\mu = 28.97$); $R = 1.987$ cal/deg mol $= 8.314 \times 10^7$ erg/deg mol is the gas constant; $T$ is the absolute temperature (Kelvin); $h$ is elevation above the sea level. The air density declines under a similar rule.

The nitrogen–oxygen composition of the atmosphere is unique among the Solar System's planets. The dry air is composed of 75.51% (by mass) nitrogen, 23.15% oxygen, 1.28% argon, 0.046% carbon dioxide, 0.00125% neon and about 0.0007% other gases. An important active component of the atmosphere is the water vapor (and the water drops in clouds). The average water vapor and water content in the atmosphere reaches $(0.12–0.13) \times 10^{20}$ g (which is equivalent to the water layer 25 mm thick all over the world or the pressure equivalent of 2.5 g/cm$^2$ on the average. If we take the average annual humidity evaporation and the precipitation (approximately 780 mm of mercury) then it may be calculated that the water vapor is renewed in the atmosphere about 30 times per year, that is, every 12 days. In the upper atmosphere affected by the solar radiation, ozone ($O_3$) is formed. Its content in the atmosphere is small, $O_3 \approx 3.1 \times 10^{15}$ g (oxygen content in the atmosphere is $O_2 = 1.192 \times 10^{21}$ g). But its role is very big as it protects life on the Earth's surface from the deadly effect of the hard solar radiation.

The UV solar radiation is absorbed in the tenuous atmospheric and mesospheric layers. This occurs mainly due to a photochemical dissociation of oxygen and water molecules accompanied by the absorption of the energy of the hard solar radiation:

$$O_2 + h\nu \rightarrow 2O, \tag{13.2}$$

$$H_2O + h\nu \rightarrow OH + O. \tag{13.2'}$$

The ozone formation, on the contrary, is an exothermal reaction whereas in its dissociation the solar UV radiation is absorbed again:

$$O_2 + O \rightarrow O_3 + 31.7\,\text{kcal/mol}. \tag{13.3}$$

$$O_3 + h\nu \rightarrow O_2 + O. \tag{13.3'}$$

The heat release in the formation of ozone molecules results in heating of the tenuous stratospheric and mesospheric air masses at elevations of about 50 km. This is demonstrated by the temperature profile in Fig. 13.2.

There are transitional layers between the troposphere and stratosphere, and between the mesosphere and thermosphere. These layers are, respectively, the tropopause (the temperatures are 190–220 K) and the mesopause (the temperatures are 180–190 K).

Over the mesosphere is located the thermosphere where the ionized gas temperature grows with the elevation to 1000 K and greater. At elevations over 1000 km the thermosphere gradually changes into the exosphere and higher up, into outer space.

The average temperature distribution in the Earth's troposphere is radically different from its distribution in the stratosphere, mesosphere, and thermosphere. It is almost linear in the troposphere whereas in the upper atmosphere it is drastically nonlinear, with a characteristic maximum at the elevations of about 50 km and the temperature growth above 90 km. The reason for that is that the temperature in the stratosphere and mesosphere is mostly determined by the heat release in the oxygen dissociation and the radiation

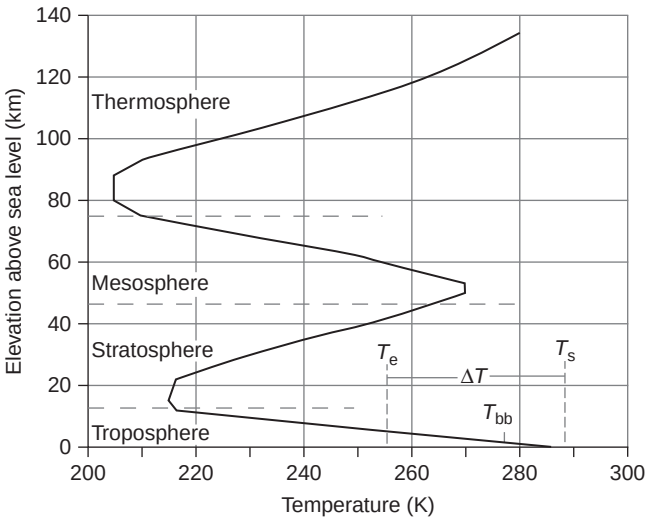


**FIGURE 13.2** Temperature distribution in the Earth's atmosphere (Atmosphere of Earth, 1988): $T_e$ is Earth's effective temperature; $T_s$ is the average Earth's temperature normalized for sea level; $\Delta T$ is greenhouse effect value; $T_{bb}$ is absolute black body temperature at the Earth from Sun distance.

mechanism of the heat transfer whereas the temperature distribution in the troposphere is determined by different processes the most important of which is the convective heat release from this dense atmospheric layer into the stratosphere where it is lost to outer space through radiation.

## 13.3 ADIABATIC THEORY OF THE GREENHOUSE EFFECT: FUNDAMENTALS

Under the classical version, at the Earth's precession angle $\psi = 0$ (which corresponds to the perpendicular position of the Earth's revolution axis toward the ecliptics), the incoming solar energy flow is characterized by the absolute black body temperature found from the Boltzmann's equation:

$$T_{bb} = \left(\frac{S}{4\sigma}\right)^{1/4}, \tag{13.4}$$

where $S = 1.367 \times 10^6$ erg/cm$^2$ s is the solar constant (incoming flow of the solar energy); $\sigma = 5.67 \times 10^{-5}$ erg/cm$^2$ s deg$^4$ is the Stefan–Boltzmann constant. Part of the solar radiation with the radiation temperature $T_r$ is reflected from Earth and is lost in outer space:

$$T_r = \left(\frac{SA}{4\sigma}\right)^{1/4}, \tag{13.5}$$

where A is the planet's reflectivity or albedo (for Earth A $\approx 0.3$). In this case (at $\psi = 0$), the Earth's radiation temperature $T_r \approx 206$ K, and only part of the solar energy with it effective temperature $T_e$ reaches Earth:

$$T_e = \left(\frac{S(1-A)}{4\sigma}\right)^{1/4}. \tag{13.6}$$

For Earth $T_e \approx 255$ K. The temperature determined by Eq. (13.6) is sometimes called the radiation temperature because it describes planet's radiation as it is seen from outer space (although it is not totally accurate).

By definition, the greenhouse effect $\Delta T$ is the difference between the planet's average surface temperature $T_s$ and its effective temperature $T_e$:

$$\Delta T = T_s - T_e. \tag{13.7}$$

The average temperature of the entire Earth is approximately 288 K or +15 °C, and its effective temperature by definition (13.6) (at $\psi = 0$) is $T_e = 255$ K or −18 °C. Thus, the classical greenhouse effect value for Earth is +33 °C.

Earth has relatively dense atmosphere. For this reason the heat transfer within its lower, densest layer (the troposphere), 12 km thick, occurs mostly through the air convection and not only through radiation as is represented by the proponents of the "classical" treatment of the greenhouse effect. In a dense atmosphere (with the pressure in excess of 0.2 atm), the dominating heat transfer in always by the air flows, that is, through the convective mass exchange where the warm air expands and rises up, and the cold air compress and goes down. The radiation heat transfer dominates only the tenuous layers of the stratosphere, mesosphere, and thermosphere. A main inference from this is that the average temperature distribution in the troposphere must by close to the adiabatic distribution, that is, to such distribution that takes into account the air expansion and cooling when it rises and, conversely, its compression and heating when it goes down.

It does not mean at all that a specific temperature distribution at a specific moment in time must always be adiabatic. What we mean is just average temperature distributions over the time intervals on the order of 1 month.

The adiabatic temperature distribution is controlled by the atmospheric pressure $p$ and by the air effective heat capacity (Landau and Lifshitz, 1979): $T^{\gamma} p^{1-\gamma} = \text{const}$ and $\gamma = c_p / c_v$, where $c_p$ and $c_v$ are the gas heat capacities, respectively, at the constant pressure and constant volume. From these, $T(p)$ is found as:

$$T = Cp^{\alpha}, \tag{13.8}$$

where

$$\alpha = \frac{\gamma - 1}{\gamma} \quad \text{and} \quad \gamma = \frac{c_p}{c_v}. \tag{13.8'}$$

It shows that under the adiabatic process the gas temperature (in K) is always proportionate with the gas pressure $p$ to a power of the adiabatic exponent $\alpha$, which depends on the effective heat capacity of the gas mixture (atm). For all triatomic gases ($CO_2$ and $H_2O$) $\gamma \approx 1.3$ and $\alpha_0 \approx 0.2308$, and for the biatomic gases ($N_2$ and $O_2$) $\gamma \approx 1.4$. In which case for the dry air without consideration of absorption of the Earth's heat (IR) radiation $\alpha_0 \approx 0.2857$.

An important fact is that humidity condensation in the atmosphere generates the cloud cover. This is the main factor determining the Earth's reflectivity (albedo). It creates strong negative feedback between the near-surface temperature $T_s$ and the effective temperature of

"absolute black body" $T_{bb}$ that characterizes the solar radiation intensity $S$ at the Earth's distance from the Sun. Indeed, any rise in the near-surface temperature increases humidity evaporation and the cloud cover. That, in turn, increases the planet's albedo and the atmosphere's reflectivity. A result is the increased Sun's heat reflection by the clouds into outer space and a decrease in heat supply to Earth. Thus, the average surface temperature lowers to the previous level again.

It is mandatory to consider that any deep negative feedback in a system results in a linear correlation between the reactions at the system's output and actions at its input. This property of the systems with negative feedback is universal and is manifested independent of the systems' nature, be it a planet's atmosphere, electron amplifier or Watt's centrifugal controller in steam engines.

Because of this the near-surface temperature is always in proportion with the "absolute black body" temperature or, which is the same, with the effective temperature $T_e$ (just with the other scaling factor) (Fig. 13.3).

It follows from this that the near-surface temperature $T_s$, or any other temperature $T_t$ on any tropospheric level, is in proportion with the revolving Earth's effective temperature and atmospheric pressure $p$ to the power of adiabat $\alpha$, which depends on the atmospheric heat capacity and composition:

$$T_t = b^{\alpha} T_e \left(\frac{p_t}{p_0}\right)^{\alpha}, \tag{13.9}$$

where $p_t$ is the troposphere's atmospheric pressure; $p_0$ the pressure unit (for instance, $p_0 = 1$ atm); $b$ is the scaling factor dependent on the adiabatic exponent and on the ratio between the planet's surface temperature to its effective temperature.

$$b^{\alpha} = \frac{T_s}{T_e}. \tag{13.9'}$$

Under the classic version of the greenhouse effect theory, the solar constant in Eqs. (13.4)–(13.6) is divided by 4 as the Sun-illuminated disk is four times smaller than the total surface of the revolving Earth. Strictly speaking, such action is valid only if the planet's revolution axis is perpendicular to the plane of the ecliptics, that is, if the precession angle $\psi = 0$.

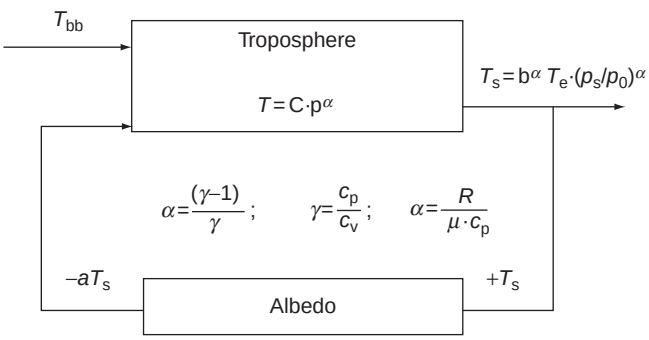


**FIGURE 13.3** Block diagram of the temperature transformation in the troposphere: $T_e$ is effective Earth's temperature (K); $p_s$ atmospheric pressure; $p_0$ pressure unit; $b$ is scale factor; $\alpha$ is adiabatic exponent; $c_p$ is the air heat capacity at constant pressure; $c_v$ is the air heat capacity at constant volume; $R$ is the gas constant; $\mu$ is the air molar weight.

A reminder: precession angle $\psi$ is the angle between the planet's revolution axis and the perpendicular to the ecliptics plane or, which is the same, between the plane of the Earth's equator and the ecliptics' plane.

Let us imagine another extreme situation of a planet "lying on its side". In this case, its revolution axis is in the plane of the ecliptics and is directed toward Sun. Then the total area of the illuminated Earth is somewhat lower than the visible Earth's circle whereas when its revolution axis is perpendicular to the direction toward Sun, the total planet's area is again 4 times the area of its illuminated circle. Thus, in this case, for the determination of the effective temperature the solar constant in Eq. (13.6) must be divided not by 4 but by a value $N$ where $4 > N > 2$. For the intermediate cases, with the Earth's revolution axis inclined to the ecliptics, it is necessary to take into account the proportionality of these two extreme cases to the inclination angle and its complement (for the modern Earth $N \approx 3.5$).

The Earth equator is presently inclined to the ecliptics at the angle $\psi = 23.44^\circ$. Therefore, the areas beyond the polar circle are illuminated by the Sun on the average half a year and are devoid of the solar light during another half. While one near-polar area is illuminated by the Sun, another one is in the dark. Because of this, while calculating the average annual effective temperature for the polar areas, we should divide the solar constant by 4, not by 2. And taking sphericity of the Sun-illuminated polar area into account, the divisor should be $2s_s/s_o$, where $s_s$ is the Earth's near-polar area beyond the polar circle and $s_o$ is the areal extent of the near-polar area projection onto the planet's equatorial plane:

$$\frac{s_s}{s_o} = 2\left(\frac{1-\cos\psi}{(\sin\psi)^2} = \frac{2}{1+\cos\psi}\right). \tag{13.10}$$

For the other Earth's areas regularly illuminated by the Sun the Eqs. (13.4)–(13.6) and (13.9) are completely valid. In which case the Earth's effective temperature is (Sorokhtin, 2006):

$$T_e = \left[\frac{S(1-A)}{\sigma\left(\frac{(\pi/2)-\psi}{\pi/2}4 + \frac{\psi}{\pi/2}2\frac{2}{1+\cos\psi}\right)}\right]^{1/4}. \tag{13.11}$$

As the current precession angle is $\psi = 23.44$, the factor in the denominator of Eq. (13.11) is

$$4\left(\frac{\pi/2-\psi}{\pi/2} + \frac{\psi}{\pi/2}\frac{1}{1+\cos\psi}\right) = 3.502. \tag{13.11'}$$

If we now assume Earth's albedo $A = 0.3$, the effective temperature turns out to be $T_e = 263.6$ K. Then the tropospheric temperature (including the surface temperature) may be expressed through the planet's effective temperature.

$$T_t = b^\alpha\left[\frac{S(1-A)}{\sigma\left(\frac{(\pi/2)-\psi}{\pi/2}4 + \frac{\psi}{\pi/2}2\frac{2}{1+\cos\psi}\right)}\right]^{1/4}\left(\frac{p_t}{p_0}\right)^\alpha. \tag{13.12}$$

Empirically, the average near-surface Earth temperature at $p = p_0 = 1$ atm and $\psi = 23.44^\circ$ is approximately 288 K or $+15\,^\circ$C (The Atmosphere, 1988; Reference Book, 1951).

We assumed $T_s = 288.2$ K. The scaling factor determined by Eq. (13.9′) is found from the conditions: at $\psi = 23.44°$, $T_e = 263.6$ K, and $T_s = 288.2$ K, and at $\psi = 0°$: $T_e = 255$ K and $T_s = 278.6$ K. Then for Earth within a wide range of the precession angles $b^{\alpha} = 1.093$.

Taking into account Eqs. (13.9′), (13.11′), the Eq. (13.12) for the modern Earth may be simplified:

$$T_t = 288.2\left(\frac{p_t}{p_0}\right)^{\alpha}. \tag{13.12′}$$

At $\psi = 23.44$ °C, the best fit of the theoretical temperature distribution (13.12) in the troposphere and the averaged empirical data occurs at $\alpha = 0.1905$.

If the gas heat capacity $c_p$ is in cal/g deg and the gas constant $R = 1.987$ cal/g deg, the adiabatic exponent's $\alpha$ correlation with the atmospheric composition and humidity is:

$$\alpha = \frac{R}{\mu(c_p + C_w + C_r)}, \tag{13.13}$$

$$c_p = \frac{p_{N_2}c_p(N_2) + p_{O_2}c_p(O_2) + p_{CO_2}c_p(CO_2) + p_{Ar}c_p(Ar)}{p}, \tag{13.13′}$$

where $R = 1.987$ cal/mol deg is the gas constant; $\mu$ is the molar weight of the atmospheric air mixture (for Earth $\mu \approx 29$); $p_{N_2} = 0.7551$; $p_{O_2} = 0.2315$; $p_{CO_2} = 0.00046$; $p_{Ar} = 0.0128$ atm are the partial pressures of, respectively, nitrogen, oxygen, carbon dioxide, and argon (Reference Book, 1990); $p \approx 1$ atm is the total pressure of all gas component in the atmosphere accepted for the calculation; $c_p(N_2) = 0.248$; $c_p(O_2) = 0.218$; $c_p(CO_2) = 0.197$; $c_p(Ar) = 0.124$ cal/g deg are heat capacities of nitrogen, oxygen, carbon dioxide, and argon at constant pressure (Reference Book, 1971). From these, the dry Earth's tropospheric heat capacity is $c_p = 0.2394$. The correction factors with the dimension of the heat capacity taking into account the total heat effect of the humidity condensation $C_w$ (in a humid atmosphere) and of the Earth's and Sun's heat radiation $C_r$ absorption by the greenhouse gases may be determined independently. Thus, it follows from Eq. (13.13) that

$$C_w + C_r = \frac{R}{\mu\alpha} - c_p. \tag{13.14}$$

At $\psi = 23.44$ °C, the best fit of the theoretical temperature distribution (13.12) in the Earth's troposphere with the averaged empiric data at $\alpha = 0.1905$. For a dry air mixture in the Earth's atmosphere $c_p = 0.2394$ cal/g deg. From that, for a humid and IR-absorbing air of the real although averaged atmosphere with the temperature gradient 6.5 deg/km, from Eq. (13.13), $C_r + C_w = 0.1203$ cal/g K. For a planet with the atmosphere of a different kind these parameters are the characteristics of any thermophysical or chemical nature leading to the heat release or absorption (at $C_w + C_r < 0$) within the troposphere.

For finding individually $C_w$ and $C_r$ factors it will be necessary to involve the planet's characteristic temperature (Sorokhtin, 2001):

$$C_r = \frac{R}{\mu\alpha}\frac{T_s - T_e}{T_s}, \tag{13.15}$$

$$C_w = \frac{R}{\mu\alpha}\frac{T_e}{T_s} - c_p. \tag{13.16}$$

Substituting the Earth's atmosphere parameter values $\alpha = 0.1905$; $\mu = 29$; $c_p = 0.2394$ cal/g K; $T_s = 288$ K and $T_e = 263.5$ K; and also $R = 1987$ cal/mol deg into Eqs. (7.15) and (7.15′), we find the radiation component $C_r = 0.0306$ cal/g K, the condensation component $C_w = 0.0897$ cal/g K and their total $C_r + C_w = 0.1203$ cal/g K. That is the same value of these parameters as from Eq. (13.14). We can also verify the accepted value of the adiabat $\alpha$ from (13.13) by substituting into it $R = 1.987$ cal/mol deg, $\mu \approx 29$. This is not an accidental coincidence but a confirmation that Eqs. (13.13)–(13.16) are right.

The heat transfer from the Earth's surface through convection, radiation, and humidity condensation in the atmosphere is obviously determined by the total heat reserve associated with the individual processes. It follows from Eq. (13.12) that at $p = p_0$ the energy of the heat transfer from the surface into the stratosphere $\dot{E}$ may be determined from:

$$\dot{E} \approx \frac{\sigma \times 3.502}{(1-A)}\left[\frac{T_s}{b^{\alpha}}\right]^4, \tag{7.16}$$

where, as previously, $T_s = 288$ K, $b = 1.597$ and the factor 3.502 takes into account the effect of the Earth's precession angle from Eq. (13.12′). For a completely dry and transparent atmosphere where the heat transfer may only be by the convection ($c_p = 0.2394$ kcal/g K), we find from Eq. (13.12) $\alpha_p = 0.286$, then $\dot{E}_p = 1.143 \times 10^6$ erg/cm$^2$s. It is possible to find in a similar way the contribution from the radiation component of the "greenhouse gases" heat transfer ($C_r = 0.0306$ kcal/g K). First, we determine $\alpha_r = 2.239$, then $\dot{E}_r = 2.249 \times 10^4$ erg/cm$^2$s, and the contribution from the humidity condensation in the convection process ($C_w = 0.0897$ kcal/g K and $\alpha_w = 0.7641$) is then $\dot{E}_w = 4.671 \times 10^5$ erg/cm$^2$s. From this we find that the contribution from the "greenhouse gases" into the convective heat transfer is just 1.8% whereas the humidity condensation is adding approximately 28.5% more. Remaining 69.7% of the convection processes are due to the direct heating of the air mass by the solar radiation or the heat reflected from Earth (see Fig. 13.4).

To verify the correctness of Eq. (13.12) it was used to calculate the temperature distribution in the Earth troposphere based on the given pressure from the standard atmosphere model (Reference Book, 1951). The results accounting for the present-day precession angle of $\psi = 23.44°$ at $p_s = p_0 = 1$ atm are included in Table 13.1 and shown in Fig. 13.5.

We can see from the table that the calculations for Earth are coincident with the temperature distribution in the troposphere model for the standard Earth's atmosphere with accuracy of about 0.1%. A reminder: the standard model of the Earth's atmosphere is actually the temperature and pressure versus the elevation over the sea level averaged for the entire Earth. This tropospheric model with gradient 6.5 K/km is commonly used for tuning the aviation altimeters and calibration of the barometers intended for the surface observations.

A much more rigid check of the universality of the derived pattern is the temperature distribution calculation within the high-density carbon dioxide atmosphere of Venus. The assigned values are: pressure, 92.1 bar = 90.9 atm; solar constant $S = 2.62 \times 10^6$ erg/cm$^2$ s; the precession angle $\psi \approx 3.18°$ and the molar weight $\mu = 43.5$, effective temperature 288 K, surface temperature 735.3 K, and $b^{\alpha} = 3.225$. The best match between the theoretical and empirical distributions was obtained with the adiabatic exponent $\alpha = 0.1786$.

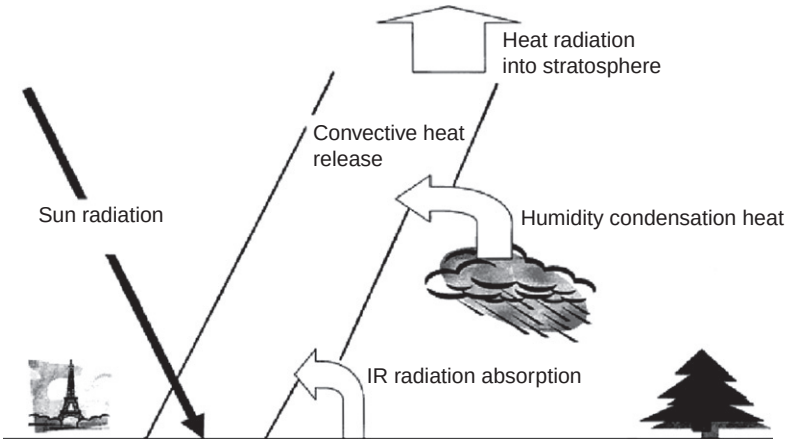


**FIGURE 13.4** Balance of heat transfer in the Earth's troposphere: 69.7% of the heat is lost through the air convection, 28.5% is lost through the humidity condensation, and only 1.8% is lost through radiation.

As Table 13.2 and Fig. 13.5 show, the theoretical temperature distribution in the Venus troposphere totally different from that of Earth matched well with the empirical measurements published in "Planet Venus" (1989). Up to the elevation of 40 km the match is 0.5–1.0%, higher up and to 60 km the theoretical temperatures are between the two series of measurements in the Venus low and high latitudes (the theoretical curve was calculated for low latitudes). Higher yet, above 60 km, at $p < 0.2$ atm, the tropopause begins, and the proposed theory no longer works.

Such a coincidence cannot be accidental. Most likely, it is a testimony to the theory's validity, especially taking into account that that was a first theoretical distribution ever obtained for Venus.

The quoted comparisons show that the average temperature distribution in a planet's troposphere is uniquely defined by the solar constant, atmosphere's mass (pressure), heat capacity of its gas mixture, and the planet's precession angle.

Averaged Venusian tropospheric parameters are: $T_s = 735.3$ K and $T_e = 228$ K. The heat capacity of the atmospheric gas mixture changes, depending on the temperature, from $c_p = 0.261$ cal/g K near the planet's surface at 735 K to 0.138 cal/g K at the elevation about 80 km at $T \approx 200$ K.

For a better match between the theoretical temperature distribution and its empirical values in the Venusian atmosphere, the experimental temperatures should be approximated by a set of the enveloping distributions. The $\alpha$ values should be determined from Eq. (13.13) and the atmosphere composition (approximately 95% $CO_2$ and 3–5% $N_2$; Marov, 1986) but with a mandatory consideration of the heat capacity temperature dependence for $CO_2$: $c_p = 10.57 + 2.1 \cdot T \times 10^{-3} - 2.06 \cdot T^{-2} \times 10^5$ and for $N_2$: $c_p = 6.83 + 0.9 \cdot T \times 10^{-3} - 0.12 \cdot T^{-2} \times 10^5$ (Reference Book, 1971). Then it is possible to determine from Eqs. (13.14)–(13.16) the correction factors accounting for the summary heat effects of the dissociation, formation, and condensation processes of chemical compounds $C_w$ in the hot Venusian atmosphere, as well as the absorption by the greenhouse gases of the Sun's and Venus's heat radiation $C_r$. See Table 13.3 for the calculation results.

**TABLE 13.1** Temperature Distribution in Earth's Atmosphere Based on the Standard Atmospheric Model and Eq. (13.12)

| Model of standard atmosphere (Bachinsky, A. I., Putilov, V. V., and Suvorov, N. P., 1951) Theoretical calculation (Eq. (13.12)) | | | | | | | |
|---|---|---|---|---|---|---|---|
| $h$ (km) | $p$ (mmHg) | $T$ (°C) | $T$ (K) | | $p$ (atm) | $T$ (K) | $T$ (°C) |
| 0.0 | 760.00 | 15.00 | 288.20 | | 1.00 | 288.20 | 15.00 |
| 0.5 | 716.01 | 11.75 | 284.95 | | 0.9421 | 284.95 | 11.77 |
| 1.0 | 674.11 | 8.50 | 281.70 | | 0.8870 | 281.70 | 8.50 |
| 1.5 | 634.21 | 5.25 | 278.45 | | 0.8345 | 278.44 | 5.24 |
| 2.0 | 596.26 | 2.00 | 275.20 | | 0.7846 | 275.20 | 2.00 |
| 2.5 | 560.16 | −1.25 | 271.95 | Troposphere | 0.7371 | 271.94 | −1.26 |
| 3.0 | 525.87 | −4.50 | 268.70 | | 0.6919 | 268.69 | −4.51 |
| 3.5 | 493.30 | −7.75 | 265.45 | | 0.6491 | 265.44 | −7.76 |
| 4.0 | 462.40 | −11.00 | 262.20 | | 0.6084 | 262.20 | −11.00 |
| 4.5 | 433.10 | −14.25 | 258.95 | | 0.5699 | 258.95 | −14.25 |
| 5.0 | 405.33 | −17.50 | 255.70 | | 0.5333 | 255.69 | −17.51 |
| 5.5 | 379.04 | −20.75 | 252.45 | | 0.4987 | 252.45 | −20.75 |
| 6.0 | 354.16 | −24.00 | 249.20 | | 0.4660 | 249.21 | −23.99 |
| 6.5 | 330.72 | −27.25 | 245.95 | | 0.4345 | 245.91 | −27.29 |
| 7.0 | 308.52 | −30.50 | 242.70 | | 0.4059 | 242.75 | −30.45 |
| 7.5 | 287.55 | −33.75 | 239.45 | | 0.3784 | 239.53 | −33.67 |
| 8.0 | 267.79 | −37.00 | 236.20 | | 0.3524 | 236.30 | −36.90 |
| 8.5 | 249.16 | −40.25 | 232.95 | | 0.3278 | 233.07 | −40.13 |
| 9.0 | 231.62 | −43.50 | 229.70 | | 0.3048 | 229.87 | −43.33 |
| 9.5 | 215.09 | −46.75 | 226.45 | | 0.2830 | 226.64 | −46.56 |
| 10.0 | 199.60 | −50.00 | 223.20 | | 0.2626 | 223.44 | −49.76 |
| 10.5 | 185.01 | −53.25 | 219.95 | | 0.2434 | 220.23 | −52.97 |
| 11.0 | 171.34 | −56.50 | 216.70 | | 0.2254 | 217.04 | −56.16 |
| 11.5 | 160.11 | −56.50 | 216.70 | Tropopause | 0.2107 | 214.27 | −58.93 |
| 12.0 | 149.64 | −56.50 | 216.70 | | 0.1969 | 211.52 | −61.68 |

As Table 13.3 shows, based on the temperature distributions quoted in "Planet Venus" (1989), the heat capacity of the heat radiation energy absorption process increases with elevation from $C_r = 0.19$ near the surface to 0.45–0.5 cal/mol K at the elevations 60–80 km.

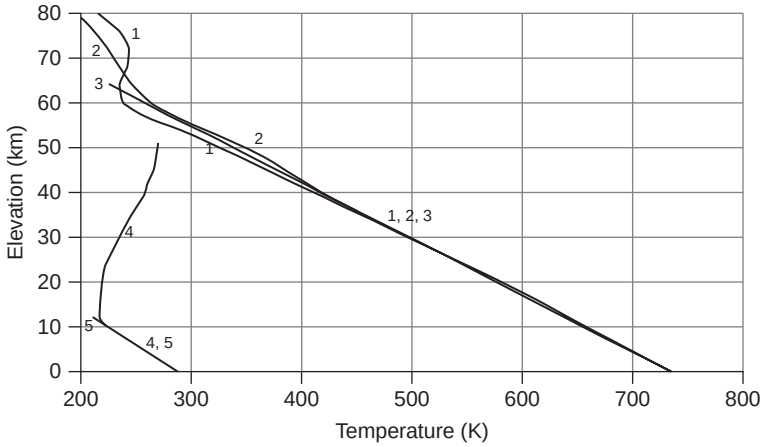


**FIGURE 13.5** Distribution of experimental temperatures in the Earth troposphere and stratosphere (curve 4) and in the Venusian troposphere (1 and 2) (Planet Venus, 1989) versus theoretical distributions (5 and 3) plotted based on the adiabatic theory of the greenhouse effect (all temperature is in absolute (physical) K).

**TABLE 13.2** Venus Temperature Distribution: Empirical and From Eq. (13.12)

| **Empirical data (Planet Venus, 1989)** | | | **Theoretical calculation (Eq. (13.12))** | | | | |
|---|---|---|---|---|---|---|---|
| ***h* (km)** | ***T* (K)** | ***p* (bar)** | ***T* (K)** | ***p* (bar)** | ***h* (km)** | ***p* (bar)** | ***T* (K)** |
| 0 | 735.3 | 92.10 | | | 0 | 92.10 | 735.43 |
| 1 | 727.7 | 86.45 | | | 1 | 86.45 | 727.4 |
| 2 | 720.2 | 81.09 | | | 2 | 81.09 | 719.37 |
| 3 | 712.4 | 76.01 | | | 3 | 76.01 | 711.35 |
| 4 | 704.6 | 71.20 | | | 4 | 71.20 | 703.33 |
| 5 | 696.8 | 66.65 | | | 5 | 66.65 | 695.32 |
| 6 | 688.8 | 62.35 | | | 6 | 62.35 | 687.33 |
| 7 | 681.1 | 58.28 | | | 7 | 58.28 | 679.33 |
| 8 | 673.6 | 54.44 | | | 8 | 54.44 | 671/35 |
| 9 | 665.8 | 50.81 | | | 9 | 50.81 | 663.36 |
| 10 | 658.2 | 47.39 | | | 10 | 47.39 | 655.39 |
| 12 | 643.2 | 41.12 | | | 12 | 41.12 | 639.46 |
| 14 | 628.1 | 35.57 | | | 14 | 35.57 | 623.59 |
| 16 | 613.3 | 30.66 | | | 16 | 30.66 | 607.73 |
| 18 | 597.1 | 26.33 | | | 18 | 26.33 | 592.28 |

*Continued*

**TABLE 13.2** Venus Temperature Distribution: Empirical and From Eq. (13.12)—(Cont'd)

| *h* (km) | *T* (K) | *p* (bar) | *T* (K) | *p* (bar) | *h* (km) | *p* (bar) | *T* (K) |
|---|---|---|---|---|---|---|---|
| 20 | 580.7 | 22.52 | | | 20 | 22.52 | 576.07 |
| 22 | 564.3 | 19.17 | | | 22 | 19.17 | 560.2 |
| 24 | 547.5 | 16.25 | | | 24 | 16.25 | 544.38 |
| 26 | 530.7 | 13.70 | | | 26 | 13.70 | 528.5 |
| 28 | 513.8 | 11.49 | | | 28 | 11.49 | 512.62 |
| 30 | 496.9 | 9.581 | | | 30 | 9.581 | 496.72 |
| Measurement latitude 0–30°; Measurement latitude 75° Theoretical calculation | | | | | | | |
| 33 | 471.7 | 7.211 | 471.7 | 7.211 | 33 | 7.211 | 472.84 |
| 36 | 448.0 | 5.346 | 446.5 | 5.345 | 36 | 5.346 | 448.93 |
| 39 | 425.1 | 3.903 | 420.5 | 3.894 | 39 | 3.903 | 425.86 |
| 42 | 403.5 | 2.802 | 394.5 | 2.78 | 42 | 2.802 | 402/06 |
| 45 | 385.4 | 1.979 | 368.7 | 1.941 | 45 | 1.979 | 378.54 |
| 48 | 366.4 | 1.375 | 343.5 | 1.321 | 48 | 1.375 | 355.38 |
| 51 | 342.0 | 0.9347 | 318.5 | 0.8741 | 51 | 0.9347 | 332.38 |
| 54 | 312.8 | 0.6160 | 290.0 | 0.5582 | 54 | 0.6160 | 309.19 |
| 57 | 282.5 | 0.3891 | 258.2 | 0.3392 | 57 | 0.3891 | 285.51 |
| 60 | 262.8 | 0.2357 | 237.5 | 0.1948 | 60 | 0.2357 | 261.74 |
| 64 | 245.4 | 0.1156 | 234.3 | 0.0895 | 64 | 0.1156 | 231.33 |
| 68 | 235.4 | 0.0545 | 242.0 | 0.0418 | 68 | 0.0545 | 203.03 |
| 72 | 224.1 | 0.0248 | 243.6 | 0.01987 | 72 | 0.0248 | 177.09 |
| 76 | 212.1 | 0.0108 | 234.9 | 0.00935 | 76 | 0.0108 | 153.39 |
| 80 | 197.1 | 0.00448 | 214.7 | 0.00418 | 80 | 0.00448 | 131.65 |

Similarly, the heat capacity of the chemical compounds dissociation and condensation processes increases from $C_w = -0.176$ to positive values $+0.064$ to $+0.12$ cal/g K at the elevations about 60–80 km. A relatively elevated value of the parameter $C_r$ (which defines the planet's heat absorption) is apparently due to a carbon dioxide atmospheric composition and a very high temperature of the Venusian troposphere. For the Venusian troposphere $C_w < 0$, that is, its thickness (especially its lower and middle layers) is dominated by endothermic dissociation reactions of some chemical compounds (such as sulfuric acid decomposition into sulfur trioxide and water). In the upper tropospheric layers, at the

elevations 40–50 km and above 60 km, usually $C_w > 0$. Therefore, these elevations are dominated by exothermic reactions of the formation of chemical compounds (for instance, the sulfuric acid) and humidity condensation in the clouds.

Thus, the lower and middle layers of the Venusian troposphere (at the elevations of 0 to approximately 60 km) are dominated by the energy absorption processes probably associated with the molecule dissociation processes, for instance, $H_2SO_4 + Q \rightarrow SO_3 + H_2O$, where $Q$ is the molecule dissociation heat (for the sulfuric acid, $Q \approx 15$ kcal/mol). Reactions of carbon dioxide and water dissociation are possible in the upper troposphere and stratosphere caused by the UV Sun radiation $CO_2 + h\nu \rightarrow CO + O$ and $H_2O + h\nu \rightarrow OH + H$. For carbon dioxide, the critical UV radiation wavelength is about 0.228 mkm (2276 Å), and for the water 0.243 mkm (2428 Å) so such reactions are quite possible in the tenuous layers of the Venusian troposphere above 60 km. However, the reverse exothermic reactions of atoms recombining into the source molecules are also possible with the formation, for instance, of carbon dioxide $CO + O \rightarrow CO_2 + 125.6$ kcal/mol and water $OH + O \rightarrow H_2O + 117.76$ kcal/mol. In fact, these reactions convert the Sun's UV radiation energy into the atmosphere's heat energy. That is exactly why the upper troposphere and lower stratosphere above 60 km are noticeably heated which is well illustrated by Fig. 13.5. At the same elevations the sum $C_q = C_r + C_w \approx 5$–$7$ cal/g K also reaches its maximum value (see Table 13.3).

In the Earth's clouds with humidity condensation, there is the release of a significant internal energy (see Eq. 13.18 and Fig. 13.7). On Venus, the clouds are likely composed of sulfuric acid aerosols (Sill, 1983). Transparency measurements of the atmospheric gas mixture on Venus indicate that the clouds there are positioned at elevations of 48–68 km (Planet Venus, 1989). Clouds, however, insignificantly affect the temperature distribution (probably, because of the low concentration of sulfur oxides in Venus's atmosphere) although parameter $C_w$ distribution at the cloud level shows some increase in its value (see Table 13.3).

**TABLE 13.3** Gradient Temperatures and Heat Capacities of the Heat Release and Absorption in the Venusian Troposphere.

| Latitudes 0–30° | | | | | Latitude 75° | | | | |
|---|---|---|---|---|---|---|---|---|---|
| **Elevation (km)** | **$C_w$ (cal/g K)** | **$C_r$ (cal/g K)** | **$C_w + C_r$ (cal/g K)** | **grad$T$ (deg/km)** | **Elevation (km)** | **$C_w$ (cal/g K)** | **$C_r$ (cal/g K)** | **$C_w + C_r$ (cal/g K)** | **grad$T$ (deg/km)** |
| 0–23 | −0.1757 | 0.1898 | 0.0142 | 7.665 | 00–23 | −0.1757 | 0.1898 | 0.0142 | 7.665 |
| 23–38 | −0.1707 | 0.1658 | −0.0049 | 8.386 | 23–51 | −0.1707 | 0.1658 | −0.005 | 8.386 |
| 38–46 | −0.1219 | 0.2424 | 0.1205 | 5.341 | 51–60 | −0.1219 | 0.1413 | −0.026 | 12.024 |
| 46–60 | −0.1163 | 0.1423 | 0.0269 | 12.508 | 60–75 | 0.1214 | 0.5083 | 7.1867 | 0.1017 |
| 60–84 | 0.0644 | 0.4502 | 0.5145 | 1.851 | 75–87 | −0.0068 | 0.2918 | 0.2849 | 4.422 |

## 13.4 CONSIDERATION OF THE TROPOSPHERIC AIR HUMIDITY AND CLOUD COVER

Eq. (13.12) may be used for plotting the temperature distribution within the humid Earth's atmosphere with the average heat capacities $(C_p)_{hum} = C_p + C_r + C_w \approx 0.361$ cal/g K $= 1.509 \times 10^7$ erg/g K and $(\alpha)_{hum} = 0.1905$. It also may be used for a dry Earth's atmosphere with the "greenhouse gases" absorbing the IR radiation.

We selected an option where the radiation component within a relatively dry troposphere remains the same and the humidity is three times lower because even a dry atmosphere (in a regular judgment) still contains some humidity. In this case: $(C_p)_{dry} = C_p + C_r + C_w/3 \approx 0.3$ cal/g K $\approx 1.25 \times 10^7$ erg/g K and $(\alpha)_{dry} = 0.2285$. Then, obviously, the temperature gradients in the humid and "dry" atmosphere (in K/km) will be:

$$\text{grad}\, T_{hum} = \frac{g}{(C_p)_{hum}} \approx 6.5\,\text{K/km}, \tag{13.17}$$

and

$$\text{grad}\, T_{dry} = \frac{g}{(C_p)_{dry}} \approx 7.8\,\text{K/km}, \tag{13.17'}$$

where $g = 981$ cm/s$^2$ is the Earth's gravity acceleration.

Relatively dry air is usually observed in anticyclones, and humid air in cyclones. Taking the above estimates into account, Fig. 13.6 shows the temperature distributions in the humid and relatively dry air. As we see, the near-surface temperature in a "dry" troposphere is usually somewhat higher than in a humid one. In our example, the average difference in the near-surface temperatures reaches $+5.2$ °C. This phenomenon may explain the temperature increase in the near-surface air layers and the droughts in the Earth's deserts and arid areas as well as in the regions where dry air masses invade with the anticyclones from the arid belts (for instance, the Trans-Volga steppes).

We will now discuss disruptions in the adiabatic temperature distributions within the cloudy troposphere. In this case, the temperature distribution below the cloud cover must be controlled by the humid air adiabat, and above the cloud cover, by the "dry" air adiabat (of course, this dry air contains about 1/3 of the initial humidity). Within the cloud cover proper, the temperature distribution must be controlled by the heat released in the humidity condensation. The average humidity mass $m_w$ in the atmosphere is determined from the already found average heat capacity of the atmospheric humidity $C_w = 0.0897$ cal/g K. Heat capacity of 1 g of the vapor is 0.49 cal/K. Then the humidity content above 1 cm$^2$ of the Earth's area is $m_w = 0.49/0.0897 \approx 5.46$ g/cm$^2$, and the average humidity content in the near-surface layers of the atmosphere is approximately: $C(H_2O) \approx 0.55\%$.

As shown above, the heat capacity of humid and heat-absorbing air is approximately $(C_p)_{hum} \approx 0.36$ cal/g K, and the heat capacity of relatively dry but IR-absorbing air is $(c_p)_{dry} \approx 0.3$ cal/g K. Let us assume for certainty that the cloud cover extends from 1 to 2.5 km and that the dew point is about $+0.5$ °C (with the surface temperature 280 K $= +7$ °C). Then the per-unit air mass in this cloud cover is approximately equal to the pressure difference on its boundaries $M_{cl} \approx \Delta p = 887 - 737.1 = 149.9$ g/cm$^2$ (see Table 13.1), and the humidity

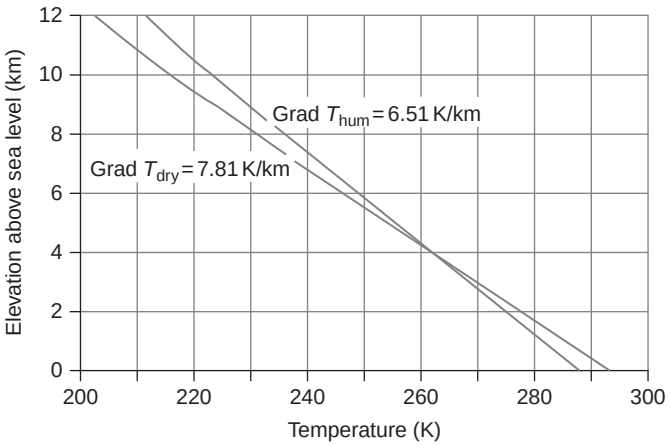


**FIGURE 13.6** Comparison of the temperature distributions plotted from (13.17) and (13.17′) in relatively dry (grad$T_{dry}$) and humid (grad$T_{hum}$) troposphere. As seen, with all other conditions equal the near-surface temperature in the humid troposphere in the cyclonic areas are always lower than the near-surface "dry" atmosphere of the anticyclonic areas.

mass in the cloud layer is $(m_w)_{cl} = 149.9 \times 0.0055 = 0.824\ g/cm^2$. Not all humidity (only about 1/3 of its mass) is concentrated in the clouds and the internal heat of the humidity condensation is $q = 595.8$ cal/g. Then we can find the average air heating within the cloud layer:

$$\Delta\bar{T} = \frac{q(m_w)_{cl}}{M_{cl}(C_w)_{\Sigma}}\frac{2}{3} \approx 6.1\,^{\circ}C. \tag{13.18}$$

Despite the air heating within the cloud cover, it does not rise up immediately as its expansion is compensated by the humidity condensation in water drops, which make the air volumes in the clouds heavier. This is an unstable situation as the water drops gradually go down. Thus, after a while the emerged cloud cover can fall apart. If, however, the clouds form over the ascending air flows which continuously feed the clouds with humidity, the cloud cover becomes more stable, and the temperature distribution above it approaches the distribution of a relatively dry air (curve 2 in Fig. 13.7). It shows that noticeable inversions of the air temperature may occur in the cloud formation.

## 13.5 CONSIDERATION OF THE "GREENHOUSE" GASES

We will now discuss the effect of the so-called "greenhouse gases" on the tropospheric temperature regimes. For this, we will conceptually replace the Earth's nitrogen–oxygen atmosphere first with a carbon dioxide and then, with a methane atmosphere (i.e., most thinkable "greenhouse atmospheres") with the same atmospheric pressure $p_s = 1$ atm but with the adiabatic exponents determined from Eq. (13.13) at $\mu_{CO_2} = 44$, $c_p = 0.197$, $\mu_{CH_4} = 16$ and $c_p = 0.528$. From these, $\alpha_{CO_2} = 0.1423$, $\alpha_{CH_4} = 0.1915$. Substituting these $\alpha$ values into Eq. (13.12), we can determine the temperature distribution within the carbon dioxide and methane tropospheres. In our case, the near-surface temperature in the hypothetical carbon dioxide atmosphere will be 281.5 K, that is, 6.4 °C lower than for the nitrogen–oxygen

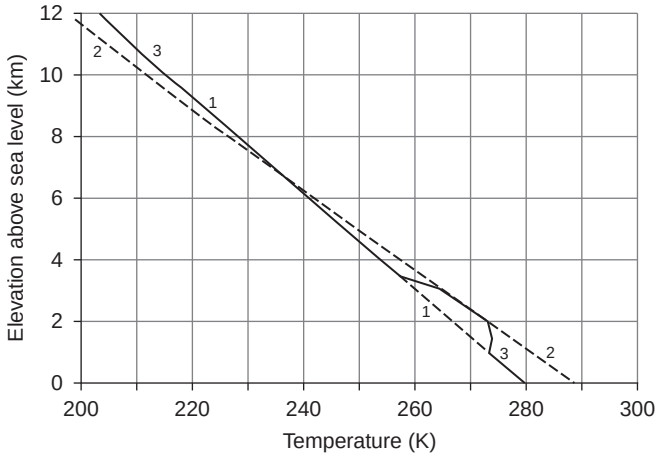


**FIGURE 13.7** Temperature versus elevation in a troposphere with cloud cover at 1–2.5 km: 1. Temperature distribution in a humid troposphere (grad$T_{hum} \approx 6.5\,^{\circ}C/km$); 2. Temperature distribution in a relatively dry troposphere (grad$T_{dry} \approx 8\,^{\circ}C/km$); 3. Theoretical temperature distribution in a troposphere with the cloud cover (the dew point temperature is assumed $\approx +0.5\,^{\circ}C$).

composition of the atmosphere, and for the methane atmosphere it will be 288.1 K, which is coincident with the usual average Earth's temperature of 288.2 K. It needs to be taken into consideration that the carbon dioxide atmosphere is denser and the methane one, conversely, lighter so the equal pressures in these atmospheres will be reached at different elevations compared with the nitrogen–oxygen atmosphere:

$$h_{CO_2} = h_{N_2+O_2}\frac{\mu_{N_2+O_2}}{\mu_{CO_2}} \quad \text{and} \quad h_{CH_4} = h_{N_2+O_2}\frac{\mu_{N_2+O_2}}{\mu_{CH_4}}, \tag{13.19}$$

where $\mu_{N+O_2} = 28.9$ is the molar weight of the nitrogen–oxygen atmosphere, and $\mu_{CO_2} = 44$ and $\mu_{CH_4} = 16$ are, respectively, the carbon dioxide and methane molar weights. The so derived temperature distributions in the carbon dioxide and methane atmospheres, in comparison with the quoted (see Fig. 13.5) temperature distribution in the nitrogen–oxygen atmosphere, are illustrated in Fig. 13.8.

Thus, mentally replacing the Earth's nitrogen–oxygen atmosphere by the carbon dioxide one with the same surface pressure 1 atm, we arrive at an average surface temperature of about 6.5° lower (accounting for Eq. (13.19)) and not substantially higher as it is conventionally thought.

Likewise, the temperature within the entire thickness of the carbon dioxide atmosphere always turns out lower than in the nitrogen–oxygen atmosphere. In replacing the atmosphere with a methane one, the surface temperature at the sea level practically does not change although within the troposphere it is higher than in the nitrogen–oxygen atmosphere with the adiabatic exponent $\alpha = 0.1905$. That is why in a purely methane atmosphere (which is hardly possible), the surface temperature in mountainous areas may substantially rise. However, the methane concentration in the atmosphere is so low (around $1.2 \times 10^{-6}$) that the realistically possible temperature distributions with methane addition are practically indistinguishable from its distribution in a purely nitrogen–oxygen Earth's atmosphere and hence do not affect the Earth's climate.

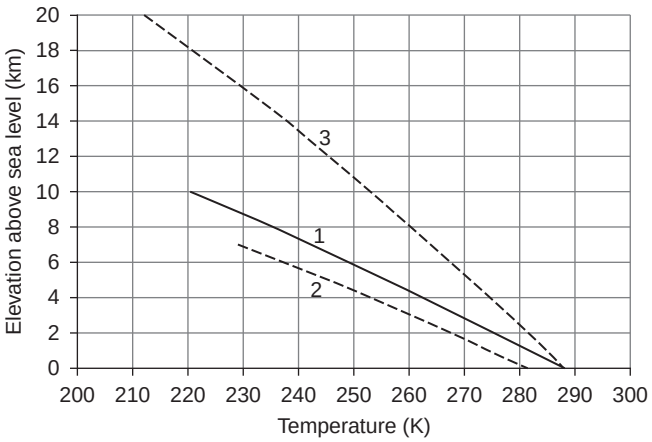


**FIGURE 13.8** Averaged temperature distributions in the Earth's troposphere under Eq. (13.12): 1. For Earth's troposphere with a regular nitrogen–oxygen air mixture; 2. For Earth's atmosphere model with the carbon dioxide air composition; 3. For Earth's atmosphere model with the purely methane composition of its gas shell (all other model 2 and 3 parameters are the same as for case 1).

Similarly, mentally replacing the Venus' carbon dioxide atmosphere by the nitrogen–oxygen at the same pressure of 90.9 atm we will raise the surface temperature from 735 to 777 K or from 462 to 504 °C (see Fig. 13.9).

The quoted examples show that saturation of the atmosphere with carbon dioxide, despite the heat radiation absorption by it, under other conditions equal always results not in a rise but in a decline of the greenhouse effect and the average temperature within the entire thickness of the planet's troposphere. The reason is simple: the molar weight of carbon dioxide is 1.5 higher and its heat capacity is 1.2 times lower than for the air. As a result, as it follows from Eq. (13.13), the adiabatic exponent for carbon dioxide atmosphere, with all other conditions equal, is about 1.34 times lower than that for a humid air of the nitrogen–oxygen composition: $\alpha(N_2+O_2)=0.1905$.

Physically, the explanation of this phenomenon is that the heat transfer from the troposphere mostly occurs through the air mass convection, which is much more efficient than the radiation heat transfer mechanism (see Fig. 13.4). It is understandable because, after the greenhouse gases absorbed the Earth's heat radiation, its energy is converted into the energy of gas molecules' heat oscillations. That, in turn, results in the expansion of the gas mixture and its rapid rise to the stratosphere (where the excessive heat is further lost through the radiation). To replace the risen warm air volumes, the cooled-down air descends from the upper troposphere, and the overall temperature changes very little.

One particular conclusion from this is that the convection mass exchange of the atmospheric gases must substantially accelerate in the troposphere with the elevated carbon dioxide content. Thus, it is possible that the intensification of the synoptic activity in the troposphere (not the temperature raise!) observed during the recent years is associated with the accumulation of the anthropogenic carbon dioxide in it.

Thus, the commonly accepted idea of a global climate warming when $CO_2$ accumulates in the atmosphere is a myth. In actuality, $CO_2$ accumulation, under all other conditions equal, may result only in the climate cooling and in a somewhat increased synoptic activity

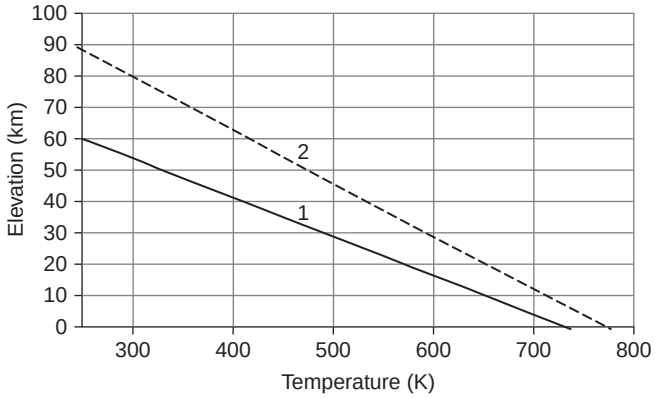


**FIGURE 13.9** Averaged temperature distributions in the Venusian troposphere under Eq. (13.12): 1. Temperature distribution for the actual carbon dioxide troposphere (above 60 km); 2. Temperature distribution for a hypothetical nitrogen–oxygen model of the Venusian troposphere with all other conditions equal.

in the Earth's troposphere. An additional explanation is that when the anthropogenic carbon dioxide is released, oxygen is also absorbed from the atmosphere, and the result may be only a climate cooling.

## 13.6 INTENSITY OF THE PRESENT-DAY EARTH'S SYNOPTIC ACTIVITY

The proposed model of the greenhouse effect is in its substance a unidimensional model. The platen is represented as a dimensionless point and the only dimension is the elevation above this point. Such a synergetic model is at the same time most accurate in the determination of the global tropospheric parameters such as its greenhouse effect, average surface temperature, and the average value of the radiation or humidity-condensational component of the tropospheric heat release, etc. Using Lambert's law of the illumination of a sphere and introducing the consideration of latitude, this model may be converted into a 2D one. By adding the longitudinal component and the seasonal fluctuations of the planet illumination, a tridimensional and quadridimensional (with time as the fourth dimension) model may be obtained. These, however, would noticeably lower the accuracy in the greenhouse effect correlation versus the composition of the planetary atmosphere.

In this case, the physical definition of the "absolute black body" temperature needs to be replaced by a concept of the "gray body" temperature:

$$T_{\mathrm{gb}}^4 = \frac{S}{4\sigma}\cos\varphi, \tag{13.20}$$

where $\varphi$ is the location's latitude.

If we also consider the convective heat transfer in the Earth's troposphere, the Earth-imitating "gray body" temperature is:

$$T_{\mathrm{gb}} = \left(\frac{S}{4\sigma}\cos\varphi + \frac{\dot{Q}}{\sigma}\right)^{1/4}, \tag{13.21}$$

where $\dot{Q}$ is the heat transfer rate by the air masses such as cyclones (in erg/cm$^2$ s). The tropospheric temperature, with the Earth's precession accounted for, under the accepted approximation will be:

$$T = b^{\alpha}\left[\frac{S(1-A)}{\sigma\left(\frac{(\pi/2)-\psi}{\pi/2}4 + \frac{\psi}{\pi/2}2\frac{2}{1-\cos\psi}\right)}\cos\varphi_{\psi} + \frac{\dot{Q}}{\sigma}\right]^{1/4}\left(\frac{p}{p_0}\right)^{\alpha}, \tag{13.22}$$

where $\varphi_{\psi} = \frac{\phi\pi}{180}\left(1 - \frac{\psi\pi}{180}\delta\right)$ is the locality's effective latitude accounting for the precession angle; $\delta$ is the delta function: $\delta = 1$ in summer in a given hemisphere and $\delta = 0$ in winter in the same hemisphere; in the determination of average annual values, $\varphi_{\psi}$ $\delta = 1/2$.

Equation (13.22) enables the determination of the near-surface temperature $T_s$ latitudinal zoning. If at the same time the latitudinal distribution of the empirical average annual or average monthly temperatures is provided, it is then possible to determine the average heat transfer rate by the air masses $\dot{Q}$ at given latitude.

$$\dot{Q} = \frac{T^4}{b^{4\alpha}}\sigma\left(\frac{p_0}{p}\right)^{4\alpha} - \frac{S(1-A)\cos\varphi_{\psi}}{\left(\frac{(\pi/2)-\psi}{\pi/2}\right)4 + 4\frac{\psi}{\pi/2}\frac{1-\cos\psi}{(\sin\psi)^2}}. \tag{13.22'}$$

Equation (13.22′) enables the determination of the synoptic processes evolution rate $\dot{Q}$ if the near-surface temperature latitudinal distributions are available. They are provided in Fig. 13.10:

Fig. 13.11 includes diagrams of the tropospheric synoptic activity $\dot{Q}$ versus latitude derived from Eq. (13.22′). The so determined $\dot{Q}$ values characterize the cyclonic activity at a given latitude $\varphi$.

As the provided diagrams show, the energy release rate by the trade winds is slightly over $4\times10^4$–$4.5\times10^4$ erg/cm$^2$·s. In the northern hemisphere, the average energy release rate by the air mass cyclonic activity gradually increases toward the high latitudes. It certainly appears that the air mass motion energy is transmitted from the tropical belt to the northern boreal and polar areas. For instance, the synoptic energy release maximum in July at 30 N (see Fig. 13.11) clearly indicates the emergence there of the summer tropical storms and hurricanes. They occur at that time, for instance, in the northern areas of the Caribbean, and in the Pacific, in the Philippines, in the South Japanese Islands and the southern China. It is quite possible that New Orleans destruction by Katrina in 2005 was exactly due to such hurricanes.

Substantial increase in the synoptic activity in the polar areas of the Northern hemisphere shown on the diagrams also correlates well with the views of the leading Russian climatologists. For instance, Khromov and Petrosyants (2001) indicate that "the intense cyclonic activity is observed in the Arctic basins in all seasons. The cyclones emerge on the Arctic fronts and also penetrate the Arctic from the lower latitudes where they develop on the polar fronts."

The Antarctic synoptic activity was measured approximately along the meridian 90°E along a profile from the Mirny Station through the continent's highest elevation (the ice

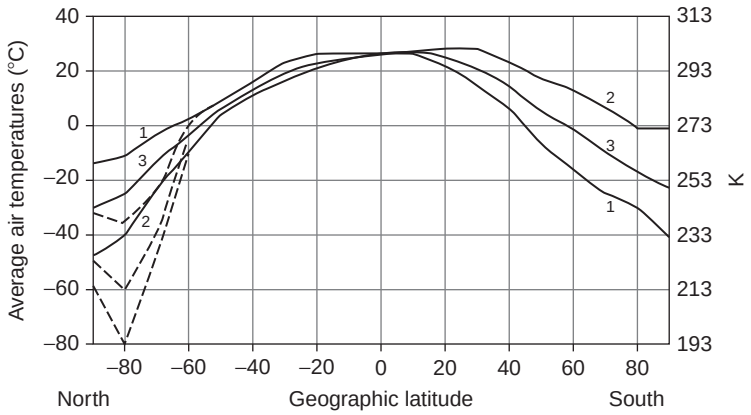


**FIGURE 13.10** Near-surface average air temperature versus latitude. Solid lines, after Khromov and Petrosyants (2001); 1. January; 2. July; 3. annual average temperatures; dashed lines (Antarctic data) are average temperatures from The Atlas of Antarctic. (1966); for the ice cover dome on the Antarctic cold pole (80 °S) are shown the calculated data from well observations in 1946 of the annual average temperature (it was −60 °C there) by O. Sorokhtin and A. Kapitsa.

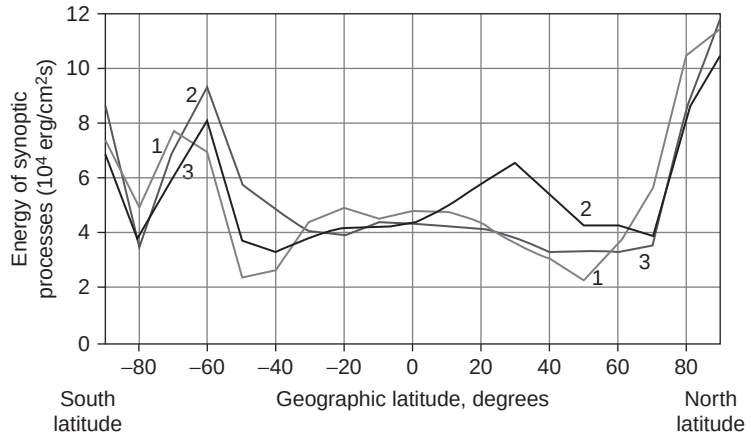


**FIGURE 13.11** Synoptic energy versus latitude calculated from Eq. (13.22′): 1. In January; 2. In July; 3. Annual average.

sheet dome at 80°S and elevation 4000 m above sea level) and to the South Pole. The Antarctic is practically always dominated by anticyclonic conditions with clear and quiet weather. Usual cyclones penetrate only the near-shore areas. Nevertheless, the synoptic activity distribution in the Central Antarctic turned out to be very peculiar: the minimal activity occurs over the dome; south of it (toward the pole) and north of it the energy of the synoptic processes drastically increases. Why, then, the observed bursts of synoptic activity over the continents?

The paradox is explained by strong katabatic winds continuously blowing from the high continental dome to the shores. They strengthen in winter (July) which was often observed

by one of the authors (O. Sorokhtin). These strong (up to 20 m/s and stronger) winds adiabatically warm up while moving over the slopes of the ice sheet. The air masses descending from the continental dome bring with them significant energy whose maximum release rate occurs over the shores near 60°S. Outside of the continent, the katabatic winds spread over the Southern Ocean and gradually die out. The katabatic winds are exactly the reason for the "double-headed" form of the synoptic activity over Antarctica.

Eq. 13.22′ calls for an interesting conclusion about the dependence of the tropospheric synoptic activity on carbon dioxide concentration in the troposphere. As the atmospheric $CO_2$ content increases, the atmospheric adiabatic exponent declines. Thus, from Eq. 13.22′, the atmospheric synoptic activity should increase. Based on our estimates, however, the currently observed $CO_2$ concentration changes can induce only the negligibly small effect on the atmospheric synoptic activity. That is why the storm activity growth over the recent years as well as the humid cyclone penetration into the internal Antarctic areas (see Fig. 13.4.4) could have occurred due to the increased solar radiation at that time.

## 13.7 EFFECT OF THE ANTHROPOGENIC FACTOR ON EARTH'S CLIMATE

The anthropogenic effect on the earth's climate is commonly an emotional perception of the heat absorption by the greenhouse gases. What we will do now is review the quantitative side of the humane-caused carbon dioxide releases to the atmosphere on the tropospheric temperature from a position of the adiabatic theory of the greenhouse effect.

According to different estimates, currently 7–10 billion tons of carbon dioxide or 1.9–2.7 billion tons of pure carbon enters the atmosphere due to burning of natural fuels. This huge amount of carbon not only affects the composition of the atmospheric gas mixture and decrease in its heat capacity but also somewhat increases the total atmospheric pressure. Both these factors work in opposite directions so that the average surface temperature is very little affected. From Eq. (13.12′), with $p_s \approx 1$ atm, we find:

$$dT_s \approx 288\alpha \frac{dp}{p_0}, \tag{13.23}$$

where, as before, the average Earth's temperature $T_s = 288$ K and the adiabatic exponent $\alpha = 0.1905$. Under doubling of the carbon dioxide concentration in the atmosphere from 0.046 to 0.092 mass percent expected by 2100, pressure rise $dp$ will reach $0.46 \times 32/44$ mbar. Then, from Eq. (13.23) we find $dT_s \approx +0.018$ °C. This temperature increase is not associated with the change in the atmospheric composition but with some rise in the atmospheric pressure. The effect of the changed composition is negligibly small, in the order of $-2 \times 10^{-3}$ °C. A conclusion is that the anthropogenic carbon dioxide releases into the atmosphere have no practical effect on the greenhouse effect.

In real life the bulk of carbon dioxide, under Henry's law, is dissolved in the oceanic water. Subsequently, in the hydration of oceanic crust rocks it is bonded in carbonates and is absorbed by plants. Together with carbon, part of the atmospheric oxygen migrates into carbonates. The end result is that instead of a slight increase in the atmospheric

pressure we should expect its slight decline, hence, slight climate cooling (and not at all its substantial warming as proposed by the orthodox environmentalists).

Besides, in hydration of rocks in the oceanic crust some carbon dioxide is reduced to methane. The total carbon dioxide presently removed from the oceans, therefore, from the atmosphere through the carbonate formation and methane generation is about $2.3 \times 10^8$ tons/year. The potential of this $CO_2$ absorption mechanism in the hydration of the oceanic crust is much higher. Although the period of this geochemical cycle is over 100 years, the effect will accumulate with time.

Thus, together with the anthropogenic carbon dioxide some oxygen is also removed from the atmosphere. Based on the stoichiometry of $CO_2$, almost 2.3 g of oxygen is removed from the atmosphere with every gram of carbon. Provided the ocean and vegetation absorb the entire excess $CO_2$, this will result after 2100 in a decline of the total atmospheric pressure by about 0.34 mbar, therefore in the climate cooling by $-8.2 \times 10^{-3}$ K $\approx -0.008$ °C. In real life, however, life activity of plants must almost totally compensate the human-disrupted equilibrium by way of accelerated biomass growth, and therefore restore the climatic balance.

An important practical conclusion from the above is that even significant technogenic carbon dioxide releases into the atmosphere practically do not affect the averaged Earth's climate parameters and its greenhouse effect. Thus, common concepts of a significant effect that the anthropogenic carbon dioxide releases have on climate warming are a myth. In actuality, these releases have no effect on the Earth's heat regime. Besides, there are very positive side effects: a carbon dioxide concentration increase in the atmosphere will certainty increase agricultural productivity and facilitate more efficient restoration of the plant mass in forest-felling areas. As Robinson et al. (1998) indicate, the growth in agricultural productivity is almost in direct proportion with the increase in carbon dioxide partial pressure.

## 13.8 VIEWS OF AMERICAN SCIENTISTS ON THE ROLE OF THE GREENHOUSE EFFECT

Many US scientists who studied climate changes in different parts of North America came to a similar conclusion of the lack of influence from the greenhouse gases on the Earth's heat regime. According to these scientists, currently there is no discernible climate warming. A well-known US scientist, a former president of the National Academy of Sciences, Professor F. Zeitz, wrote experimental data on climate change do not indicate any harmful effect of the anthropogenic hydrocarbon use. Contrary to that, there are strong indications that the increase in carbon dioxide content in the atmosphere is beneficial. F. Zeitz invited the scientific community to sign a special petition calling on the Government of the United States and other countries not to sign the Kyoto Protocol on limiting greenhouse gas emissions concluded in December of 1997 and other similar agreements. The petition says in particular that there is no convincing scientific evidence that the anthropogenic carbon dioxide, methane or other greenhouse gas release inflicts or may in the foreseeable future cause catastrophic progressive warming of the Earth's atmosphere and the destruction of its climate. Besides, there is ample scientific evidence showing the increase

of carbon dioxide in the atmosphere results in a positive effect on the plant and animal growth in the ambient Earth's medium.

A general review published by Robinson, Balinuas et al. (1998) and attached to Zeitz's petition, concludes that the increase in carbon dioxide atmospheric concentration in the twentieth century did not affect the global climate but did substantially increase the plant growth. The popular climate warming hypothesis, in view of Robinson et al., turned out to be invalid and not corresponding to modern experimental data.

## 13.9 OCEANIC EFFECT ON CARBON DIOXIDE CONTENT IN THE ATMOSPHERE

Much more carbon dioxide is dissolved in the oceanic water (as $HCO_3^-$ ions) than is contained in the atmosphere (Reference Book, 1990). The equilibrium carbon dioxide distribution between the atmosphere and the ocean is governed by the Henry's law under which the gas concentration in the oceanic water $C(CO_2)_{oc}$ is directly proportionate to its partial pressure $p(CO_2)_{atm}$ in the atmosphere:

$$C(CO_2)_{oc} = (CO_2)_{atm}, \tag{13.24}$$

where $H$ is Henry's factor substantially dependent on the temperature $T$.

In the modern ocean, the ion concentrations are: $HCO_3^{1-} = 1.427 \times 10^{-4}$ and $CO_3^{2-} = 7.02 \times 10^{-5}$, which is equivalent to $CO_2$ mass in the ocean of $2.14 \times 10^{20}$ g whereas its atmospheric content is about $2.33 \times 10^{18}$ g $CO_2$ (Reference Book, 1990). The corresponding partial pressure is $p = 4.6 \times 10^{-4}$ atm Thus, the oceanic $CO_2$ content is approximately 90 times that of the atmosphere. The average $CO_2$ concentration in the oceanic water is $1.56 \times 10^{-4}$. Based on this, from Eq. (13.24) we determine the present-day Henry's factor $H \approx 0.34$ atm$^{-1}$.

$$H = H_0 e^{-\Delta H^0/RT}, \tag{13.25}$$

where $\Delta H^0$ is the enthalpy change (heat release with the opposite sign) at dissolving one mole of $CO_2$ in the oceanic water; $R = 1.987$ cal/mol deg is, as previously, the gas constant; $T$ is temperature in degrees Kelvin; $H_0$ is maximum value of Henry's factor at $\Delta H^0 = 0$. When carbon dioxide is dissolved in water, the carbonic acid is formed:

$$CO_2 + H_2O \rightarrow {}_2CO_3. \tag{13.26}$$

The enthalpy values $\Delta H_{f(298.15)}{}^0$ of these compounds are, respectively, $-94.05$; $-68.32$ and $-167$ kcal/mol. Then enthalpy change at dissolving of one mole $CO_2$ in the water is $-167\ -(-94.05-68.32) = -4.63$ kcal/mol $= -4630$ cal/mol. Our estimate of the present-day oceanic water is close to $+7$ to $+8$ °C (280–281 K). Then, from Eq. (13.25):

$$H_0 = \frac{0.34}{e^{4360/1.987\times 280}} \approx 8.27 \times 10^{-5}\,\text{atm}^{-1}. \tag{13.27}$$

Now we can find from Eqs. (13.24) and (13.25) that the temperature change in the present-day ocean by $\pm 1$ °C results in a change in the $CO_2$ partial pressure in the

atmosphere by about $\pm 13.5 \times 10^{-6}$ atm (i.e., by $\pm 13.5$ ppm). During the Quaternary glaciations, the decline in the oceanic average temperature may have reached by 4 °C (to 276 K). Which would cause the partial pressure drop by about 52–54 mass ppm or by 79–82 volume ppmv. As Fig. 13.12 shows, that is exactly $CO_2$ content fluctuations observed in air bubbles from the Antarctic sheet ice cores at the Vostok station (nearly 80–90 ppmv).

It is important that during the warm spells in Cretaceous when the average oceanic water temperature may have risen to +17 °C (290 K), carbon dioxide partial pressure must have increased to about 740 ppm, that is, was approximately 1.6 times its current value.

Discussing the greenhouse effect issues, it is impossible not to mention the arguments by the proponents of Arrhenius's idea that the carbon dioxide concentration has a direct effect on the tropospheric temperature. For instance, the proponents usually quote the data on carbon dioxide content in the air samples from the ancient firn layers in Greenland and Antarctica. These data show that the $CO_2$ atmospheric concentration during the interglacial periods always rose (Fig. 13.12). In their view, a similar but much stronger effect was observed during warm climatic epochs such as Cretaceous. Technically, they are right.

The temperature fluctuations with carbon dioxide partial pressure changes in the air bubbles from the ice sheet at the Vostok Station indeed show a close correlation of these two atmospheric parameters. It is, however, to be clarified which is the cause and which is the effect.

A detailed study of the ice core field data showed that the temperature curve is always slightly ahead of the corresponding changes in $CO_2$ core concentrations (Monin and Sonechlin, 2005). Thus, the determinations by Mokhov et al. (2003) and Fischer et al. (1999) show that the changes in $CO_2$ concentrations lag the temperature fluctuations on the average by about 500–600 years. That is exactly the time needed for a complete stirring

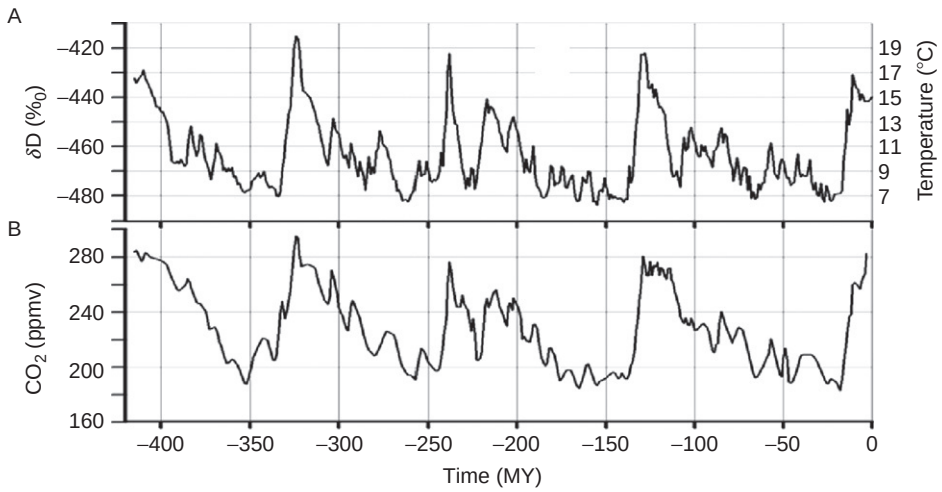


**FIGURE 13.12** Correlation of the isotopic air temperature (A) with carbon dioxide concentration (B) over the recent 420 MY at the Antarctic station Vostok. The $CO_2$ concentration and temperature data from the cores of an ice well (TD = 3623 m) were kindly provided by Kotlyakov (2000) (the scale of the Earth's average temperatures is our interpretation).

of the upper (active) oceanic layer which is the main controller of carbon dioxide partial pressure in the atmosphere.

Thus, drilling results through the Antarctic ice sheet uniquely show that the temperature changes over the recent 420,000 years were always ahead of the corresponding $CO_2$ concentration changes within the ice sheet. This is an indisputable and unique testimony to the fact that $CO_2$ concentration changes in the atmosphere are the result, not the cause of the global temperature changes.

It shows that the orthodox proponents of the classical approach are clearly confusing the cause and effect: carbon dioxide partial pressure increases and declines in the atmosphere are not the cause but only the effect.

As was shown above, the explanation is in the negative correlation of carbon dioxide solubility in the oceanic water versus temperature and in the Henry's law (13.25) which sets dynamic equilibrium between the gas partial pressure in the atmosphere and its concentration in the hydrosphere. This is the reason why the oceanic water temperature increase always results in its partial degassing and migration of some carbon dioxide from the ocean to the atmosphere and vice versa, cooling increases $CO_2$ solubility in the oceanic water so part of the atmospheric carbon dioxide is dissolved in the ocean. A consequence is that carbon dioxide partial pressure increases in the atmosphere always corresponds with the climate warming, and the decrease corresponds with its cooling. But the primary cause is always the climate temperature fluctuations and not the changes in carbon dioxide partial pressure. This pattern may be dubbed as a milder form of the "Champaign effect".

The real causes of the Earth's climate temperature fluctuations should be looked for among the other processes and phenomena such as precession of the Earth's own revolution, nonuniformity of the solar radiation (see Chapter 14), instability of the oceanic currents or changes in their circulation caused by other reasons (like the periodic salinity increases or decreases in the surficial waters of the Arctic Ocean).

Demonstrative in this respect is correlation of the observed carbon dioxide partial pressure in the air bubbles from the Antarctic ice sheet at the Vostok Station versus the calculated from the Henry's law $CO_2$ pressures (13.25) and the observed isotopic paleotemperature of the same sheet (Fig. 13.12). The correlation results are illustrated in Fig. 13.13.

As the comparison shows, the curve correlation (accounting for the experimental data accuracy) is quite acceptable. It is another testimony in favor of explaining $CO_2$ partial pressure fluctuations by the changes in the oceanic water temperature. The inverse solution is impossible as the Henry's law determines only the oceanic water (and the dissolved $CO_2$) temperature effect over carbon dioxide partial pressure in the atmosphere but not the effect of the $CO_2$ partial pressure over the oceanic water temperature.

## 13.10 SPECIAL OPINION ON THE SUBSTANCE OF KYOTO PROTOCOL

The scientific and political community must be reminded that prior to 1990s there was no theory of the greenhouse effect and of the effect of the "greenhouse gases" on the tropospheric heat regime. All talks about it were purely intuitive and speculative. Moreover,

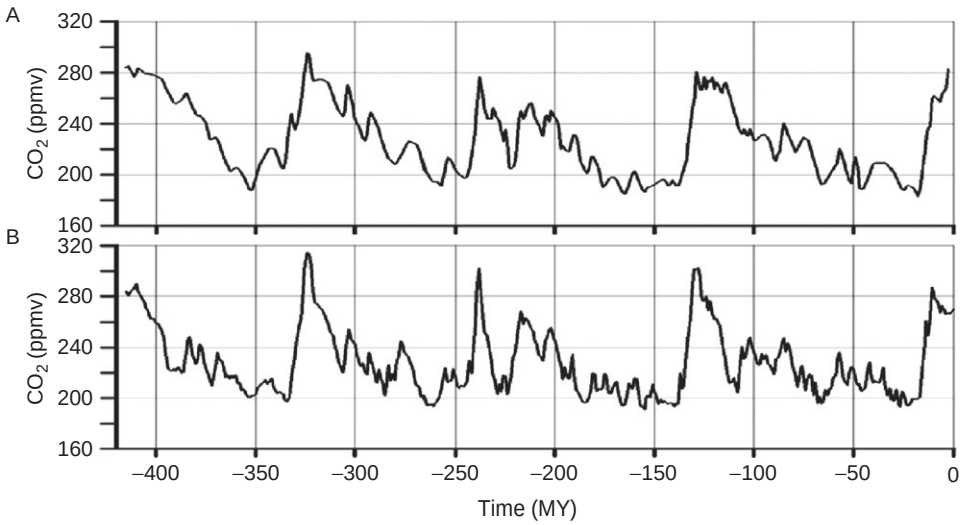


**FIGURE 13.13** Correlation of the observed $CO_2$ partial pressure in the air bubbles from the Antarctic ice sheet (A) with the calculations of the same pressure from the ice sheet isotopic temperatures (B) (see Fig. 13.12) and Henry's law (field data by Kotlyakov, 2000).

currently many experts (especially in Europe) have no idea that such theory already exists and allows for the quantitative determination of the Earth's climate dependence on the atmospheric composition and pressure (Sorokhtin, 2001; Sorokhtin et al., 2007), which we attempted to show in this book. Whereas traditional and "classical" model forecasts of climate changes associated with the atmospheric releases of the so-called "greenhouse gases" (especially carbon dioxide) are, as a rule, purely intuitive and incorrectly set problems.

Besides, currently there is not a single (we emphasize, NOT A SINGLE) reliable proof of the "greenhouse gases" effect on the Earth's climate. Usually, proponents of the traditional approach say that the current climate warming (which, if exists at all, most likely is associated with the solar activity) correlates with the carbon dioxide partial pressure increase in the atmosphere. The cause and effect relationships between these phenomena are not analyzed although carbon dioxide partial pressure rise may be a result, not the cause of the climate warming. That is why the Kyoto protocol developed in 1997 has no scientific ground. In 2004, this was officially stated, in particular, by the Russian Academy of Sciences but the Russian political authorities wouldn't listen, so Russia signed this pseudoscientific document deleterious for the country.

Over the recent years, the aforedescribed physical theory was developed. It describes the tropospheric temperature regimes and is called the adiabatic theory of the greenhouse effect. This theory was verified by a close coincidence between the theoretical temperature distributions and the accepted model of the Earth's troposphere (see Table 13.1) and, which is especially important, the experimental data for a high-density carbon dioxide Venusian atmosphere obtained by the Soviet and American cosmic apparatuses (see Table 13.2 and Fig. 13.5).

It is important that under the adiabatic theory of the greenhouse effect proposed here the accumulation of small amounts of carbon dioxide, methane, and some other "greenhouse gases" has no effect whatsoever on the climate of Earth. At the elevated $CO_2$ concentration in the atmosphere (but at the same pressure as the present-day nitrogen–oxygen atmosphere), carbon dioxide can only cause climate cooling, not warming as is usually believed and as follows from the Kyoto protocol, and a slight increase in the synoptic activity.

It is necessary to emphasize that the Kyoto protocol, besides having no scientific ground, in its substance contradicts the physics of natural processes and provides a totally wrong explanation of the anthropogenic effect on the climate. Also, it is needed to be taken into account that the increase in carbon dioxide partial pressure in the atmosphere results in an increased agricultural productivity and regrowth rate of the felled forests. The proponents of the Kyoto protocol forget about it or just do not want to know whereas Robinson et al. (1998) showed that the agricultural efficiency and forest regrowth rate increases in direct proportion with carbon dioxide partial pressure increase in the atmosphere. The same publication convincingly shows that the increase in $CO_2$ concentration improves drought-resistance of the cereals, including wheat.

Presently, mass media spread various pseudoscientific (and sometimes outright false-scientific) forecasts of a drastic climate warming, of a significant ocean level rise, of the flooding of numerous near-shore (and not only near-shore) cities and even of an ecumenical catastrophe coming with even slight future increase in carbon dioxide partial pressure. In actuality, we are now living at the peak of a relatively small local warming (see Figs. 14.22–14.24). In the nearest future, a new cooling phase will begin (possibly it has already begun). The upcoming cooling may turn out to be the deepest over the recent millenia. We need to prepare to it now because it will be a harbinger of the next ice period.

The cause of the ongoing and still upcoming cooling is quite natural. It is associated with a decrease of the Earth's precession angle and decline of the total atmospheric pressure due to the life activity of the nitrogen-consuming bacteria which gradually remove nitrogen from the air and converting it into deposits (see Section 12.4). These processes are beyond human control: we will not be able to stop them.

All the aforementioned singularly indicates that, as concerns the proposed measures against the anthropogenic releases of the "greenhouse gases", the Kyoto protocol is a wrong and harmful solution of an important environmental problem. The Protocol's stipulations are especially harmful for Russia as its economy is to a very significant extent based on the use of the hydrocarbon fuels. Besides, Russia is the "coldest" country, larger amounts of natural fuel are needed for its heating. For this reason the IPCC proposed costly (tens of billions of dollars annually) measures for stabilizing $CO_2$ concentrations are nonsense and harmful for the economy and agriculture. These monies would be better spent for the development of the economy, social spheres, and science.

We would like also to draw the reader's attention to the active propaganda by the apologists of the idea about the anthropogenic effect on "climate warming". A typical example is Mr. Al Gore who published a book with the intriguing title "An Inconvenient Truth" (2007) and created a film under the same name. Actually, both the book and the movie are collections of erroneous and illiterate climatic scares, such as melting ice covers in Greenland and Antarctica, catastrophic sea level rise, predictions of intolerably hot climates and an appeal

to fight the "windmills". As we will show in Section 14.5, the Antarctic ice and snow mass significantly increased over the last 30–40 years and has not declined as Al Gore maintains.

From the viewpoint of the physical fundamentals of the Earth's climate formation, both the book and the movie are illiterate and damaging. Nevertheless, they enjoy a wide recognition by "green ecologists" and politicians and were awarded prestigious international prizes. This is a very sad fact which emphasizes that climate change problems must be dealt with by professional scientists and not dilettantes and politicians.

CHAPTER

# 11

# Hydrosphere: The Patterns of its Origin and Evolution

The Earth's hydrosphere and atmosphere evolutionary regimes are crucial in the determination of the climate evolution, the emergence and evolution of life, and the issue of commercial deposits including combustible deposits. We now discuss the formation of these geospheres in more detail.

## 11.1 PRIMARY DEGASSING OF THE MANTLE

As previously mentioned, the Young Earth in Katarchaean was devoid of the hydrosphere and atmosphere. It is natural to suggest that these external and very mobile geospheres emerged only due to the Earth's degassing. The degassing could only begin after the heating of the upper section and the emergence of melted matter nodes within it. The Earth depths' heating at those distant times was only due to the release of the Moon-interaction tidal energy and radioactive decay. The tidal energy was released mostly in the Earth's upper section. For this reason, first melts of the Earth's matter appeared at relatively shallow depths of 200–400 km approximately 600 MMY after the emergence of Earth. Immediately upon the appearance of first melts, the Earth's matter differentiation began and first indications of the tectonomagmatic activity showed about 4 BY ago. After that, the Earth's matter differentiation was fed by the most powerful gravitational energy process of high-density melted iron separation from the Earth's matter silicates (see Section 4.3). It is to be expected that the Earth's—or rather the Earth's mantle—degassing substantially depended not only on the mantle temperature (which determined the mantle convection flow intensity) but also on its chemical composition. The main features of the evolution of the convecting mantle chemical composition are illustrated in Figs. 4.15 and 4.16.

The emergence of the lithospheric plate tectonics and especially the development of the fundamentals of the Earth's global evolution provided a real opportunity for a quantitative description of the ocean forming processes. Our quantitative models of the World Ocean

*Developments in Earth and Environmental Sciences*, Volume 10
DOI: 10.1016/S1571-9197(11)10011-7

water and the gas shell growth were based on the most general concept of the global evolution (Sorokhtin, 1974). The concept included the lithospheric plate tectonics as its component. The models took into account the direct proportionality between the Earth's degassing rates but the major contribution to the mantle convective mass exchange came from the most powerful energy process of the chemico-density differentiation of Earth's matter into a high-density iron-oxide core and a residual silicate mantle.

These earlier studies, however, were still related to the end of the planet's formation process about 4.6 BY ago.

Later models (Monin and Sorokhtin, 1984; Sorokhtin and Ushakov, 1991, 2002) were based on the aforementioned Earth's matter zonal and barodiffusion differentiation mechanisms (see Sections 4.3 and 4.4). These models were more sophisticated and took into account that the primordial Earth after its emergence was a relatively cold planet. Thus, the degassing could have started only much later (about 600 MMY after the Earth's emergence), after a preliminary heating of the originally cold Earth's depths to the temperature when the silicate melting began in the upper mantle, and the emergence of the first asthenosphere.

The primary mantle degassing is apparently associated with the solubility decline of volatile components in the silicate melts under lowering temperature and relatively low pressure. As a result, the mantle melts erupted on the surface (mostly basalts, and in Archaean also komatiite lavas) boiled and released the excess volatile elements and compounds into the atmosphere. Some of these volatile components may have been released at the weathering of the erupted rocks after their sojourn on the surface. However, the main water degassing mechanism was the decline of its solubility under the cooling and crystallization of water-containing basalt melts at low pressure (Fig. 11.1).

It follows that the Earth's degassing rate is in direct proportion with the mantle rocks mass erupted on the surface per unit of time, their content of volatile elements, and their mobility. As a first approximation, the mantle rock eruption rate is proportionate to the Earth's tectonic activity. This activity is determined by the rate of its total heat loss $\dot{Q}_{\mathrm{m}}$ (see Fig. 5.17) or the derivative over time of the Earth's tectonic parameter $\dot{z} = \left(\dot{Q}_m - Q_{4.0}\right)/\left(\dot{Q}_{\mathrm{m0}} - Q_{4.0}\right)$, where $Q_{\mathrm{m}}$ is current value of the heat flow from the mantle, $Q_{4.0} \approx 1.6 \times 10^{37}$ erg is Earth's heat loss by the start

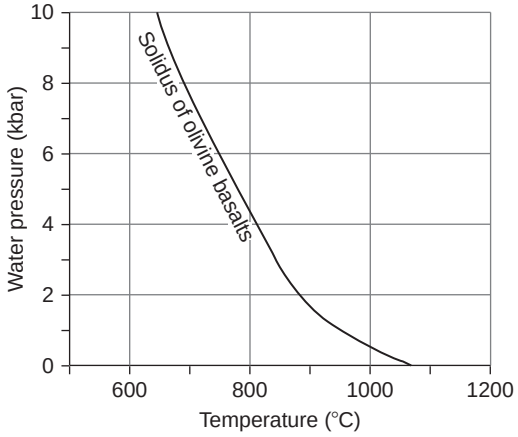


**FIGURE 11.1** Olivine basalt solidus curve versus pressure (content) of water dissolved in the basalt melt (Joly, 1929). When basalts crystallize the water dissolved in the basalt melts is released.

of its tectonic activity 4 BY ago, and $Q_{m0} \approx 10.77 \times 10^{37}$ erg is total heat loss of the Earth's mantle by the present time. Then the derivative $\dot{z} = \dot{Q}_m/(Q_{m0} - Q_{4.0})$ and its normalized value is $\dot{z}_n = \dot{Q}_m/|\dot{Q}_{m0}|$, where $|\dot{Q}_{m0}| = 3.39 \times 10^{20}$erg/s is the absolute value of the present-day Earth depth heat flow. The correlation of the Earth's tectonic parameter change rate versus time is shown in Fig. 11.2 and the value of the parameter proper is shown in Fig. 11.3.

Thus, the mantle degassing rate is in direct proportion with the component content in the mantle $(m_i)_m$, its mobility factor $\chi_i$, and the rate of the mantle convective mass exchange $\dot{z}$

$$\dot{m}_i = -(m_i)_m \chi_i \dot{z}. \tag{11.1}$$

Then the mass of an $i$th degassed volatile component and its accumulation in the Earth's external geospheres is determined as

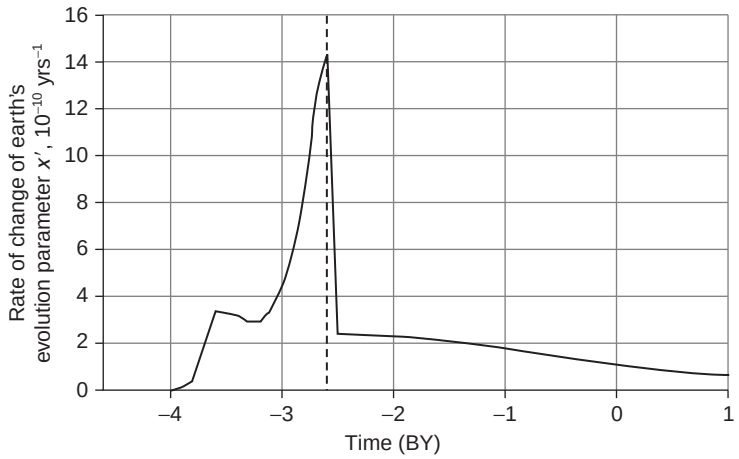


**FIGURE 11.2** Rate of change in the Earth's tectonic parameter $\dot{z}$ determining the rate of the basalt melts surface eruptions and the mantle degassing rate (the dashed line is the core separation time).

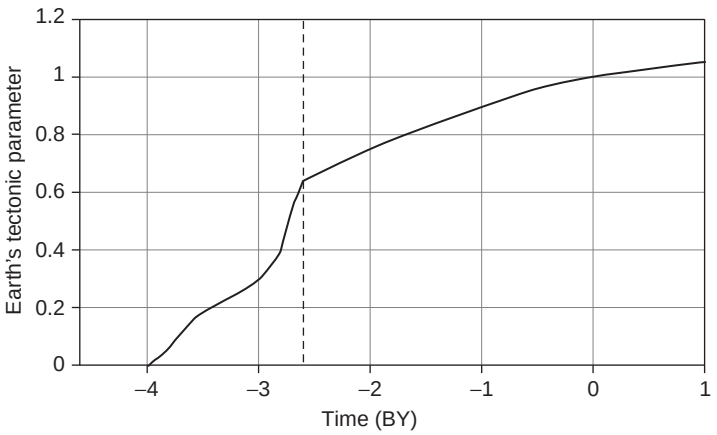


**FIGURE 11.3** Earth tectonic parameter $z$ controlling the magmatic activity products accumulation rate and the mass of the substances degassed from the mantle; the dashed line is the core separation ends.

$$m_i = (m_i)_0(1 - e^{-\chi_i z}), \tag{11.2}$$

where $(m_i)_0$ is the total mass of the $i$th volatile component in the mantle and external geospheres. In Archaean, the degassed mantle mass gradually increased. Thus, it is necessary to take into account its increase from $M_m = 0$ to its total amount at the end Archaean $M_{m\Sigma}$. The mantle mass was previously estimated (see Fig. 6.6). Then it is necessary to use a different equation for degassing of the water or any other volatile element and compound (such as $N_2$ and $CO_2$) in Archaean:

$$m_i = (m_i)_0(1 - e^{-\chi_i z})\frac{M_m(t)}{M_{m\Sigma}}, \tag{11.2'}$$

where $M_m(t)$ is the mantle mass at the time $4 < t < 2.6$ BY ago. For Proterozoic and Phanerozoic, Eq. (11.2) is valid.

To determine the mass of the volatile component $m_i$ degassed from the mantle (it may be, e.g., the water), it is necessary to insert in Eqs. (11.2) and (11.2′) the initial and boundary conditions for the content of this component (water, nitrogen, or carbon dioxide) in the Earth's external geospheres.

## 11.2 FORMATION OF THE HYDROSPHERE AND THE OCEANS

The Earth's matter differentiation mechanisms were drastically different in Archaean and in the post-Archaean time. Thus, it is to be expected that the mobility factors $\chi_i$ of the volatile components (or at least some of them) may also have been significantly different.

In Archaean, all the silicate matter from the convecting mantle, together with its volatile components, unavoidably went through the layer of a melted iron (see Fig. 4.1). The oxides, with their lower formation heat than the oxide of bivalent iron (63.64 kcal/mol), must have dissociated and released their oxygen for the iron oxidation to the bivalent oxide. The water (water vapor or fluid) molecule formation heat is 57.8 kcal/mol. Therefore, water must have dissociated on the metallic iron melts in the Earth's matter differentiation zones

$$Fe + H_2O \rightarrow FeO + H_2 + 5.84 \text{ kcal/mol}. \tag{11.3}$$

On the other hand, carbon dioxide formation heat is 94.05 kcal/mol. Thus, carbon dioxide could have crossed through this zonal differentiation layer without difficulty. Thus, in Archaean the water mobility factor in the degassing equations (11.1) and (11.2) was significantly lower than that in the post-Archaean time, whereas the carbon dioxide mobility factor could remain constant during the entire time of its degassing from the mantle. It is noteworthy that together with the water many other oxides with the low formation heat dissociated in Archaean on the iron melts. They were reduced to free elements.

The water mobility factors in Archaean and thereafter significantly differed. Thus, to estimate the mantle degassing it is necessary to put together two degassing equations (11.2) and (11.2′) with different mobility factors and combine those by the degassing process continuity condition at the Archaean–Proterozoic time boundary. In this case, the two equations include three variables: two water mobility factors and the original water mass $(m_{H_2O})_0$

in the Earth's matter. That is, to solve the problem quantitatively, it is necessary to determine and insert into the equations three independent boundary conditions.

The first boundary condition may be the total mass of water in the present-day ocean and the continental crust. Our estimates based on publications by Ronov and Yaroshevsky (1978) and amended by own observations and calculations tell us that the following water mass in the hydrosphere may be assumed. The ocean currently contains $1.42 \times 10^{24}$ g of water (in the continental crust together with the continental waters and icebergs of $0.446 \times 10^{24}$ g). The oceanic crust contains approximately $0.358 \times 10^{24}$ g of irreducible water. Altogether, the Earth's external geospheres (the hydrosphere) contains $2.23 \times 10^{24}$ g of water. This amount was degassed from the Earth's depths over its entire geological life, that is, over the last 4 BY. Strictly speaking, this is not exactly accurate because significant part of the water that reached the surface in Proterozoic and Phanerozoic was constantly returning back into the mantle through the plate subduction zones, some part of it dissociated in hydrating of the oceanic crust rocks and in the upper atmosphere (affected by the solar radiation). We, however, assume not the absolute mass but only its effective value. It is equal the difference between the masses of the degassed and the subducted water. In such a case, all calculations are valid and only the effective value of the mobility factors $\chi$ will be somewhat lower than their actual values.

A second boundary condition is the total water mass on Earth $(m_{H_2O})_0$. The first thing to do to determine it is to find out its mass in the present-day mantle. The water concentration in the mantle is a fundamental problem for the global petrology. Unfortunately, it has not been conclusively solved. The reason is that upon getting to the Earth's surface practically all the mantle water immediately (during the very rise and discharging onto the surface) is intensely contaminated by the surface water. Even the most depth-associated xenoliths (such as garnet peridotites or eclogites from the kimberlite blow pipes) turn out to be just fragments of the oceanic crust sucked-in to great depths underneath the continents through the former subduction zones (Sorokhtin, 1985; Sorokhtin et al., 1996, 2004). Nevertheless, fresh basalts of the oceanic islands (despite a possibility that they capture some marine water) which filter through the strato-volcanoes usually contain very little water, no greater than 0.3% OH (Joder and Tilly, 1962).

This and other theoretical consideration lead most modern petrologists dealing with the mantle origin rocks to believe that the mantle water content is exceptionally low. For instance, Ringwood (1981) assumed the mantle water content at 0.1%. Pugin and Khitarov (1978) believed that it is actually lower, 0.025–0.1%. Our estimates discussed in more detail in Sorokhtin and Ushakov (1991, 2002) are no greater than 0.05–0.06%, the mantle is indeed exceptionally dry. Then the total water content in the present-day mantle is $2.007 \times 10^{24}$ g and the total water mass on Earth reaches approximately $(m_{H_2O})_0 \approx 4.23 \times 10^{24}$ g.

A third pivotal point for the calculations could be the hydrosphere's water mass at an intermediate point in time (if, of course, it is doable). Using additional geological data, it is a solvable problem. As the ocean gradually increased in volume, there should have been a moment in its evolution when the oceanic water covered the mid-oceanic ridge crests with their associated rift zones. After that, hydration of the oceanic crust rocks must have been rapidly increasing and so must have been the ore element release from the rift zones to the ocean.

Therefore, the oceanic deposit geochemistry must have drastically changed after the described event as they now included abundant ore element brought out from the mantle.

The most characteristic such element and the brightest indicator of the sought-for boundary (the moment of the oceanic crust saturation with water) is certainly iron. Metallic (free) iron was still available in the Precambrian mantle in noticeable amounts (see Fig. 4.16). Rising together with the hot mantle matter into the rift zones it reacted there with the marine water in the no-oxygen environment rich with carbon dioxide:

$$Fe + H_2O + 2CO_2 \rightarrow Fe(HCO_3)_2. \quad (11.4)$$

After the ocean covered the mid-oceanic ridge crests, the dissolved iron oxide began spreading all over the ocean. In the shallow water, the bivalent iron helped by bacteria (especially cyanobacteria) was oxidized to the trivalent state and precipitated forming thick iron ore deposits:

$$2Fe(HCO_3)_2 + O \rightarrow Fe_2O_3 + 2H_2O + 4CO_2. \quad (11.4')$$

Due to such iron release from the oceanic rift zones, at least two unique mass iron ore formation deposition epochs are identified in the World Ocean history. A first one was at the end Archaean (the Kivatin-type iron ore formations, after 3 BY ago). A second one was at the end of Early Proterozoic (nearly 2.2 BY ago). It was the Krivoy Rog-type ores. The second iron accumulation stage is most identifiable in the Earth's geological record.

The area of the oceans in Proterozoic was obviously the Earth's area minus the continents' area. Assuming that the continental crust thickness little changed with time, it may be expected that the area of the continents is proportionate to their mass, and the mass evolution is illustrated in Fig. 7.7. The area of the oceans 2.2 BY ago reached $3.48 \times 10^{18}$ cm$^2$. We will later show (see Fig. 11.6) that the average ocean depths at that time was 930 m, hence, the World Ocean water mass 2.2 BY ago was approximately $0.325 \times 10^{24}$ g. The water mass bounded in the crust 2.2 BY ago was possible to determine using a reconstruction (Sorokhtin and Ushakov, 2002) of the oceanic crust structure (Fig. 7.1) and the continental crust mass at the time (see Fig. 7.7). We estimate that by the end Archaean the average irreducible water concentration in the continental crust rose to 0.6%, and in the present, to 2%. In this case we find that 2.2 BY ago the continental crust contained about $0.109 \times 10^{24}$ g of irreducible water. Assuming the average density of the pelagic deposits at about 2.2 g/cm$^3$ with 20% water, the hydrated basalts and gabbros (density about 2.9 g/cm$^3$) contain about 2.5%, and the serpentinites (density 3 g/cm$^3$), up to 11%, we find that 2.2 BY ago the oceanic crust included nearly $0.385 \times 10^{24}$ g of water. Thus, for this case the total water mass in the hydrosphere was $0.325 \times 10^{24} + 0.385 \times 10^{24} + 0.109 \times 10^{24} = 0.819 \times 10^{24}$ g.

We now put together a system of two equations of the type (11.2) and (11.2′) separately for Archaean and for the post-Archaean time. We substitute into them the water masses found in the present-day Earth, its hydrosphere, and in the Early Proterozoic hydrosphere about 2.2 BY ago. These equations have different water mobility factors. Thus, they need to be merged into a common system through the condition of the degassing continuity at the Archaean–Proterozoic time boundary. Only after that it will be possible to determine the correlation of the mantle-degassed water versus time. The water mobility factor in Archaean turned out to be $\chi_1 = 0.245$, and in Proterozoic and Phanerozoic, as it was anticipated, it was much greater: $\chi_2 = 1.27$.

The water accumulation in the Earth's hydrosphere is illustrated in Fig. 11.4. It shows that the water accumulation regime in the external geospheres changed substantially at

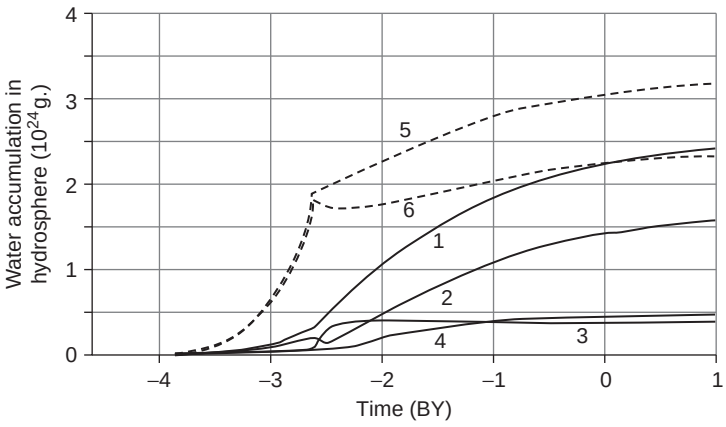


**FIGURE 11.4** Water accumulation in the Earth's hydrosphere: 1, total mass of water degassed from the mantle; 2, oceanic water mass; 3–4, water mass bonded in the oceanic and continental crust; and 5–6, water mass degassed form the mantle and the oceanic water mass under a hypothetical scenario of no water dissociation in the Earth's matter differentiation zones in Archaean under reaction (11.3).

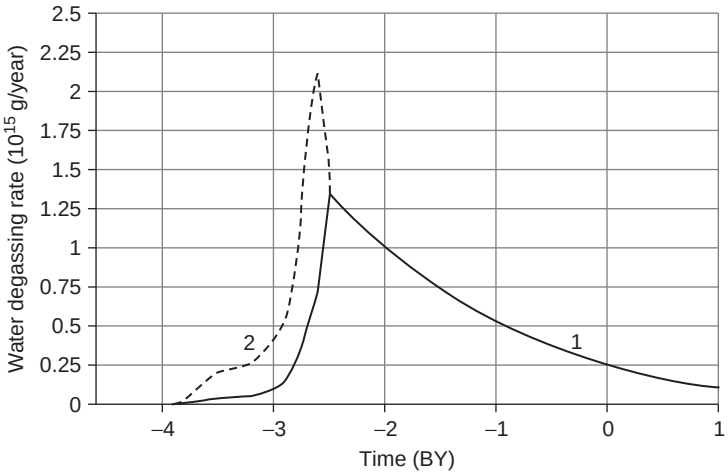


**FIGURE 11.5** Mantle-to-hydrosphere water degassing rate: 1, accounting for water dissociation in the Earth's matter differentiation zones in Archaean and 2, not accounting for such dissociation.

the Archaean–Proterozoic time boundary. This change was especially drastic for the water accumulation in the oceanic crust. It was caused by the formation in the beginning of Proterozoic of the oceanic crust's serpentinite layer which is the most capacious reservoir of the irreducible water on Earth.

Thus, we determined the total water mass in Earth and the water mobility factors in Archaean and post-Archaean time. Now, from Eq. (11.1) we can determine the water accumulation rate in the Earth's hydrosphere. The so constructed water-from-mantle degassing rate is shown in Fig. 11.5. The graph indicates that the maximum water degassing rate occurred 2.5 BY ago which is early in Proterozoic. At the same time, maximum tectonic activity occurred in Archaean. This is a seeming discrepancy. It was caused by the fact that in Archaean most of the degassed water, still within the mantle, dissociated over the iron melts in the Earth's matter

differentiation zones like this: $H_2O + Fe \rightarrow FeO + H_2$. The heavy hydrogen isotope was mostly bonded with iron, whereas the light isotope was held in the degassed water. In Proterozoic and even more so in Phanerozoic, there was no water dissociation in the mantle. In a complete compliance with Eq. (11.1), the water without any losses entered the Earth,s hydrosphere. Currently, $2.6 \times 10^{14}$ g/year or 0.26 km$^3$/year of water is degassed from the mantle.

The average depth of the oceanic depressions may be determined from the Earth's tectonic activity (see Fig. 5.17), from Eqs. (8.9), (8.9′) and from average oceanic plate longevity (see Fig. 7.3). Thus, we determined the average depth of the oceanic depressions and their areas keeping in mind that the oceans in Early Archaean were positioned only in the low latitudes. It is now possible from the determined water mass in the ocean to find the ocean surface elevation relative the average stand level of the mid-oceanic ridge crests. The results are displayed in Fig. 11.6.

The figure shows that the oceanic depression depths relative to the average stand level of the mid-oceanic ridge crests in Early Archaean were small, 80–200 m. But there was not a lot of the water in the oceans. In Early and Middle Archaean, there were no real oceans on Earth. What existed were numerous isolated shallow-water marine type basins. Over the level of these seas rose the mid-oceanic ridge crests and the Earth's primordial matter areas but especially the lithospheric plate pileup zones. The kernels of future continental massifs were being born in the centers of these zones (see Fig. 7.5). Their elevations reached 6 km (see Figs. 7.10 and 11.6).

As a reminder: the so high continent stand level in Archaean was determined by high heat flows of the time. As a result, thick and heavy lithospheric plates could not form underneath the heavy continental shields. The crust itself, as a light cork, arose high over the average mantle surface. As opposed to that, the present-day continental crust is

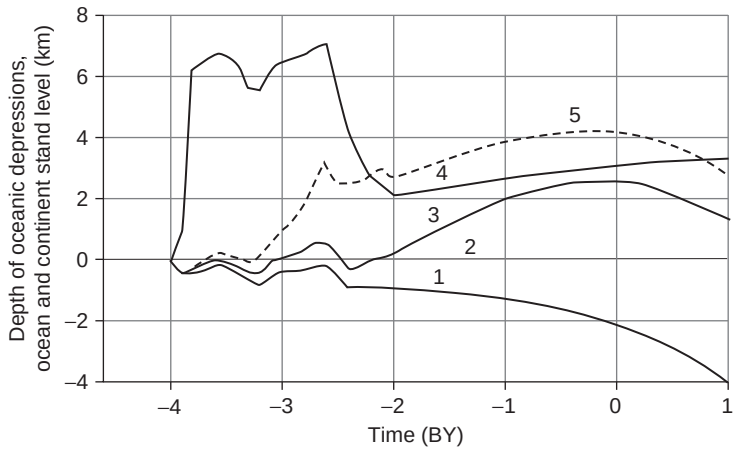


**FIGURE 11.6** Evolution in the positions of the oceanic and continental surfaces compared with the average mid-oceanic ridge crests stand level: 1, average depth of the oceanic depressions; 2, mid-oceanic ridge crests stand level; 3, World Ocean surface level; 4, average continent stand level (relative to mid-oceanic ridge crests stand level); and 5, ocean surface position in case of no water dissociation on iron melts in Archaean under reaction (11.3).

underlain by a soldered thick (up to 200 km) and dense (close to 3.3 g/cm$^3$) ultramafic lithosphere, which substantially sinks the continents into the upper mantle (see Fig. 7.9).

As stated in Chapter 7, the high stand of the continental shield in Archaean naturally resulted in intense physical erosion of their surface. This may be observed in many present-day Archaean shields on whose surface is exposed deeply metamorphosed amphibolite and granulite facies formed in their time at depths of 5–10 km. There are also examples of a deeply metamorphosed epidote–amphibolite facies, such as in the Kola Peninsula Keiva block. We demonstrated in Section 7.2 that huge masses of sedimentary rocks that had to be deposited on the ocean floor at the high stand of the Archaean continental blocks, after their remelting in the oceanic plate pileup zones, converted to huge granitoid intrusions of the Archaean granite–greenstone belts (see Fig. 7.5).

At the end Proterozoic, the surface of the growing ocean rose to the average elevation of the continental planes. After that, already in Phanerozoic, occurred first global marine transgressions on the continents. They noticeably shrank the river discharge and continental rock erosion dump areas in the oceans.

It is interesting that should no water dissociation occurred during Archaean in the Earth's matter differentiation zones, the water mass in its hydrosphere would have today exceeded its current amount 1.5 times, $3 \times 10^{24}$ g rather than $2.2 \times 10^{24}$ g (see Fig. 11.4). The ocean surface elevation would have been about 2 km above its current elevation. That would have resulted in the flooding in Archaean and Proterozoic of the largest portion of the continental areas (see Fig. 11.6), only the highest summits would have stuck over the water surface, and our planet could have been called the Oceania.

## 11.3 HYDROTHERMAL PROCESSES ON THE OCEAN FLOOR

We mentioned that the primary Earth's degassing occurred only with the eruptions of juvenile basalt magmas on the surface. The magmas were mostly fed through the rift zones of mid-oceanic ridges. In the very beginning of Archaean, when the basalts erupted from the mantle boiled, the vapor sources and hot fluid were indeed juvenile. After that, however, numerous hydrothermal springs within the very rift zones gushing through the so-called "black smokers" were not juvenile at all as all the water running through them have exclusively oceanic origin. Such mineral springs may create an illusion of being primary which is wrong.

Thus, we discuss the issue of the Earth's secondary degassing in more detail.

In the late 1970s, intense hydrothermal activity was discovered on the ocean floor. It was associated with functioning of the most active underwater volcanic belt in the World Ocean rift zones. This discovery changed many views of the origins of some economic minerals on the continents. They include, for instance, hydrothermal sulfide deposits and other mineral formations in the ophiolite zones of the Earth's folded belts. The same very discoveries indicated a large role of the exogenous matter in the hydrothermal ores' formation. They include, for instance, hydroxyl groups in hydrosilicates or the sulfide sulfur in sulfides. They also helped determine the abiogenic methane formation mechanisms in the hydrothermal springs.

By now, significant amounts of fundamental studies in the ocean floor hydrothermal activity were conducted. Since 1978, after the discovery of hydrothermal springs in the Galapagos rift (Francheteau et al., 1979), the number of studies devoted to the ocean floor

hydrotherms, massive sulfide ores, and other hydrothermal formations drastically increased. Results of some of these studies were published, for instance, by Lisitsin, Bogdanov, and Gurvich (1990): "Hydrothermal formations of the rift zones," Rona (1986): "Hydrothermal mineralization of spreading areas in the oceans," and a recent fundamental publication by Bogdanov et al. (2006): "Hydrothermal ore genesis of the ocean floor."

A first suggestion of powerful hydrotherms existing in the oceanic rift zones and proposition of the exogenic nature of the water circulating in them was made based on theoretical considerations by Lister (1972) and independently by Sorokhtin (1974). That was way ahead of the actual discoveries in 1977–1978. The latter publication provided the combined capacity of hydrothermal processes in the mid-oceanic ridges. Our theoretical forecast was based on a comparison of the calculated correlation between the per-unit area heat loss by the oceanic plates versus time with the empirically measured heat flows penetrating the very same slopes of the mid-oceanic ridges (Fig. 11.7). It was taken into account that the empirical data measured only the heat flow's conductive component, whereas the theoretical estimates encompassed the entire heat flow. Their difference accounted for the convective heat release by the oceanic waters circulating within the fractured Earth's crust in the rift zones and on the mid-oceanic ridge slopes.

The estimates of the corresponding heat loss give the idea of the grandiose scale of this convective oceanic crust "flushing" by the marine waters. It was found that about 30% of the total endogenous energy radiated by Earth is lost through the hydrothermal activity. The total radiated energy is estimated at approximately $\dot{Q} = (4.2/4.3) \times 10^{20}$ erg/s (Sorokhtin, 1974). Thus, the thermal waters currently carry out at least $\dot{\theta} = 1.29 \times 10^{20}$ erg/s or about $3.07 \times 10^9$ kw of the Earth's heat energy (30% of $4.3 \times 10^{20}$ erg/s).

Maximum water heating in the "black smokers" hot springs encountered in the rift valley of the mid-oceanic ridges is always limited by the water's critical temperature $T_{crit} = 374\ ^\circ C$. The reason is that at the temperatures above the critical value the water converts to a gas fluid whose volume $V$, as for a gas, is in direct proportion with the pressure $p$ (because for such a fluid $pV = \text{const.}$). It results in a rapid and very efficient removal of the overheated water fluids from the open fracture system due to the fact that the fluid density as it is rising decreases in proportion with the pressure decline. Besides, at $T > T_{crit}$ the water completely loses its capillary properties which play the definitive role in its saturation of the crustal

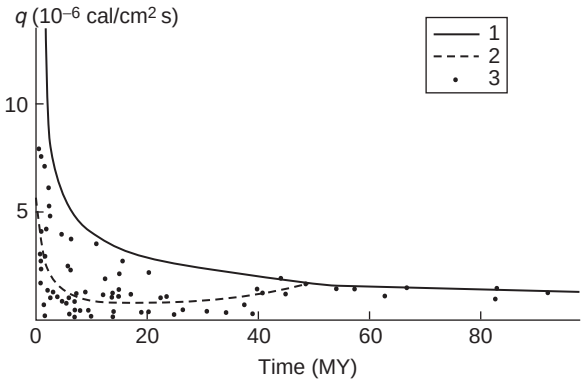


**FIGURE 11.7** Heat flow through the ocean floor versus the lithospheric plate age (Sorokhtin, 1974): 1, theoretical curve of the total heat flow; 2, heat flow conductive component (average value from experimental determinations); and 3, experimental heat flow measurements in the South Atlantic and Pacific.

rocks. As a result, the water within the fracture system communicating with the ocean floor simply cannot physically get to the levels where the temperature exceeds 374 °C. And this determines maximum temperatures of the greenstone metamorphism of the oceanic crust rocks which occurs due to the functioning of the "black smokers"-type hot springs.

This conclusion finds the total confirmation in geological data.

Thus, the rocks in the ophiolite complexes, which are fragments of the oceanic crust obducting the continents (Peyve, 1969) (and the rocks are basalts, dolerites, gabbro, and serpentinites), are altered only to the facies of greenstone metamorphism (metamorphism of the green schists) with maximum temperature not exceeding 400 °C (the figure is rounded). Therefore, the metamorphism of the oceanic crust rocks indeed occurs in the environment of the open (communicating with the ocean floor) paths of the water penetration of the crust. What it means is that all higher degrees of the thermal metamorphism, such as the amphibolite or granulite facies, can occur only in closed environments preventing the removal of the water from the system of rocks entering the reactions with this water. Such environments usually arise within the water-saturated subduction zones due to dehydration of the sucked-in oceanic crust.

Sometimes, however (although rarely), the environment for the emergence of the amphibolite metamorphic stage can occur in the rift zones. For instance, in the emergence of faults forming the rift valleys of slowly spreading ridges, the dyke complex rocks that underwent the greenstone metamorphism can sink again into the magmatic node under the rift zone. As in the rocks of greenstone metamorphism all the water are bonded, the progressive metamorphic transformations will occur with the formation of the amphibolite facies. But no matter the option, the rocks of the amphibolite metamorphic facies play insignificant role in the oceanic crust structure.

The fractured bedrock of the oceanic crust is gradually covered by the pelagic deposits. The deposits undergo diagenesis. The existing fractures are plugged-in as well as are the other migration paths of the water in the crust by chemical deposits from the hydrotherms. As a result, the crust permeability for the oceanic water gradually decreases. A comparison of the observed (conductive) heat flows with the theoretical calculations (see Fig. 11.7) shows that almost complete stoppage of the oceanic water circulation through the crustal bedrock occurs in about $\tau = 50$ MMY after the time of the crust emergence in the rift zone of a mid-oceanic ridge. It indicates that the hydrothermal springs (including the warm and "cool" seepings, that is, the springs soaking-in through the deposits) mostly exist only on the ocean floor areas with the age $\tau < 50$ MMY. The average temperature of the hydrothermal springs over the areas of this age interval is approximately $\bar{T}_{ht} \approx 42$ °C, whereas the "black smokers" maximum temperatures in the rift zones reach 370–400 °C.

An estimate of the water mass flushing through the ocean crust per unit time was done based on the balance of the heat flows. It was found that the total amount of the water annually filtering through the mid-oceanic ridges and their slopes was about $2.3 \times 10^{18}$ g/year (2300 km$^3$/year). At this hydrothermal water-exchange rate the entire oceanic water ($1.42 \times 10^{24}$ g) runs through hydrotherms and seepings of the mid-oceanic ridges and their vast slopes over 600 MY. At the same time, the rate of the rift zones "flushing" by hot hydrotherms is approximately $2.2 \times 10^{16}$ g/year (22 km$^3$/year). Therefore, the entire oceanic water is filtered through "black smokers" hot springs only within 60–70 MMY. The oceanic crust formation rate in the rift zones is about $1.46 \times 10^{16}$ g/year. Hence, the water/rock ratio within the "hot zones" is 1.5 (not counting the water associated with the rocks proper in the

reactions). The oceanic crust is, however, generated also outside the rift zones, so the total rate of it formation is somewhat greater and reaches $4.7 \times 10^{16}$ g/year, in which case the water/rock ratio within the complete hydrotherm's system reaches almost 50. This indicates a reasonable complete hydration of the oceanic crust rocks.

Therefore, the provided estimates of the exogenous water-exchange mass for the mid-oceanic ridges oceanic crust is 8500 times the present-day juvenile water degassing from the mantle (which is equal to $0.26 \times 10^{15}$ g/year (0.26 $km^3$/year). We determined the average rate of the juvenile water degassing from the mantle over the entire duration of the process, that is, 4 BY, based on the total mass of the hydrosphere of $2.18 \times 10^{24}$ g (it includes the water bonded in the Earth's crust rocks). Even in such a case the average rate of the juvenile water supply from the mantle of 0.54 $km^3$/year is 4000 times lower than the total discharge rate of the ocean floor hydrothermal springs.

All these are certain indications of the exogenous origin of the water coming from the oceanic hydrotherms.

Similarly, when the oceanic crust is heated up in the subduction zones due to the lithospheric plate friction, its dehydration is accompanied by the release of the water and carbon dioxide which got there from the ocean:

$$\underset{\text{serpentine}}{2Mg_6(Si_4O_{10})(OH)_8} + \underset{\text{calcite}}{CaCO_3} + 164 \text{ cal/mol} \rightarrow \underset{\text{olivine}}{5Mg_2SiO_4} + \underset{\text{enstatite}}{MgSiO_3} + \underset{\text{diopside}}{MgCaSi_2O_6} + 8H_2O + CO_2, \quad (11.5)$$

but still, it is also the secondary crust degassing. The total current secondary water degassing in the island arcs and Andean-type active continental margins reaches 2.5–3 $km^3$/year, which is about 10 times the present-day juvenile water degassing. The total water mass released this way through the Earth's subduction zones over its entire life reaches $1.4 \times 10^{25}$ g (14 billion $km^3$), which is about 10 times its amount in the modern oceans. It shows that al without exception currently observed surface hot and mineral water springs are not juvenile, and their water eventually always comes from the Earth's hydrosphere.

The mantle rock primary mineral ratios in the well-preserved hyperbasite samples from the East Pacific high are: 70–75% olivine, 15–20% enstatite, 5–7% diopside, and 1–2% chrom-spinelide (Savelyeva, 1987).

Serpentinization can develop only over olivines and enstatites, and that is about 85–90% of the source matter. The base silicate hydration under the greenstone metamorphism environment usually goes like this:

$$\underset{\text{forsterite}}{4Mg_2SiO_4} + 6H_2O \rightarrow \underset{\text{serpentine}}{Mg_6(Si_4O_{10})(OH)_8} + \underset{\text{brusite}}{2Mg(OH)_2} + 33 \text{ kcal/mol}, \quad (11.6)$$

and in the presence of carbon dioxide:

$$\underset{\text{forsterite}}{4Mg_2SiO_4} + 4H_2O + 2CO_2 \rightarrow \underset{\text{serpentine}}{Mg_6(Si_4O_{10})(OH)_8} + \underset{\text{magnesite}}{2MgCO_3} + 65.05 \text{ kcal/mol} \quad (11.7)$$

$$\underset{\text{anortite}}{2CaAl_2Si_2O_8} + 4H_2O + 2CO_2 \rightarrow \underset{\text{kaolin}}{Al_4(Si_4O_{10})(OH)_8} + \underset{\text{calcite}}{2CaCO_3} + 110.54 \text{ kcal/mol}. \quad (11.7')$$

The reaction of the ferrous silicate hydration is an exothermic one. It releases hydrogen, and in the presence of carbon dioxide it forms the abiogenic methane:

$$\underset{\text{fayalite}}{Fe_2SiO_4} + 3\underset{\text{forsterite}}{Mg_2SiO_4} + 5H_2O \rightarrow \underset{\text{serpentine}}{Mg_6(Si_4O_{10})(OH)_8} + \underset{\text{hematite}}{Fe_2O_3} + H_2 + 21.1\ \text{kcal/mol}, \quad (11.8)$$

$$4\underset{\text{fayalite}}{Fe_2SiO_4} + 12\underset{\text{forsterite}}{Mg_2SiO_4} + 18H_2O + CO_2 \rightarrow 4\underset{\text{serpentine}}{Mg_6(Si_4O_{10})(OH)_8} + 4\underset{\text{hematite}}{Fe_2O_3} + CH_4 + 183.4\text{kcal/mole}. \quad (11.9)$$

The oceanic water contains noticeable amount (up to 0.7‰) of $SO_4^{2-}$ ion. Thus, reacting with hot rocks may result in $H_2S$ formation, for instance, like this:

$$4\underset{\text{fayalite}}{Fe_2SiO_4} + 3\underset{\text{forsterite}}{Mg_2SiO_4} + CaSO_4 + H_2O \rightarrow 5\underset{\text{enstatite}}{MgSiO_3} + 4\underset{\text{hematite}}{Fe_2O_3} + \underset{\text{diopside}}{CaMgSi_2O_6} + H_2S + 33.0\,\text{kcal/mol}. \quad (11.10)$$

Hydrogen sulfide has high reduction potential, so sulfur rapidly bonds with transitional metals forming sulfides, for instance, pyrrhotine:

$$\underset{\text{fayalite}}{Fe_2SiO_4} + \underset{\text{forsterite}}{Mg_2SiO_4} + 2H_2S \rightarrow 2\underset{\text{enstatite}}{MgSiO_3} + \underset{\text{pyrrhotine}}{2FeS} + 2H_2O + 26.6\ \text{kcal/mol}. \quad (11.11)$$

The isotopic shifts in the sulfate sulfur are a confirmation of the abiogenic nature of methane and the formation of sulfides at the expense of the sulfate sulfur. Usually, the $\delta^{34}S$ sulfur isotopic shifts in the sulfides of the "black smokers" are within +3‰ to +5‰. It is different in the hot springs on serpentinites where the shift range is much broader, +4‰ to +16‰. This difference may be due to the sources of the sulfate sulfur and the sulfur isotope fractioning conditions in the hydrotherms. Due to a strong thermal effect in the isotope fractioning, they separate between the mineral phases:

$$^{32}SO_4^{2-} + H_2{}^{34}S \leftrightarrow {}^{34}SO_4^{2-} + H_2{}^{32}S. \quad (11.12)$$

That is exactly the reason why under usual conditions of the chemical equilibrium must occur impoverishment of the of the sulfide phase in the isotope $^{34}S$ and enrichment in this isotope of the sulfate phase.

If the sulfides form through sulfate reduction, they inherit the sulfate values of $\delta^{34}S$. In the "black smokers" emerging over a hot basalt crust the sulfate reduction occurs on the basalts' iron. It is possible that the juvenile sulfur manifestations may also occur there. In the hot springs over the serpentinites whose iron content is much higher than in the basalts the bulk of the sulfur is supplied by the oceanic water and is reduced under reactions (11.10) and (11.11). It appears that as a result the isotope density of sulfur in the oceanic water ($\delta^{34}S$ is about +18.86‰) is split so that the $H_2S$ isotope shift in a hot fluid declines to +2.4...+3.2‰, and in metal sulfides to +4...+14‰.

Now we discuss the major carbon isotope shift patterns in the "black smoker" system over the serpentinites.

The negative shifts occur in methane of such springs ($\delta^{13}C \approx -13‰ \ldots -14‰$) compared with the average isotope composition of $HCO_3^-$ and $CO_2$ in the oceanic waters ($\delta^{13}C = -5.5‰$). As with hydrogen sulfide, the reason may be carbon isotope fractioning in methane formation from carbon dioxide.

It follows from the fundamental Le Chatelier's principle that an exothermal chemical reaction always goes along the way of maximum decrease of the internal energy (enthalpy $\Delta H_T{}^0$). It is the same as the release of maximum energy per unit mass of the reaction products. For this reason, it is expected that if $CH_4$ is formed from a carbon dioxide represented by a mixture of the light and heavy carbon isotopes, mostly light isotope $^{12}C$ must participate in the reaction. Indeed, the thermal effect of carbon fractioning reaction in $^{12}C$ "consumption" by methane compared with the $^{13}C$ isotope reaches 0.412 kcal/g ($CH_4$). This is a noticeable effect which definitely helps "lighten" carbon in the forming methane. Thus, the exchange isotopic reaction

$$^{12}CO_2 + 13CH_4 \rightarrow {}^{13}CO_2 + {}^{12}CH_4 + 0.412 \text{ kcal/g } (CH_4) \tag{11.13}$$

mostly evolves from left to right.

To what extent are the methane and "black smokers" (they emerge in the oceanic crust rock serpentinization) carbon ratios comparable with those in the oceanic waters? The standard of carbon isotope ratios is the ratio $^{12}C/^{13}C = 88.99$ in the *Belemnites Americana (Morton)*. It may be determined that the marine water carbon isotopic composition of $\delta^{13}C = -5.5‰$ corresponds to the ratio $^{12}C/^{13}C = 89.48$, and the dissolved methane from the "serpentinite" source isotopic composition of $\delta^{13}C = -13.4‰$ corresponds to the ratio $^{12}C/^{13}C = 90.2$. As carbon is bonded in methane, the isotope ratio changes to $\Delta^{12}C_{mt}$. Then, per unit mass, $\Delta^{12}C_{mt}/^{13}C = 90.2 - 89.48 = 0.72$. $CH_4$ concentration in the fluids from such sources is approximately 0.14 mmol/l. In this case, after methane formation the isotope ratio in the fluid from which the carbonates form under reactions (11.9) is $89.48 - 0.143 \times 0.72 = 89.38$. This corresponds to the isotope shift $\delta^{13}C = -4.35‰$. This ratio is usual for the "black smokers" of this type. The remaining fluid at the output of the hydrothermal system should be practically devoid of carbon dioxide which is often observed in the field.

But in any case all methane emerging in hydrotherms is only exogenous. At greater depths methane is unstable as it is oxidized by oxygen released in the core matter formation under reaction

$$8FeO + CH_4 \rightarrow 4Fe_2O + CO_2 + 2H_2O. \tag{11.14}$$

To conclude this section, a reminder of the existing mantle cycle in the volatile elements and compounds turnaround. It is associated with the fact that the dehydration and decarbonatizing of the oceanic crust rocks in the subduction zones may be incomplete. Thus, part of the remaining water, carbon dioxide and other volatile and mobile elements sinks into the mantle depths together with the oceanic plates and is again included into the general mantle matter convective mass exchange. For this reason, the purely mantle degassing at close consideration is not purely juvenile but includes some elements and compounds repeatedly getting to the Earth's surface.

Unfortunately, it was not possible at this time to estimate the genuinely juvenile fraction of the degassed volatile and mobile elements. Thus, when we discuss the juvenile degassing of Earth we will always mean its effective value. The genuine juvenile degassing is somewhat lower than the effective value because part of the released volatiles sink again into the mantle through the subduction zones. The difference, however, is not great. We estimate it at 20% for the water and even smaller for the other elements and compounds.

## 11.4 NATURE OF THE GLOBAL MARINE TRANSGRESSION ON THE CONTINENTS

The provided discussion of the Earth's tectonic activity used only average parameters of this process without consideration of its periodic fluctuations. Fluctuations in the convective mass exchange intensity and rate of the lithospheric plate movement must take place in actuality. The cause may be, for instance, nonstationary nature of the chemico-density convection and reconfiguration of its structures, or the effect of the continent collision and the lithospheric plate destruction on the rate of their mutual displacements. An example: based on the age identification of the ocean floor striped magnetic anomalies, the average Pacific Plate motion rate in Late Cretaceous was 1.5 times its current value, whereas it was close to this value in Late Jurassic and Early Cretaceous.

The footprints of marine transgressions and regressions on the continents help reconstruct the fluctuations in the Earth's tectonic activity. Menard (1966), Pitman and Heys (1973), Sorokhtin (1976), and Turcotte and Burke (1978) showed that the global marine transgressions and regressions may have been caused by pulsations in the Earth's tectonic activity. Besides the relatively slow changes in the World Ocean level with periods on the order of tens of millions of years, the shorter eustatic fluctuations were identified. They lasted tens of thousands of years and were associated with substantial water amounts accumulation in sheet glaciers (during the ice periods) and their melting.

Prior to the advent of the plate tectonics theory, the nature of the global marine transgressions and regressions on the continents was explained as caused by vertical oscillatory motions of the continental platforms which ostensibly experienced uplifts and subsidence. The tradition of such approach goes far back in time to the ancient philosophers Strabo and Aristotle. The idea was so seemingly obvious that it was axiomatic, not really discussed and entered in its pure form in many textbooks on geology and tectonics. The existence of large oscillatory motions on the platforms resulting in the global transgressions and regressions was usually associated with the periodical heating and cooling of the upper mantle underneath the continents (Joly, 1929; Belousov, 1954). The very nature and especially the mechanism of such cyclical mantle overheating were unclear and could not be quantified.

The lithospheric plate tectonics open a totally different approach to the explanation of the global marine transgressions. This approach was first tried in the publications by marine geologists. Thus, Menard (1964) ventured the idea that large fluctuations in the World Ocean level could be caused by changes in the mid-oceanic ridge volumes. He demonstrated, in particular, that the emergence of the present-day ridges could raise the ocean level by 300 m.

It follows from the lithospheric plate tectonics that the oceanic lithosphere's thickness is determined by the depth of the mantle matter cooling and crystallizing. Therefore, it depends on the duration of the hot mantle matter exposure on the Earth's surface (see Eq. (8.5)). Gradual oceanic lithospheric plate spreading and the continuous buildup of their edges occur in the rift zones due to the cooling and crystallizing of the rising asthenospheric matter. Because of those, the lithospheric thickness underneath the mid-oceanic ridges regularly increases with the distance from their crests. The silicate crystallization goes with the increase in their density. Thus, as the oceanic lithosphere increases in thickness, its surface

subsides under the law of square root of the lithosphere's age (see Eqs. (8.4) and (8.5)). Therefore, the faster the ocean floor spreading in the rift zones, the flatter the mid-oceanic ridges (see Fig. 8.10). The volumes of the oceanic depressions decrease correspondingly and greater water volumes, respectively, are pushed from the oceanic areas onto the continents. It shows that the amplitude of the eustatic ocean level fluctuations associated with tectonics is totally determined by the average rate of the oceanic lithospheric plate motion, that is, by the Earth's tectonic activity.

## 11.5 EARTH'S TECTONIC ACTIVITY AS REFLECTED IN FLUCTUATIONS OF THE WORLD OCEAN SURFACE LEVEL

The inverse approach is also possible. If, from independent data, such eustatic fluctuations of the World Ocean level are known, they may be used for the determination of fluctuations in the Earth's tectonic activity. The amplitude of eustatic ocean level changes for almost entire Phanerozoic was derived from the marine sediments area on the continents and the analysis of seismostratigraphic cross sections on the ocean's continental margins (Vail et al., 1976; see Fig. 11.8).

While interpreting this curve, one has to keep in mind that the eustatic ocean level changes occur for four main reasons.

First, the water mass in the oceans gradually increases due to the mantle degassing. During the entire geological period of about 4 BY, the ocean level raise for this reason was 4.5 km.

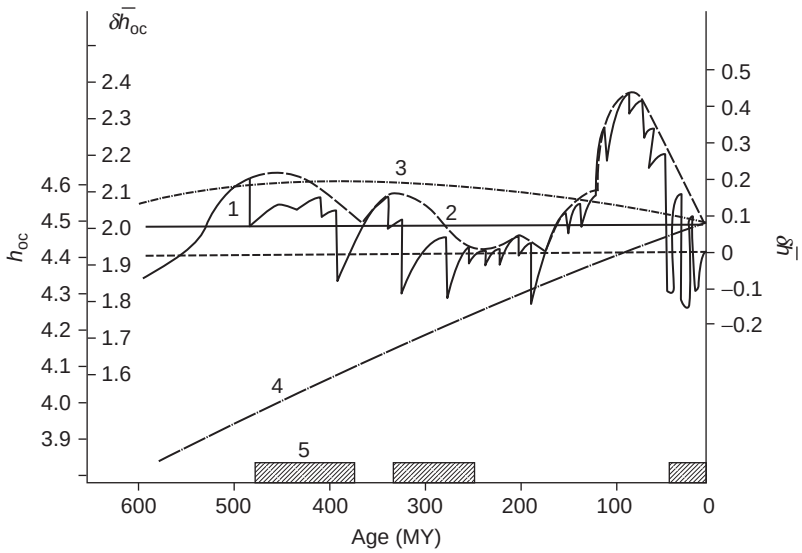


**FIGURE 11.8** Eustatic fluctuations of the World Ocean level in Phanerozoic: 1, after Vail et al. (1976); 2, the average (envelop) curve; 3, evolution of the ocean level $\delta\bar{h}$ (see Fig. 11.6); 4, ocean depth evolution counted from the mid-oceanic ridge crest average stand level $\bar{h}_{oc}$; and 5, glaciations.

Second, evolutionary changes in the Earth's tectonic activity. These are also very slow changes, with the characteristic ocean level fluctuation periods on the order of 1 BY (except for Archaean when it was 100 MMY). Their amplitude was also significant and reached ±1–2 km.

Third, the Earth's tectonic activity fluctuations due to periodical reconfiguration of the structure of the mantle chemico-density convection which resulted in the emergence and destruction of the supercontinents. The corresponding ocean level fluctuations have the characteristic period of 100–800 MMY and amplitudes $\delta h \approx \pm 200$–400 m.

And finally, the fastest ocean level changes with the period of just a few thousand years occur due to the emergence and melting of the sheet glaciers in the near-polar areas. The periods of the glacio-eustatic ocean level fluctuations are on the order of 100,000 years with the amplitude of up to ±100–150 m. The nature of the glacio-eustatic marine transgressions and regressions is discussed in more detail in Section 14.6 (see Fig. 14.25).

Curve 1 of the eustatic ocean level changes (Fig. 11.8) was averaged. The reason was that the shown drastic regressive jumps were associated either with the rapid glacio-eustatic changes or are just seeming changes that appeared due to the absence or erosion of the regressive depositional sequences. Figure 11.9A displays the recalculation results of the average World Ocean eustatic fluctuations curve (curve 2) for the average movement rate of the oceanic lithospheric plates. As the heat flow through the ocean floor is proportionate with the square root of the average rate of the oceanic plate spreading, it is possible to determine at the same time the average heat flows that penetrated the oceanic plates in Phanerozoic (Fig. 11.9B).

As the resulting diagrams show, individual pulsations of the tectonic activity may reach 15–20%. Three maximums of such pulsations are observed in Phanerozoic. The main one was manifested in Ordovician and Silurian during the Caledonian orogeny 500–400 MMY ago when the formation of the Wegenerian Pangaea began. A second, less intense

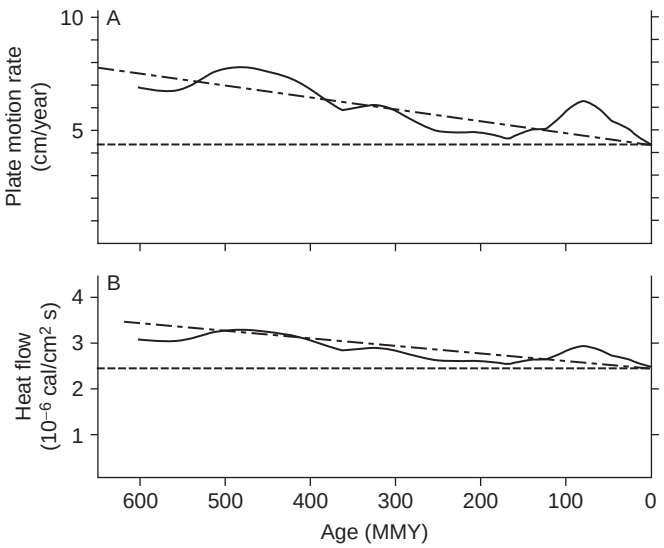


**FIGURE 11.9** Phanerozoic tectonic activity (Sorokhtin and Ushakov, 1991): (A) normalized for the lithospheric plate average movement rate; (B) normalized for the average heat flow through the ocean floor; and dashed–dotted lines are evolutionary changes corresponding to the oceanic plate movement rates and heath flow through the ocean floor.

maximum was in Carboniferous, during the Hercynian orogeny and continued Pangaea formation. These active orogenic epochs were followed in Triassic and Jurassic by a relatively quiet and brief stability period of the supercontinent Pangaea. The last, Late Cretaceous tectonic activity burst was associated with Pangaea disintegration, closing of the Tethys Paleo-ocean and emergence in its place of the grandiose Alpine-Himalayan mountain belt.

Global transgressions and regressions may cause serious restructuring of the biotic associations. An example is a rapid mass extinction of many coral species on the oceanic islands early in the Late Cretaceous. But that was a period of the last global transgression. It was caused by increased rate of the growth in the oceanic lithosphere. And it resulted in the carbonate and phosphorus compounds "pumping" from the oceans into the shallow water extremely broad epicontinental seas and in the deposition in these seas of chalk sediments and phosphorites. That is why corals and many mollusks (such as rudistas) were extinguished on the oceanic islands in the middle of Cretaceous due to the open ocean water impoverishment in calcium carbonate and phosphorus compounds (see Figs.15.6 and 15.7).

CHAPTER

# 14

# Evolution of Earth's Global Climate

## 14.1 CLIMATIC PARADOX

The most important definitive factor of the Earth's climatic conditions is its surface temperature. Temperatures during the past epochs may be deduced from the oxygen isotopic shifts, for instance, in the marine flintstones which usually form in equilibrium with the surrounding water. We know from isotope geochemistry that the $\delta^{18}O$ value in marine flintstones substantially depends on the temperature of the water where the siliceous sediments were deposited. Based on such determinations, it is usually assumed that a high atmospheric temperature occurred already in Archaean about 3.4 BY ago (Perry and Tan, 1972). By mid-Archaean, the oceanic water temperature reached $+70\,^{\circ}C$ (Knauth and Lowe, 1978). Other determinations put the oceanic water temperature in mid-Archaean 3.2 BY ago even at $90\,^{\circ}C$ (Perry, 1967), and from the isotopic composition of siliceous slates, at $+70$ to $+100\,^{\circ}C$. It is not clear to this day, however, to what extent the $\delta^{18}O$ values in ancient flintstones reflect their origin and, most important, the temperatures of the water where these flintstones formed: the isotope ratio in the flintstones may have been affected also by the same ratio in the oceanic water (Hollend, 1989; Schopf, 1980). It is possible that the observed regular decline of the $\delta^{18}O$ values in the flintstones is not only due to the oceanic water temperature change but also to other reasons causing regular $\delta^{18}O$ value decline in the Archaean oceanic waters (Sorokhtin and Ushakov, 2002).

For instance, our estimates are that, affected by the exchange reactions with iron oxides, the marine water isotopic composition declined in Precambrian to $\delta^{18}O \approx -10‰$. Galimov (1988b) estimated the Archaean oceanic water isotopic composition at $\delta^{18}O \approx -15$ to $-10‰$. The current value (SMOW scale) is at $\delta^{18}O = 0$. After the metallic iron totally disappeared from the mantle by the end of Proterozoic (Sorokhtin and Ushakov, 2002), that is, already in Phanerozoic, the $\delta^{18}O$ for the marine water may be assumed to be 0. In such a case, the near-bottom temperature in the Early Archaean basins was much more moderate, no higher than $+70\,^{\circ}C$. With this in mind, Fig. 14.1 illustrates not only the heavy oxygen isotope $\delta^{18}O$ distribution in the marine flintstones of different ages but also the corresponding isotopic temperatures of the near-bottom marine water (accounting for the aforementioned correction of $\delta^{18}O \approx -10‰$). Therefore, the World Ocean near-bottom temperature was still rather high indicating a hot Archaean climate, but it declined with time.


DOI: 10.1016/S1571-9197(11)10014-2

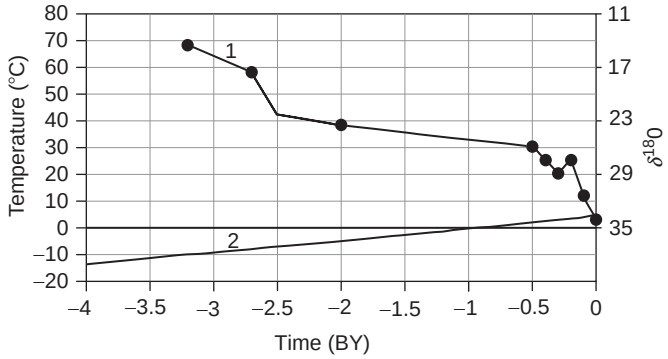


**FIGURE 14.1** Climatic paradox: the Sun's luminosity increases while the climate cools down: 1. Average isotopic temperature of marine flints formation (it characterizes the average temperature of the World Ocean's near-bottom waters; dots are $\delta^{18}O$ values from the marine flintstones from Schopf (1980); 2. Temperature of the absolute black body at the Earth's distance from the Sun characterizing the Sun's luminosity (the temperature scale is ours)

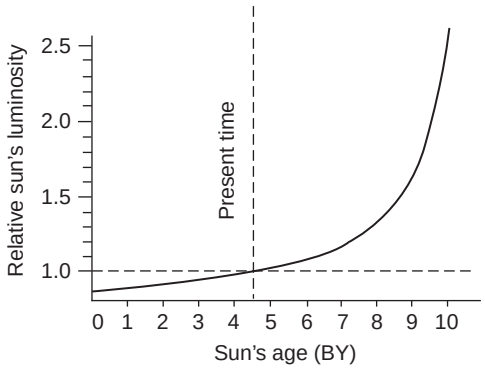


**FIGURE 14.2** Sun luminosity versus time (Aller, 1971)

What was the reason for such a regular decline in the near-surface temperatures during the planet's geological evolution?

The first factor that comes to mind is a decrease in the solar luminosity. The stellar evolution theory says, however, that upon entering the main succession of a star's evolution, the star's luminosity can only increase at an ever accelerating rate. Figure 14.2 displays a diagram of the Sun's luminosity increase after the well-known astrophysicist, Aller (1971). Calculations indicate that beginning in Archaean and through the present the Sun's luminosity increased by 20–30% (Bachall et al., 1982). This must have caused the temperature to increase approximately by 20 °C. In actuality, the near-bottom water temperature in the World Ocean over the same time interval declined almost from +70 °C to +2 °C. This is what constitutes the main climatic paradox of Earth (Fig. 14.1).

The adiabatic theory of the greenhouse effect says (see Eq. (13.12)) that besides the solar radiation, the main factor determining Earth's climate is the atmospheric pressure (Sorokhtin, 2001a,b). The higher the atmospheric density (i.e., the higher the pressure), the warmer the climate. That is why high surface temperatures in Archaean on the surface at the ocean level, with a low luminosity of the Sun, may only be the result of the elevated atmospheric pressure in Archaean, and a gradual decline with time of the oceanic water temperature, with a smooth increase in the Sun's luminosity, may only be the result of the gradual decline of the atmospheric pressure.

The Archaean atmosphere was high-density, composed of carbon dioxide and nitrogen, and with atmospheric pressure on the order of 5–6 atm (see Fig. 12.15). After the serpentinite layer of the oceanic crust formed in Early Proterozoic (see Fig. 7.1) the high-density carbon dioxide Archaean atmosphere was almost totally bonded in the carbonates of sedimentary rocks (see Chapter 12, Section 12.3). This turned the Proterozoic atmosphere into almost purely nitrogen. Nevertheless, the climate continued to cool down, and therefore the nitrogen atmospheric pressure continued to dwindle. We showed in the earlier publications (Sorokhtin, 2005a,b) that the general climate cooling in Proterozoic and Phanerozoic occurred substantially due to the life activities of the nitrogen-consuming bacteria. They continuously consumed the atmospheric nitrogen and converted it into organic compounds, which gradually accumulated in Earth's soils and depositional sequences.

A similar role belonged to thunderstorms in the humid Earth's atmosphere. Not only was there a decrease in the nitrogen partial pressure in the atmosphere but also in the total atmospheric pressure. That with time led to climate cooling and the appearance of conditions under which glaciations emerged (Sorokhtin, 2005b; Sorokhtin et al., 2007a,b).

Geological data show that the climate in Phanerozoic and especially in the entire Cenozoic gradually cooled down. There were several reasons for this, including nitrogen removal from the atmosphere and its bonding in organic compounds of the soils as mentioned in Chapter 12. A result was significant decline in atmospheric mass and pressure beginning in mid-Proterozoic and in particular over the recent 100 MMY, which caused climate cooling by 12–15 °C (see Fig. 14.3). Currently, this cooling is not compensated for even by a smooth increase in the intensity of the solar radiation.

The evolutionary climate cooling was also facilitated by the continental drift which in Cenozoic moved some continents to the high latitudes, and the precession angle decreased from approximately 34° to the present 24°. This is also indicated by abundant geological data such as the total absence of any glaciation in Mesozoic and the appearance of the first Antarctic ice sheets in the middle of Cenozoic (about 40 MMY ago), and in Quaternary (the recent 2 MMY), of periodic glaciations in the Northern Hemisphere. We are now in the period of an interglacial stadial. When it is replaced by a new glaciation phase it is expected to be very severe.

The general Cenozoic climate cooling was clearly marked by the near-bottom water temperature decline (see Fig. 14.4). The figure shows that the Antarctic glaciation began about

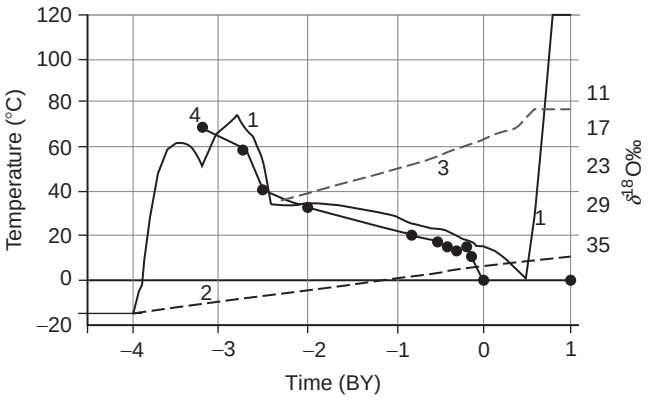


**FIGURE 14.3** Averaged evolution of Earth's climates at a constant precession angle $\psi = 24°$: 1. Earth's average surface temperature at sea level; 2. "Absolute black body" temperature at the Earth to Sun distance showing Sun luminosity increase with time; 3. Average Earth temperature on assumption of no nitrogen consumption by bacteria; 4. Temperature of the oceanic near-bottom water (dots are $\delta^{18}O$ values in marine flintstones after Schopf (1980))—(see Fig. 14.1)

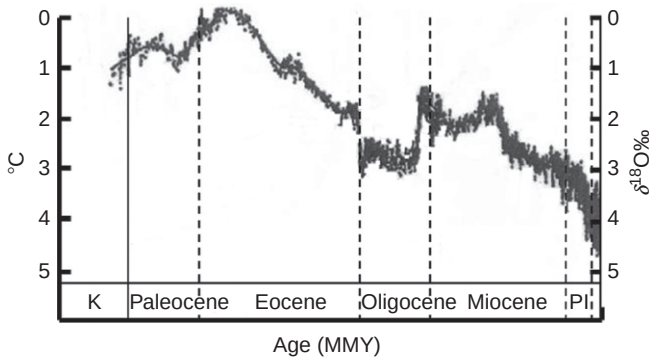


**FIGURE 14.4** Deep oceanic water temperature by $^{18}O$ isotope shifts in benthonic fauna carbonates (isotopic data after Zachos et al. (2001), temperature scale is ours)

50 MMY ago. A drastic cooling down of the water at the Eocene/Oligocene time boundary was apparently caused by the spread of the Antarctic glaciation to the edges of the continent. A new and slight temperature rise happened in Miocene. It was likely due to the closing of the Tethys Ocean and drift to the equator of some Gondwana continents. In Pliocene–Quaternary, new glaciations began, this time in the northern regions. This quickly resulted in the decline of the near-bottom temperatures, almost to 0 °C. A general temperature decline over the recent 70–60 MMY was most likely associated with the removal from the atmosphere of some nitrogen by the nitrogen-consuming bacteria and its bonding in soils, deposits, and organic matter (see Section 12.4). The result was a noticeable decline in the general atmospheric pressure in Cenozoic (see Fig. 12.15) which, in turn, unavoidably resulted in climate cooling (see Eq. (13.12)) Presently, this general climate cooling is not compensated for even by a gradual increase in the Sun's luminosity.

It is noteworthy that the accelerated Cenozoic decline in the oceanic near-bottom water temperature was associated not only with a decrease in the general atmospheric pressure but also with the glacier formation on the high-latitude continents (as mentioned previously). Indeed, the glaciers crawl from the polar continents into the oceans, cool the nearshore water and gradually melt, reaching the planet's boreal zones. The cooled-down water descends to the ocean floor, lowering the temperature of the near-bottom water. This process became especially noticeable after the glaciation epochs emerged on the northern continents in Quaternary. That was exactly the Pleistocene glaciation epochs that caused the near-bottom water cooling to almost 0 °C as seen in Fig. 14.4.

We determined the evolution in time of atmospheric pressure and composition (Fig. 12.15). Now, using the adiabatic theory of the greenhouse effect, it is possible to find the correlation between the Earth's surface temperature and time. As a first approximation, it may be performed based on the general atmospheric composition and pressure changes as shown in Fig. 12.15, and on Eq. (13.12). The first approximation, however, does not account for evolutionary parameter changes in this equation, and first of all of the atmospheric gas mixture's heat capacity $c_p$, molar weight $\mu$, adiabatic exponent $\alpha$, and the planet's albedo $A$.

The atmospheric heat capacity may be found from Eq. (13.13′), the molar weight is determined from a similar equation with the gas molar weight substituted instead of the heat

capacities. Then, using Eq. (13.13) we find the adiabatic exponent, and the values of the sum $C_w + C_r$ are found from Eqs. (13.14)–(13.16) where the $T_s$ and $T_e$ values are inserted from the first approximation solution. The Earth's albedo is assumed to be in proportion with its surface temperature counted from the present-day level of $A_0 = 0.3$ at $T_0 = 15\ ^\circ C$. Then $A = 0.3 + (T - T_0)k$. Factor $k$ is selected from the best fit of the theoretical curve and empirical data for the isotopic temperature of the marine flintstones (accounting for the oxygen isotopic shift correction $\delta^{18}O \approx -10‰$ in the water of the Archaean oceans).

The general match between the theoretical curve and empirical data on the temperature of the World Ocean near-bottom water indicates that the proposed theory solves the climatic paradox naturally, by way of decreasing the general atmospheric pressure.

## 14.2 GENERAL PATTERNS IN EARTH'S CLIMATE EVOLUTION

We will now discuss the main regularities of the Earth's averaged climate. We described in Chapter 12 a model of Earth's degassing and atmospheric evolution. The atmospheric composition and pressure are illustrated in Fig. 12.15. This model was generated in consideration of the removal from the atmosphere of some nitrogen through life activity of the nitrogen-consuming bacteria, which substantially lowered by the present time the nitrogen partial pressure and the general atmospheric pressure.

Thus, we found the correlation with time of the atmospheric composition and pressure. Now, using the adiabatic theory of the greenhouse effect we can determine averaged temperature regimes of the Earth's climates. The Earth's temperature is assigned by Eq. (13.12), its effective temperature (i.e., the temperature at which Earth is seen from the outer space), by Eq. (13.16) and the greenhouse effect, by their difference, that is, Eq. (13.7). The results are shown in Fig. 14.5. The figure also includes the temperature of the absolute black body characterizing the intensity of the solar radiation.

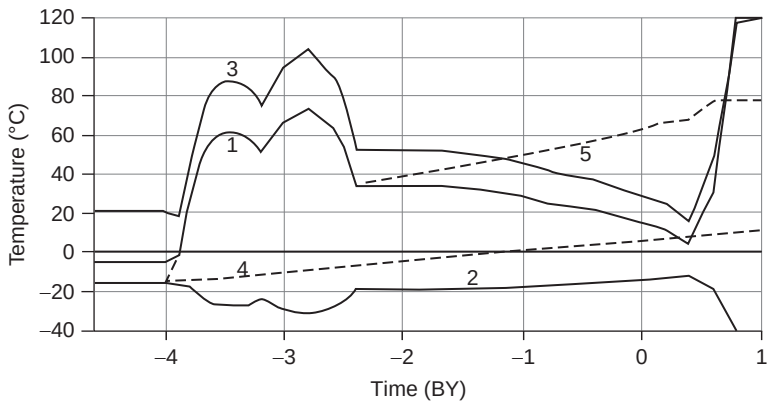


**FIGURE 14.5** Averaged evolution of Earth's climates at a constant precession angle $\psi = 24°$: 1. Earth' average surface temperature at sea level; 2. Earth's effective temperature; 3. Greenhouse effect of Earth's atmosphere; 4. Temperature of the absolute black body at the Earth distance from Sun showing Sun luminosity increase with time; 5. Average Earth's temperature on assumption of no nitrogen consumption by bacteria

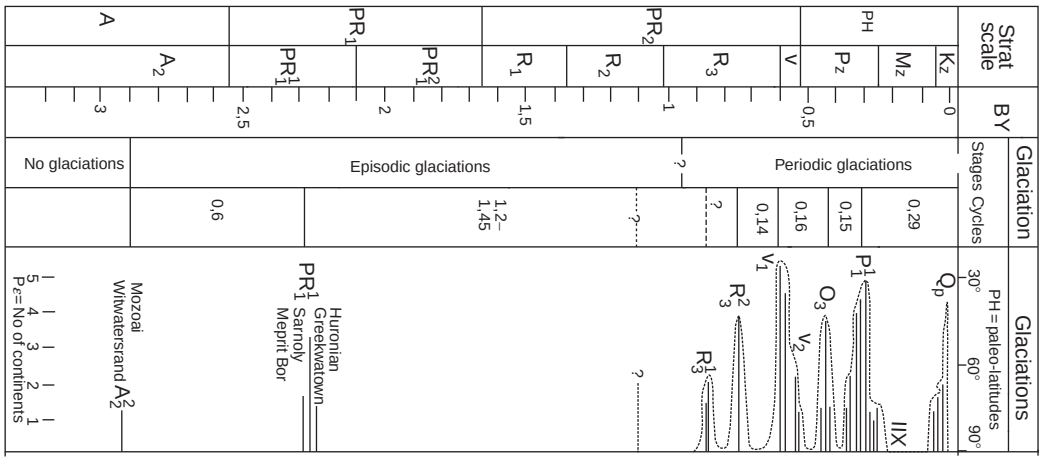


**FIGURE 14.6** Glaciations in geological history. After Chumakov (2004a,b,c)

As the figure indicates, despite growth in solar activity, both the Earth's surface temperature and the atmospheric greenhouse effect decline. Such a drop in the tropospheric temperature (mostly of bacterial origin) gradually created conditions for the emergence of glaciation eras on Earth, and of the glaciation epochs within the eras.

It appears obvious that regional glaciations on the Earth's surface occur only if the temperature within a given region declines to the freezing point of water. As one of the best glacier experts, Chumakov (2001, 2004a,b,c) noted, the onset of the glaciation periods accelerated with time. This conclusion is well illustrated by the glaciation epoch distribution in the geological history (Fig. 14.6). It needs to be taken into account that the Early Proterozoic (Huron) and even more so the Archaean glaciations were clearly high-altitude phenomena (Sorokhtin and Sorokhtin, 1997, Sorokhtin and Sorokhtin, 2002) as the continents in Archaean rose 6–7 km above sea level, and in Early Proterozoic, 5–2 km (see Fig. 11.6). At the time of a temporary tectonic slackening in Archaean about 3.2 BY ago, the general atmospheric pressure declined from 5 to almost 3.5 atm, and in Early Proterozoic, to 2–1.5 atm (see Fig. 12.15). This made it possible for the temperature during these epochs to drop below the freezing point of water (see Fig. 14.21). In this case, the conclusion that there was acceleration with time in the advent of glaciation epochs is confirmed even more convincingly because there were no normal (non-high-altitude) glaciations prior to Late Riphaean (1 BY ago).

What, then, were the reasons for so significant a drop in the global temperature that caused glaciations over large regions? We showed above that such temperature decline could not have been a result of decreased solar luminosity. The only possible explanation is a decrease in the atmospheric pressure. We made an attempt in Chapter 12 to show that the "culprits" were nitrogen-consuming bacteria and in part electrical storm activity.

We will now discuss a specific emergence mechanism of global glaciations epochs.

## 14.3 ORIGIN OF GLACIATION EPOCHS

Glaciation epochs are an oscillatory process as periods of a significant cooling are replaced by drastic warming (the interglacial stadials), and after that the cooling returns. That is why this oscillatory process cannot be explained by smooth climate cooling (such as the bacterial drop in the air pressure).

Let us now discuss the behavior of the revolving Earth's precession. We reviewed the effect of the Earth's precession angle on the tropospheric temperature in Section 13.3, Eq. (13.12). The emergence of precession is associated with the deviation in the Earth's mass distribution from the total spherical symmetry. Such deviations are caused first of all by the crust nonuniformity in its continental and oceanic segments, that is, by the continent and ocean positions on the Earth's surface. Another reason is density nonuniformities in the mantle. The average period of the Earth's axis to go over the total precession circle is presently $\tau \approx 25.7$–$26$ thousand years (Sommerfeld, 1944; Kaula, 1968). The precession motions are superposed by smaller short-period nutation ("nodding") fluctuations. They are perceived as the pole motions apparently caused by the tidal disturbances, movements of the internal Earth's core and by the Earth–Moon system revolution around the common barycenter. A result is rather complex pattern of the Earth's axis rotation. We will attempt to separate the main component of this movement.

The shape of Earth is very close to that of the revolutional ellipsoid of a liquid body with the equatorial inertial swelling. The Earth's equatorial radius $R_e = 6378.2$ km is greater than the polar radius $R_p = 6356.8$ km by 21.4 km, which corresponds to its compression $e = (R_e - R_p)/R_e = 1/298.3$. That is the reason why a greater excess mass is concentrated at the equator and can have the gravity interaction with the other celestial bodies. These interactions tend to turn Earth so that its equatorial plane would coincide with the rotation plane of the disturbing body. Still, only the gravity pull by Moon and Sun play the main role in decreasing the precession angle (Fig. 14.7).

The gravity of the Moon and Sun works simultaneously on both sides of the Earth's equatorial swelling, tending to turn its axis of revolution in opposite directions. But the gravity action on the swelling side facing the Moon or Sun is slightly greater than on the opposite side (see Fig. 14.7).

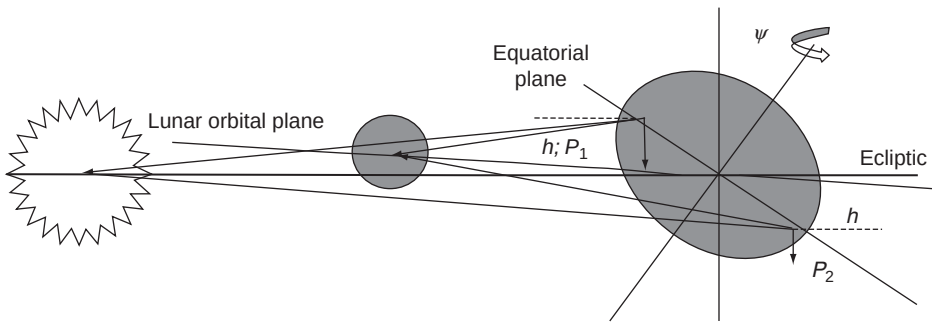


**FIGURE 14.7** Effect of Lunar–Solar gravitational pull on Earth's equatorial inertial swelling resulting in Earth's equatorial plane approach to Lunar revolution plane and to the ecliptics, that is, in a decline of Earth's precession angle (scale distorted).

The volume of the equatorial swelling is obviously equal to the difference between the Earth's revolution ellipsoid volume and the volume of a sphere inscribed in it:

$$V_{\text{swell}} = \frac{4}{3}\pi R_e^2 R_p - \frac{4}{03}\pi \times R_p^3 = 7.1 \times 10^{24}\,\text{cm}^3. \tag{14.1}$$

Then the mass of the equatorial swelling is

$$m_{\text{swell}} = V_{\text{swell}} r_{\text{swell}} \approx 2 \times 10^{25}\,\text{g},$$

where $\rho_{\text{swell}} \approx 2.8\ \text{g/cm}^3$ is the average density of the swelling accounting for the oceanic water layer about 3–4 km deep and the underlying layer of the oceanic crust and the upper mantle (about 17 km). One half of this equatorial swelling is facing the Moon, and the other half is on the opposite side of the Earth (see Fig. 14.7). Thus, the effective mass of each half is about 2 times smaller, just $m_{\text{swell}}/2 \approx 1 \times 10^{24}$ g. Then the difference of the lunar gravity forces acting on these halves $\Delta P_L = P_1 - P_2$ is:

$$\Delta P_L = \frac{2}{\pi}\gamma m_L m_{\text{swell}} \left[\frac{1}{[L_L - R\cos(\psi - \lambda)]^2} - \frac{1}{[L_L + R\cos(\psi - \lambda)]^2}\right], \tag{14.2}$$

where $\gamma = 6.67 \times 10^{-8}\ \text{cm}^3/\text{g s}^2$ is the gravitational constant; $m_L = 7.35 \times 10^{25}$ g is the Lunar mass; $L_L = 3.844 \times 10^{10}$ cm is the distance between the Earth's and Moon's centers of mass; $R = 6.371 \times 10^8$ cm is the average radius of Earth; $\psi$ is the precession angle (present value, $\psi = 23.44°$); $\lambda \approx 5°$ is the angle between Moon-around-Earth rotation plane and the plane of the ecliptics.

The result is $\Delta P_L \approx 1.3725 \times 10^{21}\ \text{cm g/s}^2$.

Similarly, the difference in the Sun gravitational forces acting on the equatorial swellings is:

$$\Delta P_\otimes = \frac{2}{\pi}\gamma m_\otimes m_{\text{swell}} \left[\frac{1}{[L_\otimes - R\cos\psi]^2} - \frac{1}{[(L_\otimes + R\cos\psi)]^2}\right], \tag{14.3}$$

where $m_\otimes = 1.99 \times 10^{33}$ g is the mass of Sun; $L_\otimes \approx 1.496 \times 10^{13}$ cm is the distance between the Sun and Earth centers of mass. Then $\Delta P_\otimes \approx 0.6088 \times 10^{21}\ \text{cm g/s}^2$.

Obviously, the lunar and solar gravitational forces must be attached to the center of mass of each half of the equatorial swelling. Each half is similar to a convex dome with the center of gravity at a distance of about 2/3 Earth radius from the center of Earth (Fig. 14.8). Therefore,

$$h \approx \frac{2}{3}R\sin\psi, \tag{14.6}$$

and the difference of the moments of force attached from the lunar side to the Earth's equatorial swelling (see Fig. 14.7) is equal to $\Delta M_L = \Delta P_L \cdot h = 3.71 \times 10^{29}\ \text{g cm}^2/\text{s}^2$, and from the solar side $\delta M_S = \delta P_S h = 1.72 \times 10^{29}\,\text{g cm}^2/\text{s}^2$. The combined effect of the Moon and Sun gravitational pull is then $\Delta M_L + \Delta M_S = 5.43 \times 10^{29}\ \text{g cm}^2/\text{s}^2$.

Beside the effect of the Moon and Sun, the Earth's precession is influenced by the asymmetry of continental positions on the globe's surface. The combined mass of the continents

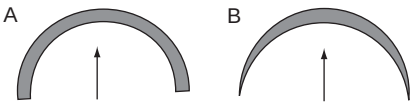


**FIGURE 14.8** Center of gravity of Earth's equatorial swelling in the cross section facing Moon: (A) In equatorial plane; (B) In meridional plane.

$m_{cont}$ is equal to approximately $2.25 \times 10^{25}$ g (Ronov and Yaroshevsky, 1978), the average thickness of the continental crust is $H_{cont} = 40$ km $= 4 \times 10^6$ cm and their average stand above sea level is $\Delta h = 875$ м $= 8.75 \times 10^4$ cm. The continent effect on the Earth's asymmetry is due to their centers of mass being positioned slightly above the center of mass of the mantle matter displaced by the continents. Obviously, under the continents' isostatic equilibrium the mass of the displaced mantle $m_{mant}$ is equal to the mass of the continents $m_{cont} = 2.25 \times 10^{25}$ g. Judging from the continent stand elevation, the continents' center of mass is above the center of mass of the displaced mantle by $\delta h \approx 500$–$600$ m. Then the continental crust excess mass is $\Delta m_{cont} \approx m_{cont} \cdot \delta h / H_{cont} \approx 3.38 \times 10^{23}$ g. With the centrifugal acceleration $g_{ctrf} = \Omega^2 R \cos\varphi$, where $\Omega = 7.27 \times 10^{-5}$ rad/s is the Earth's revolution angular velocity and $\varphi$ is the latitude of the continents' center of mass. At $\varphi = 30°$, $g_{ctrf} = 2.9$ cm/s$^2$, and $\Delta P_{cont} = \Delta m_{cont} g_{ctrf} \approx 9.8 \times 10^{23}$ g cm/s$^2$. Depending on the distance between the center of mass of the entire continental ensemble and the Earth's center, the value $\Delta M_{cont}$ is between $10^{29}$ and $10^{30}$–$10^{31}$ g cm$^2$/s$^2$. The mantle is nonuniform, especially with respect to the positions of the lighter ascending mantle flows and the heavier descending ones. Besides, the nonuniformity is added by the core surface topography (see Fig. 2.10). The result is that the combined effect of all these factors is quite fuzzy. Our indirect estimate based on a comparison of the theoretical temperature climate fluctuations in Pleistocene with the isotopic temperatures of the Antarctic ice cover (see Fig. 14.13) is that the present-day $\Delta M_{cont+m}$ is approximately equal to $(0.2$–$0.6) \times 10^{29}$ cm$^2$ g/s$^2$.

Using the theory of free gyroscopes, we will determine the average rate $\omega$ of the axial rotation of Earth's revolution about the intersection line of the equatorial plane with the lunar orbit plane around Earth and Earth orbit plane around the Sun:

$$\omega = \frac{\Delta M_L + \Delta M_S - \Delta M_{cont+m}}{I\Omega}, \tag{14.7}$$

where $I = 8.04 \times 10^{44}$ g cm$^2$ is Earth's moment of inertia; $\Omega = 7.27 \times 10^{-5}$ rad/s is angular velocity of the Earth's own revolution. The present-day Earth's rotation rate, with the precession angle of 23.44°, is $\omega \approx 4.83 \times 10^{-12}$ rad/s or $1.53 \times 10^{-4}$ rad/year (the rotation by 1° takes approximately 716.5 years). And the Earth rotation from the present precession angle 23.44° to the lunar orbit inclination angle to the ecliptics occurs asymptotically and gradually, approaching 5.1°. This approach takes millions of years, which indicates that the function of Earth's rotation rate versus the precession angle is substantially nonlinear. The Earth rotation time may be found from the following equation:

$$\tau = \frac{2\pi}{\omega}. \tag{14.8}$$

But $\omega = d\psi/dt$, wherefrom the precession angle correlation versus time is (Fig. 14.9).

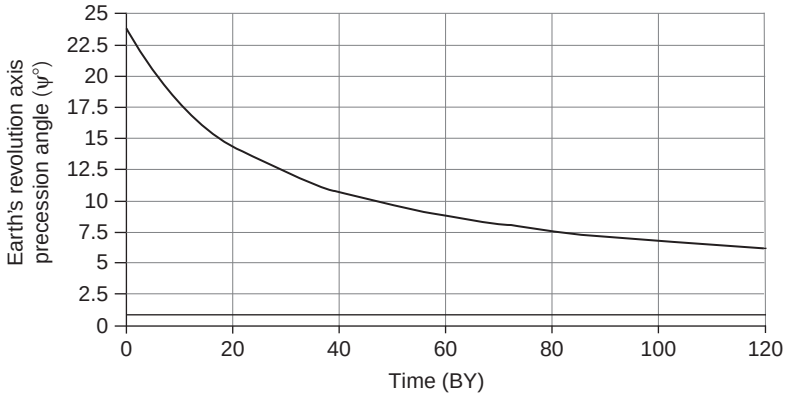


**FIGURE 14.9** Earth's precession angle change with time as affected by lunar–solar tides and asymmetric continents' locations on the Earth's surface. As an example, the initial precession angle is assumed at 24°. Minimal precession angle is determined by continents' position on the Earth's surface and by condition (14.10); its current value is about 2.5°

$$\psi = \int_0^t \omega \mathrm{d}t, \tag{14.9}$$

At the equilibrium of lunar–solar gravity pull of the Earth's equatorial swelling with the effect of the continents and mantle,

$$\Delta M_L + \Delta M_S = \Delta M_{cont+m}, \tag{14.10}$$

$\omega = 0$, and the precession angle $\psi$ acquires its equilibrium value (at $t \to \infty$). For the present-day positions of the continents, $\psi_\infty \approx 2.5°$ (Fig. 14.9). Currently, the precession angle declines at a rate of about $6 \times 10^{-4}$ deg/year.

Now we can find from Eq. (13.12) the correlation of near-surface temperature versus time (Fig. 14.10).

As the plane of the Earth's equator approaches the plane of the lunar orbit around Earth and the ecliptics, the Moon's and Sun's external action on the Earth's equatorial swelling substantially decreases. Based on Eq. (13.12), a noticeable climate cooling corresponds with this process. As soon as the temperature reaches some critical level, glaciations begin on the high-latitude continents (for the northern regions the critical value of the Earth's average temperature appears to be close to 10–11 °C).

Indeed, the ice sheets emergence and growth in the polar areas unavoidably disrupts the Earth's revolution equilibrium and leads to a renewed rapid increase of the precession angle. To determine the direction of the ice sheets action on the Earth's revolution regime, the glaciations in both Northern and Southern hemispheres must be accounted for (Figs. 14.11 and 14.12). However, the Antarctic ice mass increment was limited by the finite size of the underlying continent and mostly occurred in the near-shore areas and in the West Antarctic where humid cyclone penetration is common. The Eastern Antarctic ice dome has a high stand (up to 4 km). For this reason, it is dominated by anticyclones and

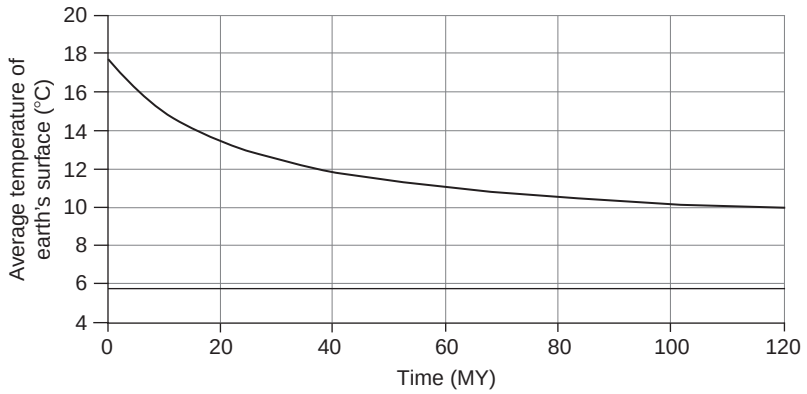


**FIGURE 14.10** Changes in the Earth's surface average temperature as affected by the gravity pull from the Moon and Sun on the equatorial swelling and by the asymmetry of the continents' positions on the Earth's surface. As the precession angle monotonously declines from 24°, the temperature curve asymptotically approaches its minimum value of $T_\infty \approx 6.5\,^\circ\mathrm{C}$ (the classical absolute black body at Earth distance to the Sun is equal to $278.6\,\mathrm{K} = 5.4\,^\circ\mathrm{C}$).

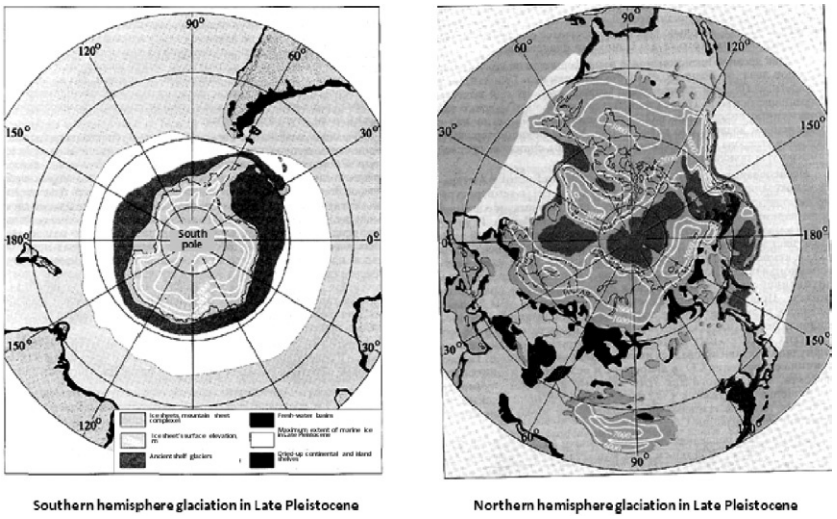


**FIGURE 14.11** Antarctic and Northern hemisphere glaciations in Late Pleistocene (after Kotlyakov, 2002). Light shading around the poles indicates maximum marine ice development areas in Lt. Pleistocene; dark-gray areas around Antarctica, in the Arctic Ocean, Northern Atlantic, Barents Sea, the Sea of Okhotsk and Bering Sea are ancient shelf glaciers.

the snow mass increment in its central areas is mostly due to the hoar-frost precipitation out of a relatively dry air. This increment is almost totally compensated by the ice plastic flow from the central areas to the shores. Besides Antarctica, the main ice accumulator in the southern hemisphere, is almost symmetrical relative to the South Pole and does not cause substantial disruptions in the Earth's axial symmetry.

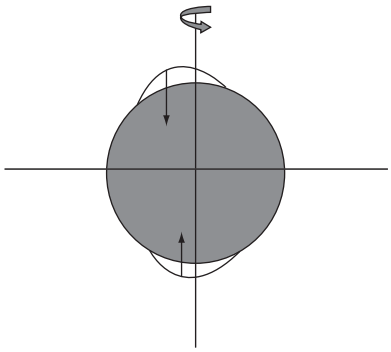

**FIGURE 14.12** Effect of inertion forces from the excess mass of ice sheets in the Northern and Southern hemispheres on the turn of the Earth's revolution axis.

Kotlyakov (2002) published data about the Late Pleistocene glaciers distribution (Fig. 14.11). The main ice mass in the Northern Hemisphere was accumulated over the Canadian Shield. If so, two moments of force directed against each other must have been acting on the body of Earth in Late Pleistocene. One was caused by the Canadian glaciation, and another one, by the West Antarctic glaciation as shown in Fig. 14.12. The moment of force from the Northern Hemisphere clearly dominated.

Ice sheets 2–3 km thick were developed in Lt. Pleistocene in the Central Antarctic, in Canada, Northern Europe, Northern Siberia and in the Arctic Ocean's shelf seas as well as in the mountainous areas of Central Asia.

In estimating the ice sheet effect on the Earth's precession, the glacier masses positioned symmetrically with respect to the poles may be disregarded as they mutually compensate and do not have any significant effect on the Earth's revolution regime.

As we estimated, the excess mass of the ice sheets (taking the southern glaciers into account) was located in Late Pleistocene at about 70° N over Canada and was approximately $2\times10^{22}$ g. The centrifugal acceleration at 70° latitude is equal to about $g_{\text{ctrf}}\approx1.15$ cm/s$^2$. In this case, $\Delta P_{\text{glacier}}\approx2.3\times10^{22}$ g cm/s$^2$, and the distance between the excess mass center of gravity and the North Pole was close to $h_{\text{glacier}}\approx2.2\times10^{8}$ cm or 2200 km. Then the additional moment of force attached to Earth is equal to $\Delta M=\Delta P_{\text{glacier}}\cdot h\approx5.1\times10^{30}$ g cm$^2$/s$^2$. Then, from Eq. (14.7), $\omega\approx7.9\times10^{-11}$ rad/s and the characteristic warming time $\tau\approx2500$ years.

This, of course, is a very approximate estimate but it provides the order of a characteristic warming and glaciers degrading time, about a few thousand years which was apparently actually observed. Quoting Kotlyakov (2002), "the disintegration of a giant Pleistocene glaciation in the Northern Hemisphere occurred geologically very rapidly, just over a few thousand years."

To calculate temperature climate change, it is necessary to estimate how it is affected by the Earth's orbit precession in its rotation around Sun (Milanković cycles). Main harmonics of the Milanković cycles have periods of about 41,000 and 23,000 years (Milanković, 1930; Bolshakov, 2003). Their effect causes temperature changes on the order of $\pm2$ to $\pm3$ °C. The average Late Pleistocene temperature in consideration of such fluctuations and in comparison with the isotopic temperature of the Antarctic ice at the Vostok Station is shown in Fig. 14.13.

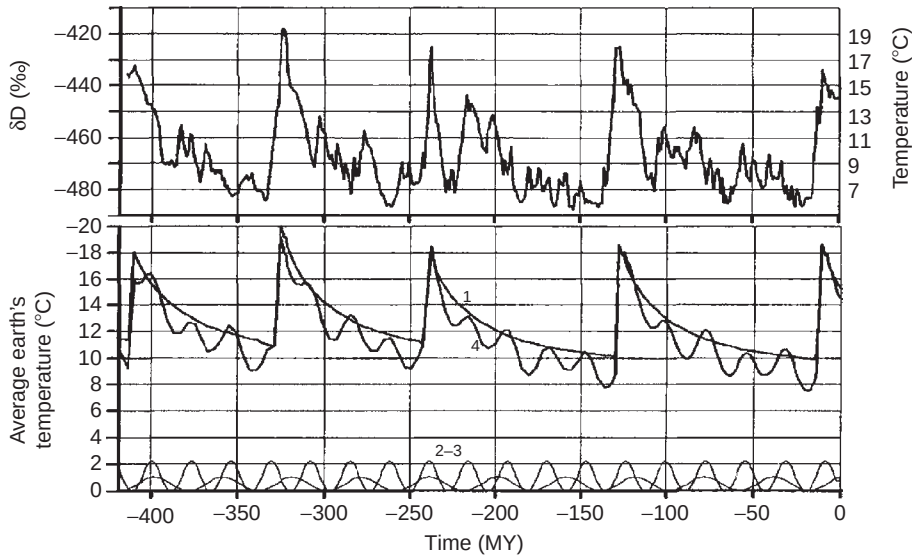


**FIGURE 14.13** Correlation of the oceanic water experimental temperature (the evaporation of this water gave birth to the Antarctic ice sheet) (upper diagram) with theoretical temperature values of the same water (lower diagram). Experimental temperatures were determined from the deuterium/hydrogen ratio (in $\delta D$‰) in cores from the Antarctic ice sheet (Vostok Station; Kotlyakov, 2000). Based on Kotlyakov's calculations, the 10–20 thousand years burst of the isotopic temperature was 8 °C, the previous temperature transition from 140 to 130 thousand years corresponded to 10 °C. (the most flabby fourth cycle is apparently distorted by the near-ocean-floor ice flows). The theoretical curve in the lower figure is plotted from equations (14.2)–(14.9) accounting for the Milankovic cycles and describes changes in the Earth's average temperatures: 1. Temperature fluctuations caused by changes in Earth's precession angle (here, the maxima of curve 1 are superposed on extrema of the experimental data); 2 and 3. Temperature fluctuations caused by the precession of the orbit of Earth-around-Sun revolution (two major harmonics with periods about 40 and 22 thousand years are the Milankovic cycles); 4. Composite temperature change as affected by all causes.

As we see, the correlation between the theoretical and experimental temperature curves is quite good although the theoretical curves are more smoothed.

We will now compare the theoretical glaciation curve of the last (Würm) climatic cycle with the independent geological data about the ice sheet distribution in Canada and the US as quoted by Imbrie and Imbrie (1979). The comparison is illustrated in Fig. 14.14, which shows that both curves are similar (with the slight deviations in ages and scales). It is also possible that some glacier traces (the end moraines) of somewhat earlier glaciation phases (for instance, the phases about 70,000 years ago) were just obliterated in the last phase of glaciation which substantially overlaid the area of earlier phases.

Obviously, the shape of the theoretical curve substantially depends on phase relationships between the main cycles of the lunar–Earth and "glacier" temperature fluctuations, precession cycles of the Earth-around-Sun revolution orbit and precession of Earth own revolution. Based on these, we select the best fit between the theory and experimental isotope temperature determinations in the Antarctic ice sheet from the phase shift of the component climatic fluctuations. After that, the future climate changes can be forecast (see an example of such forecast in Fig. 14.15).

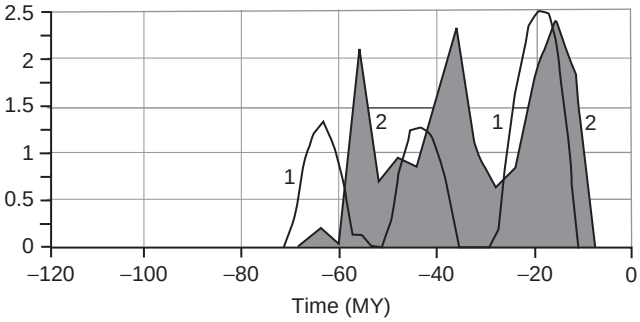


**FIGURE 14.14** Glaciations distribution in the northern continents determined from the theoretical temperature curve of the latest (Wurm) Pleistocene precession climatic cycle (curve 1). Average Earth surface temperature (10 °C) was assumed as the threshold of the glaciation start. Shaded field of curve 2 is averaged glaciations distribution in Canada and USA determined from the positions of border moraines in North America (Imbry and Imbry, 1988) (arbitrary vertical scale on both diagrams).

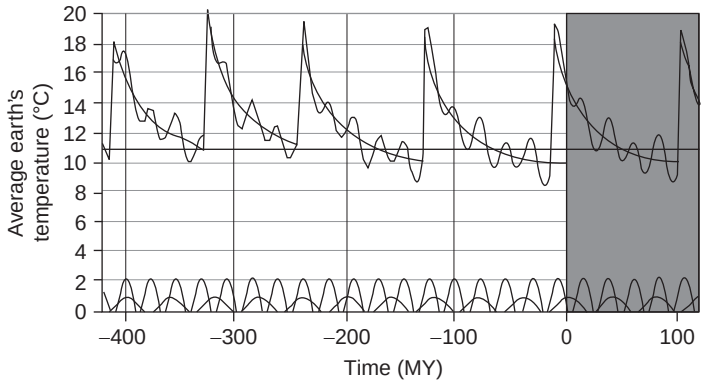


**FIGURE 14.15** Temperature forecast for the next 120 thousand years is presented by the shaded portion.

Thus, as a result of the Moon–Earth connections, slow but regular climate cooling episodes periodically occurred in Pleistocene. Every one reached 8–10 °C and lasted 100–120 thousand years. After the emergence of thick ice sheets came rapid, within just a few thousand years, climate warming by the same 8–10 °C and equally rapid glaciation degrading. Therefore, the Moon–Earth connections in combination with the Earth's glaciations excite substantially nonlinear self-oscillatory climatic processes so typical of the entire Late Pleistocene. The future climatic forecast is only a cooling, probably the most severe of all preceding cooling episodes. As a reminder, such general cooling occurs due to life activity of the nitrogen-consuming bacteria which continuously lowers the nitrogen partial pressure (Fig. 12.8) and hence the general atmospheric pressure (Fig. 12.15). The atmospheric pressure decline, under Eq. (13.12), unavoidably leads to the Earth's climate cooling which occurs under the increasing regime, at least since Riphaean (see Fig. 14.19–14.21).

The warm climate during the second half of Mesozoic was due to the formation at that time of the supercontinent Pangaea (see Section 9.6) and to the accelerated oxygen generation caused by a broad advance of the flowering plants which temporarily compensated the decline in the nitrogen partial pressure. After Pangaea began to destruct and oxygen pressure stabilized, a new cooling phase started in Cenozoic despite an increase in the solar luminosity. Calculations indicate that the average surface temperature at the end Mesozoic reached +1 to +19 °C (the present-day value is +15 °C).

## 14.4 EFFECT OF CONTINENTAL DRIFT ON EARTH CLIMATE

Thus, the continents positions on the Earth's surface can affect its spherical symmetry and temperature regimes. This effect is difficult to calculate, however, as we do not know the mantle's density anomalies and the core surface topography which was mentioned in the previous section. Presently, this contribution is relatively small, just $\Delta M_{\text{cont}+m} \approx 0.2 \times 10^{29}$–$0.6 \times 10^{29}$ cm$^2$ g/s$^2$. It was different with the supercontinents. Their component continents were compactly positioned usually in the low latitudes (see Chapter 9), with the combined centers of mass at the equator ($\varphi = 0$) (Monin, 1988, 1999). In such a case, moments of force $\Delta M_{\text{cont}+m}$ drastically increase (Monin, 1988, 1999). It is difficult to make the determination of a direct contribution from the continental drift to the Earth's precession, we used an indirect approach and determined the precession angles from the oceanic paleo-temperatures in the past geological epochs.

Chumakov (2004a) indicated that the surface temperatures of the Sargasso Sea, which was positioned 100 MMY ago in the tropical belt at about 20°N, ranged between +25 and +30 °C. Maximum temperatures (apparently at the equator) were even higher, +28 to +32 °C. The temperatures at the poles were at that time above the freezing point. We determine from Eq. (13.12) that about 100 MMY ago, at the $T_{\text{eq}} = 32$ °C and positive temperatures at the poles, the precession angle must have been 34°.

Beside the quoted Cretaceous paleo-temperatures, the determination of the precession angles during the past geological epochs may be facilitated by the data on the glaciation eras distribution as displayed in Fig. 14.6.

Thus, the stationary precession angle at the Pangaea formation reached 34°. For the other supercontinents, based on their reconstructions and smaller mass (see Fig. 9.13), the precession angles were smaller (Fig. 14.16). During the time intervals between the moments of the supercontinent formation, we assumed the precession angles close to the stationary value of 6–8°.

The precession angle drastically increased during the Monogaea formation above the descending mantle flow. The reason was that simultaneously with the emergence of the supercontinent, a depth matter from the primordial Earth's kernel, which at that time was being displaced by the core formation, was rising on the opposite side of the equatorial zone (Sorokhtin, 2004; Sorokhtin and Ushakov, 2002). Such a rise of the depth matter must have created a substantial mantle "swelling" at the equator (see Fig. 4.1-e) which significantly disrupted the Earth's spherical symmetry.

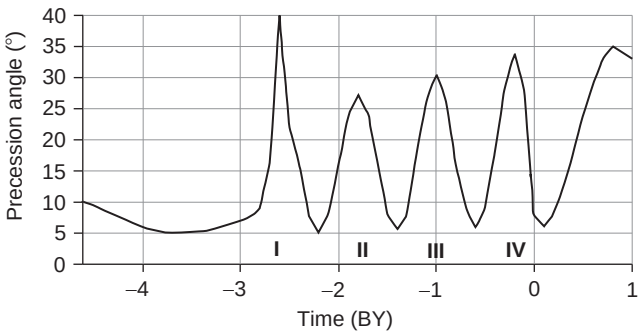


**FIGURE 14.16** Probable precession angle changes at the times of supercontinent formation: I. Monogaea; II. Megagaea; III. Mesogea (Rodinia); IV, Pangaea. It was assumed that the Monogaea, Megagaea, and Mesogea excess masses were, respectively, 0.7, 0.8, and 0.9 of the Pangaea mass and that the future supercontinent Hypergea, due to the pending weakening of the Earth's tectonic activity, will form only in about 0.8 BY.

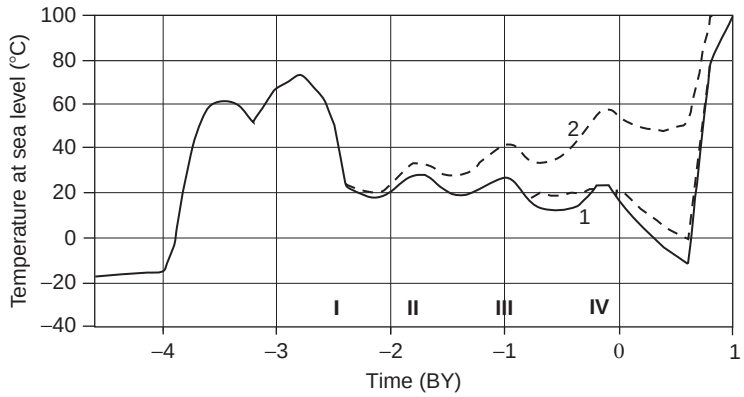


**FIGURE 14.17** Earth's climate evolution: effect of the continental drift and supercontinent formation on the Earth's average sea level temperatures: 1. Average temperature at sea level taking Earth's precession into account; 2. Average Earth's temperature in the absence of the nitrogen consumption by bacteria; thin dashed line is average Earth's temperature during interglacial stadials; Roman numerals are supercontinent formation times: I. Monogaea, II. Stille's Megagaea, III. Mesogea (Rodinia), IV. Wegener's Pangaea.

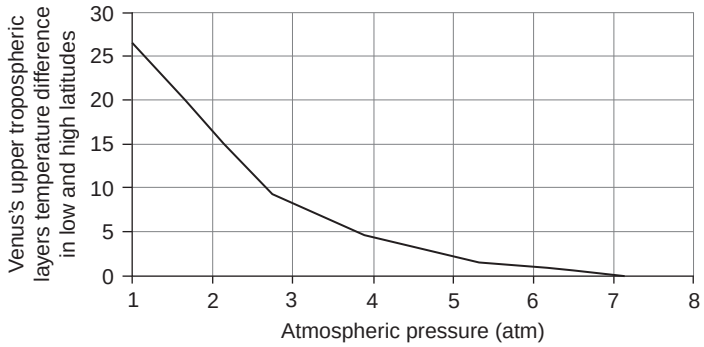


**FIGURE 14.18** Latitudinal climatic zoning in the upper Venusian atmosphere determined from the temperature difference between the low (0–30°) and high (75°) latitudes between 33 and 50 km (Planet Venus, 1989)

Using the precession angle change model (Fig. 14.16), we were able to determine the average Earth's temperature fluctuations at sea level (Fig. 14.17)

The changes in tropospheric temperatures on Earth as well as on Venus in the low (0–30°) and high (75°) latitudes, but at the elevations where pressure is commensurate with the pressure within the Earth's troposphere, show that the climatic contrasts as determined by the temperature differences at those latitudes are approximately inversely proportional to the atmospheric pressure (Fig. 14.18).

Using this pattern, we determined evolution in the latitudinal temperature distribution also in the Earth's atmosphere, that is, determined not only the average temperature but also the temperature at the equator $T_{eq}$ and at the poles $T_{pl}$:

$$T_{eq} \approx T_s + \delta T \times 0.36; \quad T_{pl} \approx T_s - \delta T \times 0.64, \tag{14.11}$$

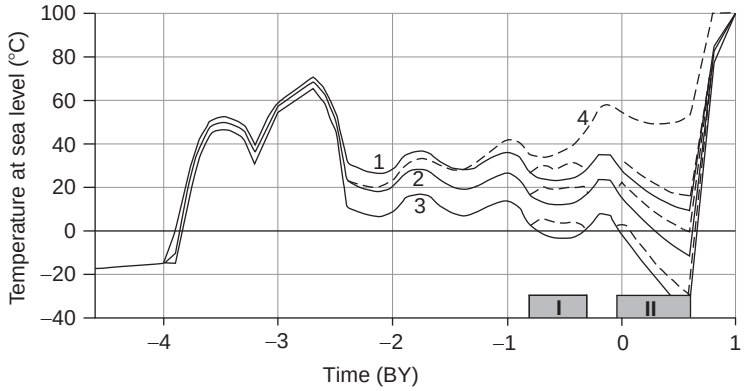


**FIGURE 14.19** World Ocean temperature evolution in connection with the superposition of joint atmospheric pressure change actions (Fig. 12.15) and of precession angles (Fig. 14.16); 1. Oceanic temperature at the equator; 2. Average oceanic temperatures; 3. Oceanic temperatures at the poles in Proterozoic and Phanerozoic (dashed lines over curves 1–3 are the temperatures at the times of interglacial stadials); Shaded blocks I and II are glaciation eras of the polar oceanic basins in Riphaean and Phanerozoic.

where $\delta T \approx \Delta T_0/p_s$; $\Delta T_0 \approx 30\,^{\circ}\mathrm{C}$ is the current temperature difference at the equator and poles (not considering the snow cover albedo effect); $p_s$ is the current near-surface Earth pressure. The $T_{eq}$ and $T_{pl}$ determination results for the World Ocean are displayed in Fig. 14.19.

Vast snow-covered polar areas with high albedo (about 0.7) must have substantially lowered temperatures. Considering that the polar areas are illuminated by Sun at half-level of the other areas (see Section 13.3) we get from Eq. (13.12) the equation for the temperatures in such snow-covered areas:

$$T_e^* = b^{\alpha}\left[\frac{S(1-A)}{\sigma \times 2\left(\frac{2}{1+\cos\psi}\right)}\right]^{1/4}\left(\frac{p}{p_0}\right)^{\alpha}. \tag{14.12}$$

This equation (14.12) enables the approximate determination of the ice sheets at various altitudes in the polar areas. We assume the present precession angle of $\psi = 23.44^{\circ}$, average albedo for the Arctic Ocean of $A_N = 0.66$, albedo for the Central Antarctic of $A_A = 0.69$, with the average temperature gradient over Antarctica at $\mathrm{grad}T = 7.8\,\mathrm{K/km}$. Then, from Eq. (14.12), and in consideration of Eq. (13.17′), we derive the average annual temperature at the North Pole of $-22.8\,^{\circ}\mathrm{C}$ (the empirical data are $-23\,^{\circ}\mathrm{C}$; Khromov and Petrosyants, 2001). Similarly, we find the temperature for the central Antarctic at the altitudes of 1, 2, 3, and 4 km above sea level: $-36.6$, $-44.7$, $-52.8$, and $-60.9\,^{\circ}\mathrm{C}$. To verify these theoretical calculations of the average temperatures, we compared them with the experimental data (in-well determinations) of annual average temperatures $\overline{T}$ in the Central Antarctic where the oceanic cyclones almost never penetrate. Kotlyakov (2000) quotes for the Dome-C, elevation 3.24 km above sea level, $\overline{T} = 53\,^{\circ}\mathrm{C}$, for the stations Komsomolskaya and Vostok, at the elevations about 3.5 km above sea level, $\overline{T} = -55$ and $-55.5\,^{\circ}\mathrm{C}$. Based on our with Kapitsa data (measurements of the average temperatures in wells), the annual average temperature at the crest of the Main Antarctic Dome (elevation about 4 km) was $\overline{T} = -60\,^{\circ}\mathrm{C}$.

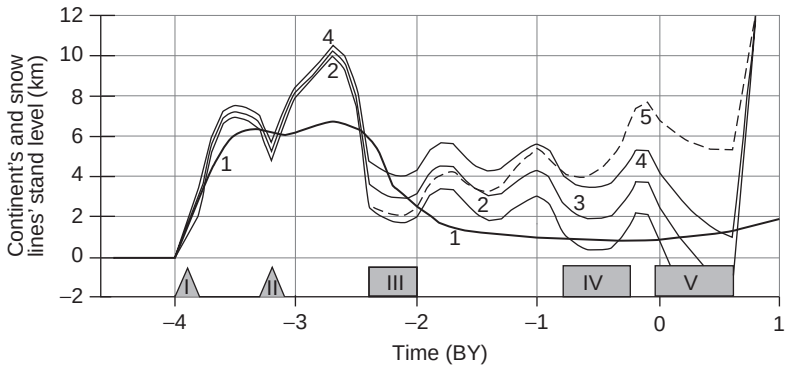


**FIGURE 14.20** Continent and snow-line elevations: 1. Average continent stand elevation; 2. Snow-line elevation at the poles; 3. Average elevation of the snow-line; 4. Snow-line elevation at the equator; 5. Snow-line elevation at the poles assuming no bacterial consumption of nitrogen; I. Early Archaean high-altitude continental glaciation at the equator; II. Middle-Archaean (3.2 BY ago) high-altitude glaciation at elevations about 6 km; III. Early Proterozoic (Huron) high-altitude glaciation at elevations about 3–4 km; IV. Late-Riphaean–Paleozoic high-latitude continental glaciation era; V. Cenozoic and future high-latitude continental and marine glaciations.

Using Eq. (14.12) at the same elevation, with the temperature gradient of 7.8 K/kmм, the theoretically determined temperatures are −54.9, −56.9, and −61.9 °C. We believe this is an acceptable fit.

It must be mentioned that our theoretical estimates can only cover relatively extended time intervals, that is, eras (see Fig. 14.20) during which individual glaciation epochs could emerge. In order to identify the glaciation epochs, we need to include the continental drift, Earth's precession angle changes and the astronomical Milanković cycles. The reason is that for a glaciation to occur the climate cooling alone is insufficient. The continents need to be located in the polar areas and also, according to the precession cycles, the solar radiation needs to be at its minimum during these epochs.

Figure 14.20 displays the continent stand elevations (see Fig. 7.10) and snow-line elevations, and Fig. 14.21, the continent surface temperature and also theoretically estimated continental glaciation eras. A comparison with the geological data on glaciation epoch distribution (Chumakov, 2004b; also see Fig. 14.6) as well shows a nice match between the calculations and empirical data.

As Figs. 14.19–14.21.21 show, each epoch of the supercontinent formation was accompanied by a rise in the near-surface temperature. For instance, during the emergence 2.6 BY ago of the first supercontinent we call Monogaea the average temperature $\overline{T}_{oc}$ at the ocean level exceeded 70 °C. When Stille's Megagaea was forming 1.8 BY ago, $\overline{T}_{oc}$ approached 30 °C, and the formation 1 BY ago of Mesogea (Rodinia) was accompanied by the temperature that declined to 26 °C, whereas 200 MMY ago Wegener'e Pangaea formed accompanied by the temperatures 24 °C and lower. Between the supercontinent formation epochs the average temperatures at the sea level declined by 7–10 °C.

We will now discuss the causes why the identified Earth's glaciation epochs emerged.

We will start with the oldest Early Archaean era. The temperatures anywhere on the Earth's surface were negative in Katarchaean. By 3.8–3.7 BY ago the temperatures at the equator became positive. Thus, the temperatures of young marine basins which were also

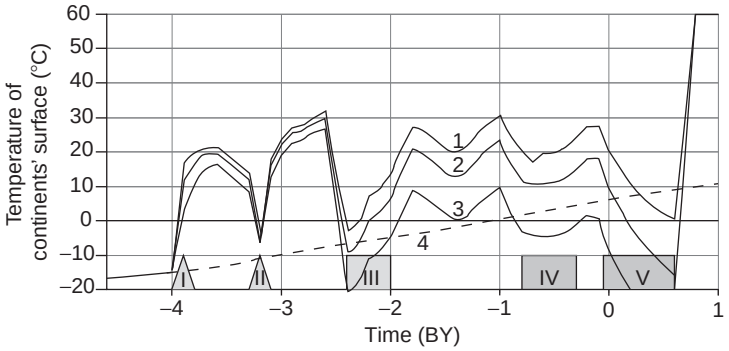


**FIGURE 14.21** Evolution of the continental glaciation eras: 1. Continental temperature at the equator; 2. Average surface continental temperature; 3. Continental temperature at the poles; 4. Temperature of the absolute black body; I. Early Archaean high-elevation continental glaciation at the equator; II. Middle-Archaean (3.2 BY ago) high-altitude glaciation at elevation of about 6 km; III. Early Proterozoic (Huron) high-altitude glaciation at elevation of 3–4 km; IV. Late-Riphaean–Paleozoic high-latitude continental glaciation era; V. Cenozoic and future high-latitude continental and marine glaciations.

located only within a narrow equatorial belt rose above zero (see Fig. 14.19). The summits of young continental formations (probably at elevations of 3–4 km), although at the equator, were within the domain of negative temperatures. Glaciations I over these formations were local and high-altitude, possibly even without the real glaciers as there was not much water on Earth at that time. This probably is why there are no traces of the Early Archaean glaciation in the geological record.

The Middle Archaean glaciation II in Fig. 14.21 occurred 3.2 BY ago due to a decrease in the tectonic activity and general atmospheric pressure (see Fig. 12.15). This glaciation could develop not only in the high latitudes but also in the moderate latitudes as by that time the width of the tectonically active zone spread to $\pm 40^\circ$ to $50^\circ$ latitude. The young continental shields could also drift to these latitudes. Along with that, their average elevation rose to about 5.5–6 km (see Fig. 7.10). In Middle Archaean, the amount of water in marine basins noticeably increased (see Fig. 11.4). The water temperature rose to $+30$ to $+40\,^\circ$C, which increased evaporation. For these reasons, the Middle Archaean high-altitude glaciation could have been accompanied by the formation of small ice sheets which left their trace in the geological record.

In Early Proterozoic, real oceans emerged. They have not been very deep, with the average depths of around 1 km. At the same time, the continent stand levels were still relatively high, on the average 3 to 4–5 km (see Fig. 7.10). In the beginning of our third glaciation era called Huron glaciation (group III in Fig. 14.21), ice sheets could develop at all latitudes. After the disintegration of the first supercontinent Monogaea, the "fragments" standing high over the ocean level were dispersed all over the surface of the globe. In the middle and at the end of the third glaciation era (2.4–2.1 BY ago), the ice sheets could arise at all latitudes regardless of the continent fragment's latitude. That is supported by the field data. The glacier deposits of that age (indicating a sheet cover nature of the glaciation) are known practically on all ancient continental massifs: in several places in North America (including the Huron Formation), in Europe (on the Baltic shield), in South Africa (in the formations of

Transvaal and Griekwaland) and in Western Australia (the Turi Formation). The glaciation age in all these regions is similar, about 2.4–2.2 BY ago.

Calculations indicate (see Fig. 14.21) that between 2 and 0.8 BY ago there were no negative annual average temperatures anywhere on the continents. Thus, there should not have been continental glaciations. That is exactly what actually happened: Chumakov (2004b) wrote that no traces of glaciations were discovered in the older horizons of Middle Proterozoic, in Early Riphaean and most of Middle Riphaean. That was a lengthy no-glaciation period in the Earth's history.

A new, fourth era of the continental glaciations began in Late Riphaean and Paleozoic. It was associated with a noticeable climate cooling (group IV in Fig. 14.21). Vast snowy expanses on the planet's poles had high albedo (about 0.7) and must have had lower temperatures. See Chumakov (2004c, 2006) for a detailed description.

What is interesting is that despite rather severe continental glaciations, apparently there were no stable marine glaciations (like the modern Arctic Ocean) neither in Late Riphaean, nor in Paleozoic. That was because at that time the polar areas of oceans and seas had only slightly negative annual average temperatures. That is why they had to melt in-between glaciations (see Fig. 14.20).

In the middle of Cenozoic (50 MMY ago) the last, fifth glaciation era began. The glaciation epochs within this era produced the most extensive ice sheets in the Earth's evolution. This fifth glaciation era will continue in the future although it will be the last one (group V in Fig. 14.21). Simultaneously, first in the Earth's history marine glaciations happened over the Arctic and part of the Southern Oceans (the Ross Sea and Weddell Sea shelf ice sheets) in Oligocene or Miocene. That, in turn, substantially lowered the near-bottom water temperature from $+16\,^{\circ}\mathrm{C}$ at the Paleocene/Eocene time boundary to $+2\,^{\circ}\mathrm{C}$ presently (see Fig. 14.4).

As a result of the climate cooling (especially in Pleistocene), stable negative annual temperatures reigned on the continents positioned close to the poles. Unavoidably, ice sheets must have emerged on such continents. If their area was significant, the snow cover albedo began to play role, and depending on the ice cover elevation the temperatures over the continents declined from $-40$ to $-60\,^{\circ}\mathrm{C}$. We verified these theoretical estimates of the average temperatures on the surface of ice sheets compared with the experimental annual average temperatures $\overline{T}$ in the Central Antarctic (where there are practically no oceanic cyclones) using Eq. (14.12).

## 14.5 EFFECT OF SOLAR ACTIVITY ON CLIMATE

As mentioned, the currently prevailing idea among the environmentalists and many climatologists is that of carbon dioxide accumulation in the atmosphere as the cause of a substantial climate warming. This idea was inculcated on many politicians and governments and is being actively pushed by the mass media. In particular, this process is placed at the root of the climate warming during the recent decades.

We showed earlier that a significant carbon dioxide accumulation (on the order of 1–0.1 bar) may only cause climate cooling (see Fig. 13.8) whereas a small accumulation (on the order of 0.001 bar or hundreds or even thousands ppm) has no discernible effect on the climate. As for the latest warming, based on the geological data it was occurring

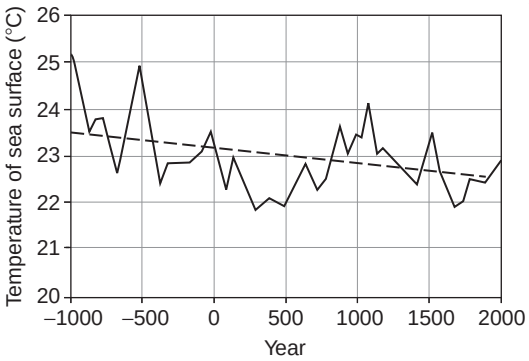


**FIGURE 14.22** Sargasso Sea surface temperatures (50 year averaging) determined from the oxygen isotopic ratios in the remains of the marine plankton from the seafloor deposits (Kegwin, 1996). Dashed line is the temperature trend about $3.3 \times 10^{-4}$ deg/year.

against the background of a general climate cooling (Fig. 14.22) with a gradient of approximately $-0.33\,^{\circ}$C/1000 years. Our theoretical calculations (Figs. 14.13 and 14.15), over about the same time interval (0–4 thousand years ago), show that the cooling gradient was $-0.32\,^{\circ}$C/1000 years which is a good fit with the experimental data.

Geological data also support the Earth's climate fluctuations against the backdrop of its general and regular cooling. For instance, oxygen isotopic shifts in the remains of plankton foraminifers and other microorganisms from the Sargasso Sea indicate a regular temperature decline of the surface waters, although with some fluctuations, during the recent 3000 years (Fig. 14.22). As this figure shows, we are now experiencing the conditions of the "summit" of a next, albeit not most significant, warming which began in the XVII century when certainly there were no technogenic carbon dioxide releases into the atmosphere. That is why a new climate cooling phase may begin in the nearest future (possibly it has already begun).

Byshev et al. (2005) noticed an interesting pattern in the modern climate. It turned out that the secular trend of the near-surface air temperatures over the continents and oceans in the XXth century was directed differently. For instance, a substantial temperature increase over the land occurred in the second half of the last century which is almost completely absent over the oceans. The tendency was discovered of returning the climatic system to the status preceding the 1970s. This indicates that in the nearest future the heating observed in recent years can stop. A rapid climate restructuring in the 1970s apparently happened due to El Nino which was accompanied by the changes in the global cloud cover and the heat flows over the oceans (Byshev et al., 2009a).

The present warming has a clearly expressed natural origin and may be soon replaced by a new cooling phase (Landscheidt, 2003). The instrumental temperature observations were conducted in the Southern England since 1749, and the instrument observations of the Sun's magnetic activity (the number of Sun spots or the Wolfe number) in France, since the mid-1750s. Comparison of these data indicates a very high degree of correlation between the near-surface air temperature and Sun's magnetic activity (Fig. 14.23). That is why it is absolutely necessary to involve the data on periodic fluctuations of the solar activity for middle-term forecasts of the climatic changes. Estimates by the Pulkovo Observatory (Abdusamatov, 2003) forecast the beginning of a slow temperature decline already in 2012–2015 годах, with the global minimum reached around 2055–2060. This situation will be maintained for 50–70 years, and in the beginning of the XXII century a new cycle of global warming will begin.

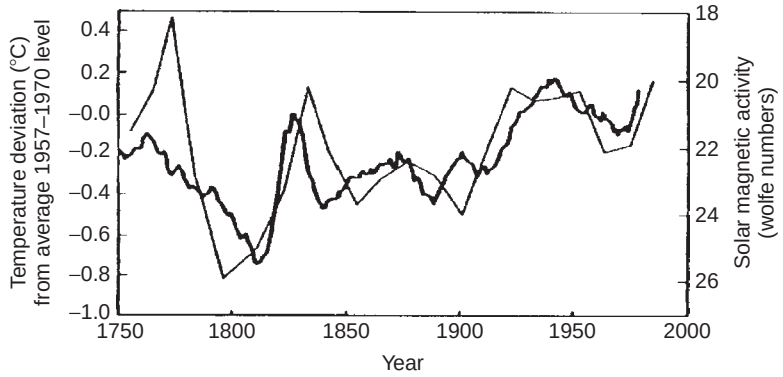


**FIGURE 14.23** Correlation between temperature fluctuation in the northern hemisphere and the solar magnetic activity (Wolfe's numbers). Left axis and heavy line are deviations of the average surface temperatures in the northern hemisphere with the current 11-year smoothing, °C. Right axis and thin line are averaged solar magnetic activity (Wolfe's numbers). Bursts of the magnetic cycles correspond to more active, hence, brighter Sun (Robinson et al., 1998).

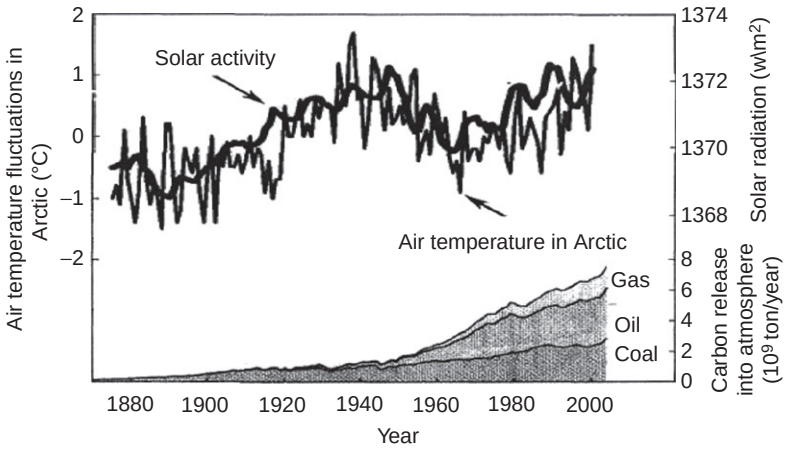


**FIGURE 14.24** Near-surface temperature in the Arctic versus solar activity compared with the carbon dioxide content increase in the atmosphere (Robinson et al., 2007).

Such climatic variations are clearly determined by periodic (pulsating) changes in the Sun's luminosity (Robinson et al., 1998) (see Fig. 14.23). These changes, in turn, are probably associated with fluctuations of Sun's size and area, and those depend on the intensity of nuclear reactions going on within it (Abdusamatov, 2003).

More detailed correlation between the near-surface temperatures in the Arctic region and the Sun's activity pulsations is displayed in Fig. 14.24 (Robinson et al., 2007).

It is also interesting that the Sun's activity curves and the temperatures in the Arctic region well match the snow accumulation in the internal Antarctic. One of these authors (O. Sorokhtin) visited the Antarctic Pole of Inaccessibility (82.1°S and 55°E) in 1958 and in 1964. There practically was no snowfall there during this 6-year interval so that even the tracks from the first visit have not been

covered by the snow. In 2008, an international expedition visited the Pole of Inaccessibility and found that over the subsequent 44 years not only the work shack on sledges but also part of the drilling rig (for drilling shot-holes in the process of a seismic survey for the determination of the snow cover thickness) were covered in snow. The total snow accumulated there over that period was 4–5 m (although it was in part caused by the snow eddies behind the shack).

The diagrams in Fig. 14.24 provide the complete explanation of a nonuniform snow accumulation in the internal Antarctic. Indeed, the late 1950s through the early 1960s was the period of a local climate cooling which caused the set-in of the anticyclonic and snowless conditions in the Central Antarctic. In the 1970s, the Sun's activity and tropospheric temperature noticeably increased. A climatic reaction was increased water evaporation from the oceans and increased synoptic activity in the troposphere as already mentioned in Section 13.7. As a result, water-soaked cyclones began to penetrate the internal Antarctic which caused the accelerated snowfall, including at the Pole of Inaccessibility.

That is why, and contrary to Gore's (2006) forebodings of the ostensible melting of the Antarctic glaciers and drastic rise of the ocean level, during the recent decades the ice intensely accumulated in the Antarctica which could have caused a drop in the ocean level and not its catastrophic (!?) rise.

We believe that the provided data irrefutably prove that all climatic fluctuations (including the recent 30-year-long warming) are caused only be the solar activity and have nothing to do with the increase in carbon dioxide partial pressure. We need to take into account that, beside the 11-year cycles, the dominant period in fluctuations of the solar activity averaged over the current 11-year interval is approximately 60 years. Based on this it is possible to make a conclusion that the climate cooling either have already begun or will begin shortly. In 30 years, a rather noticeable (by 1–1.5 °C) decline of the surface temperatures will occur (at least in the northern hemisphere).

A known German climatologist Landscheidt (2003) came to a similar conclusion. He wrote in his large article ("New Little Ice Age Instead of Global Warming?") that, despite the continuing increase in the atmospheric carbon dioxide partial pressure, our nearest future is that of a cooling and of the onset of a little ice age similar to that of the XVII–XVIII centuries with the temperature drop by one degree or greater. A first significant cooling impulse is anticipated at around 2030, and a much more severe cooling, with the temperatures declining to the early XVIIth century level, is forecast for 2200.

This conclusion by Landscheidt (2003) and the forecast by Abdusamatov (2003) perfectly match our forecast as shown in Fig. 14.15. In the mean-time, in the nearest future we anticipate a slight climate cooling because after the solar activity maximum of 2007 the transition will begin to a new quiet Sun period. What needs to be kept in mind is that, as mentioned before, due to great heat capacity of the surficial oceanic water, the climatic reaction on the decreased solar activity lags a few years relative to its 11-year cycles. In order to obtain the total picture of the future climate changes both forecasts derived from the precession climatic cycle mechanism and from the analysis of the changes in solar luminosity must be combined. This shows the importance for the Earth's climatic studies of the knowledge of the solar activity and, most of all, its forecast for the future.

Beside the solar activity, as previously mentioned, changes in the planet's precession angle strongly affect its climate. A reminder: a smooth decrease in the precession angle results in the no less smooth climate cooling (Fig. 14.10). The cycle is about 100–120

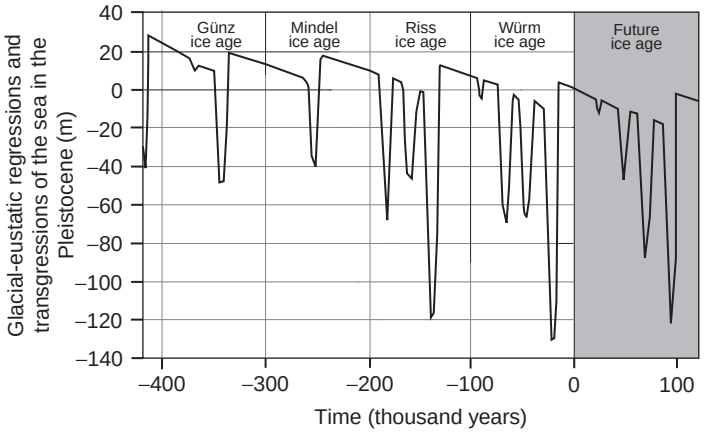


**FIGURE 14.25** Glaciological sea level fluctuations in Pleistocene. The present-day sea level is taken for the zero elevation. Regressive phases removed from the climate forecast curve for the next 120th years (see Fig. 14.15), and their alternating transgressive phases are constructed in consideration and with averaging of the terrace elevations on the oceanic islands quoted in Bowen (1981).

thousand years long, so we do not notice it. But as soon as the average surface temperature reaches the critical level (which we estimate at about 11°C; see Section 14.3), all high-latitude continents immediately become glaciated. As a result, the ocean level rapidly declines. Kotlyakov (2002) estimated that about 20 thousand years ago the World Ocean level dropped by at least 125 m. However, the subsequent postglacial transgression (10–12 thousand years ago) rapidly (over a few thousand years) raised the ocean level above the present-day elevation.

If we assume that the water mass concentrated in the ice sheets is proportionate with the difference between the critical and average Earth's temperature (Fig. 14.15), we can estimate the declines in the oceanic level corresponding o the other glaciations. In such an estimate we accepted that the oceanic level drop during the last phase of the Wurm glaciation (about 200 thousand years ago) reached 130 m. See Fig. 14.25 for the calculation results.

Just a side note: during the last phase of the Wurm (Valday) glaciation the Bering Strait dried out, and the East-Siberian tribes about 12,000 years ago could migrate over the dry land o Alaska and populate first the North and later the South America (Bowen, 1981).

Summarizing, we need to state that the problem of changes in the global climate must be solved in a systemic way and based on a strict physical theory accounting for the evolution in the atmospheric composition, the geological environments, the fluctuation in the Sun's luminosity, the Earth's precession and oceanologic data, for the feedbacks within this complex system. The explanation using a fictional correlation between the climate and the atmospheric concentration of the so-called greenhouse gases will not suffice.

## 14.6 CLIMATIC EPOCHS OF THE GEOLOGICAL PAST AND FUTURE

Analyzing the energy model of Earth's evolution we showed that its climate is determined by the solar activity as well as by the atmospheric pressure and composition. Thus, it depends not only on the external factors (intensity of the solar insolation) but also on its internal evolution which gave birth to the atmosphere and hydrosphere. In the course of

Earth's evolution, the solar activity was gradually increasing but no more than by 20–25% (see Fig. 14.2) and with relatively minor fluctuations (see Fig. 14.22). For this reason, the major and most substantial changes in the Earth's climate are associated with the global evolution per se. Therefore, the climate evolution should be discussed in a close contact with the tectonic evolution.

As a reminder, there were three fundamentally different tectonic eras in the planet's geological history.

The oldest era, Katarchaean (4.6–4.0 BY ago) experienced very low endogenous activity although the planet's surface was shuddered with intense tidal earthquakes associated with the close Earth–Moon distance at that time (see Section 3.3).

The Archaean era (4.0–2.6 BY ago) was very active. It was the time intervals of the core separation accompanied by a tempestuous tectonomagmatic activity. It began at the equator and spread by the end Archaean over the entire planet. First blocks of the continental crust (kernels of the future continents) appeared at that time. By the end Archaean (about 2.7–2.6 BY ago) the tectonic activity reached its maximum.

Beginning in Early Proterozoic (after the core separation) the planet's tectonic activity drastically declined. This decline and fade-out of the endogenous processes in Earth will continue in the future until they completely die-out about 1.5–2 BY from now.

We indicated earlier that in Katarchaean, most likely, there was no hydrosphere or a high-density atmosphere (see Section 12.1). The primary atmosphere's density may have reached $10^{-3}$ atm; the solar activity at the time was 20% below the present one. Thus, the climate was very severe, with low temperatures reigning everywhere.

With the advent of Archaean and after the core separation process had started, the mantle began to degas. At the same time, first shallow marine basins appeared, and carbon dioxide and nitrogen entered the atmosphere. Since then, the atmospheric pressure was rapidly rising (see Fig. 12.15) and 50 MMY ago exceeded 1 atm. with the near-surface temperature rising almost to 280 K (7 °C). In the middle of Early Archaean (about 3.5 BY ago) total atmospheric pressure rose almost to 5 atm, and by the end Archaean exceeded 6 atm. Naturally, increase in atmospheric pressure led to the emergence of a substantial greenhouse effect with the rise of the Archaean average temperatures to 60–70 °C. As a result, during the second Archaean climatic epoch the climate was very hot despite a weak Sun luminosity.

As was numerously mentioned above, after the core separation at the Archaean/Proterozoic time boundary Earth's tectonic activity drastically declined. Instead of thin basalt sheets, the modern-type oceanic crust emerged with a 2 km-thick serpentinite layer. Carbon dioxide was rapidly consumed from the Archaean atmosphere under reactions (11.7) and (11.7′), and the climate became moderately warm. That was the advent of the third tectonic era of Proterozoic and Phanerozoic.

In Proterozoic, the atmosphere became almost purely nitrogenous with gradually declining pressure due to the life activity of the nitrogen-consuming bacteria and to thunderstorms. Oxygen appeared in the end of the third epoch but it could not compensate the total decline of the atmospheric pressure. As a result, the third climatic epoch displayed a substantial temperature decline and general climate cooling. It led in Riphaean, Paleozoic, and especially Cenozoic to the emergence of rather severe glaciations (the previous glaciations in Archaean and Early Proterozoic were only high-altitude phenomena). The third

climatic epoch is lasting about 2.5 BY now. In its temperature regime and atmospheric composition it became most favorable (especially in its last quarter) for life on Earth.

The climate cooling will continue until about 600 MMY from now the abiogenic oxygen will start degassing from the mantle. Oxygen will be released at the core formation from the mantle iron which will be oxidized by that time to the maximum (see reactions 4.45). After that, the atmospheric pressure will start rising rapidly. It will be deadly for all living on Earth as it will burn in the oxygen atmosphere. Thereafter, the almost unlimited increase of the greenhouse effect will begin. The oceans will boil out. Earth will turn to a hot planet like Venus. There will be no life on Earth. This will be a fourth era of an extremely hot and lifeless climate.

To summarize, the proposed energy model of the global evolution enables a natural way of describing changes of climatic epochs in the geological past and future.

In the very distant future (several billion years from now), Earth will meet with a real catastrophe. The Sun-type stars in the end of their life violently expand, their brightness rapidly increases and eventually they blow up leaving after themselves a small but very bright kernel, a "white dwarf" starlet (Aller, 1971). The Sun explosion will blow away the emergent hot gas–vapor atmosphere. Thereafter, depending on the mass of the discarded solar matter, Earth will have to move to a more distant orbit or, as a slingshot, will be cast out to the edge of the Solar System or even outside it into the outer space.

CHAPTER

# 15

# Origin and Major Stages of Life Evolution on Earth

## 15.1 UNIQUENESS OF EARTH

We will now review the main stages in the emergence and evolution of life on Earth and geologo-climatic processes which led to the appearance on Earth of conditions conducive to the existence of higher life forms. Upon reviewing the aforementioned Earth's evolutionary specifics, it becomes clear that its evolutionary path was predetermined by its place within the Solar System, by the Sun's luminosity, and by Earth's mass and chemical composition. Should our Sun have belonged with the variable stars, the Earth's climate would have been alternatively intolerably hot or freezing cold. Should the Sun's mass have been substantially greater than it is, then in just a few hundred million years upon its formation it would have blown up and converted into a neutron star or even a black hole. We and all living things on Earth are very lucky that the Sun is a quiet star with an average star mass and belongs to the dwarf-stars, spectral class G2, and is a stationary star with only slightly variable luminosity over many billions of years. This is especially important because it allowed the Earth's life over the last 4 BY to travel a long evolutionary way from the nascence of primitive life to its highest forms.

The distance from Earth to the Sun also turned out to be at its optimum. At a closer distance, it would be too hot on Earth, an irreversible Venus-type greenhouse effect could have arisen. At a farther distance, Earth would be frozen into a "white" planet with a stable global glaciation.

We were also lucky with a massive satellite, Moon. Its emergence in a close near-Earth orbit substantially "pumped" the tidal energy into Earth, accelerated its tectonic evolution and span Earth in the forward direction so that the climate became more even. Without a massive satellite, Earth, like Venus, would have retarded by 2.5–3 BY in its tectonic evolution. In such a case, Earth would have been dominated now by the Late Archaean conditions with a high-density carbon dioxide atmosphere and high temperatures, and instead of the highly organized life would have been populated with primitive bacteria—single-cell prokaryotes.

*Developments in Earth and Environmental Sciences*, Volume 10
DOI: 10.1016/S1571-9197(11)10015-4

Earth, in a close interaction with the Sun and Moon, evolved into an optimal and finely balanced system which luckily provided for the emergence on our planet of comfortable conditions for the formation and evolution of highly organized life. A close review of this system shows the Earth's optimum mass capable of retaining on its surface the moderately dense atmosphere, with its exceptionally lucky chemical composition.

Indeed, even relatively minor deviations from the source concentrations within the Earth's matter of such elements and compounds as Fe, FeO, $CO_2$, $H_2O$, $N_2$, etc., could have resulted in consequences catastrophic for life. In particular, should the primordial Earth's matter have contained less water, the carbon dioxide absorption would have been less intense, and it would have accumulated in the atmosphere. That might have created as early as in Archaean an irreversible greenhouse effect, and Earth might have turned into a "hot" planet like Venus.

Should there have been noticeably more water or less free iron, Earth would have turned into an "Ocean" planet. Should the primordial Earth matter have contained less nitrogen, the planet might have as early as Early Proterozoic converted into a totally snowed-over "white" and cold planet. Should the Earth's matter have included more free (metallic) iron, the modern atmosphere, as in Proterozoic, would not be able to accumulate free oxygen, therefore, the animal kingdom could not have emerged on Earth. Conversely, had the initial iron content been lower, a profuse release of endogenous (abiogenic) oxygen would have begun presently or even earlier. Such atmosphere would have "burned" all living things. Besides, the depth oxygen degassing would have resulted in the strongest greenhouse effect, and Earth would have turned into a hot planet similar to Venus.

A conclusion from this, in particular, is that the life span of highly organized and, even more so, intelligent life on any planet in any of the Universe's stellar systems is relatively limited.

We were lucky. Earth turned out to be a harmonious planet in all respects, with a comfortable nitrogen–oxygen atmosphere and wonderful life forms. It is highly likely that a "lucky" planet like Earth is an extremely rare phenomenon in the Universe. It is unlikely that there are more such planets populated with intelligent beings in our Galaxy. We may only enjoy living on such a beautiful planet.

## 15.2 ORIGIN OF LIFE ON EARTH

The primordial Earth emerged through the accretion of the source protoplanetary matter and must have been totally devoid of life. The reason was that the very matter in the protoplanetary gas-dust cloud formed due to explosions of supernovas and was thoroughly sterilized by hard cosmic radiation way before the Solar System planets although the cloud apparently contained some simple abiogenic organic components. Besides, at that distant time there was on Earth just a very delicate atmosphere of inert gases (with a pressure of $<10^{-3}$ atm.), and there was no hydrosphere, that is, there was no medium most favorable for the emergence, habitation of life, and its protection against destruction. The reason for this is as follows. From the very beginning, the Earth's matter was drastically impoverished in volatile compounds. Those of them that were released at impacts and heat explosions of planetesimals were immediately sorbed on a very porous ground, quickly removed from

the Earth's surface and gradually buried into its depths by the continuous torrent of the protoplanetary matter. Besides, at the time of Earth's formation its surface was subjected to the exceptionally strong action of the young Sun's radiation, a powerful corpuscular flow emerging inside stars when nuclear reactions were "kindled" in them.

The Sun, like τ-Taurus stars, was in the very beginning of the main succession of its evolution. This intense flow of corpuscles (mostly the protons and helium nuclei) must have literally blown away from the Earth's surface any remains of the gas components.

After a first active evolutionary stage, the young Sun's luminosity drastically declined and about 4.6 BY ago was approximately 30–25% below the current level (Bachall et al., 1982).

By that time, at the expense of the falling planetesimals, a primordial very tenuous atmosphere was formed. The temperatures were negative even at the equator so the climatic environment on the young planet was severe. On the one hand, its surface was a cold desert. On the other hand, the planet was subjected to an intense continuous hard cosmic radiation.

The unfavorable conditions for the emergence of life were maintained on Earth until the Earth's matter degassing process had begun. This, however, could only happen after the depth temperature in the young Earth rose to the Earth's matter melting point, the asthenosphere formed and the convection motions within the upper mantle arose, that is, after the most powerful process of the Earth's matter gravity differentiation became operational. As we showed in Chapter 3, the formation of the asthenosphere and the process of Earth's matter zonal melting resulted in a drastic increase of the Earth–Moon tidal interaction and in a substantial overheating of the upper mantle in the narrow equatorial belt. All that happened approximately 4.0–3.9 BY ago.

At the early tectonic stages (Early Archaean), Earth was almost totally composed of the primordial matter. Most of the surface was covered with the primordial regolite (see Figs. 4.1-6 and 6.15). As the Earth's degassing began, carbon dioxide, nitrogen, and water started to enter the atmosphere actively. At about the same time first carbon dioxide saturated acid rains poured over the porous regolite. The bulk of humidity hitting the surface was absorbed by the primordial regolite of the young Earth. The primordial Earth's matter contained high percentage of iron, close to 13%. Water and carbon dioxide dissociated in the porous regolite and formed first links of the future organic molecules which later served the basis of life emergence on Earth. Such reactions included first of all methane formation (12.10): $4Fe + 2H_2O + CO_2 \rightarrow 4FeO + CH_4 + 41.8$ kcal/mol and formaldehyde formation (12.14): $2Fe + H_2O + CO_2 \rightarrow 2FeO + HCOH + 3.05$ kcal/mol, which also emerged at the methane photodissociation by the solar radiation (12.13): $CH_4 + CO_2 + h\nu \rightarrow 2HCOH$. Formaldehyde remained dissolved in water soaking the regolite, was washed-out of it by the rain water into the just formed and still shallow marine basins. Methane was released into the atmosphere and made it very reducing. Besides, in a humid carbon dioxide–nitrogen and methane-rich reducing Early Archaean atmosphere hydrogen cyanide (prussic acid) could form, for instance, due to the electric storms under reaction (12.15): $N_2 + 2CH_4 + Q \rightarrow 2HCN + 3H_2$, where $Q = 26.6$ kcal/mol is the reaction-used part of the thunderstorm discharges. Hydrogen was released and also was formed in the water dissociation over a hot iron in the process of the zonal differentiation under reaction (11.3): $Fe + H_2O \rightarrow FeO + H_2 + 5.84$ kcal/mol. This hydrogen, in the presence of transitional group metallic ions, played a leading role in the formation of energy basis for life on early Earth (Fedonkin, 2008).

As a result, the Earth's atmosphere became reducing. This is the most favorable condition for the emergence of life (Galimov, 2001). High porosity, the presence of transitional metals in the regolite and its sorption capacity at a sufficiently high capillary pressure could have apparently provided the conditions necessary for the formation of complex organic compounds and later on, the emergence of life.

Beside simple hydrocarbons, at the same time nitrogen oxides, nitrates, nitrites, ammonia, chlorides, ammonia sulfates, and numerous other nitrogen compounds could form in the nitrogen–carbon dioxide atmosphere due to the electric storm activity. Phosphorus compounds may have entered the solutions directly from the primordial regolite. The environment needed for the reactions under which more complex organic molecules formed in the elevated atmospheric temperature of Early Archaean was provided by the capillary pressure of water solutions in the regolite pores and by the catalytic action of the transitional metals in the regolite (Fe, Ni, Cr, Co, etc.). The formation of complex proto-organic molecules was facilitated by the following. The organoelemental compound concentration in the regolite small pores, due to their high sorbing capacity and high capillary pressure, may have reached the level necessary for the synthesis of more complex organic matter (in the marine basins these compounds would have been too diluted).

This gives a good reason to believe that life on Earth emerged within the water- or organoelemental compound-saturated primordial ground in the beginning of Early Archaean (4.0–3.9 BY ago) at the time when the reducing atmosphere formed on Earth. Thus, the emergence of life on Earth was coincident with a first and strongest tectonic and geochemical time boundary in the planet's evolution. This boundary was the beginning of the core separation (see Chapter 4) and of the Earth's matter chemico-density differentiation. These events resulted down the road in the formation of the hydrosphere, high-density atmosphere, and the continental crust. As we showed in Section 3.7, however, the beginning of Earth's tectonomagmatic activity caused the lunar basalt magmatism. Therefore, the emergence of life on Earth, paradoxical though it may sound, was clearly marked by the basalt "mares" formation on Moon.

The classical experiments by Miller (1959), Miller and Urey (1959), Wilson (1960), Oro (1965, 1966), Fox (1965) and other scientists showed that rather complex organic molecules can be synthesized from inorganic compounds heated under electric discharges or the Sun's UV radiation. A Russian scientist Oparin (1957) was also actively involved in the autochthonous emergence of life by way of organic molecules synthesizing from inorganic compounds.

Miller used a water solution of ammonia, prussic acid, and aldehyde. The solution was boiled, and electric discharges were applied to the vapors. A result was amino acids, the main building blocks of the plant and animal proteins (see Fig. 15.1)

Wilson (1960) reproduced the Miller's experiments with the addition of sulfur into the initial mixture and obtained much larger polymer molecules with 20 and more carbon atoms, and also surficial films—precursors of biological membranes.

Ponnamperuma (1965) replaced electric discharges by UV radiation. Not only the amino acids and purines were synthesized (i.e., the main components of the proteins and nucleic acids) but also, from these proteins, polymers. With the addition of the phosphoric acid, nucleotides were formed.

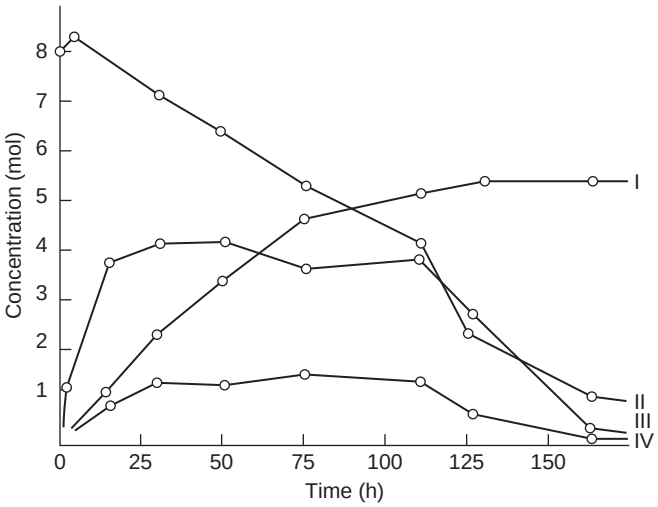


**FIGURE 15.1** Results of Miller's experiments (Miller, 1959) with electric discharges in ammonia water vapor, hydrogen cyanide, and aldehydes: I. Changes in amino-acid concentration; II. Change in ammonia concentration; III. Change in hydrogen cyanide concentration; IV. Change in aldehydes concentration.

Oro (1965, 1966) obtained large "organic" molecules by a simple heating of the source mixtures. And Fox (1965) dehydrated amino acids by heating and received compounds with the molecular weight of up to 300,000 composed of the same components as the natural proteins.

Galimov (2001), in his study dealing with the emergence and evolution of life on Earth, showed that the emergence of life must have been associated with the energy chemical reactions lowering the system's entropy. Such high-energy low-entropy reactions may occur, for instance, with the participation of adenosine triphosphate (ATF), and the synthesis of ATF was likely at the early stages on the Earth's evolution. For ATF to form, first adenine nucleobase has to be synthesized (by polymerization of prussic acid HCN) as well as ribose (by polymerization of formaldehyde HCOH). Thus, Galimov believes, ATF synthesis is the necessary step for the emergence and evolution of life on Earth.

Recently Fedonkin (2008) came up with a hypothesis of hydrogen as a leading source of protons and electrons, and also of ions of the transition group metals as primary catalysts in the formation of life's energy basis on the young Earth. That is the way for Fedonkin to reconstruct the preorganic stages in the evolution of metabolic systems, which included as the electron acceptor the nonmetals with relatively large ion radius. All these ingredients were abundant in the proposed model of the early Earth.

It was shown in all aforementioned and many other experiments of the organic matter formation out of inorganic components that for them to be successful the reducing environment in a warm atmosphere of the young Earth was necessary. Our proposed model not only suggests but also quantitatively estimates such conditions favorable for the subsequent synthesis of more complex organic and prebiological compounds. As we showed in Chapters 12 and 14, the Earth's atmosphere in the very beginning of Archaean was warm, without oxygen and reducing. It was facilitated by the presence of active catalysts (transitional metals Fe, Cr, Co, Ni, Pt, etc.) in the regolite. By that time, the most primitive associations of complex organic molecules or primitive but containing ribonucleic acids compounds could then migrate into the waters of the Early Archaean marine basins.

As Earth was degassed and its atmosphere evolved, the atmospheric reducing potential gradually decreased due to methane $CH_4$ dissociation under reaction (12.13). After a while the atmosphere became purely carbon dioxide with small methane admixture as methane was continuously generated under reactions similar to (10.4) or (12.10). This admixture could play a significant role in feeding primitive, just emerged Archaean microorganisms.

As previously mentioned, in the oceanic water methane, under reaction (12.18), is consumed by bacteria with the release, again, of carbon dioxide (especially after the microorganisms died out): $CH_4 + \text{bacteria} \rightarrow CO_2 + (\text{organic matter})$. After oxygen appeared in noticeable amounts in Late Precambrian and especially Phanerozoic, direct methane oxidation reactions (12.19) began developing: $CH_4 + 4O_2 \rightarrow 2H_2O + CO_2 + 131.2$ kcal/mol.

Further perfecting of life must have occurred due to the high-energy but low-entropy reactions (Galimov, 2001), DNA mutations, gene drift under the living matter evolution biological laws, under influence of the directional action and "filtering" properties of the ambient medium, and later, the competition.

Thus, the emergence of life on Earth may only be explained by a favorable combination of the primordial matter composition, its form on the Earth's surface (regolite with small pores), the atmospheric composition (a noticeable content of methane) and moderately high temperature in young Early Archaean basins. The first period of the emergence and existence of abiogenic organic compounds was probably short. They served as a base for the formation of the ribonucleic acids. After that, virus formation appeared. In the bio-symbiosis of such compounds and synthesis of forest amino acids and also semi-permeable membranes first cellular bacterial forms probably emerged. Subsequently, however, due to the intense Earth degassing carbon dioxide pressure rapidly increased, the atmospheric temperature rose, and the climate became hot. It is possible that it was a reason for a decline in life perfecting rate during Archaean: Archaean was dominated by only most primitive thermophilic prokaryote (nuclearless) bacterial forms like archaeobacteria of the chalcophilic or siderophilic specialization. Most likely, the energy source for these primitive life forms were then chemical reactions of the type similar to those used currently by thermophilic bacteria in hot hydrotherms ("black smokers").

As a result, probably as early as in Early Archaean, most primitive viruses and single-cell organisms (prokaryotes) emerged. The prokaryotes were separated from the ambient medium by semi-permeable membranes but did not have detached nucleus. Photosynthesizing single-cell organisms (similar to cyanobacteria) capable of oxidizing iron probably appeared somewhat later. This is supported, in particular, by the commonality in the Early Archaean sediments (3.75 BY) of iron ore formations composed of trivalent iron oxides (such as Isua Formation in West Greenland).

## 15.3 EFFECT OF GEOLOGICAL PROCESSES AND OXYGEN ACCUMULATION ON THE EVOLUTION OF LIFE

The most important factor of life on Earth is undoubtedly the environment of the habitation of live organisms in the oceans and on continents. And the habitation environment is determined first of all by the Earth's climate (Sorokhtin, 2008), that is, by the composition, state, and temperature of the atmosphere whose origin and evolution was associated with

the planet's degassing and with life activity of the organisms (see Section 12.4). As previously mentioned, the Earth's degassing begun at the Archaean/Katarchaean time boundary resulted in the formation during Archaean of a relatively high-density, substantially reducing carbon dioxide–nitrogen–methane atmosphere. In Archaean also appeared volcanoes, differentiated magmatic rocks and first isolated marine basins which joined by the end Archaean into a single albeit so far shallow-water ocean. Due to a high atmospheric pressure, 5–6 atm. (see Fig. 12.15), average oceanic water temperature, same as the troposphere temperature at sea level, rose in Archaean to +60 to +70 °C (see Fig. 14.17). As the atmosphere has a carbon dioxide composition, the oceanic water has acidic reaction with pH≈5.5–6 (see Fig. 12.6).

Despite these conditions not really being favorable for the existence of life in Archaean, beginning at approximately 3.6–3.5 BY ago stromatolite deposits are known. For example, in the Onverwacht Fm. In South Africa (3.5–3.3 BY), stromatolites have the flintstone composition and comprise thin and areally limited layers among siliceous beds in volcanic rocks of a greenstone belt (Semikhatov et al., 1999).

In the middle of Archaean, the Earthly life became more diverse which is supported, for instance, by numerous bacterial remains in the Fig Tree in South Africa. The abiogenic oxygen was released in Archaean from the water vapor under reactions (12.6). It is possible that after the emergence of cyanobacteria capable of generating small amounts of oxygen, the biogenic originated oxygen had also appeared. Thus, it is possible that a gradual oxygenation of the atmosphere began as early as in Archaean (Rosanov, 2003). This process may have been facilitated by a low free iron concentration within the convecting mantle over the Earth's differentiation zones (see Fig. 4.16) so that iron at that time was unable to absorb oxygen in noticeable amounts.

In Late Archaean (about 2.8 BY ago), the water mass in the hydrosphere increased, and individual marine basins joined together into a single World Ocean which already flooded the summits of mid-oceanic ridges (see Figs. 11.4 and 11.6). At about the same time, due to the Earth's core separation process (see Fig. 4.1d and e), the metallic iron and iron-containing silicates (fayalites) began entering the upper mantle and the oceanic crust. As a result, the abiogenic methane generation increased (see Fig. 12.13). That, in turn, must have led by the end of Archaean to an increase in mass of the stromatolites deposits in the greenstone belts of that time (see Fig. 12.12) albeit their share of volcanic formations in such Archaean belts was still insignificant (Semikhatov et al., 1999). Still, simultaneously the oxygen absorption noticeably increased and its partial pressure declined somewhat (see Fig. 12.9).

By Early Proterozoic 2.5–2.4 BY ago carbon dioxide from the atmosphere was bonded in the crustal rocks, and the atmosphere became almost purely nitrogenous, with small addition of other gases (see Fig. 12.15). Simultaneously, the temperature at the surface substantially declined. Drastic changes in the habitation environment at the Archaean/Proterozoic time boundary could not but affect the biota of the time. The cenosis of thermophilic prokaryotes must have yielded place to more cold-loving bacteria. One more revolutionary restructuring was associated with these events. Early in Proterozoic photosynthesizing microorganisms (blue-green algae) became very common, and a strong increase in growth of the stromatolites abundance occurred (see Fig. 12.12) (Semikhatov et al., 1999) during the

epoch of massive iron ore formations deposits and abiogenic methane generation (see Figs. 12.11 and 12.13).

In the beginning of Early Proterozoic, the tectonic activity drastically declined. Due to that, the depths of oceanic depressions significantly increased, and the ocean stand level dropped (see Fig. 11.6). As a result, iron supply to the hydrosphere decreased. That, in turn, caused about 2.4 BY ago a noticeable increase in the oxygen partial pressure (see Fig. 12.9), and that apparently led to the appearance and broad development of eukaryote microorganisms (Fedonkin, 2004). New form of the single-cell eukaryote organisms had a separate nucleus with the DNA molecules, carriers of the cellular genome. Eukaryotes probably emerged due to the symbiosis of more primitive prokaryote bacteria. It is likely that about the same time appeared eukaryote organisms capable to generate oxygen if influenced by the Sun's radiation, that is, first algae formed and the vegetal kingdom arose.

Since then, the further evolution of life occurred under the biological laws, under pressures from the environment and was affected by a gradual oxygenation of the atmosphere (see Fig. 12.9). The oxygenation played an exceptionally large role in the evolution of earthly life and in the appearance of its new forms (Fig. 15.2).

After the main iron ore deposition epoch had ended (see Fig. 10.5) and oxygen partial pressure rose again, a new major jump in the development of life on Earth occurred 1.9 BY ago. Based on the finds of chain-type microfossils about 1.9–1.8 BY ago, first multicellular organisms appeared (Fedonkin, 2003). At the same time at the end of Early Proterozoic 2.0 BY ago many species of single-cell bacteria and algae tempestuously evolved (see Fig. 15.3). The next deep restructuring of the ocean's biota trophic structure occurred at the Middle/Late Proterozoic time boundary. It was connected with a rapid spreading of eukaryote organisms and phytoplankton. At about the same time, bacteria populated

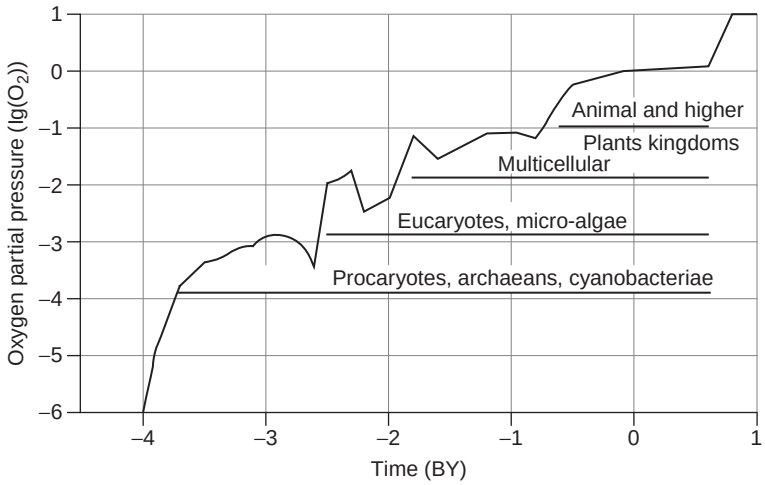


**FIGURE 15.2** Oxygen partial pressure evolution in Earth's atmosphere (to a log scale). In Precambrian, oxygen was generated only by the oceanic biota, and in Phanerozoic oxygen from the land plants was added. Besides, it is assumed that the oxygen generation by Archaean prokaryotes (cyanobacteria) was higher by one order of the magnitude than by Proterozoic eukaryote micro-algae.

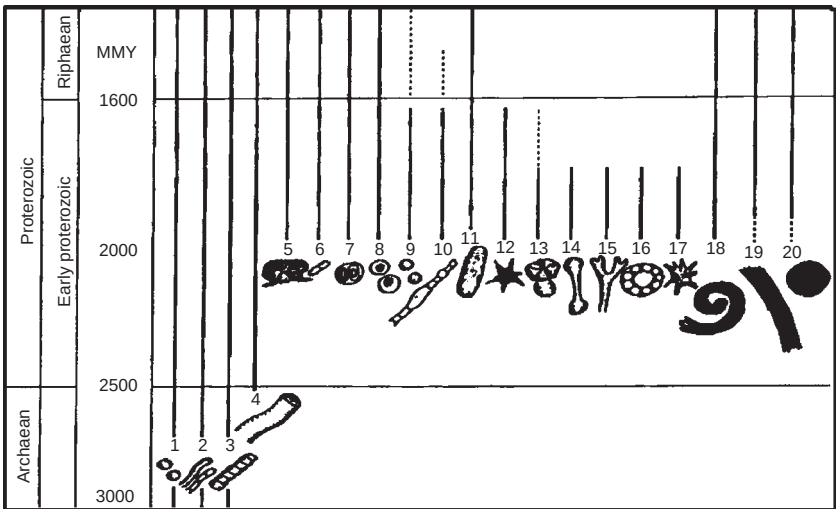


**FIGURE 15.3** Major microfossil remain distribution in Archaean and Early Proterozoic (Semikhatov et al., 1999). Common in Archaean were mostly singular globular and filamentary nanobacteria (1, 2), trichomes (3) and possibly cyanobacteria filaments (4). The diversity of Early Proterozoic microfossils extends from cyanobacteria (4); (5–7), coccoid forms (8,9), trichomes (10) to impressions of large and morphologically complex (11–17) spiral (18), tape-like (19), round and globular (20) forms.

the dry land which is indicated by the red-bed weathered crusts of continental rocks of the same age (Anatolyeva, 1978).

As Fig. 15.2 shows, iron formation deposition each epoch in Precambrian corresponded with an oxygen partial pressure minimum. This is natural as iron was the active absorbent of this gas when oxidizing. The same figure juxtaposes oxygen partial pressure with the major stages in the evolution of life. It is clear that the new life forms emerged only after the next rise in the oxygen partial pressure (i.e., after the end of the next iron ore deposition interval). That was what happened at the Archaean/Proterozoic time boundary. Probably, the replacement of thermophilic prokaryote microorganisms by more cold-loving eukaryote forms was in part due to a noticeable climate cooling in Early Proterozoic (see Fig. 14.19). The eukaryote metabolism was associated with the consumption of small amounts of oxygen so they could spread only after oxygen's partial pressure rose to about $10^{-3}$ of its present value (the Urey point). Simultaneously, the efficiency of oxygen generation by the biota improved. That also facilitated the rise in oxygen partial pressure and massive formation of new life, including at the end of Early Proterozoic about 2 BY ago (Fig. 15.3).

The total phytoplankton biomass which generates oxygen in the ocean, as mentioned earlier, is determined by the amount of the dissolved phosphorus compounds (Schopf, 1980). But its concentration in the ocean water was always in equilibrium with respect to the oceanic crust basalts and close to the present-day one. Thus, the oceanic phytoplankton mass increased with time approximately in proportion with the increase of the oceanic water mass (see Fig. 12.7). Therefore, about 2 BY ago the biomass of oceanic organisms was quite significant, nearly one-third of its present-day amount.

After the metallic iron completely disappeared from the Precambrian mantle and migrated to the core (Sorokhtin, 1974, 2002), the biogenic oxygen more actively accumulated in the Earth's atmosphere (Fig. 15.2). That resulted in the most significant restructuring of the entire Earth's biota, that is, the appearance of highest life forms. As the oxygen's partial pressure stepped over 30 mbar, the Earth's biota literally exploded in its diversity, the skeletal forms appeared and all major types of the currently existing life (Fig. 15.4). The emergence and bloom of the highest life on Earth was apparently also facilitated by a decline in the average near-surface temperature below 20 °C (see Fig. 14.19).

Along with the accumulation of oxygen, Earth's life was becoming more sophisticated. Thus, in Vendian first macroorganisms emerged, animals similar to jelly fishes whose remains are found in many Vendian rocks. In Cambrian, the skeletal animal forms appeared as well as practically all present-day types of the plant and animal kingdoms (Fig. 15.4)

Thus, a third drastic geologo-biological boundary at the transition from Proterozoic to Phanerozoic clearly reflected in Earth's biological evolution. It radically changed the environmental situation on its surface. The Earth's atmosphere now turned from a neutral or slightly acidic into the acidic one. In this new environment, the life forms whose


**FIGURE 15.4** "Tree of life" from a publication by D. Attenborough "Life on Earth: A Natural History" (Attenborough, 1984). The evolution of life at the Proterozoic/Phanerozoic time boundary was like a biological explosion.

metabolism was based on the oxidation of organic substances by oxygen synthesized by the plant domain turned out to be most effective.

It is obvious that the bloom of life on Earth occurred, among other factors, due to the comfortable climatic conditions of a moderately warm climate in slightly oxidizing atmosphere with not too high and not too low pressure. In a hot Archaean climate, with a high pressure carbon dioxide atmosphere, only most primitive and thermophilic bacterial forms could survive. After Archaean, Earth was dominated by the moderate temperature conditions most favorable for biological processes. Even a noticeable climate cooling in Pleistocene, with periodic continental glaciations in the polar and boreal zones apparently played positive role in the perfection of highest life forms including the development of modern man.

In the distant future, life on Earth will imminently die due to the degassing of the abiogenic oxygen which will begin releasing at the formation of the core matter after the oxidation of the mantle iron to the magnetite stoichiometry. That will occur due to the magnetite reduction to the oxide of the univalent iron phase and release of the free oxygen under reaction (4.45) as mentioned in Section 4.5. This, however, will happen in about 600 MMY.

## 15.4 EFFECT OF THE CONTINENTAL DRIFT AND MARINE TRANSGRESSIONS ON THE PHANEROZOIC ENVIRONMENTS

It is a tradition to associate large restructurings of large oceanic or land biological taxons with the Earth's volcanic activity or with mega-impacts. There are, however, no reliable grounds to stipulate noticeable effect of the volcanic processes or the large meteorite impacts on the global evolution of life forms. In particular, a close study did not support the dinosaur extinction hypothesis due to the impact of a large meteorite which caused the appearance in the sediments of the iridium anomaly because dinosaurs existed at least 10 MMY after it. Contrary to the volcanic hypotheses and impact events, the consequences of the continental drift or climatic changes could have resulted in substantial restructuring of the Earth's environments, therefore, render a strong and comprehensive influence on the biosphere evolution. We propose a mechanism of how the cyclical continental drift events, marine transgressions and regressions, and climatic changes affected the Earth's biota. In order to substantiate this mechanism we will first discuss in more detail the major trends in biota's space–time evolution.

The biota restructuring in Phanerozoic occurred mostly in the form of organisms' differentiation and evolution within the framework of the major taxons formed in the beginning of this eon. The main effect on the Phanerozoic life evolution was gradual increase in the oxygen's partial pressure. A noticeable effect from the ambient environment was rendered also by the continental drift, marine transgressions and regressions, climatic changes and, to a smaller extent, the Earth's geomagnetic field polarity changes. All these factors changed the established ecological niches of the biological communities and strengthened their competition for the survival.

Two major planetary transgressions occurred in Phanerozoic. A first one happened in Ordovician, Silurian, and Devonian during the Caledonian orogeny (500–350 MMY ago). Its amplitude reached 200–250 m (see Fig. 11.8). A second and larger global transgression

was caused by the disintegration of the supercontinent Pangaea and occurred in Jurassic-Cretaceous. Its amplitude was 350–400 m. Besides, in the periods of the Riphaean–Paleozoic and Cenozoic sheet glaciations, the water conservation in continental glaciers could have caused relatively short-lived regressions with the ocean level drops by 120–130 m (see Fig. 14.25).

The ocean transgressions over land and the regressions associated with the eustatic fluctuation of the ocean level must have had a significant effect on the global climate variations in the geological past. The water's heat capacity is much higher than that of the atmosphere. Thus, any significant increase in the sea surface at the expense of the dry land made the seasonal and latitudinal climate oscillations milder. In the middle of Cretaceous, the water flooded up to 30% more continental land surface. The mitigating effect of this transgression on the global climate variations in the moderate and high latitudes was quite significant. This was also facilitated by the expansion of epicontinental seas which created the marine corridors through which the heat exchange could occur between the low and high latitudes. During regressions, as the sea receded the general climate continentality increased, and the seasonal temperature oscillations grew.

Let us now review the correlation between the life evolution and the Earth's climatic zoning. We will do it using as an example the marine species distribution versus the continents' and oceans' latitude. The overwhelming majority (about 90%) of all marine animal species populate continental shelves or shallow-water areas near the underwater highs and islands at depths shallower than 200 m. Thus, we may assume that the main development of the marine fauna in Phanerozoic occurred at shallow depths. The richest shallow-water marine fauna is currently observed in the tropics where it is represented by a great number of highly specialized species.

The marine fauna diversity and numbers decrease in higher latitudes, especially in the oligotrophic oceanic waters. In high-latitude and polar waters, however, the ocean's bioproductivity significantly increases again due to a higher oxygen concentration in the cold waters. The lowermost productivity of the oceans is observed at the middle subtropical (oligotrophic) latitudes. The extent of the present-day shallow-water marine fauna correlate well with the food reserves stability change, and these reserves depend on the climatic seasons. Beside this most important latitudinal factor, the longitudinal components also affect the general diversity of the present-day marine fauna. In particular, greater fauna diversity is observed in the locations at the same latitude where the food resources are stable. That is why the greatest diversity of the marine fauna within each latitudinal belt is observed near the continental shores, major archipelagos, and large islands.

In the upwelling areas, the phosphorus and organic matter-rich water from the oceanic depths rise along the continental slope to the surface and make a plentiful food for shallow-water organisms (see Fig. 10.24). The upwellings usually occur next to the ocean's eastern shores in the tropics. Peculiar oases of life arise in these zones and bloom among the relatively empty waters of the adjacent oligotrophic aquatories. Among the examples are the Peruvian and West African upwellings in the Pacific and Atlantic oceans.

Still, the main processes affecting the global climate and its latitudinal zoning are gradual bacterial nitrogen removal from the atmosphere and fluctuations of the Earth's precession angle as affected by the continental drift and high-latitude glaciations (see Section 14.3). Besides, the continents' and oceans' positions substantially affect the climate zoning. Thus,

during glaciation eras the land areas moved together with the lithospheric plate ensemble into the high latitudes, and were gradually covered first by mountain glaciers and then by sheet glaciers which served as the global refrigerators. Therefore, the most contrasting latitudinal zoning occurred on Earth at the times when the ice and snow covered continents or frozen oceans were positioned during the glaciation epochs in the polar areas. Besides, the changes in mutual positions of the continental massifs affected the oceanic water circulation, and that had a strong effect on the global climate. The current Antarctic glaciation began due to the general climate cooling but reached its maximum only after Australia split and moved north, and the Drake Strait opened south of the Tierra del Fuego. After that, the southern circumpolar current emerged around Antarctica and totally cut the continent off the warmer counter-trade wind currents of the three surrounding oceans. This system of the climate isolation is still working in Antarctica.

As we saw earlier, beside the purely earthly factors the planet's climate was affected by the Moon and Sun. This effect always decreased the Earth's precession angle, and that in turn caused significant climate cooling. A smooth climate cooling in Proterozoic and Phanerozoic was also caused by the nitrogen removal from the atmosphere by the nitrogen-consuming bacteria. On the other hand, the supercontinent formation processes always influenced in the opposite direction, toward the climate warming. The interaction of these factors caused a general cooling in Proterozoic and Phanerozoic with individual warming epochs against this cooling backdrop. The result was the climatic fluctuations with periods 100–200 to 800 MMY, and the glaciation epochs with periods of about 100 MY and the average temperature amplitude of up to 8–10 °C (see Figs. 14.19, 14.21 and 14.15).

Thus, we proposed a geohistorical interpretation of the global climate changes. Now we can discuss the nature of major ecological boundaries in Phanerozoic, that is, during the recent 550–600 MMY of life evolution on the planet.

We will briefly review the issue following the data quoted by Fenton and Fenton (2003). Gradual increase in the oxygen partial pressure made it possible around 440 MMY ago the appearance of higher plants on land although bacteria populated the dry land in mid-Proterozoic and primitive spore plants apparently emerged in Vendian or Cambrian. After the Paleozoic transgression, the shallow-water epicontinental seas formed in Late Ordovician. Lunar tides regularly filled the near-shore areas with water and dried them up. A result was the emergence of lungfishes, and in Late Silurian and Devonian, their "posterior", dry-land animals, amphibians.

This event was a unique phenomenon. It was associated with a radical change in the metabolism of oceanic organisms and appearance in the animal kingdom of the forms with lungs, that is, the organ ideally fit for the gas exchange in the air.

The subsequent marine regression somewhat stabilized the environment. However, the continuing glaciations over the high-latitude continents made the climate more contrasting, pushed the amphibians out and replaced them with reptiles which emerged in the middle of Carboniferous. The reptilian bloom, however, happened during the Mesozoic era when the climate significantly warmed up due to the formation of the supercontinent Pangaea. First, very primitive mammals appeared in Late Triassic, and the birds, in Late Jurassic.

Pangaea disintegration began in Early Cretaceous (Fig. 15.5) initiated by a powerful ascending mantle flow (similar to the one in Fig. 9.14) underneath the central part of the supercontinent. This process was accompanied by a strong increase in the tectonic activity

**FIGURE 15.5** Initial stages of the disintegration of Pangea. Reconstruction for a period 100 MMY ago (Dalamber projection) after Smith and Briden (1977).

(see Fig. 6.8), centrifugal spreading of individual continents and the largest Phanerozoic marine transgression (see Fig. 11.8). The result was the formation of relatively shallow-water epicontinental seas (see Fig. 10.31), which subdivided a unified environmental province Pangaea into a series of isolated or semi-isolated environments. As a consequence, the animal world diversity increased and did so with the vengeance in Cenozoic as the shelf provinces of various continents separated and especially due to the occurrence of a higher contrast in the Earth's climatic zones.

Therefore, global tectonic processes and the associated marine transgressions and regressions played important role in the evolution of the climates and environments in Phanerozoic, similar to the previous eons. Indeed, changes in the spatial positions, sizes, and shapes of both continents and oceans in the Phanerozoic evolution substantially affected the oceanic currents' capacity and structure. Therefore, it affected the distribution of their biologic productivity, that is, the formation of the animal and plant communities most fit to various natural conditions and ecological environments.

Coming back to the evolution of the oceanic biota, it is noteworthy that deep-water oceanic depressions were always a significant obstacle to the spread of the oceanic fauna. Volcanic arcs emerging over the zones of the oceanic lithosphere subducting into the mantle and intraplate chains of volcanic islands are often convenient ways for the marine fauna to spread. It is especially true when such chains have sublatitudinal trend or are positioned within the same climatic belt as the Polynesian and Micronesian islands. Another mechanism of the shallow-water fauna spread is the larva migration. Nevertheless, as all large

continents are currently widely separated, the shallow-water fauna on their shelves forms currently about 30 provinces and has only a few species common for these provinces. There are estimates that the present-day shallow-water marine fauna has more species by the whole order of the magnitude than it would have in case of a single shelf faunistic province, even at the highest species diversity.

The same patterns are observed in the spread of some deep-water fauna species. For instance, the biological communities of the Pacific Ocean's "black smoker" hot springs are dominated by large tubular worms Vestimentiphera and bivalved molluscs Calyptogena. At the same time, similar hydrothermal springs in the Atlantic Ocean are totally occupied by small shrimps feeding on serobacteria.

Using these fauna spread patterns, continental drift data, information about eustatic ocean level changes and climatic consequences of these phenomena, we attempted to determine the nature of the change in numbers of the shallow-water fauna taxons in Phanerozoic, such as the mass extinction of many animal groups at the Paleozoic/Mesozoic time boundary. The separated locations in Early Paleozoic of most continental massifs, their positions spreading from the tropics to the high latitudes and the presence of the shelves in each of them resulted in the growth during Ordovician in the number of the shallow-water families. Such increased number of the families was maintained in the marine fauna evolution during most of Paleozoic. At the Permian/Triassic time boundary many continental fragments began merging into a single supercontinent Pangaea. In Jurassic, Pangaea was completely formed. The precession angle then significantly grew to 30–34°, end the Earth's climate substantially warmed up (see Figs. 14.19 and 14.21). The number of ecological provinces and ecological niches strongly contracted over the supercontinent's shelves in the very beginning of its existence. Besides, the Permian/Triassic marine regression (see Fig. 11.8) resulted in a drastic shrinking of the shallow-water areas. Under such conditions, mostly specialized genera became extinct at the Permian/Triassic boundary whereas the shallow-water fauna adjusted to varying conditions survived as they could find food in the near-bottom layers. In other words, the families which survived at the Paleozoic/Mesozoic time boundary apparently evolved under unstable environments whereas most Paleozoic populations evolved under stable environments not unlike the present-day tropical ones. They turned out less fit after the Pangaea formation and were doomed. Thus, it may be assumed that a rapid extinction of many marine fauna species at the Paleozoic/Mesozoic time boundary was caused by the decrease in the number of ecological niches surrounding the emerging supercontinent and by the decrease in the potential of bioproductivity of the shelf seas surrounding it.

Naturally, this is a much generalized view on the evolution of life. It requires substantial development and detailing. Thus, the Cretaceous transgression resulted in the bloom of carbonate-consuming fauna and microflora on shelves and in epicontinental seas, especially of foraminifera and coccolithophorids which formed unique chalk sequences. But the same transgression caused a crisis in the life of the open ocean coral atolls' biocenoses. One gets the impression that a powerful mechanism was active in the middle of Cretaceous which caused drastic decline in the oceanic deposition (see Fig. 15.6) (Davis et al., 1977), and on the other hand resulted in the accelerated transfer of calcium carbonate and phosphorus from the open ocean into the shallow-water seas in the flooded areas of the former dry land (Bogdanov et al., 1990; Sorokhtin and Ushakov, 1991). The reason was that during the

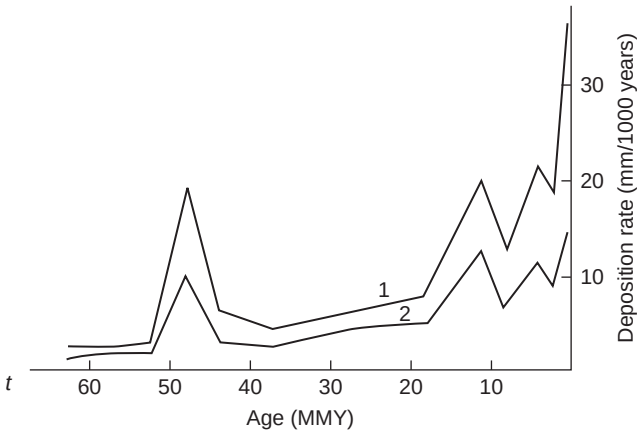


**FIGURE 15.6** Cenozoic oceanic deposit accumulation rate after Davis et al. (1977): 1. Combination rate; 2. Carbonate deposition rate.

Cretaceous transgression most epicontinental seas turned out to be located in the arid climate (see Fig. 10.31) where the water evaporation dominated the precipitation. Thus, such seas became natural pumps draining the oceanic water and its dissolved carbonates and phosphorus compounds from the ocean into the continental seas (see Fig. 15.7). Because of this, the deposition rate drastically declined in the ocean and increased one the shelves and in the shallow-water seas.

Drastic decline in calcium carbonate and phosphorus supply to the atoll biotherms in the open ocean during Aptian–Cenomanian caused the suppression and degrading of reef communities whose skeletons needed calcium carbonate. Under the carbonate hunger environment the corals, rudists, and other skeletal organisms no longer could build strong calcareous constructions capable of resisting the oceanic wave abrasion, especially in a stormy weather. In such a situation, the reef buildups of the oceanic islands (the Aptian–Cenomanian atolls and rudist banks) did not have time to build over and compensate by their growth a continuous subsidence of their volcanic bases under the ocean level as the ocean floor subsidence occurs in proportion to the square root of its age (see Fig. 8.10). At some moment in time the erosion of the former reefs totally destroyed shallow-water fauna populating them and turned the former coral atolls and rudist banks into flat-top underwater mountains guyots (Fig. 15.8) so called by Hess in memoriam of a XIXth century Swiss-born American geologist and geographer A. H. Guyot.

Three hundred previously blooming atolls died this way only in the Pacific during Aptian and Cenomanian. They turned into flat-top underwater mountains whose summits are now located at a depth of about 1500 m below the ocean level. The origin of the volcanic mountains—atoll pediments—was associated with the membrane tectonics and lithospheric plate deformations in their movements on the surface of the Earth's ellipsoid of revolution (see Section 6.7 and Fig. 6.17). The age of 82 guyots was estimated by analyzing their geomorphologic position on the ocean floor. It was shown that practically all underwater mountains emerged during a relatively narrow time range of approximately 95–105 MMY ago (Bogdanov et al., 1990). Thus, almost all numerous Pacific coral islands died practically simultaneously in Albian–Cenomanian for the same reason, the carbonate and, probably, phosphorus deprivation (Sorokhtin and Ushakov, 1991).

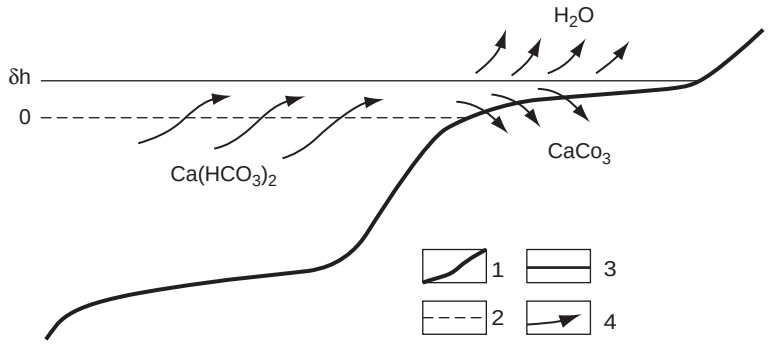


**FIGURE 15.7** Effect of a marine transgression on the redistribution of carbonate deposition areas: 1. Depth curve; 2. Present-day ocean level; 3. Ocean level at the time of the Cretaceous transgression; 4. Migration paths of carbonate matter, phosphates and water.

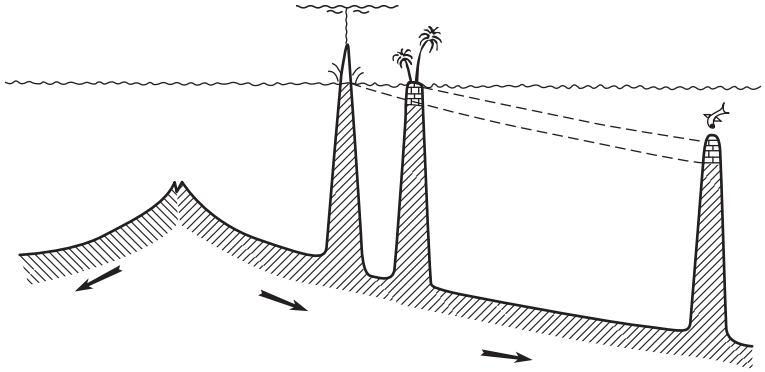

**FIGURE 15.8** Guyot formation concept.

During ice ages, the oceanic water was continuously stirred up. Near bottom water in those times is always saturated with oxygen. This facilitated the existence of deep-water fauna on the ocean floor. It was different during warm eras when glaciations were completely absent. Then, the stirring of the oceanic water almost completely stopped, the deep-water depressions were filled up with stagnant, devoid of oxygen and rather heated deep-water. Under such conditions the water often stagnated, was infected with sulfur dioxide which was accompanied by the sapropel ooze accumulation. The deep-water and benthonic fauna that existed on the ocean floor during the previous glaciation eras died off in such periods. With the advent of a new glaciation era, the benthal population and the formation of benthos communities occurred actually anew at the expense of the animals resettled into the depths from the pelagic areas (Fig. 15.9).

In particular, based on the deep-water drilling results the sapropelic oozes are found in the Pacific Ocean's Cretaceous deposits. Therefore, all benthonic animal communities of this ocean are very young, no older the Middle Cenozoic (Kuznetsov, 1991). Most likely,

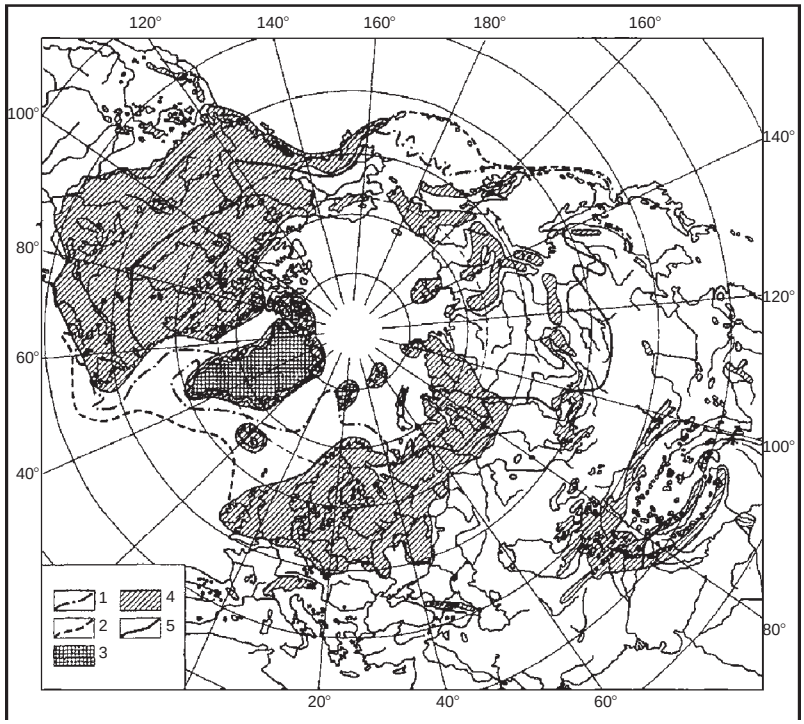


**FIGURE 15.9** Maximum extent of the Pleistocene glaciation (after Fenton and Fenton, 2003)): 1. Present-day marine ice boundary; 2. Ancient marine ice boundary; 3. Present-day onland continental ice; 4. Ancient maximum onland glaciation; 5. Present-day permafrost and underground glaciation boundary.

they are no older than 55 MMY (Nesis, 2001), that is, no older than the beginning of the Antarctic glaciation about 50 MMY ago.

Continental drift substantially affected the dry land fauna. For instance, Mesozoic and postPermian Paleozoic were the reptile era whereas Cenozoic was the mammalian era. During 200 MMY of the Permian–Mesozoic evolution, only 20 new reptilian orders emerged whereas in Cenozoic (during 65 MMY) about 30 mammalian orders emerged. This striking difference becomes clear if we compare the evolution environment of the reptiles and mammals. It is noteworthy that the initial period of a tempestuous evolution of the dry land reptilians coincided with the formation start of the fourth supercontinent Pangaea (see Figs. 9.9 and 9.10). The same interval, about 250–200 MMY ago, had a significant global regression but with relatively mild global climate which set up at the end Permian. And the bloom of the reptiles occurred during the second half of Mesozoic when, after the Earth's precession angle increased due to the Pangaea formation, the climate became warm. In Cretaceous, when Pangaea began to disintegrate, more or less stable environmental connection still existed between its fragments. Therefore, during a long interval of the reptile evolution there was a single environmental province on the dry land (or a small number of semiisolated provinces). It is clear that such environment was not conducive to the emergence of great reptilian diversity.

In the middle of Cretaceous, when some connections between the cluttering Pangaea fragments still remained, primitive mammals expanded. In Late Cretaceous—Early Cenozoic (i.e., in the beginning of the mammalian bloom) the individual continents were remote from one another, and the marine transgression was still continuing (see Fig. 11.8). At that time several large significantly or totally isolated continental ecological provinces formed (see Fig. 10.31). In particular, early in Cenozoic, as the anomalous Polar Atlantic magnetic field shows, dry land connections still existed between America and Europe (up to Eocene). However, Eurasia in Late Cretaceous and Early Cenozoic was divided by a major internal sea extending through West Siberia from the Tethys to the Arctic Ocean. The dry land connections occurred periodically between Alaska and Chukotka through the present-day Bering Strait. Thus, in the first half of Cenozoic three partially communicating ecological provinces formed within the Laurasian continents. Many mammalian orders emerged there.

The ecological subdivision of the provinces within the Gondwana continents probably began somewhat earlier that within the Laurasian ones. By the end of Late Cretaceous most of this continent was flooded with shallow-water seas which separated it into two or three dry-land areas. In the end of Cretaceous (see Fig. 10.31), South America split from Gondwana and became a rather independent ecological province. It was completely separated by a shallow sea in the present-day Amazon Basin into two dry-land areas. Besides, two other isolated dry-land provinces existed in Late Cretaceous, the Indian and Australo-Antarctic ones. Early in Cenozoic (about 40 MMY ago) the latter was separated into two independent areas.

Thus, eight to ten substantially isolated dry land ecological provinces that emerged in Cenozoic were the main precondition of the mammalian genera diversity. In Late Cenozoic, several continental fragments merged, and the number of ecological provinces shrank to five. The largest included Eurasia with Hindustan, Africa, North America, South America, and Australia. This resulted in the extinction of 13 orders of the dry-land mammals. The surviving orders were evolving in the first half of Cenozoic within partially communicating ecological provinces. The mammals which were prior to the continental merger evolving within isolated environments usually were poorer adapted and became extinct.

A more general conclusion can only be sketched now based on the Late-Mesozoic and Cenozoic evolution of the World Ocean floor. It is that all major time boundaries in the geological history (and, as a consequence, the subdivision of the geochronologic scale into eras, periods, and epochs) are substantially predetermined by such events as the continental collisions and splits in the course of the global movement of the lithospheric plate ensemble.

Indeed, the reconstructions by Smith and Briden (1977) partially included in Figs. 9.9, 9.10, 10.31 and 15.5 show that most time boundaries between the biological communities (used for the subdivision of Phanerozoic into individual periods) coincide with major stages in the Earth's tectonic restructuring. Thus, in the middle of Mesozoic all continents formed a single supercontinent Pangaea (maybe except for the Chinese Platform), and Cretaceous was the time when Pangaea began to split and is continuing to split right now.

The split of Europe and Asia began (but was not completely implemented) in Triassic in the area of the present-day western Siberian Platform. Also, North America began separating from Africa and Europe which resulted in the middle of Jurassic in the emergence of a young North Atlantic depression. Early in Cretaceous Africa split from South America and

Antarctica, which later also separated from one another. At the end of Cretaceous, Hindustan split from Antarctica and Australia. At the end of Cretaceous and beginning of Cenozoic the present-day New Zeeland Plateau and the underwater Lord Howe Ridge split from the then merged Antarctica and Australia, these continents also separated, and Australia moved toward the equator.

During the same period (at the Cretaceous/Cenozoic time boundary) in the northern hemisphere, North America, Greenland, and Europe separated. A result was the formation in Cenozoic of the polar Atlantic Ocean. In the very beginning of Cenozoic, the Arabian Plate split from the African Plate, and the formation of the Red Sea and Gulf of Aden started. In mid-Cenozoic, the Hindustan Plate collided with Asia and the major current mountain range of Hindukush–Himalaya emerged. At the Oligocene/Miocene boundary paleo-ocean Tethys continued to close. It finally closed in mid-Miocene. At the same time, the folded mountains in the European part of the Alpine–Himalayan belt arose. It is noteworthy that the closing of Tethys was clearly marked by a local temperature increase in the near-bottom waters of the World Ocean (see Fig. 14.3). In Late Miocene, the Caucasus Mountains as well as the mountains in the Central Asia and Himalaya rose. This formation process of the giant Alpine–Himalayan folded belt separating the northern Asia from its southern regions is still continuing.

The examples show that the plant and animal life evolution on continents was probably to a substantial extent determined by the continental drift and climate changes on Earth. That must have been especially demonstrative at the merging of the previously separated continents or at the separation of their fragments. The alternations of the continent consolidation and fragmentation epochs with the emergence of the unified and intercontinental oceans were undoubtedly accompanied by the formation of new and closing of old ecological niches, that is, by radical changes of the life conditions on Earth. Thus, such restructurings could have been one of the major causes of species formation, extinction, and conservation. A clear example is the endemic life forms on the isolated continents in Australia and South America.

All these events affected the paleoclimate and the evolution of the entire planet's ecological system. It was reflected in the composition of the geochronological scale and its subdivision into eras, periods, and probably epochs. Naturally, the continental drift data and the ecological balance in each area which merged or separated in the continental drift should be utilized in the geohistoric analysis of the flora evolution. In Russia, it was implemented in particular by Meyen (1971, 1981) who conducted a detailed analysis of the Siberian Platform flora evolution.

Once again, a typical feature of Phanerozoic was a long-term global climate cooling due to life activity of the nitrogen-consuming bacteria which continuously lowered nitrogen's partial pressure hence, that of the entire atmosphere. In Paleozoic and Pleistocene, such general climate cooling was superposed by the glaciation epochs associated with the self-oscillatory cycles of the Earth's precession angle.

Thus, the entire Earth's biosphere during 3.5 BY was evolving as a single system in a close interrelation with the planet's geological evolution. That is why the past biospheres should be studied in the integrated manner. It should include the analysis of the interaction between the biospheres with the past geological environments. It should take into account the tectono-geochemical boundaries in the Earth evolution, the climate evolution due to the

precession angle changes, the biota affect on the atmospheric pressure and composition, the continental drift, the emergence of new oceans and the closing of the old ones, etc.

Thus, the geological processes directly affected life evolution on Earth. However, there was also the feedback, the effect of life on the geological processes. A clear example was quoted in Sections 12.4 and 12.5 where the definitive effect of the nitrogen-consuming bacteria and of the plant forms on the formation of the present-day comfortable climatic conditions was demonstrated. That enabled the emergence on Earth of the higher life forms. Besides, beginning in Mesozoic life played a leading role in maintaining the balanced oxygen concentration in the atmosphere. That was not only a definitive factor in the climate formation but also the major factor in the evolution of the highly organized life.

The organic life played a major role in the carbonate, phosphorite, coal formations, oil and gas-bearing sequences, and pelagic deposits sedimentation. It also was significant in rock weathering processes therefore, in the crustal matter turnaround and emergence of the commercial deposits (see Sections 10.8 and 10.9).

## 15.5 EFFECT OF GLACIATIONS ON THE LIFE OF LARGE MAMMALS

We will now briefly discuss the glaciation effect on the evolution of large mammals. After a warm Mesozoic era and Pangaea disintegration, and especially after Paleocene the climate cooled down again, large reptiles (dinosaurs) got extinct, and mammals rapidly evolved and bloomed during entire Cenozoic.

The onset of the Cenozoic glaciation (see Fig. 14.6) resulted in a substantial restructuring of the boreal flora and mass extinction of many species of high-latitude fauna. Conifer and especially deciduous forests retreated far southward and were replaced by tundra and steppe landscapes. Periodic glaciations during Pleistocene affected the Earth's biota, in particular periodic fauna and flora migrations over the planet's latitudes. Besides, it appears that drastic climate changes facilitated the sharpening of evolutionary processes of species formation and extinction.

As an example, at the time boundary of the Würm (Valday) glaciation and the modern interglacial event about 12–10 thousand years ago seemingly favorable climatic conditions appeared. Nevertheless, most of the "mammoth" fauna became extinct, including mammoths proper, giant and large-horned deer, woolly rhinos, cave bears, smilodons, and many other forms of large and small animals. Man definitely played a certain role in the mammoth extinction but the anthropogenic pressure alone was insufficient for so radical a change in the fauna composition at the end of the last phase of the Würm glaciation. Vinogradov believes that during the last glaciation the environment of dry steppe reigned in the areas directly south of the sheet glaciers, the winters were not very snowy so that graminivorous representatives of the mammoth fauna could easily find pasture even in winter. At the advent of the interglacial time 12–10 MY ago the atmospheric humidity substantially grew, the winters became snowy which made the pasturage less accessible in winter, and the large animals apparently had a hard time getting south through dense forests. As a result, the graminivores died of hunger and the predators of lack of graminivores.

It is quite possible that the glaciations affected the evolution of mankind. It is a possibility that the Neanderthals became extinct 30–20 MY ago not only because of the Cro-Magnon competition but because they could not survive the cooling during the last phases of the Würm glaciation period. Drastic global climatic changes at that time determined the timing of the population migrations and the timing of the human races formation. Thus, the population of North America through the Bering Strait most likely occurred through the dry land (Fig. 14.25) during the ocean level drop caused by the last phase of the Würm glaciation which lasted approximately from 30–12 MY ago. The glaciation was at its maximum about 20 MY ago (Imbry and Imbry) but the population of New World occurred at about the same time (20–12 MY ago; Bowen, 1981).

## 15.6 FUTURE EVOLUTION OF LIFE AND THE DEATH OF THE BIOSPHERE

The climate cooling caused by the bacterial consumption of the atmospheric nitrogen will continue. For this reason, it is unlikely that the climate will warm up during the next 100–200 MMY. A reminder: the so much talked about present-day climate warming began in the XVII century (i.e., way before the industrial revolution). Most likely, it is temporary and is associated with fluctuations in the Sun's magnetic activity (see Fig. 14.23). In particular, this is supported by the temperature measurements over the recent 3000 years in the plankton foraminifer remains of the Sargasso Sea (see Fig. 14.22). They clearly indicate that the current local temperature rise is developing against the background of a general climate cooling.

The same is read from geological data. Indeed, 200–100 MMY ago there were no sheet glaciers on Earth, and the average temperatures reached almost $+20\,^{\circ}C$ whereas today they declined to $+15\,^{\circ}C$ (see Figs. 14.15 and 14.19). As a result of such seemingly slight cool-down a new glaciation era began (Fig. 14.21), the sheet glaciation emerged in Antarctica in Mid-Cenozoic, and in Quaternary, periodic glaciations in North America, Europe, and Asia (Fig. 14.15).

Despite a gradual increase in the solar activity, a slow climate cool-down will continue in the future until new cool climate equilibrium is reached. This new climatic level determined by metabolism of the nitrogen-consuming microorganisms may not be too favorable for the higher forms of life.

In our estimate, in 250 MMY the average temperature on Earth during glaciations will drop to $0\,^{\circ}C$ although during the interglacial stadials the average temperatures will still be above freezing, close to $+5$–$+8\,^{\circ}C$. Due to a general decline in the tectonic activity, the World Ocean level will simultaneously drop by about 200 m. That will expose the present-day shelves although the environment for the highly organized life in the low and middle latitudes will remain tolerable. About 400 MMY from now the average Earth's surface temperature may decline to $-5\,^{\circ}C$, and the World Ocean level, by more than 400 m (see Fig. 11.6). In this case, all northern and southern continents, even at moderate latitudes, will be covered by ice sheets. The elevated continental areas will be glaciated even at the equator.

The cooling will not be forever, however. In the previous Section dealing with the climate evolution on Earth we already touched upon the subject. We will now repeat it with a special emphasis on the destiny of life on Earth.

In about 40 MMY, a balance must be reached between the temperature decline due to the bacterial removal of nitrogen from the atmosphere and its increase as a result of the heightened solar luminosity. About 600 MMY after that this equilibrium will have been drastically disrupted by the degassing of the abiogenic oxygen released in the formation of the core matter under reaction (4.45). After that, the free oxygen will start generating within the mantle at a rate of $2.1 \times 10^{16}$ g/year, or 21 billion t/year. Should all this oxygen enter the atmosphere, its partial pressure would rise at a rate of approximately 4 atm. per 1 MMY. The real oxygen degassing rate will have been much lower but still quite noticeable. In 600 MMY, the atmospheric pressure will rapidly rise way over 10 atm. causing on Earth a very strong greenhouse effect**.** 100 MMY after that the oxygen pressure will have reached 14 atm., and the near-surface temperature, 110 °C.

Under such environment all surface life will literally "burn" soon after the degassing begins. As oxygen solubility in the water is low, the higher life forms will exist for some time in the ocean but later they will also be "boiled". After the ocean will have reached the boiling point in 700–800 MMY, and the irreversible greenhouse effect occured with a temperature of about 550 °C, even the primitive thermophilic prokaryotes will not be able to survive.

The provided analysis of the Earth's climates shows that the geodynamic conditions favorable for life are not infinite. Most likely, the total duration of life on Earth is about 4.6 BY (from 4 BY in the past to 0.6 BY in the future). The highly organized life window is much shorter, no longer than 1.2 BY in the ocean (600 MMY in the past through 600 MMY in the future) and no longer than 1 BY on dry land ($-400$ to $+600$ MMY). The time allowed for the humanity to exist (unless it self-destructs earlier) is the shortest compared to all other life forms.

Our generation is safe (unless a nuclear catastrophe strikes). We believe that a realistic estimate of the potential of the evolution of organic life on Earth is not only interesting but important from the *weltanschauung* viewpoint. That is why we made an attempt in this book not only to retrospectively review the evolution of life on the planet but also to show its possible sad development.

In the meantime, we should enjoy living on such a beautiful and unique planet.

# Conclusions

In this book, we have attempted to show that an adequate description of the Earth's geological evolution may be given based on the source physical model by Schmidt and Safronov's theory of planetary formation. The theory shows that the planets of the Earth's group emerged through a combination (adhesion) of the cosmic dust from the fragments within a cold protoplanetary gas–dust cloud. At the same time, the gaseous and volatile cloud components by that time would already have been swept away by the solar wind onto the Solar System's periphery.

It follows from this fundamental planetary formation model that the primordial Earth was uniform in its composition, without a dense core, mantle, and crust. Besides, the young Earth was totally devoid of a hydrosphere, and its fine atmosphere with a total pressure of below $10^{-3}$ atm. included only noble and inert gases.

The modern Earth went through a chemico-density differentiation, has a crust, a silicate shell (the silicate mantle), and a dense iron-oxide core. The crust composition is well studied. The mantle's chemical composition is also known from the deep-seated rocks raised from the ocean floor or from the composition of ophiolite sheets, the deep-seated rocks thrust over the continents. As to the core, we can only hypothesize based on geophysical studies and laboratory experiments. We proposed a hypothesis in Section 2.6 under which the core's external shell responsible for almost a third of the Earth's mass is composed of the oxide of univalent iron phase (such iron phase emerges at a pressure $>130$ kbar), and the central part of the core comprises an iron–nickel melt (Sorokhtin, 1972). In actuality, the proposed theory of the Earth's evolution is based only on the two fundamental assumptions: (1) the primordial Earth was compositionally uniform and (2) the external core comprises oxide $Fe_2O$ of the univalent iron phase. Besides, the model is based on a fundamental physical principle under which the greatest contribution to the planet's evolution came from those energy processes which lowered to the maximum the potential energy of the Earth–Moon planetary system.

The first assumption determines the initial condition of the Earth's evolution from a uniform planet to a laminated one. The second assumption enables the determination of the primordial Earth's chemical composition, hence, an estimate of the internal (endogenous) Earth's energy. The thermodynamic handling of the issue determines and ranks the main energy sources for the Earth's evolution and explains the irreversibility of its evolution process.

Presently, the lunar effect on the Earth's tectonic processes is negligible, no more than 1% in terms of the energy. However, at the early stages of the system's existence, the Moon rotated near the Earth, and the effect was huge and dominated all other sources of the internal energy. For this reason, no adequate analysis of the global evolution is possible without consideration of the Earth–Moon interaction.

The Moon played a certain role at the earliest stages of its existence. It is assumed that the Moon formed due to the destruction at the Roche limit of a more massive planet (three to four lunar masses) which we called Proto-Moon. In any case, this is supported by the value of kinetic momentum in the Earth–Moon system. This planet likely emerged near the Earth or, even more likely, was captured by the growing Earth from a close orbit (the probability of the capture by the growing planet of satellites from the nearby orbits is greater than zero).

Due to the tidal interaction between the planets, the distance between them should have initially decreased rapidly. This resulted in the heating of Proto-Moon. Moon melted and underwent a practically complete gravity differentiation, and the Earth was spun in the forward direction. In this process, the Earth was also somewhat heated but due to its larger mass it was insignificant. As soon as the Moon entered the Earth's Roche sphere, it began to fall apart. About 4.6 BY ago, most of the Proto-Moon matter, including its melted iron core, fell onto the Earth's surface. The Moon proper was formed out of iron impoverished silicate matter of the internal tidal hump of the destroyed protoplanet.

In the course of those catastrophic events, the Earth spun to the maximum angular velocity of the satellite rotation at the Roche limit (~one revolution every 6 h). After that, the Moon began to move rapidly away from Earth (which saved it from destruction) and the Earth's own revolution began to slow down gradually. In the very beginning of the Katarchaean (crypto-tectonic) epoch, the Earth's surface was literally shaken by intense exogenous earthquakes caused in the "solid" Earth by the lunar tides. Their amplitude reached 1 km but later rapidly declined to tens of meters and single meters (the current tides in the "solid" Earth are about 30 cm).

The tidal energy "pumped" into the Earth from its gravity interaction with the Moon and the radioactive decay in Katarchaean amounted in total to approximately $3 \times 10^7$ erg. The primary energy reserves of the young Earth was about $7 \times 10^{37}$ erg. As a result, first melts appeared at the equator about 600 MMY after the Earth's emergence. Subsequently, the process of chemico-density differentiation of the Earth matter began, which was the main process controlling the entire geological evolution. Estimations indicate that because of lunar tidal energy, the Earth's evolution was accelerated by at least 2.5–3 BY.

As the primordial matter contained nearly 13% of a relatively easily fusible iron and 24% of bivalent iron, a mechanism of the mantle matter zonal melting was active in Archaean. For that reason, Archaean was very active tectonically, up to 70% of the present-time crust was formed then.

As underneath the heavy melts a less dense (not yet differentiated) matter was located in the Earth "kernel," the Earth's zonal differentiation resulted in Archaean in severe gravity instability of the Earth's depths. Eventually, this gravity instability resulted in a catastrophic process of iron and iron-oxide melts rapid flow to the planet's center.

In our belief, that is exactly how at the very end Archaean about 2.6 BY ago, the high-density Earth core was separated. The process was accompanied by the generation of intense convective movements in the mantle. These movements grouped together all previously formed continental plates near the equator of one hemisphere with the emergence of a single supercontinent Monogea. Subsequently, the core grew under a quieter barodiffusion mechanism. At the same time, a present-day type dipole geomagnetic field arose.

The described physical model of the global evolution is based on an analysis of

the Earth's energy balance and enabled the quantitative estimation of the Earth's depths degassing rate. It provided an opportunity to determine the hydrosphere formation rate and the composition and pressure of the Earth's atmosphere, and to show that a hot Archaean climate was due to an increase in pressure of the carbon dioxide–nitrogen atmosphere. In Early Proterozoic, the atmospheric carbon dioxide was bonded in carbonates and the atmosphere became almost purely nitrogen and moderately warm.

The climate cooling, however, continued, mostly due to the life activity of nitrogen-consuming bacteria. These bacteria continuously consumed the atmospheric nitrogen, bonded it in the organic compounds, and buried in the planet's sedimentary sequences. The adiabatic theory of the greenhouse effect developed by the authors indicates that declines in atmospheric pressure resulted in further cooling and facilitated the onset of glaciation eras. Within these eras, the glaciation epochs were associated with the solar–lunar effect on the Earth's precession angle. It was also found that the emergence of the supercontinents results in substantial warming of the Earth's climates.

The physical theory of Earth and Moon global evolution developed and proposed in the book enabled the explanation from a unified position of seemingly diverse phenomena and events. The following processes and phenomena were calculated and explained:

1. A total "memory lapse" in the geological record of the young Earth, 600 MMY long (4.6–4.0 BY ago) was explained.
2. The origin of the Moon was established as a result of the destruction of its parent body at the Earth's Roche limit. This explains the considerable iron deficiency in the Moon and abnormally high ratios of radiogenic isotopes to stable isotopes in the lunar rocks, as well as the value of the total revolutional momentum in the Earth–Moon system.
3. The Earth–Moon system and evolution of Earth's revolution were determined; the cause of the Earth moving away from the Sun due to their tidal interaction was identified.
4. The time coincidence between the lunar basalt magmatism and the beginning of the Earth's tectonic evolution about 4.0–3.9 BY ago was explained.
5. The differentiation mechanism of the Earth's matter in Archaean (iron separation from the silicates) and in Proterozoic and Phanerozoic (barodiffusion mechanism) was identified and calculated.
6. The cause of the upper mantle overheating in Archaean was explained and the overheating was quantitatively estimated.
7. The mechanism of the emergence and separation of the Earth's crust was quantitatively estimated.
8. The nature of the mantle's chemico-density convection, the immediate cause of the Earth's tectonomagmatic activity, was identified.
9. The nonstationary nature of the chemico-density convection was established and the associated periodic emergence of the unified supercontinents in Proterozoic and Phanerozoic with their subsequent destruction.
10. The evolution of the Earth's energy balance was calculated and its tectonomagmatic activity was quantitatively determined.

11. The evolution of the mantle's chemical composition was defined and the formation rate of the unique Precambrian iron-ore deposits was calculated.
12. The origins of Early Proterozoic nickel, iron, titanium, copper, chromium, cobalt, platinum, and platinoid-rich unique laminated intrusions of the Bushveld and Great Dyke-type in South Africa, Sudbury in Canada, and Pechebga in Russia were explained.
13. The origins of the world's largest Early Proterozoic stratiform gold, uranium, copper, manganese, and polymetals deposits (Witwatersrand in SAR, Udokan in Siberia), gold-bearing conglomerates of ancient platforms, and other deposits of that age were identified.
14. The origins of diamonds, diamondiferous kimberlites, lamproites, carbonatites, and alkali-ultramafic rocks of the Khibin apatite syenites were explained.
15. The nature of many Phanerozoic economic deposits associated with the recycling of Early Proterozoic ore formations was established.
16. The origins of the oceanic and continental crust were explained, and the continental crust formation rate and its mass accumulation process were calculated.
17. The Earth's atmosphere and hydrosphere emergence were explained, and major patterns of formation and evolution of these geospheres were quantitatively determined.
18. Greenhouse effect physical theory of planetary atmospheres with different compositions and pressure was developed. Using this theory, the temperature distribution in the Venusian troposphere was quantitatively determined for the first time.
19. The origins of a hot climate in Archaean were explained as well as its further regular cooling despite increasing solar luminosity.
20. The effect of the nitrogen-consuming bacteria on the Earth's climate was identified. It was shown that their life activity results in the decline of the atmospheric pressure and, as a consequence, in climate cooling.
21. It was shown that the so-called greenhouse gases have no practical effect on the Earth's climate and that the climate warm-up over the recent decades is associated only with a temporary increase of the solar activity, whereas the long-term climate changes are directed toward its cooling-down and the approach of a glaciation period.
22. The origins of the grandiose Early Proterozoic Huron glaciation were explained.
23. It was shown that the lunar–solar interaction with the Earth equatorial swelling results in a decline of the Earth's precession angle and, as a result, in a gradual cooling-down of the global climate; whereas, conversely, the ice sheet formation in the northern hemisphere results in a precession angle increase and in a rapid climate warming.
24. Periodic onset of the Pleistocene glaciations was explained and quantitatively calculated.
25. Substantial influence of geologo-geochemical factors on the evolution of life was determined.
26. It was shown that the Early Archaean Earth's atmosphere was carbon dioxide-nitrogenous with a noticeable methane content. Thus, it was reducing which

predetermined the emergence of life on Earth.

**27.** It was shown that the life evolution in Precambrian was restrained by oxygen absorption in the oxidation of the Precambrian iron-ore formations.

**28.** The atmosphere oxygenation process was quantitatively estimated and shown that new forms of life on the Earth appeared only when partial pressure of the biogenic oxygen increased.

**29.** The emergence and bloom of highly organized life at the Proterozoic–Phanerozoic time boundary were explained by a drastic increase in the oxygen partial pressure after total disappearance of the metallic iron from the mantle.

**30.** The causes of the demise in Mid-Cretaceous of the previously blooming atolls and their conversion to underwater flat-crested mountains (guyots) were identified.

A number of less general phenomena and processes also found their explanation within the framework of the unified theory of the Earth's evolution. Among them are the topography of the oceanic lithospheric plates, origins of the global marine transgressions, causes of no magmatism in many subduction zones in Early Proterozoic, abiogenic origins of methane, etc.

Besides, the proposed theory enabled the explanation of the aforementioned planetary energy processes controlling the global evolution of the Earth. Also, it was shown that after the core separation at the end Archaean, the ore element-enriched primary Earth matter was squeezed from the Earth's center into the mantle. That provided a natural explanation of the origins of the Early Proterozoic unique laminated intrusions like the Bushveld Massif and Great Dyke in South Africa, Sudbury in Canada, and Pechenga and Pan intrusions in Russia. As a reminder: these intrusions are accompanied by very rich deposits of nickel, titanium, copper, chromium, cobalt, platinum, and platinoids.

A drastic decline in carbon dioxide partial pressure in the atmosphere at the Archaean–Proterozoic time boundary resulted in a no less drastic decrease in the oceanic water acidity and, as a consequence, to a massive precipitation of the dissolved ore elements. So have unique stratiform deposits of gold, uranium, copper, manganese, and polymetals arisen, like the Witwatersrand in South Africa, Udokan in Siberia or gold-bearing conglomerates of ancient platforms, and other economic deposits of that age. The theory provided a natural explanation for the origins of diamondiferous rocks through sucking-in of iron-ore pelagic deposits of the Early Proterozoic oceans to great depths underneath the ancient continental massifs. In the process, the tropical area deposits gave birth to carbonate-rich kimberlites, and the polar deposits produced lamproites. The diamonds *per se* form due to the reaction between carbon dioxide released at the dissociation of oceanic carbonates within the Early Proterozoic subduction zones with the participation of the organic methane.

It therefore follows from the proposed theory that the Earth's evolutionary path was predetermined by its position in the Solar System, its mass, specifics of its chemical composition, and by the existence of a massive satellite, the Moon. For this reason, it is totally incorrect to judge the other planets of the Solar System based on the patterns typical of Earth. Although the general energy and matter-related approach remain the same, the evolutionary problem must be solved individually for each individual planet. A clear example is given by the comparison between the evolutionary paths of sister planets, Earth and Venus.

One of the major factors that defined the difference in the evolutions of the two planets, besides the different distance from the Sun, was the emergence on the close near-Earth orbit of a massive satellite, the Moon, which significantly accelerated the tectonic activities on the Earth. If Earth did not have a massive satellite, it most likely would be slowly revolving about its axis (possibly, in the opposite direction, just as in the case of Venus). The Earth would be presently under Archaean conditions with a dense carbon dioxide atmosphere and high temperatures. Only primitive bacterial forms would be populating the Earth instead of highly organized life.

# References


Abdusamatov, Kh. I. (2003). On long-term coordinated activity variations of the luminosity, Sun radius and global climate. Proc. of internat. conf. "Climatic and ecological aspects of the Sun activity", SPB, p. 3–10.

Alfven, H. (1954). "On the Origin of the Solar System." Oxford University Press, London.

Alfven, H. (1963). On the early history of the Sun and the formation of the solar system. *Astrophys. J.* **137,** 981–996.

Alfven, H. and Arrhenius, G. (1976). "Evolution of the Solar System." Scientific and Technical Information Office National Aeronautics and Space Administration, Washington, DC.

Aller, L. H. (1971). "Atoms, Stars and Nebula." Harvard University Press, Cambridge, MA.

Almukhamedov, A. I. and Medvedev, A. Ya. (1982). "Sulfur Geochemistry in Basic Magma Evolution Processes." Nauka, Moscow, 148.

Altshuler, L. V. (1965). Application of shock waves in physics of high pressures. *Adv. Phys. Sci.* **85,** 197–258.

Altshuler, L. V. and Bakanova, A.A. (1968). Metal electron structure and compressibility at high pressure. *Adv. Phys. Sci.* **96,** 193–215.

Altshuler, L. V. and Sharipdzhanov, I. P. (1971a). Additive equations of state of the silicates at high pressures. *Izv. AN USSR Phys. Earth* **3,** 11–28.

Altshuler, L. V. and Sharipdzhanov, I. P. (1971b). On iron distribution in Earth and her chemical differentiation. *Izv. AN USSR Phys. Earth* **4,** 3–16.

Altshuler, L. V., Simakov, G. V., and Trunin, R. F. (1968). On the issue of the Earth's core chemical composition. *Izv. AN USSR. Phys. Earth* **1,** 3–6.

Anatolyeva, A. I. (1978). "Main Evolution Boundaries of the Red-Bed Formations." Nauka, Novosibirsk, 190pp.

Anderson, Don L. (1989). "Theory of the Earth." Blackwell Scientific Publications.

Anderson, R. N. and Hobart, V. A. (1976). The relation between heat flow, sediment thickness and age in the Eastern Pacific. *J. Geophys. Res.* **81,** 2968–2989.

Areshev, E. G. (2003). "Oil and Gas Potential of the Marginal Seas in the Far East and SE Asia." AVANTI, Moscow, 288pp.

Artyushkov, E. V. (1968). Gravity convection in Earth's depth. *Izv. AN USSR. Phys. Earth* **9,** 3–18.

Artyushkov, E. V. (1970). Earth's matter density differentiation and the associated phenomena. *Izv. AN USSR. Phys. Earth* **5,** 18–30.

Artyushkov, E. V. and Sobolev, S. V. (1977). Mechanisms of kimberlite magma rise from depth. *Proc. AN USSR* **236,** 3692–695.

Artyushkov, E. V. and Sobolev, S. V. (1984). Physics of kimberlite magmatism. *In* "Kimberlites I: Kimberlites and Related Rocks," pp. 309–322. Elsevier, Amsterdam.

Atlas of Antarctic (1966). Vol. 1. Moscow–Leningrad. GUGK MG USSR. 236pp.

Atmosphere of Earth (1988). "Physical Encyclopedia." Soviet Encyclopedia, Moscow, Vol. 1, pp. 133–136.

Attenborough, D. (1984). "Life on Earth." Mir, Moscow, 176pp.

Avsyuk, Yu. N. (1996). "Tidal Forces and Natural Processes." OIFZ RAN, Moscow, 188pp.

Avsyuk, Yu. N., Genshaft, Yu. S., Saltykovskii, A. Yu., and Svetlosanova, Z. P. (2005). Latitudinal zonality of sedimentation areas as a manifestation of the evolution of the Earth–Moon–Sun tidal system. *Doklady Earth Sci.* **403,** 5659–661.

Azbel, I. Ya. and Tolstikhin, I. N. (1988). *In* "Radiogenic Isotopes and Evolution of the Earth's Mantle, Crust and Atmosphere," Geol. Inst. AN USSR, Apatity, 140pp.

Bachall, J. N., et al. (1982). Standard solar models the uncertainties in predicted capture rates of solar neutrinos. *Rev. Mod. Phys.* **54,** 767–778.

Bachinsky, A. I., Putilov, V. V., and Suvorov, N. P. (1951). "Reference Book of Physics." Uchpedgiz, Moscow, 380pp.

Balanyuk, I. E. (1981). "Hydrocarbon Migration from Plate Subduction Zones to Foredeeps. Issues of Theoretical Geodynamics and Lithospheric Plate Tectonics." Institute of Oceanology of AN USSR, Moscow, pp. 168–173.

Balanyuk, I. E. and Dongaryan, L. Sh. (1994). Role of hydrothermal methane in the formation of gas-hydrate accumulations. *Geol. Geophys. Dev. Fields* **3,** 22–28.

Balanyuk, I. E., Matveyenkov, V. V., and Sedov, A. P. (1995). "Serpentinization of the oceanic upper mantle rocks as a source of the hydrocarbon formation." *In* "Geologic Exploration and Utilization of the Subsurface." RF Committee for the geology and utilization of the subsurface, Moscow, pp. 34–40.

Barazangi, M. and Dorman, J. (1968). World seismicity map of ESSA coast and geodetic survey epicenters data for 1961–1967. *Bull. Seism. Soc. Am.* **59,** 369–379.

Belousov, V. V. (1954). "Fundamentals of Geotectonics." Gosgeoltekhizdat, Moscow, 607pp.

Benioff, H. (1955a). Seismic evidence for crustal structure and tectonic activity. *Geol. Soc. Am. Spec. Paper* **62,** 67–74.

Benioff, H. (1955b). Seismic evidence for crustal structure and tectonic activity. *Geol. Soc. Am. Spec. Paper* **62,** 61–74.

Berzon, I. S. and Pasechnik, I. P. (1972). Dynamic parameters of the PcP wave in a case of a thin-layer model of the mantle to core transition area. *Izv. AN USSR. Phys. Earth* **6,** 21–33.

Berzon, I. S., Kogan, S. D., and Pasechnik, I. P. (1968). On a possibility of constructing a thin-layer model of the shell to core transition area. *Proc. AN USSR* **178,** 186–89.

Betekhtin, A. G. (1950). "Mineralogy." Gosizdat of Geologic Literature, Moscow, 957pp.

Bijy-Duval, B., Moore, J. C., Bergen, J., et al. (1981). Leg 78 A, Eastern Caribbean sea. *JOIDES J.* **VII**, 221.

Birch, F. (1958). Differentiation of the Mantle. *Geol. Soc. Am. Bull.* **69,** 4483–486.

Blackett, P. M. S. (1961). Comparison of ancient climates with ancient latitude from rock magnetic measurements. *Proc. Roy. Soc. A* **263,** 1236–248.

Boehler, R. (1993). Temperatures in the Earth's core from melting-point measurements of iron at high static pressures. *Nature* **363,** 534–536.

Boehler, R. (1996). Experimental constraints on melting conditions relevant to core formation. *Geochim. Cosmochim. Acta* **60,** 71109–1112.

Bogatikov, O. A., Ryabchikov, I. D., and Kononova, V. A. (1991). "Lamproites." Nauka, Moscow.

Bogdanov, Yu. A., Sorokhtin, O. G., Zonenshain, L. P., et al. (1990). "Iron-Manganese Crusts and Concretions of Underwater Mountains in the Pacific Ocean." Nauka, Moscow, 229pp.

Bogdanov, Yu. A., Lisitsin, A. P., Sagalevich, A. M., and Gurvich, E. G. (2006). "Hydrothermal Ore Genesis of the Ocean Floor." Nauka, Moscow, 527pp.

Bogdanova, M. N., Yefimov, M. N., and Sorokhtin, N. O. (1992). "Elements of Archaean geodynamics in the northwestern White Sea area." "Geodynamics and Deep Structure of the Soviet Part of the Baltic Shield." KNC RAN, Apatity, pp. 81–91.

Bolshakov, V. A. (2003). "New Concept of Orbital Theory of Paleo-Climate." Taurus, Moscow, 256pp.

Bolt, B. A. (1978). "Earthquakes." W. H. Freeman and Company, New York.

Bolt, B. (1984). In the depths of Earth: what the earthquakes tell us about. Moscow, Mir, 189 p.

Bondarenko, B. A., Garkalenko, I. A., Zhuravlev, A. V., et al. (1977). New data on the structure of deep crust in the Kuril-Kamchatka trough. *Proc. AN USSR* **234**.

Borukayev, Ch. B. (1985). "The Structure of Precambrian and the Plate Tectonics." Nauka, Novosibirsk, 190pp.

Borukayev, Ch. B., et al. (1977). "Precambrian of the Continents. Major Features of Tectonics." Nauka, Novosibirsk, 264pp.

Botte, M. (1974). "Internal Structure of Earth." Mir, Moscow, 373pp.

Bowen, D. Q. (1978). "Quaternary Geology: A Stratigraphic Framework for Multidisciplinary Work." Pergamon Press, Oxford-New-York, 221p.

Bowen, D. (1981). Quaternary geology, the basis of interdisciplinary studies. Moscow, Mir, 272 p.

Brosge, W. P. and Tailleur, I. L. (1971). Northern Alaska petroleum provins. *In* "American Association of Petroleum Geologists (Mem. 15,)," (I. H. Cram, ed.), pp. 68–99. American Association of Petroleum Geologists.

Broun, G. C. and Mussett, A. E. (1981). "The Inaccessible Earth." Allen and Unwin, London.

Brown, J. M. and McQueen, R. G. (1986). Phase transition, Gruneisen parameter and elasticity for shocked iron between 77 GPA and 400 GPA. *J. Geophys. Res.* **91,** 7485–7494.

Budyko, M. I. (1974). "Climate Changes." Gidrometeoizdat, Leningrad, 280pp.

Budyko, M. I. (2002). Global warming. *In* "Climate Changes and Their Consequences," (G. V. Menzhulin, ed.), pp. 7–12. Nauka, Sankt-Peterburg.

Bullard, E. C., Everett, J. E., and Smith, A. G. (1965). The fit of continents around Atlantic. A symposium on continental drift. *Phil. Trans. Roy. Soc. A* **258,** 41–51.

Bullen, K. E. (1956). Seismology and the Broad Structure of the Earth's interior. *Phys. Chem. Earth* **1,** 68–93.

Bullen, K. E. (1963). "An Introduction to the Theory of Seismology." Cambridge University Press, London.

Bullen, R. E. (1973). Cores of the terrestrial planets. *Nature* **243,** 68–70.

Bullen, K. E. (1975). "The Earth's Density." Chapman and Hall, London.

Burke, K. C. and Wilson, T. (1976). Hot spots on the Earth's surface. *Sci. Am.* **235,** 246–57.

Bykhover, N. A. (1984). "World Mineral Resource Distribution by the Ore-Formation Epochs." Nedra, Moscow, 576pp.

Byshev, V. I., Neiman, V. G. and Romanov, Yu. A. (2005). On multi-directionality of the global climatic changes on continents and in oceans. Proc. RAN, Vol. 400, 1, p. 98–104.

Cameron, A. G. W. (1972). The origin and evolution of the solar system. *Sci. Am.* **233,** 32–41.

Cameron, A. G. W. (1973). Accumulation processes in the primitive solar nebula. *Icarus* **18,** 407–450.

Cameron, A. G. W. and Benz, W. (1990). The origin of the Moon and the single impact hypothesis IV. *Icarus* **92,** 204–216.

Cameron, A. G. W. and Ward, W. R. (1976). The origin of the Moon. *Lunar Sci.* **7,** 120–132.

Carslow, G. and Yeager, D. (1964). "Heat-Conductivity of Solid Bodies." Moscow, Nauka.

Chandrasekhar, S. (1961). "Hydrodynamic and Hydromagnetic Stability." Oxford University Press, Oxford, England. Chap. VI, p.198.

Chilingar, G. V. (1956). Relationship between Ca/Mg ratio and geologic age. *Bull. Am. Assoc. Petrol. Geol.* **40,** 92256–2266.

Chumakov, N. M. (1978). "Precambrian Tillites and Tilloids." Nauka, Moscow, 2006-published by GEOS in Russia. 202pp.

Chumakov, N. M. (2001). General direction of climatic changes on Earth over the recent 3 billion years. Proc. RAN, Vol. 381, 5, p. 652–655.

Chumakov, N. M. (2004a). Climatic zoning and the climate of Cretaceous period. *In* "Climate in the Epochs of Major Biospheric Changes," pp. 105–123. Nauka, Moscow.

Chumakov, N. M. (2004b). Dynamics and possible causes of climatic changes in Late Mesozoic. *In* "Climate in the Epochs of Major Biospheric Changes," pp. 149–157. Nauka, Moscow.

Chumakov, N. M. (2004c). Glaciation and non-glaciation climate in Precambrian. *In* "Climate in the Epochs of Major Biospheric Changes," pp. 259–270. Nauka, Moscow.

Chumakov, N. M. (2006). Early-Paleozoic glaciation and Biospheric events of Late Ordovician. *In* "Proc. GIN, 580: Cause-and-Effect Associations and Factors of Global Changes in Phanerozoic," pp. 25–41. GEOC, Moscow.

Clemens, W. (1963). personal communication.

Coleman, R. G. (1971a). Petrological and geophysical nature of serpentinites. *Geol. Soc. Am. Bull.* **82,** 4897–918.

Coleman, R. G. (1971b). Plate tectonic emplacement of upper mantle peridotites along continental edges. *J. Geophys. Res.* **76,** 51212–1222.

Condie, K. C. (1981). "Archean Greenstone Belts." Elsevier, Amsterdam.

Darwin, G. H. (1898). "The Tides Kindred Phenomena in the Solar System." John Murray, London.

Davis, T. A., Hay, W. W., Southam, J. R., and Worslev, T. R. (1977). Estimates of Cenozoic oceanic sedimentation rates. *Science* **197,** 53–55.

Dawson, J. B. (1980). "Kimberlites and Their Xenoliths." Springer-Verlag, Heidelberg.

Demenitskaya, R. M. and Karasik, A. M. (1971). "Issue of the Arctic Ocean Origin. History of the World Ocean." Nauka, Moscow, 306pp.

Dewey, J. and Bird, J. (1970a). Plate tectonics and geosynclines. *Tectonophysics* **10,** 5/6625–638.

Dewey, J. and Bird, J. (1970b). Mountain belts and the new global tectonics. *J. Geophys. Res.* **75,** 142625–2647.

Dickinson, W. R. (1974). Subduction and oil migration. *Geology* **2,** 9.

Dietz, R. S. (1961). Continent and ocean basin evolution by spreading of the sea floor. *Nature* **190,** 4779854–857.

Dietz, R. S., Holden, J. C. (1972). The break up of Pangea. *In* Continents adrift. Readings from the Scientific American. San Francisco, Freeman and Co., P. 1246–1254.

Dmitriyev, L. V. (1969). On the issue of the origin of ultramafic rocks in the Indo-Oceanic ridge. *Geochemistry* **10,** 326–332.

Dmitriyev, L. V. (1973). "Mid-Oceanic Ridge Bedrock Geochemistry and Petrology." GEOCHI, Moscow, Abstract of PhD thesis, 45pp.

Dmitriyev, L. V., et al. (1969). Bedrock of the rift zones in the Indian Ocean Ridge and some features of their geochemistry. *Proc. AN USSR* **185,** 2444–446.

Dmitriyev, L. V., et al. (2000). Hydrogen and methane formation in serpentinization of the oceanic hyperbasites and the origin of oil. *Russ. Earth Sci. Mag.* **1,** 11–16.

Dodd, R. T. (1986). "Meteorites. Petrology and Geochemistry." Mir, Moscow, 384pp.

Duffield, W. A. (1972). A naturally occurring model of global plate tectonics. *J. Geophys. Res.* **7,** 2543–2555.

du Toit, A. L. (1937). Our Wandering Continents; An Hypothesis of Continental Drifting, Oliver & Boyd, London, UK.

Dzivonsky, A. M., Hales, A. L., and Lapwood, E. R. (1975). Parametrically simple Earth models consistent with geophysical data. *Phys. Earth Planet. Inter.* **10,** 12–48.

Edmond, L. M., Measures, C., McDuff, R. E., et al. (1979). Ridge crest hydrothermal activity and the balances of the major and minor elements in the

ocean: The Galapagos data. *Earth Planet. Sci. Lett.* **46,** 1–18.

Eldrdge, C. S., Compston, W., Williams, I. S., et al. (1991). Isotope evidence for the involvement of recycled sediments in diamond formation. *IBID* **353,** 649–653.

Elsasser, W. M. (1963). "Early History of the Earth. Earth Science and Meteoritics." North-Holland, Amsterdam, 1–30.

Exley, R. A., Mattey, D. P., Clague, D. A., and Pillinger, C. T. (1986). Carbon isotope systematic of a mantle "hotspot": A comparison of Loihi Seamount and MORB glasses. *Earth Planet. Sci. Lett.* **78,** 189–199.

Faure, G. (1977). "Principles of Isotope Geology." 2th ed. John Wiley and Sons, New York.

Fedonkin, M. A. (2003). The origin of the Metazoa in the light of the Proterozoic fossil record. *Paleontol. Res.* **7,** 19–41.

Fedotov, et al. (1969). Earthquakes and deep structure of the south of the Kuril Island Arc. Moscow, Nauka, 245 p.

Fedonkin, M. A. (2004). Change in the metal availability and the biosphere eukariotization in Precambrian. *In* "Proceedings of the Geological Institute, 565, Present-day Issues of Geology," pp. 426–447. Nauka, Moscow.

Fedonkin, M. A. (2008). Role of hydrogen in the evolution of metabolic systems. *In* "Issues of Emergence and Evolution of the Biosphere," pp. 417–437. House of Books "LIBROKOM", Moscow.

Fenton, G. L. and Fenton, M. A. (1989). "The Fossil Book. A Record of Prehistoric Life." Doubleday, New York.

Fenton, C. L. and Fenton, M. A. (2003). "The Rock Book." Dover Publications, Dover, De, 432pp.

Fischer, H., Wahlen, M., Smith, J., Mastroianni, D., and Deck, B. (1999). Ice core records of atmospheric $CO_2$ around the last three glacial terminations. *Science* **283,** 1712–1714.

Fish, F. (1967). Angular momenta of the planets. *Icarus* **7,** 251–256.

Fisher, O. (1889). "Physics of the Earth Crust." 2nd ed. Macmillan, London.

Fisher, D. E. (1987). "The Birth of the Earth." Columbia University Press, New York.

Forsyth, D. and Uyeda, S. (1975). On the relative importance of the driving forces of plate motion. *Geophys. J. Roy. Astr. Soc.* **43,** 163–200.

Fox, S. W. (1965). A theory of macromolecular and cellular origins. *Nature* **205,** 328–340.

Francheteau, J., Needham, H. D., Chourone, P., Juteau, T., et al. (1979). Massive deep-sea sulfide ore deposits discovered on the East Pacific Rise. *Nature* **277,** 523–528.

Frolova, T. I. and Burikova, I.A. (1992). Andesite volcanism in the Earth's history. Herald MGU. *Geology* **4,** 3–17.

Frolova, T. I., Rudnik, G. B., and Kashintsev, G. L. (1979). Some general patterns of the oceanic magmatism and issues of the magmatic rocks origins. *In* "Oceanology, Geology of the Ocean, Sediment Formation and Magmatism of the Ocean," pp. 69–87. Nauka, Moscow.

Fryer, B. J. (1977). Rare Earth evidence in iron-formations for changing Precambrian oxidation states. *Geochim. Cosmochim. Acta.*, Vol. 41, p. 361–367.

Galimov, E. M. (1984). $^{13}C/^{12}C$ ratio in diamonds. Vertical zoning of diamond formation in the lithosphere. *In* "Proceedings of 27th International Geologic Congress, Vol. 11, Section C 11. Geochemistry and Cosmochemistry," pp. 110–123. Nauka, Moscow.

Galimov, E. M. (1988a). Issues of the carbon geochemistry. *Geochemistry* **2,** 258–278.

Galimov, E. M. (1988b). On the ocean's emergence and evolution based on the data of $^{18}O/^{16}O$ ratio variations in Earth's sedimentary shell in geologic time. *Proc. AN USSR* **299,** 4977–981.

Galimov, E. M. (2001). "Phenomenon of Life: Between Equilibrium and Linearity. ORIGINS and Principles of the Evolution." Editorial URSS, Moscow, 256pp.

Galushkin, Yu. I. and Ushakov, S. A. (1978). Global image of lithospheric plate instantaneous kinematics. Herald MGU. *Geology* **4,** 20–35.

Garkalenko, I. A. and Ushakov, S. A. (1978). Earth's crust of the Kuril Region. *Soviet Geol.* **11,** 46–59.

Garrels, R. M. and Mackenzie, F. T. (1971). "Evolution of Sedimentary Rocks." W.W. Norton, New York.

Gast, P. W. (1968). Upper mantle chemistry and evolution of the Earth's crust. *In* "The History of the Earth's Crust," (R. A. Phinney, ed.), pp. 15–27. Princeton University Press, Princeton, USA.

Gast, P. W. (1972). The chemical composition of the Earth, the Moon and chondritic meteorites. *In* "The Nature of the Solid Earth," (E. C. Robertson, ed.), pp. 19–40. McGraw-Hill, New York.

Gavrilov, V. P. (1978). "Planet's "Black Gold"" Nedra, Moscow, 190pp.

Gavrilov, V. P. (1986). "Origin of Oil." Nauka, Moscow, 176pp.

Gavrilov, V. P. (2008). On possible mechanisms of natural reserves replenishment in oil and gas fields. *Geol. Oil Gas* **1,** 1–8.

Geodynamic map jf the Circum-Pacific region (1985). Free-air gravity (to degree 10). Tulsa, Oklahoma 74101, USA.

Gestenkorn, H. (1967). On the controversy over the effect of tidal friction upon the history of the Earth–Moon system. *Icarus* **7,** 2160–167.

Giuli, R. T. (1968a). Gravitational accretion of small masses attracted from large distances as a mechanism for planetary rotation. *Icarus* **9,** 186.

Giuli, R. T. (1968b). On the rotation of the Earth produced by gravitational accretion of particles. *Icarus* **8,** 301.

Glebovitsky, V. A. (ed.) (2005). Early Precambrian of the Baltic Shield, Nauka, Sankt-Peterburg, 711pp.

Glikson, A. Y. (1976). Stratigraphy and evolution of primary and secondary greenstone complexes. Data on the Southern hemisphere shields. *In* "Early History of Earth," (B. F. Windley, ed.), John Wiley and Sons, New York.

Glukhovsky, M. Z. (1990). "Geologic Evolution of Basements of the Ancient Platforms (Nuclear Concept)." Nauka, Moscow, 215pp.

Glukhovsky, M. Z. and Moralev, V. M. (1988). Tectonic position and petrogenesis of the Aldan Shield anorthosites. *Geol. Geophys.* **4,** 37–43.

Glukhovsky, M. Z., Moralev, V. M., and Kuzmin, M. I. (1994). Hot belt of the early Earth and its evolution. *Geotectonics* **5,** 3–15.

Goldreich, P. (1966a). History of the lunar orbit. *Rev. Geophys.* **4,** 411–439.

Goldreich, P. (1966b). History of the lunar orbit. *Rev. Geophys.* **4,** 411–439.

Goldreich, P. and Soter, S. (1966). Q in the solar system. *Icarus* **5,** 2.

Goldreich, P. and Toomre, A. (1969). Some remarks on polar wandering. *J. Geophys. Res.* **74,** 2555–2567.

Gore, A. (2006). An Inconvenient Truth: The Planetary Emergency of Global Warming and What We Can Do About It, Melcher Media - 2006 - 346 p.

Gorodnitsky, A. M. (1977). Thickness of the oceanic lithosphere and maximum height of the underwater volcanoes. *In* "Tectonics of the Lithospheric Plates," (A. S. Monin, ed.), pp. 24–32. USSR Institute of Oceanology, Moscow.

Gorodnitsky, A. M. and Sorokhtin, O. G. (1979). "Map of the lithospheric plate thickness," (O. G. Sorokhtin ed.), pp.181–183. Geophysics of the Ocean, Vol. 2, Geodynamics. Nauka, Moscow.

Gorodnitsky, A. M. and Sorokhtin, O. G. (1981). "Map of the calculated values of heat flow through the ocean floor." *In* "Issues of theoretical geodynamics and lithospheric plate tectonics," (O. G. Sorokhtin, ed.), pp. 122–128. USSR Institute of Oceanology, Moscow.

Gorodnitsky, A. M., Zonenshain, L. P., and Mirlin, E. G. (1978). "Reconstruction of Continents' Positions in Phanerozoic." Nauka, Moscow, 121pp.

Green, D. H. and Ringwood, A. E. (1966). Origin of the calcalkalaine igneous rock suite. *Earth Planet. Sci. Lett.* **1,** 307–316.

Green, D. H. and Ringwood, A. E. (1967a). The genesis of basaltic magmas. *Contrib. Miner. Petrol.* **15,** 103–190.

Green, D. H. and Ringwood, A. E. (1967b). The genesis of basaltic magmas. *Contr. Miner. Petrol.* **15,** 103–190.

Greenhouse effect, climate and ecosystem change. (1989). Gidrometeoizdat, Leningrad, 558pp.

Grinenko, V. A. and Grinenko, L. N. (1974). Geochemistry of Sulphur Isotopes. Nauka, Moscow, 274pp.

Gurvich, E. G. (1998). Metal bearing deposits of the word ocean. Moscow, Nauchny, Mir, 340p.

Haddon, R. A. W. and Bullen, K. E. (1969). An Earth model incorporating free Earth oscillation data. *Phys. Earth Planet. Inter.* **2,** 1.

Haken, G. (1980). "Synergistics." Mir, Moscow, 404pp.

Haken, G. (1985). "Synergistics. Hierarchy of instability in self-organizing systems and devices." Mir, Moscow, 188pp.

Hale, C. J. (1987). Palaemagnetic data suggest link between Archaean–Proterozoic boundary and inner-core nucleation. *Nature* **329,** 6136233–236.

Harris, A. W. and Kaula, W. M. (1975). A co-accretional model of satellite formation. *Icarus* **24,** 516–524.

Hartmann, W. and Davis, D. (1975). Satellite—sized planetesimals and lunar origin. *Icarus* **24,** 504–515.

Hartmann, W. and Larson, S. (1967). Angular momenta of planetary bodies. *Icarus* **7,** 257–260.

Haskell, N. A. (1935). Motion of viscous fluid under a surface load. *Physics* **6,** 265–269.

Наука, М. (1981). Essays of Comparative Planetology. Moscow, Nauka, 327–327pp.

Heirtzler, J. R., Dickson, G. O., Herron, E. M. Pitman, III, W. C., and Le Pichon, X. (1968). Marine magnetic anomalies, geomagnetic field reversals and motions of the ocean floor and continents. *J. Geophys. Res.* **73,** 62119–2136.

Heiskanen, W. A. and Vening Meinesz, F. A. (1958). "The Earth and Its Gravity Field." McGraw Hill, New York, 470pp.

Hekinian, R., Rosendahl, B. R., Cronan, D. S., et al. (1978). Hydrothermal deposits and associated basement rocks from the Galapagos spreading center. *Oceanol. Acta* **1,** 3473–482.

Hekinian, R., Francheteau, J., Renard, V., Ballard, R. D., et al. (1983). Intense hydrothermal activity at the rise axis of the East Pacific Rise near 13 N: Submersible witnesses the growth of sulfide chimney. *Mar. Geophys. Res.* **6,** 11–14.

Hess, H. H. (1962). History of ocean basins. Petrologic Students. A volume to honor A.F. Buddington. *Geol. Soc. Am.* 599–620.

Hollend, H. D. (1984). "The Chemical Evolution of the Atmosphere and Oceans." Princeton University Press, Princeton, NJ.

Holmes, A. (1928). Radioactivity and Earth movements. *Geol. Soc. Glasgow Trans.* **18,** 559–606.

Holmes, A. (1946). An estimate of the age of the Earth. *Nature* **157,** 680–684.

Houtermans, F. G. (1946). Die Isotopenhaufigkeiten im naturlichen Blei und das Alter des Urans. *Naturwissenschaften* **33,** 219185–186.

Hurley, P. M. (1968). Absolute abundance and distribution of Rb, K and Sr in the Earth. *Geochim. Cosmochim. Acta* **323,** 273–284.

Hutton, J. (1788). Theory of the Earth, Transactions Royal Society of Edinburgh, Vol. 1, p. 209-303.

Hutton, J. (1795). Theory of the Earth with Proofs and Illustrations, Edinburgh.

Ida, S., Canup, R. M., and Stewart, G. R. (1997). Lunar accretion an impact-generated disk. *Nature* **389,** 353–357.

Ilupin, I. P., et al. (1990). "Kimberlites. Reference Book." Nedra, Moscow, 248pp.

Imbrie, J. and Imbrie, K. P. (1979). "Ice Ages Solving the Mystery." Hillside, New Jersey.

Isaks, B., Oliver, J., and Sykes, L. R. (1968). Seismology and the new global tectonics. *J. Geophys. Res.* **73,** 185855–5899.

Ito, E. and Takahashi, E. (1989). Postspinel transformations in the system $Mg_2SiO_4-Fe_2SiO_4$ and some geophysical implications. *J. Geophys. Res.* **94,** 10637–10646.

Jacobs, J. A. (1975). "The Earth's Core." Academic Press, New York.

James, H. (2008). in The Guardian UK, June 23.

Janke, E., Emde, F., and Losch, F. (1960). "Tafeln Hoherer Funktionen." Stuttgart, B.G. Teubner Verlage Sellscaft.

Jaques, A. L., Lewis, J. D., and Smith, C. B. (1986a). "The Kimberlites and Lamproites of Western Australia." Government Printing Office, Perth.

Jaques, A. L., Lewis, J. D., and Smith, C. B. (1986b). The kimberlites and lamproites of Western Australia. *Geol. Surv. Australia Bull.* **32,** 268.

Jeffreys, H. (1959). "The Earth." 4th ed. Cambridge, New York, 420pp.

Jessberger, E. K., Huneke, I. C., Podosek, F. A., and Wasserburg, G. J. (1974). High resolution argon analysis of neutron-irradiated Appollo 16 rocks and separated minerals. *Proc. Fifth Lunar Sci. Conf.* **2,** 1419–1449.

Joder, H. S. and Tilley, C. E. (1962). "Origin of Basalt Magmas: An Experimental Study of Natural and Synthetic Rock Systems." Oxford University Press, Oxford.

Joly, J. (1929). "The surface history of Earth." Dublin.

Jordan, T. H. (1975), The present-day motions of the Caribbean Plate. *J. Geoph. Res.*, 80, 32.

Kalinin, V. A. and Sergeyeva, N.A. (1977). Variations in the internal structure of Earth caused by her evolution. *Izv. AN USSR, Phys. Earth* **5,** 44–51.

Kaminsky, F. V. (1984). "Diamond Bearing of Non-Kimberlite Igneous Rocks." Nedra, Moscow, 173pp.

Kapitsa, A. P. and Gavrilov, A. A. (1999). Confirmation of a hypothesis of the Antarctic ozone hole natural origin. Proc. RAN, Vol. 36, 4, p. 543–546.

Kaufmann, W. J., III. (1979). "Planets and Moons." W. H. Freeman and Company, San Francisco.

Kaula, W. M. (1968). "An Introduction to Planetary Physics: The Terrestrial Planets." Wiley and Sons, New York.

Kaula, W. M. and Harris, A. W. (1973). Dynamically plausible hypotheses of lunar origin. *Nature* **245,** 367–369.

Kay, M. (1971). North American geosynclines (Memoir 48), Geological Society of America.

Kazakov, A. V. (1939). Phosphate formations: Origin of phosphorites and the geologic factors of deposit formation. Proceedingsof NIUF **145**, Moscow. 108pp.

Kegwin, I. D. (1996). The Little Ice Age and Medieval Warm in the Sargasso Sea. *Science* **274,** 1504–1508.

Keondzhyan, V. P. and Monin, A. S. (1975). Gravity differentiation model of the planetary subsurface. *Proc. AN USSR* **220,** 4825–828.

Keondzhyan, V. P. and Monin, A. S. (1976). Calculation of the planetary subsurface evolution. *Izv. AN USSR Phys. Earth* **4,** 3–13.

Khain, V. E. (1973). "On the New Global Tectonics Issues of the Global Tectonics." Nauka, Moscow, pp. 5–26.

Khain, V. E. (1977). Particulars of the Earth's crust evolution in Early Precambrian—Real and fictitious. *In* "Issues of the Early Precambrian Geology," pp. 5–12. Nauka, Leningrad.

Khain, V. E. (2000). Issues of the Early Precambrian Tectonics. Herald MGU, Series 4. *Geology* **4,** 13–24.

Khain, V. E. (2001). "Tectonics of the Continents and Oceans." Nauchny Mir, Moscow, 606pp.

Khain, V. E. and Bozhko, N.A. (1988). "Historical geotectonics, Precambrian." Nedra, Moscow, 382pp.

Khain, V. E. and Lomidze, M. G. (1995). "Geotectonics with the Fundamentals of Geodynamics." MGU Publishers, Moscow, 480pp.

Khain, V. E. and Seslavinsky, K. B. (1994). Global rhythms in the Phanerozoic endogenous activity of Earth. *Stratigr. Geol. Correl.* **2,** 640–63.

Khain, V. E., Koronovsky, N. V. and Yasamanov, N. A. (1997). "Historical Geology," 448pp. MGU Publishers, Moscow.

Kharkiv, A. D., Zinchuk, N. N., and Kryuchkov, A. I. (1998). "Bedrock Diamond Deposits of the World." Nedra, Moscow, 555pp.

Kheskin, L. A., Frey, F. A., Schmidt, L. A., and Smith, R. H. (1968). "Rare Earths Distribution in the Lithosphere and Cosmos." Mir, Moscow, 188pp.

Khilyuk, L. and Chilingar, G. (2003). Global warming: Are we confusing cause and effect? *Energy Sour.* **25,** 357–370.

Khilyuk, L. and Chilingar, G. (2004). Global warming and long-term climatic changes: A progress report. *Environ. Geol.* **46,** 6–7970–979.

Khramov, A. N. (1976). Paleomagnetic characteristics of rocks. *In* "Physical Properties of Rocks and of Economic Deposits," pp. 189–193. Nedra, Moscow.

Khromov, S. P. and Petrosyants, M. A. (2001). "Meteorology and Climatology." MGU Publishers, Moscow, 528pp.

Kirkinsky, V.A. (1975). Decomposition of solid solutions. *In* "Experiment in Mineralogy and Petrography," Nauka, Moscow, 1735pp.

Knauth, L. P. and Lowe, D. R. (1978). Oxygen isotopic composition of cherts from the Onverwacht Group (3, 4 b. yrs), South Africa, with implications for secular variations in the isotopic composition of cherts. *Geol. Soc. Am. Abstracts Prog* **10,** 436.

Kolman, R. G. (1979). "Ophiolites." Mir, Moscow, 262pp.

Kotlyakov, V. M. (2000). Glaciology of the Antarctic. Moscow, Nauka, 432 p.

Kotlyakov, V. M. (2002). In the world of snow and ice. Moscow, Nauka, 384 p.

Kovalenko, V. I., et al. (1987). General patterns of the magmatism evolution in Earth's history. *In* "Magmatic Rocks", Magmatism Evolution in the Earth's History, (O. A. Bogatikov, ed.), Vol. 6, pp. 332–348. Nauka.

Kovalev, A. A. (1972). Plate tectonics and some aspects of metallogenetic analysis. *Geol. Ore Deposits* **5,** 90–96.

Kovalev, A.A. (1974). On the causes of a strong oil- and gas-geheration in the Middle East. *Geol. Oil Gas* **11,** 69–74.

Kovalev, A. A. (1978). "Mobilism End Exploration Geologic Criteria." Nedra, Moscow, 287c.

Kozlov, N. E. Sorokhtin, N. O., et al. (2006). "Archaean Geology of the Baltic Shield." Nauka, Sankt-Peterburg, 329pp.

Kozlovsky, E. A. (2002). "Russia: Raw Material Policy and the National Security." MGU Publishers, Moscow, 856pp.

Kratz, O. K., et al. (1981). "Evolution Stages and Types in the Precambrian Crust of the Ancient Shields." Nauka, Leningrad, 164pp.

Kropotkin, P. N. (1958). Value of paleomagnetism for stratigraphy and geotectonics. *Bull. MOIP Geol.* **38,** 457–86.

Kropotkin, P. N. (1961). Paleomagnetism, paleoclimates and the issue of Earth's crust major horizontal movements. *Soviet Geol.* **5,** 16–38.

Kucheruk, E. V. and Ushakov, S. A. (1985). "Plate tectonics and Oil and Gas Occurrences (Geophysical Analysis). Physics of Earth." VINITI, Moscow, 200c.

Kuhn, T. (1977). "Structure of the Scientific Revolutions." Progress, Moscow, 301pp.

Kuleshov, V. N. (1986). "Isotope Composition and Origin of the Depth Carbonates." Moscow, Nauka, 126pp.

Kushev, V. G. (1992). Baltic and Ukraine Shields in the general structure of the East-European basement as a system of meso- and mini-plates. *In* "Depth Structure and Geodynamics of the Crystalline Shields in the European USSR," (O. A. Bogatikova, ed.), pp. 85–94. Nauka, KNC AN USSR, Apatity.

Kuskov, O. L. and Fabrichnaya, O. B. (1990). Phase relations in the system FeO–MgO–$SiO_2$ at the transition zone—Lower mantle boundary. *Geochemistry* **2,** 266–278.

Kuskov, O. L. and Panferov, A. B. (1991a). Constitution of the mantle. 3. Density, elastic properties and the mineralogy of the 400 km discontinuity. *Phys. Earth Planet. Inter.* **69,** 85–100.

Kuskov, O. L. and Panferov, A. B. (1991b). Phase diagrams of the FeO–MgO–$SiO_2$ system and the structure of the mantle discontinuities. *Phys. Chem. Miner.* **17,** 642–653.

Kuznetsov, A. P. (1991). Once again on the old age and formation paths of the deep-water oceanic fauna. *Izv. AN USSR Biol.* **2,** 275–284.

Landau, L. D. and Lifshits, E.M. (1976). "Statistical Physics. Part 1." Nauka, Moscow, 584.

Landscheidt, T. (2003). New little ice age instead of global warming? *Energy Environ.* **14,** 327–350.

Larson, R. L., Pitman, W. C. I. I. I., Golovchenko, X., Cande, S. C., et al. (1985). "The bedrock Geology of the World." Freeman, New York, 235pp.

Lazarenko, E. K. (1971). "Course of Mineralogy." Higher Education Publishers, Moscow, 608pp.

Le Pichon, X. (1968). Sea-floor spreading and continental drift. *J. Geophys. Res.* **73,** 123661–3697.

Le Pichon, X., Francheteau, J., and Bonnin, J. (1973). "Plate Tectonics." Elsevier Scientific Publishing Company, Amsterdam.

Lehmann, I. (1934). Transmission times for seismic waves for epicentral distances around 20°. *Geodet. Inst. Skr.* **5,** 44.

Lehmann, I. (1936). *"P" Publ. Bur. Cent. Seism. Int.* A 14, 87–115.

Lehmann, I. (1959). Velocities of longitudinal waves in the upper part of the Earth's mantle. *Ann. Geophys.* **15,** 93–118.

Lein, A. Yu. and Sagalevich, A. M. (2000). Smokers of the Rainboe Field as area of a large-scale abiogenic methane synthesis. *Nature* **8,** 44–53.

Lein, A. Yu., et al. (1998). Geochemical features of gas-bearing ($CH_4$) deposits of a subwater mud volcano in the Norwegian Sea. *Geochemistry* **3,** 230–249.

Levinson-Lessing, F. Yu. (1940). "Petrography." GIZ Geological Literature, Leningrad-Moscow, 524pp.

Lisitsin, A. P. (1974a). Age and composition of the oceans' basalt bed. *Proc. AN USSR* **217,** 3561–565.

Lisitsin, A. P. (1974b). "Deposit Formations in the Oceans. Quantitative Distribution of the Depositional Material." Nauka, Moscow.

Lisitsin, A. P. (1978). "Processes of the Oceanic Sedimentation." Nauka, Moscow, 392pp.

Lisitsin, A. P. (1980). "Geology of the Ocean (Oceanology, Geophysics of the Ocean)." Nauka, Moscow, 464pp.

Lisitsin, A. P. (1984). Avalanche deposition, ocean level changes, hiatuses and the pelagic deposition as the global patterns. *In* "Paleo-Oceanology," (E. A. Kozlovsky, ed.), **3,** pp. 3–21. Nauka, Moscow.

Lisitsin, A. P. and Vinogradov, M.E. (1982). Global patterns of life distribution in the oceans and their reflection in the composition of the ocean-floor deposits. The formation and distribution of biogenic deposits. *Izv. AN USSR. Geol.* **4,** 5–24.

Lisitsin, A. P., et al. (1990). "Hydrothermal Formations in the Oceanic Rift Zones." Nauka, Moscow, 256pp.

Lister, C. R. B. (1972). On the thermal balance of a mid-ocean rise. *Geophys. J. Roy. Astron. Soc.* **26,** 516–520.

Litvin, Yu. A. (1991). "Physicochemical Studies of the Melting of Earth's Depth Matter." Nauka, Moscow, 312pp.

Lobkovsky, L. I. (1988). "Geodynamics of the Spreading and Subduction Zones and the Double-Staged Plate Tectonics." Nauka, Moscow, 251pp.

Lobkovsky, L. I. (2005). Catastrophic earthquake and tsunami 12. 26.2004 in the northern Sunda island arch, Indian Ocean: Geodynamic analysis and analogy with the central Kuril Islands. *Science* **5,** 253–61.

Lobkovsky, L. I. and Kotelkin, V. D. (2000). "Double-Stage Thermochemical Model of the Mantle Convection and Its Geodynamic Consequences. Issues of Global Geodynamics." GEOC, Moscow, pp. 29–53.

Lobkovsky, L. I. and Sorokhtin, O. G. (1976). "Plastic Deformations of the Oceanic Lithosphere in the Plate Subduction Zones. Tectonics of the Lithospheric Plates." Oceanology Institute, AN USSR, Moscow, p. 22–52.

Lobkovsky, L. I. and Sorokhtin, O. G. (1980). Tectonics of the lithospheric plates and the origin of the tsunami earthquakes. *Proc. AN USSR* **251,** 51092–1095.

Lobkovsky, L. I., et al. (2004). "Current Issues of Geotectonics and Geodynamics." Nauchny Mir, Moscow, 612pp.

Loper, D. E. (1975). Torque balance and energy budget for the precessionally driven dynamo. *Phys. Earth Planet. Inter.* **11,** 43–60.

Luriye, A. M. (1988). "Genesis of Copper Sandstone and Slates." Nauka, Moscow, 183pp.

Lutz, B. G. (1985). "Magmatism of Early Earth Mobile Belts." Nauka, Moscow.

Lyubimova, E. A. (1968a). "Thermics of Earth and of the Planets." Nauka, Moscow.

Lyubimova, E. A. (1968b). "Thermics of Earth and Moon." Nauka, Moscow, 280pp.

MacDonald, G. J. F. (1964a). Tidal friction. *Rev. Geophys.* **2,** 467–541.

MacDonald, G. J. F. (1964b). Tidal friction. *Rev. Geophys.* **2,** 3467–541.

Macdonald, C. A., Abbott, A. T., and Peterson, F. L. (1990). "Volcanes in the Sea: The Geology of Hawaii." University of Hawaii Press, Honolulu, 518pp.

Magnitsky, V.A. (1965). "Internal Structure and Physics of the Earth." Nedra, Moscow, 379pp.

Makkaveyev, P. M. and Sorokhtin, O. G. (2005). Experience in the reconstruction of the carbonate balance in the ancient ocean. *Oceanology* **45,** 3374–380.

Mason, B. (1966). "Principles of Geochemistry." 3rd ed. Wiley and Sons, New York, 329pp.

Mason, B. and Melson, W. G. (1970). "The Lunar Rocks." Wiley and Sons, New York.

Mason, B. (1971). Basics of geochemistry. Moscow, Nedra, 312 p.

Mason, B. and Melson, W. (1973). "Lunar Rocks." Mir, Moscow, 165pp.

Matveyenkov, V. V. and Sorokhtin, O. G. (1998). Petrological features on the initial evolutionary stages of the Loihi intraplate volcanism (Hawaian Islands, Pacific Ocean). *Oceanology* **38,** 5742–749.

McConnell, R. K., Jr. (1965). Isostatic adjustment in a layered Earth. *J. Geophys. Res.* **70,** 5171–5188.

McKenzie, D. and Richter, F. (1976). Convection currents in the Earth's mantle. *Sci. Am.* **235,** 572–89.

Melton, C. E. and Giardini, A. A. (1974). The composition and significance of gas released from natural diamonds from Africa and Brazil. *Am. Miner.* **59,** 7–8775–782.

Melton, C. E. and Giardini, A. A. (1975). Experimental results and theoretical interpretation of gaseous

inclusions found in Arkansas natural diamonds. *Am. Miner.* **60,** 5–6413–417.

Menard, G. U. (1966). "Geology of the Pacific Ocean Floor." Mir, Moscow, 273pp.

Meyen, R. V. (1971). Modern paleobotanics and the evolution theory. *Nature* **2,** 48–57.

Meynen, R. V. (1981). "Traces of Indian Grasses." Mysl, Moscow, 159pp.

Milankovitch, M. (1930). "Mathematische Klimatehre und Astronomische Teorie der Klimaschwan Kungen." Hundbuch der Klimatologie, **1A,** pp. 1–176. Gebrruder Borntraeger, Berlin.

Miller, S. L. (1959). Formation of organic compounds on the primitive Earth. *In* "The Origin of Life on Earth," (F. Clark and R. C. M. Synge, eds.), pp. 123–135. Pergamon, London.

Miller, S. L. and Urey, H. C. (1959). Organic compound synthesis on the primitive Earth. *Science* **130,** 245–251.

Minster, J. B., Jordan, T. N., Molnar, P., and Haines, E. (1974). Numerical modeling of instantaneous plate tectonics. *Geophys. J. Roy. Astron. Soc.* **36,** 541–554.

Minz, M. V. (1992). Paleogeodynamic reconstructions of Early Precambrian on the most ancient (eastern and northeastern) part of the Baltic Shield. *In* "-Geodynamics and Deep Structure in the Soviet Part of the Baltic Shield," (F. P. Mitrofanov, ed.), pp. 34–49. KNC RAN, Apatity.

Miyashiro, A. (1976). "Metamorphism and Metamorphic Belts." Mir, Moscow, 536pp.

Mokhov, I. I., Bezverkhniy, V.A., and Karpenko, A. A. (2003). Milankovic cycles and the evolution of climatic regime parameters and atmospheric composition based on ice cores from the Antarctic station "Vostok" *Mater. Glaciological Stud.* **95,** 3–8.

Monin, A. S. (1977). "History of Earth." Nauka, Leningrad, 228pp.

Monin, A. S. (1988). "Theoretical Fundamentals of Geophysical Hydrodynamics." Gidrometeoizdat, Leningrad, 424pp.

Monin, A. S. (1999). "Hydrodynamics of the Atmosphere, Ocean and Earth's Depths." Gidrometeoizdat, Moscow, 524pp.

Monin, A. S. and Sorokhtin, O. G. (1981). On the volumetric gravity differentiation of Earth. *Proc. AN USSR* **259,** 51076–1079.

Monin, A. S. and Sorokhtin, O. G. (1982a). Earth's evolution at volumetric differentiation in her depths. *Proc. AN USSR* **263,** 3572–575.

Monin, A. S. and Sorokhtin, O. G. (1982b). Evolution of the oceans and Precambrian metallogeny. *Proc. AN USSR* **264,** 61453–1457.

Monin, A. S. and Sorokhtin, O. G. (1982c). Heat evolution of Earth at volumetric differentiation of her depths. *Proc. AN USSR* **266,** 163–67.

Monin, A. S. and Sorokhtin, O. G. (1984). Evolution of the oceans and geochemistry of the continents. *In* "Paleo-oceanology," (E. A. Kozlovsky, ed.), 27th IGC **3,** pp. 22–35. Nauka, Moscow.

Monin, A. S. and Sorokhtin, O. G. (1986). On the deposits suck-in to great depths under the continents. *Proc. AN USSR* **286,** 3583–586.

Monin, A. S., Seidov, D. G., Sorokhtin, O. G., and Sorokhtin, Yu.O. (1987a). Numerical experiments with forms of the mantle convection. *Proc. AN USSR* **295,** 51080–1083.

Monin, A. S., Seidov, D. G., Sorokhtin, O. G., and Sorokhtin, Yu. O. (1987b). Numerical modeling of the mantle convection. *Proc. AN USSR* **295,** 158–63.

Moorbath, S. (1976). Age and isotope constraints for the evolution of Archean crust. *In* "The Early History of the Earth," (B. F. Windly, ed.), pp. 356–366. Wiley and Sons, New York.

Moralev, V. M. (1986). "Early Stages in the Evolution of the Continental Lithosphere." Nauka, Moscow, 166c.

Moralev, V. M. and Glukhovsky, M. Z. (1985). Partial melting of meta-basites and the evolution of the Precambrian lithosphere. *Proc. AN USSR* **284,** 2427–431.

Morelli, A. and Dziewonski, A. (1987). Topography of the core—Mantle boundary and lateral homogeneity of the liquid core. *Nature* **325,** 6106678–683.

Morgan, W. J. (1968). Rises, trenches, great faults and crustal blocks. *J. Geophys. Res.* **73,** 61959–1982.

Morgan, W. J. (1971). Convection plumes in the lower mantle. *Nature* **230,** 42–43.

Morgan, W. J. (1972). Deep mantle convection and plate motions. *Am. Assoc. Petrol. Geol.* **56,** 203–213.

Munk, V. (1968). Once again: Tidal friction. *J. Roy. Astron. Soc.* **9,** 4352–375.

Murbat, S. (1980). Boundary conditions of the Archaean crust evolution based on the age and isotope data. *In* "Early history of Earth", Moscow, Mir, p. 356–366.

Musatov, D. I. and Mezhelovsky, N. V. (1982). "Role of Riftogenic Structures in the Formation of Oil and Gas Basins and Fields." Moscow, VIEMS, 50pp.

Naimark, L. M. (1984a). On possible gravity differentiation mechanism in a medium which separates at heating. *Proc. AN USSR* **276,** 4846–850.

Naimark, L. M. (1984b). Zonal melting as a gravity differentiation mechanism. *Proc. AN USSR* **278,** 3580–584.

Naimark, L. M. and Sorokhtin, O. G. (1977a). "Density Distribution in Earth's Model with a Lherzolite

Mantle Composition and Oxide-Iron Core. Tectonics of the Lithospheric Plates." USSR Institute of Oceanology, Moscow, pp. 28–41.

Naimark, L. M. and Sorokhtin, O. G. (1977b). "Energy of Earth's Gravity Differentiation. Tectonics of the Lithospheric Plates." USSR Institute of Oceanology, Moscow, pp. 42–56.

Nekrasov, B. V. (1973). Fundamentals of general chemistry, Vol. 1. Moscow, Khimia, 656 p.

Naumov, G. B., Ryzhenko, B. N., and Khodakovsky, I. L. (1971). "Reference book of thermodynamic values (for geologists)." Moscow, Atmoizdat, 240pp.

Nesis, K. N. (2001). When life emerged in the ocean depths. *Nature* **4,** 68–69.

New Global Tectonics (Plate Tectonics) (1974). "Collection of Articles." Mir, Moscow, 472pp.

Ohtani, E. and Ringwood, A. (1984). Composition of the core. I. Solubility of oxygen in molten iron at high temperatures. *Earth Planet. Sci. Lett.* **71,** 185–93.

Ohtani, E., Ringwood, A., and Hibberson, W. (1984). Composition of the core II. Effect of high pressure on solubility of FeO in molten iron. *Earth Planet. Sci. Lett.* **71,** 194–103.

Ohtsuki, K. and Ida, S. (1998). Planetary rotation by accretion of planetesimals with nonuniform spatial distribution formed by the planet's gravitational perturbation. *Icarus* **131,** 393–420.

Oparin, A. I. (1957). "Origin of Life." AN USSR Publishers, Moscow.

Opik, E. J. (1961). Tidal deformation and the origin of the Moon. *Astronom. J.* **66,** 60–67.

Orlov, Yu. L. (1984). Mineralogy of the diamond. Moscow, Nauka, 264 p.

Oro, J. (1965). Investigation of organo-chemical evolution. *In* "Current Aspects of Exobiology," (G. Marnikunian and M. H. Briggs, eds.), Pergamon, London, pp. 13–76.

Oro, J. (1966). Prebiological organic systems. *In* "The Origin of Prebiological Systems," (S. W. Fox, ed.), pp. 137–162. Academic Press, New York.

Oversby, V. M. and Ringwood, A. E. (1971). Time of formation 0f the Earth's core. *Nature* **234,** 463–465.

Ozima, M. and Podosek, F. A. (1983). "Noble Gas Geochemistry." Cambridge University Press, Cambridge, London, New York, Melbourne, Sydney.

Panelli, G, F. A. (1972). Paleontological evidence on on the Earth's rotational history since early Precambrian. *Astrophys. Space Sci.* **16,** 212–237.

Pankov, V. L. and Kalinin, V.A. (1975). Thermodynamic parameters of rocks and minerals in conditions of Earth shell. *Izv. AN USSR Phys. Earth* **3,** 3–15.

Pariysky, N. N. (1960). On the effects of Earth's tides on centenarian slowdown of Earth's revolution. *Astron. J.* **37,** 543–555.

Parker, R. L. and Oldenburg, D. W. (1973). Thermal model of Ocean Ridges. *Nat. Phys. Sci.* **242,** 122137–139.

Parkinson, W. D. (1983). "Introduction to Geomagnetism." Scottish Academic Press, Edinburgh and London.

Perisypkin, V. I., Lein, A. Yu., Bogdanov, Yu. A., and Bortnikov, N. S. (1998). Lipids in hydrothermal formations in the area of 14°45′N and 29°N of the Mid-Atlantic Ridge. *Oceanology* **38,** 5.

Perry, E. C., Jr. (1967). The oxygen isotope chemistry of ancient cherts. *Earth Planet. Sci. Lett.* **3,** 62.

Perry, E. C., Jr. and Tan, F. C. (1972). Significance of oxygen and carbon isotope variations in early Precambrian cherts and carbonate rocks of southern Africa. *Geol. Soc. Am. Bull.* **83,** 647–664.

Peyve, A. V. (1969). Oceanic crust of the geologic past. *Geotectonics* **4,** 5–23.

Peyve, A. V., Knipper, N.A., Shtreys, A. A., et al. (1971). Ocean and the geosynclinal process. *Proc. AN USSR* **196,** 3657–659.

Physical properties of rocks and of economic deposits (Petrophysics) (1976). "Reference Book of Geophysicists." Nedra, Moscow, 527pp.

Physics of the Cosmos (1986). "Small Encyclopedia." Soviet Encyclopedia, Moscow, 783pp.

Piper, J. D. F. (1976). Paleomagnetic evidence for a Proterozoic supercontinent. *Phil. Trans. Roy. Soc. Lond.*, Vol. 280A, p.469–490.

Pitman, W. C. and Heys, J. D. (1973). Upper cretaceons spreading rates and the great transgression. *Geol. Soc. Am. Abstr.* **5,** 72344–2357.

Polyansky, O. P. (1987). "Mechanism of granite-gneiss domes diapiric buoying. Hydrodynamic model. Evolutionary models of the metamorphism processes on the shields and in the folded areas." IGiG, Novosibirsk, pp. 62–64.

Ponnamperuma, C. (1965). "Abiological Synthesis of Some Nucleic Acid Constituents. The Origin of Prebiological Systems." Academic Press, New York, pp. 221–236.

Pospelov, G. M. (1971). Some issues of endogenous dynamics. *In* "Issues of the General and Regional Geology," (B. N. Falaleyev, ed.), pp. 20–60. Nauka, Novosibirsk.

Precambrian of the Continents (1976a). "Australia and Africa." Nauka (Siberian Branch), Novosibirsk, 224pp.

Precambrian of the Continents (1976b). "North and South America." Nauka (Siberian Branch), Novosibirsk, 240pp.

Precambrian of the Continents (1977). "Ancient Platform of Eurasia." Novosibirsk, Nauka (Siberian Branch), 312pp.

Prigozhin, I. R. and Stengers, I. (2003). "Order from Chaos. New Dialog of Man with the Nature." Editorial URSS, Moscow, 312pp.

Pugin, V.A. and Khitarov, N. I. (1978). "Experimental Petrology of the Depth Magmatism." Nauka, Moscow, 175pp.

Pushcharovsky, Yu. M. and Pushcharovsky, D. Yu. (1999). Geospheres of the Earth's mantle. *Geotectonics* **1,** 3–14.

Ranelli, G. and Fischer, B. (1984). Diffusion creep, dislocation creep, and mantle rheology. *Phys. Earth Planet. Inter.* **34,** 77–84.

Reference book of rocks' physical constants. (1969). P. Ckarke, (ed)., Mascow, 544pp.

Reynolds, R. T. and Summers, A. L. (1969). Calculation on the composition of the terrestrial planets. *J. Geophys. Res.* **74,** 10.

Richter, F. M. (1973). Dynamical models of see-floor spreading. *Rev. Geophys. Space Phys.* **11,** 223–287.

Ringwood, A. E. (1962a). A model for the upper mantle. 1. *J. Geophys. Res.* **67,** 857–866.

Ringwood, A. E. (1962b). A model for the upper mantle. 2. *J. Geophys. Res.* **67,** 4473–4477.

Ringwood, A. E. (1966). "The Chemical Composition and Origin of the Earth. Advances in Earth Sciences." Cambridge, MIT Press, pp. 276–356.

Ringwood, A. E. (1975a). "Composition and Petrology of the Earth's Mantle." McGraw-Hill, New York.

Ringwood, A. E. (1975b). "Composition and Petrology of the Earth's Mantle." McGraw-Hill, New York.

Ringwood, A. E. (1977). Composition of the core and implications for the origin of the Earth. *Geochem. J.* **11,** 111–135.

Ringwood, A. E. (1979). "Origin of the Earth and Moon." Springer-Verlag, Berlin.

Ringwood, A. E. (1981). Composition and petrology of the Earth's mantle. Moscow, Nedra, 584 p.

Ringwood, A. E. (1982). Origins of Earth and Moon. Moscow, Nedra, 175 p.

Ringwood, A. E. and Hibberson, W. (1990). The system Fe-FeO revisited. *Phys. Chem. Miner.* **17,** 313–319.

Rosanov, A. Yu. (2003). Fossil bacteria, sedimentogenesis and early studies of the biosphere evolution. Paleontologic Journal, Moscow, MAIK, No. 6, p. 1–9.

Robinson, A. B., Baliunas, S. L., Soon, W., and Robinson, Z. W. (1998). Environmental effects of increased atmospheric carbon dioxide. *J. Am. Physicians Surg.* **3,** 171–178.

Robinson, A. B., Robinson, N. E., and Soon, W. (2007). Environmental effects of increased atmospheric cabon dioxide. *J. Am. Physicians Surg.* **12,** 79–90.

Romankevich, E. A. (1977). Geochemistry of organic matter in the ocean. Moscow, Nauka, 256 p.

Romankevich, E. A. (1984). "Geochemistry of Organic Matter in the Ocean." Springer-Verlag, Moscow, 33pp.

Rona, P. (1986). "Hydrothermal Mineralization of Spreading Areas in the Oceans." Mir, Moscow, 160pp.

Ronov, A. B. (1993). "Stratisphere or the Sedimentary Shell of Earth." Nauka, Moscow, 144pp.

Ronov, A. B. and Yaroshevsky, A.A. (1978). "Chemical Composition of the Earth's Crust and of Her Shells. Tectonosphere of Earth." Nedra, Moscow, pp. 376–402.

Rosen, O. M., Condie, K. C., Natapov, L. M., and Nozhkin, A. D. (1994). "Archaean and Early Proterozoic evolution of the Siberian Craton: A Preliminary Assessment. Archaean Crustal Evolution." Elsevier, Amsterdam, pp. 411–459.

Rudkevich, M. Ya. (1974). "Paleotectonic Criteria of Oil- and Gas-Bearing." Nedra, Moscow, 184pp.

Runcorn, S. K. (1962). Convection currents in the Earth's mantle. *Nature* **195,** 1248–1249.

Runcorn, S. K. (1963). Paleomagnetic Methods of Investigating Polar Wandering and Continental Drift: Soc. Econ. Paleon. Min. Special Pub., Tulsa, vol. 10, p.47–54.

Runcorn, S. K. (1965). Changes in the convection pattern in the Earth's mantle and continental drift: Evidence for a cold origin of the Earth. *Philos. Trans. Roy. Soc. Ser. A* **258,** 228–251.

Ruskol, E. L. (1960). On the origins of Moon. I. The formation of the near-Earth swarm. *Astronom. J.* **37,** 4690–702.

Ruskol, E. L. (1963). On the origins of Moon. II. Moon's growth within the near-Earth satellite swarm. *Astronom. J.* **40,** 2288–296.

Ruskol, E. L. (1971). On the origins of Moon. III. Some issues of the near-Earth swarm dynamics. *Astron. J.* **48,** 4819–829.

Ruskol, E. L. (1975). "On the Origins of Moon." Nauka, Moscow, 188pp.

Safronov, V. S. (1969). "Evolution of the Preplanetary Cloud and the Formation of Earth and Planets." Nauka, Moscow, 244pp.

Safronov, V. S. (1982). Current status of the Earth's origins theory. *Izv. AN USSR Phys.Earth* **6,** 5–24.

Safronov, V. S. and Vityazev, A. V. (1983). *In* "Origins of the Solar System. Results of Science and Technology, Astronomy," (G. Rives, ed.), **4,** pp. 5–93. VINITI, Moscow.

Sakai, H., Marais, D., Ueda, A., and Moore, J. (1984). Concentrations and isotope ratios of carbon, nitrogen and sulfur in ocean-floor basalts. *Geochim. Cosmochim. Acta* **48,** 122433–2441.

Salop, L. I. (1973). "General Stratigraphic Scale of Precambrian." Nedra, Leningrad, 310pp.

Savelyeva, G. N. (1987). "Gabbro-Ultramafic Complexes of the Uralian Ophiolites and Their Analogs in the Modern Oceanic Crust." Nauka, Moscow, 246pp.

Savostin, L.A., Volokitina, L. P., Zonenshain, L. P., et al. (1980). Paleobathymetry of the Pacific Ocean in Late cretaceous. *Oceanology* **XX,** 5871–881.

Schidlowski, M. (1987). Application of stable carbon isotopes to early biochemical evolution on Earth. *Ann. Rev. Earth Planet. Sci.* **15,** 47–72.

Schlichting, H. (1964). "Grenzschicht-Theorie." Verlag G. Braun, Karlsruhe.

Schmidt, O. Yu. (1946). New theory of the Earth's origins. Nature, **7**, 6–16.

Schmidt, O. Yu. (1948). "Four Lectures on the Theory of the Earth's Origins," 76pp. AN USSR Publishers, Moscow.

Schopf, T. (1980). "Paleoceanography." Harvard University Press, Cambridge, MA.

Sclater, J. G., Jaupart, C., and Galson, D. (1980). The heat flow through oceanic and continental crust and the heat loss of the Earth. *Rev. Geophys. Space Phys.* **18,** 269–311.

Sclater, J., Parsons, B., and Laupart, C. (1981). Oceans and continents: Similarities and differences in the mechanism of heat transport. *J. Geophys. Res.* **86,** 11535–11552.

Semikhatov, M. A., Raaben, M. E., Sergeyev, V. N., Veis, A. F., and Artemova, O. B. (1999). Biotic events and a positive isotopic anomaly of the carbonate carbon 2.3–2.06 BY ago. *Stratigr. Geol. Correl.* **2,** 3–27.

Shemenda, A. I. (1983). Similarity criteria at mechanical modeling of tectonic processes. *Geol. Geophys.* **10,** 10–19.

Shklovsky, I. S. (1975). "Stars: Their Birth, Life and Death." Nauka, Moscow, 368pp.

Shklovsky, I. S. (1976). "Supernovae and the Associated Issues." Nauka, Moscow, 440pp.

Sillitoe, R. H. (1972a). A plate tectonic model for the origin of porphyry copper deposits. *Econ. Geol.* **67,** 184–197.

Sillitoe, R. H. (1972b). Relation of metal provinces in Western America to subduction of oceanic lithosphere. *Bull. Deol. Soc. Am.* **83,** 813–818.

Sinitsin. (1992). Geodynamics of the Baltic shield from the position of Archean cratons and Proterozoic mobile belts. In: Geodynamics and deep structure of the Soviet portion of the Baltic shield. KNZ RAN, p. 7–16.

Singer, S. F. (1972). Origin of the Moon by tidal capture and some geophysical consequences. *The Moon* **5,** 206.

Sinyakov, V. I. (1987). "Fundamentals of the Ore Genesis Theory." Nedra, Leningrad, 192pp.

Slobodkin, A. I., et al. (1995). Magnetite formation by thermophilic micro-organisms. Proc. RAN, Vol. 345, 5, p. 694–697.

Smirnov, Ya. B. (1980). "Heat Field of the USSR Territory (Explanatory Note to the Heat Flow and Depth Temperature Maps 1:10, 000, 000)." GUGK, Moscow, 150pp.

Smirnov, V. I. (1982). Geology of commercial deposits. Moscow, Nedra, 669p.

Smirnov, V. I. (1984). Periodicity of ore formation in the geologic history. *In* "Metallogeny and ore deposits," Moscow, Nauka, p. 3–10.

Smith, A. G. and Briden, J. C. (1977). *In* "Mesozoic and Cenozoic Paleocontinental Maps," Cambridge University Press, London, New York, Melbourn, 63pp.

Smith, D. E., Kolenkiewicz, R., Dunn, P. J., Robbins, J. W., et al. (1990). Tectonic motion and deformation from satellite laser ranging. *J. Geophys. Res.* **95,** B1322013–22041.

Sobolev, R. N. (2000). Types of tin deposits and their distribution in time and space. Herald of MGV, series 4, Geology, 1, p. 30–39.

Sobolev, V. S. and Sobolev, N. V. (1980). New evidences of the Earth crust eclogite rocks subsidence to great depths. *Proc. AN USSR* **250,** 3683–685.

Sokolov, Yu. M. and Kratz, K. O. (1984). Metallogenic impulses of the Earth's crust endogenous activization in Precambrian. *In*: "Metallogeny of the USSA Early Precambrian". Leningrad, Nauka, p. 4–14.

Sommerfeld, A. (1944). "Mechanik." Zweite, Revidierte Auflage.

Sorokhtin, O. G. (1972). Differentiation of the Earth's matter and the evolution of tectonic processes. *Izv. AN USSR. Phys. Earth* **7,** 55–66.

Sorokhtin, O. G. (1973a). Correlation of the mid-oceanic ridge topography with the lithospheric plate spreading rate. *Proc. AN USSR* **208,** 6, 1338–1341.

Sorokhtin, O. G. (1973b). Possible formation mechanism of the regional overthrusts and geosynclinal folding. *Izv. AN USSR, Phys. Earth* **7**, 55–67.

Sorokhtin, O. G. (1974). "Global Evolution of Earth." Nauka, Moscow, 184pp.

Sorokhtin, O. G. (1976). Tectonics of the lithospheric plates and the nature of global transgressions. *In* "Issues of Paleohydrology," (M. V. Astaykin, ed.), pp. 59–69. Nauka, Moscow.

Sorokhtin, O. G. (1977). Contents of radioactive elements in Earth and the radiogenic energy. *In* "Tectonics of the Lithospheric Plates (Sources of the Tectonic Processes Energy and the Plate Dynamics)," (A. S. Monin, ed.), pp. 7–27. IOAN, Moscow.

Sorokhtin O. G. (editor) (1979). Geodynamics (oceanology, geophysics of the ocean), Vol. 2, Moscow, Nauka, 416 p.

Sorokhtin, O. G. (1979a). Issues of oil generation within the plate subduction zones. *In* "Oceanology, Geophysics of the Ocean, Vol. 2, Geodynamics," (O. G. Sorokhtin, ed.), pp. 377–383. Nauka, Moscow.

Sorokhtin, **O**. G. (1979b). "Geodynamics (Oceanology, Geophysics of the Ocean, Vol. 2)." Nauka, Moscow, 416pp.

Sorokhtin, O. G. (1981a). Possible physicochemical processes of the Earth's core formation. *Proc. AN USSR* **198,** 61327–1330.

Sorokhtin, O. G. (1981b). Structure of the continental lithospheric plates and the origins of kimberlites. *In* "Issues of Theoretical Geodynamics and the Tectonics of the Lithospheric Plates," (A. S. Monin, ed.), pp. 161–168. Oceanology Institute of AN USSR, Moscow.

Sorokhtin, O. G. (1984). "Tectonics of the Lithospheric Plates—A Modern Geologic Theory." Znaniye, Moscow, Russian Federation, 40pp.

Sorokhtin, O. G. (1985). "Tectonics of the Lithospheric Plates and the Origins of the Diamondiferous Kimberlites. General and Regional Geology." VIEMS, Moscow, 47pp.

Sorokhtin, O. G. (1987). "Formation of Diamondiferous Kimberlites and the Affined Rocks from a Standpoint of the Lithospheric Plate Tectonics. Geodynamic Analysis and the Patterns of Formation and Distribution of Economic Deposits." Nedra, Leningrad, pp. 92–107.

Sorokhtin, O. G. (1988). "Origins of Moon and the Initial Stages of the Earth Evolution Life of Earth." MGU Publishers, Moscow, pp. 5–24.

Sorokhtin, N. O. (1994). Theoretical aspects of the Early Precambrian geodynamics on the example of the continental crust formation in the NW White Sea region. *In* "Geologic Mapping of Early Precambrian complexes," (N. V. Mezhelovsky, ed.), pp. 438–498, Moscow.

Sorokhtin, N. O. (1997). Dual-layer model of the continental crust formation in Archaean. *In* "Abstracts of Reports at the International Conference "New Ideas in Earth Sciences," Vol. 1, Moscow," 136–137.

Sorokhtin, O. G. (1999). Early stages in the evolution of the Earth-Moon system. *Izv. Sect. Earth Sci. RAEN* **2,** 141–153.

Sorokhtin, N. O. (2001a). "Evolution of the Continental Lithosphere in Early Precambrian (on the Example of the Eastern Baltic Shield)." MGU, Moscow, PhD thesis, 368pp.

Sorokhtin, O. G. (2001b). Greenhouse effect: Myth and reality. *Herald RAEN* **1,** 18–21.

Sorokhtin, N. O. (2002). Climate of Early Precambrian and the nature of the Huron glaciation. *Herald MGU* **5,** 125–42.

Sorokhtin, O. G. (2004). Global evolution of Earth. *Herald RAEN* **4,** 43–16.

Sorokhtin, O. G. (2005a). Bacterial nature of the Earth's glaciations. *Herald RAN* **75,** 121107–1114.

Sorokhtin, O. G. (2005b). Generation of the abiogenic methane and history of Earth evolution. *Oceanology* **45,** 4531–541.

Sorokhtin, O. G. (2006a). Oceanic deposits—A "cradle" of diamonds. *Nauka in Russia* **4,** 46–56.

Sorokhtin, O. G. (2006b). "Evolution and forecast of changes in the global Earth climate. "Regular and chaotic dynamics"." Institute of Computer Studies, Moscow–Ижевск.

Sorokhtin, O. G. (2007). "Life of Earth. "Regular and Chaotic Dynamics"" Institute of computer studies, Moscow–Izhevsk, 452pp.

Sorokhtin, O. G. (2008). Causes of changes in the Earth's global climate. *Ecol. Industry Russ.* 35–40.

Sorokhtin, O. G. and Balanyuk, I. E. (1982). On the association between oil and gas occurrences and plate subduction zones. *Oceanology* **XXII,** 2236–245.

Sorokhtin, O. G. and Lobkovsky, L. I. (1976). A mechanism of pulling-in the oceanic deposits into the oceanic plate subduction zones. *Izv. AN USSR Phys. Earth* **5,** 3–10.

Sorokhtin, O. G. and Sagalevich, A.M. (1994). Hydrothermal activity on the ocean-floor. *Proc. IO RAN* **131,** 151–162.

Sorokhtin, N. O. and Sorokhtin, O. G. (1997). Continent stand level and possible nature of the Early Proterozoic glaciation. *Proc. RAN* **354,** 2234–237.

Sorokhtin, O. G. and Sorokhtin, N. O. (2005). Earth's core separation is the main planetary process controlling geologic evolution of Earth. *Izv. Sect. Earth Sci. RAEN* **13,** 99–116.

Sorokhtin, O. G. and Sorokhtin, N. O. (2006). Exogenous mechanism of the diamond origin. *In* "Smirnov Collection," (V. I. Smirnov, ed.), pp. 109–130. RAEN, Moscow.

Sorokhtin, O. G. and Ushakov, S. A. (1989a). On three stages in the tectonic evolution of Earth. *Proc. AN USSR* **307,** 177–83.

Sorokhtin, O. G. and Ushakov, S. A. (1989b). "Origin of Moon and Its Effect on the Global Evolution of Earth." MGU Publishers, Moscow, 111pp.

Sorokhtin, O. G. and Ushakov, S. A. (1990). "Process of the Earth's Core Separation. Life of the Earth, Evolution of Earth and the Planets." Izd. MGU, Moscow, 6–34.

Sorokhtin, O. G. and Ushakov, S. A. (1991). "Global Evolution of Earth." MGU Publishers, Moscow, 446pp.

Sorokhtin, O. G. and Ushakov, S. A. (1993). "Nature of Earth's tectonic activity. Results of Science and Technology. Series Physics of Earth, Vol. 12." Moscow, VINITI, p. 292.

Sorokhtin, O. G. and Ushakov, S. A. (1996). ContinentalDrift in the Geologic History of Earth. Life of Earth **29,** pp. 5–37. MGU Publishers, Moscow.

Sorokhtin, O. G. and Ushakov, S. A. (1998). Effect of the ocean on the Earth's atmosphere composition and climates. *Oceanology* **38,** 6928–937.

Sorokhtin, O. G. and Ushakov, S. A. (2002). "Evolution of Earth." MGU Publishers, Moscow, 560pp.

Sorokhtin, O. G., Dmitriyev, L. V., and Udintsev, G. B. (1971). Possible mechanism of the Earth's crust formation. *Proc. AN USSR* **199,** 2319–322.

Sorokhtin, O. G., Ushakov, S. A., and Fedynsky, V. V. (1974). Dynamics of the lithospheric plates and oil field formation. *Proc. AN USSR* **214,** 1407–1410.

Sorokhtin, O. G., Mitrofanov, F. P., and Sorokhtin, N. O. (1996). "Origin of Diamonds and Potential of Diamond Bearing of the Eastern Baltic Shield." KNC RAN, Apatity, p. 144.

Sorokhtin, O. G., Lein, A. Yu., and Balanyuk, I. E. (2001). Thermodynamics of the oceanic hydrothermal systems and the abiogenic generation of methane. *Oceanology* **41,** 6898–909.

Sorokhtin, O. G., Mitrofanov, F. P., and Sorokhtin, N. O. (2004). "Global Evolution of Earth and Origin of Diamonds." Nauka, Moscow, 269pp.

Sorokhtin, O. G., Chilingar, G. V., and Khilyuk, L. F. (2007a). "Global Warming and Global Cooling: Evolution of Climate on Earth." Elsevier, New York, 313pp.

Sorokhtin, O. G., Chilingar, G. V., Khilyuk, L. F., and Gorfunkel, M. V. (2007b). Evolution of the Earth's global climate. *Energy Sour. A* **29,** 11–19.

Stacey, J. S. and Kramers, J. D. (1975). Approximation of terrestrial lead isotope evolution by a two-stage model. *Earth Planet. Sci. Lett.* **26,** 207–221.

Standard Atmosphere. Physical Encyclopedia. (1988) Soviet Encyclopedia, Moscow, Vol. 1, pp. 140–141.

Starostin, V. I. and Ignatov, P.A. (2004). "Geology of Economic Deposits." Academic Project, Moscow, 512pp.

Starostin, V. I. and Sorokhtin, O. G. (2002). Evolution of Earth and metallogeny. *Izv. SNZ RAEN* **8,** 64–76.

Strakhov, N. M. (1963). Types of lithogenesis and their evolution in Earth's history, Moscow, Gosgeolizdat, 535 p.

Strakhov, N. M. (1976). Geochemical issues of the present-day oceanic lithogenesis, Proc. GIN AN SSSR, 292, Moscow, Nauka, p. 73–87.

Stille, H. (1944). Geotectonische Gliederung der Erdgeschichte, Abh. preuβ. Acad. Wiss. math-phys., K1. 3, Berlin.

Stille, H. (1964). Geotectonic subdivision of Earth's history. Selected works, Moscow, Mir, 888 p.

Takahashi, I. (1986). Melting of dry peridotite KLB-1 up to 14 Gpa: Implications on the origin of peridotitic mantle. *J. Geophys. Res.* **91,** 899367–9382.

Takeuchi, H. (1963). Time scales of isostatic compensations. *J. Geophys. Res.* 68, 8. p. 2357.

Takeuchi, H. and Sakata, S. (1970). Convection in a mantle with variable viscosity. *J. Geophys. Res.* **5,** 5.

Tayler, R. J. (1975). "Origins of Chemical Elements." Mir, Moscow, 232pp.

Taylor, S. R. (1964). Trace element abundances and the chondritic Earth model. *Geochim. Cosmochim. Acta* **28,** 1989–1998.

Taylor, S. R. (1973). Chemical evidence for lunar melting and differentiation. *Nature* **245,** 203–205.

Taylor, S. P. and McLennan, S. M. (1985). "The Continental Crust: Its Composition and Evolution." Blackwell Scientific, Oxford.

Teng, T. (1968). Attenuation of body waves and the Q structure of the mantle. *J. Geophys. Res.* **73,** 62195–2208.

Tera, F. and Wasserburg, G. J. (1974). U–Th–Pb systematics on lunar rocks and inferences evolution and the age of the Moon. Proceedings of the Fifth Lunar Science Conference, Elsevier, Cambridge, MA. Vol. 2, pp. 1571–1599.

Tera, F. and Wasserburg, G. J. (1975). The evolution end History of mare basalts as inferred from U–Th–Pb systematic. *Lunar Sci.* **VI,** 807–809.

Tera, F., Papanastassion, D. A., and Wasserburg, G. J. (1974). Isotopic evidence for a terminal lunar cataclysm. *Earth Planet. Sci. Lett.* **22,** 1–21.

Teslenko, T. L. and Sagautdinova, M. Sh. (2006). "Geodynamic Conditions of the Lithosphere Formation." IP, Almaty, 229pp.

Tikhonov, A. N. and Samarinsky, A.A. (1966). "Equations of Mathematical Physics." Nauka, Moscow, 724c.

Tilton, G. B. and Read, G. W. (1963). Radioactive heat production in eclogites and some ultramafic rocks. *In* "Earth Science and Meteoritics," (J. Geiss and E. D. Goldberg, eds.), *In* North-Holland PublishingCompany, Amsterdam, 31–43.

Tolstikhin, I. L. (1986). "Isotopic Geochemistry of Helium, Argon and Rare Gases." Nauka, Leningrad, 200pp.

Tozer, D. C. (1965). Thermal history of the Earth. 1: The formation of the core. *Geophys. J.* **9**95.

Trofimov, V. S. (1980). "Geology of Natural Diamond Deposits." Moscow, Nedra, 304pp.

Trubitsin, V. P. and Rykov, V. V. (2000). "Mantle Convection with Floating Continents. Issues of Global Geodynamics." GEOC, Moscow, pp. 7–28.

Trubitsin, V. P., Belavina, Tu. F., and Rykov, V. V. (1994). Interaction between the mantle convection and continental and oceanic plates. *Proc. RAN* **334,** 3368–371.

Turcotte, D. and Burke, K. (1978). Global sea-level changes and the thermal structure of the Earth. *Earth Planet. Sci. Lett.* **41,** 341–346.

Turcotte, D. L. and Oxburg, E. R. (1978). Intraplate volcanism. *Philos. Trans. R. Soc. Lond.* **288A,** 501–579.

Turcotte, D. L. and Schubert, J. (1985). "Geodynamics." Mir, Moscow, Vols. 1 and 2, 374pp., 730pp.

Tugarinov, A. I. and Voitkevich, G. V. (1970), Precambrian geochronology of the continents, Moscow, Nedra, 434 p.

Umbgrove, J. H. F. (1947). "The Pulse of the Earth." Martinus Nijhof, Hague.

Unksov, V.A. (1981). "Plate Tectonics." Nedra, Leningrad, 288c.

Urey, H. C. (1972). The origin of the Moon and the Solar system. *Moon, IAU Sympos* **47,** 429–440.

Urey, H. C. and Craig, H. (1953). The composition of the stone meteorites and the origin of meteorites. *Geochim. Cosmochim. Acta* **4,** 36–82.

Ushakov, S. A. (1968). Viscosity and dynamic processes in the crust and upper mantle. Herald MGU. *Geology* **1,** 62–75.

Ushakov, S. A. (1974). "Structure and Evolution of Earth. Results of Science and Technology. Series Physics of Earth." VINITI, Moscow, Vol. 1, 269pp.

Ushakov, S. A. and Fedynsky, V. V. (1973). Riftogenesis as a mechanism of control over the Earth's heat loss. *Proc. AN USSR* **209,** 51182–1185.

Ushakov, S. A. and Galushkin, Yu. (1978). "Earth's Lithosphere (Based on Geophysical Data). Pt. 1. Plate kinematics and the oceanic lithosphere." "Results of Science and Technology, Physics of Earth." VINITI AN USSR, Moscow, Vol. 3, 272pp.

Ushakov, S. A. and Khain, V. E. (1965). Structure of the Antarctic based on geologo-geophysical data. Herald MGU. *Geology* **1,** 3–27.

Ushakov, S. A. and Krass, M. S. (1972). "Gravity and Issues of the Depth Mechanics." Nauka, Moscow, 158pp.

Uyeda, S. and Francheteau, J. (Eds.) Chilean versus Mariana type subduction zones with remarks on arc volcanism and collision tectonics. *In* Monger, J. W. H. Circum-Pacific Orogenic Belts and Evolution of the Pacific Ocean Basin. *Amer. Geophys. Un., Geodyn. Ser.*, vol.18, pp.1–17.

Vail, P. R., Mitchum, R. M., Sr., and Thompson, S. (1976). Seismic stratigraphy and global changes in sea level, part 4: global cycles of relative changes in sea level. *Am. Assoc. Petrol. Geol. Memoir* **26,** 83–97.

Veizer, J. (1976). Evolution ratio $^{87}Sr/^{86}Sr$ in marine water. *In* "The Early History of the Earth," (B. F. Windley, ed.), pp. 363–373. Wiley, New York.

Vening Meinesz, F. A. (1948). GravityExpedition at Sea **4,** Neth. Geol. Comm, Delft.

Vening Meinesz, F. A. (1955). Plastic buckling of the Earth's crust: The origin of geosynclines. *In* "Crust of the Earth (A Symposium)," (A. Poldervaart, ed.), Spec. Papers, Vol. 62, pp. 319–330. Geological Society of America.

Verhoogen, J., Turner, F. J., Weiss, L. E., Wahrhafting, C., and Fyfe, W. S. (1970). "The Earth. An Introduction to Physical Geology." Holt, Rinehart and Winston, New York.

Vine, F. J. and Matthews, D. H. (1963). Magnetic anomalies over oceanic ridges. *Nature* **199,** 4897947–949.

Vinogradov, A. P. (1962). Average contents of chemical elements in major types of Earth's crust igneous rocks. *Geochemistry* **7,** 188.

Vinogradov, A. P. and Yaroshevsky, A.A. (1965). On physical conditions of zonal melting in Earth's shells. *Geochemistry* 7, 779–790.

Vinogradov, A. P. and Yaroshevsky, A.A. (1967). Dynamics of the zonal melting and some geochemical consequences. *Geochemistry* **12**, 79–93.

Vityazev, A. V., Pechernikova, G. V., and Safonov, V. S. (1990). "Earth's Group Planets: Origin and Early Evolution." Nauka, Moscow, 296pp.

Vogt, P. R. (1974). Volcano height and plate thickness. *Earth Planet. Sci. Lett.* **23,** 3.

Voitkevich, G. V. and Lebedko, G. I (1975). Commercial deposits and Precambrian metallogeny. Moscow, Nedra, 231 p.

Voytkevich, G. V. (1979). "Fundamentals of the Earth's Origin Theory." Nedra, Moscow, 135pp.

Voytkevich, G. V., Kokin, A. V., Miroshnikov, A.E., and Prokhorov, V. G. (1990). "Reference Book of Geochemistry." Nedra, Moscow, 480pp.

Voytkevich, G.V. et al. (1990). Reference book of Geochemistry. Moscow, Nedra, 480 p. .

Vysotsky, V. I. and Golenkova, N. P. (1980). Causes of giant hydrocarbon concentrations in the Mesopotamian trough. *In* "Geology and Oil and Gas Occurrences of the Foredeeps," (A. E. Kontorovich, ed.), pp. 208–214. Nauka, Moscow.

Wadati, K. (1935). On the activity of deep-focus earthquakes in the Japan Island and neighborhood. *Geophys. Mag.* **8,** 305–326.

Walker, J. C. G. (1974). Stability of atmospherics oxygen. *Am. J. Sci.* **274,** 193–214.

Walker, J. C. G. (1977). "Evolution of the Atmosphere." Macmillan Publishing Company, New York, 318pp.

Watanabe, S., Mishima, K., and Matsuo, S. (1983). Isotopic ratios of carbonaceous materials incorporated in olivine crystals from the Hualalai volcano Hawaii. An approach to mantle carbon. *Geochim. J.* **17,** 295–104.

Wegener, A. (1912). Die Entstehung der Kontinente. *Geol. Rundsch.* **3,** 4276–292.

Wegener, A. (1922). "Die Entstehung der Kontinente und Ozeane, 3 umgearb." Vieweg, Aufl. Braunschweig.

Weizer, Ya. (1980). Evolution of $^{87}Sr/^{86}Sr$ in sea water in geologic history and its importance as indicator of the Earth's crust evolution. *In* "Early history of Earth", Moscow, Mir, p. 565–575.

Wells, J. W. (1963). Coral growth and geochronometry. *Nature* **197,** 948–950.

Wendt, H. (1956). In Search of Adam, Houghton Mifflin, Boston, p. 144–171.

Werner, A. G. (1787). Kurze Klassifikation und Beschreibung der verschiedenen Gebirgsarten, Dresden. (Sent to press, 1777).

Wilde, S. A., Vailey, J. W., Peck, W. H., and Graham, C. M. (2001). Evidence from detrital zircons for the existence of continental crust and oceans on the Earth 4.4 BY ago. *Nature* **409,** 175–178.

Wilson, A. T. (1960). Synthesis of macromolecules. *Nature* **188,** 1007–1009.

Wilson, J. T. (1963). A possible origin of the Hawaiian islands. *Can. J. Phys.* **41,** 863–870.

Wilson, J. T. (1965). A New Class of Faults and Their Bearing on Continental Drift: Nature, vol. 207, p. 343–347.

Wilson, J. T. (1968). Convection tectonics: Some possible effects upon the earth's surface of the from the deep mantle. *Can. J. Earth Sci.* **25,** 81199–1208.

Wit, M. J. (1998). On Archean granites, greenstones, cratons and tectonics: Does evidence demand a verdict? *Precambrian. Res.* **91,** 181–226.

Wit, M. J., Roering, C., Hart, R. J., Armstrong, R. A., de Ronde, C. E. J., Green, R. W. E., Tredoux, M., Peberdy, E., and Hart, R. A. (1992). Formation of an Archaean Continent. *Nature* **357,** 553–562.

Wood, J. A. and Mitler, H. E. (1974). Origin of the Moon by a modified capture mechanism, or half a loaf is better a whole one. *Lunar Sci.* **V,** 851–853.

Wyllie, P. J. (1984). Sources of granitoid magmas at convergent plate boundaries. *Phys. Earth Planet. Inter.* **35,** 112–18.

Yeremenko, N.A. and Chilingar, G. V. (1996). "Geology of Oil and Gas on the Verge of the Century." Nauka, Moscow, 176pp.

Yoder, H. S., Jr. (1976). "Generation of Basaltic Magma." National Academy of Sciences, Washington, DC.

Yoshii, T. (1975). Regionality of group velocities of Rayleigh waves in the Pacific and thickening of the plate. *Earth Planet. Sci. Lett.* **25,** 3305–312.

Zabanbark, A. (2004). Oil and gas basin of the Bay of Bengal as a potential hydrocarbon potential for the South Asia. *Oceanology* **44**, 778–783.

Zabanbark, A. (2006). Structural features and petroleum potential of the continental slopes of Gulf of Mexico (offshore USA). *Oceanology* **46,** 4596–602.

Zabanbark, A. and Konyukhov, A. I. (2005). Oil and gas potential of the continental slopes of the World Ocean: tectonic aspects. *Geotectonics* **1,** 99–106.

Zachos, J., Paganl, M., Sloan, L., Thomas, E., and Billups, K. (2001). Trends, rhythms and aberrations in global climate 65 Ma to Present. *Science* **292,** 686–693.

Zavaritsky, A. N. (1950). "Introduction to the Petrochemistry of Igneous Rocks." 2nd ed AN USSR Publishers, Moscow, Leningrad, 400pp.

Zeldovich, Ya.B. and Novikov, I. D. (1971). "Theory of Gravitation and Evolution of Stars." Nauka, Moscow, 484pp.

Zeldovich, Ya. B. and Novikov, I. D. (1975). "Structure and Evolution of the Universe." Nauka, Moscow, 736pp.

Zerr, A. and Boehler, R. (1993). Melting of (Mg, Fe) $SiO_3$ – perovskite to 625 kilobars indication of a high temperature in the lower mantle. *Science* **262,** 553–555.

Zharikov, V.A. (1976). "Fundamentals of Physicochemical Petrology." MGU Publishers, Moscow, 420pp.

Zharkov, V. N. and Trubitsin, V. P. (1980). Physics of the Planetary Subsurface. Nauka, Moscow, 448 p.

Zharkov, V. N. (1983). "Internal Structure of Earth and Planets." Nauka, Moscow, 415pp.

Zharkov, V. N. and Kalinin, V.A. (1968). "Equations of State of Solid Bodies at High Pressure and Temperature." Nauka, Moscow, 312pp.

Zharkov, V. N. and Trubitsin, V. P. (1980). "Physics of the Planetary Subsurface." Nauka, Moscow, 448p.

Zharkov, V. N., et al. (1971). "Physics of Earth and Planets, Shapes and Internal Structure." Nauka, Moscow, p. 384.

Zharkov, V. N., et al. (1974). Test distribution of the Q (t) dissipative function in the Earth's shell. *Izv. AN USSR Phys. Earth* **12,** 3–12.

Zonenshain, L. P. and Gorodnitsky, A. M. (1977). Paleozoic and Mesozoic reconstructions of continents and oceans. *Geotectonics* **2,** 3–23.

Zonenshain et al., 1976Zonenshain, L. P., et al. (1977). "Global Tectonics, Magmatism and Metallogeny." Nedra, Moscow, 231pp.

# Index

## F



## G



## H



## I



## K



## L



## M